

Dec 13, 11, 90

CVE H02918-24 - P024448

AJR

(24)

American
Journal of
Roentgenology

September 1989

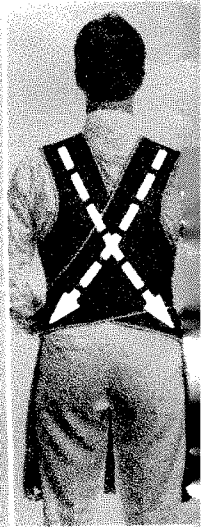
Serious side effects

Pulling forward on the sidestraps of any of E-Z-EM's Pinnacle™ Adjust-A-Weight™ protective garments has a very noticeable effect—it gradually redistributes the weight of the garment from your shoulders to your back and hips. The amount that you pull determines how the weight is spread, and spreading the load makes you feel more comfortable all over.

Our patented design uses non-snag Velcro® brand fasteners for easy adjustment, and comes in a variety of styles for radiology, cath lab, and operating room use. They're available in your choice of fabric, color, and trim.

To find out why Pinnacle has become the industry standard for comfort, contact your local representative, or call E-Z-EM toll-free at 800-645-3052. In New York call 516-333-8230.

E-Z-EM
More than barium—
much more



CIRCLE 5 ON READER SERVICE CARD

E-Z-EM, Inc.
7 Portland Avenue
Westbury, NY 11591

BING



American Journal of Roentgenology
Diagnostic Imaging and Related Sciences

Editor-In-Chief Robert N. Berk, *La Jolla, California*
University of California, San Diego
School of Medicine and Medical Center

Editor Emeritus Melvin M. Figley, *Seattle, Washington*

Associate Editor Saskia von Waldenburg Hilton, *San Diego, California*

Consulting Editor Juan M. Taveras, *Boston, Massachusetts*

Statistician Charles C. Berry, *San Diego, California*

P24,448

Editorial Board

John R. Amberg
Itamar Aviad
Mark E. Baker
Lawrence W. Bassett
Michael A. Bettmann
William G. Bradley, Jr.
N. Reed Dunnick
David K. Edwards
Ronald G. Evens
David S. Feigin
Sandra K. Fernbach
Richard H. Gold
William R. Hendee

John R. Hesselink
Charles B. Higgins
Melvyn T. Korobkin
Faye C. Laing
Thomas L. Lawson
Robert G. Levitt
Bruce L. McClennan
Richard P. Moser
Albert A. Moss
Jeffrey H. Newhouse
Donald L. Resnick
Stewart R. Reuter
Charles A. Rohrmann, Jr.

Peter M. Ronai
Sjef H. J. Ruijs
Stuart S. Sagel
David J. Sartoris
Stefan C. Schatzki
William P. Shuman
Edward A. Sickles
Barry A. Siegel
David D. Stark
Edward T. Stewart
Murali Sundaram
Eric vanSonnenberg
Robert K. Zeman

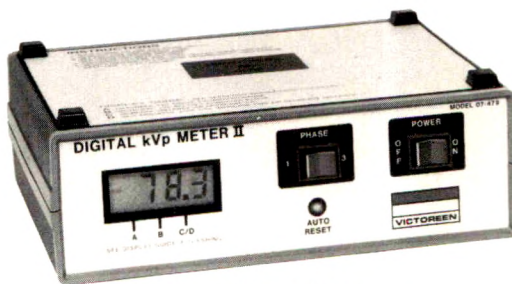
Editorial Staff: Margaret Levene, *managing editor*; Katie L. Spiller, Barbara Rose, Barbara L. Halliburton, and Janine Anderson, *manuscript editors*; Nancy Rydbeck, *office manager*; Sheri Smith, *administrative assistant*; Sandra L. Griffin, *administrative secretary*.

AJR, AMERICAN JOURNAL OF ROENTGENOLOGY (ISSN 0361 803X) is the official journal of the American Roentgen Ray Society and is published monthly by Williams & Wilkins, 428 E. Preston St., Baltimore, MD 21202. Annual dues include \$50 for journal subscription. Second-class postage paid at Baltimore, MD, and at additional mailing offices. Postmaster, send address changes (Form 3579) to AJR, 428 E. Preston St., Baltimore, MD 21202. Subscription rates \$100 (\$145 foreign); institutions \$110 (\$155 foreign); in training \$25 (\$70 foreign); single copy \$16 (\$19 foreign). Japanese rates include airfreight. Japanese yen price is available from our sole agent USACO Corporation, 13-12, Shimbashi 1-Chome, Minato-Ku, Tokyo 105, Japan, telephone 03-502-6471. Airmail rates furnished on request. Indexed by *Current Contents* and *Index Medicus*. Copyright © 1989 by American Roentgen Ray Society. 0361-803X/89\$2.00

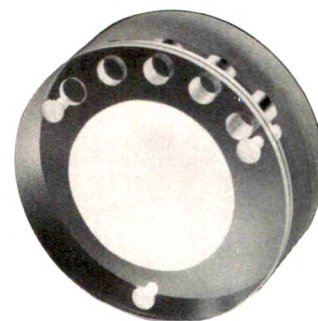
NUCLEAR ASSOCIATES...For All Your RADIOLOGY INSTRUMENTS & ACCESSORY NEEDS



Hand-Held
Dual-Reference
Digital Densitometer



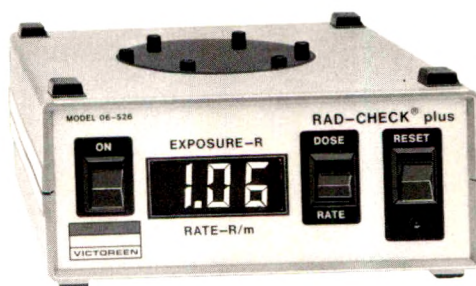
Digital kVp Meters
(Mammographic, General Purpose, Dental)



Mammographic QA Phantom



Radiglasses™ & Thyro-Shield™



RAD-CHECK® PLUS X-Ray Exposure Meter

Prima® 11b Fluoroscopy
Exposure Monitor



Precision High Voltage Divider



CLEAR-Pb® Mobile X-Ray Barriers



Hand-Held
Dual-Color Sensitometer

- Radiation Protection & Monitoring Equipment
- Quality Assurance Test Instruments

- Personal Protection & Safety Devices
- Improved Diagnostic Imaging Products

CIRCLE 36 ON READER SERVICE CARD

NUCLEAR ASSOCIATES



Division of VICTOREEN, INC.
100 VOICE ROAD • P.O. BOX 349
CARLE PLACE, NY 11514-0349 U.S.A.
(516) 741-6360 • FAX (516) 741-5414
A Member of THE TALBEX GROUP, PLC.

*For more information on our
complete line of
Radiology, MRI, CT products,
request Catalog GA-44*

AJR Guidelines for Authors

Address new and revised manuscripts, correspondence, and classified ads to the Editor:

AJR Editorial Office
2223 Avenida de la Playa, Suite 200
La Jolla, CA 92037-3218

Telephone: (619) 459-2229; FAX: (619) 459-8814

Inquiries regarding subscriptions, display advertising, reprints, or permission to republish *AJR* material should be addressed to the publisher:

The Williams & Wilkins Co.
428 E. Preston St.

Baltimore, MD 21202 Telephone: (301) 528-4133

The *AJR* publishes original contributions to the advancement of medical diagnosis and treatment. Submitted manuscripts should not contain previously published material and should not be under consideration for publication elsewhere. Papers dealing with neuroradiology should be addressed to: American Journal of Neuroradiology, Dept. of Radiology, Massachusetts General Hospital, Boston, MA 02114. At the discretion of the *AJR* Editor, *AJNR* articles that are of interest to the general reader may be republished in the *AJR*. Neuro-radiologic papers sent to the *AJR* will be forwarded to the Editorial Office of the *AJNR*.

Manuscript decisions are based on peer review. Reviewers receive manuscripts without title pages to ensure an unbiased review. Statements made in the article, including changes made by the Editor or manuscript editor, are the responsibility of the author and not of the *AJR* or its publisher. Authors will be sent the edited manuscript, galley proof, and proofs of illustrations. If the corresponding author will be unavailable to review galleys, arrangements should be made for a coauthor or colleague to read and return the proof.

The following guidelines are based on instructions set forth in the **Uniform Requirements for Manuscripts Submitted to Biomedical Journals** (*Ann Intern Med* 1988;108:258-265). Articles will be edited, however, to conform to the individual style of *AJR*.

General Guidelines for Major Papers

Abstract. Clearly state (in 200 words or less) the purpose, methods, results, and conclusions of the study. Include actual data.

Introduction. Briefly describe the purpose of the investigation, including relevant background information.

Methods. Describe the research plan, the materials (or subjects), and the methods used, in that order. Explain in detail how disease was confirmed and how subjectivity in observations was controlled.

Results. Present results in a clear, logical sequence. If tables are used, do not duplicate tabular data in text, but do describe important trends and points.

Discussion. Describe the limitations of the research plan, materials (or subjects), and methods, considering both the

purpose and the outcome of the study. When results differ from those of previous investigators, explain the discrepancy.

AUTHOR'S CHECKLIST

For priority handling, complete the following checklist, sign the copyright form on the reverse side of this page, and include both with the manuscript.

_____ Two copies of the manuscript (the original and a photocopy) and two complete sets of figures are submitted. One copy has been retained by the author.

_____ If appropriate, *AJR* Guidelines for case reports, technical notes, pictorial essays, or letters to the Editor have been followed. (See page A5.)

_____ The manuscript, including references, figure legends, and tables, is typed double-spaced on 8½ × 11 in. (21.6 × 27.9 cm) *nonerasable* paper. Right-hand margins are not justified.

_____ All manuscript pages are numbered consecutively beginning with the abstract. Authors' names do not appear on the manuscript pages.

_____ The manuscript is organized as follows: title page, blind title page (title only), abstract, introduction, methods, results, discussion, acknowledgments, references, tables, figure legends, and figures.

_____ Informed consent has been obtained from patients who participated in clinical investigations. If experiments were performed on animals, authors complied with NIH guidelines for use of laboratory animals.

_____ Use of unfamiliar acronyms and abbreviations is kept to a minimum. When abbreviations are used they are defined at first mention, followed by the abbreviation in parentheses.

_____ Metric measurements are used throughout, or the metric equivalent is given in parentheses.

_____ Names and locations (city and state only) of manufacturers are given for equipment and nongeneric drugs.

Title Page

_____ The following information is given: title of article; names and complete addresses (including zip code) of all authors; current addresses of authors who have moved since study; acknowledgment of grant or other assistance. The corresponding author is clearly identified, and a current address, phone number, and Fax number are given.

_____ Two copies of a blind title page are included giving only the title (without the authors' names) for use in the review process.

Abstract

_____ An abstract of approximately 200 words concisely states the purpose, methods, and results of the study in one paragraph. Actual data are included. Conclusions are stated in a second, summary paragraph.

_____ No abbreviations or reference citations are used.

References

References (not to exceed 35) are typed double-spaced starting on a separate page and are **numbered consecutively in the order in which they appear in the text**.

All references are cited in the text and are enclosed in brackets and typed on line with the text (not superscript).

Unpublished data are not cited in the reference list, but are cited parenthetically in the text, for example, (Smith DJ, personal communication), (Smith DJ, unpublished data). This includes papers submitted, but not yet accepted, for publication.

Inclusive page numbers (e.g., 333–335) are given for all references.

Journal names are abbreviated according to *Index Medicus*.

Style and punctuation of references follow the format illustrated in the following examples (all authors are listed when six or less; when seven or more authors, the first three are listed, followed by "et al."):

Journal article

1. Long RS, Roe EW, Wu EU, et al. Membrane oxygenation: radiographic appearance. *AJR* 1986;146:1257–1260

Book

2. Smith LW, Cohen AR. *Pathology of tumors*, 6th ed. Baltimore: Williams & Wilkins, 1977:100–109

Chapter in a book

3. Breon AJ. Serum monitors of bone metastasis. In: Clark SA, ed. *Bone metastases*. Baltimore: Williams & Wilkins, 1983:165–180

Paper presented at a meeting

4. Lau FS, Kirk AN. MR imaging of the spine. Presented at the annual meeting of the American Roentgen Ray Society, Washington, DC, April 1986

Tables

Each table is typed double-spaced on a separate page without vertical or horizontal rules; each has a short, descriptive title. Tables do not exceed two pages in length and contain at least four lines of data.

Tables are numbered in the order in which they are cited in the text.

Abbreviations are defined in an explanatory note below each table.

Tables are self-explanatory and do not duplicate data given in the text or figures.

All arithmetic (percentages, totals, differences) has been double checked for accuracy, and tabular data agree with data given in the text.

Figures and Legends

Two complete sets of original figures are submitted unmounted in labeled envelopes.

Figures are clean, unscratched, 5 × 7 in. (13 × 18 cm) glossy prints with **white borders**. A separate print is submitted for each figure *part*.

All figure parts relating to one patient have the same figure number.

Each figure is labeled on the back with the figure number and an arrow indicating "top." For black-and-white figures, labeling is done on a gummed label, which is then affixed to the back of the print. *Never* use labels on color figures, but write figure number on the back lightly in pencil. *Never* use ink on front or back of any figures.

Author's names are *not* written on the backs of figures.

Only removable (rub-on) arrows and letters are used on the figures. Symbols are uniform in size and style and are not broken or cracked.

Images are uniform in size and magnification.

Line drawings are done in black ink on a white background. They are professional in quality, and all use the same size type. (Only glossy prints are acceptable.)

Written permission has been obtained for use of all previously published illustrations (and copies of permission letters are included), and an appropriate credit line is given in the legends.

Legends are typed double-spaced, and figure numbers correspond with the order in which the figures are cited in the text.

Transfer of Copyright Agreement, Conflict of Interest Acknowledgment, Certification of Coauthors, and Exclusive Publication Statement

Complete copyright to the article entitled: _____

is hereby transferred to the American Roentgen Ray Society (for United States government employees to the extent transferable), effective if and when the article is accepted for publication in the *American Journal of Roentgenology*. In the case of the authors who are officers or employees of the United States government, the American Roentgen Ray Society recognizes that works prepared by officers or employees of the United States government as part of their official government duties are in the public domain.

Authors reserve all proprietary rights other than copyright, such as patent rights and the right to use all or part of this article in future works of their own. The authors retain the right of replication, subject only to crediting the original source of publication and receiving written permission from the publisher.

Authors guarantee that this manuscript contains no matter that is libelous or otherwise unlawful, invades individual privacy, or infringes any proprietary rights.

Authors understand that they will receive no royalty or other compensation from the American Roentgen Ray Society or the publisher.

Authors guarantee that the editor has been or will be informed of any proprietary or commercial interest or conflicts of interest the authors may have that relate directly or indirectly to the subject of this article.

All authors certify that they have made substantive and specific intellectual contributions to the article and assume public responsibility for its content.

Finally, the authors certify that none of the material in this manuscript has been published previously or is currently under consideration for publication elsewhere.

First author/date

Second author

Third author

Fourth author

Fifth author

Sixth author

This agreement must be signed by all authors in order for the manuscript to be published.

Case Reports

A case report is a brief description of a special case that provides a message that transcends the individual patient.

Format. There is no abstract. The introduction should be a short paragraph giving the general background and the specific interest of the case. No more than one case should be described in detail (similar ones can be mentioned briefly in the discussion). Emphasis should be on the radiologic aspects; clinical information must be limited to that necessary to provide a background for the radiology. The discussion should be succinct and should focus on the specific message and relevance of radiologic methods. A review of the literature is not appropriate.

Length. Maximum of five double-spaced, typewritten pages, including the references but not the title page or figure legends.

References. Maximum of eight.

Figures. Maximum of three or four, unless the text is shortened accordingly. Legends must not repeat the text.

Tables and Acknowledgments. Not appropriate in case reports.

Technical Notes

A technical note is a brief description of a specific technique or procedure, modification of a technique, or equipment of interest to radiologists.

Format. No abstract, headings, or subheadings are required. If headings are used, they should be a combination of "Case Report," "Materials and Methods," "Results," and "Discussion." A brief one-paragraph introduction should be included to give the general background. Discussion should be limited to the specific message, including the uses of the technique or equipment. Literature reviews and lengthy case reports are not appropriate.

Length. Maximum of five double-spaced, typewritten pages, including the references but not the title page or figure legends.

References. Maximum of eight.

Figures. Maximum of two, unless the text is shortened accordingly.

Tables and Acknowledgments. Not appropriate in technical notes.

Pictorial Essays

A pictorial essay is an article that conveys its message through illustrations and their legends. Unlike other *AJR* articles, which are based on original research, pictorial essays serve primarily as teaching tools, like exhibits at a scientific meeting. They are not encyclopedic book chapters. No abstract is necessary.

Length. Maximum of four double-spaced, typewritten pages, including the references but not the title page or figure legends.

References. Maximum of four.

Figures. Maximum of 30 figure parts. Number should be as few as necessary to convey the message of the paper.

Tables and Acknowledgments. Not appropriate in pictorial essays.

Letters to the Editor and Replies

Letters to the Editor and Replies should offer objective and constructive criticism of published articles. Letters may also discuss matters of general interest to radiologists. Do not end a letter with a hand-written signature.

Format. All letters should be typed double-spaced on nonletterhead paper, with no greeting or salutation. Name and affiliation should appear at the end of the letter. Titles for letters should be short and pertinent. The title for a reply is simply "Reply."

Length. Maximum of two double-spaced, typewritten pages, including references.

References. Maximum of four.

Figures. Maximum of two.

Tables and Acknowledgments. Not appropriate in Letters to the Editor and Replies.

Opinions, Commentaries, and Perspectives

Opinions, commentaries, and perspectives are special articles dealing with controversial topics or issues of special concern to radiologists.

Format. Include a title page but no abstract. Headings may be used to break up the text.

Length. Maximum of five double-spaced, typewritten pages.

References. Maximum of five.

Tables and Figures. Maximum of four.

Computer Page Articles

Articles published on the computer page deal with practical computer applications to radiology.

Format. Include a title page but no abstract.


Length. Maximum of eight double-spaced, typewritten pages.

References. Maximum of five.

Figures and Tables. Maximum of five. Computer printouts are not acceptable. Figures must be submitted as 5 × 7 in. glossy prints.

All submissions to the *AJR* must be accompanied by a completed copy of the Author's Checklist and the signed Copyright Agreement.

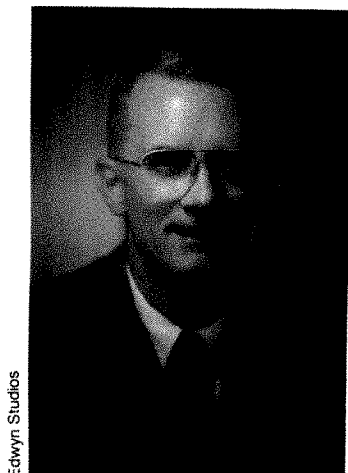
**THE
LOADER
THAT LOADS
CASSETTES
FROM
KODAK**



ARRS Presidential Address

A Time to Focus on Patients, Not Profit

Ronald G. Evens¹



Edwyn Studios

I am very appreciative of the honor placed on the president of our society by its leaders and members. Standing here today, I am very aware of my distinguished colleagues and friends in the audience before me and of the great radiologists who previously held this position. With genuine humility, I begin this year with the responsibility and challenge of a presidential address.

Our most recent president, Lee F. Rogers, titled his presidential message "The Ascendancy of Radiology" [1].

Summarizing the exciting development of our specialty since 1895 and the growth of the American Roentgen Ray Society since 1900, he eloquently described the struggles required to make radiology a prominent medical specialty and for American radiology to lead the world. Suggestions for action by President Rogers included a review of the need for subspecialty certification, a recognition of the importance of working with the political process, and constant vigilance to ensure that we do not become complacent. He summarized our current status as "the good times," yet warned of clouds on the horizon.

There has never been a better time to be a radiologist. Improved technology and the efforts of academic radiologists and scientists have expanded our role in patient care. We

have more patients, more respect, and can be highly satisfied about our contributions in improving patient care. We are also reaping the benefits of this increasingly esteemed position. As an example, we have progressed from a time when it was difficult to recruit enough medical students into our specialty to today, when we have a large and growing proportion of the very best students applying for training. Yes, these are the good times, but there are clouds on the horizon and some clouds are already overhead.

Charles Dickens began his novel *A Tale of Two Cities* with the famous phrase "It was the best of times, it was the worst of times." To many organizations and individuals in the United States, these words were never more true than when discussing medical care. Consider the following statements:

1. What irony that *today* in the United States we have the best resources for medical care available in the world, yet millions of our citizens have no access to care or cannot afford it.
2. We are increasingly successful with diagnostic and treatment methods and our understanding of disease processes is constantly improving, yet it is evident that many people are getting too many tests and too many medications.
3. Individual physicians continue to be held in high esteem by their patients, yet the "prestige" rating of physicians by the public at large is lower than it has been in years.

Presented at the annual meeting of the American Roentgen Ray Society, New Orleans, LA, May 1989.

¹ Mallinckrodt Institute of Radiology, Washington University School of Medicine, 510 S. Kingshighway Blvd., St. Louis, MO 63110. Address reprint requests to R. G. Evens.

4. Physicians have never been so financially well-off, yet there is growing evidence of fraud and abuse.

Why is there so much concern in this era of medical good times? Why are we radiologists, and other physicians, seeing increasing concern from others about the way we handle our affairs? I suggest it is because of the dollar costs associated with modern medicine. It is more evident as time passes that we cannot afford all of the medical possibilities available. Even with such an important topic as health, more and more people are beginning to realize that the sky cannot be the limit. Medical technology began its rapid advance in the 1940s, and it was quickly apparent that most individuals could not afford to pay for medical care out-of-pocket. The concept of medical insurance programs developed, with much of the financial responsibility placed on employers and local governments. The medical budget soon outgrew these resources, and federal and state governments began to bear part of the financial burden in the 1950s. Now businesses and all government agencies say they cannot afford the rising costs.

Most business or service activities have a predictable pattern of growth. Initially with a new and important technology, the growth is rapid. Later one expects a time of slower and controlled growth as the technology matures, and finally a slow reduction in activity as public interest or need is satisfied or competing programs develop. This has not been the pattern for medicine in general, and radiology in particular, as constantly improving technology has fueled the public's continuing demand for our services. It now seems likely that financial limits will force a slowing of medical expansion.

Arnold Relman, editor of the *New England Journal of Medicine*, recently sent a similar message to all medical professionals [2]. He describes three important periods in modern medicine. The first, from the 1940s to the 1960s, was the period of technological growth and seemingly unlimited funds that he calls the "era of expansion." The second phase is ongoing and is the "revolt of the payers" or the "era of cost containment." The third phase, the "era of assessment and accountability" is just beginning. Dr. Relman is convincing when he predicts that an increasing number of parties, soon to include many patients, will insist that medical professionals assess what they are doing and be accountable for the good and the bad.

The major issue is cost, but the questions and complaints are about a variety of problems. Some costs are rising for obvious reasons, for example, the aging population, inflation, and the much improved medical resources available today. Our critics focus on other reasons for increasing costs. They point to waste and inefficiency, cases where we do more than is necessary to solve a patient's problem, and fraud and abuse. Experts disagree on how serious the problems are, but whatever their magnitude, the continuing rise in health care costs will force us to respond to these issues. The challenge is to maintain our specialty in the best possible position during the next several years of adjustment from a period of rapid growth to a time of slow growth and increasing demand for assessment.

The title of this presidential address can serve as an overall guide for radiology's future. *We should focus on patients and*

not on profits. We physicians, including radiologists, have always been respected by our patients because we did not decide on our profession and the necessary long years of training in order to obtain high incomes; we became physicians to heal the sick. Suddenly, physicians have become part of a competitive and profit-oriented health care delivery system. Business training, an M.B.A. or a C.P.A., are not necessary to catch the entrepreneurial fever, there are plenty of businessmen and women who want to work with physicians for a price. Rather than trying to focus on profit making or profit taking, I firmly believe our best program for the future is to focus on what is best for our patients, as individuals and as a society.

Many in the audience will be surprised by this message. With my background in medicine, economics, and business administration, much of my academic interest has been related to the business aspects of our specialty. However, as with most radiologists, my decision to enter medicine and to become a radiologist was based on a desire to take care of patients.

The Increasing Emphasis on Money, not Medicine

An emphasis on money matters is relatively new to medicine. Radiology did not begin as a financially successful medical specialty. One of our first radiology leaders, Robert Newell of San Francisco, was so highly respected that he was asked to dedicate the Mayo Memorial Building at the University of Minnesota in 1954 [3]. He used this opportunity to discuss his concerns about the increasing emphasis on dollars and titled his presentation "Mink Coats and Cadillacs—A Discourse on the Nutrition and Hygiene of the Soul." The specialty of radiology went through difficult financial times in its early years, and it wasn't until after World War II that there was enough procedure volume and practice efficiency to become profitable. The increased volume and efficiency was due to technical improvements in film, X-ray tubes, and diagnostic equipment. The increased capacity of a radiographic room and the radiologist, plus an expanding health insurance program that was beginning to recognize reasonable charges for diagnostic procedures, placed radiologists among the higher paid physicians for the first time. Dr. Newell said, "The Cadillac and the mink coat are only symbols, emotional and I hope pointed, but only symbols. Let radiologists choose instead the payoff that is uniquely available to doctors, namely, the satisfaction of bringing the best we have to the patient who entrusts his life to our learning and our skill." Dr. Newell also noted that other physicians were beginning to be interested in performing X-ray studies because of the possible financial gain. Has anything changed since 1954?

It is bad news for patients when physicians focus excessively on the balance sheet and the income statement. Yet, it is hard not to focus on the financial bottom line when our hospitals and medical institutions are having difficulties. The daily newspaper regularly reports on reduced reimbursement, growing competition, and predictions about the closure of some hospitals. Even a few of the larger and most prestigious teaching hospitals are feeling the pinch. Many radiologists have already found difficulties with hospital and university

administrators who believe their professional future and salaries are dependent on short-term financial results. Of course, hospitals are not taking the competitive situation and financial pressures lightly. They have expanded entrepreneurial efforts, purchased physicians' practices, offered free rent to referring physicians, agreed to some forms of reimbursement that border on kickbacks, and are tempted to let other physicians provide radiology services. It has become a standard hospital administration dictum [4] that radiology has become a cost center and is no longer a profit center, as if this makes the radiology department less important to the hospital. We need to remind ourselves and others that our specialty gained its position and prestige because we help patients, not because we make a profit. We should emphasize our ability to serve patients with important diagnostic and therapeutic services in an expedient and cost-efficient manner, and not be required to make a profit for the hospital or other physicians.

Radiology is a Patient-Care Specialty

Another way to focus on patients is to emphasize that radiology is a patient-care specialty and radiologists are interested and involved in patient care. The best example of radiologists as primary care physicians is radiation oncology. For many weeks, and sometimes years, the radiation oncologist is the primary care physician or a key member of the physician team caring for the cancer patient. There are also a growing number of diagnostic procedures where radiologists should serve the patient as a primary care physician. Interventional procedures [5] and mammography [6] are examples where the radiologists can be a caring physician who is not only a source of technology, but a source of expert advice.

In this busy world of modern radiology, it is impossible for a radiologist to see every patient personally. Many patients do not need our direct intervention and advice but are best served by our sending a diagnostic report to the referring physician and our being available for consultation. Increasing pressure to control costs will require radiologists sometimes to serve as consultants when a radiograph is being considered in order to determine whether the procedure is necessary or which of several possible procedures is most cost-effective. Unfortunately, current payment mechanisms do not usually pay for a radiology consultation separate from a procedure. This is a difficulty that can be corrected by developing professional radiology consulting charges and convincing third-party payers and patients that they are appropriate expenses. We radiologists will have more control of our future with a successful program to emphasize that we are clinicians and are interested in patient care. We do not want to be considered one of "the RAPs" (i.e., radiologists, anesthesiologists, and pathologists), or hospital-based physicians, but should be associated with physicians who take care of patients directly.

Ethical Issues are Important

As we emphasize our interest and desire to be involved in patient care, we should dedicate ourselves to the highest ethical and moral values. I believe that Machiavelli was wrong

when he stated "The man who wishes to make a profession of goodness must necessarily come to grief in a world where so many are not good." Some physicians, hospital administrators, and other health care professionals seem to believe it is impossible to survive without compromising ethical standards. I do not believe this is the case and urge radiologists to support and maintain high ethical principles. Sometimes ethical principles seem hard to define and suggestions to change or compromise certain standards abound. In most cases, it is easy to define an ethical medical practice because it is what is best for the patient. Today there are several important medical controversies under consideration in which the final decision should be based on this fundamental principle: "what is best for the patient." Of great current interest is the issue of "self-referral" where a referring physician becomes the provider of a service. The potential adverse results are unnecessary procedures, expense, and risk for the patient.

When radiologists discuss "self-referral" we think of the use and abuse of obtaining radiographs, but the possibilities are endless and potentially include any technology or service where physicians refer patients. A short list includes prescription drugs, laboratory tests, physical therapy, wellness centers, psychological testing, EEGs, ECGs, and nursing homes. The potential problem did not begin with the recent organization of imaging centers but is more commonly associated with radiographic and diagnostic laboratories in physicians' offices. The risk to patients from self-referral is not limited to physician practice but can be a factor when hospitals own HMOs, PPOs, and nursing homes. Physicians are people who cannot be expected to be completely immune from financial temptation. Financial ownership in a laboratory or the direct provision of services by referring physicians that are not necessary for a physician's practice will lead to medical misconduct in some instances.

In taking a stand against self-referral and unnecessary physician ownership in health care facilities, we should review potential problems in the practice of radiology. We have to consider carefully whether it is appropriate for the radiologist to decide which diagnostic procedure should be delivered when a personal profit is the result. For example, is it ethical for a radiation oncologist to refer patients to a diagnostic radiology practice where the radiation therapist has a financial interest? The issues should be debated and the final decision be made in line with the ethical principle of what is best for the patient. Ethics should not be graded on a curve. An ethical "A" should always be a score of 100, not a score of 70 just because it is what others are doing.

Business incentives in medicine are not in themselves unethical. Much of American society is based on commerce, and it is certainly appropriate for physicians to be rewarded and appropriately compensated for their efforts and expertise. The need for proper financial incentives and rewards does not justify recent suggestions that profit making is essential to medical care and the modern practice of medicine. The very special relationship between patients and physicians is based on the principle that a sick person is highly vulnerable to the possibility of exploitation. Our patients have to rely on the fundamental premise that the doctor's first interest is in serving the patient, not personal profit [7].

A Radiologist Should be Involved in the Community

Our patients are also members of the community. Radiology is a demanding specialty, and it is easy for us to become absorbed with our professional lives. We should not forget that radiologists are among the most highly educated members of American society and have a responsibility to contribute to the community-at-large. My role model was Emmett J. Senn, a general practitioner in the small community of Herculaneum, MO. He was not only the good doctor who delivered me and took care of my family, but he was also the president of the public school board and a member and a leader in the Lions Club. He spent considerable time as a reviewer for the first-aid Boy Scout merit badge and regularly performed physical examinations for volunteer organizations at no charge.

Radiologists should be encouraged to serve others and should be recognized when they serve important roles in the community. There are many possibilities for service—scouting, church or synagogue, Red Cross, service clubs, school boards, politics, medical organizations, and so on. Radiologists who take the time to be citizen leaders will benefit our specialty.

Conclusions

This presidential address encourages our specialty and its members to focus on patients, not profit. There are four suggested areas for further consideration, discussion, debate, and action.

First, we should recognize the increasing emphasis on money, not medicine, by health care providers. We should try to change this emphasis. Fortunately, most programs and practices in radiology are based on benefit for the patient. We should be more careful in recognizing the inherent difficulties of our specialty to always "do more" with the current emphasis in technology development. Our specialty should insist on a thorough evaluation of new technology to be certain that it will result in better patient care, not higher fees.

Second, we should emphasize that radiology is a patient-care specialty. We should encourage more contact between radiologists and patients and spend more time in consultation

with referring physicians. We should develop a reasonable charge for consultation that is not associated with a procedure or treatment.

Third, we should promote and practice the highest of ethical standards. Our standard for ethics should be based on the principle of what is best for the patient. If there is confusion or ambiguity about ethics, we need to restate them and be clear about what we believe and what we do. We should not agree to participate in programs where economic abuse is likely. Ethics should not be graded on a curve.

Fourth, radiologists should play a service role in the community. We should encourage the members of our specialty to volunteer their time for medical and community programs.

Medicine and radiology are businesses but, more importantly, they are professions. Sound business practices and systems should serve a primary goal of providing better care to patients, not making a profit. Improving the financial position of a health care practice is an achievement when it improves patient care.

The specialty of radiology is on the high road, and we have never been more blessed with resources and people. We should acknowledge the public's demand for assessment and accountability, and our standard for evaluation should be what is best for the patient. With quality people, quality technology, and a goal of helping our patients, we can look at the next era as a challenge to find new ways of contributing to the community. It is not a time to rest on our achievements. The American Roentgen Ray Society and its members can be leaders, not followers.

REFERENCES

1. Rogers LF. The ascendancy of radiology. *AJR* 1988;151:393-395
2. Relman AS. Assessment and accountability: the third revolution in medical care. *N Engl J Med* 1988;319:1220-1222
3. Newell RR. Mink coats and Cadillacs: a discourse on the nutrition and hygiene of the soul. *JAMA* 1955;158:381-384
4. Evens RG. The importance of economics in academic radiology (or "money talks"). *Invest Radiol* 1988;23:227-228
5. White RJ Jr. Interventional radiology: we can't have it both ways. *Radiology* 1986;161:656
6. Monsees B, Destouet JM, Evens RG. The self-referred mammography patient: a new responsibility for radiologists. *Radiology* 1988;166:69-70
7. Pellegrino, ED. Altruism: self-interest and medical ethics. *JAMA* 1987;258:1939-1940

Eugene W. Caldwell Lecture

Health Care Choices for the Nineties

Senator Bill Bradley¹



We have made great strides in the United States health care system over the last several decades. More Americans think about health. More Americans than ever before think about wellness. More Americans than ever before are interested in medicine. Medical science itself has made enormous strides in the past few decades, as the fruits of research have manifested themselves in dramatically improved medical technology.

The human results are striking. In 1900, life expectancy at birth for the average American was 47 years. In 1985, it was 75 years. From just 1950, it had improved from 68 years to 75 years. Clearly Americans live longer, but health care costs continue to climb, now accounting for 11% of our gross national product, almost double the level of two decades ago, amounting to nearly \$550 billion annually. The per capita health expenditures in America have gone from approximately \$300 in 1970 to about \$450 in 1986, and that is in constant dollars. So we are spending more than any other country on health care, yet we cannot provide even basic primary care to all of our citizens. There are 37 million Americans today who have no health insurance at all and many more who are inadequately covered.

We have been talking about the problems in United States health care for a number of years, but we have not success-

fully resolved them. If anything, the magnitude of some of the problems has grown. But before focusing on the problems, let me try to put them in perspective.

I just got back from a trip to the Soviet Union. Since 1985, I have led a task force on the Intelligence Committee that has looked at the Soviet Union and what is happening with Mr. Gorbachev and the future course that country might take. On this trip to the Soviet Union, I paid particular attention to the health care system. I visited the health minister, a cardiologist named Chazov, and I visited many other sites of interest related to health care. In short, the quality and availability of health care in the Soviet Union is appalling. The infant and adult mortality rates are rising. In some places in central Asia, the infant mortality rate is as high as 60-70 per thousand, and the life expectancy for males in the area around the Aral Sea is 38 years. Thirteen percent of all deaths in the Soviet Union are due to bad water. Out of a pharmacologic list of a thousand drugs, the average Soviet pharmacy can provide about 80, maybe 90—on a rare day, 100. Syringes and catheters are frequently used over and over again. In fact, the first AIDS crisis that was admitted by the Soviet Union came from one AIDS-infected needle being used on 15 children.

Clearly the elite in the Soviet Union have a pretty good health care system. But the workers do not get much at all. Hospitals are overcrowded, nurses are virtually nonexistent, and doctors are not available. The average patient hospital expenditure including drugs and food is \$5.60 a day. So when we talk about health care in America and the problems we confront, let us make sure that you know, that I know, that everything is relative. In addition to the persistence of problems in the United States health care system, I really do not

Presented as the Caldwell Lecture at the annual meeting of the American Roentgen Ray Society, New Orleans, LA, May 1989.

¹ United States Senate, 731 Mart Bldg., Constitution Ave, Washington, DC 20510. Address reprint requests to Senator Bill Bradley.

want you to believe that by talking about the problems, I do not recognize the sizeable strides and the quality that exists in our country's health care system today.

But, the fact of the matter is, our health care system is not static. It changes. Because of escalating costs and the Reagan administration's emphasis on competition, we have witnessed a dramatic transformation of our health care system during the 1980s. First, we now have an increasing number of alternative delivery systems, including health maintenance organizations (HMOs), individual practice associations, and preferred provider organizations. Second, employers have restructured their health benefit plans to promote more cost-conscious behavior on the part of the employee. In other words, employees are required to pay more out-of-pocket for the health care services they receive. The employers also provide more options, such as HMOs. Third, a prudent-buyer approach to financing has led payers of health care, including Medicare, Medicaid, and private insurers, to price some health care services prospectively. For example, diagnosis-related groups create incentives to minimize costs because no matter how much care is provided for treatment of certain conditions, the reimbursement amount will be the same.

It is argued by some that these changes have helped contain health care costs. But, when you look at the health care system as a whole, rather than keeping costs down, many of these changes seem to be effectively shifting the cost burden to either different payers, such as consumers, or to different health care sectors, such as outpatient departments. These changes also expose the hidden subsidies of the reimbursement system. As a result, it is now much more difficult for the uninsured, a population that grew substantially in the early 1980s, to receive any free care. The number of uninsured grew by nearly 20% in the 1980s, because of increased competition, the recession, and the administration's attack on welfare programs. How is that so? Well, when welfare for the working poor was cut back, about a million working people lost their health insurance coverage because of the link between welfare and Medicaid.

As we have experienced it so far, the competitive approach to health care has not controlled costs. Medical prices continue to soar at a rate comparable to that during the inflationary 1970s. In the eighties, for example, prices went up 101%. As we have experienced it, a competitive approach, as I said, has not controlled costs. In addition, the competitive approach has made it increasingly unattractive for health care providers to provide care not only to the uninsured but also to poor people on Medicaid. For example, many providers seem to be saying that they cannot take all the Medicaid patients because reimbursement rates are not high enough.

The transformation in the health care environment has had another troubling impact, and all of you know this very well. Physicians' incomes have become greatly constrained and many physicians increasingly and more obviously have yielded to the profit motive in health care and have established or invested in various health care business arrangements, typically in the form of joint ventures or limited partnerships. Although some of these arrangements may indeed increase the quality of, and access to, health care services as a whole,

we cannot let these arrangements represent the norm in health care delivery.

Several studies have examined the pattern of patient referrals to these facilities, and frankly, between you and me, the findings are dismaying. One study found that patients of referring physicians known to be owners or investors in a clinical laboratory received on average 45% more clinical laboratory services than all Medicare patients in general. In an era of uncontrollable cost growth, we simply cannot afford to let this kind of abuse and overutilization continue. But as you know, that is only part of the problem. Health care is not a good that can be bought and sold as any other good in the competitive free market. The health care market is fraught with perverse incentives leading to conflicts of interest that undermine the doctor-patient relationship and the doctor's commitment to keeping the interest of the patient above all else.

Here, I would simply like to read from the American College of Physicians Ethics Manual. It states the following:

In the case of personal conflicts the moral edict is clear. The physician must avoid any personal commercial conflict of interest that might compromise his loyalty and the treatment of the patient. Collusion with nursing homes, pharmacists or colleagues for personal financial gain is morally reprehensible.

That is the ethics manual of the American College of Physicians. Congressman Pete Stark has introduced the Ethics in Patient Referrals Acts. The bill, as many of you know, would prohibit physicians from referring patients to facilities in which the doctor has an ownership interest or receives a payment for referrals. I think that this bill merits close scrutiny, and I would urge you to make your views known and improve the bill if you disagree with its present form.

Another major reform on the horizon is physician payment under Medicare. Congress is now looking at fee schedules based on the principle of ranking payments for physician service according to the financial, physical, and mental resources expended by physicians when caring for a patient. At the luncheon with the former American Roentgen Ray Society presidents today, we had a very interesting set of discussions about that subject. If enacted, this type of relative value scale, if it works right, would substantially increase payment for primary care services and decrease payment for surgery and other invasive procedures. Physicians would be more fairly reimbursed for taking the time to evaluate and counsel patients, and they would have less incentive to use high-cost medical technology inappropriately.

An emphasis on relative value and a relative-value-scale system might bring long overdue and needed change, not only because it could promote greater pay equity among physicians, but because it would better recognize the necessity of primary and preventive health care. In other words, we would be reinvesting in what should be, and perhaps at one time was, the foundation of health care delivery. But this is another subject that requires your involvement and I know

that you, more than most societies, have been directly involved in the last year in devising your own relative-value system.

But enacting major reforms of the system aimed at controlling costs, providing health care coverage to the uninsured, and shifting the focus of our health care systems is going to be a long and difficult process. We have to decide now how we as a society can provide health care that is equitable for both patients and providers, and above all is of high quality.

Walter Lippmann once said, "A rational man acting in the real world may be defined as one who decides where he will strike a balance between what he desires and what can be done. It is only in imaginary worlds that we can do whatever we wish." So how do we act rationally, and what balance are we striving to achieve? I clearly do not know all the answers, but I do have a few ideas that, given the onerous budget constraints, I believe make some sense.

In other words, in a world where the menu is large and the resources are small, where would I put some dollars? I have mentioned my support for paying for more primary care services under Medicare. I believe, to the extent possible, we need to invest in prevention and early detection. The coverage of immunizations and mammography screening under Medicare represent first steps in overcoming our health care system's almost sole focus on curative medicine. This coverage is important for the elderly and the disabled but it is absolutely critical for children and pregnant women. In no other type of service and in no other population could we better invest scarce resources than in preventive care and early detection for children and pregnant women. And if we do not have the resources to help all 37 million Americans who are uninsured, then our highest priority, I believe, should be our children.

Because of the number of uninsured, because of poverty, drug abuse, and teenage births, infant mortality and morbidity are horrendous problems in this country. From 1965 to 1982, the annual rate of infant mortality in the United States was cut in half, from 24 per thousand to 12 per thousand, but it was dropping even faster and further in other industrial countries, so that now the United States rate of infant mortality ranks about 18th on a list of 20 industrialized countries. Number one on the list, Japan, ranked first with an infant death rate that is half the infant death rate in the United States.

Each year in America 40,000 infants die and 385,000 other infants survive with serious health problems. The cost of caring for these kids in neonatal intensive care units is astronomical: hundreds of thousands of dollars per child in some cases and over two billion dollars annually, not to mention the cost of human suffering. And the fact of the matter is that we can prevent many of these deaths and illnesses. We know that lack of prenatal care is strongly associated with the birth of low-birth-weight babies and we know that infant mortality and morbidity are strongly associated with low-birth-weight babies. Therefore we know that prenatal care is an effective and cost-effective preventive tool. Immunizations, screening, and check-ups for young children are also critical for preventing illness and giving children the benefit of optimal growth

and development. So, in terms of rational choices in a real world, a real world with giant budget deficits and limited resources, I think it makes sense to invest in expanding access to prenatal care for pregnant women as well as primary services for children.

A few years ago, I wrote an article for *Women's Day* magazine about the problems of infant mortality. That was at a time when I thought the problem was primarily financial. I wrote the article and thought the answer to the problem was at least allowing Medicaid to cover prenatal care up to the level of poverty. In some states in this country, if you made more than 30% of poverty and you were a woman, you got no prenatal care covered by Medicaid. I wrote the article, one article, and I got 7,000 letters from women all across this country and their story was the same by and large, and that was: "I was pregnant. I didn't have any health insurance. I was making too much to qualify for Medicaid but I didn't have any coverage at work and therefore when I couldn't go to the doctor and have it paid, I didn't go to the doctor. I had a low-birth-weight baby and the baby died or the baby was in serious straits and remains so." Story after story. Well, Henry Waxman and I went to work, we expanded Medicaid eligibility for pregnant women and infants. First for pregnant women with incomes up to 100% of poverty and this year, we hope to raise it to 185% of poverty, so that we can get over the financial hurdle in ensuring access to prenatal care for women who are poor and near-poor.

I am a member of the National Commission to Prevent Infant Mortality, and this year we have tried to address the problem of nonfinancial barriers to receiving prenatal care, such as lack of information or poor coordination among health- and nutrition-related programs. Our proposals include some greatly needed services such as maternal and pediatric health handbooks for all pregnant women and new families, which exist in almost every other country in the world, and home-visiting programs for high-risk pregnant women and new mothers.

So, in the grand scheme of health care, the infant mortality initiatives may seem small and incremental. But I think these steps are solid and important. And in the face of severely limited health care dollars, I think investing in pregnant women and children is the right choice to make, and I hope you agree.

Our American society has created great economic prosperity, and a health care system equipped with the best and most modern technology, but we seem in some cases to neglect the basics in order to allow income to select quality of care. And we have responded more to the health needs of the elderly than to the health needs of the young. The challenge for the so-called medical-industrial complex, and for its government partner, is to devise a more humane, cost-effective and personal health care system, while at the same time to continue our technological advance. It will not be an easy task, but it will dominate the policy debate of the next decade and will shape the work that both you and I do. As Dr. Ronald Evans said in his presidential speech, he hopes that this society and its members—not only hopes, but he said that you must be a leader in this debate and a leader who never loses sight of the goal, which is helping patients.



AMERICAN JOURNAL OF ROENTGENOLOGY

MELVIN M. FIGLEY FELLOWSHIP IN RADIOLOGY JOURNALISM

The American Roentgen Ray Society announces a one-month fellowship in radiology journalism in the La Jolla editorial office of the AJR. Board-certified radiologists with special academic promise are invited to apply.

PURPOSE

The purpose of the fellowship is (1) to stimulate bright young radiologists to continue with an academic career, to accelerate their progress, and to stimulate their interest in good radiology journalism, and (2) to improve the quality of radiology journals by teaching the fundamentals of medical journalism to academicians, training manuscript reviewers and future editors, and providing core teachers of medical journalism in radiology departments around the country.

CURRICULUM

The fellow will be taught the fundamentals of medical writing, manuscript preparation, peer review, manuscript editing, the ethics of scientific journalism, and journal publication and printing in personal tutorials given by the AJR editors and editorial staff through hands-on experience in the editorial office. He or she will visit Williams & Wilkins in Baltimore to observe the publication and printing process.

STIPEND

The successful candidate will be awarded \$10,000, which includes the cost of travel to La Jolla and Baltimore, living expenses for the month, and an honorarium.

APPLICATIONS

Candidates should apply in writing to Robert N. Berk, M.D., Editor-in-Chief, AJR Editorial Office, 2223 Avenida de la Playa, Suite 200, La Jolla, CA 92037. The letter must include a curriculum vitae and a description of the candidate's goals during the fellowship. Letters of recommendation from his or her department chairman and one other senior person are required. Deadline for receipt of applications is Nov. 1, 1989. The successful candidate will be notified Dec. 1, 1989, and may choose one of the following months for the fellowship training: Jan., Feb., March, April 1990.

Review Article

Interventional Neuroradiology

Van V. Halbach,¹ Randall T. Higashida, and Grant B. Hieshima

Interventional neuroradiology has emerged as a relatively new subspecialty. In the past decade the development of small microcatheters and balloons has permitted access to a wide variety of neurovascular pathology. Some of the diseases in which this specialty is particularly beneficial are discussed in this review.

Direct Carotid-Cavernous Fistulas

Direct carotid-cavernous fistulas are acquired connections between the cavernous internal carotid artery and the cavernous sinus and most often are the result of blunt trauma associated with a basal skull fracture [1]. Other less common causes are penetrating injuries, collagen-deficiency diseases, ruptured intracavernous aneurysms, arterial dissections, fibromuscular dysplasia, and iatrogenic injuries [2]. The most common presenting symptoms are pulse synchronous bruit, proptosis, chemosis, headaches, and cranial-nerve palsies. Less commonly these patients can have epistaxis, otorrhagia, intracerebral hemorrhage, dementia, hydrocephalus, stroke, visual loss, and blindness [3]. The angiographic features that are associated with a poorer prognosis are the presence of a dilated cavernous sinus varix, cortical venous drainage into the intracerebral veins away from the cavernous sinus, the presence of a pseudoaneurysm, and obstruction of the anterior superior ophthalmic vein [3]. The earliest treatments consisted of surgically occluding the proximal carotid artery or performing a trapping procedure with carotid ligation and clipping of the supraclinoid carotid artery [4, 5]. Because the

ophthalmic artery arose from the trapped segment, where perfusion pressure is greatly reduced after trapping, and because external to internal collaterals were present within the trapped segment, these patients invariably lost vision after the trapping procedures and often the fistula would remain patent [6]. The development of detachable balloon systems by Serbinenko [7] and Debrun et al. [8] has yielded a technique in which the carotid-cavernous fistula can be occluded with preservation of the parent artery. Figure 1 is an example of a carotid-cavernous fistula due to trauma treated by transarterial balloon techniques. Several large series have demonstrated the effectiveness of the transarterial route for closure of the majority of direct carotid-cavernous fistulas [9–11]. Rarely the transarterial route is unsuccessful because of inaccessibility, previous carotid ligations or dissections, or a fistula orifice too small to allow placement of a detachable balloon in the cavernous sinus. Retrograde catheterization of the draining venous pathways through the inferior petrosal sinus or the superior ophthalmic vein can permit access to the fistula site and allow closure of the fistula by placement of balloons, coils, liquid adhesives, or combinations of these [9, 12]. With smaller fistulas, compression of the involved carotid artery and jugular vein has been shown to be an effective treatment by reducing the arterial inflow, increasing the venous pressure, and promoting thrombosis within the fistula [13]. Our own experience with endovascular treatment of over 200 symptomatic carotid-cavernous fistulas has resulted in complete closure of the fistula in 99% and preservation of the parent artery in 88% of cases with a complication rate of 4.9%, primarily for strokes or sympto-

Received March 23, 1989; accepted after revision May 15, 1989.

¹ All authors: Departments of Radiology and Neurologic Surgery, University of California, San Francisco, 505 Parnassus Ave., San Francisco, CA 94143-0628. Address reprint requests to V. V. Halbach.

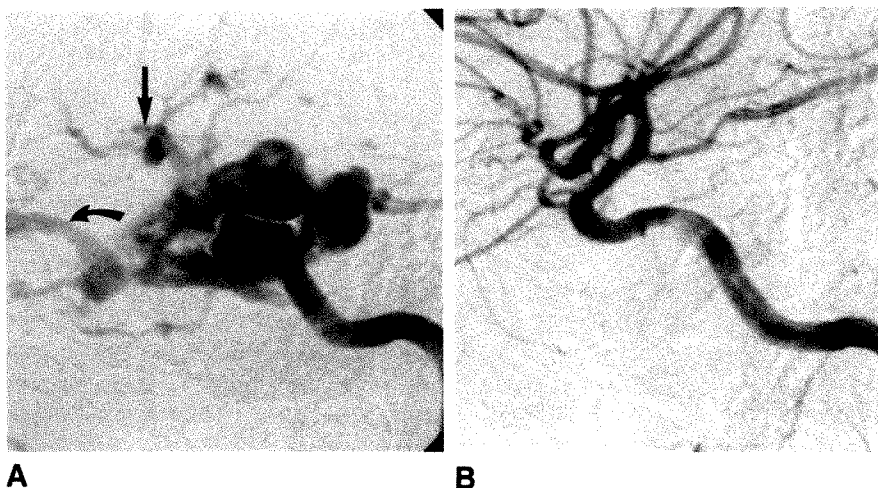


Fig. 1.—17-year-old man who sustained a basal skull fracture during a motor vehicle accident and developed rapidly progressive proptosis, chemosis, and visual loss in the right eye.

A, Right internal carotid angiogram, lateral projection, shows a carotid-cavernous fistula associated with a large cavernous sinus varix with drainage to the superior ophthalmic vein (curved arrow) and cortical venous drainage (straight arrow).

B, Right internal carotid angiogram, lateral projection, shows complete closure of fistula with preservation of parent artery after balloon embolization.

matic pseudoaneurysm formation [11]. Endovascular techniques have emerged as the primary definitive treatment of symptomatic carotid-cavernous fistulas, with acceptably low morbidity and mortality rates in experienced hands [9–11].

Vertebral Artery Fistulas

Vertebral artery fistulas are solitary connections between the vertebral artery and surrounding paravertebral veins and most often are the result of penetrating injury [14, 15]. Less often these fistulas are congenital; the result of blunt trauma [16]; or associated with neurofibromatosis [17], fibromuscular dysplasia [18], or collagen-deficiency diseases. The signs and symptoms resulting from vertebral artery fistulas are usually bruit and neck pain but can be brain or spinal cord dysfunction [19], subarachnoid hemorrhage, external hemorrhage, expanding hematomas, distal embolic events, and airway obstruction [20]. The earliest treatments for this disease consisted of surgical occlusions of the proximal vertebral artery or trapping procedures, which could aggravate symptoms and rarely resulted in fistula closure [14]. Although direct surgical exposure and repair of the vertebral artery has been described, it can be complicated by proximity to surrounding arterialized veins and adjacent critical structures. Newer endovascular techniques have included treatment with coils and detachable balloons [21–23]. Figure 2 shows a 33-year-old woman with right pulsatile tinnitus treated successfully by detachable balloon therapy. Patients with fistulas of long duration can develop tremendous vascular steal from the intracranial vessels into the fistula. The vascular territories supplied by these intracranial vessels can become ischemic and lose their ability to autoregulate cerebral blood flow. Following abrupt closure of the fistula, a relative overperfusion can occur in the ischemic vascular territory that can result in neurologic dysfunction or hemorrhage [24–26]. The closure of these fistulas should be performed in an awake patient, with careful observation for these signs and symptoms; if observed, staged or gradual occlusion can result in complete fistula obliteration without devastating complications.

In patients with complete transection of the vertebral artery, trapping of the fistula segment with balloons is often required

to achieve complete closure of the fistula. Because of retrograde flow in the distal vertebral artery above the transection, occlusion of the parent artery is always tolerated [23]. Several series have reported excellent results with endovascular treatment of vertebral artery fistulas, with low morbidities and no mortality [11, 21–23, 25]. In our series of 35 patients, the complete cure rate was 100% with only one complication (mild stroke). This technique has emerged as the definitive procedure in patients with symptomatic vertebral fistulas.

Vein of Galen Malformations

Vein of Galen malformations are congenital connections between intracerebral vessels and the vein of Galen or the adjacent midline middle cerebral vein. The arterial supply usually is from the thalamoperforator vessels, pericallosal branches of the anterior cerebral arteries, and anterior and posterior choroidal vessels, and rarely may include the superior cerebellar and middle cerebral arteries [27, 28]. These connections can be large direct fistulas or smaller, more numerous connections. The clinical presentation can be classified into three distinct groups: the neonate who has intractable congestive heart failure at birth, the infant who develops hydrocephalus and seizures, and the older child with hemorrhage [29]. The vast majority of patients fall into the first category, which has the largest degree of arteriovenous shunting and the poorest prognosis; it is nearly always fatal unless treatment is instituted [30, 31]. Medical treatment alone rarely is able to control the heart failure, although it is a useful adjunct [31]. Prior to endovascular interventional techniques, the initial treatment of this complicated disease included surgical ligation of the anomalous connections; however, the results of surgical ligation have been disappointing. A recent review of 60 neonates treated by surgical ligation of the feeding vessels revealed only six survivors, three of whom were neurologically intact [31]. Endovascular treatment has emerged as an effective initial treatment in patients who require therapy [32–34]. These endovascular treatments fall into three distinct categories: free-particle embolization; superselective catheterization and embolization of the connections with liquid adhesives, particles, platinum coils, or silk

sutures; and transvenous embolization with coils and balloons. The venous approach can be performed through a small craniotomy made over the torcular Herophili, with direct catheterization of the vein of Galen through the straight sinus or falcine sinus [33, 34], or through transvenous catheterization of the vein of Galen from a transfemoral route [35]. Figure 3A is a carotid angiogram of a neonate with severe congestive heart failure. After several staged arterial and venous embolizations the fistula was almost completely obliterated (Fig. 3B). Although some of these procedures do not result in complete cure of the arteriovenous connections, the flow is markedly reduced, allowing the neonate to develop to a point where a more definitive treatment can be performed. The complication rate reported with these techniques is approximately 15–20%; complications consist of infarction of deep structures from errant emboli, uncontrolled cardiac failure from migration of emboli to the lungs producing massive pulmonary embolism, and hemorrhage [32–35]. Endovascular techniques have emerged as excellent primary or adjunctive

techniques for the treatment of symptomatic vein of Galen malformations.

Cerebral Aneurysms

The vast majority of symptomatic intracerebral aneurysms can be managed by surgical procedures, usually clipping of the aneurysm with preservation of the parent vessel. However, in some patients either surgical clipping fails or, because of the aneurysm's size or location or the patient's underlying clinical condition, the patient is not a surgical candidate. Several series have shown that it is technically possible to treat intracranial aneurysms with detachable balloon therapy [36–40]. Some of these showed the usefulness of proximal occlusion or trapping with detachable balloons, thus eliminating the aneurysm and the parent vessel [38, 40]. More recently, several series have reported the effectiveness of placing a balloon within the aneurysm, excluding it from the

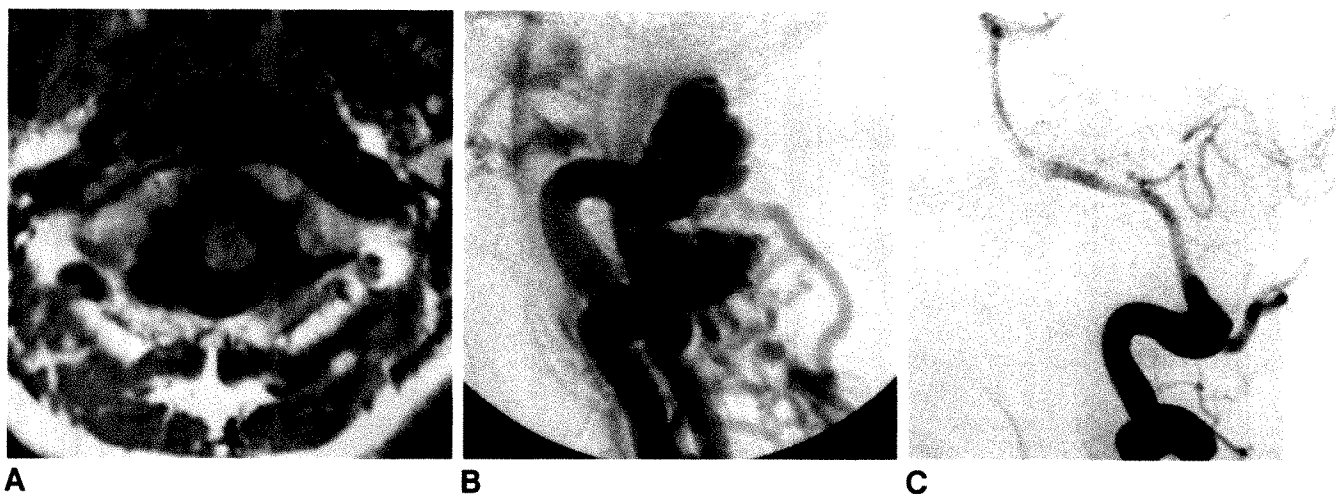


Fig. 2.—33-year-old woman with right ear tinnitus and headaches.

A, T1-weighted axial MR image (TR = 739 msec, TE = 39 msec) through the foramen magnum shows area of abnormal signal void to the right of the spinal cord.

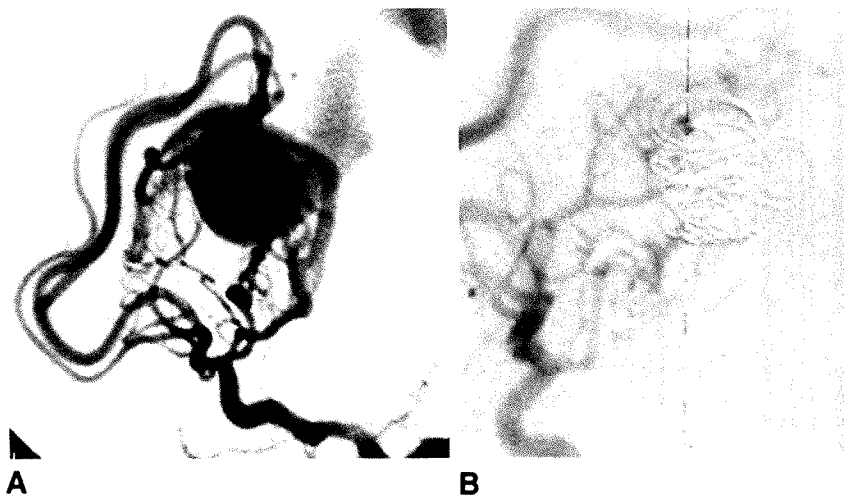
B, Right vertebral injection, lateral projection, shows vertebral fistula at C1 level with drainage to paravertebral veins and epidural venous plexus.

C, Same injection and projection 1 month after balloon embolization reveals complete closure of vertebral fistula and preservation of parent artery.

Fig. 3.—Neonate with severe intractable congestive heart failure.

A, Right common carotid angiogram, lateral projection, on day 10 shows multiple fistulas arising from lateral posterior choroidal, anterior choroidal, and pericallosal arteries supplying vein of Galen malformation.

B, Right internal carotid angiogram, lateral projection, 2 years after arterial particulate and transvenous coil embolization shows marked diminished flow in the malformation. The patient remains developmentally normal.



circulation and preserving the parent vessel [37, 41–47]. Figure 4 shows a 27-year-old woman with a symptomatic carotid-ophthalmic aneurysm in whom surgical clipping failed but transvascular embolization techniques were successful.

Figure 5 shows a 37-year-old woman who had diplopia and headaches caused by a basilar tip aneurysm. A single silicone balloon was placed into the aneurysm resulting in complete obliteration of the aneurysm (Fig. 5B).

Most of these procedures are performed under local anesthesia with IV sedation allowing continuous neurologic monitoring. If the aneurysm has fresh intraaneurysmal thrombus or the absence of a definable neck, then parent artery occlusion is performed if tolerated. If the aneurysm has a defined neck and no recent intraaneurysmal thrombus, then a balloon can be navigated into the aneurysm in the majority of cases. To ensure continued inflation and obliteration of the aneurysm, the contents of the balloon are commonly solidified with 2-hydroxyethyl methacrylate [47] or a silicone polymer [37].

In our experience with over 200 aneurysms treated by detachable balloon therapy, the parent artery was preserved in 40% of the cases. The remaining patients had either the absence of a well-defined neck, the presence of intraaneurysmal thrombus, or technical factors preventing placement of the balloon in the aneurysm. Aneurysms that have been treated by balloon embolization include petrous and cavernous-carotid aneurysms [44–46]; those in the carotid-ophthalmic [42], posterior communicating, and anterior communicating regions; middle cerebral artery aneurysms; those of posterior inferior cerebral artery origin; and vertebral artery, basilar artery, posterior inferior cerebral artery, and distal posterior cerebral artery aneurysms [43–47]. At our institution we reserve detachable balloon therapy for treatment of intracranial aneurysms in which neurosurgical clipping has failed, in patients who are not surgical candidates, or in which the projected risks of surgical clipping are excessively high. Our complications in these procedures include 6.7% transient

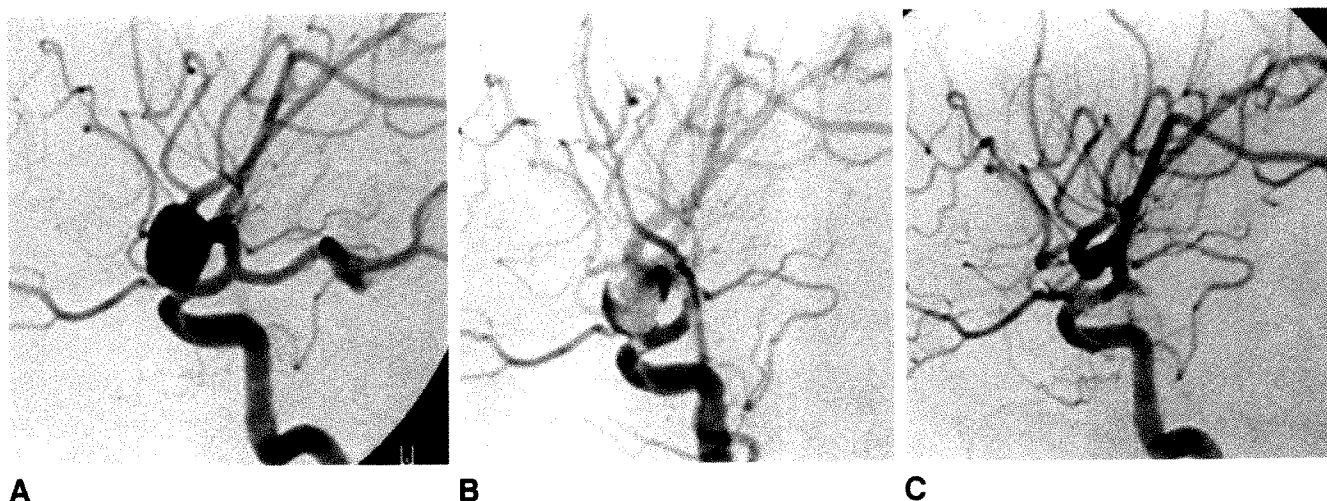


Fig. 4.—27-year-old woman with headaches caused by a carotid-ophthalmic aneurysm in which surgical clipping failed 6 years before balloon therapy. A, Left internal carotid angiogram, lateral projection, shows large carotid-ophthalmic aneurysm. B, Same injection and projection immediately after placement of a single silicone balloon within aneurysm lumen. Note residual filling between balloon and aneurysm wall. C, Same injection and projection at 6-month follow-up shows obliteration of aneurysm.

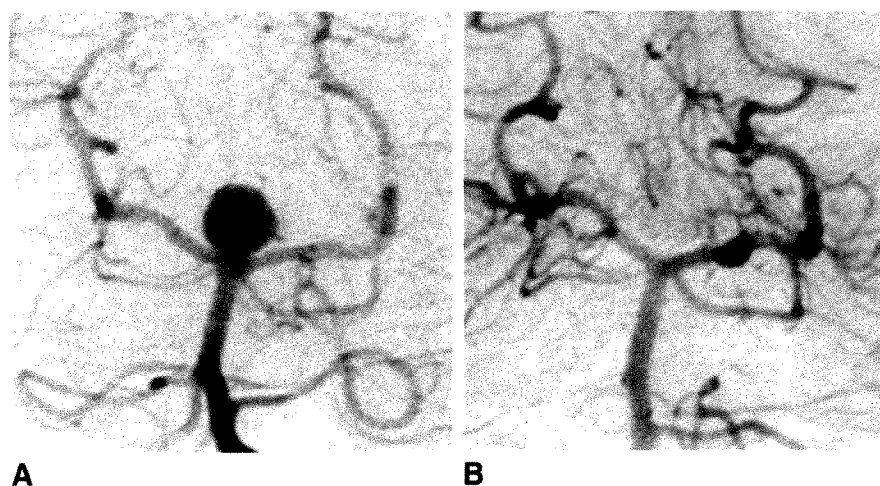


Fig. 5.—37-year-old woman with diplopia and headaches caused by a basilar tip aneurysm that could not be clipped surgically.

A, Left vertebral artery injection, Towne's projection, reveals basilar tip aneurysm extending superiorly into cerebral peduncles.

B, Same injection and projection after embolization with a single silicone balloon shows complete aneurysm obliteration and preservation of posterior cerebral arteries.

ischemic deficits, 9.3% strokes, and 4.0% hemorrhages, which have resulted in a permanent morbidity rate of 9.3% and a mortality rate of 5.6%. Romodanov and Shcheglov [37] have reported impressive results in a large series of aneurysms treated by balloon embolization techniques, many of which would be considered surgically clipable aneurysms.

Despite the impressive initial results with detachable balloon embolization therapy of intracranial aneurysms, the current surgical management of this disease is outstanding. Therefore, we believe that surgical exploration should be performed in symptomatic intracranial aneurysms whenever clipping is possible, given a reasonable risk of morbidity and mortality. Balloon embolization procedures should be reserved for patients in whom this established technique has failed or in whom surgical risks are unacceptable. Whether advances in balloon technology, delivery systems, and increased operator experience will produce balloon embolization results that surpass surgical procedures is purely speculative.

Vasospasm After Subarachnoid Hemorrhage

Symptomatic vasospasm after aneurysmal subarachnoid hemorrhage remains the major cause of delayed morbidity and mortality in patients who survive the initial hemorrhage. Despite a plethora of various pharmacologic agents and the use of volume expansion and induced hypertension, many patients continue to experience considerable morbidity and mortality from this disease. Several reports have demonstrated the efficacy of transluminal angioplasty to improve or alleviate symptoms associated with vasospasm [48, 49]. Figure 6 shows a 61-year-old man in whom a coma state requiring intubation developed 1 week after a subarachnoid hemorrhage. Following transluminal angioplasty, an immediate improvement was seen in his neurologic state. Our experience with 13 patients has shown that the angioplastied segments remain dilated unless hemorrhage recurs [49]. Often dramatic clinical improvement occurs shortly after angioplasty of severe spasm. Angioplasty can be performed in patients with an unclipped aneurysm; however, increased

perfusion and pressure can be transmitted to the recently ruptured aneurysm, thereby increasing the risk of rebleeding. Therefore, the ruptured aneurysm should be dealt with in a timely fashion if a successful angioplasty results in clinical improvement. Another complication can occur if angioplasty is performed too late after the onset of neurologic decline. Reperfusion of infarcted brain can transform a bland into a hemorrhagic infarction; therefore, these procedures should be performed in the acute phase before infarctions have occurred. Additional risks of thromboembolic complications and vascular rupture are possible with this technique but are difficult to estimate with the small size of published series. Despite these limitations, preliminary results have been encouraging. Larger series are needed to evaluate the efficacy, delayed sequelae, risks, and indications of this technique.

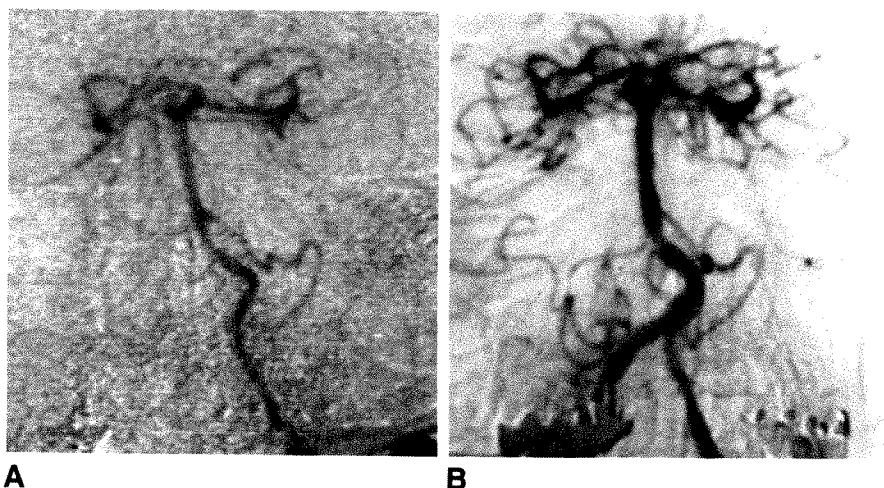
Atherosclerosis

Percutaneous transluminal angioplasty of the innominate, carotid, subclavian, vertebral, and intracranial vessels is being performed in selected cases [50–55]. Traditional medical therapy has failed in most of these patients, and they present with a variety of symptoms such as strokes, transient ischemic attacks, subclavian steal, vertebral basilar insufficiency, or progressive neurologic deterioration. Angioplasty has been reported to alleviate most of these symptoms with a low morbidity rate [50–55], except in the case of intracranial atherosclerosis [55], which has a high morbidity rate, presumably due to occlusion of critical perforator arteries in these territories. The development of endovascular stents may offer some improvement in the treatment of this disease in the future. The results of extracranial transluminal angioplasty have been quite encouraging. Of the 117 cases reported involving eight innominate, six proximal subclavian, 12 vertebral, 21 common carotid, four external carotid, and 66 internal carotid arteries, the only complications were a transient ischemic attack lasting 5 min in a patient who underwent bilateral vertebral angioplasties and two groin hematomas [51, 55]. The angiographic follow-up demonstrated return to normal luminal diameter in 40% of cases and substantial

Fig. 6.—61-year-old man who presented with a subarachnoid hemorrhage. One week later he became comatose, ventilator-dependent, and unresponsive to painful stimuli (grade 4–5 Hunt-Hess classification).

A, Left vertebral angiogram shows diffuse spasm involving intradural distal left vertebral artery, basilar artery, and both posterior cerebral arteries with aneurysm between right posterior cerebral artery and superior cerebellar artery.

B, Same injection and projection after transluminal angioplasty of both intradural right and left vertebral, basilar, and proximal posterior cerebral arteries. Marked improvement is seen within luminal caliber of these vessels. After angioplasty of distal basilar artery the patient awoke, became clinical grade 2, and was extubated.



improvement in intraluminal caliber in the remaining 60%. The clinical follow-up has averaged 27 months and all patients have been asymptomatic. Potential complications include acute stroke, subintimal dissection, vasospasm, and vessel perforation.

Dural Arteriovenous Fistulas

Dural arteriovenous fistulas can present with a wide clinical spectrum of signs and symptoms primarily related to their location and their venous drainage.

Transverse and Sigmoid Sinus Dural Fistulas

These fistulas pose the highest risk and remain the greatest therapeutic challenge. On one end of the spectrum these patients can be entirely asymptomatic or merely have headaches or bruit. On the other end of the spectrum they can present with strokes, seizures, altered mental status, hemorrhage, papilledema, and dementia [56–59]. The angiographic findings of stenosis involving the dural sinus with diversion of arterialized venous drainage into cortical veins poses a high risk of stroke, neurologic deficit, or hemorrhage [58, 59]. Surgical excision of the involved dural sinus can be performed but is not without substantial morbidity and mortality [60]. The initial endovascular treatments consisted of subselective catheterization of the external carotid arterial supply and embolization with particles or liquid adhesives [59]. Although the majority of patients had either symptomatic improvement or complete alleviation of their symptoms, approximately one-third of the patients would continue to have symptoms related to their dural fistula. More recently a transvenous embolization procedure has been described, either from direct surgical exposure [61] or a transfemoral venous access [62]. Thrombogenic material, usually platinum or steel coils, is placed directly into the involved dural fistula, producing thrombosis and often complete obliteration. Although this technique has produced complete cure in most of the patients treated, it is reserved for patients in whom cortical venous drainage away from the dural sinus is demonstrated. Our own experience with over 50 dural fistulas involving the transverse and sigmoid sinus region has yielded a complete cure rate of 59% for transarterial embolization and 82% for transvenous embolization, with a complication rate of 6–8%. Endovascular procedures are often considered a primary definitive treatment for symptomatic dural fistulas in this region.

Cavernous Sinus Dural Fistulas

Cavernous dural fistulas most often occur spontaneously in elderly women but can be associated with trauma, sinusitis, cavernous sinus thrombosis, and pregnancy [63–65]. Although spontaneous obliteration is possible [66, 67], the majority remain symptomatic producing headaches; bruit; proptosis; ophthalmoplegia; and, rarely, diminished visual acuity, blindness, and hemorrhage. Initial endovascular treatments have consisted of subselective catheterization of the external carotid dural supply, usually the ascending pharyn-

geal artery, middle meningeal artery, and distal branches of the internal maxillary artery, and embolization with a variety of embolic agents [68, 69]. Some patients remained symptomatic after these procedures because of recruitment or enlargement of the dural supply arising from the internal carotid artery. Although embolization of these branches is technically possible [70], the risk of embolic stroke makes this the less desirable treatment. Recently, transvenous embolization has been described through the inferior petrosal sinus or superior ophthalmic vein with placement of thrombogenic material, either platinum or steel coils, silk suture, or liquid adhesives, to produce complete obliteration of the fistula [71]. Figure 7 is an example of a symptomatic cavernous dural fistula treated by transvenous techniques.

Patients who do not demonstrate cortical venous drainage or progressive visual loss are begun initially on a trial of compression therapy [13, 69] to promote thrombosis at the fistula site. This will result in complete cure in one-third of the patients treated. Our own experience with endovascular treatment in over 52 patients with symptomatic cavernous dural fistulas has shown complete cure in approximately two-thirds of patients treated by either transarterial or transvenous embolization, with a complication rate (mostly transient aggravation of ocular symptoms) of 5–7%. Compression therapy and transvascular embolization techniques have emerged as the treatments of choice for symptomatic cavernous dural fistulas.

Midline Dural Fistulas

Dural fistulas can involve the superior sagittal sinus, straight sinus, and vein of Galen. These fistulas tend to present with neurologic deficits, hemorrhage, and headaches. Because of the length, multiplicity, and complexity of the arterial supply to these fistulas, combined endovascular and intraoperative embolizations often are required for complete fistula obliteration [72, 73].

Intracerebral Arteriovenous Malformations

Intracerebral arteriovenous malformations (AVMs) are congenital malformations involving the vascular development of the fetal brain and include abnormalities in arteries, capillaries, and venous structures. Clinically these lesions can present with seizures, recurrent headaches, hemorrhage, progressive neurologic deficits, hydrocephalus, and dementia. The mortality rate associated with the initial hemorrhage of an AVM is estimated to be 10% with a morbidity rate of 30–50% [74]. The early endovascular treatments of free-particle or Silastic-sphere [75, 76] embolization have largely been replaced with superselective embolization techniques. Large series have demonstrated the effectiveness of subselective embolization as an adjunct to surgical excision by reducing the flow and size of the nidus, occluding deep feeding pedicles, and reducing the risk of perfusion breakthrough [76–80]. Figure 8 is an example of a posterior fossa AVM that was preoperatively embolized, facilitating surgical removal. When transfemoral routes are ineffective, direct intraoperative

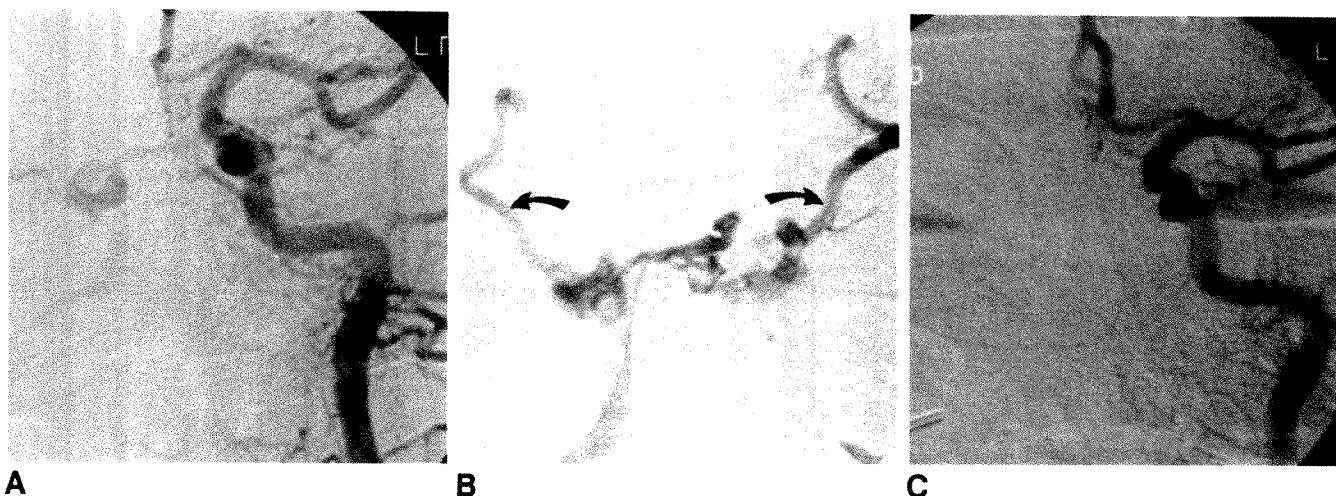
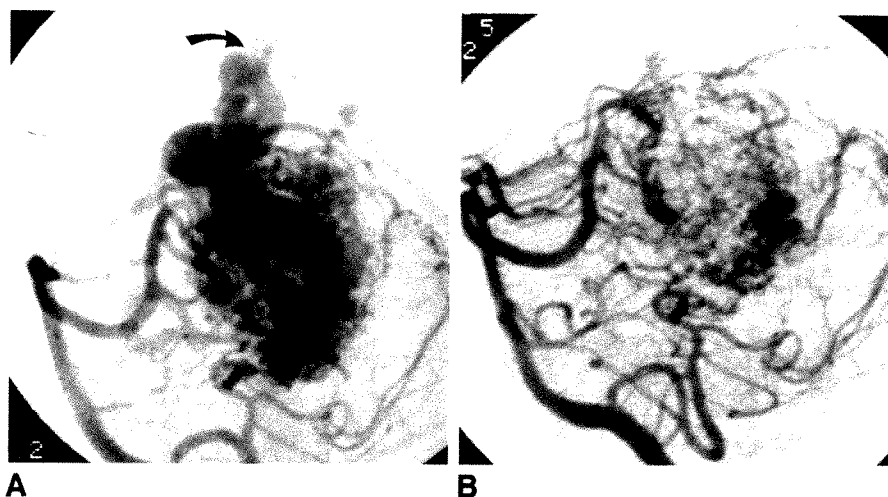


Fig. 7.—81-year-old woman with ocular symptoms caused by a dural cavernous fistula supplied by the left internal carotid artery.
A, Left common carotid angiogram, anteroposterior projection, shows dural fistula involving left cavernous sinus; fistula drains across circular sinus to contralateral superior ophthalmic vein and inferior petrosal sinus.
B, Catheter has been navigated from transfemoral venous approach up right inferior petrosal sinus across circular sinus to left cavernous sinus. This reveals fistula site as well as drainage to both superior ophthalmic veins (arrows).
C, Left common carotid angiogram, anteroposterior projection, shows complete obliteration of fistula after embolization with platinum coils and liquid adhesives from a transvenous approach.

Fig. 8.—37-year-old woman who had several subarachnoid hemorrhages caused by posterior fossa arteriovenous malformation (AVM).

A, Left vertebral angiogram, lateral projection, shows AVM in vermis draining to vein of Galen (arrow).

B, Same injection and projection show marked decreased flow after embolization of both superior cerebellar arteries and choroidal branch of posterior inferior cerebellar artery. AVM was surgically removed in 1½ hr with minimal blood loss.



embolization in an awake patient or with cortical mapping has been shown to be effective for AVMs located near critical (speech, motor strip, or visual cortex) areas [81, 82]. In patients who are not surgical candidates, staged palliative embolization may eliminate associated aneurysms in feeding vessels or within the nidus and presumably reduce the associated risk of hemorrhage [83]. Progressive neurologic deficits may be a result of arterial steal away from normal surrounding brain into a high-flow AVM or venous hypertension transmitted from the AVM to shared surrounding brain. Staged palliative embolization of the AVM often can recover these associated deficits. Patients with severe unilateral pulsatile headaches often have recruited dural supply to their parenchymal AVM. Embolization of this dural supply can be performed with relative safety and often results in improvement or alleviation of the headaches.

Surgical excision remains the gold standard for the treatment of most symptomatic AVMs. Most of the embolization procedures performed for symptomatic AVMs are performed as presurgical adjuncts. Some AVMs, because of their size or involvement with deep or essential structures, are not considered operable because of the excessive morbidity and mortality associated with surgical excision. Embolization alone has been used as a primary therapy in some of these complex lesions; however, the cure rate has been low, reportedly between 8% and 16% [84, 85], with a permanent complication rate of 13.5–22% [84, 85]. Two recent reports have shown that the prevalence of serious complications secondary to embolization is declining, presumably because of the development of better catheter and embolic agent technology and advances in operator experience [86, 87]. Subtotal occlusion of an AVM by embolization can improve

neurologic function and reduce headaches and seizures [88, 89]. However, the impact of these procedures on reduction of subsequent hemorrhages when no definable hemorrhage source is identified remains to be proven.

Stereotactically guided X-irradiation, gamma-produced intersecting beam irradiation, or Bragg-peak proton beam irradiation of AVMs has been shown to be effective in producing proliferative changes in the vessel wall of AVMs resulting in obliteration of the nidus [87, 88]. The results of treatment of smaller AVMs (less than 3 cm) followed for 2 years or more have shown complete obliteration in approximately 80% of patients [84]. The reported results of large AVMs (up to 5 cm) has shown a low rate of angiographic obliteration (20%) in patients treated with proton beam irradiation [85]. Although the complications reported with radiotherapy have been low, the major drawback has been the 1- to 2-year interval required for radiation therapy to produce obliterative changes in AVM vessels, during which the patient is at continued risk for intracranial hemorrhage. Embolization has been used as an adjunct prior to radiosurgery to reduce the size of the nidus, occlude large fistulous connections, and obliterate aneurysms or pseudoaneurysms associated with a risk of recurrent hemorrhage.

Spinal Vascular Malformations

Spinal vascular malformations can present with a wide clinical spectrum of signs and symptoms. Intramedullary malformations usually present in the second or third decade with hemorrhage. Perimedullary fistulas are connections found on the surface of the spinal cord, usually in the conus region, and can present with hemorrhage or progressive myelopathy. Spinal dural fistulas are located in the dura, usually present with radiculopathy or myelopathy, and occur in older patients [90]. Many of these diseases can be palliated or obliterated by endovascular techniques [90-94]. In patients with a spinal dural fistula whose feeding arterial supply does not contribute to the spinal cord, transvascular embolization is the primary definitive therapy [90]. Some intramedullary AVMs can be palliated or cured by embolization techniques; however, an understanding of the angioarchitecture is essential for a satisfactory outcome.

Summary

Interventional neuroradiology has made tremendous advances in the 28 years since Lussenhop and Spence [75] first reported occlusion of a cerebral AVM by embolization with radiologic guidance. This progress is largely attributable to continuing advances in imaging techniques, catheters, and embolic technology, coupled with an improved understanding of the natural history and pathophysiology of neurovascular disorders. In this evolving subspecialty there is still some variability in the consistency of results. It is hoped that subspecialty training guidelines will improve the consistency of therapeutic outcomes.

REFERENCES

- Delens E. *De la communication de la carotide interne et du sinus caverneux (aneurysme arterioveineux)* (thesis). Paris: Parent, 1870
- Dandy WE. Carotid cavernous aneurysms (pulsating exophthalmos). *Zentralbl Neurochir* 1937;2:77-113, 165-204
- Halbach VV, Hieshima GB, Higashida RT, Reicher M. Carotid cavernous fistula: indications for urgent therapy. *AJNR* 1987;8:627-633, *AJR* 1987;149:587-593
- Sattler CH. *Pulsierender exophthalmus: Handbuch der Gesamten Augenheilkunde*. Berlin: Springer, 1920:1-268
- deSchweinitz GE, Holloway TB. *Pulsating exophthalmos: its etiology, symptomatology, pathogenesis and treatment*. Philadelphia: Saunders, 1908
- Sanders MD, Hoyt WF. Hypoxic ocular sequelae of carotid cavernous fistulae. *Br J Ophthalmol* 1969;53:82-97
- Serbinenko FA. Balloon occlusion of a cavernous portion of the carotid artery as a method of treating carotid cavity anastomoses. *Zh Vopr Neurokhir* 1971;6:3-8
- Debrun G, Lacour P, Caron JP, Hurth M, Comoy J, Yervel Y. Detachable balloon and calibrated-leak balloon techniques in the treatment of cerebral vascular lesions. *J Neurosurg* 1978;49:635-649
- Debrun GM, Lacour P, Vinuela FV, et al. Treatment of 54 traumatic carotid cavernous fistulas. *J Neurosurg* 1981;55:678-692
- Goto K, Hieshima GB, Higashida RT, et al. Treatment of direct carotid cavernous sinus fistulae: various therapeutic approaches and results in 148 cases. *Acta Radiol [Suppl]* (Stockh) 1986;369:576-579
- Higashida RT, Halbach VV, Tsai FY, et al. Interventional neurovascular treatment of traumatic carotid and vertebral artery lesions: therapeutic results in 234 cases. *AJR* 1989;153:577-582
- Halbach VV, Higashida RT, Hieshima GB, Hardin C, Yang P. Transvenous embolization of direct carotid cavernous fistulas. *AJNR* 1988;9:741-749
- Higashida RT, Hieshima GB, Halbach VV, Bentson JR, Goto K. Closure of carotid cavernous sinus fistulae by external compression of the carotid artery and jugular vein. *Acta Radiol [Suppl]* (Stockh) 1986;369:580-583
- Matas R. Traumatism and traumatic aneurysms of the vertebral artery and their surgical treatment with the report of a cured case. *Ann Surg Neurol* 1993;18:477-521
- Olson RW, Hillier LB Jr, Svien HJ. Arteriovenous fistula: a complication of vertebral angiography: report of a case. *J Neurosurg* 1963;20:73
- Hayes P, Gerlock AJ Jr, Cobb CA. Cervical spine trauma: a cause of vertebral artery injury. *J Trauma* 1980;20(10):904-905
- Deans WR, Block S, Leibrock L, Berman BM, Skultety FM. Arteriovenous fistula in patients with neurofibromatosis. *Radiology* 1982;144(1):103-107
- Reddy SV, Karnes WE, Earnest F IV, Sundt TM Jr. Spontaneous arteriovenous fistulas of cerebral vessels in association with fibromuscular dysplasia. *J Neurosurg* 1981;54(3):399-402
- Nagashima C, Iwasaki T, Kawanuma S, Sakaguchi A, Kamisasa A, Suzuki K. Traumatic arteriovenous fistula of the vertebral artery with spinal cord symptoms: case report. *J Neurosurg* 1977;46:681-687
- Miller RE, Hieshima GB, Giannotta SL, Grinnell VS, Mehringer CM, Kerin DS. Acute traumatic vertebral arteriovenous fistula: balloon occlusion with the use of a contralateral approach. *Neurosurgery* 1984;14(2):225-229
- Debrun G, Legre J, Karbarian M, Tapis PL, Caron JP. Endovascular occlusion of vertebral fistulae by detachable balloon occlusion with conservation of the vertebral blood flow. *Radiology* 1979;13:141-147
- Reizine D, Laouiti M, Guimaraens L, Riche MC, Merland JJ. Vertebral arteriovenous fistulas: clinical presentation, angiographical appearance and endovascular treatment—a review of 25 cases. *Ann Radiol (Paris)* 1985;28(6):425-438
- Halbach VV, Higashida RT, Hieshima GB. Treatment of vertebral arteriovenous fistulas. *AJNR* 1987;8:1121-1128, *AJR* 1988;150:405-412
- Spetzler RF, Wilson CB, Weinstein P, et al. Normal perfusion pressure breakthrough theory. *Clin Neurosurg* 1978;25:651
- Halbach VV, Higashida RT, Hieshima GB, Norman D. Normal perfusion pressure breakthrough occurring during treatment of carotid and vertebral fistulas. *AJNR* 1987;8:751-756
- Kondoh T, Tamaki N, Takeda N, Suyama T, Oi SZ, Matsumoto S. Fatal intracranial hemorrhage after balloon occlusion of an extracranial vertebral arteriovenous fistula: case report. *J Neurosurg* 1988;69(6):945-948
- Lasjaunias P, Ter Brugge K, Lopez-Ibor L, et al. The role of dural anomalies

- in vein of Galen aneurysms: report of six cases and review of literature. *AJNR* **1987**;3:185-192
28. Steinheil SC. *Über einen Fall von Varix aneurysmaticus im Bereich der Gehirngefäße* (dissertation). Würzburg: University of Würzburg, 1895. (Cited in Dandy WE. Arteriovenous aneurysm of the brain. *Arch Surg* **1928**;17:190-243)
 29. Gold AP, Ransohoff JR, Carter S. Vein of Galen malformation. *Acta Neurol Scand [Suppl]* **1964**;40(11):5-31
 30. Amacher AL, Shillito J Jr. The syndromes and surgical treatment of aneurysms of the great vein of Galen. *J Neurosurg* **1973**;39:89-98
 31. Johnston IH, Whittle IR, Besser M, Morgan MK. Vein of Galen malformation: diagnosis and management. *Neurosurgery* **1987**;20:747-758
 31. Hoffman HJ, Chuang S, Hendrick EB, Humphreys RP. Aneurysms of the vein of Galen: experience at the Hospital for Sick Children, Toronto. *J Neurosurg* **1982**;57:316-322
 32. Berenstein A, Epstein F. Vein of Galen malformations: combined neurosurgical and neuroradiological intervention. In: McLaurin RL, Schut L, Venes, et al., eds. *Pediatric neurosurgery*. New York: Grune & Stratton, **1982**:637-647
 33. Mickle JP, Quisling RG. The transtocular embolization of vein of Galen aneurysms. *J Neurosurg* **1986**;64:731-735
 34. Edwards MSB, Hieshima GB, Higashida RT, Halbach VV. Management of vein of Galen malformations in the neonate. *Intervent Radiol* **1988**;3:184-188
 35. Halbach VV, Dowd CF, Higashida RT, Hieshima GB. Transvenous embolization of a vein of Galen malformation through a femoral vein access. Presented at the annual meeting of the World Interventional Neuroradiological Society, Val D'Isere, France, January **1989**
 36. Serbinenko FA. Balloon catheterization and occlusions of major cerebral vessels. *J Neurosurg* **1974**;41:125-145
 37. Romodanov AP, Shcheglov VI. Intravascular occlusion of saccular aneurysms of the cerebral arteries by means of a detachable balloon catheter. In: Krayenbuhl H, ed. *Advances and technical standards in neurosurgery*. Wien: Springer-Verlag, **1982**:25-49
 38. Fox AJ, Vinuela F, Pelz DM, et al. Use of detachable balloons for proximal artery occlusion in the treatment of unclippable cerebral aneurysms. *J Neurosurg* **1987**;66(1):40-46
 39. Debrun G, Fox A, Drake C, et al. Giant unclippable aneurysms: treatment with detachable balloons. *AJNR* **1981**;2:167-173
 40. Berenstein A, Ransohoff J, Kuppersmith M, et al. Transvascular treatment of giant aneurysms of the cavernous carotid and vertebral arteries: functional investigation and embolization. *Surg Neurol* **1984**;21:3-12
 41. Hieshima GB, Higashida RT, Wapenski J, et al. Balloon embolization of a large distal basilar artery aneurysm. *J Neurosurg* **1986**;65(3):413-416
 42. Hieshima GB, Higashida RT, Halbach VV, et al. Intravascular balloon embolization of a carotid-ophthalmic artery aneurysm with preservation of the parent vessel. *AJNR* **1986**;7:916-918
 43. Higashida RT, Hieshima GB, Halbach VV, et al. Intravascular detachable balloon embolization of intracranial aneurysms: indications and technique. *Acta Radiol [Suppl]* (Stockh) **1986**;369:594-596
 44. Halbach VV, Hieshima GB, Higashida RT. Treatment of intracranial aneurysms by balloon embolization. *Semin Intervent Radiol* **1987**;4(4):261-268
 45. Higashida RT, Hieshima GB, Mehringer CM, Halbach VV. Giant cavernous aneurysm associated with trigeminal artery: treatment by detachable balloon. *AJNR* **1987**;8:757-758
 46. Higashida RT, Halbach VV, Cahan L, Hieshima GB. Cavernous carotid artery aneurysm associated with Marfan's syndrome: treatment by balloon embolization therapy. *Neurosurgery* **1988**;22(2):297-300
 47. Goto K, Halbach VV, Higashida RT, Hieshima GB, Hardin CW. Low viscosity hydrophilic polymer for a detachable balloon. *Radiology* **1988**;169:787-790
 48. Zubkov YN, Nikiforov BM, Shustin VA. Balloon catheter technique for dilation of constricted cerebral arteries after aneurysmal SAH. *Acta Neurochir (Wien)* **1984**;70:665-679
 49. Higashida RT, Halbach VV, Cahan LO, Brant-Zawadzki M, Hieshima GB. Transluminal angioplasty of intracranial vessels for treatment of intracranial arterial vasospasm. *J Neurosurg* (in press)
 50. Numaguchi Y, Puyau FA, Provenza LJ, Richardson DE. Percutaneous transluminal angioplasty of the carotid artery. *Neuroradiology* **1984**;26:527-530
 51. Tsai FY, Matovich V, Hieshima G, et al. Percutaneous transluminal angioplasty of the carotid artery. *AJNR* **1986**;7:349-358
 52. Molarieme A, Keifer JW, Zuaka AJ. Percutaneous transluminal angioplasty of the brachiocephalic arteries. *AJNR* **1982**;3:169-174
 53. Theron J, Courtheoux P, Henriot JP, Pelouze G, Derlon JM, Maiza D. Angioplasty of supra-aortic arteries. *J Neuroradiol* **1984**;11:187-200
 54. Theron J, Melancon D, Ethier R. "Pre" subclavian steal syndromes and their treatment by angioplasty. *Neuroradiology* **1985**;27:265-270
 55. Higashida RT, Hieshima GB, Tsai FY, Halbach VV, Norman D. Transluminal angioplasty of the vertebral and basilar artery. *AJNR* **1987**;8:745-749
 56. Newton TH, Cronqvist S. Involvement of the dural arteries in intracranial arteriovenous malformations. *Radiology* **1969**;93:1071-1078
 57. Houser OW, Cambell JK, Cambell RJ, Sundt TM. Arteriovenous malformations affecting the transverse dural venous sinus: an acquired lesion. *Mayo Clin Proc* **1979**;54:651-661
 58. Lasjaunias P, Chiu M, Ter Brugge K, Tolia A, Hurth M, Bernstein M. Neurological manifestations of intracranial dural arteriovenous malformations. *J Neurosurg* **1986**;64:724-730
 59. Halbach VV, Higashida RT, Hieshima GB, Goto K, Norman D, Newton TH. Dural fistulas involving the transverse and sigmoid sinuses: results of treatment of 28 patients. *Radiology* **1987**;163:443-447
 60. Sundt TM, Piepgras DG. The surgical approach to arteriovenous malformations of the lateral and sigmoid dural sinuses. *J Neurosurg* **1983**;59:32-39
 61. Barnwell SL, Halbach VV, Higashida RT, Hieshima GB, Wilson CB. Complex dural arteriovenous fistulas: results of a new combined neurosurgical and interventional neuroradiology treatment in 16 patients. *J Neurosurg* (in press)
 62. Halbach VV, Higashida RT, Hieshima GB, Mehringer CM, Hardin CW. Transvenous embolization of dural fistulas involving the transverse and sigmoid sinuses. *AJNR* **1989**;10:385-392
 63. Newton TH, Hoyt WF. Spontaneous arteriovenous fistula between dural branches of the internal maxillary artery and the posterior cavernous sinus. *Radiology* **1968**;91:1147-1150
 64. Newton TH, Hoyt WF. Dural arteriovenous shunts in the region of the cavernous sinus. *Neuroradiology* **1970**;1:71-81
 65. Castaigne P, Laplane D, Djindjian R, et al. Communication arterioveineuse spontanee entre la carotide externe et le sinus caverneux. *Rev Neurol (Paris)* **1966**;114:5-14
 66. Magidson MA, Weinberg DE. Spontaneous closure of a dural arteriovenous malformation. *Surg Neurol* **1976**;6:107-110
 67. Seeger JF, Gabrielson TO, Gianotta SL, Lotz PR. Carotid cavernous sinus fistulae and venous thrombosis. *AJNR* **1980**;1:141-148
 68. Lasjaunias P, Halimi P, Lopez-Ibor L, Sichez JP, Hurth M, Triboulet ND. Traitement endovasculaire des malformation vasculaires dures (MVD) pures spontanees. *Neurochirurgie* **1983**;30:207-223
 69. Halbach VV, Higashida RT, Hieshima GB, Reicher M, Norman D, Newton TH. Dural fistulas involving the cavernous sinus: results of treatment in 30 patients. *Radiology* **1987**;163:437-442
 70. Halbach VV, Higashida RT, Hieshima GB, Hardin CW. Embolization of the dural branches arising from the cavernous internal carotid artery. *AJNR* **1989**;10:143-150
 71. Halbach VV, Higashida RT, Hieshima GB, Hardin CW, Pribram H. Transvenous embolization of dural fistulas involving the cavernous sinus. *AJNR* **1989**;10:377-384
 72. Halbach VV, Higashida RT, Hieshima GB, Cahan L, Rosenblum M. Treatment of dural arterial venous malformations involving the superior sagittal sinus. *AJNR* **1988**;9:337-343
 73. Halbach VV, Higashida RT, Hieshima GB, Wilson CB. Treatment of dural fistulas involving the deep cerebral venous system. *AJNR* **1989**;10:393-399
 74. Perret G, Nishioka HJ. Report on the cooperative study of intracranial aneurysms and subarachnoid hemorrhage: arteriovenous malformations. An analysis of 545 cases of craniocerebral arteriovenous malformations and fistulae reported to the cooperative study. *J Neurosurg* **1966**;25:467-490
 75. Lussenhop AJ, Spence WT. Artificial embolization of cerebral arteries: report of use in a case of arteriovenous malformation. *JAMA* **1960**;172:1153-1155
 76. Stein BM, Wolpert SM. Arteriovenous malformations of the brain. II: Current concepts and treatment. *Arch Neurol* **1980**;37(2):69-75
 77. Halbach VV, Higashida RT, Yang P, Barnwell S, Wilson CB, Hieshima GB.

P24448

- Preoperative balloon occlusion of arteriovenous malformations. *Neurosurgery* **1988**;22:301-308
78. Pelz DM, Fox AJ, Vinuela F, Drake CC, Ferguson GG. Preoperative embolization of brain AVMs with isobutyl-2 cyanoacrylate. *AJNR* **1988**; 9(4):757-764
 79. Spetzler RF, Martin NA, Carter LP, Flom RA, Raudzens PA, Wilkinson E. Surgical management of large AVM's by staged embolization and operative excision. *J Neurosurg* **1987**;67(1):17-28
 80. Vinuela F, Fox AJ, Debrun G, Pelz D. Preembolization superselective angiography: role in the treatment of brain arteriovenous malformations with isobutyl-2 cyanoacrylate. *AJNR* **1984**;5(6):765-769
 81. Girvin JP, Fox AJ, Vinuela F, Drake CG. Intraoperative embolization of cerebral arteriovenous malformations in the awake patient. *Clin Neurosurg* **1983**;31:188-247
 82. Vinuela FV, Debrun GM, Fox AJ, Girvin JP, Peerless SJ. Dominant hemisphere arteriovenous malformations: therapeutic embolization with isobutyl-2-cyanoacrylate. *AJNR* **1983**;4:959-966
 83. Lasjaunias P, Piske R, Terbrugge K, Willinsky R. Cerebral arteriovenous malformations (C. AVM) and associated arterial aneurysms (AA). Analysis of 101 C AVM cases, with 37 AA in 23 patients. *Acta Neurochir (Wien)* **1988**;91(1-2):29-36
 84. Moret J, Picard L. Endovascular therapy of intracranial arteriovenous malformations; results in 242 patients. Presented at the annual meeting of the World Interventional Neuroradiological Society, Val D'Isere, France, January **1989**
 85. Berenstein A, Choi I, Kuppersmith M, Flam E, Kricheff II, Madrid M. Embolization of intracranial arteriovenous malformations; results in 182 patients. Presented at the annual meeting of the World Interventional Neuroradiological Society, Val D'Isere, France, January **1989**
 86. Berenstein A, Choi IS, Kuppersmith M, Flam E, Kricheff II, Madrid M. Complications of endovascular embolization in 182 patients with cerebral AVMs. Presented at the annual meeting of the American Society of Neuroradiology, Orlando, FL, March **1989**
 87. Dion J, Vinuela F, Duckwiler G, Martin N, Jordon S, Bentson J. Impact of recent technological advances on endovascular therapy of brain arteriovenous malformations and fistulas. Presented at the annual meeting of the American Society of Neuroradiology, Orlando, FL, March **1989**
 88. Steiner L. Treatment of arteriovenous malformations by radiosurgery. In Wilson CB, Stein BM, eds. *Intracranial arteriovenous malformations*. Baltimore: Williams & Wilkins, **1984**:295-314
 89. Kjellberg RN, Hanamura T, David KR, et al. Bragg-peak proton beam therapy for arteriovenous malformations of the brain. *N Engl J Med* **1983**; 309:269-274
 90. Merland JJ, Riche MC, Chiras J. Intraspinous extramedullary arteriovenous fistulae draining into the medullary veins. *J Neuroradiol* **1980**;7:271-320
 91. Latchaw RE, Harris RD, Chou SN, Gold LH. Combined embolization and operation in the treatment of cervical arteriovenous malformations. *Neurosurgery* **1980**;6(2):131-137
 92. Doppman JL, DiChiro G, Ommaya AK. Percutaneous embolization of spinal cord arteriovenous malformations. *J Neurosurg* **1971**;34(1):48-55
 93. Theron J, Cosgrove R, Melanson D, Ethier R. Spinal arteriovenous malformations: advances in therapeutic embolization. *Radiology* **1986**;158(1): 163-169
 94. Horton JA, Latchaw RE, Gold LHA, Pang D. Embolization of intramedullary arteriovenous malformations of the spinal cord. *AJNR* **1986**;7(1):113-118

Review Article

Assessment of Myocardial Viability with SPECT and PET Imaging

Manuel D. Cerqueira¹ and Arnold F. Jacobson

In patients with acute myocardial infarction, early use of thrombolytic therapy with streptokinase or tissue plasminogen activator has shown potential for salvaging jeopardized myocardium. Although spontaneous thrombolysis occurs in many patients, thrombolytic therapy increases the percentage of patent infarct-related vessels, causes reperfusion to occur earlier, decreases infarct size, preserves ventricular function, and improves survival [1-3]. Successful thrombolysis after a period of coronary artery occlusion often establishes blood flow to areas of myocardium that are a mixture of irreversibly damaged and viable myocytes. The viable myocytes may have depressed systolic and diastolic function and depleted high-energy phosphate stores, the so-called "stunned" myocardium, but such areas are capable of regaining mechanical function over time without the need for aggressive intervention [4]. When mechanical function does not improve after several weeks, viable myocytes may still be present distal to the patent vessel but subject to chronic ischemia as a result of residual stenosis or poor collateral flow. Ventricular dysfunction due to chronic ischemia has been referred to as "hibernating" myocardium and may be very difficult to differentiate from myocardial scar [5]. A patient with hibernating myocardium may benefit from revascularization by coronary artery bypass surgery or percutaneous transluminal coronary angioplasty (PTCA), but similar interventions to improve blood flow to scar would expose the patient to possible risk of morbidity or death without potential benefit [6]. Thus, accurate identification of those patients who have viable, hiber-

nating myocardium distal to a previously occluded vessel and who will regain mechanical ventricular function and have relief of their angina after revascularization is critical for optimal clinical decision making.

²⁰¹Tl scintigraphy has been shown to have a high sensitivity and specificity in identifying patients with coronary artery disease and to be accurate in identifying areas of prior myocardial infarction [7]. Single-photon emission CT (SPECT) substantially improves image contrast, overcomes the overlap problems encountered in planar imaging, and is becoming the preferred method for performing ²⁰¹Tl scintigraphy [7]. However, recent reports suggest that the conventional stress-redistribution imaging sequence may result in underestimation of viable myocardium, and new imaging sequences have been introduced to improve differentiation of hibernating from necrotic myocardium [8]. In addition, cardiac positron emission tomography (PET), with its ability to separate blood flow from metabolism, offers promise of even more specific functional cardiac imaging [9]. We review the established role of SPECT ²⁰¹Tl scintigraphy, describe new techniques and imaging strategies with ²⁰¹Tl, and discuss the role of PET blood flow and metabolic imaging in identifying viable but ischemic myocardium.

Radiopharmaceuticals for Assessing the Myocardium

There are two major classes of tracers for measurement of myocardial blood flow: gamma emitters (²⁰¹Tl and ^{99m}Tc iso-

Received March 15, 1989; accepted after revision May 15, 1989.

This work was supported by the General Medical Research Services of the Veterans Administration, Washington, DC.

¹ Both authors: Department of Radiology, Division of Nuclear Medicine, Seattle Veterans Administration Medical Center and the University of Washington, 1660 S. Columbian Way, Seattle, WA 98108. Address reprint requests to M. D. Cerqueira.

AJR 153:477-483. September 1989 0361-803X/89/1533-0477 © American Roentgen Ray Society

nitriles) and positron emitters (^{13}N -ammonia, ^{82}Rb , and ^{15}O -water).

Gamma Emitters

Thallium.— ^{201}Tl is a potassium analog with predominantly low-energy photon emissions (69–83 keV). The kinetics of ^{201}Tl uptake and washout have been studied extensively [10]. Myocardial uptake of ^{201}Tl is directly proportional to blood flow over the physiologic range encountered in humans. Because in the resting state myocardial blood flow is low, areas with normal blood flow and areas distal to a stenosed vessel may show similar ^{201}Tl uptake. When studies are performed after exercise stress or dipyridamole-induced hyperemia, uptake is increased in areas with normal vascular supply, while areas distal to an occluded or stenosed vessel have diminished or absent ^{201}Tl uptake. Over time, areas of myocardial scar show no change in ^{201}Tl activity, but areas distal to a stenosed vessel usually show gradual accumulation of ^{201}Tl as a result of slow net wash-in of activity from the serum. Thus, at 4 hr postinjection, a time when delayed or redistribution ^{201}Tl imaging is routinely performed, areas of infarction have a persistent or fixed defect, whereas areas distal to stenoses usually have ^{201}Tl concentrations similar to normal surrounding myocardium. Thus, redistribution reflects the presence of viable but ischemic myocardium.

Isonitriles.—Since ^{201}Tl has a relatively long half-life, has high attenuation due to its low energy, achieves a low target-to-background ratio, and is cyclotron-produced, alternative perfusion agents that can be labeled with $^{99\text{m}}\text{Tc}$ have been sought. Several different isonitrile compounds have been complexed with technetium cations to produce myocardial blood flow agents. Six (hexa) molecules are attached to the $^{99\text{m}}\text{Tc}$ cation, and the unique properties of each compound are determined by the side chains. $^{99\text{m}}\text{Tc}$ -hexakis-2-methoxyisobutyl isonitrile has been the most widely used clinically, and Food and Drug Administration approval is pending [11]. It has the unique properties of permanently binding to intracellular proteins in direct proportion to blood flow and showing minimal redistribution over time. Thus, it has properties similar to microspheres, offers all the imaging advantages of $^{99\text{m}}\text{Tc}$, and the absence of redistribution makes it ideal for the longer imaging times required for SPECT. In order to differentiate exercise-induced ischemia from previous infarction, a separate resting study is required. In addition to assessing perfusion, the acquisition may be gated, which allows information on global and regional ventricular function to be obtained [12]. In a direct comparison with ^{201}Tl imaging for the detection of coronary artery disease, comparable results have been reported for $^{99\text{m}}\text{Tc}$ -hexakis-2-methoxyisobutyl isonitrile [13]. There is currently inadequate data to evaluate the role of $^{99\text{m}}\text{Tc}$ isonitriles in the assessment of myocardial viability, but the improved imaging properties and the ability to simultaneously assess both perfusion and function suggest that isonitriles will offer advantages over ^{201}Tl blood-flow imaging.

Positron Emitters

Markers of myocardial blood flow.—The three positron-emitting tracers that have been used for assessing myocardial blood flow have distinct characteristics that make each attractive for use in clinical PET imaging [14]. ^{82}Rb , a potassium analog similar to ^{201}Tl , is generator-produced, making it potentially available on a routine basis without the need for a cyclotron. For this reason, this agent has been extensively evaluated for the detection of coronary artery disease [15, 16]. ^{15}O -water is cyclotron-produced and has a very high myocardial extraction efficiency, but high blood pool and lung water activity may limit quantitative estimation of perfusion. ^{13}N -ammonia has a lower myocardial extraction efficiency than ^{15}O -water and ^{82}Rb and uptake deviates from linearity with flow at high rates, but intracellular metabolism results in extended retention of the tracer. The short half-lives of ^{82}Rb and ^{15}O (76 sec and 2 min, respectively) place greater demands on a scanner with regard to its sensitivity and speed of image acquisition. This limitation does make possible serial imaging under different physiologic conditions (e.g., before and after pharmacologic, mental, or physical stress) without the redistribution delays encountered with ^{201}Tl imaging. However, the intracellular retention of ^{13}N -ammonia, in addition to the longer half-life of ^{13}N (11 min), has made this agent generally preferred for blood flow imaging with PET.

Markers of myocardial metabolism.—The primary metabolic substrates for normal myocardial cells are fatty acids, but under hypoxic conditions, glucose metabolism increases and may become the primary energy source [17–21]. Use of fatty acid and glucose analogs labeled with positron emitters thus provides a noninvasive means for evaluating regional myocardial oxygenation status.

The fatty acid ^{11}C -labeled palmitate is avidly extracted by the myocardium, and the relatively long half-life of ^{11}C (20 min) makes PET imaging practical. This agent has proved useful for studying the kinetics of fatty acid uptake under normal and ischemic conditions and to obtain good-quality PET images [17]. Because labeled fatty acids undergo beta oxidation, there is fast washout from areas of normal myocardium and back diffusion in areas of ischemia. These properties impose limitations on modeling kinetics and the performance of imaging studies. Several fatty acid analogs are being investigated for clinical imaging [18]. These agents are partially metabolized in myocytes and remain trapped intracellularly and thus facilitate imaging and modeling. Phenylpentadecanoic acid has also been labeled with iodine-123 and may be used for SPECT imaging [22].

Deoxyglucose labeled with ^{18}F (half-life, 109 min) has been shown to be an accurate marker of regional glucose utilization [14]. ^{18}F -fluorodeoxyglucose has gained wide acceptance for its ability to identify ischemic but still viable myocardium, often in areas with markedly diminished blood flow on ^{201}Tl or ^{13}N -ammonia imaging and decreased aerobic metabolism on ^{11}C -palmitate studies. An example of such a study is shown in Figures 1 and 2. Those areas with decreased or undetectable blood flow and preserved metabolism represent a blood flow–metabolism mismatch and are consistent with ischemic, but

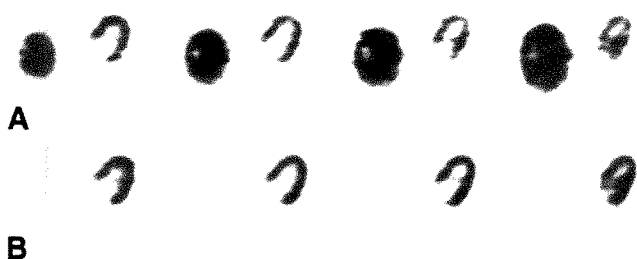


Fig. 1—A and B, Serial transaxial positron emission tomographic slices of ^{13}N -ammonia blood flow (A) and ^{18}F -fluorodeoxyglucose metabolism (B) in a normal volunteer. There is uniform distribution of blood flow and metabolism throughout the myocardium. (Images were acquired on a CTI 831 15-slice ECAT scanner and provided courtesy of G. T. Smith and M. Besozzi, University of Tennessee Medical Center, Knoxville).

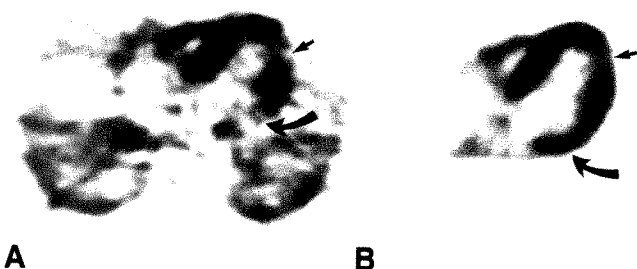


Fig. 2—A and B, Single transaxial ^{13}N -ammonia (A) and ^{18}F -fluorodeoxyglucose (FDG) (B) images in a patient with a prior myocardial infarction. A, ^{13}N -ammonia image shows diminished blood flow to inferolateral (straight arrow) and posterobasal (curved arrow) walls. B, ^{18}F -FDG image shows matched decrease in metabolism in inferolateral wall (straight arrow), consistent with infarction, and normal uptake (mismatch) in posterobasal wall (curved arrow), consistent with ischemia. (Images were acquired on a CTI 831 15-slice ECAT scanner and provided courtesy of G. T. Smith and M. Besozzi, University of Tennessee Medical Center, Knoxville).

viable myocardium. Areas with normal blood flow and metabolism represent normal myocardium, and areas where both are absent represent scar.

Imaging Techniques

Gamma Camera Systems

Thallium.—In over 10 years of clinical use, planar ^{201}Tl imaging has demonstrated a high sensitivity and specificity for the detection of coronary artery disease and offers simple image acquisition using conventional gamma cameras [7]. However, planar ^{201}Tl imaging suffers from both the general resolution limitations that affect all planar techniques as a result of superimposition of overlying structures, as well as from the increased attenuation and low target-to-background ratio specifically due to the low photon energy of ^{201}Tl . This has led to increasingly widespread use of SPECT techniques in myocardial imaging.

The earliest tomographic methods used for ^{201}Tl myocardial imaging relied on seven-pin-hole and rotating-slant-hole collimators. These techniques offered the convenience of using

existing large-field-of-view stationary gamma cameras, but, because of their dependence on incomplete view sampling, produced images with substantial spatial distortion [23]. Clinical studies using these limited-angle tomographic methods were unable to show a major advantage over planar imaging, and these techniques have been abandoned [7].

Tomographic techniques using a rotating gamma camera have overcome the limitations of other tomographic techniques and have gained wide acceptance in myocardial perfusion imaging. SPECT is most often performed with a single-headed detector, but two- and three-headed systems are also commercially available [24]. Ring detector systems for scintigraphic acquisition have also been developed but are not used for cardiac imaging. The multiheaded and ring systems offer the advantages of higher count rates and more accurate attenuation and scatter correction, but acquisition and reconstruction are more complex. Existing SPECT systems have spatial resolutions varying from 14 to 16 mm. The technical demands in performing good-quality SPECT imaging are greater than those in planar imaging. SPECT requires greater attention to details such as initial acceptance testing of the equipment; daily, weekly, and quarterly quality control; and greater training for technologists and physicians [7].

Cardiac SPECT studies are generally acquired using a 180° rotation from right anterior oblique to the left posterior oblique. After reconstruction of the transaxial plane, the long axis of the heart is defined, and for visual analysis images may be displayed in serial slices at 90° angles relative to the long axis of the heart. This allows optimal display of the ventricular chambers and assignment of perfusion abnormalities to specific coronary arteries. Several methods of displaying serial SPECT slices and the results of quantitative analysis have been developed [7]. The bull's-eye format is used widely; several examples are shown in Figures 3–5. Quantitative methods are used extensively for cardiac SPECT because they make interpretation more reproducible and less dependent on the skills and training of the interpreter, and localization of disease to a specific vascular territory is improved.

The value of SPECT ^{201}Tl scintigraphy for the identification of coronary artery disease has been well established using visual and quantitative interpretation. SPECT studies are 90–95% sensitive and have a lower specificity [25–30]. Thallium SPECT also has been shown to have greater sensitivity than planar imaging in identifying patients with previous myocardial infarction, especially for the inferior wall and small subendocardial infarcts [31].

PET Systems

The basic design of a modern PET imaging system is analogous to that of a CT scanner [24, 32–38]. A series of adjacent rings of scintillation detectors surrounds the patient and provides the capability for 180° coincidence counting of the paired 511-keV photons produced by positron annihilation. The resolution element of the scanner is established by the field of view of individual paired opposing detectors, with

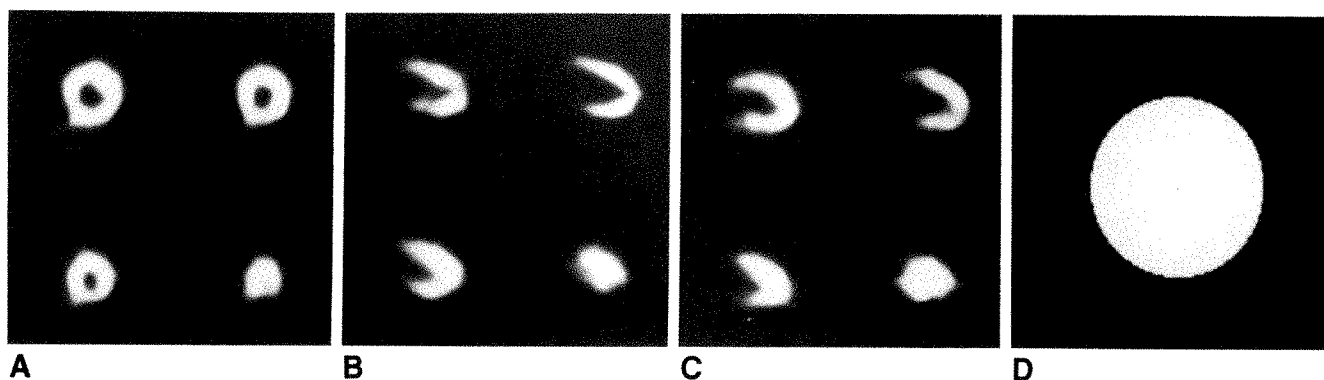


Fig. 3.—Four representative ^{201}Tl tomographic slices in a resting patient with normal coronary arteries.

A, Short axis view.

B, Superior long axis view.

C, Right anterior oblique long axis view.

D, Quantitation view.

In quantitative display, each tomographic slice was compared with a population of normal subjects and found to be within 3 SD of the mean. (Reprinted with permission from Cerqueira et al. [7].)

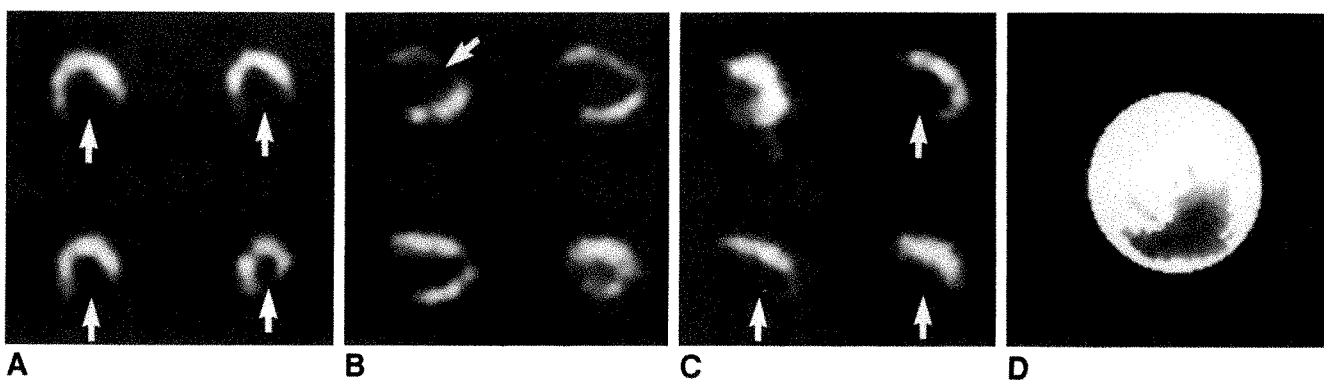


Fig. 4.— ^{201}Tl tomograms in a resting patient with a prior inferior myocardial infarction.

A, Short axis view.

B, Superior long axis view.

C, Right anterior oblique long axis view.

D, Quantitation view.

Large inferior defect (arrows) is seen on all tomographic slices and includes part of apex. Quantitative display localizes defect representing 32% of left ventricle (black area).

(Reprinted with permission from Ritchie et al. [25].)

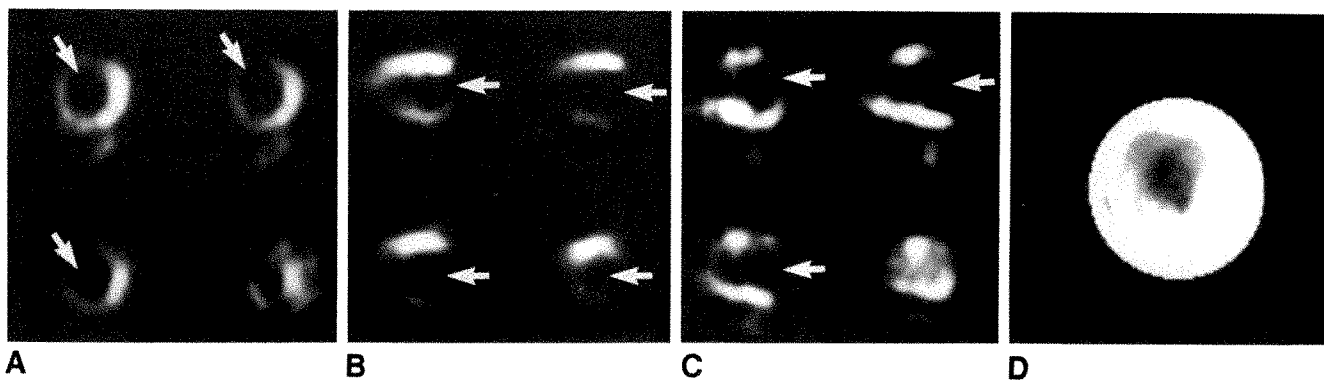


Fig. 5.— ^{201}Tl tomograms in patient with prior anterior myocardial infarction.

A, Short axis view.

B, Superior long axis view.

C, Right anterior oblique long axis view.

D, Quantitation view.

Portions of anterior wall, septum, and apex are involved (arrows). This patient's defect comprised 29% of left ventricle.

(Reprinted with permission from Ritchie et al. [25].)

improved resolution achieved by using a larger number of smaller detectors. Whole-body scanners have from 200 to 512 detectors per ring, with the rectangular imaging surface of each detector being 5–9 mm wide and 13–24 mm high. As a result of generation of cross-plane image slices through use of coincidence detection between detectors in adjacent rings, image plane spacing is 7–14 mm, about half the overall height of a single crystal. Systems with two to eight detector rings, providing three to 22 individual image slices over an axial field of view of 5–16 cm, are available. In-plane resolution for the current generation of whole-body PET scanners, specified in terms of full width at half maximum, is typically 5–10 mm. Axial resolution ranges from 6 to 14 mm depending on crystal dimensions, gantry translation, and configuration of interplane shields.

Clinical Assessment of Myocardial Viability

²⁰¹Tl Scintigraphy

In areas of prior myocardial infarction or severe ischemia, regional loss of mechanical function may improve after revascularization. This has been shown by several groups using planar ²⁰¹Tl techniques. Rozanski et al. [39] performed exercise ²⁰¹Tl imaging and regional wall motion analysis by gated blood pool imaging in 25 patients before coronary artery bypass grafting (CABG). Regional wall motion was studied after surgery, and 54% of segments with abnormal ²⁰¹Tl distribution had improvement in regional wall motion after CABG. Improvement in function was more likely to occur in areas with ²⁰¹Tl redistribution at 4 hr (90%), but also occurred in 24% of areas with fixed defects at 4 hr. Similar findings were reported by Gibson et al. [40] with quantitative planar ²⁰¹Tl imaging before and after CABG in 47 consecutive patients. Forty-two defects were fixed at 4 hr; after surgery, 45% of these segments had normal ²⁰¹Tl activity and improved regional contractility.

These studies showed that myocardial segments with ²⁰¹Tl redistribution at 4 hr have increased ²⁰¹Tl uptake and improvement in ventricular function after CABG. Fixed defects may also show improvement in regional function (24%) and ²⁰¹Tl uptake (45%), suggesting that these areas are a mixture of scar tissue and viable myocytes. As the time course of thallium redistribution is directly related to the severity of

coronary artery stenosis, severely ischemic areas of myocardium may require longer than 4 hr to show redistribution [41].

Late Redistribution

Several studies have shown that extending ²⁰¹Tl imaging to 24 or even 48 hr will help differentiate severely ischemic but viable areas of myocardium from scar. This time dependence of redistribution is shown in Figure 6 in a patient with prior inferior myocardial infarction and collateral flow from a left anterior descending coronary artery with a high-grade lesion. The major problem with delaying imaging this long after administration of ²⁰¹Tl is the paucity of counts. Increasing the imaging time increases the counts but also increases the opportunity for the patient to move, thereby degrading the image.

Kiat et al. [8] studied 21 patients who had exercise ²⁰¹Tl SPECT scintigraphy before and after CABG or PTCA. Patients were imaged immediately after exercise and at 4 hr; delayed imaging was performed at 18–72 hr. Of 201 individual myocardial segments that had defects on immediate imaging, 79 (39%) had reversible defects at 4 hr, and 67 (85%) of these showed improved perfusion after CABG. Of 122 segments with fixed defects at 4 hr, 88 (72%) also showed improved perfusion following revascularization. Statistically there was no difference in improvement after revascularization between reversible and fixed defects at 4 hr. Of the 122 fixed segments at 4 hr, 74 (61%) showed late redistribution, and 95% of these segments improved after revascularization. Of the 48 segments that remained fixed at 18–72 hr, 18 (37%) still showed improvement in regional perfusion after CABG.

Cloninger et al. [42] performed quantitative stress SPECT ²⁰¹Tl scintigraphy in 141 patients before and after PTCA. In patients without prior myocardial infarction, 67% had partial redistribution on delayed imaging. After PTCA, 76% of these patients show improved ²⁰¹Tl uptake in the areas with partial redistribution. This study documents that in patients without prior infarction, but with high-grade lesions, two-thirds have incomplete redistribution at 4 hr and improvement after PTCA. In a separate group of 40 patients with partial redistribution at 4 hr, imaging was repeated at 8–24 hr. In 28 with prior myocardial infarction, 13 (46%) had additional redistribution

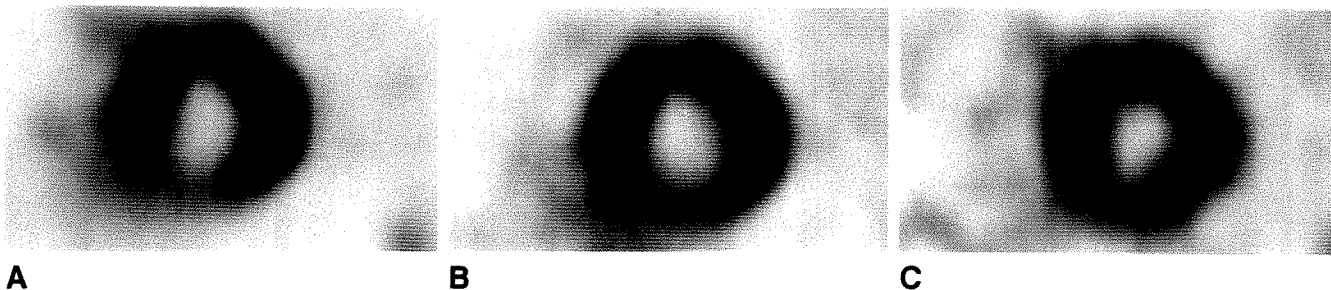


Fig. 6.—A–C, Exercise stress single-photon emission CT ²⁰¹Tl study shows short-axis slice imaged immediately after stress (A) and at 4 (B) and 24 (C) hr. Anterior and inferior walls have progressive redistribution over time. These changes are consistent with severe ischemia and markedly delayed redistribution of ²⁰¹Tl activity.

on delayed imaging. In 12 without prior infarction, four had complete redistribution and seven had additional redistribution. Performing delayed imaging at 8–24 hr will show complete or additional redistribution in patients with and without myocardial infarction.

Thus, in patients with or without prior myocardial infarction, severe reductions in flow may cause ^{201}Tl defects at 4 hr that show improvement after revascularization. If imaging is performed at 8–72 hr, late redistribution occurs in some patients; they have a higher probability of showing benefit from revascularization. In patients with fixed defects, even on late imaging, improvements in ^{201}Tl uptake and ventricular function may still result from revascularization, but the percentage is lower. While this limitation of SPECT ^{201}Tl imaging may be due in part to the resolution limits of this technique, it may also reflect a more general limitation of imaging that examines perfusion alone and suggests the need for evaluating myocardial metabolism.

Comparisons Between PET and SPECT

Several studies of ^{201}Tl and PET imaging in the same group of patients have been done. Brunken et al. [43] studied 12 patients, 10 with a clinical history of myocardial infarction, with stress planar ^{201}Tl and ^{13}N -ammonia and ^{18}F -2-deoxyglucose PET imaging. A total of 51 myocardial segments had defects on immediate poststress ^{201}Tl imaging, and at 4 hr, 36 were fixed, 11 had partial redistribution, and four had complete redistribution. In 21 (58%) of 36 patients with fixed defects and seven (64%) of 11 patients with partially redistributing ^{201}Tl defects, residual glucose metabolism consistent with the presence of viable myocardium was seen. In a similar study using SPECT and PET imaging, Tamaki et al. [44, 45] found that 38% of patients with fixed defects on ^{201}Tl imaging at 4 hr had evidence of preserved metabolic activity when ^{18}F -2-deoxyglucose was used. Thus, fixed defects on ^{201}Tl imaging at 4 hr may contain viable myocardium that can be detected by a mismatch between blood flow and metabolic activity on PET imaging. These findings are clinically important because areas of myocardium with preserved glucose uptake can regain function after revascularization.

New Approaches to Identifying Ischemic Myocardium

Available PET imaging agents can define myocardial perfusion and metabolism, but new compounds may be able to measure the actual oxygen concentration in the area of the ischemic or hibernating myocardium. Nitroimidazoles make up a class of compounds that are enzymatically trapped inside cells at a rate inversely proportional to the oxygen concentration [46–48]. As binding is enzyme-mediated, binding does not occur in normal, necrotic, or irreversibly damaged cells. Fluoromisonidazole can be labeled with ^{18}F , and it has been shown in isolated myocytes that binding is dependent on oxygen concentration [46]. In a dog model of myocardial ischemia/infarction, the uptake of this agent had an excellent correlation with microsphere measurements of myocardial blood flow [47]. Thus, this agent shows promise as a selective

marker of oxygen concentration and may prove clinically useful in identifying viable but ischemic myocardium.

Summary

The use of thrombolytic therapy for the treatment of acute myocardial infarction has increased the number of patients presenting for assessment of myocardial viability. Stress SPECT ^{201}Tl perfusion imaging performed in the conventional manner with delayed imaging at 4 hr can identify a large percentage of patients with ischemic but viable areas of myocardium. In some patients, delayed imaging up to as long as 24–48 hr after exercise may be required to show ^{201}Tl redistribution indicative of viability. Thus, in most patients, stress ^{201}Tl scintigraphy will correctly identify the presence of viable myocardium.

PET imaging, with its ability to assess blood flow and metabolism separately, offers the ability to identify myocardial areas with diminished blood flow but preserved metabolism. Areas with such a blood flow–metabolism mismatch may benefit from revascularization, even in the absence of ^{201}Tl redistribution. The exact role PET will play in the initial evaluation of patients presenting for assessment of myocardial viability remains to be established as more clinical data are accumulated.

REFERENCES

1. Kennedy JW, Martin GV, Davis KB, et al. The western Washington intravenous streptokinase in acute myocardial infarction randomized trial. *Circulation* **1988**;77:345–352
2. Gruppo Italiano per lo studio della streptochinasi nell'infarto miocardico. Long term effects of intravenous thrombolysis in acute myocardial infarction: final report of the GISSI study. *Lancet* **1987**;1:871–874
3. I.S.I.S. collaborative group. Randomised trial of intravenous streptokinase, oral aspirin, both, or neither among 17,187 cases of suspected acute myocardial infarction: ISIS-2. *Lancet* **1988**;1:349–359
4. Braunwald E, Kloner RA. The stunned myocardium: prolonged, postischemic ventricular dysfunction. *Circulation* **1982**;66:1146–1149
5. Braunwald E, Rutherford JD. Reversible ischemic left ventricular dysfunction: evidence for the "hibernating myocardium." *J Am Coll Cardiol* **1986**;8:1467–1470
6. Tillisch J, Brunken R, Marshall R, et al. Reversibility of cardiac wall-motion abnormalities predicted by positron tomography. *N Engl J Med* **1986**;314:884–888
7. Cerqueira MD, Harp GD, Ritchie JL. Evaluation of myocardial perfusion and function by single photon emission computed tomography. *Semin Nucl Med* **1987**;17:200–213
8. Kiat H, Berman DS, Maddahi J, et al. Late reversibility of tomographic myocardial ^{201}Tl defects: an accurate marker of myocardial viability. *J Am Coll Cardiol* **1988**;12:1456–1463
9. Gould KL. Identifying and measuring severity of coronary artery stenosis: quantitative coronary arteriography and positron emission tomography. *Circulation* **1988**;78:237–245
10. Berman DS, Garcia EV, Maddahi J, Rozanski A. Thallium-201 myocardial perfusion scintigraphy. In: Freeman LM, ed. *Freeman and Johnson's clinical radionuclide imaging*, 3rd ed. Orlando, FL: Grune & Stratton, **1984**:479–537
11. Okada RD, Glover D, Gaffney T, Williams S. Myocardial kinetics of technetium-99m-hexakis-2-methoxy-2-methylpropyl-isonitrile. *Circulation* **1988**;77:491–498
12. Kahn JK, Henderson EB, Akers MS, et al. Prediction of reversibility of perfusion defects with a single post-exercise technetium-99m RP-30A gated tomographic image: the role of residual systolic thickening. *J Am Coll*

- Cardiol* 1988;11:31A
13. Wackers FJ, Berman DS, Maddai J, et al. Technetium-99m hexakis 2-methoxyisobutyl isonitrite: human biodistribution, dosimetry, safety, and preliminary comparison to thallium-201 for myocardial perfusion imaging. *J Nucl Med* 1989;30:301-311
 14. Jacobson HG. Application of positron emission tomography in the heart. *JAMA* 1988;259:2438-2445
 15. Demer LL, Gould KL, Goldstein RA, et al. Assessment of coronary artery disease severity by positron emission tomography. *Circulation* 1989;79:825-835
 16. Gould KL, Goldstein RA, Mullani NA, et al. Noninvasive imaging of coronary stenoses by myocardial perfusion imaging during pharmacologic coronary vasodilation. VIII. Clinical feasibility of positron cardiac imaging without a cyclotron using generator-produced ^{82}Rb . *J Am Coll Cardiol* 1986;7:775-789
 17. Schelbert HR. Assessment of myocardial fatty acids metabolism with [^{11}C] palmitic acid. In: Heiss HW, ed. *Advances in clinical cardiology, regional myocardial metabolism by positron tomography*, vol. 3. Mahwah, NJ: Foundation for Advances in Clinical Medicine, 1987:85-96.
 18. Elmassah DR, Livni E, Brownell GL, Strauss HW. Biochemical rationale for the use of fatty acid analogs as agents for studying myocardial metabolism. In: Heiss HW, ed. *Advances in clinical cardiology, regional myocardial metabolism by positron tomography*, vol. 3. Mahwah, NJ: Foundation for Advances in Clinical Medicine, 1987:97-101.
 19. Schon HR, Schelbert HR, Robinson G, et al. ^{11}C labeled palmitic acid for the noninvasive evaluation of regional myocardial fatty acid metabolism with positron-computed tomography. I. Kinetics of ^{11}C palmitic acid in normal myocardium. *Am Heart J* 1982;103:532-547
 20. Schon HR, Schelbert HR, Robinson G, et al. ^{11}C labeled palmitic acid for the noninvasive evaluation of regional myocardial fatty acid metabolism with positron-computed tomography. II. Kinetics of ^{11}C palmitic acid in acutely ischemic myocardium. *Am Heart J* 1982;103:548-561
 24. Schwaiger M, Schelbert HR, Keen R, et al. Retention and clearance of ^{11}C palmitic acid in ischemic and reperfused canine myocardium. *J Am Coll Cardiol* 1985;6:311-320
 22. Kahn JK, Pippin JJ, Akers MS, Corbett JR. Estimation of jeopardized left ventricular myocardium in symptomatic and silent ischemia as determined by iodine-123 phenylpentadecanoic acid rotational tomography. *Am J Cardiol* 1989;63:540-544
 23. Williams DL, Ritchie JL, Harp GD, et al. In vivo simulation of thallium-201 myocardial scintigraphy by seven-pinhole emission tomography. *J Nucl Med* 1980;21:821-828
 24. Sorenson JA, Phelps ME. *Physics in nuclear medicine*. Orlando, FL: Grune & Stratton, 1987
 25. Ritchie JL, Cerqueira MD, Maynard C, Davis K, Kennedy W. Ventricular function and infarct size: the western Washington intravenous streptokinase in myocardial infarction trial. *J Am Coll Cardiol* 1988;11:689-697
 26. Tamaki N, Mukai T, Ishii Y, et al. Clinical evaluation of thallium-201 emission myocardial tomography using a rotating gamma camera: comparison with seven-pinhole tomography. *J Nucl Med* 1981;22:849-855
 27. Tamaki N, Yonekura Y, Mukai T, et al. Stress thallium-201 transaxial emission computed tomography: quantitative versus qualitative analysis for evaluation of coronary artery disease. *J Am Coll Cardiol* 1985;4:1213-1221
 28. Nohara R, Kambara H, Suzuki Y, et al. Stress scintigraphy using single-photon emission computed tomography in the evaluation of coronary artery disease. *Am J Cardiol* 1984;53:1250-1254
 29. DePasquale EE, Nody AC, DePury EG, et al. Quantitative rotational thallium-201 tomography for identifying and localizing coronary artery disease. *Circulation* 1988;77:316-327
 30. Fintel DJ, Links JM, Brinker JA, Frank TL, Parker M, Becker L. Improved diagnostic performance of exercise thallium-201 single photon emission computed tomography over planar imaging in the diagnosis of coronary artery disease: a receiver operating characteristic analysis. *J Am Coll Cardiol* 1989;13:600-612
 31. Ritchie JL, Williams D, Harp G, Stratton JR, Caldwell J. Transaxial tomography with ^{201}Tl for detecting remote myocardial infarction: comparison with planar imaging. *Am J Cardiol* 1982;50:1236-1241
 32. Muehllehner G, Colsher J. Positron computed tomography. I. Instrumentation. In: Ell PJ, Holman BL, eds. *Emission computed tomography*. New York: Oxford University, 1982:3-41
 33. Muallani NA, Wong WH, Hartz R, et al. Preliminary results with TOF-PET. *IEEE Trans Nucl Sci* 1983;30:739
 34. Hoffman EJ, Ricci AR, van der Stee LMAM, et al. ECAT III: basic design considerations. *IEEE Trans Nucl Sci* 1983;NS-33:729-733
 35. Senda M, Tamaki N, Yonekura Y, et al. Performance characteristics of Positologica III: a whole-body positron emission tomograph. *J Comput Assist Tomogr* 1985;9(5):940-946
 36. Hoffman EJ, Phelps ME, Huang SC, et al. Dynamic gated and high resolution imaging with the ECAT III. *IEEE Trans Nucl Sci* 1986;NS-33:453-455
 37. Phelps ME, Mazziotta JC, Schelbert HR. *Positron emission tomography and autoradiography: principles and application to the brain and heart*. New York: Raven, 1986
 38. Jacobson HG. Instrumentation in positron emission tomography. *JAMA* 1988;259:1531-1536
 39. Rozanski A, Berman DS, Gray R, et al. Use of ^{201}Tl redistribution scintigraphy in the preoperative detection of reversible and nonreversible myocardial asynergy. *Circulation* 1981;64:936-944
 40. Gibson RS, Watson DD, Taylor GJ, et al. Prospective assessment of regional myocardial perfusion before and after coronary revascularization surgery by quantitative ^{201}Tl scintigraphy. *J Am Coll Cardiol* 1983;1:804-815
 41. Gutman J, Berman DS, Freeman M, et al. Time to completed redistribution of ^{201}Tl in exercise myocardial scintigraphy: relationship to the degree of coronary artery stenosis. *Am Heart J* 1983;106:989-995
 42. Cloninger KG, DePuey G, Garcia EV, et al. Incomplete redistribution in delayed ^{201}Tl single photon emission computed tomographic (SPECT) images: an overestimation of myocardial scarring. *J Am Coll Cardiol* 1988;12:955-963
 43. Brunken R, Schwaiger M, Grover-McKay M, Phelps ME, Tillisch J, Schelbert HR. Positron emission tomography detects tissue metabolic activity in myocardial segments with persistent thallium perfusion defects. *J Am Coll Cardiol* 1987;10:557-567
 44. Tamaki N, Yonekura Y, Yamashita K, et al. Relation of left ventricular perfusion and wall motion with metabolic activity in persistent defects on ^{201}Tl tomography in healed myocardial infarction. *Am J Cardiol* 1988;62:202-208
 45. Tamaki N, Yonekura Y, Senda M, et al. Value and limitation of stress ^{201}Tl single photon emission computed tomography: comparison with ^{13}N ammonia positron tomography. *J Nucl Med* 1988;29:1181-1188
 46. Cerqueira MD, Martin GV, Embree L, Caldwell JH, Krohn K, Rasey J. Enhanced binding of fluoromisonidazole in isolated adult rat myocytes during hypoxia (abstr). *J Nucl Med* 1988;29:806
 47. Martin GV, Caldwell JH, Rasey JS, Grunbaum Z, Cerqueira M, Krohn KA. Enhanced binding of the hypoxic cell marker [^3H] fluoromisonidazole in ischemic myocardium. *J Nucl Med* 1989;30:194-201
 48. Shelton ME, Dence CS, Hwang DR, Welch MJ, Bergmann SR. Myocardial kinetics of ^{18}F -misonidazole: a marker of hypoxic myocardium. *J Nucl Med* 1989;30:351-358

Book Review

General Thoracic Surgery, 3rd ed. Edited by Thomas W. Shields. Philadelphia: Lea & Febiger, 1251 pp., 1989. \$150

Comprehensive textbooks on nonimaging subspecialties are principally used by imagers as reference works. At their best, such textbooks provide specific information outside the scope of subspecialty imaging textbooks. Of equal importance is that they provide the point of view of a specific group of our clinical colleagues. Such perspective increases our understanding of the clinical problems with which we deal and provides knowledge that increases our rapport with those for whom the textbook is specifically intended.

This book is one of the principal texts on thoracic surgery. It differs from similar works in that it concentrates on surgery of the chest wall, lungs, and mediastinum. Shields' book excludes the subject of cardiovascular surgery, which is often covered—and even featured—in thoracic surgery textbooks because many surgeons practice both general thoracic and cardiovascular surgery.

Excellent introductory chapters cover anatomy and, exceedingly briefly, physiology. The new 3rd edition includes a markedly expanded discussion of radiologic and imaging studies. This section is probably of the least use to radiologists, who have access to much more complete discussions of chest imaging. It is, however, remarkable that this text includes a thorough discussion of thoracic MR imaging by Gordon Gamsu. Dr. Gamsu's coverage is unusually detailed for a text of this type, and it is reasonably up-to-date with inclusion of material through the early months of 1988.

Discussions of nonimaging diagnostic procedures and the preoperative, postoperative, and anesthetic management of the patient are all done well and only minimally complicated by overlapping subject matter. Descriptions of surgical procedures are sufficiently terse to be readable by nonsurgeons; it strikes me that a specialist would find these descriptions insufficient, and I would hesitate to recommend a surgeon whose knowledge of a procedure was limited to the material found in this book.

Long sections discuss the diseases of the chest wall, diaphragm, pleura, trachea, lung, esophagus, and mediastinum. These sections are comprehensive and generally well written, and the discussions of "medium rare" and uncommon diseases are particularly useful. Excellent discussions, for example, cover each of the parasitic diseases, including *Paragonimus* and hydatid disease. Particularly strong is the

section on the esophagus, an organ often poorly covered in other subspecialty texts.

A pleasing feature of this work is its division into 100 short chapters. This organization makes specific topics easy to find. In addition, it is delightful to find an index that is both comprehensive and easy to use. My repeated attempts to find missing items and errors resulted in my becoming increasingly impressed that this index had been prepared with care and intelligence.

As one might expect, there is a general tendency to emphasize surgery over other possible methods of treatment. This is reflected by relatively brief mention of such important innovations as percutaneous drainage of abscesses under imaging control. The discussion of diffuse lung disease is particularly archaic: it retains the conventional concept that there are no particular differences in the images of the many diseases that can infiltrate the lungs diffusely.

This text must be compared with the other standard thoracic surgery text, *Gibbon's Surgery of the Chest* by Sabiston and Spencer. The *Gibbon's* text includes far more detail concerning specific surgical procedures, including cardiovascular procedures, and is thus a much better reference for the specifics of how surgery is performed. It does, however, lack the basics and principles that are so well covered by Shields. The *Gibbon's* text is also due for revision; its fourth edition was published in 1983. In general, Shields' book seems preferable for basic and general information and for terse discussions of surgical procedures, whereas *Gibbon's* is stronger in describing surgical specifics.

Should a radiologist have a copy of *General Thoracic Surgery* on his or her bookshelf? The general answer is no, unless one has frequent, detailed discussions with thoracic surgeons (e.g., during thoracic surgery rounds and conferences). However, it is nearly as illuminating to remind ourselves of the point of view of our clinical colleagues as it is to know their practice, as well as our own.

David S. Feigin
University of California, San Diego
La Jolla, CA 92093

Bronchial Impaction in Lobar Collapse: CT Demonstration and Pathologic Correlation

Harvey S. Glazer¹
Dixie J. Anderson
Stuart S. Sagel

Bronchial (or mucoid) impaction refers to the accumulation of inspissated secretions (mucus and/or inflammatory products) within a bronchus, usually accompanied by bronchial dilatation. This process may be caused by abnormal mucociliary transport and excessive production of mucus. In other cases, a discrete lesion may be present that obstructs the bronchus with inspissated secretions accumulating distal to the obstructing lesion. Lobar collapse may result in either case if a lobar bronchus is occluded by the excessive mucus or a discrete obstructing lesion. The CT manifestations of bronchial impaction in four patients with lobar collapse are described. In two patients, the lobar collapse and distal bronchial impaction were produced by a central obstructing bronchogenic carcinoma, whereas the other two patients had an abnormal mucus accumulation without a discrete bronchial obstruction. On CT, the impacted bronchi, best seen on postcontrast images, appeared as relatively low-attenuation branching structures extending from the hilum peripherally into the more opaque enhancing atelectatic lung. In the three patients who had surgical resection of the involved lobe, pathologic examination confirmed the dilated bronchi, filled with mucus (one patient), fibrinopurulent exudate (one), or mucous plugs with *Aspergillus* hyphae (one).

This unique pattern of impaction within a collapsed lobe should be recognized on CT and prompt a search for a possible central obstructing lesion.

AJR 153:485-488, September 1989

Bronchial (or mucoid) impaction refers to the accumulation of inspissated secretions (mucus and/or inflammatory products) within a bronchus, usually accompanied by bronchial dilatation [1-5]. This process may involve lobar or segmental bronchi and may be caused by abnormal mucociliary transport and excessive production of mucus (e.g., allergic bronchopulmonary aspergillosis, asthma, bronchiectasis, cystic fibrosis). In other cases, a discrete lesion (e.g., bronchogenic carcinoma, bronchial atresia, tuberculous bronchostenosis) may be present that obstructs the bronchus with inspissated secretions accumulating distal to the obstructing lesion. In patients with a neoplasm obstructing the bronchus and causing bronchial impaction, the dilated distal bronchi may contain neoplastic cells in addition to or instead of inspissated secretions [2].

Lobar collapse may result if a lobar bronchus is occluded by either the excessive mucus or a discrete obstructing lesion [6, 7]. Little attention has been directed specifically to the recognition of bronchial impaction within a collapsed lobe [7]. The CT appearance of bronchial impaction associated with lobar collapse in four patients is described.

Materials and Methods

Lobar collapse in two of the four patients (two men and two women) was caused by a central bronchogenic carcinoma with bronchial impaction developing distal to the central tumor. The other two patients had excessive mucus occluding the bronchus (one with allergic

Received January 20, 1989; accepted after revision April 19, 1989.

¹ All authors: Mallinckrodt Institute of Radiology, Washington University School of Medicine, 510 S. Kingshighway Blvd., St. Louis, MO 63110. Address reprint requests to H. S. Glazer.

0361-803X/89/1533-0485
© American Roentgen Ray Society

bronchopulmonary aspergillosis and one with nonspecific mucous plugging). The left lower lobe and left upper lobe were collapsed in two patients each.

CT was performed on a Siemens Somatom DR3 (three patients) or EMI 7070 (one patient) with scanning times of 5 sec or less. Noncontrast contiguous scans were obtained during suspended inspiration at 1-cm intervals throughout the thorax by using 8–10 mm collimation. In two patients, dynamic scanning also was performed at two preselected levels after the bolus administration of 50 ml of Conray 60 (Mallinckrodt, Inc., St. Louis, MO). In the remaining two patients a bolus of 50 ml of Conray 60 was administered, and the thorax was rescanned during a rapid infusion of 150 ml of Conray 60.

Pathologic correlation was achieved via surgical resection (two lobectomy, one pneumonectomy) in three patients and by bronchoscopy in the patient with nonspecific mucous plugging. Pathologic specimens were inflated and fixed with 10% buffered formalin before sectioning.

Results

In all four patients, CT images obtained after IV contrast administration showed multiple low-attenuation tubular branching structures within the enhancing atelectatic lung (Figs. 1 and 2). The branching structures followed the course of bronchi and could be seen extending peripherally from the

hilum. When imaged in cross section they were oval or circular. Similar findings were barely perceptible in two of four patients on the noncontrast images. In two patients (one with bronchogenic carcinoma and one with allergic bronchopulmonary aspergillosis), dilated air-filled bronchi were seen also.

In the three patients (two with bronchogenic carcinoma and one with allergic bronchopulmonary aspergillosis) who underwent surgical resection, the relatively low-density tubular branching structures seen on CT corresponded to dilated bronchi seen pathologically. Thickened bronchial walls seen pathologically in two patients could not be distinguished on CT from the adjacent enhancing atelectatic lung. In one patient with a centrally obstructing bronchogenic carcinoma resulting in lobar collapse, the distal bronchi were filled with mucus (Fig. 1). In the other patient with a centrally obstructing bronchogenic carcinoma, many of the distal bronchi were filled with fibrinopurulent exudate surrounded by areas of bronchopneumonia. Multiple mucous plugs containing a few scattered *Aspergillus* hyphae were seen in the patient with allergic bronchopulmonary aspergillosis (Fig. 2).

Discussion

Varying amounts of atelectasis may occur distal to obstruction of a segmental or lobar bronchus. A combination of

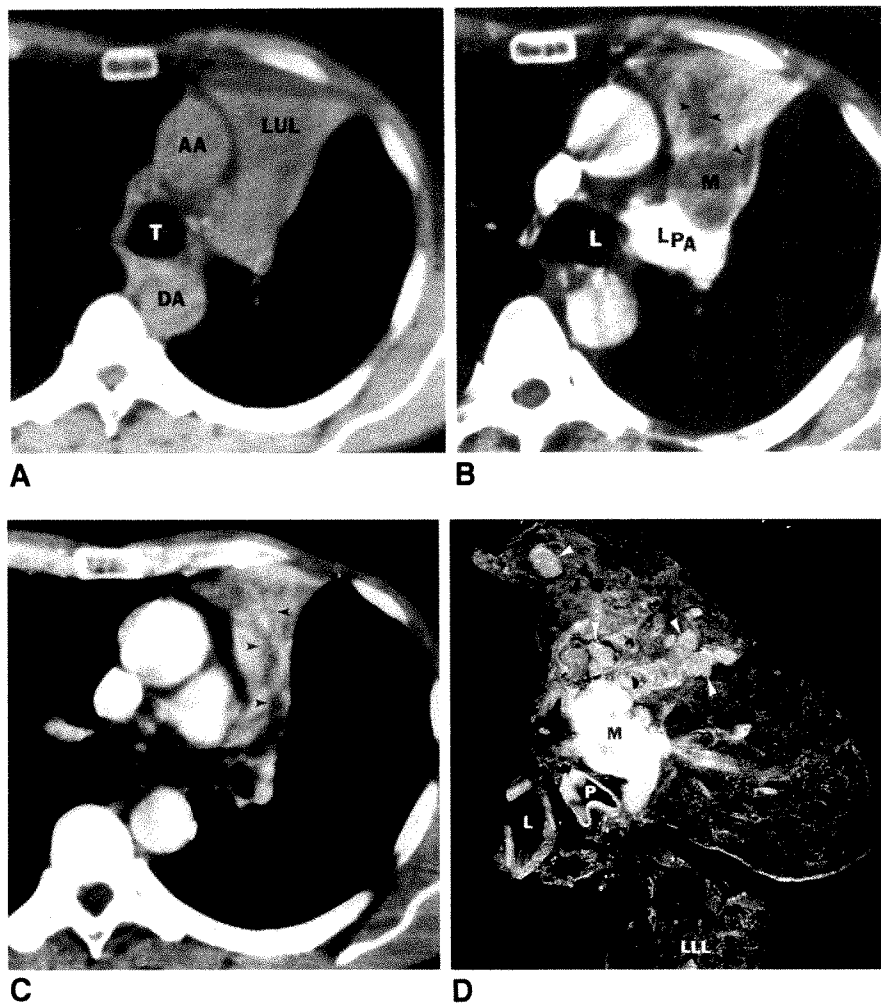


Fig. 1.—Left upper lobe collapse in bronchogenic carcinoma.

A, Precontrast CT scan shows left upper lobe (LUL) collapse. AA = ascending aorta; DA = descending aorta; T = trachea.

B and C, Postcontrast images at same level as A (B) and 1 cm caudad (C) show multiple low-attenuation branching structures (arrowheads) within atelectatic lung, as well as 3-cm mass (M) compressing left pulmonary artery (LPA). L = left mainstem bronchus.

D, After left pneumonectomy, pathologic specimen was sectioned transversely. Pathologic specimen is at a slightly different orientation and level than B. Multiple, dilated, mucus-filled bronchi (arrowheads) are seen mostly in anterior segment of left upper lobe distal to central neoplastic mass (M). Bronchial walls are slightly thickened. Adjacent lung was firm and golden brown from postobstructive pneumonia. Note more normal appearance of left lower lobe (LLL). L = left mainstem bronchus; P = left pulmonary artery.

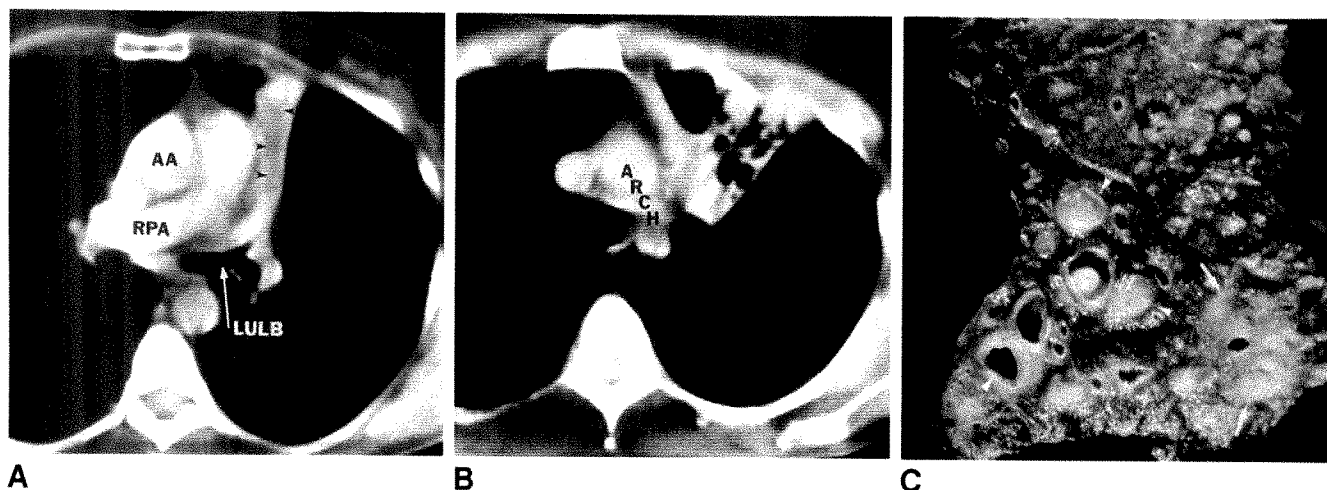


Fig. 2.—Left upper lobe collapse in allergic bronchopulmonary aspergillosis.

A, Postcontrast CT scan shows relatively low-attenuation tubular structure (arrowheads) extending from left upper lobe bronchus (LULB). Subtle branching is seen peripherally. RPA = right pulmonary artery; AA = ascending aorta.

B, CT scan at level of top of aortic arch (ARCH) shows multiple, dilated, air-filled bronchi within collapsed left upper lobe.

C, Lobectomy specimen, sectioned sagittally, shows multiple, dilated, thick-walled bronchi filled with mucus and air (arrowheads) adjacent to pulmonary artery branches. Focal areas of acute pneumonia (arrows) also are present. Several long strands of mucous plugs, which were removed from bronchi, showed segmental and subsegmental branching. Extensive bronchiolitis was seen microscopically. Histologic sections of mucous plugs showed scattered *Aspergillus hyphae*.

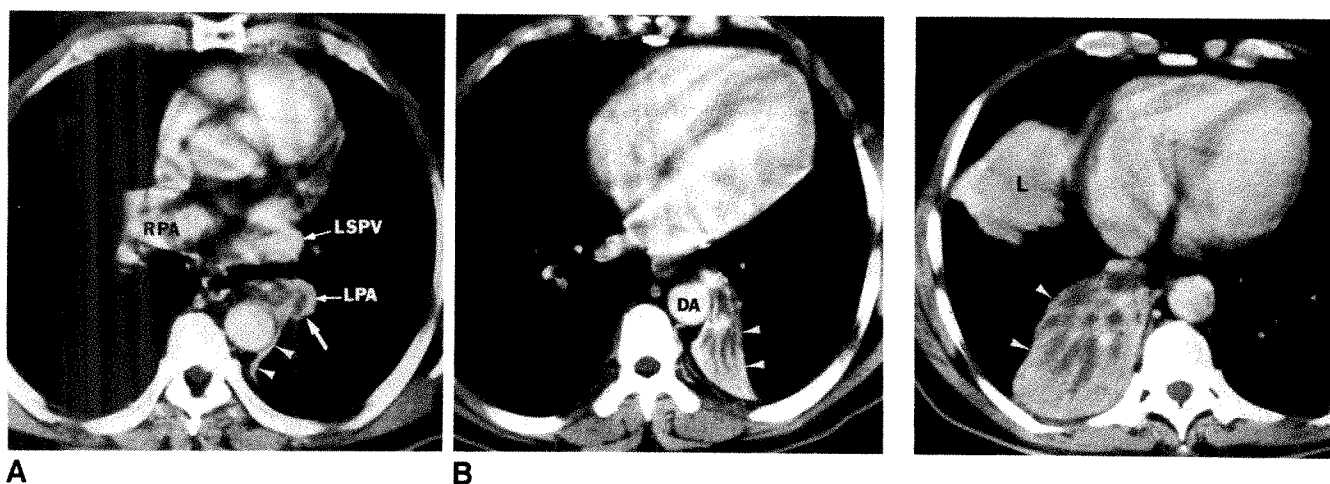


Fig. 3.—Left lower lobe collapse in bronchogenic carcinoma.

A, Postcontrast CT scan through level of right pulmonary artery (RPA) shows relatively low-attenuation soft-tissue mass (large arrow) obstructing left lower lobe bronchus, resulting in left lower lobe collapse (arrowheads). LSPV = left superior pulmonary vein; LPA = compressed left lower lobe pulmonary artery.

B, CT scan through base of heart shows multiple low-attenuation branching structures (most likely representing mucus-filled bronchi) within enhancing collapsed left lower lobe (arrowheads). DA = descending aorta.

Fig. 4.—Right lower lobe collapse in bronchogenic carcinoma. Postcontrast CT scan shows multiple, relatively low-attenuation branching structures (most consistent with dilated, mucus-filled bronchi) within enhancing collapsed right lower lobe (arrowheads). More cephalad images showed large mass obstructing right lower lobe bronchus. L = top of liver.

pathologic features in the lung (e.g., mucous plugging, intraalveolar fluid, interstitial pneumonitis, interstitial fibrosis, and infection) may account for the opacification seen on plain chest radiographs [8]. Mucous glands continue to function after an obstruction of a bronchus unless they are destroyed by tumor or infection [1]. Mucus is produced until the bronchial pressure exceeds the secretory pressure. Cilia transport the mucus proximally to the site of obstruction, where it overdistends the bronchi. Bronchiectasis and bronchiolectasis with mucous plugging were found distal to central obstructing

neoplasms in 13 of 16 patients in one series [8]. Changes of bronchial impaction may be less apparent with neoplasms seen at an early stage or with only partial bronchial obstruction.

With segmental bronchial impaction, one or more tubular structures with the long axis pointing toward the pulmonary hilum are seen on chest radiographs or CT scans. In a review of 30 cases of bronchogenic carcinoma obstructing a segmental bronchus, bronchial impaction was found in 12 (40%) [1]. Bronchial impaction distal to a bronchogenic carcinoma

partially obstructing a lobar or mainstem bronchus has been described also [4].

Bronchial impaction within a completely collapsed lobe usually is not visible on conventional chest radiographs because the bronchi are surrounded by an airless lung. Several authors have described the CT features of lobar collapse and shown that CT may be useful in clarifying confusing plain film findings as well as in confirming the presence and extent of a proximal obstructing lesion [9–13]. A recent study of pulmonary atelectasis illustrated one case of bronchial impaction ("mucous bronchograms") on CT and described seeing it in 12 of 20 patients with central hilar masses and distal atelectasis [7].

Bronchial impaction was not described in early CT studies of lobar collapse [9–11]. This, in part, may be because IV contrast material often was not used. We have shown that differentiation between the dilated bronchi and adjacent atelectatic lung was accentuated by the administration of IV contrast material. The atelectatic lung enhanced relative to the inspissated secretions within the dilated bronchi. Because of the small number of patients in this study, the optimal technique for demonstrating these findings could not be assessed. Conceivably, bronchial impaction might be difficult to see within a collapsed lobe despite the proper use of IV contrast material. Obstruction of the blood supply to the collapsed lobe by tumor might prevent adequate enhancement of the atelectatic lung. Associated abscess or necrosis within the collapsed lobe could obscure the findings of mucoid impaction on CT because that region would enhance relatively less than the more normal surrounding parenchyma.

Two of our four cases of bronchial impaction were caused by bronchogenic carcinoma. Several other cases suggestive of bronchial impaction in patients with an obstructing bron-

chogenic carcinoma and lobar collapse have been seen at our institution, but these patients did not undergo surgical resection (Figs. 3 and 4). Abnormal secretion of mucus or mucociliary transport also can demonstrate this finding without a central bronchial mass or obstruction [7].

REFERENCES

1. Felson B. Mucoid impaction (inspissated secretions) in segmental bronchial obstruction. *Radiology* 1979;133:9–16
2. Aronberg DJ, Sagel SS, Jost RG, Levitt RG. Oat cell carcinoma manifesting as a bronchocele. *AJR* 1979;132:23–25
3. Pugatch RD, Gale ME. Obscure pulmonary masses: bronchial impaction revealed by CT. *AJR* 1983;141:909–914
4. Woodring JH, Bernardy MO, Loh FK. Mucoid impaction of the bronchi. *Australas Radiol* 1985;29:234–239
5. Bowen AD, Oujhane K, Odagiri K, Liston SL, Cumming WA, Oh KS. Plastic bronchitis: large branching, mucoid bronchial casts in children. *AJR* 1985;144:371–375
6. Geffer WB, Epstein DM, Miller WT. Allergic bronchopulmonary aspergillosis: less common patterns. *Radiology* 1981;140:307–312
7. Woodring JH. Determining the cause of pulmonary atelectasis: a comparison of plain radiography and CT. *AJR* 1988;150:757–763
8. Burke M, Fraser R. Obstructive pneumonitis: a pathologic and pathogenetic reappraisal. *Radiology* 1988;166:699–704
9. Naidich DP, McCauley DI, Khouri NF, Leitman BS, Hulnick DH, Siegelman SS. Computed tomography of lobar collapse: endobronchial obstruction. *J Comput Assist Tomogr* 1983;7:745–757
10. Naidich DP, McCauley DI, Khouri NF, Leitman BS, Hulnick DH, Siegelman SS. Computed tomography of lobar collapse: collapse in absence of endobronchial obstruction. *J Comput Assist Tomogr* 1983;7:758–767
11. Glazer HS, Aronberg DJ, VanDyke JA, Sagel SS. CT manifestations of pulmonary collapse. *Contemp Issues Comput Tomogr* 1984;4:81–119
12. Raasch BN, Heitzman ER, Carsky EW, Lane EJ, Berlow ME, Witwer G. A computed tomographic study of bronchopulmonary collapse. *RadioGraphics* 1984;4:195–232
13. Khoury MB, Godwin JD, Halvorsen RA Jr, Putman CE. CT of obstructive lobar collapse. *Invest Radiol* 1985;20:708–716

Case Report

Fibrosing Mediastinitis in the Posterior Thorax

Paul D. Kountz,¹ Paul L. Molina, and Stuart S. Sagel

Fibrosing mediastinitis and retroperitoneal fibrosis are rare conditions of uncertain cause in which proliferating connective tissue encases and compresses adjacent structures. Some cases have been associated with a malignant neoplasm, infection, drug ingestion (e.g., methysergide), or retroperitoneal hematoma and thus are considered by many to represent an autoimmune hypersensitivity response to various antigens [1]. Mediastinal fibrosis typically presents as a middle mediastinal and/or hilar mass [2, 3]. A unique case is described that manifested initially as a predominantly posterior mediastinal mass and subsequently extended into adjacent pulmonary parenchyma and the retroperitoneum, and developed other manifestations of a systemic fibrosclerosis syndrome.

Case Report

A 63-year-old man presented initially with complaints of chronic mild dyspnea, coughing, and occasional hemoptysis. Relevant medical history included a 50-pack-year history of smoking, lifelong residence in the Mississippi River Valley, and Peyronie disease. Physical examination was remarkable only for mild bilateral wheezes. Serologic tests for recent exposure to *Histoplasma*, *Aspergillus*, *Blastomyces*, and *Coccidioides* were negative, as was a second-strength tuberculin skin test (with positive controls). Chest radiographs at that time revealed a posterior mediastinal mass. Evaluation by CT (Figs. 1A and 1E) showed a soft-tissue mass in the posterior mediastinum that contained scattered foci of calcification. The mass extended from just below the aortic arch into the retrocrural space, but not below the celiac trunk. Percutaneous needle biopsy and subsequent biopsy at thoracotomy confirmed the diagnosis of sclerosing mediastinitis with extension into the adjacent pulmonary parenchyma.

The patient was treated conservatively with bronchodilators, but his symptoms progressed minimally over the next 3 years. On read-

mission, chest radiography revealed an 8 × 18 cm irregular, posterior mediastinal mass with streaky bilateral extension into the adjacent pulmonary parenchyma (Figs. 1C and 1D). There was no osseous involvement. A second CT study (Figs. 1E and 1F) documented progression of the fibrosis during the 3-year interval. The mass contained extensive calcification and involved the posterior mediastinum from the thoracic inlet and extended caudally through the retroperitoneum to the level of the aortic bifurcation. The bronchus intermedius and, to a lesser extent, the bronchus of the left lower lobe were narrowed. Ventilation-perfusion scintigraphy confirmed significant obstructive ventilatory abnormality of the right middle and lower lobes. Nevertheless, there remained little involvement of the middle mediastinum or hila and no significant compression of the superior vena cava. The esophagus appeared normal on barium-swallow examination.

Discussion

Idiopathic mediastinal fibrosis may be a localized manifestation of a group of systemic fibrosclerosing syndromes, including retroperitoneal fibrosis, sclerosing mediastinitis, sclerosing cholangitis, systemic sclerosis, Riedel thyroiditis, Peyronie disease, and tumefactive inflammatory lesions of the head and neck [1, 4]. Involvement of more than one organ has been termed *multifocal fibrosclerosis* [5]. The features of our case support this concept of multiple manifestations of a common underlying fibrosclerotic predisposition. The patient had been treated for Peyronie disease 15 years before, presenting with mediastinal fibrosis, and later developing pulmonary parenchymal and retroperitoneal involvement. Although no specific cause was identified, prior infection by *Histoplasma capsulatum* is most likely because it is the commonest proved cause of fibrosing mediastinitis [6], and normal

Received January 24, 1989; accepted after revision March 22, 1989.

¹ All authors: Mallinckrodt Institute of Radiology, Washington University School of Medicine, 510 S. Kingshighway Blvd., St. Louis, MO 63110. Address reprint requests to P. L. Molina.

AJR 153:489-490, September 1989 0361-803X/89/1533-0489 © American Roentgen Ray Society

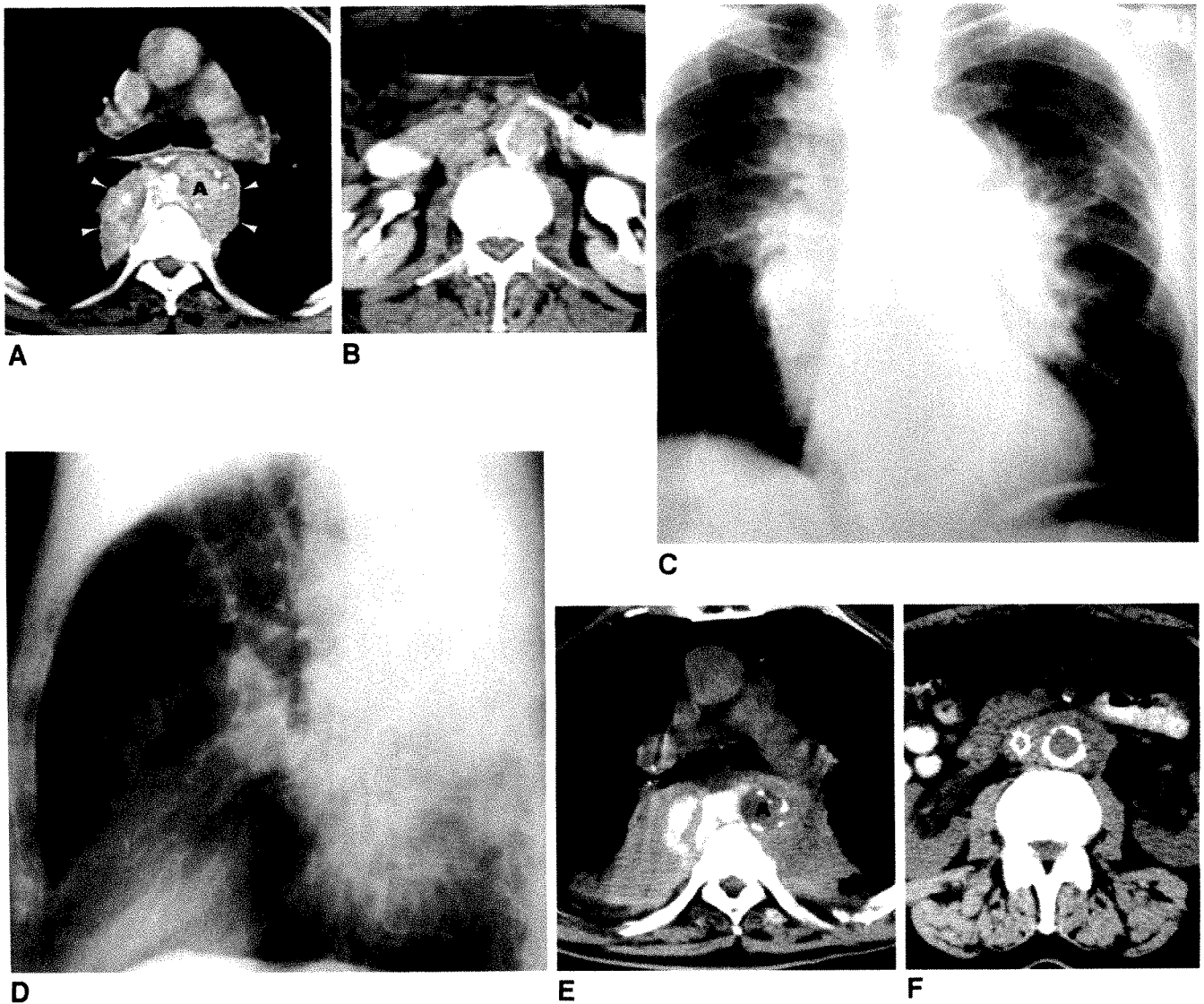


Fig. 1.—A, Contrast-enhanced CT scan at level of carina shows a large bilateral paraspinal soft-tissue mass (arrowheads) containing scattered calcifications and encasing descending aorta (A).
 B, At level of renal hila, fat planes around aorta and inferior vena cava are preserved. No fibrotic mass was identified at any level in retroperitoneum.
 C and D, Posteroanterior (C) and lateral (D) chest radiographs show large irregular mass extending from posterior mediastinum into adjacent pulmonary parenchyma bilaterally.
 E, Non-contrast-enhanced CT scan at level of carina 3 years after study in A and B. Mass has enlarged and extends more laterally into hemithoraxes. Dense, irregular calcifications within mass have also increased. A = aorta with extensive atherosclerotic calcification.
 F, At level of renal hila, aorta is now surrounded by a homogeneous soft-tissue-density mass. A caval umbrella had been placed after an episode of deep venous thrombosis in lower extremity.

serologic findings do not necessarily exclude this possibility. Furthermore, *Histoplasma* is endemic in the Mississippi River Valley.

The atypical chest radiographic findings of a primarily posterior mediastinal mass undoubtedly account for the absence of clinical findings usually associated with extensive mediastinal fibrosis (e.g., superior vena cava syndrome or esophageal obstruction). Occasionally, pulmonary parenchymal involvement may be associated with mediastinal fibrosis. In this reported case, the radiographic and histologic evidence of direct extension of the mediastinal mass into adjacent lung is unusual. The serial CT scans show interval incorporation of contiguous lung parenchyma into the progressive fibrotic process. Recognition of this atypical pattern of mediastinal

fibrosis may be important in differentiating this condition from other causes of masses in the posterior thorax.

REFERENCES

1. Kittredge RD, Nash AD. The many facets of sclerosing fibrosis. *AJR* 1974;122:288-298
2. Feigin DS, Eggleston JC, Siegelman SS. The multiple roentgen manifestations of sclerosing mediastinitis. *Johns Hopkins Med J* 1979;144:1-8
3. Weinstein JB, Aronberg DJ, Sagel SS. CT of fibrosing mediastinitis: findings and their utility. *AJR* 1983;141:247-251
4. Cameron DG, Ing ST, Boyle M, Matthews WH. Idiopathic mediastinal and retroperitoneal fibrosis. *Can Med Assoc J* 1961;85:227-232
5. Comings DE, Skubi KB, Van Eyes J, Motulski AG. Familial multifocal fibrosclerosis. *Ann Intern Med* 1967;66:884-892
6. Strimlan CV, Dines DE, Payne WS. Mediastinal granuloma. *Mayo Clin Proc* 1975;50:702-705

Pictorial Essay

MR Imaging of Congenitally Corrected Transposition of the Great Vessels in Adults

Jae Hyung Park,¹ Man Chung Han, and Chu-Wan Kim

Congenitally corrected transposition of the great vessels is a rare congenital heart disease in which atrioventricular discordance and transposition of the great arteries occur [1]. In the absence of associated anomalies, or in the case of mild hemodynamic derangement with the anomalies, the disease often is not suspected clinically until adulthood [1, 2].

The diagnosis of congenitally corrected transposition of the great vessels in adults can be suspected on the basis of plain chest radiography, electrocardiography, and echocardiography [2]. Recently, MR imaging has been applied in the diagnosis of various congenital heart diseases, facilitating noninvasive diagnosis because of the good anatomic delineation it provides [3, 4].

We retrospectively analyzed MR findings in eight adults with this defect.

Materials and Methods

ECG-gated MR imaging was performed in eight adult patients with congenitally corrected transposition of the great vessels. Six were men and two were women. Their age range was 18 to 45 years. Cineangiocardiology was done in all patients. Six patients had situs solitus, and two had situs inversus. Associated anomalies included ventricular septal defect (three patients), atrial septal defect (three patients), and pulmonary stenosis (two patients).

MR imaging was performed with a 0.15-T resistive unit (KAIST, Seoul, Korea) in four cases and with a 2.0-T superconducting system (Spectro-20000, Gold Star, Korea) in four cases. An ECG-gated multislice technique was used to obtain transverse, sagittal, and coronal images in all cases. Repetition time (TR) was gated to the R-R interval, with a range of 600–1000 msec, and echo time (TE) was

30 msec. The reconstruction matrix was 128×256 . The signal was averaged two times; the spatial resolution was 1.6 mm. Slice thickness was 10 mm, and the interslice gap was 3 mm.

Results

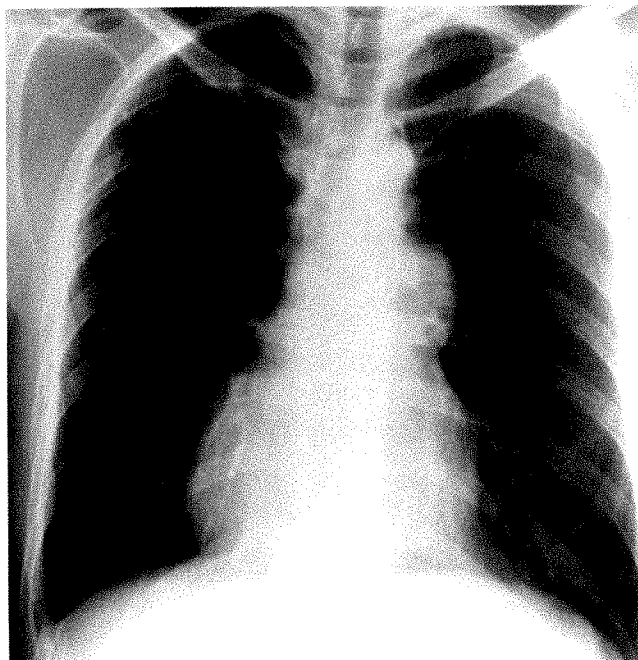
MR images in six patients showed the left transposed ascending aorta along the upper left cardiac border (Fig. 1). The left atrial appendage occupied the lower left cardiac border in four cases, covering the free lateral wall of the morphologic right ventricle (Fig. 1). In one case, the lower left cardiac border showed double convexities caused by the left atrial appendage. The upper right cardiac border was composed of superior vena cava in five cases. The right atrial appendage was found at the upper right cardiac border in three cases.

MR images showed coarse trabeculation in the morphologic right ventricle, and fine trabeculation in the morphologic left ventricle, especially in coronal images (Fig. 2). In three cases, transverse images showed the moderator band crossing the morphologic right ventricle (Fig. 2). In five patients, transverse images showed valvular attachment to the atrioventricular septum. In one patient, the septal leaflet was displaced toward the apex of the ventricle, suggesting Ebstein anomaly of the morphologic right ventricle (Fig. 3). Discordant connections of the great vessels to the ventricles were identified in all cases (Figs. 1–3). The ascending aorta arose anteriorly from the left ventricle in seven cases. All cases had associated findings of atrial septal defect, ventricular septal defect, and valvular pulmonary stenosis (Fig. 2).

Received April 7, 1989; accepted after revision May 15, 1989.

¹ All authors: Department of Radiology, Seoul National University Hospital, 28 Yeongun-Dong, Chongro-Ku, Seoul 110-744, Korea. Address reprint requests to J. H. Park.

AJR 153:491–498, September 1989 0361–803X/89/1533–0491 © American Roentgen Ray Society



A

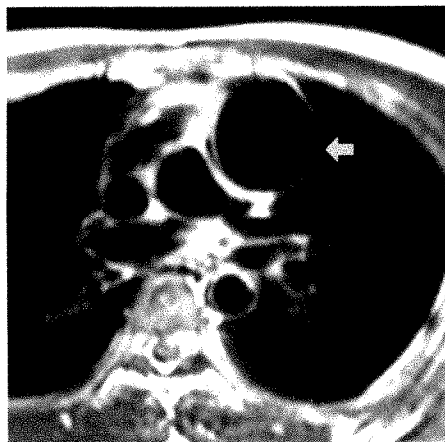
Fig. 1.—30-year-old man with congenitally corrected transposition of great vessels.

A, Chest radiograph shows typical convexity along upper left cardiac border.

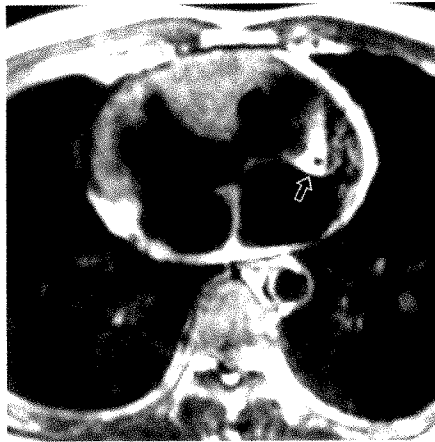
B, Transverse MR image shows anterolaterally transposed ascending aorta (arrow), forming upper left cardiac border.

C, Lower transverse MR image shows left atrial appendage lateral to morphologic right ventricle. Note epicardial fat containing coronary artery (arrow) between cardiac structures.

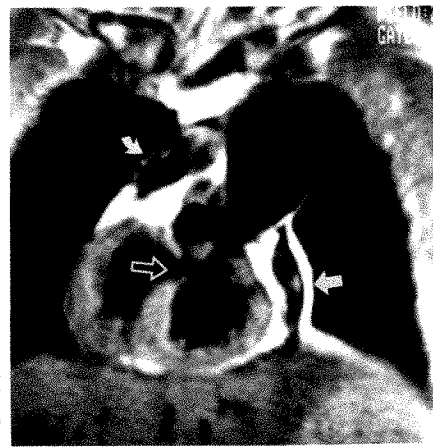
D, Coronal MR image shows structures composing left cardiac border on chest radiograph. Left atrial appendage (solid arrow) is surrounded by epicardial fat, covering lateral aspect of morphologic right ventricle. Right atrial appendage is seen in upper right cardiac border (curved arrow). An associated ventricular septal defect is evident (open arrow).



B



C



D

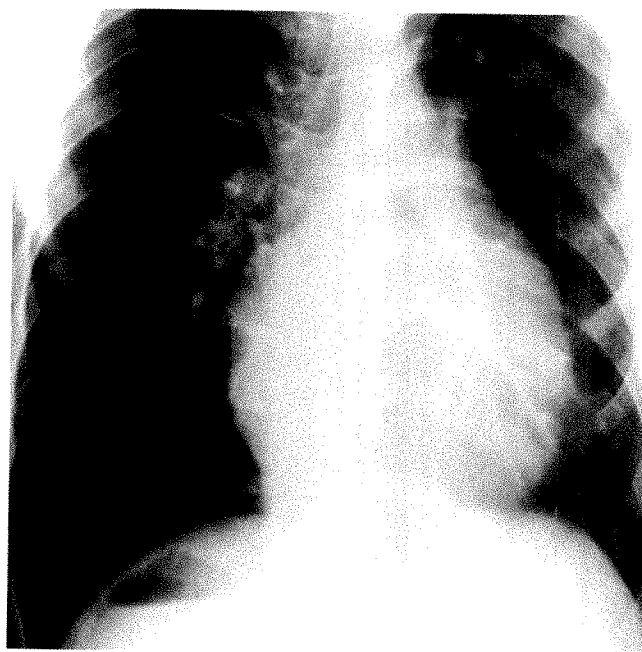
Fig. 2.—18-year-old man with congenitally corrected transposition of great vessels.

A, Preoperative chest radiograph shows gastric air bubble under right hemidiaphragm, suggesting situs inversus.

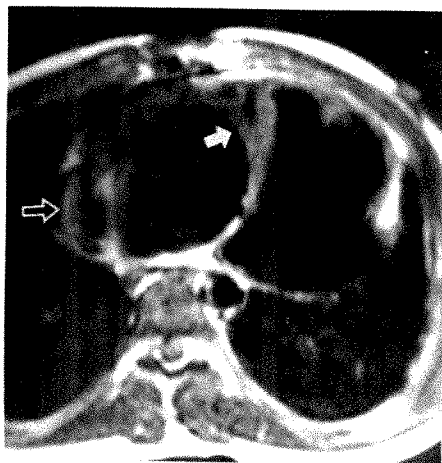
B, Postoperative transverse MR image shows moderator band (solid arrow) in apical area of morphologic right ventricle. Lateral border is occupied by right atrial appendage (open arrow).

C, Coronal MR image shows difference of trabeculation of ventricles. Note irregularity of septal surface (solid arrow) of morphologic right ventricle, compared with smoothness of left ventricular septum. Venous atrial appendage composes upper left cardiac border (open arrow).

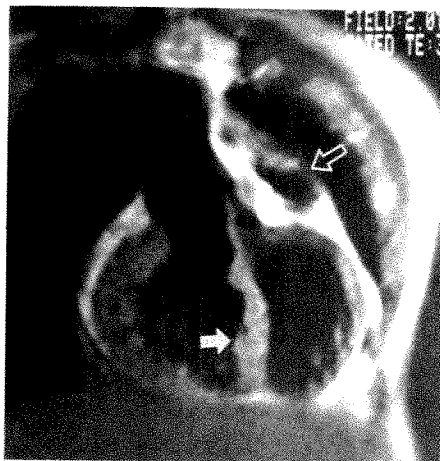
D, Coronal MR image shows left superior vena cava draining into left-sided ventricle. A hepatic vein (arrow) drains into inferior vena cava, which eventually drains into left-sided atrium.



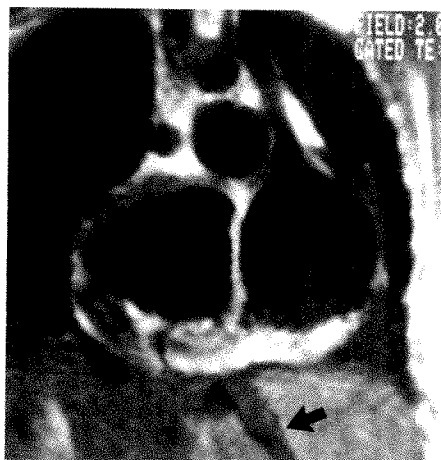
A



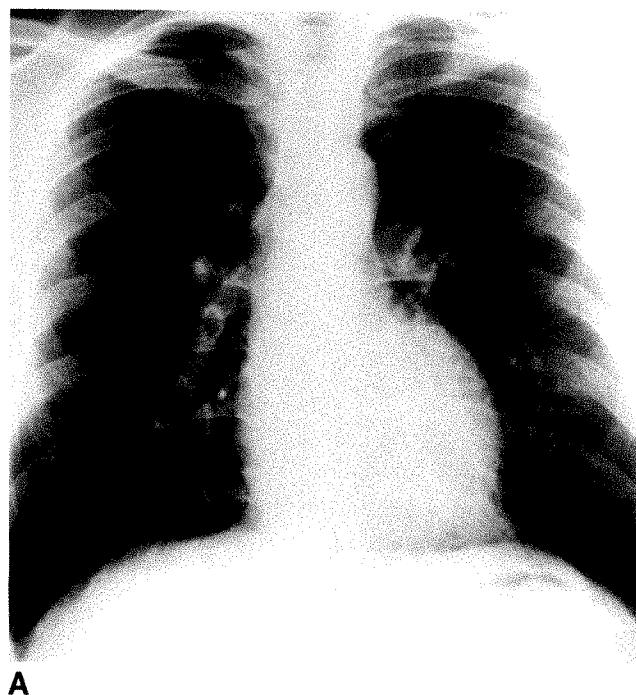
B



C



D



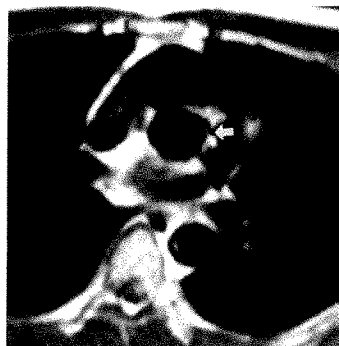
A

Fig. 3.—28-year-old man with congenitally corrected transposition of great vessels.

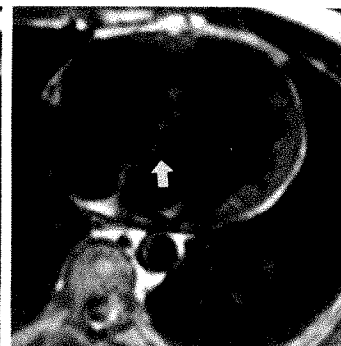
A, Chest radiograph shows a normal cardiac contour.

B, MR image shows anteroposterior relation of great vessels due to transposition. Ascending aorta (arrow) is posterior to pulmonary artery.

C, Transverse MR image shows difference of valvular attachment to atrioventricular septum. Septal leaflet of tricuspid valve (arrow) of morphologic right ventricle is attached more anteriorly toward cardiac apex than that of mitral valve, suggesting presence of an associated Ebstein anomaly.



B



C

Discussion

Cardiac morphology, viscerotrial situs, and the relationship of the ventricles and the great vessels can be detected by MR imaging to diagnose congenitally corrected transposition of the great vessels in adults [4]. In addition, ECG-gated cardiac MR imaging delineates the specific anatomic structures composing the cardiac contours on plain chest radiographs. MR imaging also can show both atrioventricular valves, not only to identify both ventricles but also to show Ebstein anomaly of the tricuspid valves in the morphologic right ventricle.

REFERENCES

1. Allwork SP, Bental HH, Becker AE, et al. Congenitally corrected transposition of the great arteries: morphologic study of 32 cases. *Am J Cardiol* 1976;38:910-923
2. Tonkin IL, Kelley MJ, Bream PR, Elliott LP. The frontal chest film as a method of suspecting transposition complexes. *Circulation* 1976;53:1016-1025
3. Didier D, Higgins CB, Fisher MR, Osaki L, Silverman NH, Cheitlin MD. Congenital heart disease: gated MR imaging in 72 patients. *Radiology* 1986;158:227-235
4. Guit GL, Blueman R, Rohmer J, et al. Levotransposition of the aorta: identification of segmental cardiac anatomy using MR imaging. *Radiology* 1986;161:673-679

Case Report

MR Diagnosis of Lipomatous Infiltration of the Interatrial Septum

Kenneth R. Kaplan¹ and Matthew D. Rifkin

Lipomatous infiltration of the interatrial septum is associated with obesity and advancing age, and it has been identified as a cause of supraventricular arrhythmias in elderly people [1–3]. The diagnosis of this entity has been limited, until recently, to pathologic and histologic observations at autopsy. In this report, we describe the MR imaging findings and in vivo diagnosis of an unusual case of lipomatous infiltration of the interatrial septum with encasement, compression, and deviation of the superior vena cava by paracardiac extension of the lipomatous mass.

Case Report

A 69-year-old mildly obese woman with an 11-year history of congestive heart failure presented with a chief complaint of palpitations and worsening dyspnea on exertion during a 2-week period before admission. Physical examination revealed an irregular cardiac rhythm with a rate of 120–140 beats per minute and a II/VI systolic murmur at the left sternal border. Auscultation of the lungs revealed bibasilar rales. The rest of the physical examination was unremarkable. An ECG obtained on admission revealed multifocal atrial tachycardia. Subsequent ECGs obtained over a 1-week hospital stay revealed rhythms ranging from atrial fibrillation, to wandering pacemaker, to abundant atrial premature contractions. A chest radiograph showed moderate cardiomegaly. Two-dimensional echocardiography showed marked hypertrophy of the interatrial septum of uncertain cause and significance.

Further investigation of the echocardiographic findings was undertaken with ECG-gated MR imaging. The MR imaging study was performed with a 1.5-T superconducting magnet (GE Signa, Milwaukee, WI). Cardiac-gated MR images were obtained in axial and coronal planes by using multiple spin-echo pulse sequences. T1-weighted

images revealed homogeneous high signal intensity within a markedly thickened interatrial septum, which measured approximately 4 cm in maximal transverse diameter. The posterior walls of the right and left atria also were infiltrated by the same process (Fig. 1A). Furthermore, paracardiac extension of the mass resulted in encasement, compression, and lateral deviation of the superior vena cava; however, signal void in the vessel suggested that there was neither significant fixed obstruction to caval blood flow nor intracaval extension (Figs. 1B–1D). The signal characteristics of the mass were comparable to subcutaneous and subepicardial adipose tissue, namely, high signal on T1-weighted images (Figs. 1A–1C) and intermediate signal on T2-weighted images (Fig. 1D). Therefore, the lesion was felt to represent lipomatous hypertrophy of the interatrial septum with fatty infiltration of the posterior walls of the atria and paracardiac extension resulting in encasement of the superior vena cava.

Discussion

Lipomatous infiltration/hypertrophy of the interatrial septum has been identified as a cause of supraventricular arrhythmias in obese, elderly patients [1–3]. Documentation of this entity has, until recently, been limited to autopsy studies. Cases of in vivo diagnosis are reported rarely in the medical literature [4, 5]. Although a histologic diagnosis is not available for the present case, we believe that the MR appearance of this lesion is characteristic, if not pathognomonic, of lipomatous infiltration of the interatrial septum. Recent studies suggest that cardiovascular MR imaging may be able to provide as much clinical information as echocardiography, CT, and angiography combined in the evaluation of cardiac and paracardiac masses [6–8]. Our report supports this premise.

Received February 6, 1989; accepted after revision April 7, 1989.

¹ Both authors: Department of Radiology, Thomas Jefferson University Hospital, 111 S. 11th St., Philadelphia, PA 19107. Address reprint requests to K. R. Kaplan.

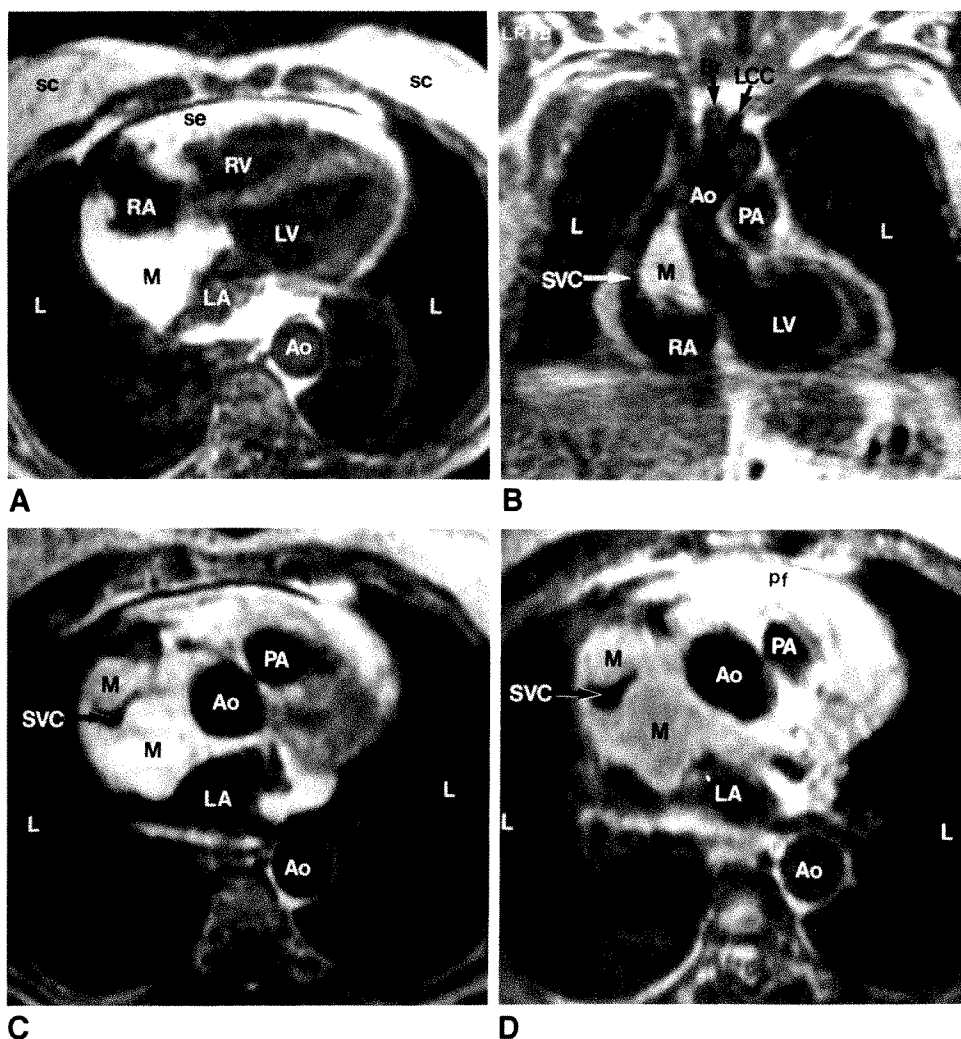


Fig. 1.—A, T1-weighted (570/20), ECG-gated axial MR image shows high signal intensity in atrial septal mass and adjacent thickened posterior walls of right and left atria. Mass is homogeneous and isointense to subepicardial fat, but has generally higher signal intensity than inhomogeneous subcutaneous fat.

B–D, T1-weighted (870/20), ECG-gated coronal (B) and axial (C) MR images and a T2-weighted (1846/70), ECG-gated axial MR image (D) show encasement, compression, and lateral deviation of superior vena cava by mass. C and D show signal characteristics of lesion on T1- and T2-weighted images, respectively. A crescent of high signal seen anterior to aorta and pulmonary artery on T2-weighted image (D) represents pericardial fluid. Signal void is noted in superior vena cava, cardiac chambers, and great vessels on all images.

Ao = aorta, Br = brachiocephalic artery, L = lung, LA = left atrium, LCC = left common carotid artery, LV = left ventricle, M = atrial septal mass, PA = pulmonary artery, pf = pericardial fluid, RA = right atrium, RV = right ventricle, sc = subcutaneous fat, se = subepicardial fat, SVC = superior vena cava.

A two-dimensional echocardiogram showed thickening of the interatrial septum and increased echogenicity in the posterior walls of the right and left atria. However, the cause and significance of these findings were not readily apparent. A contrast-enhanced CT scan, obtained after MR characterization of the lesion, did not provide any additional diagnostic information and did not have the advantage of assessment in the coronal plane. In summary, MR imaging was able to (1) greatly expand on the echocardiographic anatomic findings, (2) provide tissue characterization of the lesion, (3) evaluate the paracardiac extent of the lesion in both axial and coronal planes, and (4) assess the effect of the lesion on blood flow in the superior vena cava.

MR imaging is rapidly gaining acceptance as a powerful diagnostic imaging technique in the evaluation of cardiovascular disease [6–8]. The multiplanar capabilities, high degree of intrinsic soft-tissue contrast, and ability to evaluate mediastinal vasculature on an anatomic and physiologic level make MR imaging well suited for cardiovascular imaging. In the case presented here, MR imaging offered a noninvasive means of making a tissue diagnosis of a clinical entity formerly limited to the realm of the surgeon or pathologist. Although this is by no means a histologic diagnosis, MR tissue char-

acterization not only provided an anatomic basis for the patient's cardiac rhythms, but also may have circumvented the need for invasive diagnostic studies.

REFERENCES

1. Prior JT. Lipomatous hypertrophy of the cardiac interatrial septum: a lesion resembling hibernoma, lipoblastomatosis and infiltrating lipoma. *Arch Pathol* 1964;78:11–15
2. Page DL. Lipomatous hypertrophy of the cardiac interatrial septum: its development and probable clinical significance. *Hum Pathol* 1970;1:151–163
3. Hutter AM Jr, Page DL. Atrial arrhythmias and lipomatous hypertrophy of the cardiac interatrial septum. *Am Heart J* 1971;82:16–21
4. Isner JM, Channing SS II, Mikus JP, Carter BL. Lipomatous hypertrophy of the interatrial septum: in vivo diagnosis. *Circulation* 1982;66:470–473
5. Levine RA, Weyman AE, Dinsmore RE, et al. Noninvasive tissue characterization: diagnosis of lipomatous hypertrophy of the atrial septum by nuclear magnetic resonance imaging. *J Am Coll Cardiol* 1986;7:688–692
6. Amparo EG, Higgins CB, Farmer D, Gamsu G, McNamara M. Gated MRI of cardiac and paracardiac masses: initial experience. *AJR* 1984;143:1151–1156
7. Reed JD Jr, Soulen RL. Cardiovascular MRI: current role in patient management. *Radiol Clin North Am* 1988;26:589–606
8. Higgins CB, Byrd BF II, McNamara MT, et al. Magnetic resonance imaging of the heart: a review of the experience in 172 subjects. *Radiology* 1985;155:671–679

MR Appearance of Gallstones in Vitro at 1.5 T: Correlation with Chemical Composition

Richard L. Baron¹
 William P. Shuman¹
 Sum P. Lee²
 Charles A. Rohrmann, Jr.¹
 Robert N. Golden¹
 Todd L. Richards¹
 Michael L. Richardson¹
 James A. Nelson¹

Gallstones from 63 patients were evaluated by in vitro 1.5-T MR imaging, with T1- and T2-weighted images, and in 14 cases, a fat-suppression sequence (short-T1 inversion recovery imaging). Subsequent chemical analysis was performed on 43 gallstones. In vitro proton MR spectroscopy was performed on 14 stones. On T1-weighted MR images, foci of increased signal were seen in 46 of 63 stones (faint in 17, moderate in nine, and bright in 20). T2-weighted images showed areas of increased signal in 18 of 63 stones (faint in 15, moderate in three). T1-weighted MR imaging patterns were homogeneously dark (17), homogeneously bright (two), homogeneously faint (three), rimmed (dark rim and bright center, 32), and laminated (nine). Short-T1 inversion recovery imaging suppressed the foci of increased signal in 13 of 14 cases. Despite imaging characteristics suggestive of high lipid content, spectroscopy revealed only a single peak corresponding to a large water-proton signal. The T1 relaxation times of the water were shortened, ranging from 0.006 to 0.92 sec, explaining the increased signal seen on MR images of the gallstones.

MR imaging characteristics (signal intensity, relative signal area, or imaging patterns) did not correlate with chemical composition. We hypothesize that different structural relationships must exist within gallstones of similar chemical content that alter the water bonding and hence the MR imaging characteristics.

AJR 153:497-502, September 1989

The development of nonsurgical gallstone therapies such as chemical dissolution and extracorporeal shock-wave lithotripsy has generated renewed interest in the use of imaging procedures to predict gallstone composition and susceptibility to such nonoperative therapies. Although sonography has become the accepted standard for diagnosing cholelithiasis, it cannot be used to differentiate among gallstone types [1, 2]. Preliminary studies have shown that CT can be used to predict gallstone chemical composition [3, 4] and susceptibility to chemical dissolution [3, 5].

Limited low-field-strength MR investigations have shown increased gallstone signal in a minority of gallstones [6, 7]. No prior reports have studied whether the MR appearances of gallstones correlate with gallstone chemical composition. We undertook this in vitro study to investigate the MR appearances of gallstones at 1.5 T and to determine whether these MR gallstone signals correlate with gallstone chemical composition.

Materials and Methods

Gallbladder stones removed surgically from 63 consecutive patients were maintained in normal saline until undergoing MR imaging, MR spectroscopy, and chemical analysis. One gallstone from each patient was selected for imaging studies. In patients with multiple stones, the stone to be imaged was selected randomly. Gallstone size varied from 2 to 32 mm in maximal diameter.

Received March 30, 1989; accepted after revision May 15, 1989.

¹ Department of Radiology (SB-05), University of Washington School of Medicine and University Hospital, Seattle, WA 98195. Address reprint requests to R. L. Baron.

² Department of Medicine, University of Washington School of Medicine, Seattle, WA 98195.

0361-803X/89/1533-0497

© American Roentgen Ray Society

MR Imaging

Gallstones were placed in a normal saline suspension within individual chambers of a custom Plexiglas and water body phantom. Because the in vivo MR signal-intensity characteristics of bile are known to vary with hydration state and concentration of bile [8], normal saline was chosen as a suspension agent within the phantom to standardize the background MR signal intensity. MR images were obtained with a 1.5-T GE SIGNA scanner with T1-weighted, 600/25 (TR/TE), and T2-weighted, 2000/80, spin-echo sequences. A short-T1 inversion recovery (STIR) sequence, 2000/40/110 (TR/TE/TI), with the inversion time chosen to optimize fat-signal suppression, was used to investigate further the foci of increased signal intensity seen within gallstones from 14 patients. All sequences were performed in the body coil with two excitations, a 30-cm field of view, and a 256×128 matrix.

Gallstone images were analyzed for the presence, intensity, and area of visualized MR signal, as well as the organization of MR signals into imaging patterns.

Gallstone Signal Intensity

Gallstones were evaluated with T1- and T2-weighted sequences for foci of increased MR signal when compared with the dark MR signal void also seen in most gallstones [6, 7]. Also in order to compare signal intensities, the gallstone signal intensity was measured and compared with the intensity of the surrounding saline, resulting in a stone/saline signal-intensity ratio for each gallstone on both T1- and T2-weighted images. If the intensity of gallstone MR signal varied throughout a stone, it was measured at its most intense region (single pixel). A large circular region of interest excluding the gallstone was used to obtain an average signal intensity for the surrounding saline. For purposes of comparing our findings with those of prior studies [6, 7], stones were grouped by T1 signal-intensity ratios as follows (Fig. 1): dark (stone/saline signal-intensity ratio < 0.40), faint (stone/saline signal-intensity ratio $0.40-0.60$), moderate (stone/saline signal-intensity ratio $0.61-1.05$), and bright (stone/saline signal-intensity ratio > 1.05). These corresponded to visually apparent grouping of gallstone signal intensities.

Gallstone Signal Area

The area of the visibly increased gallstone signal on T1-weighted images was compared with the area of the entire stone. The relative area of higher intensity gallstone signal was estimated on the basis of the proportion of the diameter of visualized signal to the total stone

diameter (Fig. 2). Visualized signal with a diameter less than 25% of the stone diameter was classified as small. A medium-sized signal comprised 26–50% of stone diameter. Gallstones with a large signal were those comprising more than 50% of stone diameter, retaining, however, areas of signal void. When the increased signal occupied the entire stone without areas of signal void, the area of increased signal was considered total.

Gallstone MR Patterns

Gallstones were categorized into one of five patterns determined by their T1-weighted MR images (Fig. 3): dark (homogeneously dark stones with stone/saline ratio < 0.40), rimmed (visibly increased central signal intensity with a stone/saline ratio ≥ 0.40 and a surrounding rim of signal void), laminated (more complex variations of alternating layers of visible signal and signal void), homogeneously bright (homogeneously bright gallstone signal without regions of signal void), and homogeneously faint (homogeneously faint gallstone signal without a peripheral rim of signal void).

MR Spectroscopy

Proton MR spectroscopy was performed on 14 stones with a 2-T GE CSI imager/spectrometer. Stones were chosen to represent the spectrum of gallstone imaging appearances. Stones were dried with forced air for 60 sec and placed directly within a four-turn 2-cm solenoid coil to obtain spectra. T1 relaxation times were measured with this same system by using a standard inversion recovery sequence with eight or nine increments of time delay between the 180° and 90° RF pulses. T1 values were obtained by fitting peak heights with a three-parameter function by using a nonlinear least squares algorithm (provided as part of the GEMCSI software for the GE CSI imager/spectrometer).

Chemical Analysis

After imaging, 43 stones were selected as representative of the different MR patterns of signal distribution and of signal intensity; these stones underwent subsequent chemical analysis. Each gallstone was pulverized and desiccated to constant weight. Dried gallstone powder was then extracted with acidified methanol-chloroform mixture (1:1; v/v). The insoluble material (residue) was desiccated to dry weight and was not analyzed further. Cholesterol was measured by the method of Abell et al. [9]. Calcium was determined by atomic absorption spectrometry. Composition was expressed as milligrams per gram of dry initial weight.

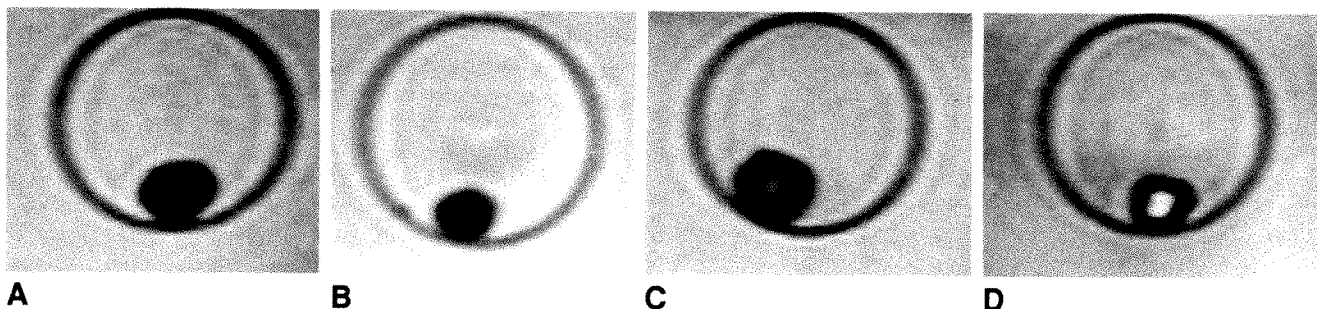


Fig. 1.—Spectrum of gallstone MR signal intensities seen on in vitro T1-weighted MR images.

A, Dark: The maximal ratio of gallstone/saline signal intensity is < 0.4 .

B, Faint: This gallstone shows a rimmed pattern with faint increased signal in center. Maximal stone/saline signal-intensity ratio is 0.46.

C, Moderate: This gallstone shows moderate central signal intensity. Maximal stone/saline signal-intensity ratio is 0.8.

D, Bright: This gallstone shows bright central signal intensity. Maximal stone/saline signal-intensity ratio is 1.6.

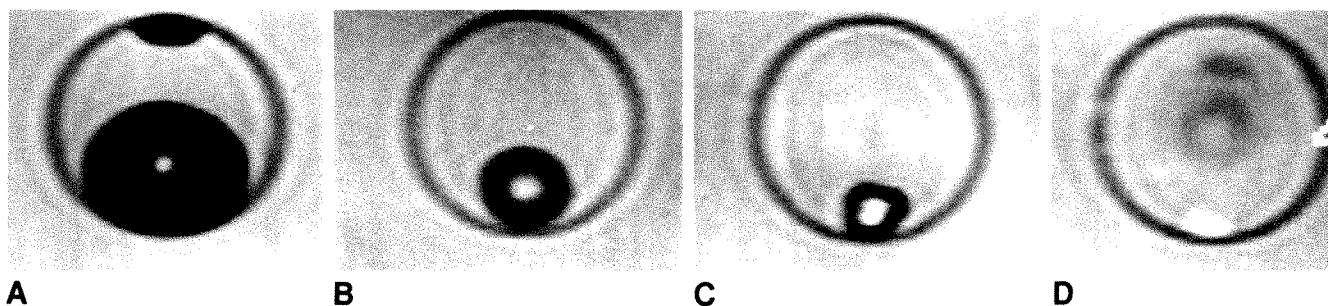


Fig. 2.—Size (area) of increased gallstone signal intensity on T1-weighted MR images was estimated by comparing diameter of area of visible increased MR signal with entire gallstone diameter. An area of increased signal <25% was considered small (A); areas of 25–50% were considered medium (B) and 51–99%, large (C). When area of increased MR signal occupied entire gallstone without areas of signal void, area was considered total (D).

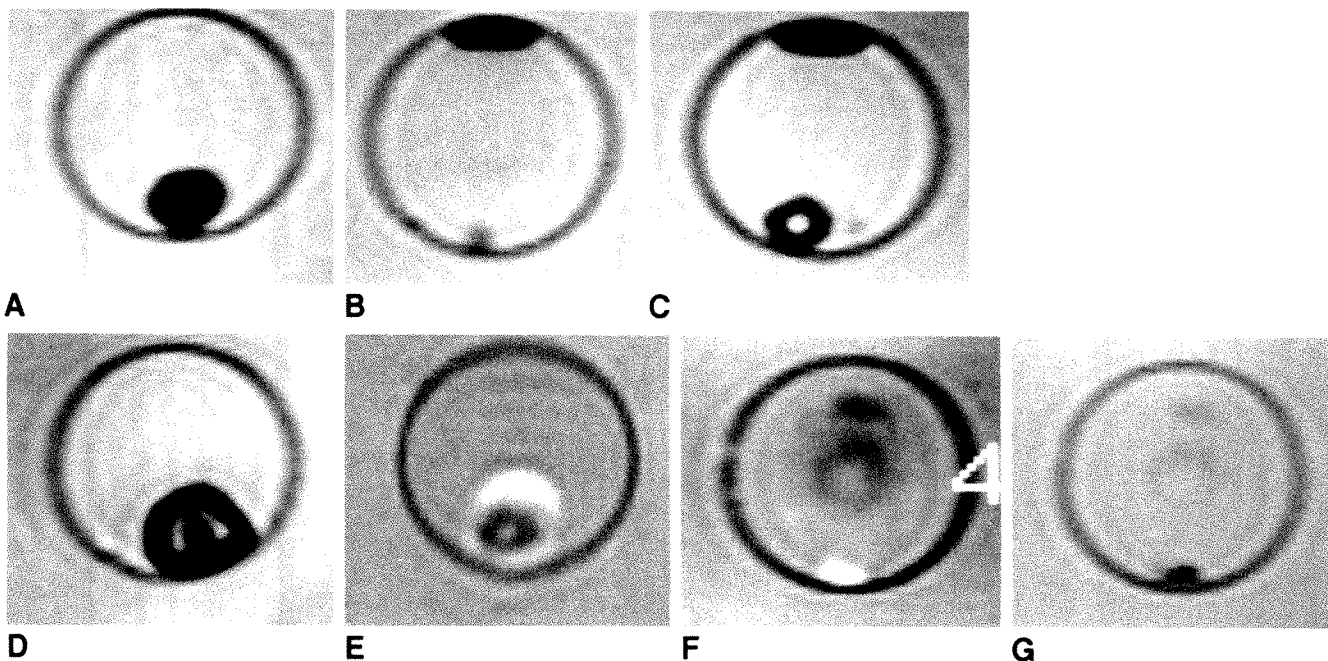


Fig. 3.—Gallstone patterns seen on in vitro T1-weighted MR images.

- A, Homogeneously dark: All areas of gallstone had a gallstone/saline signal-intensity ratio less than 0.4.
 B, Homogeneously faint: Homogeneously low signal intensity with maximal gallstone/saline signal-intensity ratio of 0.4–0.6.
 C, Rimmed: Gallstone has areas of visible increased signal intensity surrounded by a peripheral rim of signal void.
 D and E, Laminated: Gallstone shows more complex variations of alternating layers of increased and low signal intensities. Peripheral layer may be of increased signal intensity (E).
 F and G, Homogeneously bright gallstone without a rim of signal void is shown on T1-weighted image (F). T2-weighted image of this stone (G) showed no visible signal.

Statistical Analyses

All correlation coefficients mentioned in this study refer to the Pearson product-moment correlation coefficient.

Analysis of variance was used to test for statistically significant differences among gallstone groups for cholesterol, calcium, and T1 relaxation time.

Results

MR Gallstone Appearances

All gallstones could be visualized within the saline bath on both T1- and T2-weighted images. T1-weighted images revealed foci of increased signal intensities in 46 of 63 gallstones

(faint, 17; moderate, nine; bright, 20), and no signal (dark) in 17 of 63. T2-weighted images showed visible increased signal intensities in 18 of 63 gallstones (faint, 15; moderate, three). In all but one stone, the gallstone/saline signal-intensity ratio was greater on the T1- than on the T2-weighted images. The visualized MR signal patterns on T1-weighted images were dark (17), rimmed (32), laminated (nine), homogeneously bright (two), and homogeneously faint (three).

A STIR sequence was used to examine stones from 14 patients that had shown increased T1 signal intensity (faint, two; moderate, four; bright, eight). The STIR sequence suppressed the signal in 13 of 14 stones (Fig. 4). One stone with faint T1 signal showed similar faint signal intensity with the STIR sequence.

Correlation with Chemical Analysis

Poor correlation was found between cholesterol concentration within gallstones and the gallstone/saline signal-intensity ratio from T1-weighted ($r = .06$) or T2-weighted ($r = .22$) images (Fig. 5).

Poor correlation existed between calcium content within gallstones and gallstone/saline signal-intensity ratio from T1-weighted ($r = .10$) or T2-weighted ($r = .17$) images (Fig. 6).

A comparison of chemical composition among gallstones grouped by MR pattern is shown in Table 1. There were wide variations of chemical contents within each MR pattern. Analysis of variance showed no significant difference in cholesterol ($p = .70$) or calcium ($p = .76$) content among stones grouped by MR pattern.

A comparison of the MR signal area with chemical composition is shown in Table 2. Again, wide variations of chemical composition were seen within each group. Analysis of variance showed no significant difference in calcium ($p = .77$) or cholesterol ($p = .96$) content among stones grouped by MR signal area.

TABLE 1: Cholesterol and Calcium Content vs Gallstone MR Pattern

MR Pattern (No.)	Mean Cholesterol in mg/g (1 SD)	Mean Calcium in mg/g (1 SD)
Dark (15)	748 (271)	27 (51)
Rimmed (17)	735 (199)	18 (29)
Laminated (6)	858 (105)	6 (3)
Homogeneous bright (2)	825 (185)	5 (5)
Homogeneous faint (3)	659 (229)	13 (13)

Proton MR Spectroscopy and T1 Measurements

Fourteen stones were selected for proton MR spectroscopy. The MR gallstone patterns investigated included dark (seven), laminated (two), rimmed (four), and homogeneously bright (one). All fourteen stones undergoing spectroscopy showed only a single peak corresponding to a large water-proton signal (Fig. 7). No other peaks were identified on spectra of any of the stones tested.

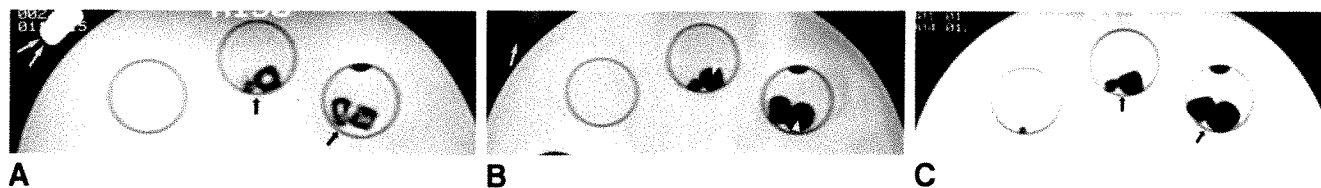


Fig. 4.—Effect of short-T1 inversion recovery (STIR) sequence on gallstone signal intensity.

A, T1-weighted sequence with several gallstones from each patient placed within individual chambers of the body phantom. Gallstones in two chambers (black arrows) show bright central signal intensity. Note that a lipid capsule (white arrows) applied externally to phantom shows bright signal intensity.

B, Same gallstones in phantom as in A. T2-weighted sequence shows central gallstone intensity (white arrowheads) to have decreased markedly to a faint level. Signal intensity in lipid capsule (white arrows) also has decreased markedly.

C, Same gallstones in phantom as in A and B. STIR sequence shows absence of visible signal within gallstones (arrows), as well as from lipid capsule (located under the identifying series data in the same location as in A), indicating optimal fat suppression.

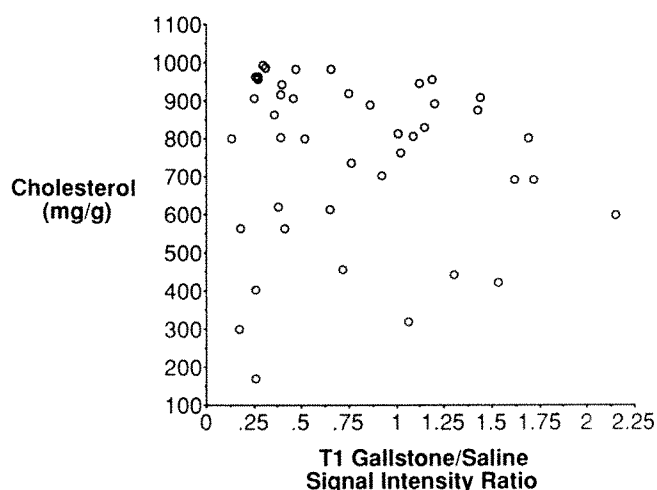


Fig. 5.—Graph shows poor correlation between cholesterol content and gallstone/saline signal-intensity ratio on T1-weighted MR images.

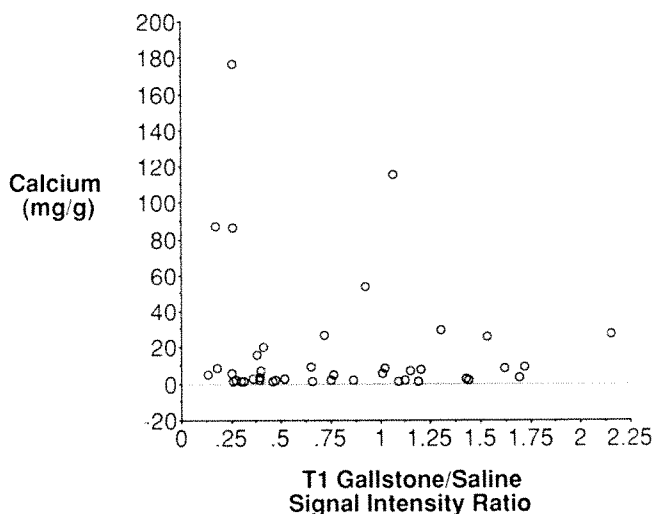


Fig. 6.—Graph shows poor correlation between calcium content and gallstone/saline signal-intensity ratio on T1-weighted MR images.

TABLE 2: Correlation of MR Signal Area with Gallstone Chemical Composition

Gallstone Signal Area (No.)	Mean Cholesterol Content in mg/g (1 SD)	Mean Calcium Content in mg/g (1 SD)
Dark (5)	748 (271)	27 (51)
Small (2)	683 (171)	12 (12)
Medium (13)	760 (198)	20 (33)
Large (9)	800 (182)	8 (8)
Total (35)	725 (207)	10 (11)

Measurements of the T1 relaxation times of the water peak from the 14 stones on the GE CSI spectrometer ranged from 0.006 to 0.98 sec (mean = 0.27 sec), with a saline control measuring 2.8 sec. Table 3 shows the mean T1 relaxation times for each signal-intensity group of the 14 stones tested. Of stones with any increased signal seen on T1-weighted images, there was a decrease in the mean T1 relaxation time with increasing T1 signal intensity. However, three homogeneous dark stones had the shortest T1 relaxation times (0.006–0.019 sec), with the T1 values of the other four dark stones averaging 0.411 sec (0.11–0.92 sec). Gallstone T1 relaxation time measurements correlated poorly with either cholesterol ($r = .3$) or calcium ($r = .4$) content.

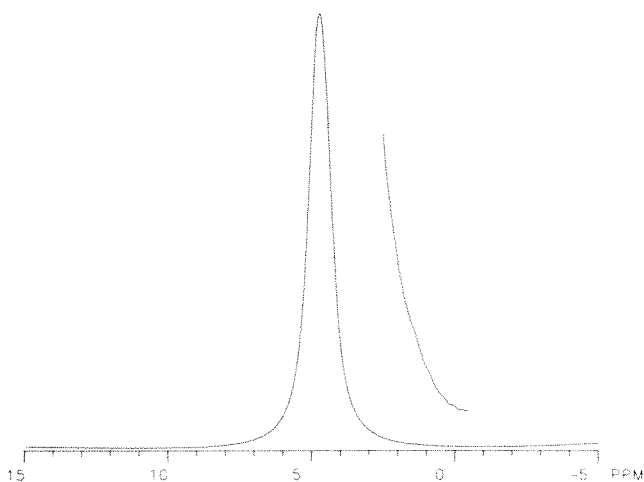


Fig. 7.—Typical proton MR spectrum of gallstone showing a single, broad water peak at 4.7 ppm. Region of expected lipid signal (0–2.5 ppm) is magnified 32 times and shows lack of any lipid signal.

TABLE 3: Gallstone T1 Relaxation Time Values

Gallstone Intensity (No.)	Mean T1 Relaxation Time in sec (1 SD)
Dark (7)	0.230 (0.34)
Faint (1)	0.980
Moderate (2)	0.255 (0.13)
Bright (4)	0.153 (0.07)

Discussion

There have been few reports of MR imaging characteristics of gallstones. In an in vitro study at 0.35 T, Moon et al. [6] reported that most gallstones were visualized as a signal void, and only 17% of stones showed faint increased signal seen centrally within gallstones. More recently, Moriyasu et al. [7], also using low-field-strength MR (0.2 T), reported in vivo strong central signal intensity in six of 34 gallstones and concluded that these signals were due to water-filled cavities within mixed-type gallstones with high cholesterol content. Neither study, however, correlated gallstone MR signal intensity or pattern with chemical composition.

Unlike these prior MR studies, we found gallstones to exhibit a variety of MR imaging patterns. The present study also showed a visibly increased gallstone signal on T1-weighted images in 73% of gallstones, compared with 17–18% reported by other investigators [6, 7]. Several factors may explain this difference. Both prior studies used low-field-strength MR imaging rather than the high-field 1.5 T used in the current study. In addition, Moriyasu et al. [7] noted that visualized central signals in gallstones were more intense in vitro than in vivo. Still, the investigations by Moon et al. [6], also performed in vitro, found only 17% of stones to have faint central signals. Gallstones in the study by Moon et al. also had been desiccated and then rehydrated before their investigations, which could affect the MR appearances. Different populations of patients with underlying physiologic differences also may affect stone structure, composition, and MR appearance. Thus, the factors that influence the MR appearances of gallstones are varied and complex, and comparison of different study populations may be difficult.

We also found differences in the location of the visualized MR signals within gallstones compared with gallstones described in prior studies. Although most gallstone MR signals in our study were central in location and surrounded by a rim of signal void, other less common locations were seen. Five stones showed a homogeneous increase in signal intensity on T1 images (faint, three; bright, two), and three laminated stones had peripheral rims of increased T1 signal (Fig. 3). These MR appearances are not consistent with the hypothesis of Moriyasu et al. [7] that gallstone MR signals result from water accumulating within a central cavity of gallstones.

The predominant MR imaging characteristics of gallstones at 1.5 T (brightest on T1-weighted images, less bright or dark on T2-weighted images, and suppressed on STIR sequence images) reflect shortening of T1 and T2 relaxation times and simulate the imaging characteristics of fat or lipids. However, our spectroscopy data showed only a water signal and no significant lipid signal. This apparent conflict between the imaging and spectroscopic characteristics is explained by the gallstone T1 relaxation times measured with the spectrometer.

Signal intensity in spin-echo MR images is a function of both T1 and T2. For T1-weighted images, signal intensity should increase in structures with shorter T1 relaxation times, as long as T2 values do not get significantly smaller than TE. However, T2 is always equal to or less than T1, and as T1

becomes significantly less than TE, so do the T2 values, decreasing signal intensity because the MR signal decays as a result of T2 relaxation before the spin echo is formed.

The water protons in gallstones were found to have shortened T1 relaxation times (mean, 0.27 sec) compared with water in saline (2.8 sec). T1 relaxation times of water protons are decreased when bonding to relatively immobile nucleotides or proteins. As explained above, the shorter T1 relaxation times would be expected to produce increased signal intensity with T1-weighted images, compared with free water. These findings are similar to those previously described in bile [8], where a shortened T1 relaxation time of water protons in concentrated bile was found to account for the bright T1 signal intensity of bile. However, when the T1 of water in gallstones becomes very short (<20 msec), so does T2, and signal intensity should decrease in these instances so that no signal is recorded even at short echo times. This was confirmed in our studies by the three stones with extremely short T1 values (<20 msec), which all imaged as a signal void. However, four stones with longer T1 values were relatively dark. Our hypothesis is that this is caused by very short T2 relaxation times due to some structural or chemical property of the stone. Further investigations with T2 measurements and high-resolution spectroscopy of gallstones may clarify these issues.

Thus, although cholesterol forms a large fraction of total stone weight in many stones, it plays a relatively small role in determining MR imaging characteristics of the stones. Rather, these imaging characteristics are dominated by the effects of water in the gallstone's internal environment, which does not appear to relate to absolute chemical composition. We found no statistically significant differences in cholesterol, calcium, or T1 relaxation time among the various groupings of gallstones by MR appearance.

In summary, we found that most gallstones showed increased MR signal in vitro at 1.5 T. Whether these in vitro

findings are similar to in vivo MR appearances of gallstones must be determined. The in vitro gallstone MR imaging characteristics (signal intensity, imaging patterns, and area of the visualized signals) did not correlate with chemical composition. We hypothesize that different structural relationships must exist within gallstones of similar chemical content, altering the water bonding and hence the MR imaging characteristics. Why some gallstones have MR signals of different intensity and size and why others have persistently high signal on T2-weighted images remains unknown and awaits further investigation. Although different MR imaging patterns do not correlate well with chemical composition, they may reflect other underlying chemical or structural differences.

REFERENCES

1. Carroll BA. Gallstones: in vitro comparison of physical, radiographic, and ultrasonic characteristics. *AJR* **1978**;131:223-226
2. Filly RA, Moss AA, Way LW. In vitro investigation of gallstone shadowing with ultrasound tomography. *JCU* **1979**;7:255-262
3. Hickman MS, Schwesinger WH, Bova JD, Kurtin WE. Computed tomographic analysis of gallstones. *Arch Surg* **1986**;121:289-291
4. Baron RL, Rohrmann CA, Lee SP, Shuman WP, Teefey SA. Computed tomographic evaluation of gallstones in vitro: correlation with chemical analysis. *AJR* **1988**;151:1123-1128
5. Baron RL, Kuyper S, Lee SP, Rohrmann CA, Shuman WP, Nelson JA. Chemical dissolution of gallstones in vitro: correlation with CT/MR imaging characteristics. *Radiology* (in press)
6. Moon KL Jr, Hricak H, Margulis AR, et al. Nuclear magnetic resonance imaging characteristics of gallstones in vitro. *Radiology* **1983**;148:753-756
7. Moriyasu F, Ban N, Nishida O, et al. Central signals of gallstones in magnetic resonance imaging. *Am J Gastroenterol* **1987**;82:139-142
8. Demas BE, Hricak H, Moseley M, et al. Gallbladder bile: an experimental study in dogs using MR imaging and proton spectroscopy. *Radiology* **1985**;157:453-455
9. Abell LL, Levy BB, Brodie BB, Kendall FE. A simplified method for estimation of total cholesterol in serum and demonstration of its specificity. *J Biol Chem* **1952**;195:357-366

Routine Sonographic Techniques Fail to Quantify Gallstone Size and Number: A Retrospective Study of 111 Surgically Proved Cases

James A. Brink¹
 Joseph F. Simeone
 Peter R. Mueller
 Sanjay Saini
 Glenn A. Tung
 Nathan O. Spell
 Joseph T. Ferrucci

We analyzed sonographic images retrospectively to determine their value in quantifying gallstone size and number in 111 surgically proved stone-containing gallbladders for which routine preoperative sonograms were available. The number and size of stones found on pathologic examination were correlated with the results of image analysis. In patients with more than one stone, observable size differences were recorded if the smallest stone diameter was less than 50% of the largest stone diameter. Estimates of gallstone size and number from preoperative sonograms were correct in only 23 (21%) of 111 cases. Stone size and number were overestimated as often as they were underestimated. Stones of a uniform size were recognized correctly in 59 (92%) of 64 cases. Stones of two different sizes were correctly identified in only 14 (30%) of 47 cases; the second, smaller stones were missed in 26 (79%) of 33 cases.

These findings indicate poor sonographic characterization of gallbladder contents when imaging studies are performed solely to determine the presence or absence of gallstones.

AJR 153:503-506, September 1989

Traditionally, the principal diagnostic issue in patients with suspected cholelithiasis has been limited to the presence or absence of gallstones. The decision to use the only form of therapy available, cholecystectomy, was based on the presence or lack of gallstones rather than on their number or size. However, with new nonsurgical forms of gallstone therapy (extracorporeal shock-wave lithotripsy [ESWL], bile salt dissolution with oral ursodeoxycholic acid [Actigal, Ciba-Geigy, Summit, NJ], and direct contact solvent dissolution with methyl *tert*-butyl ether [MTBE]), quantitative assessment of gallstone size and number has assumed increased diagnostic significance.

Gallstone size and number have a direct impact on eligibility and expected success with ESWL [1] and oral bile acid therapy [2]. For example, the current Food and Drug Administration (FDA) protocol for United States trials of the Dornier gallbladder lithotripter excludes patients with more than three stones and patients with stones of less than 0.5 cm or greater than 3.0 cm diameter [3]. The FDA/Ciba-Geigy protocol for the United States trials of oral bile acid therapy with ursodeoxycholic acid (recently approved by the FDA) excludes patients if the size of the largest gallstone exceeds 2.0 cm. At present, there is no practical limit on the number of stones when therapy is with oral bile acids [4]. Ultimately, the success of all nonsurgical therapies is determined by the number and size of the gallstones or their fragment residua.

Sonography is important in evaluation of cholelithiasis both before and after therapy. However, the accuracy with which routine gallbladder sonography can be used to determine gallstone size and number has not been investigated. In an earlier study [3], we examined the number, size, and degree of calcification of gallstones in 100 patients undergoing cholecystectomy to predict the number of surgical patients who would have been eligible for ESWL. In this study, we

Received February 6, 1989; accepted after revision May 1, 1989.

Presented at the 18th annual meeting of the Society of Gastrointestinal Radiologists, Palm Desert, CA, February 1989.

¹All authors: Department of Radiology, White 2, Massachusetts General Hospital, Boston, MA 02114. Address reprint requests to J. T. Ferrucci.

0361-803X/89/1533-0503
 © American Roentgen Ray Society

retrospectively analyze routine preoperative gallbladder sonograms in 111 surgically proved stone-containing gallbladders to assess the accuracy of conventional sonographic techniques for use in quantifying gallstone size and number.

Materials and Methods

The gallbladder contents in 200 consecutive patients undergoing cholecystectomy between June 1987 and April 1988 were collected for analysis. Routine preoperative sonograms obtained within 4 weeks before surgery were available in 111 patients.

Each case was analyzed by counting stones individually when they numbered fewer than five; when more than five, they were counted collectively as 5–10 or as more than 10.

An estimate of gallstone size was made for each patient according to the following categories: ≤ 0.5 cm, >0.5 – 1.0 cm, >1.0 – 1.5 cm, >1.5 – 2.0 cm, >2.0 – 3.0 cm, and >3.0 cm. In oval stones or stones that were irregular in shape, the largest diameter was recorded.

In patients who had more than one stone, observable size differences were recorded if the diameter of the smallest stone was less than 50% of the diameter of the largest stone. The major stone family included stones with diameters that were within 70% of that of the largest stone; the minor stone family included the rest of the smaller stones. The two stone families were counted separately.

Sonograms were obtained routinely by technologists with staff or fellows and residents in attendance. Real-time 3.5- or 5.0-MHz sector scans were obtained by using either G.E. 3600 or Radius scanners

(General Electric Medical Systems, Milwaukee, WI). Patients' gallbladders were imaged routinely in the supine and left posterior oblique positions. Upright and magnification views were not used routinely. Hard-copy films from the sonograms were reviewed by an experienced abdominal radiologist. The sonograms were categorized as showing one or two stone-size families within the gallbladder, and the number and size of the gallstones were recorded.

Results

Analysis of the preoperative sonograms revealed that gallstone size and number were displayed correctly in 23 (21%) of 111 cases (Table 1).

Of 64 patients with stones of a single size, sonography was used correctly to identify one stone-size family in 59 (92%) cases. However, the correct size and number of gallstones were identified in 22 (34%) of 64 cases. Stone size was overestimated in 15 (36%) of 42 cases and underestimated in 16 (38%) of 42 cases. Of 14 cases with small stones of uniform size (<0.5 cm), stone size was overestimated in six (75%) of eight missed cases. Of 16 cases with large stones of uniform size (>2.0 cm), stone size was underestimated in seven (88%) of eight missed cases. Stone number was overestimated in nine (21%) of 42 missed cases, and underestimated in 12 (29%) of 42 missed cases. In two (5%) of 42 missed cases, the patients' gallstones were not visible on the preoperative sonogram.

Two stone-size families were identified correctly in only 14 (30%) of 47 cases. The smaller stone family was missed in 26 (79%) of 33 missed cases, and the larger stone family was missed in six (18%) of 33 missed cases. In patients with two stone families, the gallstone size and number for each stone family were defined correctly in only one (2%) of 47 cases. Figure 1 is a preoperative sonogram that correctly shows two stones of dissimilar size in the gallbladder.

In two (2%) of 111 cases, a curvilinear echogenic focus with shadowing was seen in the gallbladder fossa without visualization of the gallbladder lumen. Although cholelithiasis was diagnosed correctly, gallstone size and number could

TABLE 1: Retrospective Sonographic Accuracy of Gallstone Size and Number As Estimated from Routine Preoperative Sonograms in 111 Cholecystectomy Patients

Stone Category	Sonographic Accuracy
Single stone family ($n = 64$)	
One family identified correctly	92 (59/64)
Size and number correct	34 (22/64)
Two stone families ($n = 47$)	
Two families identified correctly	30 (14/47)
Size and number correct	2 (1/47)
Total stone size and number correct ($n = 111$)	21 (23/111)



Fig. 1.—Preoperative sonogram correctly shows two stones of dissimilar size within gallbladder.

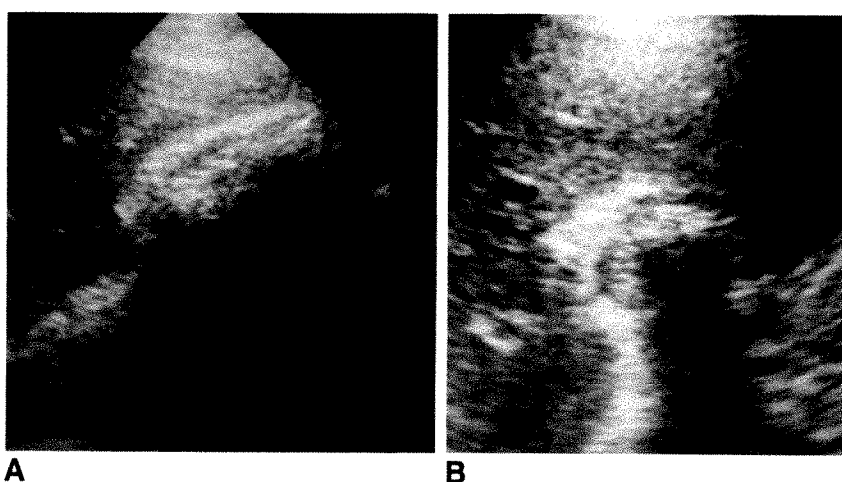
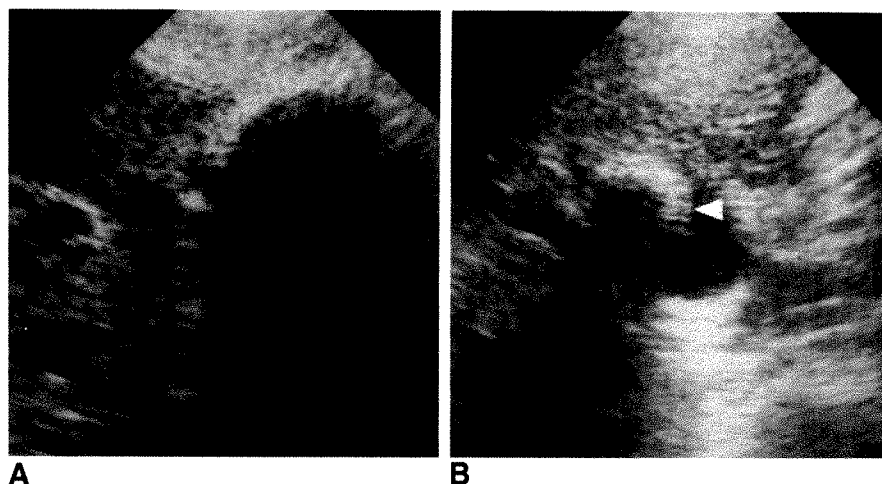


Fig. 2.—A and B, Preoperative sagittal (A) and transverse (B) sonograms show a shadowing, curvilinear echo within gallbladder fossa without visualization of gallbladder lumen. Although gallbladder is filled with innumerable small calculi, their number and size cannot be discerned.

Fig. 3.—A, Sagittal sonogram shows a shadowing, curvilinear echo within gallbladder fossa without visualization of gallbladder lumen.

B, Transverse sonogram correctly shows a thin rim of bile around margin of a single large gallstone (arrowhead).



not be assessed. Figure 2 shows such a patient with multiple stones in whom a diffuse echo in the gallbladder fossa precluded assessment of gallstone size and number. Another patient had a similar finding on sagittal views of the gallbladder (Fig. 3A). The transverse image, however, correctly revealed a thin rim of bile around the margin of a single large calculus (Fig. 3B).

Discussion

To date, refinements in the sonographic assessment of cholelithiasis have been limited to improved detection of gallstones. Cholelithiasis can be diagnosed confidently in patients whose gallbladders contain echogenic structures that are associated with posterior acoustic shadowing. Crade et al. [5] found that such type I cholecystosonograms were virtually 100% diagnostic of gallstones. Acoustic shadowing depends on the size of the stone, the angle between the stone surface and the incident beam, the proximity of the stone to the beam focus, and the ultrasonic frequency used [6–8]. However, it is independent of composition, calcium content, shape, surface characteristics, and specific gravity of the stone [9–11].

As not all stone-containing gallbladders display such classic findings, Crade and coworkers [5] defined two additional sonographic patterns. The type II pattern included sonographic nonvisualization of the gallbladder, or visualization of only an echogenic focus with shadowing in the region of the gallbladder fossa. The type III pattern consisted of small nonshadowing echogenic foci in the gallbladder. Although less specific than the type I pattern, cholelithiasis can be diagnosed correctly in 88–98% of sonograms with the type II pattern [5, 12, 13] and in 60–80% of sonograms with the type III pattern [5, 14].

With the recent emergence of alternative, nonsurgical modes of gallstone therapy, the diagnosis of cholelithiasis is no longer the primary issue of gallstone presence. The size, number, and composition of the stones are now critical to eligibility of the patient and expected success with ESWL, oral bile acid therapy, and percutaneous contact dissolution techniques.

Our retrospective study indicates poor sonographic characterization of gallbladder contents when imaging studies are performed solely to determine the presence or absence of gallstones. Analysis of preoperative sonograms revealed the correct size and number of stones in only 21% of cases. Among gallbladders with single stone families, the accuracy was only 34%; stone size and number were underestimated as often as they were overestimated. However, multiple smaller stones (<0.5 cm) were overestimated in size in 75% of missed cases because often they were imaged in aggregate and not separated from each other. Larger stones (>2.0 cm) were underestimated in size in 88% of missed cases. We have found that stones larger than 1.5 cm in maximal diameter tend to be ellipsoid. As such, these larger stones may have been underestimated in size because of the acoustic reflection and absorption of the ultrasound beam obscuring the deep and polar surfaces of the stone [4].

We previously reported the importance of two stone sizes within the gallbladder with respect to ESWL [3]. In that study, 44% of our patients had second, smaller stones within the gallbladder that reduced by 30% the number of patients eligible for ESWL on the basis of stone size. Although review of the preoperative sonograms in this study correctly revealed a single stone family in 92% of cases, two stone families were identified correctly in only 30% of cases. The smaller stone family was missed with much greater frequency (79%) than the larger stone family (18%). As most stones (55%) in the smaller stone families measure less than 0.5 cm in diameter, they are more likely to show a type III sonographic pattern: nonshadowing echogenic foci within the gallbladder, usually less than 5 mm in size, which may or may not move [14]. As such, they suffer from the same 20–40% reduction in detection accuracy on in vivo sonography as stones with a type III pattern [5, 14].

Although the accuracy of gallstone detection is only slightly reduced in the type II cholecystosonographic pattern [5, 12, 13], such findings pose a greater problem in the emerging era of nonsurgical therapies. Visualization of an echogenic focus in the gallbladder fossa without visualization of the gallbladder lumen (Fig. 2) may permit the diagnosis of cholelithiasis;

however, the number and size of the gallstones remain unknown. A thin rim of bile outlining even a small portion of the stone mass (Fig. 3), however, may permit discrimination of a single large gallstone from multiple smaller stones seen in aggregate.

Quantification of gallstone size and number may be improved when special technical maneuvers for cholecystosonography are used. Simeone et al. [4] have advocated the use of magnified high-frequency sonograms for stone measurement in the axial (anteroposterior) rather than lateral dimension. In addition, patients must be positioned optimally to separate multiple stones. Although sonography can be used to detect gallstones with 28% greater sensitivity than is possible with oral cholecystography [15], it is less accurate for counting stones when more than three to five stones are present in a gallbladder [4]. This is an inherent limitation of the sectional tomographic nature of B-mode sonography as opposed to the projection imaging used in conventional radiographic cholecystography. Thus, in patients with multiple gallstones, direct correlation of sonographic with oral cholecystographic findings will be necessary to determine best the number and size of gallstones.

REFERENCES

1. Sackmann M, Delius M, Sauerbruch T, et al. Shock-wave lithotripsy of gallbladder stones: the first 175 patients. *N Engl J Med* **1988**;318:393-397
2. Tint GS, Salen G, Colalillo A, et al. Ursodeoxycholic acid: a safe and effective agent for dissolving cholesterol gallstones. *Ann Intern Med* **1982**;97:351-356
3. Brink JA, Simeone JF, Mueller PR, Richter JM, Prien EL, Ferrucci JT. Physical characteristics of gallstones removed at cholecystectomy: implications for extracorporeal shock-wave lithotripsy. *AJR* **1988**;151:927-931
4. Simeone JF, Mueller PR, Ferrucci JT. Nonsurgical therapy of gallstones: implications for imaging. *AJR* **1989**;152:11-17
5. Crade M, Taylor KJW, Rosenfield AT, deGraaff CS, Miniham P. Surgical and pathologic correlation of cholecystosonography and cholecystography. *AJR* **1978**;131:227-229
6. Colhoun EN, Fitzgerald EJ, McKnight L. The importance of appropriate frequency selection in sonographic gallstone detection. *Br J Radiol* **1987**;60:645-648
7. Grossman M. Cholelithiasis and acoustic shadowing. *JCU* **1978**;6:182-184
8. Sommer FG, Taylor KJW. Differentiation of acoustic shadowing due to calculi and gas collections. *Radiology* **1980**;135:399-403
9. Good LI, Edell SL, Soloway RD, Trotman BW, Mulhern C, Arger PA. Ultrasonic properties of gallstones: effect of stone size and composition. *Gastroenterology* **1979**;77:258-263
10. Carroll BA. Gallstones: in vitro comparison of physical, radiographic, and ultrasonic characteristics. *AJR* **1978**;131:223-226
11. Filly RA, Moss AA, Way W. In vitro investigation of gallstone shadowing with ultrasound tomography. *JCU* **1979**;7:255-262
12. Harbin WP, Ferrucci JT, Wittenberg J, Kirkpatrick RH. Nonvisualized gallbladder by cholecystosonography. *AJR* **1979**;132:727-728
13. Conrad MR, Leonard J, Landay MJ. Left lateral decubitus sonography of gallstones in the contracted gallbladder. *AJR* **1980**;134:141-144
14. Simeone JF, Mueller PR, Ferrucci JT, Harbin WP, Wittenberg J. Significance of nonshadowing focal opacities at cholecystosonography. *Radiology* **1980**;137:181-185
15. Gelfand DW, Wolfman NT, Ott DJ, Watson NE, Chen YM, Dale WJ. Oral cholecystography vs gallbladder sonography: a prospective blinded reappraisal. *AJR* **1988**;151:69-72

Biliary Cystadenoma and Cystadenocarcinoma: CT and Sonographic Findings

Melvyn Korobkin¹
 David H. Stephens²
 Joseph K. T. Lee³
 Robert J. Stanley⁴
 Elliot K. Fishman⁵
 Isaac R. Francis⁶
 Michael B. Alpern⁶
 Mark Rynties¹

Biliary cystadenomas and cystadenocarcinomas are rare cystic neoplasms, usually intrahepatic in location, that are characterized pathologically by a multilocular appearance. We report the CT and sonographic findings in eight cases of biliary cystadenoma and three cases of biliary cystadenocarcinoma and correlate them with the surgical and pathologic findings. CT showed internal septa in eight of the 10 multiloculated lesions, whereas sonography showed septa in all five cases in which it was used. CT in two of the three cystadenocarcinomas showed thick and coarse mural and septal calcifications as well as large solid soft-tissue masses in one. CT showed mural soft-tissue nodules in the single case of a unilocular cystadenocarcinoma.

Sonography and CT usually show the multilocular nature of biliary cystadenomas and cystadenocarcinomas. The presence of mural or septal nodules, discrete soft-tissue masses, and possibly thick and coarse calcifications increase the likelihood of a cystadenocarcinoma.

AJR 153:507-511, September 1989

Biliary cystadenoma is a rare cystic neoplasm occurring primarily in middle-aged women. Although usually benign, it tends to recur after subtotal excision and can develop into a malignant cystadenocarcinoma [1, 2].

The most striking feature of the gross pathologic specimen of a biliary cystadenoma or cystadenocarcinoma is its multiloculated appearance. Even in the exceptional tumor where the lesion appears to be primarily unilocular, gross or microscopic loculi can be identified in the cyst wall [2].

Scattered case reports and small series describing the CT and sonographic appearances of these lesions suggest that they have a characteristic appearance [3-9]. Most reports describe a septated, multiloculated cystic mass with varying degrees of mural and septal thickening and nodularity. We report eight patients with biliary cystadenomas and three patients with biliary cystadenocarcinomas in whom the appearance of the tumors on CT and sonography was correlated with the surgical and pathologic features.

Materials and Methods

Eleven patients with a surgically proved diagnosis of biliary cystadenoma or cystadenocarcinoma who had undergone CT and/or sonography were included in a retrospective study. The cases were collected from several different medical centers. No attempt was made to include all of the patients with these lesions seen at these institutions.

There were 10 women and one man, with a mean age of 55 years (range, 26-76 years old). Abdominal pain and/or distension was the major clinical symptom. Duration of symptoms ranged from 2 weeks to 5 years. In two patients a liver "cyst" had been partially excised 5 and 30 years earlier, respectively. In three additional patients there had been multiple episodes of percutaneous aspiration of upper abdominal or liver "cysts" over a period ranging from 4 months to 5 years.

Received February 21, 1989; accepted after revision April 28, 1989.

¹ Department of Diagnostic Imaging/Radiology, Sinai Hospital of Detroit, 6767 W. Outer Dr., Detroit, MI 48235. Address reprint requests to M. Korobkin.

² Department of Radiology, Mayo Clinic, Rochester, MN 55905.

³ Mallinckrodt Institute of Radiology, Washington University, St. Louis, MO 63110.

⁴ Department of Radiology, University of Alabama at Birmingham, Birmingham, AL 35233.

⁵ Department of Radiology and Radiologic Sciences, The Johns Hopkins Medical Institutions, Baltimore, MD 21205.

⁶ Department of Radiology, University of Michigan Medical Center, Ann Arbor, MI 48109.

0361-803X/89/1533-0507
 © American Roentgen Ray Society

CT and sonography were performed on a wide variety of instruments. CT units with scanning times of 5 sec or less were used. Four patients had both CT and sonography, six patients had only CT, and one patient had only sonography. Of the 10 patients who had CT, five studies were performed only with IV contrast enhancement, two only without IV contrast enhancement, and three both before and after contrast enhancement. A variety of methods was used to inject the IV contrast agents.

At surgery a large cystic mass was found in or contiguous with the liver in each case. The cyst was totally excised in four cases and partially excised in two others. Hepatic lobectomy or segmentectomy was performed in the remaining five patients. One of the patients undergoing hepatic lobectomy had had a partial resection several weeks earlier. Mucinous fluid was present in all or some portions of the lesion in most patients. A final histologic diagnosis of biliary cystadenoma was made in eight patients and a diagnosis of biliary cystadenocarcinoma in three patients.

A pathologic diagnosis of biliary cystadenoma was made when the cyst wall and septa were lined primarily by tall columnar epithelium similar to the lining of normal bile ducts. Three cases were diagnosed as papillary cystadenocarcinoma: in all three there was evidence of malignant papillary epithelium coexisting with other regions of benign columnar epithelium. The malignant portion typically consisted of hyperchromatic columnar cells with prominent nucleoli and frequent mitoses, forming disordered papillary projections and pleomorphic glands. The thick and coarse calcifications shown on CT in the two cystadenocarcinomas were confirmed on histologic examination. Cal-

cification was not mentioned in the patient with a benign cystadenoma in whom CT showed a single focus of thin calcification.

The medical records and imaging studies of the 11 patients were reviewed. From the medical charts of each patient we reviewed the discharge summaries, surgical reports, pathologic reports, and reports of all CT scans and sonograms. One of the authors reviewed the CT scans and sonograms of each patient and compared the retrospective interpretation with the initial report; no major discrepancies were apparent. The CT and sonographic findings were then compared with the clinical, surgical, and pathologic data.

Results

CT scans and sonograms showed a large cystic liver mass in 10 patients; an upper abdominal cyst in or adjacent to the liver was noted in the other patient. The size of the mass ranged from 5 to 27 cm in greatest diameter. No masses were localized to the bile ducts. In 10 of the 11 patients the imaging studies indicated a lesion more complex than a simple cyst: one or more septa were shown in nine patients and mural nodules were shown in the other. In the four patients who had both CT and sonograms the findings agreed in three and disagreed in one: septa shown on both examinations were confirmed in three patients, whereas in the other patient septa shown by sonography were not visualized on CT and

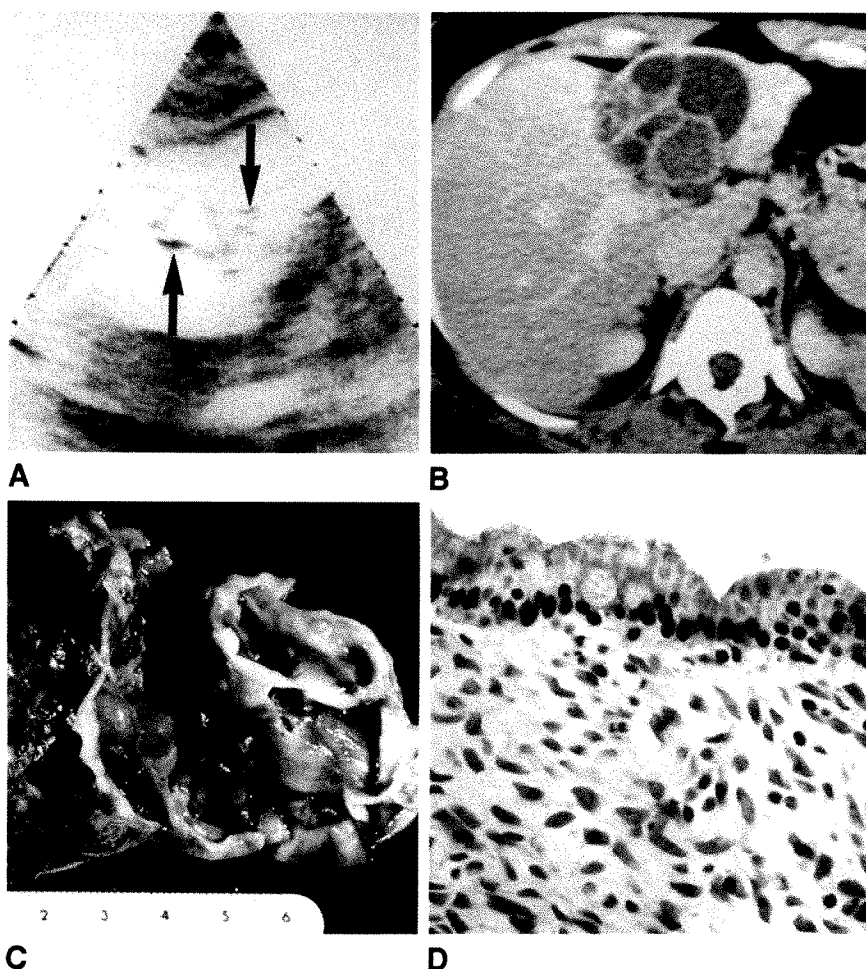


Fig. 1.—Biliary cystadenoma.

A, Sonogram shows cystic mass with thin echogenic septa (arrows).

B, CT scan shows multiloculated cyst in medial segment of left lobe. Note density of some loculations is higher than others.

C, Multiple septa and loculations are seen in unroofed half (right side) of gross pathologic specimen.

D, Microscopic section of typical septum shows benign tall columnar epithelium (top) overlying cellular stroma (H and E, $\times 500$).

were denied on the pathology report. The gross morphologic features of the complicated cysts were described in the CT and sonographic reports, but a histologic diagnosis usually was not offered. Specifically, the possibility of biliary cystadenoma or cystadenocarcinoma was mentioned only in a minority of the cases.

A final pathologic diagnosis of biliary cystadenoma was made in eight patients. In seven of these CT and/or sonography showed a septated multilocular cyst without gross nodules or soft-tissue masses (Figs. 1 and 2). A single focus of thin subtle calcification was seen in one of these seven cases. In the eighth patient, a discrete nodular echogenic structure associated with the internal septa was seen (Fig. 3). In three patients, all studied with CT only, the final pathologic diagnosis was biliary cystadenocarcinoma. In one, prominent soft-tissue mural nodules lined a unilocular cyst (Fig. 4). Thick, coarse mural and septal calcifications were seen in both multilocular cystadenocarcinomas, one of which also showed large soft-tissue masses within the cyst (Figs. 5 and 6).

Discussion

In order to analyze a series of patients with cystic biliary neoplasms we collected cases from several institutions using different CT and sonographic scanners and nonstandardized techniques. Although this is an unselected group representing all known patients from our institutions with a proven diagnosis of biliary cystadenoma or cystadenocarcinoma who underwent CT scans and/or sonography, this report is limited by its retrospective assessment of imaging features of a specific entity. In addition, the radiologic-pathologic correlation is based only on the surgical and pathologic reports, rather than the better approach in which the imaging studies are compared directly with the surgical and gross and micro-

scopic findings. This latter limitation may partially explain the few discrepancies between imaging and pathologic findings of internal septa.

Our series confirms that CT and sonography accurately demonstrate the internal morphologic features characteristic of cystic biliary neoplasms. Unequivocal septa and multilocularity within the cyst were shown in nine patients and confirmed by surgical and gross pathologic observations in seven of these. Of the other two patients, the cyst aspiration performed at surgery in one could have disrupted internal septa; in the other there was no specific comment about either the presence or absence of septa in the surgical and pathologic reports. Although not confirmed on this retrospective review, we believe it is likely that the highly characteristic appearance of septa on sonography in one case and on CT in the other correctly mirrored the internal morphology.

In one case imaged with CT but not sonography, multiple septa described in the surgical report were not visible on the CT scans. Overall we interpret the results of our study to indicate that CT failed to show definite or probable septa in two of 10 cases, whereas sonography correctly showed internal septa in all five cases in which it was used. As suggested in other reports, we believe that sonography is somewhat more sensitive than CT in the detection of septa in a cystic lesion [10].

Several previous reports of sonographic findings in benign cystadenoma have included a description of mural nodules and papillary projections in addition to the usual presence of septa within a liver cyst [4, 5]. It is difficult to explain what these sonographic nodules or projections represent: most authorities state that solid nodular projections, although common in biliary cystadenocarcinoma, are rare in cystadenoma [1, 2]. Even microscopically, papillary proliferation of benign epithelium is uncommon in cystadenoma. Only one of the cystadenomas in our series showed an unequivocal nodular mass on sonography.

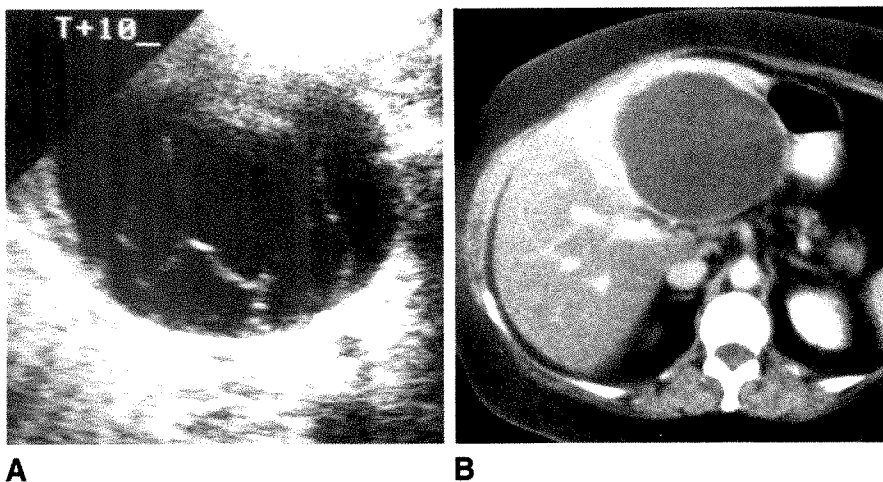


Fig. 2.—Biliary cystadenoma.

A, Sonogram shows septated liver cyst.

B, CT scan shows unilocular cyst with no evidence of internal septa.

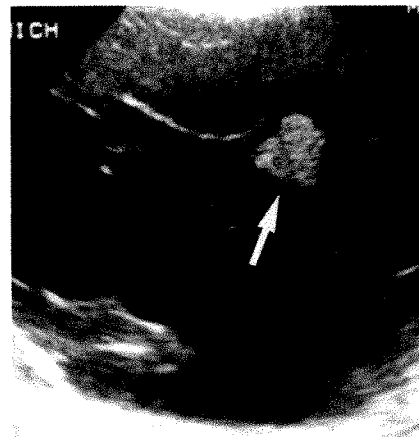


Fig. 3.—Biliary cystadenoma. Sonogram shows echogenic nodule (arrow) within septated multilocular cyst. This was the only discrete nodule or mass seen in the eight benign cystadenomas.

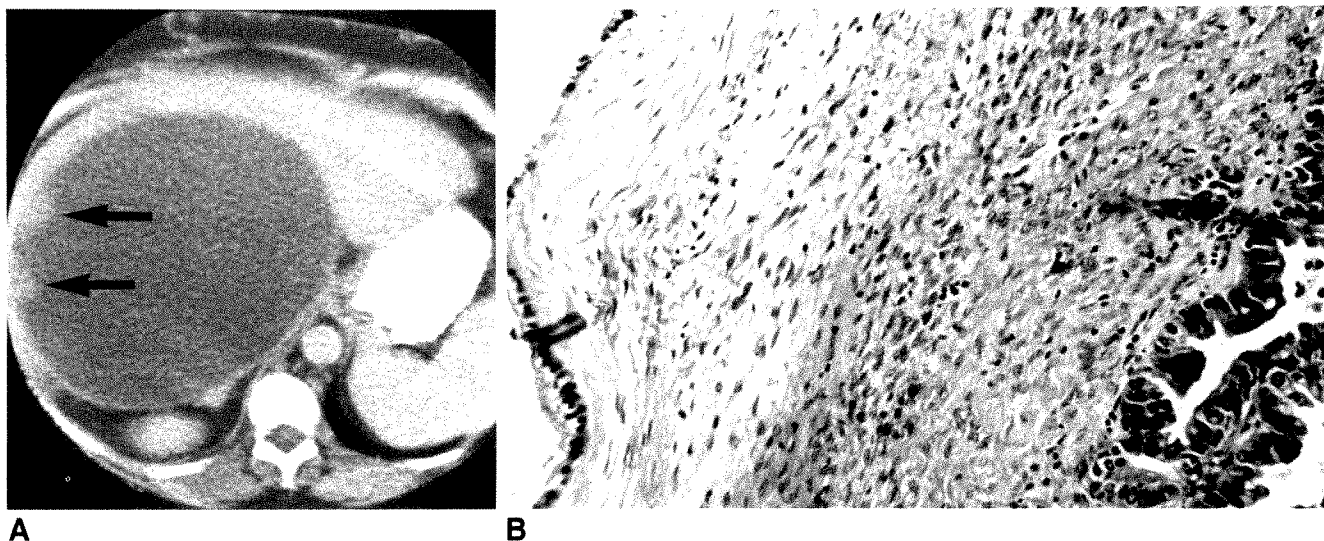


Fig. 4.—Biliary cystadenocarcinoma.

A, CT scan shows discrete mural nodules (arrows) lining unilocular hepatic cyst.

B, Histologic section shows both benign (left) and malignant (right) epithelium in the same mural nodule (H and E, $\times 250$).

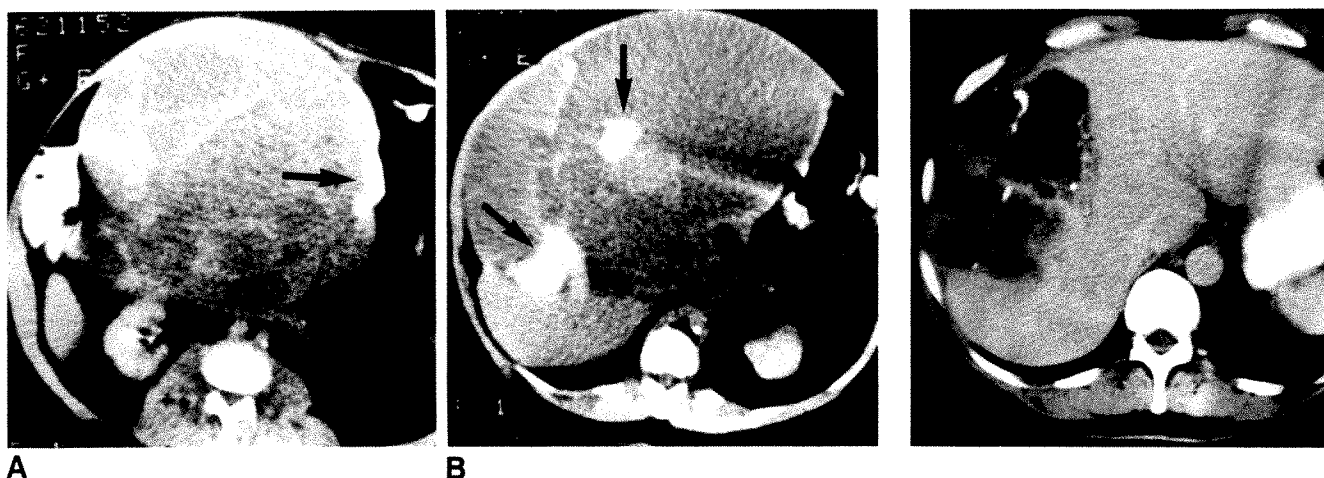


Fig. 5.—Biliary cystadenocarcinoma.

A, CT scan shows multiple septa poorly. Thick and coarse mural calcification is evident (arrow).

B, At a higher level, large, solid soft-tissue masses (arrows) are within septated cyst.

Fig. 6.—Biliary cystadenocarcinoma. CT scan shows coarse calcification of multiple thick septa.

Macroscopic nodules or solid elements were present on the CT scans in two of our three patients with biliary cystadenocarcinoma. These findings correspond to the grossly solid malignant tissue ranging up to 3.5 cm in diameter that Wheeler and Edmondson [2] described protruding from the internal cyst lining in their review of the pathologic features of malignant biliary cystadenocarcinoma. Multiple coarse and thick mural and septal calcifications were also shown on the CT scans of two of our three cases of cystadenocarcinoma, but a thin simple focus of mural calcification was also seen in one of our eight patients with cystadenoma. Although differentiation of cystadenoma from cystadenocarcinoma by imaging criteria may not be possible in many cases, our small series

suggests that the presence of solid nodular masses or coarse calcifications along the wall or septa in a multilocular cystic mass indicates a more likely diagnosis of biliary cystadenocarcinoma. Even if it is possible to distinguish biliary cystadenocarcinoma from cystadenoma by CT in some cases, the therapeutic implication of this distinction is minimal. The probable premalignant nature of biliary cystadenoma means that total surgical excision is the preferred treatment for both lesions. The essential point is that both neoplasms can almost always be differentiated from a simple hepatic cyst by CT and sonographic criteria.

Biliary cystadenoma must be differentiated from other cystic liver masses detected by CT and sonography. Solitary

simple hepatic cysts are sometimes shown on routine screening examinations of the upper abdomen. Although they are much less common than the ubiquitous renal cyst, similar care must be taken that the criteria for a simple cyst on CT and sonography are rigidly satisfied before other diagnoses are excluded. Unlike septa that are occasionally seen in otherwise benign-appearing renal cysts [11], in our experience septa are less commonly shown within hepatic cysts discovered as an incidental finding on CT or sonography. Mesenchymal hamartoma [12] and undifferentiated (embryonal) sarcoma [13] are rare hepatic neoplasms that can have a multiloculated cystic appearance on CT scans and sonograms, but their occurrence almost exclusively in children and teenagers differentiates them from cystic biliary neoplasms. A cystic hepatoma or metastasis [10] can rarely simulate a unilocular cystadenoma or cystadenocarcinoma.

Liver abscess and hydatid disease of the liver are the two entities most likely to be confused with biliary cystadenoma. Between 20% and 30% of liver abscesses, whether pyogenic or amebic in etiology, have a septated or multilocular appearance on CT images [14]. Hydatid liver cysts caused by *Echinococcus granulosus* are commonly multilocular in appearance because of the presence of daughter cysts within the original cyst [15]. The diagnosis of both infectious diseases is usually easily made by a combination of clinical and laboratory findings, including serologic tests and/or Gram stain and culture of cystic fluid obtained by percutaneous aspiration.

ACKNOWLEDGMENTS

We thank James Bova for assistance in this project and Dawn Hutton for typing the manuscript.

REFERENCES

1. Ishak K, Willis GW, Cummins SD, Bullock AA. Biliary cystadenoma and cystadenocarcinoma: report of 14 cases and review of the literature. *Cancer* 1977;38:322-338
2. Wheeler D, Edmondson A. Cystadenoma with mesenchymal stroma (CMS) in the liver and bile ducts: a clinicopathologic study of 17 cases, 4 with malignant change. *Cancer* 1985;56:1434-1445
3. Carroll BA. Biliary cystadenoma and cystadenocarcinoma: grey scale ultrasound appearance. *JCU* 1978;6:337-340
4. Forrest ME, Cho KJ, Shields JJ, Wicks JD, Silver TM, McCormick TL. Biliary cystadenomas: sonographic-angiographic-pathologic correlations. *AJR* 1980;135:723-727
5. Frick MP, Feinberg SB. Biliary cystadenoma. *AJR* 1982;139:393-395
6. Stanley J, Vujic I, Schabel SI, Gobien RP, Reines HD. Evaluation of biliary cystadenoma and cystadenocarcinoma. *Gastrointest Radiol* 1983;8:245-248
7. Itai Y, Araki T, Furui S, Yashiro N, Ohtomo K, Iio M. Body computed tomography: computed tomography of primary intrahepatic biliary malignancy. *Radiology* 1983;147:485-490
8. Kokubo T, Itai Y, Ohtomo K, Itoh K, Kawauchi N, Minami M. Mucin-hypersecreting intrahepatic biliary neoplasms. *Radiology* 1988;168:609-614
9. Choi BI, Lim JH, Han MC, et al. Biliary cystadenoma and cystadenocarcinoma: CT and sonographic findings. *Radiology* 1989;171:57-61
10. Federle MP, Filly RA, Moss AA. Cystic hepatic neoplasms: complementary roles of CT and sonography. *AJR* 1981;136:345-348
11. Rosenberg ER, Korobkin M, Foster W, Silverman PM, Bowie JD, Dunnick NR. The significance of septations in a renal cyst. *AJR* 1985;144:593-595
12. Giyanani VL, Meyers PC, Wolfson JJ. Mesenchymal hamartoma of the liver: computed tomography and ultrasonography. *J Comput Assist Tomogr* 1986;10:51-54
13. Ros PR, Olmstead WW, Dachman AH, Goodman ZD, Ishak KG, Hartman DS. Undifferentiated (embryonal) sarcoma of the liver: radiologic-pathologic correlation. *Radiology* 1986;160:141-145
14. Halvorsen RA, Korobkin M, Foster WL, Silverman PM, Thompson WM. The variable CT appearance of hepatic abscesses. *AJR* 1984;141:941-946
15. Lewall DB, McCorkell SJ. Hepatic echinococcal cysts: sonographic appearance and classification. *Radiology* 1985;155:773-775

Book Review

Atlas of Duplex Scanning. Carotid Arteries. By John J. Cranley, William S. Karkow, and E. Douglas Baldrige, Jr. Philadelphia: Saunders, 352 pp., 1989. \$125

The authors' introductory statements speak to the importance of the quality of the image—that this is paramount and that the Doppler signal is of lesser importance in the evaluation of the carotid arteries. I cannot agree. The image defines plaque and indicates the correct areas to be sampled to determine the vascular hemodynamics. Image alone is subject to error in interpretation (e.g., an occluded vessel may look perfectly normal sonographically). Indeed, the title of the book is a misnomer: Duplex scanning refers to both sonographic image and velocity profile or spectral analysis, and the atlas is concerned only with the imaging component.

The atlas consists of a series of illustrations and minimal text. On the left-hand side of the page is a description; on the right-hand side, a sonographic image superiorly and a colored drawing inferiorly. The colored drawings of the sonographic images are superb and are more representational than exact tracings of the image. The terminology of sonographic effects tends to be descriptive, rather than scientifically precise (e.g., "pigtail effect" for refraction). The authors need, in my opinion, to address in the introduction the question of resolution of the system and the transducer frequency used, inasmuch as the introduction states that image is a prime consideration. Some sonograms are coarse and grainy; the technology has advanced since these images were obtained. Interfaces are not always well distinguished. The carotid artery is aligned vertically, and its orientation always is defined, but sometimes the distal part is superior and in other instances inferior, which can be disconcerting. The usual convention is to align the artery horizontally with the head of the patient on the left.

For someone starting out in this field, this atlas presents a broad range of what can be expected in a group of patients with athero-

sclerosis. Although no examples of carotid dissection or fibrous dysplasia are included, a large range of examples of atherosclerotic change before and after surgery is included, with examples of endarterectomy sites, grafts, and artifacts. The reader is not always enlightened as to whether examples of images called ulcerated plaque have been verified by surgery, and sonography has been shown to be relatively ineffective in distinguishing ulcers from nonulcerated areas. Two adjacent heaped up plaques may mimic a single ulcerated plaque.

An excellent discussion of the various ways to calculate the percentage of stenosis is presented, which reiterates the difficulties of precision in this realm, particularly as plaque often is not seen well in the images on which the measurements of residual lumen are based. This points out the need for spectral analysis as well to determine what the effects of plaque are on velocity and flow. No color images are shown although Doppler color flow imaging is becoming the technique of choice because of the ease in localization and the visual sighting of the narrowed stream.

This work can serve as a guide to beginners in this field, whether physicians or sonographers. It gives an overview of the delineation of sonographic abnormalities of the carotid artery.

Gretchen A. W. Gooding
University of California, San Francisco
Veterans Administration Medical Center
San Francisco, CA 94121

Identification of a Patent Paraumbilical Vein by Using Doppler Sonography: Importance in the Diagnosis of Portal Hypertension

Robert N. Gibson¹
 Peter R. Gibson²
 John D. Donlan¹
 David A. Clunie¹

The aim of this study was to determine if the addition of pulsed Doppler imaging to conventional sonography allows discrimination between true paraumbilical veins of portal hypertension and the apparent vein sometimes seen in the ligamentum teres in normal subjects. Conventional sonography and Doppler sonography of the ligamentum teres were performed in 33 normal subjects and in 39 patients with portal hypertension due to chronic liver disease. An apparent ligamentum teres vessel (i.e., hypoechoic channel) was identified on sonograms in 32 (97%) normal subjects (diameter 0.6–1.9 mm) and in 35 (90%) patients with portal hypertension (diameter 1.1–22 mm). In the portal hypertension group, the apparent vessel had a diameter of greater than 3 mm in only 20 patients (51%), but in 32 patients (82%) it was shown on Doppler examination to be a patent paraumbilical vein (i.e., hepatofugal venous signal).

A patent paraumbilical vein on duplex Doppler sonography is therefore a specific sign of portal hypertension. The addition of Doppler imaging to conventional sonographic examination significantly increases the sensitivity for the diagnosis of portal hypertension by demonstration of a paraumbilical vein.

AJR 153:513–516, September 1989

A number of sonographic findings have been described in patients with portal hypertension, including the demonstration of portosystemic collateral veins [1]. One site of collateral flow is in the ligamentum teres, via a vein that has been termed a recanalized umbilical vein [2–7], but which is probably more accurately referred to as a paraumbilical vein [8]. It is well recognized that an enlarged paraumbilical vein is seen on sonography in some patients with portal hypertension, but the frequency of the finding is not well documented. Furthermore, a hypoechoic band of uncertain nature is seen in the ligamentum teres in some normal subjects. It has been suggested that a vessel apparent on sonograms within the ligamentum teres must measure more than 3 mm in diameter to be regarded as a sign of portal hypertension [9]. Duplex Doppler sonography now allows more precise identification and characterization of vessels compared with conventional sonography. The aim of this study is to determine if the addition of Doppler to conventional sonography allows discrimination between true paraumbilical collateral veins of portal hypertension and the ligamentum teres vessels sometimes seen in normal subjects.

Materials and Methods

The study included 103 consecutive patients referred by the gastroenterological unit for sonography. Of these patients, 39 had clinically unequivocal portal hypertension (27 men, 12 women; age range, 17–85 years; median age, 57 years) and 33 patients had no evidence of portal hypertension or chronic liver disease (23 men, 10 women; age range, 16–80 years; median age, 59 years). The remaining 31 patients had some evidence of liver disease but did not fulfill the criteria applied to portal hypertension. The criteria used for the diagnosis of

Received March 9, 1989; accepted after revision May 1, 1989.

¹ Department of Radiology, The Royal Melbourne Hospital, Victoria 3050, Australia. Address reprint requests to R. N. Gibson.

² Department of Gastroenterology, The Royal Melbourne Hospital, Victoria 3050, Australia.

0361-803X/89/1533-0513
 © American Roentgen Ray Society

portal hypertension were (1) the presence of chronic liver disease (with or without splenomegaly) and (2) the presence of either non-malignant ascites or endoscopically proved gastroesophageal varices. All patients in the portal hypertension group had cirrhosis, which was due to alcoholism in 24 patients, was cryptogenic in seven, and was associated with chronic active hepatitis in six, primary sclerosing cholangitis in one, and Wilson disease in one. Upper gastrointestinal endoscopy was performed in 20 of the patients with portal hypertension. Patients with sonographic evidence of prehepatic portal hypertension (i.e., main portal vein obstruction) were excluded.

All patients were examined in a supine position, after fasting for at least 4 hr, with an ATL Ultramark 8 sonography unit (ATL, Bothell, WA). In each patient an attempt was made to image the ligamentum teres in its long axis as it courses forward from the anterior aspect of the umbilical portion of the left portal vein (Fig. 1). Imaging was attempted with three probes in every patient, namely 3-MHz, 5-MHz annular array, and 7.5-MHz mechanical sector probes. If a hypoechoic band was identified with one or more of the probes within either the intrahepatic or the extrahepatic portion of the ligamentum teres, it was regarded as possibly representing a vessel and a positive result was recorded. The maximum internal diameter of any such apparent vessel was measured with the cursors of the scanning unit. An average measurement was recorded if the measurements varied between the three probes. Apparent ligamentum teres vessels that were visible only within 1 cm of the left portal vein were disregarded because small vessels normally may be present in this region [8]. Doppler sampling this close to the left portal vein could produce misleading signals arising from a portal vein or hepatic artery branch.

Pulsed Doppler sonography of any apparent ligamentum teres vessels was performed with both 3-MHz and 5-MHz probes, by using a 1.5-mm or 2.0-mm sampling gate and an angle of insonation of between 30° and 75°. Doppler signals were recorded in velocity mode and classified into one of five categories (Fig. 2): venous, arterial, thump, noise, and no signal. A positive result for a patent paraumbilical vein was recorded only if Doppler sonography showed a venous signal with hepatofugal flow from within the apparent ligamentum teres vessel.

Each study was performed by one of two experienced operators, and interpretation was made during the examination with images and Doppler tracings also being recorded on film. At the time of examination, the operator necessarily had access to other sonographic and some clinical information and therefore was not truly blinded, but the operator was not told whether the clinical criteria for portal hypertension had been fulfilled in each patient.

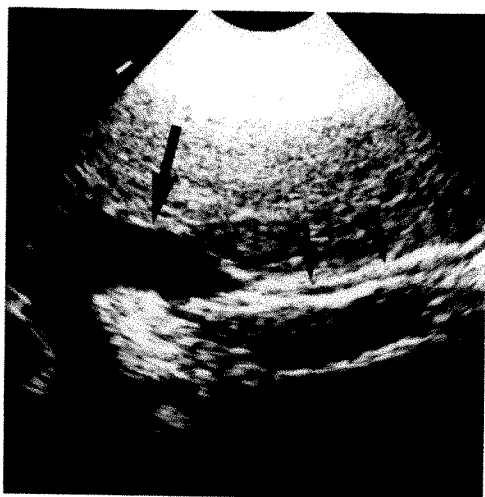


Fig. 1.—Longitudinal sonogram in a normal subject shows ligamentum teres (small arrows) coursing anteroinferiorly from umbilical portion of left portal vein (large arrow). Ligamentum teres in this case contains an apparent vessel (i.e., hypoechoic channel) from which no Doppler signal was obtained.

Results

In the control group, adequate studies were achieved in all 33 patients. An apparent ligamentum teres vessel was imaged in 32 patients (97%) with a range of diameter from 0.6 to 1.9 mm and a median diameter of 1.3 mm (Fig. 3). In these 32 patients, the Doppler signals obtained were arterial in 12 (all hepatofugal), absent in 10, thump in eight, and noise in two. Most importantly, no venous signals were obtained; therefore, none of the normal patients had Doppler evidence of a patent paraumbilical vein.

In three of the 39 patients with portal hypertension, the studies were technically inadequate because the patients were obese, unable to cooperate in breath-holding, or both. Of the remaining 36 patients, sonograms showed an apparent ligamentum teres vessel in 35. Doppler studies showed this was a patent paraumbilical vein in 32 patients (Fig. 3). In the other three patients, two had an arterial waveform (diameters, 0.5 mm and 2.0 mm) and one had no signal (diameter, 2.4 mm). Therefore, in the patients with portal hypertension, the Doppler examination was positive for a patent paraumbilical vein in 82% of the total group and in 89% of those with a technically adequate scan. Hence, the Doppler study had a scanning sensitivity of 82% and specificity of 100% for diagnosis of portal hypertension.

The diameter of the Doppler-positive paraumbilical veins in the portal hypertension group had a median of 4.5 mm, but more importantly, showed a wide range from 1.1 mm to 22 mm. In fact, in 34% it measured 3 mm or less, and 22% measured 2 mm or less in diameter. It has been suggested that an apparent ligamentum teres vessel should measure more than 3 mm in diameter before it is regarded as a sign of portal hypertension [9]. In the portal hypertension group in this study, only 51% had a paraumbilical vein diameter of more than 3 mm and, indeed, in only 59% was it more than 2 mm.

In 17 patients with Doppler-positive paraumbilical veins, at least one of the probes gave a negative result, either for conventional sonography alone (11 patients) or for sonography and Doppler imaging (six patients). These false-negative results were seen with all of the probes at some time, and no single probe performed significantly better than the others with respect to conventional sonography or Doppler imaging. In five of the 32 patients with patent paraumbilical veins, the vein was more easily studied in its extrahepatic course than in its intrahepatic segment (Fig. 4).

The venous waveform observed in the patent paraumbilical veins showed low-amplitude pulsatility in four patients (Fig. 5A), which was quite different from the arterial waveform (Fig. 2B), but closely paralleled a pulsatile waveform obtained from the left portal vein (Fig. 5B). (In our experience, low-amplitude pulsatility of portal venous flow may be seen on Doppler studies both in normal subjects and in patients with portal hypertension.)

Upper gastrointestinal endoscopy was performed in 20 patients, 16 of whom had gastroesophageal varices. Of these, a Doppler-positive paraumbilical vein was found in 13 (two findings were negative and one study was technically inadequate). No varices were seen at endoscopy in four, all of whom had a Doppler-positive paraumbilical vein. No correlation was seen between paraumbilical vein size and the presence of varices on endoscopy.

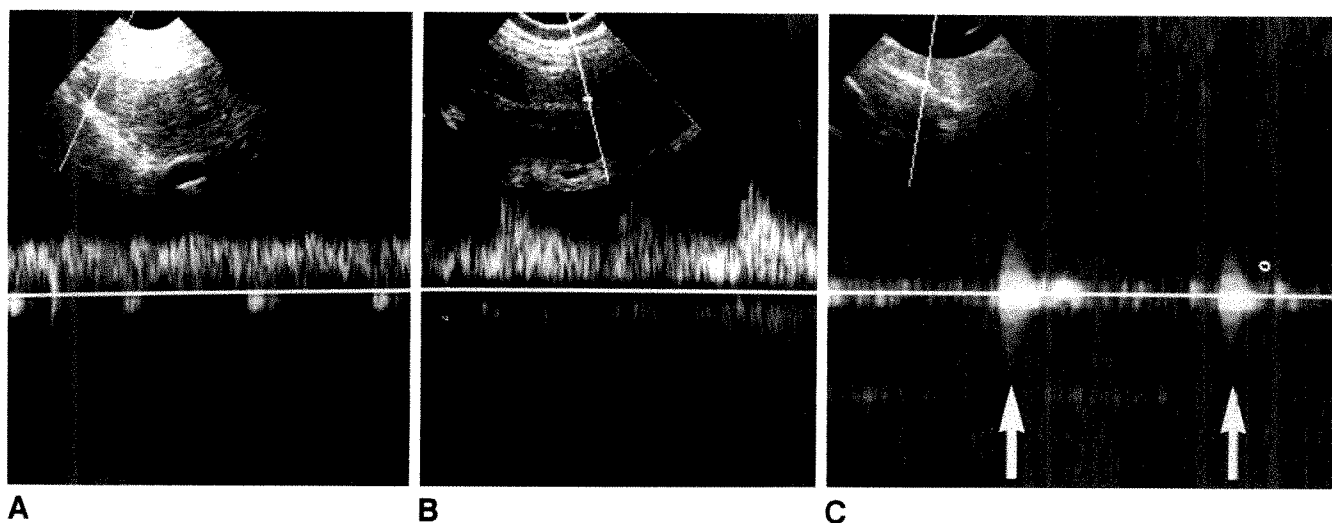


Fig. 2.—Doppler signals obtained from apparent ligamentum teres vessels included (A) venous (approximately uniform, low-amplitude hepatofugal flow), (B) arterial (with obvious systolic and diastolic components), (C) thump (transmitted cardiac or aortic pulsation—indicated by arrows) and noise (low-amplitude bidirectional signal between arrows).

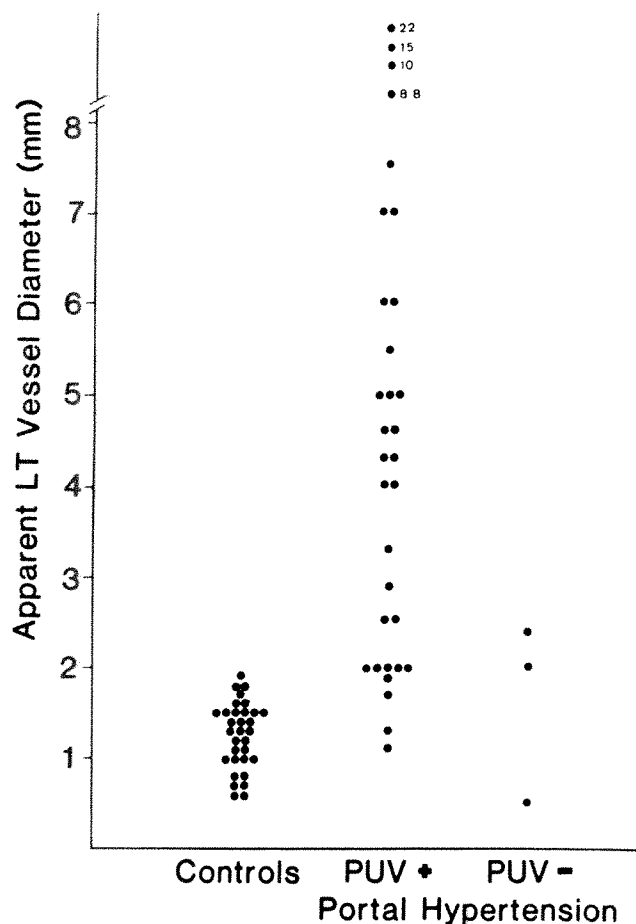


Fig. 3.—Diameters of apparent ligamentum teres (LT) vessels in control subjects and portal hypertension patients. PUV+ = venous signal obtained from apparent ligamentum teres vessel; PUV- = no venous signal obtained.

Discussion

The results indicate that demonstration of a patent paraumbilical vein in the ligamentum teres by duplex Doppler sonography is a specific sign (specificity, 100%) of portal hypertension of hepatic and posthepatic cause. The specificity of the sign, which has not been shown before, together with the noninvasive nature of the test, make it an attractive method for the diagnosis of portal hypertension.

The sensitivity of the test was 82% (32/39 patients) or 89% if technically inadequate studies were excluded. As the patients in the study had clear clinical evidence of portal hypertension, the sensitivity of the technique for the diagnosis of mild portal hypertension remains undetermined, but might be expected to be less. Nevertheless, the sensitivity shown is greater than that reported in other studies evaluating sonographic imaging of portosystemic collateral veins without the use of Doppler sonography [10–12].

An apparent vessel (i.e., hypoechoic channel) in the ligamentum teres of greater than 3-mm diameter noted on sonograms has been suggested as a specific sign of portal hypertension [9]. Our study confirms this specificity, but demonstrates a low sensitivity (51% in the present study) in the diagnosis of portal hypertension. Indeed, apparent ligamentum teres vessels of more than 2-mm diameter were seen in this study only in patients with portal hypertension, and all but one vessel (which measured 2.4 mm in diameter) were Doppler-positive for a patent paraumbilical vein. Of the 32 patients with portal hypertension who had Doppler-positive paraumbilical veins, the veins measured less than or equal to 3 mm in 11 patients (34%) and less than or equal to 2 mm in seven (22%). The overlap with the diameter range of the apparent ligamentum teres vessels in normal subjects (0.6–1.9 mm) diminishes its diagnostic value (Fig. 3) and is the main reason for adding pulsed Doppler sonography to imaging of the ligamentum teres in patients with suspected portal hypertension. The addition of Doppler sonography increased

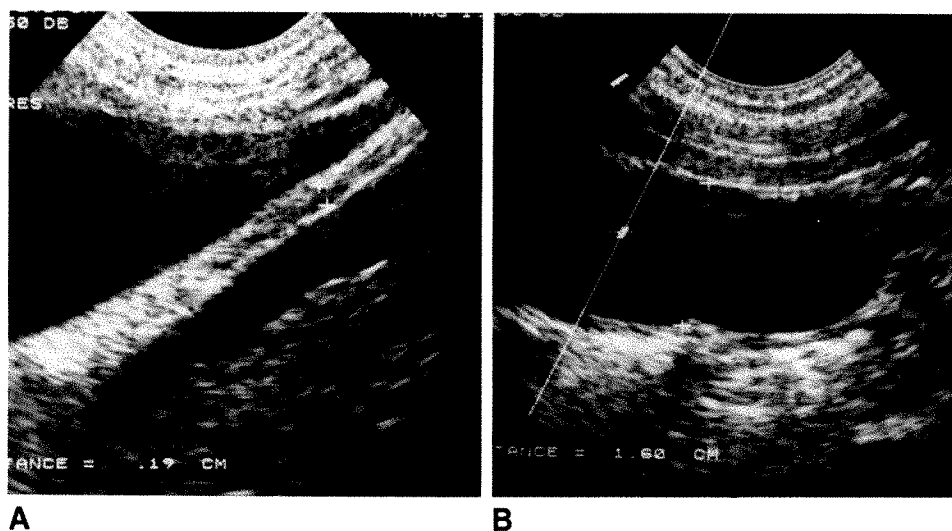


Fig. 4.—A, Longitudinal sonogram shows a small paraumbilical vein (between cursors). Vessel is more easily seen in extrahepatic portion of ligamentum teres, which is surrounded by ascites.

B, Longitudinal sonogram shows extrahepatic portion of a 16-mm-diameter paraumbilical vein (between cursors), which could be traced to a smaller intrahepatic paraumbilical vein.

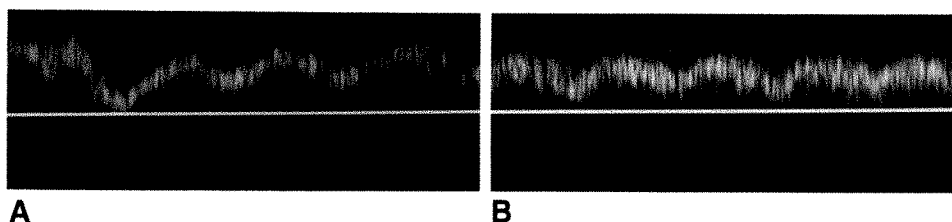


Fig. 5.—A, and B, Doppler tracing shows pulsatile venous signal in a patent paraumbilical vein (A). Pulsatility is not of arterial type and is similar to that seen in left portal vein (B) in same patient.

the sensitivity for the diagnosis of portal hypertension in this series from 51% to 82% while maintaining specificity.

This study failed to show any correlation between the size of the paraumbilical vein and the presence of varices on endoscopy. The significance of this is uncertain; it may reflect merely a relatively small sample population (only 20 patients with portal hypertension underwent endoscopy).

The nature of the apparent ligamentum teres vessels in normal subjects is only partially answered by this study. In some patients, the hypoechoic bands represent small arteries (38% in this study) and in others they presumably represent interfaces between layers of fibrous or fatty tissue. In patients with portal hypertension, but with Doppler-negative ligamentum teres vessels, the explanation for the apparent vessel is probably the same in some patients, although other explanations may apply. It is possible, for example, that some patients with portal hypertension develop a patent paraumbilical vein that subsequently undergoes thrombosis. This may have been the case in the single patient in the portal hypertension group who had an apparent ligamentum teres vessel of greater than 2-mm diameter (2.4 mm) from which no signal could be obtained.

Two important aspects of the examination technique are evident from our results. First, the use of more than one probe frequency for both conventional sonography and Doppler imaging increases the likelihood of detection of a patent paraumbilical vein. Imaging frequencies of 3 to 7.5 MHz and Doppler frequencies of 3 and 5 MHz were used in this study, and no single probe performed significantly better overall. Factors influencing the optimal probe in a given patient were, as one would expect, the degree of obesity, the presence of ascites, and the degree of echogenicity and attenuating properties of the liver parenchyma. The second finding relating to technique was that in some patients the paraumbilical vein was more easily seen in the extrahepatic course of the

ligamentum teres. This occurred in five patients and appeared to be caused by one or more of the following: difficult sonographic access to the intrahepatic ligamentum teres in small highly placed livers, including those patients with ascites; the presence of a very echogenic and beam-attenuating cirrhotic liver; or a real increase in size of the paraumbilical vein in the extrahepatic segment of the ligamentum teres, where it may be more distensible.

REFERENCES

- Hill MC, Dach JL, Shawker TH. Ultrasonography in portal hypertension. *Clin Gastroenterol* **1985**;14:83-103
- Weill F. Ultrasonic visualisation of an umbilical vein. *Radiology* **1976**;120:159-160
- Funston MR, Goudie E, Richter IA, et al. Ultrasound diagnosis of the recanalized umbilical vein in portal hypertension. *J Clin Ultrasound* **1980**;8:244-246
- Glazer GM, Laing FC, Brown TW, et al. Sonographic demonstration of portal hypertension: the patent umbilical vein. *Radiology* **1980**;136:161-163
- Schabel SI, Rittenberg GM, Javid LH, et al. The "bull's-eye" falciform ligament: a sonographic finding of portal hypertension. *Radiology* **1980**;136:157-159
- Aagaard J, Jensen LI, Sorensen TIA, et al. Recanalized umbilical vein in portal hypertension. *AJR* **1982**;139:1107-1109
- Bolondi L, Gandolfi D, Arienti V, et al. Ultrasonography in the diagnosis of portal hypertension: diminished response of portal vessels to respiration. *Radiology* **1982**;142:167-172
- Lafortune M, Constantin A, Breton G, et al. The recanalized umbilical vein in portal hypertension: a myth. *AJR* **1985**;144:549-553
- Saddekni S, Hutchinson DE, Cooperberg PL. The sonographically patent umbilical vein in portal hypertension. *Radiology* **1982**;145:441-443
- Dach JL, Hill MC, Pelaez JC, et al. Sonography of hypertensive portal venous system: correlation with arterial portography. *AJR* **1981**;137:511-517
- Dokmeci AK, Kimura K, Matsutani S, et al. Collateral veins in portal hypertension: demonstration by sonography. *AJR* **1981**;137:1173-1177
- Subramanyam BR, Balthazar EJ, Madamba MR, et al. Sonography of portosystemic venous collaterals in portal hypertension. *Radiology* **1983**;146:161-166

Pictorial Essay

Cross-sectional Imaging of Abdominal Wall Hernias

Richard J. Wechsler,¹ Alfred B. Kurtz, Laurence Needleman, Bradley W. Dick, Rick I. Feld, Pamela L. Hilpert, and Lorna Blum

Abdominal wall hernias are one of the more common conditions for which patients seek surgical intervention. These hernias involve the passage of a peritoneal sac, with or without abdominal contents, through a site of congenital or acquired weakness in the abdominal wall. The diagnosis of hernias is often straightforward. They may, however, cause diagnostic problems, particularly in obese patients, patients with scars, or in those in whom a herniated sac protrudes between muscle layers (Fig. 1). A variety of abdominal wall lesions such as tumors, hematomas, undescended testes, aneurysms, or abscesses can be confused with hernias (Fig. 2) [1]. The purpose of this essay is to illustrate the findings on cross-sectional imaging of abdominal wall defects that may be clinically occult or confusing.

Groin and Pelvic Hernias

Inguinal Hernias

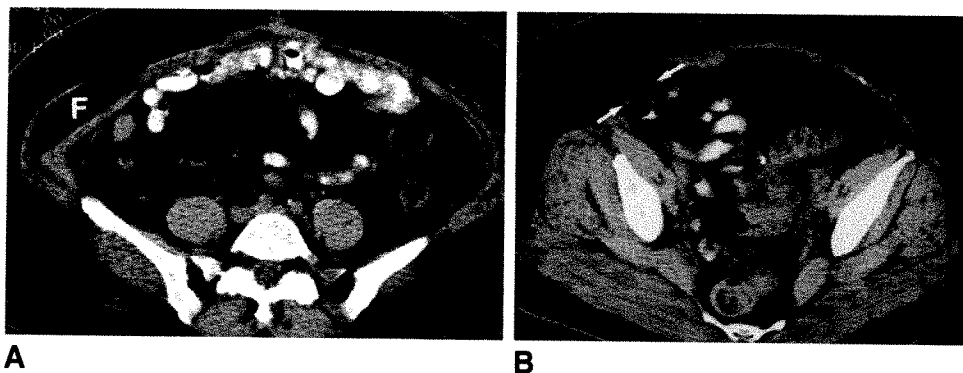
Inguinal hernias are either direct or indirect, depending on their relationship to the inferior epigastric vessels. In an indirect hernia, the peritoneal sac passes down the course of the inguinal canal anterior to the spermatic cord and lateral to the inferior epigastric vessels (Fig. 3). In females, the hernia sac follows the course of the round ligament into the labium. The sac usually contains omentum and small bowel and occasionally ascites.

A direct hernia is almost always acquired, rather than congenital. The neck of the hernia is medial to the inferior

Fig. 1.—Interstitial spigelian hernia. An interstitial hernia is one in which hernia sac protrudes between two abdominal wall layers.

A, CT scan shows space between external oblique and internal oblique muscles is distended by fat (F).

B, CT scan at lower level shows a defect (arrows) at linea semilunaris, indicative of a spigelian hernia.



Received March 6, 1989; accepted after revision April 28, 1989.

¹ All authors: Department of Radiology, Thomas Jefferson University Hospital, 111 S. 11th St., Philadelphia, PA 19107. Address reprint requests to R. J. Wechsler.

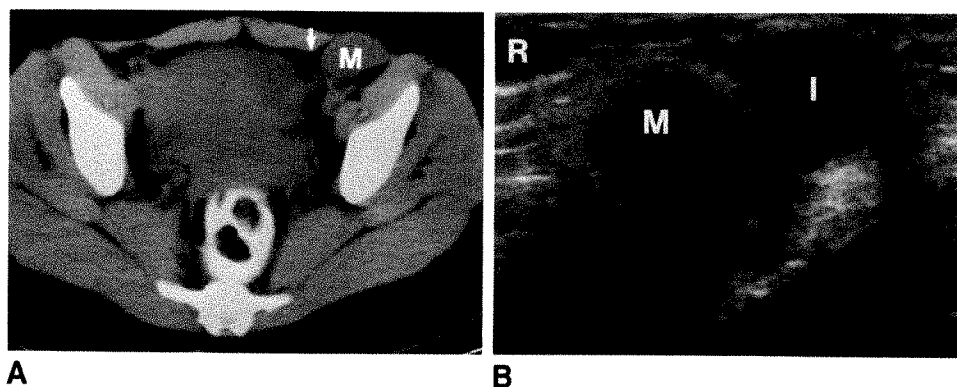


Fig. 2.—Desmoid tumor simulating an inguinal hernia.

A, CT scan shows a soft-tissue mass (M) in inguinal canal just lateral to inferior epigastric vessels (arrow). This was mistaken for a hernia because of its location and continuity with small bowel.

B, On transverse sonogram, mass (M) is between rectus abdominis (R) and iliopsoas (I) muscles. Mass was separate from bowel and there was no peristalsis.

At surgery, a desmoid tumor in inguinal canal was found.

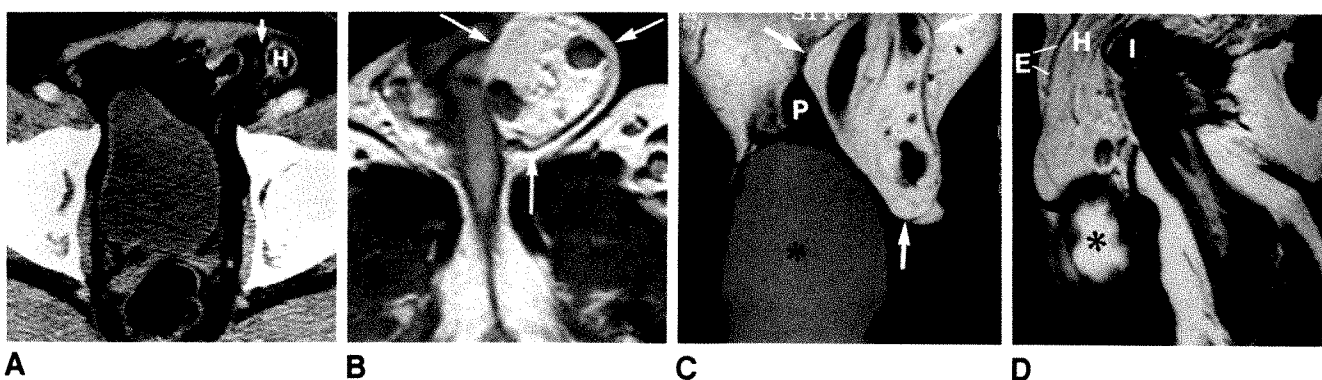


Fig. 3.—Indirect hernia.

A, CT scan shows neck of indirect inguinal hernia (H) just lateral to inferior epigastric vessels (arrow).

B, Axial MR image at level of base of penis shows bowel contents (arrows) in left scrotal sac.

C, Coronal MR image at level of base of penis (P) shows bowel contents (arrows) in left hemiscrotum.

D, Sagittal MR image shows indirect hernia (H) extending into scrotum between anterosuperior external oblique muscle (E) and posterior iliopsoas (I) muscle.

Asterisk = contralateral right hydrocele. MR has advantage over CT of defining a hernia in sagittal and coronal planes.

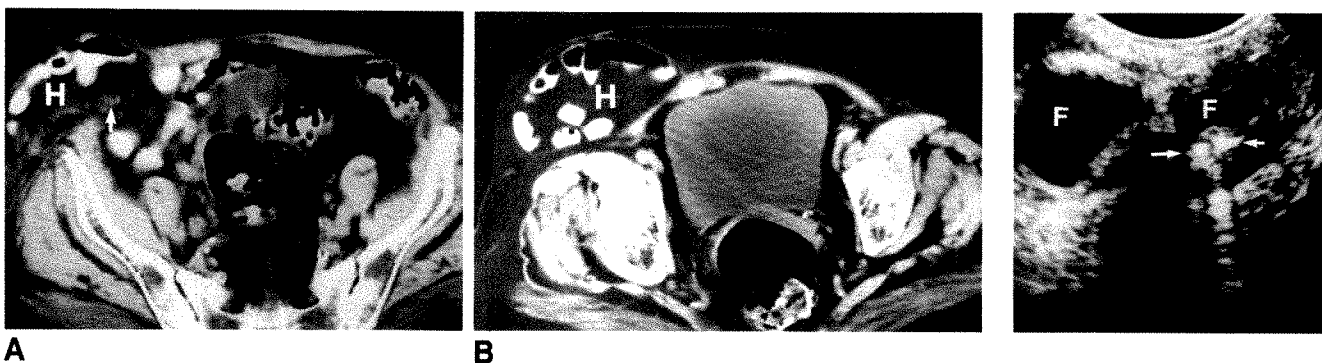


Fig. 4.—Direct hernia.

A, CT scan shows neck of large inguinal hernia (H) medial to inferior epigastric vessels (arrow).

B, CT scan at lower level shows hernia (H) as it extends toward labium.

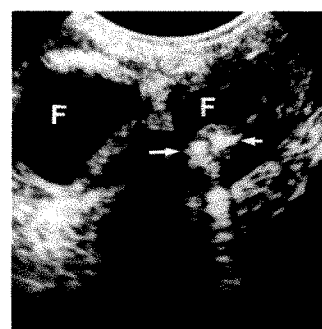


Fig. 5.—Congenital inguinal hernia. Transverse sonogram shows fluid (F) and hyperechoic foci (arrows) in scrotum of an infant. Plain film showed scrotal calcification associated with meconium peritonitis, which had extended through processus vaginalis. (Courtesy of Henrietta Rosenberg, Philadelphia).



Fig. 6.—Femoral hernia. CT scan shows fluid-filled loops of bowel (asterisk) along course of saphenous vein, indicative of a femoral hernia.



Fig. 7.—Sciatic hernia. CT scan shows that recurrent rectal carcinoma (asterisk), herniating through sciatic foramen, lies behind ischial spine deep to gluteus maximus muscle (G).

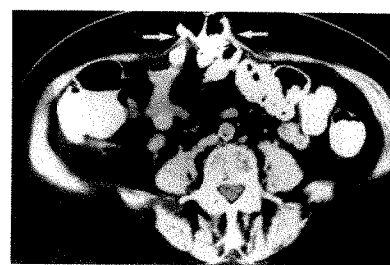


Fig. 8.—Paraumbilical hernia. CT scan shows midline abdominal wall defect in paraumbilical region with bowel (arrows) extending to skin.

epigastric vessels, and it generally does not traverse the inguinal canal (Fig. 4). Therefore bowel strangulation is seldom a complication because of the blunt and diffuse character of the protrusion. CT and MR imaging both define the relationship of the inferior epigastric vessels to the hernia sac. Sonography, although useful in diagnosing an inguinal hernia (Fig. 5), usually does not visualize these vessels.

Femoral Hernias

Femoral hernias occur less frequently than inguinal hernias and are more common in women. The hernia protrudes through the femoral ring and canal and appears at the saphenous opening. The hernia may be lateral to the femoral vessels. However, the sac may turn upward and involve the superficial epigastric vessels, or it may turn toward the labium or scrotum. Bowel strangulation is common.

The clinical findings of femoral hernias may mimic those of inguinal adenitis, lipoma, varicosities, psoas abscess, hydroceles, and other abdominal wall masses. The diagnosis is easily made by CT (Fig. 6). A femoral hernia may be distinguished from an inguinal hernia on CT because its sac lies below and lateral to the pubic tubercle as it emerges from the femoral canal. Conversely, the inguinal hernia lies above and medial to the tubercle.

Obturator Hernias

Obturator hernias protrude through the obturator foramen alongside the obturator vessels. They occur most frequently in thin, elderly women. About one third of the patients have neuralgia involving the thigh as a result of compression of the obturator nerve in the obturator canal [2]. The diagnosis of this hernia is made by showing herniated bowel protruding through the obturator canal on CT scans or MR images.

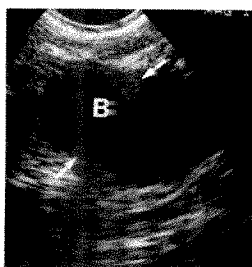
Sciatic Hernias

Sciatic hernias are hernias that pass from the pelvis through the sciatic foramina into the buttocks. These hernias may involve the ureter, bowel, bladder, or ovary. CT or MR imaging shows the involved organ behind the ischial spine (Fig. 7).

Abdominal Trunk Hernias

Paraumbilical Hernias

Acquired infantile umbilical hernias are usually small and caused by weakness in the umbilical scar. Most disappear as the child grows. Acquired adult umbilical hernias are more correctly termed paraumbilical; they protrude through the linea alba in the region of the umbilicus, occur mostly in



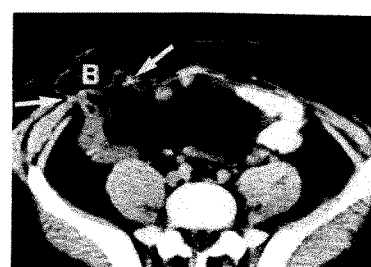
9



10



11



12

Fig. 9.—Paraumbilical hernia. Transverse infraumbilical sonogram shows loops of bowel (B) in anterior abdominal wall that are identified by valvulae conniventes (arrows).

Fig. 10.—Paraumbilical hernia. Sagittal midline MR image shows hernia (H) through linea alba and rectus abdominis muscle (L), with bowel contents in anterior abdominal wall.

Fig. 11.—Epigastric hernia. CT scan shows large hernia (H) through linea alba above level of umbilicus, indicative of an epigastric hernia.

Fig. 12.—Spigelian hernia. CT scan shows bowel (B) herniating through linea semilunaris (arrows), indicative of a spigelian hernia.

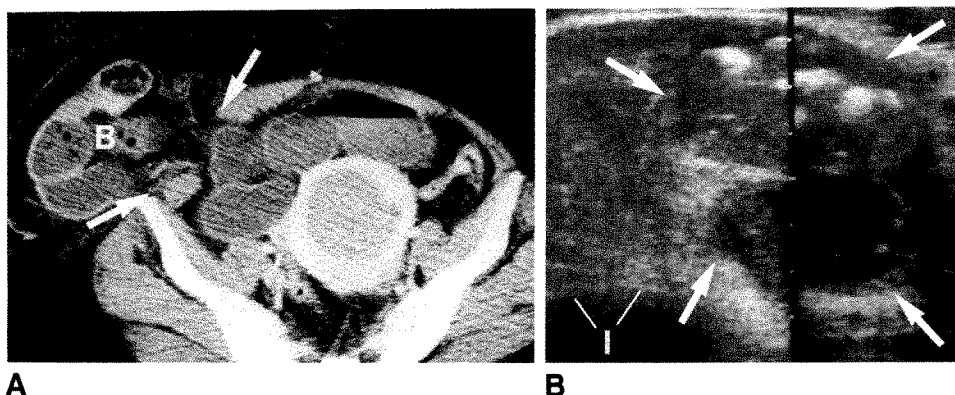


Fig. 13.—Obstructed incisional hernia.

A, CT scan shows defect in region of linea semilunaris (arrows) with dilated loops of bowel (B) extending into abdominal wall. This was at site of a previous incision.

B, Transverse oblique sonogram shows fluid- and gas-filled loops of bowel (arrows) within abdominal wall. I = anterior surface of iliac bone.

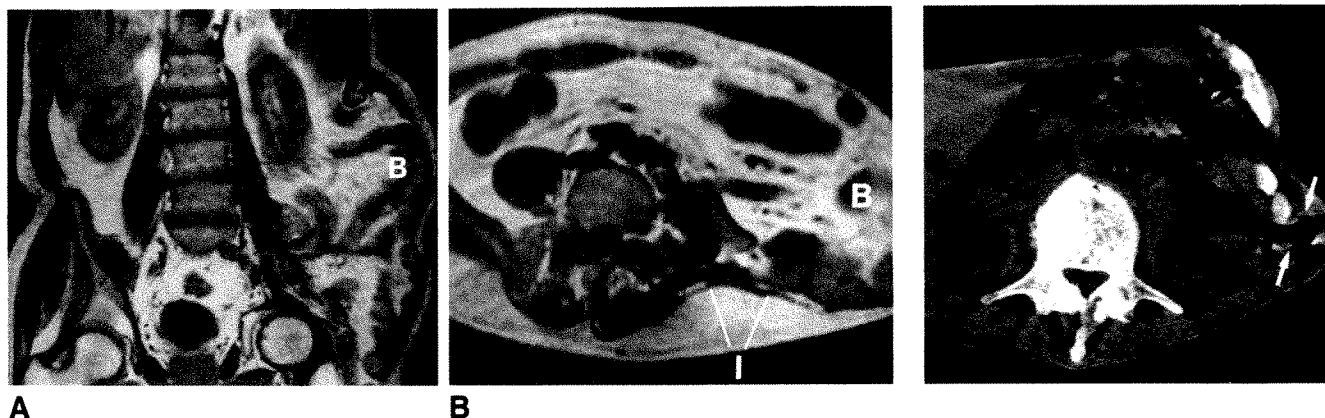


Fig. 14.—Hernia through iliac crest defect.

A, Coronal MR image after iliac wing surgery reveals large amount of bowel (B) extending into buttocks and along posterior lateral thigh.

B, Axial MR image reveals large amount of bowel (B) extending through defect in iliac bone (I) into buttock and thigh.

Fig. 15.—Lumbar hernia. CT scan shows part of colon (arrows) herniating into lateral abdominal wall inferior to 12th rib.

middle-aged women, and are associated with obesity or a history of multiple pregnancies. They may result in part from diastasis of the rectus abdominis muscle. CT (Fig. 8), sonography (Fig. 9), or MR (Fig. 10) clearly visualizes diastasis of the rectus abdominis and resulting omental fat or bowel contents in the anterior abdominal wall.

Epigastric Hernias

Epigastric hernias emerge through the linea alba between the umbilicus and the xyphoid process. In most instances, only omental and preperitoneal fat are involved. These hernias may cause upper abdominal pain that simulates ulcer or gallbladder symptoms. Both CT and sonography visualize the defects easily and confirm the diagnosis (Fig. 11).

Spigelian Hernias

Spigelian hernias are those that protrude through the linea semilunaris. They are associated with a high risk of bowel incarceration and strangulation. These hernias are difficult to diagnose clinically because of their rarity and insidious presentation. They have been mistaken for abdominal ab-

scesses, seromas, hematomas, ovarian masses, pseudocysts, and malignant omental or peritoneal implants [1].

Cross-sectional imaging techniques are important in establishing the diagnosis of a spigelian hernia. On CT scans, a hernia sac protruding through the linea semilunaris and containing bowel or fat is identified (Fig. 12). If it contains only peritoneal fat, it can be mistaken for an abdominal wall lipoma. However, careful inspection of the images reveals the muscular defect at the linea semilunaris (Fig. 1). Sonography shows a complex mass within the anterolateral aspect of the abdominal wall, which may contain fluid or gas-filled loops of bowel.

Incisional Hernias

Abdominal incisions cause weakened areas in the abdominal wall through which hernias can protrude. These hernias can be confused with other types of ventral hernias [3]. Most of these hernias develop within 4 months of surgery but may remain clinically inapparent for years. CT or sonography reveals the herniated sac protruding into the abdominal wall (Fig. 13). This is an important diagnosis to make, because incisional hernias cause intermittent abdominal pain and other symptoms of intestinal obstruction.

Lumbar Hernias

Lumbar hernias occur in the flank. They either result from postoperative iliac crest defects or are spontaneous. Hernias through an iliac crest defect may be seen as a gluteal soft-tissue mass. Hernia symptoms may begin as early as 15 days to as late as 15 years after creation of the osseous defect (e.g., those defects created after removal of bone for grafting or tumor involvement) [4]. Conventional radiographs reveal the bone defect, but the herniation is rarely apparent. Cross-sectional imaging clearly delineates the contents of the hernia and its anatomic relation to the bone defect (Fig. 14).

Spontaneous lumbar hernias occur through two areas of weakness in the flank. These areas are (1) the inferior lumbar triangle, which is bounded by the free border of the latissimus dorsi muscle posteromedially, the external oblique muscle anterolaterally, and the iliac crest inferiorly; and (2) the superior lumbar triangle, which is bounded above by the 12th rib and inferior margin of the inferior serratus posterior muscle, inferolaterally by the internal oblique muscle, and posteriorly by the erector spinae muscle. Common signs and symptoms of lumbar hernias are discomfort, muscle weakness, and a

bulge in the flank. Although these hernias can contain bowel, omentum, kidney, spleen, or stomach, strangulation is rare because of the wide neck of the hernia. As in other hernias, CT defines the wall and contents of the hernia (Fig. 15). It is the only imaging method needed to confirm or exclude this diagnosis.

ACKNOWLEDGMENTS

The authors thank Ann Prather Hunter and Lisa Massanova for their secretarial assistance in preparation of this manuscript.

REFERENCES

1. Wechsler RJ. *Cross-sectional analysis of the chest and abdominal wall*. St. Louis: Mosby, 1989.
2. Cubillo E. Obturator hernia diagnosed by computed tomography. *AJR* 1983;140:735-736.
3. Weiss Y, Lernau OZ, Nissan S. Spigelian hernia. *Ann Surg* 1974;1180:836-839.
4. Kane VG, Silverstein GS. CT demonstration of hernia through an iliac crest defect. *J Comput Assist Tomogr* 1986;10:432-434.

Book Review

Endovaginal Ultrasound. By Steven R. Goldstein. New York: Alan R. Liss, 175 pp., 1988. \$55

This slender volume is presented as an overview of techniques and applications of endovaginal ultrasound in both obstetric and gynecologic examinations, providing both normal anatomy and a survey of pathologic entities. The book contains 12 chapters: "How to Begin: Basic Instrumentation and Method of Examination;" "Normal Pelvic Anatomy: What You Can Expect to See;" "Pelvic Masses: Endovaginal Sonographic Appearance;" "Pregnancy I: Embryo;" "Pregnancy II: Something Is Wrong;" "Pregnancy III: Fetus, First Trimester;" "Pregnancy IV: After the First Trimester;" "Ectopic Pregnancy;" "Routine Use of Ultrasound Prior to First-Trimester Termination;" "Ovulation Induction and Follicle Surveillance;" "In Vitro Fertilization and Embryo Transfer;" and "Incorporating Endovaginal Ultrasound into the Practitioner's Examining Room."

The first chapter contains a simply written and brief discussion of the physical principles of ultrasound that will be understood easily by practitioners who have no previous exposure to these concepts. Coverage of technique includes many useful practical hints, and normal anatomy is well demonstrated. Because the orientation of endovaginal scans is different from that of the familiar transabdominal views, addition of small orientation diagrams adjacent to the scans may be of value. A list of indications for endovaginal ultrasound accompanies a survey of the more commonly encountered gynecologic masses, with brief descriptions of each. Here, as elsewhere through the book, the intent does not seem to be encyclopedic coverage of the field but rather presentation of representative entities, an appropriate focus for a work of this size.

The obstetric sections are well documented with a liberal number of scans and considerable clinical obstetric information. Much of this may be obvious to the practicing obstetrician, but it is of particular value to radiologists who sometimes are forced to operate in something of a clinical void. For example, in dealing with the use of ultrasound before first-trimester termination, the author points out that precise estimation of the gestational age will aid significantly in determining how much cervical dilatation will be required. To the obstetrician, this is a given; to the radiologist, not so.

The discussion of ectopic gestation, a particularly important application of ultrasound, is complete, well documented with scans, and realistic. For example, the author observes, "Endovaginal ultrasound will be more successful at imaging (ectopic) pregnancies than traditional transabdominal techniques. It is unclear exactly how often this will be true." One of the most common and deleterious tendencies with a new technology is to oversell its capabilities and thus inevitably disappoint the referring clinicians, so such circumspection (and it is found throughout this book) is refreshing and well advised.

The chapters on infertility and in vitro fertilization are well written and documented; some of the historical perspective, although interesting, is perhaps less essential to the mission of the book. Somewhat the same is true of the last chapter, "Incorporating Endovaginal Ultrasound into the Practitioner's Examining Room." Some of this section is editorial, albeit probably accurate, and some elements (e.g., preparation of the patient and preparation and orientation of the probe) appear misplaced and would be more useful incorporated into chapter 1, "Basic Instrumentation and Method of Examination."

Overall, this is a timely, pertinent, well-written, and useful volume. It can provide a balanced introduction to endovaginal applications in two evenings of comfortable reading. The author and contributors are well-recognized authorities in the field and have produced their characteristic high-quality work. References are pertinent and not overwhelming, and reproduction of the scans is of good quality. The encouragement by the obstetrician-author of increased clinical involvement on the part of the radiologist (he dares to suggest the possibility of a pelvic examination by the radiologist!) is a thoughtful, mature position that only can result in improved communication and, ultimately, better care of patients.

Andrew M. Fried
Albert B. Chandler Medical Center
Lexington, KY 40536-0084

Endovaginal Sonographic Diagnosis of Dilated Fallopian Tubes

Franklin N. Tessler¹
 Rita R. Perrella¹
 Arthur C. Fleischer²
 Edward G. Grant¹

Twelve cases of fallopian tube dilatation were diagnosed in 10 patients by using endovaginal sonography. The diagnosis was confirmed by surgery in seven patients and by hysterosalpingography in three. A tubular shape was present in every case. Other sonographic features included a well-defined echogenic wall, a folded configuration, and linear echoes protruding into the tube lumen. Dilated tubes were distinguished from bowel loops by a lack of peristaltic activity and from pelvic veins by a lack of moving low-level echoes on real-time sonography.

We conclude that the findings of dilated fallopian tubes on endovaginal sonography are sufficiently characteristic to allow the diagnosis to be made with this technique.

AJR 153:523-525, September 1989

Sonography is a well-established technique for evaluating the female pelvis. Apart from abnormalities associated with ectopic pregnancy, however, few reports concern the sonographic features of fallopian tube abnormalities [1-6]. On conventional transabdominal sonograms, dilated tubes appear as complex cystic masses [2, 4]; hemosalpinx appears as a solid, echogenic mass [5]. No specific features have been identified that can distinguish tubal abnormalities from other pelvic abnormalities and normal structures [2, 4]. Because of its superior resolution, endovaginal sonography has the potential to characterize tubal abnormalities better. Using this technique, we identified four features that distinguish dilated fallopian tubes.

Materials and Methods

The sonograms and medical records of all women who underwent endovaginal sonography between 1986 and 1989 were reviewed. We identified 65 patients in whom fallopian tube dilatation was suspected at the time of the sonogram. No confirmation was available in 55 patients. The final study group consisted of 10 women in whom tubal dilatation was confirmed by surgery (five patients), laparoscopy (two patients), or hysterosalpingography (three patients). Of the five women who underwent surgery, hydrosalpinx was found in three, pyosalpinx in one, and hemosalpinx in one. The women ranged in age from 20 to 62 years. All patients were scanned with dedicated 5.0- or 3.0-MHz endovaginal transducers (Advanced Technology Laboratories, Bothell, WA, and Toshiba, Tustin, CA) by using standard technique.

The sonograms were reviewed retrospectively by one author, who was aware of the diagnosis of fallopian dilatation in every case. On each sonogram, a structure that was proved to represent a dilated fallopian tube was identified and analyzed for four specific features: (1) tubular shape, (2) a well-defined echogenic wall, (3) a folded configuration, and (4) short, linear echoes protruding into the lumen.

Results

Twelve dilated fallopian tubes were diagnosed in 10 patients. The degree of dilatation ranged from 1 to 4 cm (mean, 2 cm). A tubular structure was present on

Received March 7, 1989; accepted April 4, 1989

¹ Department of Radiological Sciences, UCLA School of Medicine, CHS BR-272, 10833 Le Conte Ave., Los Angeles, CA 90024-1721. Address reprint requests to F. N. Tessler.

² Department of Radiology, Vanderbilt University Medical Center, Nashville, TN 37232.

0361-803X/89/1533-0523

© American Roentgen Ray Society

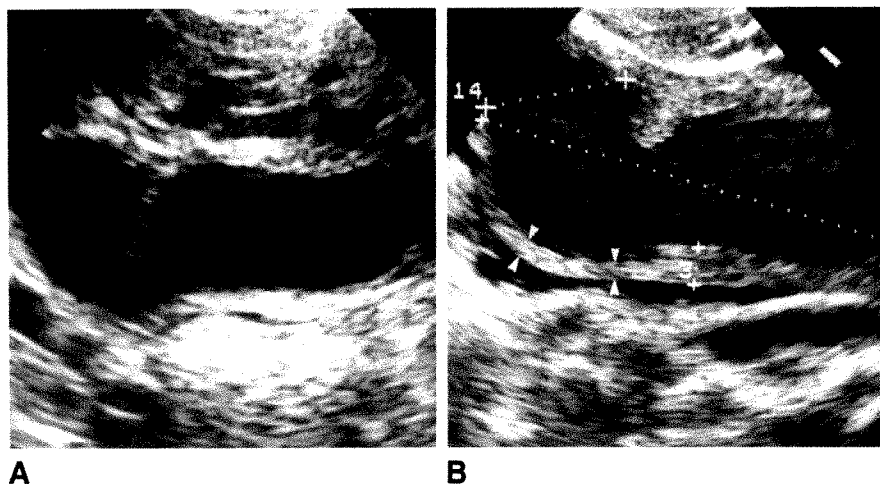


Fig. 1.—A, Sagittal endovaginal sonogram of left adnexal region shows a 1.6-cm tubular structure characteristic of a dilated fallopian tube, which proved to be pyosalpinx at surgery.

B, Right sagittal endovaginal sonogram shows a 2.3-cm tubular structure with a well-defined echogenic wall (between arrowheads), which proved to be pyosalpinx at surgery.

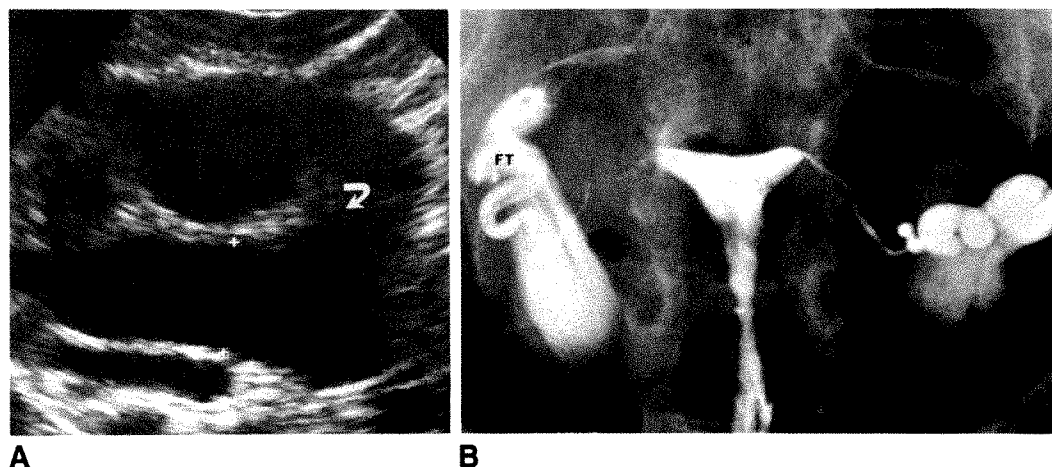


Fig. 2.—A, Oblique endovaginal sonogram of right adnexal region shows a 2.7-cm tubular structure with a folded appearance (curved arrow).

B, Hysterosalpingogram confirms dilated right fallopian tube (FT).

every sonogram (Fig. 1A). In eight cases, the structure had a well-defined, echogenic wall, and in six cases it had a folded configuration (Figs. 1B and 2). Linear echoes protruded into the tube lumen in five cases (Fig. 3). Three of the four features were found in seven tubes, and two features were seen in the other five cases.

Discussion

Considering their narrow diameter (1–4 mm) [7], the inability to identify normal fallopian tubes on sonograms is not surprising. When distended by a sufficient amount of fluid, however, the tubes should be easily visible. On standard trans-abdominal sonograms, dilated fallopian tubes usually have a nonspecific appearance and often are indistinguishable from other pelvic fluid collections and masses [2, 4]. Lande et al. [8] described five of 12 patients with tubo-ovarian abscesses in whom tubular fluid collections were seen on endovaginal sonograms. Aside from a cylindrical shape, however, they did not describe specific findings that would distinguish dilated fallopian tubes from other pelvic abnormalities.

As expected, the most consistent sonographic feature of fallopian tube dilatation in our patients was a tubular structure with a folded configuration. The wall of the structure was

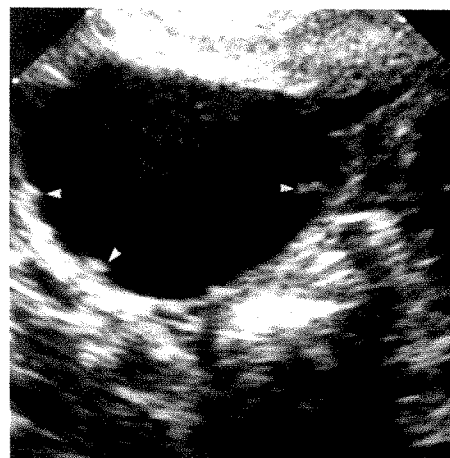


Fig. 3.—Transverse endovaginal sonogram of right adnexal region shows a fluid-filled structure with short, linear echoes protruding into lumen (arrowheads). Dilated fallopian tube was seen at laparoscopy.

typically well defined and echogenic. This echogenic appearance has been described in patients with acute salpingitis [9]. Half of our cases had short, linear echoes protruding into

the lumen, a feature that may be related to the wrinkled nature of the fallopian tube epithelium [7].

Distended pelvic veins, a common finding on endovaginal sonography, have a tubular appearance when imaged along their long axis. However, blood flow within them usually causes multiple low-level moving echoes on real-time sonography. Bowel loops also can resemble dilated fallopian tubes. However, peristaltic motion is almost always evident in bowel loops, even if only transiently. The rectosigmoid colon is easily identified by administering a water enema, and the colon often has distinctive haustral markings. Adnexal masses may have some of the features of dilated fallopian tubes. However, if an ovarian origin can be established, fallopian tube dilatation can be excluded. Moreover, in our experience, adnexal masses are rarely elongated and do not possess a well-defined echogenic wall. We conclude that the findings of dilated fallopian tubes on endovaginal sonography are sufficiently characteristic to allow the diagnosis to be made with this technique.

REFERENCES

1. Warner MA, Fleisher AC, Edell SL, et al. Uterine adnexal torsion: sonographic findings. *Radiology* **1985**;154:773-775
2. Reuter K, Cohen S, Daly D. Ultrasonic presentation of giant hydrosalpinges in asymptomatic patients. *JCU* **1987**;15:45-50
3. Meyer JS, Kim CS, Price HM, et al. Ultrasound presentation of primary carcinoma of the fallopian tube. *JCU* **1987**;15:132-134
4. Russin LD. Hydrosalpinx and tubal torsion: a late complication of tubal ligation. *Radiology* **1986**;159:115-116
5. Subramanyam BR, Raghavendra BN, Balthazar EJ, et al. Hematosalpinx in tubal pregnancy: sonographic-pathologic correlation. *AJR* **1983**;141:361-365
6. Richman TS, Viscomi GN, deCherney A, Polan ML, Alcebo LO. Fallopian tubal patency assessed by ultrasound following fluid injection. *Radiology* **1984**;152:507-510
7. Warwick R, Williams PL. *Gray's anatomy*. London: Longman, **1973**:1354-1356
8. Lande IM, Hill MC, Cosco FE, Kator NN. Adnexal and cul-de-sac abnormalities: transvaginal sonography. *Radiology* **1988**;166:325-332
9. Terry J, Forrest T. Sonographic demonstration of salpingitis: potential confusion with appendicitis. *J Ultrasound Med* **1989**;8:39-41



The Radiology Outreach Foundation (ROF) is a nonprofit corporation whose goal is to help disadvantaged countries improve their health care by providing radiology equipment, books, consultation, education, and training to their practitioners. This assistance is on an application basis that is independent of political, ethnic, or religious orientation of the grantee. It depends on the need of the people and the ability of the ROF to meet that need. The ROF is approved by the U.S. Internal Revenue Service as a tax-exempt organization. It is endorsed by the following radiologic societies: American Association of Women Radiologists, American College of Radiology, American Roentgen Ray Society, Association of University Radiologists, Radiological Society of North America, Society of Chairmen of Academic Radiology Departments, Society for Pediatric Radiology, European Society of Pediatric Radiology.

All donations to the ROF are tax deductible. Persons who would like to contribute financially to the ROF, would be interested in being a visiting professor, would like to send books or journals to any of the institutions supported by the ROF, or would like further information about the ROF should write to Charles A. Gooding, M.D., President, Radiology Outreach Foundation, 3415 Sacramento St., San Francisco, CA 94118 USA.

Book Review

Applied Pathology for Radiographers. By Paul F. Laudicina. Philadelphia: Saunders, 326 pp., 1989. \$32.95

This text has been written for "second year and graduate radiographers with a basic working knowledge of pathology as it pertains to diagnostic medical radiography." Each chapter begins with objectives and ends with a quiz; at the end of the book is a large glossary. The eight chapters deal with principles of pathology, the respiratory system, the alimentary tract, the hepatobiliary system, the genitourinary system, the osseous system and joints, the CNS, and neoplasia. There is no chapter on the cardiovascular system.

The first chapter deals with various pathologic processes in a rudimentary manner. In general, this chapter deals with mortality and not with morbidity. In fact, morbidity is not discussed throughout the book. The other chapters follow the format: general information, diagnosis and identification, and treatment.

Although the goals of the text are admirable, certain deficits permeate the book and deter the author from achieving his goals. First, the book does not deal with the effects of new technology in showing pathology and, to a greater extent, ignores nuclear medicine. The author discusses the IV pyelogram as the best test of renal function. The sonograms in the text are not of high quality, and their white background shows them to be quite old. No CT scans of the chest are shown. Second, the indications for examinations and the technique that will bring out the pathology are not discussed. These considerations seem crucial to a radiographer who is trying to learn pathology. Third, in many instances, the general information given either is not correct or is outdated. For example, diagnosis of cystic fibrosis now can be made before birth. Also, the mortality rate with hyaline membrane disease is not 50% nor is there a higher incidence of hyaline membrane disease with cesarean section; and the incidence of retrolental fibroplasia or retinopathy of prematurity is increas-

ing now, not decreasing. The recommendation shown in the illustrations of Gastrografin as a primary agent in esophageal atresia (page 54) is clearly wrong, because aspiration of such contrast will cause pulmonary edema immediately. The discussion about Meckel diverticulum is erroneous: Meckel diverticulum is rarely seen on an upper gastrointestinal series, and the most common presentation in children is painless bleeding. Fourth, many of the findings in the radiographs are not described. Figures 2-11 and 2-14 show the same neonate with hyaline membrane disease. The caption reads "16 month old boy with hyaline membrane disease." A pneumomediastinum is not described, nor is a subcutaneous emphysema described in Figure 2-13. Figure 3-23 shows pyloric stenosis, but the classic findings are not present nor is any description of them given. Figures 3-30, 3-31, and 5-18 are printed backward. In the chapter on bone, a discussion concerning achondroplasia includes an illustration of a thanatophoric dwarf; the caption of the figure is correct, but there is no discussion of thanatophoric dwarfs.

Several of the technologists in our department reviewed this text in a cursory manner. They found it was easy reading, but they could not evaluate the areas of my concern (those areas in which the information is not correct). In fact, they skipped some of the discussion because "it was too much to read" and without apparent value.

The concept of a book on applied pathology for radiographers is a good one. However, I think that, for the above-mentioned reasons, this text does not reach its mark.

Thomas L. Slovis
Children's Hospital of Michigan
Detroit, MI 48201

Case Report

Papillary Cystadenoma of the Broad Ligament in a Patient with von Hippel-Lindau Disease

Kevin C. Funk¹ and Jay P. Heiken²

Papillary cystadenoma of the epididymis is a rare tumor seen in men with von Hippel-Lindau disease. The mesonephric (wolffian) origin of this benign tumor suggests a female counterpart located in the broad ligament, near the fallopian tube [1]. We present a case of papillary cystadenoma of the broad ligament in a woman with von Hippel-Lindau disease and illustrate its appearance on CT.

Case Report

A 46-year-old woman with von Hippel-Lindau disease diagnosed 25 years earlier presented for evaluation of an abdominal mass in the left upper quadrant. Urinalysis showed five RBCs per high-power field. CT of the abdomen and pelvis showed the mass to be a 20-cm simple cyst arising from the upper pole of the left kidney. Numerous smaller cysts were present throughout both kidneys in addition to a 4-cm solid mass in the lower pole of the right kidney, consistent with a renal cell carcinoma. Cysts also were present in the liver, pancreas, and right ovary. A 2.5 × 3.0 cm mass in the left adnexal region contained areas of water attenuation and soft-tissue attenuation (Fig. 1). Several curvilinear calcifications were at the periphery of the mass.

A right nephrectomy was performed to remove the renal cell carcinoma from the lower pole. The right ovarian cyst and left adnexal mass also were identified at surgery and excised.

On pathologic examination, the adnexal mass was found to be located within the left mesosalpinx and separate from the ovary and the fallopian tube. It was multicystic with partially calcified walls. Centrally, the cysts contained papillary structures composed of his-

tologically benign, relatively vacuolated cuboidal cells covering stromal pegs. The cytologic features of the neoplasm suggested a mesonephric derivation, and the appearance was identical to that of the epididymal cystadenomas seen in men with von Hippel-Lindau syndrome.

Discussion

Von Hippel-Lindau disease is an autosomal dominant disorder with variable penetrance. The lesions primarily responsible for morbidity and mortality in patients with the disease are retinal angiomas, CNS hemangioblastomas, renal cell carcinomas, and paragangliomas [2]. In addition, patients with von Hippel-Lindau syndrome may develop cystic lesions involving numerous body organs, including the lung, liver, spleen, pancreas, kidney, ovary, omentum, and epididymis [2].

Papillary cystadenoma of the epididymis is a rare tumor seen in 10–40% of men with von Hippel-Lindau disease [2, 3]. The mesonephric (wolffian) origin of this benign tumor has led some investigators to postulate the existence of a female counterpart [1]. Brief mention is made in the case records of the Massachusetts General Hospital [4] of bilateral broad ligament papillary cystadenomas in a woman with von Hippel-Lindau disease.

Mesonephric remnants in females include the epoophoron, paroophoron, and Gartner duct [5]. Lesions of mesonephric

Received February 24, 1989; accepted after revision April 4, 1989.

¹ Department of Radiology, Eastern Idaho Regional Medical Center, 3100 Channing Way, Idaho Falls, ID.

² Mallinckrodt Institute of Radiology, Washington University School of Medicine, 510 S. Kingshighway Blvd., St. Louis, MO 63110. Address reprint requests to J. P. Heiken.

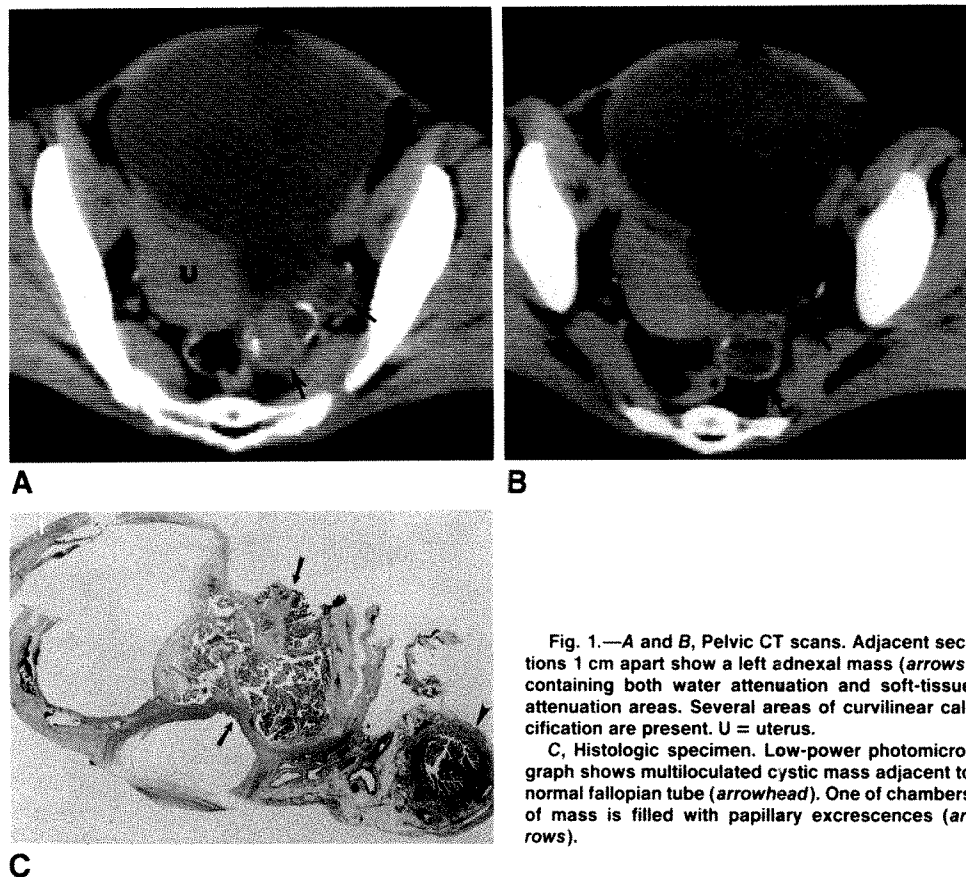


Fig. 1.—A and B, Pelvic CT scans. Adjacent sections 1 cm apart show a left adnexal mass (arrows) containing both water attenuation and soft-tissue attenuation areas. Several areas of curvilinear calcification are present. U = uterus.

C, Histologic specimen. Low-power photomicrograph shows multiloculated cystic mass adjacent to normal fallopian tube (arrowhead). One of chambers of mass is filled with papillary excrescences (arrows).

and paramesonephric origin are found in the portion of the broad ligament near the fallopian tube (the mesosalpinx). Histologic criteria exist to classify parovarian lesions as being of mesonephric (wolffian), paramesonephric (müllerian), or mesothelial derivation, although occasionally the distinction is difficult [6]. Benign epithelial parovarian cysts of paramesonephric origin are very common, but usually are small and clinically insignificant [7]. During pathologic examination of over 2000 specimens, parovarian cysts were identified in nearly 92% of cases [8]. Benign and malignant papillary serous parovarian neoplasms with microscopic paramesonephric (müllerian) features have been described [6, 8]. However, broad ligament papillary cystadenomas of mesonephric (wolffian) origin, analogous to the epididymal lesion seen in men with von Hippel-Lindau disease, have rarely been documented before.

Our case shows a papillary cystadenoma of mesonephric origin in a woman with von Hippel-Lindau disease and depicts the CT appearance of this lesion. On the basis of CT features alone, it would be impossible to differentiate this mass from a small cystic ovarian neoplasm (cystadenoma or cystaden-

ocarcinoma) or from ovarian cysts complicated by old hemorrhage or chronic infection.

REFERENCES

1. Witten FR, O'Brien DP III, Sewell CW, Wheatley JK. Bilateral clear cell papillary cystadenoma of the epididymides presenting as infertility: an early manifestation of von Hippel-Lindau's syndrome. *J Urol* **1985**;133:1062-1064
2. Horton WA, Wong V, Eldridge R. Von Hippel-Lindau disease: clinical and pathological manifestations in nine families with 50 affected members. *Arch Intern Med* **1976**;136:769-777
3. Price EB Jr. Papillary cystadenoma of the epididymis. A clinicopathologic analysis of 20 cases. *Arch Pathol Lab Med* **1971**;91:456
4. Scully RE, Galdabini JJ, McNeely BU. Case records of the Massachusetts General Hospital. *N Engl J Med* **1978**;298:95-101
5. Moore KL. *The developing human*, 2nd ed. Philadelphia: Saunders, **1977**:239
6. Genandry R, Parmley T, Woodruff JD. The origin and clinical behavior of the parovarian tumor. *Am J Obstet Gynecol* **1977**;129:873
7. Honoré LH. Pathology of the fallopian tube. In: Fox H, ed. *Haines and Taylor obstetrical and gynecological pathology*, 3rd ed. New York: Churchill Livingstone, **1987**:510-513
8. Honoré LH, O'Hara KE. Serous papillary neoplasms arising in paramesonephric parovarian cysts. *Acta Obstet Gynecol Scand* **1980**;59:525-528

Occult Fractures of the Carpals and Metacarpals: Demonstration by CT

B. W. Hindman¹
W. J. Kulik
G. Lee
R. E. Avolio

Occult fractures of the carpals and metacarpals occur frequently and are associated with major disability. The cross-sectional display and superior resolution of CT are well suited to the demonstration of these fractures. Sixteen patients with persistent pain and negative conventional radiographs were chosen for further evaluation by CT. Imaging was performed in two planes and showed 21 fractures. The transaxial plane was the most revealing imaging plane. Coronal imaging was equal or superior to the transaxial plane in most fractures of the scaphoid, lunate, capitate, and pisiform bones and of the bases of the metacarpal bones. The direct sagittal plane was the best imaging plane in one patient with fractures of the scaphoid and lunate bones. After discovery of the fracture on CT, surgical removal of the avulsed fracture fragment was recommended in seven patients and fusion was recommended in three. Eight patients had a marked decrease in pain after the surgical procedure.

The accuracy of CT for the demonstration of occult fractures may result in earlier recognition of these fractures and a reduction in the associated disability.

AJR 153:529-532, September 1989

The hand and wrist are the most commonly injured body parts [1], and these injuries are frequently work-related. Fractures of the carpals and metacarpals account for 6% of all fractures [2], and occult fractures would substantially increase this percentage if their prevalence could be accurately determined. These fractures may be associated with long-term disability, consisting of persistent pain, weakness, or limitation of motion, and these fractures may be missed for a prolonged period of time or never found. The cross-sectional display and superior resolution make high-resolution CT an important imaging technique in the evaluation of the radiographically negative wrist with persistent pain. CT can facilitate early recognition of these occult fractures and may thereby reduce the associated disability.

Materials and Methods

A retrospective review of over 200 CT scans of the wrist revealed 16 patients with 21 occult fractures. These 16 patients had a history of trauma and persistent pain in the presence of negative radiographs. CT was performed to rule out the existence of an occult fracture. The fractures usually were imaged in subacute or chronic periods. In some cases a fracture was unsuspected clinically. Conventional radiography of the wrist included the standard posteroanterior, lateral, and pronation oblique views. Additional views, determined by the fracture suspected, included ulnar deviation views for patients who clinically were suspected of having scaphoid fractures and carpal tunnel views for hamate fractures. Radiographic findings were suspicious in three of the 16 patients. Possible fractures of the hamate, lunate, and triquetral bones were noted. In these cases, CT was used to confirm the actual existence and extent of the fracture. In two cases, the fractures of the scaphoid and triquetral bones could be identified retrospectively.

CT was performed on a General Electric 9800 scanner (General Electric, Milwaukee, WI). The wrist was supported with an extremity positioning device (Omega Scan Systems, Los

Received April 7, 1989; accepted after revision May 15, 1989.

Presented at the annual meeting of the American Roentgen Ray Society, New Orleans, May 1989.

¹ All authors: Flower Imaging Medical Group, 2300 S. Flower St., Suite 100, Los Angeles, CA 90007. Address reprint requests to B. W. Hindman.

0361-803X/89/1533-0529
© American Roentgen Ray Society

Angeles, CA) that allowed comfortable immobilization of the wrist throughout the period of the examination (Fig. 1). Contiguous 1.5-mm-thick slices were obtained by using a fast-scan technique of 120 kV, 70 mA, and 3-sec scan time with interscan delay of 4.5 sec. Axial imaging of both wrists was performed, and the symptomatic wrist was also imaged in the semicoronal plane. Occasionally, direct semisagittal images of the wrist were added (Fig. 1). The images were displayed by using a bone algorithm and a small displayed field of view (12.8–14 cm). The images were photographed at level and window settings for bone detail. Four skeletal radiologists reviewed the studies, and the radiographs, history of previous trauma, and site of pain accompanied their review.

Results

Twenty-one fractures of the carpal bones and metacarpal bases in 16 patients were diagnosed on the basis of CT findings between November 1984 and August 1988. Injury to the wrist had occurred as recently as 11 days and as long ago as 4 years before the CT study. Fractures were identified on CT in all of the carpal bones except the trapezoid. The hamate bone was the most commonly fractured bone. There were four fractures of the hook of the hamate bone and one fracture of the medial volar surface (Fig. 2). Unsuspected fractures of the scaphoid bone occurred in three patients (Fig. 3). In five cases, there were fractures of more than one bone. The three occult scaphoid fractures were associated with fractures of the lunate bone. In one case, the pisiform and triquetral bones were fractured (Fig. 4), and in the other case the hook of the hamate and the second metacarpal bones were fractured.

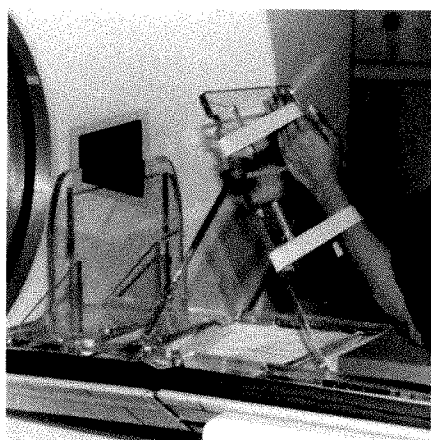
Healing of the fracture could be clearly identified in two patients and there was evidence of nonunion in two patients. One fracture occurred through a cystic area in the capitate bone (Fig. 5), and CT showed a sclerotic fragment consistent with a focus of avascular necrosis. Three patients had fractures of the metacarpal bases (Fig. 6).

The importance of finding the fractures can be inferred from the clinical improvement following the surgical removal of the avulsed fragment in six patients and the fusion of two or more carpal bones in two patients. Two patients had clinical improvement with evidence of fracture healing after immobilization.

Discussion

Carpal and metacarpal fractures may go unrecognized and result in major disability. Conventional radiography has been the principal technique for demonstrating these fractures, but well-positioned studies may be difficult to perform because of pain associated with the injury. Fractures may not be shown because of superimposition of the bony parts. CT, because of its cross-sectional display and superior resolution, is well suited to the evaluation of small bony parts. In our experience, CT is best performed in two imaging planes. In this series, the transaxial plane was the most revealing. The ability to compare the normal and abnormal sides resulted in the diagnosis of fractures that otherwise might have been missed. Partial voluming of the carpal bones was a potential deficiency of cross-sectional imaging. When partially volumed, carpal and metacarpal prominences can appear to represent small avulsed fragments. This problem can be minimized by imaging the opposite wrist for comparison and by the use of a second imaging plane. Patient comfort and immobilization of the wrist are important considerations. The use of a rigid platform is key to achieving images that display crisp trabecular detail and decrease the need to repeat studies. A positioning device is well suited for this task and provides comfortable immobilization of the patient's wrist. A two-plane study can be performed in about 30 min.

In seven of eight cases, fractures of the hamate, triquetral, and trapezium bones were best imaged in the transaxial plane. In three cases, fractures of the triquetral, capitate, and



A



B

Fig. 1.—Immobilization and positioning of wrist for CT scanning.

A, Photograph shows wrist supported in extremity positioning device for scanning in semisagittal plane.

B, Digital scan of wrist shows plane of semisagittal sections. Off-axis plane for sagittal images reduces streak artifact from long-bone cortices.



Fig. 2.—Hamate fractures were the most common occult fractures. Transaxial CT scan reveals small avulsed fragment from ulnar side of hamate bone (arrow).

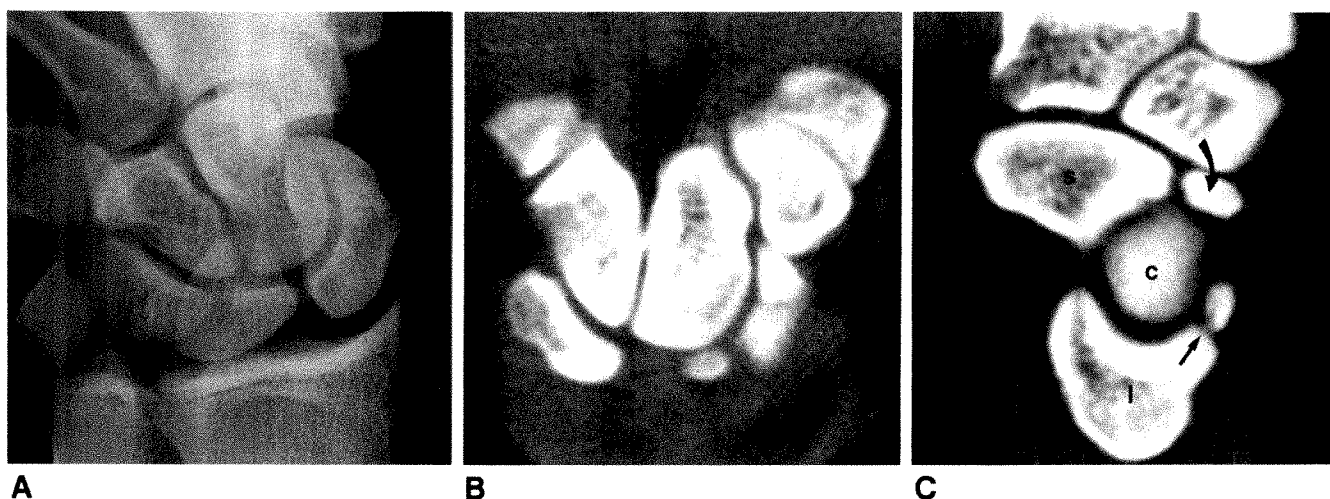


Fig. 3.—Off-axis sagittal and coronal imaging of scaphoid bone can be helpful in demonstrating occult fracture.

A, Posteroanterior radiograph with ulnar deviation shows dissociation at scapholunate joint but no evidence of scaphoid fracture. Oval fragment between scaphoid and lunate bones represents avulsed lunate fracture fragment.

B, Transaxial CT scan shows fractures of midportion of scaphoid bone and avulsed fragment from lunate bone.

C, Semisagittal CT scan shows avulsed fragments from lunate (straight arrow) and scaphoid (curved arrow) fractures. l = lunate bone; s = scaphoid bone; c = capitate bone. (Refer to digital image, Fig. 1B.)

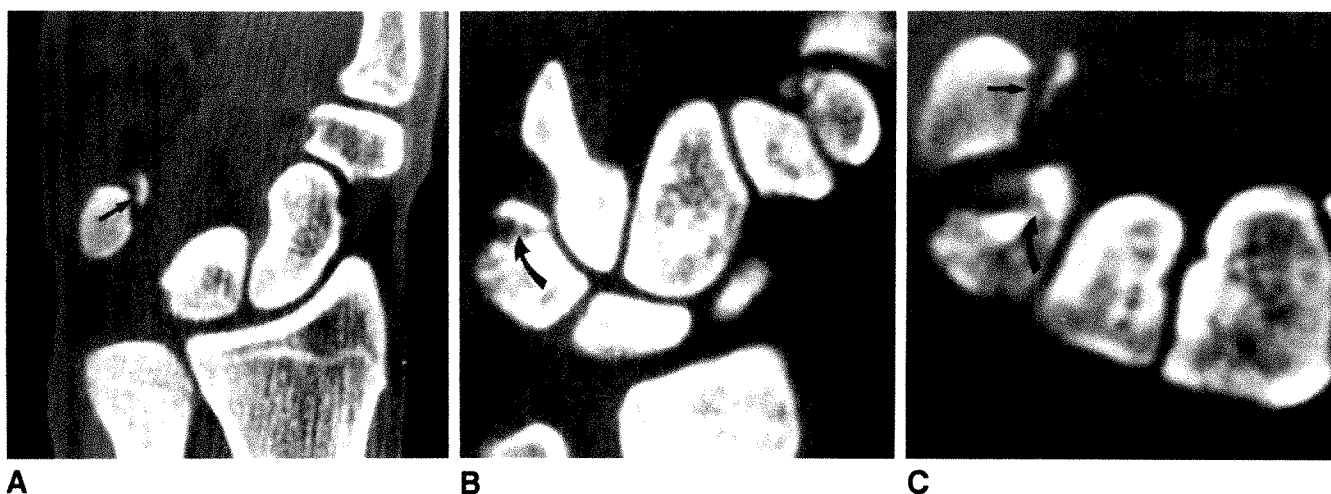


Fig. 4.—CT may show second fracture in hand or wrist with one radiographically apparent fracture. Oblique radiograph showed fracture of os triquetrum.

A and B, Coronal CT scans at levels of pisiform (A, straight arrow) and triquetrum (B, curved arrow) fractures.

C, Transaxial CT scan shows fractures of both pisiform (straight arrow) and triquetrum (curved arrow) bones.

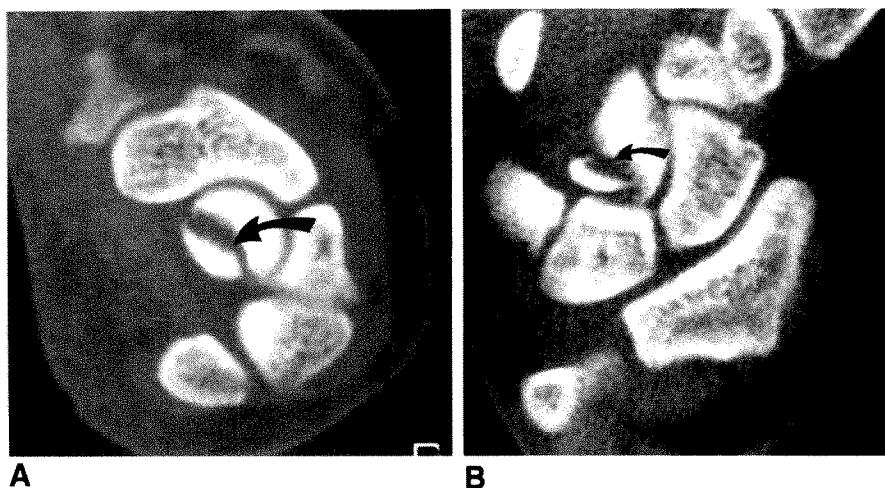


Fig. 5.—CT can identify underlying process in occult pathologic fractures. All radiographs were normal.

A and B, Transaxial (A) and coronal (B) CT scans show fracture in area of lucency in capitate bone (arrows).

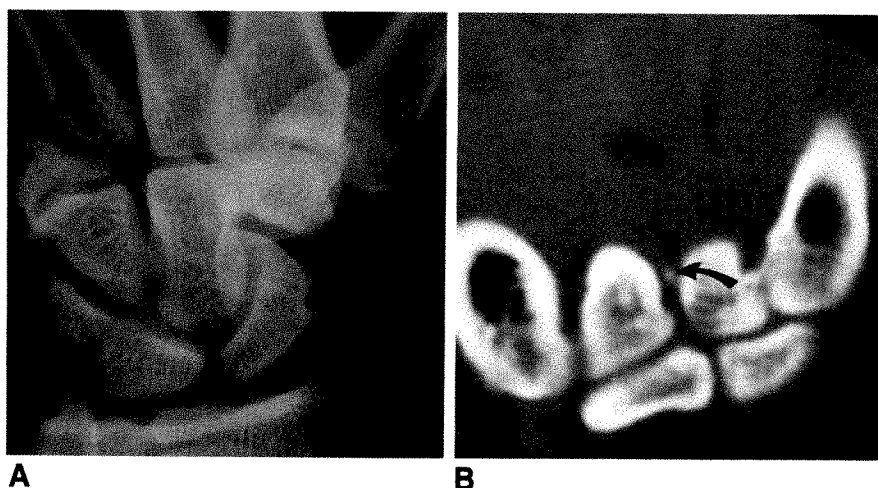


Fig. 6.—Occult metacarpal fractures are difficult to show radiographically.

A, Oblique radiograph shows widened space between third and fourth metacarpal bones resulting from ligamentous tear, but no evidence of fracture.

B, Coronal CT scan at level of metacarpal bases shows avulsed fracture fragment (arrow) from one metacarpal base.

pisiform bones could be identified well in either the coronal or transaxial plane. Fractures of the scaphoid bone were best imaged in the coronal plane in two cases and in the sagittal plane in one. Fractures of the lunate bone were best identified in the coronal plane in two cases, in the transaxial plane in one, and in the sagittal plane in another. Fractures of the metacarpal bases were best shown in the coronal plane in two cases and in the transaxial plane in one. Biondetti et al. [3] reported their experience with CT of the wrist in 23 patients. They found the coronal plane the most helpful, and indicated that examination in this single plane was sufficient. This observed difference from our series probably reflects the type of fractures studied, as only four of their 23 cases appear to be occult fractures. The optimal imaging plane should be perpendicular to the fracture line. The selection of the imaging planes should be determined by the fracture clinically suspected, but should always include the transaxial plane.

CT is a rapid and comfortable method of examining the wrist. The occult fracture, which may be associated with substantial disability, can be shown more easily with CT. CT can be a valuable diagnostic tool in the evaluation of the patient with wrist trauma in which an explanation for the patient's symptoms cannot be shown with conventional imaging studies.

REFERENCES

1. Curtis DJ. Injuries of the wrist: an approach to diagnosis. *Radiol Clin North Am* 1981;19:625-644
2. Emmett JE. A review and analysis of 11,000 fractures seen in a private practice of orthopaedic surgery. *J Bone Joint Surg [Am]* 1958;40-A:1169-1175
3. Biondetti PR, Vannier MW, Gilula LA, Knapp R. Wrist: coronal and transaxial CT scanning. *Radiology* 1987;163:149-151

Anatomic Relations Between the Median Nerve and Flexor Tendons in the Carpal Tunnel: MR Evaluation in Normal Volunteers

Jacob Zeiss¹
 Martin Skie²
 Nabil Ebraheim²
 W. Thomas Jackson²

To ascertain the dynamic changes between the median nerve and flexor tendons in the carpal tunnel, MR images of 16 wrists in eight volunteers were studied in flexion, extension, and neutral positions. T1-weighted axial images, 600/20 (TR/TE), were obtained with the wrists straight, extended at 45°, and flexed at 45°. Each scan was evaluated with regard to positional changes of the median nerve and flexor tendons in the carpal tunnel as well as alterations in nerve shape. In the neutral position, the median nerve was found in one of two standard positions: either anterior to the superficial flexor tendon of the index finger or interposed more posterolaterally between this tendon and the flexor pollicis longus. During extension, the nerve always maintained or assumed an anterior position between the superficial index finger flexor and the flexor retinaculum, while the flexor tendons moved posteriorly. With flexion, the tendons shifted anteriorly toward the retinaculum, and the median nerve was found in one of three positions. It either remained in its anterior position between the superficial index finger flexor and retinaculum or became interposed between the superficial flexor tendons of the index finger and thumb or middle finger and ring finger. Nerve shape varied with its position. Anteriorly positioned nerves were flattened in the anteroposterior plane between the tendon and flexor retinaculum; this was greatest with flexion and least with extension. Interposed nerves were flattened in the mediolateral plane or rounded in configuration.

In conclusion, the alignment of the median nerve in the carpal tunnel, its shape, and its relationship to the flexor tendons were variable and dependent on wrist positioning. These findings may explain why certain wrist motions, flexion in particular, predispose a person to carpal tunnel syndrome.

AJR 153:533-536, September 1989

MR imaging of the carpal tunnel has become a widely accepted means of investigating the median nerve entrapment syndrome, with the nerve consistently identifiable on standard axial views [1, 2]. Its relationship and proximity to the transverse carpal ligament (flexor retinaculum) and flexor tendons result in some flattening, lobulation, or even slight triangulation of its usually rounded shape, even in normal instances [3].

One of the presumed mechanisms of carpal tunnel syndrome is an exaggeration of these extrinsic effects on the median nerve [4]. Initial studies proposed repeated wrist extension as a major mechanism in the production of median nerve neuropathy [5]. Subsequent investigations, however, indicated wrist flexion to be a much more likely predisposing mechanism [6-8].

The purpose of this study was to examine the normal relationships of the median nerve and flexor tendons in the carpal tunnel that exist when the wrist is in neutral position and when the wrist is in flexion and extension.

Subjects and Methods

A total of 16 wrists from three men and five women, 25-32 years old, were evaluated. All subjects but two were chosen at random from a healthy and asymptomatic volunteer pool of

Received March 20, 1989; accepted after revision May 15, 1989.

¹ Department of Radiology, Medical College of Ohio, P.O. Box 10008, Toledo, OH 43699-0008. Address reprint requests to J. Zeiss.

² Department of Orthopaedic Surgery, Medical College of Ohio, Toledo, OH 43699-0008.

0361-803X/89/1533-0533
 © American Roentgen Ray Society

medical students, physicians, and radiology department staff members. Two additional volunteers were included who had had previous episodes of conservatively treated carpal tunnel syndrome. MR scans were obtained with the wrists secured in prefabricated splints in neutral position, 45° extension, and 45° flexion. In eight of the examinations the fingers were gently flexed; in the other eight, the fingers were straight in a neutral position.

Imaging was performed on a 1.5-T General Electric Signa MR scanner using a General Electric extremity coil. T1-weighted axial images, 600/20 (TR/TE), were obtained as 3-mm-thick slices in an interleaved fashion. A 12-cm field of view was used with a 256 × 128 matrix and two excitations.

The shape and position of the median nerve and the orientation of the flexor tendons were studied on all scans. The effect of finger flexion was also evaluated by comparing scans obtained with the fingers in different positions. Separate evaluations were done by three of the authors who were aware of wrist position only. All evaluations were done directly off a physician console monitor so that window and level settings could be used to optimize correct anatomic identification. Discrepancies were resolved by majority opinion during a subsequent group evaluation with the use of monitor images and hard copies. The effect of finger position was evaluated on hard copies only by side-to-side comparison in group discussion.

Key to Abbreviations Used in Figures

FPL	flexor pollicis longus
FR	flexor retinaculum
MN	median nerve
P2	profundus 2
P3	profundus 3
P4	profundus 4
S2	sublimis 2
S3	sublimis 3
S4	sublimis 4

Results

The right and left wrists in each individual were essentially mirror images with only minor positional variations. Therefore, they could be treated as paired sets.

In the neutrally positioned wrists the median nerve was found in one of two positions: 12 were anterior to the superficial flexor tendon of the index finger (sublimis 2) and four were interposed more posterolaterally in the "slot" between sublimis 2 and the flexor pollicis longus. In the anterior location, side-to-side positioning was variable: eight nerves were anterolateral to sublimis 2, two were immediately anterior to it, and two were anteromedial to sublimis 2. In the more posterolateral interposed location, front-to-back positioning was variable, with two nerves anterior to the deep flexor tendon of the index finger (profundus 2) and two nerves adjacent to its lateral aspect. Figures 1 and 2 show the anterior and posterolateral interposed positions, respectively. Nerve shape in both locations was oval, but the long axis of the anterior nerves was in the mediolateral direction, while in the lateral interposed nerves, the long axis was in the antero-posterior direction. The effect of finger flexion in the neutral wrist was negligible.

With wrist extension all nerves were found anteriorly between sublimis 2 and the flexor retinaculum, while the flexor tendons made a slight posterior shift. Again some side-to-side variability in nerve position was noted: six were anterolateral to sublimis 2, six were anteromedial to it, and four were directly anterior to it. Figure 3 illustrates the extension position. Nerve shape was more rounded than in the neutral position though still slightly oval, long axis mediolaterally. Finger position had no discernible effect.

With wrist flexion, a slightly variable but consistent volar shift of flexor tendons occurred. As a result the tendons were lined up more closely to the flexor retinaculum, and the usual

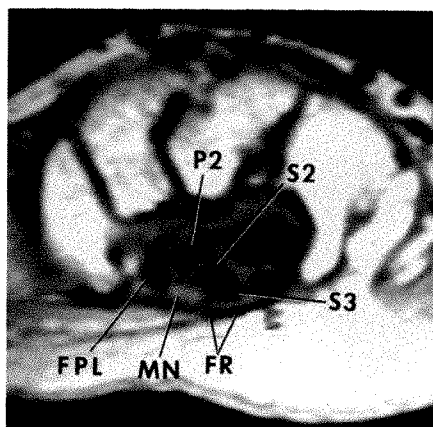


Fig. 1.—MR image (600/20) shows most common position of median nerve in a neutral wrist. It is just anterior and slightly radial to sublimis 2. (See key for abbreviations.)

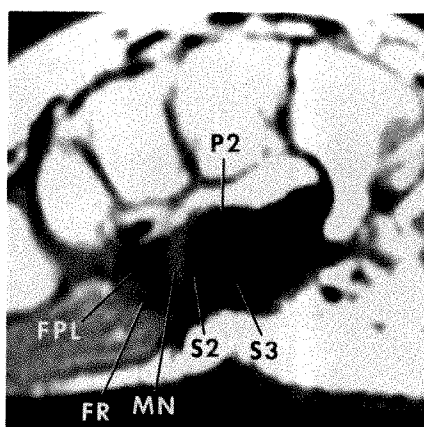


Fig. 2.—MR image (600/20) shows median nerve interposed between flexor pollicis longus and sublimis 2 and bordered dorsally by profundus 2 when wrist is in neutral position. (See key for abbreviations.)

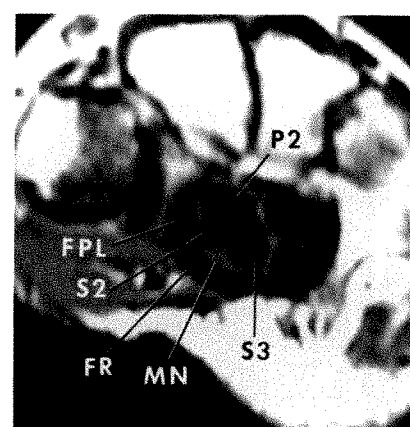


Fig. 3.—MR image (600/20) of wrist in 45° extension shows dorsal shifting of flexor tendons relative to neutral and anterior positioning of median nerve. Both anterior and interposed neutral nerves assume this position on extension. (See key for abbreviations.)

2–3 mm of free space between tendons and retinaculum in neutral and extension was attenuated. The median nerve was found in one of three positions: four were anterior to sublimis 2, eight were interposed posterolateral to this position between sublimis 2 and the flexor pollicis longus, and four were interposed posteromedially between sublimis tendons 3 and 4. Figures 4–6 are respective MR examples. Table 1 denotes the position changes of each nerve in neutral, extension, and flexion. Nerve shape was flattened anteroposteriorly for anterior nerves, flattened mediolaterally for laterally interposed nerves, and rounded for the medially interposed nerves. The degree of nerve flattening was greatest with flexion, intermediate in neutral position, and least with extension. The effect of finger positioning was subtle, but flexion slightly exaggerated the volar tendon shift and flattening of nerve shape.

Discussion

In a neutral wrist the median nerve was typically anterior to sublimis 2, especially anterolateral, as illustrated in Figure 1. This is the "standard" position described in previous anatomic and radiographic studies that used CT and MR [1–3, 9]. The laterally interposed position shown in Figure 2 with the nerve lying between sublimis 2 and the flexor pollicis longus is a variant of normal; examples of this have been described in previous anatomic [3] and MR [1, 10] studies.

Our examination of the wrist in flexion and extension indicated that the neutral alignment is not necessarily maintained throughout a range of motion. Wrist extension produced a posterior shift of flexor tendons and a uniformly anterior location of the median nerve between the flexor retinaculum and sublimis 2. Flexion, however, produced an anterior shift of the tendons toward the flexor retinaculum. The median nerve either became flattened against the flexor retinaculum

anterior to sublimis 2 or became interposed between individual flexor tendons, most commonly sublimis 2 and the flexor pollicis longus, but also sublimis tendons 3 and 4. The flexed position, therefore, placed the median nerve, flexor tendons, and flexor retinaculum in closer proximity to each other than the neutral position did, while the extended position increased the space between these structures. The flattened nerve configuration on flexion vs a more rounded shape with extension was a reflection of these relative proximity changes. This anatomic crowding during flexion is not inconsistent with previous publications, which have proposed wrist flexion rather than extension as a predisposing mechanism to carpal tunnel syndrome, despite carpal tunnel pressure increases with both [1, 4, 7, 11].

The two volunteers who had previous episodes of carpal tunnel syndrome showed different nerve-tendon alignments. In one, median nerves remained in the anterior location be-

TABLE 1: Changes in Position of Median Nerve with Changes in Wrist Position

Finger Position/Wrist Nos.	Position of Nerve with Wrist in:		
	Neutral	Extension	Flexion
Flexion			
1 and 2	Anterior	Anterior	Lateral
3 and 4	Anterior	Anterior	Medial
5 and 6	Lateral	Anterior	Lateral
7 and 8	Lateral	Anterior	Lateral
Straight			
9 and 10	Anterior	Anterior	Anterior
11 and 12	Anterior	Anterior	Anterior
13 and 14	Anterior	Anterior	Medial
15 and 16	Anterior	Anterior	Lateral

Note.—Anterior = anterior to sublimis 2; Lateral = lateral interposition between sublimis 2 and flexor pollicis longus; Medial = medial interposition between sublimis tendons 3 and 4.

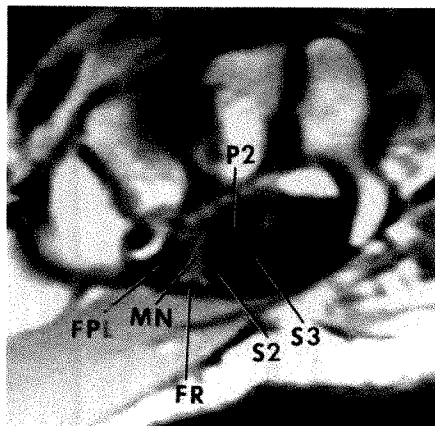


Fig. 4.—MR image (600/20) of wrist in 45° flexion shows volar shift of flexor tendons in comparison with neutral and especially extension images. Median nerve is interposed between flexor pollicis longus and sublimis 2. Appearance is similar to neutral interposed position of Fig. 2 except for volar tendon arrangement in flexion. (See key for abbreviations.)

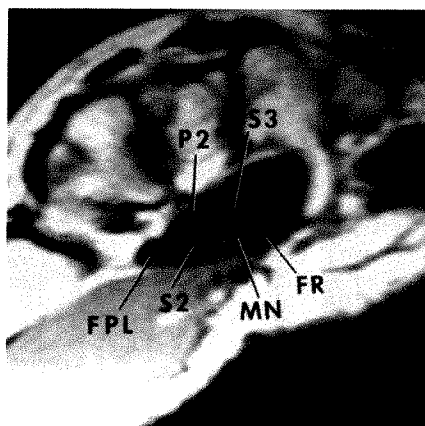


Fig. 5.—MR image (600/20) of flexed wrist shows volar tendon shift with median nerve remaining anteriorly between sublimis tendons 2 and 3 and flexor retinaculum. (See key for abbreviations.)

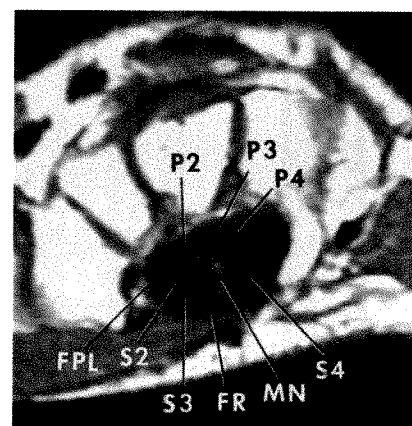


Fig. 6.—MR image (600/20) of flexed wrist shows median nerve interposed between and deep to sublimis tendons 2 and 3, immediately volar to profundus tendons 2 and 3. (See key for abbreviations.)

tween sublimis 2 and the flexor retinaculum in all three positions. In the other, the median nerves were anterior to sublimis 2 in neutral position and with extension, and became interposed between sublimis 2 and the flexor pollicis longus with flexion.

Further studies are needed to evaluate dynamic interactions of the median nerve and flexor tendons in symptomatic patients to determine their role among the wide variety of factors contributing to carpal tunnel syndrome.

REFERENCES

1. Middleton W, Kneeland J, Kellman G, James C. MR imaging of the carpal tunnel: normal anatomy and preliminary findings in the carpal tunnel syndrome. *AJR* **1987**;148:307-316
2. Weiss KL, Beltran J, Shamam OM, Still RF, Levey M. High-field MR surface-coil imaging of the hand and wrist. Part I. Normal anatomy. *Radiology* **1986**;160:143-146
3. Robbins H. Anatomical study of the median nerve in the carpal tunnel and etiologies of the carpal tunnel syndrome. *J Bone Joint Surg [Am]* **1963**;45-A:953-966
4. Kendall D. Non-penetrating injuries of the median nerve at the wrist. *Brain* **1950**;73:84-94
5. Brain W, Wright A, Wilkerson M. Spontaneous compression of both median nerves in the carpal tunnel: six cases treated surgically. *Lancet* **1947**;1:277-282
6. Love J. Median neuritis; carpal tunnel syndrome; diagnosis and treatment. *NC Med J* **1955**;16:463-469
7. Tanzer R. The carpal tunnel syndrome. *J Bone Joint Surg [Am]* **1959**;41-A:626-634
8. Cooney WP, Dobyns JH, Linscheid RL. Complications of Colles' fractures. *J Bone Joint Surg [Am]* **1980**;62-A:613-619
9. Zucker-Pinchoff B, Hermann G, Srinivasan R. Computed tomography of the carpal tunnel: a radioanatomical study. *J Comput Assist Tomogr* **1981**;5(4):525-528
10. Mesgarzadeh M, Schneck CD, Bonakdarpour A. The wrist and hand. In: Bassett LW, Gold RH, Seeger LL, eds. *MRI atlas of the musculoskeletal system*. London: Martin Dunitz, **1989**:152-157
11. Gelberman R, Szabo R, Mortensen W. Carpal tunnel pressures and wrist position in patients with Colles' fractures. *J Trauma* **1984**;24:477-479

MR Imaging of the Knee in the Sagittal Projection: Comparison of Three-Dimensional Gradient-Echo and Spin-Echo Sequences

John D. Reeder¹
 Samuel O. Matz²
 Larry Becker³
 Samuel M. Andelman¹

Fifty patients with suspected internal derangement of the knee had arthroscopic examinations after MR imaging with both a standard T1-weighted spin-echo (SE) sequence and a three-dimensional (3-D) gradient-echo sequence. This series permitted correlative evaluation of 100 menisci and 50 anterior cruciate ligaments. Meniscal tears were diagnosed when intrameniscal signal communicated with the meniscal surface. Criteria for diagnosing anterior cruciate ligament disruption included absence or discontinuity of the ligament, ligamentous laxity, and hyperflexion of the posterior cruciate ligament. Arthroscopic surgery confirmed the presence of 39 meniscal tears and 11 anterior cruciate ligament tears in this population. The sensitivity and specificity of the SE sequence for the diagnosis of meniscal tears were 77% and 98%, respectively. The 3-D gradient-echo sequence had a sensitivity of 87% and a specificity of 88%. For disruption of the ligament, the SE technique had a sensitivity of 82% and a specificity of 95% and the 3-D technique had a sensitivity of 64% and a specificity of 100%. Although these differences in sensitivity and specificity are not statistically significant at the $p < .05$ level, probably because of the small sample size, the results show the relative strengths and weaknesses of the two imaging sequences.

These data suggest that because of the complementary results of the two MR techniques, both the SE and the 3-D gradient-echo sequences have a role in the diagnosis of knee injuries.

AJR 153:537-540, September 1989

Previous reports have emphasized the ability of MR to accurately define cartilaginous and ligamentous injuries of the knee, stimulating interest in refining and improving imaging techniques [1-4]. The design of tailored surface coils and three-dimensional (3-D) imaging have resulted in dramatic improvements in image quality [5-8]. We determined the sensitivity and specificity of a 3-D gradient-echo sequence compared with that of a spin-echo (SE) sequence for the diagnosis of injuries to the meniscus and the anterior cruciate ligament (ACL). Arthroscopic findings were used as the gold standard.

Subjects and Methods

Three-dimensional gradient-echo images and T1-weighted SE MR images were obtained in 50 patients referred for suspected internal derangement of the knee, permitting evaluation of 100 menisci and 50 ACLs. The SE and 3-D images were interpreted independently; the reader did not know the results of the complementary imaging sequence or the surgical findings. Meniscal signal was graded according to a previously described method [1, 2]. Specifically, a meniscal tear was diagnosed only when an abnormal signal in the meniscus clearly communicated with the meniscal surface. Intrameniscal signal that did not communicate with the surface was considered to represent internal meniscal degeneration.

Criteria used to diagnose ACL disruption included absence of an identifiable ACL, ACL laxity or discontinuity, and bowing or hyperflexion of the posterior cruciate ligament [4]. Surgical correlation was obtained for all 50 patients, permitting computation of the sensitivity

Received February 16, 1989; accepted after revision May 4, 1989.

¹ Department of Radiology, Franklin Square Hospital, Baltimore, MD 21237. Address reprint requests to J. D. Reeder, Magnetic Imaging Associates, Suite T19, 1700 Reisterstown Rd., Baltimore, MD 21208.

² Carroll County Center for Orthopaedic Surgery and Sports Medicine, Westminster, MD 21157.

³ Department of Orthopedic Surgery, Sinai Hospital, Baltimore, MD 21215.

0361-803X/89/1533-0537

© American Roentgen Ray Society

and specificity for the two imaging sequences relative to arthroscopic examination. Statistical significance was evaluated with the McNemar Exact Test.

All of the MR studies were performed on a 1.0-T magnet (Siemens Medical Systems, Iselin, NJ). Two sets of interleaved (contiguous interleaved series), relatively T1-weighted sagittal images were obtained with a TR of 800 msec, a TE of 20 msec, and a slice thickness of 3 mm. With one acquisition, imaging time was about 7 min. Patients also had sagittal imaging with a 3-D fast imaging with steady precession (FISP) technique that used a 40-msec TR, a 15-msec TE, and a flip angle of 40°. This volume-acquisition sequence provided contiguous images with an effective slice thickness of 1.5 mm. With one acquisition, the imaging time for the 3-D series was about 11 min. For both the SE and 3-D sequences an imaging matrix of 256 × 256 was used. A Siemens extremity resonator coil with a 21.4-cm field of view was used and knees were imaged in slight (10–15°) external rotation.

Results

Of the 100 menisci studied by MR imaging, 61 were normal and 39 had tears on arthroscopy. Eleven of the 50 ACLs had

tears on arthroscopy. Thirty of the meniscal tears and 60 normal menisci were correctly identified on T1-weighted SE images. Nine results were false-negative and one was false-positive. This yielded a sensitivity of 77% and a specificity of 98%. With respect to ACL tears, the SE technique successfully showed nine of the 11 tears, and in 37 cases, the ACL was correctly interpreted as being normal. There were two false-positive and two false-negative results. For ACL tears, the SE sequence had a sensitivity of 82% and a specificity of 95%.

The 3-D FISP sequence correctly identified 34 of the 39 surgically confirmed meniscal tears and 54 of the 61 arthroscopically normal menisci. The results of this technique included seven false-positives and five false-negatives, yielding a sensitivity of 87% and a specificity of 88%. The 3-D FISP sequence identified only seven of the 11 tears but allowed correct identification of all 39 normal ACLs with no false-positive results. There were four false-negatives. Applying the 3-D FISP technique to ACL tear evaluation resulted in a sensitivity of 64% and a specificity of 100%.

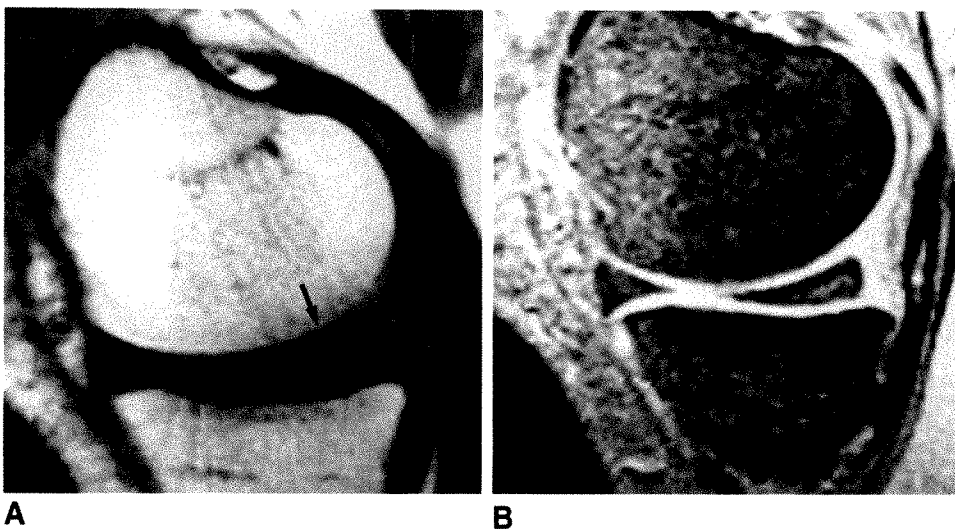


Fig. 1.—A, Internal signal is observed within posterior horn of medial meniscus (arrow) with SE technique. B, Increased contrast between signal and surrounding fibrocartilage is obtained with 3-D FISP sequence in comparison with SE image.

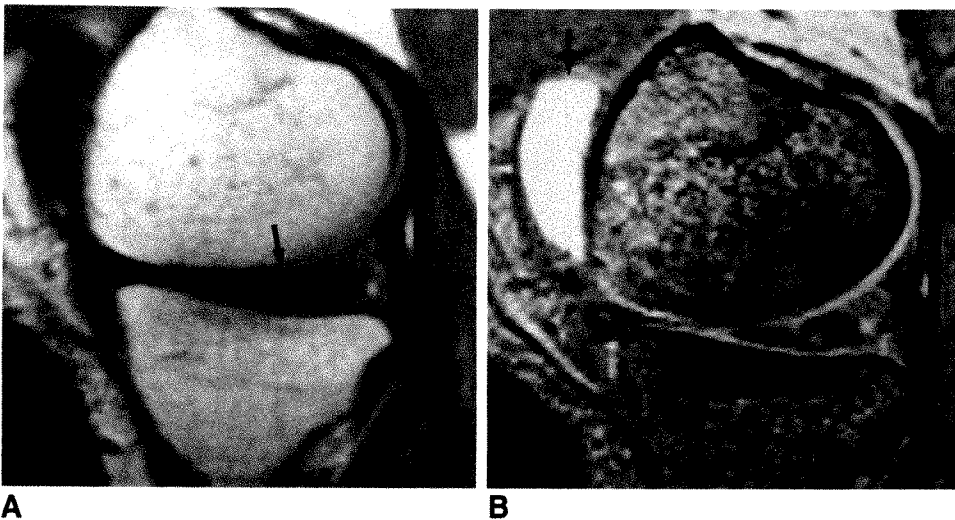


Fig. 2.—A, Surgically confirmed meniscal tear is identified on SE image (arrow). B, Tear appears similar in pattern but more intense relative to normal fibrocartilage on 3-D FISP image. Also, note hyperintensity of effusion (arrow), reflecting T2* contrast.

All five of the torn menisci missed on the 3-D sequence were also missed by the SE technique. The other four tears not identified by the SE sequence were identified on the 3-D images. The single false-positive case on the SE sequence was also positive on 3-D images. The remaining six 3-D false-positive cases were normal on SE images.

As determined by the McNemar Exact Test, the differences in sensitivity and specificity for detection of meniscal tear and ACL disruption fail to demonstrate statistical significance at the $p < .05$ level.

Discussion

In our series, both the SE and the 3-D FISP sequences provided subjectively high-quality images with comparable anatomic detail. Internal meniscal degeneration was shown equally well with both techniques, although the degenerative signal tended to be brighter with the 3-D technique (Fig. 1). Meniscal tears maintained a similar appearance on both sequences (Fig. 2). Absence of an identifiable ACL, in general,

correlated well with surgically confirmed ACL tears. However, diagnostic differences between the two protocols did emerge. With respect to meniscal tears, the superior sensitivity of the 3-D FISP technique became evident (Fig. 3). The thinner slice thickness and resultant diminution in volume-averaging may have been responsible for this observation, especially in the case of small tears. Although obtaining two interleaved sets of SE slices is almost gapless imaging, 3-D volume acquisition permits examination of truly contiguous slices. Similarly, optimization of slice profile relative to SE imaging also may contribute to increased 3-D sensitivity. However, the heightened sensitivity to intrameniscal signal afforded by the 3-D technique also contributes to its decreased specificity relative to SE imaging. Because a greater volume of signal could be identified within the meniscus, it often became more difficult to determine whether the abnormality communicated with the meniscal surface, thus differentiating internal degeneration from actual tear (Fig. 4).

With a specificity of 100%, the 3-D protocol was accurate in the identification of a normal ACL (Fig. 5). This may have

Fig. 3.—A, Signal within posterior horn on SE image was considered to represent degeneration rather than tear because no surface communication was observed. A tear was discovered at surgery.

B, 3-D FISP image correctly identifies inferior surface communication (arrow), indicative of tear.

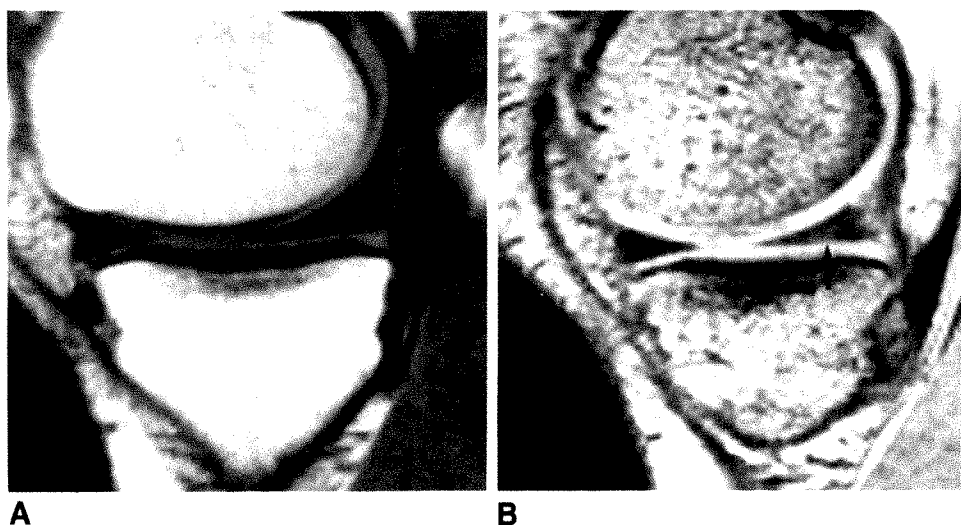
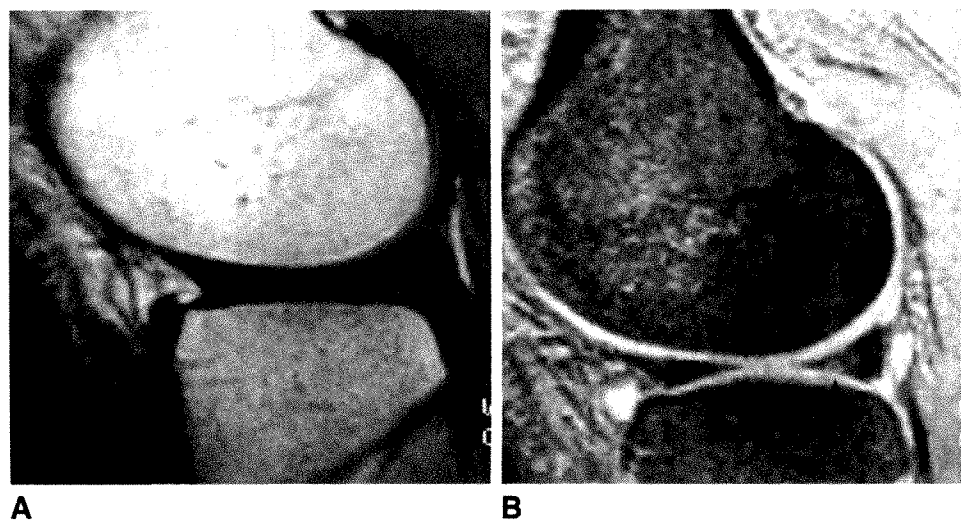


Fig. 4.—A, SE image correctly identifies only signal within posterior horn of this surgically normal meniscus.

B, 3-D FISP image suggests presence of surface contact (arrow), rendering a false-positive diagnosis of tear.



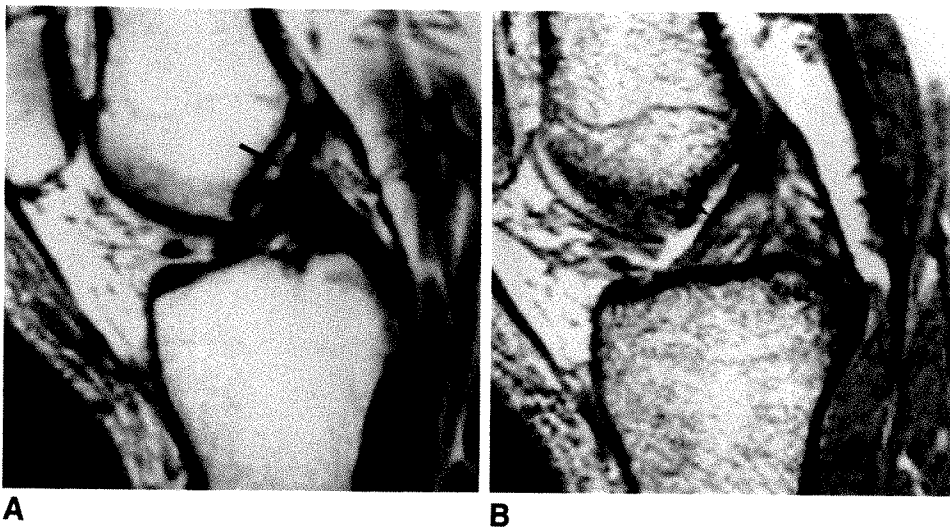


Fig. 5.—A and B, Normal anterior cruciate ligament (arrows) is seen on both SE (A) and 3-D FISP (B) sequences. 3-D technique, however, provides greater contrast between anterior cruciate ligament and surrounding tissue and fluid, and thinner sections obtained with 3-D sequence permit evaluation of ligament on more images with less volume averaging.

been because of the thin (1.5-mm) contiguous slice acquisition possible with the technique. During SE imaging, particularly with thicker slices, slight rotational changes in positioning or the presence of an effusion may substantially affect the visibility of the ligament [9].

There may have been selection bias in our study, because all patients selected had had arthroscopy. These patients generally have more complex clinical findings. This study is also limited in that only sagittal images were considered in comparing the two techniques. Although other authors have recommended axial, radial, or coronal images, the sagittal plane may offer the most diagnostic information for the diagnosis of meniscal and ACL injuries [1, 3, 10]. A third limitation is the fact that only a T1-weighted sequence was used with the SE technique. T2-weighted images may improve the accuracy of the technique for the diagnosis of ACL tears but not meniscal tears [4, 9]. Finally, arthroscopy is not infallible for the detection of these abnormalities [1, 3].

Both the SE sequence and the 3-D FISP protocol have advantages in the evaluation of the knee. The SE images have greater specificity for meniscal tears and greater sensitivity for ACL tears. The 3-D FISP sequence provides greater sensitivity with regard to meniscal tears and greater specificity for ACL tears. Because the 3-D FISP images reflect T2* data, they provide enhanced fluid-soft tissue contrast. Although the observed differences in sensitivity and specificity lack statistical significance, probably because of the small sample size,

the results emphasize the relative strengths and weaknesses of these two imaging sequences. Our results suggest that both techniques have a role in the evaluation of the knee.

REFERENCES

1. Crues JV III, Mink J, Levy TL, Lotysch M, Stoller DW. Meniscal tears of the knee: accuracy of MR imaging. *Radiology* 1987;164:445-448
2. Stoller DW, Martin C, Crues JV III, Kaplan L, Mink JH. Meniscal tears: pathologic correlation with MR imaging. *Radiology* 1987;163:731-735
3. Reicher MA, Hartzman S, Duckwiler GR, Bassett LW, Anderson LJ, Gold RH. Meniscal injuries: detection with MR imaging. *Radiology* 1986;59:753-757
4. Lee JK, Yoo L, Phelps CT, Wirth CR, Czajkaj, Lozman J. Anterior cruciate ligament tears: MR imaging compared with arthroscopy and clinical tests. *Radiology* 1988;166:861-864
5. Tyrrell RL, Gluckert K, Pathria M, Modic MT. Fast three dimensional MR imaging of the knee: comparison with arthroscopy. *Radiology* 1988;166:865-872
6. Konig H, Sauter R, Deimling M, Vogt M. Cartilage disorders: comparison of spin-echo, CHES, and FLASH sequence MR images. *Radiology* 1987;164:753-758
7. Spritzer CE, Vogler JB, Martinez S, et al. MR imaging of the knee: preliminary results with a 3DFT GRASS pulse sequence. *AJR* 1988;150:597-603
8. Harms SE, Muschler G. Three dimensional MR imaging of the knee using surface coils. *J Comput Assist Tomogr* 1986;10:773-777
9. Mink JH, Levy T, Crues JV III. Tears of the anterior cruciate ligament and menisci of the knee: MR imaging evaluation. *Radiology* 1988;167:769-774
10. Beltran J, Noto AM, Mosure JC, Weiss KL, Zuelzer W, Christoforidis AJ. The knee: surface coil MR imaging at 1.5 T. *Radiology* 1986;159:747-751

Soft-Tissue Masses: Diagnosis Using MR Imaging

Mark J. Kransdorf^{1,2}
 James S. Jelinek^{1,2}
 Richard P. Moser, Jr.^{2,3}
 Joseph A. Utz^{1,2,4}
 Anne C. Brower^{2,3}
 Terry M. Hudson³
 B. Hudson Berrey^{5,6}

The MR images of 112 soft-tissue masses of various causes were retrospectively reviewed. Pathologic diagnosis by biopsy was available in 96 cases. Diagnosis in the remaining 16 cases was established by characteristic radiographs, CT scans, and/or arteriograms, in conjunction with appropriate history and clinical follow-up. All masses were evaluated with both T1-weighted, 300–600/20–30 (TR/TE), and T2-weighted, 2000/80–100, images. They were reviewed to determine (1) if these images were sufficiently unique to allow a preoperative diagnosis based exclusively on the MR appearance and (2) if benignity vs malignancy could be predicted on the basis of the analysis of the MR image characteristics of the lesion. Concerning the latter, attention was directed to the margins of the lesions, to the impact of the lesion on the surrounding tissues (edema, infiltration, etc.), and to the intensity and homogeneity of the MR signal of the lesion.

MR images were sufficiently characteristic to allow a specific diagnosis in 27 (24%) of the 112 cases (10 lipomas, eight hemangiomas, six pigmented villonodular synovitis, two hematomas, and one arteriovenous malformation). MR was incapable of reliably distinguishing between benign and malignant soft-tissue tumors.

AJR 153:541–547, September 1989

Received March 6, 1989; accepted after revision May 1, 1989.

The opinions or assertions contained herein are the private views of the authors and are not to be construed as official or as reflecting the views of the Department of the Army, the Department of Defense, or the Uniformed Services University of the Health Sciences.

¹ Department of Radiology, Walter Reed Army Medical Center, Washington, DC 20307-5001. Address reprint requests to M. J. Kransdorf.

² Department of Radiology and Nuclear Medicine, Uniformed Services University of the Health Sciences, Bethesda, MD 20814.

³ Department of Radiologic Pathology, Armed Forces Institute of Pathology, Washington, DC 20306-6000.

⁴ Present address: Drs. Mori, Beau, and Brooks, PA, 3599 University Blvd. S., Jacksonville, FL 32216.

⁵ Department of Orthopedic Surgery, Walter Reed Army Medical Center, Washington, DC 20307-5001.

⁶ Department of Surgery, Uniformed Services University of the Health Sciences, Bethesda, MD 20814.

0361-803X/89/1533-0541

MR is currently considered superior to CT for imaging soft-tissue tumors [1–15], although we are unaware of any specific studies to evaluate its diagnostic accuracy and ability to differentiate benign from malignant lesions. Weekes et al. [16] reviewed the CT scans of 84 patients with untreated soft-tissue tumors, 75 primary (41 malignant and 34 benign) and nine secondary neoplasms, and found these images sufficiently characteristic to suggest a histologic diagnosis in only 13 tumors. In their series, CT imaging characteristics correctly distinguished benign from malignant neoplasms in 88% of cases, but one type of malignancy could not be distinguished from another.

We retrospectively reviewed the MR images of 112 soft-tissue masses (occurring in 105 patients), in a fashion similar to that used by Weekes et al. for CT, to determine if MR imaging characteristics could establish a preoperative diagnosis and if any reliable MR criteria exist to differentiate benign from malignant lesions.

Materials and Methods

The MR images of 112 soft-tissue masses found in 105 patients were reviewed retrospectively. All patients were initially referred for evaluation of a soft-tissue mass. One hundred two masses were imaged before any treatment. Seven masses were imaged after fine-needle aspiration or biopsy. Two cases of plantar fibromatosis were recurrent. MR images were obtained in one patient because of a mass in an area previously treated with radiation therapy. All scans were obtained on a 1.5-T Signa (General Electric, Milwaukee, WI), a 1.5-T Teslacon (Technicare, Solon, OH), or a 0.5-T Picker (Picker International, Highland Heights, OH) scanner. Typical scanning sequences included spin-echo T1-weighted, 300–700/20–34 (TR/TE), and T2-weighted, 2000–2800/80–100, pulse sequences. At least two orthogonal planes were imaged in every case.

Pathologic diagnosis by biopsy was available in 96 cases. Diagnosis in the remaining 16 cases was established by characteristic plain radiographs, CT scans, and/or arteriograms, in conjunction with appropriate history and clinical follow-up. Entities in the latter category included arteriovenous malformations, hemangiomas, and myositis ossificans.

For each lesion, both T1- and T2-weighted images were reviewed and evaluated for the following features: margin definition, intensity and homogeneity of MR signal, presence or absence of surrounding edema, and involvement of adjacent bone or neurovascular tissues. The MR images also were analyzed to determine if they were sufficiently characteristic to suggest a specific preoperative diagnosis. Scans were reviewed by two radiologists. To eliminate bias, characteristic images for each lesion also were reviewed independently by three radiologists who were unfamiliar with any of the case material and were without knowledge of history, diagnosis, or other imaging studies. Discrepancies in interpretation were decided by consensus.

The 112 soft-tissue masses (arising in 105 patients) included 85 benign lesions and 27 malignant neoplasms. The former included both benign neoplasms and inflammatory and tumorlike masses (such as myositis ossificans, synovial osteochondromatosis, and pseudoaneurysm). The 27 malignancies included 24 primary neoplasms (one of which was recurrent) and three cases of soft-tissue lymphoma. These patients were included because the clinical presentation for their lymphoma was a soft-tissue mass. Specific diagnoses are listed in Table 1. There were 63 male and 42 female patients. The 85 benign lesions occurred in 80 patients: 53 males and 27 females. In one patient with neurofibromatosis (complicated by a neurofibrosarcoma), three additional neurofibromas were imaged incidentally on MR. This was the only patient in the series with coexistent benign and malignant soft-tissue lesions. In a second patient with neurofibromatosis, two neurofibromas were imaged. One patient had both an arteriovenous malformation in one thigh and an intramuscular hemangioma in the contralateral thigh. One patient had plantar fibromatosis with a recurrence approximately 13 months after initial surgery.

The 27 malignancies (which included one recurrence) occurred in 26 patients: 16 females and 10 males. One patient had a synovial sarcoma in the thigh and 2 months later a lesion in the shoulder developed. Because no evidence in this patient of metastases existed elsewhere (e.g., lungs, liver, bone marrow, or regional lymph nodes), it is unclear if the shoulder lesion represented a metastasis or, less likely, a metachronous primary synovial sarcoma.

At presentation, the 105 patients ranged in age from 5 months to 73 years. Of those with benign soft-tissue masses, the average age at presentation was approximately 30 years, ranging from 5 months (lipomatosis) to 73 years (hematoma). Of the patients with soft-tissue malignancies, the average age at presentation was approximately 37 years, ranging from 9 (synovial sarcoma) to 72 (liposarcoma) years old.

Results

There were 112 soft-tissue masses, of which 85 were benign and 27 were malignant. The MR images were sufficiently characteristic to allow a confident specific diagnosis of benignity in 27 (24%) masses (10 benign fatty masses, eight hemangiomas, six pigmented villonodular synovitis, two hematomas, and one arteriovenous malformation). Of the remaining 58 benign lesions, MR images were indeterminate in 37 cases, favored a benign cause in 16 cases, and incorrectly suggested a malignant cause in five cases.

Of the 27 pathologically confirmed malignancies, none were sufficiently characteristic on MR to allow a specific diagnosis. Overall, the MR images were indeterminate in 12 cases,

TABLE 1: Diagnoses of Soft-Tissue Masses Studied with MR Imaging

Type of Mass	No.
Benign	
Arteriovenous malformation	2
Abscess	3
Angiomatosis	1
Chondroma	2
Devitalized muscle	1
Epidermal inclusion cyst	2
Fibroosseous pseudotumor	1
Fibromatosis	8
Fibrous proliferation	1
Ganglion cyst	5
Hemangioma	10
Hematoma	2
Lipoma	10
Lipomatosis	1
Lymphangioma	3
Myositis ossificans	2
Myxoma, intramuscular	1
Neurofibroma	7
Nodular fasciitis	3
Pigmented villonodular synovitis	8
Pseudoaneurysm	2
Schwannoma	3
Synovial cyst	1
Synovial (oste)chondromatosis	3
Synovitis, chronic	2
Rheumatoid arthritis	1
Subtotal	85
Malignant	
Chondrosarcoma, myxoid	2
Ewing sarcoma	1
Fibrosarcoma	2
Hemangiopericytoma	1
Liposarcoma	4
Lymphoma	3
Malignant fibrous histiocytoma	2
Malignant schwannoma	4
Neurofibrosarcoma	1
Rhabdomyosarcoma	1
Synovial sarcoma	6
Subtotal	27
TOTAL	112

Note.—Pathologic diagnosis was established by biopsy in 96 cases. Diagnosis in the remaining 16 cases was established by characteristic radiographs, CT scans, and/or arteriograms.

correctly suggested a malignant cause in 11 cases, and incorrectly suggested a benign cause in four cases. Fat was identified on MR in two of four liposarcomas, suggesting the correct diagnosis, although the diagnosis of liposarcoma was incorrectly suggested in four additional cases (one malignant fibrous histiocytoma, one synovial sarcoma, one soft-tissue myxoid chondrosarcoma, and one intramuscular myxoma).

Margin Definition

For any given mass, regardless of cause, margins were typically better defined on the T2-weighted image. Four categories of margins were established, ranging from circumferentially well-defined to infiltrating. Benign and malignant causes were not readily distinguished on the basis of margins. These results are summarized in Table 2.

TABLE 2: Margin Analysis, Signal Intensity, and Homogeneity of Benign and Malignant Soft-Tissue Masses as Determined on T1- and T2-weighted MR Images

MR Characteristic	No. (%)			
	Benign		Malignant	
	T1	T2	T1	T2
Margin^a				
Circumferentially well defined	20 (24)	26 (31)	7 (26)	7 (26)
Relatively well defined	25 (29)	22 (26)	8 (30)	10 (37)
Discrete mass, poorly defined	16 (19)	14 (16)	5 (18)	4 (15)
Infiltrating	24 (28)	23 (27)	7 (26)	6 (22)
Total	85 (100)	85 (100)	27 (100)	27 (100)
Signal intensity^b				
Greater than that of fat	2 (2)	37 (43)	0	16 (59)
Equal to that of fat	13 (15)	19 (22)	1 (4)	7 (26)
Between that of fat and muscle	23 (27)	6 (7)	9 (33)	2 (7)
Equal to that of muscle	24 (28)	4 (5)	14 (52)	1 (4)
Less than that of muscle	8 (10)	4 (5)	7 (26)	0
Complex	15 (18)	15 (18)	1 (4)	1 (4)
Total	85 (100)	85 (100)	27 (100)	27 (100)
Homogeneity^c				
Homogeneous	27 (32)	21 (25)	8 (29)	4 (15)
Mild inhomogeneity	34 (40)	30 (35)	14 (52)	12 (44)
Moderate inhomogeneity	8 (9)	17 (20)	4 (15)	8 (30)
Complex	16 (19)	17 (20)	1 (4)	3 (11)
Total	85 (100)	85 (100)	27 (100)	27 (100)

^a Circumferentially well defined = mass with cystlike or nearly cystlike margins; relatively well defined = discrete mass with readily identified margins, though not cystlike or nearly cystlike; discrete mass, poorly defined = discrete mass in which margins are not readily discernible from surrounding soft tissues; infiltrating = mass blends into surrounding tissue without readily identifiable margins.

^b The signal intensity of the tumor was compared with that of muscle and subcutaneous fat. If no dominant signal was present, the mass was considered complex.

^c Homogeneous = completely homogeneous, cystlike, or nearly cystlike mass; mild inhomogeneity = less than 25% of the mass showing inhomogeneity; moderate inhomogeneity = 25–50% of the mass showing inhomogeneity; complex = more than 50% of the mass showing inhomogeneity.

Signal Intensity

The overwhelming majority of both benign and malignant lesions displayed a signal intensity equal to or less than that of skeletal muscle on T1-weighted pulse sequences and equal to or greater than that of fat on T2-weighted pulse sequences. Absence of increased signal intensity on T2-weighted images was not an indication of benignity. Seven malignant tumors (three synovial sarcomas, two soft-tissue myxoid chondrosarcomas, one neurofibrosarcoma, and one hemangiopericytoma) had a signal intensity on T2 approximating that of subcutaneous fat; two malignant tumors (one synovial sarcoma and one malignant fibrous histiocytoma) had a signal intensity on T2 intermediate between that of fat and muscle; and one tumor (a malignant schwannoma) had a signal intensity on T2 approximating that of skeletal muscle. Only two of four liposarcomas had an MR signal suggesting fat. These results are summarized in Table 2.

Homogeneity of the MR Signal

Regardless of cause, the soft-tissue masses were more homogeneous on T1-weighted images. With respect to this variable, four categories were established: completely homo-

geneous, mildly inhomogeneous (less than 25% of the mass showing inhomogeneity), moderately inhomogeneous (approximately 25–50% of the mass showing inhomogeneity), or complex (more than 50% of the mass showing inhomogeneity). Two malignancies, a synovial sarcoma and a malignant fibrous histiocytoma, displayed coexistent hemorrhage. These results are summarized in Table 2.

Surrounding Soft-Tissue Edema

Surrounding edema was apparent in four (15%) of the malignant tumors and in two (2%) of the benign masses. Extensive edema was noted in one patient with recurrent synovial sarcoma, although these changes probably resulted from previous radiation therapy. The remaining three malignancies that showed edema were all lymphomas. None of the primary malignancies showed surrounding edema. In the benign group, extensive edema was seen surrounding an abscess and a hematoma.

Involvement of Adjacent Bone or Neurovascular Tissue

MR evidence of bone or neurovascular involvement was apparent in six (22%) of 27 malignancies. Three of these were

lymphomas, which presented as soft-tissue masses. There also was one each high-grade malignant fibrous histiocytoma, malignant schwannoma, and soft-tissue Ewing sarcoma. Only three (13%) of 24 primary malignancies had bone involvement. Bone involvement was noted in seven benign masses (8%): four cases of pigmented villonodular synovitis, two cases of chronic synovitis, and one periosteal arteriovenous malformation.

Discussion

To our knowledge there have been no previous reports concerning the diagnostic value of MR in the evaluation of soft-tissue tumors. Weekes et al. [16] reviewed the CT scans of 84 patients with untreated soft-tissue tumors and found these scans sufficiently characteristic to suggest a correct histologic diagnosis in only 13 cases (15%) (nine lipomas, three hemangiomas, and one neurofibroma). Regardless of histology, the malignant neoplasms were indistinguishable. The authors did note, however, that the CT appearance allowed for the differentiation of benign from malignant neoplasms in 88% of cases. Similar results have not been reported in the MR literature, and no unique MR features have been identified to reliably distinguish benign from malignant soft-tissue lesions [3, 8, 17]. Petasnick et al. [12] did suggest, however, that clearly defined margins and uniform (homogeneous) signal intensity on T2-weighted MR images were indicative of benignity, with the latter feature considered the most reliable indicator.

Our results, based on a large number of cases of various causes (Table 1), suggest that there are no reliable MR criteria for differentiating benign from malignant soft-tissue masses. Furthermore, histologically high-grade malignancies may appear on MR as well-defined, homogeneous soft-tissue masses without surrounding edema or involvement of adjacent bone (Fig. 1). Conversely, benign soft-tissue lesions may appear on MR as poorly defined, inhomogeneous masses with surrounding edema and apparent involvement of adjacent bony structures (Figs. 2 and 3).

In addition to the important broad distinction between benignity and malignancy, these 112 masses also were analyzed to determine if the MR images were sufficiently characteristic to allow a specific diagnosis. The diagnosis of 10 of 11 benign fatty tumors was easily determined on MR, where the signal intensity of the mass approximated that of subcutaneous fat. Six of these fatty tumors were intramuscular lipomas, in which the fatty elements predominated, although the tumor was inhomogeneous on MR because of interspersed regions of decreased signal on both pulse sequences. The latter was believed to represent either muscle or fibrous tissue within the lipoma. Benign fatty tumors are easily identified on both CT and MR [18], although atypical lipomas may be indistinguishable from liposarcomas on both studies [19]. Of the four soft-tissue liposarcomas, two were of particular interest because their MR appearance was nonspecific and failed to show evidence of fat. One of these tumors had an MR appearance of a synovial cyst (Fig. 1). One intramuscular myxoma had signal characteristics compatible with a fatty component on MR and, therefore, was misdiagnosed preoperatively as a liposarcoma (Fig. 2).

The MR appearance of pigmented villonodular synovitis also was sufficiently characteristic to allow successful preoperative diagnosis in six of eight cases. Pigmented villonodular synovitis was suspected when the lesion showed areas of significantly decreased (or absent) signal intensity on both T1- and T2-weighted pulse sequences owing to deposition of hemosiderin within the mass (Fig. 4). Coexistent joint effusion and/or bone erosions (particularly when evident on both sides of the joint) supported the diagnosis of pigmented villonodular synovitis [20–24].

Two subacute hemorrhages (one hematoma and one popliteal artery pseudoaneurysm) were diagnosed easily because of high signal intensity on both T1- and T2-weighted pulse sequences [25–27]. Although readily apparent clinically, one hematoma was misdiagnosed on MR as an infiltrating neoplasm because MR had been performed too early to show typical findings that would have suggested subacute blood [28]. One popliteal artery pseudoaneurysm failed to show

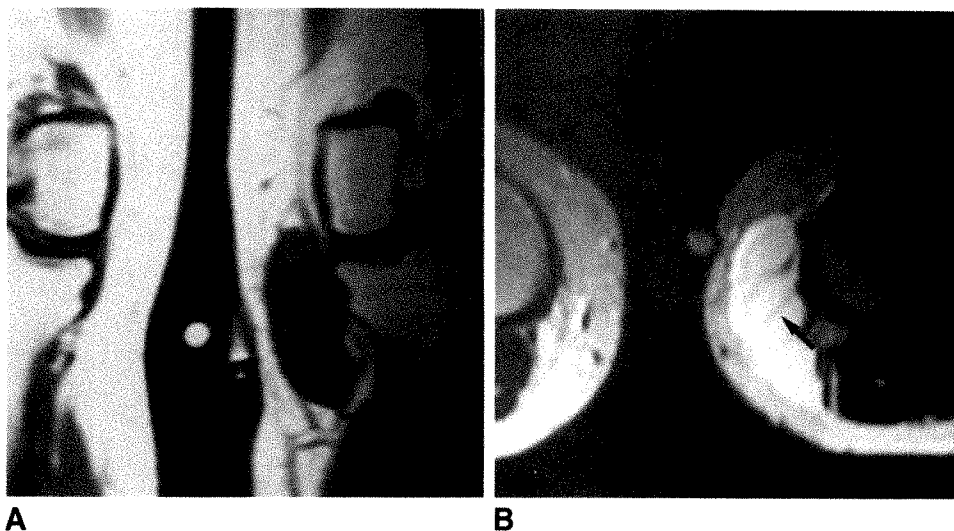


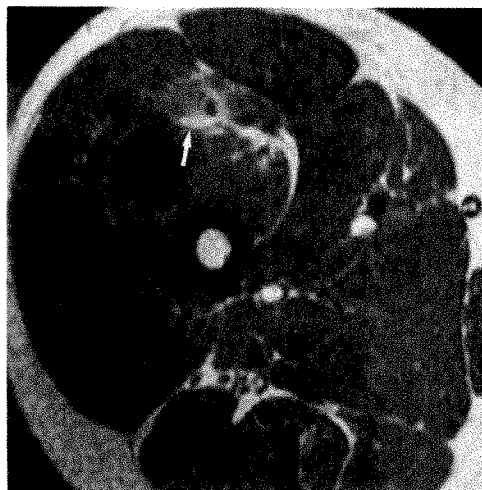
Fig. 1.—Myxoid liposarcoma in a 28-year-old woman.

A, Coronal T1-weighted MR image (600/20) shows well-defined, homogeneous soft-tissue mass in subcutaneous fat on medial aspect of left knee. Signal intensity of mass approximates that of skeletal muscle.

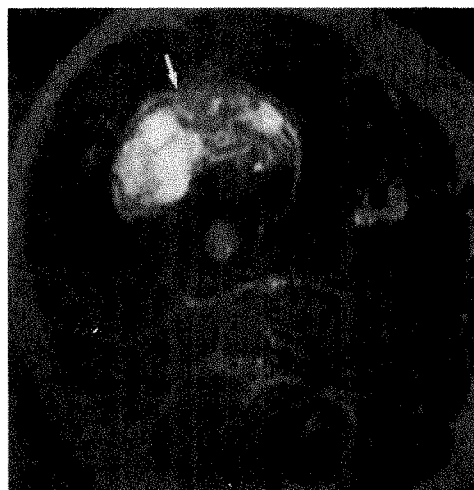
B, Axial T2-weighted MR image (1800/80) shows septa (arrow) not appreciated on T1-weighted image.

Fig. 2.—Intramuscular myxoma in a 41-year-old man.

A and B, Axial T1-weighted (500/20) (A) and T2-weighted (3200/80) (B) MR images show poorly defined, complex soft-tissue mass in right thigh. Fat is noted within mass (arrows); preoperative diagnosis of liposarcoma was suggested.



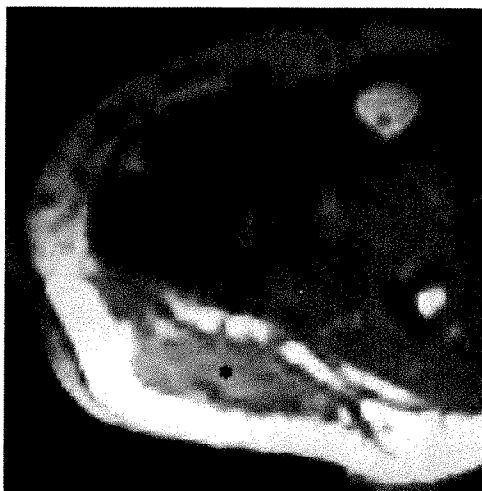
A



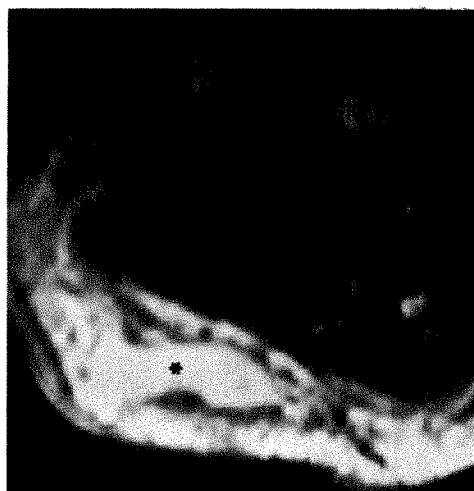
B

Fig. 3.—*Staphylococcus aureus* abscess in a 29-year-old man.

A and B, Corresponding axial T1-weighted (690/32) (A) and T2-weighted (2000/80) (B) MR images of lower leg show infiltrating soft-tissue mass (asterisks) with surrounding edema. Mass is within gastrocnemius muscle. Edema and skin thickening were seen equally well on corresponding axial CT scan (not shown).



A



B

Fig. 4.—Pigmented villonodular synovitis in a 26-year-old woman.

A and B, Coronal T1-weighted (480/22) (A) and T2-weighted (2000/80) (B) MR images reveal well-defined soft-tissue mass (arrows) of markedly decreased signal intensity on both pulse sequences. This suggests hemosiderin deposition, flowing blood, or calcification.



A



B

either subacute blood or hemosiderin deposition. Review of this patient's history indicated that the lesion was clinically apparent for approximately 8 years before acquisition of the MR scan. Furthermore, surgery detected coexistent infection because the mass contained pus, although no organisms were identified on either Gram stain or culture.

The MR appearance of the 10 hemangiomas was sufficiently characteristic to suggest a diagnosis in eight cases (Fig. 5). All showed markedly increased signal on T2-weighted pulse sequences [5, 8, 10, 29, 30]. Signal intensity approximating that of skeletal muscle was noted on the T1-weighted pulse sequence with areas of fat interspersed within the tumor. The latter may reflect the fibrous/fatty septa interspersed between the endothelium-lined vascular channels of the tumor, as identified by Cohen et al. [29].

Schwannomas and neurofibromas tended to be homogeneous [12] on the T1-weighted pulse sequence, with signal intensities somewhat greater than those of skeletal muscle. This was noted in six of 10 cases (Fig. 6). Hyperintensity relative to skeletal muscle on T1-weighted images was non-

specific and was also seen in pyogenic and sterile abscesses, fibromatosis, myositis ossificans, lymphangioma, fibroosseous pseudotumor, fibrosarcoma, malignant schwannoma, and soft-tissue myxoid chondrosarcoma. The inability of MR to differentiate between benign and malignant nerve-sheath neoplasms has been noted previously [31].

The absence of signal from calcification and cortical bone makes their MR images more difficult to interpret [4, 14]. The MR images in two cases of synovial chondromatosis and two cases of myositis ossificans were quite difficult to interpret. The associated plain films were diagnostic and extremely helpful in the interpretation of MR images. In addition, phleboliths, which were readily apparent on plain films in five hemangiomas, were identified clearly on only one MR image.

One case of epidermal inclusion cyst showed a large amount of dependent debris on the T2-weighted sequence. This was not seen in other tumors (Fig. 7).

In summary, the MR images of benign fatty tumors, pigmented villonodular synovitis, hemangiomas, and hematomas can be quite characteristic, although not pathognomonic.

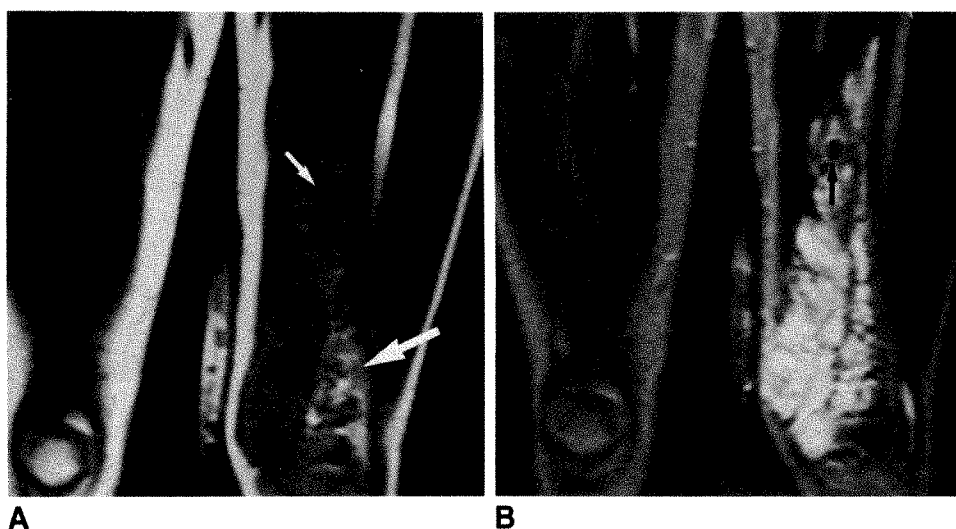


Fig. 5.—Intramuscular hemangioma in a 6-year-old girl.

A and B, Coronal T1-weighted (600/20) (A) and T2-weighted (2000/80) (B) MR images of soft-tissue mass in medial aspect of left thigh. Mass has infiltrating margins. Areas of increased signal on T1-weighted image are compatible with fat (long arrow); rounded areas of signal void on both pulse sequences (short arrows) correspond to phleboliths. Signal voids are nonspecific and could represent vessels (flowing blood) as well as phleboliths. CT scan (not shown) clearly showed these to be phleboliths.

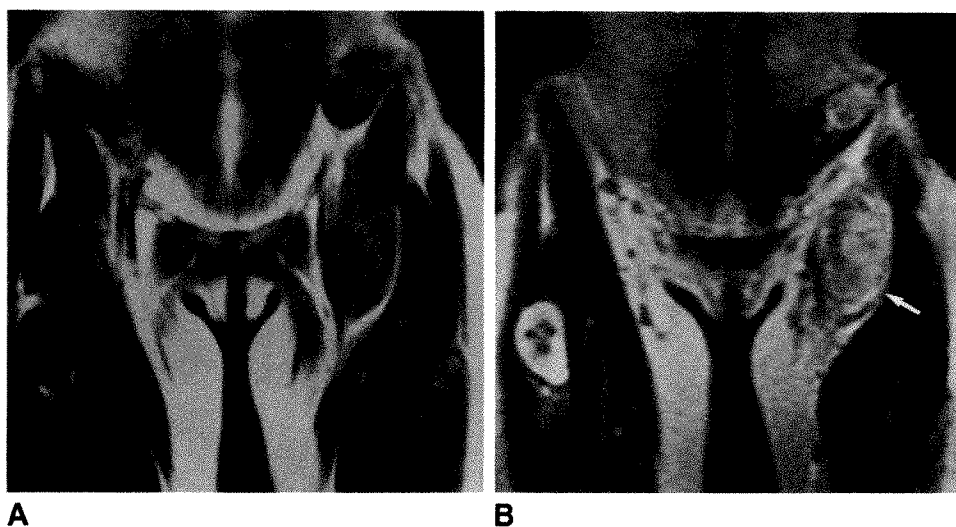
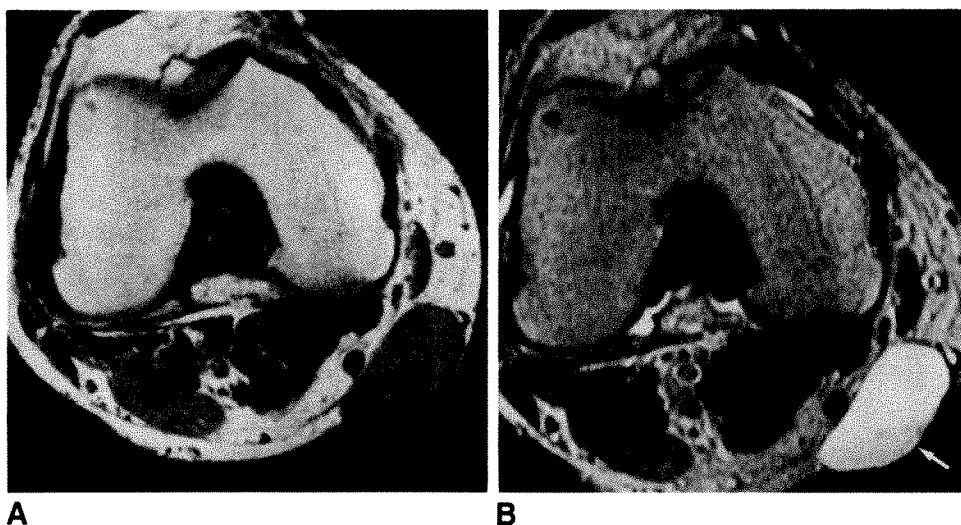


Fig. 6.—Neurofibrosarcoma and two neurofibromas in a 28-year-old woman with neurofibromatosis.

A and B, Corresponding coronal T1-weighted (700/32) (A) and T2-weighted (2000/80) (B) MR images show multiple tumors. Lesions are homogeneous on T1-weighted image and show minimally increased signal relative to skeletal muscle. Large sarcoma in left groin (white arrow) has signal characteristics almost identical to those of benign neurofibroma in lower abdominal wall (black arrow).

Fig. 7.—Epidermal inclusion cyst in a 49-year-old man.

A and B, Axial T1-weighted (700/32) (A) and T2-weighted (2000/80) (B) MR images of knee show circumferentially well-defined soft-tissue mass in subcutaneous fat. Debris is noted in dependent portion of mass on T2-weighted image (arrow). Corresponding sonogram (not shown) showed that mass did not meet criteria for a simple cyst.



There are no reliable criteria to distinguish the MR images of malignant from benign soft-tissue tumors or tumorlike masses. The MR imaging characteristics most likely reflect the underlying lesion morphology (fat content, hemosiderin deposition, cyst formation, hemorrhage, etc.) and not the specific histology. Because of the absence of MR signal from calcification, all scans should be interpreted with corresponding radiographs or CT scans.

REFERENCES

1. Aisen AN, Martel W, Braunstein EM, McMillin KI, Phillips WA, Kling TF. MRI and CT evaluation of primary bone and soft-tissue tumors. *AJR* 1986;146:749-756
2. Burk DL, Dalinka MK, Schiebler ML, Cohen EK, Kressel HY. Strategies for musculoskeletal magnetic resonance imaging. *Radiol Clin North Am* 1988;26:653-672
3. Chang AE, Matory YL, Dwyer AJ, et al. Magnetic resonance imaging versus computed tomography in the evaluation of soft tissue tumors of the extremities. *Ann Surg* 1987;205:340-348
4. Cohen MD, Wæetman RM, Provisor AJ, et al. Efficacy of magnetic resonance imaging in 139 children with tumors. *Arch Surg* 1986;121:522-529
5. Cohen JM, Weinreb JC, Redman HC. Arteriovenous malformations of the extremities: MR imaging. *Radiology* 1986;158:475-479
6. Demas BE, Heelan RT, Lane J, Marcove R, Hajdu S, Brennan MF. Soft-tissue sarcomas of the extremities: comparison of MR and CT in determining the extent of disease. *AJR* 1988;150:615-620
7. Hudson TM, Hamlin DJ, Enneking WF, Pettersson H. MRI of bone and soft-tissue tumors: early experience in 31 patients compared with CT. *Skeletal Radiol* 1985;13:134-146
8. Kaplan PA, Williams SM. Mucocutaneous and peripheral soft-tissue hemangiomas: MR imaging. *Radiology* 1987;163:163-166
9. Kilcoyne EF, Richardson ML, Porter BA, Olson DO, Greenlee TK, Lanzer W. Magnetic resonance imaging of soft tissue masses. *Clin Orthop* 1988;228:13-19
10. Pearce WH, Rutherford RB, Whitehill TA, Davis K. Nuclear magnetic resonance imaging: its diagnostic value in patients with congenital vascular malformations of the limbs. *J Vasc Surg* 1988;8:64-70
11. Pettersson H, Gillespy T, Hamlin DJ, et al. Primary musculoskeletal tumors: examination with MR imaging compared with conventional modalities. *Radiology* 1987;164:237-241
12. Petasnick JP, Turner DA, Charters JR, Gitelis S, Zacharias CE. Soft-tissue masses of the locomotor system: comparison of MRI with CT. *Radiology* 1986;160:125-133
13. Sundaram M, McGuire MH, Fletcher J, Wolverson MK, Heiberg E, Shields JB. Magnetic resonance imaging of lesions of synovial origin. *Skeletal Radiol* 1986;15:110-116
14. Sundaram M, McGuire MH, Herbold DR. Magnetic resonance imaging of soft tissue masses: an evaluation of fifty-three histologically proven tumors. *Magn Reson Imaging* 1988;6:237-248
15. Wetzel LH, Levine E, Murphey MD. A comparison of MR imaging and CT in the evaluation of musculoskeletal masses. *RadioGraphics* 1987;7:851-874
16. Weekes RG, McLeod RA, Reiman HM, Pritchard DJ. CT of soft-tissue neoplasms. *AJR* 1985;144:355-360
17. Totty WG, Murphy WA, Lee JKT. Soft-tissue tumors: MR imaging. *Radiology* 1986;160:135-141
18. Doms GC, Hricak H, Solitto RA, Higgins CB. Lipomatous tumors and tumors with fatty component: MR imaging potential and comparison of MR and CT results. *Radiology* 1985;157:479-483
19. Bush CH, Spanier SS, Gillespy T. Imaging of atypical lipomas of the extremities: report of three cases. *Skeletal Radiol* 1988;17:472-475
20. Weisz GM, Gal A, Kitchener PN. Magnetic resonance imaging in the diagnosis of aggressive villonodular synovitis. *Clin Orthop* 1988;236:303-306
21. Mandelbaum BR, Grant TT, Hartzman S, et al. The use of MRI to assist in diagnosis of pigmented villonodular synovitis of the knee joint. *Clin Orthop* 1988;231:135-139
22. Jelinek JS, Kransdorf MJ, Utz JA, et al. Imaging of pigmented villonodular synovitis with emphasis on MR imaging. *AJR* 1989;152:337-342
23. Spritzer CE, Dalinka MK, Kressel HY. Magnetic resonance imaging of pigmented villonodular synovitis: a report of two cases. *Skeletal Radiol* 1987;16:316-319
24. Kottal RA, Vogler JB, Matamoros A, Alexander AH, Cookson JL. Pigmented villonodular synovitis: a report of MR imaging in two cases. *Radiology* 1987;163:551-553
25. Sundaram M, McGuire MH, Herbold DR, Beshany SE, Fletcher JW. High signal intensity soft tissue masses on T1 weighted pulse sequences. *Skeletal Radiol* 1987;16:30-36
26. Unger EC, Glazer HS, Lee JKT, Ling D. MRI of extracranial hematomas: preliminary observations. *AJR* 1986;146:403-407
27. Doms GC, Fisher MR, Hricak H, Higgins CB. MR imaging of intramuscular hemorrhage. *J Comput Assist Tomogr* 1985;9:908-913
28. Rubin JI, Gomori JM, Grossman RI, Gefter WB, Kressel HY. High-field MR imaging of extracranial hematomas. *AJR* 1987;148:813-817
29. Cohen EK, Kressel HY, Perosio T, et al. MR imaging of soft-tissue hemangiomas: correlation with pathologic findings. *AJR* 1988;150:1079-1081
30. Levine E, Wetzel LH, Neff JR. MR imaging and CT of extrahepatic cavernous hemangiomas. *AJR* 1986;147:1299-1304
31. Levine E, Huntrakoon M, Wetzel LH. Malignant nerve-sheath neoplasms in neurofibromatosis: distinction from benign tumors by using imaging techniques. *AJR* 1987;149:1059-1064

Book Review

Computed Tomography of the Abdomen in Adults. 85 Radiological Exercises for Students and Practitioners. By A. Wackenheim and A. Badoz. (Translated by Marie-Therese Wackenheim.) New York: Springer-Verlag, 159 pp., 1988. \$19.50

The aim of *Computed Tomography of the Abdomen in Adults* is to provide an easy and simplistic approach to the CT morphology of some of the lesions affecting upper abdominal organs. This is a small (8 × 5 in. [20.3 × 12.7 cm]), unpretentious, softcover book of 85 exercises, translated from French, containing exercises in abdominal CT diagnosis. It contains CT images illustrating common pathologic entities involving the liver, biliary ducts, pancreas, spleen, and kidneys. The illustrations are uneven but mostly adequate in quality. The book has no references and no bibliography. In the first part, normal CT anatomy and a variety of pathologic conditions are presented as challenging unknown cases in numerical order without labels or associated text. Corresponding diagrams with appropriate explanations and a succinct description, diagnosis, and differential diagnosis are provided in the second section of the book. The English translation suffers from some odd medical expressions but generally poses no significant difficulties in understanding the text.

To the uninitiated reader or beginner, this book provides a fast access to basic concepts of CT interpretation and illustrates the most common pathologic conditions affecting upper abdominal organs.

This is basic, not state-of-the-art, CT pathology useful in the daily practice of a gastroenterologist, internist, or abdominal surgeon. For the diagnostic radiologist, however, this is already an outdated book offering limited new or useful information. In addition, some of the CT images are confusing, pathologic changes are not always well demonstrated, and some of the statements made in the explanatory text are overstated. For instance, the authors claim that 80–90% of common duct stones are visualized by CT and that the diagnosis of a duodenal tumor can be made because contrast material is not seen in the duodenum.

Notwithstanding some of these limitations, the exercises can be useful to the medical student, resident in radiology, and the busy medical or surgical practitioner. Obviously, all this information and state-of-the-art techniques in CT diagnosis are easily available in recently published CT textbooks.

Emil J. Balthazar
Bellevue Hospital
New York, NY 10016

Expert Advice

Technical Aspects of Abdominal CT in Infants and Children

Robert A. Kaufman^{1,2}

As a result of remarkable advances in equipment, technique, sedation, and general availability, CT plays a central role in the diagnosis of pediatric abdominal disease and injury. This article focuses on those techniques and strategies that produce successful examinations in infants and children. The practical aspects of technique are emphasized, including preparation of the patient, sedation, immobilization and positioning, dynamic scanning with rapid table incrementation, technical factors, choice of contrast medium, and delivery of contrast medium. The discussion includes hints to help avoid pitfalls and traps that may spoil an examination in whole or in part. This practical technique is designed for the investigation of tumor, trauma, and infection in the infant and child [1].

The following presentation reflects 7 years experience with body CT in a large, tertiary-care, free-standing pediatric hospital with a wide referral area and a busy trauma service. Approximately 2700 examinations are performed annually, of which 75% are cranial and 25% are extracranial. The distribution of outpatients to inpatients is 55% to 45%.

Basic Principles

High-quality CT examinations of the infant and child are obtained easily by dynamic scanning at incremental levels during a bolus injection of IV contrast medium. This method shortens the examination, provides excellent vascular and tissue opacification, and produces accurate and reproducible

images. For dynamic scanning to be successful, however, meticulous attention to technique is required.

The technique for obtaining high-quality CT scans of the abdomen is based on the following general principles. First, the patient must be cooperative. If a child is unable to follow breath-holding instructions or unable to lie motionless on the scanner table because of discomfort or young age, the patient should be sedated so that the radiologist, not the child, controls the examination. Second, faster scanning times produce better results. Although a shorter scanning time reduces photon flux (and radiation dose), the outcome is generally a better quality scan because artifacts from respiratory motion and movement of the patient are minimized. Conversely, an excessively long scanning time increases photon flux (and radiation dose) but also enhances the likelihood of image degradation due to motion. Third, opacify everything. Oral and IV contrast media are usually necessary in order to provide satisfactory tissue contrast, which is inherently lacking in the infant and child. At times, a rectal contrast enema also is useful. When these principles are followed, CT can be a very accurate and useful tool for evaluating the abdomen in infants and children.

Preparation of the Patient

Food and liquids must be withheld from all infants and children who will receive IV contrast medium or sedation

Received January 23, 1989; accepted after revision March 28, 1989.

Presented at the American College of Radiology Categorical Course in Body CT with MR Imaging Correlation, September 24, 1988, Cincinnati, OH.

¹ Departments of Radiology and Pediatrics, University of Cincinnati College of Medicine, and Department of Radiology, Children's Hospital Medical Center, 240 Bethesda, Cincinnati, OH 45229-2899.

² Present address: Le Bonheur Children's Medical Center, Department of Radiology, 848 Adams Ave., Memphis, TN 38103. Address reprint requests to R. A. Kaufman.

(Table 1). It is preferable to do the same for patients receiving only alimentary tract contrast medium, although such cases are infrequent in our experience. As such, virtually all patients having abdominal CT examinations forego food and liquids for some length of time before the examination (Table 1).

Two additional benefits are derived from making the older child and teenager fast after midnight for a morning examination. Although the intent of this measure is not to dehydrate the patient, it virtually guarantees that the patient will be thirsty enough to drink the oral contrast medium, which is less than tasty to some. Second, it avoids having the energetic teenager arise at 4 a.m. to gobble down a 12-course breakfast only to become nauseated at 8 a.m. during a bolus IV contrast injection!

Venipuncture

A large-bore butterfly needle or a 22-gauge intravascular cannula is inserted into a vein in (preferably) the upper extremity and attached to a heparin well. It is secured with tape to an extremity that has been firmly immobilized on an arm board. Venipuncture is not routinely performed in the lower extremity, particularly when the liver or upper abdomen is being examined, in order to avoid artifacts caused by dense contrast medium in the inferior vena cava, which is subject both to respiratory and cardiac motion near the diaphragm. Venipuncture is performed first, as soon as the patient arrives to be scanned, so that the child's fears of a "shot" are not prolonged unduly.

Oral Contrast Medium

Almost all patients receive oral contrast medium to opacify the upper gastrointestinal tract because unopacified bowel loops may be mistaken for an abnormal fluid collection, and conversely, abnormal fluid collections may be mistaken for unopacified bowel loops.

We use a diluted solution of ionic contrast medium (Hypaque Sodium Oral Solution, Winthrop-Breon Laboratories, New York) dissolved in a flavored, clear liquid (grape or rainbow punch Kool-Aid, orange Tang), which masks the unpleasant taste moderately well. A 1.5% concentration of Hypaque Oral liquid is dense enough to opacify the small bowel, but is usually not so concentrated in the colon that it creates artifacts. The usual volume of liquid administered is 4–16 oz (118–473 ml) of this solution, given according to an arbitrary dose regimen (Table 2).

TABLE 1: Suggested Schedule for Withholding Food and Liquid Before CT

Age	When to Withhold
Premature	Consult neonatologist
Neonate	One feeding
Infant < 1 year	For 3 hr
Over 1 year	For 4 hr
Older children and adolescents	After midnight for morning examinations

TABLE 2: Oral Contrast Medium, Single-Dose Regimen

Age	Volume of 1.5% Solution
Neonate	Per neonatologist
Under 1 year	4 oz (118 ml)
1–5 years	8 oz (237 ml)
6–12 years	12 oz (355 ml)
Over 12 years	16 oz (473 ml)

Note.—Each ounce (29.6 ml) of 1.5% oral contrast medium contains 1.1 ml of stock solution Hypaque Oral liquid.

When to Use a Nasogastric Tube

If liquid cannot be taken orally, it may be necessary to use a nasogastric tube to deliver the oral contrast medium. The same is true for a young child who refuses to drink the oral contrast medium as the time of examination nears. If praise and encouragement and help from the child's parent do not elicit success, an 8-French feeding tube is placed into the stomach to deliver the contrast medium. Additives for flavoring are not used in this case. This may save a greater deal of time and anguish, and gives control of the gastrointestinal tract opacification to the radiologist rather than leaving it to the whim of the child (Fig. 1). It also provides the opportunity to aspirate swallowed air from the child's stomach, which may cause an artifact because of its interface with high-density oral contrast medium.

Timing of Oral Contrast Medium

In order to opacify the small bowel for an upper abdominal examination, a single dose of oral contrast medium (Table 2) is administered 45 min before scanning. This opacifies the gastrointestinal tract from the stomach to the terminal ileum. If an examination of the abdomen and pelvis is to be performed (e.g., in Hodgkin disease staging), then a single dose of oral contrast medium is given the preceding evening (12–14 hr before scanning) [2] and a second dose the morning of (45 min before) scanning. Additional oral or rectal supplementation is given if needed.

When upper abdominal injury is suspected [3], the examination is begun only 10–15 min after administration of oral contrast medium. This allows contrast medium to reach the upper small bowel if ileus is not present. The time interval between contrast administration and scanning may be lengthened if lower abdominal injury is suspected and it is safe to do so. Occasionally, emptying the stomach can be expedited by placing the child in the right lateral decubitus position on the gurney or scanner table. In addition, when examining a patient with blunt trauma, we reduce the volume of oral contrast medium in the suggested dose schedule (Table 2) by one third to one half. This is particularly important if splenic injury is suspected, because distension of the stomach in a child with a ruptured spleen commonly causes pain and nausea. In addition, most emergency circumstances dictate a short examination time, which does not allow the usual 45 min for contrast medium to opacify the entire upper gastrointestinal tract.

Fig. 1.—CT scan of 19-month-old girl with splenic granulomatous abscesses from histoplasmosis. Oral contrast medium given through nasogastric tube produces no air-contrast level in stomach.

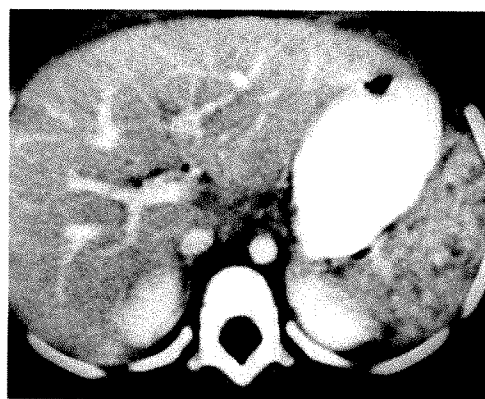
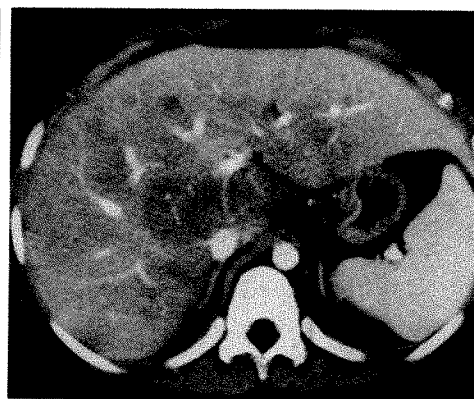


Fig. 2.—Bolus effect. An aortocaval contrast density difference of greater than 30 H allows detection of infiltrative disease throughout liver on CT scan of 7-year-old boy. Note bolus effect in Fig. 1 also.



1

2

Vomiting of contrast medium is a problem that occurs occasionally, particularly in oncology patients who are receiving chemotherapeutic drugs and often are nauseated. In this case, we try to schedule an elective CT examination either the week before or sufficiently after chemotherapy administration so that the tendency for nausea is minimized. The injured child may become nauseated if the stomach is rapidly distended. In this circumstance, we infuse the oral contrast medium slowly via a nasogastric tube in order to obtain good opacification, while avoiding excessive gastric distension.

When Not to Use Oral Contrast Medium

Oral contrast medium is usually given for most examinations of the abdomen for trauma, tumor, and infection. However, if only the liver, spleen, or kidney parenchyma is to be scanned, it may be useful *not* to opacify the upper gastrointestinal tract when an air-contrast level in the stomach interferes with lesion detection in the left lobe of the liver; when bowel distension is severe enough to cause artifacts that hinder interpretation of the inferior edges of the left and right lobes of the liver; and when a nauseated patient will most likely vomit during injection of IV contrast material, causing delay in or interruption of scanning. For example, we do not think it necessary to administer oral contrast medium for examination of the liver, spleen, and kidneys in the immunosuppressed patient when looking for microabscesses [4].

Related contraindications to the use of oral contrast medium include the lack of a gag or cough reflex and a patient who is intubated without a cuffed endotracheal tube. This is particularly important, in our opinion, in the patient with head injury who is comatose or unresponsive. In most institutions, oral contrast medium is contraindicated if general anesthesia is planned.

Renal Contrast Enema

When opacification of the distal colon is needed, a 1.5% solution of Hypaque Oral liquid in tap water is administered *slowly* via a small-caliber barium enema tip. The volume of contrast solution should be limited to less than 200 ml: 50 ml for infants, 100 ml for young children, 150 ml for older children.

If sedation is required for the examination, the contrast enema is given after the patient is sedated. The liquid is usually retained very consistently even if the child is asleep. The key to success is a *small volume*, given through a *small tube*, *slowly*.

Sedation

Sedation is necessary in most children under 4 years of age, especially when IV contrast medium is used. Most infants and children in this age group are best examined while asleep. Although some 4 and 5 year olds are mature enough to breath-hold on command or remain motionless for the entire examination, many will require sedation. With children over 5 years of age, less sedation is needed. Our most successful drug regimen is based on IV pentobarbital, IV phentanyl, or (in the infant 1 month to 18 months of age) oral chloral hydrate.

IV pentobarbital is given initially in a dose of 2 mg/kg. If this is insufficient, additional pentobarbital is given to a maximum of 6 mg/kg [5]. After an *initial* dose of pentobarbital, if the child is very close to sleep but awakens when positioned or when the scanner table moves, IV phentanyl is administered by titrating 1 μ g/kg until sedation and/or analgesia is achieved. We rarely exceed a 2 μ g/kg dose. If the child has already received a second dose of pentobarbital, such that the total pentobarbital dose is ≥ 5 mg/kg, then we are very judicious about the use of any additional phentanyl and generally do not exceed 2 μ g/kg, especially if there is oral contrast medium in the gastrointestinal tract. Occasionally, phentanyl is used alone if only calming and analgesic effects are needed, such as in the child with a skeletal injury or other painful condition that precludes cooperation. Phentanyl and pentobarbital must be administered cautiously and according to the manufacturers' recommendations. As with any potent narcotic or barbiturate, substantial risks are associated with their use and the patient must be monitored closely and carefully. There is an increased risk of respiratory depression and arrest when phentanyl and pentobarbital are combined. In our group, this sedation protocol has been 98% successful, with a very small complication rate of 2% (R. Towbin and R. Kaufman, unpublished data in 1020 cases). Recently, Strain et al. [5, 6] have reported a similar success and safety rate in their use of IV pentobarbital for CT sedation.

Sedation Failures

In our experience, sedation is most likely to fail in the severely mentally retarded child, the organ or bone marrow transplantation patient, and the patient receiving chronic barbiturate medication. In the last two categories, the hepatic metabolism of the sedatives we commonly use may be increased to such a level that doses far in excess of our usual regimen are required for successful sedation. When we encounter a sedation failure or anticipate unusual sedation difficulties, we consult our colleagues in pediatric anesthesiology for help and advice, believing that circumstances out of the routine are best handled by pediatric experts in sedation.

Monitoring of the Patient

All patients undergoing sedation for CT are carefully monitored, both visually by nursing and medical personnel, as well as by mechanical means using a pulse-oximeter or a cardiorespiratory monitor with ECG recording capability. Periodic recording of vital signs is done according to institutional guidelines. Blood pressure recording is not done routinely unless the patient is critically ill or injured, as this tends to wake up the sedated child, and thus adds to the examination time, the radiation dose, and the amount of sedation required for an adequate study.

Psychological Preparation: The Three Es

For the child who will remain awake for the procedure, it is important to provide a simple and truthful *explanation* of the procedure to be performed. Information should be provided in a reassuring and nonthreatening manner. Speaking softly and in a friendly tone is less frightening. The scanning room should be relatively quiet, noise kept at a minimum. The child should not be left alone for any length of time, as this often adds to the anxiety level and increases the likelihood of improper positioning and unexpected movement.

Giving the child an *expectation* of what will occur decreases the likelihood that "surprise" will ruin the study. This is particularly important for the injection of contrast medium during dynamic scanning with table incrementation. In those children well enough and mature enough to follow instructions on command and who can repeatedly suspend respiration for 5 sec, we practice breath-holding before the examination begins. Kuhns et al. [7] have shown that most 5-year-old children can voluntarily suspend respiration for 5 sec or more. Our experience supports that finding. In children 4 to 5 years old who cannot do this, quiet breathing in an otherwise motionless child may be satisfactory. Sometimes, however, it becomes obvious during "practice" that sedation will be necessary to avoid unacceptable motion.

Finally, all young children generally want to know "When will we be done?" Accurately predicting the *end point* of the examination is important in maintaining the child's concentration and cooperation throughout the examination. Virtually all

children old enough and well enough to breath-hold on command are capable of counting from one to 20 or so. Thus, we tell each child how many scans ("pictures") will be taken so that he can count along with us through the critical part of the examination.

Immobilization and Positioning

All children undergoing abdominal CT are positioned supine with both arms elevated above the head, elbows slightly flexed. For the trauma patient who may have a clavicle or humerus fracture, the orthopedist or surgeon is asked to help move the injured extremity safely into a position out of the field of view of the X-ray beam. We do not scan the abdomen or chest with an upper extremity in the X-ray beam. The upper extremities are then immobilized by using tape or velcro wristlets with enough tension to make even the sleeping child feel secure. A velcro strap is placed across the chest and another across the thighs and knees. All extraneous tubes, catheters, and monitor leads are removed from the field of view before scanning. Care is taken to position and align the patient as perfectly as possible.

Technique

Scout Digital Radiographs

An anteroposterior digital radiograph is made from above the diaphragm to the iliac crests or lower, if warranted, for examination of the lower abdomen and pelvis. The digital radiograph is used for localizing a specific anatomic area, for planning the noncontrast and contrast scans to be taken, for determining the presence of gastric and bowel dilatation, and for determining the adequacy of distribution of oral contrast medium. A lateral digital radiograph is occasionally useful in blunt trauma if free intraperitoneal air has not been excluded beforehand by plain radiographs.

Scout Scans Made Without Contrast Medium

Because infants and younger children have little fat or inherent contrast of their own, there is little need for extensive noncontrast abdominal scanning in children, especially if the contemplated lesion(s) is (are) small. Although unenhanced sections in the abdomen may be useful when detection of calcification or hemorrhage is important, if diffuse infiltrative disease is suspected in the liver, and when a known solitary lesion is being investigated, they are most useful for checking the distribution of oral contrast medium in the bowel, for determining positioning and technical factors to be used, and as another opportunity to test of the level of cooperation of intermittent breath-holding during the exposures. In the usual upper abdominal CT examination, we make an average of four to five evenly spaced non-contrast-enhanced slices through the area of interest. An important exception to this is the workup of a new abdominal tumor, or an examination to look for calculi in the kidneys or urinary tract.

IV Contrast Medium: Strategies for Use

In our opinion, the most successful CT examination of the abdomen in an infant or child is obtained by injecting a bolus of contrast material with dynamic scanning and rapid table incrementation [8]. Other contrast strategies, including delayed scanning, infusion, and postinfusion scanning techniques, are less reliable for most lesions [9–13].

The "bolus effect" after rapid injection of contrast medium is a rapidly changing rather than uniform phase. The concentration of contrast material differs between the aorta and the inferior vena cava by more than 30 H (bolus effect), which enhances lesion detectability (Fig. 2). Equilibrium phase (difference in iodine concentration between aorta and inferior vena cava of less than 10 H) is reached 2 min after bolus injection and almost immediately after an infusion [12]. Equilibrium phase scanning does not improve lesion detectability and it carries the risk of lesion isodensity [12]. Delayed scanning also heightens the risk of isodensity of nonhypervascular lesions [12, 13].

Dynamic Scanning with Table Incrementation

The key part of each examination is the dynamic scanning with table incrementation during a bolus injection of IV contrast medium. Contrast medium is injected as rapidly as possible while consecutive scans are taken and the table is incremented (Fig. 3). If the child is sedated, the table is incremented as rapidly as possible. If the child is breath-holding, a 6-sec (to 8-sec) interscan delay is programmed between exposures.

Thus, if one is using a sub-5-sec scanner (e.g., GE 8800) with a 4.8-sec scanning time, the total "slice unit" (scanning time + table incrementation) per table location varies between 7.3 and 10.8 sec (Table 3). For a sub-2-sec scanner (e.g., GE 9800) the slice unit varies between 5.5 and 8.0 sec. By multiplying the slice-unit time by the number of scans programmed, the total scanning time can be calculated. Most examinations in infants and children will take 60–120 sec for the dynamic scanning with table incrementation. Ultrafast CT scanners have exposure times up to 20 times shorter than most conventional scanners, which may reduce the slice-unit

time considerably, as well as decrease the radiation dose and the need for sedation.

Scanning Time

We advocate the use of the shortest scanning time available. With our scanner, the 2-sec scan or 1.2-sec partial arc scan (Fig. 4) are used routinely. It may be necessary to increase the milliamperage setting when using the partial scanning time in older children in order to generate high-quality images.

Slice Thickness and Interval

Routine abdominal examinations are performed by using contiguous 10-mm sections. If wide respiratory excursion is present in breathing infants and young children, overlapping 10-mm scans at 7.5-mm table increments helps avoid gaps in information in both the abdomen and the chest. Thinner sections are reserved for the very detailed work, such as pancreatic examinations, and are rarely used.

Choice of Contrast Medium

We prefer to use a nonionic contrast agent such as iohexol or iopamidol (300 mg/ml), usually at a dose of 2 ml/kg to a maximum of 100 ml, for all body CT examinations. The nonionic agents have the advantage of causing less nausea and vomiting during administration of the bolus of contrast medium; reduced local sensation on injection (important both in the sedated and the awake child); and subjectively, less of an unpleasant feeling, in general, is reported. Any or all of these factors could otherwise potentially ruin an examination in a marginally cooperative or mildly sedated patient.

Because of the viscosity of nonionic contrast agents, a bolus injection may be difficult if the IV cannula is small. Warming the contrast medium to body temperature (98.6°F) in a continuous temperature contrast-material warmer is useful to reduce viscosity during injection. Avoidance of larger volume syringes in preference to smaller sizes also allows for a faster injection of contrast medium. If multiple smaller

Fig. 3.—Dynamic CT scanning with rapid table incrementation in a 9-year-old boy with head injury and blunt abdominal trauma. "Slice-unit" time is 5.5 sec. Scan was made in corticomedullary junction differentiation (arterial) phase of injection of contrast medium. Note complex, central laceration of liver parenchyma, and halo of blood around inferior vena cava.



3

Fig. 4.—1.2-sec partial arc scanning time provides high-quality CT image in a 15-month-old abused infant. Note splenic infarct, perigastric hematoma, and blood in fissure for ligamentum teres.



4

TABLE 3: Slice Unit Time

Patient	Sub-5-Sec Scanner (e.g., GE 8800)				Sub-2-Sec Scanner (e.g., GE 9800)			
	Scanning Time		Table Incrementation	Total	Scanning Time		Table Incrementation	Total
Sedated	4.8 sec	+	2.5 sec (minimum)	= 7.3 sec	2.0 sec	+	3.5 sec (minimum)	= 5.5 sec
Breath-holding	4.8 sec	+	6.0 sec	= 10.8 sec	2.0 sec	+	6.0 sec	= 8.0 sec

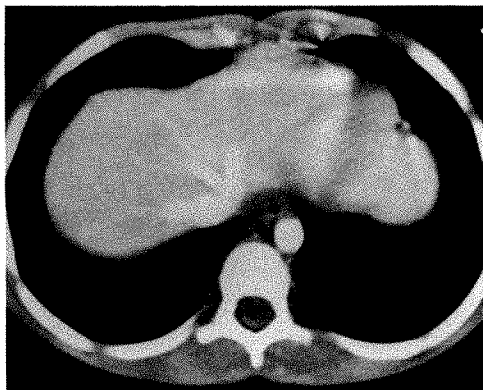


Fig. 5.—Rapid bolus injection of more than 50% of total IV contrast dose before CT scanning allows excellent vascular enhancement of inferior vena cava and hepatic veins, as well as liver parenchyma in dome of liver.

volume syringes are used, they may be connected to a three-way stopcock so that the flow of IV contrast medium is interrupted as little as possible during syringe changes. As nonionic contrast medium is expensive, unused contrast medium can be saved and refrigerated in the original vial to be used later for preparation of oral or rectal solutions of contrast medium.

How to Administer A Bolus

For upper abdominal examinations, 50% of the total dose of contrast material is injected as rapidly and evenly as possible, then scanning is begun while the second half of the dose is injected (Fig. 5). If the total scanning time is very short and the total number of scans is quite small, 60% to 65% of the dose may be injected before the scanning is begun.

For examinations of the abdomen and pelvis, scanning is begun after 40% to 50% of the total dose of contrast material is injected rapidly. The injection is completed as quickly as possible. Occasionally in older children, a small additional aliquot of contrast medium (0.5 ml/kg) is helpful when injected at the level of the umbilicus during rapid table incrementation from the diaphragm to the symphysis pubis in order to supplement the enhancement of the pelvis.

When visualization of the renal collecting systems and ureters is essential, the technique is modified to ensure modest but adequate pyelographic excretion of contrast medium in the urinary tract. This involves injecting from 2 to 5 ml of IV contrast medium approximately 3 to 5 min before the bolus

injection. Collecting system density will be sufficient, but not enough to cause an artifact in the breathing patient.

A Strategy for Successful Results

Although the time spent in preparation, sedation, and positioning of the child forms a strong foundation for high-quality results, the 2 min needed for the dynamic scanning and table incrementation is the most critical period of the examination. If the radiologist is present within or immediately outside of the scanning room, monitoring and supervising the procedure, then there is a greater chance of anticipating difficulty, correcting problems, and potentially saving an examination that otherwise may be spoiled. It is time and effort well spent.

ACKNOWLEDGMENTS

My thanks to Patty Felix for preparing the manuscript and to J. Scott Dunbar for his support and encouragement.

REFERENCES

1. Kaufman RA. Liver-spleen computed tomography: a method tailored for infants and children. *J Comput Tomogr* 1983;7:45-47
2. Cranston PE. Colon opacification by oral water-soluble contrast medium administration the night prior to CT examination. *J Comput Tomogr* 1982;6:413-415
3. Kaufman RA, Towbin R, Babcock DS, et al. Upper abdominal trauma in children: imaging evaluation. *AJR* 1984;142:449-460
4. Shirkhoda A. CT findings in hepatosplenic and renal candidiasis. *J Comput Assist Tomogr* 1987;11:795-798
5. Strain JD, Harvey LA, Foley LC, Campbell JB. Intravenously administered pentobarbital sodium for sedation in pediatric CT. *Radiology* 1986;161:105-108
6. Strain JD, Campbell JB, Harvey LA, Foley LC. IV Nembutal: safe sedation for children undergoing CT. *AJR* 1988;151:975-979
7. Kuhns LR, Berger PE, Zierolf E, Spielman S. Duration of voluntary apnea in children. *Radiology* 1979;132:355
8. Kaufman RA. Liver disease in the infant and child. In Silverman PM, Zeman RK, eds. *Contemporary issues in computed tomography, CT and MRI of the liver and biliary system*. New York: Churchill Livingstone (in press)
9. Zeman RK, Clements LA, Silverman PM, et al. CT of the liver: a survey of prevailing methods for administration of contrast material. *AJR* 1988;150:107-109
10. Phillips VM, Erwin BC, Bernardino ME. Delayed iodine scanning of the liver: a promising CT technique. *J Comput Assist Tomogr* 1985;9:415-416
11. Foley WD, Berland LL, Lawson TL, Smith DF, Thorsen MK. Contrast enhancement technique for dynamic hepatic computed tomographic scanning. *Radiology* 1983;147:797-803
12. Burgener FA, Hamlin DJ. Contrast enhancement of hepatic tumors in CT: comparison between bolus and infusion techniques. *AJR* 1983;140:291-295
13. Marchal GY, Baert AL, Wilms GE. CT of noncystic liver lesions: bolus enhancement. *AJR* 1980;135:57-65

Pictorial Essay

CT of Blunt Abdominal Trauma in Children

George A. Taylor,¹⁻³ Christopher J. Guion,^{1,4} Barry M. Potter,^{1,2} and Martin R. Eichelberger^{2,5}

CT has become the imaging method used most often in the evaluation of children with suspected abdominal injury after blunt trauma. Its utility in the determination of the presence and extent of injury has been well documented [1-3]. Familiarity with patterns of injury in childhood and their appearance on CT is important for the radiologist involved in imaging acutely injured children. In this essay we present our experience with 615 consecutive children evaluated with CT for blunt abdominal injury over a 5-year period.

Technique

CT scans were obtained on either a GE 8800 (before June, 1983) or GE 9800 CT scanner (General Electric, Milwaukee, WI), with 1-cm-thick slices at 1-cm intervals. All children received 3 ml/kg of iohalamate 43% (Conray, Mallinckrodt, St. Louis, MO) by rapid IV infusion for contrast enhancement. Gastrointestinal contrast material was not used routinely but reserved for situations in which an injury to the intestinal tract was strongly suspected clinically but not shown on standard CT images (two patients). Appropriate positioning, removal of overlying metallic hardware, and a sufficiently large radius of reconstruction are keys to accurate CT diagnosis in the traumatized child (Fig. 1).

Solid-Organ Injury

One hundred twenty-three children (20%) had solid-organ injuries. Of these, 45 children (37%) had injuries to more than one abdominal organ. In contrast to experience reported in

the literature [1], the liver was the most commonly injured solid viscus in this series (47%), followed by the spleen (44%), kidney (34%), and pancreas (6%). Although CT was useful in the detection and delineation of most parenchymal injuries (Figs. 1-5), pancreatic injury occasionally was difficult to identify with CT. The plane of fracture through the pancreas and peripancreatic soft-tissue changes were often subtle and nonspecific in the acute phase of injury (Figs. 6-8).

Hollow-Organ Injury

The CT diagnosis of hollow viscus rupture usually depends on the presence of extravasated air or contrast material. Pneumoperitoneum was detected in four of six intestinal perforations (Figs. 9 and 10). In two children, thickened bowel wall and unexplained peritoneal fluid collections were the only CT indications of intestinal perforation (Fig. 11). Intraperitoneal bladder perforation was identified on CT in two children by the presence of extravasated contrast material in the peritoneal cavity (Fig. 12). Although the specific site of rupture was not identified on CT, the presence of air or extravasated contrast material in the peritoneal cavity was an indication for surgical exploration of the abdomen.

Physiologic Instability

Recently, we have recognized a complex of findings on abdominal CT that are associated only with profound shock in young traumatized children [4]. This "hypoperfusion com-

Received February 8, 1989; accepted after revision April 24, 1989.

¹ Department of Radiology, Children's Hospital National Medical Center, Washington, DC 20010.

² Department of Pediatrics, Children's Hospital National Medical Center, Washington, DC 20010.

³ Present address: Department of Radiology, The Johns Hopkins Hospital, 600 N. Wolfe St., Baltimore, MD 21205. Address reprint requests to G. A. Taylor.

⁴ Present address: Department of Radiology, The Children's Hospital, 1600 7th Ave., S., Birmingham, AL 35233.

⁵ Department of Surgery, Children's Hospital National Medical Center, Washington, DC 20010.



Fig. 1.—8-year-old boy injured in fall.
A, CT scan at another hospital with patient in oblique position, and with a small radius of reconstruction. Significant motion was present on scans above and below this level. Peripheral splenic lucencies were interpreted as beam-hardening artifacts related to overlying ribs.
B, CT scan 4 hr later at our institution shows a shattered spleen and small amount of peritoneal fluid surrounding liver (arrow).

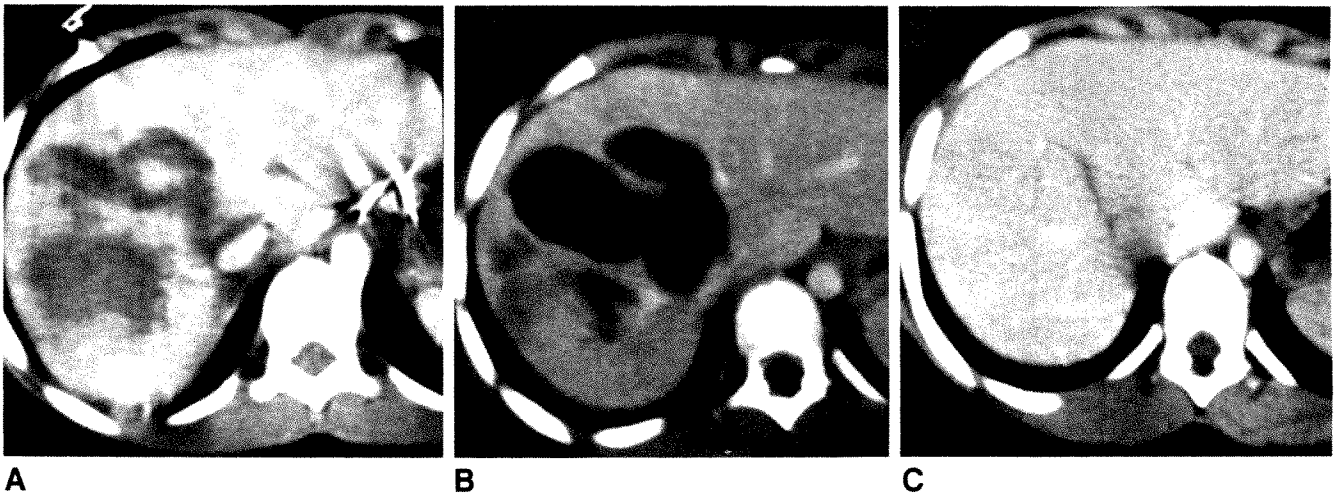


Fig. 2.—9-year-old boy struck by car.
A, Initial CT scan shows complex injury to right lobe of liver, extending to and surrounding inferior vena cava. Patient was hemodynamically stable and was treated nonoperatively.
B, Follow-up CT scan at 1 month shows partial resolution and liquefaction of hematoma.
C, CT scan at 3 months shows almost complete resolution of injury. Only a thin, irregular lucency remains.

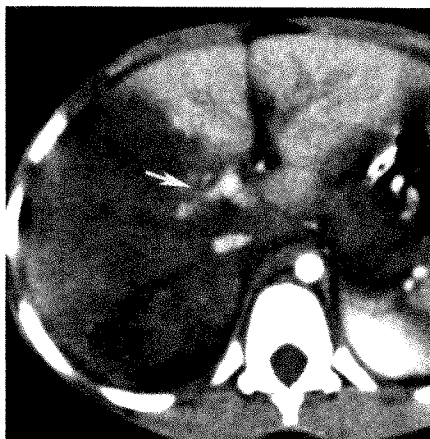
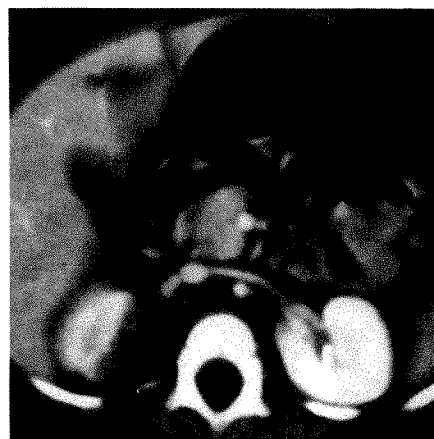
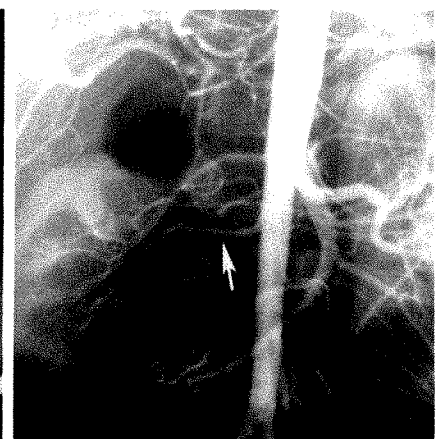


Fig. 3.—5-year-old boy crushed by dumpster. CT scan shows vascular compromise of most of right lobe of liver and right kidney. Note sharp cutoff of right portal vein (arrow) and flattening of inferior vena cava. Fever, abdominal pain, and leukocytosis developed 1 week later; a partial hepatectomy was required because of infection in infarcted portions of liver.



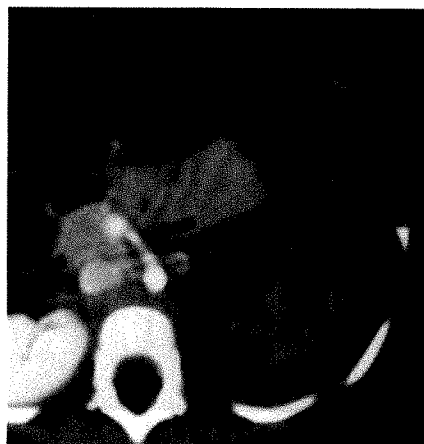
A



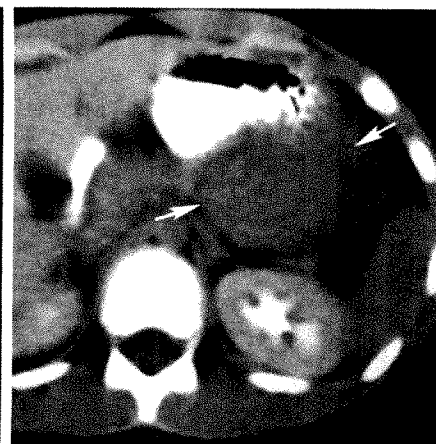
B

Fig. 4.—1-year-old girl injured in motor vehicle accident.
A, CT scan shows vascular compromise of lower pole of right kidney.
B, Arteriogram 1 week later shows intimal tear of accessory right renal artery (arrow). Balloon angioplasty and surgical repair of the vessel were unsuccessful, and the patient required a heminephrectomy for control of blood pressure.

Fig. 5.—2-year-old girl injured in motor vehicle accident. CT scan 2 days after injury shows poorly functioning, macerated left kidney and a moderate amount of peritoneal fluid. Follow-up DTPA renal scan (not shown) showed minimal return of function.

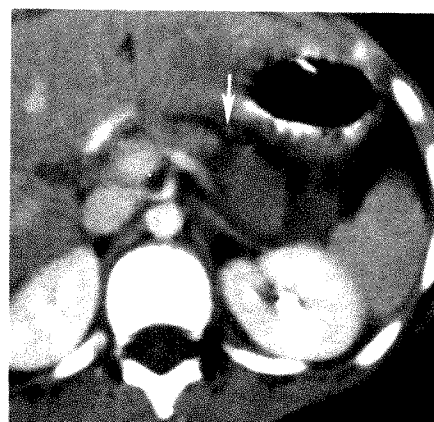


5



6

Fig. 6.—13-year-old girl injured in fall. Hematoma of pancreatic tail was suspected on initial CT scan (arrows). At surgery, a hemorrhagic papillary cystic tumor was removed from pancreas.



A

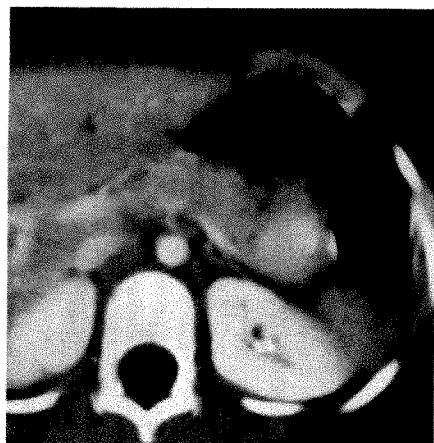


B

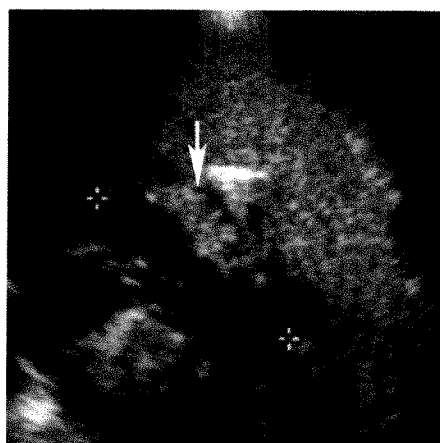
Fig. 7.—11-year-old boy injured in motor vehicle accident.

A, Initial CT scan shows transection of body of pancreas (arrow).

B, Follow-up CT scan obtained because of persistent abdominal pain shows well-defined pseudocyst (arrow). Fever and leukocytosis developed, and surgical cyst drainage was required.



A



B

Fig. 8.—5-year-old boy run over by trailer.

A, Initial CT study. Pancreas was interpreted as normal.

B, Follow-up sonogram 12 days later shows poorly defined pseudocyst (measured by cursors) near tail of pancreas (arrow).



Fig. 9.—10-year-old boy who fell against handlebars while riding bicycle. Small bubble of free peritoneal air is seen adjacent to ligamentum teres (arrow). Perforation of proximal jejunum was found at surgery.

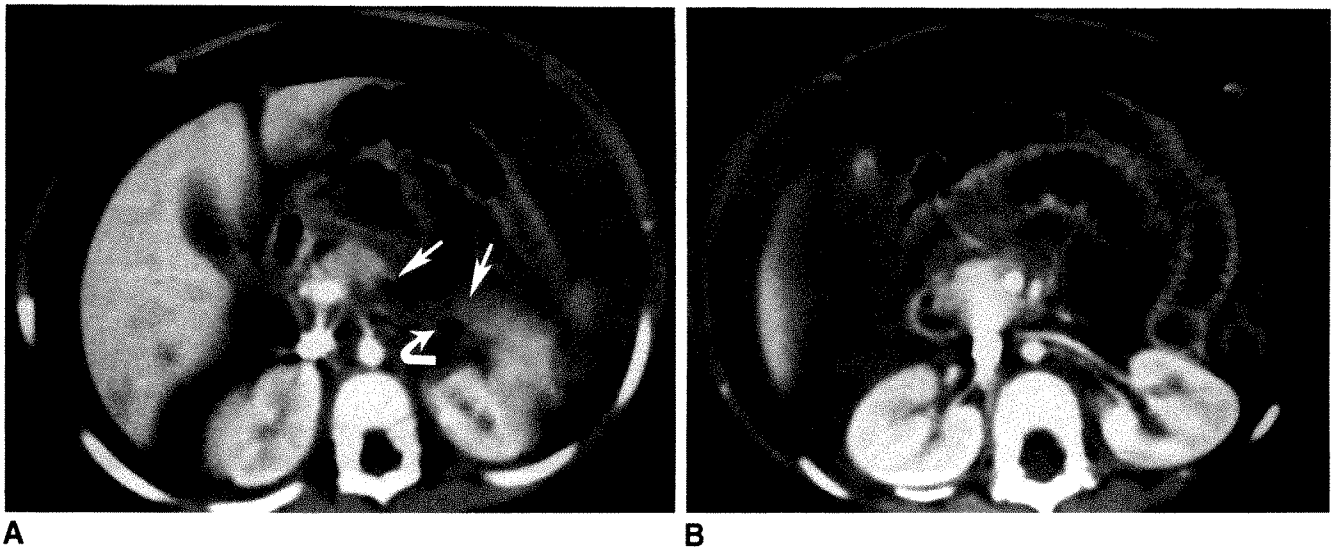


Fig. 10.—2-year-old abused girl. Her blood pressure was unobtainable on arrival at emergency room. She responded to resuscitative measures and appeared to be clinically stable at the time of CT. She had a severe metabolic acidosis (pH, 6.84; base deficit, -28).

A, CT scan shows large hemoperitoneum, transection of pancreas (straight arrows), and small bubbles of gas in retroperitoneum (curved arrow).

B, CT scan shows markedly dilated loops of abnormally enhancing bowel; dense nephrograms; and small caliber of aorta, superior mesenteric artery, and vein. Aortic diameter below renal arteries was 3.0 mm. At surgery, transections of pancreas and duodenum were identified and repaired. Acute respiratory distress developed, and the patient died 20 hr after surgery.

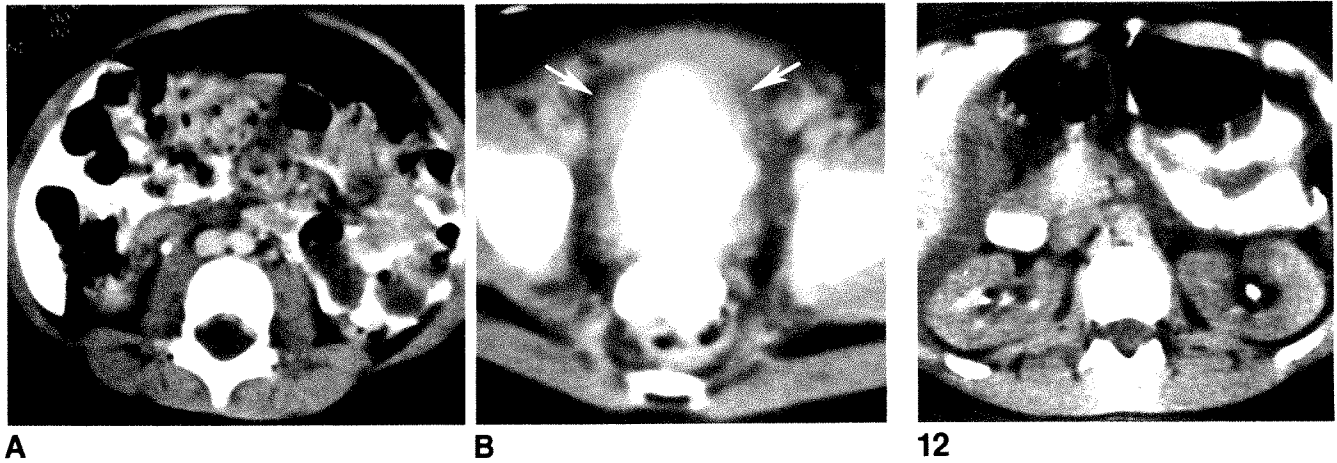


Fig. 11.—2-year-old girl with gross hematuria after motor vehicle accident.

A and B, CT scans show intraperitoneal contrast material (A) and contracted, irregular bladder wall (B, arrows). Perforation of bladder was repaired at surgery.

12

Fig. 12.—16-year-old girl injured in motor vehicle accident. Diffusely thickened and abnormally enhancing small bowel was present on initial CT scan (not shown). Because of strong suspicion of intestinal injury, barium was administered orally and CT was repeated. Diffuse thickening of small bowel and peritoneal fluid are present. No extravasation is evident. A jejunal perforation was identified at surgery. Diffuse edema of small bowel was confirmed and thought to be related to vascular injury.

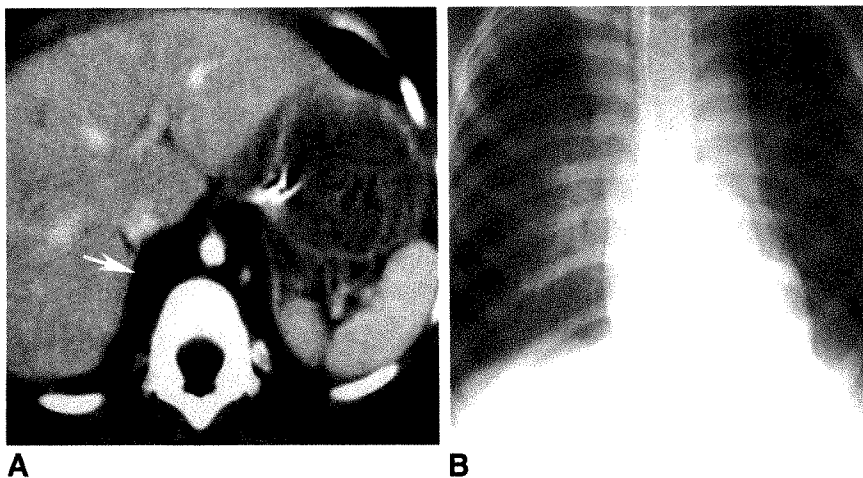


Fig. 13.—7-year-old boy struck by car. Initial chest radiograph (not shown) was overexposed and did not allow evaluation of mediastinum.

A, CT scan shows evidence of retrocrural hematoma (arrow), suggesting a possible mediastinal hematoma.

B, Repeat chest radiograph after CT shows bilateral paraspinal and mediastinal widening consistent with vascular injury. The patient died next day of severe head injuries. Autopsy showed a transection of aortic arch and left pulmonary vein.

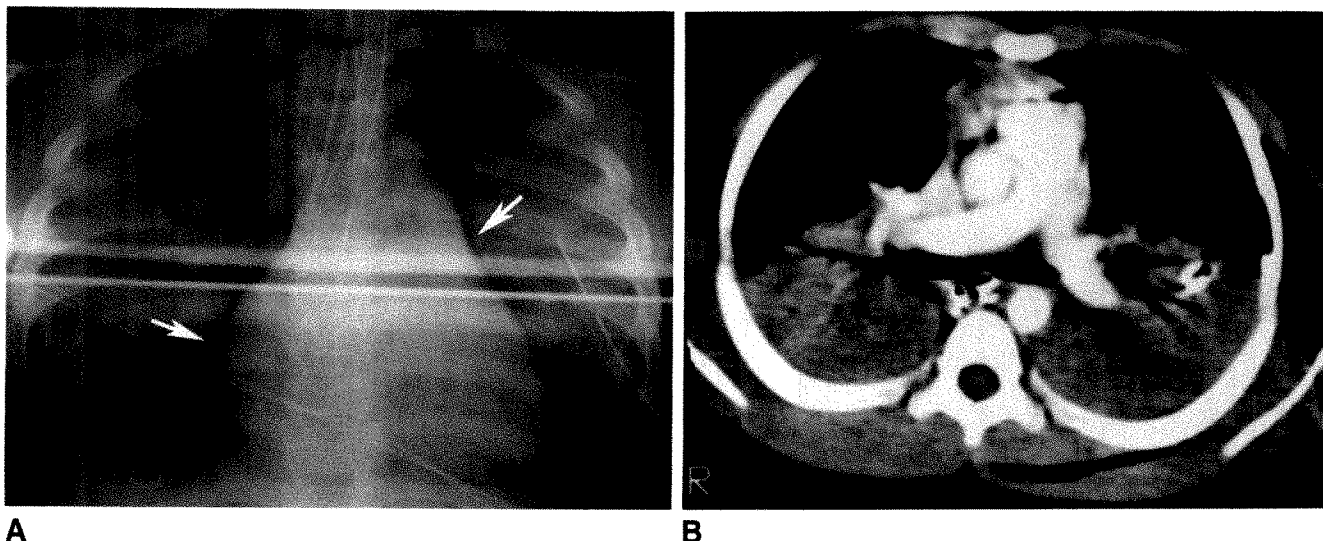


Fig. 14.—10-year-old boy struck by car.

A, Portable chest radiograph shows small bilateral pneumothoraces (arrows). Pleural tubes are present. Nasogastric tube is coiled in esophagus, and tip of endotracheal tube is in right main bronchus.

B, CT scan obtained within 30 min of radiograph shows large bilateral pneumothoraces with marked loss of volume in both lungs and moderate subcutaneous emphysema. Left pleural tube was thought to be in major fissure.

plex" consists of marked, diffuse dilatation of the intestine with fluid; abnormally intense contrast enhancement of the bowel wall, mesentery, kidneys, and/or pancreas; decreased caliber of the abdominal aorta and inferior vena cava; and moderate to large peritoneal fluid collections (Fig. 12). This complex was present in 13 patients. All appeared clinically stable at the time CT was performed but died within 36 hr of presentation.

Chest Injuries

The lower chest is often included in the CT imaging of the upper abdomen. Associated parenchymal or mediastinal in-

juries were detected in 15% of children examined with CT. Plain radiographs of the chest often missed or underestimated the degree of abnormality present (Figs. 13 and 14).

REFERENCES

1. Kaufman RA, Towbin R, Babcock DS, et al. Upper abdominal trauma in children: imaging evaluation. *AJR* 1984;142:449-460
2. Taylor GA, Fallat ME, Potter BM, Eichelberger MR. The role of computed tomography in blunt abdominal trauma in children. *J Trauma* 1988;28:1660-1664
3. Kane NM, Cronan JJ, Dorfman GS, DeLuca F. Pediatric abdominal trauma: evaluation by computed tomography. *Pediatrics* 1988;82:11-15
4. Taylor GA, Fallat ME, Eichelberger MR. Hypovolemic shock in children: abdominal CT manifestations. *Radiology* 1987;164:479-481

Book Review

Diagnostic Imaging of the Acute Abdomen. A Clinico-Radiologic Approach. By Dieter Beyer and Ulrich Mödder. (Translated by Terry C. Telger.) New York: Springer-Verlag, 445 pp., 1988. \$130

This work is divided into six chapters encompassing clinical features, imaging techniques, imaging findings, specific disease entities, pediatrics, and charts giving relative values of studies in specific clinical contexts. The contributors are 11 German radiologists and one German surgeon. The quality of the English translation is excellent; for the most part the reader is unaware that this book was originally a German text. The images are mostly plain films, sonograms, and CT scans, with some contrast gastrointestinal examinations and angiograms. The image quality is excellent, especially the sonograms. The line drawings illustrating anatomic points are also excellent. The quality of the binding and paper is first-rate. The cost is high. The references at the end of each chapter are not specific citations; they are in the form of suggested reading lists and include mostly texts and some older and more recent journal articles.

This book was designed to "serve as a quick reference aid in daily practice," assist the attending physician in tailoring imaging studies to the problems of the given patient, and "show the current status of diagnostic radiology in the investigation of the acute abdomen." The authors' aim is to provide short, clear presentations emphasizing relevant signs and symptoms and clinical problems, with some unavoidable overlap between chapters emphasizing, in turn, methods, signs and symptoms, and diseases.

The first chapter, on clinical examinations and signs and symptoms, is short and superficial, consisting mostly of lists of signs and symptoms and diagnoses. I disagree with the statement that the physician must know location and character of pain, rigidity, and peristalsis in order to interpret radiographs, sonograms, and CT scans of the acute abdomen correctly. The second chapter, on imaging techniques and systematic analysis, is also short and superficial. In this chapter and the subsequent chapter, use of water-soluble material in studies of the upper gastrointestinal tract is recommended for diagnosis of suspected partial or complete obstruction of the small bowel and for "therapeutic effect" in paralytic ileus. Most gastrointestinal radiologists would use barium in these patients and would dispute any therapeutic effect of water-soluble contrast material in paralytic ileus. Enemas with water-soluble contrast material are recommended for patients with clinical or radiologic findings that suggest perforation or

obstruction of the colon. I prefer barium for diagnosis of obstruction and would not use any enemas with contrast material if free air were present. If localized colonic perforation is suspected and no free air is present, I prefer barium. The authors advocate a left lateral decubitus view of the abdomen in addition to the supine view for evaluation of the acute abdomen. The most common practice in the United States for patients who can stand is to take chest and abdominal films with the patient erect in addition to the film taken with the patient supine.

Chapter 3, on radiologic findings, is quite good at an elementary level. The statement that "duodenal distension is present on the left lateral decubitus x-ray in 90% of patients with pancreatitis" I find hard to believe. One illustration on plain film, sonogram, and CT scan of duodenal distension allegedly due to pancreatitis shows a normal pancreatic head on the CT scan. Most would disagree with the recommendation that every renal CT study should include scanning both before and after administration of IV contrast material. Chapter 4, on specific disease processes, is a good elementary overview. If radiologists followed literally the authors' recommendation that "when abscess is suspected and plain films and sonography are negative, always do CT or operate," the result would be a lot of laparotomies with normal findings. Chapter 5, on pediatrics, is good. The sixth chapter consists of a long list of clinical impressions and relative values of imaging studies that is fairly worthless to anyone with common sense who has read the preceding text.

I can recommend this book to medical students rotating through radiology, surgery, or emergency medicine; surgical residents; and beginning radiology residents. Because of its price, I recommend they take it out of the library rather than buy it. Because the illustrations are excellent, and the text is a good, albeit superficial, overview, I will put my copy in our departmental library and insist that our medical students and beginning residents read it, and I will encourage our senior residents to leaf through the pictures.

Arnold C. Friedman
Temple University Hospital
Philadelphia, PA 19140

The Value of CT in Detecting Bowel Perforation in Children After Blunt Abdominal Trauma

Dorothy I. Bulas^{1,2}
George A. Taylor¹⁻³
Martin R. Eichelberger^{2,4}

In this era of conservative management for most infants and children with blunt abdominal trauma, there is a concern that the diagnosis of bowel perforation may be missed or delayed. To determine the sensitivity of CT in the detection of perforated viscus in this population, we reviewed the CT examinations of 547 consecutive children who had had blunt abdominal trauma. Of six patients (1%) with documented bowel perforation, four (67%) had free intraperitoneal air detected preoperatively by CT. The remaining two cases had secondary signs of bowel thickening and unexplained peritoneal fluid. Free intraperitoneal air was not a specific indicator for bowel perforation. Of nine patients in whom CT studies showed pneumoperitoneum, only four (44%) had a ruptured bowel. The remaining five patients had pneumoperitoneum from sources other than bowel perforation including pneumomediastinum, bladder perforation, and previous peritoneal lavage.

This experience shows that the CT finding of pneumoperitoneum is useful, although not specific for the detection of bowel perforation in children with blunt abdominal trauma. When free air is not present, secondary signs of bowel wall thickening and unexplained peritoneal fluid suggest a bowel perforation.

AJR 153:561-564, September 1989

The use of CT in the diagnosis of solid organ injury after blunt abdominal trauma has been well established [1-4]. However, little information is available on the accuracy of CT in the detection of bowel perforation [5-7]. We reviewed our experience with CT evaluation of children with blunt abdominal trauma to determine the sensitivity and specificity of various CT findings in the diagnosis of intestinal perforation.

Materials and Methods

Since January 1983, 547 consecutive children have been examined with CT at our hospital after blunt abdominal trauma. Indications for CT scans included physical signs and symptoms such as tenderness, distension, abrasions or contusions; hematuria; suspected bleeding (decreasing or low hematocrit); and high-risk mechanism of injury. CT scans also were obtained if physical examination was considered unreliable because of neurologic impairment of the patient.

CT scans were performed on a GE 9800 scanner (General Electric, Milwaukee, WI) by using 10-mm-thick slices at 10-mm intervals. Rapid IV infusion of 43% iohalamate sodium (Conray, Mallinckrodt, St. Louis, MO) was administered to all children at a dose of 3 ml/kg. Scans were obtained immediately through the upper abdomen with delayed scanning (5 min) through the pelvis to allow filling of the urinary bladder with contrast material.

Oral contrast material was not used routinely. One child, in whom intestinal perforation was strongly suspected clinically but was not shown on nonenhanced CT scans, received oral contrast material.

We excluded three patients with intestinal perforations who were taken immediately to surgery without having CT scans because of their clinical instability.

Received March 9, 1989; accepted after revision April 18, 1989.

¹ Department of Radiology, Children's Hospital National Medical Center (CHNMC) and George Washington University School of Medicine and Health Sciences, Washington, DC 20010. Address reprint requests to D. I. Bulas at CHNMC, 111 Michigan Ave., N.W., Washington, DC 20010.

² Department of Child Health and Development, Children's Hospital National Medical Center and George Washington University School of Medicine and Health Sciences, Washington, DC 20010.

³ Present address: Department of Radiology, The Johns Hopkins Hospital, 600 N. Wolfe St., Baltimore, MD 21205.

⁴ Department of Surgery, Children's Hospital National Medical Center and George Washington University School of Medicine and Health Sciences, Washington, DC 20010.

0361-803X/89/1533-0561
© American Roentgen Ray Society

All CT examinations were reviewed at the time of initial injury. The scans were analyzed for the presence and severity of solid organ injury, peritoneal fluid, pneumoperitoneum, and bowel wall thickening. CT signs suggestive of bowel wall injury included the presence of pneumoperitoneum, focal or diffuse thickening of the bowel wall, and unexplained peritoneal fluid. Clinical information collected included demographic data and a description of the mechanism of injury.

Of 11 patients with CT findings suggestive of bowel perforation, nine underwent surgery and two underwent peritoneal lavage. Six of 547 children (1%) were found at surgery to have perforations of the bowel. Ages ranged from 2 to 16 years (mean, 9 years). Four patients were girls, and two were boys. Four children were involved in motor vehicle accidents while wearing lap-style seat belts, one was injured falling on the handlebars of his bicycle, and one was a victim of abuse.

Results

Pneumoperitoneum was detected on CT scans in four (67%) of six cases of bowel perforation. Only one patient had obvious pneumoperitoneum shown on plain radiographs. The remaining three patients had unsuspected bowel perforation before CT scanning. Although CT scans showed obvious pneumoperitoneum in one patient (Fig. 1), in two patients CT showed only subtle amounts of free air anterior to the ventral edge of the liver requiring careful observation at wide window settings (Fig. 2).

Pneumoperitoneum was not present in two of the six patients with bowel perforation. CT showed multiple thickened loops of bowel in one patient (Fig. 3) and a focally thickened duodenum in the other (Fig. 4). In addition, both of these patients had moderate to large amounts of peritoneal fluid without evidence of significant solid organ injury.

The size of bowel laceration noted at surgery, which ranged from 0.3 cm to complete transection, did not correlate with the amount of free air found on the CT scan.

Pneumoperitoneum was detected on CT scans in nine (2%) of the 547 patients who underwent CT. Of these nine patients four (44%) had a perforation of the bowel. The five remaining patients had other recognizable causes for peritoneal free air.

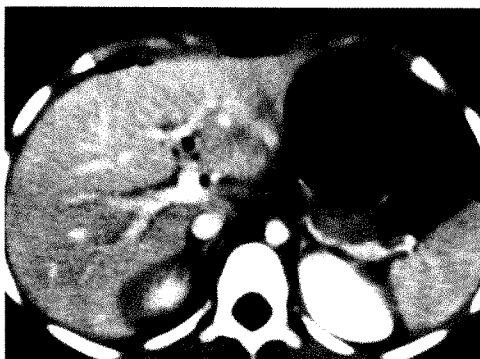


Fig. 1.—Pneumoperitoneum noted on CT scan was not recognized on supine abdominal radiograph in this 5-year-old girl who was involved in a motor vehicle accident while wearing a lap belt. CT findings include free air anterior to the liver and air and fluid tracking along left portal vein. At surgery a 1.5-cm jejunal perforation was found.

Two had an associated pneumomediastinum, which presumably dissected into the peritoneal cavity. Both of these patients underwent further studies, laparotomy in one case and peritoneal lavage in the other, with no evidence of intestinal injury.

A third child had a pneumoperitoneum caused by a peritoneal lavage with negative results performed before CT scanning. This patient did well under close observation, with no evidence of an occult perforation.

One child with a ruptured urinary bladder had extravasation of both air and contrast material into the peritoneal cavity. Air was most likely introduced into the peritoneum during placement of a Foley catheter. No bowel injury was found at surgery.

The last patient with pneumoperitoneum presented with a small bubble of air anterior to the liver. At surgery, a duodenal hematoma was found with air bubbles adjacent to this region. No perforation was identified. The child did well after surgery.

When only "unexplained" pneumoperitoneum is considered (no associated pneumomediastinum, pneumothorax, or previous peritoneal lavage), four of five patients with pneumoperitoneum identified on CT scans had an associated perforation (sensitivity, 67%; positive predictive value, 80%).

Two of six children with bowel perforation were not identified prospectively because of the absence of pneumoperitoneum. Both cases, however, showed bowel wall thickening and unexplained peritoneal fluid. Of 547 patients in whom abdominal CT scans were obtained for blunt abdominal trauma, 18 patients (3%) had findings of unexplained peritoneal fluid or bowel wall thickening. Thirteen cases met the clinical and CT criteria for "shock bowel" as described by Taylor et al. [8]. Of the remaining five children, two had bowel perforations, and three with unexplained peritoneal fluid had uncomplicated hospital stays with no evidence of bowel injury.

Discussion

Bowel injury in children with blunt abdominal trauma is infrequent (1–9%), and accurate and prompt diagnosis remains difficult [9–11]. Early physical findings and laboratory results may be equivocal [9, 12]. Pneumoperitoneum is shown on plain radiographs of the abdomen in less than 40% of children with intestinal perforations [9, 12–15]. Upper gastrointestinal series may be false-negative because of early sealing of a bowel laceration [9]. Peritoneal lavage may be used to diagnose bowel perforation [16, 17]. However, early lavage may miss an isolated injury to the bowel because of a delay in WBC response [17]. In addition, because hemoperitoneum is no longer an absolute indication for surgery in children, lavage is an oversensitive tool in the evaluation of blunt abdominal trauma [18–20].

Although the question of whether gastrointestinal perforations can be detected reliably by CT has been discussed by several authors, only a limited number of series actually have studied the sensitivity and specificity of CT [21–23]. Cook et al. [6] had little success in detecting bowel injuries, reporting three false-negative and two false-positive CT scans. No bowel perforations were identified correctly prospectively in

Fig. 2.—Jejunal perforation with free intraperitoneal air in a 16-year-old who was wearing a seat belt when involved in a car accident.

A. A small collection of free air (arrow) anterior to ventral edge of liver could be mistaken for fat on CT scan.

B. Lower CT scan shows lucency to be of lower attenuation than adjacent fat in rectus sheath. A jejunal tear was identified at surgery.



A



B

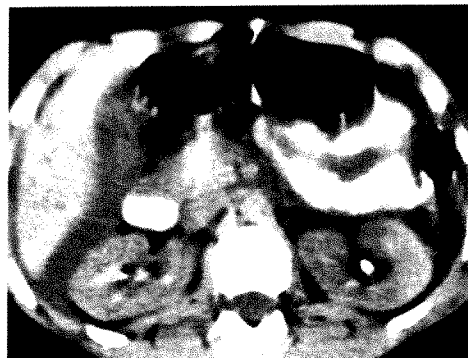


Fig. 3.—CT scans show free fluid and thickened bowel loops in a 14-year-old girl who was involved in a motor vehicle accident while wearing a seat belt. Because of high suspicion of bowel injury, CT with oral contrast medium was performed with patient in supine and in lateral decubitus positions. No evidence of extravasation of contrast material or pneumoperitoneum was seen. Upper gastrointestinal series done again next day was normal. On third day, because symptoms continued to worsen, patient was taken to surgery. A jejunal perforation 30 cm distal to ligament of Treitz was found.

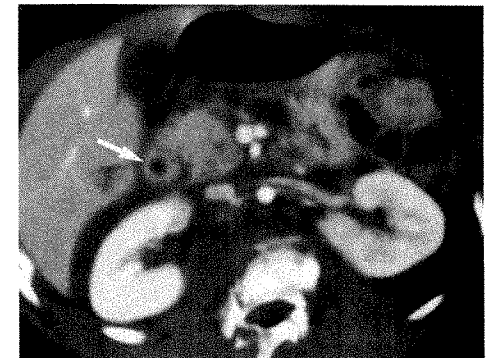


Fig. 4.—CT scan shows thickening of second part of duodenum (arrow) and a retroperitoneal hematoma in a 7-year-old girl who has been paraplegic since she was involved in a car accident while wearing a lap belt. L2 vertebra is shattered. No solid organ injuries were identified. At surgery, a transection of the second part of duodenum was found.

83 patients examined [6]. Fabian et al. [7] correctly identified only one of two bowel perforations.

Our data show that CT is a useful tool in the detection of bowel perforation in infants and children. However, the use of pneumoperitoneum as the sole indication for surgery can lead to false-negative and false-positive results. The finding of peritoneal free air may be subtle. The differentiation of free air from fat or intraluminal air may be difficult if window widths and levels are not altered appropriately. When free air is documented, pneumoperitoneum caused by dissection of air from the chest or by previous lavage must be excluded. Pneumoselective leaks resulting in pneumoperitoneum without peritonitis can make the accurate diagnosis of ruptured bowel difficult. Reported after endoscopy and barium enemas, these leaks of air are benign, with no true perforations found at surgery [24, 25]. Theoretically, small valvular perforations may allow air but not bowel contents to escape. A sudden increase in intraluminal pressure from blunt trauma with a resultant pneumoselective leak may explain our one false-positive case in which pneumoperitoneum was identified on CT but only a duodenal hematoma was found at laparotomy.

Excluding this one false-positive case, pneumoperitoneum was correctly identified as arising from extraintestinal sources in the remaining four cases. Once these sources were excluded, the findings of free peritoneal air became a strong indicator of underlying bowel perforation (sensitivity, 67%, positive predictive value, 80%).

The absence of pneumoperitoneum did not exclude the possibility of an intestinal tear (false-negative rate, 33%). Tears may seal quickly with no chance of air escaping into the peritoneum. Conversely, only bowel contents may extravasate, and the sole sign of rupture may be free fluid within the peritoneal cavity. We did not routinely administer oral contrast material for CT examination of the abdomen after blunt trauma. CT scans after oral administration of contrast material and upper gastrointestinal series may aid in confirming perforation. Unfortunately, perforations may seal off quickly, and even these studies may yield false-negative results (Fig. 3).

Donohue et al. [5] improved the sensitivity of CT in the evaluation of bowel injury by using bowel wall thickening and significant amounts of peritoneal fluid as criteria for lesions

requiring surgical intervention. In their series, all eight cases of perforation were identified correctly. An additional six cases identified as having surgical lesions were found at surgery to have bowel hematomas. Although these lesions may have required surgical intervention in adults, most bowel hematomas can be treated conservatively in infants and children. Thus, although the finding of bowel wall thickening and unexplained intraperitoneal fluid can improve the sensitivity of CT identification of bowel perforations, specificity will drop in infants and children.

In this series, the CT scans of two patients with intestinal perforation showed only bowel wall thickening and unexplained peritoneal fluid. Although these signs are not specific, they indicate a subset of children at risk of having a perforation. Peritoneal lavage then may be performed. Children with an equivocal peritoneal lavage still warrant close monitoring in view of reported false-negative results of peritoneal lavage [16, 17].

Conclusions

CT is helpful in the diagnosis of bowel perforation in infants and children. Pneumoperitoneum, when present, suggests a viscus rupture. However, the source of the free air often is not associated with bowel perforation. Conversely, pneumoperitoneum may not be present, and secondary signs such as bowel wall thickening and unexplained peritoneal fluid should suggest the possibility of an occult perforation. In these cases, peritoneal lavage may be useful in identifying the injury.

REFERENCES

- Goldstein AS, Sclafani SJA, Kupferstein NH, et al. The diagnostic superiority of computerized tomography. *J Trauma* **1985**;25:938-946
- Federle MP, Crass RA, Jeffrey RB, Trunkey DD. Computed tomography in blunt abdominal trauma. *Arch Surg* **1982**;117:645-650
- Peitzman AB, Makaroun MS, Slasky BS, Ritter P. Prospective study of computed tomography in initial management of blunt abdominal trauma. *J Trauma* **1986**;26:585-592
- Karp MP, Cooney DR, Berger PE, Kuhn JP, Jewett TC. The role of CT in the evaluation of blunt abdominal trauma in children. *J Pediatr Surg* **1981**;16:316-323
- Donohue JH, Federle MP, Griffiths BG, Trunkey DD. CT in the diagnosis of blunt intestinal and mesenteric injuries. *J Trauma* **1987**;27:11-17
- Cook DE, Walsh JW, Vick CW, Brewer WH. Upper abdominal trauma: pitfalls in CT diagnosis. *Radiology* **1986**;159:65-69
- Fabian TC, Mangiante EC, White TJ, Patterson CR, Boldreghini S, Britt LG. A prospective study of 91 patients undergoing both computed tomography and peritoneal lavage following blunt abdominal trauma. *J Trauma* **1986**;26:602-608
- Taylor GA, Fallat ME, Eichelberger MR. Hypovolemic shock in children: abdominal CT manifestations. *Radiology* **1987**;164:479-481
- Cobb LM, Vinocur CD, Wagner CW, Weintraub WH. Intestinal perforation due to blunt trauma in children in an era of increased nonoperative treatment. *J Trauma* **1986**;26:461-463
- Kaufman RA, Towbin R, Babcock DS, et al. Upper abdominal trauma in children: imaging evaluation. *AJR* **1984**;142:449-460
- Fischer RP, Miller-Crotchett P, Reed RL. Gastrointestinal disruption: the hazard of nonoperative management in adults with blunt abdominal injury. *J Trauma* **1988**;28:1445-1449
- Maul KI, Reath DB. Impact of early recognition on outcome in nonpenetrating wounds of the small bowel. *South Med J* **1984**;77:1075-1077
- Donohue JH, Crass RA, Trunkey DD. The management of duodenal and other small intestinal trauma. *World J Surg* **1985**;9:904-913
- Roh JJ, Thompson JS, Harned RK, Hodgson PE. Value of pneumoperitoneum in the diagnosis of visceral perforation. *Am J Surg* **1983**;146:830-833
- Winek TG, Mosely HS, Grout G, Lualin D. Pneumoperitoneum and its association with ruptured abdominal viscus. *Arch Surg* **1988**;123:709-712
- Hawkins ML, Scofield WM, Carraway RP, Laws HL. Diagnostic peritoneal lavage in blunt trauma. *South Med J* **1988**;81:293-296
- Alyono D, Perry JF. Value of quantitative cell count and amylase activity of peritoneal lavage fluid. *J Trauma* **1981**;21:345-348
- Rothenberg S, Moore EE, Marx JA, Moore FA, McCroskey BL. Selective management of blunt abdominal trauma in children—the triage role of peritoneal lavage. *J Trauma* **1987**;27:1101-1106
- Marx JA, Moore EE, Jordan RC, Eule J Jr. Limitations of computed tomography in the evaluation of acute abdominal trauma: a prospective comparison with diagnostic peritoneal lavage. *J Trauma* **1985**;25:933-937
- Powell RW, Green JB, Ochsner MG, Barttelbort SW, Shackford SR, Sise MJ. Peritoneal lavage in pediatric patients sustaining blunt abdominal trauma: a reappraisal. *J Trauma* **1987**;27:6-10
- Jeffrey RB, Federle MP, Wall S. Value of computed tomography in detecting occult gastrointestinal perforation. *J Comput Assist Tomogr* **1983**;7:825-827
- Glazer GM, Buy JN, Moss AA, Goldberg HI, Federle MP. CT detection of duodenal perforation. *AJR* **1981**;137:333-336
- Karnaze GC, Sheedy PF II, Stephen DH, McLeod RA. Computed tomography in duodenal rupture due to blunt abdominal trauma. *J Comput Assist Tomogr* **1981**;5:267-269
- Chandler JG, Berk RN, Goldan GT. Misleading pneumoperitoneum. *Surg Gynecol Obstet* **1977**;144:163-174
- Madura MJ, Craig RM, Shields TW. Unusual causes of spontaneous pneumoperitoneum. *Surg Gynecol Obstet* **1982**;154:417-420

MR Imaging of the Craniovertebral Junction, Cranium, and Brain in Children with Achondroplasia

Simon C. S. Kao¹
 Mary H. Waziri²
 Wilbur L. Smith¹
 Yutaka Sato¹
 William T. C. Yuh¹
 Edmund A. Franken, Jr.¹

MR imaging of the craniovertebral junction, cranium, and brain was performed in 10 patients (aged 3 months to 16 years) with achondroplasia. All patients had narrowing of the subarachnoid space at the level of the foramen magnum and five had compressive deformities of the cervicomedullary junction. Apparent upward displacement of the brainstem and a relatively vertical course of the optic nerve were seen in all patients. Dilated lateral and third ventricles were seen in five patients and bifrontal widening of the subarachnoid space was evident in four. Skull asymmetry was seen in two patients and an empty sella (confirmed by metrizamide cisternography) was present in one individual. In one patient, foci of abnormal signal intensity were seen in the cervicomedullary region.

Our experience indicates that MR imaging is useful in delineating the many abnormalities of the cranial, cerebral, and cervicomedullary junction present in children with achondroplasia.

AJR 153:565-569, September 1989

In achondroplasia, endochondral bone formation is inhibited. The base of the skull, the only part of the cranium formed by endochondral bone, is affected whereas the membranous bones of the calvaria develop and grow normally. This disharmonious development of the basicranium results in a relatively large skull with a small base and stenosis of the foramen magnum [1]. When this causes compression of the medulla oblongata and upper cervical spinal cord, it may result in neurologic and respiratory complications, including quadriplegia, sleep apnea, and sudden death [2-6]. We report a study of 10 children with achondroplasia who underwent MR evaluation of the cranium, brain, and craniovertebral junction (CVJ).

Materials and Methods

From September 1984 to May 1988, 10 children with achondroplasia (five boys and five girls, 3 months to 16 years old) were examined by MR of the head and neck. At the time of evaluation, all patients had neurologic and/or respiratory symptoms, or were considered at risk for complications. Follow-up MR studies were performed in three patients from 3 to 16 months after the initial evaluation.

All patients were sedated with oral chloral hydrate (Roxane Laboratories, Columbus, OH) at an average dose of 80 mg/kg body weight 45 min before the examination. They were carefully monitored during the examination. None of our patients required general anesthesia. There were no complications.

All but one MR study were performed with a 0.5-T superconducting system (Picker International, Highland Heights, OH). Initial T1-weighted, 350-550/20-40 (TR/TE), 5- or 10-mm sagittal images were obtained in all patients by using a spin-echo (SE) technique. Corresponding T2-weighted (1200-2500/100-120) sagittal images were obtained in six patients. T1-weighted (200-350/20-25) and T2-weighted (2000/100) 10-mm axial images

Received February 9, 1989; accepted after revision April 26, 1989.

¹ Department of Radiology, The University of Iowa College of Medicine, Iowa City, IA 52242. Address reprint requests to S. C. S. Kao.

² Department of Pediatrics, The University of Iowa College of Medicine, Iowa City, IA 52242.

0361-803X/89/1533-0565
 © American Roentgen Ray Society

were obtained through the brain in five patients and CVJ in six patients at 10-mm intervals. Inversion recovery, 1200/400 (TR/TI), axial brain images were obtained in one patient. T2-weighted (2000/100) 10-mm coronal images of the brain also were obtained in five patients. One follow-up examination was performed on a 1.5-T system (Signa, General Electric Medical Systems, Milwaukee, WI). T1-weighted (600/20) 5-mm sagittal and coronal and T2-weighted (2000/90) 5-mm axial images were obtained through the CVJ by using the SE technique. Interleaved 5-mm sagittal images were acquired by using a gradient-refocused echo sequence (150/13, flip angle = 7°).

The size of the ventricular system and the width of the subarachnoid space were evaluated and correlated with head circumference, by using standard graphs for achondroplasia [7]. Position of the brainstem was related to the base of the skull by using the fat pad in the posteroinferior portion of the sella as a landmark of the skull base (Fig. 1). The angle (optic nerve–base angle) formed by the optic nerve with the floor of the anterior cranial fossa (line joining tuberculum sellae and nasion) was measured. The MR images of 25 age-matched normal controls were evaluated for position of the brainstem and optic nerve–base angle. Skull symmetry and the size and position of the straight sinus and the fourth ventricle were noted. The position of the straight sinus was assessed by measuring the "tentorial angle" (the angle between the slope of the straight sinus and a line joining the nasion to the tuberculum sellae) [8]. The position of the fourth ventricle was noted in relation to Twining's point (midpoint between the tuberculum sellae and torcular Herophili). The basal angle was determined in the conventional fashion [9]. The cervicomedullary junction (CMJ) was evaluated for compressive deformity, abnormal signal intensity, and surrounding subarachnoid space.

Results

Ventricles and Subarachnoid Space

The cisterna magna was extremely small or not visible in all patients. Nine of the 10 patients had enlargement of the suprasellar cistern (Fig. 2). An empty sella, confirmed by metrizamide cisternography, was present in one individual.

Five of the 10 patients had enlargement of the third and lateral ventricles. One of these patients had a dilated fourth

ventricle. Among the six patients with axial or coronal T2-weighted images, MR evidence of transependymal CSF resorption was seen in only one, suggesting increased intraventricular pressure. Four patients had bifrontal widening of the subarachnoid space associated with a widened interhemispheric fissure frontally, a constellation of findings indicating external hydrocephalus (Fig. 3) [10]. Head circumferences, all within 2 SD of the mean for achondroplasia, were larger in patients with dilated ventricles and/or external hydrocephalus compared to those without these findings, but there was considerable overlap.

Position of Brainstem and Optic Nerves

The sellar fat pad, normally opposite the pontomesencephalic junction, was related to the mid pons in six patients, lower pons in three, and pontomedullary junction in one (Fig. 1). The optic nerve–base angle was less obtuse than usual and varied from 115° to 140° (Fig. 4). This angle in 25 age-matched controls was found to be between 140° and 160°. None of these patients had visual complaints, and detailed ophthalmologic examinations in three revealed no abnormality.

Skull Symmetry

Two of the 10 patients showed asymmetry in the outline of the cranium and brain, best noted on the axial or coronal sections (Fig. 5). Both had marked delay in motor development and were profoundly hypotonic on clinical examination. The deformity was considered to be related to clinical status rather than intrinsic brain abnormality.

Size and Position of Straight Sinus and Fourth Ventricle

The straight sinus was best seen on the T1-weighted midsagittal image as a flow-void linear structure. By visual comparison with age-matched controls, it appeared to be large in five and its course to be more vertical in all 10 patients (Fig. 4). The "tentorial angle," normally 27–52° [8], measured 55–70° (Fig. 1). In the normal individual, Twining's point lies within the fourth ventricle. In our patients, the center of the fourth ventricle was up to 1.3 cm above this point.

Cervicomedullary Junction

All patients showed virtual obliteration of the subarachnoid space at the CMJ (Fig. 6). The foramen magnum was considerably narrowed and appeared triangular (Fig. 7). Compressive deformity of the CMJ, present in five patients, was best documented on T1-weighted sagittal sections. Indentations were posterior in two, anterior in one, and both anterior and posterior in two. Foci of abnormal signal intensity were noted in the upper cervical cord and medulla in one patient with unexpected but monitored respiratory arrest (Fig. 8A). This patient had marked clinical improvement after surgical decompression of the CVJ. Follow-up MR examination 16

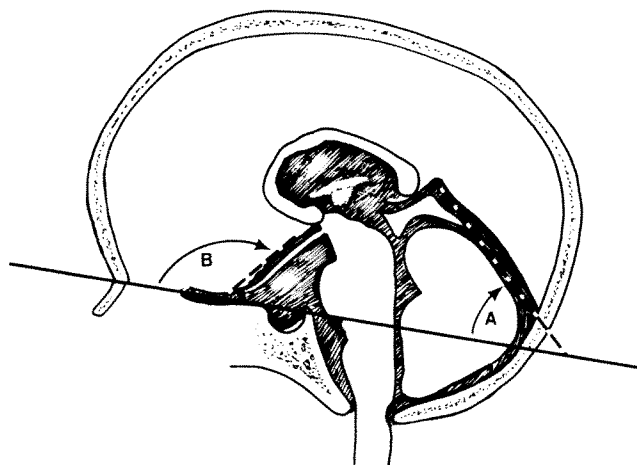


Fig. 1.—Diagram of midsagittal section of skull and craniocervical junction shows sellar fat pad, tentorial angle (A), and optic nerve–base angle (B) between slope of optic nerve and line joining nasion with tuberculum sellae.



Fig. 2.—Sagittal MR image (SE 483/20) in a 3-year-old boy shows large suprasellar cistern, small cisterna magna, and short clivus with sellar fat pad related to mid pons. Pituitary stalk (arrowhead) is markedly stretched.

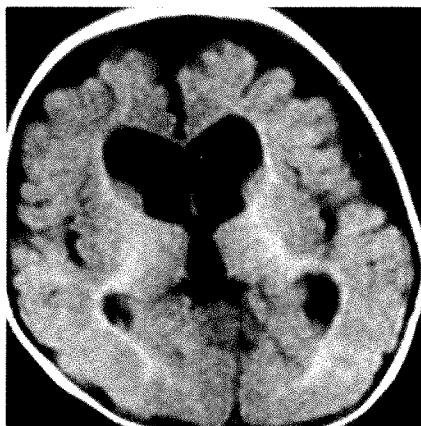


Fig. 3.—Axial MR image (SE 550/20) in an 8-month-old girl shows dilated third and lateral ventricles with widening of frontal sulci and interhemispheric fissure.

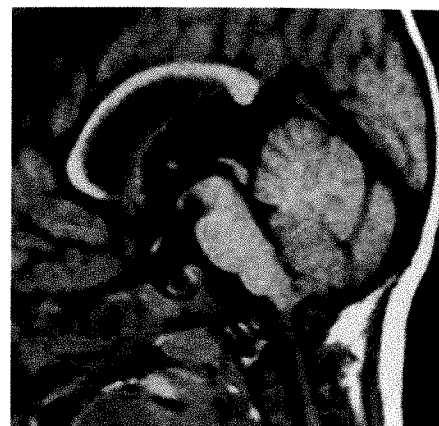


Fig. 4.—Sagittal MR image (SE 483/20) in a 10-month-old girl shows position of optic nerve and prominent straight sinus. Tentorial angle (angle A, Fig. 1) measured 70° and optic nerve–base angle (angle B, Fig. 1) measured 140° .

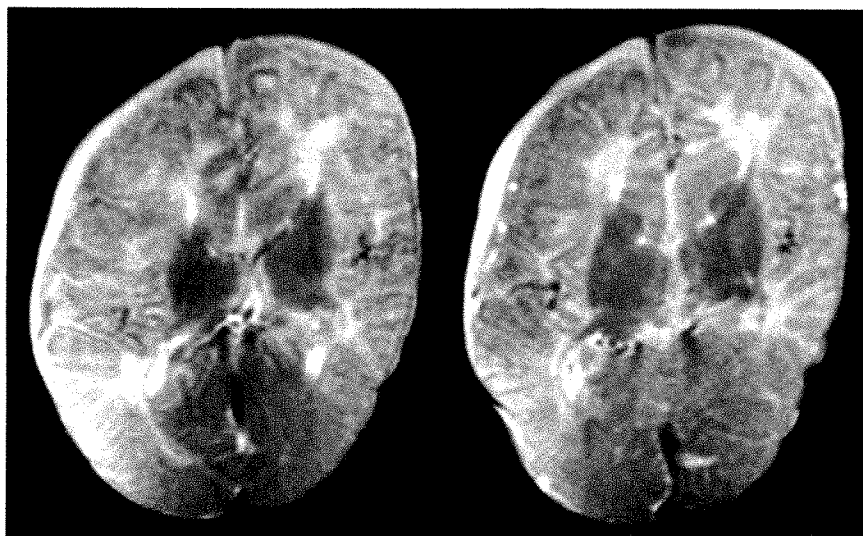


Fig. 5.—Contiguous 10-mm axial MR images (SE 1900/100) in a 3-month-old boy with marked hypotonia show skull asymmetry and a prominent straight sinus.

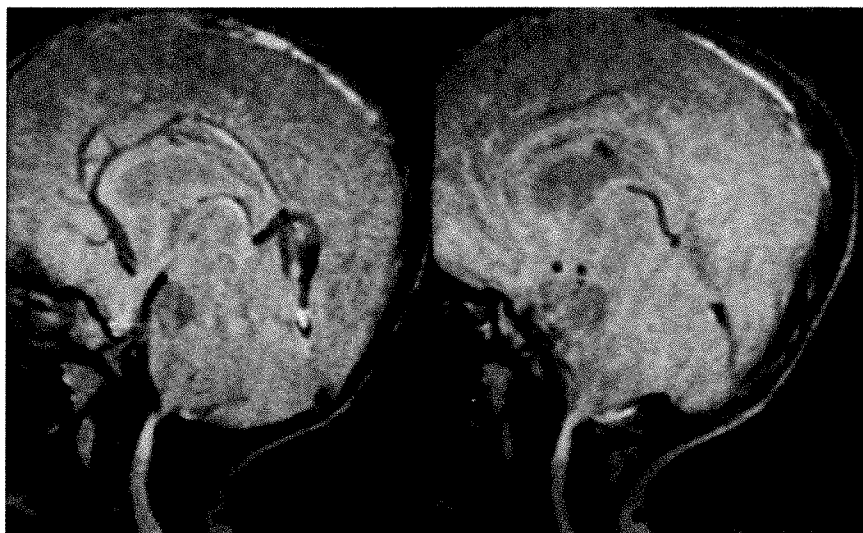


Fig. 6.—Contiguous 5-mm sagittal T2-weighted MR images (SE 1700/100) in an 11-month-old girl show marked narrowing of subarachnoid space at craniocervical junction and prominence of deep cerebral veins.



Fig. 7.—Axial MR image (SE 550/20) of skull base in an 8-month-old girl shows narrow and triangular foramen magnum (arrowheads).



A



B

Fig. 8.—MR images in patient with respiratory arrest.

A, Sagittal T1-weighted image (SE 416/20) at 11 months of age shows deformity at cervicomedullary junction with abnormal signal intensity. Marked clinical improvement followed surgical decompression.

B, Follow-up image (SE 400/20) at 27 months of age shows persistent signal abnormality despite disappearance of deformity.

months postoperatively showed a focus of abnormal signal intensity in the upper cervical cord, despite disappearance of the compressive deformity at the CMJ (Fig. 8B).

Basal Angle

The basal angle, normally 123–152°, was between 120° and 125° in eight patients and measured 130° and 140° in the remaining two patients.

Discussion

Considerable interest has been focused on the neurologic and respiratory complications in achondroplasia, which include hydrocephalus, cervicomedullary compression, sudden unexpected death, and unexplained apnea [2–6]. Prediction of likelihood for these complications is of great clinical importance because most patients with achondroplasia lead an active and productive life.

MR imaging provides a major advance in neuroimaging of achondroplasia. Although plain radiography and CT provide precise definition of the bony abnormalities, the medulla and cervical cord are not well visualized without the use of intrathecal contrast medium [11]. MR imaging provides multiplanar evaluation of the brain and CMJ without the use of ionizing radiation and IV or intrathecal contrast injection [12, 13]. The direct MR sagittal views allow better visualization of the brainstem and upper cervical cord than do reformatted CT myelograms.

Recent comprehensive neurologic and respiratory evaluations of achondroplastic children show a close relationship between respiratory abnormalities and cervicomedullary compression, despite a heterogeneity of respiratory symptoms [14]. Moreover, the neurologic and respiratory problems attributed to cervicomedullary compression are alleviated by

surgical decompression [2, 6]. Necropsy studies have documented instances of central cystic myelomalacia and medullary gliosis associated with cervicomedullary compression [15]. In our patient with respiratory arrest, the foci of abnormal signal intensity in the cervicomedullary region probably represented these findings. Further clinicoradiologic studies are necessary regarding the development and evolution of abnormal signal in the cervicomedullary region of symptomatic achondroplastic patients.

The head enlargement (macrocephaly) in achondroplasia is thought to be the result of macrencephaly (excessive size of the brain) and/or hydrocephalus. The pathogenesis of the latter finding is still a subject of controversy [2, 16–18]. Obstruction of the fourth ventricular outlets, obstruction of the extraventricular spaces, and elevation of venous sinus pressure due to stenosis of the jugular foramen have all been implicated as possible contributory factors. In our patients, the presence and degree of ventricular dilatation and external hydrocephalus were shown well. Most patients with dilated ventricles and/or bifrontal widening of the subarachnoid space had head circumferences larger than those without these findings, with some overlap. The relatively large straight sinus might reflect an elevation of venous pressure, which partly explained the ventricular dilatation and external hydrocephalus.

All our patients had apparent upward displacement of the brainstem due to shortening of the chondrocranium at the skull base. This resulted in optic nerves with a relatively vertical course from the optic chiasm to the optic canals. These findings were best seen on T1-weighted sagittal images and were better appreciated by MR than any other currently available imaging technique.

In conclusion, the pathologic findings seen by MR imaging may help us to understand the various secondary effects of the abnormal endochondral ossification at the skull base. MR

imaging provides information not appreciated by other currently available imaging techniques, such as the relatively high brainstem with stretching of optic nerves and pituitary stalk. Demonstration of substantial cervicomedullary compression and cystic myelomalacia is of value in decisions regarding operative intervention in the management of children with achondroplasia.

ACKNOWLEDGMENTS

We thank LuAnn Osdoba for secretarial assistance, Phyllis Bergman for editorial assistance, Frank Sindelar for drawing Figure 1, and John Johnson and Carla Stevens for photographic assistance in the preparation of this manuscript.

REFERENCES

1. Marin-Padilla M, Marin-Padilla TM. Developmental abnormalities of the occipital bone in human chondrodystrophies (achondroplasia and thanatophoric dwarfism). *Birth Defects* 1977;13(3D):7-23
2. Yamada H, Nakamura S, Tajima M, Kageyama N. Neurological manifestations of pediatric achondroplasia. *J Neurosurg* 1981;54:49-57
3. Hecht JT, Butler LJ, Scott CI. Long-term neurological sequelae in achondroplasia. *Eur J Pediatr* 1984;143:58-60
4. Stokes DC, Phillips JA, Leonard CO, et al. Respiratory complications of achondroplasia. *J Pediatr* 1983;102:534-541
5. Pauli RM, Scott CI, Wassman ER, et al. Apnea and sudden unexpected death in infants with achondroplasia. *J Pediatr* 1984;104:342-348
6. Fremion AS, Garg BP, Kalsbeck J. Apnea as the sole manifestation of cord compression in achondroplasia. *J Pediatr* 1984;104:398-401
7. Horton WA, Rotter JL, Rimoin DL, Scott CI, Hall JG. Standard growth curves for achondroplasia. *J Pediatr* 1978;93:435-438
8. Wolpert SM. Dural sinus configuration: measure of congenital disease. *Radiology* 1969;92:1511-1516
9. Lusted LB, Keats TE. *Atlas of roentgenographic measurement*, 4th ed. Chicago: Year Book Medical, 1978:51
10. Maytal J, Alvarez LA, Elkin CM, Shinnar S. External hydrocephalus: radiologic spectrum and differentiation from cerebral atrophy. *AJR* 1987;148:1223-1230
11. Wang H, Rosenbaum AE, Reid CS, Zinreich SJ, Pyeritz RE. Pediatric patients with achondroplasia: CT evaluation of the craniocervical junction. *Radiology* 1987;164:515-519
12. Lee BCP, Deck MDF, Kneeland JB, Cahill PT. MR imaging of the craniocervical junction. *AJNR* 1985;6:209-213
13. Thomas IT, Frias JL, Williams JL, Friedman WA. Magnetic resonance imaging in the assessment of medullary compression in achondroplasia. *Am J Dis Child* 1988;142:989-992
14. Reid CS, Pyeritz RE, Kopits SE, et al. Cervicomedullary compression in young patients with achondroplasia: value of comprehensive neurologic and respiratory evaluation. *J Pediatr* 1987;110:522-530
15. Yang SS, Corbett DP, Brough AJ, Heidelberger KP, Bernstein J. Upper cervical myelopathy in achondroplasia. *Am J Clin Pathol* 1977;68:68-72
16. Mueller SM, Bell W, Cornell S, Hamsher K deS, Dolan K. Achondroplasia and hydrocephalus. *Neurology* 1977;27:430-434
17. Mueller SM. Enlarged cerebral ventricular system in infant achondroplastic dwarf. *Neurology* 1980;30:767-769
18. Pierre-Kahn A, Hirsch JF, Renier D, Metzger J, Maroteaux P. Hydrocephalus and achondroplasia. *Childs Brain* 1980;7:205-219

Book Review

Digital Subtraction Imaging in Infants and Children. Edited by Eric N. Faerber. Mount Kisco, NY: Futura, 193 pp., 1989. \$42

This text was written with the aid of 15 contributors under the direction of Dr. Faerber. It includes nine chapters and an appendix that concern both the clinical and technical aspects of designing and staffing a pediatric digital angiographic suite.

The first chapter presents briefly the basic physics and instrumentation for digital subtraction angiography and is useful for a general understanding of the digital technique. It also serves as an introduction for the remainder of the text.

Chapters 2 and 3 discuss not only the techniques but also the design of appropriate units. These chapters contain discussions of the application of each technique to clinical problems. The authors clearly state the advantages and disadvantages of each technique as it relates to the examination of the child.

Chapters 4 through 8 discuss the use of digital subtraction in angiocardiology, imaging of the aorta and great vessels, cerebral angiography, renal angiography, and peripheral angiography. Each chapter demonstrates the usefulness of digital subtraction and underscores the importance of using particular techniques to produce

the best image quality. The case selection within the chapters clearly shows normal and morbid anatomy. In some circumstances, the content in one chapter overlaps that of another chapter; however, duplication is minimal for a book with this number of contributors. The illustrations are usually satisfactory.

The last chapter deals with future applications and trends in digital imaging; it provides information about storage, retrieval, and display of stored information, and it discusses network design. This book serves as a primer on the use of digital imaging in children, and it presents an overview of the spectrum of selected pediatric disorders for which digital imaging may be helpful. The book is, however, more concerned with the preliminary role of digital subtraction angiography and should not be considered a reference text.

John R. Sty
Children's Hospital of Wisconsin
Milwaukee, WI 53201

Brain Abnormalities in Infants on Extracorporeal Membrane Oxygenation: Sonographic and CT Findings

Diane S. Babcock^{1,2}
 Bokyoung Kim Han¹⁻³
 Richard G. Weiss^{2,4,5}
 Frederick C. Ryckman^{2,4}

The findings of cranial sonography performed before and during extracorporeal membrane oxygenation (ECMO) in 50 near-term infants and CT findings after ECMO in 18 of those patients are reported. Hemorrhage is uncommon in patients being considered for ECMO: subependymal hemorrhage was seen in one case and subependymal cyst possibly due to in utero hemorrhage was seen in five cases. Hypoxic ischemic injury is more common: severe cerebral edema was seen in two cases, occipital hemorrhagic infarct in one case, and mild cerebral edema in 17 cases. During ECMO, sonograms showed that the hemorrhage in patients with small subependymal hemorrhage or cyst before ECMO did not extend while on ECMO. Typical germinal matrix/intraventricular hemorrhage was seen uncommonly (three cases). Unusual parenchymal hemorrhage did occur. Hypoxic ischemic brain injury was more common: parenchymal hemorrhage was seen in three cases, severe cerebral edema in three cases, and infarction in three cases. Hypoxic ischemic brain injury probably occurs before ECMO, with a delay in visualization. CT after ECMO detected additional abnormalities, particularly peripheral areas of hemorrhage and infarction not visible on sonograms, and is now being performed on all patients.

More emphasis should be placed on better screening of infants being considered for ECMO treatment to identify irreversible anoxic brain injury, not just hemorrhage.

AJR 153:571-576, September 1989

Extracorporeal membrane oxygenation (ECMO) is a method of treating acute reversible respiratory disease in infants who have a high likelihood of death. The procedure requires ligation and cannulation of the right common carotid artery and internal jugular vein. Continuous heparinization and thrombocytopenia during ECMO result in an increased risk of intracranial hemorrhage [1-3]. Because previous authors have reported a high frequency of hemorrhage in premature infants [1-3], only patients of greater than 34 weeks gestation have been placed on ECMO at our institution.

The purpose of our study was to determine the prevalence of intracranial hemorrhage (ICH) and other abnormalities in near-term infants treated with ECMO.

Materials and Methods

Fifty consecutive infants with life-threatening respiratory failure unresponsive to conventional treatment methods were placed on ECMO between July 1985 and December 1987. Forty-nine of the patients were neonates born after 34 weeks gestation. The average age of the neonates at the time of institution of ECMO was 68 hr (range, 12-138 hr). One was a 10-month-old cardiac patient unable to be weaned from cardiopulmonary bypass. The diagnoses requiring ECMO support included meconium aspiration syndrome (16 cases), respiratory distress syndrome (15), persistent pulmonary hypertension (five), congenital diaphragmatic hernia (seven), sepsis (four), irreversible perinatal asphyxia (two), and cardiac failure (one). Intake criteria included an alveolar-arterial oxygenation (A-aPO₂) gradient greater than 620 mm Hg for more than 12 hr in 27 patients, more than 6 hr accompanied by acidosis

Received September 23, 1988; accepted after revision April 26, 1989.

¹ Department of Radiology, Children's Hospital Medical Center and the University of Cincinnati College of Medicine, Elland & Bethesda Aves., Cincinnati, OH 45229-2899. Address reprint requests to D. S. Babcock.

² Department of Pediatrics, Children's Hospital Medical Center and the University of Cincinnati College of Medicine, Cincinnati, OH 45229-2899.

³ Present address: Department of Radiology, Rush-Presbyterian-St. Luke's Medical Center, 1635 W. Congress Pkwy., Chicago, IL 60612.

⁴ Department of Surgery, Children's Hospital Medical Center and the University of Cincinnati College of Medicine, Cincinnati, OH 45229-2899.

⁵ Present address: Department of Surgery, New York University Medical Center, 550-560 First Ave., New York, NY 10016.

0361-803X/89/1533-0571
 © American Roentgen Ray Society

and hypotension in seven patients, and association with severe barotrauma in three patients. These criteria were used to identify a group of patients with a 90% mortality risk. Three patients were placed on ECMO during or shortly after cardiopulmonary resuscitation for cardiac arrest. The average time on ECMO was 132 hr (range, 49–231 hr).

All infants with respiratory failure were supported by using venoarterial bypass with cannulation of the right common carotid artery and the right internal jugular vein through a neck incision. The patient unable to be weaned from cardiopulmonary bypass was perfused through the preexisting aortic root and right atrial cannulas. A Sci-Med 0.8 M2 membrane oxygenator, roller pump, and countercurrent heat exchanger (Sci-Med Life Systems, Minneapolis, MN) were used in all cases. Platelet counts were maintained at 100,000–200,000/ml, and systemic heparin was administered to prolong the activated clotting time 2 1/2-fold. Hypertension was treated vigorously to maintain mean blood pressures of 55–65 mm Hg. The details of the ECMO procedure are described in previous publications [4].

All cranial sonograms were obtained with sector real-time (Advanced Technology Laboratories, Inc., Bothell, WA) equipment by using standard technique and 5- to 7.5-MHz transducers [5]. Standard coronal and sagittal views as well as magnified coronal views of the interhemispheric fissure were obtained. Sonograms were routinely obtained within 6 hr before ECMO, within 12 hr after starting ECMO, during ECMO as clinically indicated (not necessarily every day), and within 24 hr after ECMO was stopped.

Cranial CT scans were obtained after ECMO on GE 9800 equipment both before and after infusion of contrast material in the last group of patients. CT scans were obtained after ECMO when the patient was stable enough to be transported to the scanner.

Cranial sonograms and CT scans were reviewed retrospectively by two of the authors who had no knowledge of clinical information. Sonograms were evaluated for size and configuration of the ventricles; presence of extraaxial fluid, particularly in the interhemispheric fissure; hemorrhage; brain parenchymal echogenicity; relative sulco-parenchymal differentiation; and presence of cystic areas within the brain. CT scans were evaluated for ventricular size and configuration; size of the extraaxial fluid spaces; overall density of the brain parenchyma; gray-white matter differentiation; and presence of areas of hemorrhage, infarction, or cysts.

Results

Forty-one patients (82%) survived and were discharged after an average hospital stay of 24 days. Nine patients died, three of multisystem failure, two of pulmonary hypoplasia associated with congenital diaphragmatic hernia, two of sepsis, and two of massive intracranial hemorrhage. Only one death occurred during ECMO.

Sonograms obtained before ECMO on 49 of the 50 patients were normal in 23 patients and were abnormal in 26. The abnormalities included subependymal hemorrhage (one), subependymal cysts suggesting in utero subependymal hemorrhage (five), severe cerebral edema (two) (Fig. 1), occipital hemorrhage/infarct (Fig. 2) diagnosed retrospectively (one), and mild cerebral edema as defined by slit like ventricles with slight increase in brain parenchymal echogenicity (17) (Fig. 3). No patients were excluded because of intracranial hemorrhage.

Sonograms during ECMO documented the development of additional abnormalities in 14 patients as follows: small bilateral subependymal hemorrhages (two); intraventricular hem-

orrhage and hydrocephalus (two); hemorrhage in the right cerebellum, which subsequently became cystic (one) (Fig. 4); hemorrhage in the left temporooccipital lobes with subsequent intraventricular hemorrhage (two) (Fig. 5); severe bilateral cerebral edema/infarction (three); focal infarction in the distribution of the left middle cerebral artery (two) (Fig. 6); infarction in the left basal ganglia (one) (Fig. 7); unilateral increase in the extraaxial fluid (one); and mild ventricular dilatation that resolved during ECMO (one). The one patient with subependymal hemorrhage and the five patients with cysts before ECMO did not develop further hemorrhage while on ECMO.

Eighteen neonates had CT examinations performed within 1 week after ECMO and within 1 week of their last sonogram. In seven neonates the CT scan was normal, and in 11 the CT scan was abnormal. Correlation between the sonographic findings and the CT findings were good in 13 patients and discrepant in five. Seven patients were normal on both studies. Six patients were abnormal on both, including two with infarction in the distribution of the left middle cerebral artery, one with severe bilateral edema shown on sonograms and multiple low-density areas shown on CT scans. One patient had right-sided increased extraaxial fluid of unknown significance on both examinations. Two patients had intraventricular hemorrhage and hydrocephalus on both studies.

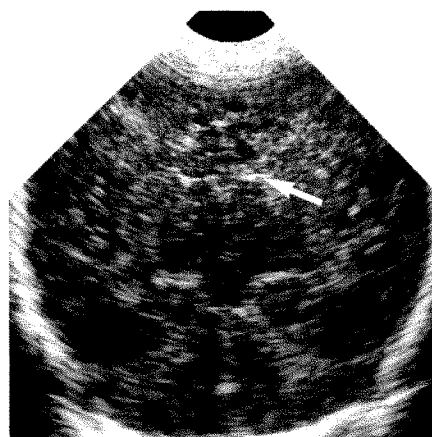
Five patients had a discrepancy in findings between sonography and CT. In one patient, the CT scan showed several small areas of bilateral occipital and cerebellar hemorrhages not identified on sonograms. These were peripheral in location and, on retrospectively reviewing the sonogram, one small suspicious area of increased echogenicity was seen (Fig. 8). An earlier sonogram had shown periventricular increased echogenicity, suggesting periventricular leukomalacia or edema. Another patient had mild increased extraaxial fluid shown on a CT scan, which had not been visible on the sonogram obtained 3 days earlier. One patient had small bilateral areas of hemorrhage in the periventricular area shown on a CT scan, which were not recognized on the sonogram although in retrospect the sonogram showed several suspicious areas of increased echogenicity (Fig. 9). One patient had low density in the right parietal area shown on the CT scan, suggesting an old infarct not shown on the sonogram. One patient had increased gray-white matter differentiation on the CT scan, whereas the sonogram had shown mild ventricular dilatation and echogenic endyma.

Follow-up Sonograms and CT

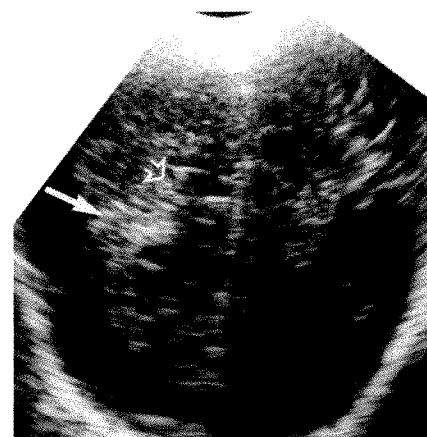
Of the 23 patients with normal sonograms before ECMO, 17 (74%) had subsequent normal sonograms and/or CT scans, and six (26%) developed abnormalities. Three neonates with normal sonograms died of nonneurologic causes.

Of the 17 patients with mild cerebral edema on sonography before ECMO, 10 (59%) had normal follow-up sonograms and/or CT scans, and seven (41%) developed abnormalities. Five of these 17 patients died. Two had normal sonograms and died of nonneurologic causes. One had severe cerebral

Fig. 1.—Severe cerebral edema. Coronal sonogram shows slitlike ventricles (*arrow*) and diffuse increase in brain parenchymal echogenicity obliterating normal sulci and gyri.

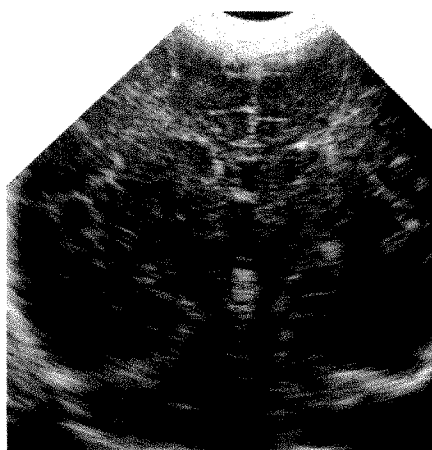


1

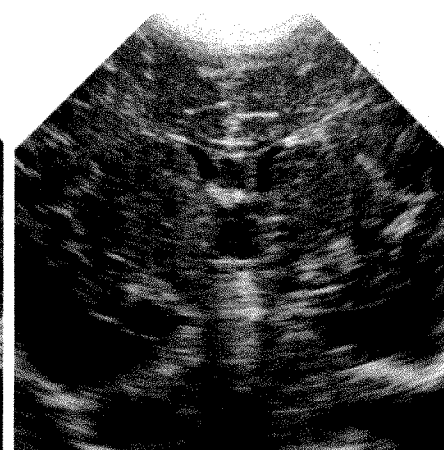


2

Fig. 2.—Posterior parietal hemorrhage/infarct. Coronal sonogram through posterior brain shows increased echoes in right periventricular area (*closed arrow*) adjacent to normal halo of corona radiata (*open arrow*).



A

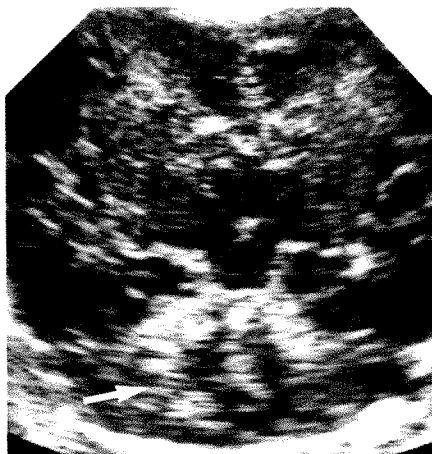


B

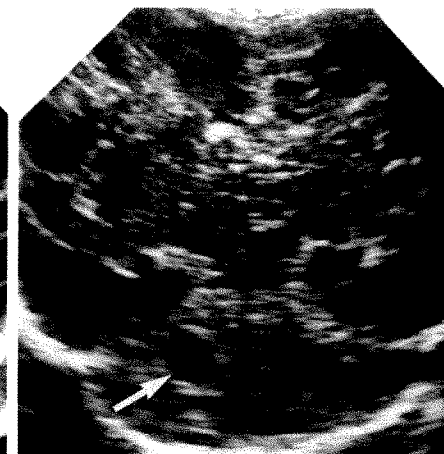
Fig. 3.—Mild cerebral edema.

A, Coronal sonogram obtained before extracorporeal membrane oxygenation (ECMO) shows slitlike ventricles with slight diffuse increase in brain parenchymal echogenicity. Normal sulci and gyri are still visible.

B, Sonogram obtained after 24 hr on ECMO shows resolution of cerebral edema with ventricles now visualized and parenchymal echogenicity normal.



A



B

Fig. 4.—Cerebellar hemorrhage.

A, Coronal sonogram on day 2 of extracorporeal membrane oxygenation (ECMO) shows increased echoes in right cerebellum (*arrow*). This was recognized only in retrospect.

B, Coronal sonogram on day 7 of ECMO shows cystic area of hemorrhage in right cerebellum (*arrow*), representing a liquefying hematoma.

A

B

edema but died of nonneurologic causes, and two died from massive intracranial hemorrhage.

One patient with a subependymal hemorrhage on the pre-ECMO sonogram progressed to having a subependymal cyst, but the hemorrhage did not extend and a parietal infarct was seen later on a CT scan of the opposite hemisphere. Five

patients showing subependymal cysts on pre-ECMO cranial sonograms did not develop hemorrhage on ECMO. One of these patients died of pulmonary disease, and two developed infarcts or severe edema.

The two patients with severe cerebral edema before ECMO had abnormal CT scans on follow-up, with low-density areas

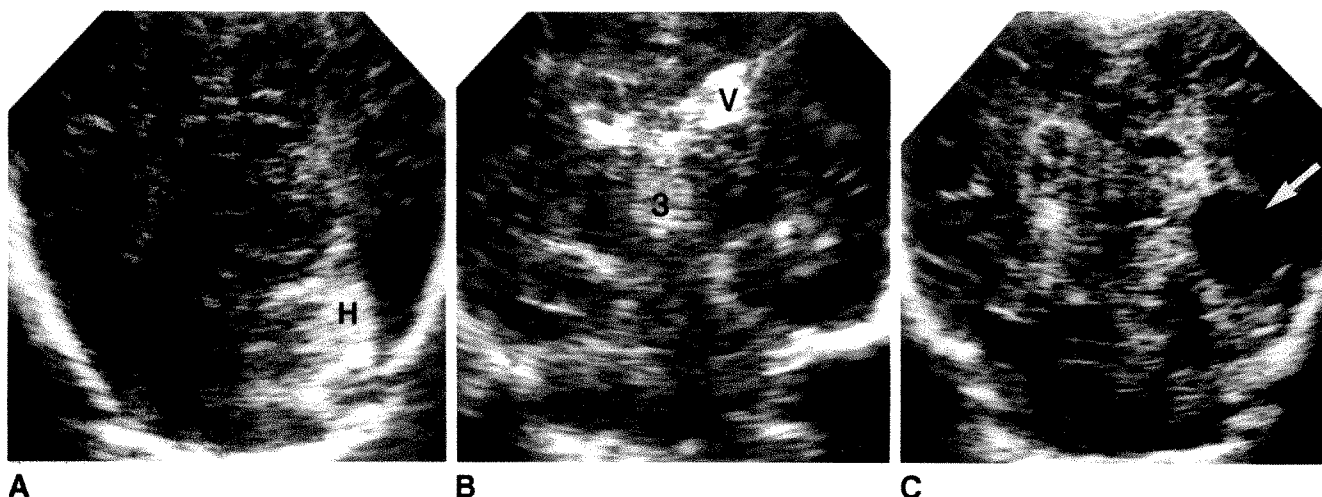


Fig. 5.—Left temporooccipital hemorrhage and intraventricular hemorrhage.

A, Posterior coronal sonogram on day 4 of extracorporeal membrane oxygenation (ECMO) shows normal ventricles and echogenic hemorrhage (H) in left temporooccipital region.

B and C, Coronal sonograms on day 5 of ECMO show left temporooccipital intraparenchymal hemorrhage now partially cystic (arrow) and partially echogenic. Echogenic clot is now seen filling the lateral (V) and third (3) ventricles, which are slightly dilated.

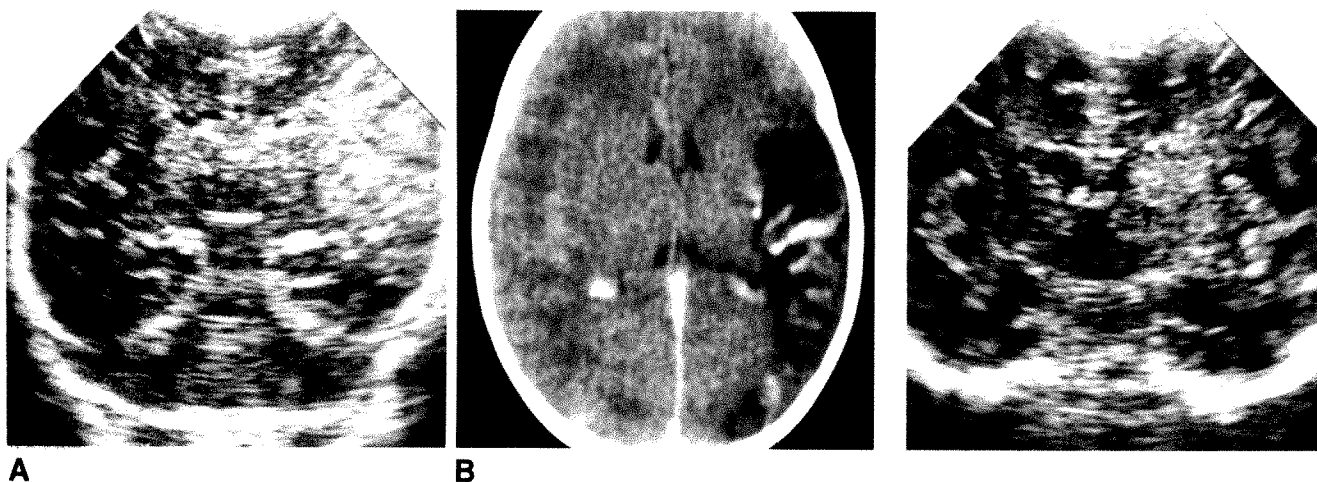


Fig. 6.—Middle cerebral artery infarct.

A, Coronal sonogram on day 6 of extracorporeal membrane oxygenation (ECMO) shows increased parenchymal echoes in distribution of left middle cerebral artery.

B, Contrast-enhanced cranial CT scan after ECMO shows partially enhancing brain infarct.

Fig. 7.—Basal ganglia infarct. Coronal scan on day 5 of extracorporeal membrane oxygenation shows increased parenchymal echogenicity in left thalamus (T), representing infarct.

suggesting infarction. One of these developed a left middle cerebral artery infarction during ECMO. The patient with occipital hemorrhages and infarctions before and during ECMO showed abnormalities on the follow-up CT scan as well.

Overall, of the 50 patients, 44% (22/50) showed abnormalities either on sonograms or on CT scans obtained during or after ECMO. There was a 16% (8/50) prevalence of hemorrhage with 6% (3/50) representing typical subependymal and/or intraventricular hemorrhages. Ten percent (5/50) had other parenchymal hemorrhages. There was an 18% prevalence of severe cerebral edema and infarction. The remaining 10% had subependymal cysts or increased extraaxial fluid. The focal brain abnormalities did not occur significantly more

frequently in the right (three patients) than in the left (four patients) side of the brain.

Discussion

ECMO has become an accepted method for treating acute reversible respiratory disease that is refractory to medical management in infants. As presently performed in most ECMO centers [6], the procedure requires ligation of the right common carotid artery and internal jugular vein for cannulation. Originally there was concern that this would result in injury, particularly infarction, of the right cerebral hemisphere. Right-sided preponderance was not seen in any of our pa-

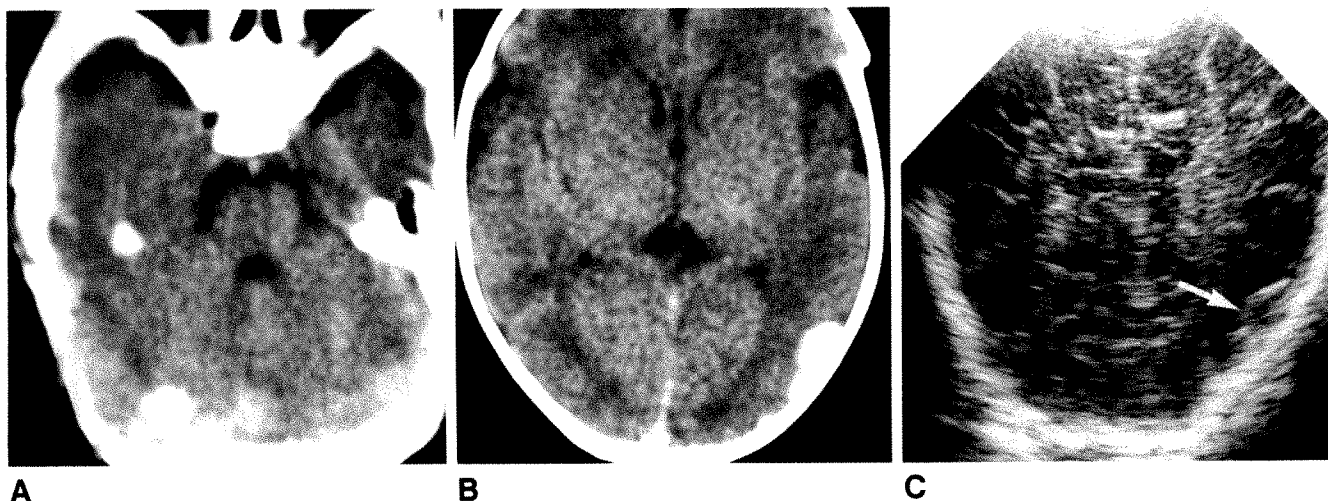


Fig. 8.—Bilateral occipital and cerebellar hemorrhage.

A and B, Non-contrast-enhanced cranial CT scans after extracorporeal membrane oxygenation (ECMO) show small hemorrhages in cerebellum and occipital lobes.

C, Coronal sonogram on day 4 of ECMO shows area of increased echogenicity (arrow) in left occipital lobe peripherally. This was recognized only after CT was performed.

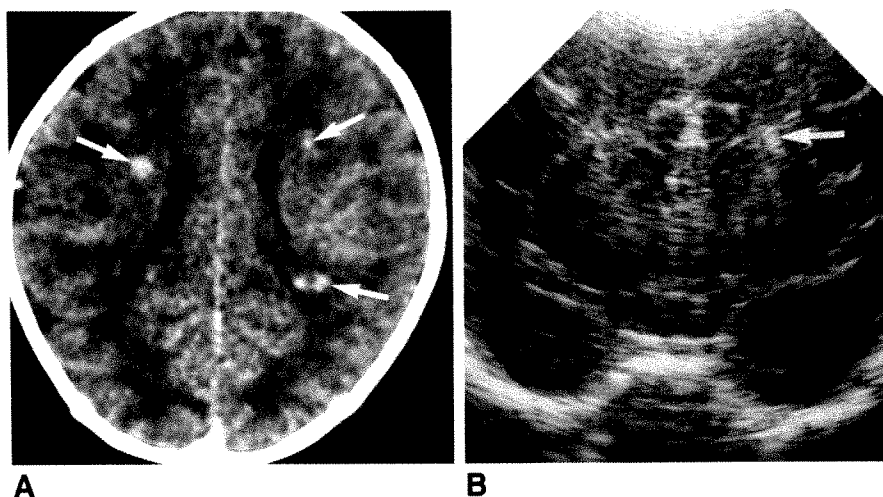


Fig. 9.—Small periventricular hemorrhages not seen on sonography.

A, Non-contrast-enhanced CT scan after extracorporeal membrane oxygenation (ECMO) shows bilateral small hemorrhages (arrows).

B, Coronal sonogram during ECMO shows small periventricular area of increased parenchymal echogenicity (arrow) corresponding to small hemorrhage on CT. This was recognized only in retrospect after CT.

tients nor was it seen in reports from other institutions [7]. The injuries that occur do not preponderate in either cerebral hemisphere.

Systemic heparinization while on ECMO and potential thrombocytopenia from platelet aggregation in the ECMO circuit or sepsis increases the risk of hemorrhage, including intracranial hemorrhage. Routine imaging of these patients before and during ECMO was originally instituted to detect hemorrhage. Early reports from institutions in which even small premature patients were treated with ECMO showed a high prevalence of intracranial hemorrhage (28%) [1–3]. Premature infants less than 32 weeks gestational age have a higher prevalence of intracranial hemorrhage, often arising from the germinal matrix [8]. Because of the increased morbidity and mortality rates in this group, only patients born after 34 weeks gestation are now being placed on ECMO at many centers.

The platelet count was maintained by transfusion at $>100,000/\text{ml}$ in our patients. In full-term infants, germinal matrix and intraventricular hemorrhage are less common and were seen in only 8% of our patients. The pre-ECMO sonogram is obtained primarily to exclude a preexisting hemorrhage that may extend after anticoagulation. Hemorrhage was uncommonly seen before ECMO in our patients (one in 49), and the germinal matrix hemorrhage did not extend while on ECMO. Hemorrhage occurred in an additional eight patients while on ECMO. Three were typical germinal matrix/intraventricular hemorrhages as seen in premature infants, and five were unusual intraparenchymal hemorrhages.

Patients are placed on ECMO therapy only after failure of vigorous medical therapy and may be hypoxic, hypotensive, or both for several days. Brain perfusion also may be decreased because of hypocarbia, and patients may have episodes of cardiac arrest before treatment with ECMO. The

sonographic findings of hypoxic/ischemic injury in term infants not on ECMO have been described [9]. They include cerebral edema, large vessel infarction, and smaller focal areas of infarction or hemorrhage. Delayed findings included diffuse brain atrophy, diffusely abnormal brain echogenicity, brain calcifications, and cystic encephalomalacia. Findings similar to those of acute hypoxic/ischemic brain injury were seen in 28% of our patients, including 10% with nongerminal matrix parenchymal hemorrhages and 18% with severe cerebral edema or infarctions.

In our study, patients born after 34 weeks gestation were more likely to suffer cerebral edema, infarction, and parenchymal hemorrhages associated with hypoxic injury than primary germinal matrix hemorrhage. As hypoxia and ischemia occur early and are treated with ECMO, the brain injury most likely occurs before the start of ECMO. Hypoxic injury may not be visible on initial sonograms and may only appear later. Our earlier study [9] reported a relatively low sensitivity of cranial sonography (46%) for detecting abnormalities in the first week after the asphyxial episode.

Additional abnormalities could be detected in those patients who underwent CT, particularly peripheral areas of hemorrhage and infarction not visible on sonograms (five patients). CT is now being performed on all patients within 1 week after ECMO therapy. The peripheral brain is more difficult to image by sonography through the fontanelle. MR imaging and positron emission tomography scanning may show additional abnormalities not detected by sonography or CT [10].

Hypoxic/ischemic brain injury is a significant problem in patients being considered for ECMO. There should be more emphasis on sonographic screening of infants before ECMO to identify irreversible hypoxic brain injury in addition to hemorrhage. Brain parenchymal abnormalities such as infarction and cerebral edema need to be assessed, and the peripheral brain parenchyma, posterior fossa, and periventricular region should be scrutinized for abnormalities. Brain injury such as severe cerebral edema, large infarctions, and large hemorrhages results in a devastating neurologic outcome, and such

patients should be offered ECMO support at this time only with significant reservations. The outcome with less severe hypoxic abnormalities such as mild cerebral edema and small infarctions is not predictable pending long-term follow-up studies, and these patients could continue to be treated with ECMO. As more experience and confidence with this technique is gained, earlier institution of ECMO should be considered to prevent hypoxic/ischemic brain injury.

ACKNOWLEDGMENTS

We thank Marsha Chapman, Theresa Adams, Debra Root, and Kim Dunn for technical assistance; Marlena Tyre for secretarial assistance; and William Ball and Donald Kirks for editorial assistance.

REFERENCES

1. Bowerman RA, Zwischenberger JB, Andrews AF, Bartlett RH. Cranial sonography of the infant treated with extracorporeal membrane oxygenation. *AJR* 1985;145:161-166
2. Cilley RE, Zwischenberger JB, Andrews AF, Bowerman RA, Roloff DW, Bartlett RH. Intracranial hemorrhage during extracorporeal membrane oxygenation in neonates. *Pediatrics* 1986;78:699-704
3. Slovis TL, Sell LL, Bedard MP, et al. Ultrasonographic findings (CNS, thorax, abdomen) in infants undergoing extracorporeal oxygenation therapy. *Pediatr Radiol* 1988;18:112-117
4. Bartlett RH, Gazzaniga AB. Extracorporeal circulation for cardiopulmonary failure. *Curr Probl Surg* 1978;15(5):5-24
5. Babcock DS, Han BK. *Cranial ultrasonography of infants*. Baltimore: Williams & Wilkins, 1981:23-26
6. Bartlett RH, Gazzaniga AB, Toomasian J, Corwin AG, Roloff D, Rucker R. Extracorporeal membrane oxygenation (ECMO) in neonatal respiratory failure: 100 cases. *Ann Surg* 1986;204:236-235
7. Taylor GA, Fitz CR, Miller MK, Garin DB, Catena LM, Short BL. Intracranial abnormalities in infants treated with extracorporeal membrane oxygenation: imaging with US and CT. *Radiology* 1987;165:675-678
8. Pape KE, Wigglesworth JS. *Hemorrhage, ischemia and the perinatal brain*. Philadelphia: Lippincott, 1979:133-148
9. Babcock DS, Ball WS Jr. Postasphyxial encephalopathy in full-term infants: ultrasound diagnosis. *Radiology* 1983;148:417-423
10. McArdle CB, Richardson CJ, Hayden CK, Nicholas DA, Amparo EG. Abnormalities of the neonatal brain: MR imaging. Part II. Hypoxic-ischemic brain injury. *Radiology* 1987;163:395-403

Interventional Neurovascular Treatment of Traumatic Carotid and Vertebral Artery Lesions: Results in 234 Cases

Randall T. Higashida¹
 Van V. Halbach¹
 Fong Y. Tsai²
 David Norman¹
 Henry F. Pribram³
 C. Mark Mehringer⁴
 Grant B. Hieshima¹

Traumatic injuries to the head and neck that result in arteriovenous fistulae are often difficult to treat by direct surgical access. This is because of anatomic location, instability of the acutely injured patient, and difficulty in localizing the exact site of injury. Between 1974 and 1988, 234 consecutive cases of traumatic injuries to the carotid or vertebral artery were evaluated by our group for intravascular embolization therapy. This included 206 cases of direct and seven cases of indirect carotid-cavernous sinus fistulae and 21 cases of traumatic vertebral fistulae. A variety of devices including detachable balloons, liquid tissue adhesives, microcoils, and silk suture were used with the goal of fistula occlusion and preservation of the parent vessel. This was achieved in 193 cases (82%). In the remaining 41 cases (18%), the carotid or vertebral artery had to be occluded by endovascular occlusion techniques because of extensive vascular injury in 28 cases and subtotal occlusion of the fistula in 13 cases. Complications included transient cerebral ischemia in six cases, pseudoaneurysm formation in five cases, stroke in five cases, and peripheral nerve injury in one case.

The development of interventional neurovascular techniques has altered the management of these acutely injured patients. The preferred method for treatment has shifted from direct surgical access under general anesthesia to endovascular therapy under local anesthesia.

AJR 153:577-582, September 1989

Carotid-cavernous sinus fistulae (CCFs) result from an abnormal communication of the carotid artery to the adjacent cavernous sinus. They may be direct or indirect [1, 2]. Either type of fistula can produce symptoms of increased orbital venous pressure resulting in chemosis, exophthalmos, ophthalmoplegia, and decreased visual acuity. If left untreated, patients may develop hypoxic ocular sequelae leading to blindness [3]. Posttraumatic CCFs and vertebral arteriovenous fistulae (AVFs) are usually a result of closed head injury, often from a motor vehicle accident, and are usually associated with adjacent basilar skull or vertebral body fractures. Signs and symptoms of the fistula may develop immediately or they may be delayed, with symptoms manifesting days to weeks after the initial injury [4, 5].

Over the past four decades, the treatment technique has radically altered. Surgical techniques for treating CCFs and AVFs in the past have carried an excessively high risk of thromboembolic and ischemic complications, often leading to stroke or blindness, and often not curing the fistula [4].

In 1971, Prolo and Hanberry [6] described the use of a fixed balloon catheter inserted directly into the neck and placed across the fistula site to block a CCF. In 1974, Serbinenko [7] reported the use of detachable balloons for occlusion of the fistula and preservation of the carotid artery. These reports ushered in a new era for treatment of traumatic carotid and vertebral fistulae by interventional neurovascular techniques.

We report our experience in the treatment of 234 consecutive traumatic carotid and vertebral artery fistulae treated by a variety of these newer interventional methods.

Received April 7, 1989; accepted after revision May 4, 1989.

¹Departments of Radiology and Neurosurgery, Interventional Neuroradiology Section, 505 Parnassus Ave., L352, San Francisco, CA 94143. Address reprint requests to R. T. Higashida.

²Department of Radiology, Truman Medical Center, 2301 Holmes St., Kansas City, MO 64108.

³Department of Radiology, University of California at Irvine, Irvine, CA 92664.

⁴Department of Radiology, Harbor-UCLA Medical Center, Torrance, CA 90509.

0361-803X/89/1533-0577

© American Roentgen Ray Society

Materials and Methods

Between 1974 and 1988, 228 patients with 234 vascular injuries were evaluated and treated by our group for either a traumatic CCF or a traumatic vertebral AVF. The patients ranged in age from 14 to 84 years of age (mean, 49 years). Of the 234 cases, 206 had a direct CCF, seven had an indirect CCF, and 21 had a traumatic vertebral AVF. Unusual presentations for the CCF patients included five cases of bilateral fistulae and one patient with a double ipsilateral CCF. Twelve patients had complete transection of the carotid artery, and 16 patients had transection of the vertebral artery.

Patients with CCFs presented with clinical symptoms of pulsating exophthalmos, chemosis, retroorbital bruit, ophthalmoplegia, and/or diminution of visual acuity. Diplopia due to ophthalmoplegia was common because of injury or compression of the adjacent cranial nerves III, IV, and VI. Four patients with massive head trauma presented with severe epistaxis and hemorrhage. In general, patients with direct fistulae presented with more acute and severe symptoms than those with indirect fistulae. Patients with traumatic fistulae of the vertebral artery presented with symptoms of hemorrhage, expanding hematomas, pseudoaneurysm formation, airway obstruction, and/or bruit.

Most procedures were performed in the neuroangiography section of our hospital under local anesthesia. The initial radiologic evaluation consisted of a CT head scan to evaluate the extent of head trauma and associated skull fractures. A complete four-vessel cerebral angiogram was obtained to evaluate the location and extent of vascular injury, as well as collateral circulation. A variety of maneuvers were used to identify the exact location of the fistula orifice and size. This included compression of the ipsilateral carotid artery during injection of the vertebral artery and subtotal compression of the cervical carotid artery during injection of the ipsilateral internal carotid artery for direct high-flow CCFs. If the parent artery was not transected and no intimal damage was present, every attempt was made to preserve flow to that vessel.

Transarterial Embolization by Detachable Balloons

All patients with direct CCFs and vertebral AVFs were treated initially by transarterial detachable balloon embolization therapy. From a transfemoral approach, a 7.3-French nontapered catheter is placed into the internal carotid or vertebral artery to be treated. Five thousand units of heparin is then given IV to prevent thrombus formation on the catheter and balloon system. The detachable balloon system used for most cases is the ITC Detachable Balloon Occluder System (Interventional Therapeutics Corp., San Francisco, CA) [8]. The balloon is composed of silicone and has an internal miter valve to prevent deflation when detached. It is available in a variety of sizes and detachment strengths. The medium-sized balloon, which is used most frequently, measures 1.5×4.0 mm uninflated, will accept a 0.50-ml volume, and expands to 7.5×13.5 mm. Often more than one balloon may be used to occlude large compartments of the cavernous sinus or pseudoaneurysm, or to trap a vessel. The balloon is attached to a 2.0-4.0-French coaxial polyethylene catheter and the set is placed through the larger 7.3-French introducing catheter. The balloon is then partially inflated and is flow-directed to the fistula orifice. In 12 cases, the Becton-Dickinson (Fairfield, NJ) 2.0-mm balloon catheter system was used for therapy.

Usually because of the high flow of the fistula, the balloon will easily traverse the tear of the vessel. However, in some instances where the fistula is small or on an unfavorable curve of the vessel, the 2.0-French catheter can be shaped into a more geometrically favorable curve. Once the balloon is in the correct position, a second arteriogram is obtained to ensure that the fistula is completely occluded and that the parent artery is patent. The patient is reexamined neurologically, and if stable, the balloon is detached by gentle traction on the 2.0-French catheter (Figs. 1 and 2).

All patients are followed up by clinical evaluation and radiologic studies including skull radiographs and/or CT head scans at 1, 3, and 12 months after the procedure to ensure that the balloon has not shifted or deflated. Neurologic and ophthalmologic examinations also are performed at these times to ensure that the fistula remains clinically closed.

Transarterial Embolization with Other Embolic Materials

The goal of therapy has been to occlude the traumatic fistulous connection while preserving the normal vessel. Patients with traumatic dural CCFs have been treated by superselective catheterization of the feeding arterial pedicles to the cavernous sinus. These consisted of distal branches of the external carotid artery including the internal maxillary artery, middle meningeal artery, and ascending pharyngeal artery and the two main branches of the cavernous internal carotid artery, the meningohypophyseal trunk and inferolateral trunk artery. The development of newer microcatheters and steerable guidewires and the availability of digital subtraction angiography with road-mapping techniques have made these approaches to treatment possible. Road-mapping allows the neurovascular architecture to be visualized on the monitor with simultaneous visualization of the movement of the catheter and guidewire. This allows highly selective catheterization of vessels measuring less than 2.0 mm in diameter.

A variety of embolic agents have been used depending on catheter location in relationship to the fistula orifice, flow characteristics, number of pedicles involved, and normal adjacent vessels and structures. Early on, polyvinyl alcohol particulate emboli; barium-impregnated silicone spheres; and isobutyl 2-cyanoacrylate (IBCA), a liquid tissue adhesive, were used for occlusion therapy [9]. In more recent years, newer microembolic steel and platinum coils (Target Therapeutics Corp., Los Angeles, CA), silk suture, and normo-butyl-cyanoacrylate (NBCA) (CRX Medical Corp., Raleigh, NC) have become the preferred materials for treatment (Fig. 3) [10, 11].

Transvenous Embolization Therapy

In selected cases where the fistula could not be safely approached from the arterial route, transvenous embolization therapy has been highly effective. Most embolizations were performed from a transfemoral venous access. Selective catheterization could be performed, by using a 7.0-French polyurethane catheter, in the proximal inferior petrosal sinus for

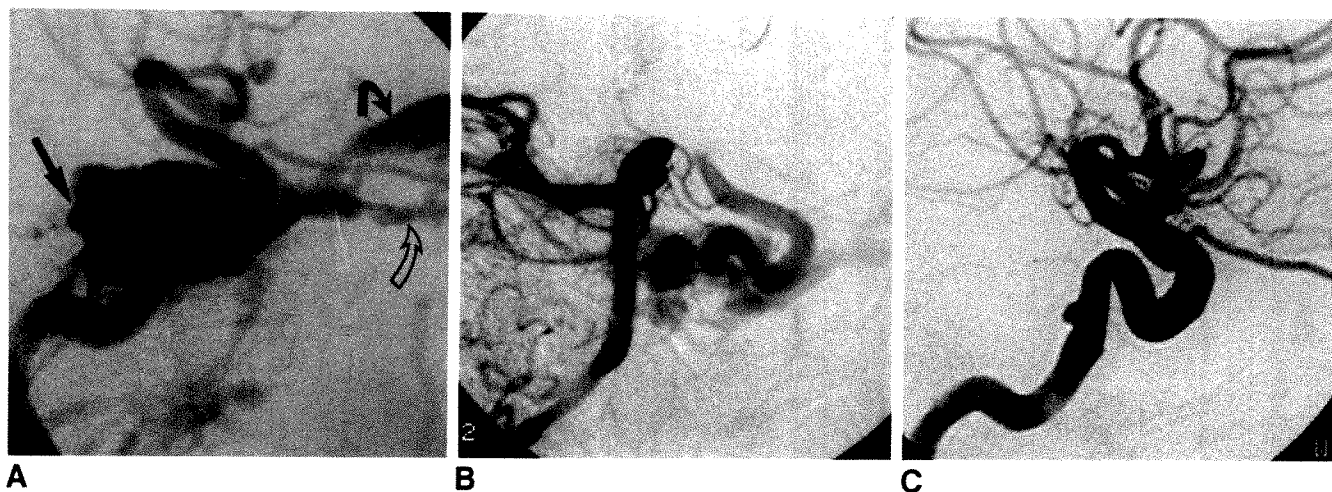


Fig. 1.—A, Left internal carotid arteriogram, lateral view, shows typical findings of traumatic carotid-cavernous sinus fistula. There is rapid opacification of cavernous sinus (straight arrow) and filling of superior (solid curved arrow) and inferior (open arrow) ophthalmic veins.

B, Left vertebral artery angiogram, lateral view. To help delineate exact site of traumatic laceration, injection of vertebral artery with simultaneous compression of involved carotid artery best shows fistula site (arrow).

C, Left internal carotid angiogram, lateral view. Follow-up angiogram 3 days after placement of a single detachable balloon into cavernous sinus fistula. There is obliteration of the fistula with preservation of the intracranial vessels.

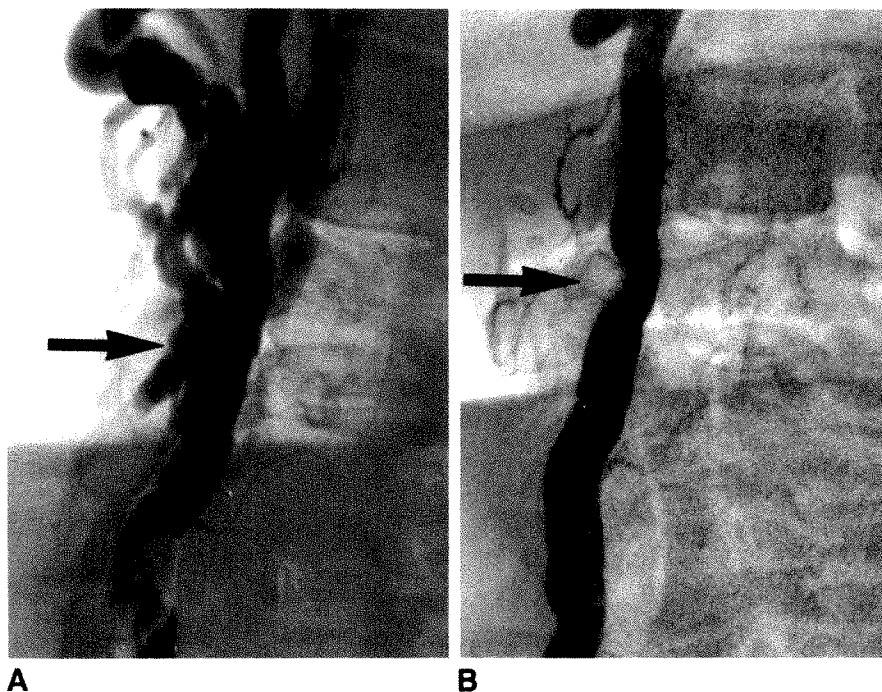


Fig. 2.—A, Right vertebral artery angiogram shows traumatic vertebral arteriovenous fistula at level of C4 due to stab wound of the neck (arrow).

B, Placement of a single detachable balloon at fistula site (arrow) results in total obliteration of fistula with preservation of distal vertebral artery.

CCF therapy. Through this, a 3.2-French Tracker catheter (Target Therapeutics) could be selectively guided through the inferior petrosal sinus and into the fistulous compartment of the cavernous sinus. Coils, silk suture, and/or NBCA were

then used to close the fistula while preserving the carotid artery (Fig. 4).

The inferior petrosal sinus approach has been used successfully when arterial access has been difficult. When the

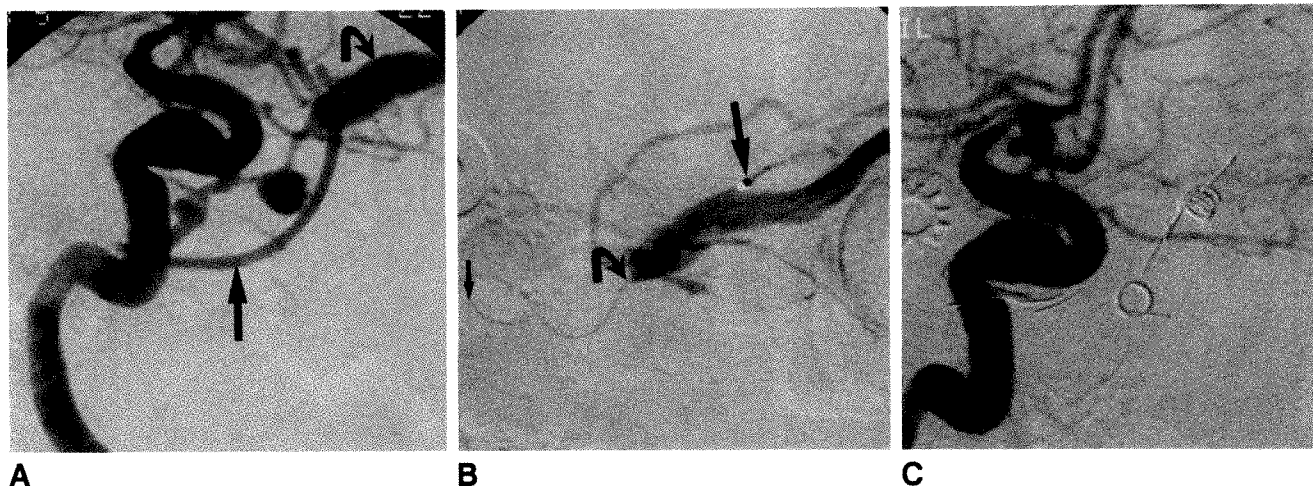


Fig. 3.—A, Left internal carotid arteriogram, lateral view, shows direct, traumatic carotid-cavernous sinus fistula. Drainage is to sphenoparietal sinus (straight arrow) and superior ophthalmic vein (curved arrow).

B, Superselective angiogram through a 2.2-French microcatheter that traverses internal carotid artery (small straight arrow) and fistula site (curved arrow) and is in proximal superior ophthalmic vein (large straight arrow).

C, Postembolization angiogram shows occlusion of fistula with multiple steel and platinum minicoils within ophthalmic vein, sphenoparietal sinus, and cavernous sinus.

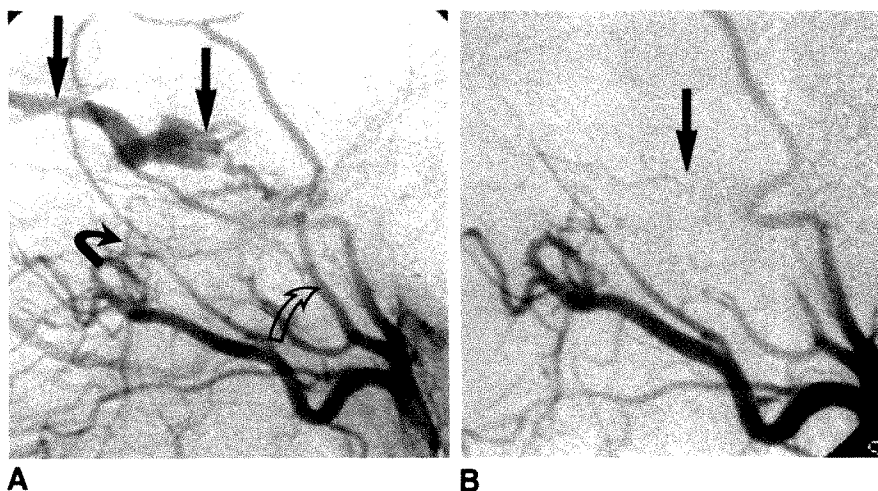


Fig. 4.—A, External carotid angiogram, lateral view, shows dural type of carotid-cavernous sinus fistula. There is early opacification of cavernous sinus and superior ophthalmic vein (straight arrows) from distal internal maxillary (solid curved arrow) and middle meningeal (open arrow) arteries.

B, After embolization of external carotid artery branches with Ivalon particulate emboli and transvenous embolization of cavernous sinus with liquid tissue adhesive, fistula is obliterated (arrow).

ipsilateral inferior petrosal sinus could not be traversed, we have been successful in using a contralateral venous approach from the opposite inferior petrosal sinus, across the circular sinus, and to the fistulous compartment.

When both inferior petrosal sinuses were not accessible, we were able to guide a catheter from the external jugular vein, to the facial vein and angular vein, and into the superior or inferior ophthalmic vein to the cavernous sinus for occlusion therapy [12, 13].

Results

Two hundred thirty-four cases were treated by a variety of intravascular embolization techniques for traumatic lesions of the carotid and/or vertebral artery. Of this total, 206 cases were for direct CCFs, 21 for vertebral AVFs, and seven for dural CCFs.

For direct CCFs, the treatment of choice was intravascular detachable balloon embolization as the first therapy technique. In 181 (88%) of 206 cases, the fistula was occluded and the internal carotid artery preserved. Of the remaining 25 patients, 12 had angiographic evidence of complete transection, seven had subtotal occlusion of their fistula, five had pseudoaneurysm formation, and one had multiple and extensive carotid injuries requiring carotid occlusion therapy. In one of the 25 patients, an extracranial to intracranial bypass graft was required because of delayed onset of cerebral ischemia 12 hr after carotid artery occlusion. Six patients (3%) could not be treated by a transarterial approach and required a transvenous approach for fistula occlusion. In five patients, extensive head trauma caused bilateral traumatic CCFs requiring both carotid arteries to be treated by balloon embolization therapy. In one patient, two different sites of communication between the carotid artery and the cavernous sinus

required two procedures. Complications associated with endovascular therapy included transient cerebral ischemia during or after the procedure in five patients and thromboembolic or ischemic strokes in five patients.

Twenty-one patients had traumatic vertebral AVFs. These patients were all treated by detachable balloon embolization therapy. Sixteen patients with vertebral artery transection presented with rapidly expanding hematoma of the cervical region or pseudoaneurysm formation. The vertebral artery was occluded in these patients. In one patient there was mild cerebellar dysfunction from delayed ischemia to a posterior inferior cerebellar artery associated with ipsilateral vertebral artery occlusion. In five patients, the fistula was occluded with preservation of the vertebral artery.

Seven patients were treated for a traumatic dural CCF. These patients were initially treated by selective catheterization of the feeding external carotid artery pedicles and embolization performed with Ivalon particulate emboli and/or liquid tissue adhesives. Occlusion was accomplished in four patients. In three patients, this approach resulted in incomplete closure. For this group a closure was completed by a transfemoral venous approach to the inferior petrosal sinus and cavernous sinus resulting in fistula obliteration. One patient developed a partial facial sensory deficit due to compromise of the internal maxillary artery vascular supply to the trigeminal nerve by liquid tissue adhesive embolization. This resolved over a 6-month period.

Discussion

Traumatic carotid and vertebral artery lesions often present in an acute setting with life-threatening consequences. Injury of the carotid artery can result in (1) massive hemorrhage and epistaxis; (2) stroke from cerebral ischemia due to vascular steal to the fistula from the contralateral carotid artery or through the posterior communicating artery from the vertebral artery; (3) dilatation of the cavernous sinus, which may result in subarachnoid hemorrhage; (4) abnormal venous drainage into cortical veins, which has an increased prevalence of parenchymal hemorrhage and venous hypertension; and (5) rapidly progressive visual deterioration leading to blindness. These are all indications for urgent treatment [14]. Vertebral fistulae also can result in massive hemorrhage, subarachnoid bleeding, expanding hematomas with resultant neurologic deficits, brain and spinal cord dysfunction related to vascular steal and compression, venous hypertension, and airway obstruction [15]. In these cases, it is necessary to rapidly evaluate the extent of injury, the site of pathology, and the role that interventional neurovascular techniques may have to alleviate symptoms [16, 17].

When there is extensive damage to the blood vessel, active hemorrhage, or a rapidly expanding hematoma of the soft tissues, it is usually not possible to preserve the parent vessel. In these instances, test occlusion across or distal to the tear should first be performed, if possible, to determine the individual tolerance of each patient to occlusion of a major cerebral vessel.

When long-standing fistulae have impaired the brain's ability to autoregulate its perfusion, abrupt closure of the fistula can result in relative overperfusion, termed normal perfusion pressure breakthrough. This was first described in 1978 by Spetzler et al. [18] and may occur because of rapid alteration in intracranial blood flow during resection of cerebral vascular malformations. This syndrome is more common in chronic long-standing fistulae, and may result in cerebral hemorrhage, edema, and neurologic dysfunction. It is postulated that perfusion breakthrough occurs because of loss of normal autoregulation from chronic arteriolar distension associated with vascular steal. If perfusion is reestablished acutely with the closure of a fistula, this may result in malignant cerebral edema or uncontrollable cerebral hemorrhage. Although rare, we observed this phenomenon in five of our patients with carotid and vertebral fistulae [19].

In acute posttraumatic injuries leading to pseudoaneurysm formation, we have found that placement of detachable balloons or coils directly into the pseudoaneurysm does not prevent further expansion or dissection. This is because there is no wall or tissue plane, except for thrombus, to keep the embolic material in place against the fistula orifice. Therefore, it is necessary to trap the fistula segment, obliterating both the inflow and outflow. Occlusion of only the proximal segment of the carotid or vertebral artery may be effective transiently but is not sufficient. With time, a vascular steal phenomenon from the supraclinoid carotid or contralateral vertebral artery will develop. Appropriate therapy, which would have been readily accomplished at the time of the initial treatment, now becomes quite difficult and carries a higher morbidity [15].

Several series have been published describing therapeutic embolization of traumatic carotid and vertebral fistulas. These include reports by Serbinenko [7], Debrun et al. [5, 20], Vinuela et al. [2, 10], Scialfa et al. [17], Kendall and Hoare [21], Norman et al. [22], and Halbach et al. [12, 13, 15]. Of note are the excellent results obtained by a variety of different techniques and embolization methods for treating traumatic injuries of the head and neck and the acceptable morbidity and mortality rates as compared with direct surgical intervention. Clearly, as more experience and expertise is gained in the field of interventional neuroradiology, the morbidity and mortality statistics will continue to improve.

Endovascular therapy has several advantages: (1) These procedures can be performed under local anesthesia, thereby allowing continuous neurologic monitoring of the patient's condition. This is particularly important if parent vessel occlusion is necessary. (2) In the acutely injured patient, time is of the essence, and if life-threatening hemorrhage, airway compromise, or cerebral ischemia has developed, then therapy can be rendered immediately after adequate diagnostic angiography. (3) Recovery time is faster and there is less trauma of adjacent cranial nerves and vessels.

Complications associated with embolization therapy include (1) thromboembolic and ischemic events due to catheter and balloon manipulation, injury to the blood vessel, or inadvertent balloon detachment; (2) pseudoaneurysm formation due to balloon deflation or migration; and (3) alteration of arterial flow

resulting in hemorrhage, edema, or worsening of ocular symptoms [17, 23].

Controversy still exists over the natural history and treatment of dural CCFs. Several authors have reported that many of these patients will have alleviation of symptoms from spontaneous thrombosis with time, and therefore treatment should not be instituted [24]. Although dural CCFs tend to be low-flow and low-pressure lesions, as compared with direct CCFs, we have also followed many patients with serial ophthalmologic examinations who have developed progressive visual deterioration. Our current recommendation is that in patients with dural CCFs without rapidly progressive visual deterioration, evidence of abnormal cortical venous drainage, hypoxic ocular changes involving the retina and optic nerve, or ischemic keratopathy, a trial of manual carotid artery-jugular vein compression therapy should be attempted first [25]. If patients do not respond to this therapy and continue to have symptoms of visual disturbance, headache, diplopia, and chemosis, then embolization therapy may be warranted.

A variety of therapeutic options are now available to the interventional neuroradiologist to treat traumatic CCFs and AVFs. For direct carotid and vertebral fistulae, a transarterial approach with detachable balloons is usually attempted first. However, if this technique fails, treatment with a variety of newer embolic agents, as well as newer microcatheters and guidewires, has greatly facilitated treatment by the transvenous approach.

Conclusions

Interventional neurovascular techniques to treat traumatic injuries of the carotid and vertebral artery have become accepted forms of therapy. Particularly in the acute setting, these techniques may be lifesaving in preventing uncontrollable hemorrhage. The goal of therapy for fistulae involving the carotid artery should be preservation of vision and preservation of the carotid artery. For traumatic injuries involving the vertebral artery, every effort should be made to close the fistula and preserve the parent vessel. If complete transection of the vertebral or carotid artery is present, then test occlusion, followed by a trapping procedure, should be performed to ensure that both the distal and proximal portions of the fistula are completely treated.

REFERENCES

1. Newton TH, Hoyt WF. Dural arteriovenous shunts in the region of the cavernous sinus. *Neuroradiology* 1970;1:71-81
2. Vinuela F, Fox AJ, Debrun GM, Peerless SJ, Drake CG. Spontaneous carotid-cavernous fistulas: clinical, radiological, and therapeutic considerations. *J Neurosurg* 1984;60:976-984
3. Sanders MD, Hoyt WF. Hypoxic ocular sequelae of carotid-cavernous fistulae. *Br J Ophthalmol* 1969;53:82-97
4. Hosobuchi Y. Carotid-cavernous fistulas. In: Wilson C, Stein BM, eds. *Intracranial arteriovenous malformations*. Baltimore: Williams & Wilkins, 1984:246-258
5. Debrun GM, Lacour P, Fox AJ, Vinuela F, Davis KR, Ahn HS. Traumatic carotid cavernous fistulas: etiology, clinical presentation, diagnosis, treatment, results. *Semin Intervent Radiol* 1987;4:242-248
6. Prolo DJ, Hanberry JW. Intraluminal occlusion of a carotid cavernous sinus fistula with a balloon catheter: technical note. *J Neurosurg* 1971;35:237-242
7. Serbinenko FA. Balloon catheterization and occlusion of major cerebral vessels. *J Neurosurg* 1974;41:125-145
8. Hieshima GB, Grinnell VS, Mehringer CM. A detachable balloon for therapeutic transcatheter occlusion. *Radiology* 1981;138:227-228
9. Bank WO, Kerber CW, Drayer BP, et al. Carotid cavernous fistula: endoarterial cyanoacrylate occlusion with preservation of carotid flow. *J Neurosurg* 1978;5:279-285
10. Vinuela F, Fox AJ. Interventional neuroradiology and the management of arteriovenous malformations and fistulas. *Neurol Clin North Am* 1983;1(1):131-155
11. Yang P, Halbach VV, Higashida RT, Hieshima GB. Platinum wire: a new transvascular embolic agent. *AJNR* 1988;9:547-550
12. Halbach VV, Higashida RT, Hieshima GB, Hardin CW, Yang PJ. Transvenous embolization of direct carotid cavernous fistulas. *AJNR* 1988;9:741-747
13. Halbach VV, Higashida RT, Hieshima GB, Reicher M, Norman D, Newton TH. Dural fistulas involving the cavernous sinus: results of treatment in 30 patients. *Radiology* 1987;163:437-442
14. Halbach VV, Hieshima GB, Higashida RT, Reicher M. Carotid cavernous fistulae: indications for urgent treatment. *AJNR* 1987;8:627-633
15. Halbach VV, Higashida RT, Hieshima GB. Treatment of vertebral arteriovenous fistulas. *AJNR* 1987;8:1121-1128
16. Mehringer CM, Hieshima GB, Grinnell VS, et al. Therapeutic embolization for vascular trauma of the head and neck. *AJNR* 1983;4:137-142
17. Scialfa G, Vaghi A, Valsecchi F, Bernard L, Tonon C. Neuroradiological treatment of carotid and vertebral fistulas and intracavernous aneurysms: technical problems and results. *Neuroradiology* 1982;24:13-25
18. Spetzler RF, Wilson CB, Weinstein P, et al. Normal perfusion pressure breakthrough theory. *Clin Neurosurg* 1978;25:651-672
19. Halbach VV, Higashida RT, Hieshima GB, Norman D. Normal perfusion pressure breakthrough occurring during treatment of carotid and vertebral fistulas. *AJNR* 1987;8:751-756
20. Debrun GM, Vinuela F, Fox AJ, Davis KR, Ahn HS. Indications for treatment and classification of 132 carotid-cavernous fistulas. *Neurosurgery* 1988;22:285-289
21. Kendall B, Hoare R. Percutaneous transvenous balloon occlusion of arteriovenous fistula. *Neuroradiology* 1980;20:203-205
22. Norman D, Newton TH, Edwards MS, DeCaprio V. Carotid-cavernous fistula: closure with detachable silicone balloons. *Radiology* 1983;149:149-157
23. Tsai FY, Hieshima GB, Mehringer CM, Grinnell V, Pribram HW. Delayed effects in the treatment of carotid-cavernous fistulas. *AJNR* 1983;4:357-361
24. Barrow DL, Spector RH, Braun IF, Landman JA, Tindall SC, Tindall GT. Classification and treatment of spontaneous carotid-cavernous sinus fistulas. *J Neurosurg* 1985;62:248-256
25. Higashida RT, Hieshima GB, Halbach VV, Bentson JR, Goto K. Closure of carotid cavernous sinus fistulae by external compression of the carotid artery and jugular vein. *Acta Radiol [Suppl]* (Stockh) 1986;369:580-583

Paragangliomas of the Jugular Bulb and Carotid Body: MR Imaging with Short Sequences and Gd-DTPA Enhancement

T. Vogl¹
R. Brünig¹
H. Schedel¹
K. Kang¹
G. Grevers²
D. Hahn¹
J. Lissner¹

Twenty-six patients with glomus jugulare (16), glomus tympanicum (three), or carotid glomus (seven) tumors were examined with contrast-enhanced CT scans and MR scans without and with Gd-DTPA. MR and CT scans had similar sensitivities, but the enhanced MR scans were diagnostically more specific than either CT or nonenhanced MR. Dynamic MR scanning permitted measurement of the degree of Gd-DTPA enhancement over time.

We recommend contrast-enhanced MR with short sequences and a dynamic approach in patients with suspected carotid, tympanic, and jugular paragangliomas.

Before the introduction of MR imaging, the radiologic diagnosis of glomus tumors was based on CT findings [1–3]. MR imaging shows some advantages over CT in the diagnosis of lesions in the skull base and surrounding structures. Our experience indicates that these advantages are particularly evident in patients with suspected carotid, tympanic, and jugular paragangliomas. The following is a discussion of the diagnostic value of MR imaging of glomus tumors, particularly with short sequences and with the paramagnetic contrast medium Gd-DTPA.

Subjects and Methods

Twenty-six patients examined with MR and CT are included in this study. When clinical symptoms indicated a lesion in the middle ear or neck, prospective MR and CT were performed. Patients lacking objective clinical findings were excluded from the study. CT was performed with a Somatom DRH scanner* before and, except in five patients, after injection of a nonionic contrast agent.

MR examinations were carried out on a 0.35-T (seven cases) and later on a 1.0-T (19 cases) unit. In 16 patients with suspected jugular bulb tumors, the standard head coil was used. For suspected masses in the neck, a specially constructed Helmholtz coil was used to improve the signal-to-noise ratio. Axial images with a 5-mm slice thickness were obtained by using a long, 1600/30, 90 (TR/first-echo TE, second echo TE), and a short, 500/30 (TR/TE), spin-echo sequence. Eighteen patients were examined with the fast imaging technique. The time dependence of the Gd-DTPA enhancement was recorded by repeating the same slice eight times, one image every 30 sec. A 40° flip-angle sequence, 30/12, was used with acquisition times of 7 sec each, beginning at the time of bolus injection of Gd-DTPA. The enhancement/time ratio was analyzed and used for differential diagnosis. Similar to the denseness/time profile in dynamic CT, the enhancement/time ratio described the variation of the intensity of the region of interest vs time [3, 4].

There were 16 paragangliomas of the jugular bulb, three glomus tympanicum tumors, and seven tumors in the neck. A subjective evaluation system was developed to analyze our results (Table 1). Three categories of assessment were developed. The first category dealt with the quality of the MR images, with a range of grades from satisfactory (grade 1) to optimal (grade 3). Satisfactory image quality was defined as allowing anatomic display and recognition of tumor masses 5.0 mm in diameter. Good image quality was defined as allowing clear delineation of the tumor. Optimal information was defined as offering not only clear

This article appears in the July/August 1989 issue of *AJNR* and the September 1989 issue of *AJR*.

Received August 8, 1988; revision requested October 17, 1988; revision received December 1, 1988; accepted December 14, 1988.

¹ Department of Radiology, University of Munich, Klinikum Grosshadern, Marchioninstr. 15, 8000 Munich 70, W. Germany. Address reprint requests to T. Vogl.

² Department of Head and Neck Surgery, University of Munich, Klinikum Grosshadern, 8000 Munich 70, W. Germany.

AJR 153:583–587, September 1989

0361-803X/89/1533-0583

© American Roentgen Ray Society

* Siemens AG, Erlangen, W. Germany.

display of the anatomy and tumor delineation but also information on tissue necrosis and vascularity of the neoplasm.

The second category of assessment dealt with the use of Gd-DTPA. The post-Gd-DTPA image quality was deemed satisfactory (grade 1) if modest improvement was attained in comparison with nonenhanced images, good (grade 2) if significant tumor enhancement allowed better delineation of tumor extent, and optimal (grade 3) if mucosal structures and vascularity could be visualized in detail. The third category of assessment dealt with the results of CT and the comparison of MR and CT.

TABLE 1: MR and CT Assessments of Glomus Tumors

Tumor Type	Rating ^a		MR vs CT ^b
	Nonenhanced MR	Gd-DTPA MR	
Glomus jugulare (<i>n</i> = 16)	2	3	+
Glomus tympanicum (<i>n</i> = 3)	2	3	0
Glomus caroticum (<i>n</i> = 7)	3	3	+

^a 3 = optimal; 2 = good; 1 = satisfactory.

^b + = MR superior to CT; 0 = MR equal to CT; - = MR inferior to CT.

Results

The results of the MR studies and other examinations were divided between tumors in the skull base and neck.

Glomus Jugulare and Glomus Tympanicum Tumors

We found 16 glomus jugulare tumors. The clinical symptoms associated with paragangliomas were unilateral "deafness," tinnitus, pulsation, vertigo, and pain. Paralysis of cranial nerves VII, IX, and XI was evident in some.

The MR study was done before and after IV injection of Gd-DTPA. In tumors smaller than 1.5 cm, nonenhanced MR was not able to delineate masses in three of five cases. In all paragangliomas we found a remarkable increase in signal intensity in the first 60 sec after injection. Maximum signal intensity in tumor tissue was found after 150 sec with an enhancement factor of 1.8; after this peak, the intensity diminished gradually until the end of measurement at 360 sec. We attribute this to the "washout effect" of the highly vascularized tumor tissue.

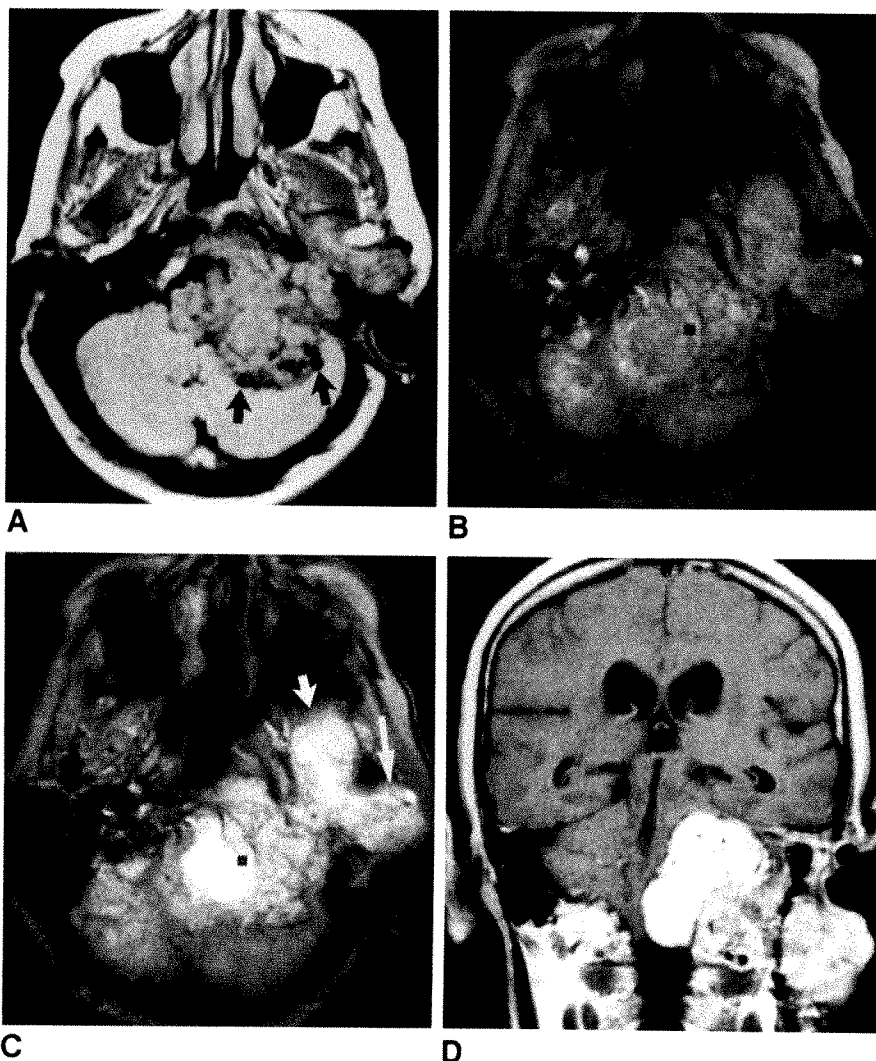


Fig. 1.—Large glomus jugulare tumor with intracranial involvement and bony erosion.

A, Axial plain MR image, 500/30, shows mass in left temporal bone and posterior fossa extending across midline. Large veins (arrows) are seen on surface of tumor.

B, Nonenhanced FLASH (fast scan) image, 30/12, 40° flip angle.

C, Gd-DTPA-enhanced FLASH image, 30/12, 40° flip angle, shows marked enhancement of tumor. Extent into infratemporal fossa (short arrow) and parotid area (long arrow) is appreciated.

D, Coronal Gd-DTPA image, 500/28, shows displacement of brainstem, bony erosion from large enhanced mass, and parotid involvement.

The T1-weighted sequence (500/30) was carried out after completion of the fast imaging technique. Enhancement with Gd-DTPA increased the signal intensity to 205% in tumor tissue, 132% in muscles, and 119% in fatty tissue. In 16 patients with glomus jugulare or glomus tympanicum tumors this led to significant additional information; only in three patients with very large tumors were no additional facts discovered (Table 1).

In analyzing the results of MR and CT, diagnostic reliability, completeness of the topographic description, and histologic diagnosis were compared. MR was superior in 13 patients with paragangliomas and equal to CT in three. Especially in tumors eroding the skull base (Figs. 1 and 2), in tumors with

surrounding edema, and in very small tumors (Figs. 3 and 4), contrast-enhanced MR demonstrated its value.

Glomus Caroticum Tumors

Nonenhanced MR imaging was sufficient in six patients with glomus caroticum tumors, but information improved further after application of Gd-DTPA. Because it provided better soft-tissue contrast, MR was superior to CT. MR was able to demarcate the tumor from the carotid bifurcation as well as from surrounding structures (Fig. 5). The characteristic vascularity of the tumors could be partly seen on nonenhanced MR, but was seen better on the early postinjection

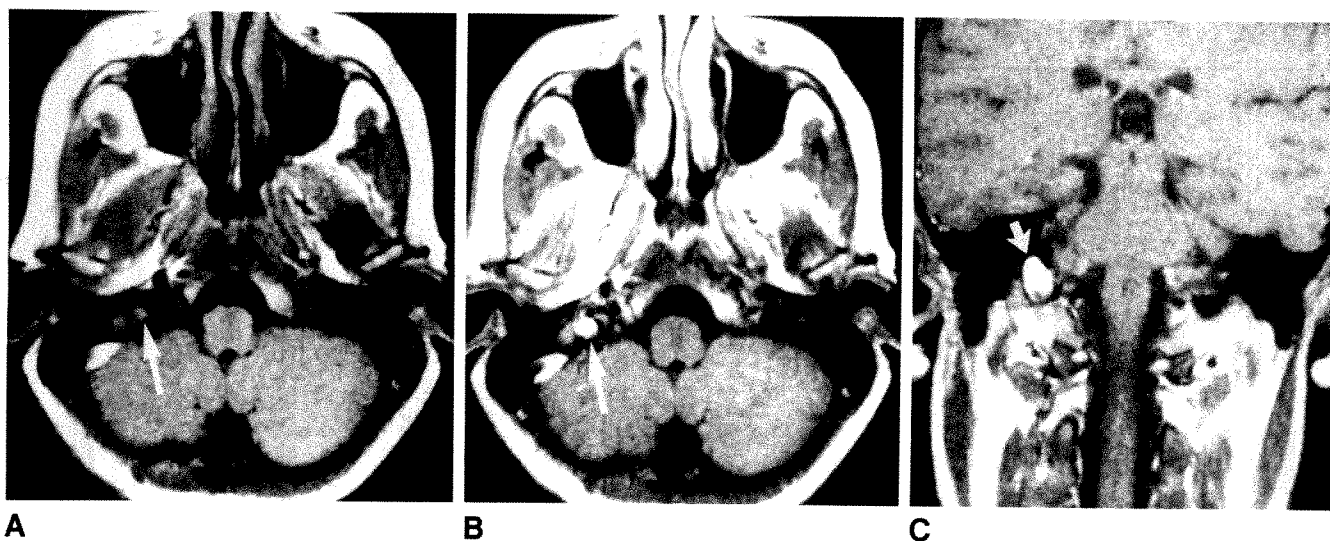


Fig. 2.—Small glomus jugulare tumor on right.

A, Nonenhanced axial image, 500/28, shows mass (arrow) in temporal bone measuring 1 × 1.5 cm in diameter. Lesion shows medium signal intensity. B, Gd-DTPA-enhanced axial image, 500/28, shows increase in signal intensity of mass (arrow) and optimum contrast in relation to surrounding tissues. C, Gd-DTPA-enhanced coronal image, 500/28, shows hyperintense mass (arrow).

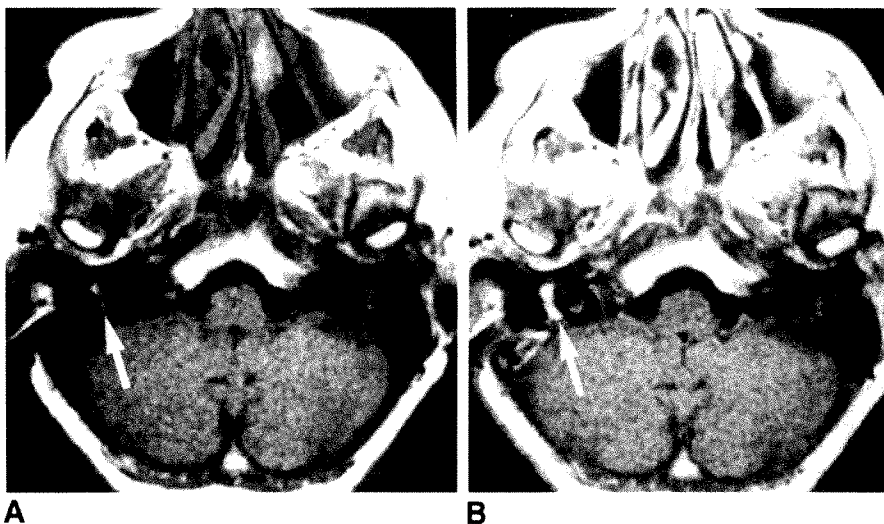


Fig. 3.—Recurrent tumor of glomus tympanicum after radiation therapy.

A, Nonenhanced axial image, 500/28, shows very small lesion (arrow) of intermediate signal intensity in mesotympanum.

B, Gd-DTPA-enhanced axial image, 500/28, shows marked increase in signal intensity in glomus tympanicum tumor (arrow), which measures 11 × 3 mm.

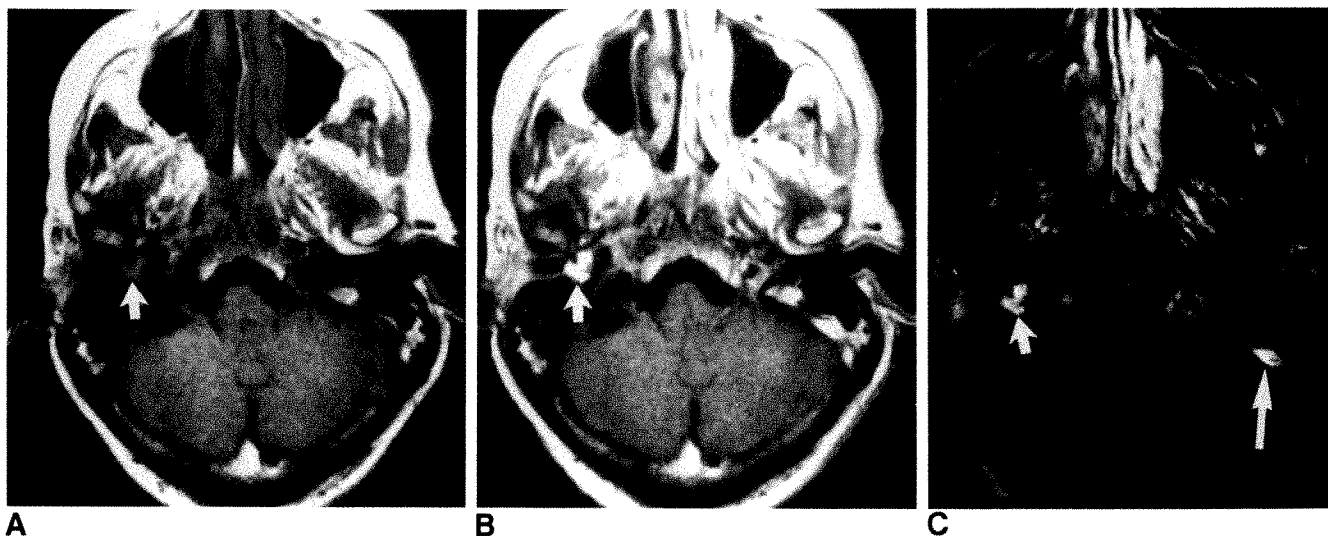


Fig. 4.—Glomus tympanicum tumor on right side.

A, Nonenhanced axial image, 500/28. Medial end of external auditory canal is obstructed by tumor (arrow) growing from middle ear.

B, Gd-DTPA-enhanced axial image, 500/28, shows marked enhancement of tumor (arrow).

C, Image obtained after subtracting A from B. Enhanced structures are glomus tympanicum tumor (short arrow), transverse sinus (long arrow), and nasal mucosa and turbinates.

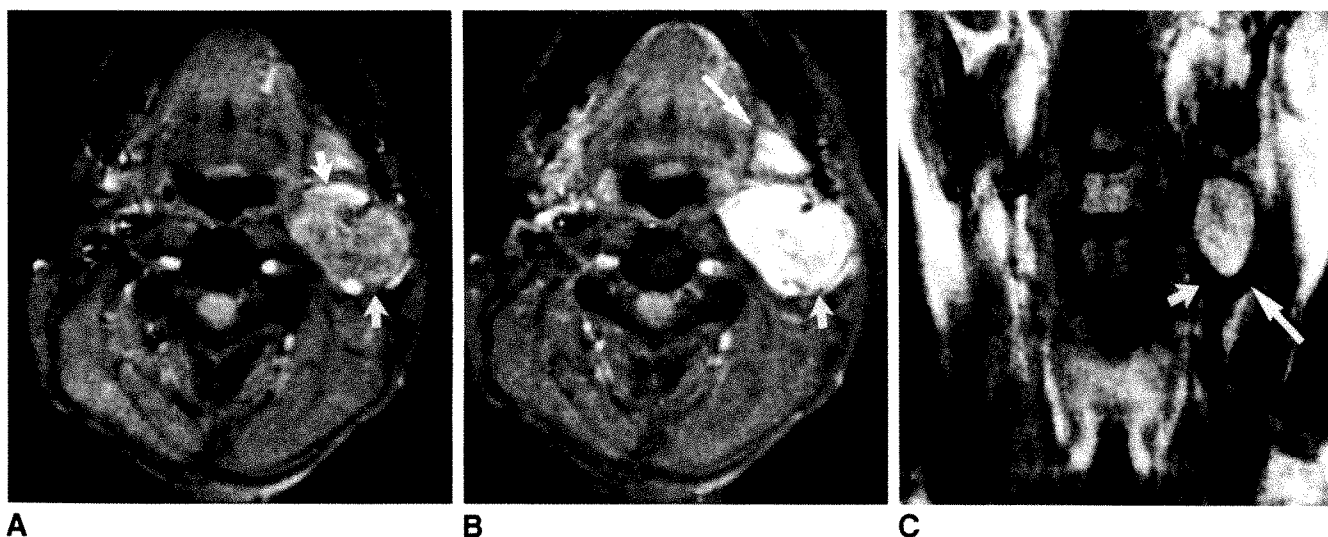


Fig. 5.—Glomus caroticum tumor.

A, Nonenhanced axial FLASH image, 30/12, 40° flip angle, shows large mass of heterogeneous intensity in carotid sheath (arrows).

B, Gd-DTPA-enhanced axial FLASH image, 30/12, 40° flip angle, shows homogeneous increase in signal intensity in glomus tumor (short arrow) and submandibular gland (long arrow). Salivary glands usually show marked enhancement.

C, Gd-DTPA-enhanced coronal image, 1600/30, provides optimum localization of tumor. Inferior aspect of mass is delineated by external (long arrow) and internal (short arrow) carotid artery.

sequences of the fast imaging technique. The signal/time pattern in one case is shown in Figure 6.

Discussion

Glomus tumors arise from paraganglia, which exist in various places in the human body. The precapillary arteriovenous shunts and nonchromaffin cells are characteristic of the histologic appearance of these tumors. Although glomus tissue

is found in different locations in the body, the histology and functions are the same [1, 5–7]. In the literature these tumors are called either chemodectomas, paragangliomas, or glomus tumors. Characteristic signs are their slow progression and the mostly benign, nonmetastatic growth. We did not find metastatic spread in our patients, but it is described in the literature [7, 8].

CT with thin slices and contrast enhancement so far has been the method of choice to diagnose glomus tumors and

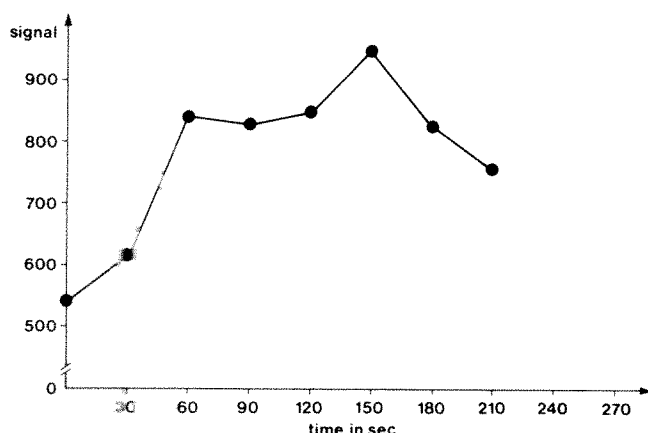


Fig. 6.—Enhancement/time profile typical of glomus caroticum tumor. Signal intensity was measured every 30 sec.

their growth in the skull base. Before the introduction of CT the preoperative diagnosis of glomus tumors was based on selective angiography [5, 7].

Coronal CT scanning is desirable and is recommended by various authors [1, 3, 5, 9–11]. Contrary to the findings of Larson et al. [1], our CT investigations with a high-resolution technique have yielded lower sensitivity and also lower specificity. The diagnosis of small tumors, especially those found at the glomus tympanicum without bone erosion, proved to be difficult, especially the differentiation from inflammatory changes.

MR as a new imaging tool shows some advantages for the diagnosis of lesions in the skull base and surrounding structures. In comparison with CT, MR provides superb soft-tissue contrast as well as soft-tissue/bone differentiation [12, 13]. This and the flow phenomenon are two reasons for the superiority of MR.

Generally, in the conventional spin-echo techniques, flowing blood has a low signal intensity; therefore, the lumina of vessels are easily distinguished from surrounding tissue [13, 14]. By using thin slices and individually adapted head or surface coils with a high signal-to-noise ratio, the carotid artery and the jugular bulb and vein are easily identified on nonenhanced MR. MR enables demonstration of even smaller vessels within the tumor [12].

The advantages of noninvasive investigation are forfeited when the contrast medium Gd-DTPA is used; however, MR with Gd-DTPA is considerably less invasive than angiography. The paramagnetic contrast medium helps to differentiate inflammatory lesions from tumors in the tympanum and mastoid. In our series, inflammatory lesions showed a significantly lower enhancement by Gd-DTPA than tumors did. Even more important is the use of Gd-DTPA for detecting tumors of the glomus jugulare and tympanicum with a diameter of 5 mm or less.

As in dynamic CT, it is possible to measure an enhancement/time pattern with the fast imaging technique. Short exposure sequences (gradient-echo sequences) repeated in a standardized pattern allow measurement of the degree of enhancement as well as its time dependence. Typically, par-

agangliomas show a take-up immediately after injection of the paramagnetic contrast medium, and a gradual decrease until the end of measurement at 7 min. Peak enhancement is reached after approximately 150 sec. This enhancement/time pattern with the washout effect helps to differentiate paragangliomas from meningiomas and neuromas.

MR of the glomus caroticum offers the same advantages described for skull-base glomus tumors. However, because these lesions may be difficult to detect clinically, an imaging study is of particular importance. The possibility of multiplanar imaging and the high soft-tissue contrast make MR the primary diagnostic tool when a carotid body tumor is suspected [15]. MR is able to define the position of the common, external, and internal carotid arteries. Carotid body tumors 5 mm in diameter can be identified by MR, while CT examination with iodine contrast medium only allows detection of carotid glomus tumors greater than 8 mm in diameter.

In conclusion, our experience has shown the advantages of MR in patients with suspected carotid, tympanic, and jugular paragangliomas. For the detection of glomus tumors in the head and neck area, the use of contrast-enhanced MR including short sequences and a dynamic imaging approach is recommended.

REFERENCES

- Larson TC, Reese DF, Baker HL, McDonald TJ. Glomus tympanicum chemodectomas: radiographic and clinical characteristics. *Radiology* 1987;163:801–806
- Chakeres DW, La Masters DL. Paragangliomas of the temporal bone: high-resolution CT studies. *Radiology* 1984;150:749–753
- Mafee MF, Valvassori GE, Shugar MA, Yanias DA, Dobben GD. High resolution and dynamic sequential computed tomography. *Arch Otolaryngol Head Neck Surg* 1983;109:691–696
- Mafee MF, Valvassori GE, Kumar A, et al. Tumors and tumor-like conditions of the middle ear and mastoid: role of CT and MRI. *Otolaryngol Clin North Am* 1988;21:349–375
- Carmody RF, Seeger JF, Harsley WW, Smith JRL, Miller RW. Digital subtraction angiography of glomus tympanicum and jugulare tumors. *AJNR* 1983;4:263–265
- Lo WWM, Solti-Bohmann LG, Lambert PR. High-resolution CT in the evaluation of glomus tumors of the temporal bone. *Radiology* 1984;150:737–742
- Lundgren N. Tympanic body tumors in the middle ear: tumors of carotid body type. *Acta Otolaryngol (Stockh)* 1949;37:367–379
- Manefte C, Rouleau J, Julian A, Guidicelli G. Glomus tympanicum tumors: early diagnosis by arteriography. *Neuroradiology* 1972;4:226–232
- Lo WWM, Solti-Bohmann LG. High-resolution CT of the jugular foramen: anatomy and vascular variants and anomalies. *Radiology* 1984;150:743–747
- Som PM, Reede DL, Bergeron RT, Parisier SC, Shugar JMA, Cohen NL. Computed tomography of glomus tympanicum tumors. *J Comput Assist Tomogr* 1983;7:14–17
- Mafee MF, Campos M, Raju S, et al. High field magnetic resonance imaging versus CT. *Otolaryngol Clin North Am* 1988;21:513–546
- Lee BC, Kneeland JB, Deck MD, Cahill PT. Posterior fossa lesions: magnetic resonance imaging. *Radiology* 1984;153:134–143
- Flannigan BD, Bradley WG, Mazzotta JC, et al. Magnetic resonance imaging of the brainstem: normal structure and basic functional anatomy. *Radiology* 1985;154:375–383
- McGinnis BD, Brady TJ, New PF. Nuclear magnetic resonance (NMR). Imaging of tumors in the posterior fossa. *J Comput Assist Tomogr* 1983;7:575–584
- Stark DD, Moss A, Gamsu G. MR imaging of the neck. Part 1: Anatomy. Part 2: Pathologic findings. *Radiology* 1984;150:447–461

Book Review

Magnetic Resonance Imaging, 2nd ed.; vol. I, Clinical Principles. By C. Leon Partain, Ronald R. Price, James A. Patton, Madan V. Kulkarni, and A. Everette James, Jr. Philadelphia: Saunders, 967 pp., 1988. \$400/set

Written by MR imaging experts, this book comprises 11 subdivisions with a total of 58 chapters. After a historical review and basic sciences introduction, there are sections on clinical imaging experiences in various parts of the body, special applications including contrast media, and a concluding section that forecasts and analyzes future expectations. Also included are a chapter on legal aspects of MR, an excellent index, and a glossary of MR terms at the end of the book. Edward Purcell and Felix Block, the fathers of nuclear magnetic resonance (NMR), wrote the foreword and chapter 1, respectively. Basic NMR physics and imaging principles are discussed only briefly in volume I and are covered in greater depth in volume II of this set.

Clinical principles of MR imaging are extensively discussed, and some material is duplicated. Several chapters discuss tissue characterization and optimization of MR image contrast by using the pulse sequence parameters. I was particularly impressed with the clinical chapters that presented biological explanations for the changes seen in MR intensities and studies in which the effects were confirmed with histology or other non-MR techniques. For example, tumor enhancement in brain tumors by paramagnetic compounds was explained by a break in the blood-brain barrier, and this effect was confirmed by animal studies with Evans blue dye. In another example, the oxidation state of hemoglobin and RBC membrane integrity are used to describe the changes in T1 and T2 relaxation times observed in aging hemorrhage. Also, I was impressed with the discussions that covered limitations and artifacts of MR imaging.

Several chapters presented detailed descriptions of the pathologic, physiologic, and biochemical bases of the disease before describing the MR changes. In some chapters, however, only the MR changes in the various disease states were described without any pathologic description. I realize that pathologic analysis cannot always be performed on patients, but parallel animal and/or in vitro studies should be done to understand the biophysical basis of the MR signal-intensity changes. I was not particularly impressed with nonquantitative descriptions of MR intensity changes that were found in several chapters. All MR images are digital, and therefore the intensity numbers should be used to describe the changes seen.

Comparisons of MR with other imaging techniques received considerable emphasis. For example, the author of chapter 23 states that positron emission tomography currently provides the best measurements of myocardial perfusion. Also, in chapter 53, 5000 MR cases were used to construct a table of sensitivity and specificity of MR vs CT, angiography, sonography, nuclear medicine, myelography, mammography, and radiography.

In summary, I would recommend this book to physicians interested in clinical MR imaging principles.

Todd Richards
University of Washington
Seattle, WA 98195

MR Characteristics of Subdural Hematomas and Hygromas at 1.5 T

Edward S. Fobben¹
 Robert I. Grossman
 Scott W. Atlas
 David B. Hackney
 Herbert I. Goldberg
 Robert A. Zimmerman
 Larissa T. Bilaniuk

MR images of 24 patients with 33 subdural collections were retrospectively reviewed to determine the spectrum of MR findings associated with such lesions. The lesions were dated by history, when available. Hematomas were grouped as follows: acute, four; early subacute, four; late subacute, four; chronic, 13. Six collections were classified as rehemorrhage; and two patients had CSF hygromas. Subdural hematomas evolved in a pattern similar to intracerebral hemorrhage with the exception of chronic subdural hematomas, in which isointensity or hypointensity relative to gray matter was observed on short TR/TE images compared with the persistent very high signal intensity noted in chronic parenchymal hematomas. Hemosiderin was rarely seen in chronic hematomas. These findings are most likely the result of the absence of a blood-brain barrier, which allowed clearance and dilution of blood products. Subdural hematomas with repeat hemorrhage demonstrated multiple phases of bleeding with layering phenomenon and more frequent hemosiderin deposition. It is possible that the clearance of blood products, as observed in chronic subdural hematomas, is impaired or poorly functional when rehemorrhage occurs. The persistence of high signal from methemoglobin in a hematoma that is expected to be in the chronic phase also suggests repeated hemorrhage. Acute CSF subdural hygromas had signal intensities identical to CSF without MR evidence of blood products. At surgery, clear fluid under pressure was found.

MR imaging, with its unique ability to delineate the various phases of hemorrhage, is well suited to the evaluation of subdural hemorrhage.

Although the appearance and evolution of hemorrhage in the brain on high-field MR images is well established [1], subdural hemorrhage is less well characterized. Physiologically and anatomically, the subdural space differs from the brain parenchyma. It is a potential space-lacking tissue as well as a blood-brain barrier. Such differences may alter the MR appearance and evolution of subdural hemorrhage when compared with bleeding into the cerebral parenchyma. The known propensity for repeat hemorrhage in subdural hematomas may further complicate the MR signal intensity patterns. Our study is an attempt to categorize and understand the MR appearance of subdural hemorrhage.

This article appears in the July/August 1989 issue of *AJNR* and the September 1989 issue of *AJR*.

Received August 22, 1988; revision requested October 31, 1988; revision received December 20, 1988; accepted December 27, 1988.

Presented at the annual meeting of the American Society of Neuroradiology, Chicago, May 1988.

¹ All authors: Department of Radiology, Hospital of the University of Pennsylvania, 3400 Spruce St., Philadelphia, PA 19104. Address reprint requests to R. I. Grossman.

AJR 153:589-595, September 1989

0361-803X/89/1533-0589

© American Roentgen Ray Society

Materials and Methods

The MR images of 24 patients (ages 1 month to 70 years) with subdural hematomas and hygromas were reviewed retrospectively. Imaging was performed on a 1.5-T GE imager using spin-echo (SE) sequences with 600/20 (TR/TE) and 2500-3000/30-80/2 and a matrix size of 128 × 256. Serial imaging was performed in four patients. Hemorrhages were classified by the patients' clinical history (i.e., time interval between insult and MR scan) as acute (<1 week old), early subacute (>1 week and <2 weeks old), late subacute (>2 weeks old and <1 month old), or chronic (>1 month old). These categories, which follow those developed by Gomori et al. [1, 2] for parenchymal hematomas, can be summarized as follows: Acute hematomas are characterized by hypointensity on long TR images. Early subacute hematomas have peripheral hyperintensity on short TR images and hypointensity centrally on long TR/TE sequences. The late subacute subdural hematoma is hyperintense on both long and

short TR images. Chronic parenchymal hematomas are hyperintense on long and short TR images and are surrounded by a hemosiderin rim. In subdural hematomas the presence of hemosiderin is indicated by susceptibility changes (hypointensity on long TR/TE images) in thickened membranes or clumps of material.

Results

Thirty-three subdural collections were present in 24 patients and were grouped as follows: acute, four; early subacute, four; late subacute, four; chronic, 13; and rehemor-

TABLE 1: Summary of 24 Patients with Subdural Hematomas*

Case No.	Age	Interval	Comment
Acute SDH (<1 week old)			
1.	55 yr	1 day	MVA
2.	8 yr	3 days	Hemophilia
3.	2 mo	5 days	(patient also had a late subacute SDH)
4.	33 yr	5 days	Skull fracture MVA
Early subacute SDH (>1 week and <2 weeks old)			
5.	5 yr	9 days	Preop debris
6.	1 mo	13 days	MVA
7.	55 yr	14 days	MVA
8.	59 yr	14 days	Shunt out
Late subacute SDH (>2 weeks and <1 month old)			
9.	6 mo	10 days	Abuse
10.	4 mo	Unknown*	Abuse
11.	5 yr	23 days	MVA
Chronic SDH (>1 month old)			
12.	2 yr	30 days	Postop
13.	70 yr	>30 days, est	On Coumadin
14.	9 wk	>30 days, est	Abuse
15.	4 mo	>30 days, est	Abuse
16.	4 mo	>30 days, est	Abuse
17.	5 mo	>30 days, est	Abuse
18.	15 mo	>30 days, est	Abuse
Subdural hygroma			
19.	7 wk	3 days	Head trauma
20.	4 yr	15 days	MVA
Rehemorrhage			
21.	4 yr	8 mo	(Follow-up scan 4 months later). New bleeding in known chronic collections.
22.	8 yr	9 mo	(Follow-up scan 42 days later). New bleeding in known chronic collections.
23.	31 yr	7 mo	Since initial trauma, 2-week history of headache, presented with papilledema.
24.	41 yr	Unknown	Autopsy revealed chronic SDH with acute rehemorrhage.

Note.—est = estimate (in some cases the exact date of injury was unknown but a reasonable estimate could be made); unknown* = interval from injury to examination was unknown, classified with SDH of similar signal intensities; MVA = motor vehicle accident.

* Hematomas were bilateral in nine patients, for a total of 33.

rhage, six. There were two hygromas. The results are presented in Table 1. Subdural hematomas evolved in a pattern similar to parenchymal hematomas in the acute and subacute stages. Acute subdural hematomas were characterized by

the presence of hypointensity on long TR/TE images (Fig. 1). In the early subacute stage we noted a rim of high signal intensity, presumably due to free methemoglobin, on all pulse sequences surrounding a center of low signal intensity most

Fig. 1.—Case 2: hemophiliac with acute right suboccipital SDH and incidentally discovered left subacute SDH.

A, CT scan shows hyperdense acute right occipital SDH.

B, MR image, 2500/80, shows low signal intensity of deoxyhemoglobin in acute right SDH and high signal from methemoglobin in subacute left SDH. Note absence of hemosiderin in left subacute SDH.

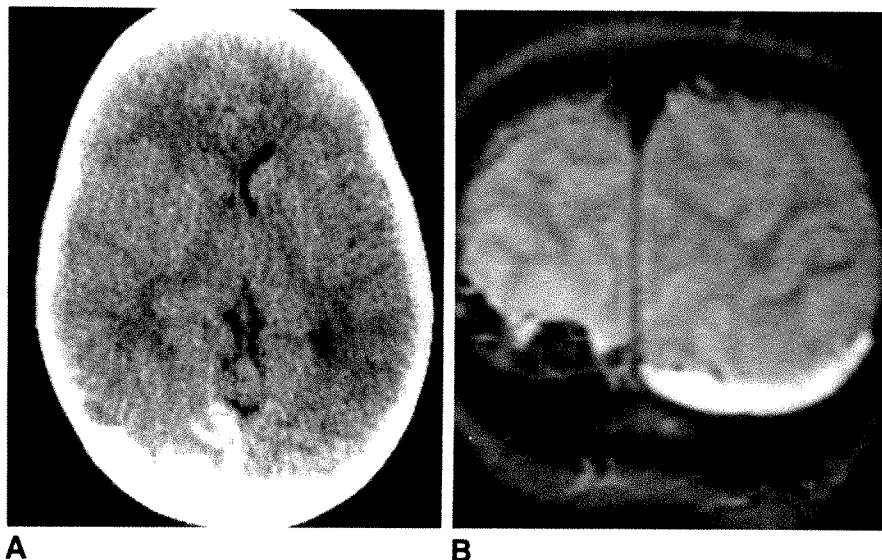


Fig. 2.—Case 7: early subacute SDH 14 days after motor vehicle accident.

A, Sagittal MR image, 600/20, shows peripheral high signal intensity of extensive frontotemporal SDH.

B, MR image, 2500/80, shows peripheral hyperintensity of methemoglobin surrounding a center of low signal intensity deoxy- or intracellular methemoglobin (arrows).

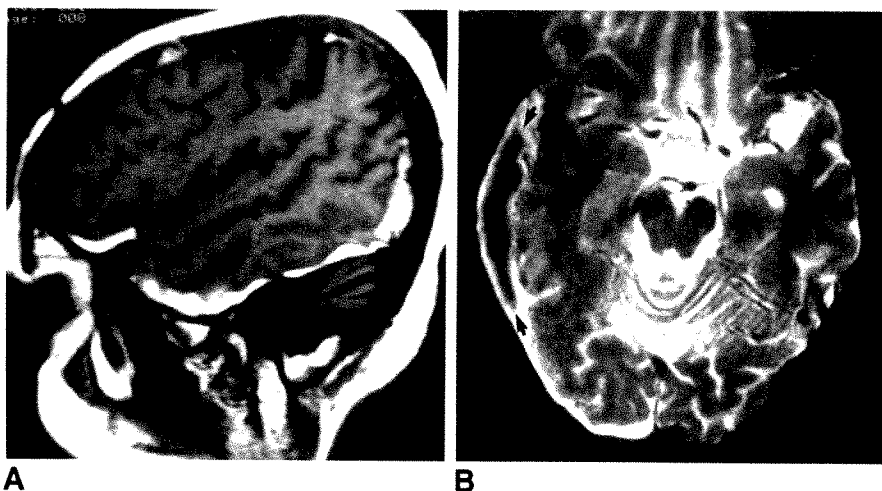
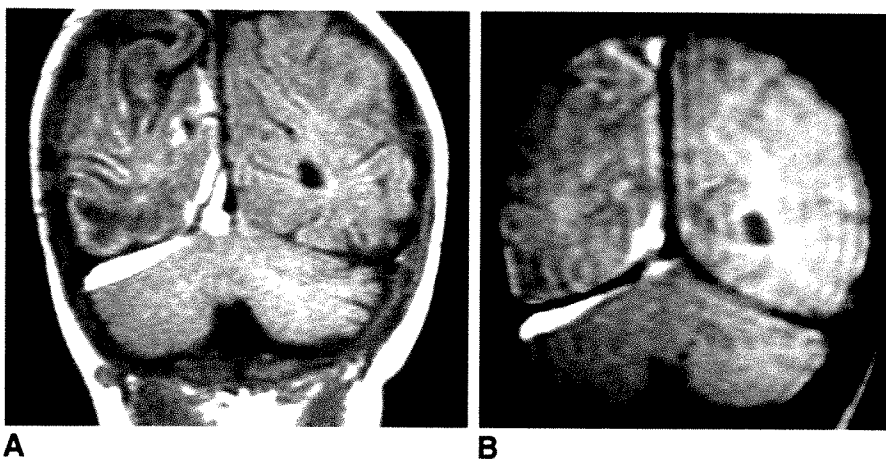


Fig. 3.—Case 10: late subacute SDH in a case of child abuse. Exact interval from injury to examination is uncertain.

A, Coronal MR image, 600/20, shows high signal intensity in small right tentorial SDH.

B, Coronal MR image, 3000/30, also shows high signal intensity in right tentorial SDH.



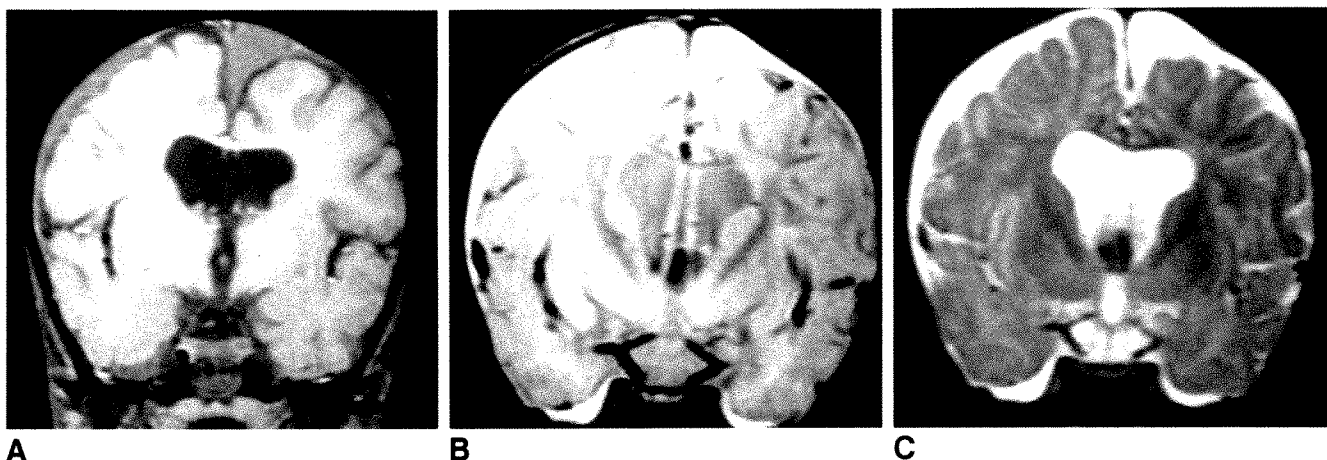


Fig. 4.—Case 14: chronic SDH in a case of child abuse. Injury interval estimated at >30 days.

A, Coronal MR image, 600/20, shows extracerebral collection with signal intensity isointense relative to gray matter in vertex and convexities.

B, Coronal MR image, 3000/30, shows hyperintensity of bilateral chronic SDH while ventricular CSF remains hypointense.

C, Coronal MR image, 3000/80, shows hyperintensity of SDH.

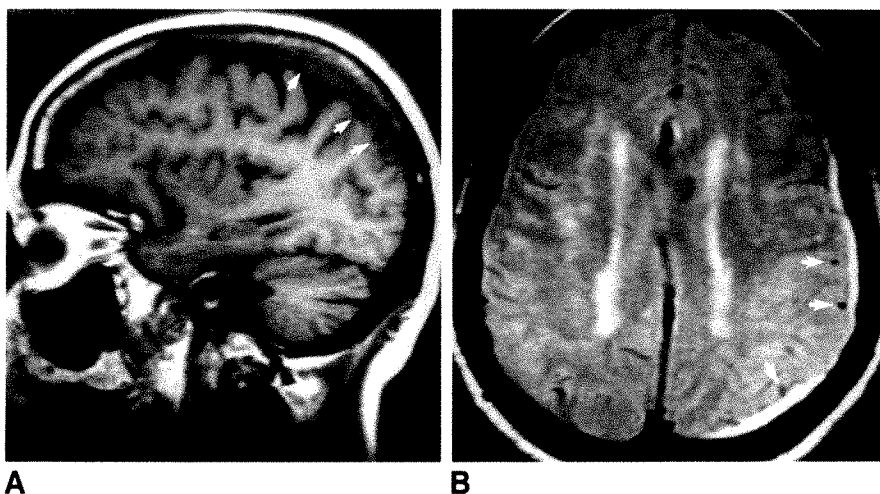


Fig. 5.—Case 13: elderly patient on Coumadin.

A, Sagittal MR image, 600/20, of a small chronic SDH in an elderly patient with large sulci showing inward displacement of veins (arrows) by SDH, a useful anatomic criterion for distinguishing subdural collections from simply enlarged CSF spaces.

B, Axial MR image, 3000/80, shows hyperintense chronic SDH and inwardly displaced veins (arrows).

marked on long TR/TE images (Fig. 2). In the late subacute hematoma, the entire volume of the collection had high signal intensity on all pulse sequences (Fig. 3). No hemosiderin was seen in acute or subacute collections.

Subdural hematomas differed significantly from parenchymal hematomas in the chronic phase (Fig. 4). The signal intensity ranged from slightly hypointense to isointense relative to gray matter on short TR/TE images, in contrast to the persistent high signal intensity seen in chronic parenchymal hematomas on both long TR/short TE and long TR/TE images [1]. In contrast to brain hemorrhage, hemosiderin was detected in only one of 13 chronic subdural hematomas. The presence of hemosiderin was noted to occur in the presence of either thickened membranes or was associated with clumps of material, which demonstrated susceptibility changes on long TR images. An anatomic observation in MR images of subdural hematomas that has proved useful in angiography is the inward displacement of superficial veins against the

brain by the subdural collection. Although this sign is not needed to diagnose the presence of subdural hematomas on MR, it can be useful in differentiating chronic subdural collections from enlarged CSF spaces resulting from atrophy (Fig. 5).

Chronic subdural hematomas with rehemorrhage demonstrated several unique characteristics, including layering phenomenon and more consistent hemosiderin deposition. The evolution from acute to subacute rehemorrhage and from the subacute to the chronic phase was demonstrated on serial scans in one patient (Fig. 6). Persistence of high signal intensity, typical of the subacute stage, beyond its expected time interval was present in two collections, which were repeatedly rehemorrhaging, as documented either clinically or by CT (Fig. 7). This patient also showed membranous deposition of hemosiderin (Fig. 7B).

In one patient, a surgically proved bilateral acute subdural CSF hygroma was present, which contained no blood prod-

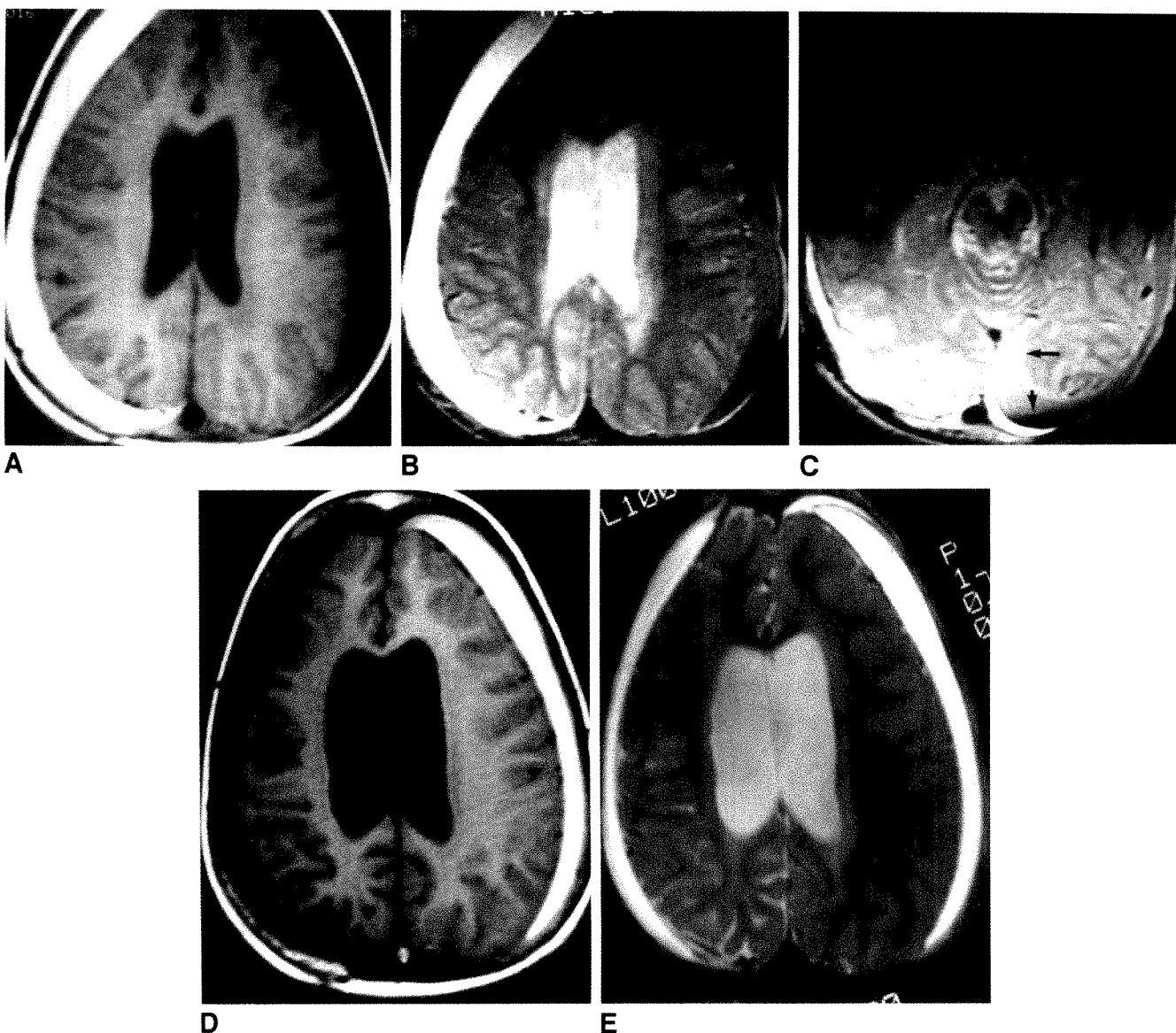


Fig. 6.—Case 21: routine follow-up scan in patient with known chronic SDH of 8 months duration after shunting for a tectal glioma shows acute rehemorrhage on the left and a right-sided subacute rehemorrhage. Although clinically asymptomatic, this bleeding into preexisting chronic subdural collections was new compared with prior CT scans.

A, MR image, 600/25, shows a high-intensity, right-sided subacute SDH as well as a low-intensity acute rehemorrhage of left SDH. On this scan alone it cannot be determined whether the low signal intensity on the left is due to a CSF collection or deoxyhemoglobin.

B, MR image, 3000/80, shows diffuse low-intensity susceptibility effects in the collection on the left, confirming the presence of deoxyhemoglobin in an acute rehemorrhage. The right-sided subacute rehemorrhage remains high in signal intensity.

C, MR image, 3000/80, shows layering effect and loculations. There is a dependent layer of low-intensity deoxyhemoglobin (*short arrow*) and a plasma supernatant of high signal intensity (*long arrow*). There is also an area of loculated high signal fluid posteromedially.

D–E, Repeat scans 4 months after initial scan show the evolution from subacute to chronic SDH on the right and from acute to subacute on the left. The persistence of the high signal from methemoglobin on the left over 4 months is most likely due to repeated hemorrhage.

D, MR image, 600/25, shows evolution of right-sided SDH from high intensity subacute to low-intensity chronic SDH. The left-sided collection has evolved from acute to subacute.

E, MR image, 3000/80, shows high signal intensity in both collections.

ucts. These collections demonstrated signal intensities that were identical to CSF (Fig. 8). In this case, surgery revealed clear CSF under pressure in the subdural space.

Discussion

The MR characteristics of acute and subacute subdural hematomas are similar to those of intraparenchymal hemor-

rhage [1, 2], whereas chronic subdural hematomas differ from parenchymal hematomas in several ways. As opposed to the typical parenchymal hematoma, which is markedly hyperintense on short TR/TE images, a chronic subdural hematoma will usually be slightly hypointense to isointense relative to gray matter on short TR/TE images. This loss of the T1 shortening effect appears to result from a decrease in the concentration of free methemoglobin by either dilution, ab-

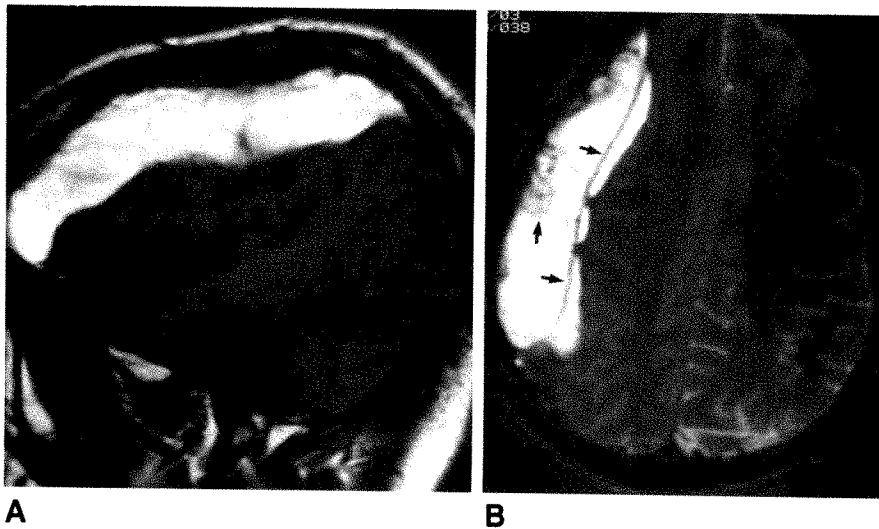
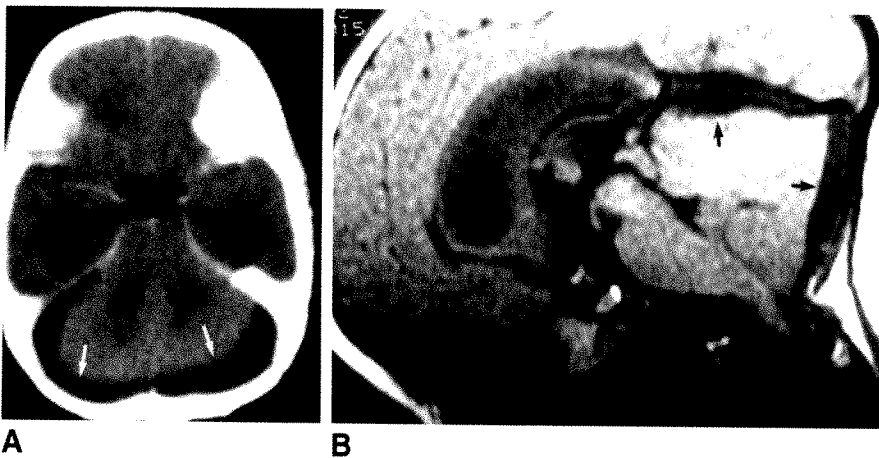


Fig. 7.—Case 23: patient with head trauma 7 months previously presented with a 2-week history of increasing headache and papilledema.

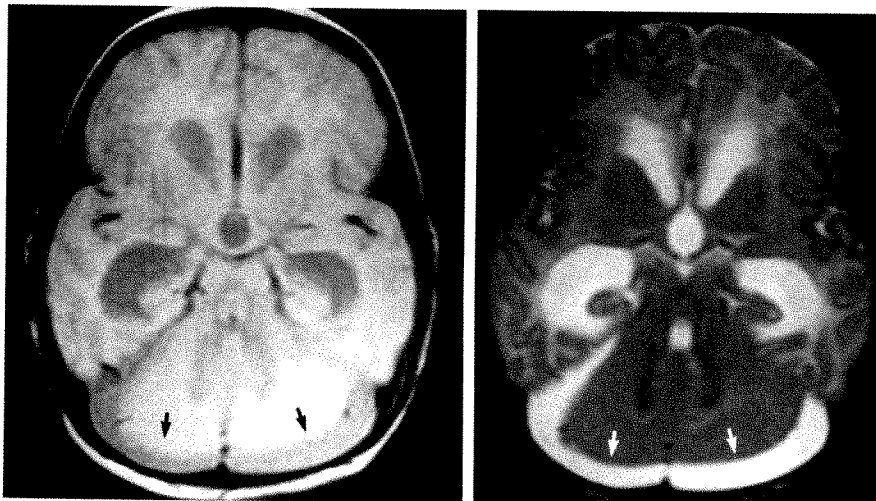
A, Sagittal MR image, 600/20, shows high signal intensity subacute rehemorrhage.

B, Axial MR image, 3000/80, demonstrates high signal intensity collection with thickened membranes showing hypointensities characteristic of hemosiderin (arrows).



A

B



C

D

Fig. 8.—7-week-old girl was accidentally dropped on her head and presented to the emergency room 3 days later obtunded and with cerebellar signs.

A, CT scan shows hypodense bilateral posterior fossa fluid collections (arrows) and acute hydrocephalus with temporal horn dilatation.

B, Sagittal MR image, 600/20, shows collections around cerebellum identical in signal intensity to CSF (arrows).

C and D, Axial MR images, 3000/30 (C) and 3000/80 (D), show that signal intensity of collections is identical to CSF (arrows).

sorption, and/or degradation. This is clearly shown on longitudinal imaging of the subdural hematoma shown in Figure 6, where hyperintensity on short TR/TE images converts to isointensity 4 months later.

The infrequent presence of hemosiderin, manifested by hypointensity on long TR/TE images, in chronic subdural hematomas as noted in this study is quite different from that in chronic intraparenchymal hematomas, in which it is a constant feature [3]. However, the marked hypointensity of hemosiderin was seen in thickened membranes and multiple clumps in three of four of the subdural collections that had rehemorrhaged. It is possible that, owing to the absence of a blood-brain barrier in the subdural space, hemosiderin is largely resorbed into the bloodstream. In repeat hemorrhages the clearance mechanism may be poorly functional, resulting in greater hemosiderin deposition.

Rehemorrhage is a frequent phenomenon with subdural hemorrhage and MR offers excellent visualization of this process. Because of the presence of a vascular membrane, subdural hematomas are prone to rehemorrhaging even without clinically evident trauma [4, 5]. Studies utilizing radio-nuclide-tagged red blood cells indicate that repeat hemorrhage in chronic subdural hematomas occurs at the average rate of 10.2% of the subdural hematoma's volume per day [5]. MR demonstrated repeat hemorrhages with layering and dilution of deoxyhemoglobin (MR changes of acute hemorrhage) in known chronic collections. Subacute hemorrhage was also seen in hematomas known to be chronic by clinical history.

Much of the previous literature emphasized the superior ability of MR to visualize subdural hematomas that were isodense on CT with little emphasis on the appearance or evolution of hemorrhage [6-8]. Hosoda et al. [9], using a much broader classification of chronic SDH, described a series of 20 chronic subdural hematomas that varied in appearance from hyper- to hypointensity on short TR images. However, if their individual cases are categorized by our time criteria, the hyperintense collections are subacute and the hypointense collections are chronic, as in our cases.

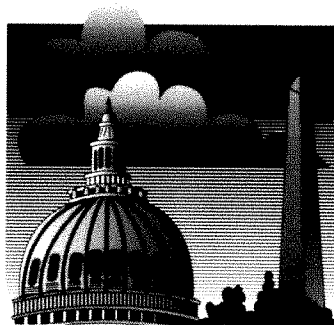
In addition to the observations made on the appearance and evolution of subdural hemorrhages, MR demonstrated nonhemorrhagic acute subdural hygromas in two cases. These collections displayed signal intensities that followed CSF without MR evidence of hemorrhage. In one of these

cases fluid analysis demonstrated nonhemorrhagic, clear CSF. Such collections are presumably due to tears in the arachnoid membrane [10].

In conclusion, acute and subacute subdural hematomas follow the signal intensity pattern at 1.5 T of intraparenchymal brain hemorrhage, but they differ in the chronic phase. As opposed to the typical chronic parenchymal hematoma, which is markedly hyperintense on short TR/TE images, the chronic subdural hematoma may be slightly hypointense to isointense relative to gray matter on short TR/TE images. We hypothesize that these signal intensity changes are the result of a decrease in the concentration of free methemoglobin by either dilution, absorption, and/or degradation. Hemosiderin, which is a constant feature of parenchymal hematomas, was seen only rarely in chronic subdural hematomas. The phenomenon of repeated hemorrhage was characterized by layering effects as well as more frequent hemosiderin deposition. MR, with its unique ability to image the various phases of hemorrhage, is well suited to the evaluation of subdural hemorrhage.

REFERENCES

1. Gomori JM, Grossman RI, Goldberg HI, Zimmerman RA, Bilaniuk LT. Intracranial hematomas: imaging by high-field MR. *Radiology* 1985; 157:87-93
2. Gomori JM, Grossman RI, Hackney DB, Goldberg HI, Zimmerman RA, Bilaniuk LT. Variable appearances of subacute intracranial hematomas on high-field spin-echo MR. *AJNR* 1987;8:1019-1026
3. Grossman RI, Gomori JM, Goldberg HI, et al. Magnetic resonance imaging of hemorrhagic conditions. *Acta Radiol [Diagn] (Stockh) [Suppl]* 1986; 369:53-55
4. Markwalder T-M. Chronic subdural hematomas: a review. *J Neurosurg* 1981;54:637-645
5. Ito H, Yamamoto S, Komai T, Mizukoshi H. Role of local hyperfibrinolysis in the etiology of chronic subdural hematoma. *J Neurosurg* 1976;45: 26-30
6. Sipponen JT, Sepponen RE, Sivula AS. Chronic subdural hematoma: demonstration by magnetic resonance. *Radiology* 1984;150:79-85
7. Young IR, Bydder GM, Hall AS, et al. Extracerebral collections: recognition by NMR imaging. *AJNR* 1983;4:833-834
8. Moon KL, Brant-Zawadzki M, Pitts LH, Mills CM. Nuclear magnetic resonance imaging of CT-isodense subdural hematomas. *AJNR* 1984;5: 319-322
9. Hosoda K, Tamaki N, Masmura M, Matsumoto S, Maeda F. Magnetic resonance images of chronic subdural hematomas. *J Neurosurg* 1987; 67:677-683
10. Hoff J, Bates E, Barnes B, Glickman M, Margolis T. Traumatic hemosiderin hygroma. *J Trauma* 1973;13:10; 870-876



Come to the
American Roentgen Ray Society

90th

ANNUAL MEETING

Washington, D. C.

Sheraton Washington Hotel
May 13-18, 1990

Scientific Program (200 papers)

Instructional Courses (60 hours)

Categorical Course on Cardiovascular Imaging

The Caldwell Lecture

Award Papers

Scientific Exhibits

Social, Golf, and Tennis Programs

Guest Programs



MR Imaging of Intracranial Fluid Levels

James J. Abrahams¹
Mika Lidov
Carlos Artiles

Six patients with seven intracranial fluid levels were evaluated with both CT and MR at 1.5 T. A surgical diagnosis was obtained in six of the seven instances. MR was found to be superior to CT in detecting intracranial fluid levels, and the MR signal characteristics were helpful in identifying their contents. These cases demonstrate the necessity for a slightly different approach to lesions with fluid levels. In one patient, imaging in the prone position allowed detection of a solid component; in several others, detection of the fluid level was dependent on the selection of nonroutine windows and levels. Fluid levels are classified with respect to their components and MR features.

MR is superior to CT in imaging fluid levels. The appearance of fluid levels on MR varies with their composition, the ratio of the components, the sequence parameters, and the position of the patient.

Some intracranial lesions that have a cystic appearance on MR and CT are later demonstrated at surgery to be solid. A fluid level is the only preoperative radiographic finding that unequivocally proves a lesion is cystic. The impact this finding can have on the differential diagnosis and the surgical technique is obvious. We describe the MR characteristics of fluid levels in a variety of intracranial lesions and demonstrate the superior ability of MR in comparison with CT in detecting and characterizing them. The fluid levels are categorized according to their components, and the MR features of the three most common kinds (air-fluid, fluid-precipitate, and fat-fluid) are discussed.

Materials and Methods

Six patients with seven intracranial fluid levels were evaluated by MR, and the findings were compared with those on CT (Table 1). A surgical diagnosis was obtained in six of the seven instances. Patients who did not have both a CT and MR scan were excluded from the study. The study included five males and one female 10–72 years old.

A high-field-strength (1.5-T) superconducting MR scanner was used.* T1-weighted, 400, 600/20 (TR/TE), and T2-weighted multiecho, 2000, 2500/20, 80, sequences were acquired. The width and level were adjusted for maximum visualization of the fluid levels. One patient (case 1) was scanned in both the supine and prone positions.

CT scans were obtained 1 day before the MR scans in cases 5 and 6 and 2 and 3 days before the MR scans in cases 1 and 3, respectively. In case 2, sequential CT scans were obtained, with the last CT scan being obtained 2½ months prior to MR. In case 4, a CT scan was obtained 3 weeks after the MR scan.

Case Reports

Case 1

A 42-year-old man was seen with recent onset of slowly progressive cranial-nerve deficits. A CT scan demonstrated questionable areas of low and high attenuation in the left pons without evidence of a fluid level (Fig. 1A). MR, initially performed on a low-field-strength (0.15-

This article appears in the July/August 1989 issue of *AJNR* and the September 1989 issue of *AJR*.

Received September 1, 1988; revision requested November 1, 1988; revision received November 14, 1988; accepted December 19, 1988.

Presented at the annual meeting of the American Society of Neuroradiology, New York City, May 1987.

¹ All authors: Department of Diagnostic Radiology, Yale University School of Medicine, NF2-123, 333 Cedar St., New Haven, CT 06510. Address reprint requests to J. J. Abrahams.

AJR 153:597–604, September 1989

0361–803X/89/1533–0597

© American Roentgen Ray Society

* General Electric, Milwaukee, WI.

TABLE 1: Summary of Patients with Intracranial Fluid Levels Evaluated by CT and MR

Classification/ Case No.	Pathology	Detection of Fluid Level	
		CT	MR
Fluid-precipitate			
1	Vascular malformation with hemorrhagic cyst	Not seen	T1: seen well after width & level adjustment T2: seen well
2	Arachnoid cyst resection with hemorrhagic surgical bed	Not seen initially ^a	T1: seen poorly after width & level adjustment T2: seen well after width & level adjustment
3	Cystic schwannoma of hypoglossal nerve	Not seen initially ^a	T1 & T2: seen well
4	Chromophobe adenoma with hemorrhagic cyst	Not seen	T1 & T2: seen well
5	Recurrent craniopharyngioma with hemorrhagic cyst	Not seen	T1: seen well after width & level adjustment T2: seen well
6	Intraventricular blood	Seen well	T1 & T2: seen well
Air-fluid			
6 ^b	Intraventricular epithelial cyst	Seen well	T1: seen well after width & level adjustment T2: seen well

^a After the fluid level was seen on MR, retrospective review of CT showed subtle findings suggesting a fluid level.

^b This patient had two fluid levels.

T) scanner, showed a smooth, round, homogeneous high-signal pontine mass, but did not show a fluid level. A subsequent high-field-strength MR scan, however, clearly revealed a fluid level on the T2-weighted sequence, with a lower-signal-intensity component in the dependent position and a heterogeneous high-signal component in the nondependent layer (Figs. 1B, 1C, and 1E).

The complexity of the nondependent high-signal portion of the lesion suggested the possibility of a solid nodule. A repeat examination, performed with the patient in the prone position (Fig. 1D), readily revealed a fixed solid nodule that did not shift position while the fluid layers did.

The precise MR localization of the solid component of the lesion and the demonstration of its cystic nature changed what was believed to be an inoperable lesion into an operable one.

At surgery, a cystic lesion was entered, and a small arteriovenous malformation with adherent clot was excised. This clot corresponded exactly to the location of the nodule seen on the MR scan. Six months later the patient had resumed work and was playing tennis again.

Case 2

A 60-year-old woman had a left parietal arachnoid cyst resected at another hospital; the postoperative CT scan revealed a hemorrhagic surgical bed. Sequential CT scans over the next month showed resolution of the hemorrhage. At our institution, a fluid level, which was not initially appreciated on CT, was clearly demonstrated on MR (Fig. 2B). Retrospective review of the CT scan suggested a fluid level (Fig. 2A).

Case 3

A 59-year-old man was seen for MR evaluation of a complex posterior fossa lesion that was demonstrated on CT. No cystic component or fluid level was initially appreciated on CT (Fig. 3A). The MR scan that followed, however, beautifully demonstrated a large cystic area with a fluid level (Figs. 3B and 3C). The surgical approach was greatly facilitated by the ability of MR to differentiate the cystic from solid portions of the lesion.

At surgery, the cystic component contained a viscous yellow fluid. No blood was seen in the cyst and no hemosiderin was demonstrated histologically. The pathologic diagnosis was a cystic schwannoma.

Case 4

A 72-year-old man followed by ear, nose, and throat specialists for chronic vertigo and tinnitus had an MR scan of the internal auditory canal that revealed an incidental pituitary lesion with a fluid level composed of a very hypointense dependent layer and a hyperintense nondependent layer on the T2-weighted sequence (Fig. 4A). A subsequent CT scan failed to demonstrate this fluid level (Fig. 4B). Further questioning elicited two recent episodes of severe headache and nausea, which were believed to be consistent with pituitary apoplexy. The patient underwent transsphenoidal surgery, and a cyst containing subacute blood was encountered within the lesion. The pathologic diagnosis was chromophobe adenoma.

Case 5

A 10-year-old boy who had undergone debulking of a craniopharyngioma when he was 4 years old presented with signs and symptoms of hydrocephalus. CT and MR scans 1 day apart revealed recurrent tumor and hydrocephalus (Fig. 5). A fluid level was once again identified within the lesion on MR but not on CT. The dependent layer was hyperintense relative to brain on T1 images and markedly hypointense on T2 images, while the nondependent layer was very hyperintense on both T1- and T2-weighted images. It was believed from CT and MR that these findings represented hemorrhage with recurrent tumor, but the patient refused surgery.

Case 6

A 52-year-old man had a 1½-year history of right-sided headaches that occasionally were positional in nature. His neurologic examination was unremarkable. CT and MR scans demonstrated a cyst in the trigone of the right lateral ventricle (Fig. 6A). An attempt at rupturing

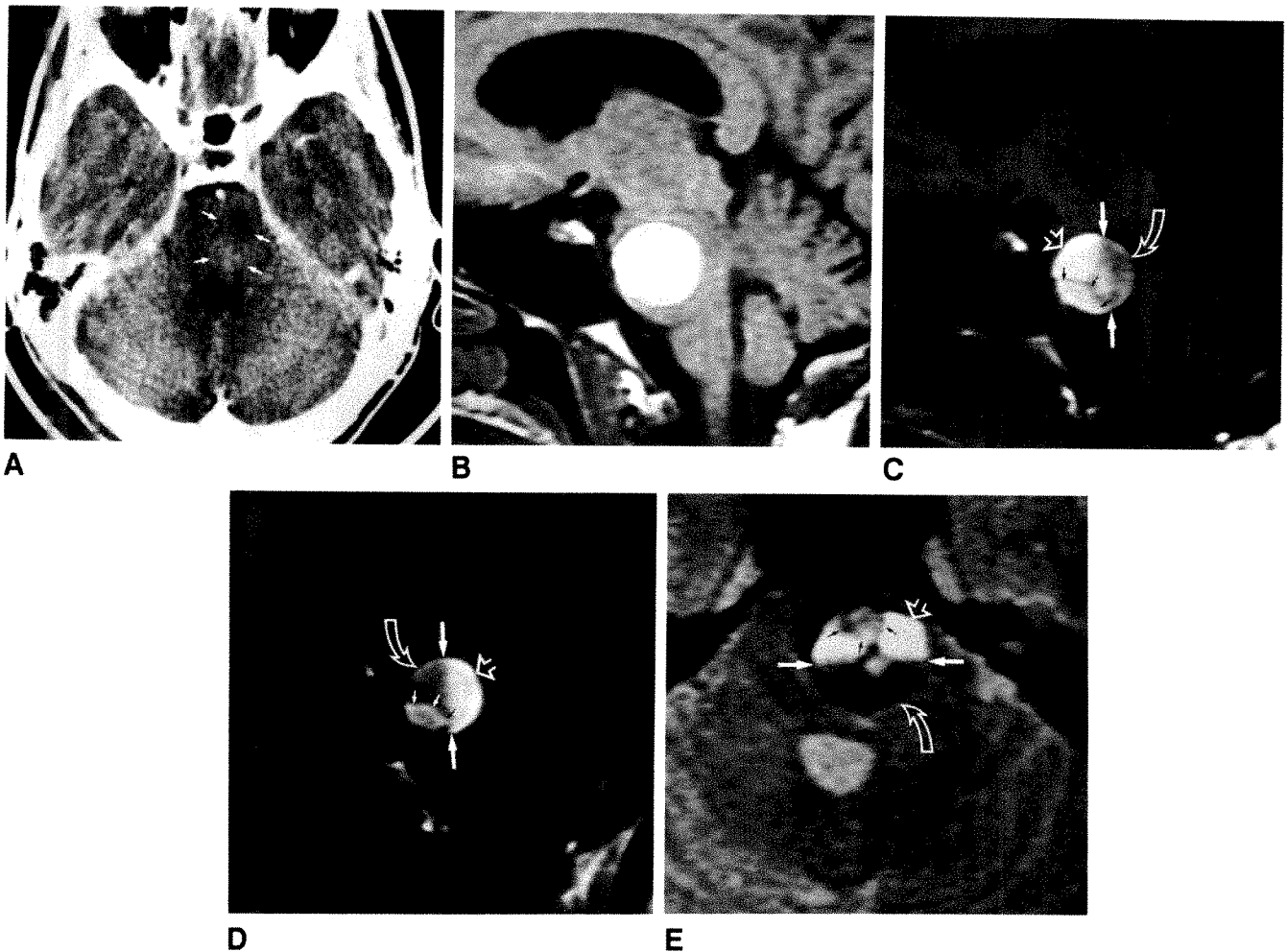


Fig. 1.—Case 1: Vascular malformation with a hemorrhagic cyst.

A, Axial contrast-enhanced CT scan. Areas of low and high attenuation (arrows) suggest a lesion in this location. No fluid level is seen.

B, Sagittal T1-weighted image (600/20) shows high-signal lesion in pons.

C, With width and level adjusted to allow visualization of fluid level (compare with B). High-signal free methemoglobin layer is in nondependent position (straight open arrow), while lower-signal intracellular deoxyhemoglobin and/or intracellular methemoglobin layer assume dependent position (curved arrow). Fluid level (solid white arrows). Nodule (black arrows).

D, Sagittal T1-weighted image (400/20) with patient in prone position. This causes fluid layers to swap positions while high-signal nodule (small straight solid arrows) remains fixed. Nodule is now better visualized against relatively lower-signal layer (curved arrow). (Compare with C.) Free methemoglobin (straight open arrow); fluid level (long straight solid arrows).

E, Axial T2-weighted image (2500/80). Low-signal intracellular deoxyhemoglobin and/or intracellular methemoglobin layer (curved arrow) have dropped further in signal intensity on this T2-weighted image. (Compare with C.) Nodule (black arrows); free methemoglobin (straight open arrow); fluid level (solid white arrows).

the cyst was made by passing a needle through a burr hole under sonographic guidance. Only partial decompression of the cyst was achieved. His symptoms resolved transiently, but recurred 4 months later. A CT and MR scan at that time showed that the cyst had enlarged. Therefore, the patient underwent surgical deroofting of the cyst. This lesion was diagnosed as an epithelial cyst at pathology and the patient did well postoperatively. The anterior portion of the cyst wall, which was left intact, allowed the formation of an air-fluid level, which was seen on postoperative CT and MR scans (Figs. 6B–6D). The nondependent air produced a signal void on all pulse sequences, while the dependent CSF layer behaved like CSF on all pulse sequences.

In addition to the air-fluid level demonstrated on the postoperative CT and MR scans, a blood-CSF level formed in the occipital horn of the lateral ventricle (Figs. 6E–6G). The fluid level was composed of a

dependent layer that was slightly hypointense relative to brain on T1-weighted images and markedly hypointense on T2 images, and of a nondependent layer that behaved like CSF (Figs. 6F and 6G). On CT, the dependent layer was highly attenuating and the nondependent layer again behaved like CSF (Fig. 6E).

Results

MR was superior to CT in imaging fluid levels (Table 1). In cases 1–5, the fluid levels were readily seen on MR, but not on CT. In case 6, the fluid levels were seen equally well on MR and CT. Retrospective review of the CT scans did show subtle findings suggesting fluid levels in cases 2 and 3 (Figs. 2A and 3A), but these were not appreciated initially.

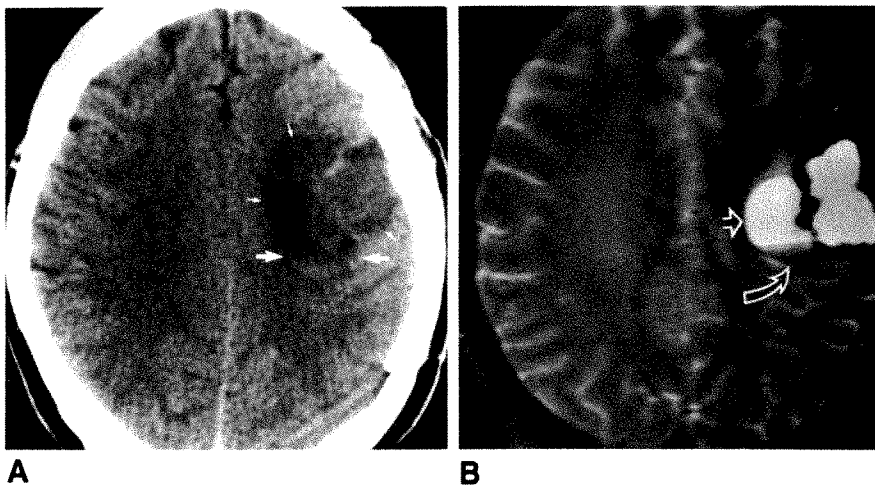


Fig. 2.—Case 2: Hemorrhagic surgical bed after resection of arachnoid cyst.

A, Axial CT scan. Retrospective review revealed findings suggestive of fluid level (large arrows). Lesion (small arrows).

B, Axial T2-weighted image (2500/80) clearly shows fluid level. High-signal free methemoglobin assumes nondependent position (straight arrow). Intracellular deoxyhemoglobin and/or intracellular methemoglobin (curved arrow).

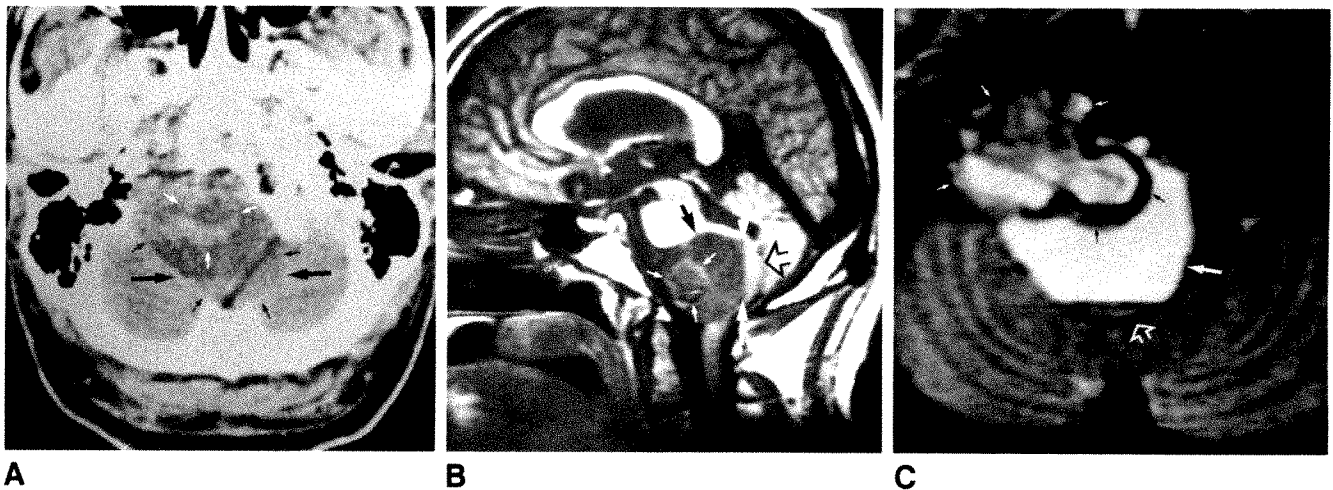


Fig. 3.—Case 3: Cystic schwannomas of hypoglossal nerve. Fluid level comprising proteinaceous cyst fluid and necrotic debris is evident.

A, Axial CT scan shows complex posterior fossa mass. Retrospective review revealed findings suggestive of fluid level (large black arrows). Solid component of lesion (white arrows); cystic component (small black arrows).

B, Sagittal T1-weighted image (600/20). Nondependent proteinaceous fluid layer (solid black arrow) has a slightly higher signal intensity than CSF in ventricles and cisterns. Dependent layer is presumed to be composed of necrotic debris (open arrow). Solid portion of lesion (small white arrows); fluid level (large white arrows).

C, Axial T2-weighted image (2500/80). Proteinaceous fluid has slightly higher signal than CSF (large solid white arrow), while necrotic debris is isointense relative to brain (open arrow). Solid portion of lesion (solid arrows).

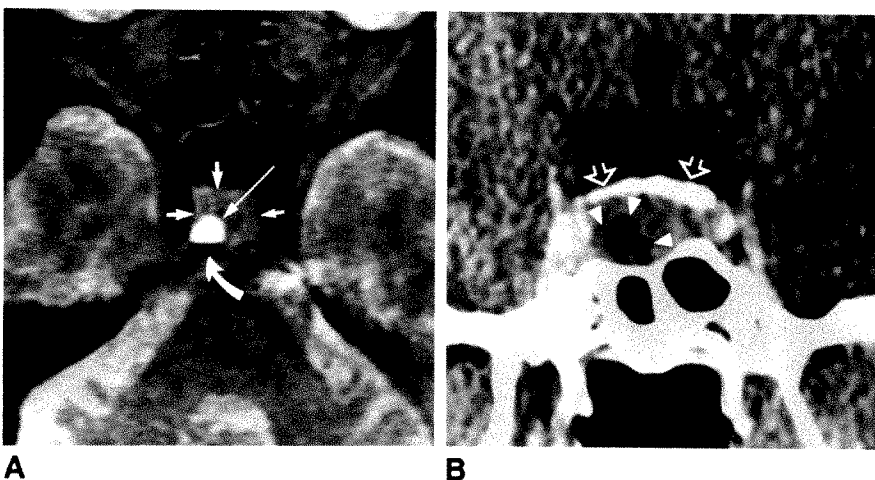


Fig. 4.—Case 4: Chromophobe adenoma with hemorrhagic cyst.

A, Axial T2-weighted MR image (2000/80). Fluid level is noted within lesion. Chromophobe adenoma (short straight arrows). Free methemoglobin layer (long straight arrow). Intracellular deoxyhemoglobin and/or intracellular methemoglobin (curved arrow).

B, Coronal CT scan through posterior sella turcica shows chromophobe adenoma with low-attenuating hemorrhagic cyst (arrowheads). Dorsum sellae (arrows).

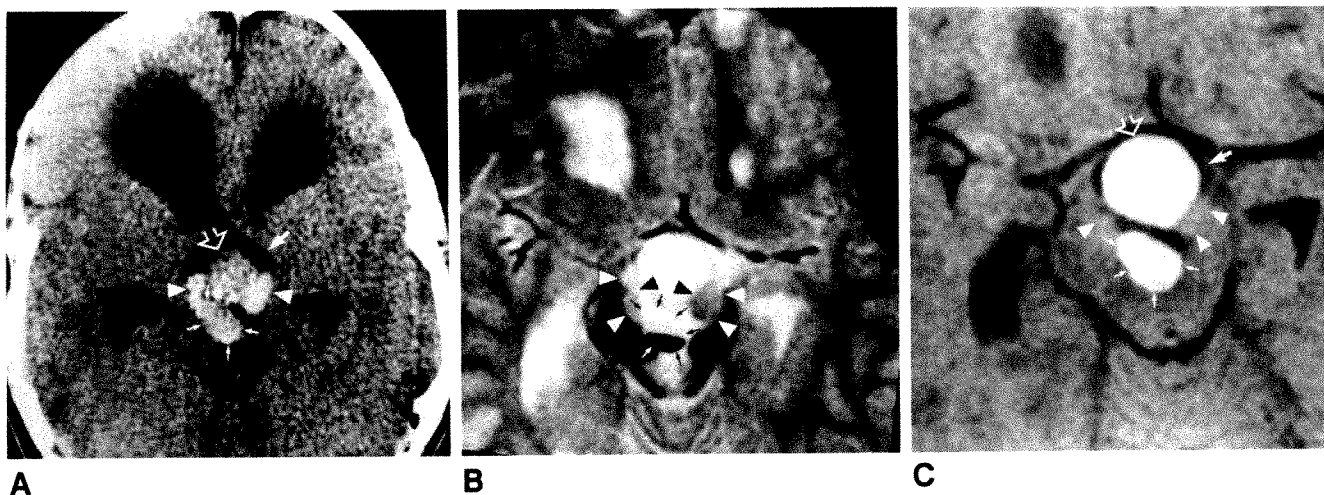


Fig. 5.—Case 5: Recurrent craniopharyngioma with fluid level.

A, Axial CT scan. Posterior cystic component (small solid arrows). Fluid level is not seen. Solid calcified portions of craniopharyngioma are seen (arrowheads). Anterior hemorrhagic component, without fluid level (open arrow). Third ventricle (large solid arrow).

B, Axial T2-weighted MR image (2000/80) corresponding to A. Two solid, calcified portions of lesion are noted (arrowheads). (Compare with A.) Within posterior cystic portion (arrows), fluid layer is seen. High-signal free methemoglobin layer assumes nondependent position.

C, Axial T1-weighted MR image (600/20) through circle of Willis. Note that when width and level are adjusted for brain parenchyma, as in this image, fluid level is not seen clearly. Solid portions of lesion (arrowheads); cystic portion (small solid arrows). Third ventricle invaginated by tumor (large solid arrow). Large, round, high-signal area (open arrow) in upper portion of lesion was also believed to be hemorrhagic focus, because it had high attenuation on concurrent CT scan (A) and low attenuation on previous CT scan. No fluid level was seen in this portion.

The MR signal characteristics of the fluid levels were helpful in identifying their contents in all cases. In addition, several other observations were made. It was found that adjusting the width and level was necessary, in some sequences, for visualization of the fluid levels (Table 1). When the level and width were adjusted for normal brain imaging, the fluid levels were not initially visualized on the T1 sequences in cases 1, 2, and 5 (Figs. 1B, 1C, and 5C) or on the T2 sequence in case 2. The air-CSF level in case 6 was seen with difficulty on the T1-weighted sequence (Fig. 6D). Changing the width and level, however, enabled us to detect these fluid levels readily. This point deserves special emphasis since widths and levels are routinely selected by technologists, who, with batch filming, will not adjust the parameters for each image. Cases 1, 2, 5, and 6, in particular, showed that the demonstration of these sometimes subtle findings will depend on the use of nonroutine parameters. In addition, contrast between fluid levels might be enhanced by gradient-refocused imaging techniques, particularly in areas of hemorrhage.

The fluid levels composed of blood in different stages (cases 1, 2, and 4–6) were seen best on the T2-weighted sequence (Figs. 1E, 2B, 4A, 5B, and 6G). The more pronounced hypointensity of the dependent layer on the T2-weighted sequences compared with the T1 sequences resulted in superb contrast between the two components of the fluid level. The relatively blacker appearance of the dependent layer on T2-weighted images is believed to be related to the selective T2 shortening caused by intracellular paramagnetic substances such as intracellular deoxyhemoglobin or intracellular methemoglobin [1, 2].

Lastly, imaging in the prone position in case 1 (Fig. 1D) was extremely helpful in defining a solid nodule that was not clearly seen in the supine position. The relatively high signal intensity

of the nodule on the T1-weighted sequence made its visualization difficult against the high signal intensity of the surrounding free methemoglobin. In the prone position, however, the solid nodule remained fixed while the component fluid layers swapped positions. This enabled the nodule to be clearly seen against the surrounding layer of low signal intensity.

Discussion

MR Characteristics in Reported Cases

The MR signal characteristics in our six patients were helpful in identifying the contents of the fluid levels. Similar signal characteristics were seen in cases 1, 2, 4, and 5 (Figs. 1, 2, 4, and 5). In these cases the nondependent layers had high signal intensities on T1- and T2-weighted sequences. The dependent layers were hyperintense relative to brain on T1-weighted sequences (although less hyperintense than the nondependent layer) and became hypointense on T2-weighted sequences (Figs. 1C, 1E, 2B, 4A, and 5B). These signal characteristics were consistent with those described for various phases of subacute blood, as described in depth by other authors [1–6]. Subacute blood in the dilute methemoglobin phase has been shown to have high signal intensity on all pulse sequences. Intracellular methemoglobin has been described as having high signal on T1 sequences and low signal on T2 sequences, while intracellular deoxyhemoglobin appears hypointense to isointense on T1 sequences and hypointense on T2 sequences. However, as the hematoma evolves, intermediate stages are found containing both intracellular deoxyhemoglobin and intracellular methemoglobin, which may be variably hyperintense on the T1 images. Blood, as predicted, was demonstrated in all these cystic lesions,

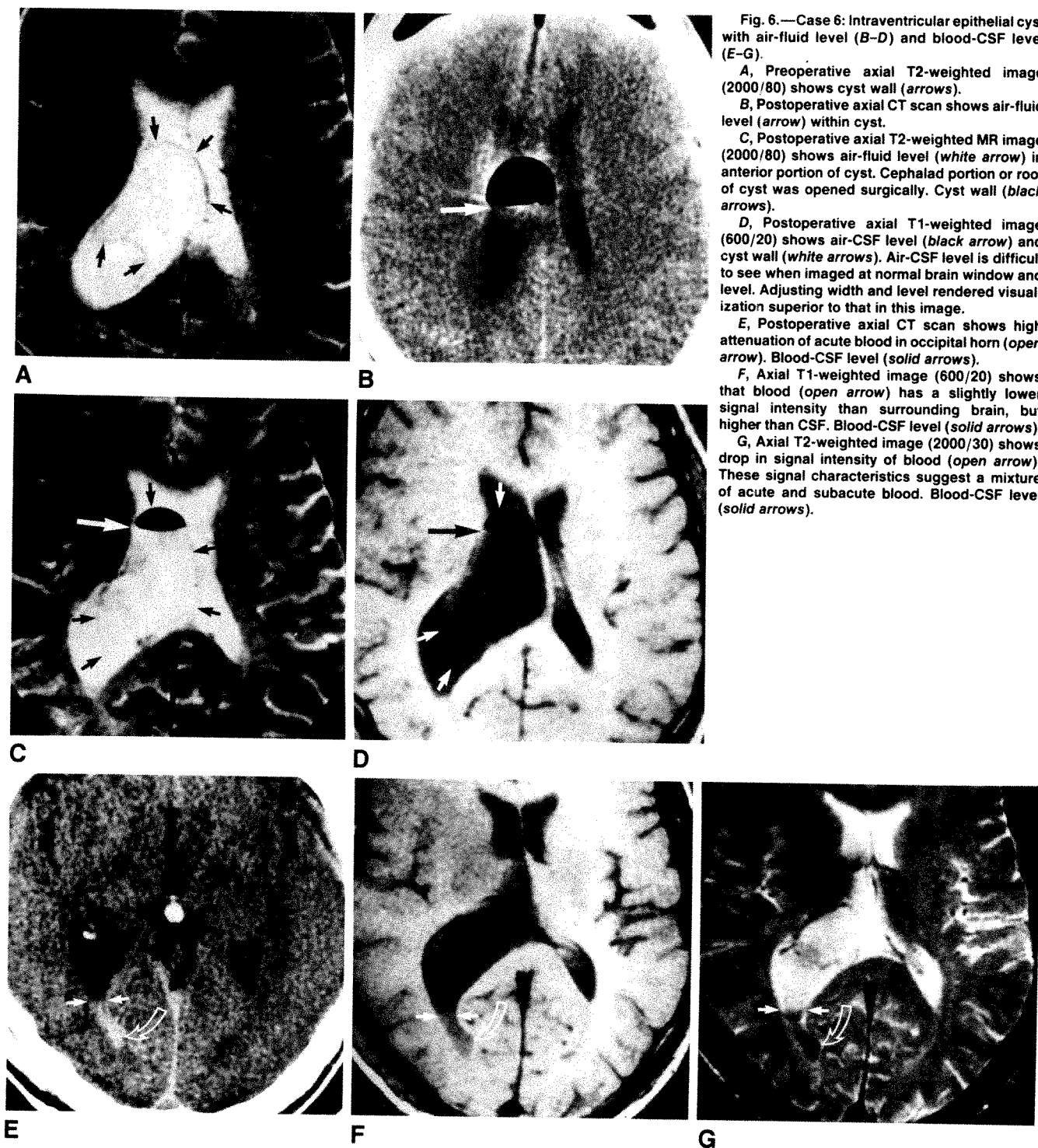


Fig. 6.—Case 6: Intraventricular epithelial cyst with air-fluid level (B–D) and blood-CSF level (E–G).

A, Preoperative axial T2-weighted image (2000/80) shows cyst wall (arrows).

B, Postoperative axial CT scan shows air-fluid level (arrow) within cyst.

C, Postoperative axial T2-weighted MR image (2000/80) shows air-fluid level (white arrow) in anterior portion of cyst. Cephalad portion or roof of cyst was opened surgically. Cyst wall (black arrows).

D, Postoperative axial T1-weighted image (600/20) shows air-CSF level (black arrow) and cyst wall (white arrows). Air-CSF level is difficult to see when imaged at normal brain window and level. Adjusting width and level rendered visualization superior to that in this image.

E, Postoperative axial CT scan shows high attenuation of acute blood in occipital horn (open arrow). Blood-CSF level (solid arrows).

F, Axial T1-weighted image (600/20) shows that blood (open arrow) has a slightly lower signal intensity than surrounding brain, but higher than CSF. Blood-CSF level (solid arrows).

G, Axial T2-weighted image (2000/30) shows drop in signal intensity of blood (open arrow). These signal characteristics suggest a mixture of acute and subacute blood. Blood-CSF level (solid arrows).

except in case 5 (recurrent craniopharyngioma). In case 5, where the patient refused repeat surgery, the presence of blood was inferred by its appearance on CT. In case 6 (intraventricular blood) the blood had slightly different signal characteristics. On the T1-weighted sequence, the blood had a slightly lower signal intensity than brain parenchyma, and on the T2-weighted sequence it dropped even further (Figs. 6F and 6G). This was consistent with blood in a more acute

phase (intracellular deoxyhemoglobin), the presence of which was readily explained by surgery the previous day. The signal intensity on the T1-weighted sequence being higher than that of CSF suggests a mixture with some subacute blood.

The appearance in cases 3 and 6 (air-fluid level), in which there was no blood, was completely different. In case 3 (cystic schwannoma), the nondependent layer had a low signal intensity on the T1-weighted sequence that was slightly higher in

intensity than CSF (Fig. 3B). On the T2-weighted sequence, the signal flipped to an intensity that was higher than that of CSF (Fig. 3C). These signal characteristics were typical of those described for nonhemorrhagic proteinaceous cysts [7], and at surgery a cystic schwannoma with proteinaceous fluid was encountered. No blood or hemosiderin was demonstrated at pathology. The dependent layer had a signal intensity that was similar to that of surrounding brain on both the T1- and T2-weighted sequences (Figs. 3B and 3C). It was not studied separately at pathology but was considered radiographically to represent necrotic debris. In case 6, an air-CSF level was present within an intraventricular epithelial cyst (Figs. 6A–6D). The nondependent air layer naturally had a signal void on all sequences, while the CSF layer demonstrated the usual characteristics of CSF.

Classification of Fluid Levels

Although MR signal characteristics are helpful in identifying the contents of the fluid levels, their formation is actually related to density differences within the layers. Fluid levels occur when two or more immiscible substances of unequal density coexist. In the human body we commonly encounter four "substances" with different densities: water, air, fat, and solids. The fluid levels we confront most frequently can therefore be classified into three groups: air-fluid, fat-fluid, and fluid-solid (precipitate) (Fig. 7).

Fluid-precipitate level.—Every patient in our series is included in the fluid-precipitate category. In the cystic schwannoma (case 3), the precipitate layer was composed of necrotic debris that settled to the bottom of the proteinaceous cyst, a finding that has been reported also in a cystic glioma [8]. In the fluid levels that contained blood in various stages of evolution, the precipitate layer was composed of cellular blood elements (cases 1, 2, 4, 5, and 6). Cohen et al. [9] have been able to demonstrate this phenomenon in vitro. They showed that both serum and plasma assume a nondependent position and have a high signal intensity of T1- and T2-weighted

images. RBCs assume a dependent position and have a low signal intensity on T2-weighted images. Therefore, while various stages of methemoglobin and deoxyhemoglobin are responsible for the signal characteristics, the physical formation of the fluid level is due to settling of the relatively denser cellular components. Other fluid-precipitate levels might also be seen in cerebral abscesses when inflammatory cells layer or in calcified cystic lesions when calcified products settle to the bottom.

Air-fluid level.—The MR appearance of an air-fluid level is nicely illustrated by case 6. The nondependent air layer should always have a signal void, while the dependent fluid layer could vary in signal intensity according to the amount of fat, protein, or blood within the fluid (Fig. 7).

An air-fluid level containing subacute blood might even have three layers: a nondependent air layer, a dependent layer containing intracellular methemoglobin or intracellular deoxyhemoglobin, and, in between, a layer containing free methemoglobin or free deoxyhemoglobin (Fig. 7). The air and free methemoglobin would have a signal void and a high signal intensity, respectively, on both the T1- and T2-weighted sequences, while the intracellular methemoglobin or intracellular deoxyhemoglobin would become markedly hypointense on the T2-weighted sequence. This would account for the appearance demonstrated in Figure 7.

Fat-fluid level.—None of our patients had intracranial fat-fluid levels on MR; however, they have been seen on CT in epidermoid tumors in the brain [10], ventricles [11], and subarachnoid spaces [11]. On MR we would expect a pure fat-fluid level to have a nondependent fatty layer characterized by high signal intensity on the T1-weighted sequence with a slight loss of signal intensity on the T2-weighted sequence. This is due to the relatively short T1 and T2 relaxation times of fat [12]. It is important to keep in mind, however, that the predicted appearance of the fatty layer may not always conform to this model [13]. With high-field-strength magnets we would also expect a chemical-shift artifact to occur between the lipid and aqueous interface in the frequency-encoding direction. On a multiecho axial scan the anterior aspect of the fatty component would have a rim of low signal (signal gap) while the posterior aspect would be expected to have a rim of high signal (signal overlap).

The dependent fluid layer in a fat-fluid level, as with CSF, would be expected to have a low signal intensity on the T1-weighted sequence and a high signal intensity on the T2-weighted sequence (Fig. 7). This is due to the long T1 and T2 relaxation times of relatively pure fluids [3, 7, 12]. Again, one must also keep in mind that not all fluids are in a relatively pure state like CSF. An increase in the protein content of a fluid shortens its T1 and T2 relaxation times [3, 7]. Under these conditions the fluid layer on the T1 sequence may have a signal intensity higher than CSF has, but usually lower than that of the surrounding brain parenchyma. At TRs used in routine T2-weighted imaging sequences, the signal intensity of a fluid with a high protein content may become brighter than CSF. This results from the relatively greater contribution of T1 shortening on signal intensity at routine imaging parameters [7]. Therefore, we can see that the predicted MR appearance of a fat-fluid level may vary, particularly in the

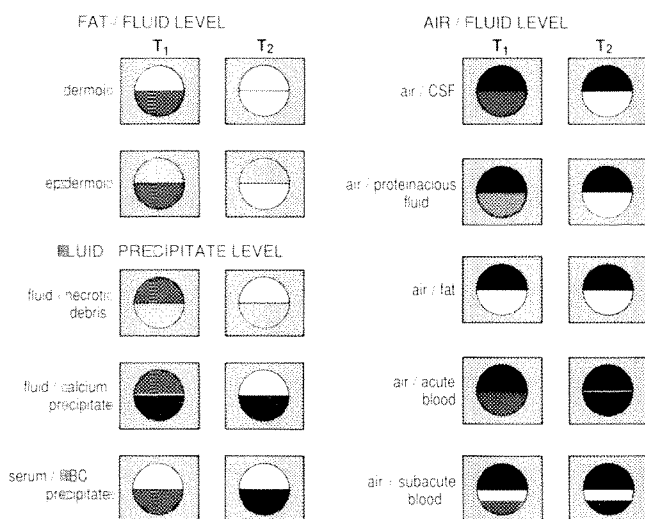


Fig. 7.—MR appearances of fluid levels.

case of an epidermoid tumor. Dermoid tumors seem to behave more like pure fat-fluid levels (Fig. 7) [14].

Conclusions

We have described the MR characteristics of fluid levels and have classified fluid levels into three main groups: fat-fluid, air-fluid, and fluid-precipitate. It is important to remember, however, that the MR appearance of a specific lesion may vary according to the exact contents of the fluid level. For example, the fluid layers of two cystic lesions with the same pathologic diagnosis may appear different if the protein, fat, or blood contents of the fluid are different. It also seems clear, from this limited series, that MR is superior to CT in imaging fluid levels, and that analysis of MR signal characteristics can be most helpful in attempting to identify the contents of the fluid layers.

ACKNOWLEDGMENTS

We thank Eve VanDine, Carolyn Meloling, Tom McCarthy, Geri Mancini, Wendolyn Hill, and the MR staff for making this article possible.

REFERENCES

1. Gomori JM, Grossman RI, Goldberg HI, Zimmerman RA, Bilaniuk LT. Intracranial hematomas: imaging by high field MR. *Radiology* **1985**; 157:87-93
2. Gomori JM, Grossman RI, Hackney DB, Goldberg HI, Zimmerman RA, Bilaniuk LT. Variable appearance of subacute intracranial hematomas on high-field spin-echo MR. *AJNR* **1987**;8:1019-1026, *AJR* **1988**;150: 171-178
3. Bradley WG. Pathophysiologic correlates of signal alterations. In: Brant-Zawadzki M, Norman D, eds. *Magnetic resonance imaging of the central nervous system*. New York: Raven, **1986**:23-42
4. Norman D. Vascular disease: hemorrhage. In: Brant-Zawadzki M, Norman D, eds. *Magnetic resonance imaging of the central nervous system*. New York: Raven, **1986**:209-220
5. Gomori JM, Grossman RI. Mechanisms responsible for the MR appearance and evolution of intracranial hemorrhage. *RadioGraphics* **1988**;8:427-440
6. Grossman RI, Gomori JM, Goldberg HI, et al. MR imaging of hemorrhagic conditions of the head and neck. *RadioGraphics* **1988**;8:441-454
7. Kjos BO, Brant-Zawadzki M, Kucharczyk W, Kelly WM, Norman D, Newton TH. Cystic intracranial lesions: magnetic resonance imaging. *Radiology* **1985**;155:363-369
8. Brant-Zawadzki M, Kelly W. Brain tumors. In: Brant-Zawadzki M, Norman D, eds. *Magnetic resonance imaging of the central nervous system*. New York: Raven, **1986**:151-185
9. Cohen MD, McGuire W, Cory DA, Smith JA. MR appearance of blood and blood products: an in vitro study. *AJR* **1986**;146:1293-1297
10. Cornell SH, Graf CJ, Dolan KD. Fat-fluid level in intracranial epidermoid cyst. *AJR* **1977**;128:502-503
11. Laster WD, Moody DM, Marshall RE. Epidermoid tumors with intraventricular and subarachnoid fat: report of two cases. *AJR* **1977**;128:504-507
12. Pavlicek W, Modic M, Weinstein M. Pulse sequence and significance. *RadioGraphics* **1984**;4:49-65
13. Vion-Dury J, Vincentelli F, Jiddave M, et al. MR imaging of epidermoid cysts. *Neuroradiology* **1987**;29:333-338
14. Batnitzky S, Price HI, Gresick RJ, McMillan JH, Danziger A, Rosenthal S. Intracranial pearly tumors: radiologic evaluation, past and present. *Radiology* **1987**;165P[suppl]:401-402

The Acetazolamide Challenge: Imaging Techniques Designed to Evaluate Cerebral Blood Flow Reserve

Jeffrey Rogg¹
Michael Rutigliano²
Howard Yonas³
David W. Johnson⁴
Susan Pentheny⁴
Richard E. Latchaw³

Cerebral blood flow was analyzed by the stable xenon (Xe)/CT scanning technique in 29 patients with significant vascular lesions before and after administration of an acetazolamide (Diamox) vasodilatory challenge. Three response types were identified: I, normal flow before Diamox with flow augmentation after Diamox; II, low flow before Diamox with flow augmentation after Diamox; and III, low or normal flow before Diamox with no augmentation or decreased flow after Diamox. Twenty-four percent of the patients studied qualified for category III. We believe that patients in this category represent a group of individuals without blood flow reserve whose clinical management should include careful consideration of their hemodynamic status.

The Xe/CT scanning technique with the addition of Diamox flow challenge is a clinically accessible and effective method for assessing cerebral blood flow and blood flow reserve.

The development of a clinically accessible means to identify patients with neurologic symptoms caused by transient focal or global low cerebral blood flow (CBF) has important potential therapeutic implications [1-3]. Signs and symptoms of decreased cerebrovascular reserves and episodic low CBF are generally non-specific and may be difficult to recognize [4]. Angiography is imprecise in establishing the diagnosis because this technology is unable to provide the physiologic information necessary to assess the adequacy of primary or collateral regional blood supply [5]. Ideally, this analysis is performed by positron emission tomography (PET), which requires the measurement of both CBF and metabolism [6, 7]. PET is, however, available at relatively few centers. This article describes the use of stable xenon (Xe)/CT performed before and after a vasodilatory challenge to identify patients with low cerebral blood flow and blood flow reserve.

The strategy we followed was derived in part from PET studies that determined that the cerebral arteries maintain CBF in response to decreased perfusion pressure by dilatation [2]. After vessels are maximally dilated, any further compromise in perfusion pressure results in a progressive decrease in blood flow and an accompanying increase in oxygen extraction. When this condition, termed "misery perfusion" [3], has been achieved, additional vasodilatory challenges would not be expected to augment flow. When CBF falls below 20 ml/100 g/min in normal cortical tissue, metabolism and neurologic function become compromised as the regional oxygen and glucose supply to the brain is expended [8, 9].

Although local cerebral blood flow values may be reduced by proximal vascular compromise and inadequate supply, CBF can also be reduced by decreased metabolic demand caused by either neuronal loss or deafferentation. Therefore, a single measurement of CBF, regardless of the method—Xe-133, single photon emission CT (SPECT), or stable Xe/CT—does not give nonspecific information in this regard. However, the addition of a second measurement obtained during a vasodilatory challenge can assess whether territorial reserves have been compromised. That is, CBF augmentation would not be expected in regions that already

This article appears in the July/August 1989 issue of *AJNR* and the September 1989 issue of *AJR*.

Received June 24, 1988; revision requested August 22, 1988; revision received November 11, 1988; accepted December 5, 1988.

¹ Department of Radiology, Brown University School of Medicine, Rhode Island Hospital, Providence, RI 02902.

² University of Pittsburgh School of Medicine, Pittsburgh, PA 15213.

³ Department of Radiology and Neurological Surgery, University of Pittsburgh School of Medicine, Pittsburgh, PA 15213. Address reprint requests to H. Yonas.

⁴ Department of Radiology, University of Pittsburgh School of Medicine, Pittsburgh, PA 15213.

AJR 153:605-612, September 1989

0361-803X/89/1533-0605

© American Roentgen Ray Society

TABLE 1: Summary of Clinical Histories, Significant Vascular Anatomy by Doppler or Angiographic Investigation, and Categorization by Xe Diamox Analysis in 29 Patients

Case No.	Clinical History	Significant Vascular Anatomy	Age	Pre-pCO ₂ /Post-pCO ₂	Baseline Cerebral Blood Flow	Xe Diamox	Type*
1	L hemiparesis expressive aphasia	R MCA occlusion	59	39/30	Focal R MCA distr.; low flow	No change	III
2	L facial and upper extremity weakness; symptoms related to decreased blood pressure	R ICA occlusion; bilateral moderate VA stenosis	78	38/30	Diffuse low	Diffuse increase	II
3	Transient L hemisphere symptoms	L ICA occlusion	55	31/27	Focal L ICA distr.; low flow	No change	III
4	L hemisphere TIAs after endarterectomy		74	38/32	Normal	Diffuse increase	I
5	L TIA	R & L VA stenosis	72	33/30	Diffuse low	Diffuse increase	II
6	Aphasia	R ICA occlusion	64	32/24	Normal	Diffuse increase	I
7	Syncope	L ICA occlusion		37/32	Normal	Diffuse increase	I
8	R hemiparesis	L ICA occlusion, 80–90%; R ICA stenosis	66	30/28	Focal R MCA distr.; low flow	No change	III
9	L carotid bruit	Doppler 80% L ICA stenosis	50	39/37	Normal	Diffuse increase	I
10	Transient R hemiparesis & expressive aphasia	Doppler severe L ICA stenosis	57	42/40	Focal L MCA decreased flow	Unchanged	III
11	Transient R hemiparesis	40–50% L ICA stenosis	66	34/24	Normal	Diffuse increase	I
12	L occipital infarct; light-headedness	>80% L ICA stenosis; >80% L subclavian stenosis; R subclavian occlusion	54	42/34	Normal	Diffuse increase	I
13	R CVA	R ICA occlusion	63	30/26	Low flow R ACA; R MCA distr.	Diffuse increase	II
14	Transient R hemiparesis & aphasia	>70% L ICA stenosis		32/28	Periinfarct; normal	Diffuse increase	I
15	Syncope	R ICA occlusion		41/38	Normal	Diffuse increase	I
16	Episodic dizziness	>70% L & R VA stenosis	67	36/30	Normal	Diffuse increase	I
17	Asymptomatic	L ICA occlusion	66	30/27	Global low flow	Diffuse increase	II
18	Asymptomatic	L ICA & R ICA occlusion	60	36/30	Global low flow	Diffuse increase	II
19	R hemiparesis; L caudate infarction	L MCA occlusion			Low normal flow (periinfarct)	Diffuse increase except in infarct	I
20	Vertigo	L ICA, R ICA, R VA occlusion; L EC-IC bypass	70		Global low	Diffuse increase	II
21	R hemisphere TIAs; R amaurosis fugax	R ICA occlusion R ICA stenosis			Focal low R ICA distr. flow	Focal low R ICA distr.	III
22	R amaurosis fugax	L ICA occl; R VA occl; R ICA pseudooocclusion	64	35/28	Diffuse low flow	Diffuse increase	
23	R amaurosis fugax	R ICA 80% stenosis; R subclavian occlusion	54	35/26	Normal	Diffuse increase	I
24	R hemiparesis	>80% L ICA stenosis	67	32/28	Low normal	Diffuse increase	I

Table 1—Continued

Case No.	Clinical History	Significant Vascular Anatomy	Age	Pre-pCO ₂ /Post-pCO ₂	Baseline Cerebral Blood Flow	Xe Diamox	Type*
25	Vertigo	Doppler; R ICA stenosis	62	32/32	Diffuse low flow	Focal low	III
26	L carotid bruit	90% L ICA stenosis	69		Normal	Diffuse increase	I
27	R amaurosis fugax	L ICA & R ICA occlusion; 80% L VA stenosis; 60% R VA stenosis	63		Diffuse low flow	Diffuse increase	II
28	L bruit; old MCA infarct	99% L ICA stenosis; 50% R ICA stenosis	42		Focal low flow (perinfarct)	Diffuse increase	II
29	L upper extremity weakness	99% R ICA stenosis; L ICA occlusion; 50% L & R VA stenosis	55		Normal	Focal decrease (R ICA distr.)	III

* Type: I = normal baseline with post-Diamox flow augmentation; II = low-flow baseline with post-Diamox augmentation; III = low or normal baseline with no response or decreased flow post-Diamox. Low = 20–35, normal = 35–60, high = >60 (as defined in text).

Note.—ACA = anterior cerebral artery; MCA = middle cerebral artery; PCA = posterior cerebral artery; subclav = subclavian artery; VA = vertebral artery; ICA = internal carotid artery; R = right; L = left; EC-IC = extracranial to intracranial; TIA = transient ischemic attack; CVA = cerebrovascular accident.

have maximum vasodilation, while augmentation would be expected in regions with reduced CBF secondary to decreased metabolic demand.

On the basis of this theory, some investigators have measured CBF before and after a flow challenge to identify patients with "misery perfusion." Various methods have been used to create a flow challenge: (1) elevating or lowering blood pressure, (2) having patients inhale a 3–5% carbon dioxide mixture, or, more recently, (3) administering an IV acetazolamide (Diamox) bolus [9–12].

Acetazolamide is easy to administer, safe, and provokes a predictably potent vasodilatory challenge [13–15]. The specific action of the drug that causes vasodilation is unclear, but it is believed that vasodilation is mediated by the drug's inhibition of carbonic anhydrase [12, 13]. The vasodilatory effect appears to be localized to the brain [13, 15, 16], and the activity of the drug remains potent despite baseline increased tissue levels of pCO₂ [13, 14]. The degree of CBF augmentation found in the normal individual has ranged from 70–90% [12, 13]. With advancing age, activated flows may not increase as dramatically, but flow symmetry will remain preserved [12].

Materials and Methods

CBF was determined by the Xe/CT CBF method. The Xe/CT method is a relatively new CBF technology that provides tomographic, quantitative CBF information with direct anatomic correlation.* This methodology has been addressed in detail previously [1, 17–19].

Xe/CT CBF with an acetazolamide challenge can be performed on an outpatient as well as inpatient basis. The average time to complete a double CBF study—before and 20 min after the administration of

TABLE 2: Cerebral Blood Flow* Analysis in Four Representative Cases: The Effect of Diamox by Vascular Territory

		R ACA	L ACA	R MCA	L MCA	R PCA	L PCA
Type I	Baseline	46	44	49	52	49	47
Case 26	Diamox	63	63	67	67	63	66
	% Change	35%	43%	37%	29%	30%	39%
Type II	Baseline	26	26	31	28	32	32
Case 27	Diamox	37	46	41	41	53	51
	% Change	43%	73%	31%	50%	65%	60%
Type II	Baseline	33	25	35	23	37	37
Case 28	Diamox	44	32	44	31	47	47
	% Change	35%	28%	23%	35%	25%	27%
Type III	Baseline	34	36	34	41	47	44
Case 29	Diamox	34	32	32	48	47	54
	% Change	1%	–11%	–5%	18%	0%	23%

* Cerebral blood flow measured as ml/100 g/min.

Note.—R = right; L = left; ACA = anterior cerebral artery; MCA = middle cerebral artery; PCA = posterior cerebral artery.

acetazolamide—is 60 to 90 min. Patient cooperation is required for this study, which also demands direct involvement of a health care professional. Immediately after the initial CBF study, 1 g of IV acetazolamide is administered. The second study is begun 20 min after drug delivery. Typically, acetazolamide results in a reduction of measured end tidal CO₂ (see Table 1) without alteration of vital signs or other associated symptoms.

We studied 29 patients with significant vascular disease diagnosed by either noninvasive studies or angiography. Twenty-three individuals had at least one significantly stenosed or occluded carotid artery, and 12 had occlusion in two or more major vessels (Table 1). Three patients were asymptomatic and underwent these studies because they were found to have a carotid bruit. Twenty-six patients had experienced transient ischemic attacks (TIAs) or fixed neurologic compromise. The latter patients were studied at least 3 weeks after a stroke. This allowed time for the recoupling of CBF and metabolism to occur.

* General Electric Medical Systems, Milwaukee, WI.

We compared pre- and postacetazolamide CBF studies by using standard contrast-mode software and region-of-interest density software for blood flow analysis (see Fig. 1). In the contrast mode, all values above the designated flow level are displayed as white, and all values below as black (see Figs. 2E and 2F). Regions of interest for regional cerebral blood flow (rCBF) were consistent with vascular territories reported by Damasio [20]. Pre- and postacetazolamide blood flow maps were compared for evidence of flow change in corresponding vascular territories. We generally considered rCBF to be within normal limits when flows ranged between 35 and 60 ml/100 g/min. Acceptable limits of normal were somewhat dependent on patient age, however, as flows of 35 ml/100 g/min were considered low in a 20-year-old but acceptable in an 80-year-old. An rCBF between 20 and 35 was generally considered low; an rCBF greater than 60 was generally considered elevated.

Results

The results are summarized in Table 1. This table provides clinical information and significant vascular anatomy for each of the 29 patients in the study. All patients had at least one major vessel with greater than 50% stenosis. Twelve (41%) had multivessel disease. pCO_2 values are provided to demonstrate that Diamox was physiologically active, blocking carbonic anhydrase and thereby decreasing pCO_2 in all cases.

Three basic types of responses to Diamox are defined: type I, normal CBF before Diamox with flow augmentation after Diamox; type II, diffuse or focal low CBF before Diamox with augmentation after Diamox; type III, low or normal CBF before Diamox with no response or decreased CBF after Diamox. Thirteen patients (45%) had a type I response, nine patients (31%) had a type II response, and seven patients (24%) had a type III response. The following four cases are representative of each response type and are described in greater detail in Table 2.

Type I (case 26, Table 1): A 69-year-old man was evaluated after being diagnosed, during a routine physical examination, as having an asymptomatic left carotid bruit. Noninvasive studies showed severe stenosis of his left internal carotid artery (ICA). Angiography confirmed 80–90% stenosis at the origin of the proximal left ICA; the remainder of the intracranial vasculature and the circle of Willis were normal. A CT scan (Fig. 1A) was unremarkable, and the baseline Xe/CT CBF study (Fig. 1B) was normal. Flow was symmetrical in all territories, with most values ranging between 45 and 55 ml/100 g/min. Twenty minutes after the patient received 1 g of IV acetazolamide, we performed a second CBF study (Fig. 1C), which showed an average flow increase of 36% in all vascular territories (Table 2).

Type II (case 27, Table 1): A 63-year-old woman presented with a sudden onset of blindness in the right eye that resolved partially over the next 6 weeks. Angiography demonstrated 90% stenosis at the origin of the left common carotid artery and occlusion of the left internal carotid artery (ICA). The right ICA also was occluded, and the right external carotid artery was moderately stenotic at its origin. The origin of the left vertebral artery had an 80% stenosis, and the origin of the right vertebral artery had 50–60% stenosis. Collateral supply to the right ICA siphon was supplied by ethmoidal vessels. In addition to flow from the right ICA, the right anterior cerebral artery (ACA) and middle cerebral artery (MCA) also received collateral flow through the right posterior communicating artery and leptomeningeal collaterals from the right posterior cerebral distributions. The baseline Xe/CT CBF study demonstrated lower flow values bilaterally than would be expected in a 63-year-old person (a mean of 29, Table 2). The introduction of acetazolamide, however, caused a symmetrical flow augmentation of 55% (up to 44.9 ml/100 g/min).

Type II (case 28, Table 1): A 42-year-old man presented with an asymptomatic bruit found after a significant left hemi-

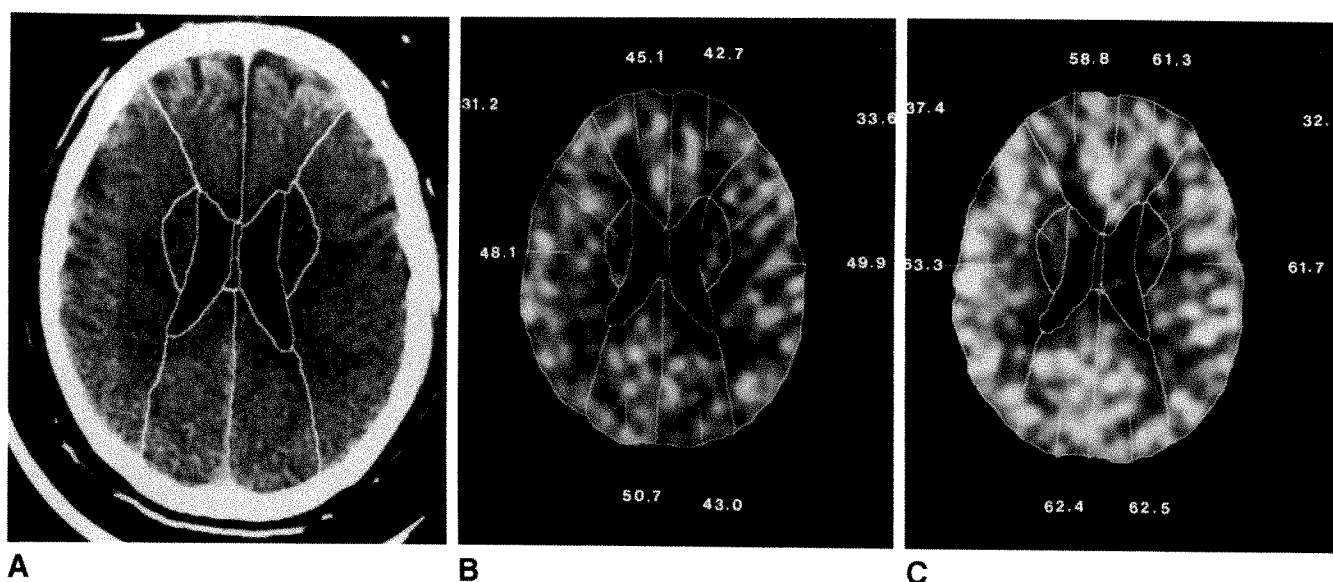


Fig. 1.—A–C, Case 26. Xe/CT scans demonstrate a representative type I normal scan series.

A, The middle of the usual three levels selected for evaluation.

B, Baseline Xe/CT image with superimposed vascular territory map and region of interest blood flows (ml/100 g/min).

C, Repeat Xe/CT CBF evaluation after Diamox (1 g IV). Flow augmentation has occurred in all vascular territories.

sphere, closed head injury. His examination revealed a mild residual expressive aphasia. CT images disclosed an area of encephalomalacia in the left middle cerebral artery distribution, consistent with a remote infarction (Fig. 2A). Angiography demonstrated 99% stenosis at the origin of the left ICA and 50% stenosis at the origin of the right ICA. Collateral flow to the left hemisphere occurred by retrograde ophthalmic artery flow to the carotid siphon, and by posterior communicating artery and leptomeningeal collaterals from the posterior circulation. The baseline Xe/CT CBF study showed an area of hypoperfusion corresponding to the site of previous infarction, but also showed compromised flow values in the remainder

of the left middle cerebral artery (Figs. 2B, 2E, and Table 2). After receiving 1 g of acetazolamide, there was an increase of CBF in all territories, including the region immediately posterior to the infarction within the distal distribution of the middle cerebral artery (Figs. 2C, 2F, and Table 2).

Type III (case 29, Table 1): A 55-year-old man presented with left upper extremity weakness and left facial paresis of recent onset. An angiogram defined a 95% stenosis at the proximal right ICA, and complete occlusion of the left ICA. The left and right anterior and middle cerebral arteries were supplied by the stenotic right ICA. The left middle cerebral artery was supplied by collateral vessels from the left external

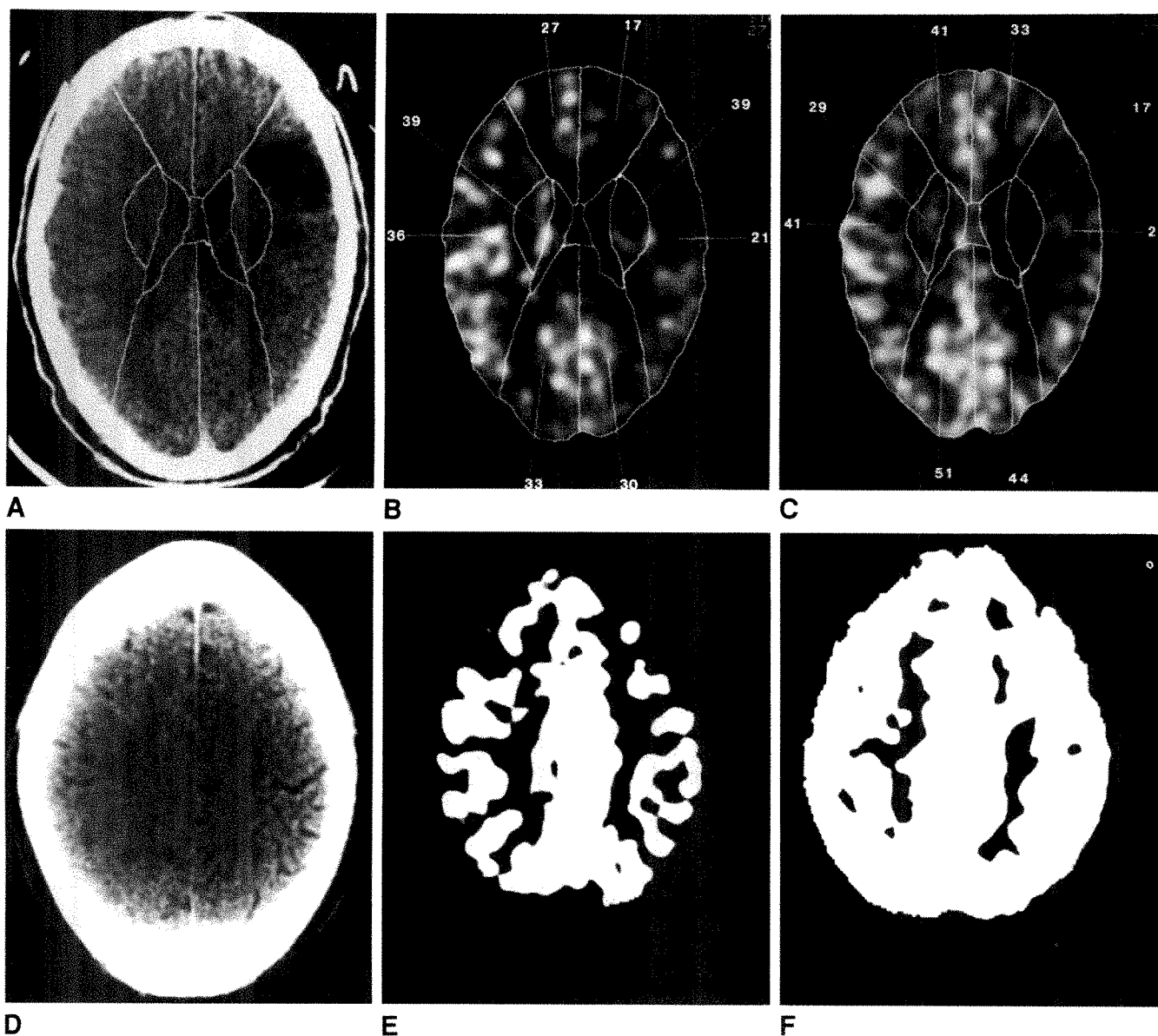


Fig. 2.—A–F, Case 28. Xe/CT scans demonstrate a representative type II scan series.

A shows an area of encephalomalacia in left frontoparietal region from a previous infarction. The level above, D, appears normal.

In B and E, Xe/CT shows that the area of decreased CBF is greater than that expected from plain CT. Flows are decreased in the left frontal and mid-parietal regions anterior and posterior to the old infarction, as well as in the frontoparietal region above the site of the infarct.

In C and F, Post-Diamox flow augmentation is seen in periinfarct zone at level of, and cephalad to, the known area of encephalomalacia. E and F were filmed at a level of 20 (white = flow greater than 20 ml/100 g/min) to accentuate flow differences before and after Diamox.

carotid and left posterior cerebral arteries. The origins of both vertebral arteries were moderately stenotic. A CT scan was unremarkable (Fig. 3A). The baseline Xe/CT CBF study disclosed normal baseline flow values within all territories, but with mild asymmetry ($R < L$) (Figs. 3B, 3C, and Table 2). After the addition of acetazolamide, flow remained unchanged or decreased in all right anterior circulation territories and in the left anterior cerebral artery territory (Figs. 3D, 3E, and Table 2).

Discussion

The diagnostic utility and specificity provided by the use of acetazolamide as a vasodilatory challenge were suggested

by Vorstrup et al. [21], who used Xe-133 with SPECT imaging to evaluate patients before and after extracranial-intracranial bypass operations [21, 22]. These researchers noted post-operative augmentation of resting CBF in only one of the 13 patients with preoperative regional hypoperfusion; this patient was also the only patient in the study whose CBF was not increased after preoperative acetazolamide flow challenge. These findings support the contention that acetazolamide flow challenge can identify those patients who already have maximal vasodilation and minimal flow reserves.

On the basis of our experience, we defined three types of responses to an acetazolamide challenge: I, an increase in normal baseline flow values; II, an increase in focal or diffuse low flow values; and III, no change or a decrease in low or normal flow values. Type III is the only group that would

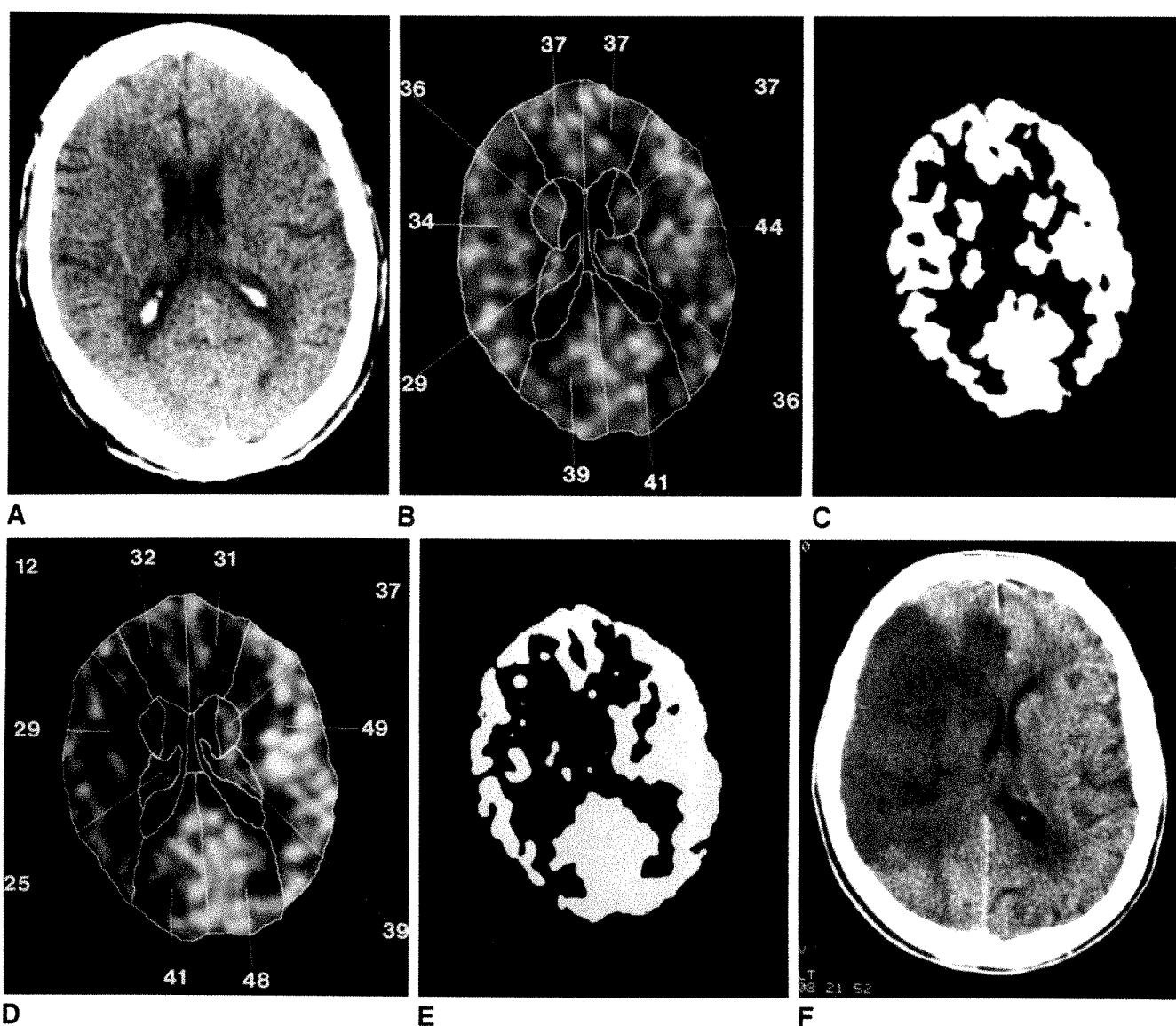


Fig. 3.—A–F, Case 29. Xe/CT scans demonstrate a representative type III scan series.

A shows a baseline CT with low-normal right hemispheric CBF (B) on baseline Xe/CT scans. C displays the CBF data shown in B at a flow threshold of 20 ml/100 g/min. The post-Diamox (D and E) scans demonstrate decreased CBF from baseline in right and left anterior cerebral and right middle cerebral artery territories. F, obtained 48 hr after xenon evaluation, shows massive area of infarction corresponding to region of predicted CBF compromise.

include the single patient reported by Vorstrup et al. [21] and the group with "misery perfusion" reported by Baron et al. [3]. Each of these categories is represented by one or two of the cases described earlier. Case 26 is an example of type I: normal baseline CBF that increased significantly after the administration of acetazolamide. This patient is typical of many patients (13 of 29) we studied who had normal flow despite angiographic evidence of significant stenosis or occlusion.

Cases 27 and 28 exemplify type II: diffuse or focal low flow in baseline studies but with maintained reserves of CBF as demonstrated by the ability to augment flow with acetazolamide. Nine of our 29 patients fell into this group. Although angiography suggested that the supply of blood was severely compromised in case 27, the patient's retention of blood flow reserves suggested that the low flow areas were appropriate to the decreased demand. The patient's absence of further symptoms while on anticoagulation therapy in the 6 months following this assessment supports our assumption of an embolic origin of her symptoms.

Case 28 illustrates reduced CBF, and presumably reduced metabolism, due to deafferentation. Figure 2B shows a region with relatively low flow posterior to the CT-defined infarction, despite the relatively normal appearance of this region on the CT images. After acetazolamide administration, the flow in this area increased, providing evidence for adequate availability of blood flow, but reduced demand. The presence of a larger area of flow and metabolic disturbance than suggested by the CT-defined injury has been widely reported [23].

Case 29 represents type III, low or normal baseline flow values that decreased in a potentially compromised vascular distribution after the patient received acetazolamide, despite an elevation of CBF in other areas. This finding suggested that there is little potential for collateral flow to the portion of the brain that angiography has shown to be supplied preferentially by the right ICA. If the right ICA were further compromised, the patient would be at a significant risk of sustaining a massive infarct [24]. The patient was scheduled for emergency right carotid endarterectomy but before this could be performed, 36 hr after the study, the predictive value of the acetazolamide challenge was substantiated by the onset of a massive stroke in the territory of the right middle cerebral artery (Fig. 3F). Seven (24%) of our 29 patients with significant occlusive vascular disease were in this category.

Despite angiographic and/or noninvasive evidence of significant occlusive vascular disease, 76% of the patients studied by Xe/CT CBF had, at rest, flow values that increased significantly with acetazolamide. This finding is consistent with earlier reports that emphasize the imprecision of existing anatomic methods for predicting hemodynamic compromise [5], and is supported by Sullivan et al. [13], who found that 40% of patients with significant vascular disease on angiography had normal CBF when given an acetazolamide flow challenge and studied by Xe-133 scintillation counting. The studies of Vorstrup and others along with our own limited experience indicate that patients who have type III responses are those most likely to benefit from medical or surgical efforts to augment CBF delivery.

Although the international study of extracranial-intracranial

bypass operations suggested that flow augmentation procedures were not of significant clinical benefit [25, 26], a recent review of that study suggests that a subgroup of critically flow-dependent patients may have been excluded [27]. Our experience indicates that the Xe/CT CBF technique combined with a challenge of flow reserve is a useful clinical means to identify a hemodynamically compromised subgroup of individuals who may have transient symptoms due to a marginal basal level of perfusion that transiently drops to a level inadequate to maintain function. Once such persons are identified, future studies are needed to define their prognosis and determine whether they may benefit from either medical or surgical approaches.

In summary, we believe that Xe/CT CBF measurements used with an acetazolamide challenge provide an objective, clinically accessible method of assessing cerebral blood flow and blood flow reserve.

REFERENCES

1. Yonas H, Gur D, Good B, et al. Stable xenon CT blood flow mapping for evaluation of patients with extracranial-intracranial bypass surgery. *J Neurosurg* 1985;62:324-333
2. Grubb RL Jr, Ratcheson R, Raichich M, et al. Regional cerebral blood flow and cerebral oxygen utilization in superficial temporal middle cerebral artery anastomosis patients. *Acta Neurol Scand* 1979;60:502-503
3. Baron JC, Boussier MG, Rex A, et al. Reversal of focal "misery perfusion syndrome" by extra-intracranial arterial bypass in hemodynamic cerebral ischemia: a case study with 0-15 positron emission tomography. *Stroke* 1981;12:454-459
4. Kistler PJ, Popper AH, Heres RC. Therapy of ischemic cerebral vascular disease due to atherothrombosis. *N Engl J Med* 1984;311:22-34, 1984; 311:100-105
5. Latchaw RE, Ausman JI, Lee M. Superficial temporal-middle cerebral artery bypass: a detailed analysis of multiple pre- and post-operative angiograms in 40 consecutive patients. *J Neurosurg* 1979;51:455-465
6. Lebrun-Grandie P, Baron JC, Soussaline F, et al. Coupling between regional blood flow and oxygen utilization in the normal human brain: a study with positron tomography and oxygen-15. *Arch Neurol* 1986;4: 230-236
7. Lenzi GL, Frackowiak RS, Jones T. Cerebral oxygen metabolism and blood flow in human cerebral ischemic infarction. *J Cereb Blood Flow Metab* 1982;2:321-335
8. Jones TH, Morawetz RB, Crowell RM, et al. Thresholds of focal cerebral ischemia in awake monkeys. *J Neurosurg* 1981;54:773-782
9. Yonas H, Gur D, Claassen D, Wolfson SK Jr, Moossy J. Stable xenon-enhanced computed tomography in the study of clinical and pathologic correlates of focal ischemia in baboons. *Stroke* 1988;19:228-238
10. Norving B, Bengt N, Risberg J. rCBF in patients with carotid occlusion; resting and hypercapnic flow related to collateral pattern. *Stroke* 1982;13:155-162
11. Grubb RI, Reichle ME, Erchling JO, et al. The effects of changes in PaCO₂ on cerebral blood volume, blood flow and vascular mean transit time. *Stroke* 1974;5:630-639
12. Auge A, Thoresen M, Walle L. Changes in cerebral blood flow during hyperventilation and CO₂-breathing measured transcranially in humans by pulsed bidirectional ultrasound Doppler blood velocity meter. *Acta Physiol Scand* 1980;110:167-173
13. Sullivan HG, Kingsbury TB, Morgan MS, et al. The rCBF response to Diamox in normal subjects and cerebrovascular disease patients. *J Neurosurg* 1987;67:525-534
14. Hauge A, Nicolaysen G, Thoresen M. Acute effects of acetazolamide on cerebral blood flow in man. *Acta Physiol Scand* 1983;117:233-239
15. Cotev S, Lee J, Severinghaus JW. The effects of acetazolamide on cerebral blood flow and cerebral tissue PCO₂. *Anesthesiology* 1968;29:471-477
16. Macri JJ, Politoff A, Rubin R, Dixon R, Rall D. Preferential vasoconstrictor properties of acetazolamide on the arteries of the choroid plexus. *Int J*

- Neuropharmacol* **1966**;5:109-115
17. Gur D, Wolfson SK, Yonas H, et al. Progress in cerebrovascular disease: local cerebral blood flow by xenon-enhanced CT. *Stroke* **1982**;13:750-758
 18. Yonas H, Good WF, Gur D, et al. Mapping cerebral blood flow by xenon-enhanced computed tomography: clinical experience. *Radiology* **1984**;152:435-442
 19. Yonas H, Wolfson SK Jr, Gur D, et al. Clinical experience with the use of xenon-enhanced CT blood flow mapping in cerebral vascular disease. *Stroke* **1984**;15:443-450
 20. Damasio H. A computed tomographic guide to the identification of cerebral vascular territories. *Arch Neurol* **1983**;40:138-142
 21. Vorstrup S, Paulson OB, Lassen NA. How to identify hemodynamic cases. In: Spetzler, Carter, Selman, Martin, eds. *Cerebral revascularization for stroke*. New York: Theme-Stratton, **1985**
 22. Batjer HH, Devous MD, Purdy PD, et al. Improvement in regional cerebral blood flow and cerebral vasoreactivity after extracranial-intracranial arterial bypass. *Neurosurgery* **1988**;22:913-919
 23. Kuhi DE, Phelps ME, Kowell AP, Metter EJ, Selin C, Winter J. Effects of stroke on local cerebral metabolism and perfusion: mapping by emission computed tomography of ^{18}F FDG and ^{13}N H₂. *Ann Neurol* **1980**;8:47-60
 24. Yonas H, Steed D, Latchaw R, Gur D, Peitzman A, Webster M. Relief of nonhemispheric symptoms in low flow states by anterior circulation revascularization: a physiologic approach. *J Vasc Surg* **1987**;5:289-297
 25. EC/IC Bypass Study Group. Failure of extracranial-intracranial arterial bypass to reduce the risk of ischemic stroke. *N Engl J Med* **1985**;313:1191-1200
 26. Plum F. Extracranial-intracranial arterial bypass and cerebral vascular disease. *N Engl J Med* **1985**;313:1221-1223
 27. Sundt TM Jr. Was the international randomized trial of EC/IC arterial bypass representative of the population at risk? *N Engl J Med* **1987**;316:814-816

IV Injection of Air-Filled Human Albumin Microspheres to Enhance Arterial Doppler Signal: A Preliminary Study in Rabbits

Pamela L. Hilpert^{1,2}
Robert F. Mattrey¹
Roxane M. Mitten¹
Thomas Peterson¹

When air-filled human albumin microspheres are injected IV, they have been shown to traverse the pulmonary circulation and markedly influence the echogenicity of the left atrium and ventricle. We studied the possibility that the microspheres can be used to enhance the Doppler signal from systemic arteries and the portal vein. Doppler sonography of the aorta, renal artery, intrarenal branch, and portal vein was performed after the IV injection of saline or microspheres in doses of 1.0, 0.5, 0.3, and 0.1 ml in four rabbits. With appropriate blinding of the observers, subjective estimates of enhancement of the Doppler signal were made in each case. All injections of saline had no detectable effect. All four doses of microspheres enhanced the Doppler signal in the aorta in all rabbits. Signals from the renal artery enhanced in all rabbits after injections of 0.3 ml or greater, but in only two rabbits after 0.1 ml. Although the 1.0-ml dose enhanced the Doppler signal from the intrarenal arterial branch in all rabbits, the 0.5- and 0.3-ml doses enhanced signals in two and the 0.1-ml dose in one. The effect was typical for bolus IV injections. The mean time from injection to onset of enhancement was 5 sec and the effect lasted for 12 sec. Portal venous signals were evaluated in three rabbits. Ten injections were made, four at 1.0 ml and two at each of the lesser doses. Portal vein signals enhanced after all four injections of 1.0 ml of microspheres but after only one of the six injections of lower doses.

Our results show that the IV injection of air-filled human albumin microspheres enhances the Doppler signal from systemic arteries and the portal vein and that the microspheres have the potential to serve as a contrast agent for Doppler sonography in humans.

AJR 153:613-616, September 1989

Received March 21, 1989; accepted after revision May 1, 1989.

R. F. Mattrey is the recipient of Research Career Development Award KO8-CA01319.

This work was supported in part by National Cancer Institute grants NCI-CA36799 and NCI-KO8-CA01319.

¹ Department of Radiology, University of California, San Diego, Medical Center, 225 Dickinson St., San Diego, CA 92103. Address reprint requests to R. F. Mattrey.

² Present address: Department of Radiology, Thomas Jefferson Hospital, 111 S. 11th St., Philadelphia, PA 19107.

0361-803X/89/1533-0613

© American Roentgen Ray Society

The need for a contrast agent to enhance the Doppler signal from systemic vessels has been recognized by a number of authorities [1-6]. Such an agent should flow freely through capillaries in order to traverse the lung, be stable long enough to persist for the time required to inject the agent and make the images, be sufficiently reflective to cause enhancement of the sonographic image that is detectable with conventional equipment, and be nontoxic.

Stable air-filled human albumin microspheres (Albunex, Molecular Biosystems, Inc. [MBI], San Diego, CA) has been shown to traverse the lungs in sufficient quantity after IV administration to produce striking changes in the echogenicity of the left atrium and ventricle [7, 8]. Clinical trials are underway to study the value of the microspheres as a contrast agent for sonography of the heart (J. L. Barnhart, MBI, personal communication, October 1988).

The aim of this study was to evaluate the effect of IV administration of various doses of microspheres on the Doppler signal from the aorta, renal artery, intrarenal arterial branches, and portal vein in rabbits and to determine the dose-response relationship.

Materials and Methods

A stable preparation of air-filled human albumin microspheres (Albunex) processed by sonication of a 5% solution of human serum albumin was used. The microspheres ranged in size from 1 to 10 μm , with 99% of particles smaller than 10 μm . The mean size was 5 μm , which is small enough to pass freely through the pulmonary capillary circulation. There were 4×10^8 particles/ml. Albunex was supplied in 5-ml vials.

Four 2- to 3-kg New Zealand white rabbits were sedated with intramuscular injections of 35 mg/kg ketamine (Parke-Davis, Morris Plains, NJ) and 35 mg/kg xylazine (Miles Laboratory, Elkhart, IN). In these rabbits, a femoral vein was exposed and a 20-gauge catheter was inserted and advanced to the level of the inferior vena cava. In one rabbit, microspheres were administered through a 20-gauge catheter placed in an ear vein. The animals were sacrificed at the completion of the experiment, and gross necropsy was performed immediately.

Four doses of Albunex, 0.1, 0.3, 0.5, and 1.0 ml, were used. Control studies with injections of similar volumes of saline were performed in three of the four rabbits. Because the capacity of the catheter was 1.0 ml, bolus injections of microspheres were given by preloading the catheter with the appropriate dose and immediately flushing the catheter with 1.0 ml of saline. The time between any two consecutive injections was at least 2–3 min. If a technical failure occurred such as a change in the position of the sampling volume, or if bowel entered the field of view or activity in the inferior vena cava was prolonged, the injection was repeated. In order to ensure the integrity of the microspheres, a small dose was injected into the inferior vena cava of the rabbit being studied while the heart was being viewed. If opacification of the left ventricle was not observed, the vial was discarded.

Duplex sonography was performed with a 5-MHz pulsed-wave linear transducer (Acuson, Mountain View, CA). In each rabbit, the portal vein, aorta, main renal artery, and an intrarenal arterial branch were examined. The selected arteries represented a large, a medium, and a small vessel. Each dose of microspheres and each dose of saline were given at each site evaluated. For each trial, the Doppler signal was optimized, and continuous duplex imaging and videotape recordings were obtained for a 10-sec baseline period and a 40-sec postinjection period while the transducer was held fixed and without further manipulation of imaging or Doppler variables. When the bolus injection was given, a cursor was illuminated on the screen that marked the end of the injection on the image and video recording. The sonographer did not know the type of solution and the volume injected.

Evaluation of the portal vein was possible in three of the four rabbits. Ten injections of Albunex were given, four of 1.0 ml and two each of 0.5, 0.3, and 0.1 ml.

The duplex images of each vessel were evaluated for the presence and degree of enhancement by two observers who viewed the videotape recordings. They had no knowledge of the type of solution or volume injected. They rated the degree of enhancement independently by assigning a grade of 0–3 as follows:

0 = no response, 1 = mild, 2 = moderate, and 3 = marked Doppler enhancement.

Because the time when the bolus injection was given was marked on the video recording, it was possible to measure the interval between the end of the injection and the onset of arterial Doppler enhancement. The duration of enhancement was measured also. Mean and standard deviation of the time of onset and duration were then calculated.

The subjective data were examined by using the Friedman analysis of variance of ranks at each site with dose and animal as the dependent variables [9]. A Wilcoxon sign test was performed when the analysis of variance indicated a significant main effect for animal or dose.

Results

On real-time studies, the microspheres were visualized in the inferior vena cava as they were being injected. They appeared as tiny echogenic foci that coalesced at larger doses and caused acoustic shadowing. Though the activity in the inferior vena cava interfered at times with acquisition of Doppler signals from the aorta and renal artery in these small animals, it usually subsided as the arterial Doppler enhancement became apparent. After IV administration of microspheres, gray-scale enhancement of cardiac chambers on both the right and left sides was observed in all four rabbits. Gray-scale opacification of the aorta or any vessel other than the vena cava and sonographic enhancement of abdominal organs was not apparent at any time during the experiment.

For all arteries studied in all four rabbits, a total of 48 Albunex and 36 saline injections were given. Both observers gave the same grade for 62 of 84 trials and were one grade apart in 21 trials and two grades apart in one.

Whereas activity in the inferior vena cava was detected after saline injections, no detectable Doppler signal enhancement was observed at any of the arterial sites studied. Doppler enhancement after administration of microspheres, as rated by both observers, was present in 77% of injections (Figs. 1–3). At the 1.0-ml dose, a response was present in all of the vessels studied in all four rabbits. The Doppler signal from the abdominal aorta was enhanced after the injection of all four doses of microspheres in all rabbits. Volumes less than 1.0 ml produced a less consistent response in arteries smaller than the aorta. Whereas the 0.3- and 0.5-ml injection of microspheres produced detectable enhancement of the Doppler signal sampled from the renal artery in all four rabbits, the 0.1-ml dose caused enhancement in only two rabbits. Doppler signals from the intrarenal artery branch were enhanced after the injection of 1.0 ml of microspheres in all four rabbits. The 0.3- and 0.5-ml doses caused enhancement in only two rabbits and the 0.1-ml dose in only one rabbit. Whereas the 0.1-ml dose injected into the vena cava enhanced the Doppler signal of the abdominal aorta in all four rabbits, a 1.0-ml dose injected into the ear vein of one of the rabbits had no effect on signals obtained from the same vessel. Doppler signals acquired from the portal vein were enhanced after all four injections of 1.0 ml of microspheres. Of all six injections of lower doses, only one (0.5 ml) produced detectable enhancement (Fig. 4).

The mean time interval between IV injection of microspheres to onset of enhancement of Doppler signal was 5 ± 2 sec. The duration of Doppler enhancement was 12 ± 4 sec. No significant differences in onset or duration of response related to the dose given or the vessel examined were seen. Once the effect produced by the passage of the bolus of microspheres subsided, no effect from recirculation was detected during the 40-sec postinjection observation period.

Friedman's nonparametric analysis of variance by ranks indicated that the magnitude of Doppler enhancement varied significantly with the IV dose of microspheres administered at $p < .05$ in the aorta and $p < .001$ in the renal artery and intrarenal arterial branch. Of all possible pair-combinations of doses given, the Wilcoxon test showed a significant difference in the degree of enhancement produced by the lowest dose and all other doses (0.1 vs 0.3 ml, $p < .003$; 0.1 vs 0.5 ml, $p < .006$; and 0.1 vs 1.0 ml, $p < .001$).

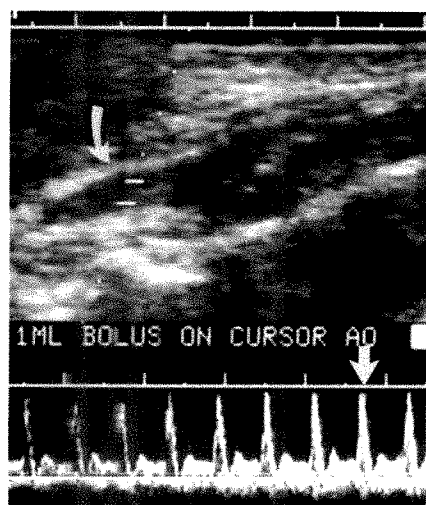


Fig. 1.—Duplex sonogram oblique to abdominal aorta (curved arrow) shows effect of 0.1 ml of microspheres on aortic Doppler signal. Note increased brightness of velocity waveform when microspheres reach sampling volume. Peak effect (straight arrow) was at 3 sec after onset. Brightness returned to baseline 8 sec after onset (not shown).

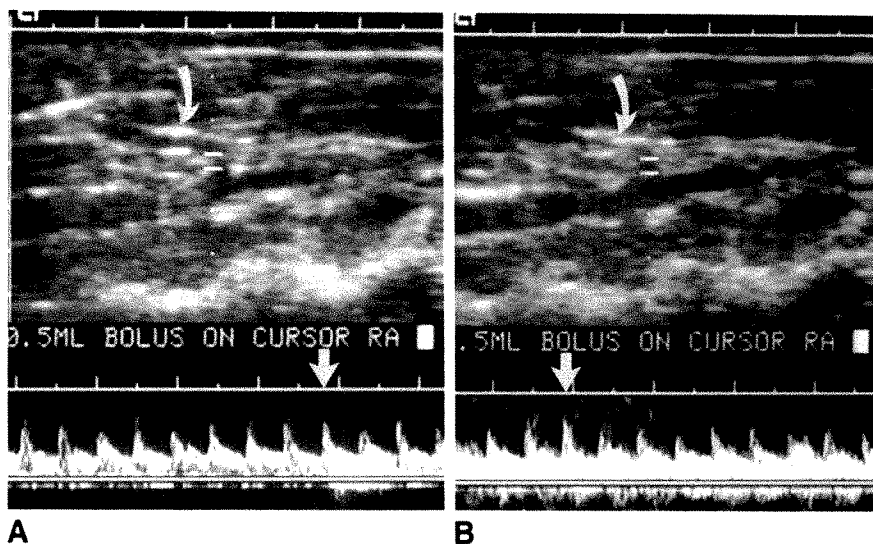


Fig. 2.—Coronal sonograms of left main renal artery (curved arrow) show effect of 0.5 ml of microspheres on renal arterial Doppler signal.

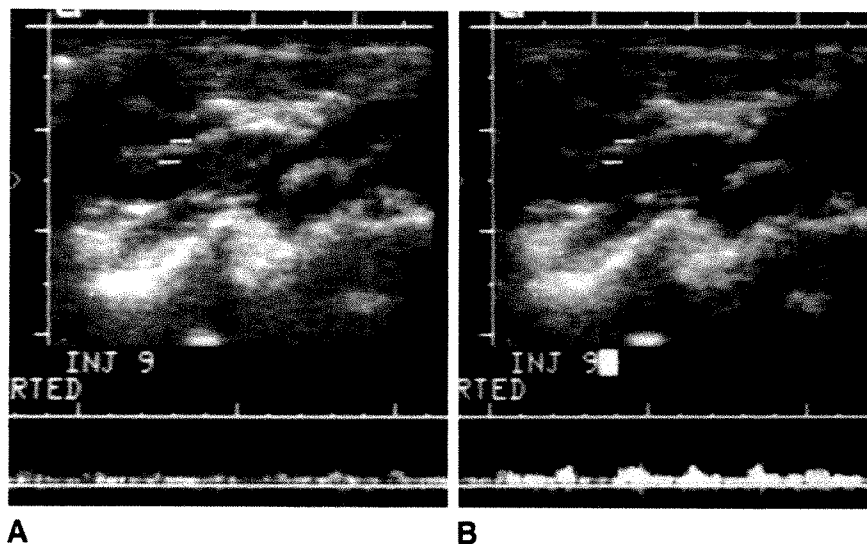
A, Arrival of microspheres to sampling volume causes increased brightness of Doppler tracing (right of straight arrow) relative to baseline (left of straight arrow).

B, Peak effect (straight arrow) occurred 5 sec after onset. Brightness of Doppler waveform returned to baseline level in 12 sec (not shown).

Fig. 3.—Longitudinal oblique sonograms of upper pole of kidney with sampling volume placed over small intrarenal arterial branch show effect of 1.0 ml of microspheres.

A, Baseline Doppler waveform.

B, Doppler waveform during peak effect. Brightness returned to baseline levels a few seconds later (not shown).



No obvious adverse effects on rabbit cardiovascular function were noted after administration of Alunex. Gross necropsy revealed no abnormalities of the intrathoracic or intraabdominal viscera.

Discussion

The Doppler waveform is a display of frequency shift on the y-axis (or velocity of the reflective interfaces [RBCs] if the angle between the sound beam and direction of flow is known), time on the x-axis, and intensity of the reflected signal from these interfaces as brightness. IV injection of air-

filled human albumin microspheres, which are much more reflective than RBCs, produced consistent Doppler enhancement or increase in the brightness of the waveform. This effect was observed when signals were recorded from small, medium, or large arteries, represented by an intrarenal branch, the main renal artery, and aorta. All doses evaluated, 0.1–1.0 ml, consistently enhanced the Doppler signal in the aorta. Regardless of the vessel studied, including the portal vein, a 1.0-ml dose was sufficient to reproducibly enhance the Doppler signal in this animal model. Although small doses resulted in a consistent effect in larger vessels, aorta, and main renal artery, larger doses were necessary to enhance

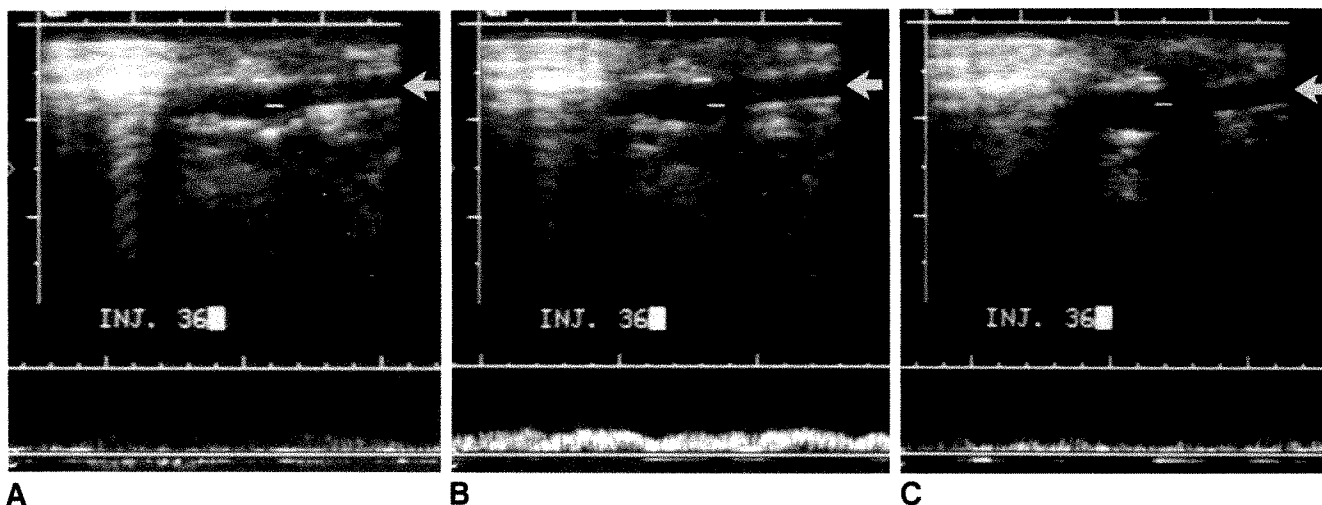


Fig. 4.—Longitudinal sonograms of portal vein (arrows) show effect of 0.5 ml of microspheres. This was the only injection less than 1.0 ml that was effective.

A, Baseline tracing shows faint Doppler signal.

B, As bolus of microspheres passed through sampling volume, Doppler signal became markedly bright.

C, After microspheres exited sampling volume, brightness returned to baseline.

signals in the small (<1 mm) intrarenal branches. A dose-response effect was noted; larger doses produced greater enhancement. Whereas 1.0 ml of microspheres was required to produce a consistent effect in rabbits, the effective human dose for consistent filling of the left ventricle is approximately 5.0 ml (J. L. Barnhart, personal communication, October 1988). The 5.0-ml dose might be sufficient for Doppler enhancement in humans.

The left atrium and ventricle, as has been previously described [7, 8], were opacified when the air-filled human albumin microspheres were injected in the inferior vena cava of all four rabbits. The consistent enhancement of Doppler signal of arteries and the portal vein suggests not only that the microspheres had to survive the splanchnic circulation in addition to the pulmonary circulation in the case of the portal vein, but that their intravascular half-life was sufficiently long to allow their detection several seconds after they traversed the left ventricle. However, in the portal vein, which is more distant from the site of injection, a larger dose was required to produce consistent enhancement. This suggests that either the bolus of microspheres became sufficiently dispersed as it traveled toward the portal vein, decreasing the concentration of microspheres, or the intravascular half-life was short enough that only a small population of microspheres reached the portal vein. Evidence that existed in favor of the former reason was the inability to induce enhancement of Doppler signal in the aorta when 1.0 ml of microspheres was given through an ear vein. Because the ear vein is distant from the central circulation and because it is small, requiring slower injection rates, the bolus became diluted as it traveled centrally. Evidence suggesting that the survival of the microspheres might be short is the absence of detectable Doppler enhancement when the microspheres recirculated back through the heart.

The time between the injection of microspheres and the onset of Doppler enhancement and the duration of enhanced signal suggest that the response was based mostly on a bolus effect. In the rabbit, the ear vein was too small and too peripheral to allow the delivery of a compact population of

microspheres. A central vein had to be used in this animal model.

The first-pass effect of the Doppler enhancement suggests the possible clinical uses of Alburnex microspheres. Because the response is short-lived, the use of microspheres to help in the search for vessels or vascular signal will be limited. However, when a vessel is visualized and its Doppler signals are near the noise level, microspheres, at the proper dose, will enhance the signal. Examples of such weak Doppler signals include signals from small or deep vessels, vessels partially hidden by atherosclerotic plaques, and vessels located in the porta hepatis of patients with severe hepatic cirrhosis or fatty infiltration.

To our knowledge this is the first report describing the ability of IV administered microspheres to intensify systemic arterial and portal venous Doppler signals.

REFERENCES

1. Ziskin MC, Bonakdarpour A, Weinstein DP, Lynch PR. Contrast agents for diagnostic ultrasound. *Invest Radiol* **1972**;7:500-505
2. Carroll BA, Young SW, Rasor S, Briller B, Cassel M. Ultrasonic contrast enhancement of tissue by encapsulated microbubbles. *Radiology* **1982**; 143:747-750
3. Feinstein SB, Ten Cate FJ, Zwehl W, et al. Two-dimensional contrast echocardiography. I. In vitro development and quantitative analysis of echo contrast agents. *J Am Coll Cardiol* **1984**;3:14-20
4. Ten Cate FJ, Feinstein S, Zwehl W, et al. Two-dimensional contrast echocardiography. II. Transpulmonary studies. *J Am Coll Cardiol* **1984**; 3:21-27
5. Ophir J, Gobuty A, Maklad N, Tyler T, Jaeger P, McWhirt R. Quantitative assessment of in vivo backscatter enhancement from gelatin microspheres. *Ultrason Imaging* **1985**;7:293-299
6. Gramiak R, Shah PM. Echocardiography of the aortic root. *Invest Radiol* **1986**;3:356-366
7. Keller MN, Feinstein SB, Watson DD. Successful left ventricular opacification following peripheral venous injection of sonicated contrast agent: an experimental evaluation. *Am Heart J* **1987**;114:570-575
8. Berwing K, Schlepper M. Echocardiographic imaging of the left ventricle by peripheral intravenous injection of echocontrast agent. *Am Heart J* **1988**;115:399-408
9. Siegel S, ed. *Nonparametric methods for behavioral sciences*. New York: McGraw-Hill, **1956**

Laser Catheter Thermal Angioplasty: Technique and Early Results in 34 Patients

Harold A. Mitty¹
 Timothy A. Sanborn²
 John S. Train¹
 Sol J. Dan¹

The laser catheter is a nylon vascular catheter with a metal tip that has an end hole as well as side holes. The metal tip is heated by laser energy delivered through an optical fiber embedded in the catheter wall. The catheter may be advanced over a guidewire for use as an adjunct to balloon angioplasty or for use in smaller vessels as the exclusive method of recanalization. We used the catheter to treat 34 patients with 54 discrete vascular lesions in 35 extremities. Twenty patients were treated for clinically significant claudication and 14 for ischemic changes. Laser catheter-assisted balloon angioplasty was used to treat six iliac artery occlusions, two iliac artery stenoses, 10 superficial femoral artery occlusions, 12 superficial femoral stenoses, four popliteal artery occlusions, and three popliteal stenoses. Initial technical and clinical success in these patients, with follow-up periods of 3–6 months, was equivalent to the results of previous reports of laser probe-assisted balloon angioplasty. In 11 patients, 15 of 17 popliteal or tibial-peroneal lesions were treated with the laser catheter without subsequent balloon angioplasty. The treatment was successful in eight of these patients, with follow-ups for up to 6 months.

Our results suggest that the laser catheter is a useful device for the treatment of vascular stenosis or occlusion when used either as an adjunct to balloon angioplasty or in smaller vessels as the exclusive method for angioplasty.

AJR 153:617–621, September 1989

Thermal (hot-tip) laser-assisted balloon angioplasty has been investigated as a means of recanalizing vessels and possibly improving long-term patency [1–3]. Metal probes on the end of optical fibers are heated by laser energy. These probes are passed through atherosclerotic occlusions or severe stenoses. The channel that is produced as a result of the thermal effect can then be traversed by a standard angioplasty balloon catheter, and conventional dilatation can be performed. Although thermal recanalization usually is an adjunct to balloon angioplasty, it can be used as the exclusive method of establishing an adequate lumen in smaller vessels.

Early thermal probes were difficult to guide through vessels. Recently, a new laser catheter (Trimedyn, Santa Ana, CA) was developed that allows true coaxial passage of the metal-tipped catheter over a guidewire. The new catheter also allows direct injections of contrast material through the distal metal tip. Thus, locations of obstructions relative to the catheter tip can be visualized quickly and accurately.

This report concerns our initial clinical experience with the laser catheter in treating 54 lesions in 35 limbs in 34 patients both as an adjunct to balloon angioplasty (23 patients) and as the sole means of angioplasty in smaller-caliber vessels (11 patients).

Materials and Methods

Thirty-four patients, 17 men and 17 women, were treated with the laser catheter between October 1987 and November 1988. Angioplasty was indicated to control clinically significant

Received March 16, 1989; accepted after revision May 3, 1989.

¹ Department of Radiology, Mount Sinai School of Medicine of the City University of New York, 1 Gustave L. Levy Pl., New York, NY 10029. Address reprint requests to H. A. Mitty.

² Department of Medicine, Mount Sinai School of Medicine of the City University of New York, New York, NY 10029.

0361-800X/89/1533-0617
 © American Roentgen Ray Society

claudication in 20 patients, to treat gangrene in six patients, to heal ischemic ulcers in five patients, and to relieve rest pain in three patients. Sixteen of the 34 patients had diabetes mellitus. Nineteen had a history of heavy cigarette smoking. Informed consent for use of the laser catheter with or without subsequent balloon angioplasty was obtained from all patients.

Fifty-four discrete lesions were treated in 35 extremities in 34 patients. Six iliac artery occlusions were present in four patients. Two of these occlusions were 1 cm long and were separated by a 4-cm patent segment in the same vessel. One patient had bilateral 1-cm common iliac artery occlusions. Two patients had single occlusions, 3 and 8 cm long, respectively. Two patients had severe 1-cm-long common iliac stenoses.

The 10 superficial femoral artery occlusions ranged from 1 to 3 cm in six cases and from 4 to 7 cm in four cases. Twelve superficial femoral artery stenoses ranged from 1 to 3 cm in eight cases and from 4 to 6 cm in the remaining four.

In 11 patients selected for laser catheter angioplasty without subsequent balloon dilatations, 17 popliteal or tibial-peroneal lesions were treated. These included six popliteal stenoses—two 1 cm long, one 2 cm long, one 7 cm long, and two 12 cm long; six anterior tibial artery stenoses—three 1 cm long, two 2 cm long, and one 3 cm long; and peroneal artery stenoses—two 3 cm long, one 1 cm long, and one 4 cm long. Angioplasty was also attempted in one 4-cm posterior tibial artery stenosis.

Four additional popliteal artery occlusions 1–3 cm long and three stenoses 1–2 cm long were treated by laser catheter–assisted balloon angioplasty.

The laser catheter consists of a 7-French nylon catheter with a 2.5-mm-diameter metal cap attached to the end by metal prongs. There is enough flexibility in the catheter to allow a gradual change in direction as the catheter is advanced in the iliac and femoral circulation. There is not enough flexibility to allow more abrupt changes in direction, as would be necessary to enter a renal artery or cross over the aortic bifurcation. A 200- μ m optical fiber is embedded in one wall of the catheter and joins the metal cap, with a safety wire in the opposite wall welded to the metal cap. The metal cap has multiple side holes for injection of contrast material. In addition, these side holes facilitate cooling after each period of laser heating. The proximal end of the 80-cm catheter has a standard Luer lock fitting. The laser fiber is 4.5 m long and exits the catheter shaft proximal to the Luer lock fitting to allow junction with the laser. The laser system is a 14-W argon laser generator (Optilase, Model 900, Trimedyn, Santa Ana, CA).

Use of the laser catheter requires the placement of a standard 8-French vascular sheath. Although the central lumen theoretically would allow one to perform the Seldinger technique, the blunt shape of the metal cap and the danger of loosening or dislodging the metal tip from the catheter shaft requires that a sheath be used. Before use, each device is visually inspected to be sure that the metal cap–catheter junction is smooth and there is no separation at this point. The tip is immersed in water, and laser energy is applied to confirm that the device is functioning and that the optical fiber has not been damaged. Appropriate safety goggles are worn while testing and using all laser devices.

All patients in this series were pretreated with aspirin, 325 mg per day. Patients with lesions of the superficial femoral artery or more distal vessels were heparinized, with an initial average dose of 5000 units. After the procedure, protamine was not used and no further heparin was administered. Aspirin was continued on a long-term basis. Patients in whom iliac lesions were treated received aspirin but were not heparinized during the procedure.

We reserve use of the laser catheter for those cases in which the occlusion or stenosis can be traversed initially by a guidewire. Sten-

otic lesions are crossed with a 0.035-in. (0.89-mm) angled steerable guidewire (USCI, Billerica, MA) or with an angled polymer-coated wire (Medi-Tech, Watertown, MA, or Glidewire, Terumo, Tokyo, Japan). Often a 5-French catheter with a gentle 10° distal bend is used in conjunction with the guidewire to facilitate the change in direction necessary to allow the wire to enter the stenosis. In no case should the heated tip be passed over the "Glidewire," as the polymer coating may melt and shred in the vessel when the laser energy is applied. Occlusions are usually traversed with a Teflon-coated J wire. In some instances, additional support for the wire is provided by a 5-French vascular catheter so that greater force may be applied in order to cross a dense or calcified occlusion. In four instances a 0.014-in. (0.35-mm) steerable guidewire was used to cross anterior tibial stenoses. The remaining cases were treated over a 0.035-in. (0.89-mm) wire. Once the lesion has been crossed with a Teflon-coated guidewire, the laser catheter is advanced to the lesion, at which point resistance to further advance is felt and seen fluoroscopically. At this point, the laser is activated and the heated tip gently advanced through the obstruction. The Teflon coating on the guidewire is not damaged by the heated metal probes. Short pulses of 5–10 sec were used. The laser catheter is moved to and fro continuously so that cooling down is facilitated and no adherence to the vessel wall occurs. If an approach over the guidewire is not possible because of failure of the guidewire to pass through an occlusion or stenosis, then one of the solid metal probes (2.0-mm flex or Spectraprobe, Trimedyn, Santa Ana, CA) are used. This was necessary in three patients who are not included in the series.

Results

In the classification of results we defined technical success as improvement in the luminal diameter to less than 30% residual stenosis. Clinical success was defined as appearance of distal pulses and persistent improvement of 0.15 in the Doppler ankle-arm index.

Six iliac artery occlusions treated in four patients were technical and clinical successes after laser catheter–assisted balloon angioplasty. One reocclusion 1 month after recanalization was treated surgically. The remaining five occluded vessels remained patent, with a mean follow-up period of 4.6 months. Treatment of two severe iliac artery stenoses was also technically and clinically successful, with a mean follow-up of 3 months.

Ten superficial femoral artery occlusions were treated with laser catheter–assisted balloon angioplasty. Treatment was technically and clinically successful in eight. There was failure to recanalize the vessels in two. One reocclusion 4 months after recanalization was treated by femoral popliteal bypass. The remaining seven vessels remained patent for a mean of 5.3 months. Twelve superficial femoral artery stenoses were treated. There was initial technical success in 11 patients, including one in whom diffuse disease in a small-caliber vessel was treated by laser catheter angioplasty only. The one technical failure was in a patient in whom the stenosis could not be crossed. In another patient, the procedure was a technical success but a clinical failure, presumably due to poor distal vessels. In the patient in whom the vessel was recanalized only by laser catheter, the vessel reoccluded 24 hr after the procedure. Of the remaining nine patients with stenoses and clinically successful angioplasties, seven

treated vessels remained patent, with a mean follow-up of 6 months. In two of this group of nine, the treated stenoses reoccluded at 5 and 6 months, respectively, and femoral-popliteal artery bypasses were performed.

In 11 patients, 15 of 17 popliteal or tibial-peroneal lesions were treated only with the laser catheter (Fig. 1). One 4-cm posterior tibial artery occlusion and one short anterior tibial stenosis could not be crossed with the laser catheter, but the results in both patients were clinically successful because of recanalization of associated popliteal artery lesions. In addition, balloon dilatation of the anterior tibial lesion was successful after the laser catheter failure. Initial clinical and hemodynamic improvement (mean Doppler ankle-arm index increased 0.27) was noted in eight (73%) of 11 patients. Treatment in three patients was technically successful, but the patients failed to improve clinically because of poor runoff. Two of the eight patients in whom treatment was clinically successful required femoral-popliteal bypasses because of subsequent occlusions of the superficial femoral artery. At that time, the distal vessels treated by the laser catheter were still patent. Short-term (mean, 6 months) clinical follow-up of the eight patients with clinical success is consistent with continued patency at the site of laser catheter thermal angioplasty.

Four additional popliteal artery occlusions and three stenoses were treated by laser catheter-assisted balloon angioplasty; technical and clinical successes were recorded in all seven cases, with a mean follow-up period of 5.9 months.

Two substantial hematomas occurred at the femoral artery puncture site. One required transfusion with two units of blood.

In two instances the metal cap partially separated from the catheter shaft (Fig. 2). In no case was there total dislodgment or embolization of the metal tip. Two other laser catheters

were rejected for use because small spaces were present between the metal tip and the catheter shaft.

Two episodes of laser burn-through of the catheter shaft occurred after fracture of the optical fiber just proximal to the metal cap (Fig. 3). No harm to either patient in the form of vessel damage or perforation was documented.

Discussion

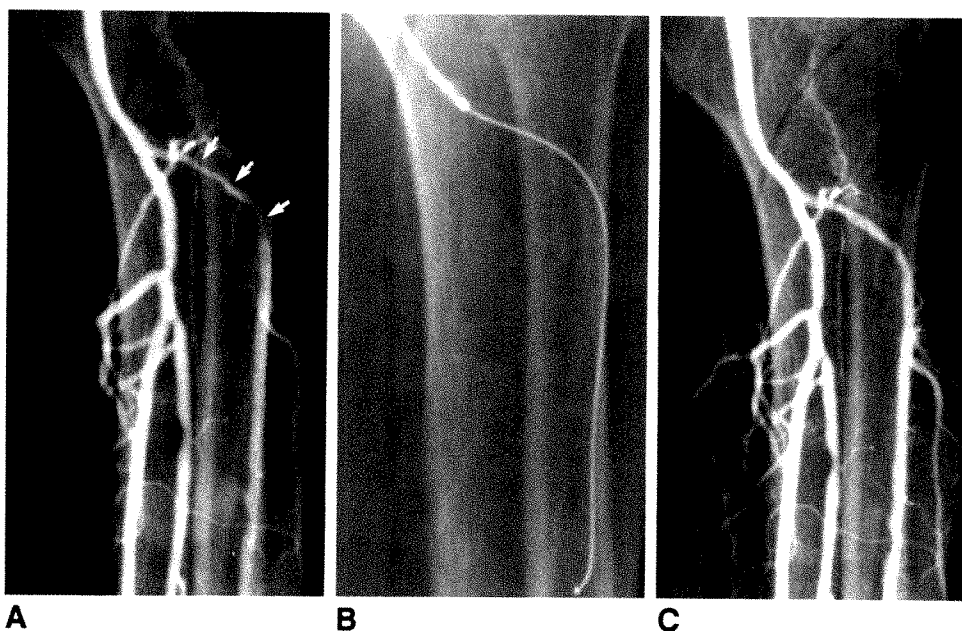
The laser catheter was designed to allow true coaxial passage over a guidewire. In addition, it has the advantage of providing a means for local injections of contrast material, vasodilators, or other drugs through the metal tip. The advantage of this new design is apparent when compared with the original thermal probes, which were fastened directly to the optical fiber. These devices were passed through a vascular sheath and advanced to the point of stenosis or occlusion. Their major drawback was that they had no mechanism by which one could change direction within the vessel lumen. This problem was partly solved by welding a wire at the point where the probe was bonded to the optical fiber. Thus, by gently bending this wire distally, a slight curve at the end of the shaft can be achieved. Torquing this modified device then results in a change in direction of the probe in the vessel. Nevertheless, perforation rates of 4–10% have been reported with the solid probes [1, 2]. Further improvement consisted of placing an eccentric hole in the solid-metal probe tip. This allowed passage of the probe over a guidewire. The relationship of the probe to the wire with this design is not optimal because the guidewire channel is eccentric. An additional problem that all of the solid probes have relates to visualization of their path through the diseased vessel. As these probes have no lumen, one must depend on prior fluoroscopic

Fig. 1.—Laser catheter angioplasty of stenosis of anterior tibial artery.

A, Pretreatment angiogram shows 3-cm stenosis of proximal anterior tibial artery (arrows).

B, Laser catheter is seen following guidewire.

C, Posttreatment angiogram shows marked improvement in size of vessel lumen. Balloon dilatation was not necessary.



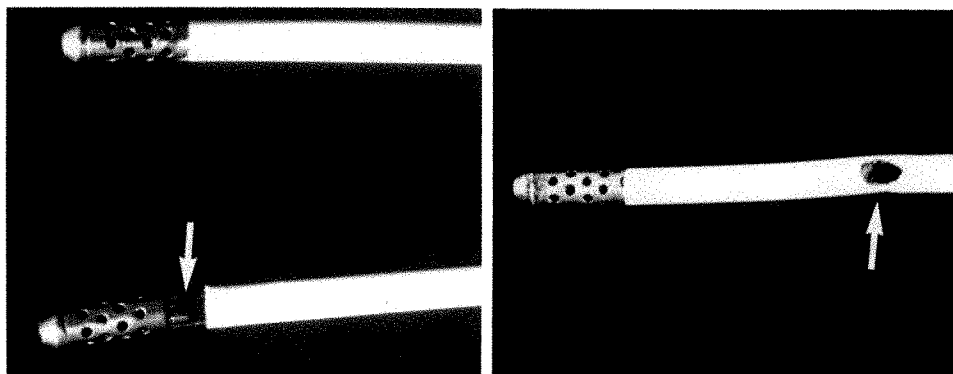


Fig. 2.—Laser catheter separation. Correct relationship of metal cap and catheter shaft is seen in upper device. Metal cap has partially separated from catheter shaft in bottom laser catheter. Metal prongs and optical fiber also are visible (arrow).

Fig. 3.—Catheter “burn-through.” Fracture of optical fiber occurred after flexion of shaft while traversing resistant calcified lesion. Note resultant charred hole in catheter (arrow).

road-mapping, if available, or wait for slow collateral filling from a proximal vascular sheath injection to assess the position of the laser probe in the vessel. This may result in a critical delay in distal small vessels, where there is the most concern about vessel spasm and thrombosis.

The laser catheter solves most of the shortcomings of previous solid metal probes. The central lumen allows passage over a guidewire so that the coaxial course in the vessel is sure to be maintained. Thus, there were no perforations in our patients. In addition, one can inject contrast material through the laser catheter and be sure of the location of the metal tip, guidewire, and area to be treated. This design of the laser catheter requires placing the optical fiber and safety wire in the wall of the catheter without substantially compromising the catheter lumen. This task has been accomplished in the 2.5-mm laser catheter, which easily accepts a 0.035-in. (0.89-mm) guidewire. Recently, a 1.7-mm laser catheter with the same design has become available.

The major problem related to the physical properties of the laser catheter appears to result from the tendency of the catheter to flex at or near the point where it is joined to the metal cap. This problem is most apparent during fluoroscopy when a hard fibrotic or calcified obstruction is encountered. Thus, the two instances of partial separation were in lesions that were particularly resistant to thermal laser recanalization. Although total separation did not occur, there is always a danger of dislodging the metal cap. The metal cap–catheter interface should be visually inspected before it is inserted in the vascular sheath. If there is any separation at this site, that particular laser catheter should not be inserted. Small amounts of metal cap–catheter separation may not be apparent during subsequent fluoroscopy. In such cases, during withdrawal the metal cap can be caught on the distal rim of the vascular sheath causing further separation. This problem occurred in one case. For this reason, it is recommended that a guidewire be placed through the laser catheter tip if there is any resistance while withdrawing the device through the vascular access sheath. Use of the guidewire will realign the metal cap–catheter relationship and facilitate withdrawal of the laser catheter. The manufacturer has indicated that design modifications are being made so that the mechanical bond between the metal tip and catheter will be more secure.

The same tendency to flexion near the metal tip–catheter junction was the most likely cause of our two cases of optical fiber fracture with secondary catheter burn-through. This event became apparent during the procedures by the odor of burning plastic. In both instances there was no evidence of any adverse effect to the patient. If any undue flexion of the catheter shaft occurs, the mechanical and functional integrity of the device should be confirmed by visual inspection followed by application of laser energy with the catheter outside of the patient and the distal 5 cm in water. Appropriate protective goggles must be worn.

The problems inherent in delivering the laser energy have been approached in a variety of ways. Bare fiber devices are apt to perforate vessels, particularly when the vessels are not straight. This problem has been addressed with centering balloons [4, 5], wider angled beams, and computer-assisted analysis of the structures in continuity with the fiber [6]. These promising systems are under clinical investigation. The hot-tip or thermal probe also may represent a compromise by converting the laser energy to heat. Experimental evidence indicates that thermal probes cause less perforation and charring of the vessel wall than do poorly controlled bare fiber devices [7]. In addition, thermal probes distribute heat in a more circumferential manner than do most bare fibers. This circumferential heating effect may be applied more reliably in small vessels with a coaxial device like the laser catheter. Finally, there is evidence that a smoother intimal surface is obtained with thermal angioplasty when compared with balloon angioplasty [8].

Previous reports have described laser thermal recanalization as an aid to balloon angioplasty because it provides channels through lesions that might not be crossed by conventional guidewire and catheter techniques [1–3]. In addition, Sanborn et al. [2] reported that cumulative 1-year patency rates with laser-assisted balloon angioplasty may be better than with conventional balloon angioplasty in the femoropopliteal vessels. As yet, no controlled trials have been undertaken comparing laser-assisted balloon angioplasty and standard balloon angioplasty. Our early experience with laser catheter–assisted balloon angioplasty is similar to that reported by those using conventional solid probes. We have had technical success using the laser catheter as an adjunct

to balloon angioplasty in six iliac occlusions, two iliac stenoses, eight of 10 superficial femoral artery occlusions, 11 of 12 superficial femoral artery stenoses (includes patient treated by laser catheter only), four popliteal artery occlusions, and three popliteal stenoses. Our follow-up period has been short, but it is unlikely that use of the laser catheter will result in better patency rates than solid thermal probes of the same diameter used as an adjunct to balloon angioplasty. The major advantage of the laser catheter is its reliable coaxial relationship to the guidewire and its use as a direct route for injecting contrast material or vasodilating drugs at the level of a lesion. The coaxial passage of the catheter over a guidewire allows advancement through small vessels with confidence. Thus, we were successful in 11 other patients in our series in opening 15 of 17 popliteal and infrapopliteal lesions solely with laser thermal angioplasty using the laser catheter. Clinical success was achieved in eight of these patients, with a mean patency of 6 months. These results lend support to the concept of exclusive thermal recanalization with this device. The results presented here support the feasibility of the laser catheter as a useful clinical device. Controlled trials and long-term follow-up in a larger group of patients must follow. The possibility of thermal angioplasty without balloon angioplasty in larger vessels awaits the development of larger-diameter devices for percutaneous and/or intraoperative use. Other laser devices may become available for recanalization when

the problems inherent in maintaining the intraluminal position of the beam are solved.

REFERENCES

1. McCowan TC, Ferris EJ, Barnes RW, Baker ML. Laser thermal angioplasty for treatment of obstruction of the distal superficial femoral or popliteal arteries. *AJR* **1988**;150:1169-1173
2. Sanborn TA, Cumberland DC, Greenfield AJ, Walsh CL, Gubera JK. Percutaneous laser thermal angioplasty: initial results and 1-year follow-up in 129 femoropopliteal lesions. *Radiology* **1988**;168:121-125
3. Cumberland DC, Sanborn TA, Tayler DI, et al. Percutaneous laser thermal angioplasty: initial clinical results with a laserprobe in total peripheral artery occlusions. *Lancet* **1986**;1:1457-1459
4. Nordstrom LA, Castañeda-Zuniga WR, Young EG, VonSeggern KB. Direct argon laser exposure for recanalization of peripheral arteries: early results. *Radiology* **1988**;168:359-364
5. Nordstrom LA, Castañeda-Zuniga WR, Greive DD, Schoster DVM. Laser-enhanced transluminal angioplasty: the role of coaxial fiber placement. *Semin Intervent Radiol* **1986**;3:47-52
6. Leon MB, Lu DY, Prevosti LG, et al. Human arterial surface fluorescence: arteriosclerotic plaque identification and effects of laser atheroma ablation. *J Am Coll Cardiol* **1988**;12:94-102
7. Sanborn TA, Faxon DP, Handenschild CC, Ryan TJ. Experimental angioplasty: circumferential distribution of laser thermal energy with a laser probe. *J Am Coll Cardiol* **1985**;5:934-938
8. Sanborn TA, Handenschild CC, Garber GR, Ryan TJ, Faxon DP. Angiographic and histologic consequences of laser thermal angioplasty: comparison to balloon angioplasty. *Circulation* **1987**;75:1281-1286

George Patrick Genereux, 1935–1989



Canada lost one of its most skilled pulmonary radiologists, a man of world-class accomplishments, on April 10, 1989.

George Patrick Genereux was born in Saskatoon March 1, 1935, the son of A. G. Genereux, a highly respected Saskatoon ophthalmologist. George was an outstanding athlete, especially in baseball and hockey. A talent scout from the Toronto Maple Leafs tried to enlist him for one of their junior teams in Ontario. But his greatest achievements were in trap shooting, culminating, when he was 17 years old, in a gold medal at the 1952 Olympic Games at Helsinki, Finland. He won the Lou Marsh Memorial Trophy as Canada's outstanding athlete that year.

George achieved world-class stature once again in his chosen field of diagnostic radiology. He obtained his B.A. from the University

of Saskatchewan and his M.D. from McGill University. He studied pathology for 1 year at St. Paul's Hospital, Saskatoon, and did his postgraduate training in radiology at the University of Minnesota Hospitals in Minneapolis and the Royal Victoria Hospital in Montreal. At the Royal Victoria, he became a protégé of the head of the radiology department, R. G. Fraser, who was then writing the first edition of the world's definitive and best-selling four-volume textbook on chest radiology, *Diagnosis of Diseases of the Chest*.

George's professional career was based at the University Hospital in Saskatoon, where he began as a lecturer in 1966. Because of his outstanding scientific contributions, including "best article of the year" in 1968 and 1970 in the *Journal of the Canadian Association of Radiologists*, the University of Saskatchewan quickly promoted him to assistant professor in 1968, associate professor in 1971, and professor in 1974.

George had unusual perceptual skills that enabled him to see and interpret subtle findings on a chest radiograph that would lead to a specific, correct diagnosis. As an interpreter of plain chest films and CT scans, he had few competitors anywhere. George made an important contribution to the training of radiology and respirology residents, but his teaching to medical students was often somewhat above their level of understanding. During his career, he wrote six book chapters and more than 20 scientific papers.

His carefully prepared talks, with superb pathologic-radiologic correlation, were much in demand. He was a visiting professor at the Universities of British Columbia (twice), Cal-

gary, Manitoba, Western Ontario, Toronto, and McGill, as well as at the Universities of California, Los Angeles, and Alabama. He was a featured speaker at lecture courses at the Universities of Washington, Minnesota, and California, San Francisco; at the Nova Scotia Association of Radiologists; the Aspen Radiological Conference; and the Mexican Society of Radiology. George was a member of the Fleischner Society, a select, worldwide group of physicians devoted to the study of chest disease. Beginning in 1971, he made outstanding annual presentations to this group, meeting in Williamsburg, Boston, London, San Diego, San Francisco, Miami, Stockholm, New Orleans, Vienna, Santa Fe, New York, and Washington. This culminated with the honor of giving the prestigious Fleischner Lecture at San Francisco in 1987: *Computed Tomography of Diffuse Pulmonary Disease: State-of-the Art*.

The sad side of the story is that, beginning in 1952, George had continuous pain throughout his spine and in many of his major joints from unremitting ankylosing spondylitis. In his last year, he was able with difficulty to summon sufficient energy to spend several hours a day working on the third edition of *Diagnosis of Diseases of the Chest*, of which he was now a coauthor. He saw volume 1 appear in 1988 and volume 2 early in 1989. Volume 3 is in press, and volume 4 is in preparation. These four volumes will be his memorial. He is survived by his son, George, and his daughter, Andrea.

C. Stuart Houston
University Hospital Saskatoon,
Saskatchewan S7N 0J8, Canada

Technical Note

Dissecting Renal Artery Aneurysm: Treatment with an Endovascular Stent

W. P. Th. M. Mali,¹ G. G. Geyskes² and R. Thalmann³

Treatment of renal artery stenosis by percutaneous transluminal angioplasty has gained widespread acceptance [1]. The method is relatively easy and safe, and the technical and clinical results are generally good. Certain patients, such as those with atherosclerotic stenoses at the origin of the renal arteries [2] and children with certain renal artery stenoses [3], have arteries that are difficult to dilate. New endovascular methods would be useful in these cases. Recently we encountered a hypertensive patient with renal artery stenosis due to a dissecting aneurysm in whom the angiographic results from percutaneous transluminal angioplasty alone were unsatisfactory. Placement of an endovascular stent corrected the stenosis and resulted in partial thrombosis of the aneurysm.

Case Report

A 58-year-old man had been in good health until he experienced severe headache 2 months before presentation. His blood pressure was 230/130 mm Hg at admission. A renogram showed 83% of the renal function in the left kidney and 17% in the right kidney. An angiogram showed a small right kidney with a spontaneous dissecting aneurysm of the renal artery, which caused severe stenosis of the lumen (Fig. 1A). The abdominal aorta showed no signs of atherosclerosis. After obtaining informed consent, we planned to dilate the stenosis and, if this proved impossible, to place an endovascular stent. During the procedure, the stenosis could be passed easily and dilatation with a 5-mm balloon was done without significant improve-

ment of the stenosis. Next, an endovascular stent of the Wallstent type (Medinvent AG, Zurich), with 5.5-mm diameter and a length of 25 mm, was inserted. This self-expanding stainless steel stent was loaded on a 5-French catheter and was advanced easily into the renal artery. An angiogram showed a widely patent lumen of the renal artery, but there was still filling of the aneurysm (Fig. 1B). The next day, the patient was normotensive without antihypertensive medication. The renogram now showed 25% function in the right kidney. Ten days after the procedure, a follow-up angiogram showed that the lumen was still patent and the aneurysm was almost completely thrombosed (Fig. 1C). The patient remains normotensive.

Discussion

Although references to endoluminal stenting can be found dating from the 19th century [4], it was not until 1969 that Dotter reported the use of endovascular stents in canine arteries [5]. Experiments in animals in the 1980s showed that high patency rates could be achieved in healthy vessels [6]. One of the first clinical reports appeared in 1987 [7]. It is still too early to make any judgment on the efficacy of stents given the limited experience and the enormous spectrum of potential indications both in the vascular and nonvascular systems. On the basis of the animal data, it appears that the purely mechanical function of the stent for supporting dissected healthy tissue should be straightforward and highly beneficial. The flow in the renal artery is generally high and the diameter of the artery favors a low risk of thrombosis or

Received February 1, 1989; accepted after revision April 7, 1989.

¹ Department of Radiodiagnosis, University Hospital Utrecht, Catharijnesingel 101, 3511 GV Utrecht, the Netherlands. Address reprint requests to W. P. Th. M. Mali.

² Department of Nephrology, University Hospital Utrecht, Heidelberglaan 100, 3584 CX Utrecht, the Netherlands.

³ Department of Medinvent AG, Zurich, Switzerland.

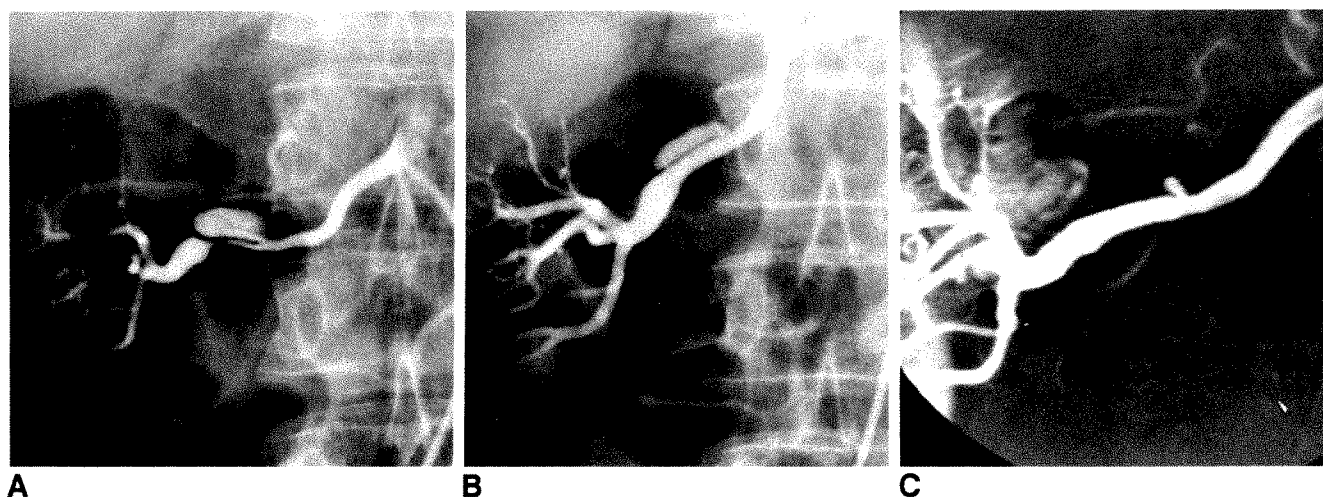


Fig. 1.—A, Selective angiogram of right renal artery shows dissecting aneurysm and intimal flap causing marked narrowing of lumen. B, Selective renal angiogram after stent placement shows that normal lumen has been restored. Aneurysm is still visible. C, Selective angiogram made 10 days after stent placement shows patency of lumen has been maintained. Aneurysm is now nearly completely obliterated.

excessive intimal hyperplasia. Although percutaneous transluminal angioplasty of the renal arteries is a highly successful procedure, it is well known that dissecting aneurysms in the renal artery can result from guidewire or catheter manipulations and can acutely occlude the artery. In such cases a stent could be of value.

In our patient, a dissecting aneurysm occurred in the renal artery. Arteries with dissecting aneurysms cannot be dilated easily, because the intimal flap falls back into the lumen as in our case. This lesion also could have been treated with bypass surgery or reimplantation of the kidney in the pelvis. Apart from being a major operation, such treatment had a high complication rate because the kidney was relatively small (17% of the renal function was on this side). Consequently, after the unsuccessful dilatation with a 5-mm balloon, the stent was used. As expected, the lumen of the renal artery increased considerably and the aneurysm remained, although decreased in size. The stent pushed the intimal flap partly into the aneurysm, but retained its preselected diameter of 5.0 mm. Because the aneurysm was excluded from the circulation, it nearly completely thrombosed. Stent placement

appears to be a simple and effective approach to the treatment of dissecting aneurysms of the renal artery.

REFERENCES

1. Sos TA, Pickering TG, Sniderman K, et al. Percutaneous transluminal renal angioplasty in renovascular hypertension due to atheroma or fibromuscular dysplasia. *N Engl J Med* **1983**;309:274-279
2. Cicuto KP, McLean GK, Oleaga JA, Freiman DB, Grossman RA, Ring EJ. Renal artery stenosis: anatomic classification for percutaneous transluminal angioplasty. *AJR* **1981**;137:599
3. Mali WPTHM, Puijlaert CBAJ, Kouwenberg JJ, et al. Percutaneous transluminal renal angioplasty in children and adolescents. *Radiology* **1987**;165:391-394
4. Kuhn F. Klinischen Diagnostik, in besondere des Magen Darm Kanals. *Munch Med Wschr* **1896**;43:865-868
5. Dotter CT. Transluminally placed coilspring endarterial grafts: longterm patency in canine popliteal artery. *Invest Radiol* **1969**;4:329-332
6. Rousseau H, Puel J, Joffre F, et al. Self-expanding endovascular prosthesis: an experimental study. *Radiology* **1987**;164:709-714
7. Sigwart U, Puel J, Mirkovitch V, Joffre F, Kappenberg L. Intravascular stents to prevent occlusion and restenosis after transluminal angioplasty. *N Engl J Med* **1987**;316:701-706

Case Report

Balloon Occlusion of a Pseudoaneurysm in a Below-the-Knee Amputation Stump

J. Bayne Selby, Jr.,¹ Gloria M. Bittner,¹ Charles J. Tegtmeier,¹ and Curtis G. Tribble²

Embolotherapy is now well established for the treatment of aneurysms, arteriovenous malformations, arteriovenous fistulas, tumors, and uncontrollable hemorrhage [1, 2]. Materials used for embolization include Gelfoam (Upjohn, Kalamazoo, MI) and other particulate matter for small vessels and coils or balloons for larger vessels. In particular, the use of detachable balloons for embolization has gained rapid acceptance in the past decade [3-5]. Their use has been primarily in the treatment of pulmonary arteriovenous malformations and varicoceles and in interventional neuroradiology. We present a case in which a detachable balloon was used to treat a pseudoaneurysm of the popliteal artery.

Case Report

A 68-year-old man with diabetes was admitted to the hospital because of pain and swelling in the stump of his right leg. He had had bilateral amputations below the knee 18 months earlier. His rehabilitation had been successful, and before admission he had been walking with the aid of prostheses. One month before admission, he was treated at another hospital for an apparent infection of the stump. His symptoms persisted, and on the day before admission a pulsatile mass was noted behind the knee. A sonogram showed a large pseudoaneurysm arising from the distal popliteal artery with rapid flow into it. Arteriography showed a pseudoaneurysm approximately 9 × 10 cm arising from the mid popliteal artery (Figs. 1A and 1B). Ligation of the popliteal artery was considered, but because the risk of stump necrosis was high, balloon occlusion was attempted. An antegrade puncture was made into the right common femoral artery and a 9-French guiding catheter was placed into the proximal super-

ficial femoral artery. A 2-mm detachable balloon (Becton Dickinson & Co., Franklin Lakes, NJ) was injected through the guiding catheter and into the pseudoaneurysm. The balloon then was withdrawn until it just occluded the tip of the popliteal artery. In order to minimize the risk of inadvertent detachment of the balloon, a blood pressure cuff was placed around the thigh to occlude arterial flow before the balloon was inflated. After the balloon was inflated (Fig. 1C), the blood pressure cuff was deflated, and contrast material was injected through the guiding catheter. This showed complete occlusion of the distal popliteal artery with no filling of the pseudoaneurysm. Placement of the balloon was such that no collateral branches of the popliteal artery were occluded. The balloon was then detached successfully. A second injection of contrast material confirmed that the balloon had not moved and was still occluding the vessel (Fig. 1D).

After the procedure, the stump decreased markedly in size but no evidence of ischemia was seen. The patient became asymptomatic and was discharged on the seventh day after embolization. At follow-up 2 months later, the stump remained free of infection or necrosis. A sonogram showed localized thrombosis in the mid popliteal vein. No treatment was indicated.

Discussion

The use of balloon embolotherapy has increased remarkably in recent years. It is now standard treatment for carotid cavernous fistulas, pulmonary arteriovenous malformations, varicoceles, and many intracranial aneurysms and arteriovenous malformations. Balloons also are frequently used in conjunction with coils to control bleeding from large vessels. Although our case is somewhat unusual, it is presented to

Received February 10, 1989; accepted after revision March 22, 1989.

¹ Department of Radiology, University of Virginia Health Sciences Center, Charlottesville, VA 22908. Address reprint requests to J. B. Selby, Jr. at Box 170.

² Department of Surgery, University of Virginia Health Sciences Center, Charlottesville, VA 22908.

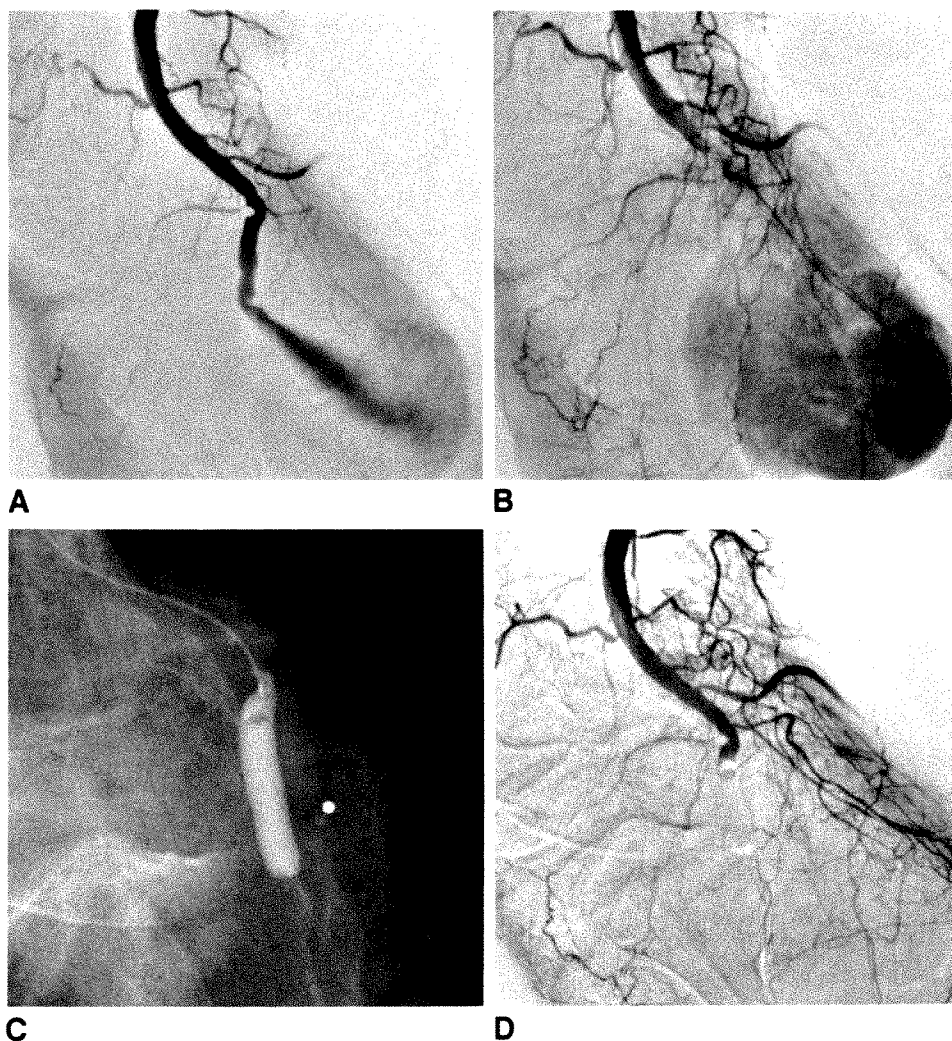


Fig. 1.—Balloon occlusion of a pseudoaneurysm in a below-the-knee amputation stump.

A, Lateral view of knee. Early phase of popliteal arteriogram shows rapid flow from distal popliteal artery into pseudoaneurysm.

B, Later phase shows large size of pseudoaneurysm.

C, Balloon has been inflated in popliteal artery just proximal to pseudoaneurysm but has not yet been detached.

D, Follow-up arteriogram shows no filling of pseudoaneurysm but good perfusion to remainder of stump.

show yet another application of this technique. Surgical ligation was thought to be an unacceptable risk. Primary considerations in placement and detachment of the balloon included avoiding premature release of the balloon and positioning the balloon properly to maximize survival of the stump.

We thought that inadvertent early release of the balloon might be a problem because this was a high-flow system. The balloon is at highest risk for premature release during inflation and before it has approximated the walls of the vessel [1]. To minimize this possibility, we placed a blood pressure cuff around the thigh. Once the balloon was in proper position, the cuff was inflated to occlude arterial flow. Then the balloon was inflated until it completely filled the vessel lumen. The blood pressure cuff was slowly deflated while the balloon was observed fluoroscopically. No movement of the balloon was noted, indicating that it was anchored satisfactorily.

Despite the technical success of the procedure, our major concern was that the popliteal artery would thrombose proximal to the balloon, causing ischemia to the stump. To minimize this risk, we placed the balloon at the very tip of the native popliteal artery below the collateral branches shown on the diagnostic arteriogram. Follow-up arteriography after detachment of the balloon confirmed that all collateral vessels

were patent. In this regard, the balloon has a theoretical advantage over other types of occlusive material because it seems to induce less of a foreign-body reaction in the vessel. Barth et al. [6] showed experimentally that balloon occlusion was similar to surgical ligation, with only a thin thrombus covering the ends of the balloon.

The large size of the pseudoaneurysm precluded placement of the balloon directly into it. Glanz et al. [7] tried to thrombose a pseudoaneurysm in the common femoral artery by packing it with coils. The initial result was good, but within 24 hours the pseudoaneurysm had enlarged. Occlusion of the feeding vessel proximal and distal to the pseudoaneurysm was successful subsequently. No distal continuation of the popliteal artery occurred in our case, so only occlusion proximal to the pseudoaneurysm was necessary.

Clinically, the stump showed no evidence of ischemia during the succeeding week and, in fact, showed marked improvement as evidenced by symptomatic relief and reduction in size. The stump showed no evidence of vascular insufficiency at the 2-month checkup.

Although this exact situation is unusual, many similar applications for balloon embolotherapy are not realized routinely. This form of treatment should be considered whenever spon-

taneous, congenital, traumatic, or iatrogenic pseudoaneurysms or arteriovenous fistulas are encountered. Accurate percutaneous placement can be accomplished, thereby sparing the patient a more invasive and often more risky surgical procedure.

REFERENCES

1. Castañeda-Zuniga WR, Tadavarthy SM. *Interventional radiology*. Baltimore: Williams & Wilkins, 1988:13-101
2. Berenstein A, Kircheff II. Catheter and material selection for transarterial embolization: technical considerations. II. Materials. *Radiology* 1979;132:631-639
3. White RI, Kaufman SL, Barth KH, DeCaprio V, Strandbert JD. Embolotherapy with detachable silicone balloons: technique and clinical results. *Radiology* 1979;131:619-627
4. DeBrun G. Balloon catheter techniques in neuroradiology. In: Athanasoulis CH, Pfister RC, Greene RE, Roberson GH, eds. *Interventional radiology*. Philadelphia: Saunders, 1983:707-730
5. Barth KH, White RI, Kaufman SL, Terry PB, Roland J. Embolotherapy of pulmonary arteriovenous malformations with detachable balloons. *Radiology* 1982;142:599-606
6. Barth KH, White RI Jr, Kaufman SL, Strandberg JD. Metrizamide, the ideal radiopaque filling material for detachable silicon balloon embolization. *Invest Radiol* 1979;14:35-40
7. Glanz S, Gordon D, Sclafani S. Percutaneous coil embolization in the management of peripheral mycotic aneurysms. *Cardiovasc Intervent Radiol* 1987;10:134-137

American Roentgen Ray Society Residents' Award Papers, 1990

The ARRS announces competition for the 1990 President's Award and two Executive Council Awards for the best papers concerning the clinical application of the radiologic sciences.

Awards

The winner of the President's Award will receive a certificate and a \$2000 prize. The winners of the two Executive Council Awards will each be given a certificate and a prize of \$1000. The winners will be announced on March 15, 1990. Winning papers will be presented at the ARRS annual meeting at the Sheraton Washington Hotel, Washington, D.C., May 13-18, 1990. Winning papers will be submitted for early publication in the *American Journal of Roentgenology*. All other papers will be returned to the authors.

Regulations

Eligibility is limited to residents or fellows in radiology who have not yet completed 4 years of approved training in a radiologic discipline. A letter from the resident's department chairman attesting to this status must accompany the manuscript. The resident must be the sole or senior author and be responsible for all or most of the project.

Submitted manuscripts must not exceed 5000 words and have no more than 10 illustrations. Four copies of the manuscript and illustrations are required. Submitted manuscripts should not contain previously presented or published material and should not be under consideration for publication elsewhere.

Deadline for submissions is February 16, 1990. Send papers to

B. G. Brogdon, M.D.
Chairman, Committee on Education & Research
American Roentgen Ray Society
Department of Radiology
University of South Alabama Medical Center
2451 Fillingim Street
Mobile, AL 36617

FORTHCOMING ARTICLES

NEUHAUSER LECTURE

Reflections of men and machines from red goggles and spin wobblers. *Baker DH*

PROGRESS IN RADIOLOGY

High resolution carotid sonography: past, present, and future.

O'Leary DH, Polak JF

Sonography of the male genital tract. *Benson CB, Doubilet PM, Richie JP*

CARDIOPULMONARY RADIOLOGY

Serial assessment of myocardial infarction by gated MR imaging and Gd-DTPA. *Nishimura T, Kobayashi H, Ohara Y, et al.*

Case report. Diagnosis of a myocardial lipoma by using CT. *Conces DJ, Vix VA, Tarver RD*

Chronic eosinophilic pneumonia: CT findings in six cases. *Mayo JR, Müller NL, Road J, Sisler J, Lillington G*

MAMMOGRAPHY

Minimal volume excision of nonpalpable mammographic lesions.

Gallagher WJ, Cardenosa G, Rubens JR, McCarthy KA, Kopans DB

GASTROINTESTINAL RADIOLOGY

1989 ARRS President's Award. The validity and utility of sonography in the diagnosis of appendicitis in the community setting. *Larson JM, Peirce JC, Ellinger DM, et al.*

Case report. Typhoid fever: diagnosis by using sonography. *Puy-laert JBCM, Kristjánsdóttir S, Golterman KL, de Jong GM, Knecht NM*

Gastric fluid detected by sonography in fasting patients: relation to duodenal ulcer disease and gastric-outlet obstruction. *Smithuis RHM, Op den Orth JO.*

Positive predictive value and posttest probability of a diagnosis of colonic polyp on the single-contrast and double-contrast barium enema. *Ott DJ, Scharling ES, Chen YM, Gelfand DW, Wu WC*

Primary small bowel malignancies: a comparison of the small-bowel enema and conventional follow-through examination. *Bessette JR, Maglinte DDT, Kelvin FM, Chernish SM*

Localized clotted blood as evidence of visceral trauma on CT: the sentinel clot sign. *Orwig D, Federle MP*

Arterial perfusion abnormalities of the liver after hepatic arterial infusion chemotherapy and their correlation with metastatic changes: evaluation using CT and angiography. *Roth J, Wallner B, Safi F*

MR angiography and dynamic flow evaluation of the portal venous system. *Edelman RR, Zhao B, Liu C, et al.*

Choledochal cyst: findings on cholangiopancreatography with emphasis on ectasia of the common channel. *Wiedmeyer DA, Stewart ET, Dodds WJ, Geenen JE, Vennes JA, Taylor AJ*

GENITOURINARY RADIOLOGY

Renal imaging in long-term dialysis patients: a comparison of CT and sonography. *Taylor AJ, Cohen EP, Erickson SJ, Olson DL, Foley WD*

Commentary. Imaging studies for screening native kidneys in long-term dialysis patients. *Mindell HJ*

The pars infravaginalis gubernaculi: importance in the identification of the undescended testis. *Rosenfield AT, Blair DN, McCarthy S, Glickman M, Rosenfield NS, Weiss R*

Benign prostatic hypertrophy: treatment with a metallic stent.

Machan L, Jäger HR, Adam A, Gill K, Williams G, Allison DJ

Technical note. Biocompatible copolymer ureteral stent: maintenance of patency beyond 6 months. *Rackson ME, Mitty HA, Lossef SV, Dan SJ, Train JS*

MUSCULOSKELETAL RADIOLOGY

1989 ARRS Executive Council Award. Exercise-enhanced MR imaging of variations in forearm muscle anatomy and usage: importance in MR spectroscopy. *Fleckenstein JL, Bertocci LA, Nunnally RL, Parkey RW, Peshock RM*

The enthesopathic changes of hypophosphatemic osteomalacia in adults: radiologic findings. *Burnstein MI, Lawson JP, Kottamasu SR, Ellis BI, Micho J*

Radiation-induced sarcoma of bone: CT findings in 19 cases. *Lorigan JG, Libshitz HI, Peuchot M*

Optimal plain-film imaging of the shoulder impingement syndrome. *Kilcoyne RF, Reddy PK, Lyons F, Rockwood CA Jr*

PEDIATRIC RADIOLOGY

Findings on chest radiographs after prophylactic pulmonary surfactant treatment of premature infants. *Clarke EA, Siegle RL, Gong AK*

CT evaluation of blunt abdominal trauma in children: comparison of ultrafast and conventional CT. *Brody AS, Seidel FG, Kuhn JP*

Diagnostic reliability of voiding cystourethrography. *Jequier S, Jequier J-C*

Pictorial essay. The radiographic evaluation of velopharyngeal incompetence in childhood. *Barr LL, Hayden CK, Hill LC, Swischuk LE*

FETAL AND OBSTETRICAL RADIOLOGY

Placental abnormalities and oligohydramnios in women with elevated alpha-fetoprotein: comparison with normal controls. *Kelly RB, Nyberg DA, Mack LA, Fitzsimmons J, Uhrich S*

Intrauterine shelves in pregnancy: sonographic observations. *Brown DL, Felker RE, Emerson DS*

Case report. Sonographic diagnosis of omphalocele during tenth week of gestational age. *Brown DL, Emerson DS, Shulman LP, Carson SA*

Case report: prenatal sonographic diagnosis of harlequin ichthyosis. *Mihalko M, Lindfors KK, Grix AW, Brant WE, McGahan JP*

NEURORADIOLOGY

The cerebellum in sagittal plane: anatomic-MR correlation. 1. the vermis. *Courchesne E, Press GA, Murakami J, et al.*

The cerebellum in sagittal plane: anatomic-MR correlation. 2. the cerebellar hemispheres. *Press GA, Murakami J, Courchesne E, et al.*

MR imaging of muscles of mastication. *Schellhas KP*

MR imaging of neurocysticercosis. *Teitelbaum GP, Otto RJ, Lin M, et al.*

CT of nasopharyngeal carcinoma: significance of widening of the preoccipital soft tissue on axial scans. *Hoe J*

COMPUTER PAGE

Cost-effective development of a computer-assisted instruction system. *McGhee RB, Bennett WF, Morris CS, Witanowski LS*

PERSPECTIVE

Restrictive covenants in professional employment contracts. *Rooper RR*

Diagnostic Significance of Interslice Gap and Imaging Volume in Body MR Imaging

Bernhard W. Schwaighofer¹
 Kyle K. Yu
 Robert F. Mattrey

Thin interslice gaps and large imaging volumes are detrimental to MR signal and contrast, especially when the body coil is used. To show the influence of these two factors on fat and water signal and contrast, we performed a series of in vitro experiments. A cylinder filled with water and another filled with oil were imaged transaxially (TR = 2000 msec; TE = 20 and 70 msec) with different interslice gaps (0–150% slice thickness). A series of images was obtained to cover a 40-cm imaging volume. Increasing interslice gap thickness increased water signal without affecting fat signal, resulting in a decrease in fat/water contrast on TE = 20 msec (less T1-weighting) and increasing contrast on TE = 70 msec (more T2-weighting). Contrast nearly doubled when the interslice gap was increased from 10% to 75%. As slices moved away from the central slice, fat and water signals decreased slowly to 12.5 cm off center. Signal loss was significant with offsets greater than 12.5 cm.

These results emphasize that to obtain proper contrast on T2-weighted images, the optimal interslice gap should be used and the region of interest should be near the central slice. Otherwise, images should be interpreted with caution.

AJR 153:629–632, September 1989

The detection and characterization of lesions by MR imaging are dependent on both spatial and contrast resolution [1–3]. Most publications have addressed the issue of optimizing the repetition and echo times (TR and TE) to maximize contrast between lesion and background tissue on the basis of differences in T1 and T2 [4, 5]. However, two frequently overlooked variables interfere with contrast: the interslice gap and the slice position relative to isocenter (best position within the magnet when the center of the imaged volume is positioned) [6]. When the radiologist is looking for small lesions, it is tempting to use thin interslice gaps to avoid missing the lesion. This could be detrimental to contrast (Fig. 1). It is also tempting in body imaging with transaxial images to use large imaging volumes in order to cover the region of interest and the other parts of the abdomen and/or pelvis, potentially placing tissues that require characterization at one end of the imaged volume or the other. Increased distance from isocenter can substantially affect the signal-to-noise ratio and therefore the contrast resolution (Fig. 2).

Although the physical principles behind these effects are well understood, their importance is commonly overlooked in practice. We performed in vitro experiments designed to highlight the effect of these factors on MR images.

Materials and Methods

A phantom was constructed consisting of two parallel tubes 2.5 cm in diameter, one filled with vegetable oil and the other filled with water, submerged in a water bath. The phantom was positioned in the magnet parallel with the static magnetic field. A 1.5-T Signa system (General Electric, Milwaukee, WI) equipped with a quadrature body coil and 3.0 software was used. Thirteen transaxial series were obtained: 2000/20, 70 (TR/TE), four excitations, 30-cm

Received March 9, 1989; accepted after revision May 1, 1989.

B. W. Schwaighofer is the recipient of fellowship JO283M (Erwin Schrodinger Stipendium), Austria. R. F. Mattrey is the recipient of Research Career Development Award KO8-CA01319.

¹ All authors: Department of Radiology, University of California, San Diego, Medical Center, and the UCSD/AMI Magnetic Resonance Institute, 410 Dickinson St., San Diego, CA 92103. Address reprint requests to R. F. Mattrey at the Magnetic Resonance Institute.

0361-803X/89/1533-0629
 © American Roentgen Ray Society

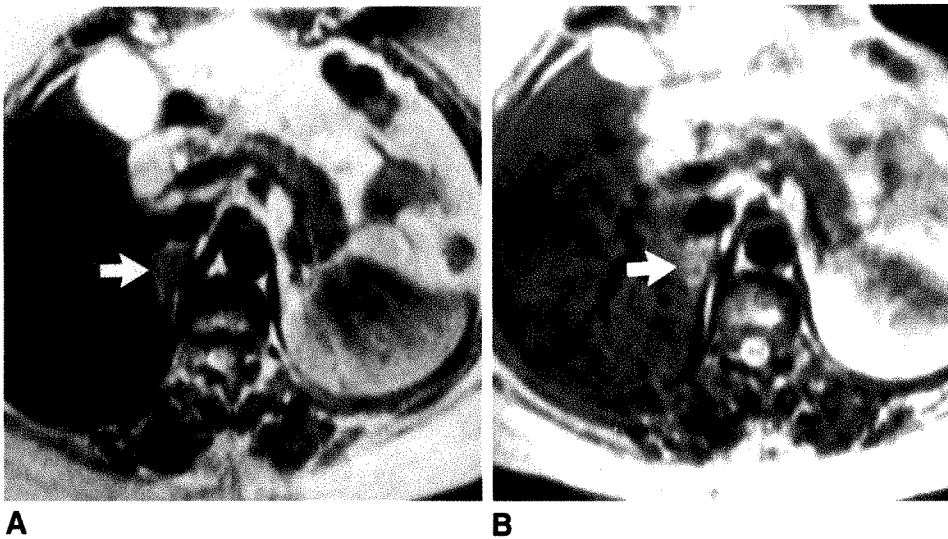


Fig. 1.—T2-weighted MR images (3000/70, 256 × 128 matrix, two excitations) of adrenal metastasis. Lesion was not present on a CT study obtained 2 months before MR.

A, On 20% interslice gap, adrenal lesion (arrow) is slightly brighter than liver but darker than surrounding fat.

B, On 50% interslice gap with all other imaging parameters unchanged, lesion (arrow) is markedly brighter than liver and nearly isointense relative to fat, indicating more T2-weighting than in A.

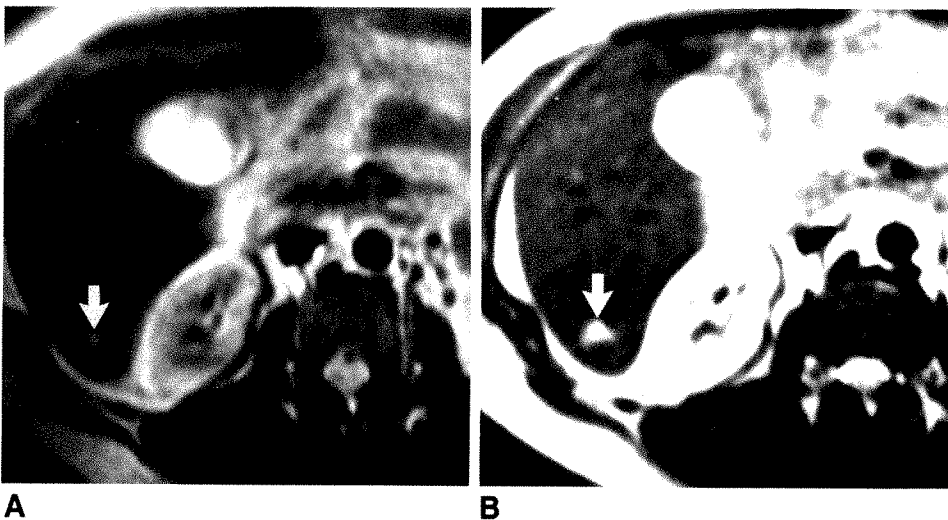


Fig. 2.—T2-weighted MR images (2000/70, 256 × 128 matrix, four excitations) of a presumed liver hemangioma.

A, On slice location 11 cm cephalad from isocenter located at mid pelvis, lesion (arrow) is poorly defined and mildly brighter than liver.

B, On slice location 8 cm caudal to isocenter located at mid liver, lesion (arrow) is markedly brighter than liver, compatible with hemangioma, and image is sharper.

field of view, 256 × 128 matrix, and 10-mm slice thickness. Series 1–11 were obtained with different interslice gaps (0–150% slice thicknesses or 0–15 mm) and the same central 12-cm imaging volume. The 12th series was obtained over the same volume with interleaved slices. This series required twice the time because two series are done automatically by the system, with one series offset by one slice thickness from the other. The 13th series used the same variables as before but imaged a 40-cm volume with 10-mm interslice gap. The signal intensity of fat and water on the central slice was measured for series 1–12 and all images of series 13. Fat/water contrast was calculated as $100 \times (\text{fat intensity} - \text{water intensity}) / (\text{fat intensity} + \text{water intensity})$.

Results

The effect of interslice gap on fat and water signal and contrast is shown in Figure 3. Although the change in interslice gap had no effect on the fat signal, it resulted in a sigmoid response for the water signal. This increased with increasing gap and reached a plateau at 75% slice thickness. The fat/water contrast decreased with increasing interslice gap when TE was 20 msec and increased when TE was 70 msec. The

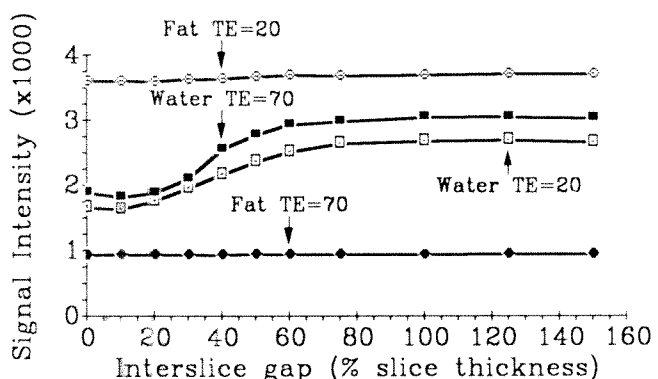
contrast nearly doubled when the interslice gap was increased from 10% to 100% slice thickness. As anticipated, the interleaved technique resulted in signals identical to those obtained with a 100% interslice gap.

For both fat and water, signal intensity decreased progressively with increasing distance from isocenter (Fig. 4). Although signal loss was less than 10% for the central 25-cm imaging volume, slices outside this volume showed substantial deterioration in signal for both fat and water.

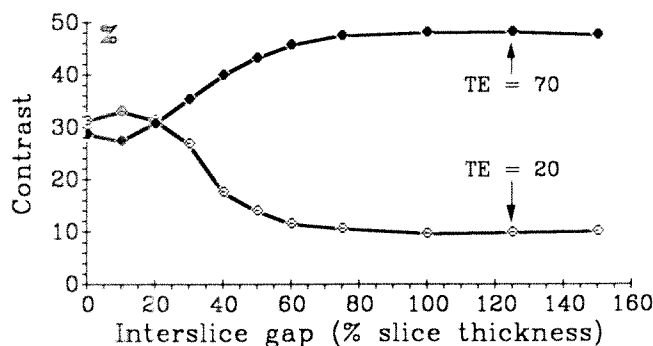
Discussion

MR images rely on differences in T1, T2, and hydrogen density among tissues to display contrast based on the TR and TE used. Variations in TR and TE have been exploited to maximize contrast. However, other variables also affect contrast. These include the field of view, slice thickness, and matrix. Less intuitive and less often considered are two additional variables: the interslice gap and the distance from isocenter.

The effect of interslice gap on MR signal has been exten-



A



B

Fig. 3.—Graphs show effect of interslice gap on signal intensity and fat/water contrast.

A. Signal intensity of fat and water imaged with TR = 2000 msec and TE as shown. Note that whereas signal remains constant for fat (material with short T1), it increases with increasing gap for water (material with long T1).

B. Contrast between fat and water calculated from signal shown in A. Note that contrast decreases on TE = 20 msec and increases on TE = 70 msec because signal becomes less T1-weighted with increasing gap.

sively reviewed [7–9]. In brief, the 90° and 180° RF pulses used in most pulse sequences are slice-selective. These pulses ideally should result in a square slice profile so that protons located near or outside the slice of interest remain unaffected. However, because the slice profiles are not really square, they do affect neighboring slices. This phenomenon is called cross-talk and is worse for the 180° pulse because it lasts twice as long as the 90° pulse. If protons affected by cross-talk are incorporated into adjacent slices, they will influence signal and contrast. This occurs because hydrogen nuclei affected by cross-talk experience an RF pulse before their scheduled time, shortening their effective TR. A shorter TR decreases signal, increases T1-weighting, and therefore, decreases relative T2 contrast. As cross-talk decreases by increasing the gap, contrast becomes less T1-weighted. Cross-talk decreases contrast at short TE and increases contrast at long TE times (Figs. 1 and 3).

Also shown in this study is the effect of distance from isocenter on signal. This phenomenon has important clinical implications, particularly in body imaging when frequent attempts are made to cover a large imaging volume on trans-

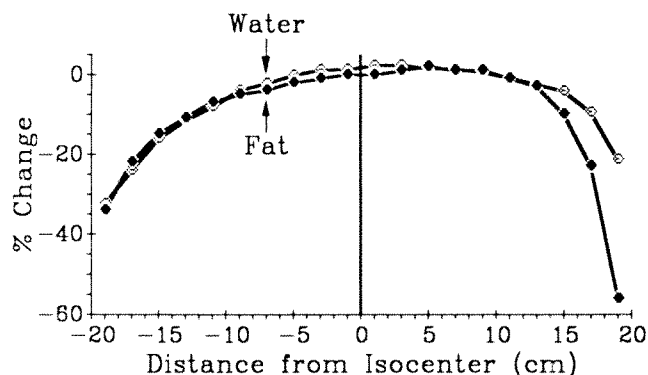


Fig. 4.—Graph shows effect of distance from isocenter on signal. Note that fat and water signals decrease on slices farther from isocenter. Degrees of signal loss for fat and water were similar for the central 26-cm volume, so contrast should not be significantly affected but contrast-to-noise ratio should decrease.

axial series. Although the advantage of a large imaging volume is obvious, as distance increases from isocenter the signal-to-noise ratio decreases and so does contrast resolution (Figs. 2 and 4). Attempts at interpreting contrast should be done with caution if evaluated on slices distant from isocenter. In our in vitro experiment, this loss was nearly 35% when the slice was 20 cm away from isocenter. On transaxial series the central slice of the imaging volume is advanced automatically to isocenter where the RF power is adjusted to achieve optimal tip angle over the whole slice to maximize signal. The RF power is less than optimal for slices away from the center slice because of RF and magnetic field inhomogeneity that yield less than or greater than 90° tip angle and therefore less signal. Our experiment used a homogeneous medium that kept magnetic field inhomogeneity to a minimum. In human subjects, tissues with markedly different magnetic susceptibilities are included in the imaging volume, and greater inhomogeneity is expected, yielding more complex results than observed in our experiment (Fig. 4).

Although cross-talk occurs in all systems, the interslice gap at which maximal signal is achieved may vary. This was at 75% slice thickness on our system. Similarly, all systems experience signal falloff from isocenter; however, the maximum imaging volume (volume over which signal loss will be less than 10%) may vary. This maximal volume on our system was 25 cm when the body coil was used. The phantom and the imaging protocol described here are simple. Further, this study evaluated the influence of slice position in the axial direction. Signal falloff may be steeper in the sagittal and coronal directions [10]. Therefore, it is important to determine the effect of cross-talk and slice position on contrast as part of quality assurance. Ideally this should be done before the precise signal intensity ratio is defined that discriminates benign from malignant lesions.

The effect of interslice gap and slice position on contrast is similar on all MR systems. However, the exact relationship of signal to these two variables presented above is unique to the equipment used here.

When contrast is critical for discrimination, a single slice obtained over the lesion is the ideal solution. However, as this is not practical, the lesion should be positioned as close to isocenter as possible, and a large interslice gap should be used.

ACKNOWLEDGMENTS

We thank Joel F. Martin and his research group for useful suggestions.

REFERENCES

1. Glazer GM. MR imaging of the liver, kidneys, and adrenal glands. *Radiology* **1988**;166:303-312
2. Reinig JW, Doppman JL, Dwyer AJ, Frank J. MRI of indeterminate adrenal masses. *AJR* **1986**;147:493-496
3. Glazer GM, Aisen AM, Francis IR, Gyves JW, Lande I, Adler DD. Hepatic cavernous hemangioma: magnetic resonance imaging. *Radiology* **1985**;155:417-420
4. Bradley WG, Tsuruda JS. MR sequence parameter optimization: an algorithmic approach. *AJR* **1987**;149:815-823
5. Darwin RH, Drayer BP, Riederer SJ, Wang HZ, MacFall JR. T2 estimates in healthy and diseased brain tissue: a comparison using various MR pulse sequences. *Radiology* **1986**;160:375-381
6. Bradley WG, Glenn BJ. The effect of variation in slice thickness and interslice gap on MR lesion detection. *AJNR* **1987**;8:1057-1062
7. Kucharczyk W, Crawley AP, Kelly WM, Henkelman RM. Effect of multislice interference on image contrast in T2- and T1-weighted MR images. *AJNR* **1988**;9:443-451
8. Kneeland JB, Shimakawa A, Wehrli FW. Effect of intersection spacing on MR image contrast and study time. *Radiology* **1986**;158:819-822
9. Runge VM, Wood DM, Kaufman DM, Silver MS. MR imaging section profile optimization: improved contrast and detection of lesions. *Radiology* **1988**;167:831-834
10. Marcu A, Prince JR, Wilson DA. Temporal and spatial characteristics of a global index of uniformity for a 1.5-Tesla magnetic resonance imager (abstr). *Magn Reson Imaging [Suppl]* **1989**;7:165

Meeting News

American Roentgen Ray Society: 89th Annual Meeting, May 1989

The 89th annual meeting of the American Roentgen Ray Society was held May 7–12, 1989, at the New Orleans Hilton Hotel, New Orleans, LA. Approximately 200 scientific presentations, over 400 instructional courses, and a wide selection of scientific and technical exhibits were available to the 2700 attendees. This year's categorical course was on genitourinary radiology and the topic of the Friday morning symposium was gastrointestinal radiology.

This review of the 1989 ARRS meeting is intended to provide readers with a short summary of most of the scientific papers presented at the meeting. Unfortunately, page limitations do not allow coverage of all presentations or an analysis of them.

Mammography

The scientific session on breast imaging included papers on three main topics: breast localization and aspiration cytology, implications of breast augmentation, and breast imaging technique. B. D. Fornage of Houston, TX, reported success in obtaining diagnostic fine-needle aspirates of nonpalpable breast lesions by using sonographic guidance. Diagnoses based on aspirates obtained in the 38 patients had an overall sensitivity of 94%. The value of sonographic guidance was emphasized, including the unique capability of sonography to confirm precisely the entry of the needle into the lesion. Two other papers also concerned localization of nonpalpable lesions through the use of stereotaxic guidance. Laurie L. Fajardo from Tucson, AZ, presented impressive results with

aspiration cytology performed under stereotaxic guidance in 61 patients with 46 benign lesions and 15 carcinomas. All of the aspirates obtained were regarded as adequate. Six of the carcinomas produced aspirates diagnosed as malignant, three as suspicious, two as atypical, two as probably benign, and two as benign. Christopher R. B. Merritt of New Orleans, LA, presented initial results in 50 patients with a prototype stereotaxic guidance device. All lesions were localized with an average accuracy of less than 5 mm and an average time for localization of less than 25 min.

The implications of breast augmentation on mammographic detection of carcinoma was discussed in two papers. Jill Liebman and Beth D. Kruse of Atlanta, GA, reviewed mammographic findings in 12 patients who developed breast carcinoma after augmentation mammoplasty. Ten of the 12 patients with cancer had suspicious mammograms and one patient had a cancer detected with sonography. Cancer staging indicated that patients with breast augmentation did not have a more advanced stage of cancer than patients without augmentation. The sensitivity of mammographic detection of cancers after augmentation was considerably less in the paper presented by K. P. Douglas of New Orleans, LA. In this study, only two of six cancers were seen on mammograms. Both authors noted that the cancers that developed in women with implants were not more advanced than those in the normal population and emphasized the importance of special mammographic techniques to optimize visualization of breast tissue after augmentation.

Editor's note.—"Meeting News" articles will report the highlights of important national radiology meetings on a regular basis. The intent is to provide Journal readers with succinct, substantive, and accurate reviews of topics of current interest—written in a readable fashion and published promptly.

The articles will not undergo the peer review usually required of *AJR* publications nor will they offer a critique of the information provided. The sole purpose of the series is to apprise *AJR* readers of topics of current concern in an interesting and timely fashion.

I thank Horacio B. D'Agostino, Amy Beth Goldman, Peter Hahn, Eric K. Lang, Christopher R. B. Merritt, William D. Middleton, Mark D. Murphey, Charles A. Rohrmann, Ernst Rummeny, David D. Stark, Franklin N. Tessler, Rudi F. Thoeni, Eric vanSonnenberg, and Robert L. Vogelzang for contributing to this summary.

AJR 152:633–640, September 1989 0361–803X/89/1533-0633 © American Roentgen Ray Society

The follow-up evaluation of patients after tylectomy (lump-ectomy) and radiation treatment was the subject of a paper by Arlene Baratz and colleagues from Pittsburgh, PA. Recurrent carcinoma after radiation treatment was evaluated in 25 patients, and the problems of differentiation of recurrence from posttreatment changes were discussed. All but one of the recurrences had the same pathology as the original cancer, and two thirds of the recurrences were in the site of the original tumor. A baseline mammogram 6 months after treatment was suggested to aid in the early identification of recurrence.

Gastrointestinal Radiology

W. E. Torres and colleagues, Atlanta, GA, reviewed 67 patients who underwent biliary extracorporeal shock-wave lithotripsy (ESWL) done under the Dornier protocol for relative contributions of sonography and oral cholecystography (OCG) in determining the number and size of gallstones. Sonography was equal to OCG in determining stone number in 52 of 67 patients, sonography showed fewer stones than OCG in 11 patients, and sonography showed more stones than OCG in four patients. The mean size determined by OCG was greater than that on sonography. They concluded that OCG is better than sonography in evaluation of patients for lithotripsy because it can be used to evaluate gallbladder function and to determine the number of stones.

Joseph E. Bernstein of Chicago presented a postmortem study in which 20 cadavers had sonographically guided transhepatic puncture of the gallbladder to determine the frequency with which the gallbladder was entered through the extraperitoneal portion of the gallbladder (bare area) and to determine anatomic correlates of success. Despite the transhepatic puncture, only 32% of entries were through the bare area, 52% did not enter the gallbladder through the bare area, and the remainder (16%) entered through the free surface of the gallbladder. It was noted that guidewire dislodgement occurred more frequently when the bare area was not entered. A transhepatic entry site also occasionally yielded potential complications. Anatomic correlation was attempted to define the measurements of the bare area and to determine whether or not sonography or CT could visualize it well. No consistent measurements of the bare area were obtained because it was variable and no CT or sonographic landmarks were found to identify the bare area. Dr. Bernstein and colleagues concluded that transhepatic gallbladder puncture frequently does not enter the gallbladder in the bare area, but they believe that transhepatic puncture does stabilize the gallbladder for percutaneous intervention.

R. G. Gibney of Vancouver, Canada, discussed the results of a study of gallstone recurrence after cholecystolithotomy. Sixty-three patients treated with cholecystolithotomy were followed up for 2–48 months. Forty-eight patients had adequate follow-up. There was recurrence in 27% (13/48). However, most patients (10/13) with recurrent stones were asymptomatic; only two of 13 had symptoms. The results confirm a relatively high frequency of stone disease recurrence. The absence of symptoms leads Dr. Gibney and col-

leagues to conclude, however, that cholecystolithotomy need not be followed by routine interval cholecystectomy in high-risk patients.

J. H. Oldershaw of Boston presented an in vitro experiment showing dissolution rates of various types of gallstones with methyl *tert*-butyl ether (MTBE) and monooctanoin in various combinations. The most rapid dissolution occurred by using monooctanoin followed by MTBE. MTBE only was the second most active agent. Monooctanoin only and MTBE followed by monooctanoin were not effective in dissolving gallstones. The authors believe that monooctanoin may fissure calcium bilirubinate shells and allow better penetration of MTBE. One implication for current clinical protocol is that all gallstone patients should have monooctanoin instilled overnight before MTBE administration.

H. V. Steinberg of Atlanta, GA, presented a study in which the gallstones of 54 patients undergoing biliary ESWL were separated according to the Dalgin criteria into primarily cholesterol stones and primarily pigmented stones. No difference in ESWL fragmentation rate between types of gallstone was found.

Genitourinary Radiology

The efficacy of transrectal, sonographically guided biopsy in the diagnosis of prostate cancer was discussed by J. Llerena from Minneapolis, MN. The findings confirm reports in the literature that sonographic abnormalities are not present in all carcinomas. Fifty-seven of the biopsies were performed in peripheral areas featuring abnormal echogenicity; 38 were used as controls on the contralateral side in a region without sonographic abnormalities. Malignancies were found in 23 of the biopsy specimens obtained from areas of abnormal echogenicity, but they also were found in six of the 38 biopsy specimens taken largely at random from regions that featured no sonographic abnormalities. Dr. Llerena concluded that although not all malignant sites may be sonographically apparent, sonographic abnormalities suggest malignancy somewhere in the gland.

F. Castañeda from Minneapolis, MN, reported the results of prostatic balloon urethroplasty in a series of 130 patients. This procedure was performed on an outpatient basis under topical anesthesia. The success rate in patients with predominantly lateral lobe hypertrophy was 75%, with follow-up of 6 months to 3 years. In patients with median bar hypertrophy, the success rate was only 25%. No adverse effects were noted.

In another paper, Dr. Castañeda and his colleagues hypothesized that stretching of the prostatic capsule, tissue compression with subsequent atrophy, and separation of the prostatic lobes by splitting the anterior posterior commissures are the mechanisms that bring about relief of obstruction of the urethra. They suggest that separation of the prostatic lobes should be the goal of the procedure.

Jeffrey Quam and his colleagues from Rochester, MN, reported that 38% of their patients have impotence of a vasculogenic cause. The patients were studied with conventional duplex Doppler sonography and spectral analysis. Both

corpora cavernosal arteries were evaluated in the flaccid state and then 5 min after intracavernosal injection of 60 mg of papaverine. The main peak systolic value was important in determining the presence of arterial vasculogenic impotence, and the diastolic velocity was important in determining the venous causes of impotence. The data suggest that there is an important role for color flow and spectral Doppler sonography as the screening method for vasculogenic impotence of both arterial and venous origin.

Musculoskeletal Radiology

In a study presented by B. W. Hindman, Los Angeles, CT studies of the wrist were performed with an extremity positioning device. Contiguous scans (1.5 mm) were obtained on both transaxial and coronal images. In some patients, semisagittal studies were added or replaced the coronal images. Dr. Hindman emphasized the necessity of obtaining two views and the particular accuracy of the transaxial study. Sixteen patients with normal plain films after trauma were selected on the basis of persistent pain. Twenty-one occult fractures were identified. The four most frequent sites were the hamate (5), the lunate (3), the scaphoid (3), and the bases of the metacarpals.

Eight patients with hyperextension dislocation of the neck were studied with plain films and MR imaging by Joel W. Yeakley and colleagues, Houston, TX. John H. Harris, Jr., who presented the paper, emphasized the subtle plain film findings (diffuse severe prevertebral soft-tissue swelling and, in two thirds of the cases, a small triangular avulsion fragment at the anterior inferior corner of the vertebral body). Malalignment was not obvious because the dislocations reduced spontaneously. Clinically, the patients have acute central cervical cord syndrome of varying severity. The combination of diffuse prevertebral swelling on plain films and the physical findings indicates the need for MR imaging. The MR image clearly outlines the soft-tissue injuries associated with hyperextension dislocation. The anterior longitudinal ligament and anterior fibers of the annulus are disrupted. The disk space is widened, the signal of the disk is changed by hemorrhage, and disk material is herniated posteriorly. The posterior longitudinal ligament is avulsed. The spinal cord is impinged on anteriorly by the herniated disk and posteriorly by the lamina of the subjacent vertebrae.

In reviewing emergency room films of the spine, Stanley P. Bohrer and Y. M. Chen of Winston-Salem, NC, found gas in the annulus of intervertebral disks in 27 patients (38 disks), or 4% of the cases. Most were related to degenerative disk disease and not acute trauma. In cases with multiple levels, contiguous disks were affected. Drs. Bohrer and Chen postulate that the cause of the degenerative vacuum is associated with changes in Sharpey fibers, which attach the disk to the vertebral body. Spurs or variants of the corner of the body (e.g., flat corner) may predispose the cervical spine to the vacuum phenomenon.

A. M. Rijke and colleagues, from Charlottesville, VA, evaluated stress radiographs of the ankle obtained on the Telos device by comparing the results with arthrography and/or

surgery. The object of the study was to determine if stress studies could differentiate accurately between isolated anterior talofibular ligament tears and the more serious combined calcaneofibular and anterior talofibular ruptures. Films were obtained in the anteroposterior projection to measure the talar tilt angle with 5, 10, 15, and 20 kg of stress. Films were obtained in the lateral projection to evaluate anterior draw with 5, 10, 15, and 20 kg of stress. The studies were performed with lidocaine anesthesia. Twenty-five patients were evaluated, and the 16 patients with significant calcaneofibular ligament tears had increased displacement of the mortise on stress views when compared with normal volunteers and/or patients with isolated anterior talofibular ligament tears.

Amy Beth Goldman of New York reviewed 119 cases of calcific tendonitis of the shoulder. Twenty patients had calcifications related to the tendon of the long head of the biceps brachii. In nine cases, the deposit was adjacent to the superior glenoid rim at the origin of the tendon, a site well described in the literature. However, in 11 cases, the calcification was extraarticular, adjacent to the proximal humeral shaft, and close to the tendon/muscle junction. This more distal site of calcific tendonitis of the long head of the biceps has not been well described. The 11 cases of extraarticular calcific tendonitis of the biceps all had a single calcification near the proximal humeral shaft. On the internal rotation view, the density was medial to the shaft; on the external rotation view, the density was lateral to the shaft; and on the axillary view, it was anterior to the shaft. Dr. Goldman concluded that including a small portion of the proximal humeral shaft on shoulder films will increase the diagnostic yield in cases of calcific tendonitis.

The advantages of MR imaging in the characterization of skeletal lesions is well documented; however, the preferred technique of evaluation continues to be investigated. Karen L. Harkens of Iowa City, IA, presented a study describing the value of Gd-DTPA-enhanced MR in evaluating both neoplastic and nonneoplastic musculoskeletal lesions in 30 patients. Long TR/TE images were adequate for tumor definition, but several advantages of Gd-DTPA-enhanced short TR images were apparent. These included differentiation of cystic regions (including hemorrhage or necrosis) from neoplasm and distinction of edema from tumor.

CT arthrography of the shoulder is currently the most accurate radiologic method for evaluating causes of glenohumeral instability. David R. Pennes of Ann Arbor, MI, presented a study evaluating the optimal positioning of the patient, comparing internal and external humeral rotation, in 42 patients. The results indicate that anterior joint abnormalities (capsular detachment and labral tears) generally were best assessed on internal rotation; however, in 10% of cases, anterior lateral abnormalities were solely or optimally shown on external rotation. Posterior joint structures were evaluated best on external rotation, with 40% of the abnormalities seen only in this position. Dr. Pennes and colleagues concluded that CT arthrography of the shoulder should be performed with both internal and external humeral rotation.

The use of uncemented hip arthroplasties and bipolar endoprostheses has presented difficulties in the radiographic

diagnosis of loosening. John Shannon Swan and colleagues of Indianapolis, IN, used contrast and nuclear arthrography to assess loosening of uncemented femoral components. Seventeen patients with surgical confirmation were evaluated, and nuclear arthrograms were performed with 100 μ Ci of indium-111 chloride. Sensitivity for detection of loosening was 50% for contrast arthrography and 70% for nuclear arthrography, whereas specificity was 100% for both. However, when either examination was positive, the sensitivity of the combined procedures was 90%. These results indicate that combination contrast and nuclear arthrography is an accurate method for determination of loosening of uncemented femoral components in hip arthroplasty or bipolar endoprostheses.

Computed Tomography

Janet E. Kuhlman and colleagues from Baltimore, MD, discussed CT of enterovaginal and vesicovaginal fistulas. Twenty-six patients with 18 enterovaginal and eight vesicovaginal fistulas were examined. The fistulas were caused by gynecologic malignancies in 15 (58%), by inflammatory bowel disease (mostly Crohn disease and diverticulitis) in eight (31%), and by miscellaneous causes in three (11%). Cervical cancer with radiation therapy was the most common cause of fistulas in the neoplastic group. The CT diagnosis of fistula was based on the presence of contrast medium in the vagina (strict criterion in 58% or 15/26) and was suggested by air in the vagina in 85% (22/26) and by fluid in the vagina in 19% (5/26). Recent surgery and recent vaginal examination, either of which can produce intravaginal air, must be excluded. Communication between vagina and bladder or between vagina and rectum often could be seen on CT. Associated findings were adjacent radiation changes in 38% (10/26), contiguous pelvic mass from recurrent tumor in 23% (6/26), and adherent bowel loops with thickened wall due to inflammatory bowel disease or radiation enteritis in 42% (11/26). Conventional studies (excretory urography, cystography, and barium enema) showed abnormalities in 44% (7/16). CT had an overall detection rate of 58% (15/26) for fistula if strict criteria were used, and the detection rate was higher if the suggestive findings were used also. CT, therefore, can be considered a successful method for showing fistulas. For detection of enterovaginal fistulas, no IV contrast material but sufficient oral and rectal contrast material should be administered. Delay of scans 20 min after contrast administration often is useful, particularly with small fistulas. For detection of vesicovaginal fistulas, no oral contrast material is given but IV contrast material should be used.

Dr. Kuhlman also discussed CT features and growth characteristics of Krukenberg tumors. The most common cause of metastases to the ovary is colonic cancer. This outnumbers other causes by a ratio greater than 2:1. Three to eight percent of women with colonic cancer have ovarian metastases at surgery. Metastases to ovaries often cannot be distinguished from primary ovarian tumors. In this study, the CT examinations of 12 patients with pathologically proved ovarian metastases (colon, seven; stomach, two; and one each, carcinoma of appendix, carcinoma of endometrium, and carcinoid) were reviewed. The most common CT features of

Krukenberg tumors were bilateral adnexal masses (9/12). Masses that presented as cystic and solid structures were frequently multiloculated with septa. Calcification was seen in two patients. The diameter of the masses ranged from 3 cm to more than 15 cm. Associated findings included carcinomatosis in 9/12, hydronephrosis in 5/12, and ascites in 4/12. Liver metastases and periaortic adenopathy were not common. In five patients with histories of pelvic mass, a primary ovarian tumor was suspected, and a genitourinary primary tumor was found either later or at surgery. Seven patients presented with pelvic masses and previous cancer surgery. Nine had serial scans over 6 to 28 months that showed disproportionate growth of the ovarian metastases as compared with the remaining metastases. This often was associated with ascites and diffuse carcinomatosis. Dr. Kuhlman concluded that Krukenberg tumors cannot be distinguished from primary ovarian tumors by CT. Because of the high frequency of ovarian metastases, CT scans made in women with primary colonic or gastric cancer should be extended to the pelvis.

M. J. Milos and colleagues from Los Angeles tested an abbreviated protocol for CT of the abdomen and pelvis in patients with blunt abdominal trauma. From 30 cases with abnormal full abdominal-pelvic scans obtained at 1-cm intervals before and after injection of contrast medium, a postcontrast sequence was selected at 1-cm increments from the dome of the liver through the spleen and then at 2-cm increments through the liver. Further scans to the midsymphysis were selected at 3-cm increments. The abbreviated scanning sequence and the long initial scanning sequence were blindly and separately reviewed and correlated with final interpretative results and histologic findings. The accuracy was over 90% for the long scanning sequence (65 slices) and less than 90% for the short sequence (22 slices). Although the specificity was high for both scanning sequences (over 90%), the sensitivity was very high (over 90%) for detecting injuries to solid organs, but it was low (61%) for pelvic fluid. Presence of fluid within the pelvis was missed with the short scanning sequence in 9 of 10 cases. Five transverse process fractures, sternal fractures, and anterior mediastinal and lung base abnormalities also were missed on the short scanning sequence. The results suggest that the short scanning format may be used in combination with routine radiographs of the spine and pelvis and may provide sufficient information for immediate patient management. However, some reports suggest that certain acetabular and spinal fractures may be detected only by CT. Therefore, the authors do not recommend the use of the abbreviated CT trauma protocol for staging, triage, or management of patients because of the false-negative results in detecting pelvic fluids or bone fractures.

Ruedi F. Thoeni and colleagues from San Francisco, CA, discussed the value of pouchogram (barium enema), CT, and 111 In-labeled leukocyte study (Lk) for detecting postoperative complications such as pouchitis, abscess, or fistula in 40 patients with ileoanal pouches after total colectomy for severe ulcerative colitis. Twenty-four S-pouches and 16 J-pouches were present, and 51 sets of examinations were analyzed. In

these 51 sets, a proved diagnosis of pouchitis was found in 21, abscess in 12, fistula in three, and no abnormality in 18. CT scans were obtained after administration of oral and rectal contrast material. Pouchogram with hypaque and Lk were obtained on the same day. Among the patients with S-pouches, 23 of 31 CT studies showed round pouches and eight of 31 showed undulated pouches. Eight of 16 J-pouches had cloverleaf appearances, and undulated or round pouches were found in three of 16. A stump was visible in eight of 16 patients with J-pouches but was not present in any patients with S-pouches. Distinctions between S- and J-pouches were made correctly in 46 of 51 cases. Based on results in 29 patients with all three tests, Lk had the highest sensitivity (75%) and the highest accuracy (84%). CT and Lk had similar specificities (100%). For detection of pouchitis, Lk was the best, with an accuracy of 89%, but it could diagnose only inflammatory change and could not distinguish among pouchitis, abscess, and fistula. For detection of abscess, CT was the best with an accuracy of 100%. Fistulas frequently were missed by all three procedures, probably because of their small size and/or early sealing of the orifice. A combination of CT and Lk appeared to be best for detection of complications, with an accuracy of 91%.

Kimble B. Dolenz and colleagues, Gainesville, FL, studied 22 patients with various hepatic masses in whom dynamic incremental CT with arterial contrast infusion was performed to determine optimal injection rate and site of injection. Selective hepatic arterial infusion was found to be best, with a sensitivity of 89%, compared with angiography alone (sensitivity, 50%). Also, this technique was as accurate as hepatic arteriography in predicting pathologic diagnoses.

S. J. Schulte and coworkers of Seattle, WA, evaluated the extrahepatic biliary system with CT. In 100 consecutive normal subjects, the common hepatic and common bile ducts were identified in 67% and 80%, respectively. Mean duct wall thickness was 1.0–1.5 mm. Forty-eight patients with thickened bile duct wall (>2.0 mm) had diagnoses including cholangitis, cholangiocarcinoma, pancreatic cancer, pancreatitis, and common bile duct stones.

To determine the usefulness of CT in predicting survival of patients with liver metastases from colorectal carcinoma, R. Halvorsen and colleagues of Minneapolis, MN, compared pretherapy CT scans of 32 patients with subsequent survival data. No significant relationship was found between the length of survival and the number and size of the metastases or the percentage of liver involvement. The only significant correlation found was that involvement in both segments of the left lobe correlated inversely with survival.

The CT findings in 61 cases of severe and 87 cases of mild acute pancreatitis were correlated with clinical outcome by J. Llauger and colleagues of Barcelona, Spain. When the CT findings were of greater severity (extensive involvement, peripancreatic fatty infiltration, peripancreatic fluid collections), the development of abscesses or pseudocysts was more common. When these findings were not present, patients had a better clinical course.

R. F. Thoeni and colleagues of San Francisco, CA, used CT to detect asymptomatic pancreatitis after ERCP. CT scans

were obtained after ERCP was performed with or without interventional maneuvers. The scans showed signs of pancreatic inflammation including gland enlargement, fluid collections, and poorly defined pancreatic margins. Eighty percent of patients who underwent ERCP with therapeutic interventions and 25% of patients who did not have interventional maneuvers showed evidence of pancreatitis. This is compared with 48% of all patients who had clinical evidence of postprocedure pancreatitis.

Sonography

Papers presented in this session focused on noninvasive vascular diagnosis by use of Doppler sonography. Although spectral Doppler analysis remains essential for quantitative evaluation, color flow imaging shows great promise for qualitative characterization of flow dynamics.

A major concern in carotid Doppler examinations—reproducibility of velocity determinations—was addressed by Joseph F. Polak of Boston. In a study of 51 carotid bifurcations, it was determined that interobserver error was less frequent for internal carotid peak systolic velocity determinations than for internal carotid/common carotid velocity ratios. Reproducibility in all measurements was decreased in patients with large calcified plaques.

In a study of 38 proved pseudoaneurysms, William D. Middleton of St. Louis, MO, showed color Doppler sonography to be a valuable method of evaluation. In all cases, blood was seen flowing within the pseudoaneurysm in a pulsatile pattern varying with the cardiac cycle. The amount of thrombus and size of the neck could be assessed easily. Waveform analysis was needed only in equivocal cases. There were no false-positive and two false-negative studies (one a 1.5-mm aneurysm and one that had inadequate acoustic access). Color Doppler sonography should be the primary technique for evaluating patients with suspected pseudoaneurysms. In most cases, surgery can be performed on the basis of the color Doppler sonography results alone.

The results of duplex sonography studies of parathyroid masses in 25 patients was discussed by K. Riedy, Evanston, IL. Parathyroid adenomas often have areas of increased flow, which helps in their detection, especially when they are ectopic or when the thyroid gland is multinodular. Many of the parathyroid adenomas showed frequency shifts greater than 4 kHz, whereas none of the other neck masses did.

Duplex and color flow sonography are gaining widespread acceptance in the workup of patients with suspected lower extremity deep venous thrombosis. Similar success in evaluating veins in the upper extremity was reported by Greg J. Knudson, Milwaukee, WI. The patency of the brachial, basilic, axillary, subclavian, innominate, and internal jugular veins was assessed with 7.5- and 5.0-MHz transducers. Complete filling of the vessel lumen by color was used as the criterion for a normal examination. In 22 examinations with venographic correlation, only one false-positive examination was encountered (due to extrinsic tumor compression); six studies were false-negative. Similar results were obtained in 121 examinations for which clinical correlation was available. Venous

collateral formation was a helpful secondary sign of thrombosis. Color flow imaging was unable to visualize either the superior vena cava or the proximal innominate vein. The authors suggest that venography be reserved for those patients with normal color flow studies but with strong clinical indications for thrombosis.

The presence of gallbladder wall perforation can change the early management of a patient with cholecystitis. Howard Levy and colleagues, New York, reviewed 117 patients with acute cholecystitis who had preoperative sonographic examinations. Twenty of these cases had perforations. The patients with perforations had a significantly greater gallbladder wall thickness (mean, 7.0 vs 4.8 mm), larger pericholecystic fluid collections (mean, 16.9 vs 4.8 mm), and a greater frequency of other fluid collections such as ascites and pleural effusion (25% vs 2.5%) when compared with patients without perforations. Although overall differences were present between the two groups of patients, in most individual cases the predictive value of these differences was not high enough to be helpful.

Stenosis of the donor artery may lead to significant hypertension in renal transplantation patients. Although angiography remains the gold standard for diagnosis, it is invasive and may adversely affect renal function. In their study of 11 patients with suspected renal artery stenosis, Franklin N. Tessler and colleagues, Los Angeles, found that all eight patients with turbulent flow had significant stenosis at angiography, whereas none of three patients without turbulent flow did. Two patients with Doppler shifts of greater than 4.0 kHz had no significant stenosis.

In contrast, J. F. Snider and coworkers, Minneapolis, MN, found a Doppler shift of greater than 7.5 kHz to be 94% sensitive and 87% specific in diagnosing renal artery stenosis in renal transplants. In their study, turbulence was a less reliable indicator, especially in patients with end-to-side anastomoses between the renal and iliac vessels. Despite the disagreement regarding the relative importance of diagnostic criteria, both investigators concluded that duplex Doppler sonography is an excellent screening technique for patients with suspected renal transplant artery stenosis. However, the criteria remain somewhat subjective, and further research is needed to refine the technique and to assess the possible role of color flow imaging.

Transvaginal sonography (TVS) is becoming indispensable in the evaluation of the female pelvis. It has excellent resolution and helps overcome some of the limitations of transabdominal sonography (TAS) such as bowel gas, obesity, and poor bladder filling. Jill Leibman of Atlanta, GA, discussed her study, done with Beth D. Kruse, comparing TVS to TAS in 65 patients with benign palpable pelvic masses. TVS provided more information in 79% of patients. In six patients with cysts and four patients with endometriomas, the diagnosis was made only on TVS.

In a study of 193 patients with suspected ectopic pregnancy, Kristin Thorsen and colleagues, Milwaukee, WI, showed that TVS was capable of significantly decreasing the number of indeterminate examinations as compared with TAS. By using the strict criterion of finding an ectopic gestational sac with a visible fetal pole, 38% (23/60) of ectopic

pregnancies were definitely identified with TVS, whereas only 22% (13/60) were diagnosed with TAS. Of the 83 patients with normal intrauterine pregnancies, TAS made a definite diagnosis in 34 cases; TVS correctly diagnosed all 83. Overall, TVS was able to establish a definite diagnosis in 113 patients, whereas TAS did so in 52.

Cheryl Sisler and Marilyn J. Siegel from St. Louis, MO, reviewed the sonographic features of 18 ovarian teratomas in 17 pediatric patients. Twelve were complex masses. Of these, nine showed a dermoid plug, two had internal septa, six had solid central components, and one had a fluid-fluid level. Three lesions were purely cystic, and three were entirely solid. Overall, 77% had features that allowed accurate preoperative diagnosis of teratoma.

Color flow imaging may become the method of choice to evaluate patients with acute scrotal pain. In a study of 15 patients, R. M. Lerner and colleagues of Rochester, NY, found increased testicular blood flow in all cases of epididymo-orchitis and detorsion. None of five patients with surgically proved torsion showed flow in the affected testis with color flow sonography. Similar success was reported by F. Fobbe and coworkers from W. Berlin, W. Germany, who were unable to show flow in 41 patients with acute torsion by using a 7.5-MHz transducer. Both investigators emphasized the need for close attention to technique, particularly when imaging young patients in whom normal flow may be very slow. Color flow imaging also could be used to show varicoceles reliably. Flow was increased considerably during Valsalva maneuver. Flow patterns in testicular neoplasms were not sufficiently characteristic to distinguish one tumor type from another.

Color flow imaging also was used to characterize the vascular events that occur during erection. In a study presented by Alan N. Schwartz, Seattle, WA, flow in the cavernosal artery in 10 normal volunteers was assessed by using color flow imaging and spectral analysis, both at rest and during pharmacologically and psychologically induced erection. The authors identified six distinct phases of arterial flow. Further investigation will be required to demonstrate applications in patients with erectile dysfunction.

MR Imaging

Several speakers discussed the advantages of MR imaging in delineating soft-tissue injuries that are not shown well on plain films. F. Feldman of New York presented examples in the neck, shoulder, chest, hip, knee, and ankle.

A. M. Rijke and colleagues of Charlottesville, VA, studied MR imaging of the ankle, examining the anterior talofibular ligament in neutral position and the calcaneofibular ligament in plantar flexion, using a three-dimensional gradient-echo imaging with steady precession (FISP) technique. They were able to show tears in these ligaments and found good correlation with the stress radiograph examination.

MR evaluation of partial tears of the anterior cruciate ligament (ACL) was the subject of another presentation by Dr. Rijke. By using a knee-stressing device, changes in the appearance of the ACL before and after stress were studied. The results showed that laxity is difficult to distinguish from a tear.

Techniques for detection of hepatic metastases were the topic of six presentations. B. Hamm and M. Taupitz of W. Berlin, W. Germany, used an induced rat tumor to study four IV contrast agents: Gd-DTPA, Gd-DTPA-albumin, Fe-EHPG, and a superparamagnetic iron oxide. In a 2-T animal imager, he followed the administration of each agent with repeated 20-sec gradient-echo images and, after 7 min, with spin-echo T1-weighted scans. Gd-DTPA required as much as 1.2 mmol/kg for enhancement, which lasted only 2 min. T1 shortening predominates at a dose of 1.0 mmol/kg. The albumin-Gd-DTPA compound maintained enhanced tumor-liver contrast for several hours, at a dose of 0.01 mmol/kg. Higher doses were less effective because contrast material leaked into the tumor. Relatively poor enhancement occurred with the hepatobiliary agent because of the lower relaxivity (potency) of iron compared with gadolinium and because, unexpectedly, contrast material leaked into the tumor. The best enhancement was produced by the iron particles and lasted for many hours. The signal intensity of the liver returned to normal in 10 days.

C. J. Fretz and colleagues (Boston and Chicago) compared the performance of a superparamagnetic iron oxide (AMI-25) in clinical trials with unenhanced MR imaging and CT, using receiver-operator-characteristic (ROC) analysis of the capacity to detect liver metastases. Sixteen patients were included, and the dose varied from 5 to 40 μ mol Fe/kg. Contrast-enhanced MR outperformed CT (statistically significant) and non-contrast-enhanced MR (not statistically significant).

Ernst Rummeny and coworkers, Boston, compared phase contrast (PC, Dixon method) T2-weighted pulse sequences with conventional, in-phase, T1- and T2-weighted pulse sequences at 0.5 T for detection of focal hepatic lesions. Because many patients with metastases have hepatic steatosis, PC pulse sequences can be used to enhance tumor-liver contrast. On average, the PC 2350/60/2 (TR/TE/excitations) pulse sequence was found to perform as well as a short-TR/short-TE T1-weighted SE sequence in detecting metastases. Hepatocellular carcinomas often undergo fatty degeneration and, unlike metastatic cancer, can show decreased contrast on PC images.

J. J. Phillips of Torrance, CA, gave evidence that the MAST gradient motion nulling technique implemented at both 0.5 T and 1.5 T improves detection of liver lesion. He described the normal pattern of signal arising from patent blood vessels. Naturally, variation of the technique, such as application of saturation pulses, may change the normal pattern.

Finally, in the tumor-detection group of papers, Harvey V. Steinberg of Atlanta, GA, gave results comparing high-field (1.5 T) with low- or intermediate-field (0.5 T) MR imaging in 29 patients (18 with lesions) who underwent both. Except for the poor performance of the high-field T1-weighted SE images, all pulse sequences on both scanners allowed comparable lesion detection rates.

Interventional Radiology

Significant improvement in patency and hemodynamics of atherosclerotic stenosis in peripheral vessels is achieved by percutaneous atherectomy. M. Maynar and colleagues, Min-

neapolis, MN, reported their experience with the Simpson atherectomy device, including wire atherectomy of the popliteal artery, in a series of patients with peripheral vascular disease. An overall patency rate of 70% of the treated vessels was found after 18 months of follow-up. The authors believe this type of atherectomy should provide improved long-term patency over treatment with percutaneous transluminal angioplasty (PTA) alone, especially if large atherectomy catheters are used.

Curtis W. Bakal, Bronx, NY, described the beneficial effects obtained with PTA of intrapopliteal vessels for limb salvage, healing of amputation wound, graft salvage, and as an adjunct to planned surgery in a group of patients, 85% of whom were diabetics. The clinical response after technically successful dilatation of the arterial stenosis was directly related to the state of the distal vessels. Excellent results were obtained in patients in whom PTA restored straight-line flow to the foot; there was no effect on those with no distal vessels.

Effects of parenteral steroids administered to prevent early restenosis after PTA were found in preliminary laboratory experiments reported by T. V. Myers, Kansas City, MO. Dr. Myers and coworkers found less subintimal fibrosis in a group of dogs that had PTA of their carotid arteries and received steroids, in contrast to fibroblastic and capillary proliferation with fibrin and collagen deposition in the control group. It appears that steroids influence the cellular and luminal response to inflammation, preventing neointimal fibroplasia. Further studies and clinical correlation are needed to assess fully this potentially beneficial effect for patients undergoing PTA.

Regardless of the causes of the Budd-Chiari syndrome, treatment is directed at relieving portal hypertension. L. G. Martin, Atlanta, GA, described the utility and safety of balloon dilatation of the hepatic veins, inferior vena cava, and portosystemic shunts in prolonging the patency of veins and shunts. This technique can reduce the severity of the disease, allowing collateral venous pathways to develop and relieving hepatic congestion. Balloon dilatation alone does not provide definitive patency. Metallic endovascular stents may improve long-term results.

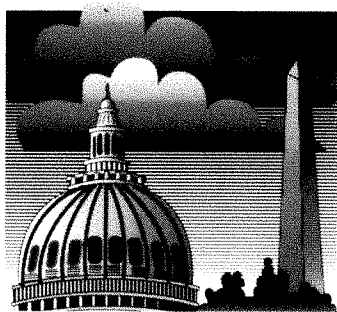
Total patient time in the lithotripsy suite, positioning of the patient, and the effectiveness of shock-wave treatment were analyzed and studied by Rendon C. Nelson and colleagues of Atlanta, GA, to aid in planning of biliary extracorporeal shock-wave lithotripsy (ESWL). Focusing the shock-wave path toward the stone is critical; this important aspect stresses the primary role of the radiologist when performing biliary ESWL. Ease of focusing on larger stones may explain why treatment time is shorter with larger stones than with smaller and multiple stones.

J. R. Mathieson and colleagues of Vancouver, Canada, studied the ability of sonography to assess the number and size of gallstones and their fragments after ESWL. They concluded that sonography is accurate for counting and measuring up to six stones. By sonography, one can ascertain that more than six stones are present, but one cannot be specific if the number is greater than six. Gallstone fragmentation after lithotripsy can be assessed in some cases; however, substantial errors can be made when many stones or fragments are present or when the gallbladder is contracted.

Dissolution time of gallstones may vary depending on the solvent and the technique used. J. Cox and colleagues from San Diego, CA, described in vitro experiments with a variety of solvents and methods to dissolve simulated gallstones (100% cholesterol pellets). Dissolution was augmented by increased rapidity of ingress and egress of methyl *tert*-butyl ether (MTBE). The study confirms the effectiveness of MTBE over other solvents and demonstrates the potential of a newly designed catheter-agitation system. This project provides laboratory support for the agitation of MTBE to dissolve cholesterol stones.

Guidelines for the selection of patients, procedural considerations, and follow-up for percutaneous gallstone dissolution with MTBE were discussed by Eric vanSonnenberg, San

Diego, CA. The radiologic workup includes plain film radiography, sonography, oral cholecystography, and CT. Exclusion criteria include stones with significant calcification or a thick gallbladder wall. The need to stop the procedure if the amount of MTBE injected is not retrieved was stressed. Evacuation of MTBE is required to prevent sedation, hemolysis, and renal failure. Basketing may be needed as a supplementary procedure for stones or fragments that do not dissolve. Percutaneous cholecystostomy was successful in 23 of 25 patients, dissolution alone in 15 of 20, dissolution and basketing in three of three, and percutaneous stone removal alone in three of three patients. Dissolution of bile duct stones occurred in three of five patients.



Scientific Program (200 papers)

Instructional Courses (60 hours)

Categorical Course on
Cardiovascular Imaging

The Caldwell Lecture

Award Papers

Scientific Exhibits

Social, Golf, and Tennis Programs

Guest Programs



Come to the
American Roentgen Ray Society

90th

ANNUAL MEETING

Washington, D. C.

Sheraton Washington Hotel

May 13-18, 1990

1989 ARRS Gold Medals

Ronald G. Evens

Jules Blouin & Associés



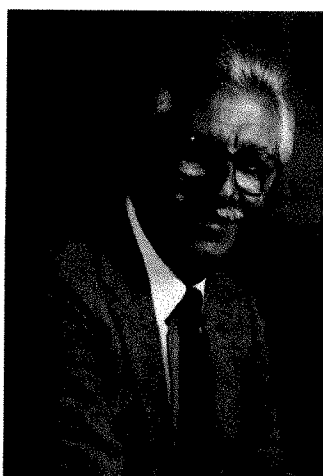
Robert Gordon Fraser

Only a few professors can influence a generation of physicians by their scholarly work. Robert Gordon Fraser is such an individual. Nearly every practicing radiologist has read his textbook on diagnosis of diseases of the chest, which was first published in 1970 and is now in its third edition. Medical texts of importance are based on a scholarly career of clinical experience and research. Dr.

Fraser is a product of Canada with early experience in Toronto and Winnipeg and a brief visit to the United States in 1947 (a year of residency in pathology at Washington University School of Medicine in St. Louis). This early year in pathology was undoubtedly important to a radiologist who has influenced tens of thousands of physicians of all specialties about the importance of radiologic and pathologic correlation. In association with Professor Paré at McGill University in Montreal, he created the subspecialty of chest radiology to the benefit of millions of patients worldwide.

Dr. Fraser has been a member of the American Roentgen Ray Society since 1959 and has served the Society in a variety of roles, including delivering the Caldwell Lecture in 1973. We are not the first society or organization to honor him; he has delivered more than 20 named lectures throughout the world and has been honored by more than 20 scientific societies. His scholarship is extraordinary and his leadership is well known. He has been the president or vice-president of the Canadian Association of Radiologists, the Fleischner Society, and the American Roentgen Ray Society. The chest radiograph has been the most common radiologic examination for at least 90 years and is likely to remain a major examination into the next century. The ability of radiologists to interpret chest radiographs and relate the findings to an interpretation appropriate for all clinicians is strongly influenced by the scholarly work of Dr. Fraser. For contributions to our specialty and our society, we give our gold medal to Robert Gordon Fraser.

Elison-Alexandre



Raymond A. Gagliardi

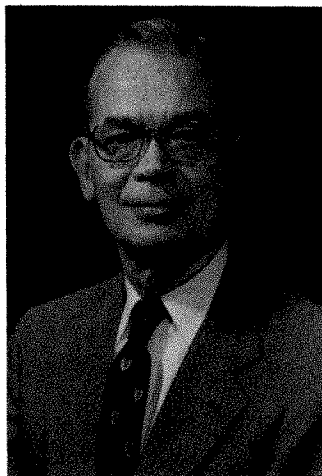
Ray Gagliardi was elected to membership in the American Roentgen Ray Society in 1972, and the society soon changed for the better. His leadership skills were recognized quickly, and he has held increasingly responsible positions for the past 15 years. As chairman of the Publications and Editorial Policy Committee (1974–1980), he became the driving force in making the *American*

Journal of Roentgenology a scientific publication in the very top echelon of peer-reviewed journals. Critical changes in people, policy, and publishers were all brought to reality under his leadership. As secretary of the society (1980–1986), he was "Mr. Roentgen Ray" and stimulated the Executive Council and its officers to bring new life to the oldest radiologic society in the United States. This society dramatically increased its membership, developed a new meeting format, and expanded its role in the specialty of radiology. His influence continued as he became the chairman of the Program Committee (1987–1988) and president (1987–1988).

Dr. Gagliardi is more than a leader of this society. His personal interest in gastrointestinal radiology is demonstrated by an impressive curriculum vitae of clinical papers focusing on the gallbladder and intestinal tract. He also serves as a clinical professor at Wayne State University and as a senior examiner in gastrointestinal radiology for the American Board of Radiology. A graduate of Yale University and Medical School, he obtained his residency and training in radiology at the same institution. Moving to Michigan in 1954, he began his distinguished career with continuing associations at St. Joseph's Mercy Hospital (serving as Radiologist-in-Chief for the last 30 years) and at Wayne State University.

The American Roentgen Ray Society has been blessed by a series of prominent radiologists and scientists who have devoted significant portions of their professional career to its mission of education. Only a few of the society's members are worthy of the gold medal. For leadership to our specialty,

and especially to the American Roentgen Ray Society, Raymond A. Gagliardi is awarded our highest honor, the gold medal.



Harry Z. Mellins

Most radiologists would find success by influencing one facet of radiology or one of its subspecialties—a rare individual is a man (or woman) “of all seasons.” Harry Z. Mellins is a clinician, teacher, researcher, and leader extraordinaire. His professional career has been primarily associated with New York and Massachusetts but includes important responsibilities in Minnesota, Michigan, and Mississippi. In every location,

he has been honored as a teacher and scientist. Making important contributions in subspecialties of gastrointestinal radiology, chest radiology, and especially noted for genitou-

rinary radiology, he also has published important papers about lymph nodes and microcirculation. His career has influenced hundreds of radiologists and thousands of medical students.

A member of the American Roentgen Ray Society since 1956, he served in many leadership positions, ultimately as our president in 1977–1979, a term of more than 1 year during the important transition from a fall to a spring meeting. He also has been a leader of other organizations, dedicating the time to serve as the president of several societies, including the Brooklyn Radiological Society, New York Roentgen Ray Society, the Association of University Radiologists, and the Society of Uroradiologists. He has given more than 15 named lectures throughout the country, including for example, lectures dedicated to such famous radiologists as Sosman, Stauffer, Rigler, and Holmes.

In 1959, Dr. Mellins was named the outstanding teacher of the year by the medical students of the State University of New York in Brooklyn. What an honor for any radiologist. This radiologist was again honored 20 years later by the medical students at Harvard, when he received the Boylston award.

How fortunate is our specialty to have a dedicated clinician/scientist/teacher. The American Roentgen Ray Society has the privilege of honoring a former president and internationally known physician with its gold medal.

89th Annual Meeting of the ARRS: Secretary's Report

Glen W. Hartman¹

The 89th annual meeting of the American Roentgen Ray Society (ARRS) was held May 7–12, 1989, at the New Orleans Hilton Riverside and Towers Hotel in New Orleans, LA. The meeting drew a record number of registrants who selected from a diverse menu of excellent scientific sessions, scientific exhibits, and refresher courses by day; superb cuisine in the evening; and fine weather all week.

The meeting officially began on Monday morning with the installation of Ronald G. Evens of St. Louis, MO, as the 89th president of the ARRS. He was installed in his new office by retiring President Lee F. Rogers and Executive Council Chairman A. Everette James, Jr. In his presidential address, Dr. Evens identified several challenges facing our specialty and proposed innovative initiatives. His thoughtful comments are published in this issue of the *AJR*, and you are encouraged to read his address in its entirety.

Dr. Evens and his Scientific Program Committee selected papers covering all phases of radiology for the scientific program, which began on Monday. One hundred eighty-nine papers covering all recent developments in diagnostic radiology were presented at the meeting.

Under the direction of Joseph T. Ferrucci, Jr. and Robert J. Stanley, 60 instructional courses were offered. These sessions continue to be highly popular segments of the program, and the total attendance at the courses easily eclipsed prior records.

The categorical course for 1989 on genitourinary radiology was arranged by Howard M. Pollack and attracted over 600 attendees. A thorough update on genitourinary radiology is provided in the syllabus prepared by the faculty and edited by Dr. Pollack. The categorical course will remain an important element of the educational program next year, when William J. Casarella will arrange a course on cardiovascular disease.

The Friday symposium, "Gastrointestinal Radiology 1989: New Problems, New Solutions" featured an outstanding faculty under the direction of Dennis M. Balfe. Musculoskeletal radiology will be the focus of the 1990 Friday symposium.

Over 200 scientific exhibits were viewed daily by a large number of attendees. John E. Madewell and the Scientific Exhibits Committee selected superb exhibits, which were well arranged with ample room for deliberate viewing and study. The Case of the Day was centrally located in the hall, and

several challenging cases were presented under the direction of Marilyn J. Siegel.

The abstracts of the award-winning scientific exhibits appear elsewhere in this issue. The three major awards were Gold Medal for "Applications of Color-Flow and Spectral Doppler Ultrasound in the Evaluation of Vasculogenic Impotence," by Jeffrey P. Quam, Bernard F. King, Duane M. Brakke, E. Meredith James, and Ronald W. Lewis of Rochester, MN; the Silver Medal for "Lasers in Biliary Obstruction: Feasibility of Fluoroscopically Guided Application," by Abraham H. Dachman, James A. McGehee, Thomas E. Beam, Anthony C. Venbrux, Robert Hoyt, and Jennifer A. Burris of Bethesda, MD; and the Bronze Medal for "Reassessment of Factors Governing Interface Resolution," by Enrique Pantoja, Candace L. Kabler, and Ching P. Li of Dayton, OH.

The Special Awards Program was held on Wednesday, and three award papers were presented by radiology residents. The President's Award, with an honorarium of \$1000, was given to James M. Larson for his paper, "The Validity and Utility of Ultrasound in the Diagnosis of Appendicitis in the Community Setting." Co-authors were John C. Peirce, Douglas M. Ellinger, Gregory H. Parish, Dennis C. Hammond, and Clifton F. Ferguson. The Executive Council Award papers, each with an honorarium of \$500, were "Biochemical Correlation of the Magnetic Resonance Appearance of Experimentally Induced Cerebral Hemorrhage in the Rat," by Keith R. Thulborn, A. Gregory Sorenson, Neil W. Kowall, Ann McKee, Albert Lai, Robert C. McKinstry, John Moore, Bruce R. Rosen, and Thomas J. Brady, and "Variations in Forearm Muscle Structure and Function: Importance in MR Spectroscopy," by James L. Fleckenstein, Loren A. Bertocci, Ray L. Nunnally, Robert W. Parkey, and Ronald M. Peshock. The Executive Council Awards were given in memory of Franklin L. Angell and Thomas C. Beneventano.

The Gold Medal of the ARRS for distinguished service to radiology was presented by President Evens to Robert G. Fraser of Birmingham, AL; Raymond A. Gagliardi of Pontiac, MI; and Harry Z. Mellins of Boston, MA. The three recipients were recognized not only for their contributions to the ARRS, but also for their outstanding service to the field of radiology.

The 68th Caldwell Lecture was presented by the Honorable Bill Bradley, United States senator from New Jersey. His

¹ Secretary, American Roentgen Ray Society, Dept. of Radiology, Mayo Clinic, 200 First St., S.W., Rochester, MN 55901.

speech, "Health Care Choices for the Nineties," and a follow-up question-and-answer session were well received by a large, attentive audience. Senator Bradley's appearance was an exciting addition to the program, and the society owes a debt of gratitude to President Evens and John K. Crowe for arranging his visit.

A record number of attendees and guests actively participated and enjoyed the social programs arranged by Abner M. Landry, Jr., who served as chairman of the Committee on Local Arrangements. He also organized the annual golf tournament, which was held at the English Turn Country Club in New Orleans. The Manges and the Exhibitor trophies were both claimed by Carl J. Zylak. The award for the tennis championship was given in honor of Robert N. Cooley and was claimed by Richard Jacobs. The winner of the ladies' tennis tournament was Renata Rigney.

Once again, the ARRS/ACR luncheon speakers presented timely and informative topics, which included "Mammography Screening" by Gerald D. Dodd, "RVS Update" by James M. Moorefield, "Standard Setting" by Jerome H. Shapiro and "Government Issues" by Otha Linton.

The entire Executive Council joins me in expressing appreciation to all faculty members, committees, and directors of various programs for their contributions to the success of the annual meeting. Meetings of superb quality such as this annual meeting of the ARRS can occur only when everyone

involved fulfills their commitments. This is especially appreciated because it is done on a volunteer basis.

During the ARRS business meeting, the following officers were elected for 1989-1990: President-Elect, M. Paul Capp; First Vice President, John A. Kirkpatrick; Second Vice President, A. Everette James, Jr.; Secretary, Glen W. Hartman; and Treasurer, Beverly P. Wood. Committee members elected were Executive Council, Albert A. Moss (5-year term); Publications and Editorial Policy Committee, William J. Casarella (5-year term); Annual Meeting Committee, John K. Crowe (5-year term); Scientific Exhibits Committee, Ruth G. Ramsey (3-year term); Finance and Budget Committee, John R. Thornbury (3-year term); and Advisory Committee on Education and Research, William M. Thompson (5-year term).

The Society was pleased to welcome 419 new active members, 32 corresponding members, and a large number of members-in-training.

Plans are under way for the 1990 meeting at the Sheraton Washington, Washington, DC, May 13-18. This hotel is located in a quiet section of Washington, DC, and will provide excellent facilities for a springtime meeting in the nation's capital. President-Elect M. Paul Capp will be the director of what promises to be an outstanding educational experience. Watch for future announcements of the program in this Journal.

The 1989 ARRS Annual Meeting Sets New Records: Administrative Report

Paul R. Fullagar¹

The 89th annual meeting of the American Roentgen Ray Society (ARRS), held May 7–12, 1989, in New Orleans, LA, set meeting attendance records for the second year in a row. Nearly 2700 registrants were present, of whom 1943 were radiologists.

The biggest impact in attendance was in the instructional courses, with over 10,200 persons attending the 60 courses during the 4 days. The program, expanded by four afternoon courses this year, was partly responsible for the increase, but as Joseph Ferrucci, chairman of instructional courses, pointed out: "There were more courses selected by each registrant and for more days." This is shown by the large number of registrants still attending on the last day, reversing past trends of reduced attendance on that day.

When the 648 registrants for the categorical course on uro-radiology and the 556 registrants for the Friday symposium on gastrointestinal radiology are considered, total net course attendance was 11,425, up from the previous record of 10,869 of last year.

The number of scientific exhibits remained constant at the 1988 number of 245. There were more exhibits submitted, but the number of exhibits that can be displayed is dictated solely by the space available in the meeting hotel. This year the maximum amount of available space was used again, and the exhibit area remained a major draw for attendees. The number of technical exhibitors held constant; however, several exhibitors could not be accommodated because of conflicting dates. This year, we will be providing a planning prospectus to the technical exhibitors several months earlier than in the past to avoid potential conflicts.

A distinct highlight of the meeting was the Caldwell Lecture, delivered by Senator Bill Bradley (D-NJ). The ballroom was

nearly filled to its capacity with 1500 attentive listeners, who gave the senator a rousing standing ovation. His many comments on health care issues and his several possible solutions to many existing problems also were greeted with the same enthusiastic ovation. The content of Senator Bradley's lecture is contained elsewhere in this issue of the *AJR*.

The 90th annual meeting, scheduled for May 13–18, 1990, in Washington, DC, promises to maintain the trend of the last 2 years of continued growth in meeting attendance and the quality of the scientific programs presented. Washington has always been a successful meeting location because of the hotel site and the attractiveness of the city and all it has to offer.

As pointed out in the past, the success of the meeting goes beyond the simple accumulation of numbers as presented here, but this seems to be the only objective way to make the analysis. We recognize all of the member and volunteer efforts that must be made for many months before and during the meeting, and the many favorable comments from attendees to that effect must be mentioned although such comments are difficult to quantify. We believe that through this committed effort the meeting has been able to remain enjoyable while maintaining the highest scientific and educational goals.

The officers, Executive Council, and committee members join me in an open invitation to join us in Washington in 1990 for what promises to be another superb meeting, under the guidance of M. Paul Capp, president-elect and chairman of the Program Committee.

Detailed information about the 1990 meeting will be in the February issue of the *AJR* and will be available from the ARRS office in Reston, VA, after February 1, 1990.

¹ American Roentgen Ray Society, 1891 Preston White Dr., Reston, VA 22091.

ARRS Award-Winning Scientific Exhibits, 1989

More than 215 scientific exhibits were displayed at the ARRS 1989 meeting in New Orleans. The Committee on Awards selected three medal winners and named 26 exhibits for certificates of merit.

Elsewhere in this issue are an application form and instructions for submitting scientific exhibits for the 1990 ARRS meeting in Washington, DC, May 13–18.

Gold Medal Exhibit

Applications of color flow and spectral Doppler sonography in the evaluation of vasculogenic impotence. Quam JP, King BF, Brakke DM, James EM, Lewis RW (Rochester, MN).

Vasculogenic impotence may result from arterial or venous insufficiency. Recent reports have described the utility of duplex Doppler with spectral analysis in the evaluation of this entity. One hundred twenty patients with suspected vasculogenic impotence (age range, 21–82 years; mean, 55.8 years), were evaluated at the Mayo Clinic from October 1987 to July 1988. All patients were studied with conventional duplex Doppler with spectral analysis and color Doppler imaging (Acuson, Mountain View, CA). Both corpora cavernosal arteries were evaluated in the flaccid state and 5 min after the intracavernosal injection of 60 mg of papaverine. Peak systolic velocity and lowest diastolic velocity were measured in addition to the diameter of each cavernosal artery, before and after papaverine. Of the 120 patients studied with duplex Doppler and color Doppler, 69 had cavernosometry and cavernosography, 84 had nocturnal penile tumescence evaluation, 77 had brachial penile index measurements, and five had arteriography. Fifty-four patients were treated surgically, 28 patients had vein ligation, 22 had prosthesis implantation, three had microvascular surgery, and one had aortic balloon dilatation. The data obtained with color flow and spectral Doppler studies are compared with the findings on cavernosometry, arteriography, and clinical studies to determine the role of Doppler in the evaluation of these patients.

Silver Medal Exhibit

Lasers in biliary obstruction: feasibility of fluoroscopically guided application. Dachman AH, McGehee JA, Beam TE, Venbrux AC, Hoyt R, Burris JA (Bethesda, MD).

Fluoroscopic guidance of the Nd:YAG laser has been limited to intravascular work. We devised an animal model and applied the laser to the common bile duct in dogs, in order to study the factors affecting a controlled laser burn with fluoroscopic guidance. If control can be achieved, this technique might be applied to tumors of the common bile duct in humans.

We controlled and limited the damage by using fibers with artificial sapphire contact probes and applying the laser only while pulling the probe retrograde. Fourteen laser applications were done in 13 dogs. Laser energies of 15, 20, and 25 watts, and pull back rates of 0.3 and 0.5 cm/sec were used. Pre and post laser cholangiograms and

videotapes of the fluoroscopy were used to measure tension on the duct wall by the probe (angular torque). The gross specimen was resected, photographed, and sectioned for microscopy. The depth and circumference of laser damage was estimated from the superficial burn to frank perforation. Angular torque seems to be the most important factor determining damage, followed by power and pull-back rate.

Bronze Medal Exhibit

Reassessment of factors governing interface resolution. Pantoja E, Kabler CL, Li CP (Dayton, OH).

Since radiography is but a graphic record of tissue interfaces, knowledge of the factors governing their resolution should facilitate interpretation. Most factors are well known (tissue contrast, beam quality, etc.) but two are not: (1) length of beam tangency to the interface along the path of the rays and (2) the ratio of interface thickness to total thickness of the part. This exhibit is based on a study of interfaces of various materials and shapes, carefully machined and x-rayed with accurate beam alignment. It demonstrates with experiments and clinical examples the effect of the last two factors on interface resolution.

Certificate of Merit Exhibits

Velopalatine incompetence: the radiologist's role. Barr LL, Hayden CK Jr, Hill LC, Swischuk LE (Galveston, TX).

Developmental defects of the diaphragm. Robinson AE, Eberly SM, Palmon L, Varma DGK, Mulvihill DM (New Orleans, LA).

MR in pediatric head and neck lesions. Yuh WTC, Sato Y, Kao SCS, Gray SD, Smith WL (Iowa City, IA).

Unusual causes of polyhydramnios. Belfar HL, Britton CA, Hill LM, Martin J, Longley DG (Pittsburgh, PA).

Pitfalls in the ultrasonographic diagnosis of pyloric stenosis. Swischuk LE, Hayden CK (Galveston, TX).

Comparison of CT and MR imaging in musculoskeletal neoplasm (complementary or overkill). Tehranzadeh J, Mnaymneh W, Ghavan C (Miami, FL).

MR imaging of the temporomandibular joint: correlation with operative findings. Port RB, Mikhael MA, Canzona JE (Evanston, IL).

The role of duplex sonography in the evaluation of groin masses in the intravenous drug abuser. Endress C, Gray D, Guyot DR, Tolliver J (Detroit, MI).

Approach to lytic bone lesions: a computer-based interactive tutorial. Mayer JS, Dittrich DL, Nayeri A, Hite M, Sabatelli FW, Seotin AG, Moore E, Madewell JE (Hershey, PA).

Abnormalities of the azygos system: CT evaluation. Dudiak CM, Olson MC, Posniak HV (Maywood, IL).

Hand arteriography: a forgotten study revisited. Tishado J (Richmond, VA).

Political trends in vascular and interventional radiology: a randomized survey. Smith TP, Cragg AH, Berbaum KS (Iowa City, IA).

Intraventricular mass lesions in children: CT and MR imaging characteristics. Fanney DR, Altman N (Miami, FL).

MR imaging of the basal ganglia. King DE, Mawad ME, Goodman JC, Bryan RM (Houston, TX).

Duplex and color flow analysis of the vertebral artery: the sonographic spectrum of subclavian steal syndrome. Magnuson JE, Reading CC, James EM (Rochester, MN).

Pulmonary arterial hypertension. Randall PA, Heitzman ER, Gordon L, Scalzetti E, Williams S, Markarian B, Bull M (Syracuse, NY).

Anatomic variations in the chest simulating disease. Proto AV (Richmond, VA).

Radiographic features of recurrent breast carcinoma after segmental resection and radiation therapy. Baratz AB, Harris KM, Greco MG, Britton C, Fukui M, Poller WR (Pittsburgh, PA).

CT and MR of the pericardium. Olson MC, Posniak HV, McDonald V, Monuada R (Chicago, IL).

Diffuse lung disease: nongravitational physiologic analysis. Gurney JW, Bates FT, Krasnow AZ, Goodman LR, Isitman AT (Omaha, NE).

Multiple nonpalpable breast lesions: should all lesions undergo biopsy? Linden CN, King PS, Cox CE, Clark RA (Tampa, FL).

Mammographic-pathologic correlations: malignancies and benign conditions that mimic malignancy. Bassett LW, Jahanshahi R, Chang B, Gold RH (Los Angeles, CA).

Pitfalls and differential diagnosis in biliary sonography. Rosenthal SJ, Cox GG, Wetzel LH, Batnitzky S (Kansas City, KS).

Endorectal sonographic staging of rectal carcinoma. Coffey SL, Jochem RJ, Reading CC, Charboneau JW, James EM, Dozois RR, Wolf BG (Rochester, NY).

Renal sinus sonography: anatomy, pitfalls, and pathologic conditions. Patel N, Kumar R, Kinkhabwala M, Wengrover S (Newburgh, NY).

Pitfalls in CT appearance of adrenal metastases. Halvorsen RA, Parker AL, Pierre A, Yankaskas BC (Minneapolis, MN).

American Roentgen Ray Society New Members

At the 1989 annual meeting of the American Roentgen Ray Society (ARRS) in New Orleans, LA, 419 applicants were elected to active membership and 32 to corresponding membership. Five hundred eleven applicants were added to in-training membership during the year preceding the 1989 annual meeting. The following member was elected to life membership in recognition of his contributions to the society and the specialty of radiology: Jerome F. Wiot.

Active members of the society must be graduates in good standing of an approved medical or osteopathic school or hold an advanced degree in one of the physical, chemical, or biologic sciences. They must be board certified, active in

radiology or one of its branches in the United States or Canada, and sponsored by two ARRS members.

Members-in-training are physicians in a radiology residency or in a postresidency fellowship program.

Corresponding members are physicians residing in foreign countries who are active in the science of radiology or allied sciences.

An application form is printed elsewhere in this issue or may be obtained by writing: Paul Fullagar, Executive Director, American Roentgen Ray Society, 1891 Preston White Dr., Reston, VA 22091.

Active Members

Kenneth H. Abbott, II, Smithville, TN
 Paul Joseph Daniel Abramson, Decatur, GA
 Jagan M. Ailani, Carbondale, IL
 Abbas Alaghemand, Yonkers, NY
 H. Russell Albright, New Orleans, LA
 Clyde R. Allen, Laurel, MS
 Nancy Allen, Middletown, CT
 Anna Marie Arenson, Toronto, Canada
 Ashokkumar R. Babaria, Cherry Hill, NJ
 Daniel R. Backlas, Metairie, LA
 John H. Bair, Boulder, CO
 Emmet H. Balch, Euless, TX
 John W. Barr, Orinda, CA
 Ira Eugene Bell, III, NCMH Chapel Hill, NC
 Debbie L. Belovich, Camp Hill, PA
 Yoram Ben-Menachem, Seattle, WA
 Lawrence N. Bennett, North Wilkesboro, NC
 Joel S. Benveniste, North Palm Beach, FL
 Richard Thomas Bergeron, Brooklyn, NY
 David Lynn Berry, Upland, CA
 Korth E. Bingham, Coronado, CA
 Brent Betts Birkin, Las Vegas, NV
 Bradley A. Blackburn, Chesterland, OH
 Gail Elizabeth Blakeley, Las Cruces, NM
 Stephen Michael Blum, Chicago, IL
 Carl Robert Bogardus, Jr., Oklahoma City, OK
 Sherwin Morton Borsuk, Meriden, CT
 Robert E. Boucher, Bow, NH
 Michael B. Brady, Memphis, TN
 Marshall Lee Brewer, Sioux Falls, SD
 R. Barton Bridges, Belleville, IL
 Paula W. Brill, New York, NY
 William R. Brody, Baltimore, MD
 Valerie A. Brookeman, Charlottesville, VA
 Jerry M. Brown, San Antonio, TX
 Steven A. Brown, Los Angeles, CA
 Ruth Govier Brush, Houston, TX
 Charles Edward Buckley, Potomac, MD
 Deland Darrell Burks, San Diego, CA
 Robert Andrew Burris, Kenner, LA
 George William Butz, Jr., Winter Haven, FL
 Gilberto Cadavid, San Antonio, TX
 Arthur Alphonso Castagno, Edmonds, WA
 Dennis Michael Chalus, Englewood, CO
 Judith Lynn Chezmar, Atlanta, GA
 Tilden Lafayette Childs III, Fort Worth, TX
 Kedar N. Chintapalli, San Antonio, TX
 Octavio Gregorio Choy, Fairfield, CT
 Pauline Kae Chu, Redlands, CA
 Peter Douglas Clarke, Boston, MA
 William Max Cloud, Springfield, MA
 Jessica Margaret Cohn, Boston, MA
 Ralph M. Colburn, Madison, WI
 Richard F. Cooper, Northville, MI

Alfred Benjamin Coren, East Syracuse, NY
 Luther H. Creed, Las Vegas, NV
 Bradley K. Cruz, Vacaville, CA
 Rand James Cuthbertson, West Point, NY
 Dvora Cyriak, Santa Ana, CA
 Frank Thomas Daly, Jr., Atlanta, GA
 Joseph J. Dariak, New Orleans, LA
 Charles M. Davis, Americus, GA
 Deborah Lee Day, Minneapolis, MN
 Baz P. DeBaz, Beachwood, OH
 Ronald E. DeCesare, Edina, MN
 Joseph H. Delaney, Seattle, WA
 Todd Andrew Denholm, Hanover, NH
 Bruce James Derauf, Mendota Heights, MN
 Rajendrakumar M. Desai, Houston, TX
 Drew H. Deutsch, Fox Island, WA
 Rosalind Brown Dietrich, Glendale, CA
 Jacques Edgar Dion, Mailibu, CA
 Robert Henry Dorwart, Shelburne, VT
 Richard R. Drummond, Potomac, MD
 Charles C. D. DuMontier, Belleville, IL
 David Marc Einstein, Orange Village, OH
 Gail Eliot, Bloomfield, NJ
 Jacob A. Epstein, Berkeley, CA
 Yasoda Eranky, San Antonio, TX
 Adel S. G. S. Escarous, Katonah, NY
 Gregory N. Famum, Garden Grove, CA
 Timothy P. Farrell, Mechanicsburg, PA
 Jeffrey M. Feinstein, Hinsdale, IL
 John J. Fennessy, Chicago, IL
 Solon L. Finkelstein, Palo Alto, CA
 John J. Fitzpatrick, Oak Lawn, IL
 Anthony E. Foderaro, Harleysville, PA
 Robert C. Fortenberry, New Orleans, LA
 Isaac Rajumar Francis, Ann Arbor, MI
 Siobodan E. Franic, Oakville, Canada
 Harris A. Freed, Orange Village, OH
 Joseph L. Frerkes, Belen, NM
 Geoffrey D. Friefeld, Denver, CO
 David Jay Frolich, Macon, GA
 Dean R. Fullingim, Tulsa, OK
 Milton Gallant, West Orange, NJ
 Jeffrey Reed Galvin, Iowa City, IA
 Edward L. Garman, Spokane, WA
 Spencer B. Gay, Charlottesville, VA
 Cornelia Golimbu, New York, NY
 Denise G. K. Gray, Detroit, MI
 William H. Green, Wallingford, PA
 S. Bruce Greenberg, Cheltenham, PA
 Thomas Lee Greer, Hamlin, NY
 David Christopher Gregg, Milwaukee, WI
 William E. Greiner, Seattle, WA
 Henry John Louis Griffiths, Minneapolis, MN
 Larry A. Grissom, Houston, TX
 Kevin David Gustafson, Eden Prairie, MN
 Ralph Aaron Gutierrez, San Antonio, TX
 Betsy Hauge Guyer, Portland, OR

Dean D. Hageman, Belleville, IL
 Dwight Perry Hager, Edina, MN
 Julia E. Halasz, Valencia, CA
 William Joseph Halden, Jr., Reston, VA
 Gary Lane Halversen, Salt Lake City, UT
 Jefferson Daniel Hanks, Jr., Rome, GA
 David Robert Hassell, Mobile, AL
 Donald Ross Hawes, Iowa City, IA
 Michael Robert Hay, Sylvania, OH
 Leonard M. Heinz, Sylvania, OH
 Robert Park Henderson, Jackson, MS
 Alan T. Hennessey, Dearborn, MI
 John Francis Hennessey, Meriden, CT
 Robert Edward Charles Henry, Jr., Eagle River, AK
 Stephen Marc Hershowitz, Washington, DC
 Frank Ronald Hetrick, Napa, CA
 Robert C. Hewes, Kettering, OH
 Cheryl Susan Hicks, Americus, GA
 Alice O. Hinton, Nashville, TN
 Angelena Ho, Ann Arbor, MI
 Brian Yow Bun Ho, Richmond, Canada
 Mark J. Hoffman, St. Louis, MO
 Paul A. Holdener, Belleville, IL
 Hiroshi Honda, Iowa City, IA
 Joseph R. Hooyman, Waterloo, IA
 Patricia A. Hudgins, Atlanta, GA
 Henry Hen Lee Huey, Vancouver, Canada
 Rebecca Lee Hulet, Wichita Falls, TX
 Clifford R. Jack, Jr., Rochester, MN
 Richard Peter Jacobs, Hopkinton, MA
 James Anthony Jagodzinski, Toledo, OH
 Meade B. Johnson, San Marino, CA
 Trent Andrew Johnson, Franklin, NC
 Patrick Francis Joyce, St. Louis, MO
 Paul R. Julsrud, Rochester, MN
 Herbert J. Kadison, Wichita, KS
 Daniel C. Karnicki, Beaumont, TX
 Joseph A. Kearney, Greensburg, PA
 Bernadette Keefe, Chapel Hill, NC
 Leland Kellerhouse, San Diego, CA
 Robert K. Kerlan, Jr., Del Mar, CA
 Arfa Khan, Muttontown, NY
 Kenneth L. Kidd, Santa Barbara, CA
 Bernard F. King, Rochester, MN
 Joseph G. King, Lexington, KY
 Nina B. Klionsky, Rochester, NY
 Robert E. Knack, Binghamton, NY
 Walter James Knickerbocker, Vancouver, Canada
 Herbert J. Koerner, Peru, NY
 David Kramer, San Jose, CA
 Steven Thomas Krueckeberg, St. Paul, MN
 Wayne S. Kubal, Pittsburgh, PA
 Barbara K. Kunkel, Harrisburg, PA
 William Arthur Ladd, Chula Vista, CA
 Barry M. Lamont, Slingerlands, NY
 John C. Lappas, Indianapolis, IN
 Joseph L. LaRosa, Columbus, OH

Joan L. Lasser, Warwick, RI
 William L. Lavidas, Tulsa, OK
 Stephen Paul Lee, Dallas, TX
 Hemlata K. Lepkowski, Columbia, MO
 Robert M. Lerner, Rochester, NY
 James W. Lester, Lackland AFB, TX
 Bertram Levin, Chicago, IL
 Van L. Lewis, Roanoke, VA
 Frederick C. Lindemann, Sheridan, WY
 William K. Littman, Cincinnati, OH
 Edward Michael Liu, San Jose, CA
 Thomas G. Loflin, Birmingham, AL
 Ian Leslie Love, Joplin, MO
 Bruce Paul Lovett, Albuquerque, NM
 Robert L. Ludwig, Briarcliff Manor, NY
 Alan Leslie Lurie, San Diego, CA
 James D. MacGibbon, Minneapolis, MN
 Thomas Edward MacIsaac, Leawood, KS
 Steven Mark Mandelblat, Tampa, FL
 Alfred A. Mansour, Jr., Monroe, LA
 Alberto Jose Martinez, San Diego, CA
 M. Victoria Marx, St. Louis, MO
 Lynn Harris McCorkle, Baltimore, MD
 Timothy John McCormack, Concord, NH
 Thomas F. McKay, Rupert, ID
 Gary Shannon McKee, Scottsdale, AZ
 Michael A. McKusick, Rochester, MN
 John H. McMillan, Kansas City, KS
 Robert Gerald Messell, Flushing, NY
 David G. Meyer, Greensburg, PA
 Jean-Guy Michaud, Longueuil, Canada
 Daniel L. Miller, The Woodlands, TX
 Joseph Paul Miller, San Antonio, TX
 Stephen Michael Miller, Beverly Hills, CA
 William B. Miller, Jr., Mechanicsburg, PA
 Michael Raymond Milner, Lake Park, GA
 Steven P. Mitchell, Palo Alto, CA
 Robin J. Mitnick, New York, NY
 Yusuf Mryusiwalla, Waterloo, Canada
 Timothy E. Moore, Iowa City, IA
 Jonathan Spaulding Moulton, Cincinnati, OH
 Michael Eugene Mulligan, Honolulu, HI
 Mark D. Murphy, Overland Park, KS
 Hasan Nabhani, Washington, DC
 Jo Ann Neely, San Francisco, CA
 Courtney Cardell Neff, Warblehead, MA
 Kenneth M. Neigus, Philadelphia, PA
 David W. Nelson, Portland, OR
 Martha C. Nelson, Washington, D.C.
 Donald Eric Newman, Vancouver, Canada
 Dale Christopher Newton, Seattle, WA
 Vung D. Nguyen, San Antonio, TX
 James J. Norconk, Jr., Seattle, WA
 Yuji Numaguchi, Baltimore, MD
 John F. O'Connor, Westwood, MA
 Louise S. O'Shaughnessy, San Diego, CA
 John Carl Osmer, Castro Valley, CA
 J. Hal Owsley, Hickory, NC
 Richard Luis Pajares, Albuquerque, NM
 Robert H. Paley, Washington, D.C.
 John Steven Pallin, Little Rock, AR
 Jorge G. Pardes, Brooklyn, NY
 Thomas Holman Parker, Longmeadow, MA
 Suhas Gajanan Perulekar, Cleveland, OH
 Parashuram R. Pimpapureddy, Staten Island, NY
 Etta D. Pisano, Newton, MA
 John J. Pittari, Bainbridge, GA
 Joseph F. Polak, Jamaica Plain, MA
 Joseph J. Porada, Homewood, IL
 Prasanna S. Prabhu, Jacksonville, FL
 Amalya Premkumar, Oradell, NJ
 Harry C. Press, Jr., Washington, D.C.
 William Edmund Prominski, Fayetteville, NC
 Stephen F. Quinn, Portland, OR
 Mitchell Rabinowitz, Easton, PA
 Irene Phillips Raisis, Greenville, DE
 Kumudha Ramanathan, Garden City, NY
 John Frederick Rasmussen, Gainesville, FL
 Janak K. Raval, Long Beach, CA
 David D. Reed, Wichita, KS
 Lester Russ Reichsk, Ft. Bragg, CA
 John E. Reifsteck, Charleston, WV
 Mark S. Reinsel, Tulsa, OK
 Russell J. Reit, San Diego, CA
 Karen L. Reuter, Worcester, MA
 William Leggett Ritchie, Edmonton, Canada
 James Alan Robinson, York, PA
 Jeff M. Robinson, Rome, GA
 Edward Victor Ross, Metairie, LA
 Peter A. Ross, Island Park, NY
 David Jerome Rotzfeld, Riverdale, MD
 Scott J. Rowen, Irvine, CA
 Stephen Eli Ruben, Newton Square, PA
 Robert James Rust, Granger, IN
 Ronald Melvin Rust, College Station, TX
 Elliot J. Sandberg, Aurora, CO
 Lyle Thomas Saylor, Owings Mills, MD
 Kurt P. Schellhas, St. Louis Park, MN

Mark L. Schiebler, Carrboro, NC
 Joel A. Schneider, Hollywood, FL
 Carl N. Schofield, Lexington, KY
 Daniel G. Schwartzberg, Atlanta, GA
 Robert Anthony Scott, Villa Hills, KY
 Purna Sharma, Tucker, GA
 Chung I. Shaw, Richmond, VA
 Steven E. Sheffner, Ann Arbor, MI
 Carol V. Sheldon, Oklahoma City, OK
 Hang Chang Shen, Chesterfield, MO
 J. Robert Shepherd, Lindale, TX
 John J. Siess, Hastings-on-Hudson, NY
 Oscar David Silverstein, Birmingham, MI
 David Michael Simms, Auburn, ME
 Stuart M. Simms, Huntingdon Woods, MI
 Rolando D. Singson, New York, NY
 Roberta Moore Slater, Valdosta, GA
 Gene Carl Smigocki, Lititz, PA
 Daniel G. Sommer, Oak View, CA
 David A. Sparks, Charleston, WV
 Gerald E. Staab, Shawnee Mission, KS
 Jehuda J. Steinbach, Gainesville, FL
 James R. Stevenson, Albuquerque, NM
 Richard P. Stewart, Camp Hill, PA
 Martin James Strandness, North Oaks, MN
 Natalie Strutytsky, New York, NY
 Stephen William Subber, Denver, CO
 David Albert Swanson, Edina, MN
 Steven K. Teplick, Haddonfield, NJ
 Deborah C. ter Meulen, Concord, MA
 Robert John Douglas Tuttle, Hamilton, Canada
 Roger Headley Tutton, New Orleans, LA
 Ira Mark Taylor, New York, NY
 Terrence A. Tyrrell, Belleville, IL
 Evan Charles Unger, Tucson, AZ
 Robert R. Varney, Leucadia, CA
 Ashok Kumar Verma, Regina, Canada
 Andrei Vermont, Cambridge, MA
 Inna Vilinsky, Moreland Hills, OH
 Ronald C. Walker, San Francisco, CA
 Ellen M. Ward, Rochester, MN
 Jennifer J. Warner, Northbrook, IL
 Michael David Weaver, Greenville, NC
 Kenneth Lee Weiss, City Island, NY
 Scott Morrison Whiddon, Atoksis, NC
 Charles G. Wieland, Belleville, IL
 Daryl R. Wierda, Sioux Falls, SD
 Nathaniel H. Wiesenfeld, Wilkes-Barre, PA
 Charles R. Williams, III, Brookline, MA
 Kenneth David Williams, Rochester, NY
 C. Amy Wilson, Philadelphia, PA
 Keith David Wilson, Sylvania, OH
 Alan Wirk, Xenia, OH
 Robert H. Wise, Jr., Valdosta, GA
 Gerhard R. Wittich, Portola Valley, CA
 Kevin Keith Woisard, El Paso, TX
 Mary J. Wood, Shreveport, LA
 David Murray Woods, Dundas, Canada
 Donald R. Yandow, II, Madison, WI
 K. K. Hsiao-Fang Yen, Wichita, KS
 Horatio H. Yeung, Chadds Ford, PA
 John Robert Yoder, Toledo, OH
 Thomas J. Zambarano, Mechanicsburg, PA
 Hilary Zarnow, Wichita, KS
 Kenneth Zirinsky, New York, NY

Active Members (Formerly In-Training)

Marita B. Acheson, Seattle, WA
 Julie L. Adam, Woodinville, WA
 Gregory J. Allen, Everett, WA
 Stephen G. Babel, Albuquerque, NM
 Wanda I. Benitez-Lopez, Little Rock, AR
 Marc A. Bernstein, Rockford, IL
 Erol M. Beytas, Durham, NC
 Ann G. Bjorkengren, Lund, Sweden
 George O. Borrero, Pembroke Pines, FL
 Cecilia M. Brennecke, Baltimore, MD
 Jeffrey M. Brody, Arlington, VA
 Alan S. Brody, Buffalo, NY
 Patrick B. Brown, Seattle, WA
 Thomas K. Burkhard, San Diego, CA
 James D. Cates, Tampa, FL
 Felix Sza-Kway Chew, Syracuse, NY
 Layne R. Clemenz, Columbia, SC
 Lawrence M. Cohen, Chevy Chase, MD
 Michael Crain, Portland, CT
 Michael J. Cullenward, Madison, WI
 Nathaniel W. Cuthbert, Roanoke, VA
 Jeffrey Dwight Dieden, Lafayette, CA
 George R. Edmonson, Worcester, MA
 Audrey L. Eisenstadt, Brooklyn, NY
 Brian S. Fiedler, Milwaukee, WI
 Michael A. Foster, Aurora, CO
 Harold Friedman, Chicago, IL
 Kevin C. Funk, Idaho Falls, ID

Mitchell E. Gallagher, Billings, MT
 Lawrence E. Ginsberg, Riverdale, NY
 Margaret D. Gore, Chicago, IL
 Jon K. Guben, Miami, FL
 Carl W. Hardin, San Antonio, TX
 William Hastrup, Jr., Fresno, CA
 Jeremy J. Hollerman, Edina, MN
 Joseph G. Jackson, Macon, GA
 Craig B. Karsama, Utica, MI
 Debra A. Kimball, Fall River, MA
 Pamela J. Koch, Lancaster, PA
 James J. Kochkodan, Dearborn, MI
 Mark J. Kransdorf, Rockville, MD
 Richard B. Lawdahl, Greenville, SC
 David P. Lawrence, Mt. Pleasant, SC
 Scot A. LeBolt, Burke, VA
 Bradley D. Lewis, Rochester, MN
 Lien-Ching Lin, Powell, OH
 Roger C. Lind, Jr., Jackson, MS
 Sarah S. Linden, Ponte Vedra Beach, FL
 Karen R. Lundquist, Rochester, MN
 Marcia McAvoy, Baltimore, MD
 Kevin T. McManus, Toms River, NJ
 Bradley W. Miller, Bristol, TN
 Cassim Moola, Sault Ste. Marie, Canada
 Donald P. Mueller, Oklahoma City, OK
 David Joshua Mullen, New York, NY
 Peter L. Munk, Vancouver, Canada
 Lakshmana D. Narla, Richmond, VA
 Jeffrey S. Noodleman, Yorba Linda, CA
 William K. O'Neal, N. Quincy, MA
 Tien T. Peng, Arcadia, CA
 David N. Rabin, Glenview, IL
 Ranji N. Samaraweera, Chestnut Hill, MA
 Manash K. Sarcar, Shreveport, LA
 Rae W. Sawyer, White Stone, VA
 Leanne L. Seeger, Studio City, CA
 Lee A. Shratter, Walnut Creek, CA
 Marc F. Siegel, Sanford, FL
 Donald C. Simon, Okemos, MI
 Anne A. Smid, Springfield, MO
 Denise J. Smith, Phoenix, AZ
 Edward N. Smith, Silver Spring, MD
 Fred L. Steinberg, Boston, MA
 Sharon L. Stocking, Grand Blanc, MI
 Jana L. Sulzer, Tampa, FL
 Philip A. Templeton, Baltimore, MD
 F. Leland Thaele, Pittsburgh, PA
 Robert H. Thomas, Hoover, AL
 Beverly A. Trombley, Edina, MN
 Julian R. Vainright, Jr., Greenville, NC
 Ellsworth Weatherby, III, Gaithersburg, MD
 Harvey M. Wiener, Melbourne, FL
 James A. Wiese, Missoula, MT
 David A. Williamson, Jackson, MS
 Paul Wozney, Pittsburgh, PA
 Andrew Yang, Baltimore, MD
 Bradford A. Yeager, Allentown, PA
 Ronald J. Zagoria, Winston-Salem, NC
 Jeffrey H. Zapolsky, Wilbraham, MA

Corresponding Members

Bouaoun Amor, Paris, France
 Nicholas Charles George Bathurst, Box, Gloucestershire, England
 Johannes L. L. Bester, Fairland, Johannesburg, South Africa
 Johan L. Bloem, Voorsihoten, The Netherlands
 Eamann S. Breatnach, Dublin, Ireland
 Jose Caceres, Barcelona, Spain
 Young D. Cho, Pusan, Korea
 Byung Ihn Choi, Seoul, Korea
 Renzo Del Dabbro, Alzingen, Luxembourg
 Go Tjong Han, Rotterdam, The Netherlands
 Philip Hung, Sydney, Australia
 Jurgen Kollath, Frankfurt, West Germany
 Jose A. Perez Mendizabal, Naucalpan de Juarez, Mexico
 Edgar F. Mohr, Linz, Austria
 Yashiro Naoburni, Tokyo, Japan
 Henricus A. J. M. Overtoom, Amsterdam, The Netherlands
 Timothy T. C. Overtoom, Nieuwegein, The Netherlands
 Luc P. Paredis, Genk, Belgium
 Jae Hyung Park, Seoul, South Korea
 Marco Tulio Polanco, Guatemala City, Guatemala
 Michael Rado, Berghem, West Germany
 Hartmut Reiner, Offenbach, West Germany
 Helmut E. Riemann, Frankfurt, West Germany
 Jan Rijkmans, Akkmaar, The Netherlands
 Fabio Jose Rodriguez, Santiago, Dominican Republic
 Franz J. Schweden, Mainz, West Germany
 Mulan Shi, Beijing, China
 Tudor Sutton, Payenne, Switzerland
 Shigeo Takebayashi, Yokohama, Japan
 Jorge L. Vazquez, Tlalpan, Mexico
 Hermine J. Wieringa, Amsterdam, The Netherlands
 Chong Hyun Yoon, Seoul, Korea

Information and Application for Membership in the American Roentgen Ray Society

General Information

The American Roentgen Ray Society, founded in 1900, has been a forum for progress in radiology since shortly after the discovery of x-rays. From its beginning and continuing to today, the ARRS has been guided by dedication to the goal of the advancement of medicine through the science of radiology and its allied sciences.

The goal of the ARRS is maintained through an annual scientific and educational meeting, and through publication of the *American Journal of Roentgenology*.

The annual meeting consists of instructional courses, scientific sessions, a symposium, scientific exhibits, and commercial exhibits. A special categorical course is also offered. Category I CME credits are available on an hour-for-hour basis.

The monthly *American Journal of Roentgenology* is a highly respected peer review journal with a worldwide subscription base. For over 75 years the *AJR* has been accepted as one of the best specialty journals available in the world, and this reputation grows each month.

A recently developed quarterly ARRS newsletter keeps members informed of events and general Society news.

Application Instructions

Candidates for Active Membership

1. An Active member must be a graduate of an approved medical school or hold an advanced degree in one of the physical, chemical or biological sciences and be certified by the American Board of Radiology, the American Osteopathic Board of Radiology, the Royal College of Physicians of Canada, or document training and credentials that are adequate to qualify for membership. Active members shall actively practice radiology or one of its branches in the United States or Canada. Such members are eligible to participate in all activities of the Society, including membership on committees, and have full voting privileges.
2. Application must be on an official form, signed by the applicant and at least two members of the American Roentgen Ray Society, active or emeritus, in good standing, who endorse the applicant.
3. Application fee is \$50 (payable when billed for dues).
4. Annual dues are \$125, payable on January 1 of each year following the initial year. First year dues will be invoiced following candidate election at the annual meeting. Of this amount, \$50 is for a 1-year subscription to the *American Journal of Roentgenology*, beginning with the July issue following election to membership.
5. Application must be received by February 1 for action during the current year's meeting.

Candidates for In-Training Membership

1. In-training members must be serving in a radiology residency program approved by the Radiology Residency Review Committee, the American Osteopathic Board of Radiology, or the Royal College of Physicians of Canada, or in an approved post-residency fellowship, or be a postgraduate student in an allied science. Training status must be verified by the program director. In-training members have special consideration in fees and subscription rates to the Society journal. Such members cannot hold Society offices or vote.
2. Application must be on an official form and signed by the applicant and by the applicant's training or residency program director.
3. In-training status is limited to a maximum of five years starting with the entrance date into the radiology residency. In the last year, each in-training member will receive an application for active membership from the Society. Those who do not apply for transfer to active membership shall be dropped from membership at the end of the fifth year, but can later apply as a new member through the process outlined for active status.
4. There is no application fee. Annual dues are \$25. Membership includes a subscription to the *American Journal of Roentgenology* and admission to the annual meeting without payment of the registration fee.
5. Membership applications will be acted on when received.

Corresponding Membership

A corresponding member must meet the qualifications of active membership, but reside and practice in a foreign country. Corresponding members shall pay dues and fees, but shall not have the privileges of voting nor of holding elective office.

All Applicants

1. Do not remit application fee or dues until requested.
2. Send completed forms to: American Roentgen Ray Society
1891 Preston White Drive
Reston, Virginia 22091

For ARRS
Office Use

Date Rec'd _____

I.D.# _____

AMERICAN ROENTGEN RAY SOCIETY APPLICATION FOR MEMBERSHIP

Date: _____

Category of Membership: ☐ Active
(Check One) ☐ Corresponding
☐ In-Training

Name (Please Print) _____ Degree(s) _____
First Initial Last

Mailing Address _____ Date of Birth _____
Street/Box

City/State/Country _____ Zip Code _____ Telephone () _____

A. Education: (List name of institution, years attended, and degree and type received.)

Undergraduate: _____

Graduate (Medical School, Graduate School, etc.):

Postgraduate (Internship, Residency, Fellowship, etc.):

B. Licensure:

Licensed to practice _____ in _____ since _____
(Type) (State, Province, etc.)

C. Appointments/Memberships: (In-Training applicants: skip to Section F on reverse.)

Present Appointments: Academic _____

Hospitals _____

Memberships in Scientific Societies: _____

Offices or Committee Assignments: _____

Government Service (Military or Civilian) _____
(Position) (Years)

Continued on Reverse Side

D. Credentials:

I hereby certify that I was issued a certificate of qualification in _____
(Specialty)

in _____ by the _____
(Year) (Name of Qualifying Board)

Other Credentials: _____

Signature: _____

E. References:

We, active or emeritus members in good standing of the American Roentgen Ray Society, and acquainted with the applicant, do recommend him/her for membership in the Society. (Two references are required.)

Name (Please Print) 1. _____ 2. _____

Address _____

Signatures: _____

F. IN-TRAINING APPLICANTS MUST COMPLETE THIS SECTION**Credentials:**

I certify that I am serving as a Resident/Fellow in _____
(Specialty)

at _____ Date program began (begins): _____
(Name of Institution)

date program to end: _____ I understand that in-training membership is limited to
maximum of 5 years.

Applicant Signature: _____

Verification: (Program Director or Department Chairman *only*)

I certify that the applicant is in training at the institution named and qualifies for enrollment as a member-in-training of the American Roentgen Ray Society.

Name (Please Print) _____

Address: _____

Signature _____

Send completed form to: **American Roentgen Ray Society**
1891 Preston White Drive
Reston, Virginia 22091

Letters

Diagnostic Specificity: Proper Use

It has become increasingly apparent that confusion exists in the radiologic literature regarding the appropriate use of the term *specificity*. A representative example of this problem is the use of this term in the recent article, "Efficacy of MR vs CT in Epilepsy," by Heinz et al. [1]. The authors report in their conclusion that "MR is the most efficacious imaging test in the evaluation of seizure patients. . . . However, as MR has a high sensitivity but *poor specificity* [italics mine], CT may be done as a second procedure to try to distinguish neoplasm from thrombosed vascular malformations and other lesions."

When used in association with *sensitivity* and without any modifying adjective, the *specificity* of a diagnostic test or imaging technique is the true-negative rate of that test, that is, the percentage of nondiseased (normal) patients with a normal (negative) test result [2]. This important test characteristic is obtained by dividing the number of true-negative results by the sum of the true-negative and false-positive results. *Specificity* is the complement of the false-positive rate ($\text{specificity} = 1 - \text{false positive rate}$). In contradistinction to the statement by Heinz et al., the current MR literature and experience suggest a *high specificity* of the technique in evaluating the brain; few normal patients appear to have false-positive findings when this technique is used. Rarely, MR artifacts may result in false-positive studies, particularly with inexperienced observers. In reality, valid specificity data for brain MR are difficult to obtain because of the problems associated with confirming normal or negative studies with surgical or autopsy proof, the conventional gold standards. However, experience with imaging normal volunteers and studies that include clinical follow-up support a high specificity of MR of the brain.

In the context of their conclusion, it appears that Heinz et al. intended *specificity* to mean the limited ability of MR to characterize or differentiate between various types of epilepsy-producing lesions that share a similar appearance on standard MR pulse sequences. Most radiologists probably are aware of this intent, as the application of *specificity* in this manner is fairly common in the radiologic community: A survey of the abstracts presented at the 7th annual meeting of the Society of Magnetic Resonance Imaging [3] revealed that four of the eight abstracts that reported *specificity* used the term as a synonym for lesion characterization. Clinicians or epidemiologists may not be as familiar with or as tolerant of this application of *specificity*. If a study does not include normal subjects or patients without the disease being evaluated by a certain test, the specificity (true-negative rate) of that diagnostic test cannot be determined. Investigators

attempting to classify the imaging findings in a study of abnormal patients without a normal or control group, a common format of radiologic studies, should append the prefix *lesion* or *tissue* to the term *specificity*, or, more preferably, use the terms *tissue characterization* or *lesion discrimination*.

The need and rationale for radiologists to be precise in the use of statistical terms have been noted [4]. As diagnostic radiology and the radiologic literature, in particular, come under more zealous scrutiny by other physicians, biostatisticians, and governmental agencies [5], it becomes increasingly important for investigators and editors to insist on proper statistical terminology in order to maintain scientific credibility. The correct use of *specificity* is a small but significant step toward that goal.

Robert D. Harris
Dartmouth-Hitchcock Medical Center
Hanover, NH 03756

REFERENCES

1. Heinz ER, Heinz TR, Radtke R, et al. Efficacy of MR vs CT in epilepsy. *AJR* 1989;152:347-352
2. Sox HC, Blatt MA, Higgins MC, Marton KI. *Medical decision making*. Stoneham MA: Butterworth, 1988:109-110
3. *Magn Reson Imaging* 1989;7(Suppl 1) (abstracts)
4. Shuman WP. Incidence and prevalence: proper use (editorial). *AJR* 1985;145:649
5. Cooper LS, Chalmers TC, McCally M, Berrier J, Sacks HS. The poor quality of early evaluations of magnetic resonance imaging. *JAMA* 1988;259:3277-3280

Reply

As Dr. Harris has suggested, *specificity* was used in our paper [1] to mean the limited ability of MR to characterize or differentiate between various types of epilepsy-producing lesions that share a similar appearance on standard MR pulse sequences. *Lesion characterization* probably would have been a better term.

E. Ralph Heinz
Duke University Medical Center
Durham, NC 27710

REFERENCE

1. Heinz ER, Heinz TR, Radtke R, et al. Efficacy of MR vs CT in epilepsy. *AJR* 1989;152:347-352

Contrast Agents and the Ozone Layer

A recent "Progress in Radiology" report by Mattrey [1] reviews the use of perfluorooctylbromide (PFOB) as a contrast agent for CT, sonography, and MR imaging. The article fails to mention the environmental controversy surrounding this class of compounds.

Chlorofluorocarbons (CFCs) are man-made chemicals developed in the 1930s as refrigerator coolants. They are still used (sometimes under the brand name Freon) for this purpose and as blowing agents for styrofoam, solvents to clean computer chips, and propellants in aerosol cans. They are the agents principally responsible for destroying the ozone layer of the atmosphere. When released into the environment, CFCs eventually filter up into the stratosphere. There they are broken down by ultraviolet light, liberating chlorine, which in turn breaks down ozone. Ozone is the only gas in the atmosphere capable of blocking harmful ultraviolet B radiation. In addition, CFC molecules are 2000 times more efficient than CO₂ molecules at trapping heat from the earth, and they are estimated to account for up to 20% of global warming.

PFOB is a halon. Halons are closely related to CFCs, containing bromine as well as fluorine and/or chlorine atoms. They increasingly are used in fire fighting because they cause no water or chemical damage. Bromine is 100 times more destructive to the ozone layer than is chlorine.

The United States has banned these agents in aerosol cans and slowed their production for some other uses. However, worldwide production is increasing, particularly for automobile air conditioners. An international treaty to protect the ozone layer, the Montreal Protocol, went into effect in 1989, but it is already recognized as inadequate, and many scientists are calling for a total ban on the manufacture of CFCs and halons.

Ferris M. Hall
Beth Israel Hospital
Harvard Medical School
Boston, MA 02215

REFERENCE

1. Mattrey RF. Progress in radiology. Perfluorooctylbromide: a new contrast agent for CT, sonography, and MR imaging. *AJR* 1989;152:247-252

Reply

The lack of mention of the controversy surrounding the environmental impact of fluorochemicals in my report [1] was not an oversight; the role of perfluorooctylbromide (PFOB) in this controversy is trivial.

The fluorochemicals suspected of harming the ozone layer are the low molecular weight, highly volatile chlorofluorocarbons (CFCs) [2]. The 1987 Montreal Protocol calls for a 50% cut in consumption and production of the one- and two-carbon CFCs by 1999. Although it has been shown that CFCs can cause depletion of ozone, the percentage of change in ozone that is caused by CFCs as compared with that caused by nitrogen oxides and other gaseous substances released by industry, domestic heating, vehicles, volcanoes, and algae and by the natural variations between the peak and the trough of the solar sunspot cycle is controversial [3, 4]. More reliable measurement techniques than are presently available are needed to monitor the ozone layer and to determine the share of each offending agent [3]. The apparently lax timetable set by the Montreal Protocol is to give industry the opportunity to find replacements for these thermodynamically efficient, nontoxic, nonflammable, nonreactive, stable compounds with others that have similar properties but lack

the ability to harm the ozone layer [5]. CFCs were singled out from the various other offenders because their source is obvious and controllable. However, their replacement is proving to be difficult, expensive, and nontrivial. Alternative agents must permit smooth transition and yet not require the replacement of existing equipment such as refrigerators, air conditioners, and so forth [5].

It is true that the presence of bromine in the stratospheric ozone layer is potentially more destructive than chlorine because the two act synergistically. However, the very low levels of bromine detected in the ozone layer cannot account for the recorded depletion of ozone [2]. The halons implicated are the ones capable of reaching the ozone stratosphere in sufficient volumes. These agents are also made up of one or two carbon chains and are used mostly for fire fighting because of their favorable physicochemical properties. These halons also have been included in the Montreal Protocol and are subject to the same timetable set therein.

Although PFOB is a potential hazard to the ozone layer because of its molecular structure, its effect is insignificant for two reasons. The first is its molecular weight, which influences the volatility and the ability of PFOB to reach the stratosphere. Of the highly volatile low molecular weight CFCs, CHFCI₂ and CHF₂Cl, it is estimated that up to 3% and 12% of the volumes released reach the troposphere, respectively [6]. From the troposphere, where they are inert, a certain amount is carried upward by eddy diffusion to the stratosphere, where they are exposed to intense ultraviolet light. The low volatility of PFOB (17 mbar at 20°C), which is 100 to 1000 times less than that of the implicated CFCs, and its high molecular weight (499), which is five to six times heavier than the low molecular weight CFCs, decrease significantly its likelihood of reaching the troposphere or higher altitudes.

The second reason for the insignificant effect of PFOB is the volume that potentially will be released. Even if PFOB could reach the troposphere, the volumes used are minimal when compared with the volumes of CFCs used as refrigerants, aerosols, cleansers, solvents, fire extinguishers, for foam blowing, and so forth, which are estimated to be near 2 million tons each year, or even the nitrogen oxides that occur naturally or from combustion that have been detected in the stratosphere and implicated in the depletion of ozone [4, 6]. Usage of PFOB in diagnostic imaging would be as an oral contrast agent for MR and as an IV agent for CT and sonography. It is estimated that by 1995, the volumes of PFOB used for diagnostic imaging would be on the order of 400 tons/year (Alliance Pharm. Inc., La Mesa, CA, personal communication). The dosage or volume of PFOB required for MR is 10 times that required for CT or sonography. Because the probability that other agents may become available to compete with PFOB as an oral contrast agent is much greater than those that could compete with its CT or sonographic applications, the exact tonnage that will be used is uncertain. If 400 tons is the volume used, it would constitute 0.025% of the total amount of fluorocarbons used by 1995 and 0.05% by 1999, after the Montreal Protocol takes effect.

Given the small volumes that will be used and the low volatility and high molecular weight of PFOB that will limit its presence in the stratosphere, and its important and needed contributions to diagnostic imaging, the benefits far outweigh the risk. Indeed, in medical applications we face these issues daily. Regard, for example, the use of many radioisotopes with long half-lives in diagnostic and research applications and the gas anesthetics that are highly volatile, one- to three-carbon halons such as halothane (CF₃CHBrCl), teflurane (CF₃CHBrF), or halopropane (CF₂HCF₂CH₂Br) that are used in millions of procedures. Would we prefer to go back to ether?

Robert F. Mattrey
University of California, San Diego, Medical Center
San Diego, CA 92103

REFERENCES

1. Mattrey RF. Progress in radiology. Perfluorooctylbromide: a new contrast agent for CT, sonography, and MR imaging. *AJR* 1989;152:247-252
2. Thrush B. Causes of ozone depletion. *Nature* 1988;332:784-785
3. Where the world stands on ozone. *Nature* 1988;332:291
4. Bamber DJ, Healey PGW, Jones BMR, Penkett SA, Tuck AF, Vaughan G. Vertical profiles of tropospheric gases: chemical consequences of stratospheric intrusions. *Atmos Environ* 1984;18:1759-1766
5. Stevensen R. CFCs: alternatives on the starting blocks. *Chem Br* 1988;23:629-630
6. Seigneur C, Caram H, Carr RW Jr. Atmospheric diffusion and chemical reaction of the chlorofluoromethanes CHFCl_2 and CHF_2Cl . *Atmos Environ* 1977;11:205-214

Clinical Significance of Traumatic Pneumorrhachis

Traumatic cervical pneumorrhachis (air in the spinal canal) originally was described in a patient with basilar skull fracture [1]; the air was in the cervical subarachnoid space. A second example occurred in a patient who had fracture dislocation of the lumbar spine with entrapment and perforation of the jejunum [2]. It was not possible to determine whether the air was extradural or intradural. We have detected pneumorrhachis in a patient with traumatic pneumothorax.

A 25-year-old man complained of neck and chest pain after an automobile accident. A chest radiograph showed a left-sided pneumothorax and fractures of the left first and second ribs. A CT scan of the cervical spine (Fig. 1) showed air outlining the left C8 nerve root and pneumorrhachis. CT scans of the brain and abdomen were normal.

Pneumothorax should be considered an additional cause of pneumorrhachis. In this case, we think that air dissected from the pneumothorax into the soft tissues of the neck, along the nerve root sheath, and subsequently into an extradural location within the spinal canal.

On CT examination, extradural pneumorrhachis is difficult to differentiate from subarachnoid pneumorrhachis. Therefore, in patients with traumatic pneumothorax, the finding of pneumorrhachis on plain films or CT scans of the cervical spine should prompt further workup to rule out basilar skull fracture.

James N. Place
Roger T. Pezzuti
Maine Medical Center
Portland, ME 04102

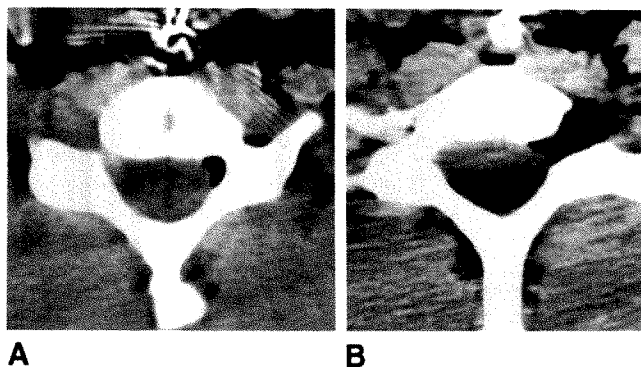


Fig. 1.—Traumatic pneumorrhachis.
A, CT scan of cervical spine at level of C8 nerve root shows air in lateral recess on left. Note marked soft-tissue emphysema.
B, CT scan 5 mm caudal to A shows air extending within left C8 neural foramen and around nerve root.

REFERENCES

1. Newbold RG, Wiener MD, Vogler JB, Martinez S. Traumatic pneumorrhachis. *AJR* 1987;148:615-616
2. Silver SF, Nadel HR, Flodmark O. Pneumorrhachis after jejunal entrapment caused by fracture dislocation of the lumbar spine. *AJR* 1988;150:1129-1130

MR Detection of Probable Hematopoietic Hyperplasia Involving the Knees, Proximal Femurs, and Pelvis

Before the publication of the recent article by Deutsch et al. [1], we saw a 36-year-old, moderately obese woman who had been having increasing pain in the left distal femur since removal of a giant cell tumor from the left lateral tibial plateau 1.5 years earlier. Frontal and lateral radiographs of the knee were normal except for the postsurgical bone packing changes in the left tibia.

A lower extremity $^{99\text{m}}\text{Tc}$ -MDP bone scan showed increased uptake only in the area of previous surgery. Because of persisting pain with ambulation, MR imaging was performed. The findings were interpreted as mixed signal changes in the area of bone packing. The patient was reassured that her pain was most likely postsurgical and that loss of weight should decrease the discomfort.

Seven months later, MR imaging of the knee was performed again because of persistent pain in the left knee. The mixed signal intensity at the previous surgical site was unchanged, when compared with the previous MR images. Mottled confluent areas of decreased signal intensity involving the bone marrow of the metaphysis of the left tibia, sparing the epiphysis, were seen on all pulse sequences (T1, T2, and proton density). These changes were present on the previous images and appeared to have increased in size. Similar MR findings were observed within the marrow space of the contralateral knee. Subsequent MR of the pelvis showed similar findings in the iliac crests, left acetabulum, and proximal femurs (Fig. 1).

The results of a peripheral blood smear, CBC with differential, and hemoglobin electrophoresis were all normal. A biopsy specimen of bone marrow from the left ilium initially was interpreted as normocellular with negative iron balance. The patient refused open femoral biopsy, and deeper sections of the original biopsy specimen were evaluated. They showed numerous well-circumscribed vascular sinusoidal spaces filled with erythrocytes that were thought to be

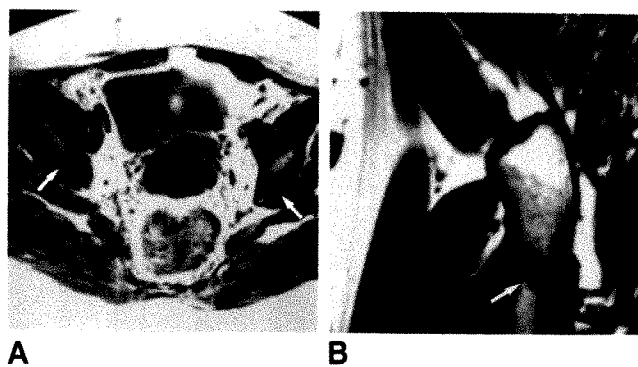


Fig. 1.—Probable hematopoietic hyperplasia.
A, Coronal MR image, 650/25, of pelvis shows mottled areas of decreased signal (arrows) within bone marrow of iliac bones.
B, Sagittal MR image, 800/20, of proximal right femur shows decreased signal (arrow) in bone marrow in metadiaphyseal region.

atypical but benign. A ^{99m}Tc -albumin colloid marrow scan showed increased uptake in the bone marrow of the distal humeri and femurs.

These findings are strikingly similar to those described by Deutsch et al. This patient is a moderately obese woman with areas of low signal within the bone marrow adjacent to the knees that were found incidentally on MR. This case differs in that the changes also were seen in the proximal femurs and pelvis, particularly the iliac crests, and in the left acetabulum. In addition, a bone marrow scan revealed changes consistent with hematopoietic marrow extension into the distal femurs and humeri. It is uncertain whether the apparent increase in the area of involvement over 7 months is related to the differences in pulse sequences from different MR units or is a result of increasing hematopoietic hyperplasia. It is known that the hyperplasia or fatty marrow reconversion occurs in the distribution shown by our MR images and marrow scans [2]. Interestingly, this patient's hematocrit was 31% (normal 35–47%) at the time of the surgery and is now normal. Finally, the vascular sinusoidal spaces seen on deeper sectioning of the bone marrow sections may, in part, account for the decreased signal observed on the MR images. It seems reasonable to extrapolate these findings to include the remainder of the involved bone marrow.

John E. Schuck
David J. Czarnecki
St. Luke's Medical Center
Milwaukee, WI 53215

REFERENCES

1. Deutsch AL, Mink JH, Rosenfelt FP, Waxman AD. Incidental detection of hematopoietic hyperplasia on routine knee MR imaging. *AJR* 1989;152:333–336
2. Vogler JB, Murphy WA. Bone marrow imaging. *Radiology* 1988;168:679–693

Reply

We thank Drs. Schuck and Czarnecki for sharing with us their recent experience with a case of hematopoietic hyperplasia encountered incidentally on an MR examination performed for evaluation of pain after removal of a giant cell tumor of the proximal tibia. We agree that the MR findings are similar to those described in our recent article [1] and are representative of hematopoietic hyperplasia. Interestingly, the patient described by Schuck and Czarnecki also was a moderately obese female, a clinical finding shared by a majority of the patients in our original report. A marrow scan performed with ^{99m}Tc -sulfur colloid showed increased uptake in the bone marrow of both the distal humeri and femora. MR of the pelvis also showed characteristic findings of hematopoietic hyperplasia in the pelvis and proximal femora.

Although in our experience with knee imaging we have continued to observe hematopoietic hyperplasia most commonly in obese women, we wish to emphasize that similar findings have been observed in several male patients, not all of whom have been obese. Although we have not had the opportunity to perform marrow scans on any of our patients, the increased uptake encountered in the patient reported by Schuck and Czarnecki is what would be expected with this process of marrow hyperplasia. Additionally, the findings within the pelvis and proximal femora on MR are entirely consistent with this process of hematopoietic hyperplasia. Since our original report, we also have performed "survey" MR on one patient, and we saw characteristic findings in the pelvis and the proximal femora and humeri. We often find small areas of decreased signal intensity in the medullary bone of the proximal humeri in patients undergoing shoulder MR for evaluation of suspected abnormalities of the rotator cuff.

We have presumed that these findings represent isolated foci of hematopoietic marrow, but we have not studied these patients critically.

As we suggested in our paper, it is likely that the incidental depiction of marrow abnormalities will be encountered more often, paralleling the increased use of MR in musculoskeletal imaging. Although the findings of hematopoietic hyperplasia eventually may be found to represent normal variants in most patients, we remain cautious in this regard, particularly when the findings are extensive.

Andrew L. Deutsch
Jerrold H. Mink
Cedars-Sinai Medical Center
Los Angeles, CA 90048

REFERENCE

1. Deutsch AL, Mink JH, Rosenfelt FP, Waxman AD. Incidental detection of hematopoietic hyperplasia on routine MR imaging. *AJR* 1989;152:333–336

Semiautomated Slide Identification by Using a Personal Computer and Printer

I read with interest Dr. Feuerstein's description [1] of his program for semiautomated slide identification by using a personal computer and printer. It is an excellent example of the usefulness of the personal computer for the professional needs of the everyday working radiologist. His article does not directly address the issues of slide storage and retrieval. I have found that the most efficient method for storage and retrieval of slides is to assign each slide a unique number and then store the slides in ascending numerical order in notebooks [2]. In my own case, I wrote a simple database program in which key words or subjects are entered for each slide, and the program then assigns the slide a number. For example, a slide showing a bronchogenic cyst on CT might be given the number 206 and have the following subjects entered into the program: chest, lung, mediastinum, anomaly, CT, bronchogenic cyst. The label on the slide itself would be "206, 57 y/o male with a bronchogenic cyst." There is no need to put CT on the slide label as it is evident from looking at the slide.

Retrieval of slide information is performed through sorting by the slide "subjects." I have found that using and searching on well-thought-out key words is far easier than using the American College of Radiology (ACR) Index for Radiologic Diagnoses. I do not have to look up or try to remember a complex numeric code. The important concept is the idea of numbering and storing slides in notebooks or boxes in consecutive numeric order rather than storing them by subjects. This has been advocated for a long time for journal reprints [3]. If a person is meticulous about labeling and placing slides in the proper place, the slides will never get out of order. If you store slides by the ACR index or by diagnoses, where do you place a slide that shows two disparate diagnoses? How would you store a slide showing a CT image of the pelvis with the presence of a pelvic abscess from diverticulitis and the presence of lymphoma involving pelvic lymph nodes? Is it stored with your CT slides, your pelvis slides, your abscess talk, or with its ACR index for lymphoma? In the consecutive numbering scheme, this slide would have its own unique number, and its location and the diagnoses would be available through the computer.

If you have 200 slides of various abscesses, they may be scattered from slide number 7 to number 3000. The computer remembers the exact location of each one. It is no real problem to walk over to the storage cabinet or bookshelves and pull down the proper boxes or notebooks to retrieve them. You can use any straightforward data-

base program to keep track of them, or write your own [2]. Dr. Feuerstein's program takes the work out of making labels for slides. It also allows for a filing code. Because he has made his program available to others, its code could be modified to give each slide its own number, and you would then have a program that does most of your slide housekeeping for you.

Tim B. Hunter
Arizona Health Sciences Center
Tucson, AZ 85724

REFERENCES

1. Feuerstein IM. Semiautomated slide identification by using a personal computer and printer. *AJR* 1989;152:861-863
2. Hunter TB. Managing one's slide collection. *Appl Radiol* 1987;16:25-26, 104
3. Reiman AS. Ripping and filing Journal articles. *N Engl J Med* 1984;311:925

Reply

I thank Dr. Hunter for his insightful commentary on my recent article [1]. His comments graphically illustrate the prime reason I wrote that paper. The beauty of home-grown computer programs is that they serve the individual programmer, performing specifically needed functions in a manner ideally suited to the user's requirements.

No one program can satisfy everyone's purposes, but persons might improve their own programs by assimilating small pieces from other programs. Extensively eliminating information about the case that appears on a slide would not work for me or for a helper who makes slides for other people. I trade a lot of slides, which would make the numbers meaningless, and I like filing slides by diagnoses because this method makes it much easier for me to assemble slides for lectures, and seeing material in one place helps me think about that material. It is a great feeling to reach into just one place and pull out the appropriate slides or articles on a subject, and for me that outweighs the potential disadvantages. On the other hand, I could incorporate Dr. Hunter's computer-generated number into the American College of Radiology (ACR) index line, or perhaps even better, I could modify Dr. Hunter's program to return the ACR index code that the slide is filed under.

I suspect that there is a great deal of useful, home-grown software in the offices of radiologists. If my article and these letters lead to an exchange of ideas and programs and promote development of other useful utilities, then some good has been done. For now, I am the proud owner of a copy of Dr. Hunter's SLIDE program, which I hope to modify and put to good use.

Irwin M. Feuerstein
Georgetown University
Washington, DC 20007

REFERENCE

1. Feuerstein IM. Semiautomated slide identification by using a personal computer and printer. *AJR* 1989;152:861-863

Subhepatic Abscess Caused by Appendicitis

A 22-year-old man had had progressive umbilical pain, vomiting, and fever for 2 days. At the time of admission, the pain had localized in the right upper quadrant. The body temperature was 39°C. Physical examination showed decreased bowel sounds and guarding with rebound tenderness in the right upper quadrant. WBC was 16,200/ μ l, and the differential count was normal. Plain films of the abdomen

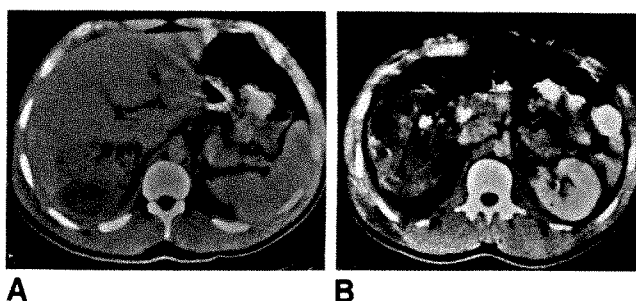


Fig. 1.—A and B, CT scans show heterogeneous collection in subhepatic space extending to level of upper pole of right kidney. Stippled gas collection within complex mass contains a focus of calcification (arrow).

showed calcifications in the right upper quadrant. A sonogram of the gallbladder was normal. CT scans showed a heterogeneous collection in the subhepatic space extending to the level of the upper pole of the right kidney. Stippled gas collection was noted within this complex mass, which contained a focus of calcification (density, 250 H) (Fig. 1).

At surgery, a subhepatic abscess associated with a perforated appendix and incomplete colonic malrotation was found. The appendix was in the right upper quadrant adjacent to the gallbladder and contained a large fecalith. Incision and drainage of the abscess and appendectomy were performed.

Anatomic variations in the position of the appendix result in unusual signs and symptoms of appendicitis. This is illustrated in this patient whose clinical findings initially suggested gallbladder disease.

Caroline Ngo
University of California, Los Angeles
Los Angeles County-Olive View Medical Center
Sylmar, CA 91342

Calcification of Metastatic Mucinous Carcinoma of the Liver After Embolization

We report a rare case of calcification after chemotherapy and therapeutic embolization of metastatic mucinous carcinoma. A 32-year-old woman had bloody stool and abdominal pain. Cancer of the sigmoid colon with hepatic metastases was detected by barium enema and sonography at another hospital. She was referred to our hospital for treatment. On admission, the serum level of carcinoem-

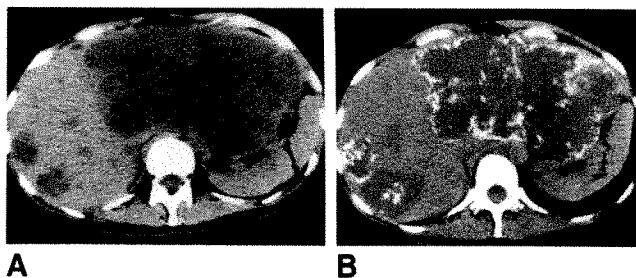


Fig. 1.—Calcification of metastatic mucinous hepatic carcinoma after embolization.

A, Initial CT scan shows metastases in both lobes of liver. No calcification is present, and approximate attenuation value of masses is 25 H.

B, CT scan made 7 months later, after embolization and chemotherapy, shows extensive calcification in periphery of metastases.

bryonic antigen (CEA) was 423 ng/ml (normal, <5.0 ng/ml). Unenhanced CT scans showed homogeneous low-density masses in both lobes of the liver without calcification (Fig. 1A). Pathologic examination of the resected sigmoid lesion showed mucinous carcinoma. Chemotherapy with cisplatin and 5-fluorouracil was administered for 1 month, but the CEA level did not decrease. Therefore, the appropriate hepatic artery was embolized with gelatin sponge. The CEA level decreased to 13.9 ng/ml during the next 4 months. The patient was readmitted 7 months after her first admission because of an increasing level of CEA. CT showed calcified deposits in the periphery of the hepatic tumors, especially in the left lobe (Fig. 1B).

The initial CT appearance of the hepatic metastases was that of metastatic mucinous carcinoma. The lesions had homogeneous low density, with no peripheral low-density areas on late enhanced scans [1]. Also, little or no change in the internal density of the tumors was observed on late enhanced scans. A few cases of calcified hepatic metastases from colorectal mucinous cancer have been reported, but the calcification occurred in the center of the metastases [2]. Scatarige et al. [3] noted that the calcification had no relation to medical treatment in two-thirds of cases. In the other one-third, the patients had had chemotherapy or external radiotherapy. The calcifications that occurred in our case appear to be the result of therapeutic embolization.

Yukio Muramatsu
Noriyuki Moriyama
Kenichi Takayasu
Tatsuya Yamada
National Cancer Center Hospital
Tokyo, 104 Japan

REFERENCES

1. Muramatsu Y, Takayasu K, Moriyama N, et al. Peripheral low-density area of hepatic tumors: CT-pathologic correlation. *Radiology* 1986;160:49-52
2. Lecky DM, Stein GN. Diagnostic procedure in evaluation of hepatic diseases: computed tomography. *Lab Res Methods Biol Med* 1983;7:317-354
3. Scatarige JC, Fishman EK, Saksouk FA, Siegelman SS. Computed tomography of calcified liver masses. *J Comput Assist Tomogr* 1983;7:83-89

Note.—The study reported in the preceding letter was supported in part by the Foundation for the Promotion of Cancer Research.

Obstructive Jaundice in Polycystic Disease of the Liver

A 56-year-old man had had progressively increasing jaundice for 1 month. Results of liver function tests indicated obstructive jaundice. A sonogram showed multiple hepatic cysts of various sizes; the largest was 5 cm and was near the porta (Fig. 1). The diameter of the common bile duct was 15 mm. Bilateral polycystic kidneys were seen also. An endoscopic cholangiopancreatogram showed medial displacement of the common hepatic bile duct with encasement and splaying of the intrahepatic radicles. The patient died before percutaneous aspiration of the cyst at the porta could be performed.

Though one-third of patients with polycystic disease of the kidney have cysts in the liver, compression of the bile ducts by these cysts sufficient to produce obstructive jaundice is uncommon and has been reported in only seven cases [1]. Surgical unroofing of the cysts is the recommended mode of treatment [1]; however, needle puncture and aspiration of the cyst compressing the bile duct are useful to alleviate jaundice temporarily [2].

Priti Shah
Ravi Ramakantan
King Edward Memorial Hospital
Bombay, India

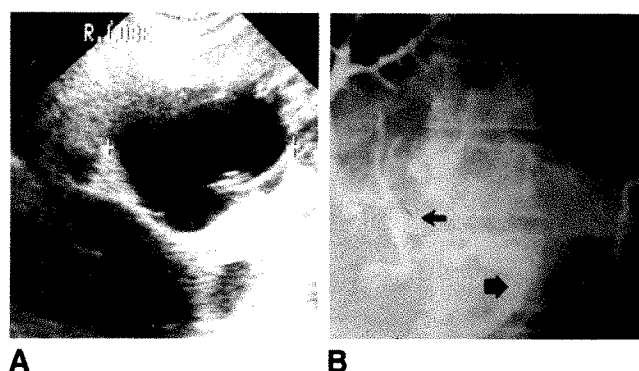


Fig. 1.—Obstructive jaundice in polycystic hepatic disease.
A, Sonogram of liver shows multiple cysts. Cursor delineates largest cyst near porta.
B, Frontal view from endoscopic cholangiopancreatogram shows extrinsic mass displacing common bile duct (large arrow) with poor opacification of a long segment of common hepatic bile duct (small arrow).

REFERENCES

1. Wittig JH, Burns R, Logmire WP. Jaundice associated with polycystic liver disease. *Am J Surg* 1978;136:383-386
2. Jones WL, Mountain JC, Warren KW. Symptomatic non-parasitic cyst of the liver. *Br J Surg* 1974;61:118-119

Transcatheter Arterial Embolization for the Treatment of Ruptured Hepatocellular Carcinoma

Rupture of the tumor is not a rare complication of hepatocellular carcinoma [1]. Partial hepatectomy, ligation of the hepatic artery, packing, and suture are treatment choices [1]. However, these procedures cannot be performed in patients who have severe liver dysfunction or poor general condition. We present a case of ruptured hepatocellular carcinoma with marked liver dysfunction that was treated successfully with transcatheter arterial embolization.

A 36-year-old man was admitted because of abdominal pain. He had been followed in the outpatient clinic for advanced cirrhosis and hepatocellular carcinoma. Laboratory data before admission included the following: prothrombin time, 22.6%; serum albumin, 3.4 g/dl; total bilirubin, 4.2 g/dl; SGOT, 72 IU/dl; and SGPT, 49 IU/dl. Pleural effusion and ascites had persisted despite administration of diuretics and albumin supplements. On admission, the patient was in acute distress. Because he was known to have hepatocellular carcinoma, rupture of the tumor was suspected. Paracentesis revealed bloody ascites. He soon became hypotensive and unconscious. Transcatheter arterial embolization was performed without delay to control the bleeding. Right hepatic angiography showed a tumor stain 10 cm in diameter in the right lobe. Transcatheter arterial embolization was performed by using 2-mm cubes of gelatin sponge. A minimal amount of contrast medium was used. After treatment, the bleeding ceased, and the vital signs became stable. The patient was discharged on the 28th day of hospitalization.

Transcatheter arterial embolization has been performed widely for the treatment of hepatocellular carcinoma [2]. A few reports have described its use for treatment of a ruptured tumor [3, 4]. Although it is less invasive than surgical procedures, embolization is not used in patients who have severe liver dysfunction because of the possibility of causing hepatic failure.

However, prognosis in cases of ruptured tumor that are treated conservatively is extremely poor; the mean survival time is approximately 2 weeks [3]. Thus, transcatheter arterial embolization should be considered for immediate treatment of ruptured hepatocellular

carcinoma even in patients who have severe liver dysfunction or are in poor general condition.

Shuichiro Shiina
Kenji Ibukuro
Mitsui Memorial Hospital
Tokyo, 101 Japan

REFERENCES

1. Chearanai O, Plengvanit U, Asavanich C, Damrongsak D, Sindhvananda K, Boonyapisit S. Spontaneous rupture of primary hepatoma: report of 63 cases with particular reference to the pathogenesis and rationale treatment by hepatic artery ligation. *Cancer* 1983;51:1532-1536
2. Yamada R, Sato M, Nakatsuka H, Nakamura K, Takashima S. Hepatic artery embolization in 120 patients with unresectable hepatoma. *Radiology* 1983;148:397-401
3. Nouchi T, Nishimura M, Maeda M, Funatsu T, Hasumura Y, Takeuchi J. Transcatheter arterial embolization of ruptured hepatocellular carcinoma associated with liver cirrhosis. *Dig Dis Sci* 1984;29:1137-1141
4. Ohta H, Nomoto M, Ozaki T, et al. A clinical study of ruptured hepatocellular carcinoma. *Jpn J Gastroenterol* 1987;84:690-697

Scrape Biopsy of Malignant Biliary Stricture: What Advantage Does the New Technique Offer?

Yip et al. [1] describe a do-it-yourself technique for converting a smooth vessel dilator into a barbed biopsy instrument. During the course of biliary drainage procedures, they were able to pass this jagged device through the strictured duct, and they obtained cytologic samples indicative of malignancy in nine of 15 patients. As pointed out by the authors, the results were equal to those obtained by using a standard biopsy brush [2, 3]. We would like the authors to explain the advantages of this device compared with the biopsy brush. Why do they encourage readers to use this new technique?

James B. Naidich
Kenneth S. Crystal
North Shore University Hospital
Manhasset, NY 11030
Cornell University Medical College
New York, NY 10021

REFERENCES

1. Yip CKY, Leung JWC, Chan MKM, Metreweli C. Scrape biopsy of malignant biliary stricture through percutaneous transhepatic biliary drainage tracts. *AJR* 1989;152:529-530
2. Mendez G Jr, Russell E, Levi JU, Koolpe H, Cohen M. Percutaneous brush biopsy and internal drainage of biliary tree through endoprosthesis. *AJR* 1980;134:653-659
3. Cropper LD, Gold RE. Simplified brush biopsy of the bile ducts. *Radiology* 1983;148:307-308

Reply

We thank Drs. Naidich and Crystal for their letter about our recent article [1]. By the technique described, nine (60%) of 15 biopsy

specimens were positive for malignant cells; four (27%) showed cellular atypia suggestive of malignancy, and two (13%) were negative for malignant cells. Retrospectively, the results in chronologic order were A, +, A, A, +, +, -, A, +, - (lymphoma), +, +, +, +, +. (A = cellular atypia, + = malignant cell positive, - = malignant cell negative.) We noted that the cases of cellular atypia occurred in the first half of the study. This may be explained by improvements in the fashioning of the scraper and technique used during the biopsy in the second half of the study. The sensitivity in the second half of the study was 6/7 (85%). The Cook Company (William A. Cook, Melbourne, Australia) is going to make a kit, and this will be helpful to standardize the biopsy instruments.

For brush biopsy, Mendez et al. [2] inserted the brush into a 6-French catheter, and the biopsy specimen was taken near the stricture. Cropper and Gold [3] modified the technique by first inserting a guidewire through the biliary stricture and then inserting a 9-French sheath above the stricture. Then the brush, which is inside a 5- to 6-French catheter, is advanced alongside the guidewire and through the stricture, and the biopsy is performed. As the brush and the supporting catheter are inserted only alongside the guidewire, we find the brush/catheter sometimes difficult to engage or to negotiate into the stricture. Prolonged manipulations may be needed, or the brushings can be taken only near but not in the stricture. The scraper, however, is a hollow instrument and can follow the guidewire through the stricture without difficulty. It is faster and more direct. It scrapes through the stricture instead of near the stricture. The scraper's flaps are sturdier than the brush and more likely to scrape cells from the submucosal layer. The scrape biopsy technique may be superior if the bile duct lesion is still covered by a mucosal layer. In the study by Cropper and Gold [3], four (57%) of seven cases were positive for malignant cells, and three (43%) were false-negatives. For the scraper's technique, the false-negative rate was only 13%, and one of the two false-negatives was lymphoma, in which cytologic diagnosis may be difficult. The scrape biopsy technique has fewer false-negatives. Although cellular atypia (27%) was not counted as positive, its discovery prompts further investigation, such as fine-needle aspiration.

In conclusion, we have found the scrape biopsy technique a simple, speedy, safe, and inexpensive technique.

C. K. Y. Yip
J. W. C. Leung
M. K. M. Chan
C. Metreweli
Prince of Wales Hospital
Shatin, New Territories, Hong Kong

REFERENCES

1. Yip CKY, Leung JWC, Chan MKM, Metreweli C. Scrape biopsy of malignant biliary stricture through percutaneous transhepatic biliary drainage tracts. *AJR* 1989;152:529-530
2. Mendez G Jr, Russell E, Levi JU, Koolpe H, Cohen M. Percutaneous brush biopsy and internal drainage of biliary tree through endoprosthesis. *AJR* 1980;134:653-659
3. Cropper LD, Gold RE. Simplified brush biopsy of the bile ducts. *Radiology* 1983;148:307-308

Letters are published at the discretion of the Editor and are subject to editing.

Letters to the Editor must not be more than two double-spaced, typewritten pages. One or two figures may be included. Abbreviations should not be used. See Author Guidelines, page A5.

Material being submitted or published elsewhere should not be duplicated in letters, and authors of letters must disclose financial associations or other possible conflicts of interest.

Letters concerning a paper published in the *AJR* will be sent to the authors of the paper for a reply to be published in the same issue. Opinions expressed in the Letters to the Editor do not necessarily reflect the opinions of the Editor.



AMERICAN JOURNAL OF ROENTGENOLOGY

MELVIN M. FIGLEY FELLOWSHIP IN RADIOLOGY JOURNALISM

The American Roentgen Ray Society announces a one-month fellowship in radiology journalism in the La Jolla editorial office of the AJR. Board-certified radiologists with special academic promise are invited to apply.

PURPOSE

The purpose of the fellowship is (1) to stimulate bright young radiologists to continue with an academic career, to accelerate their progress, and to stimulate their interest in good radiology journalism, and (2) to improve the quality of radiology journals by teaching the fundamentals of medical journalism to academicians, training manuscript reviewers and future editors, and providing core teachers of medical journalism in radiology departments around the country.

CURRICULUM

The fellow will be taught the fundamentals of medical writing, manuscript preparation, peer review, manuscript editing, the ethics of scientific journalism, and journal publication and printing in personal tutorials given by the AJR editors and editorial staff through hands-on experience in the editorial office. He or she will visit Williams & Wilkins in Baltimore to observe the publication and printing process.

STIPEND

The successful candidate will be awarded \$10,000, which includes the cost of travel to La Jolla and Baltimore, living expenses for the month, and an honorarium.

APPLICATIONS

Candidates should apply in writing to Robert N. Berk, M.D., Editor-in-Chief, AJR Editorial Office, 2223 Avenida de la Playa, Suite 200, La Jolla, CA 92037. The letter must include a curriculum vitae and a description of the candidate's goals during the fellowship. Letters of recommendation from his or her department chairman and one other senior person are required. Deadline for receipt of applications is Nov. 1, 1989. The successful candidate will be notified Dec. 1, 1989, and may choose one of the following months for the fellowship training: Jan., Feb., March, April 1990.

Review of Current Literature

Initials and addresses of corresponding authors are provided in parentheses for each article so that the reader can obtain reprints directly. Abstracts are printed verbatim from each journal.

The New England Journal of Medicine

Analgesic use and chronic renal disease. Sandler DP, Smith JC, Weinberg CR, et al. (DPS, Epidemiology Branch, MD A3-05, National Institute of Environmental Health Sciences, P. O. Box 12233, Research Triangle Park, NC 27709). *N Engl J Med* 320:1238-1243, May 1989

To examine the use of analgesics as a cause of chronic renal disease, we performed a multicenter case-control study of 554 adults with newly diagnosed kidney disease (serum creatinine, $\geq 130 \mu\text{mol}$ per liter [1.5 mg per deciliter]) and 516 matched control subjects selected randomly from the same area of North Carolina. Histories of use of analgesics (phenacetin, acetaminophen, and aspirin) were obtained by telephone interview with the patients or their proxies.

Daily users of analgesics had significantly more renal disease than infrequent users (odds ratio, 2.79; 95 percent confidence interval, 1.85 to 4.21). The risk of renal disease was highest in daily users of phenacetin (odds ratio, 5.11; confidence interval, 1.76 to 14.9, after adjustment for the effects of other analgesics). The risk of renal disease was also increased in daily users of acetaminophen; after adjustment for the use of aspirin and phenacetin, the odds ratio was 3.21 (confidence interval, 1.05 to 9.80). There was no increased risk in daily aspirin users (adjusted odds ratio, 1.32; confidence interval, 0.69 to 2.51). The risks with daily use of either phenacetin or acetaminophen changed little after adjustment for diabetes, hypertension, and the indication for analgesic use.

We conclude that the long-term, regular use of phenacetin may increase the risk of chronic renal disease. The long-term, daily use of acetaminophen, the major metabolite of phenacetin, is associated independently with an increased risk of chronic renal disease. We could find no increased risk in daily users of aspirin.

Bronchial hyperresponsiveness to methacholine in patients with impaired left ventricular function. Cabanes LR, Weber SN, Matran R, et al. (LRC, Service de Cardiologie, Hôpital Cochin, 27 rue du Faubourg St-Jacques, 75014 Paris, France). *N Engl J Med* 320 (20):1317-1322, 1989

To elucidate the pathogenesis of bronchospasm in congestive heart failure, we studied 23 patients with chronic impairment of left ventricular function due to coronary artery disease or dilated cardiomyopathy. In 21 of them we found marked bronchial hyperresponsiveness to methacholine. The mean dose (\pm SD) of methacholine that elicited a 20 percent decrease in the forced expiratory volume in

one second (FEV₁) was $421 \pm 298 \mu\text{g}$, nearly the same as in patients with symptomatic asthma. In contrast, there was no bronchial response to methacholine in 9 of 10 patients who had coronary artery disease but normal left ventricular function.

Administration of the bronchodilator albuterol led to a partial (43 percent) reversal of the methacholine-induced bronchial obstruction. In 12 patients, pretreatment with the alpha-adrenergic agonist methoxamine (10 mg by inhalation), a potent vasoconstrictor, fully prevented the methacholine-induced decrease in FEV₁. The protective effect of methoxamine was blocked by the alpha-adrenergic antagonist phentolamine in all six patients who received this agent.

We conclude that bronchial hyperresponsiveness to cholinergic agonists is frequent in patients with impaired left ventricular function and may contribute to the wheezy dyspnea commonly observed in such patients. The bronchoconstriction may be mediated at least in part by dilatation of the bronchial vessels.

Cancer

Epidural metastases in prospectively evaluated veterans with cancer and back pain. Ruff RL, Lanska DJ (RLR, VA Medical Center 127(W), 10701 East Blvd., Cleveland, OH 44016). *Cancer* 63:2234-2241, 1989

Ninety-five male veterans with cancer and back pain were prospectively evaluated for epidural metastases. The evaluation included vertebral roentgenograms and a myelogram. The most common cancers were lung and prostate. Forty-three percent of the patients had an epidural metastasis, including 73% of the 37 patients with myelopathy and 48% of the 29 patients with radiculopathy. None of the 29 patients who had back pain without radiculopathy or myelopathy had an epidural metastasis. Thirty-seven patients were treated with only radiation therapy and dexamethasone and four also had surgical decompression. Nineteen of the 20 patients who could walk at diagnosis walked after completion of therapy, whereas, only 11 of the 21 patients who were not ambulatory at the time of diagnosis walked after completion of therapy. The probability of surviving 12 months was 73% for patients who could walk after treatment and 9% for nonambulatory patients. Emergency spinal canal imaging is warranted in cancer patients with back pain and signs or symptoms of radiculopathy or myelopathy.

Reprinted by permission from the American Cancer Society.

Gastroenterology

Costs of medical and surgical treatment of duodenal ulcer. Sonnenberg A (AS, Dept. of Medicine, Veterans Administration Medical Center, Milwaukee, WI). *Gastroenterology* 96:1445-1452, 1989

Proximal gastric vagotomy and intermittent and maintenance therapy with H_2 -antagonists have all been claimed to be effective in long-term management of duodenal ulcer disease. The model of a Markov chain was used to compare their costs by a medical decision analysis. The high price of the initial procedure made proximal gastric vagotomy the most expensive therapy, its costs rising from \$10,600 after 1 yr to \$12,200 after 15 yr. The average costs of intermittent therapy per patient rose from \$500 to \$7500. Maintenance therapy cost as much as intermittent therapy but provided 8% and 4% more time spent free of ulcer relapse and pain, respectively. In a sensitivity analysis, the order of the therapeutic options regarding their cost-effectiveness remained robust to changes in the assumptions underlying the model. In a European health care system, the initial surgical procedure cost only one-seventh of the average annual income compared with two-thirds in the United States, and proximal gastric vagotomy turned out to be the cheapest therapy after 6 yr. These results suggest that maintenance therapy provides the best long-term management. Gastric surgery may represent a cost-effective measure of ulcer prevention in Europe but not in the United States.

Reprinted with permission by the American Gastroenterological Association.

Endosonography and computed tomography of esophageal carcinoma: preoperative classification compared to the new (1987) TNM system. Tio TL, Cohen P, Coene PP, Udding J, Jager FCADH, Tytgat GNJ (TLT, Dept. of Gastroentero-hepatology, Academic Medical Center, Amsterdam, the Netherlands). *Gastroenterology* 96: 1478-1486, 1989

Transesophageal endosonography and computed tomography were performed preoperatively in 74 patients with an esophageal carcinoma. The results were correlated with the histology of resected specimens according to the new (1987) TNM classification. Endosonography was superior to computed tomography in the evaluation of the depth of tumor infiltration, especially in the early stages and in nonresectable carcinoma (overall accuracy: endosonography 89%, computed tomography 59%). Endosonography was also more accurate than computed tomography in the assessment of regional lymph node metastases (overall accuracy: endosonography 80%, computed tomography 51%). The incidence of lymph node metastasis increased with the progression of the depth of tumor infiltration. The definitive exclusion factor for endosonography is severe stenosis, which cannot be passed with the instrument (26% of the cases). In these cases computed tomography was superior to endosonography in diagnosing celiac lymph node metastasis (overall accuracy: computed tomography 82%, endosonography 68%).

Reprinted with permission by the American Gastroenterological Association.

Digestive Diseases and Sciences

Upper esophageal sphincter tone and reactivity to stress in patients with a history of globus sensation. Cook IJ, Dent J, Collins SM (SMC, Room 3N5C, Intestinal Diseases Research Unit, McMaster University Medical Centre, 1200 Main St. W., Hamilton, Ontario, L8N 3Z5, Canada). *Dig Dis Sci* 34(5):672-676, May 1989

Anxiety and abnormal upper esophageal sphincter function have been ascribed ill-defined roles in the etiology of globus sensation. In this study, we examined the psychological profile and effect of acute mental stress (dichotic listening task) on UES tone in seven patients reporting to the clinic with globus sensation and 13 healthy controls. Alterations in heart rate, blood pressure, frontalis EMG, and skin conductance confirmed the effectiveness of the stress test in patients and controls. During resting conditions, UES pressure (mean \pm SE) in patients (40.4 ± 4.6 mm Hg) did not differ significantly from controls (46.5 ± 4.7 mm Hg). In response to stress, UES pressure rose by 31% in patients ($P = 0.04$) and by 25% in controls ($P = 0.002$). The stress-induced rise in UES pressure in patients (9.5 ± 3.8 mm Hg) was not significantly different to that observed in controls (11.8 ± 3.0 mm Hg). Psychological profiles of globus patients presenting to the clinic revealed them to be more introverted, anxious, neurotic, and depressed than normal controls. We conclude that in patients with a

history of globus sensation, resting UES pressure and its response to stress is normal. Although individuals presenting to the clinic with globus sensation showed increased levels of psychoneurosis, acute, predictable stress is not a factor in the genesis of globus sensation. UES hyperresponsiveness to other stimuli or subjective intolerance to changes in UES pressure could account for symptoms of globus sensation.

Intestinal infections in patients with acquired immunodeficiency syndrome: a prospective study in 132 patients. René E, Marche C, Regnier B, et al. (ER, Service de Gastroentérologie, Hôpital Bichat, 46, rue Henri Huchard, 75877 Paris Cedex 18, France). *Dig Dis Sci* 34(5):773-780, May 1989

We studied prospectively 132 patients with acquired immunodeficiency syndrome to define the spectrum of enteric pathogens during this disease, with special reference to the correlation between the lesions, the infections, and the symptoms. Forty-four percent of the patients harbored at least one enteric pathogen: the most frequently recovered were *Cryptosporidium* (28), cytomegalovirus (16), *Entamoeba histolytica* (13), *Giardia lamblia* (9), and *Mycobacterium avium intracellulare* (7). Patients harboring pathogens were more likely to be diarrheics (69%) than patients without a pathogen (38%; $P = 0.01$) and more likely to have endoscopic lesions (29%) than patients without a pathogen (4%; $P < 0.001$). The most common pathogen associated with diarrhea was *Cryptosporidium*. Cytomegalovirus, *Entamoeba histolytica*, and *Salmonella typhimurium* were each significantly associated with endoscopic lesions. Patients with cytomegalovirus infection tended to have a greater incidence of ulcer than patients without cytomegalovirus infection. Stool analysis diagnosed 61% of the infections, while endoscopy diagnosed 44%. Seven percent were recognized by stool analysis and endoscopy. When considering the 24 patients in whom accurate diagnosis warranted endoscopic biopsies, stool examination alone would have given an incomplete diagnosis in 14 patients (due to the presence of polyinfection). The frequency of inaccurate diagnosis of infection by stool determination alone, plus the development of new antiviral agents that suppress cytomegalovirus, may favor the earlier application of endoscopic evaluation in these patients.

Gastrointestinal Endoscopy

Hepatic clonorchiasis—study by endoscopic retrograde cholangiopancreatography. Leung JWC, Sung JY, Chung SCS, Metreweli C (JWCL, Dept. of Medicine, Prince of Wales Hospital, Shatin, NT, Hong Kong). *Gastrointest Endosc* 35:226-231, 1989

An endoscopic retrograde cholangiographic study of 31 consecutive cases of hepatic clonorchiasis was performed. Filamentous wavy and/or elliptical appearance of the worm is a pathognomonic finding on ERCP examination. Significant dilation of the second and third generation bile ducts, and dilation and blunting of the terminal branches of the biliary tree are also common findings.

Endoscopic ultrasonography in esophageal diseases. Danczygier H, Classen M (HD, Medizinische Klinik und Poliklinik der Technischen Universität München, Klinikum rechts der Isar, Ismaninger Str. 22, 8 Munich 80, Federal Republic of Germany). *Gastrointest Endosc* 35:220-225, 1989

Endoscopic ultrasonography (EUS) was performed prospectively in 38 patients with various esophageal disorders. Twenty-four had a histologically proven carcinoma and EUS was done to assess its ability in preoperative staging. In 9 of 24 patients (37.5%), tumor stenosis could be passed with the endoscope and EUS preoperative findings regarding tumor extension and the presence of enlarged periesophageal lymph nodes were confirmed in those operated on ($n = 4$). In five patients with achalasia, a periesophageal tumor was reliably excluded by EUS. In one of four patients with Barrett's esophagus, EUS demonstrated a small (<1 cm) carcinoma that could not be visualized with any conventional technique. For differentiation

of cancer recurrence after operation from periesophageal scar tissue EUS-guided transmural biopsies are needed. Our experience shows that at the present time EUS is the most reliable method to demonstrate small (≤ 1 cm) intra- and extramural esophageal lesions and that it should therefore be applied early in the work-up of patients with dysphagia.

Endoscopic ultrasonography in the differential diagnosis of pancreatic disease. Kaufman AR, Sivak MV Jr (MVS, The Cleveland Clinic, 9500 Euclid Ave., Cleveland, OH 44106). *Gastrointest Endosc* 35:214-219, 1989

Endoscopic ultrasonography was performed in 25 patients with suspected pancreatic disease. Cancer of the pancreas was recognized in 9 of 10 cases with 1 false negative and 2 false positive diagnoses. Chronic pancreatitis was recognized in 89% of cases. Technical difficulties limited the success of the examination in 24% of cases. The presence or absence of pancreatic disease can be determined in most cases by endoscopic ultrasonography. Differential diagnosis by endoscopic ultrasonography (EUS) is correct in the majority of cases. We have not discovered any specific EUS finding(s) that are pathognomonic for pancreatic cancer or chronic pancreatitis.

Effect of aging on the pancreatic ducts: a study based on endoscopic retrograde pancreatography. Anand BS, Vij JC, Mac HS, Chowdhury V, Kumar A (BSA, G. B. Pant Hospital, New Delhi, 110 002 India). *Gastrointest Endosc* 35:210-213, 1989

Studies in the West have shown that with advancing age there is progressive atrophy and fibrosis of the pancreas. In addition, there is a gradual increase in diameter of the main pancreatic duct (MPD) with age. However, there is a discrepancy between the findings at autopsy and findings at endoscopic retrograde pancreatography (ERP). To examine this issue, ERP of subjects who were found not to show any abnormality of the biliary and pancreatic ducts were selected. They were divided by decade from 10 to 70 years and for statistical analysis into young (<40) and older (≥ 40) patients. There was no difference in length of the MPD between the two groups. However, the width of the MPD in the head was significantly greater in the older subjects (group 2; mean \pm SD = 3.78 ± 0.97 mm) compared with those who were <40 years (group 1; 2.97 ± 0.71 mm; $p < 0.001$). Similarly, in the midbody the width of the MPD in group 2 (2.86 ± 0.9 mm) was significantly greater compared with group 1 (2.36 ± 0.51 mm; $p < 0.02$). However, there was no difference in width of the MPD in the tail between the two groups. Length of the accessory pancreatic duct (APD) did not show any alteration with age but width was significantly greater in group 2 (1.94 ± 0.69) compared with group 1 (1.49 ± 0.51 ; $p < 0.05$). No difference was observed in the length and width of the MPD or APD between male and female subjects of either group. It is concluded that aging results in the dilation of both the MPD and APD; this alteration is seen mainly after the sixth decade.

Scandinavian Journal of Gastroenterology

Correlation between gallstones and abdominal symptoms in a random population: results from a screening study. Glambek I, Arnesjø E, Søreide O (IG, Dept. of Surgery, University of Bergen, 5021 Haukeland sykehus, Bergen, Norway). *Scand J Gastroenterol* 24:277-281, 1989

A population sample of 2464 persons between 20 and 70 years of age was included in a screening study designed for establishing gallstone prevalence rates and the frequency distribution of abdominal symptoms in groups with and without gallstone(s). The response rate was 55.6%. Two hundred and eighty-five persons had unoperated gallstone disease, as diagnosed by ultrasound. They were compared with 1044 individuals without ultrasonographically detected gallstones. The frequency distribution of epigastric and/or substernal burning, upper or lower abdominal pain, intolerance to fatty food, nausea and/or vomiting, and jaundice was similar for the

two groups. Of the screened population 35% have had to see a physician for abdominal symptoms, with no difference between the two groups. In conclusion, abdominal symptoms are common in individuals with and without gallstone(s), but no differences were found in frequency distribution of symptoms between the groups. Consequently, gallstone disease is asymptomatic in the vast majority of individuals. The high proportion of abdominal symptoms in the population with gallstone(s) combined with increasing ultrasonographic activities may lead to unjustifiable cholecystectomies.

Intestinal cancer in patients with Crohn's disease: a population study in central Israel. Fireman Z, Grossman A, Lilos P, et al. (T. Gilat, Dept. of Gastroenterology, Ichilov Hospital, Tel Aviv 64239, Israel). *Scand J Gastroenterol* 24:346-350, 1989

A population study of Crohn's disease (CD) during the years 1970-1980 was performed in a defined area in central Israel with 1,400,000 inhabitants. Three hundred and sixty-five patients with definite CD were identified, and a complete follow-up was obtained with particular attention to intestinal cancer. The mean follow-up time was 9.95 years (range, 1-49 years). Forty-four per cent of the patients were operated on, but only a few had total colectomy or bypass operations. Only one patient developed colorectal cancer after 7 years of disease. The observed to expected ratio for this cancer was 1.14 at 10 years of disease and 0.73 at 20 years of disease. The incidence of colorectal cancer was not significantly different from the expected in the population. None of the patients developed small-bowel cancer. At least five patients had extraintestinal malignancies. A review of the literature showed conflicting results with regard to cancer risk in CD. The risk was not significantly increased in the two existing population studies, including the present one.

Clinical Orthopaedics and Related Research

Osteogenesis imperfecta: perspectives. Stoltz MR, Dietrich SL, Marshall GJ (MRS, Orthopaedic Hospital, 2400 S. Flower St., Los Angeles, CA 90007). *Clin Orthop* 242:120-136, May 1989

Osteogenesis imperfecta is a heterogenous group of inherited conditions arising from a variety of biochemical and morphological collagen defects. The broad manifestations of abnormalities in bones, teeth, scleri, ligaments, and other collagen-containing tissues point to the heterogeneity of the condition. Diagnosis in the neonatal period is based on clinical characteristics, roentgenograms, and a detailed family history. Treatment is conservative when possible, and particular attention is paid to the social development of the growing child as well as to genetic counseling for parents. Modes and surgical treatment include osteoclasts and percutaneous pinning for long-bone deformities in the infant and, in the child older than two years of age, segmentation and the use of telescoping rods. Surgical treatment of spinal deformity is dependent on the age of the patient and the severity of the condition. Biochemical research is being conducted using direct tissue analyses and analyses of cultured fibroblasts and osteoblasts.

The Journal of Urology

Radiographic assessment of renal trauma: a 10-year prospective study of patient selection. Mee SL, McAninch JW, Robinson AL, Auerbach PS, Carroll PR (JWM, Dept. of Urology, University of California, San Francisco, CA 94143-0738). *J Urol* 141:1095-1098, May 1989

To develop criteria to determine which patients require radiographic assessment after blunt renal trauma, we studied prospectively 1,146 consecutive patients with either blunt (1,007) or penetrating (139) renal trauma between 1977 and 1987. Based on our preliminary results from 1977 to 1983, in which none of the 221 patients with blunt trauma and microscopic hematuria without shock had significant renal injuries, we designed a prospective study to determine if such

patients could be managed safely without radiographic staging. During the last 10 years significant renal injuries were found in 44 patients (4.4 per cent) with blunt trauma and gross hematuria or microscopic hematuria associated with shock, and in 88 patients (63 per cent) with penetrating trauma. No significant injuries occurred in the 812 patients with blunt trauma and microscopic hematuria without shock, 404 of whom had complete radiographic assessment and 408 of whom did not. There were no delayed operations or significant sequelae related to the renal injury in these patients.

We conclude that complete radiographic staging is mandatory in patients with penetrating trauma to the flank or abdomen and in patients with blunt trauma associated with either gross hematuria or microscopic hematuria and shock. However, patients with blunt trauma, microscopic hematuria and no shock who do not have associated major intra-abdominal injuries can be managed safely without excretory urography.

Pediatrics

Continuous infusion of low-dose urokinase in the treatment of central venous catheter thrombosis in infants and children. Bag-nall HA, Gomperts E, Atkinson JB (JBA, Division of Pediatric Surgery, Children's Hospital, 4650 Sunset Blvd., Los Angeles, CA 90027). *Pediatrics* 83(6):963-966, June 1989

Thrombotic occlusion is a frequent complication associated with the use of central venous catheters. The purpose of this study was to evaluate the efficacy of a continuous infusion of low-dose urokinase (200 U/kg/h) in clearing catheters that had not cleared after two bolus doses of urokinase in a pediatric oncology population. Fifty-eight incidents of catheter-related occlusions (49 Hickman-type catheters/nine implantable ports) as documented by radiographic dye study occurred in 227 pediatric oncology patients with 254 central venous catheters during a 1-year period. Fourteen of 58 catheters failed to clear after two bolus instillations of urokinase (5,000 U and 10,000 U). Thirteen catheters were treated for 24 hours with urokinase, 200 U/kg/h, and one catheter with urokinase, 100 U/kg/h for 24 hours. Twelve catheters were used for study. Coagulation studies were monitored preinfusion, 12 hours into the infusion, and postinfusion. Patency was reestablished in 11/12 catheters (92%) with a mean infusion time of 28.7 hours. No coagulation abnormalities or clinical bleeding associated with the urokinase infusion occurred. Only one patient exhibited a prolonged partial thromboplastin time (>150 seconds); this was associated with a heparin effect. These data indicate that low-dose urokinase may be a safe and effective means to clear occluded central venous catheters in children.

Reprinted by permission of PEDIATRICS © 1989.

The Journal of Pediatrics

Serum vitamin D metabolites in very low birth weight infants with and without rickets and fractures. Koo WWK, Sherman R, Succop P, Ho M, Buckley D, Tsang RC (WWKK, University of Alberta Hospitals, 3A3 Walter Mackenzie Health Sciences Centre, Edmonton, Alberta T6G 2B7, Canada). *J Pediatr* 114:1017-1022, 1989

Seventy-one very low birth weight (≤ 1500 gm) infants were studied to determine the sequential changes in serum vitamin D metabolite concentrations between infants with and without radiographically documented rickets, fractures, or both (R/F). Usual intake of vitamin D included 20 IU/kg/day from parenteral nutrition or 400 IU/day supplementation with enteral feeding. Radiographs of both forearms and serum samples were obtained at 3, 6, 9, and 12 months. Twenty-two infants had R/F. At 3 months, significantly lower mean (\pm SEM) serum phosphorus levels (4.5 ± 0.4 vs 6.1 ± 0.2 mg/dl), higher 1,25-dihydroxyvitamin D ($1,25\text{-[OH]}_2\text{D}$) concentrations (96 ± 5 vs 77 ± 4 pg/ml), and higher free $1,25\text{-[OH]}_2\text{D}$ index ($1,25\text{-[OH]}_2\text{D}$:vitamin D binding protein ratio; $5.2 \pm 0.3 \times 10^5$ vs $4.0 \pm 0.2 \times 10^5$) were found in the R/F group. These values returned to normal and were similar between groups on subsequent measurements. Serum calcium, mag-

nesium, and 25-hydroxyvitamin D (25-OHD) concentrations were normal and similar between groups. In both groups, serum vitamin D binding concentrations increased initially but remained stable and normal beyond 6 months. We conclude that in very low birth weight infants with R/F, the vitamin D status (as indicated by serum 25-OHD concentrations) is normal, and that lowered serum phosphorus levels, higher serum $1,25\text{-[OH]}_2\text{D}$ levels, and a higher free $1,25\text{-[OH]}_2\text{D}$ index support the thesis that mineral deficiency (especially of phosphorus) may be important in the pathogenesis of R/F in small preterm infants.

The Journal of Nuclear Medicine

Penile blood flow by xenon-133 washout. Haden HT, Katz PG, Mulligan T, Zasler ND (PGK, Urology Section, Veterans Administration Medical Center, Richmond, VA 23249). *J Nucl Med* 30(6):1032-1035, June 1989

Penile erectile failure is often attributed to abnormalities of vascular supply or drainage, but few direct measurements of penile blood flow have been made. We describe the xenon washout method for measurement of penile blood flow, and present the results obtained in a group of normal and impotent subjects. The procedure was performed with standard nuclear imaging equipment. Flaccid-state penile blood flow in the impotent patients studied was not significantly different from the normal group, suggesting that flaccid-state measurements may not be helpful in evaluation of erectile failure. However, this method can be used to measure penile venous outflow with stimulated or induced erection, and may provide a method for detecting abnormal venous leakage.

Beta dose point kernels for radionuclides of potential use in radioimmunotherapy. Prestwich WV, Nunes J, Kwok CS (CSK, Hamilton Regional Cancer Centre, Ontario Cancer Foundation, 711 Concession ST., Hamilton, Ontario, L8V 1C3, Canada). *J Nucl Med* 30(6):1036-1046, June 1989

Beta dose point kernels for ^{32}P , ^{67}Cu , ^{90}Y , ^{131}I , ^{186}Re , and ^{188}Re nuclides appropriate for radioimmunotherapy are calculated based upon Monte Carlo results. The calculations are shown to differ significantly from values based upon solutions to the electron transport equation. Agreement with experiment for ^{32}P is found to be improved for the former as compared with the latter. Values of the scaled dose point kernels are tabulated at 4% intervals of the continuous slowing down approximation range for each of the six radionuclides. Beta dose distributions are also tabulated at corresponding distances from the source. This data may be used to calculate the spatial dose distribution expected following administration of radiolabeled monoclonal antibodies, aiding in optimum selection of the appropriate radionuclide. Parameters for functions providing analytic representation of the calculated scaled dose point kernels of individual beta groups are presented.

Gastrointestinal Radiology

Atrophic gastritis in pernicious anemia: diagnosis by double-contrast radiography. Levine MS, Paiman CL, Rubesin SE, Laufer I, Herlinger H (MSL, Dept. of Radiology, Hospital of the University of Pennsylvania, 3400 Spruce St., Philadelphia, PA 19104). *Gastrointest Radiol* 14:215-219, 1989

A retrospective study was performed to determine whether the areae gastricae pattern in the stomach or other radiologic features could be used on double-contrast upper gastrointestinal examinations to accurately diagnose atrophic gastritis in pernicious anemia. The double-contrast studies from 21 patients with pernicious anemia and 55 age-matched controls were interspersed and reviewed blindly to assess gastric size, mucosal folds, and the areae gastricae pattern in the stomach. The best set of criteria for differentiating the pernicious anemia group from the controls included a fundal diameter of 8 cm or less, absent mucosal folds in the fundus or body, and small

(i.e., 1–2 mm in size) or absent areae gastricae. This combination of findings was present in 81% of patients with pernicious anemia but it also was present in 11% of the controls, so that atrophic gastritis in pernicious anemia could not be reliably diagnosed on radiologic criteria. Nevertheless, patients with pernicious anemia invariably had small or absent areae gastricae in the stomach, so that the presence of prominent areae gastricae, particularly in the fundus, may be a useful criterion for excluding this disease.

Sonographic characteristics of small hepatocellular carcinoma.

Choi BI, Kim C-W, Han MC, et al. (BIC, Dept. of Radiology, College of Medicine, Seoul National University, 28, Yeongun-Dong, Chongro-Ku, Seoul, 110-744, Korea). *Gastrointest Radiol* 14:255–261, 1989

Fifty-four lesions of small hepatocellular carcinoma under 5 cm in diameter detected by real-time sonography were reviewed to characterize the sonographic feature. Twenty-nine lesions were smaller than 3 cm in diameter and 25 were between 3 and 5 cm in diameter. Sonographic characteristics of hepatocellular carcinoma were peripheral hypoechoic halo (52%), lateral shadow (26%), posterior acoustic enhancement (44%), and mosaic pattern (24%) of the mass. Small tumors less than 3 cm in diameter showed a hypoechoic pattern in half of the cases, whereas most of the tumors between 3 and 5 cm in diameter showed a hyperechoic or mixed pattern. Posterior acoustic enhancement was commonly seen in small tumors less than 3 cm in diameter, while a mosaic pattern was commonly seen in large tumors between 3 and 5 cm in diameter. These results suggest that sonography might be useful for the characterization of small hepatocellular carcinoma.

Digital videofluorography for direct digital spot filming of gastrointestinal studies.

Steiner E, Mueller PR, Hahn PF, Taafe J, Ferrucci JT (JTF, Dept. of Radiology, Massachusetts General Hospital, Fruit St., Boston, MA 02114). *Gastrointest Radiol* 14:193–201, 1989

Digital videofluorography (DVF) refers to a new computer-aided televised fluoroscopy technique that uses short (10–20 ms) intense pulses of radiation to produce a motion-free latent image, which is then transferred into digital storage. Because gastrointestinal imaging has lagged behind other body systems in the evaluation of digital acquisition, we investigated the potential utility of this technique for direct digital fluoroscopic spot filming of gastrointestinal examinations.

In order to assess the level of clinical image quality achieved by this technique, we conducted an observer performance comparison study of digitally acquired and conventional analog 100 mm spot films. Sequentially acquired spot films and digital radiographs of 111 anatomic regions in 60 patients undergoing routine barium and cholangiographic examinations were compared. Evaluation was made of on-line interactive performance as well as side-by-side analysis of digital and analog hard copy images. Parameters evaluated include detection of normal and pathologic features, image contrast, image resolution, and image sharpness. Direct digital and analog spot films were of comparable diagnostic quality in all parameters studied. Added benefits of the digital mode included postprocessing to enhance detail in regions of low contrast and accommodation of a large field of view (14 inch) image intensifier format.

Pediatric Radiology

The CT and MR evaluation of migrational disorders of the brain.

Part II. Schizencephaly, heterotopia and polymicrogyria. Byrd SE, Osborn RE, Bohan TP, Naidich TP (SEB, Division of Neuroimaging, Dept. of Radiology, Children's Memorial Hospital, Northwestern Uni-

versity Medical School, Chicago, IL). *Pediatr Radiol* 19:219–222, 1989

The migrational disorders are a rare group of congenital malformations of the brain. They consist of the following entities – lissencephaly (agyria – pachygyria), pachygyria, schizencephaly, heterotopia and polymicrogyria. We studied 40 children with migrational disorders radiologically with CT and MR. This article (Part II) deals with our patients with schizencephaly, heterotopia and polymicrogyria. These patients presented clinically with a variety of symptoms. The most common were seizures, delayed development, failure to thrive and hydrocephalus. CT and MR both demonstrated the characteristic findings in all of our patients except the polymicrogyria group. The gray matter and cleft abnormalities seen in these disorders were demonstrated with CT and MR. However, MR provided better delineation of these disorders than CT. Because some forms of migrational disorders can be inherited, it is extremely important for the radiologist to understand the characteristic findings for correct diagnosis which is essential for parental counseling.

Radiographic findings in liveborn triploidy.

Silverthorn KG, Houston CS, Newman DE, Wood BJ (KGS, Dept. of Radiology, University Hospital, Saskatoon, Saskatchewan, Canada). *Pediatr Radiol* 19:237–241, 1989

The detailed radiographic features of triploidy, a fatal congenital disorder with 69 chromosomes, have not previously been reported. Radiographs of ten liveborn infants with chromosomally confirmed triploidy showed six findings highly suggestive of this diagnosis: harlequin orbits, small anterior fontanelle, gracile ribs, diaphyseal overtubulation of long bones, upswept clavicles and antimongoloid pelvis. Sixteen other less specific findings showed many similarities to those found in trisomy 18.

Journal of Ultrasound in Medicine

Chromosomal abnormalities in fetuses with omphalocele: significance of omphalocele contents.

Nyberg DA, Fitzsimmons J, Mack LA, et al. (DAN, Dept. of Radiology, 1229 Madison St., Ste. 1150, Seattle, WA 98104). *J Ultrasound Med* 8(6):299–308, June 1989

Twenty-six consecutive fetuses with a sonographically detectable omphalocele and known karyotype were reviewed to identify risk factors that might be associated with chromosomal abnormalities. Risk factors that were analyzed included contents of the omphalocele sac, maternal age, fetal sex, sonographically detectable concurrent anomalies, and any major concurrent anomaly. Chromosomal abnormalities were found in 10 cases (38%) from trisomy 18 ($n = 4$), trisomy 13 ($n = 4$), trisomy 21 ($n = 1$), or 45, X ($n = 1$). The absence of liver from the omphalocele sac (intracorporeal liver) was strongly associated with an abnormal karyotype; chromosomal abnormalities were present in all 8 fetuses with an intracorporeal liver compared to 2 of 18 fetuses with an extracorporeal liver ($p < .0001$, two-tailed Fisher exact test). Other risk factors that were statistically associated with chromosomal abnormalities included advanced maternal age (≥ 33 year, $p = .03$) and sonographically detectable concurrent malformations ($p = .05$).

We conclude that sonographic findings can help determine the relative risk of chromosomal abnormalities in fetuses with omphalocele; abnormal karyotypes were significantly associated with the absence of liver from the omphalocele sac and sonographically detectable concurrent malformations in this series. Sonographers should also be aware that omphaloceles that contain bowel alone tend to be small and can be missed or mistaken for other abdominal wall defects (gastroschisis or umbilical hernia).

Reprinted with permission by the American Institute of Ultrasound in Medicine.

AAWR Distinguished Resident Award

The American Association of Women Radiologists (AAWR) has announced that an AAWR Distinguished Resident Award will be presented each year, beginning in 1990, at the AAWR annual meeting. A prize of \$500 and expenses (air fare and per diem) to accept the award will be included. Nominations are being solicited from directors of residency programs. Nominees must be members of the AAWR. One nomination per residency program is the limit. The completed application should include a nominating letter from the residency director, with a notation of what year the candidate will be in residency at the time of the award ceremony; a letter of concurrence from the departmental chair; a letter from the candidate requesting consideration, with the reasons defined; and a copy of the candidate's curriculum vitae. Nominees will be evaluated on the basis of outstanding contributions, whether in clinical care, teaching, research, or public service. Candidates must be in residency training for the year of the award. Nominations should be sent by July 1, 1990, to Executive Director, American Association of Women Radiologists, 1891 Preston White Dr., Reston, VA 22091.

Harry Fischer Award

The Harry Fischer Award has been established to recognize research in contrast agents that enhance the value of imaging technologies. Funds have been donated by manufacturers around the world who produce contrast media for diagnostic imaging. Appropriately, the first winner is Harry Fischer, who has been active in research and teaching in this field for the past 35 years. Dr. Fischer will give a speech and accept the award at the International Contrast Medical Research Symposium in Sydney, Australia, October 1989. An international committee will review nominations for future winners. The award includes a venue for presenting the Fischer Lecture at an international gathering, a significant stipend, expenses for the winner and an accompanying person to travel to accept the award, and an attractive silver commemorative medal. Information: Gerald L. Wolf, Ph.D., M.D., Ad Hoc Chairman of the Harry Fischer Award, Pittsburgh NMR Institute, 3260 5th Ave., Pittsburgh, PA 15213; telephone: (412) 647-NMRI; fax: (412) 647-8520.

Visiting Fellowship in Interventional Radiology

The Johns Hopkins Hospital is offering a 5-day course, for radiologists only, on interventional radiology. The course is tailored to the

needs of the fellow, who will participate in morning conferences, patient rounds, and laboratory observations. A newly developed teaching file is available for study. A wide range of interventional procedures will be included: angiography, angioplasty, percutaneous atherectomy, use of thrombolytic agents, embolization of varicoceles and arteriovenous malformations, biliary and urologic procedures, and use of intravascular lasers. Category 1 credit: 40 hr. Fee: \$1000. Information: Program Coordinator, The Johns Hopkins Medical Institutions, Office of Continuing Education, Turner Bldg., 720 Rutland Ave., Baltimore, MD 21205; (301) 955-3839.

Clinical Medical Physics Residency Program

The Dept. of Diagnostic Radiology, Mayo Graduate School of Medicine, Mayo Clinic, Rochester, MN, is offering a 2-year training program in clinical medical physics for a person who recently has received a doctoral degree in medical physics, physics, or engineering. The purpose of the program is to provide training and experience for those who wish to pursue careers in clinical diagnostic imaging. The program provides 2 of the 3 years of special training required for eligibility for the American Board of Radiology certification in Diagnostic Radiological Physics or Medical Nuclear Physics. Facilities include Mayo Clinic Rochester, Mayo Jacksonville (FL), and Mayo Scottsdale (AZ). Information: Joel E. Gray, Ph.D., Dept. of Diagnostic Radiology, Mayo Clinic, Rochester, MN 55905; (507) 284-4292.

Visiting Fellowships at UCSF

The Dept. of Radiology and Extended Programs in Medical Education, University of California, San Francisco, are sponsoring a number of visiting fellowships in radiology. Most programs are for 1 week. Areas of training include MR imaging (general fundamentals and applications, neuro, and advanced neuro), head and body CT, echocardiography, and ultrasound. Program chairman: Alexander R. Margulis. Category 1 credit: 40 hr. Fee: \$800-\$1350. Information: Radiology Postgraduate Education, University of California, San Francisco, School of Medicine, Visiting Fellowship Program, Rm. C-324, San Francisco, CA 94143-0628; (415) 476-9776.

Preceptorship in Transrectal Ultrasound of the Prostate

Huron Valley Radiology and the Catherine McAuley Health Center, Ann Arbor, MI, are offering monthly preceptorships in transrectal

ultrasound of the prostate. Category 1 credit: 14 hr. Fee: physicians, \$500; technologists, \$350. Information: Jerry Dowty, R.D.M.S., Manager of Ultrasound, McAuley Clinic Corp., 5333 McAuley Dr., Ste. 1015, Ann Arbor, MI 48106; (313) 572-5251.

Ultrasound Review Seminar for Technologists

The Dept. of Radiology, West Penn Hospital, will present Ultrasound Review Course for Technologists, Sept. 7-9, at the Pittsburgh Green Tree Marriott, Pittsburgh, PA. Participants will gain relevant clinical knowledge of ultrasound, review the pathophysiology and physics of ultrasound, update and enhance technical sonographic skills, and prepare for certification. Program coordinators: Marcela Bohm-Velez, Harvey L. Neiman, Lori Davidson, and Charles M. Rowe. Guest faculty: Albert Goldstein and D. A. Willard. The course has been approved for 18.5 hr of CME by the Society of Diagnostic Medical Sonographers. Fee: \$225. Information: Dept. of Continuing Medical Education, The Western Pennsylvania Hospital, 4800 Friendship Ave., Pittsburgh, PA 15224; (412) 578-6926.

Gastrointestinal Imaging 1989

The Dept. of Radiology, Toronto General Hospital, in cooperation with the Division of Gastroenterology and the Dept. of Radiology, University of Toronto, is sponsoring Gastrointestinal Imaging 1989, Sept. 8. The symposium will provide updates on barium examinations; CT; ultrasound; and endoscopy, including an introduction to endoscopic ultrasonography. Course director: Stephanie Wilson. Guest faculty: Clive Bartram and Giancarlo Caletti. Category 1 credit: 6 hr. Fee (Canadian dollars): physicians, \$150; residents, fellows, and technologists, \$50. Information: Stephanie Wilson, M.D., F.R.C.P.(C), Dept. of Radiology, Toronto General Hospital, 200 Elizabeth St., Toronto, Ontario, Canada M5G 2C4; (416) 595-3874.

MR Imaging Seminar for Technologists

The Dept. of Radiology, Hospital of the University of Pennsylvania, is sponsoring MRI for Technologists Seminar: A Practical Introduction, Sept. 9-10, at the Penn Tower Hotel in Philadelphia. The seminar will include lectures, workshops, and a roundtable discussion. Course director: Felix Wehrli. Category 1 credit: 12 hr (pending). Fee: \$300. Information: Janice Ford or Nancy Fedullo, Dept. of Radiology, Hospital of the University of Pennsylvania, 3400 Spruce St., Philadelphia, PA 19104; (215) 662-6904 or 662-6982.

1989 Interventional Neuroradiology

The Dept. of Radiology and Radiological Sciences, The Johns Hopkins University, School of Medicine, is sponsoring 1989 Interventional Neuroradiology, Sept. 11-13, at the Johns Hopkins Medical Institutions in Baltimore. The program will include detailed discussion of state-of-the-art interventional neurologic procedures used in the treatment of cerebral aneurysms, fistulas, and brain arteriovenous malformations. Course director: Gerard Debrun. Category 1 credit: 26.5 hr. Fee: physicians, \$550; residents, fellows and technicians, \$350 (letter required). Information: Program Coordinator, The Johns Hopkins Medical Institutions, Office of Continuing Education, Turner Bldg., 720 Rutland Ave., Baltimore, MD 21205; (301) 955-2959.

3-D Imaging: Theory and Clinical Applications

The Dept. of Radiology and Radiological Sciences, The Johns Hopkins Medical Institutions, Baltimore, MD, is sponsoring 3D Imaging: Theory and Clinical Applications, Sept. 15-17. The course will be a lecture series on the theory, clinical applications, and business aspects of three-dimensional imaging. The intent is to provide practical and relevant information to practicing radiologists and referring surgeons who are interested in the use of this imaging technique. Category 1 credit: 20 hr. Fee: physicians, \$300; residents and fellows, \$200. Information: Program Coordinator, The Johns Hopkins Medical Institutions, Office of Continuing Education, Turner Bldg., 720 Rutland Ave., Baltimore, MD 21205; (301) 955-2959.

Automated Percutaneous Discectomy Workshops

Radiology Postgraduate Education, University of California, San Francisco, is offering several workshops on automated percutaneous discectomy. Workshops will be held at the Hyatt Regency Hotel Embarcadero in San Francisco on Sept. 16-17, Dec. 9-10, Jan. 13-14, 1990, and Feb. 17-18, 1990; at the Vanderbilt Plaza Hotel, Nashville, TN, Nov. 18-19; and at the Marriott Hotel, Washington, DC, Oct. 21-22, and April 7-8, 1990. The course is designed to teach physicians to comprehend and perform accurately the basic technique of automated percutaneous discectomy. Attendees will work closely with an instructor, enabling them to gain an appreciation for the identification of uncomplicated lumbar herniated discs and the percutaneous surgical approach. Workshop chairmen: Clyde A. Helms and Gary Onik. Category 1 credit: 11.5 hr. Fee: \$800. Information: Radiology Postgraduate Education, University of California, Rm. 569-U, San Francisco, CA 94143-0766; (415) 476-5731.

Abdominal Ultrasound

The Division of Diagnostic Ultrasound, Dept. of Radiology, Thomas Jefferson University Hospital, Philadelphia, is offering Abdominal Ultrasound, Sept. 18-21 and Nov. 13-16. Emphasis is on an integrated approach that combines recognition of normal sonographic anatomy and typical ultrasound patterns of abdominal disorders. Specific topics include a review of the principles of ultrasound physics; instrumentation and imaging techniques, including Doppler sonography; aspiration and biopsy techniques; and ultrasound evaluation of prevertebral vessels, liver, biliary system, kidneys and retroperitoneum, pancreas, spleen, thyroid and parathyroid, and abdominal collections. The program includes lectures, demonstrations, case reviews, and hands-on experience with a variety of sonographic instrumentation. Course director: Wolfgang Dähnert. Category 1 credit: 27 hr. Fee: \$550. Information: Judith Superior, Education Coordinator, Division of Diagnostic Ultrasound, Thomas Jefferson University Hospital, 7th Floor, Main Bldg., Philadelphia, PA 19107; (215) 928-8533.

Prostate Ultrasound

The Division of Diagnostic Ultrasound, Dept. of Radiology, Thomas Jefferson University Hospital, Philadelphia, is offering the course, Prostate Ultrasound, Sept. 22 and Nov. 17. The program provides an overview of established and recently developed approaches to ultrasound of the prostate; special emphasis is given to endorectal scanning. Practical hands-on experience with a variety of instruments for endorectal scanning is a part of the course. Course director: M.

D. Rifkin. Category 1 credit: 9 hr. Fee: \$325. Information: Judith Superior, Education Coordinator, Division of Diagnostic Ultrasound, Thomas Jefferson University Hospital, 7th Floor, Main Bldg., Philadelphia, PA 19107; (215) 928-8533.

Neurologic and Musculoskeletal Radiology

The Dept. of Radiology, University of Minnesota, Medical School, is sponsoring the 52nd annual course, Radiology/89: Neuro and Musculoskeletal Radiology, Sept. 25–29, at the Hyatt Regency Hotel, Minneapolis, MN. Course directors: William M. Thompson, Harry J. Griffiths, and Benjamin Lee. Category 1 credit: 31.5 hr. Fee: \$550. Information: Continuing Medical Education, University of Minnesota, Box 202 UMHC, 420 Delaware St., S. E., Minneapolis, MN 55455; (612) 626-5525.

Annual Washington Imaging Conference

The Dept. of Radiology, Alexandria Hospital, Alexandria, VA, and the American College of Radiology are cosponsoring the 9th Annual Washington Imaging Conference: Advances in Imaging: Neuro/Body MRI, Ultrasound/Doppler, and CT, Sept. 25–29, at the Hotel Washington, Washington, DC. The conference is designed to provide state-of-the-art information. Topics in MR imaging will include detailed review of current neurologic applications and abdominal, pelvic, cardiac, and soft-tissue MR. Advanced review of ultrasound will include high-risk obstetric ultrasound fetal anomalies, duplex and Doppler imaging, and transvaginal and prostatic ultrasound techniques. Selected topics in other imaging techniques will be presented. Program director: Arina van Breda. Guest faculty: S. W. Atlas, E. K. Fishman, Mokhtar Gado, S. E. Harms, Faye Laing, T. C. McCloud, H. L. Neimann, Roger Sanders, H. D. Sostman, G. K. Sze, W. G. Totty, and Robert Zeman. Category 1 credit: 25 hr. Fee: physicians, \$600; residents, \$350 (letter required). Information: Arina van Breda, M.D., Course Director, Alexandria Hospital, 4320 Seminary Rd., Alexandria, VA 22304; (703) 379-3102.

Obstetrics and Gynecology

The Division of Diagnostic Ultrasound, Dept. of Radiology, Thomas Jefferson University Hospital, Philadelphia, is offering Obstetrics and Gynecology, Sept. 25–29, Oct. 30–Nov. 3, and Dec. 4–8. The course covers the full range of ultrasound applications used in evaluation of the fetus and the female pelvis. Approximately two-thirds of the program is devoted to obstetrics and one-third to gynecology. The obstetric component includes a thorough review of current techniques of fetal measurements and presents an orderly approach to assessment of fetal growth and well-being, identification of abnormal echo patterns, and establishing a differential diagnosis. The gynecologic part emphasizes recognition of normal anatomy and characterization of gynecologic masses. Hands-on scanning of pregnant patients is not part of the course. Course director: Alfred Kurtz. Category 1 credit: 30 hr. Fee: \$625. Information: Judith Superior, Education Coordinator, Division of Diagnostic Ultrasound, Thomas Jefferson University Hospital, 7th Floor, Main Bldg., Philadelphia, PA 19107; (215) 928-8533.

Tutorial Course in Ireland

Cornell University Medical College, The New York Hospital, and the Royal College of Surgeons in Ireland are sponsoring a tutorial

course at Adare Manor, Adare, Ireland, Oct. 1–5. Topics will include body imaging (sonography, CT, and MR), imaging of the head and spine (CT and MR), interventional radiology, surgical considerations and interventional approach to trauma, and technologic considerations in imaging. Category 1 credit: 24 hr. Fee: physicians, \$450; residents and fellows, \$275. Information: Joseph P. Whalen, M.D., Cornell University Medical College, 1300 York Ave., New York, NY 10021; (212) 746-2522.

Clinical Magnetic Resonance Imaging

Radiology Postgraduate Education, University of California, San Francisco, is sponsoring Clinical Magnetic Resonance Imaging, Oct. 2–6, at the Hyatt Regency San Francisco. The course is designed to provide comprehensive instruction in the new developments and instrumentation used for MR imaging. It also will provide an updated demonstration of the role of MR imaging in the assessment of all organ systems. Controversial questions in MR imaging and equipment choices will be explored by panels composed of university and industrial scientists. Program chairman: Charles B. Higgins. Course directors: David Norman, Hedvig Hricak, and Harry K. Genant. Guest faculty: Richard Underwood, G. S. Bissett III, D. R. Enzmann, H. Y. Kressel, and W. A. Murphy. Category 1 credit: 33 hr. Fee: physicians, \$515; residents, fellows, nurses, and technologists, \$415 (letter required). Information: Radiology Postgraduate Education, University of California, Rm. 569U, San Francisco, CA 94143-0766; (415) 476-5731.

MRI: Clinical State of the Art

MRI: Clinical State of the Art will be presented at the NYU Medical Center, New York, NY, Oct. 4–7. The course will provide a practical, clinically oriented review and analysis of the state-of-the-art of MR imaging and will introduce some of the promising new developments. Anatomy, applications, and techniques will be emphasized, and the role of MR in relation to other radiologic studies will be discussed. Category 1 credit: 24 hr. Fee: \$450. Information: NYU Post-Graduate Medical School, 550 First Ave., New York, NY 10016; (212) 340-5295.

Pediatric Neuroradiology Seminar

Radiology Postgraduate Education, University of California, San Francisco, is sponsoring Pediatric Neuroradiology Seminar, Oct. 7, at the Hyatt Regency San Francisco. The course is designed to provide an up-to-date and thorough overview of pediatric neuroradiology. Both congenital and acquired CNS disorders will be covered. Examinations of the CNS by sonography, CT, and MR will be compared and contrasted. The course will emphasize state-of-the-art imaging techniques. Program director: A. James Barkovich. Guest faculty: Derek Harwood-Nash, R. U. Bokelman, and D. E. Fadjo. Category 1 credits: 7 hr. Fee: Physicians, \$105; residents, fellows, nurses, and technologists, \$75 (letter required). Information: Radiology Postgraduate Education, University of California, Rm. 569U, San Francisco, CA 94143-0766; (415) 476-5731.

Color Doppler 1990

An intense 2.5-day course, Color Doppler 1990, will be conducted at the Beverly Hilton Hotel, Beverly Hills, CA, Oct. 12–14. Topics to

be covered include physics, flow dynamics, and color Doppler equipment. The use of color Doppler sonography in the assessment of cranial, cerebrovascular, and upper and lower extremity arterial and venous disease; deep venous thrombus; and obstetric, gynecologic, genitourinary, and abdominal disorders will be discussed also. Category 1 credit: up to 15 hr. Fee: physicians, \$495; residents, fellows, and technologists, \$395. Information: Edward Grant, M.D., UCLA Medical Center, Dept. of Radiological Sciences, Los Angeles, CA 90024-1721; (213) 825-8813.

Clinical MR Imaging Course

The Dept. of Radiology, Yale University, School of Medicine, is offering a 3-day course in clinical MR imaging, Oct. 16-18, at the Yale-New Haven Hospital MRI Center. Topics will include neurologic, musculoskeletal, and abdominal applications of MR imaging. Category 1 credit: 21.5 hr. Fee: physicians, \$550; residents, fellows, and technologists, \$400. Information: Office of Post-Graduate & Continuing Medical Education, Yale University, School of Medicine, 333 Cedar St., P. O. Box 3333, New Haven, CT 06510; (203) 785-4578.

Neonatal Neurosonography

The Division of Ultrasound, Dept. of Radiology, Thomas Jefferson University Hospital, Philadelphia, is sponsoring Neonatal Neurosonography, Oct. 19-20. This program is designed to provide a complete introduction to sonographic evaluation of the neonatal brain. Topics will include physical principles and instrumentation, scanning techniques and infection control procedures, recognition of normal anatomic structures, identification of abnormal echo patterns, natural history and sequelae of intracranial hemorrhage, and detection and classification of hemorrhage. The course will have lectures, case analyses, and video demonstrations, but participants will not do any hands-on scanning of infants. Course directors: Donald Mitchell and Matthew Pasto. Category 1 credit: 13.5 hr. Fee: \$325. Information: Judith Superior, Education Coordinator, Division of Diagnostic Ultrasound, Thomas Jefferson University Hospital, 7th Floor, Main Bldg., Philadelphia, PA 19107; (215) 928-8533.

CT and MR of the Brain, Head, Neck, and Spine

The Dept. of Diagnostic Radiology, Rush-Presbyterian-St. Luke's Medical Center, will present its 16th annual course on CT and MR of the brain, head, neck, and spine Oct. 19-20 at the Westin Hotel, Chicago. The course will provide instruction in the performance and interpretation of CT and MR examinations of the brain, head, neck, and spine. It is recommended that course registrants familiarize themselves in advance with the basic physical principles of CT and MR imaging. Guest faculty: H. L. Baker, Jr., R. T. Bergeron, R. N. Bryan, D. O. Davis, M. H. Gado, D. C. Harwood-Nash, S. K. Hilal, Enrique Palacios, R. M. Quencer, R. G. Ramsey, E. J. Russell, P. M. Som, and J. M. Taveras. Category 1 credit: 15 hr. Fee: physicians, \$435; residents and fellows, \$300. Information: Michael S. Huckman, M.D., Director of Neuroradiology, Rush-Presbyterian-St. Luke's Medical Center, 1753 W. Congress Parkway, Chicago, IL 60612; (312) 942-5781.

New Orleans Fall Radiology Conference

Louisiana State University School of Medicine, New Orleans, will present the New Orleans Fall Radiology Conference, Nov. 6-8, at Le Meridien New Orleans. This 12th LSU fall radiology conference will

emphasize various aspects of clinical radiology. The course is designed for practicing radiologists who deal with the problems of the management of patients. Special feature sessions will highlight interventional radiology of the biliary, genitourinary, and gastrointestinal tracts; the diagnostic impact of MR of the musculoskeletal system; and the expanded use of sonography in the management of the acute abdomen. A plenary session, "Management of Biliary Calculi," will cover epidemiology, selection and triage of patients, dissolution of gallstones by percutaneous techniques, extraction of gallstones, technical aspects of biliary lithotripsy, and results and complications of all these procedures. Category 1 credit: 20 hr. Fee: physicians, \$395; residents, \$295 (letter required). Information: Office of Continuing Medical Education, LSU Medical Center, 1542 Tulane Ave., New Orleans, LA 70112; (504) 568-6085.

Diagnostic Radiology Seminar in Hawaii

The Dept. of Radiology, University of California, San Francisco, is offering its 8th annual fall Hawaii Postgraduate Course in Diagnostic Radiology, Nov. 6-10, in Maui, HI. The course is designed primarily for radiologists in clinical practice. Topics to be covered include the role of CT and MR imaging in diagnosis of disorders in infants and children; problems of false-positive diagnoses in mammography; usefulness of high-resolution CT of the lungs for detecting interstitial and pleural disease; practical aspects of the obstetric ultrasound examination and its pitfalls; value of MR imaging in evaluation of pelvic disorders; current knowledge on MR imaging for diagnosis of shoulder, knee, and spine diseases; role of MR in evaluation of suspected liver disease; and uses of CT in detection of inflammatory diseases of the gastrointestinal tract. Program director: Henry I. Goldberg. Category 1 credit: 24 hr. Fee: physicians, \$515; residents, fellows, nurses, and technologists, \$415 (letter required). Information: Radiology Postgraduate Education, Rm. C-324, University of California, San Francisco, School of Medicine, San Francisco, CA 94143-0628; (415) 476-5731.

Magnetic Resonance Imaging: Techniques and Imaging Methodology

The Dept. of Radiology, Hospital of the University of Pennsylvania, is sponsoring Magnetic Resonance Imaging: Techniques and Imaging Methodology, Nov. 6-10, at the Sheraton Society Hill, Philadelphia. The course provides a good mix of clinical and technical aspects of MR imaging. Each day is devoted to a particular theme: "Principles and Imaging Methodology," "Advances in Rapid Scan Imaging," "Blood Flow," "Musculoskeletal MR," and "Contrast Agents, Body Imaging, and Quantitative MR." Course director: Felix W. Wehrli. Category 1 credit: 32 hr (pending). Fee: physicians, \$595; residents, \$375. Information: Janice Ford, CME Coordinator, Dept. of Radiology, Hospital of the University of Pennsylvania, 3400 Spruce St., Philadelphia, PA 19104; (215) 662-6904 or 662-6982.

Color Doppler Ultrasound

The Division of Diagnostic Ultrasound, Dept. of Radiology, Thomas Jefferson University Hospital, Philadelphia, is offering Color Doppler Ultrasound, Nov. 13. The principles and applications of color Doppler imaging will be presented through lectures and case reviews. A working knowledge of hemodynamics and of the principles and applications of duplex Doppler sonography is assumed. Specific topics will include pitfalls of color Doppler imaging, cerebrovascular scanning techniques, peripheral arterial and venous scanning tech-

niques, superficial vascular masses, neonatal brain, abdomen, and obstetrics. Course directors: Donald Mitchell, Peter Burns, and Laurence Needleman. Category 1 credit: 9 hr. Fee: \$200. Information: Judith Superior, Program Coordinator, Division of Diagnostic Ultrasound, Thomas Jefferson University Hospital, 7th Floor, Main Bldg., Philadelphia, PA 19107; (215) 928-8533.

CT and MRI—Head to Toe

The Post-Graduate Medical School, NYU Medical Center, will present CT and MRI—Head to Toe, Dec. 11–16, at the Grand Hyatt Hotel, New York City. This intensive program is intended to be an annual updating of the entire field of CT and MR imaging. Plenary lectures will be complemented by small-group, in-depth workshops on CT and MR of diseases of the head, neck, sinuses, thorax, abdomen and pelvis, spine, and musculoskeletal system. Relevant interventional techniques will be included. Registrants will be able to attend eight different workshops. Category 1 credit: 38.5 hr. Fee: \$675. Information: NYU Medical Center, Post-Graduate Medical School, 550 First Ave., New York, NY 10016; (212) 340-5295.

MR Imaging Seminar

The Dept. of Radiology, Cornell University Medical College and The New York Hospital, is sponsoring a course on MR imaging, Dec. 14–16, at Cornell University Medical College, New York, NY. The course will discuss MR imaging of the neurologic system, the body, and the extremities. Program chairman: John A. Markisz. Guest faculty: J. B. Kneeland and M. T. Modic. Category 1 credit: 15 hr. Fee: physicians, \$295; residents and fellows, \$150. Information: John A. Markisz, M.D., Ph.D., Program Chairman, Dept. of Radiology, Cornell University Medical College, 1300 York Ave., New York, NY 10021; (212) 746-6880.

Thoracic Imaging '90

The Society of Thoracic Radiology will present Thoracic Imaging '90, Jan. 7–11, 1990, at the Ritz Carlton Resort Hotel, Naples, FL, as part of the society's annual meeting. This course will be an in-depth review of the state-of-the-art in cardiopulmonary radiology. Program chairman: David J. Delaney. Category 1 credit: 34 hr. Fee: physicians, \$450; residents, fellows, and technologists, \$325. Information: Dawne Ryals, Ryals & Associates, P. O. Box 1925, Roswell, GA 30077-1925; (404) 641-9773.

Society of Gastrointestinal Radiologists Annual Meeting and Postgraduate Course

The 19th annual meeting and postgraduate course of the Society of Gastrointestinal Radiologists will be Jan. 14–19 at the Hyatt Regency Waikoloa, Hawaii, HI. Information: Lynne K. Tiras, CMP, International Meeting Managers, Inc., 4550 Post Oak Pl., Ste. 248, Houston, TX 77027; (713) 965-0566.

Diagnostic Radiology Seminar in Ixtapa, Mexico

The Dept. of Radiology, University of California, San Francisco, is offering the 7th annual Ixtapa postgraduate course in diagnostic radiology, Jan. 22–26, 1990, in Ixtapa, Mexico. The course has been designed primarily for the radiologist in general practice. It provides

a survey of selected subdivisions of diagnostic radiology. Course director: Susan D. Wall. Category 1 credit: 25 hr. Fee: physicians, \$515; residents, fellows, nurses, and technologists, \$415 (letter required). Information: Radiology Postgraduate Education, Rm. C-324, University of California, San Francisco, School of Medicine, San Francisco, CA 94143-0628; (415) 476-5731.

Midwinter Radiological Conference

The Los Angeles Radiological Society (LARS) will present the 42nd annual Midwinter Radiological Conference, Jan. 26–28, 1990, at the Century Plaza Hotel, Los Angeles. The new meeting format will have 15 30-min main lectures and 45 45-min seminars. The lectures and seminars will cover six subject areas: body imaging, general radiology, mammography, musculoskeletal imaging, neuroradiology, and nuclear radiology. Category 1 credit: up to 16 hr. Fee: physicians: \$395 (3 days), \$350 (2 days), and \$175 (1 day); LARS members: \$315 (3 days), \$270 (2 days), and \$135 (1 day); residents and technologists (letter required): \$125 (3 days), \$100 (2 days), and \$50 (1 day); LARS resident member: \$100 (3 days), \$70 (2 days) and \$35 (1 day). Information: Los Angeles Radiological Society—MWRC, P. O. Box 91215, Los Angeles, CA 90009-1215; (213) 827-9078.

Coronary Atherosclerosis: New Diagnostic and Therapeutic Approaches

The Depts. of Radiology and Cardiology, Mount Sinai Medical Center, Miami Beach, FL, are sponsoring the 27th annual seminar, Coronary Atherosclerosis: New Diagnostic and Therapeutic Approaches, Jan. 28–Feb. 1, 1990, at the Contemporary Hotel, Walt Disney World, Orlando, FL. The purpose of the conference is to explore the various diagnostic and therapeutic techniques available to prevent, diagnose, and treat coronary atherosclerosis at all its stages. The conference will look at new diagnostic imaging techniques applicable to the diagnosis of coronary artery disease and its complications. Program director: Manuel Viamonte, Jr. Guest faculty: Bruce Brundage, R. C. Detrano, W. D. Edwards, Valentine Fuster, R. B. Goldberg, R. J. Herfkens, S. B. King III, R. P. Martin, H. R. Schelbert, and R. S. Schwartz. Category 1 credit: 20.5 hr. Fee: physicians, \$495; residents, fellows and technologists, \$325. Information: Lucy R. Kelley, Program Coordinator, Radiology Seminars Inc., P. O. Box 143762, Coral Gables, FL 33114-3762; (305) 674-2810.

Mid-Pacific Radiological Conference

The Los Angeles Radiological Society will sponsor the 16th annual Mid-Pacific Radiological Conference, Jan. 30–Feb. 3, 1990, at the Maui Marriott Hotel, Maui, HI. A total of 20 45-min lectures and two 30-min question-and-answer sessions will make up the mornings' activities. Topics will include mammography, neuroradiology, and thoracic and interventional radiology. Category 1 credit: up to 16 hr. Fee: physicians, \$395; residents, \$150 (letter required). Information: Los Angeles Radiological Society—MWRC, P. O. Box 91215, Los Angeles, CA 90009-1215; (213) 827-9078.

American Roentgen Ray Society New Officers

The American Roentgen Ray Society installed its new officers for 1989–1990 at the annual meeting in New Orleans, LA, May 7–12: Ronald G. Evens, president; M. Paul Capp, president-elect; John A.

Kirkpatrick, first vice-president; A. Everette James, second vice-president; Glen W. Hartman, secretary; and Beverly P. Wood, treasurer.

A Primer on the Theory and Operation of Linear Accelerators

The Medical Physics Publishing Corp. (MPPC) has announced publication of *A Primer on the Theory and Operation of Linear Accelerators*, by Robert Morton and C. J. Karzmark. The book provides an overview of the components of the linear accelerator and how they function and interrelate. It promotes an understanding of the safe and effective use of these devices. The book is available for \$13 from MPPC, 27B, 1300 University Ave., Madison, WI 53706; (608) 256-3300.

The American Board of Radiology Examinations

Written examinations for the American Board of Radiology (ABR) are scheduled for Oct. 12-13, 1989, and Sept. 27-28, 1990. Oral examinations will be held at the Executive West Hotel in Louisville, KY, June 4-8, 1990. The ABR will accept applications for admission to the examinations after July 1, but not later than Sept. 30, in the year preceding the year in which the examination is to be taken. For application forms and further information: Office of the Secretary, The American Board of Radiology, 300 Park, Ste. 440, Birmingham, MI 48009.

Meeting and Course Review

For the reader's convenience, a summary of upcoming meetings and courses is provided. Detailed listings are given in the *AJR* issue given in parentheses.

Basic and Advanced Training in MRI, times arranged, Baltimore (Dec 1988)

Visiting Fellowships in Radiology at MGH, times arranged, Boston (April)

Biliary Lithotripsy Visiting Fellowships, times arranged, Philadelphia (April)

Radiation, Physics, and Biology, Aug. 28-Sept. 1, New York City (May)

Imaging on Lake Coeur d'Alene, Aug. 31-Sept. 2, Coeur d'Alene, ID (June)

Imaging, Intervention, Ireland—1989, Sept. 2-10, Dublin, Cong. and New Market, Ireland (Feb)

Sonography Update, Sept. 7-10, San Diego (June)

Physics of Diagnostic Radiology, Nuclear Medicine, and Radiation Biology, Sept. 7-10, Sacramento, CA (Aug)

Registry Preparation Courses for Sonographers: Physics, Sept. 8-10, Dallas; Sept. 22-24, Washington, DC; Sept. 29-Oct. 1, Los Angeles; Oct. 6-8, Chicago; **Doppler Physics**, Sept. 21, Washington, DC; Oct. 2, Los Angeles; **Abdomen**, Sept. 26-27, Washington, DC; **Obstetrics and Gynecology**, Sept. 25, Washington, DC (May)

Abdominal Doppler Ultrasound and Workshop on Hepatic Hemodynamics, Sept. 11-12, Bologna, Italy (Aug)

Pathological Effects of Radiation, Sept. 11-13, Bethesda, MD (April)

1989 Interventional Neuroradiology, Sept. 11-13, Baltimore (May)

Practicums in MR Imaging: Advanced Practicum, Sept. 11-15;

Basic Practicum, Oct. 23-27; Baltimore (March)

Re-Learning Chest Radiology, Sept. 11-22, England and Scotland (July)

Refresher Course on Musculoskeletal Disorders, Sept. 13-16, New York City (July and Aug)

Transrectal Ultrasound and Prostate Cancer, Sept. 14-16, Chicago (May)

Mammography and the Search for Breast Cancer, Sept. 15-17, Vancouver, B.C. (June)

Mammography for the General Radiologist, Sept. 18-21 and Oct. 23-26, Boston (March)

Harvard Postgraduate Courses, Sept. 18-22, Boston (June)

Nuclear Cardiology Symposium and Workshop, Sept. 20-22, Milwaukee, WI (June)

Weekend MRI Seminar, Sept. 23-24, Los Angeles (July)

Applied Duplex Ultrasound, Sept. 23-25, Birmingham, AL (June)

Radiology on Ischia, Sept. 23-Oct. 1, Lacco Ameno, Island of Ischia, Bay of Naples, Italy (May)

Mozart and Masters International Diagnostic Radiology Conference, Sept. 24-29, Salzburg, Austria (Aug)

Wendell G. Scott Lecture, Sept. 25, St. Louis (Aug)

Society of Uroradiology Postgraduate Course, Sept. 25-28, Hilton Head, SC (Dec 1988)

Cardiovascular Imaging and Interventional Radiology, Sept. 25-28, Boston (July)

MR Course in Riyadh, Saudi Arabia, Oct. 2-5, Riyadh, Saudi Arabia (June)

Current Trends in Diagnostic Radiology, Oct. 2-5, Boston (June)

Update in Pediatric Imaging, Oct. 2-5, Laguna Niguel, CA (June)

Seminar in Diagnostic Ultrasound, Oct. 5-7, Ann Arbor, MI (May)

Biomedical Image Processing with Microcomputers, Oct. 5-7, St. Louis (Aug)

Breast Imaging: Problems and Solutions, Oct. 6, Boston (June)

Practical Radiology, Oct. 9-12, Charlottesville, VA (May)

Introduction to Comparative Imaging for Urologic Lithotripsy, Oct. 12, Denver (Aug)

Practical Magnetic Resonance Imaging 1989, Oct. 12-15, Las Vegas, NV (April)

Renal and Biliary Lithotripsy, Oct. 12-15, Denver (Aug)

The Lungs and Heart: Imaging Answers to Clinical Problems, Oct. 14-29, Bangkok, Chiangmai, and Phuket, Thailand; Hong Kong; and Taipei, Taiwan (July)

Organ Imaging Review 1989, Oct. 15-20, Toronto, Ontario (Aug)

Chest Disease, Oct. 16-19, Boston (July)

World Congress for Bronchology, Oct. 18-20, Tokyo, and Oct. 21-22, Kyoto, Japan (Nov 1988)

Farwest Image Perception Conference, Oct. 19-20, Tucson, AZ (June)

Royal Australasian College of Radiologists Annual Meeting, Oct. 19-23, Melbourne, Australia (March)

MRI Review '89, Oct. 20-22, Toronto, Ontario (Aug)

Visiting Fellowship in Mammography, Oct. 23-27, Los Angeles (March)

Magnetic Resonance Imaging and CT Update, Oct. 23-27, Boston (July)

Advanced Neuroradiology Seminar, Oct. 26-28, Orlando, FL (June)

Advanced Imaging of the Musculoskeletal System, Oct. 28-29, Coronado (San Diego), CA (June)

San Diego Postgraduate Course, Oct. 30-Nov. 3, Coronado (San Diego), CA (July)

International Seminar of Medical Imaging, Oct. 30-Nov. 5, Shatin, Hong Kong, the New Territories (May)

Interventional Radiology, Nov. 3-5, Coronado (San Diego), CA (July)

3-D Imaging in Medicine, Nov. 16-19, San Diego (Aug)

Advances in Chest, Interventional, and Ultrasound, Nov. 25–Dec. 10, South America (Caracas, Isla Margarita, Manaus, Recife, Rio de Janeiro, Buenos Aires, and Bariloche) (March)

Advanced Seminars in Diagnostic Imaging, Dec. 8–10, Laguna Niguel, CA (July)

Genitourinary Radiology, Dec. 15–17, Scottsdale, AZ (Aug)

XV Interamerican Congress of Radiology, Feb. 11–16, 1990, Caracas, Venezuela (Aug)

International Conference on Gallstones and Their Management, Feb. 25–28, 1990, Jerusalem, Israel (May)

Interventional Radiology in Cardiovascular Pathology, Feb. 28–March 2, 1990, Toulouse, France (Aug)

Congress of the European Federation of Societies for Ultrasound in Medicine and Biology, May 6–11, 1990, Jerusalem, Israel (May)

AJR carries announcements of courses, symposia, and meetings of interest to its readers if received a minimum of 5 months before the event. There is no charge; receipt of items by the *AJR* Editorial Office is not acknowledged. Submit items for publication typed double-spaced. Provide title, date, location, brief description, sponsor, course directors, fees, category I credit, and address and telephone number for additional information. Faculty from the host institution will not be listed. Guest faculty names will appear **only** if initials are provided. Mail news items to *AJR* Editorial Office, 2223 Avenida de la Playa, Suite 200, La Jolla, CA 92037-3218.

American Roentgen Ray Society: Officers, Committees, and Membership Information

Officers

President: Ronald G. Evens

President-elect: M. Paul Capp

1st Vice-president: John A. Kirkpatrick, Jr.

2nd Vice-president: A. Everette James, Jr.

Secretary: Glen W. Hartman

Treasurer: Beverly P. Wood

Executive Council: R. J. Alfidi, R. N. Berk, B. G. Brogdon, M. P. Capp, W. J. Casarella, R. G. Evens, J. T. Ferrucci, Jr., R. A. Gagliardi, G. W. Hartman, J. A. Kirkpatrick, Jr., A. Landry, Jr., G. R. Leopold, J. E. Madewell, A. A. Moss, L. F. Rogers, J. H. Thrall, K. H. Vydareny, B. P. Wood, A. K. Poznanski, chairman

Committees

Editorial Policy: R. N. Berk, S. V. Hilton, C. A. Rohrmann, Jr., S. S. Sagel, R. J. Stanley, J. M. Taveras, N. O. Whitley, W. J. Casarella, chairman

Education and Research: C. B. Higgins, B. J. Hillman, R. A. McLeod, W. M. Thompson, B. G. Brogdon, chairman

Finance and Budget: R. J. Alfidi, R. C. Gedgaudas-McClees, G. R. Leopold, J. R. Thornbury, J. Thrall, chairman

Nominating: R. A. Gagliardi, N. O. Whitley, R. J. Alfidi, chairman

Publications: C. A. Rohrmann, Jr., S. S. Sagel, R. J. Stanley, N. O. Whitley, W. J. Casarella, chairman

Membership: R. J. Alfidi, A. A. Moss, K. H. Vydareny, G. R. Leopold, chairman

Representatives to Other Organizations

American Board of Radiology: J. A. Kirkpatrick, Jr., E. C. Klatte, L. F. Rogers

American College of Radiology: R. A. Gagliardi, G. A. Kling, J. E. Madewell, L. F. Rogers

American Medical Association House of Delegates: S. F. Ochsner, K. L. Krabbenhoft, alternate

American National Standards Institute: M. Haskin

National Council on Radiation Protection and Measurements: H. L. Friedell, E. L. Saenger

Meeting Arrangements

Annual Meetings: May 13-18, 1990, Sheraton Washington, Washington, DC; May 5-10, 1991, Sheraton Boston, Boston

Annual Meeting Committee: H. C. Carlson, J. K. Crowe, G. P. Janetos, R. R. Lukin, A. Landry, Jr., chairman

Instruction Courses: R. J. Stanley, associate chairman, J. T. Ferrucci, Jr., chairman

Scientific Program: R. J. Alfidi, E. Buonocore, D. O. Davis, W. A. Murphy, Jr., A. E. Robinson, J. H. Thrall, M. P. Capp, chairman

Scientific Exhibits: R. J. Churchill, A. A. Moss, R. G. Ramsey, J. E. Madewell, chairman

ARRS Membership

An application form is printed in this issue of the Journal. For consideration at the 1990 ARRS meeting, send completed forms before February 1, 1990, to American Roentgen Ray Society, 1891 Preston White Dr., Reston, VA 22091. Active members are graduates of an approved medical or osteopathic school or hold an advanced degree in an allied science. They must practice radiology or work in an associated science in the United States or Canada and be certified by the American Board of Radiology, American Osteopathic Board of Radiology, or Royal College of Physicians of Canada or otherwise adequately document training and credentials. Corresponding members are foreign radiologists or scientists who are active in radiology or an allied science. Members-in-training are residents or fellows in radiology or postgraduate students in an allied science. Additional application forms can be obtained from the ARRS offices in Reston, VA.

Business Office

Paul Fullagar, Executive Director, American Roentgen Ray Society, 1891 Preston White Dr., Reston, VA 22091; (703) 648-8900

American Roentgen Ray Society 90th Annual Meeting May 13-18, 1990, Washington, DC Sheraton Washington Hotel

Registration and Hotel Reservations

Forms for advance registration and hotel reservations will be in the February and March 1990 issues of the *AJR*.

Scientific Program

Abstracts of papers to be considered for the program must be submitted by December 1, 1989. Forms on which to submit abstracts are in this issue of the *AJR*. The ARRS Program Committee will select papers and notify authors in early January. The *AJR* has first rights to all papers accepted for presentation at the ARRS meeting. Send abstract, application, and four copies of the abstract to

M. Paul Capp, M.D.
c/o Paul R. Fullagar
American Roentgen Ray Society
1891 Preston White Dr.
Reston, VA 22091

Refresher Course Program

A summary of the refresher courses will appear in the *AJR* in February along with advance registration forms. Early registration is an advantage in assuring preferred courses in this popular program. Dr. J. T. Ferrucci, Jr., is program director.

Scientific Exhibits

Proposals for scientific exhibits must reach the Chairman of Exhibits by December 1, 1989. Forms, which may be photocopied, are in this issue of the *AJR*. Send completed form to

John E. Madewell, M.D.
The Pennsylvania State University
The Milton S. Hershey Medical Center
P.O. Box 850
Hershey, PA 17033
Telephone (717) 531-8044

Caldwell Lecture

Sandra Day O'Connor, U.S. Supreme Court Justice, will be giving the Caldwell Lecture. The title of her lecture and the date and time will be announced in a future issue of the *AJR*.

Local Program

A program of sightseeing, shopping, and entertainment will be developed by the Local Arrangements Chairman, Dr. Abner M. Landry, Jr. Information and advance registration forms will be in the February issue of the *AJR*.

Residents' Award Papers

The society offers several cash awards for the best scientific papers prepared by residents in radiology. The President's Award has a \$2000 prize. There are two Executive Council awards of \$1000 each. All are presented at the annual meeting. Papers should be submitted by February 16, 1990, for consideration in this competition. Send entries to

B. G. Brogdon, M.D.
Dept. of Radiology
University of South Alabama Medical Center
2451 Fillingim Street
Mobile, AL 36617

Deadlines

Abstracts of papers: December 1, 1989
Scientific exhibit proposals: December 1, 1989
Residents' Award papers: February 16, 1990

Call for Papers

**American Roentgen Ray Society
1990 Annual Meeting:
May 13-18, 1990, Washington, DC**

ADDRESS OF PRESENTING AUTHOR

Department _____

Institution _____

Street _____

City, State _____

Zip _____

Phone: _____

Type title, authors, and abstract in the space provided below. (Instructions are on reverse side of this page. Abstract should not exceed 300 words.)

Select one category: _____Angio/Interventional _____Breast _____Chest _____CT _____Gastrointestinal Tract _____Genitourinary Tract _____MR .
Neuroradiology _____Skeletal _____Sonography

Projection Requirements: _____35 mm, single or double (circle one) _____16 mm silent film _____1/2" VHS _____3/4"

Has this been presented elsewhere? _____yes _____no. If yes, please describe on reverse side of this page.

Instructions for Scientific Abstracts

1. Type the information single-spaced within the lines. Underline the name of the presenting author. Append as a last line of the abstract any research grant support, if applicable (e.g., Supported by USPHS Grant HE-80144). If the abstract is accepted, it will not be proofread; it will appear exactly as typed. Use the following format:

MR IMAGING OF THE SPINE AND NECK
F. S. Lau, M.D., A. N. Kirk, M.D., and R. A. Beck, Ph.D.
University of California, Bakersfield, Bakersfield, CA 92338
2. Abstracts should include four paragraphs devoted sequentially to the following topics: (1) object or purpose of the study, (2) materials, methods, and procedures, (3) results, (4) significance of the results and conclusions. The text should not exceed 300 words. Specific data are essential. The abstract should be a succinct summary of work done rather than a promissory note.
3. The Program Committee will grade each abstract and determine acceptance. Further information will be forwarded to those whose abstracts are accepted for presentation.

Deadline for submission of abstract is December 1, 1989. Mail abstract and two copies to

M. Paul Capp, M.D.
c/o Paul R. Fullagar
American Roentgen Ray Society
1891 Preston White Dr.
Reston, VA 22091

Call for Scientific Exhibits

**American Roentgen Ray Society
1990 Annual Meeting:
May 13-18, 1990, Washington, DC**

FOR COMMITTEE USE ONLY

Date Received _____ Application No. _____
Subject _____ Score _____
Rejected _____ Accepted _____
Assigned _____ Space No. _____

Principal Exhibitor's Mailing Address

Name _____ Institution _____
Department _____ Street Address _____ City _____
State _____ Zip Code _____ Telephone: Office () home ()

Names of Exhibitors (List principal exhibitor first and telephone number of each person.)

Last	First	Middle	Telephone	Degree (one only)	Member ARRS?
_____	_____	_____	_____	_____	_____
_____	_____	_____	_____	_____	_____
_____	_____	_____	_____	_____	_____
_____	_____	_____	_____	_____	_____

Title of Exhibit _____

Type abstract single-spaced in the space provided below. (See instructions on the reverse side of this page.)

Instructions for Abstract

The abstract should be a brief paragraph that states the purpose, principal information, and conclusions of the exhibit. Promissory statements are not acceptable. Type single-spaced in the space provided on the reverse side. Brevity is desirable but not at the expense of specific information. **The abstract will appear in the program book as submitted.** Please use typewriter and complete the application form on both sides. List space requirements.

What Sort of Exhibit Is Proposed? (Check one and fill in all appropriate blanks.)

_____ **Free-standing.** This is a self-contained display created in total by the exhibitor. It may be a fold-open unit, a unit shipped in cases and assembled on site, or a tabletop unit. Linear feet required _____.

_____ **Poster Board (backboard panels).** Backboard panels are 4 × 6 or 4 × 8 ft. (1.2 × 1.8 or 1.2 × 2.5 m). Number of panels required _____ 4 × 6 or _____ 4 × 8. If two panels are needed, there will be a ¼-in. frame separating the panels, thus requiring a separation in the presentation.

_____ **Viewbox.** Mounted materials (radiographs and other transparencies) for display on the society's illuminators. Each illuminator is 39.5 × 59.5 in. (100 × 151 cm). Number of illuminators required _____. Slides should not be glass mounted.

_____ **Audiovisual.**

Please Indicate Most Appropriate Category.

Diagnostic Radiology

_____ Bone _____ Cardiovascular System _____ Chest _____ Pediatric Radiology _____ Gastrointestinal Tract
_____ Genitourinary Tract _____ Neuroradiology _____ Mammography

Other

_____ Medical Physics _____ Nuclear Medicine _____ Radiation Oncology _____ Radiobiology _____ Sonography

Has the exhibit been shown in whole or in part at any previous meeting? _____ (Previous display does not preclude acceptance.)

If so, where? _____ When? _____

Nature of meeting or name of society _____

Signature of Principal Exhibitor _____

Exhibitors will receive instructions for exhibit preparation.

Applications must be received no later than December 1, 1989. Mail original and five copies to

John E. Madewell, M.D.
The Pennsylvania State University
The Milton S. Hershey Medical Center
P. O. Box 850
Hershey, PA 17033

Telephone: (717) 531-8044

Classified Advertisements

Positions Available

ISRAEL, DIAGNOSTIC RADIOLOGY. Opportunities for 3-4 week or longer working vacations in a number of Israeli medical centers, on a volunteer basis. Positions varied, arrangements flexible. For information contact: Jonathan H. Fish, M.D., 1844 San Miguel Dr., #302, Walnut Creek, CA 94596; (415) 947-0560. 8-10ap

DIAGNOSTIC RADIOLOGIST, ABDOMINAL IMAGING.—The University of Missouri-Columbia Hospital and Clinics is seeking a radiologist with expertise in abdominal imaging (GI, CT, ultrasound, and MRI). Board certification required. Fellowship desirable. Tenured and nontenured tracks available at assistant and associate professor levels. Address inquiries to Robert J. Churchill, M.D., Dept. of Radiology, University of Missouri-Columbia Hospital and Clinics, One Hospital Dr., Columbia, MO 65212. An equal opportunity/affirmative action employer. 9-12a

NEURORADIOLOGIST.—A position is available in the Dept. of Radiology, at the University of Rochester Medical Center, Strong Memorial Hospital, a 750-bed tertiary-care facility. An appointment as assistant professor or higher is available at a level appropriate to experience. A fellowship is required. Research and teaching opportunities are available in a strong academic dept. with state-of-the-art radiologic equipment. Send CV to Daniel K. Kido, M.D., Diagnostic Radiology, Box 648, University of Rochester Medical Center, Rochester, NY 14642. EO/AA/M-F employer. 9-11a

PEDIATRIC RADIOLOGIST.—The University of Rochester Medical Center, Strong Memorial Hospital, a 750-bed tertiary-care facility has an opening within the Pediatric Section of the Dept. of Radiology. State-of-the-art equipment, a high volume of neonatal and oncology work, research, and teaching opportunities are available in a strong academic dept. Faculty rank depends on qualifications. Send CV to Robert E. O'Mara, M.D., Chairman, Dept. of Radiology, Box 648, University of Rochester Medical Center, Rochester, NY 14642. EO/AA/M-F employer. 9-11a

DIAGNOSTIC RADIOLOGIST WITH SPECIAL INTEREST IN ANGIOGRAPHY AND INTERVENTIONAL RADIOLOGY.—The Dept. of Radiology at The University of Texas Medical School at Houston has an immediate opening for an experienced interventionist/angiographer with strong interest in patient care and teaching. Research interest and experience are important, but not essential. While the principal responsibilities will be in intervention/angiography, there will be an opportunity to be involved in other clinical areas of the candidate's interest. The position will include teaching at the medical student and resident levels. Candidate must be a diplomate of the American Board of Radiology and have completed at least a 1-yr interventional/angiography fellowship, have a Texas state medical license, and have had at least 1 yr post-fellowship experience. Candidates with the qualifications for a senior assistant professor or associate professor appointment are preferred. Academic rank and salary will be commensurate with qualifications. Please submit CV, along with the names and addresses of 3 references to John H. Harris, Jr., M.D., Dept. of Radiology, The University of Texas Medical School of Houston, 6431 Fannin St., Ste. 2.132, Houston, TX 77030. The University of Texas Health Science Center at Houston is an equal opportunity employer. Women and minorities are encouraged to apply. 9-12a

TWO DIAGNOSTIC RADIOLOGISTS.—Four-person, private practice group seeks 2 BC/BE radiologists with expertise in CT, angio/interventional, ultrasound, and mammography. MRI/neuro/trauma experience helpful. Practice includes 225-bed private hospital plus 2 smaller hospitals. University affiliation, some teaching. Duluth is a pleasant northern community which combines proximity to outdoor recreation with the advantages of a small urban center. Competitive salary/fringe leading to early partnership. Send CV or call F. Ekberg, M.D., 915 E. 1st St., Duluth, MN 55805; (218) 726-5222. 9-11ap

NUCLEAR RADIOLOGIST.—A newly created staff position with medical school appointment is available for a board-certified radiologist with subspecialty training. Certification in nuclear radiology desirable. Join a progressive, expanding dept. with state-of-the-art gamma cameras with SPECT and a computerized image-processing system in a 450-bed teaching hospital with accredited radiology residency. Many clinical and research opportunities. Must be able to obtain licensure in Massachusetts. Please contact Elizabeth Oates, M.D., Director, Division of Nuclear Medicine, Box 228, Tufts-New England Medical Center, 750 Washington St., Boston, MA 02111; (617) 956-6342. 9a

NEURORADIOLOGIST AND BODY IMAGER.—Immediate openings for a neuroradiologist and a body imager at Montefiore Medical Center. Montefiore is a 740-bed, tertiary-care hospital with state-of-the-art equipment. At least 1 yr of neuro-radiology fellowship is required for the neuro-radiology position. Fellowship experience is desirable for the body imaging position. Please send CV to Seymour Sprayregen, M.D., Acting Chairman, Dept. of Radiology, Montefiore Medical Center/Albert Einstein College of Medicine, 111 E. 210th St., Bronx, NY 10467. 9ap

POSITION AVAILABLE.—Two diagnostic radiologists seek a BE/BC radiologist to join them in a growing practice in northeast Michigan. Our 176-bed, regional referral hospital serves an area population of 80,000-100,000. All diagnostic modalities with the exception of MRI are represented. Equipment includes Acuson ultrasound, Siemens, Somatom CT, and dedicated Phillips mammography. Our location on Lake Huron offers immediate access to sailing, fishing, scuba diving, etc. Excellent hunting, snowmobiling, and cross-country skiing are favorite fall and winter activities. This is an outstanding opportunity for someone seeking a small town atmosphere, a dynamic radiology practice with early partnership in a beautiful outdoor area. Please respond to Box T5, AJR (see address this section). 9-11a

CHAIRPERSON, DEPT. OF RADIOLOGY.—The Albert Einstein College of Medicine/Montefiore Medical Center are seeking a chairperson for their Dept. of Radiology. The chairperson has the academic responsibility for the radiology programs at all of the affiliated hospitals of the medical school and the clinical responsibility for the 4 major teaching hospitals which, with the college, comprise the Bronx campus of the Albert Einstein College of Medicine. Candidates must have demonstrated leadership and broad experience in the clinical practice of radiology, experience in teaching and research, and a proficiency in administration. Applications and nominations for the position should be sent to Lawrence W. Davis, M.D., Chairman, Radiology Search Committee, Chairman, Dept. of Radiation Oncology, Montefiore Medical Center/Albert Einstein College of Medicine, 1825 Eastchester Rd., Bronx, NY 10461. An equal opportunity employer. 9a

ASSISTANT PROFESSOR OF NEURORADIOLOGY.—The University of Texas Medical School at Houston has an opening for a neuroradiologist who will perform clinical neuroradiology. Candidate will participate in resident and medical student teaching and will have the opportunity to do basic or clinical research. Candidates must have completed an approved residency in diagnostic radiology and must have successfully completed 2 yr of a neuroradiology fellowship. Candidates must be board-certified by the American Board of Radiology or equivalent and must have a Texas medical license. Applicants should send a CV, along with the names and addresses of 3 references, to John H. Harris, Jr., M.D., D.Sc., Professor and Chairman, Dept. of Radiology, The University of Texas Medical School at Houston, 6431 Fannin St., Ste. 2.132, Houston, TX 77030. The University of Texas Health Science Center at Houston is an equal opportunity employer. Women and minority candidates are encouraged to apply. 9-12a

DIAGNOSTIC RADIOLOGIST.—State-of-the-art practice includes ultrasound, nuclear medicine, digital subtraction angiography, CT, and MRI. Excellent practice. Excellent financial package. Send CV to Robert L. Dever, M.D., 1416 Big Bend Rd., Poplar Bluff, MO 63901; (314) 785-0125. 9-12ap

VASCULAR RADIOLOGIST.—Board-certified vascular radiologist to join dept. in a university-affiliated hospital in western Pennsylvania. Applicant should have fellowship training or past residency experience in vascular and interventional procedures. The radiologists are organized as a professional corporation offering excellent salary and fringe benefits. Send inquiries and CV to Radiologist-in-Chief, Montefiore Hospital, 3459 Fifth Ave., Pittsburgh, PA 15213. 9ap

ULTRASONOLOGIST.—Board-certified radiologist with fellowship training in ultrasound to join dept. in a university-affiliated hospital in western Pennsylvania. Position immediately available. The radiologists are organized as a professional corporation offering excellent salary and fringe benefits. Send inquiries and CV to Radiologist-in-Chief, Montefiore Hospital, 3459 Fifth Ave., Pittsburgh, PA 15213. 9ap

CHIEF, BREAST IMAGING CENTER.—The Dept. of Diagnostic Radiology at William Beaumont Hospital is seeking a radiologist with mammography experience to head its modern breast imaging center which includes breast ultrasound. There will be some rotation in general radiology. Beaumont Medical Center is a 940-bed, modern, tertiary-care teaching hospital in southeastern Michigan with residency and fellowship in most subspecialties including radiology. Excellent remuneration and fringe benefits. For further information, write to Jalil Farah, M.D., Chairman, Diagnostic Radiology, William Beaumont Hospital, 3601 W. 13 Mile Rd., Royal Oak, MI 48072; (313) 551-6064. 9-11a

INTERVENTIONAL RADIOLOGIST.—A tenure-track position at the rank of assistant professor to professor is available in the Dept. of Radiology at the University of Virginia Health Sciences Center. Salary and academic rank commensurate with experience and qualifications. Minimum requirements include M.D. with board certification in radiology and competence in angiography, interventional radiology, and special procedures. Starting date is negotiable. Please provide CV and names and addresses of 3 references. Contact Charles J. Tegtmeyer, M.D., Professor and Director, Division of Angiography, Interventional Radiology and Special Procedures, Box 170, University of Virginia Health Sciences Center, Charlottesville, VA 22908; (804) 924-9401. Equal opportunity/affirmative action employer. 9-11a

SOUTH FLORIDA, IMMEDIATE OPENING—

Rapidly expanding, 10-person group with 3 hospitals, MRI center, and imaging office desires an additional well-trained radiologist. Interventional radiology fellowship and/or equivalent interventional experience a must. This is a highly desirable private practice with partnership potential. Please send CV to Lee M. Katims, M.D., Dept. of Radiology, 21644 State Rd. 7, Boca Raton, FL 33428. 9-11ap

APPROVED "B" READER to interpret chest x-rays on- or off-site in central New Jersey. Contact Joel Namm, M.D., 838 W. State St., Trenton, NJ 08618. 9-11ap

RADIOLOGIST, IMMEDIATE OPENING—New York City imaging center seeks board-certified radiologist, specialty MRI, with experience in CT. General Electric equipment. Replies to Box T9, AJR (see address this section). 9-11ap

DIRECTOR, DIVISION OF RADIATION ONCOLOGY—

Emory University School of Medicine invites nominations and applications for the position of director of the Division of Radiation Oncology. The division is an autonomous unit of the Dept. of Radiology with teaching, research, and patient care responsibilities in a variety of clinical settings throughout the Woodruff Health Sciences Center. Responsibilities include the direction, management, and continued development of a division committed to excellence in these areas. Candidates must hold an M.D. degree from an accredited institution, be board-certified, and be eligible for medical licensure in Georgia. Also required are demonstrated leadership capabilities, previous academic and administrative responsibilities, a strong record in research, and excellent clinical skills. Salary is negotiable. Applications should include a current CV and the names of 3 references and should be submitted by Oct. 1, 1989 to Radiation-Oncology Search Committee, 409 Woodruff Health Sciences Center, Emory University School of Medicine, Atlanta, GA 30322. Emory University is an equal opportunity/affirmative action employer. 9a

MRI PHYSICIST—The Dept. of Radiology at the University of Minnesota has a full-time, tenure-track position available as an MRI physicist at the rank of assistant or associate professor beginning Nov. 1, 1989. At the assistant professor level, minimum requirements are a Ph.D., board certification or eligibility for certification in radiological physics, and 2-yr experience in MRI and spectroscopy. Appointment at the rank of associate professor requires a minimum of 4-yr experience in radiological physics, 2-yr experience in MRI and spectroscopy, and a demonstrated record of research, publication, and teaching, in addition to the other qualifications listed for the assistant professor status. Responsibilities will include working with a spectroscopy research group on small-bore systems, participation in research on a 4.0-T, full-size (1.25-m bore) patient imaging and spectroscopy system, and participation in both graduate and undergraduate medical instruction. The candidate also will have access to a number of departmental and university computer facilities including image-processing workstations and several supercomputers. Research performance will be strongly encouraged and evaluated. Salary is negotiable and competitive, and is dependent on past scholarly productivity and experience. Applications will be accepted through Oct. 31, 1989. Send letters to Dr. E. Russell Ritenour, Director, Physics Section, Dept. of Radiology, Box 292 UMHC, 420 Delaware St., S.E., Minneapolis, MN 55455. The University of Minnesota is an equal opportunity and affirmative action educator and employer and specifically encourages applications from women and minorities. 9a

DIAGNOSTIC RADIOLOGIST—Immediate opening for a board-certified radiologist to join young, dynamic, 4-person group in the Miami area. All modalities including special procedures, CT, nuclear medicine, and MRI. Community hospital-based practice with adjacent outpatient facility. Competitive salary and benefits with partnership opportunity. Location convenient to Florida Keys, with easy access to downtown, cultural, and recreational facilities. Please contact Roberto J. Calderon, M.D.P.A., 730 N.W. 107 Ave., Ste. 108, Miami, FL 33172. 9-11ap

PEDIATRIC RADIOLOGIST—Full-time faculty position, Dept. of Radiology, Children's Hospital Medical Center, Cincinnati OH, at academic rank of assistant professor to professor, Dept. of Radiology and Pediatrics, University of Cincinnati College of Medicine, available July 1, 1990. Salary and fringe benefits are highly competitive. Candidates must be certified in diagnostic radiology by the American Board of Radiology or its equivalent, must have completed a fellowship in pediatric radiology, and must be eligible for active membership in the Society for Pediatric Radiology. Children's Hospital Medical Center is a 355-bed institution where approximately 95,000 radiologic exams are performed annually by 12 full-time faculty radiologists. Professional coverage includes conventional radiography, ultrasonography, CT, MRI, nuclear medicine, and digital radiography. The candidate must have a demonstrated interest and qualifications in basic and/or clinical pediatric imaging research. Children's Hospital Medical Center and University of Cincinnati are affirmative action/equal opportunity employers. Address inquiry and CV to Donald R. Kirks, M.D., Director, Dept. of Radiology, Children's Hospital Medical Center, Cincinnati, OH 45229-2899; (513) 559-8058. 9ap

IMMEDIATE OPENING, DIAGNOSTIC RADIOLOGIST—Large, private practice, 3 hospitals, northeast Philadelphia suburbs and Trenton, NJ, between Philadelphia and Princeton. Two positions to start preferably Dec. 1989 or later. Practice requires all areas of diagnostic radiology; expertise in angio-interventional, MRI, or cross-sectional imaging desired. Fellowship or practice experience preferred. Send letter and CV to S. Meshkov, M.D., 838 W. State St., Trenton, NJ 08618. 9-11ap

NEURORADIOLOGIST DIRECTOR, MRI AND NEURORADIOLOGY—This outstanding opportunity within an established, free-standing imaging center is available to an experienced neuro-radiologist. Directorship of this center requires extreme commitment and offers meaningful rewards. Desirable greater Los Angeles area location. To discuss this further, please send your CV in confidence to our management group, Med-Eval Services, 8447 Wilshire Blvd., Ste. 113, Beverly Hills, CA 90211, Attn: Edward Giron. 9a

CHAIRMAN, DEPT. OF RADIOLOGY—West Virginia University School of Medicine invites applicants for chair of the Dept. of Radiology. This endowed position, vacant because of the retirement of the chairman, requires the leadership of a nationally recognized radiology educator with strong clinical, teaching, and research credentials to administer the clinical and academic programs of the dept. The dept. enjoys superb facilities and state-of-the-art diagnostic equipment in a beautiful new teaching hospital on the campus of the Health Sciences Center of the parent university. The deadline for receipt of applications is Oct. 1, 1989. Interested candidates should forward CV to William A. Neal, M.D., Chairman of the Search Committee, Dept. of Pediatrics, WVU School of Medicine, Morgantown, WV 26506. An equal opportunity employer. 9a

PERMANENT HOSPITAL PRACTICE AND RADIOLOGY GROUP POSITION—

Immediate opening for board-certified, nuclear medicine physician in 12-person, fee-for-service radiology group with medical school affiliation and 2 clinic offices. Expertise in nuclear cardiology necessary. Teaching involved. Midwestern location at St. Francis Medical Center, a 700-bed, tertiary-care medical center with 12 radiologists and 130 radiology dept. personnel. Outpatient clinic. There are 84,000 inpatient and 56,000 outpatient radiologic exams/yr. Nuclear medicine division consists of 5000 sq. ft. with approximately 7500 nuclear medicine procedures performed per yr. Excellent starting salary (negotiable) with full partnership anticipated in 12 mo. Send confidential inquiries to T. J. Cusack, M.D., Dept. of Radiology, St. Francis Hospital, 530 N.E. Glen Oak Ave., Peoria, IL 61637. 9ap

DIAGNOSTIC RADIOLOGIST, GEORGIA—

Group of 5 board-certified radiologists affiliated with 300-bed, acute-care hospital in Savannah, GA, seeks BC/BE associate. Excellent facilities include CT, nuclear medicine with SPECT, general and vascular ultrasonography, mammography, neuro/angio/interventional, and MRI. Practice includes new private office, liberal benefits, and early partnership. Demographics include an expanding economy in an attractive community with outstanding recreational resources. Please include CV with letter of inquiry to Thomas Philbrick, M.D., Savannah Radiologists, P. O. Box 14444, Savannah, GA 31499. 9-11ap

THE DEPT. OF RADIOLOGY AT THE UNIVERSITY OF MISSOURI-COLUMBIA

is seeking a full-time NMR spectroscopist at the assistant professor level. The candidate must have a Ph.D. in NMR spectroscopy. Duties include setting up an in vivo spectroscopy program for a whole body scanner and an animal imager/spectrometer. Address inquiries to Robert J. Churchill, M.D., Dept. of Radiology, University of Missouri-Columbia Hospital and Clinics, One Hospital Dr., Columbia, MO 65212. An equal opportunity/affirmative action employer. 9ap

THE DEPT. OF DIAGNOSTIC RADIOLOGY AND NUCLEAR MEDICINE AT STANFORD UNIVERSITY SCHOOL OF MEDICINE

is seeking an academic radiologist to coordinate activities related to extracranial MRI. The individual must be clinically expert in this area and be capable of leading the teaching of the subject to house staff and medical students. The candidate should be able to establish an independent research program. We are particularly interested in recruiting an individual with interests in cardiovascular MRI/MRS. The position will be at the level of associate professor or professor. Stanford University is committed to increasing representation of women and members of minority groups on its faculty and particularly encourages applications from such candidates. All interested candidates should send a letter of inquiry and CV to Gary M. Glazer, M.D., Chairman, Dept. of Diagnostic Radiology and Nuclear Medicine, Stanford University Medical Center, Stanford, CA 94305-5105. 9a

DIAGNOSTIC RADIOLOGIST, NORTHEASTERN PENNSYLVANIA—

Opportunity available for board-certified/eligible general radiologist with experience in MRI, ultrasound, CT scanning, nuclear medicine, and mammography in a 130-bed, community hospital located in the pleasant Pocono Mountain Resort region of northeast Pennsylvania. Competitive salary and early partnership. The area offers outstanding recreational opportunities and is within a reasonable distance of New York and Philadelphia. Contact Fred C. Van Natta, M.D., Dept. of Radiology, Wayne County Memorial Hospital, Honesdale, PA 18431. 9-10a

THE DEPT. OF RADIOLOGY, VIRGINIA COMMONWEALTH UNIVERSITY/MEDICAL COLLEGE OF VIRGINIA, Richmond, VA, seeks faculty for positions in diagnostic radiology: chest, GI, mammography, CT/ultrasound/MRI, neuroradiology, pediatrics, ER, angio/interventional, and general radiology. Our 1958-bed facility (205 for pediatric patients) is a Level 1 trauma center. ABR certification of eligibility required. Academic rank and salary commensurate with experience. Submit CV to A. V. Proto, M.D., Diagnostic Radiology, Medical College of Virginia, MCV Box 47, Richmond, VA 23298-0047. VCU/MCV is an equal opportunity/affirmative action employer. Women and minorities are encouraged to apply. 9-12a

IMMEDIATE OPENING IN PHILADELPHIA, PA—Excellent opportunity for diagnostic radiologist to join newly formed private group in 260-bed, south Philadelphia hospital. Prefer starting date Dec. 1989; would consider later. Expertise in angio-interventional or cross-sectional imaging desired. Practice requires all areas of diagnostic radiology. Fellowship or practice experience preferred. Send letter and CV to Box 77, AJR (see address this section). 9-11ap

NEURORADIOLOGIST—The University of Missouri-Columbia Hospital and Clinics is seeking a second neuroradiologist. Board certification required. Junior or senior member of ASNR. Tenured and nontenured tracks available at assistant and associate professor levels. Address inquiries to Robert J. Churchill, M.D., Dept. of Radiology, University of Missouri-Columbia Hospital and Clinics, One Hospital Dr., Columbia, MO 65212. An equal opportunity/affirmative action employer. 9-12a

SOLO RADIOLOGIST IN QUIET, RURAL WESTERN OREGON PRACTICE SEEKING BC/BE ASSOCIATE, SUMMER 1990—Full-time as locum tenens first yr, then share practice. General radiology, ultrasound, and mammography. Planning CT. Time, lifestyle, and conscientious quality care must be as important as income. Send CV to Hugh McMahan, M.D., 1312 Chestnut Ave., Cottage Grove, OR 97424; (503) 942-0511 PDT. 9ap

RADIOLOGIST—Expanding radiology practice has an opening for a radiologist with fellowship or postgraduate experience in interventional radiology. Exceptional general radiology talents also needed. Special competency in nuclear medicine and MRI a plus, but not mandatory. Practice is located in Albuquerque, NM and consists of 13 physicians serving 3 major hospital facilities and a separate MRI center. Climate and living conditions are outstanding. Qualified applicants may send CV and references to Radiology Associates of Albuquerque, P.A., 4001 Indian School Rd., N.E., Ste. 300, Albuquerque, NM 87110, Attn: J. R. Ellison, Business Manager. 8-10ap

VASCULAR/INTERVENTIONAL RADIOLOGIST—Fellowship training or equivalent postgraduate experience in all aspects of vascular and interventional radiology required. Practice at 120-bed, JCAHO acute-care hospital near Walt Disney World in central Florida. Qualified applicants may send CV to President, Kissimmee Memorial Hospital, P. O. Box 2103, Kissimmee, FL 32742-2108. 8-9a

DIAGNOSTIC RADIOLOGIST to associate with 6-person group at county hospital (major trauma center) and private office. Partnership after 2 yr. Start early September or by arrangement. Equal opportunity employer. Contact L. Preger, M.D., Highland Hospital, 1411 E. 31st St., Oakland, CA 94602; (415) 437-4205. 8-9ap

MAINE—General radiologist to join busy practice affiliated with modern, 92-bed, acute-care hospital. Diagnostic modalities include ultrasound, mammography, angiography, nuclear medicine, and mobile CT. Beautiful 4-season recreation area close to skiing, hunting, and fishing. Excellent school system. Competitive first yr salary with partnership available by the second yr. For further information, send CV to New England Health Search, 63 Forest Ave., Orono, ME 04473; (207) 866-5680 or (207) 866-5658. 8-11ap

DIAGNOSTIC RADIOLOGIST—BC/BE diagnostic radiologist to join established radiologist in Lexington, KY. Practice includes community hospital, pediatric orthopedic hospital, and office. No interventional radiology. Procedures include MRI (1.0 T), MRA, CT, mammography, fluoroscopy, radiography, ultrasound, and nuclear medicine. Siemens equipment throughout office. Candidate desired for fall 1989 to coincide with reopening of office at a new site. Locum tenens desired in interim. Terms negotiable. Contact James C. King, Jr., M.D., 3313 Overbrook Dr., Lexington, KY 40502; (606) 278-7329 or (606) 229-3330. 8-9ap

VASCULAR/INTERVENTIONAL RADIOLOGIST—The Dept. of Radiology of Emory University Hospital, Atlanta, GA, has a faculty position available for a board-certified vascular/interventional radiologist with fellowship training. Academic rank depends on qualifications and experience. A strong interest in care of patients, teaching, and research is required. Submit application and CV to Stephen L. Kaufman, M.D., Director of Vascular and Interventional Radiology, Emory University Hospital, 1364 Clifton Rd., N.E., Atlanta, GA 30322. Emory University is an equal opportunity/affirmative action employer. 8-10a

EUGENE, OR—BC/BE, general, and axial imaging radiologist. Group of 9 radiologists in Pacific Northwest seeking a new associate for a growing radiology practice. All imaging modalities represented are state-of-the-art. Practice is in a 400-bed hospital with an excellent referring staff. A very democratic, fair radiology group and a great environment to raise a family make this opening especially desirable. Two yr to full partnership. Prepartnership compensation negotiable, commensurate with experience. Prefer fellowship experience in MRI, CT, or ultrasound with Doppler. Please send CV to L. Paul Wilson, M.D., 667 E. 12th Ave., Ste. 110, Eugene, OR 97401. 8-10ap

INTERVENTIONAL/DIAGNOSTIC RADIOLOGIST—Immediate opening for a board-certified diagnostic radiologist in Providence, RI. Well-established private practice of 5 radiologists encompassing a tertiary-care hospital and 1 private office. Interventional fellowship, interest in general diagnostic radiology, and teaching skills required. Address CV and inquiries to Allan M. Deutsch, M.D., Director, Dept. of Radiology, Miriam Hospital, 164 Summit Ave., Providence, RI 02906; (401) 274-3700, ext. 4408. 8-10ap

RADIOLOGIST—Board-certified/eligible. Opportunity to join a multispecialty group that is affiliated with the University of Alabama School of Medicine. Candidate must be experienced in general diagnostic radiology, arteriography, ultrasound, nuclear medicine, and CT. Attractive base salary and fringe benefits package. Write or call Neal M. Miller, M.D., P. O. Box 55845, Birmingham, AL 35255-5845; (205) 934-5942. 8-9ap

RADIOLOGIST—Associate diagnostic radiologist to join a group of 4. Hospital and private practice. All imaging capabilities. Angiography and nuclear medicine. One hr from Boston. Reply Box R12, AJR (see address this section). 7-9ap

DIAGNOSTIC RADIOLOGIST—Two positions: 1 full-time leading to early partnership; 1 full-time salary for 1 yr. We are a private practice group of 7 full- and 2 part-time board-certified radiologists, all with prior fellowship and/or faculty status, practicing general radiology with specialty interests accommodating all diagnostic and interventional modalities, including MRI. Our 350-bed hospital is a primary teaching affiliate of University of Massachusetts Medical School with year-round medical students and house staff in several dept. The Berkshire Mountains are a desirable summer, winter, and fall foliage resort community, less than 3 hr drive to all major northeastern cities. Quality of our practice, hospital, affiliated office, and style of life are superior. Please respond with CV to Stuart Masters, M.D., Chairman, Dept. of Radiology, Berkshire Medical Center, 725 North St., Pittsfield, MA 01201. 8-11ap

DIAGNOSTIC RADIOLOGIST sought to join a fee-for-service group practice in a 458-bed Bronx hospital. Board certification with expertise in ultrasound, MRI, CT, special procedures, and general diagnostic radiology preferred. Send CV to St. Barnabas Radiological Associates, P. O. Box 4332, Great Neck, NY 11027, or call M. Gade, M.D.; (212) 960-6171. 8-1ap

BC/BE DIAGNOSTIC RADIOLOGIST needed to join a 3-member group at a 210-bed community hospital in mid-Michigan. Practice includes general radiography, mammography, CT, nuclear medicine, ultrasound, and invasive procedures. Generous salary and benefits as well as vacation and conference time. Early partnership and investment opportunity. Send CV to Owosso Radiology Associates, 826 W. King St. Owosso, MI 48867. 8-9ap

SAN FRANCISCO BAY AREA, DIAGNOSTIC RADIOLOGY—Full-time position available as of July 1989 for BC/BE radiologist to join established group based in growing SF Bay area communities. Competence in all modalities including MRI and angiography required; fellowship training desirable. Contact J. Fish, M.D., c/o Walnut Creek Radiology, 1844 San Miguel Dr., #302, Walnut Creek, CA 94596; (415) 947-0560. 7-9a

ON JULY 1, 1990 THE FACULTY OF THE UNIVERSITY OF TEXAS MEDICAL SCHOOL AT HOUSTON will assume clinical practice, teaching, and research at the Lyndon Baines Johnson (LBJ) General Hospital, newly constructed by the Harris County Hospital District, in Houston, TX. LBJ General will be a principal medical student teaching affiliation of the UTMSH, is certified for 307 beds, and is projected to perform approximately 130,000 imaging procedures the first yr. The Dept. of Radiology at LBJ is fully-equipped with new state-of-the-art GE equipment, including a 9800 Quick CT scanner with 3-D software and an LU angiographic unit, comparable routine, R and F, ultrasound, and nuclear equipment. Full-time UTMSH faculty positions exist for 5 associate professors and 10 assistant professors with clinical, teaching, and research interests in all aspects of diagnostic imaging. Compensation, based upon the most recent AAMC survey, will be commensurate with training and experience. Candidates must be diplomates of the American Board of Radiology or its equivalent, and must have a Texas medical license. Applicants are requested to send their CV to John H. Harris, Jr., M.D., D. Sc., and John S. Dunn, M.D., Chairman, Dept. of Radiology, the University of Texas Medical School at Houston, 6431 Fannin, Ste. 2.132, Houston, TX 77030. The University of Texas Health Science Center at Houston is an equal opportunity employer. Women and minorities are encouraged to apply. 8-11a

ABDOMINAL RADIOLOGY—Tulane University Medical Center has a position available for an experienced radiologist with clinical and research interests in all aspects of abdominal imaging including ultrasound. Applicants must be ABR-certified and eligible for Louisiana licensure. Tulane University is an AA/EOE and particularly encourages applications from qualified women and minority candidates. Please contact Arvin E. Robinson, M.D., Chairman, Radiology, Tulane University Medical Center, 1430 Tulane Ave., New Orleans, LA 70112; (504) 587-7567. 8-10ap

ALEXANDRIA, VA GROUP seeks BC associate for hospital/office practice. Candidate should have expertise in all areas of noninterventional radiology including nuclear medicine and MR. Present 8-person group staffs 400-bed hospital, MR center, and active offices. Submit CV to William V. Hindle, M.D., Chairman, Dept. of Radiology, Alexandria Hospital, 4320 Seminary Rd., Alexandria, VA 22304. 8-10ap

NEW HAMPSHIRE—Excellent opportunity for young, BC/BE, general radiologist with MRI experience to join well-established, busy, small group. Live and work in beautiful Connecticut Valley Region close to lakes and skiing. Competitive compensation package leading to partnership. Please send CV to New England Health Search, 63 Forest Ave., Orono, ME 04473; (207) 866-5680 or (207) 866-5685. 8-10ap

TWO RADIOLOGISTS, BC/BE to join 2 others in N.E. Florida location of St. Augustine. Two hospitals, imaging center, and mobile MRI. Excellent salary in lovely beach community. Send CV to Dr. Lewis or Dr. Mendenhall, St. Augustine General Hospital, U.S. 1 South, Box 2208, St. Augustine, FL 32085; (904) 824-8431. 7-10ap

NEURORADIOLOGIST—The University of Texas Health Science Center at San Antonio is seeking a qualified academic neuroradiologist to fill an immediate opening. Send cover letter and CV to John R. Jinkins, M.D., Director of Neuroradiology, University of Texas Health Science Center, 7703 Floyd Curl Dr., San Antonio, TX 78284-7800. 6-11ap

NORTHWEST TEXAS—Four-person group, servicing a 356-bed adult medical-surgical hospital and a 16-physician internal medicine clinic, has need for a radiologist with particular interest and/or training in ultrasound including Doppler. Hospital has 2 new ATL Mark IX units. 1600 ultrasound exams, including 325 Doppler exams, performed this past yr. Radiology dept. getting new CT scanner and special suite this yr. Interested parties send CV to Radiological Associates, 1901 Medi-Park, Ste. 101, Amarillo, TX 79106. 7-9ap

MINNEAPOLIS, MN—Practice opportunity for a board-certified radiologist with subspecialty interest in musculoskeletal imaging. MR expertise and procedural skills mandatory. Large volume of invasive spine and orthopedic procedures. Practice is based at a rapidly growing, privately owned, freestanding, outpatient imaging center equipped with GE 9800 Quick and 8800 CT scanners, 2 GE Signa 1.5-T MR scanners, and related fluoroscopic-radiographic and ultrasound equipment. Practice also includes coverage of a 750-bed, tertiary-care medical center. Three radiologists in practice currently. One distant MR facility operating, another under construction, and plans for more. Investment opportunities for radiologists involved in the practice as well as academic orientation and opportunity for subspecialization. Outstanding benefits. Send CV and responses to Kurt P. Schellhas, M.D., Center for Diagnostic Imaging, 5775 Wayzata Blvd., Ste. 190, Minneapolis, MN 55416. No telephone calls please. All inquiries confidential. 6-9ap

BREAST IMAGING RADIOLOGIST, THOMAS JEFFERSON UNIVERSITY HOSPITAL—The Dept. of Radiology at Thomas Jefferson University Hospital in Philadelphia has an immediate opening in a faculty position with emphasis on mammography and breast ultrasound. Some work in the general diagnostic division also is included. Jefferson has a large new Breast Imaging Center currently averaging about 85 studies/day, as well as active research and teaching programs. Excellent salary and benefits are offered. Contact either Stephen A. Feig, M.D., Director of Breast Imaging, or David C. Levin, M.D., Professor and Chairman, Dept. of Radiology, Thomas Jefferson University Hospital, Philadelphia, PA 19107. Thomas Jefferson University is an equal opportunity/affirmative action employer. 6-11ap

PEDIATRIC RADIOLOGIST—Vacancies are available in various parts of the Pediatric Radiology Dept. at The Hospital for Sick Children, Toronto. The hospital is a 560-bed, tertiary-care, pediatric center situated in downtown Toronto and affiliated with the University of Toronto. 100,000 exams are performed each yr, and the staff includes 17 full-time pediatric radiologists and 7 fellows. Positions are available in general pediatric radiology areas as well as in more specialized areas such as neuroradiology. The dept. is equipped with state-of-the-art equipment. Applicants must have pediatric radiology experience, including 1- and preferably 2-yr fellowship, and staff radiologists with greater experience are certainly most welcome. For further information, please contact A. Daneman, M.D., Radiologist-in-Chief, Dept. of Radiology, The Hospital for Sick Children, 555 University Ave., Toronto, Ontario, M5G 1X8, Canada; (416) 598-6026. 9-12a

DIAGNOSTIC RADIOLOGIST—Radiologists seek board-certified radiologist with experience in CT, nuclear medicine, general radiology, and ultrasound including Doppler, for a hospital-based, private practice in 225-bed general hospital in Forest Hills, NY. MRI pending. Immediate opening leading to partnership. Contact M. Tartell, M.D.; (718) 544-5858. 9-10ap

DIAGNOSTIC RADIOLOGIST—Two board-certified, university-trained, diagnostic radiologists seek a third general diagnostic radiologist for a suburban community hospital practice in North Central Ohio, 20 min from boating, sailing, and fishing of Lake Erie and its islands. Interested applicants please call or write to Matthew Gutowicz, M.D., or Luong Tuong, M.D., 23 Patricia Dr., Norwalk, OH 44857; (419) 668-8101, ext. 6208, 6209, or 6210. 7-9ap

POSITION OPEN IMMEDIATELY—Forty-physician multispecialty clinic, serving central and western Kansas, is seeking a board-eligible/certified radiologist. Excellent facilities include diagnostic radiology, CT, diagnostic ultrasound, nuclear medicine, and mobile MR services. An excellent opportunity in a dynamic practice setting. Please send CV to Administrator, Hutchinson Clinic, 2101 N. Waldron, Hutchinson, KS 67502; (316) 663-5121. 6-12ap

PEDIATRIC RADIOLOGIST—The Dept. of Radiology at Tulane University Medical Center has an open position for section chief in pediatric radiology. Academic opportunities include all areas of pediatric imaging. Applicants must be eligible for LA state licensure and be ABR-certified. Tulane University is an AA/EOE and particularly encourages applications from qualified women and minority candidates. Please contact Arvin E. Robinson, M.D., Chairman, Radiology, Tulane University Medical Center, 1430 Tulane Ave., New Orleans, LA 70112; (504) 587-7567. 8-10ap

RADIOLOGIST—Board-certified/eligible radiologist wanted to join 3 board-certified radiologists in busy, university-affiliated, community hospital near Boston. Area offers many educational and recreational opportunities. We seek a general radiologist with demonstrated ability in mammography, angio/interventional, ultrasound, and CT. MR experience a plus. Liberal benefits, vacation, and educational leave. Competitive salary leading to full partnership in professional corporation. Address inquiries to Steven Sitzman, M.D., The Malden Hospital, One Hospital Rd., Malden, MA 02148; (617) 322-7560, ext. 5164. 7-10ap

THE OREGON HEALTH SCIENCES UNIVERSITY, Dept. of Radiology, Portland, OR, invites applications for faculty positions in MRI, neuro-radiology, general radiology, skeletal radiology, vascular and interventional radiology, GU radiology, pediatric radiology, computed body tomography, and ultrasound. A second Ph.D. NMR scientist also is being sought. The Oregon Health Sciences University is an affirmative action, equal opportunity employer. Send CV to Richard W. Katzberg, M.D., Chairman of Diagnostic Radiology, L340, The Oregon Health Sciences University, 3181 S.W. Sam Jackson Park Rd., Portland, OR 97201-3098. 5-4ap

TEXAS, DIAGNOSTIC RADIOLOGIST—Three board-certified radiologists seek compatible associate for growing group practice in attractive N.E. Texas community. Excellent health resources. Modalities include MRI and angiography. Comfortable call arrangement; good salary and benefits. Early partnership. Area has strong, diversified economy, excellent schools, and many social and recreational opportunities. Enjoy great location, weather, and people. Extraordinary opportunity! Please send CV in confidence, or call Vicki Truitt, Physician Resource Network, P. O. Box 37102, Fort Worth, TX 76117; (817) 595-1128. 7-10ap

ATLANTA, GA—One radiology position. The Southeast Permanente Medical Group, Inc., Georgia Region, is seeking an additional radiologist for a growing radiology dept. serving several medical centers throughout the Atlanta area. Interested and qualified candidates must be board-certified in radiology with expertise in general radiology to include CT, ultrasound, and mammography. Address inquiries and CVs to Alex Daley, M.D., Chief of Radiology, c/o The Southeast Permanente Medical Group, Inc., 3355 Lenox Rd., Ste. 1000, Atlanta, GA 30326; (404) 233-0555, ext. 192. 5-10ap

DIAGNOSTIC RADIOLOGIST—Combined hospital/office position available at a large, tertiary-care hospital in Phoenix, AZ. The radiology group seeks a new associate who is board-certified, and preferably has had an imaging fellowship and/or academic experience. Competitive salary and benefits leading to partnership offered. Please call Theodore Ditchek, M.D., or Aubrey Palestrant, M.D.; (602) 239-4601 or write c/o Dept. of Radiology, Good Samaritan Regional Medical Center, 1111 E. McDowell Rd., Phoenix, AZ 85006. 8-12ap

LARGE, COMMUNITY-BASED RADIOLOGY GROUP seeks board-certified radiologist interested in part-time position. No night or weekend call. Long-term commitment desired. Responsibilities include general radiography, fluoroscopy, mammography, CT (body), and ultrasound. Ideal practice situation for semiretired radiologist. Desirable Southwest community. Competitive salary and benefits. Send CV to Radiology, Ltd., P. O. Box 12249, Tucson, AZ 85732-2249. 6-9ap

ULTRASOUND STAFF RADIOLOGIST, THOMAS JEFFERSON UNIVERSITY HOSPITAL—The Dept. of Radiology at Thomas Jefferson University Hospital in Philadelphia has an immediate faculty opening in its Division of Diagnostic Ultrasound. This is an exciting opportunity for a person with combined clinical, research, and teaching interests. Our ultrasound division is 1 of the largest and best-equipped in the world, with responsibility for the full range of ultrasound exams, including obstetrical, vascular, endorectal and endovaginal, interventional, Doppler, operative, and gallstone and kidney stone lithotripsy. Excellent salary and benefits are provided. Interested applicants should contact Barry Goldberg, M.D., Director of Diagnostic Ultrasound, or David Levin, M.D., Chairman, Dept. of Radiology, Thomas Jefferson University Hospital, Philadelphia, PA 19107. Thomas Jefferson University is an equal opportunity/affirmative action employer. 8-1ap

POSITION AVAILABLE IMMEDIATELY for a general diagnostic radiologist with interest in MRI and vascular/interventional radiology to complete staffing for new VA Medical Center in Minneapolis, MN. Dept. includes MRI, CT, cyclotron with PET scanner, interventional vascular suite, neuroradiology suite, mammography, Doppler ultrasonography, plus more. Affiliated with the University of Minnesota with non-tenure-track appointment available at appropriate level. Research and teaching opportunities available. Board certification mandatory. One yr fellowship training or equivalent experience in MRI or interventional radiology desirable. Send letters of inquiry with CV to Donovan B. Reinke, M.D., Chief of Diagnostic Radiology Service (114), VA Medical Center, One Veterans Dr., Minneapolis, MN 55417. EOE. 7-9a

FACULTY POSITIONS AVAILABLE NYU MEDICAL CENTER, RADIOLOGY DEPT.—Director of Ultrasound; ultrasound junior faculty position; bone and joint radiology junior faculty position. Contact Norman E. Chase, M.D., Professor and Chairman, Dept. of Radiology, NYU Medical Center, 550 First Ave., New York, NY 10016. An equal opportunity affirmative action employer. 7-9ap

NEW HAMPSHIRE—Join BC diagnostic radiologist affiliated with modern, 90-bed, acute-care hospital in White Mountains region. Enjoy state-of-the-art general practice that includes in-house CT and nuclear medicine. Dept. does over 17,000 procedures annually. Hiking and skiing at your doorstep. Associateship leading to partnership. Competitive first yr salary and benefit package. Please send CV to New England Health Search, 63 Forest Ave., Orono, ME 04473; (207) 866-5680 or (207) 866-5685. 7-9ap

SOUTHERN CALIFORNIA—Group of 6 radiologists requires permanent, general diagnostic radiologist with MRI training. Modern hospital dept. and imaging center with all modalities. Contact B. Goler, M.D., Dept. of Radiology, 2101 N. Waterman Ave., San Bernardino, CA 92404. 7-9ap

Fellowships and Residencies

CARDIOVASCULAR AND INTERVENTIONAL RADIOLOGY—Two-yr fellowship starting July 1, 1990. Peripheral and coronary angiography, cardiac catheterization, digital vascular imaging, all types of interventional procedures, noninvasive vascular techniques, and cardiovascular MRI. Research time available for participation in original or ongoing clinical and/or laboratory projects. Contact Donald P. Harrington, M.D., Dept. of Radiology, Harvard Medical School, Brigham and Women's Hospital, 75 Francis St., Boston, MA 02115. 9-10c

RESEARCH FELLOWSHIP IN DIAGNOSTIC ONCOLOGY, UNIVERSITY OF CALIFORNIA, SAN FRANCISCO—A 1- or 2-yr research fellowship in diagnostic imaging techniques for evaluation of oncology, sponsored by the NCI, is available beginning July 1990 at the University of California, San Francisco. Under the guidance of faculty preceptors, the fellow pursues research in the application and evaluation of newer imaging techniques for the detection and characterization of cancer. The fellowship also includes opportunity for some clinical and academic course exposure in the fellow's field of interest. The University of California is an equal opportunity/affirmative action employer. Minority groups, women, and handicapped individuals are encouraged to apply. This program is actively recruiting minorities. For further information, contact Henry Goldberg, M.D., Professor of Radiology, Dept. of Radiology, UCSF, San Francisco, CA 94143-0628. 9c

ULTRASOUND—The Dept. of Radiology at the University of Minnesota has two 1- to 2-yr post-residency fellowship training positions in ultrasound available at the rank of instructor (temporary, annual renewable) beginning July 1, 1990. Minimum requirements include successful completion of an accredited radiology residency and board certification in radiology by beginning date of fellowship appointment. In addition to clinical practice and training, responsibilities will include graduate and undergraduate medical instruction in ultrasound as well as assisting with related departmental research projects. The clinical practice will provide experience in general abdominal, obstetrical, gynecologic, and vascular ultrasound using conventional, as well as color Doppler, intracavitary, and intravascular technology. It also will provide experience with interventional procedures under sonographic guidance. Salary is negotiable and competitive and dependent on past scholarly productivity and post-M.D. experience. Applicants must be licensed or able to obtain license to practice medicine in the state of Minnesota before appointment date. Applications for these positions will be accepted through Feb. 28, 1990. Send letters to Janis Letourneau, M.D., Dept. of Radiology, Box 292 UMHC, University of Minnesota, 420 Delaware St. S.E., Minneapolis, MN 55455. The University of Minnesota is an equal opportunity and affirmative action educator and employer and specifically encourages applications from women and minorities. 9c

NUCLEAR MEDICINE—The Dept. of Radiology at the University of Minnesota has 1- to 2-yr post-residency fellowship training positions in nuclear medicine available at the rank of instructor (temporary, annual renewable) beginning July 1, 1990. Minimum requirements include successful completion of an accredited radiology residency and board certification in radiology by beginning date of fellowship appointment. In addition to clinical practice and training, responsibilities will include graduate and undergraduate medical instruction in nuclear medicine as well as assisting with related departmental research projects. Salary is negotiable and competitive and dependent on past scholarly productivity and post-M.D. experience. Applicants must be licensed or able to obtain license to practice medicine in the state of Minnesota before appointment date. Applications for these positions will be accepted through Feb. 28, 1990. Send letters to Robert Boudreau, M.D., Dept. of Radiology, Box 292 UMHC, University of Minnesota, 420 Delaware St. S.E., Minneapolis, MN 55455. The University of Minnesota is an equal opportunity and affirmative action educator and employer and specifically encourages applications from women and minorities. 9c

BODY CT—The Dept. of Radiology at the University of Minnesota has 1- to 2-yr postresidency fellowship training positions in body CT available at the rank of instructor (temporary, annual renewable) beginning July 1, 1990. Minimum requirements include successful completion of an accredited radiology residency and board certification in radiology by beginning date of fellowship appointment. In addition to clinical practice and training, responsibilities will include graduate and undergraduate medical instruction in abdominal, thoracic, and musculoskeletal CT imaging as well as assisting with related departmental research projects. Percutaneous biopsy and drainage techniques using CT guidance will be emphasized. Salary is negotiable and competitive and dependent on past scholarly productivity and post-M.D. experience. Applicants must be licensed or able to obtain license to practice medicine in the state of Minnesota before appointment date. Applications for these positions will be accepted through Feb. 28, 1990. Send letters to Robert Halvorsen, M.D., Dept. of Radiology, Box 292 UMHC, University of Minnesota, 420 Delaware St. S.E., Minneapolis, MN 55455. The University of Minnesota is an equal opportunity and affirmative action educator and employer and specifically encourages applications from women and minorities. 9c

FELLOWSHIPS IN ABDOMINAL IMAGING—The Dept. of Radiology at The University of Texas Medical School at Houston has openings for 2 fellowships to begin in July 1991 in abdominal imaging. Under faculty direction and supervision, candidates will further their training in the specialty of abdominal imaging including CT, ultrasound, and MRI through 4-mo rotations in each service. Candidates will participate in teaching in each section at the medical student and resident levels, will have the opportunity to conduct basic or clinical research, and will be expected to prepare and submit at least 1 scientific article to an appropriate refereed journal. Candidate must be a graduate of an approved U.S. medical school or its equivalent, must have completed an approved residency in diagnostic radiology, must be a diplomate of the American Board of Radiology, and must have a Texas medical license. Please submit CV, along with the names and addresses of 3 references to John H. Harris, Jr., M.D., Dept. of Radiology, The University of Texas Medical School at Houston, 6431 Fannin, Ste. 2.132, Houston, TX 77030. The University of Texas Health Science Center at Houston is an equal opportunity employer. Women and minorities are encouraged to apply. 9-12c

FELLOWSHIPS IN NEURORADIOLOGY—The Dept. of Radiology at The University of Texas Medical School at Houston has openings for 1- and 2-yr fellowships to begin in July 1990 and July 1991 in neuroradiology. Under faculty supervision, candidates will be responsible for neuroradiologic exams and procedures (i.e., angiograms, myelograms, CT and MR imaging, and *in vivo* spectroscopy). The candidate will participate in teaching at the medical student and resident levels and will conduct basic or clinical research. Candidate must be a graduate of an approved U.S. medical school or its equivalent, must have completed an approved residency in diagnostic radiology, must be a diplomate of the American Board of Radiology, and must have a Texas medical license. Please submit CV, along with the names and addresses of 3 references to John H. Harris, Jr., M.D., Dept. of Radiology, The University of Texas Medical School at Houston, 6431 Fannin, Ste. 2.132, Houston, TX 77030. The University of Texas Health Science Center at Houston is an equal opportunity employer. Women and minorities are encouraged to apply. 9-12c

CARDIOVASCULAR/INTERVENTIONAL RADIOLOGY—The Dept. of Radiology at the University of Minnesota has four 1- to 2-yr postresidency fellowship training positions in cardiovascular/interventional radiology available at the rank of instructor (temporary, annual renewable) beginning July 1, 1990. Minimum requirements include successful completion of an accredited radiology residency and board certification in radiology by beginning date of fellowship appointment. In addition to clinical practice and training, responsibilities will include graduate and undergraduate medical instruction in cardiovascular/interventional radiology as well as assisting with related departmental research projects. Salary is negotiable and competitive and dependent on past scholarly productivity and post-M.D. experience. Applicants must be licensed or able to obtain license to practice medicine in the state of Minnesota before appointment date. Applications for these positions will be accepted through Feb. 28, 1990. Send letters to Kurt Amplatz, M.D., Dept of Radiology, Box 292 UMHC, University of Minnesota, 420 Delaware St. S.E., Minneapolis, MN 55455. The University of Minnesota is an equal opportunity and affirmative action educator and employer and specifically encourages applications from women and minorities. 9c

MRI FELLOWSHIP AT THOMAS JEFFERSON UNIVERSITY HOSPITAL—A new MRI fellowship position has been created in the Dept. of Radiology of Thomas Jefferson University Hospital, Philadelphia. This 1-yr position encompasses a full range of clinical and research activities. The MRI division includes 6 staff physicians, 2 MRI physicists, and 3 Signa systems (1.5 T). The position is available as of Jan. 1990, but applications will also be taken for the academic year beginning July 1990. Send inquiries to Matthew Rifkin, M.D., Dept. of Radiology, Thomas Jefferson University Hospital, Philadelphia, PA 19107. Jefferson is an equal opportunity/affirmative action employer. 9-6c

FELLOWSHIPS AT THOMAS JEFFERSON UNIVERSITY HOSPITAL—The Dept. of Radiology at Thomas Jefferson University Hospital in Philadelphia offers 6 different fellowship programs each yr: ultrasound/CT/MRI - contact Barry Goldberg, M.D.; cardiovascular/interventional - contact Geoffrey Gardiner, Jr., M.D.; neuroradiology/ENT - contact Carlos Gonzalez, M.D.; chest/breast imaging - contact Robert Steiner, M.D. or Stephen Feig, M.D.; MRI - contact Matthew Rifkin, M.D.; and musculoskeletal (including MRI) - contact David Karasick, M.D. We have a large and well-equipped dept. performing 180,000 exams/yr. Our ultrasound division occupies a spacious new facility and provides training in all phases of ultrasound, including obstetrical, vascular, lithotripsy, and endoluminal. The dept. has 3 modern CT scanners and operates 3 GE 1.5-T MRI units also. The interventional radiology division recently has opened an entirely new angio suite housing state-of-the-art Philips units with DSA. This division performs the full range of both vascular and nonvascular interventional procedures. The neuroradiology division is housed in a neurosciences imaging center containing all imaging modalities in a single comprehensive facility. A large new breast imaging center now operates 5 mammography units and performs breast ultrasound studies also. All program directors listed above can be contacted at the Dept. of Radiology, Thomas Jefferson University Hospital, Philadelphia, PA 19107. Jefferson is an equal opportunity/affirmative action employer. 9xc

ABDOMINAL IMAGING—The Dept. of Radiology at the University of Minnesota has five 1- to 2-yr postresidency fellowship training positions in abdominal imaging including body MRI, body CT, and ultrasound available at the rank of instructor (temporary, annual renewable) beginning July 1, 1990. Minimum requirements include successful completion of an accredited radiology residency and board certification in radiology by beginning date of fellowship appointment. The fellowship will consist of body MRI, CT, and ultrasound rotations. Fellows will perform biopsy and drainage procedures using CT and ultrasound guidance. State-of-the-art equipment is available in all of these imaging areas. In addition to clinical practice and training, responsibilities will include graduate and undergraduate medical instruction in abdominal, thoracic, and musculoskeletal CT imaging as well as assisting with related departmental research projects. Salary is negotiable and competitive and dependent on past scholarly productivity and post-M.D. experience. Applicants must be licensed or able to obtain license to practice medicine in the state of Minnesota before appointment date. Applications for these positions will be accepted through Feb. 28, 1990. Send letters to Robert Halvorsen, M.D., Dept of Radiology, Box 292 UMHC, University of Minnesota, 420 Delaware St. S.E., Minneapolis, MN 55455. The University of Minnesota is an equal opportunity and affirmative action educator and employer and specifically encourages applications from women and minorities. 9c

FELLOWSHIP, VASCULAR AND INTERVENTIONAL RADIOLOGY—The University of South Florida, Dept. of Radiology, will offer a 1-yr fellowship in vascular and interventional radiology to begin July 1, 1990. Clinical experience will include the full range of interventional procedures including vascular, biliary, and endourologic procedures, as well as abscess drainage and percutaneous biopsy. The fellow will rotate between the H. Lee Moffitt Cancer Center and Research Institute, the James A. Haley VA Hospital, and possibly a third affiliated hospital. There is active, ongoing clinical research with potential for animal work if desired. Interested candidates please contact Steven S. Morse, M.D., Associate Professor of Radiology, University of South Florida, Director of Vascular Radiology, H. Lee Moffitt Cancer Center and Research Institute, P. O. Box 280179, Tampa, FL 33682-0179; (813) 972-8425. 7-9cp

NEURORADIOLOGY—The Dept. of Radiology at the University of Minnesota has four 1- to 2-yr postresidency fellowship training positions in neuroradiology available at the rank of instructor (temporary, annual renewable) beginning July 1, 1990. Minimum requirements include successful completion of an accredited radiology residency and board certification in radiology by beginning date of fellowship appointment. In addition to clinical practice and training, responsibilities will include graduate and undergraduate medical instruction in neuroradiology as well as assisting with related departmental research projects. Salary is negotiable and competitive and dependent on past scholarly productivity and post-M.D. experience. Applicants must be licensed or able to obtain license to practice medicine in the state of Minnesota before appointment date. Applications for these positions will be accepted through Feb. 28, 1990. Send letters to Benjamin C. P. Lee, M.D., Dept of Radiology, Box 292 UMHC, University of Minnesota, 420 Delaware St. S.E., Minneapolis, MN 55455. The University of Minnesota is an equal opportunity and affirmative action educator and employer and specifically encourages applications from women and minorities. 9c

MRI—The Dept. of Radiology at the University of Minnesota has two 1- to 2-yr postresidency fellowship training positions in MRI available at the rank of instructor (temporary, annual renewable) beginning July 1, 1990. Minimum requirements include successful completion of an accredited radiology residency and board certification in radiology by beginning date of fellowship appointment. In addition to clinical practice and training, responsibilities will include graduate and undergraduate medical instruction in MRI as well as assisting with related departmental research projects. We have 2 MR scanners (a 1-T and a 1.5-T) and apart from experience with MR scanning of the brain and spine, a large amount of experience with musculoskeletal and body MR will be possible. Salary is negotiable and competitive and dependent on past scholarly productivity and post-M.D. experience. Applicants must be licensed or able to obtain license to practice medicine in the state of Minnesota before appointment date. Applications for these positions will be accepted through Feb. 28, 1990. Send letters to Harry Griffiths, M.D., Dept of Radiology, Box 292 UMHC, University of Minnesota, 420 Delaware St. S.E., Minneapolis, MN 55455. The University of Minnesota is an equal opportunity and affirmative action educator and employer and specifically encourages applications from women and minorities. 9c

MUSCULOSKELETAL RADIOLOGY—The Dept. of Radiology at the University of Minnesota has 1- to 2-yr postresidency fellowship training positions in musculoskeletal radiology available at the rank of instructor (temporary, annual renewable) beginning July 1, 1990. Minimum requirements include successful completion of an accredited radiology residency and board certification in radiology by beginning date of fellowship appointment. In addition to clinical practice and training, responsibilities will include graduate and undergraduate medical instruction in musculoskeletal radiology as well as assisting with related departmental research projects. This fellowship will encompass all aspects of musculoskeletal radiology including CT, arthrography, and MR. Salary is negotiable and competitive and dependent on past scholarly productivity and post-M.D. experience. Applicants must be licensed or able to obtain license to practice medicine in the state of Minnesota before appointment date. Applications for these positions will be accepted through Feb. 28, 1990. Send letters to Harry Griffiths, M.D., Dept of Radiology, Box 292 UMHC, University of Minnesota, 420 Delaware St. S.E., Minneapolis, MN 55455. The University of Minnesota is an equal opportunity and affirmative action educator and employer and specifically encourages applications from women and minorities. 9c

FELLOWSHIP IN ULTRASOUND/CT/ANGIO-INTERVENTIONAL—Available July 1, 1990. A 1-yr fellowship program is available at the Lehigh Valley Hospital Center in Allentown, PA, a 492-bed, acute-care facility with Level I Trauma Center designation. The fellowship program offers training in CT (head and body), ultrasound, angiography (neuro and visceral), and interventional radiography. MRI experience also is available. For further information, contact Robert Kricun, M.D., Dept. of Radiology, Lehigh Valley Hospital Center, P. O. Box 689, Allentown, PA 18105. 8-9cp

RADIOLOGY RESIDENCY IN SAN FRANCISCO BAY AREA—Unexpected, immediate opening available at 2nd, 3rd, or 4th yr level. Please send CV to Edward A. Lebowitz, M.D., Dept. of Diagnostic Radiology, Santa Clara Valley Medical Center, 751 S. Bascom Ave., San Jose, CA 95128; (408) 299-6370. 9-10cp

FELLOWSHIP POSITIONS AVAILABLE IN NEURORADIOLOGY, PEDIATRIC RADIOLOGY, AND BODY IMAGING (CT/ULTRASOUND/MRI) at Baylor College of Medicine, Texas Medical Center, Houston, TX, beginning July 1990. For information and applications, contact Marvin Chasen, M.D., Dept. of Radiology, Baylor College of Medicine, One Baylor Plaza, Houston, TX 77030; (713) 798-6362. 7-9c

FELLOWSHIP POSITIONS—Applications are invited now for July 1991. Positions are available in neuroradiology, vascular/interventional radiology, and body imaging (CT/ultrasound/MRI). For information, contact James R. Schmidgall, M.D. or Richard W. Katzberg, M.D., Chairman, Dept. of Radiology, L-340, Oregon Health Sciences University, 3181 S. W. Sam Jackson Park Rd., Portland, OR 97201. 7-6c

Tutorials/Courses

FIFTH ANNUAL LONDON-PARIS FALL ULTRASOUND—Sept. 17-23, 1989. Category I accreditation, international faculty. For information, contact Medical Seminars International, 9800 D Topanga Canyon Blvd., Ste. 232, Chatsworth, CA 91311; (818) 700-9821. 3-9d

Other

FOURTEENTH ANNUAL BODY IMAGING CONFERENCE—Hyatt Regency Waikoloa Hotel, October 14-21, 1989. MRI, CT, and ultrasound. Category I accreditation, university faculty. For registration and information, contact Annual Body Imaging Conference, 9800 D. Topanga Canyon Blvd., Ste. 232, Chatsworth, CA 91311; (818) 700-9821. 6-8dp

AJR Classified Advertisements Information

Box Responses and Address for Ad Placement

Write Box _____, AJR, 2223 Avenida de la Playa, Suite 200, La Jolla, CA 92037-3218; (619) 459-2229; FAX: (619) 459-8814.

How to Place an Ad

AJR accepts classified advertising for Positions Available, Positions Desired, Fellowships and Residencies, and Tutorials/Courses. Ads are accepted by mail or FAX.

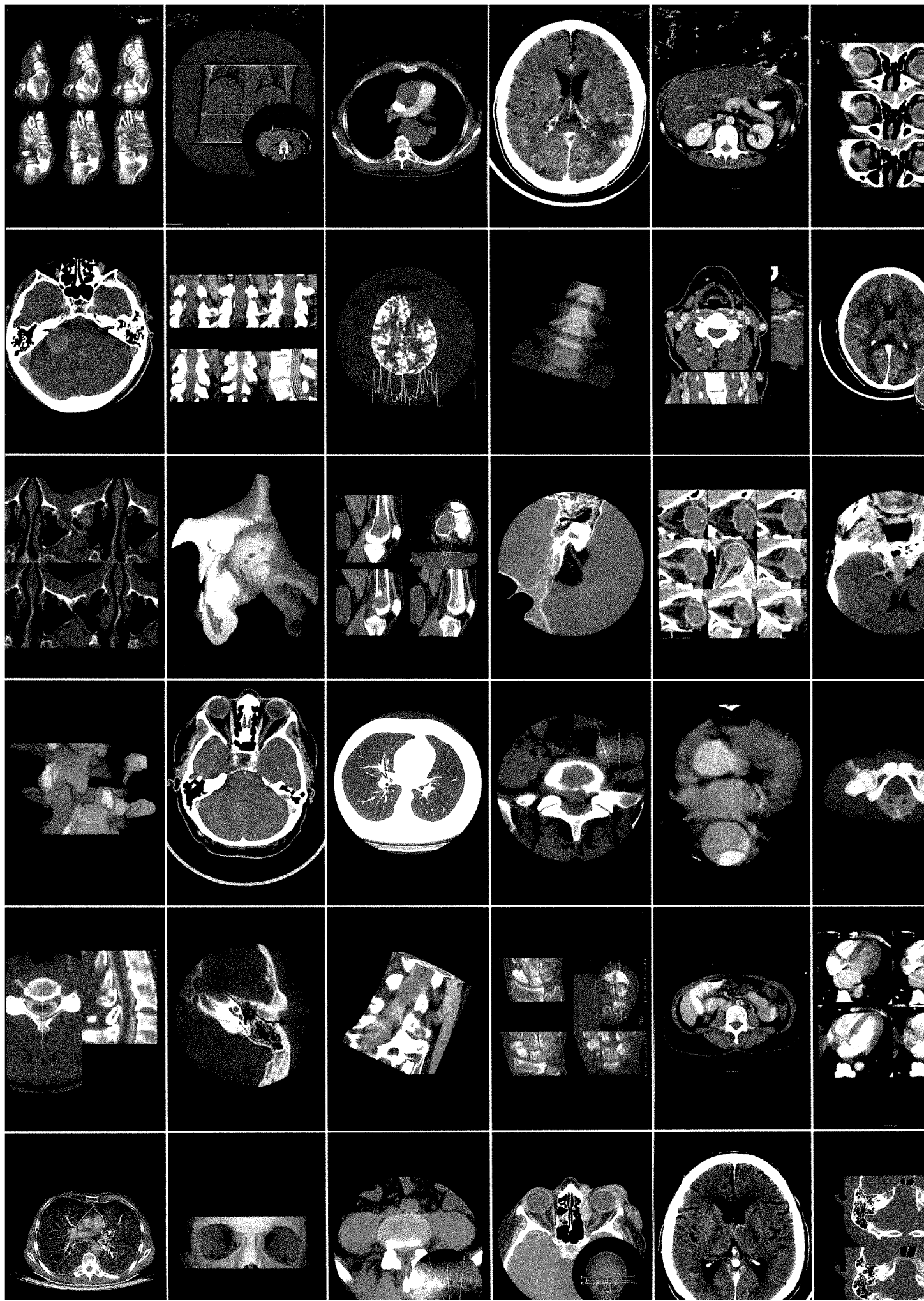
Rates: \$6.00/line with a \$30 minimum charge. Box service is \$10 additional for each month the ad appears. There are discounts for multiple insertions: 10% for 2-3 insertions; 20% for 4 or more. To estimate lines, count all words and divide by 7.

Billing: Ads *must* be prepaid, or advertisers will be billed after the ad appears *providing* a purchase order number is submitted with the advertising copy. Terms are net 30 days.

Deadlines: 6 weeks prior to issue date. For specific deadlines, telephone the AJR editorial office.

Estimating Ad Charges

Line charge: divide total words by 7 and multiply by \$6.00	\$
Multiple insertions? If so, multiply by number	x
Subtotal	\$
Discount applies to two or more insertions. Subtract 10% if ad appears 2-3 months, 20% if 4 months or more	-
Subtotal	\$
Box response requested? If so, multiply number of months by \$10.00	+
Approximate advertising charge	\$





Fuji sets the standard

Super HR Series Films, The Ultimate in Sharpness.

Fuji's quest for the ultimate sharpness in medical imaging films has produced yet another breakthrough in emulsion technology and set a new standard for image quality.

Fuji's Sharpest X-ray Film Ever

Σ (Sigma) Localized Latent Image Centers (Σ LIC) grain technology and Crossover Control Technology (CCT) increase the efficiency of the film emulsion and significantly reduce the adverse effects of crossover exposure, resulting in Fuji's sharpest x-ray film ever.

Superior Processing Stability

Specific Localized Latent Image speck formation with high development potential (Σ LIC Grain) results in increased tolerance to changes in developer temperature. This means Fuji Super HR Series Films provide exceptional processing stability for more consistent results.

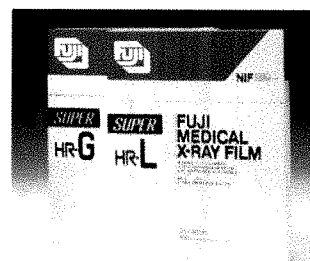
Ask your local Fuji representative or call (800)431-1850 [in CT (203) 353-0300].

CIRCLE 7 ON READER SERVICE CARD



The Reason for Change!

Burbank - Chicago - Stamford, CT.



1989 ARRS PRESIDENTIAL ADDRESS

- 459 A time to focus on patients, not profit. *Evens RG*

EUGENE W. CALDWELL LECTURE

- 463 Health care choices for the nineties. *Bradley W*

STATE OF THE ART

- 467 Interventional neuroradiology. *Halbach VV, Higashida RT, Hieshima GB*
 477 Assessment of myocardial viability with SPECT and PET imaging. *Cerqueira MD, Jacobson AF*

CARDIOPULMONARY RADIOLOGY

- 485 Bronchial impaction in lobar collapse: CT demonstration and pathologic correlation. *Glazer HS, Anderson DJ, Sagel SS*
 489 Case report. Fibrosing mediastinitis in the posterior thorax. *Kountz PD, Molina PL, Sagel SS*
 491 Pictorial essay. MR imaging of congenitally corrected transposition of the great vessels in adults. *Park JH, Han MC, Kim C-W*
 495 Case report. MR diagnosis of lipomatous infiltration of the interatrial septum. *Kaplan KR, Rifkin MD*

GASTROINTESTINAL RADIOLOGY

- 497 MR appearance of gallstones in vitro at 1.5 T: correlation with chemical composition. *Baron RL, Shuman WP, Lee SP, et al.*
 503 Routine sonographic techniques fail to quantify gallstone size and number: a retrospective study of 111 surgically proved cases. *Brink JA, Simeone JF, Mueller PR, et al.*
 507 Biliary cystadenoma and cystadenocarcinoma: CT and sonographic findings. *Korobkin M, Stephens DH, Lee JKT, et al.*
 513 Identification of a patent paraumbilical vein by using Doppler sonography: importance in the diagnosis of portal hypertension. *Gibson RN, Gibson PR, Donlan JD, Clunie DA*
 517 Pictorial essay. Cross-sectional imaging of abdominal wall hernias. *Wechsler RJ, Kurtz AB, Needleman L, et al.*

GENITOURINARY RADIOLOGY

- 523 Endovaginal sonographic diagnosis of dilated fallopian tubes. *Tessler FN, Perrella RR, Fleischer AC, Grant EG*
 527 Case report. Papillary cystadenoma of the broad ligament in a patient with von Hippel-Lindau disease. *Funk KC, Heiken JP*

MUSCULOSKELETAL RADIOLOGY

- 529 Occult fractures of the carpals and metacarpals: demonstration by CT. *Hindman BW, Kulik WJ, Lee G, Avolio RE*
 533 Anatomic relations between the median nerve and flexor tendons in the carpal tunnel: MR evaluation in normal volunteers. *Zeiss J, Skie M, Ebraheim N, Jackson WT*
 537 MR imaging of the knee in the sagittal projection: comparison of three-dimensional gradient-echo and spin-echo sequences. *Reeder JD, Matz SO, Becker L, Andelman SM*
 541 Soft-tissue masses: diagnosis using MR imaging. *Kransdorf MJ, Jelinek JS, Moser RP Jr, et al.*

PEDIATRIC RADIOLOGY

- 549 Expert advice. Technical aspects of abdominal CT in infants and children. *Kaufman RA*
 555 Pictorial essay. CT of blunt abdominal trauma in

children. *Taylor GA, Guion CJ, Potter BM, Eichelberger MR*

- 561 The value of CT in detecting bowel perforation in children after blunt abdominal trauma. *Bulas DI, Taylor GA, Eichelberger MR*
 565 MR imaging of the craniovertebral junction, cranium, and brain in children with achondroplasia. *Kao SCS, Waziri MH, Smith WL, Sato Y, Yuh WTC, Franken EA Jr*
 571 Brain abnormalities in infants on extracorporeal membrane oxygenation: sonographic and CT findings. *Babcock DS, Han BK, Weiss RG, Ryckman FC*

NEURORADIOLOGY

- 577 Interventional neurovascular treatment of traumatic carotid and vertebral artery lesions: results in 234 cases. *Higashida RT, Halbach VV, Tsai FY, et al.*
 583 Paragangliomas of the jugular bulb and carotid body: MR imaging with short sequences and Gd-DTPA enhancement. *Vogl T, Bruning R, Schedel H, et al.*
 589 MR characteristics of subdural hematomas and hygromas at 1.5 T. *Fobben ES, Grossman RI, Atlas SW, et al.*
 597 MR imaging of intracranial fluid levels. *Abrahams JJ, Lidov H, Artiles C*
 605 The acetazolamide challenge: imaging techniques designed to evaluate cerebral blood flow reserve. *Rogg J, Rutigliano M, Yonas H, Johnson DW, Penhney S, Latchaw RE*

VASCULAR RADIOLOGY

- 613 IV injection of air-filled human albumin microspheres to enhance arterial Doppler signal: a preliminary study in rabbits. *Hilpert PL, Mattrey RF, Mitten RM, Peterson T*
 617 Laser catheter thermal angioplasty: technique and early results in 34 patients. *Mitty HA, Sanborn TA, Train JS, Dan SJ*
 623 Technical note. Dissecting renal artery aneurysm: treatment with an endovascular stent. *Mali WP ThM, Geyskes GG, Thalman R*
 625 Case report. Balloon occlusion of a pseudoaneurysm in a below-the-knee amputation stump. *Selby JB Jr, Bittner GM, Tegtmeyer CJ, Tribble CG*

MR IMAGING

- 629 Diagnostic significance of interslice gap and imaging volume in body MR imaging. *Schwaighofer BW, Yu KK, Mattrey RF*

ARRS 1989 ANNUAL MEETING

- 633 Summary of scientific program
 641 Gold medal recipients. *Evens RG*
 643 Secretary's report. *Hartman GW*
 645 Administrative report. *Fullagar PR*
 646 Award winning exhibits
 648 New members
 650 Membership invitation and application

OTHER CONTENT

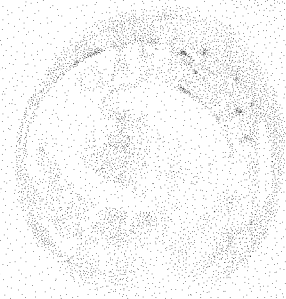
- Book reviews 484, 512, 522, 526, 548, 560, 570, 588
 622 Memorial, George Patrick Genereux
 627 ARRS 1990 resident award papers information
 628 Forthcoming articles
 653 Letters
 661 Review of current literature
 666 News
 673 American Roentgen Ray Society information
 674 ARRS 1990 meeting announcement, calls for papers and exhibits
 679 Classified advertisements
 A3 Guidelines for authors
 A10 AJR business and subscriber information

Acc 13.11.90

UCM

AJR

American
Journal of
Roentgenology



October 1989

Procedure trays to control costs ...new from E-Z-EM

The objective:

Respond to the demand for a set of disposable trays to help hospitals and private practices control biopsy costs on a per-procedure basis.

The result:

E-Z-EM's new PercuSet line of disposable biopsy trays creating a system of procedure trays—a system of trays which offers the doctor progressive degrees of procedure capability.

The PercuSet Skin Prep Tray includes every implement and agent needed to cleanse, asepsitize, and anesthetize the procedure area—for biopsy, or for any percutaneous procedure.

The PercuSet Basic Biopsy Tray includes all the elements of the Prep Tray, *plus* a needle stop, and a ruler/protractor, *and* the option of an E-Z-EM biopsy needle.

The PercuSet Expanded Biopsy Tray adds a specimen-handling section, for complete biopsy procedure capability, also with the option of an E-Z-EM biopsy needle.

PercuSet Biopsy Trays assure absolute sterility, minimize component handling, eliminate cross-contamination, and are laid out in a logical procedural sequence.

They provide effective cost control, and reduce inventory management of components.

For additional information and a color brochure that details the PercuSet System, contact your local representative, or call E-Z-EM toll-free at 800-645-3052. In New York call 516-333-8230.

E-Z-EM

More than barium—
much more

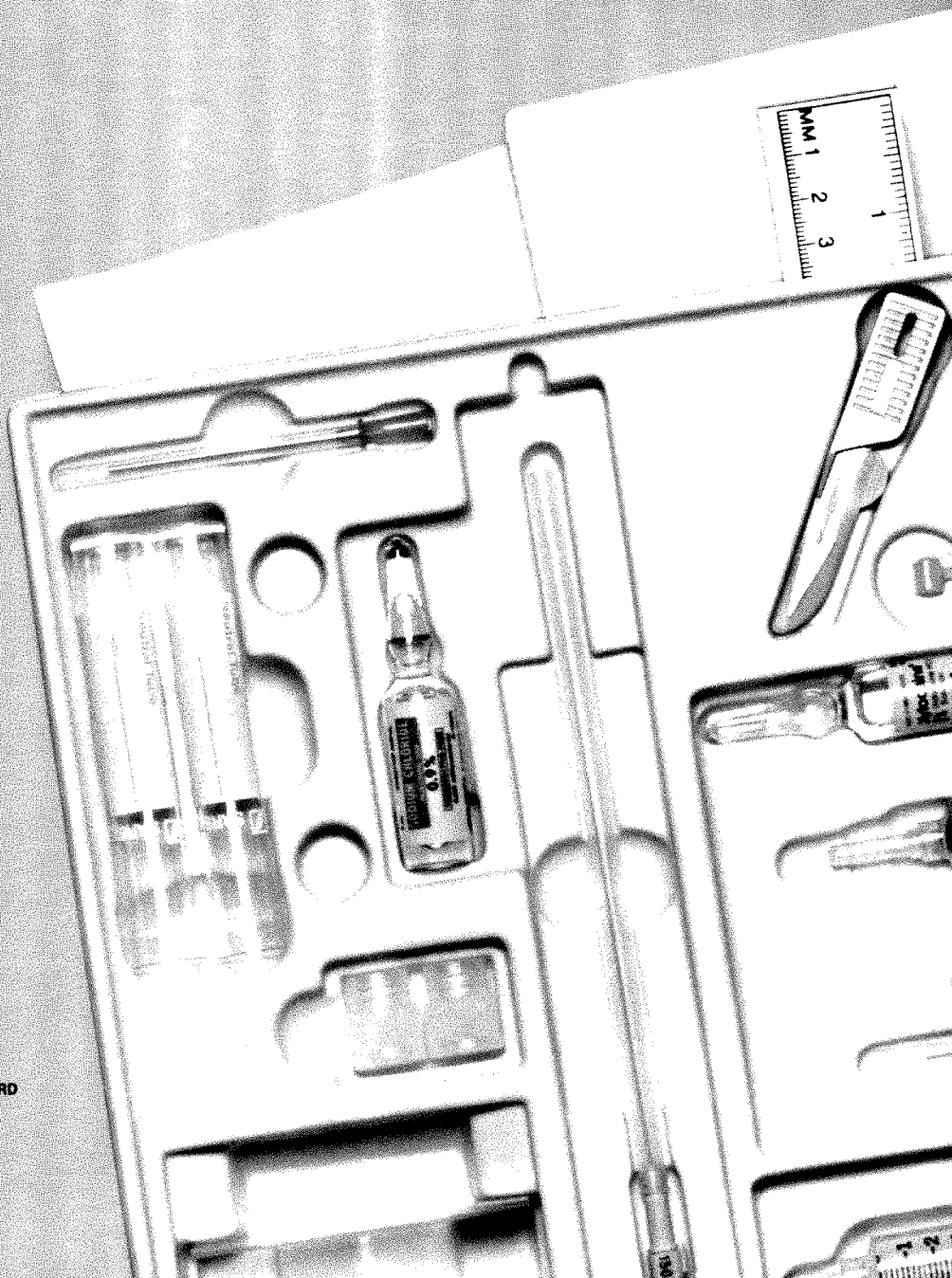


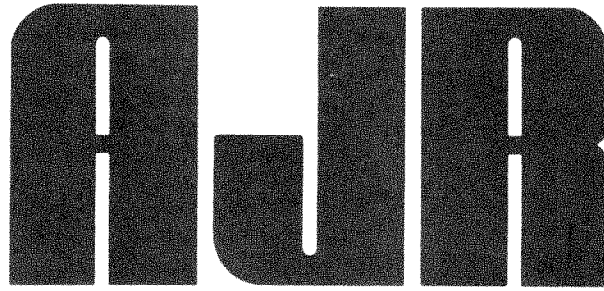
CIRCLE 30 ON READER SERVICE CARD

E-Z-EM, Inc.
7 Portland Avenue
Westbury, N.Y. 11590

© 1986 E-Z-EM, Inc.

PercuSet





American Journal of Roentgenology
Diagnostic Imaging and Related Sciences

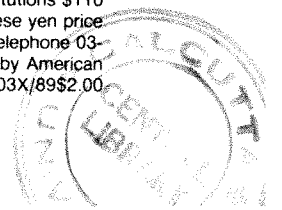
- Editor-In-Chief** Robert N. Berk, *La Jolla, California*
University of California, San Diego
School of Medicine and Medical Center
- Editor Emeritus** Melvin M. Figley, *Seattle, Washington*
- Associate Editor** Saskia von Waldenburg Hilton, *San Diego, California*
- Consulting Editor** Juan M. Taveras, *Boston, Massachusetts*
- Statistician** Charles C. Berry, *San Diego, California*

Editorial Board

- | | | |
|-------------------------|--------------------------|--------------------|
| John R. Amberg | John R. Hesselink | Peter M. Ronai |
| Itamar Aviad | Charles B. Higgins | Sjef H. J. Ruijs |
| Mark E. Baker | Melvyn T. Korobkin | Stuart S. Sagel |
| Lawrence W. Bassett | Faye C. Laing | David J. Sartoris |
| Michael A. Bettmann | Thomas L. Lawson | Stefan C. Schatzki |
| William G. Bradley, Jr. | Robert G. Levitt | William P. Shuman |
| N. Reed Dunnick | Bruce L. McClennan | Edward A. Sickles |
| David K. Edwards | Richard P. Moser | Barry A. Siegel |
| Ronald G. Evens | Albert A. Moss | David D. Stark |
| David S. Feigin | Jeffrey H. Newhouse | Edward T. Stewart |
| Sandra K. Fernbach | Donald L. Resnick | Murali Sundaram |
| Richard H. Gold | Stewart R. Reuter | Eric vanSonnenberg |
| William R. Hendee | Charles A. Rohrmann, Jr. | Robert K. Zeman |

Editorial Staff: Margaret Levene, *managing editor*; Katie L. Spiller, Barbara Rose, Barbara L. Halliburton, and Janine Anderson, *manuscript editors*; Nancy Rydbeck, *office manager*; Sheri Smith, *administrative assistant*; Sandra L. Griffin, *administrative secretary*.

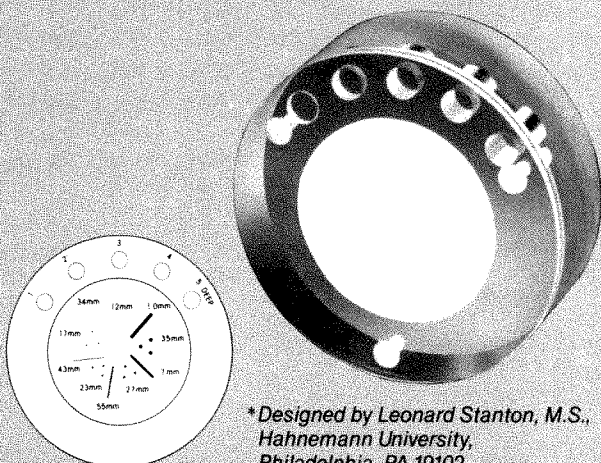
AJR, AMERICAN JOURNAL OF ROENTGENOLOGY (ISSN 0361 803X) is the official journal of the American Roentgen Ray Society and is published monthly by Williams & Wilkins, 428 E. Preston St., Baltimore, MD 21202. Annual dues include \$50 for journal subscription. Second-class postage paid at Baltimore, MD, and at additional mailing offices. Postmaster, send address changes (Form 3579) to AJR, 428 E. Preston St., Baltimore, MD 21202. Subscription rates \$100 (\$145 foreign); institutions \$110 (\$155 foreign); in training \$25 (\$70 foreign); single copy \$16 (\$19 foreign). Japanese rates include airfreight. Japanese yen price is available from our sole agent USACO Corporation, 13-12, Shimbashi 1-Chome, Minato-Ku, Tokyo 105, Japan, telephone 03-502-6471. Airmail rates furnished on request. Indexed by *Current Contents* and *Index Medicus*. Copyright © 1989 by American Roentgen Ray Society.



Ensure Mammographic Diagnostic Quality

Easy to Use... Easy to Interpret

MAMMOGRAPHIC QA PHANTOM*



*Designed by Leonard Stanton, M.S.,
Hahnemann University,
Philadelphia, PA 19102.

For Evaluating the Overall Imaging Performance of a Mammographic System

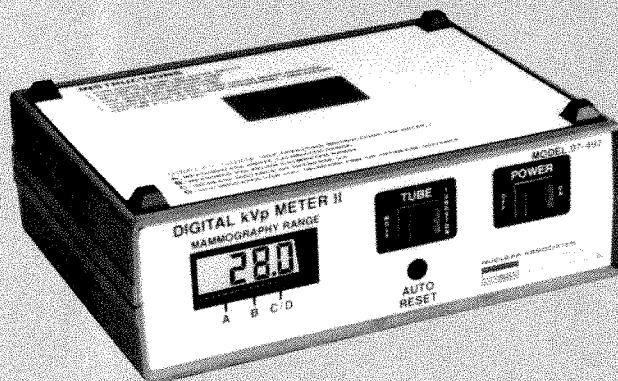
- Intended as an integral part of a complete mammography QA program: evaluates x-ray generator, screen-film combination and film processor.
- Contains calcium carbonate specks which better simulate actual clinical conditions ("punctate calcifications") in breast cancer.
- Uses nylon fibers to simulate "soft tissue fibrillar extensions in adipose tissue."
- Includes two additional attenuators to check phototiming linearity.
- Includes 5-step air wedge to gauge for image contrast.

For more details,
request
Bulletin 4053-44

CIRCLE 36 ON READER SERVICE CARD

Affordable, Non-Invasive

MAMMOGRAPHIC DIGITAL kVp METER



For Quick and Accurate Measurements of X-Ray Generator Tube Potential

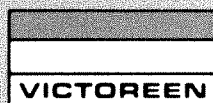
- Accuracy ± 1.5 kVp.
- Range 22-50 kVp (0.1 kVp resolution).
- Automatic display reset.
No remote control cables.
- Mo/W selector switch.
- Scope output for waveform analysis.
- Compact, lightweight, battery-operated.

SO EASY TO USE

1. Place instrument on x-ray table.
2. Set the Mo/W selector switch for your type of tube.
3. Make an exposure.
4. Read the kVp.

For more details,
request
Bulletin 421-44

NUCLEAR ASSOCIATES



A Division of VICTOREEN, INC.
100 VOICE ROAD
CARLE PLACE, NY 11514-1593 U.S.A.
(516) 741-6360
FAX (516) 741-5414

WE CARRY A COMPLETE LINE OF MAMMOGRAPHIC QA PRODUCTS

AJR Guidelines for Authors

Address new and revised manuscripts, correspondence, and classified ads to the Editor:

AJR Editorial Office
2223 Avenida de la Playa, Suite 200
La Jolla, CA 92037-3218
Telephone: (619) 459-2229; FAX: (619) 459-8814

Inquiries regarding subscriptions, display advertising, reprints, or permission to republish AJR material should be addressed to the publisher:

The Williams & Wilkins Co.
428 E. Preston St.
Baltimore, MD 21202 Telephone: (301) 528-4133

The AJR publishes original contributions to the advancement of medical diagnosis and treatment. Submitted manuscripts should not contain previously published material and should not be under consideration for publication elsewhere. Papers dealing with neuroradiology should be addressed to: American Journal of Neuroradiology, Dept. of Radiology, Massachusetts General Hospital, Boston, MA 02114. At the discretion of the AJR Editor, AJNR articles that are of interest to the general reader may be republished in the AJR. Neuro-radiologic papers sent to the AJR will be forwarded to the Editorial Office of the AJNR.

Manuscript decisions are based on peer review. Reviewers receive manuscripts without title pages to ensure an unbiased review. Statements made in the article, including changes made by the Editor or manuscript editor, are the responsibility of the author and not of the AJR or its publisher. Authors will be sent the edited manuscript, galley proof, and proofs of illustrations. If the corresponding author will be unavailable to review galleys, arrangements should be made for a coauthor or colleague to read and return the proof.

The following guidelines are based on instructions set forth in the **Uniform Requirements for Manuscripts Submitted to Biomedical Journals** (*Ann Intern Med* 1988;108:258-265). Articles will be edited, however, to conform to the individual style of AJR.

General Guidelines for Major Papers

Abstract. Clearly state (in 200 words or less) the purpose, methods, results, and conclusions of the study. Include actual data.

Introduction. Briefly describe the purpose of the investigation, including relevant background information.

Methods. Describe the research plan, the materials (or subjects), and the methods used, in that order. Explain in detail how disease was confirmed and how subjectivity in observations was controlled.

Results. Present results in a clear, logical sequence. If tables are used, do not duplicate tabular data in text, but do describe important trends and points.

Discussion. Describe the limitations of the research plan, materials (or subjects), and methods, considering both the

purpose and the outcome of the study. When results differ from those of previous investigators, explain the discrepancy.

AUTHOR'S CHECKLIST

For priority handling, complete the following checklist, sign the copyright form on the reverse side of this page, and include both with the manuscript.

_____ Two copies of the manuscript (the original and a photocopy) and two complete sets of figures are submitted. One copy has been retained by the author.

_____ If appropriate, AJR Guidelines for case reports, technical notes, pictorial essays, or letters to the Editor have been followed. (See page A5.)

_____ The manuscript, including references, figure legends, and tables, is typed double-spaced on 8½ × 11 in. (21.6 × 27.9 cm) *nonerasable* paper. Right-hand margins are not justified.

_____ All manuscript pages are numbered consecutively beginning with the abstract. Authors' names do not appear on the manuscript pages.

_____ The manuscript is organized as follows: title page, blind title page (title only), abstract, introduction, methods, results, discussion, acknowledgments, references, tables, figure legends, and figures.

_____ Informed consent has been obtained from patients who participated in clinical investigations. If experiments were performed on animals, authors complied with NIH guidelines for use of laboratory animals.

_____ Use of unfamiliar acronyms and abbreviations is kept to a minimum. When abbreviations are used they are defined at first mention, followed by the abbreviation in parentheses.

_____ Metric measurements are used throughout, or the metric equivalent is given in parentheses.

_____ Names and locations (city and state only) of manufacturers are given for equipment and nongeneric drugs.

Title Page

_____ The following information is given: title of article; names and complete addresses (including zip code) of all authors; current addresses of authors who have moved since study; acknowledgment of grant or other assistance. The corresponding author is clearly identified, and a current address, phone number, and Fax number are given.

_____ Two copies of a blind title page are included giving only the title (without the authors' names) for use in the review process.

Abstract

_____ An abstract of approximately 200 words concisely states the purpose, methods, and results of the study in one paragraph. Actual data are included. Conclusions are stated in a second, summary paragraph.

_____ No abbreviations or reference citations are used.

References

References (not to exceed 35) are typed double-spaced starting on a separate page and are **numbered consecutively in the order in which they appear in the text**.

All references are cited in the text and are enclosed in brackets and typed on line with the text (not superscript).

Unpublished data are not cited in the reference list, but are cited parenthetically in the text, for example, (Smith DJ, personal communication), (Smith DJ, unpublished data). This includes papers submitted, but not yet accepted, for publication.

Inclusive page numbers (e.g., 333–335) are given for all references.

Journal names are abbreviated according to *Index Medicus*.

Style and punctuation of references follow the format illustrated in the following examples (all authors are listed when six or less; when seven or more authors, the first three are listed, followed by “et al.”):

Journal article

1. Long RS, Roe EW, Wu EU, et al. Membrane oxygenation: radiographic appearance. *AJR* 1986;146:1257–1260

Book

2. Smith LW, Cohen AR. *Pathology of tumors*, 6th ed. Baltimore: Williams & Wilkins, 1977:100–109

Chapter in a book

3. Breon AJ. Serum monitors of bone metastasis. In: Clark SA, ed. *Bone metastases*. Baltimore: Williams & Wilkins, 1983:165–180

Paper presented at a meeting

4. Lau FS, Kirk AN. MR imaging of the spine. Presented at the annual meeting of the American Roentgen Ray Society, Washington, DC, April 1986

Tables

Each table is typed double-spaced on a separate page without vertical or horizontal rules; each has a short, descriptive title. Tables do not exceed two pages in length and contain at least four lines of data.

Tables are numbered in the order in which they are cited in the text.

Abbreviations are defined in an explanatory note below each table.

Tables are self-explanatory and do not duplicate data given in the text or figures.

All arithmetic (percentages, totals, differences) has been double checked for accuracy, and tabular data agree with data given in the text.

Figures and Legends

Two complete sets of original figures are submitted unmounted in labeled envelopes.

Figures are clean, unscratched, 5 × 7 in. (13 × 18 cm) glossy prints with **white borders**. A separate print is submitted for each figure *part*.

All figure parts relating to one patient have the same figure number.

Each figure is labeled on the back with the figure number and an arrow indicating “top.” For black-and-white figures, labeling is done on a gummed label, which is then affixed to the back of the print. *Never* use labels on color figures, but write figure number on the back lightly in pencil. *Never* use ink on front or back of any figures.

Author’s names are *not* written on the backs of figures.

Only removable (rub-on) arrows and letters are used on the figures. Symbols are uniform in size and style and are not broken or cracked.

Images are uniform in size and magnification.

Line drawings are done in black ink on a white background. They are professional in quality, and all use the same size type. (Only glossy prints are acceptable.)

Written permission has been obtained for use of all previously published illustrations (and copies of permission letters are included), and an appropriate credit line is given in the legends.

Legends are typed double-spaced, and figure numbers correspond with the order in which the figures are cited in the text.

Transfer of Copyright Agreement, Conflict of Interest Acknowledgment, Certification of Coauthors, and Exclusive Publication Statement

Complete copyright to the article entitled: _____

is hereby transferred to the American Roentgen Ray Society (for United States government employees to the extent transferable), effective if and when the article is accepted for publication in the *American Journal of Roentgenology*. In the case of the authors who are officers or employees of the United States government, the American Roentgen Ray Society recognizes that works prepared by officers or employees of the United States government as part of their official government duties are in the public domain.

Authors reserve all proprietary rights other than copyright, such as patent rights and the right to use all or part of this article in future works of their own. The authors retain the right of replication, subject only to crediting the original source of publication and receiving written permission from the publisher.

Authors guarantee that this manuscript contains no matter that is libelous or otherwise unlawful, invades individual privacy, or infringes any proprietary rights.

Authors understand that they will receive no royalty or other compensation from the American Roentgen Ray Society or the publisher.

Authors guarantee that the editor has been or will be informed of any proprietary or commercial interest or conflicts of interest the authors may have that relate directly or indirectly to the subject of this article.

All authors certify that they have made substantive and specific intellectual contributions to the article and assume public responsibility for its content.

Finally, the authors certify that none of the material in this manuscript has been published previously or is currently under consideration for publication elsewhere.

First author/date

Second author

Third author

Fourth author

Fifth author

Sixth author

This agreement must be signed by all authors in order for the manuscript to be published.

Case Reports

A case report is a brief description of a special case that provides a message that transcends the individual patient.

Format. There is no abstract. The introduction should be a short paragraph giving the general background and the specific interest of the case. No more than one case should be described in detail (similar ones can be mentioned briefly in the discussion). Emphasis should be on the radiologic aspects; clinical information must be limited to that necessary to provide a background for the radiology. The discussion should be succinct and should focus on the specific message and relevance of radiologic methods. A review of the literature is not appropriate.

Length. Maximum of five double-spaced, typewritten pages, including the references but not the title page or figure legends.

References. Maximum of eight.

Figures. Maximum of three or four, unless the text is shortened accordingly. Legends must not repeat the text.

Tables and Acknowledgments. Not appropriate in case reports.

Technical Notes

A technical note is a brief description of a specific technique or procedure, modification of a technique, or equipment of interest to radiologists.

Format. No abstract, headings, or subheadings are required. If headings are used, they should be a combination of "Case Report," "Materials and Methods," "Results," and "Discussion." A brief one-paragraph introduction should be included to give the general background. Discussion should be limited to the specific message, including the uses of the technique or equipment. Literature reviews and lengthy case reports are not appropriate.

Length. Maximum of five double-spaced, typewritten pages, including the references but not the title page or figure legends.

References. Maximum of eight.

Figures. Maximum of two, unless the text is shortened accordingly.

Tables and Acknowledgments. Not appropriate in technical notes.

Pictorial Essays

A pictorial essay is an article that conveys its message through illustrations and their legends. Unlike other *AJR* articles, which are based on original research, pictorial essays serve primarily as teaching tools, like exhibits at a scientific meeting. They are not encyclopedic book chapters. No abstract is necessary.

Length. Maximum of four double-spaced, typewritten pages, including the references but not the title page or figure legends.

References. Maximum of four.

Figures. Maximum of 30 figure parts. Number should be as few as necessary to convey the message of the paper.

Tables and Acknowledgments. Not appropriate in pictorial essays.

Letters to the Editor and Replies

Letters to the Editor and Replies should offer objective and constructive criticism of published articles. Letters may also discuss matters of general interest to radiologists. Do not end a letter with a hand-written signature.

Format. All letters should be typed double-spaced on nonletterhead paper, with no greeting or salutation. Name and affiliation should appear at the end of the letter. Titles for letters should be short and pertinent. The title for a reply is simply "Reply."

Length. Maximum of two double-spaced, typewritten pages, including references.

References. Maximum of four.

Figures. Maximum of two.

Tables and Acknowledgments. Not appropriate in Letters to the Editor and Replies.

Opinions, Commentaries, and Perspectives

Opinions, commentaries, and perspectives are special articles dealing with controversial topics or issues of special concern to radiologists.

Format. Include a title page but no abstract. Headings may be used to break up the text.

Length. Maximum of five double-spaced, typewritten pages.

References. Maximum of five.

Tables and Figures. Maximum of four.

Computer Page Articles

Articles published on the computer page deal with practical computer applications to radiology.

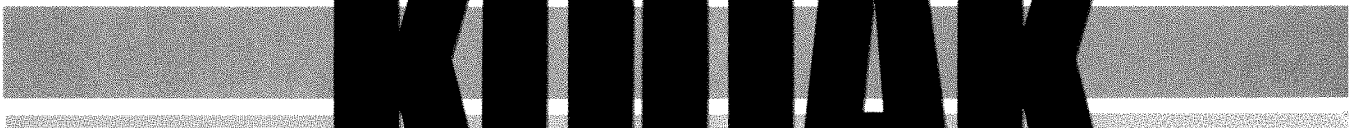
Format. Include a title page but no abstract.

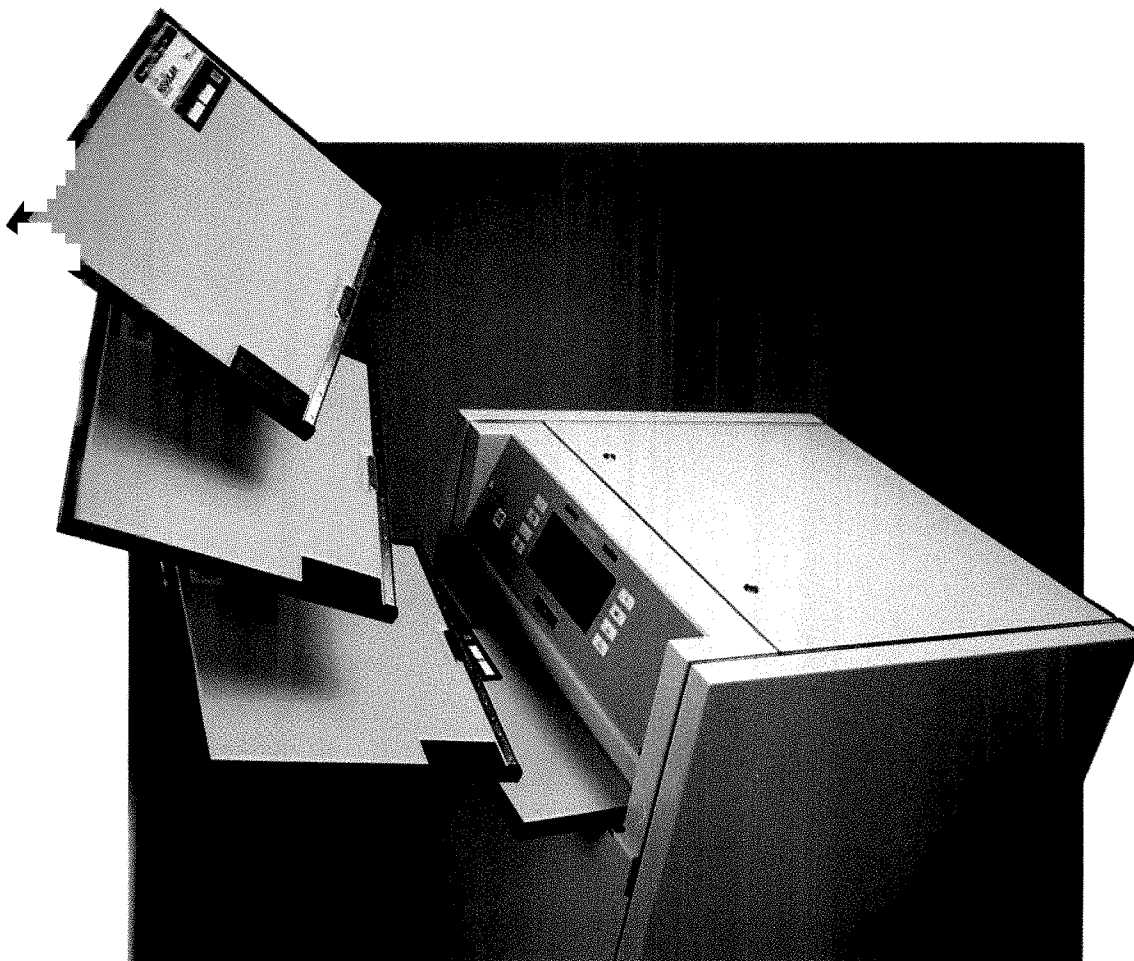
Length. Maximum of eight double-spaced, typewritten pages.

References. Maximum of five.

Figures and Tables. Maximum of five. Computer printouts are not acceptable. Figures must be submitted as 5 × 7 in. glossy prints.

**THE
LOADER
THAT LOADS
CASSETTES
FROM
KODAK**





Introducing the Kodak multiloader 700. It's the roomlight loader that works with Kodak X-Omatic cassettes... and Kodak processors.

Here is the automated roomlight film handling system that makes better use of your staff and floor space, and works with high quality Kodak X-Omatic cassettes and Kodak RP X-Omat processors. Designed around an intelligent micro-processor, the Kodak multiloader 700 comes with seven film magazines—one for each standard size. And it handles mammography cassettes and video film holders as well. Plus the built-in inventory management feature produces up-to-the-minute reports on film consumption.

This latest multiloader fits in anywhere. For more details, talk to your Kodak representative. Or, in the U.S., call 1 800 242-2424, Ext. 50.

The new vision of Kodak



AJR Business and Subscriber Information

The American Roentgen Ray Society

AJR, *American Journal of Roentgenology*, is published monthly to disseminate research on current developments in the radiologic sciences and commentary on topics related to radiology. It is published by the American Roentgen Ray Society, 1891 Preston White Dr., Reston, VA 22091; (703) 648-8992. Inquiries regarding society business, the annual ARRS meeting, and membership should be addressed to the Society at the above address.

Correspondence Concerning the *AJR*

Correspondence regarding display (not classified) advertising, subscriptions, address changes, reprints, and permission requests should be addressed to Williams & Wilkins, 428 E. Preston St., Baltimore, MD 21202; (301) 528-4000.

Correspondence regarding editorial matters and classified advertising should be addressed to Editorial Office, *AJR*, 2223 Avenida de la Playa, Ste. 200, La Jolla, CA 92037-3218; telephone (619) 459-2229; FAX (619) 459-8814. For information on manuscript submission, see Guidelines for Authors, pages A3-A5.

Subscriber Information

Subscription requests and inquiries should be sent to Williams & Wilkins, 428 E. Preston St., Baltimore, MD 21202. ARRS annual dues include \$50 for journal subscription. Subscription rates are as follows: nonmembers, \$100/year (\$145 foreign); institutions, \$110 (\$155 foreign); nonmember in-training, \$25 (\$70 foreign). Single copies of the Journal may be purchased for \$16 (\$19 foreign). Airmail rates will be furnished on request.

Japanese rates include airfreight. Japanese yen price is available from our sole agent, USACO Corporation, 13-12, Shimbashi 1-Chome, Minato-Ku, Tokyo 105, Japan; telephone 03-502-6471.

Call toll-free, 1-800-638-6423 (in Maryland call 1-800-638-4007), with subscription questions or problems. Please have the mailing label from your latest issue available when you call.

If a subscriber receives a damaged copy of the *AJR* or fails to receive an issue, the subscriber should notify Williams & Wilkins (428 E. Preston St., Baltimore, MD 21202) within 60 days of publication (90 days for foreign subscribers) and that issue will be replaced.

Change of address information should be sent to Williams & Wilkins, 428 E. Preston St., Baltimore, MD 21202. Allow 90 days for address changes.

Copyrights, Permissions, and Reprints

The American Roentgen Ray Society holds the copyright for all material published in the *AJR*. No part of this publication may be reproduced without permission from the ARRS. Requests for such permission should be addressed to Williams & Wilkins, 428 E. Preston St., Baltimore, MD 21202.

For reprints of a particular article, please contact the author designated in the footnotes for that article.

Indexes

The *AJR* provides volume and yearly indexes (subject and author) in the June and December issues each year. *AJR* articles are also indexed in *Current Contents*, *Index Medicus*, and the cumulative index published by *Radiology*.

1989 ARRS President's Award

The Validity and Utility of Sonography in the Diagnosis of Appendicitis in the Community Setting

James M. Larson¹
John C. Peirce²
Douglas M. Ellinger¹
Gregory H. Parish¹
Dennis C. Hammond³
Clifton F. Ferguson⁴
Francis J. Verde⁵
Henry L. Vander Kolk⁶

Two hundred six patients with suspected appendicitis were examined with sonography over a 6-month period in three community teaching hospitals. Of 41 patients in whom the surgeons judged the clinical findings severe enough to warrant immediate surgery (group A), 34 (83%) had appendicitis, and sonography had a sensitivity of 0.76, a specificity of 0.71, and an accuracy of 0.76. Of 165 patients in whom the surgeons judged the clinical findings severe enough to warrant hospitalization for observation but not immediate surgery (group B), 51 (31%) had appendicitis at subsequent surgery. Sonography had a sensitivity of 0.96, a specificity of 0.94, and an accuracy of 0.95. Of 49 surgeons surveyed, the mean testing threshold (i.e., the probability of appendicitis below which they would send the patient home without further tests or observation) was 0.11, and the mean treatment threshold (i.e., the probability of appendicitis above which they would operate immediately) was 0.82. The posttest probability of appendicitis with findings indicating appendicitis present on sonography was 0.93 in group A and 0.88 in group B, and with findings absent on sonography it was 0.62 in group A and 0.02 in group B.

We conclude that in group A patients, the use of sonography remains controversial in the diagnosis of appendicitis, but in group B patients it is both valid and useful.

AJR 153:687-691, October 1989

Received March 6, 1989; accepted after revision May 19, 1989.

Presented at the annual meeting of the American Roentgen Ray Society, New Orleans, LA, May 1989.

¹ Radiology Residency, Michigan State University/Grand Rapids Area Medical Education Center, 240 Cherry St. S.E., Grand Rapids, MI 49503. Address reprint requests to J. M. Larson.

² Department of Medicine, St. Mary's Health Services, Michigan State University College of Human Medicine, 200 Jefferson St. S.E., Grand Rapids, MI 49503.

³ General Surgery Residency, Blodgett Memorial Medical Center, 1840 Wealthy St. S.E., Grand Rapids, MI 49503.

⁴ Department of Radiology, Butterworth Hospital, 100 Michigan St. N.E., Grand Rapids, MI 49503.

⁵ Department of Radiology, St. Mary's Health Services, 200 Jefferson St. S.E., Grand Rapids, MI 49503.

⁶ Department of Radiology, Blodgett Memorial Medical Center, 1840 Wealthy St. S.E., Grand Rapids, MI 49503.

0361-803X/89/1534-0687
© American Roentgen Ray Society

The diagnosis of appendicitis is often straightforward with classic clinical findings. However, there are many diseases that do not require surgery that can mimic appendicitis. In order to prevent complications associated with delayed appendectomy, surgeons accept a false-positive diagnosis rate of 15-20% [1-3].

The purpose of our study was to assess the validity and utility of sonography in diagnosing appendicitis in the population of patients arriving at acute-care general hospitals with possible appendicitis. Emphasis was given to determining how the sonographic findings affected the decisions made by the surgeons. The threshold model of decision making described by Pauker and Kassirer [4] was used as a basis for dividing patients into two populations: those in whom the clinical findings warranted immediate surgery without further observation or testing and those in whom the clinical findings warranted hospitalization with monitoring. We determined the sensitivity, specificity, and accuracy (validity) of the sonographic examination in diagnosing appendicitis and compared the posttest probabilities of appendicitis to the surgeons' threshold probabilities in both populations (utility).

Subjects and Methods

The study was performed in three large metropolitan acute-care general hospitals in Grand Rapids, MI, serving a population of approximately 500,000. Each is a major teaching hospital of Michigan State University College of Human Medicine.

For 6 months, January through June 1988, sonography for the diagnosis of appendicitis was made available on a 24-hr basis at all three hospitals. During these months, 206 patients

were evaluated sonographically for appendicitis on their initial visit to the hospital. We estimated this to be about 50% of such cases seen during that time.

Patients evaluated were divided into two groups: group A comprised those who, in the judgment of the attending surgeon, had clinical findings sufficient to warrant immediate surgery without further testing, and group B comprised those who, in the judgment of the attending physician, had clinical findings that warranted hospitalization and monitoring but were not sufficient to warrant surgery. The group A patients warranted surgery without sonography; sonograms were performed only as part of the study. By the threshold model of decision making, group A included those patients who had exceeded the treatment threshold and group B included those patients who exceeded the testing threshold but not the treatment threshold. No standard criteria were used to include a patient in either group; this was left to each surgeon's individual judgment.

At sonography, patients were asked to point to the most painful area. An Acuson (Mountain View, CA) 5-MHz linear-array transducer was placed over this area. When an appendix was not recognized immediately, oblique, transverse, and longitudinal scans of the right lower quadrant were obtained by using transducer-applied graded compression as described by Puylaert [5]. A sonogram was interpreted as indicative of appendicitis if one wall of the visualized compressed appendix was more than 2-mm thick or the total outer wall-to-wall diameter of the appendix was greater than 6 mm. Sonographic findings were interpreted as normal if after careful examination the appendix was not seen or, if seen, each single-wall thickness was less than 2 mm and the outer wall-to-wall diameter was less than 6 mm.

The diagnosis of appendicitis was established by histologic examination in those patients undergoing an appendectomy. Uncomplicated appendicitis had polymorphonuclear leukocytic infiltration of the wall without necrosis; gangrenous appendicitis had necrosis in part of the wall; and a perforated appendix had through-and-through necrosis of the appendiceal wall. It was determined that patients who did not undergo surgery did not have appendicitis if their clinical findings resolved, as determined by telephone follow-up from 2 to 16 weeks after the sonographic examination.

Sensitivity, specificity, and accuracy were used to determine validity. These, along with prevalence and predictive values, were calculated by using standard epidemiologic definitions [6] and are defined in the appendix. In this article, we use the probability of appendicitis when sonograms are indicative of appendicitis as the positive predictive value, and the probability of appendicitis when sonographic findings are normal as the complement of the negative predictive value ($1 - \text{negative predictive value}$). Prevalence is the same as pretest probability.

At surgical section meetings, 49 surgeons were asked two questions: (1) What is the probability of appendicitis *below* which you would send the patient home without further testing? (2) What is the probability of appendicitis *above* which you would take the patient to the operating room without further testing? The answer to the first question determined their testing threshold; the answer to the second, their treatment threshold. Utility, or usefulness, was ascertained by comparing the postsonography probabilities of appendicitis with these threshold probabilities.

Proportions were compared statistically with the chi-square test. Of the 206 patients, 41 were taken to the operating room immediately and thus constituted group A. Twenty-six surgeons were involved. One hundred sixty-five patients were admitted to the hospitals for observation for possible appendicitis and constituted group B. These patients were initially examined by 37 physicians, some of whom were not surgeons, for example, emergency physicians. The proportion of females in group A, 20 (49%) of 41, was significantly different

($p < .015$) from that in group B, 111 (67%) of 165. The mean age was 29 years in group A (range, 11–62 years) and 28 years in group B (range, 2–84 years).

Results

Of the 41 patients in group A, 34 had appendicitis, yielding a prevalence of 0.83 (Table 1). Of the seven patients who had a normal appendix at surgery, five had no additional findings, one was found to have a ruptured ovarian cyst, and one was found to have a ruptured colonic diverticulum. Appendicitis was diagnosed sonographically in 26 of the 34 patients, for a sensitivity of 0.76. Of the seven patients with a normal appendix, the sonographic diagnosis was accurate in five, for a specificity of 0.71. In group A, the overall accuracy for the test was 0.76. The probability of appendicitis after a sonogram indicative of appendicitis in this group was 0.93, and that after a sonogram with normal findings was 0.62. Potentially correctable causes of incorrect normal readings were marked obesity of greater than 250 pounds (two patients) and extreme pain (one patient).

There were 165 patients in group B (Table 2). Fifty-one had appendicitis, for a prevalence of 0.31, which is significantly different ($p < .001$) from the prevalence of 0.83 in group A. Appendicitis was diagnosed correctly by sonography in 49 of those 51 patients, yielding a sensitivity of 0.96; of the 114 patients without appendicitis, the sonographic diagnosis was correct in 107, for a specificity of 0.94. The accuracy of 0.95 in group B was significantly different ($p = .0002$) from that in group A. The probability of appendicitis with a sonogram indicative of appendicitis was 0.88, which is an increase of 0.57 over the prevalence. The probability of appendicitis with a sonogram with normal findings was 0.02, which is a decrease of 0.29 from the prevalence.

Of the 111 females in group B, 27 had appendicitis for a prevalence of 0.24 as compared with the 54 males who had a prevalence of 0.44, which was statistically significant at $p < .01$. The sensitivity, specificity, accuracy, and the post-sonographic probabilities of appendicitis were not significantly different between the males and females.

TABLE 1: Findings Indicating Appendicitis in 41 Patients Immediately Taken to Surgery (Group A)

Findings Indicating Appendicitis	No. of Patients
Present on sonography and present on histology	26
Present on sonography and absent on histology	2
Absent on sonography and present on histology	8
Absent on sonography and absent on histology	5
Total present on histology	34
Total absent on histology	7
Total present on sonography	28
Total absent on sonography	13

Note.—Prevalence of appendicitis = 0.83, accuracy of sonography = 0.76, sensitivity = 0.76, specificity = 0.71, probability of appendicitis with findings present on sonography = 0.93, probability of appendicitis with findings absent on sonography = 0.62.

TABLE 2: Findings Indicating Appendicitis in 165 Patients Hospitalized and Observed (Group B)

Findings Indicating Appendicitis	No. of Patients		
	Total (n = 165)	Males (n = 54)	Females (n = 111)
Present on sonography and present on histology	49	24	25
Present on sonography and absent on histology	7	3	4
Absent on sonography and present on histology	2	0	2
Absent on sonography and absent on histology or in clinical course	107	27	80
Total present on histology	51	24	27
Total absent on histology or in clinical course	114	30	84
Total present on sonography	56	27	29
Total absent on sonography	109	27	82

Note.—Prevalence of appendicitis = 0.31 (males, 0.44; females, 0.24; $p \leq .01$, chi-square, $df = 1$), accuracy of sonography = 0.95 (males, 0.94; females, 0.95), sensitivity = 0.96 (males, 1.00; females, 0.93), specificity = 0.94 (males, 0.90; females, 0.95), probability of appendicitis with findings present on sonography = 0.88 (males, 0.88; females, 0.85), probability of appendicitis with findings absent on sonography = 0.02 (males, 0.00; females, 0.03).

Table 3 depicts the frequency distribution of the probabilities of the 49 surgeons' testing thresholds (i.e., that probability below which they would send the patient home without further testing). The mode and median are both 0.10, the mean is 0.11, and the 25th percentile is 0.05. Table 4 depicts the frequency distribution of the 49 surgeons' treatment threshold probabilities (i.e., that probability above which they would take the patient to surgery immediately). The mode and median are 0.80, the mean is 0.82, and the 75th percentile is 0.90.

In group A, two (6%) of the 34 patients with appendicitis had a perforation on histologic examination. In group B, 13 (25%) of the 51 patients with appendicitis had a perforation on histologic examination. This difference was statistically significant at $p < .001$. In both groups, appendicitis had been diagnosed correctly by sonography in every case of perforation.

Discussion

Recent studies have shown that sonography is accurate for diagnosing appendicitis and that it can accurately identify other diseases, regardless of whether they require surgical treatment [5, 7–15]. However, the use of sonography in the diagnosis of appendicitis remains controversial among surgeons. We felt that by determining the postsonography probabilities of appendicitis and comparing these with the testing and the treatment threshold probabilities of surgeons, we could help resolve this controversy.

In order for postsonography results to be useful they have to relate to surgical decision making. The surgical management of abdominal pain in which appendicitis is a prime consideration appeared to lend itself to the threshold model of decision making [4]. The surgeons intuitively felt comfortable with the concept of the thresholds because sending a person home, admitting them for observation, or immediately operating on them described accurately what they do. The major difficulty lay in placing a numerical probability on these thresholds. As has been found elsewhere, they preferred descriptive or qualitative phrases to express the probabilistic

TABLE 3: Frequency Distribution of Surgeons' Testing Thresholds

Probability	No. of Surgeons
0.00	3
0.03	1
0.05	12
0.10	19
0.15	2
0.20	10
0.25	1
0.30	1
Total	49

Note.—25th percentile = 0.05, 50th percentile (median) = 0.10, 75th percentile = 0.15, mode = 0.10, mean = 0.11.

TABLE 4: Frequency Distribution of Surgeons' Treatment Thresholds

Probability	No. of Surgeons
0.50	1
0.60	1
0.65	1
0.70	6
0.75	1
0.80	16
0.85	5
0.90	13
0.95	5
Total	49

Note.—25th percentile = 0.80, 50th percentile (median) = 0.80, 75th percentile = 0.90, mode = 0.80, mean = 0.82.

aspects of their clinical judgment [16]. However, in order to compare these values with the postsonography probabilities we needed to obtain from the surgeons their subjective probabilities for these thresholds. These subjective probabilities varied considerably. For the testing threshold, 33 (67%) of the surgeons had probabilities from 0.05 to 0.15, 43 (88%) had probabilities from 0.05 to 0.20, and 45 (92%) had probabilities at or above 0.05. Similarly for the treatment threshold, 34 (69%) had probabilities from 0.80 to 0.90 and 44 (90%)

had probabilities of 0.90 or below. We anticipate that with greater familiarity and use of probabilities, threshold probabilities will become more precise and take on greater meaning for the surgeon.

The prevalence of appendicitis in group B of 0.31 was unequivocally in the range between the surgeons' testing and treatment threshold probabilities, above their highest testing threshold probability and below their lowest treatment threshold probability. It was significantly different from the prevalence in group A of 0.83, which exceeded the treatment threshold probabilities of 53% of the surgeons. In group A, after a sonogram indicative of appendicitis, the probability of appendicitis increased to 0.93, exceeding the treatment threshold probabilities of all but the five surgeons who had a treatment threshold of 0.95. After a sonogram with normal findings, the probability of appendicitis fell to 0.62, entering the range between the two thresholds where further testing is warranted. These patients may benefit from further monitoring and testing rather than immediate surgery; however, because of the high number of false-negative cases (24%), it is uncertain whether surgeons will put much faith in a sonogram with normal findings, particularly when other clinical findings appear compelling. The accuracy of the test in the group A patients (0.76) was significantly different from that in the group B patients (0.95). It was not known whether this decreased accuracy was due to clinical factors that made the examination more difficult or whether it was due to the examination being hurried because the surgeon was impatient to take the patient to the operating room.

In group B patients, after a sonogram indicative of appendicitis the probability of appendicitis increased to 0.88, exceeding the treatment threshold probabilities of 31 (63%) of the 49 surgeons. After a sonogram with normal findings, the probability of appendicitis decreased to 0.02, falling below the testing threshold probabilities of all the surgeons except the three who had a threshold of 0.00.

Among the females in group B, the prevalence of appendicitis is 0.24 which was significantly different from the 0.44 prevalence in the males. This was most likely due to the higher prevalence of other pelvic disease that is confused with appendicitis. After any sonogram, the probability of appendicitis in females is not significantly different from that in group B as a whole.

Because these were not consecutive cases, selection bias is a major concern. The parameters that could be affected by this bias include the sensitivity, specificity, accuracy, prevalence, proportion of females, and the probabilities of appendicitis after normal or abnormal sonographic findings. Our group B patients were very similar to the patients studied by Jeffrey, Laing, and Townsend [9]. That study reported the following characteristics: sensitivity, 0.90; specificity, 0.96; accuracy, 0.94; prevalence, 0.36; and the probability of appendicitis after normal or abnormal sonographic findings as 0.06 and 0.93, respectively. None of these was significantly different from our values. Only the proportion of females was significantly different ($p = .005$) with 0.55 in their study and 0.64 in our study. They did not examine the test characteristics by gender. As our test characteristics are similar to theirs,

it is doubtful that selection bias caused much distortion. Whether the difference in proportion of females is from selection bias or from a true difference cannot be determined.

The efficacy of sonographic evaluation in appendicitis depends on how it affects outcome. Our finding of a higher perforation rate in group B suggests that outcome might be improved if definitive action were taken immediately on the basis of the sonographic findings. Determining efficacy would require a clinical trial in which patients warranting hospitalization for observation for appendicitis would be randomized into a group in which the results of sonography would dictate appendectomy or into another group in which conventional diagnostic evaluation would take place. Outcome measures would include important measures of morbidity rate such as perforation rates, length of hospital stay, hospital costs, and disability days, as well as mortality rate, should any patients die.

In conclusion, the use of sonography in those patients in whom the clinical findings of appendicitis strongly suggest immediate surgery remains controversial and will probably be useful only for those surgeons who demand a very high probability of appendicitis before they operate. In those patients in whom the clinical findings of appendicitis are ambiguous (i.e., not sufficiently lacking to send a patient home, but not sufficient to warrant immediate surgery), we find that sonography has high accuracy and that the posttest probability of a sonogram indicative of appendicitis exceeds the treatment threshold probabilities and the probability of appendicitis with normal sonographic findings is less than the testing threshold probabilities of most of the surgeons in our study. Of those patients with ambiguous clinical findings, sonographic examination seems particularly useful in women. Whether sonographic examination of patients with suspected appendicitis will improve outcomes remains to be determined.

ACKNOWLEDGMENT

We thank Atis Fremanis for his reviews of the manuscript.

Appendix

Sensitivity = $a/(a+c)$, specificity = $d/(b+d)$, probability of appendicitis after a sonogram indicative of appendicitis (positive predictive value) = $a/(a+b)$, probability of appendicitis after a sonogram with normal findings (1 - negative predictive value) = $c/(c+d)$, accuracy = $(a+d)/(a+b+c+d)$, prevalence (prior probability) = $(a+c)/(a+b+c+d)$, where:

- a = number of persons with findings indicating appendicitis present on sonography and on histology
- b = number of persons with findings indicating appendicitis present on sonography and absent on histology or clinical follow-up
- c = number of persons with findings indicating appendicitis absent on sonography and present on histology
- d = number of persons with findings indicating appendicitis absent on sonography and on histology or clinical follow-up

- (a+c) = total number of persons with appendicitis (proved by histology)
 (c+d) = total number of persons with no appendicitis (proved by histology or clinical follow-up)
 (a+b) = total number of persons with findings indicating appendicitis present on sonography
 (c+d) = total number of persons with findings indicating appendicitis absent on sonography
 (a+d) = total number of persons with a correct diagnosis by sonography

REFERENCES

- Berry J, Malt RAI. Appendicitis near its centenary. *Ann Surg* 1984; 200:567-575
- Lewis FR, Holcroft JW, Boey J, Dunphy JE. Appendicitis: a critical review of diagnosis and treatment in 1000 cases. *Arch Surg* 1975;110:677-684
- Knissem J, Eskin E, Fletcher S. Increasing accuracy in the diagnosis of acute appendicitis with modern diagnostic techniques. *Am Surg* 1988;52:222-225
- Pauley SG, Kassirer JP. The threshold approach to clinical decision making. *N Engl J Med* 1980;302:1109-1116
- Puylaert JBCM. Acute appendicitis: ultrasound evaluation using graded compression. *Radiology* 1986;158:335-360
- Fletcher RH, Fletcher SW, Wagner EH. *Clinical epidemiology: the essentials*, 2nd ed. Baltimore: Williams & Wilkins, 1988:42-60
- Jeffrey RB Jr, Laing FC, Lewis FR. Acute appendicitis: high resolution real-time ultrasound findings. *Radiology* 1987;163:11-14
- Abu-Yousef MM, Bleicher JJ, Maher JW, Urdaneta LF, Franken EA Jr, Metcalf AM. High-resolution sonography of acute appendicitis. *AJR* 1987;149:53-58
- Jeffrey RB Jr, Laing FC, Townsend RR. Acute appendicitis: sonographic criteria based on 250 cases. *Radiology* 1988;167:327-329
- Puylaert JBCM. Mesenteric adenitis and acute terminal ileitis: US evaluation using graded compression. *Radiology* 1986;161:691-695
- Puylaert JBCM, Lalisang RI. *Campylobacter* ileocolitis mimicking acute appendicitis: differentiation with graded-compression US. *Radiology* 1988;166:727-740
- Parulekar SG. Ultrasonographic findings in diseases of the appendix. *J Ultrasound Med* 1983;2:59-64
- McNamara MJ, Chalmers AG, Morgan M, Smith SE. Typhlitis in acute childhood leukaemia: radiological features. *Clin Radiol* 1986;37:83-86
- Puylaert JBCM, van der Werf SDJ, Ulrich C, Veldhuizen RW. Crohn disease of the ileocecal region: US visualization of the appendix. *Radiology* 1988;166:741-743
- Puylaert JBCM, Rutgers PH, Lalisang RI, et al. A prospective study of ultrasonography in the diagnosis of appendicitis. *N Engl J Med* 1987;317:666-669
- Poses RM, Cebul RD, Centor RM. Evaluating physicians' probabilistic judgments. *Med Decis Making* 1988;8:233-240



MELVIN M. FIGLEY FELLOWSHIP IN RADIOLOGY JOURNALISM

The American Roentgen Ray Society announces a one-month fellowship in radiology journalism in the La Jolla editorial office of the AJR. Board-certified radiologists with special academic promise are invited to apply.

PURPOSE

The purpose of the fellowship is (1) to stimulate bright young radiologists to continue with an academic career, to accelerate their progress, and to stimulate their interest in good radiology journalism, and (2) to improve the quality of radiology journals by teaching the fundamentals of medical journalism to academicians, training manuscript reviewers and future editors, and providing core teachers of medical journalism in radiology departments around the country.

CURRICULUM

The fellow will be taught the fundamentals of medical writing, manuscript preparation, peer review, manuscript editing, the ethics of scientific journalism, and journal publication and printing in personal tutorials given by the AJR editors and editorial staff through hands-on experience in the editorial office. He or she will visit Williams & Wilkins in Baltimore to observe the publication and printing process.

STIPEND

The successful candidate will be awarded \$10,000, which includes the cost of travel to La Jolla and Baltimore, living expenses for the month, and an honorarium.

APPLICATIONS

Candidates should apply in writing to Robert N. Berk, M.D., Editor-in-Chief, AJR Editorial Office, 2223 Avenida de la Playa, Suite 200, La Jolla, CA 92037. The letter must include a curriculum vitae and a description of the candidate's goals during the fellowship. Letters of recommendation from his or her department chairman and one other senior person are required. Deadline for receipt of applications is Nov. 1, 1989. The successful candidate will be notified Dec. 1, 1989, and may choose one of the following months for the fellowship training: Jan., Feb., March, April 1990.

1989 ARRS Executive Council Award

Exercise-Enhanced MR Imaging of Variations in Forearm Muscle Anatomy and Use: Importance in MR Spectroscopy

James L. Fleckenstein¹
Loren A. Bertocci¹
Ray L. Nunnally¹
Robert W. Parkey¹
Ronald M. Peshock^{1,2}

³¹P MR spectroscopic studies of forearm exercise frequently assume that the volume sampled is appropriate for the muscle of interest and that individual variations in muscle anatomy and use are not important. Postexercise MR imaging was used to assess variations in the size, location, and use of forearm flexors and the accuracy of palpation as a method for locating the muscle of interest. By using the information obtained with MR, the effects of errors in surface-coil position relative to the muscle of interest on ³¹P MR spectroscopy were examined. In the midforearm of seven men, the greatest diameter of the flexor carpi ulnaris was 29 ± 4 mm, and that of the flexor digitorum superficialis was 28 ± 6 mm. However, in the proximal forearm, $58 \pm 10\%$ of the diameter was covered by the palmaris longus, when present (79% of subjects). An unexpected finding was that a focal portion of the superficial finger flexor was used primarily as a wrist flexor in 26% of subjects. Palpation incorrectly identified flexor muscle margins by more than 15 mm in 50% of attempts. When a surface coil was positioned over wrist flexors during handgrip, attenuation of exercise-induced changes in ³¹P spectra resulted.

Exercise-enhanced MR imaging reveals variations in forearm muscle anatomy and use that are common and difficult to appreciate by palpation. It therefore allows improved localization of the sensitive volume for MR spectroscopic studies of muscle physiology.

AJR 153:693-698, October 1989

MR spectroscopy has great potential as a noninvasive probe of skeletal muscle physiology [1-12]. However, implicit in these studies is the assumption that the sensitive volume samples only muscles actually active during the exercise. Variations in muscular anatomy are generally not acknowledged, and muscles are assumed to respond to exercise homogeneously. Simple palpation is the primary method of localizing muscles of interest.

We used brief exercise, which causes a transient increase in signal intensity of activated muscles on MR imaging [13], to help assess the appropriate sensitive volume in MR spectroscopy studies of forearm exercise. Specifically, we asked the following questions: (1) Are there normal variants in forearm musculature apparent on MR images that could influence spatial localization of those muscles for MR spectroscopy? (2) How accurate is palpation in locating forearm flexor muscles? and (3) What is the effect of slightly different positions of the RF coil relative to the muscles of interest?

Subjects and Methods

Studies were performed under protocols approved by the Institutional Review Board for Human Experimentation at the University of Texas Southwestern Medical Center and informed consent was obtained in each case. Fourteen men and five women 22-54 years old participated in the study. No subject regularly engaged in forearm exercise prior to the study.

Variations in muscle anatomy and use were assessed from finger flexion (handgrip) and wrist flexion data. All subjects performed intermittent handgrip exercise to fatigue (2-3

Received March 6, 1989; accepted after revision May 18, 1989.

Presented at the annual meeting of the American Roentgen Ray Society, New Orleans, May 1989.

This work was supported in part by Ischemic SCOR grant HL-17669, the Moss Heart Fund, a grant from the Alcoholic Beverage Medical Research Foundation, and a grant from Diasonics, Inc. R. M. Peshock is the recipient of a Clinical Investigator Award, National Institutes of Health, HL-01157.

¹ Department of Radiology, University of Texas Southwestern Medical Center at Dallas, 5201 Harry Hines Blvd., Dallas, TX 75235. Address reprint requests to J. L. Fleckenstein, NMR Imaging Center, 1311 Record Crossing, Dallas, TX 75235-9085.

² Department of Internal Medicine, University of Texas Southwestern Medical Center at Dallas, Dallas, TX 75235.

0361-803X/89/1534-0693
© American Roentgen Ray Society

minutes) within the bore of the imaging device. Five wrist flexion experiments were performed in three men. For this, the wrist was placed adjacent to a hinged board attached to a pulley and weight that hung over the end of the magnet. The weight was adjusted to 10% of the subject's body weight. The wrist flexed 45° repetitively once per second for 1 min.

MR imaging was performed before and after exercise in all cases. A Diasonics 0.35-T imaging device and 18-cm-diameter quadrature detection coil were used. The sequences used were (1) a gradient reversal, partial-flip-angle sequence, 500/30 (TR/TE), 30°, with a $0.95 \times 0.95 \times 10$ mm voxel, a matrix of 256×256 , and one average; (2) short tau inversion recovery (STIR) sequence, 1500/100/40 (TR/TI/TE), with a voxel size of $1.25 \times 1.25 \times 5$ mm, a matrix 128×256 , and $\frac{1}{2}$ acquisition. Scan times were 2.0–3.5 min.

The muscles used in each exercise were identified on the basis of increased signal intensity on MR images obtained after exercise [13]. By using software on the imaging device, the transverse diameters of the flexor carpi ulnaris and flexor digitorum superficialis were measured at the proximal and middle portions of the forearm. The percentage of the flexor digitorum superficialis that was covered by the palmaris longus also was determined (Fig. 1).

Palpation of the forearm flexors as a localization technique prior to spectroscopy was assessed in six subjects. The radial margin of the flexor carpi ulnaris and the ulnar margin of the flexor carpi radialis were palpated during wrist flexion against resistance, and, as previously described, the flexor digitorum superficialis is assumed to lie between these muscles [1]. These margins were marked with oil-filled tubing. The skin was also marked at the junction of the proximal and second thirds of the length of the forearm, as defined by easily palpated bony landmarks, the medial epicondyle of the humerus and the pisiform. A similar axial level was marked halfway along this line. Subsequent MR images were then obtained in conjunction with handgrip exercise to assess the accuracy of palpation in detecting the flexors' margins and to measure the diameters of the flexor carpi ulnaris and flexor digitorum superficialis at the two levels described.

The accuracy of palpation as a method for defining the margins of forearm flexor muscles was examined by measuring the distance between the oil-filled markers and the true margin of the flexor muscles as shown by MR imaging after exercise (Fig. 1).

To assess effects of surface-coil location relative to activated muscles, a submaximal exercise protocol was used in a 37-year-old healthy man. The submaximal protocol is a standard approach that allows repeated exercise at a single sitting without substantial fatigue. A single handgrip contraction was maintained at approximately 30% of the maximal voluntary force for 4 min; this was repeated four times, with a resting interval of 10–30 min between each bout. Force was measured by using a transducer connected to a chart recorder as previously described [13]; this was done to verify that the same force was maintained for each exercise period during both imaging and spectroscopy.

MR images were obtained before and after exercise and inspected for evidence of different recruitment patterns with successive bouts of exercise. The same protocol was then used in conjunction with MR spectroscopy. Forearm flexors were precisely identified with MR imaging and marked in the proximal and midforearm. ^{31}P spectroscopy data were acquired after each of four of the submaximal handgrip protocol described above. Four coil positions were studied: (1) position 1—palmaris longus, proximal; (2) position 2—flexor carpi ulnaris, proximal; (3) position 3—flexor digitorum profundus, proximal; and (4) position 4—flexor digitorum superficialis, middle. After MR spectroscopy, a faint impression made on the skin by the surface coil was marked with ink. MR imaging was again performed with oil-filled, mock surface coils to confirm the position of the coil in relation to the muscles of interest.

^{31}P MR spectroscopy was performed on a 30-cm-diameter, 1.9-T, horizontal bore magnet (Oxford Instruments, Oxford, U.K.) interfaced to an NT-80 console (General Electric Instruments, Fremont, CA). A 2-cm-diameter, single-turn surface coil was used at 32.5 MHz to collect ^{31}P spectra. Shimming was performed on the proton signal obtained from the surface coil at 80.4 MHz. For each data acquisition,



Fig. 1.—Handgrip exercise-enhanced short tau inversion recovery (STIR) image of proximal forearm facilitates identification and measurement of forearm flexor muscles. Transverse diameter of flexor digitorum superficialis was measured both at level deep to subcutaneous fascia (short black line) and deep to palmaris longus (long black line). Flexor carpi ulnaris diameter was also measured (white line). Oil-filled tubing (arrows) indicates predicted, but incorrect, margins of flexor digitorum superficialis, as determined by palpation.

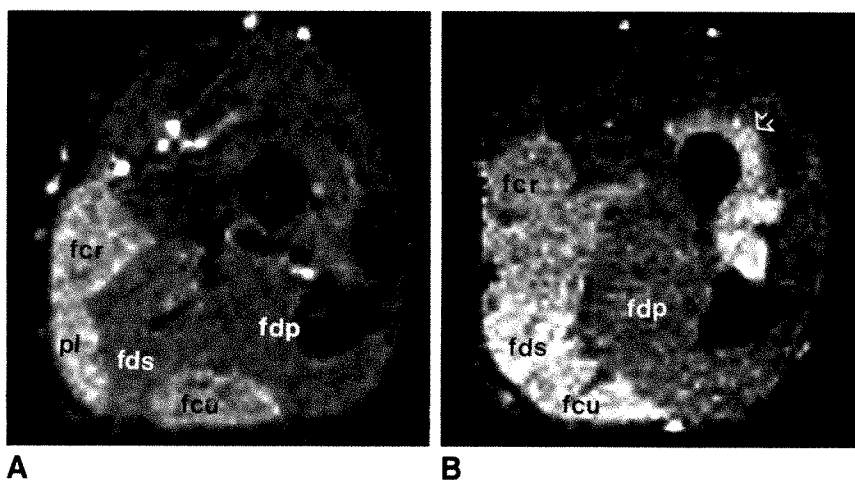


Fig. 2.—Variations in muscle brightening after comparable wrist flexion.
A, In one subject, flexor digitorum profundus (fdp) and superficialis (fds) remain less bright than wrist flexors, flexor carpi radialis (fcr), palmaris longus (pl), and flexor carpi ulnaris (fcu).
B, In another subject, who lacks palmaris longus, signal intensity increased in the flexor digitorum superficialis, similarly to that in wrist flexors. Note also recruitment of supinator (arrow) and abductor pollicis longus.

In a third subject (not shown), finger flexors and wrist flexors became similarly bright during wrist flexion.

the magnetic field was shimmed to obtain a proton line width for the water peak of less than 30 Hz. Free induction decays were acquired after a 20-msec pulse with a cycle time of 2.5 sec. Data were collected into a 4000 block. After baseline correction and a trapezoidal multiplication (line broadening, approximately 12 Hz), the data were transformed and displayed by using Fourier analysis.

Before each experiment, two 1-min control spectra were collected with normal pulse repetition rates and compared for peak saturation effects with a 10-min block acquired with a 15-sec recycle time. Each exercise bout was preceded by a 1-min control collection, then eight consecutive 1-min blocks were collected during a 4-min exercise period and a 4-min recovery period.

^{31}P spectra obtained at each position were analyzed, and the exercise-induced changes in phosphocreatine, inorganic phosphate, and pH were measured. Peak areas were quantitated by using software triangulation/integration routines available under the Nicolet Magnetics Corp. software. Areas were standardized against 1 ml of 100-mmol/l methylene diphosphonate in a vial positioned at the coil center opposite the arm. Calculations of adenosine triphosphate (ATP) concentration were made relative to the ATP concentration during the preexercise rest period and assume a concentration of 5.5 mmol/kg wet weight muscle.

The data obtained at each coil position were compared with the images acquired immediately after exercise to examine the spectrum with respect to the underlying muscles.

Results

Exercise-enhanced MR imaging revealed that the palmaris longus was present in 15 (79%) of 19 subjects. When present, it was superficial to the flexor digitorum superficialis, covering $59 \pm 10\%$ of the transverse diameter of that muscle in the proximal forearm and $20 \pm 16\%$ of the diameter in the midforearm. The palmaris longus lay adjacent to the flexor carpi radialis in all but one case. In that variant, it was adjacent to the flexor carpi ulnaris.

The sizes of the two muscles most commonly studied in forearm spectroscopy, flexor digitorum superficialis and flexor carpi ulnaris, are shown in Table 1. In the midforearm of seven men, the diameter of both muscles was approximately 28 mm.

Postexercise images revealed variations in muscle use. In all subjects, handgrip was associated with increased proton signal intensity in flexor digitorum superficialis and profundus and extensor carpi radialis. The supinator and extensor carpi ulnaris were brighter after exercise in only 47% of subjects. Wrist flexors and finger extensors did not brighten with handgrip in any subject. Wrist flexion was associated with increased signal intensity in wrist and finger flexors; however, the relative degrees of brightness of these muscles varied (Fig. 2).

An unexpected aspect of use of the flexor digitorum superficialis was identified by MR imaging. In five of 19 subjects, a focal portion of the flexor digitorum superficialis showed no increase in signal intensity during finger flexion. In the one subject with this finding who also performed wrist flexion, the portion of the muscle that did not brighten with handgrip did so on wrist flexion (Fig. 3).

The average distance between predicted and actual muscle margins was 14.5 ± 14.6 mm for the ulnar margin of the

TABLE 1: Transverse Diameters of Two Forearm Flexor Muscles Measured at Two Standard Levels

Gender/Position	Mean Diameter \pm SD (mm)		
	Flexor Carpi Ulnaris	Flexor Digitorum Superficialis	Flexor Digitorum Superficialis ^a
Male (<i>n</i> = 7)			
Proximal	26.8 \pm 3.3	15.8 \pm 7.2	24.6 \pm 3.4
Middle	28.6 \pm 4.3	27.6 \pm 5.6	27.8 \pm 5.7
Female (<i>n</i> = 3)			
Proximal	21.3 \pm 2.5	7.3 \pm 1.2	16.7 \pm 1.7
Middle	21.7 \pm 3.1	23.7 \pm 4.2	23.7 \pm 4.2

^a Surface width measured deep to palmaris longus.

flexor carpi radialis and 14.8 ± 12.2 mm for the radial margin of the flexor carpi ulnaris. Palpation was within 5 mm of the designated flexor muscle margins in five of 12 muscles but missed by more than 15 mm in six of 12. In only one of six were both margins localized within 5 mm.

The effect of errors in coil position was assessed by using MR imaging to define different muscles for subsequent MR spectroscopy. With the coil positioned precisely over the flexor digitorum profundus in the proximal forearm or the flexor digitorum superficialis in the middle forearm, normal peak-exercise spectra were obtained showing the expected large inorganic phosphate accumulation and phosphocreatine depletion (Fig. 4 and Table 2).

When the coil was placed at positions that may result from typical palpation errors, such as over wrist flexors, MR spectroscopic estimates of inorganic phosphate increases ranged from 1.5- to 5.7-fold above control level, and the phosphocreatine level fell 9–42%, depending on the coil position. These values yielded changes in the phosphocreatine/inorganic phosphate ratio, which ranged from approximately one-half to one-tenth the resting value depending solely on the position of the coil relative to the muscle of interest.

Discussion

Despite the acknowledged importance of knowing the location and size of the sensitive volume in ^{31}P MR spectroscopy [14], few studies of forearm exercise address the question of the appropriate physiologic location or size of the sample volume [1–3]. We found that MR imaging of the exercised limb identified variations of forearm musculature that may affect the appropriate location and size of the sensitive volume in forearm spectroscopy.

An anatomic variant relevant to MR spectroscopy is the palmaris longus, present in 79% of subjects. The variability of this muscle is well known [15], but its importance in MR spectroscopy is not. Like other wrist flexors, it is inactive during handgrip and will attenuate the apparent metabolic changes reflected in ^{31}P MR spectra induced in an overlying coil.

Size is another anatomic variable relevant to MR spectroscopy because it fundamentally limits the maximal appropriate sensitive volume in MR spectroscopic studies. Because the mean diameter of finger flexors and wrist flexors was approx-

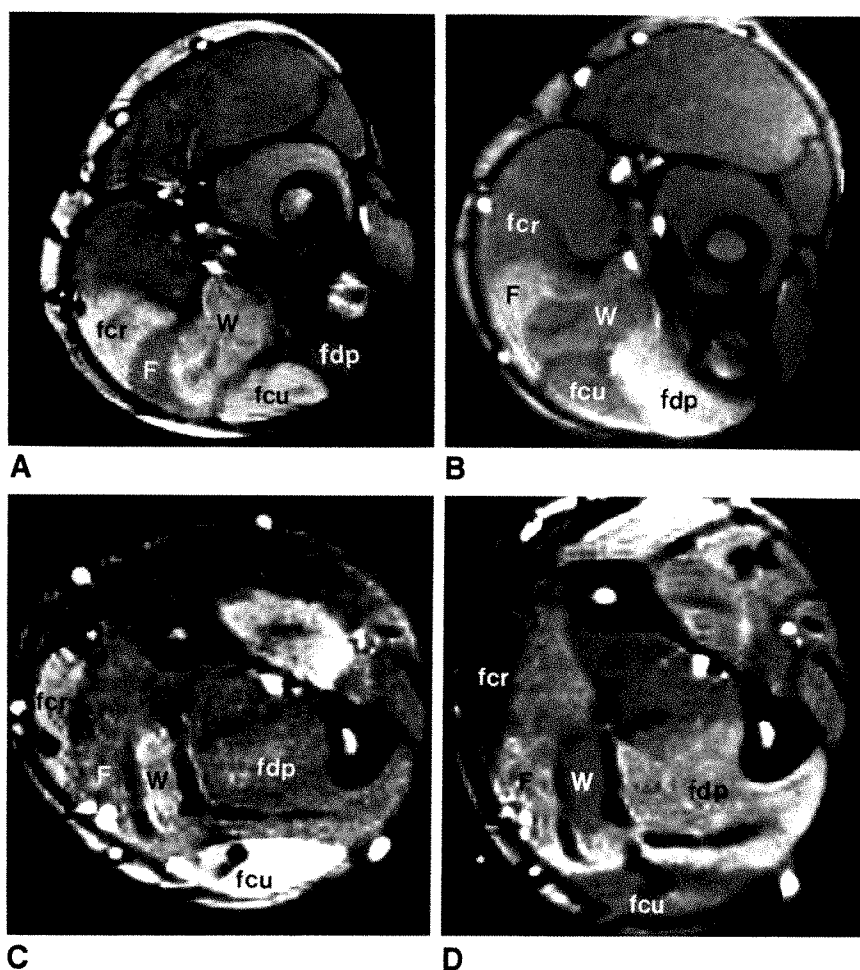


Fig. 3.—Common variant in forearm muscle use, shown at proximal (A and B) and middle (C and D) forearm levels during wrist flexion (A and C) and finger flexion (B and D). Flexor digitorum superficialis includes a portion that is used as a finger flexor (F) and one that is used as a wrist flexor (W). fcr = flexor carpi radialis; fcu = flexor carpi ulnaris; fdp = flexor digitorum profundus.

imately 28 mm in healthy men, sensitive volumes more than 28 mm wide sample an inappropriately large volume. Smaller volumes would be indicated in smaller muscles, such as those of women, children, the chronically ill, and the aged. The dimensions of the maximum physiologically acceptable sample volume is of particular relevance in that present techniques for volume-localized spectroscopy frequently use sample volumes on the order of $3 \times 3 \times 3 \text{ cm}^3$ or larger [14]. Our results indicate that there will be admixture of signal from active and inactive muscles if these volumes are used in forearm spectroscopy.

Variations in forearm muscle use were revealed by exercise-enhanced MR imaging. In wrist flexion, the same exercise protocol resulted in different muscles becoming bright in different subjects. Not only was there variation in apparent recruitment of muscles lying beside each other, but commonly, a focal portion of the flexor digitorum superficialis did not brighten during finger flexion but did appear to be used during wrist flexion.

On the basis of the small size of forearm muscles and their frequent variability, one would predict that palpation of the individual flexor muscles would be difficult. To our knowledge, there is only one primary method for localizing the muscle of interest [1]. In that study, the margins of the flexor carpi ulnaris and flexor carpi radialis were palpated during wrist

flexion against resistance. It was assumed that wrist flexors were accurately located and that the muscle between these margins was the flexor digitorum superficialis.

We compared the predicted position of the flexor digitorum superficialis based on palpation with the actual muscle position determined by using exercise-enhanced MR imaging. In the proximal forearm, palpation was accurate (within 5 mm) in defining wrist flexor margins in only five of 12 cases. Palpation was performed in young, normal-weight subjects with normal amounts of subcutaneous fat by an investigator with a thorough knowledge of forearm anatomy. Thus, it is unlikely that the result was due to investigator technique but that more fundamental factors were at work.

Examination of the exercise-enhanced images provided reasons for the inaccuracy of palpation, even with a trained examiner. First, MR imaging shows that the finger flexors may be recruited during wrist flexion. Hence, they become tense and cannot be differentiated from wrist flexors on physical examination. Second, the primary muscle of interest, the flexor digitorum superficialis, is actually not superficial but lies in the middle muscle layer of the anterior forearm, deep to the palmaris longus, and therefore is difficult to distinguish on palpation. Third, the assumption made by others that the flexor digitorum superficialis is the muscle between the palpated margins of flexor carpi radialis and ulnaris [1, 9, 10]

Fig. 4.—Effect of coil position on spectra.

A and B, Pcssthandgrip short tau inversion recovery (STIR) images show coil positions used for forearm spectroscopy relative to activated muscles in proximal (A) and mid (B) forearm.

C–F, Coil positions 1–4, respectively, were chosen in proximal forearm to sample palmaris longus (C), flexor carpi ulnaris (D), and flexor digitorum profundus (E) and in middle forearm to sample flexor digitorum superficialis (F). Although comparable exercise was performed at each of the four coil positions, ^{31}P spectra show markedly different results depending solely on coil position. This is most obvious for the variability of inorganic phosphate accumulation and phosphocreatine breakdown; ^{31}P peaks represent, from left to right, methylene diphosphonate (external standard), inorganic phosphate, phosphocreatine, gamma adenosine triphosphonate (ATP), alpha ATP, and beta ATP.

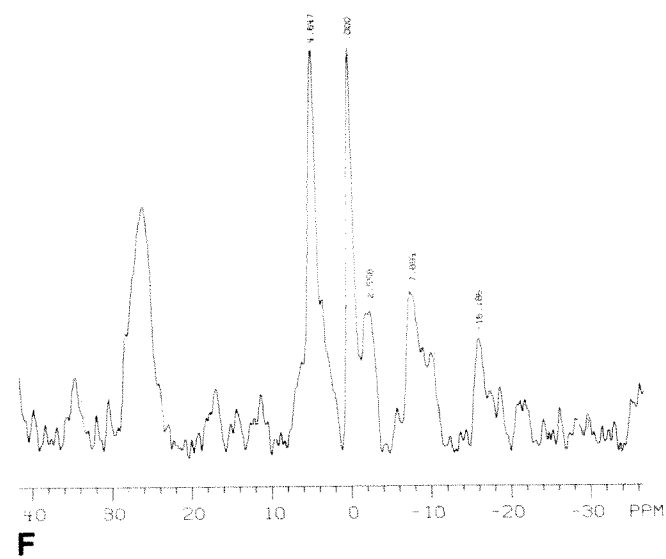
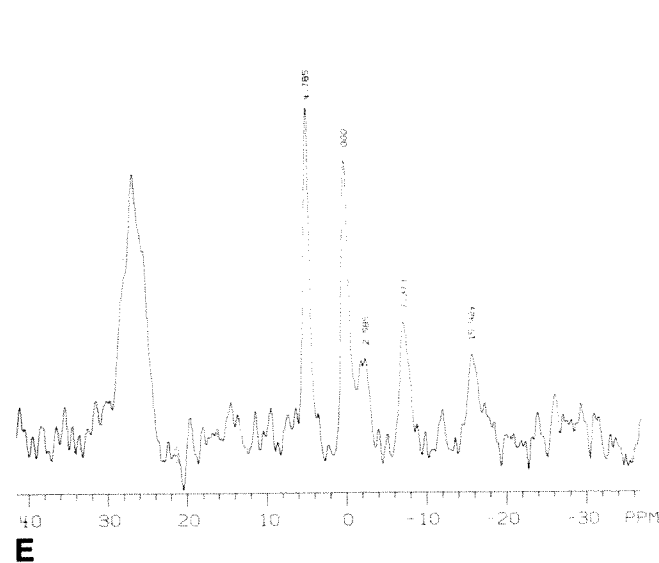
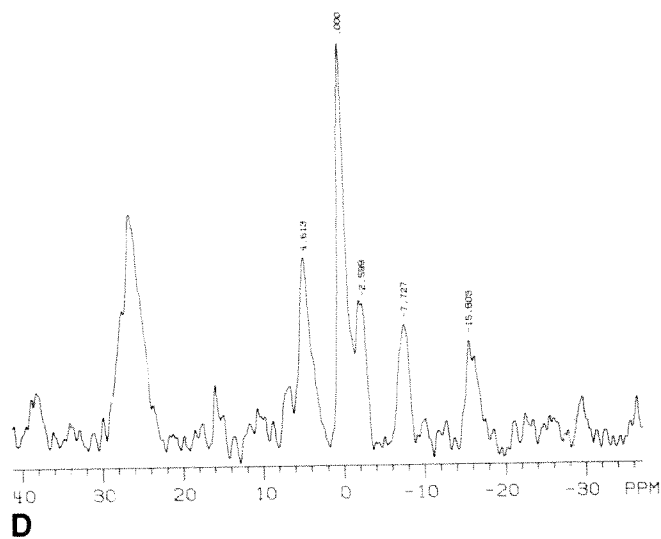
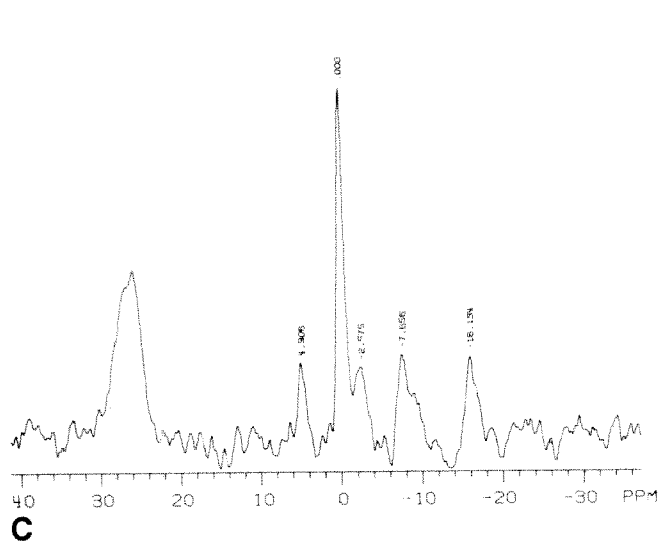
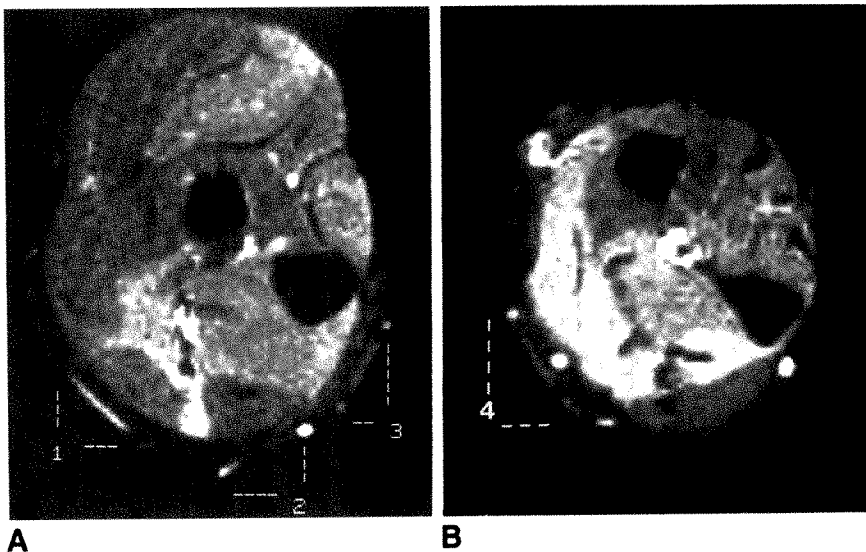


TABLE 2: MR Spectroscopy-Derived Estimates of Phosphorus Metabolites Depending on Coil Position

Group/Position No.	Pi	PCr	PCr/Pi	ATP	ADP	pH
Control	3.1	24.8	8	5.5	5.8	7.06
1 (at rest)						
Exercise						
1	4.8	22.6	4.7	5.5	10.5	7.07
2	11.1	20.1	1.8	5.5	9.6	6.84
3	15.2	16.3	1.1	5.5	24.1	6.97
4	17.6	14.3	0.8	5.6	25.3	6.87

Note.—All phosphorus estimates are in mmol/kg. Pi = inorganic phosphate; PCr = phosphocreatine; ATP = adenosine triphosphate; ADP = adenosine diphosphate.

was shown by MR imaging to be correct only in the minority of persons in whom the palmaris longus is absent.

On the basis of these findings, one would predict considerable variability in MR spectroscopic data due to errors in positioning the sample volume. Our data corroborate those of others [1] that this is indeed the case. Coils placed over muscles that did not show a change on MR imaging produced attenuated spectral changes with exercise due to admixture of active and inactive muscle within the sensitive volume. Coils placed over muscles that became bright on MR imaging showed the expected normal spectral changes. It is obviously important to determine if an attenuated metabolic response is due to coil position or to a true metabolic defect. Hence, the underlying anatomy, size, and use of the exercising muscles must be known for interpretation of MR spectra to be meaningful.

We conclude that normal variations of forearm muscle anatomy and use affect MR spectroscopy in important ways. Therefore, regardless of the spectral localizing technique used, a means of confirming the position of the sensitive volume within the muscle of interest is needed for meaningful results to be reliably obtained. Because exercise-enhanced MR imaging is unhampered by the inadequacy of palpation to define the muscles of interest, it can be used to direct physiologically appropriate sampling in ^{31}P MR spectroscopy studies of forearm exercise and should be useful in future investigations.

ACKNOWLEDGMENTS

We thank Dorothy Gutekunst, Ginny Vaughn, Jerry Cheek, Cindy Miller, Suzanne Newkirk, Maria Morgan, Janice Hall, and Kevin Baker for technical expertise.

REFERENCES

1. Taylor DJ, Bore PJ, Styles P, Gadian DG, Radda GK. Bioenergetics of intact human muscle. *Mol Biol Med* 1983;1:77-94
2. Mole PA, Coulson RL, Caton JR, Nichols BG, Barstow TJ. In vivo ^{31}P -NMR in human muscle: transient patterns with exercise. *J Appl Physiol* 1985;59(1):101-104
3. Zochodne DW, Thompson RT, Driedger AA, Strong MJ, Gravells D, Bolton CF. Metabolic changes in human muscle denervation: topical ^{31}P NMR spectroscopy studies. *Magn Reson Med* 1988;7:373-383
4. Ross BD, Radda GK, Gadian DG, Rocker G, Esiri M, Falconer-Smith J. Examination of a case of unsuspected McArdle's syndrome by ^{31}P nuclear magnetic resonance. *N Engl J Med* 1981;304(22):1338-1342
5. Chance B, Eleff S, Bank W, Leigh JS, Warnell R. ^{31}P -NMR studies of control of mitochondrial function in phosphofructokinase-deficient human skeletal muscle. *Proc Natl Acad Sci USA* 1982;79:7714-7718
6. Lehmann-Horn F, Hopfel D, Rudel R, Ricker K, Kuther G. In vivo P-NMR spectroscopy: muscle energy exchange in paramyotonia patients. *Muscle Nerve* 1985;8:606-610
7. Lewis SF, Haller RG, Cook JD, Nunnally RL. Muscle fatigue in McArdle's disease studied by ^{31}P -NMR: effect of glucose infusion. *J Appl Physiol* 1985;59(6):1991-1994
8. Wilson JR, Fink L, Maris J, et al. Evaluation of energy metabolism in skeletal muscle of patients with heart failure with gated P-31 nuclear magnetic resonance. *Circulation* 1985;71(1):57-62
9. Bogusky RT, Taylor RG, Anderson LJ, Angelos KL, Lieberman JS, Walsh DA. McArdle's disease heterozygotes. *J Clin Invest* 1986;77:1881-1887
10. Bevington A, Mundy KI, Yates AJP, et al. A study of intracellular orthophosphate concentration in human muscle and erythrocytes by ^{31}P nuclear magnetic resonance spectroscopy and selective chemical assay. *Clin Sci* 1986;71:729-735
11. Lunt JA, Allen PS, Brauer M, et al. An evaluation of the effect of fasting on the exercise-induced changes in pH and Pi/PCr from skeletal muscle. *Magn Reson Med* 1986;3:946-952
12. Duboc D, Jehenson P, Dinh T, Marsac C, Syrota A, Fardeau M. Phosphorus NMR spectroscopy study of muscular enzyme deficiencies involving glycogenolysis and glycolysis. *Neurology* 1987;37:663-671
13. Fleckenstein JL, Canby RC, Parkey RW, Peshock RM. Acute effects of exercise on MR imaging of skeletal muscle. *AJR* 1988;151(2):231-237
14. Aue WP. Localization methods for in vivo nuclear magnetic spectroscopy. *Rev Magn Reson Med* 1986;1(1):21-72
15. Hollinshead WH, Jenkins DB. *Functional anatomy of the limbs and back*, 5th ed. Philadelphia: Saunders, 1981:138-140

Review Article

High-Resolution Carotid Sonography: Past, Present, and Future

Daniel H. O'Leary¹ and Joseph F. Polak

Carotid sonography has proved to be highly accurate in detecting and quantifying carotid atherosclerosis. By far the most common indication for these examinations is for triage of patients at risk for stroke. In the absence of significant carotid stenosis, surgery usually is not contemplated. An abnormal study, on the other hand, may lead to angiography and, possibly, endarterectomy. Thus, noninvasive testing has focused on the accurate detection and quantification of high-grade lesions. Yet the prevalence of 50% or greater stenoses in the general population is low. This article discusses how evolving medical therapies and technology are reshaping the role of noninvasive carotid sonography, with increasing emphasis on early identification of wall abnormalities.

Carotid Endarterectomy and Noninvasive Studies

The perception that carotid endarterectomy can prevent stroke has been the driving force for the steady increase in the use of noninvasive carotid imaging. It was C. Miller Fisher, a neurologist, who first contemplated the possibility that surgery might be effective in treating the signs and symptoms of extracranial carotid occlusion [1]. In 1954, Eastcott et al. [2] described the first successful carotid endarterectomy. The operation caught on quickly because it was relatively easy to perform and had low reported associated morbidity and mortality rates. Also it appeared beneficial to certain groups of patients, particularly those with transient ischemic attacks (TIAs) and a significant stenosis in the extracranial carotid

artery. In 1971, about 15,000 carotid endarterectomies were performed in nonfederal hospitals in the United States. In 1985, the number had grown to 107,000 [3]. Carotid endarterectomy had become the second most common vascular procedure performed in the United States; coronary bypass surgery is the most common.

Initial Noninvasive Studies

Because not all patients with TIAs have an operable lesion, and because angiography carries its own risks, early on there was interest in developing noninvasive tests that could identify flow-reducing lesions. It was found that a hemodynamically significant decrease in flow to the brain did not occur until narrowing of the carotid artery exceeded 75% of the cross-sectional area or 50% of the diameter [4]. The first noninvasive studies developed to identify such stenoses were indirect ones. They detected alterations in vascular beds distal to the carotid bifurcation, principally in and around the orbit. They offered high specificity, poor sensitivity, and no clue as to the site of the abnormality [5].

Duplex Sonography

Later, systems that used either continuous-wave or pulsed-wave Doppler sonography with probes placed on the neck were used to detect directly obstructing lesions of the carotid bifurcation by identifying abnormal flow patterns. In 1974,

Received December 19, 1988; accepted after revision June 12, 1989.

¹ Both authors: Department of Radiology, Harvard Medical School and Brigham and Women's Hospital, 75 Francis St., Boston, MA 02115. Address reprint requests to D. H. O'Leary.

Doppler and B scans were first linked and given the name duplex imaging [6]. Because the quality of B-mode scanning at that time was poor, sonograms were used mostly to assist in the placement of the Doppler sample volume. This tendency to emphasize the Doppler component of the duplex study, and not the anatomic image, was reinforced by the fact that extensive plaque often makes the sonogram suboptimal because of acoustic shadowing and reverberation artifacts [7].

This approach found further support because of the high accuracy reported with Doppler grading of stenoses. For stenoses of greater than 50%, accuracies of greater than 90% were routinely achieved with noninvasive testing when compared with angiography [5, 7–13]. A well-functioning noninvasive carotid laboratory, by appropriately screening patients, has been shown to decrease significantly the proportion of negative arteriograms obtained [14]. In some centers, selected patients with symptoms and positive duplex imaging studies may proceed to surgery without angiography [13, 15].

Sonographic Characterization of Plaque

Although emphasis has been on the use of duplex sonography to study the disturbed hemodynamics of significant stenosis, its potential for studying plaque morphology has not been overlooked. Ulcerated, although not highly stenotic, plaques at the carotid bifurcation can serve as the nidus for the formation of emboli that cause both TIAs and stroke [16, 17]. Also, on the basis of analysis of plaques removed at the time of carotid endarterectomy, it has been postulated that recent hemorrhage in plaque is a stroke risk [18–20]. Thus, the finding on sonography of an irregular surface that could suggest ulceration or an anechoic area within plaque that could suggest recent hemorrhage can serve as justification for surgery, particularly in symptomatic patients [21, 22]. However, the clinical significance of plaque morphology remains uncertain [23, 24]. Furthermore, the ability of sonography to quantify reliably and reproducibly specific morphologic features of plaque is controversial [25–27]. Although the use of sonography in this setting is one of the more exciting developments in noninvasive testing, its clinical utility remains under active investigation.

Current Trends in the Surgical Treatment of Carotid Stenosis

Through 1985, the number of carotid endarterectomies performed and noninvasive carotid studies ordered grew steadily. The indications justifying surgical intervention broadened. Much of this growth was related to the availability of noninvasive technology, which could be used to screen many asymptomatic patients and to detect significant extracranial atherosclerosis in those with symptoms. Then in 1986 there was an abrupt change. The number of endarterectomies performed actually fell for the first time from 107,000 in 1985 to 83,000. The drop was even more dramatic when regression estimates using data from 1971 to 1985 estimated that 127,000 endarterectomies should have been performed in

1986 [28]. The reason for this sudden reversal is that over the three decades since its inception, carotid endarterectomy had become one of the most controversial procedures in medicine [29, 30]. As the number of surgical interventions increased, articles began to appear that called attention to the fact that there was scant proof that the operation was effective, that the indications for the procedure were not well defined, and that the complication rates were excessive in some institutions and communities. Other articles appeared defending carotid endarterectomy; all of this resulted in increasing uncertainty among clinicians about how best to manage patients with suspected carotid atherosclerosis [31].

This has important implications for the imaging community. Currently, noninvasive testing focuses on identifying and quantifying significant stenoses, particularly in symptomatic patients. Yet it is estimated that only about 35,000 new patients are seen each year in the United States who experience TIAs and have carotid stenosis [32]. It is clear that most of those undergoing endarterectomy do so for other reasons, and estimates are that about half of those undergoing this operation are neurologically asymptomatic. Most asymptomatic or minimally symptomatic patients probably were first diagnosed as having carotid disease by noninvasive testing. Clearly, surgery in either symptomatic or asymptomatic patients can be justified only if surgically treated patients have a better long-term prognosis than those managed conservatively. Although the complication rate for experienced surgeons is 1–2%, the overall combined mortality and morbidity rate after carotid endarterectomy has been estimated to fall between 5% and 10% [29, 31, 33]. This makes it hard to justify surgery, particularly in asymptomatic individuals, unless there is convincing evidence of benefit to the patient.

The Future of Carotid Endarterectomy

Two prospective randomized multicenter studies recently were funded by the National Institutes of Health, one to evaluate the efficacy of endarterectomy in asymptomatic patients with carotid stenosis and the other to evaluate the efficacy of endarterectomy in patients presenting with TIAs. From these and similar studies, more precise answers should be forthcoming as to what criteria identify those patients for whom carotid endarterectomy is indicated. Whatever subset of patients might remain candidates for surgery, the total number of carotid endarterectomies done in the United States has probably peaked and probably will continue to decline, possibly precipitously.

Cardiovascular Disease and Carotid Atherosclerosis

Because the demand for noninvasive carotid testing paralleled the growth of carotid endarterectomy, a decline in the need for these tests might now be anticipated. However, this may not occur because of the growing realization that carotid sonography can be important in the early prevention of cardiovascular disease. In a recent review of controversies in the management of cerebral vascular disease, Scheinberg [34] noted that almost submerged in the intense arguments about

carotid endarterectomy is the evidence that TIAs, strokes, and asymptomatic carotid stenoses are powerful indicators for coronary artery disease. Because patients with extracranial carotid atherosclerosis are at high risk of dying from a myocardial infarction, Scheinberg suggested that the medical community evaluate therapeutic techniques that might reduce this risk factor rather than concern themselves only with medical or surgical treatment directed at the cerebrovascular system. Such a focus would be less dramatic than surgical intervention but might be substantially more helpful. Medical intervention could take many forms, including searching for and managing risk factors, medication, exercise, and diet. Yet TIAs, strokes, and asymptomatic carotid stenoses are for the most part manifestations of late-stage atherosclerosis. It is far more important to identify evidence of extracranial carotid atherosclerosis early rather than late in any individual at risk for significant atherosclerotic disease. Sonography is the obvious means of accomplishing this, and, unlike in the past, the critical component of the examination will be analysis of early changes in the arterial wall, rather than analysis of flow disturbances detected by Doppler imaging.

Wall Changes and Cardiovascular Risk Factors

The identification of carotid arterial wall abnormalities by using sonography has already been shown to correlate strongly with the presence of cardiovascular risk factors. In a study by Poli et al. [35], computer-assisted measurements of the intima-media thickness derived from sonograms of 36 hypercholesterolemic patients were compared with those of 31 normal controls. These investigators found a significant increase in the wall-thickness measurements of the hypercholesterolemic patients compared with those of the matched controls. They also showed that in the control group, wall thickness correlated significantly with age. In a study of 412 Finnish men (42, 48, 54, or 60 years old) who were assessed with high-resolution, B-mode carotid sonography for arterial wall thickening, plaque, or stenosis, Salonen et al. [36] observed a strong and graded relationship between serum low-density lipoprotein cholesterol concentration and the prevalence of carotid atherosclerosis. Forty-nine percent of those studied were found to have abnormal sonographic studies. For 75%, the abnormal sonographic finding consisted of "intima-media thickening" of the arterial wall, defined as a distance of more than 1.2 mm between the lumen/intima interface and the media/adventitia interface. For the remaining 25%, the abnormal sonographic finding was the presence of recognizable plaque or actual stenosis with a 20% or greater obstruction of the lumen diameter. The authors concluded that the early phases of atherosclerosis can be assessed best by B-mode sonography of selected arterial segments. Similarly, a strong relationship between the extent of extracranial carotid atherosclerosis graded by sonography and the presence of coronary heart disease was found by Crouse et al. [37], who examined 376 volunteers hospitalized for elective coronary angiography. Preliminary results from a sonographic study of the original Framingham Heart Study cohort [38] also have shown a strong correlation between the presence

of extracranial carotid disease and cardiovascular risk factors. The appreciation that early changes seen in the vessel wall by using sonography can have a major impact on medical treatment of individuals is already well understood by epidemiologists. Two large prospective multicenter studies are sponsored currently by the National Heart, Lung, and Blood Institute; these studies involve more than 20,000 subjects and are aimed at evaluating risk factors for coronary heart disease and stroke. In both of these studies, sonography of selected arterial beds is being performed on all participants with emphasis on analysis of the arterial wall.

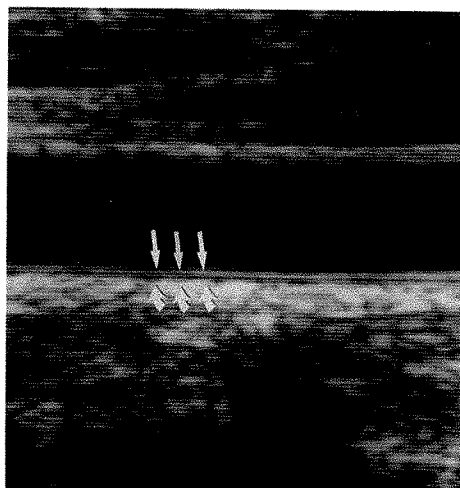
The Prevalence of Carotid Atherosclerosis

In all of the studies mentioned, the prevalence and severity of carotid disease is related to age. It is well recognized that the most important risk factor for ischemic heart disease and stroke is age. Yet the prevalence of 50% or greater diameter stenosis, even in the very oldest population groups studied, has proved low. Although only 18% of the oldest group examined in the Finnish study, people aged 60 years, had normal sonographic studies, only 5% had a 20% or greater obstruction at the most severely affected site. Of 722 individuals examined so far in the Framingham study, with a mean age of 75 years, only 9% had lumen diameter narrowing of 50% or greater [39]. Thus, the changes that must be sought on analysis sonograms are fairly subtle. They will be identified reliably only if images are acquired and analyzed carefully and uniformly. Detection of high-grade arterial stenoses has been made relatively simple, particularly with the introduction of color Doppler imaging. Early detection and quantification of wall abnormalities is not simple, and yet the benefit to the medical well-being of the individual is certainly much greater.

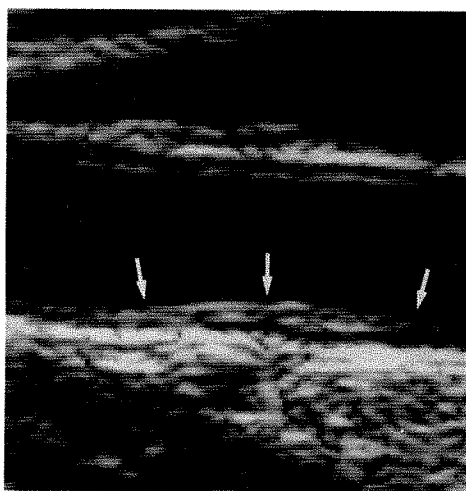
Carotid Artery Wall Anatomy: Normal and Abnormal

In normal individuals, the boundaries between the different layers of the arterial wall can be shown on high-resolution sonograms. These boundaries appear on longitudinal views of the carotid arteries as two parallel echogenic lines, separated by a hypoechoic space (Fig. 1). This observation is made more consistently in the common carotid artery, where the vessel courses parallel to the skin surface and thus presents a target at right angles to the sonographic beam. Pignoli et al. [40], using gross and microscopic techniques, have shown that the first echo along the far wall is derived from the lumen/intima interface and the second, normally brighter, echo originates from the media/adventitia interface. Between these lies the media, which appears as an anechoic zone. The distance between these first two lines corresponds to the combined thickness of the intima and media. The adventitia is quite echogenic and appears as a bright zone highlighted along its inner margin by the media. These same interfaces also can be seen along the near wall.

Three factors may affect the accuracy and reproducibility of arterial wall thickness measurements. The first is the angle of interrogation of the insonating beam. The acoustic interfaces between the different layers of the arterial wall are best



1



2

Fig. 1.—B-mode sonogram of normal carotid artery shows good definition of far-wall boundaries. Initial bright echo along far wall (straight arrows) defines lumen/intima interface. Second echogenic line (curved arrows) corresponds to media/adventitia interface. Distance between first echogenic line and second corresponds to combined width of intima and media.

Fig. 2.—B-mode sonogram of abnormal carotid artery. Widening of intima and media with focal protrusion of wall into lumen of artery (arrows) represents early carotid atherosclerosis. Near wall appears to be uninvolved on this image.

distinguished if the beam is perpendicular to the wall. The second is the order in which the ultrasound beam crosses the different interfaces. A transition between a high acoustic impedance region to a low-impedance zone tends to cause a gain-dependent reverberation and blurring of the interface. For this reason, the periadventitia/adventitia and the media/intima interfaces are detected more accurately on the near wall, whereas the lumen/intima and the media/adventitia interfaces are best seen on the far wall. The third is the algorithm used for determining wall thickness. As holds true for sonography in general, the thickness or distance measurement must be obtained with a line perpendicular to the interfaces of interest. Point-by-point measurements rely on the operator to make a best estimate of the perpendicular. An alternative scheme is to have the operator trace out each interface and then have an algorithm determine either the minimal distance between interfaces or the best fit to the perpendicular.

When near- and far-wall interfaces are not at right angles to the ultrasound beam they present a more difficult target. It is harder to demonstrate interfaces in vessel segments that are curvilinear. In the carotid bulb, where the walls flare, only short segments of the wall may be seen on any single frame. This same phenomenon may be observed in the proximal portion of the internal carotid artery, where the walls may not be parallel. Still, by using good-quality equipment and good scanning technique, wall lumen/intima and media/adventitia interfaces can be identified and measured in both the common and internal carotid arteries in normal individuals.

The earliest changes that can be seen in the arterial wall indicating the onset of the atherosclerotic process are fatty streaks. The relationship between fatty streaks and mature atherosclerosis is unknown. Nor is it clear if this finding can be detected with sonography. Fat is weakly echogenic and would not be expected to generate a signal. Picano et al. [41] pointed out that gaps seen with sonography in the lumen/intima interface of 75 fresh human aorta specimens, the "first interface" of the double-line echo pattern, might be a reflection of the presence of fatty plaques. Clearly, however, there are

many other potential explanations for this finding, including purely technical ones. Widening of the distance between the lumen/intima interface and the media/adventitia interface above 1.2 mm does appear to represent an abnormal finding, as does focal plaque, however small, and both correlate with increased risk for subsequent cardiovascular events (Fig. 2). Thus, either finding should be ranked with, and initiate a search for, other risk factors such as hypertension, plasma concentrations of high-density lipoproteins, and family history. The finding of carotid arterial wall abnormalities may well provide the rationale for initiating medical therapy with antiatherogenic drugs that are now being developed. Already, large multicenter drug trials have been initiated that use carotid sonography both to determine entry into the study and to monitor progression and regression of disease.

Scoring the Extent of Atherosclerosis

Two important issues still need to be resolved before high-resolution sonography can be used routinely to measure and track the severity of atherosclerosis. The first is a careful definition of what constitutes an atherosclerotic lesion. A functional definition of the extent of atherosclerotic change must encompass both diffuse subintimal thickening and more focal changes, which represent plaques. The second is the selection of the location where measurements are to be performed. Diffuse wall thickening is quantified best in the far wall of the common carotid artery. Here, the intima/media interfaces are clearly defined, the vessel is parallel to the transducer, and changes in the vessel wall are distributed more evenly. A maximal wall thickness therefore serves as a good measurement. Discrete plaque formation usually originates in the carotid bulb and proximal internal carotid artery. Attention must therefore be given to the projection or view that best delineates the focal abnormality. Although there are no steadfast rules, and despite certain difficulties, scoring of the extent of atherosclerotic change can be done successfully [37].

The Use of Sonography to Track Disease over Time

Measurement of arterial wall thickness has not been a routine element in the usual noninvasive vascular study. It cannot be done casually or carelessly, because it carries implications that will span decades for the patient. Tracking changes in wall thickness over time will very likely become a major tool for determining the efficacy of a given treatment for an individual. Thus, measurements must be precise, having a high degree of reproducibility. Taking a picture and using hand-held calipers to make one or two measurements at an undefined point will not work in the future.

Manufacturers of sonographic equipment are beginning to provide direct access to the digital signal before digital-to-analog conversion. Thus, the image can be transferred to optical disk with no loss in information for sophisticated off-line computer-assisted measurement. The image can be displayed on a high-resolution monitor, and, by using a mouse or similar device, highly reproducible measurements of discrete boundary interfaces are possible. The identification of possible change in wall thickness over time is somewhat more problematic, because repeat measurements should be made at the same site on repeat examination. Unfortunately, there are only two reliable internal landmarks in the carotid system, one being the tip of the flow divider and the other being the origin of the carotid bulb. The site of maximum disease may not be easily related to either point in a given patient. This can be partly circumvented by making measurements over segments of vessel rather than at single points, as this will result in averaging of results and lessen the variability of the measurement. Preliminary data from the multicenter Atherosclerosis Risk in Communities [42] study have shown that measurements performed in this fashion on large numbers of subjects are highly reproducible.

Most of the newer sonographic imagers already have computer-assisted image analysis programs. With the introduction of higher-resolution linear-array transducers free of geometric distortion, it becomes feasible to measure accurately and routinely arterial wall thickness. The availability of the instrumentation, the clinical recognition of the importance of the early subintimal changes in the arterial wall, and the possibility of early therapeutic interventions on the natural progression of atherosclerosis have combined to redefine the role of the noninvasive laboratory of the future.

ACKNOWLEDGMENT

We thank M. Gene Bond, Division of Vascular Ultrasound Research, Bowman Gray School of Medicine, for all he has taught us about the wall anatomy of normal and diseased arteries.

REFERENCES

1. Fisher CM. Occlusion of the carotid arteries: further experience. *Arch Neurol Psychiatry* 1954;72:187-204
2. Eastcott HHG, Pickering GW, Rob CG. Reconstruction of internal carotid artery in a patient with intermittent attacks of hemiplegia. *Lancet* 1954;2:994-996
3. Dyken ML, Pokras R. The performance of endarterectomy for disease of the extracranial arteries of the head. *Stroke* 1984;15:943-950
4. May AG, Vandeberg L, DeWeese JA, Rob CG. Critical arterial stenosis. *Surgery* 1963;54:250-257
5. O'Leary DH, Persson AV, Clouse ME. Noninvasive testing for carotid artery stenosis: 1. Prospective analysis of three methods. *AJNR* 1981;2:437-442
6. Barber FE, Baker DW, Nation AWC, Strandness DE Jr, Reid JM. Ultrasonic duplex echo-Doppler scanner. *IEEE Trans Biomed Eng* 1974;21:109-113
7. Jacobs NM, Grant EG, Schellinger D, Byrd MC, Richardson JD, Cohan SL. Duplex carotid sonography: criteria for stenosis, accuracy, and pitfalls. *Radiology* 1985;154:385-391
8. Shoumaker RD, Bloch S. Cerebrovascular evaluation: assessment of Doppler scanning of carotid arteries, ophthalmic Doppler flow and cervical bruits. *Stroke* 1978;9:563-566
9. Crummy AB, Zwiebel WJ, Barriga P, et al. Doppler evaluation of extracranial cerebrovascular disease. *AJR* 1979;132:91-93
10. Blackshear WM, Phillips DJ, Chikos PM, Harley JD, Thiele BL, Strandness DE. Carotid artery velocity patterns in normal and stenotic vessels. *Stroke* 1980;11:67-71
11. Kenagy JW. Comparison of duplex scanning and contrast angiography: a community hospital experience. *J Vasc Surg* 1985;2:591-593
12. Harward TRS, Bernstein EF, Fronek A. Continuous-wave versus range-gated pulsed Doppler power frequency spectrum analysis in the detection of carotid arterial occlusive disease. *Ann Surg* 1986;204:32-37
13. Goodison SF, Flanigan DP, Bishara RA, Schuler JJ, Kikta MJ, Meyer JP. Can carotid duplex scanning supplant arteriography in patients with focal carotid territory symptoms? *J Vasc Surg* 1988;5:551-557
14. O'Leary DH, Clouse ME, Potter JE, Wheeler HG. The influence of noninvasive tests on the selection of patients for carotid angiography. *Stroke* 1985;16:264-267
15. Ricotta J, Hoen J, Schenk E, et al. Is routine angiography necessary prior to carotid endarterectomy? *J Vasc Surg* 1984;1:96-102
16. Dixon S, Pais SO, Raviola C, et al. Natural history of nonstenotic, asymptomatic ulcerative lesions of the carotid artery. *Arch Surg* 1982;117:1493-1498
17. Mohr JP. Asymptomatic carotid artery disease. *Stroke* 1982;13:431-433
18. Edwards JH, Kricheff II, Gorstein F, Riles TF, Imperato A. Atherosclerotic subintimal hematoma of the carotid artery. *Radiology* 1979;133:123-129
19. Imperato AM, Riles TS, Gorstein F. The carotid bifurcation plaque: pathologic findings associated with cerebral ischemia. *Stroke* 1979;10:238-245
20. Lusby RJ, Ferrell LD, Ehrenfeld WK, et al. Carotid plaque hemorrhage: its role in production of cerebral ischemia. *Arch Surg* 1982;117:1479-1488
21. Reilly LM, Lusby RJ, Hughes L, Ferrell LD, Stoney RJ, Ehrenfeld WK. Carotid plaque histology using real-time ultrasonography: clinical and therapeutic implications. *Am J Surg* 1983;146:188-193
22. O'Donnell TF Jr, Erdoes L, Mackey WC, et al. Correlation of B-mode ultrasound imaging and arteriography with pathologic findings at carotid endarterectomy. *Arch Surg* 1985;120:443-449
23. Leahy AL, McCollum PT, Feeley TM, et al. Duplex sonography and the selection of patients for carotid endarterectomy: plaque morphology or luminal narrowing? *J Vasc Surg* 1988;8:558-562
24. Bassiouny HS, Davis H, Massawa N, Gewertz BL, Glagov S, Zarins CK. Critical carotid stenosis: morphologic and chemical similarity between symptomatic and asymptomatic plaques. *J Vasc Surg* 1989;9:202-212
25. O'Leary DH, Hoen J, Ricotta JJ, Roe S, Schenk EA. Carotid bifurcation disease: prediction of ulceration with B-mode ultrasound. *Radiology* 1987;162:523-525
26. Bluth EI, Kay D, Merritt CRB, et al. Sonographic characterization of carotid plaque: detection of hemorrhage. *AJNR* 1986;7:311-315
27. O'Leary DH, Bryan FA, Goodison MW, et al. Measurement variability of carotid atherosclerosis: real-time (B-mode) ultrasonography and angiography. *Stroke* 1987;18:1011-1017
28. Pokras R, Dyken ML. Dramatic changes in the performance of endarterectomy for diseases of the extracranial arteries of the head. *Stroke* 1988;19:1289-1290
29. Barnett HJM, Plum F, Walton JN. Carotid endarterectomy—an expression of concern. *Stroke* 1984;15:941-943
30. Winslow CM, Solomon DH, Chassin MR, Kosecoff J, Merrick NJ, Brook RH. The appropriateness of carotid endarterectomy. *N Engl J Med* 1988;318:721-727
31. Grotta JC. Current medical and surgical therapy for cerebrovascular disease. *N Engl J Med* 1987;317:1505-1516

32. Whisnant JP. Role of neurologist in the decline of stroke. *Ann Neurol* **1983**;14:1-7
33. Richardson JD, Main KA. Carotid endarterectomy in the elderly population: a statewide experience. *J Vasc Surg* **1989**;9:65-73
34. Scheinberg P. Controversies in the management of cerebrovascular disease. *Neurology* **1988**;38:1609-1616
35. Poli A, Tremoli E, Colombo A, Sirtori M, Pignoli P, Paoletti R. Ultrasonographic measurement of the common carotid arterial wall thickness in hypercholesterolemic patients. *Atherosclerosis* **1988**;70:253-261
36. Salonen R, Seppanen K, Rauramaa R, Salonen JT. Prevalence of carotid atherosclerosis and serum cholesterol levels in eastern Finland. *Atherosclerosis* **1988**;8:788-792
37. Crouse JR, Toole JF, McKinney, et al. Risk factors for extracranial carotid artery atherosclerosis. *Stroke* **1987**;18:990-996
38. O'Leary DH, Anderson KM, Kase CS, Wolf PA, Kannel WB. Extracranial atherosclerosis in a general population: the Framingham Heart Study. *Stroke* **1988**;19:143
39. Poehlmann HW, O'Leary DH, Anderson KM, Christiansen JC, Kase CS, Wolf PA. The prevalence of carotid artery disease in the Framingham study cohort as determined by ultrasound. *J Ultrasound Med* **1988**;7:272
40. Pignoli P, Tremoli E, Poli A, Oreste P, Paoletti R. Intimal plus medial thickness of the arterial wall: a direct measurement with ultrasound imaging. *Circulation* **1986**;6:1399-1406
41. Picano E, Landini L, Lattanzi F, Salvadori M, Benassi A, L'Abbate A. Time domain echo pattern evaluations from normal and atherosclerotic arterial walls: a study in vitro. *Circulation* **1988**;3:654-659
42. Bond MG, Evans GW, Howard G, et al. Noninvasive measurement of arterial wall characteristics using high resolution B-mode ultrasonography. Presented at the International Symposium on Atherosclerosis, Rome, October **1988**

Review Article

Sonography of the Male Genital Tract

Carol B. Benson,¹ Peter M. Doubilet,¹ and Jerome P. Richie²

Advances in sonographic technology and equipment have led to major increases in the clinical applications of sonography. This is particularly evident in the field of urologic sonography, in which transducers have been developed for transrectal scanning of the prostate; higher-resolution transducers are now available for evaluation of the external genitalia; and pulsed-wave Doppler imaging has been added to high-resolution scanners, permitting direct evaluation of blood flow in the penis and scrotum. Imaging with color Doppler sonography adds yet another dimension to the evaluation of blood flow, which has yet to be fully explored in urologic diagnosis.

Scrotal Sonography

The scrotum and its contents are best evaluated by using high-resolution transducers with frequencies of 5–10 MHz. Because the scrotal contents lie close to the skin surface, imaging is performed with either a linear-array transducer or a sector scanner with a standoff device. In addition, Doppler sonography, both duplex and color, can be used to evaluate blood flow in the scrotum in normal and pathologic states.

Focal Lesions

A major role of sonography of the scrotum is to detect and define intrascrotal masses, to differentiate intra- from extratesticular lesions, and to distinguish cystic from solid masses. Sonography has a high degree of accuracy in each of these areas; it has a sensitivity for tumor detection of close to 100%

and a 98–100% accuracy for distinguishing cystic from solid and intra- from extratesticular lesions [1–5]. The latter capability is critical to the evaluation and subsequent management of a patient with suspected testicular cancer, because the large majority of extratesticular lesions are benign, while most intratesticular tumors are malignant [6–9]. Sonography also plays an important role in the evaluation of patients with large retroperitoneal masses or an enlarged supraclavicular lymph node by depicting small, nonpalpable testicular “primaries,” thus distinguishing extragonadal tumors from primary gonadal tumors with metastases [1].

Ninety to 95% of malignant testicular tumors are of germ-cell origin. Among these, seminomas (40–50%) are the most common, followed by mixed germ-cell tumors (40%). Embryonal carcinoma (15–20%), malignant teratoma (5–10%), and, rarely, pure choriocarcinoma account for the rest [6, 10]. On sonographic examination, germ-cell tumors tend to be well-defined lesions surrounded by normal testicular parenchyma (Fig. 1). Most have areas of decreased echogenicity and are heterogeneous, but a small minority are predominantly hyperechoic. Cystic areas are commonly seen in any of the germ-cell tumors except seminoma (Fig. 2). The cystic areas are round and smooth with mixed germ-cell tumors, malignant teratomas, and embryonal cell tumors. In choriocarcinomas the cystic areas tend to be irregular, because they result from hemorrhage and necrosis within the tumors. Calcifications may be seen in any cell type (Fig. 3), but are most common with teratocarcinomas. Seminomas are usually more homogeneous and hypoechoic than the other cell types

Received March 20, 1989; accepted after revision May 23, 1989.

¹ Department of Radiology, Harvard Medical School, Brigham and Women's Hospital, 75 Francis St., Boston, MA 02115. Address reprint requests to C. B. Benson.

² Department of Urology, Harvard Medical School, Brigham and Women's Hospital, Boston, MA 02115.

AJR 153:705–713, October 1989 0361–803X/89/1534–0705 © American Roentgen Ray Society

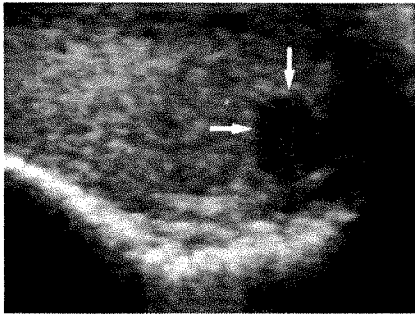


Fig. 1.—Seminoma. Longitudinal image shows well-defined hypoechoic mass (arrows) in lower pole of testis surrounded by normal testicular parenchyma.



Fig. 2.—Mixed germ cell tumor. Most of left testicle is replaced by tumor, which contains anechoic cystic areas.

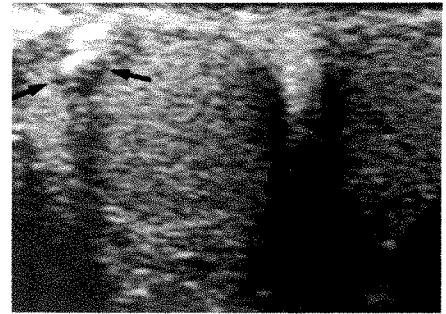


Fig. 3.—Embryonal cell carcinoma. Transverse image of both testicles shows small hypoechoic mass (arrows) in right testicle, which contains shadowing calcifications.

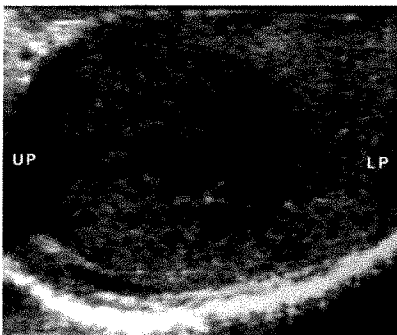


Fig. 4.—Leukemia. Left testicle is enlarged because of leukemic infiltration with decreased echogenicity in upper pole (UP), gradually fading into normal echogenicity of lower pole (LP).

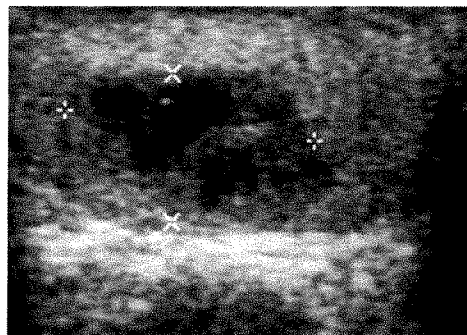


Fig. 5.—Infarct. Sonogram shows well-defined hypoechoic mass (cursors) with irregular cystic spaces mimicking tumor.



Fig. 6.—Intratesticular cyst. Transverse image shows simple well-defined, thin-walled anechoic cyst (arrow) with acoustic enhancement.

are. Embryonal cell carcinomas are aggressive tumors that may be quite large. Pure choriocarcinomas are also very aggressive and metastasize early. As a result, patients with these tumors commonly present with symptoms caused by metastases [1, 6].

Although most malignant tumors of the testicle are of germ-cell origin, metastases, leukemia, and lymphoma also may involve the testicles. Sometimes these lesions, like the germ-cell tumors, are well-defined intraparenchymal masses on sonographic examination [11]; however, others may appear as poorly defined areas of decreased or altered echogenicity that gradually fade into normal testicular tissue (Fig. 4) [1]. The latter appearance is similar to the appearance of orchitis and may present a diagnostic dilemma. A number of benign intratesticular processes, including infarct, hematoma, abscess, and orchitis, also may appear as focal intratesticular lesions. All of these can appear as intraparenchymal, round, well-defined masses that mimic a tumor (Fig. 5). In some such cases, no reliable criteria can differentiate a benign process from malignant tumor. In many cases, however, specific sonographic features and clinical presentation may strongly suggest the diagnosis. In particular, a peripheral wedge-shaped lesion suggests infarct [12], a history of substantial recent trauma suggests hematoma, and fever and an elevated WBC

count suggest orchitis or abscess. In these cases, conservative management with clinical and sonographic follow-up is often prudent.

One type of focal lesion that can be diagnosed correctly sonographically is a cyst, which can be intratesticular, tunical, or epididymal in location. These are very well-defined, anechoic, round lesions with thin smooth walls and distal acoustic enhancement. Simple intratesticular cysts are benign lesions that often are not palpable [13]. Usually located on the lateral side of the testicle near the mediastinum (Fig. 6), testicular cysts are uncommon in younger patients [1, 14], but may be seen in 8–10% of men over 60 years old [15, 16].

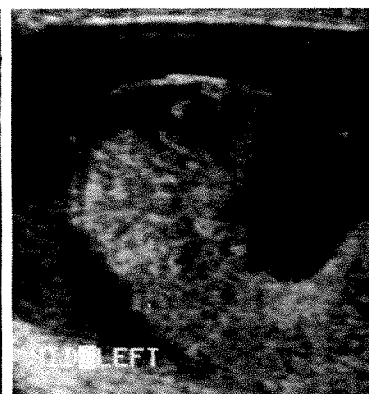
Epididymitis and Orchitis

Infection of the epididymis causes thickening of the epididymis, most commonly of the head, but occasionally of the body or tail. The involved portion of the epididymis will have a heterogeneous echotexture with either increased or decreased echogenicity. Sonographic evaluation is helpful in looking for associated testicular involvement with orchitis or abscess formation. Focal orchitis is usually located in an area of the testicle adjacent to the thickened part of the epididymis (Fig. 7). Decreased echogenicity at the periphery of the testis,

Fig. 7.—Focal orchitis. Hypoechoic area at periphery of testicle (cursors) near thickened epididymis mimics tumor.



Fig. 8.—Severe scrotal trauma. Disrupted testicle is contained within its capsule with irregular areas of hemorrhage and damaged tissue. A hematocoele, fluid containing echoes, surrounds testicle.



7

8

gradually fading into a normal parenchymal echotexture, will be seen [17, 18]. Cystic areas within the affected parenchyma suggest the presence of an abscess [17–20]. Diffuse orchitis without epididymal involvement sometimes may be seen with infections such as mumps or tuberculosis. In these cases the testicle is enlarged with diffuse and usually homogeneous decreased echogenicity.

Trauma

Scrotal hematomas are seen most often in patients with a substantial history of trauma. They may be seen in the scrotal wall, between the layers of the tunica vaginalis (a hematocele), within the epididymis, or within the testicle. As was mentioned earlier, when a focal hematoma occurs within the testicle, the lesion may mimic a tumor on sonography. The sonographic features of a hematoma, however, change rapidly with time. Acutely, it will be heterogeneous, often with increased echogenicity. As the lesion resolves, anechoic cystic spaces with internal septa will replace the heterogeneous mass. Besides localizing and following focal hematomas, sonographic examination is important in the management of scrotal trauma to diagnose or exclude testicular rupture, a condition that requires surgical intervention [17, 21]. After testicular rupture, disruption of the capsule of the testicle and disorganization of the parenchyma occur (Fig. 8). An associated hematocele is commonly present.

Hydrocele

A hydrocele is a congenital or acquired collection between the parietal and visceral layers of the tunica vaginalis lining the scrotum. Acquired hydroceles may be idiopathic or result from intrascrotal inflammation or, rarely, tumor [22]. Sonography is useful in assessing the scrotum for an underlying cause or, in the presence of a large hydrocele, to evaluate the testicle because physical examination may be impossible. Most hydroceles are anechoic collections surrounding the testicle. Occasionally, scattered echoes due to cholesterol crystals or floating calculi are seen. Septa may also be found in some cases.

Cryptorchidism

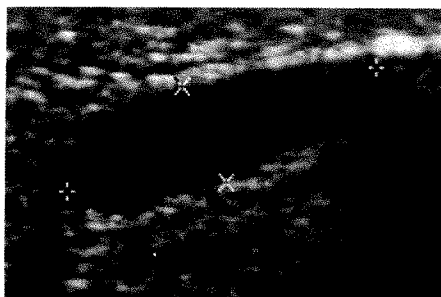
In patients with cryptorchidism, sonography is 80% successful in locating the undescended testicle because most are located at or below the inguinal ring [6, 23, 24]. Undescended testes usually are smaller than normal testes and may have diffusely decreased echogenicity because of atrophy (Fig. 9). Because both testicles are at increased risk for cancer, sonographic examination allows assessment of the parenchyma bilaterally while locating the cryptorchid testicle. It has been advocated by some that sonography be used to screen patients with a history of cryptorchidism to detect early cancers [25].

Infertility

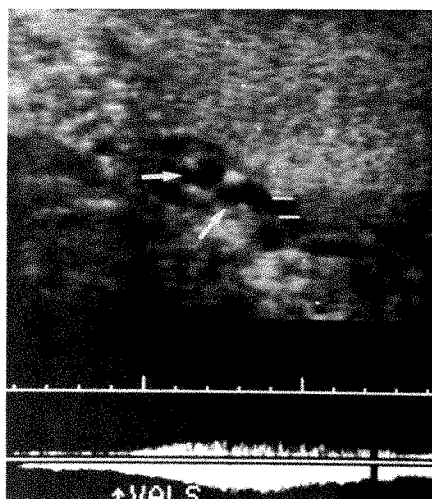
Scrotal sonography has become an integral part of the workup of cases of infertility for detecting unilateral or bilateral varicoceles [26]. These lesions may substantially affect sperm production and motility. Sonographically, varicoceles appear as tubular serpiginous structures more than 2 mm in diameter within the scrotum. Venous flow within these structures, especially during or immediately after Valsalva maneuvers, can be documented in some cases with Doppler sonography (Fig. 10); when seen, the presence of flow prevents confusion with other extratesticular fluid-filled lesions such as epididymal cysts.

Torsion

The sonographic appearance of testicular torsion depends on the time passed since the acute event. In the first few hours, the testicle becomes enlarged, usually with diffusely and homogeneously decreased echogenicity. In rare instances, the acutely twisted testicle may be diffusely hyperechoic [27]. The epididymis also may be enlarged. After about 10 hr, the testicle develops a heterogeneous echotexture as necrosis and hemorrhage occur. Hydroceles may develop as well. Since these findings may be similar to those seen in epididymo-orchitis, a companion study that documents absence of blood flow to the twisted testicle may be necessary for accurate diagnosis. This can be accomplished by using



9



10

Fig. 9.—Undescended testicle. Longitudinal image shows small hypoechoic testicle (*cursors*) in left groin.

Fig. 10.—Varicocele. Dilated veins (*arrows*) surround left testicle. Altered flow with Valsalva maneuver is detected by Doppler imaging.

Doppler sonography (conventional or color) [28] or by radio-nuclide imaging [29].

Transrectal Sonography of the Prostate

Transrectal sonography has been available for over 20 years [30], but only in the last few years have high-frequency (7–10 MHz), high-resolution transducers been developed for evaluation of the prostate gland. Most transrectal transducers are equipped with a water-bath system, consisting of an inflatable balloon surrounding the transducer that is filled with water once it is placed in the rectum. The balloon offers a stand-off for improved sonographic resolution and permits mobility of the transducer within the rectum with minimal discomfort to the patient. Several different types of probes are available. Transverse imaging of the gland can be accomplished by using a radial probe, which images 360° around the rectum, or via a sector probe oriented in a plane perpendicular to the shaft of the transducer. Sagittal imaging of the gland may be performed with a linear or sector probe aligned parallel to the shaft of the transducer.

The prostate gland can vary in size and shape, depending on the patient. (Fig. 11). The central part of the gland consists of hypoechoic periurethral tissue surrounding the proximal urethra; glandular tissue surrounds that. The central portion is often heterogeneous in echotexture, particularly in older patients with benign prostatic hypertrophy (Fig. 12). The peripheral zone surrounds the gland posteriorly, laterally, and inferiorly and has a homogeneous echotexture. Echogenic foci, which may shadow, are often seen at the junction of the peripheral zone and the central portion of the gland toward midline. These represent crystalline deposits called corpora amylacea.

The seminal vesicles are paired structures located superiorly to the prostate behind the bladder. They are more hypoechoic than the prostate gland and may contain tiny cystic areas.

Prostatic sonography has a number of uses: (1) evaluation of patients in whom prostatic cancer is suspected on the

basis of digital examination, abnormal laboratory values (e.g., elevated prostate-specific antigen), or metastases from an unknown primary tumor [31]; (2) biopsy guidance; (3) cancer staging; (4) monitoring response to radiation therapy; (5) diagnosis and drainage of prostatic abscesses; and (6) evaluation of congenital anomalies of the prostate and seminal vesicles. Screening asymptomatic men for prostatic cancer is another potential, although still controversial, application of transrectal sonography. Each of these uses is considered later in this paper.

Prostatic carcinoma arises in the peripheral zone in approximately 80% of cases [32]. These lesions, when small, tend to be well defined and hypoechoic with respect to surrounding tissue (Fig. 13) [33, 34]. Some authors claim that small tumors also can appear as hyperechoic lesions [35], but this finding has been disputed by others [33]. In either case, as the cancer enlarges, mixed or increased echogenicity may be seen as the tumor invades the central portion of the gland [36].

Once a suspicious lesion has been detected in the peripheral zone of the prostate gland, a transrectal biopsy can be performed with sonographic guidance. Sonographic guidance is especially important for nonpalpable lesions. When the lesion is palpable, sonographic guidance can ensure that the abnormal area is sampled [37, 38]. Minor complications, especially hematuria, are common, occurring in 37% of cases. More serious complications such as infection are rare, occurring in less than 1% [39]. When hypoechoic lesions are sampled by biopsy, 21–58% will prove to be carcinoma; the remainder are benign [31, 38, 40].

In addition to guiding biopsies of suspicious lesions, transrectal sonography may be valuable for defining the extent of disease and determining tumor stage [41]. Tumor spread to the seminal vesicles is assessed sonographically by scanning longitudinally to identify the superior extent of the tumor. A clearly demarcated separation should be seen between the prostate gland and seminal vesicles. If it is not, tumor invasion may have occurred. Sensitivity for seminal vesicle invasion has been found to be 33–60% [42, 43]; specificity of 84%



Fig. 11.—Normal prostate. Transverse image of prostate (cursors) shows homogeneous peripheral zone and hypoechoic periurethral tissue centrally.

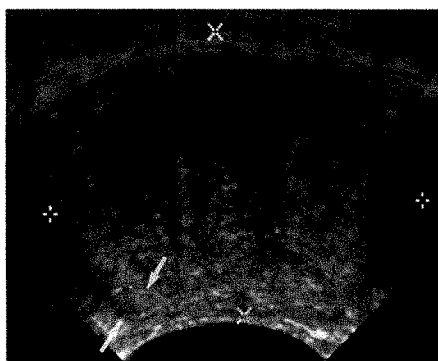


Fig. 12.—Benign prostatic hypertrophy. Transverse image shows markedly enlarged central portion of gland (cursors) with compression of peripheral zone (arrows). Hypertrophied tissue is heterogeneous, hypoechoic, and strongly attenuates ultrasound beam.

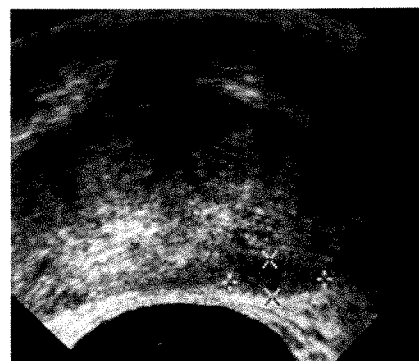


Fig. 13.—Prostate cancer. Transverse image shows hypoechoic lesions in left peripheral zone (cursors).

was reported in one study [42]. Assessment for capsular invasion is another important step in evaluating tumor extent. When the tumor has grown through the capsule, the bright border of the prostate gland is obliterated on sonography (Fig. 14) [36]. An 89% sensitivity for detection of capsular invasion by transrectal sonography was reported in one study [42]. Larger studies need to be done before the accuracy of staging prostate cancer by transrectal sonography is determined.

Transrectal sonography can be used to monitor gland and tumor size in patients with prostate cancer treated with radiation therapy. The average size of the gland appears to be the best parameter for assessing the success of treatment [44]. After radiation therapy, the entire prostate gland usually shrinks and becomes hypoechoic. A separate peripheral zone may no longer be distinguishable, and the tumor may no longer be visible.

The utility of transrectal sonography as a screening tool for prostate cancer remains controversial. Lee et al. [38] recently compared sonography and digital rectal examinations to screen for prostate cancer; they found that sonography detected twice as many cancers as the rectal examinations did. In 784 men aged 60 and over, 22 cancers were found by one or both diagnostic approaches; of these, 20 were detected by sonography and 10 by digital examination [38]. When used in combination with digital rectal examination and prostate-specific antigen measurement, the positive predictive value of an abnormal transrectal sonogram increases [45]. These studies and others, however, leave unanswered several important questions that relate to the value of sonography as a screening study. What is the sensitivity of sonography for early prostate cancer? The study by Lee et al. and other studies do not resolve this issue, because they provide no information concerning the number of cancers missed by both sonography and digital examination. More importantly, what is the impact of a screening program on life expectancy? This depends on several factors, including one about which little is known: the natural history of small, nonpalpable prostate cancer if left untreated. Are the costs of screening justified by

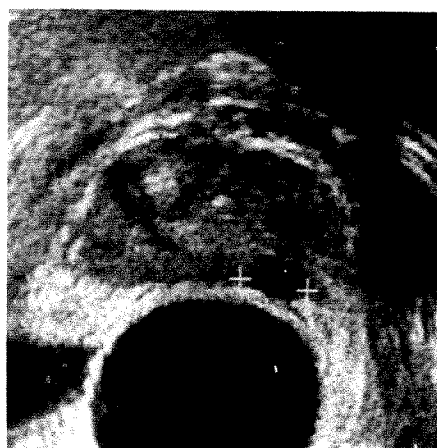
the benefits? This depends on the cost per year of life saved, not the more commonly estimated cost per cancer detected. Finally, how closely would the results achieved by dedicated researchers be duplicated by less interested and expert practitioners if screening became widespread? In less experienced hands, the accuracy of sonography and the reliability and safety of sonographically guided biopsy may suffer. The answers to these questions will require a long-term prospective study, ideally a multicenter randomized controlled trial. Only if such a study is performed will it be possible, based on data instead of conjecture, to justify or reject the use of sonography as a screening study for prostate cancer.

Imaging of the prostate gland may be important in clinical situations other than cancer evaluation. Prostatitis may develop into an abscess requiring more aggressive therapy. The sonographic appearance of a prostatic abscess is of a very hypoechoic or anechoic area with acoustic enhancement (Fig. 15 [46]). In addition to establishing the diagnosis, sonographic guidance may be useful for abscess drainage procedures.

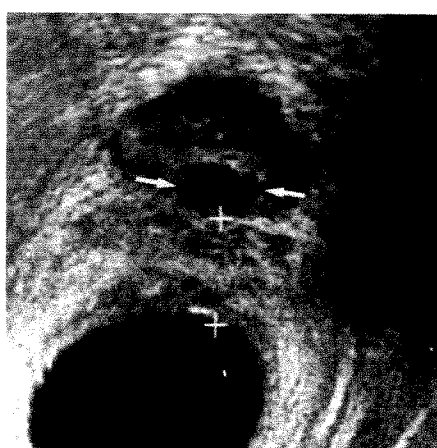
Transrectal sonography can also be used to assess the seminal vesicles and prostate in patients with suspected congenital anomalies, such as a seminal vesicle or ejaculatory duct cyst or absence of a seminal vesicle. These anomalies may account for infertility in some patients [47].

Sonourethrography

The anterior urethra can be studied with high-resolution sonography. The examination requires distension of the urethra with fluid, which can be achieved via antegrade or retrograde filling [48, 49]. The antegrade method requires the patient to begin voiding. When a full stream of urine is achieved, a Zipser clamp is applied to the distal penis. Distension of the urethra by the retrograde method is achieved by injecting lidocaine urologic jelly via a wide-tipped syringe in the meatus. The Zipser clamp is again used to sustain distension. We prefer the latter technique, as the antegrade method requires substantial patient cooperation, which may not be possible. Furthermore, with the retrograde technique, real-



14



15

Fig. 14.—Prostate cancer invading capsule. Hypoechoic lesion in left peripheral zone (cursors) bulges posteriorly and lacks bright line of capsule outside it.

Fig. 15.—Prostatic abscess. Radial image from rectum shows marked thickening of rectal wall and periprostatic tissue (cursors). Abscess within prostate gland (arrows) is hypoechoic with some through-transmission.

time scanning can be performed during actual distension by injection.

Once the urethra is distended, the penis is scanned in transverse and longitudinal planes to study the penile urethra. The bulbar urethra is studied through the scrotum and perineum. The normal urethra has smooth walls and measures more than 4 mm when fully distended (Fig. 16) [50]. By scanning in both the transverse and longitudinal planes, three-dimensional analysis of any lesion can be performed.

Sonourethrography has several clinical indications: evaluation of strictures of the anterior urethra, detection and localization of stones or foreign bodies, evaluation for urethral disruption after trauma, evaluation for urethral diverticula, and evaluation of a penile mass. In preliminary studies the sonographic findings have correlated well with results from conventional urethrography [49]. Further studies are warranted to determine the exact place of sonourethrography among the various diagnostic tests available for evaluation of the urethra. The sonographic technique has several advantages over conventional radiographic studies. Sonography involves no ionizing radiation. This is important for patients with strictures who may require multiple examinations. Iodinated contrast agents are not needed, removing the risk of contrast reactions. A three-dimensional evaluation of the urethra is possible, rather than the two-dimensional radiographic images. With sonography, the soft tissues surrounding the urethra can be examined for scarring and other wall abnormalities, as well as for abnormalities in the surrounding corpus spongiosum and corpora cavernosa. The disadvantage of this technique is its inability to evaluate the posterior prostatic urethra. Fortunately, most strictures occur in the anterior urethra [51, 52]. Furthermore, when evaluation of the prostatic urethra is indicated, it can be accomplished sonographically by using a transrectal approach.

On sonographic examination, a stricture of the anterior urethra appears as a segment of narrowed lumen, with irregularity and thickening of the urethral wall due to fibrosis and scarring (Fig. 17). The length of the stricture can be accurately measured, and urethral dilatation may be seen proximal to it [48, 49]. Intraoperative guidance of stricture dilatation can be performed with real-time sonography [48].

Stones or foreign bodies may be found in the urethra. The bulbar and penile urethra should be scanned prior to distension of the urethra to locate a stone or foreign body (Fig. 18), as it may be dislodged during retrograde filling. The urethra can be observed sonographically as the lidocaine jelly is injected.

After trauma, the penis can be scanned by high-resolution sonography to detect, locate, and measure a hematoma [51]. Sonourethrography can be performed in search of false channels communicating with the urethra as a result of urethral disruption. In the normal patient, no extravasation of fluid will be seen with filling of the urethra.

Urethral diverticula are acquired outpouchings from the anterior urethra, probably as a result of previous infection [50]. On sonography, these outpouchings are fluid-filled collections abutting the urethra that change in size with distension and emptying of the urethra.

Palpable nondermatologic penile masses can be studied by using sonography to determine the nature of the mass (e.g., cystic vs solid); its location; and, with urethral distension, its relationship to the urethra. Many benign solid tumors may be seen, such as angiomas, fibromas, and neuromas. Other penile lesions include inflammatory lesions and inclusion or retention cysts of the periurethral glands (Fig. 16) [52].

Evaluation of Impotence

Organic impotence in patients with normal endocrine balance and a normal CNS may be due to scarring of the corpora cavernosa, arterial insufficiency, or venous incompetence. Sonography can be used to distinguish among these three causes of impotence.

Scarring and fibrosis of the corpora cavernosa prevent sinusoidal relaxation and filling, even in the presence of adequate arterial inflow and competent veins [53, 54]. On sonography, poorly defined focal areas of increased echogenicity are observed in the corpora cavernosa (Fig. 19) [54].

Focal plaques of fibrosis along the tunica albuginea of the corpora cavernosa, with or without calcification, cause Peyronie disease: scarring of the penis that causes pain with the

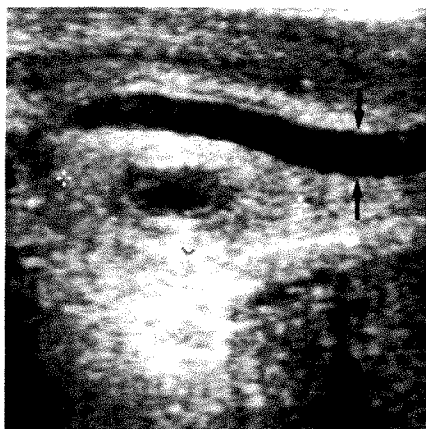


Fig. 16.—Normal penile urethra with adjacent inflammatory mass. Distended urethra (arrows) has smooth walls and uniform distension. Poorly defined mass with hypoechoic cystic center (cursors) is separate from urethra.



Fig. 17.—Urethral stricture. Sonogram shows focal narrowing of distended urethra (cursors) with thickened urethral wall.

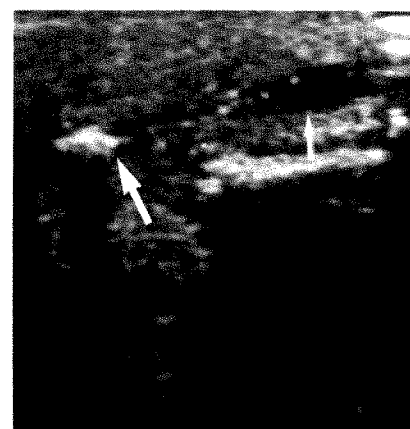
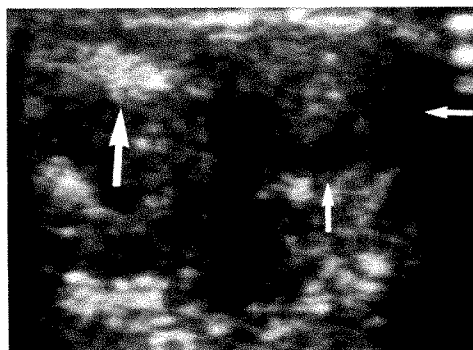
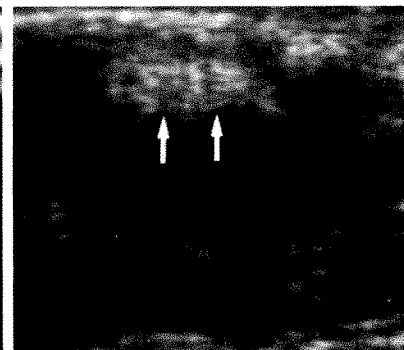


Fig. 18.—Urethral calculus. Brightly echogenic and shadowing stone (long arrow) is located proximal to urethral stricture. Urethra distal to stricture is incompletely distended (short arrow).

Fig. 19.—Scarring in corpus cavernosum.
A, Transverse image of penis shows normal echogenicity of left corpus cavernosum (short arrows). Within right corpus cavernosum is echogenic area (long arrow) caused by scarring.
B, Longitudinal image of right corpus cavernosum shows echogenic fibrosis (arrows).



A



B

development of an erection. These plaques are visible sonographically as areas of increased echogenicity, sometimes with shadowing [55, 56].

The hemodynamic function of the penis can be evaluated with duplex sonography, which combines two-dimensional and pulsed Doppler imaging. The examination is performed in conjunction with pharmacologic vasoactive agents, such as papaverine and phenoxybenzamine, which are injected into the penis to induce erection [53, 57–60]. The penis is scanned before injection, and each cavernosal arterial diameter is measured. Two minutes after intracorporal injection of the vasoactive agent, the cavernosal arterial diameters are measured again. Doppler imaging is then used to measure the maximum systolic velocity in each vessel. The protocol at our institution also includes Doppler assessment of the dorsal and cavernosal veins and measurement of the penile erectile angle.

The normal cavernosal artery (Fig. 20) before injection ranges in diameter from too small to measure (less than 0.3 mm) to 0.7 mm. After injection, the normal cavernosal artery dilates an average of 0.6 mm to reach a diameter of about 1 mm. The mean maximum systolic velocity in the artery ranges from 35 to 60 cm/sec (mean, 47 cm/sec). No venous flow is

detectable in normal patients, and the erectile angle reaches greater than 90°C.

We have found the mean peak systolic velocity to be the best diagnostic variable for identifying patients with arterial insufficiency. A mean peak velocity of 25–35 cm/sec indicates mild to moderate arterial insufficiency, which will most likely respond to medication rather than require surgery. Peak velocities less than 25 cm/sec are seen in patients with severe arterial impairment requiring surgical revascularization or prosthetic implantation (Fig. 21) [60].

It has been reported that patients with arterial insufficiency have larger preinjection diameters of the cavernosal arteries and less dilatation of these arteries after injection, when compared with normal controls [53, 57–59]. In our study of 45 patients, however, we found no statistically significant difference in either preinjection diameter or postinjection dilatation in patients with and without arterial impairment [60].

The ability of duplex sonography to detect venous incompetence has been disappointing. In our study, flow was detected in the dorsal vein in fewer than 50% of patients with dorsal venous leaks (Fig. 22), and no patients with cavernosal venous incompetence were detected with Doppler imaging [60]. The diagnosis of venous incompetence can be strongly

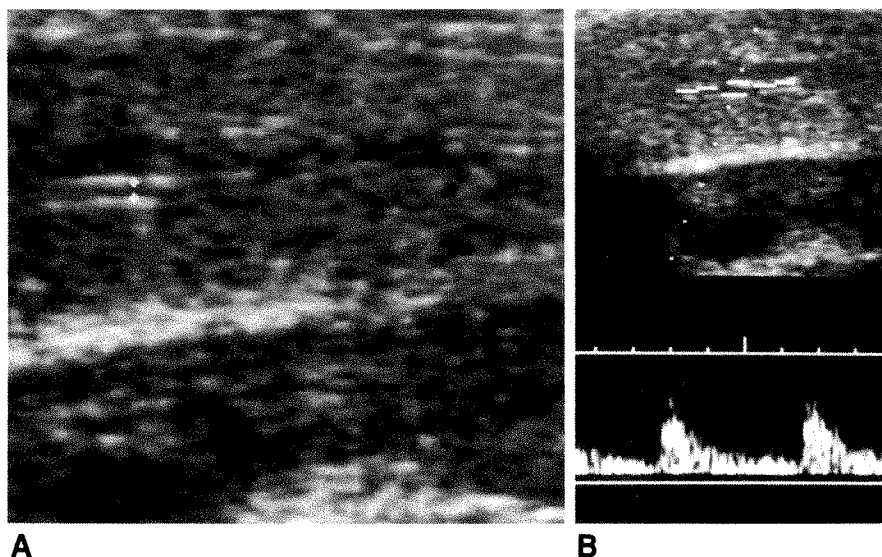


Fig. 20.—Normal cavernosal artery.

A, Right cavernosal artery (cursors) after injection of papaverine measures 1.0 mm on longitudinal image.

B, Doppler image of flow in right cavernosal artery. Peak velocity measures 0.59 m/sec (59 cm/sec).

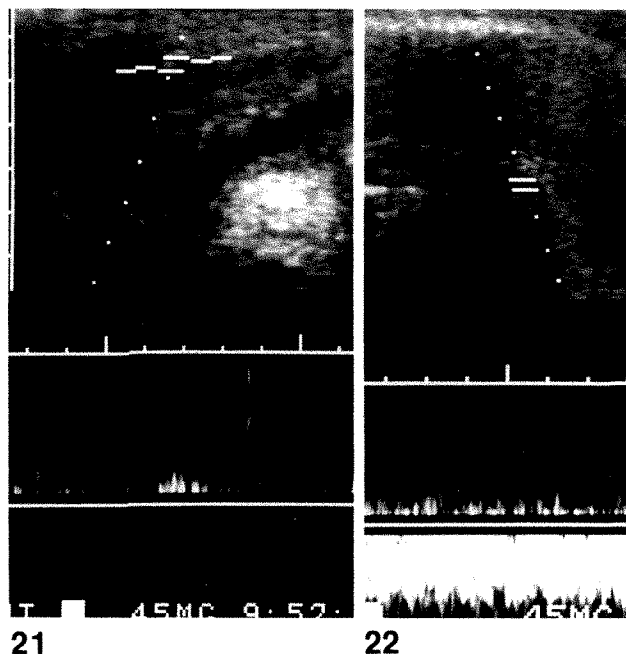


Fig. 21.—Severe arterial insufficiency. Doppler signal of right cavernosal artery after papaverine injection shows minimal flow (peak velocity, 20 cm/sec).

Fig. 22.—Dorsal venous leak. Doppler assessment of dorsal vein shows large amount of venous flow after injection of papaverine.

suggested when the mean peak velocity is within the normal range (greater than 35 cm/sec) and a less-than-90° erection is obtained, but cavernosography and cavernosometry are recommended for confirmation of the diagnosis and for anatomic definition [59, 60].

REFERENCES

1. Benson CB. The role of ultrasound in diagnosis and staging of testicular cancer. *Semin Urol* 1988;6:189-202
2. Rifkin MD, Kurtz AB, Pasto ME, Goldberg BB. Diagnostic capabilities of high-resolution scrotal ultrasonography: prospective evaluation. *J Ultrasound Med* 1985;4:13-19
3. Schwerk WB, Schwerk WN, Rodeck G. Testicular tumors: prospective analysis of real-time US patterns and abdominal staging. *Radiology* 1987;164:369-374
4. Rifkin MD, Kurtz AB, Pasto ME, et al. The sonographic diagnosis of focal and diffuse infiltrating intrascrotal lesions. *Urol Radiol* 1984;6:20-27
5. Hoddick WK, Hricak H, Jeffrey RB. Scrotal sonography. *Semin Urol* 1985;3:146-157
6. Krone KD, Carroll BA. Scrotal ultrasound. *Radiol Clin North Am* 1985;23:121-139
7. Paulson DF, Einhorn L, Peckham M, Williams SD. Cancer of the testis. In: DeVita VT, Hellman S, Rosenberg SA, eds. *Cancer—Principles and practice of oncology*. Philadelphia: Lippincott, 1982:786-800
8. Oyen R, Marchal G, Van Holsbeeck M, et al. Sonography of normal and pathological scrotal contents. *J Belge Radiol* 1986;69:43-50
9. Hill MC, Sanders RC. Sonography of benign disease of the scrotum. *Ultrasound Annu* 1986:197-237
10. Garnick MB, Prout GR, Canellos GP. Germinal tumors of the testis. In: Holland JF, Frei E, eds. *Cancer medicine*. Philadelphia: Lea & Febiger, 1982:1937-1954
11. Benson CB, Deligdisch CK, Loughlin KR. Sonographic detection of testicular plasmacytoma. *JCU* 1987;15:490-493
12. Bird K, Rosenfield AT. Testicular infarction secondary to acute inflammatory disease: demonstration by B-scan ultrasound. *Radiology* 1984;152:785-788
13. Hamm B, Fobbe F, Loy V. Testicular cysts: differentiation with ultrasound and clinical findings. *Radiology* 1988;168:19-23
14. Rifkin MD, Jacobs JA. Simple testicular cyst diagnosed preoperatively by ultrasound. *J Urol* 1983;129:982-983
15. Gooding GAW, Leonhardt W, Stein R. Testicular cysts: US findings. *Radiology* 1987;163:537-538
16. Leung ML, Gooding GAW, Williams RD. High-resolution sonography of scrotal contents in asymptomatic subjects. *AJR* 1984;143:161-164
17. Martin B, Conte J. Ultrasonography of the acute scrotum. *JCU* 1987;15:37-44
18. Lentini JF, Benson CB, Richie JP. Sonographic features of focal orchitis. *J Ultrasound Med* 1989;8:361-365
19. Rifkin MD, Kurtz AB, Pasto ME, Rubenstein JB. The sonographic diagnosis of focal and diffuse infiltrating intrascrotal lesions. *Urol Radiol* 1984;6:20-26
20. McVorach RA, Lerner RM, Dvoretzky PM, Rabinowitz R. Testicular abscess: diagnosis by ultrasonography. *J Urol* 1986;136:1213-1216
21. Jeffrey RB, Laing FC, Hricak H, McAninch JW. Sonography of testicular trauma. *AJR* 1983;141:993-995

22. LaNasa JA, Lang EK. Disorders of the scrotum and its contents. In: Resnick MJ, Older RA, eds. *Diagnosis of genitourinary disease*. New York: Thieme-Stratton, 1982:433-486
23. Weiss RM, Carter AR, Rosenfield AT. High resolution real-time ultrasonography in the localization of the undescended testis. *J Urol* 1986;135:936-938
24. Friedland GW, Chang P. The role of imaging in the management of the impalpable undescended testis. *AJR* 1988;151:1107-1111
25. Lenz S, Giwerzman A, Skakkebaek NE, Bruun E, Frimodt-Moller C. Ultrasound in detection of early neoplasia of the testis. *Int J Androl* 1987;10:187-190
26. Gonda RL, Kato JJ, Fonte RA, O'Donnell KT. Diagnosis of subclinical varicocele in infertility. *AJR* 1987;148:71-75
27. Chinn DH, Miller EI. Generalized testicular hyperechogenicity in acute testicular torsion. *J Ultrasound Med* 1985;4:495-496
28. Bickerstaff KI, Sethia K, Murie JA. Doppler ultrasonography in the diagnosis of acute scrotal pain. *Br J Surg* 1988;75:238-239
29. Chan DCP, Holder LE, Kaplan GN. Correlation of radionuclide imaging and diagnostic ultrasound in scrotal diseases. *J Nucl Med* 1986;27:1774-1781
30. Watanabe H, Kato H, Kato T, Morita M, Tanaka M, Terasawa Y. Diagnostic application of ultrasonotomography to the prostate. *Nippon Hinyokika Gakkai Zasshi* 1988;59:273-279
31. Rifkin MD, Choi H. Implications of small, peripheral hypoechoic lesions on endorectal US of the prostate. *Radiology* 1988;166:619-622
32. McNeal JE. Origin and development of carcinoma of the prostate. *Cancer* 1969;23:24-34
33. Griffiths CJ, Clements R, Jones DR, Roberts EE, Peeling WB. The ultrasound appearances of prostatic cancer with histological correlation. *Clin Radiol* 1987;38:219-227
34. Sanders RC, Hamper UM, Dahnert WF. Update on prostatic ultrasound. *Urol Radiol* 1987;9:110-118
35. Rifkin MD, Friedland GW, Shortliffe L. Prostatic evaluation by transrectal endosonography: detection of carcinoma. *Radiology* 1986;158:85-90
36. Rifkin MD. Endorectal sonography of the prostate: clinical implication. *AJR* 1987;148:1137-1142
37. Lee F, Littrup PJ, McLeary RD, et al. Needle aspiration and core biopsy of prostate cancer: comparative evaluation with biplanar transrectal US guidance. *Radiology* 1987;163:515-520
38. Lee F, Littrup PJ, Torp-Pedersen ST, et al. Prostate cancer: comparison of transrectal US and digital rectal examination for screening. *Radiology* 1988;168:389-394
39. Torp-Pedersen S, Lee F, Littrup PJ, et al. Transrectal biopsy of the prostate guided with transrectal US: longitudinal and multiplanar scanning. *Radiology* 1989;170:23-27
40. Burks DD, Drolshagen LF, Fleischer AC, et al. Transrectal sonography of benign and malignant prostatic lesions. *AJR* 1986;146:1187-1191
41. Lee F, Gray JM, McLeary RD, et al. Prostatic evaluation by transrectal sonography: criteria for diagnosis of early carcinoma. *Radiology* 1986;158:91-95
42. Pontes JE, Eisenkraft S, Watanabe H, Saitoh M, Murphy GP. Preoperative evaluation of localized prostatic carcinoma by transrectal ultrasonography. *J Urol* 1985;134:289-291
43. Hricak H, Doms GC, Jeffrey RB, et al. Prostatic carcinoma: staging by clinical assessment, CT and MR imaging. *Radiology* 1987;162:331-336
44. Fujino A, Scardino PT. Transrectal ultrasonography for prostatic cancer: its value in staging and monitoring the response to radiotherapy and chemotherapy. *J Urol* 1985;133:806-810
45. Lee F, Torp-Pedersen S, Littrup PJ, et al. Hypoechoic lesions of the prostate: clinical relevance of tumor size, digital rectal examination, and prostate-specific antigen. *Radiology* 1989;170:29-32
46. Papanicolaou N, Pfister RC, Stafford SA, Parkhurst EC. Prostatic abscess: imaging with transrectal sonography and MR. *AJR* 1987;149:981-982
47. Lipshultz LI, Cunningham GR, Howards SS. Differential diagnosis of male infertility. In: Lipshultz LI, Howards SS, eds. *Infertility in the male*. New York: Churchill-Livingstone, 1983:249-264
48. McAninch JW, Laing FC, Jeffrey RB. Sonourethrography in the evaluation of urethral strictures: a preliminary report. *J Urol* 1988;139:294-297
49. Gluck CD, Bundy AL, Fine C, Loughlin KR, Richie JR. Sonographic urethrogram: comparison to roentgenographic techniques in 22 patients. *J Urol* 1988;140:1404-1408
50. Ney C, Friedenbergh RM. Radiographic atlas of the genitourinary system, 2nd ed. Philadelphia: Lippincott, 1981
51. Dierks PR, Hawkins H. Sonography and penile trauma. *J Ultrasound Med* 1983;2:417-419
52. Schellhammer PF, Grabstald H. Tumors of the penis. In: Walsh PC, Gittes RF, Perlmutter AD, Stamey TA, eds. *Campbell's urology*. Philadelphia: Saunders, 1986:1583-1606
53. Lue TF, Tanagho EA. Physiology of erection and pharmacological management of impotence. *J Urol* 1987;137:829-836
54. DuPlessis DJ, Bornman MS, Koch Z, Van der Merwe CA. Penile ultrasonography in impotence. *S Afr J Surg* 1987;25:69-71
55. Chou YH, Tiu CM, Pan HB, et al. High-resolution real-time ultrasound in Peyronie's disease. *J Ultrasound Med* 1987;6:67-70
56. Hamm B, Friedrich M, Kelami A. Ultrasound imaging in Peyronie disease. *Urology* 1986;28:540-545
57. Mueller SC, Lue TF. Evaluation of vasculogenic impotence. *Urol Clin North Am* 1988;15:65-76
58. Lue TF, Hricak H, Marich KW, Tanagho EA. Vasculogenic impotence evaluated by high-resolution ultrasonography and pulsed Doppler spectrum analysis. *Radiology* 1987;59:777-781
59. Collins JP, Lewandowski BJ. Experience with intracorporeal injection of papaverine and duplex ultrasound scanning for assessment of arteriogenic impotence. *Br J Urol* 1987;59:84-88
60. Benson CA, Vickers MA. Diagnostic value of duplex ultrasonography with intracavernous papaverine in patients with erectile dysfunction. *Radiology* 1988;169(p):83



Book Review

Pocket Atlas of Cardiac and Thoracic MRI. By Jeffrey J. Brown and Charles B. Higgins. New York: Raven, 63 pp., 1989. \$13.95, softcover

Quick-reference, pocket medical manuals and atlases have been increasingly popular in recent years. Medical bookstores have dozens of focused diminutive treatises devoted to such topics as approaches to treatment in emergency care; recognition of dermatologic lesions; and various aspects of diagnostic imaging, particularly sonography. The *Pocket Atlas of Cardiac and Thoracic MRI* easily fits into this category. It is attractive, carefully printed, and well illustrated.

The table of contents lists two sections: "Normal Anatomy" and "Abnormal Cases." The section on normal anatomy consists of T1-weighted spin-echo images in the axial plane obtained with a 0.35-T scanner. The mediastinal structures in each image are labeled carefully with numerical codes. A key is provided with each page for convenience, together with a line drawing for slice orientation. Excellent-quality sagittal, coronal, and sagittal oblique (equivalent to lateral anterior oblique) images follow. Finally, a shorter series of 1.5-T axial images and a series of axial, short- and long-axis gradient-refocused echo images are included.

The section on abnormal cases consists of a small panoply of images of cardiac and mediastinal pathologic changes, including six images, in multiple planes, of the left superior vena cava and one image each of pericardial hematoma, atrial septal defect, patent ductus arteriosus, and constrictive pericarditis. An image of a malignant tumor metastatic to the left atrium is included also.

The goal of this pocket atlas is fulfilled as far as the heart and great vessels are concerned. However, there is no special need to recapitulate the anatomic levels by showing images obtained with both medium and high field strengths. The 0.35-T images are quite

adequate for this purpose. The muscles of the chest wall, however, are not always labeled, and the images do not always show the muscles well, either because the contrast resolution is suboptimal or the muscles are partially cropped out of the image. The spin-echo, coronal, and sagittal images are of excellent quality and are useful to the reader, but additional sagittal and coronal gradient-refocused echo images would be particularly helpful to sort out the normal anatomy as seen with this technique. Only one long-axis image is provided, which does not include the left ventricular outflow tract and aortic root, so the section would benefit from multiple long-axis views.

The book has multiple planar images of persistent left superior vena cava and axial scans of tetralogy of Fallot and pulmonary atresia. However, it has no sagittal or coronal studies of atrial septal defect, patent ductus arteriosus, and, particularly, aortic dissection, which would benefit greatly from these views.

Perhaps this volume would be most useful if it were incorporated into a pocket atlas that encompassed the entire trunk and appendicular skeleton without information about pathologic changes but with examples of anatomic pitfalls. In its current state, it will be most useful to radiologists who see a high percentage of thoracic MR cases or to medical students and nonradiologic residents who are unfamiliar with MR and cross-sectional anatomy.

Robert M. Steiner
Thomas Jefferson University Hospital
Philadelphia, PA 19107

Serial Assessment of Myocardial Infarction by Using Gated MR Imaging and Gd-DTPA

Tsunehiko Nishimura¹
 Hideki Kobayashi²
 Yuichi Ohara²
 Naoaki Yamada¹
 Kazuo Haze²
 Makoto Takamiya¹
 Katsuhiko Hiramori²

In order to assess the usefulness of Gd-DTPA in the evaluation of myocardial infarction, 17 patients were examined with gated MR imaging. Scans were made by using a spin-echo pulse sequence before and after IV administration of 0.15 mmol/kg of Gd-DTPA. The images were made at four intervals (average of 5, 12, 30, and 90 days) after the onset of the infarction. Gd-DTPA uptake at the infarcted area was graded as marked, moderate, or no increase in signal intensity by visual inspection. At these four time intervals, an area of increased signal intensity in the infarcted myocardium was detected on T1-weighted images after administration of Gd-DTPA in 14 (82%) of 17 cases, 16 (94%) of 17 cases, six (38%) of 16 cases, and three (21%) of 14 cases, respectively. Markedly increased signal intensity in infarcted areas was shown on T1-weighted images with Gd-DTPA at 5 and 12 days. The ratio of gadolinium uptake in the infarcted area to that in normal myocardium also was evaluated. At 5 and 12 days, the mean increase in signal intensity in the infarcted area was significantly higher than that in a normal area, but not at 30 and 90 days. Increased signal intensity also was apparent on T2-weighted images without Gd-DTPA at 5 and 12 days; however, the use of late echo reduced the signal-to-noise ratio, leading to image degradation.

Uptake of Gd-DTPA was a positive marker in acute myocardial infarction, but no significant uptake of Gd-DTPA occurred in chronic myocardial infarction.

AJR 153:715-720, October 1989

Gated MR imaging has potential as a noninvasive procedure for the identification and quantification of acute myocardial infarction. Previous studies have shown that acutely infarcted myocardium can be visualized on T2-weighted images without paramagnetic contrast agents [1, 2]. The use of long echo times, however, reduces the signal-to-noise ratio and degrades the image. In addition, slowly flowing blood in the ventricle and artifactual variations of signal intensity due to respiratory or residual cardiac motion create significant pitfalls [3]. It has been shown that the use of Gd-DTPA [4] as an MR contrast material serves to identify acute myocardial infarction in dogs [5-8]. The present study was undertaken to determine whether Gd-DTPA can be used for the serial assessment of myocardial infarcts in humans. Gated MR imaging with Gd-DTPA was performed serially in 17 patients at four intervals (average of 5, 12, 30, and 90 days) after the infarction.

Materials and Methods

Patients

Seventeen patients with acute myocardial infarction were included in the study. Myocardial infarction was confirmed in all patients by electrographic, serum enzymatic, and cardiac catheterization findings. There were nine patients with anterior, five with inferior, and three with nontransmural myocardial infarction according to electrocardiographic criteria. All patients were stable enough to be moved safely to the MR imaging unit from the coronary care unit. The group consisted of 16 men and one woman; their mean age was 54 ± 8 years (range,

Received January 13, 1989; accepted after revision May 15, 1989.

¹ Department of Radiology, National Cardiovascular Center, 5-7-1, Fujishirodai, Suita, Osaka 565, Japan. Address reprint requests to T. Nishimura.

² Department of Cardiology, National Cardiovascular Center, Suita, Osaka 565, Japan.

0361-803X/89/1534-0715

© American Roentgen Ray Society

39–67 years). There were 14 patients with single, one with double, and two with triple vessel disease (>75% stenosis) as determined by coronary angiography. Eleven patients had occlusion of an infarct-related coronary artery.

Data Acquisition

Gated MR imaging was done with a Magnetom H 15 (1.5 T, Siemens, Erlangen, W. Germany). Three to four contiguous axial sections were obtained by using a spin-echo technique with TE of 35 and 70 msec. The TR was dependent on the heart rate, the time

being equivalent to the R-R interval of the ECG (usually 600–1000 msec). The thickness of each section was 10 mm, and the images were gated with two excitations. On the axial image at the midventricular level, we selected the "short axis," which is perpendicular to the interventricular septum. This image plane is similar to the left anterior oblique view. Three or four contiguous short axis (left anterior oblique) scans from the base to the apex of the heart also were made. The scans were repeated with the same pulse sequences 5–10 min after IV administration of 0.15 mmol/kg of Gd-DTPA. The total scanning time was approximately 1 hr. The scan obtained after Gd-DTPA administration was compared with the regular scan for further

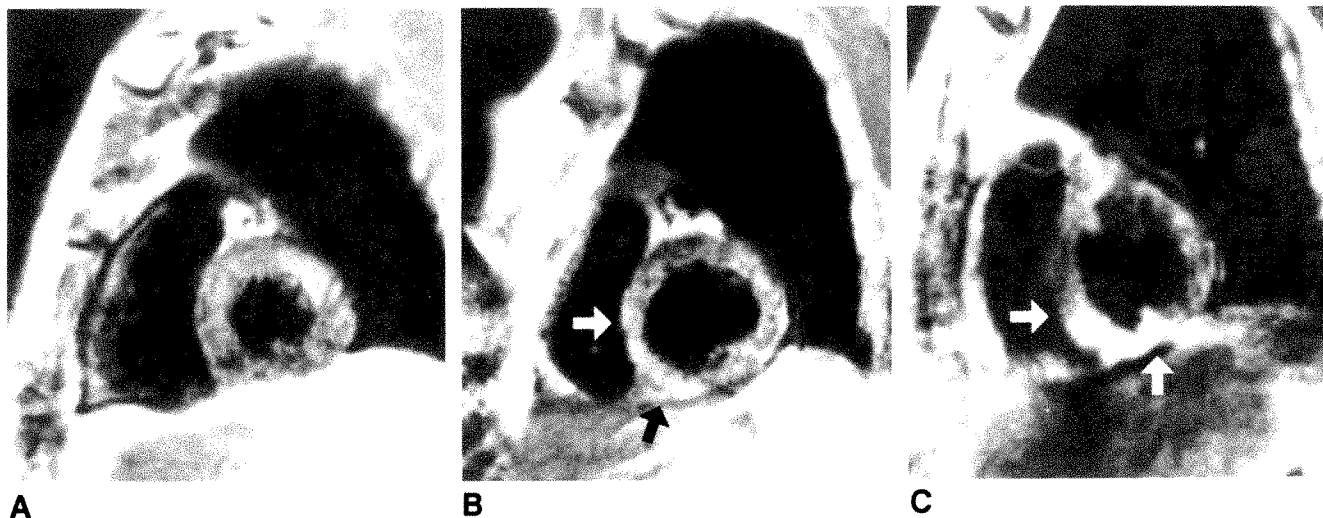


Fig. 1.—T1-weighted MR images of myocardial infarction (arrows) used in qualitative analysis of Gd-DTPA contrast enhancement. Typical patterns of no enhancement (A), moderate enhancement (B), and marked enhancement (C) are shown.

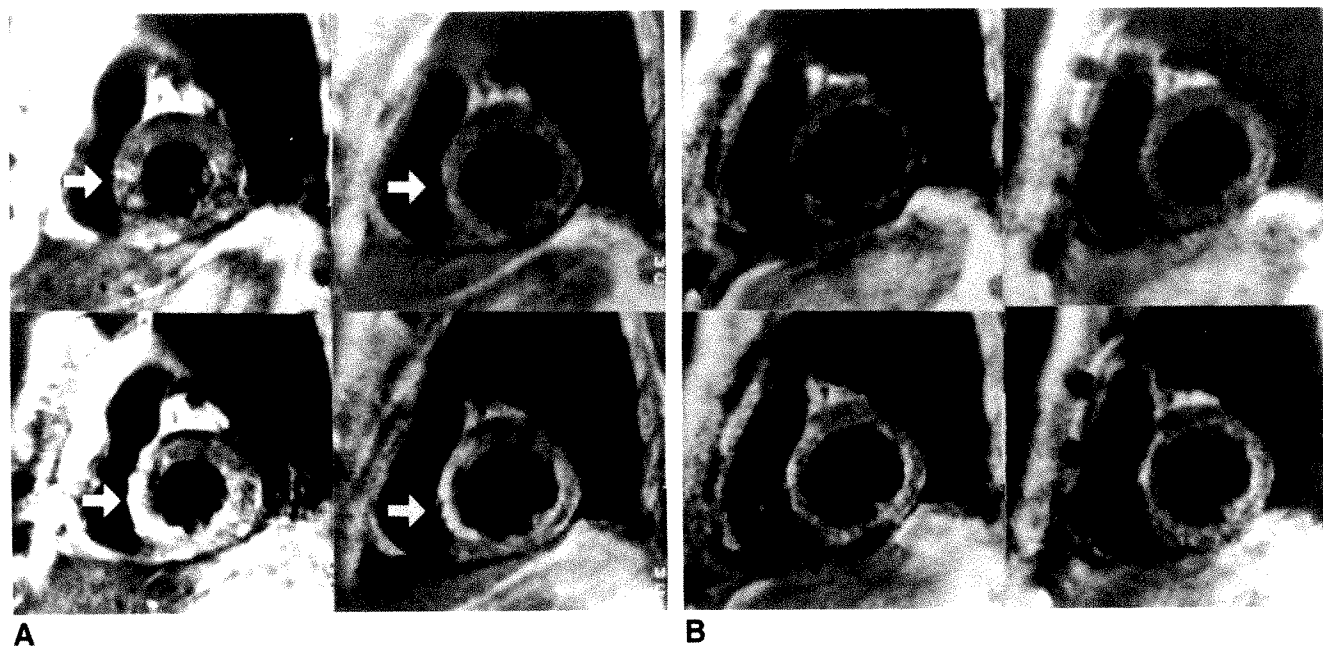


Fig. 2.—Serial assessment of acute anteroseptal myocardial infarction (arrows) by using gated MR imaging with Gd-DTPA. Pulse sequences were SE 800/35, SE 800/35, SE 820/35, and SE 820/35 at 5, 12, 30, and 90 days, respectively.

A, MR scan shows faintly increased signal intensity at anteroseptal region on T1-weighted image before Gd-DTPA administration (top) on days 5 (left) and 12 (right). This area is shown more clearly on T1-weighted image after Gd-DTPA administration (bottom).

B, Conversely, there was no increase in signal intensity and no contrast enhancement on days 30 (left) and 90 (right).

analysis. Gated MR imaging was carried out serially at four intervals after the infarction (5 ± 1 days [<1 week], 12 ± 2 days [<2 weeks], 30 ± 5 days [1 month], and 90 ± 8 days [3 months]). Fourteen patients underwent all four scans; two patients had scans made at 5, 12, and 30 days; and one patient had scans made only at 5 and 12 days.

Data Analysis

Images were assessed visually by three independent observers for increased signal intensity at the infarcted area. The intensity was graded as marked (++), moderate (+), or no (-) increase in signal intensity (Fig. 1). The ratio of the signal intensity of the infarcted area (I) to that of the normal myocardium (N) in the same tomographic slice was assessed quantitatively by using the operator-defined region-of-interest method (usually 50 voxels in each region) from the television monitor on T1-weighted images before and after Gd-DTPA administration. The statistical significance of the difference in contrast enhancement before and after Gd-DTPA administration was evaluated by using the paired *t* test.

Results

The qualitative score correlated well with the quantitative value ($r = .84$). The mean values of the I/N ratio were 1.24 ± 0.16 , 1.46 ± 0.28 , and 1.68 ± 0.24 at no, moderate, and marked increase in signal intensity, respectively. Intraobserver variability and interobserver variability of quantitative analysis were .92 and .94 in 10 selected cases. Serial assessment of a typical case by using gated MR imaging and Gd-DTPA is shown in Figure 2. The anteroapical region showed slightly increased signal intensity on T1-weighted images obtained before Gd-DTPA administration at 5 and 12 days from the

onset. This infarcted area was clearly shown to be of increased signal intensity on T1-weighted images after Gd-DTPA was administered. On the other hand, no increase in signal intensity was seen before Gd-DTPA administration, and no contrast enhancement was seen after Gd-DTPA administration at 30 and 90 days. Serial changes in the area of increased signal intensity after acute myocardial infarction on T1-weighted images, T2-weighted images, and T1-weighted images after Gd-DTPA administration are shown in Figures 3, 4, and 5, respectively. On the T1-weighted image without Gd-DTPA, increased signal intensity was observed at 5 and 12 days in six and 11 cases, respectively. On the other hand, on the T2-weighted images, these results were observed in 13 and 16 cases, respectively. Thus, signal intensity increased more often on T2-weighted images than on T1-weighted images. These areas of increased signal intensity generally disappeared at 30 and 90 days on both images. After Gd-DTPA administration, the infarct area could be visualized markedly on the T1-weighted images at 5 and 12 days in 14 and 16 cases, respectively. Considering all patients, an area of increased signal intensity was shown at 5, 12, 30, and 90 days in 35%, 65%, 25%, and 14% of cases on T1-weighted images and in 76%, 94%, 38%, and 14% of cases on T2-weighted images. After Gd-DTPA administration, the frequency of appearance of an area of increased signal intensity on T1-weighted images was highest; the results at 5, 12, 30, and 90 days were 82%, 94%, 38%, and 21% of cases, respectively. Markedly increased signal intensity was observed most often on the T1-weighted images with Gd-DTPA at 5 and 12 days (Fig. 6). The signal-intensity ratio after Gd-DTPA administration was significantly higher than before, 1.78 ± 0.48 at 5 days ($p < .01$) and 1.80 ± 0.28 at 12 days

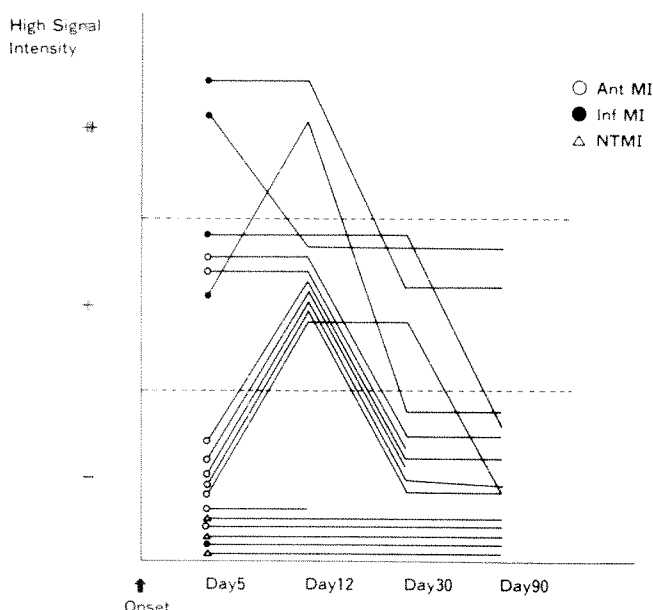


Fig. 3.—Serial changes of area of increased signal intensity after acute myocardial infarction on T1-weighted image (SE 600–1000/35). Ant MI = anterior myocardial infarction, Inf MI = inferior myocardial infarction, NTMI = nontransmural myocardial infarction.

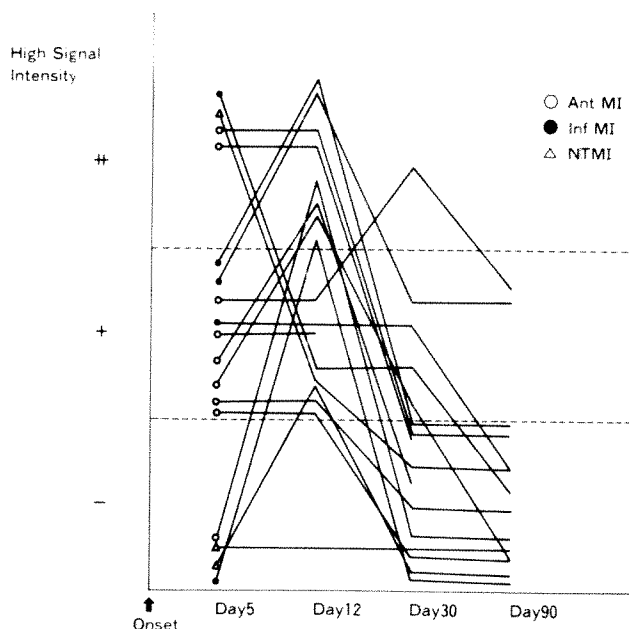


Fig. 4.—Serial changes of area of increased signal intensity after acute myocardial infarction on T2-weighted image (SE 600–1000/70). Ant MI = anterior myocardial infarction, Inf MI = inferior myocardial infarction, NTMI = nontransmural myocardial infarction.

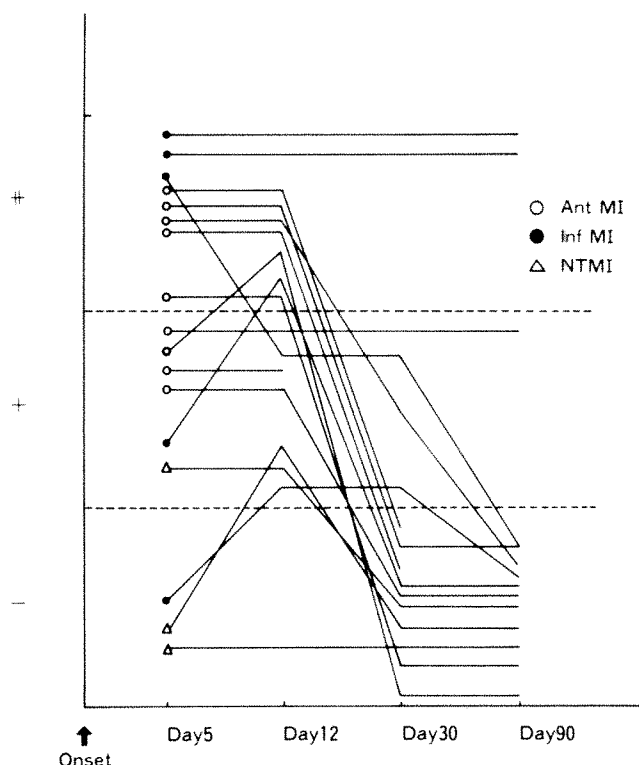


Fig. 5.—Serial changes of increased signal intensity after acute myocardial infarction on T1-weighted image with Gd-DTPA (SE 600–1000/35). Ant MI = anterior myocardial infarction, Inf MI = inferior myocardial infarction, NTMI = nontransmural myocardial infarction.

($p < .01$). This same ratio measured only 1.32 ± 0.48 at 30 days and 1.25 ± 0.46 at 90 days (Fig. 7). Furthermore, image quality on T1-weighted images after Gd-DTPA administration was superior to that on T2-weighted images (Fig. 8).

Discussion

Because signal intensity is sensitive to changes in water content, acutely infarcted myocardium can be distinguished from normal myocardium by using MR imaging [9, 10]. It has been shown that the infarcted area appears to be more distinct on T2-weighted images [11, 12]. Thus, a long T2 relaxation time, which reflects the increased water content at the infarcted area, results in high signal intensity compared with the normal myocardium. In a study by Fisher et al. [3], the acute infarcted area was visualized as high signal intensity on T2-weighted images in 23 (92%) of 25 patients with acute myocardial infarction 3–17 days from the onset of acute chest pain. Our study shows that acute myocardial infarction is detected more frequently on T2-weighted images (76% and 94%) than on T1-weighted images (35% and 65%) at 5 and 12 days, respectively. Thus, MR imaging can be used without Gd-DTPA to visualize acute infarcts. In addition, infarct location by MR imaging was compatible with that by ECG criteria. There are still, however, several potential pitfalls including the need to differentiate the signal from slowly flowing blood in

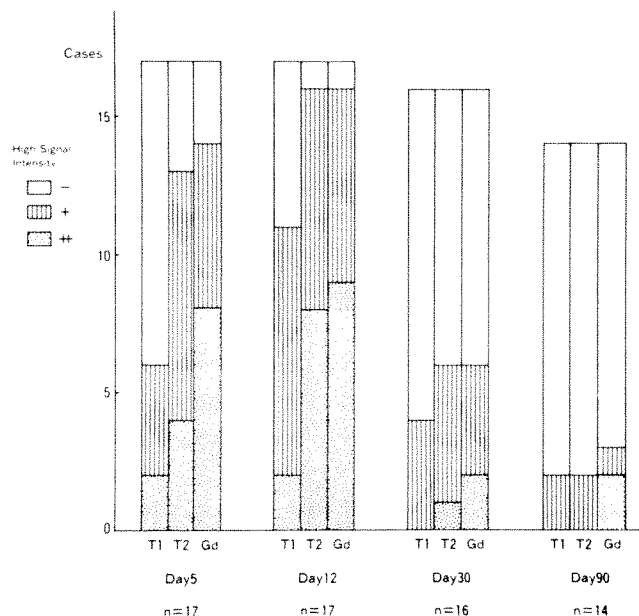


Fig. 6.—Qualitative assessment of area of increased signal intensity in acute myocardial infarction by using gated MR imaging with Gd-DTPA. Gd-DTPA contrast was observed more clearly after 5 and 12 days than after 30 and 90 days. T1 = T1-weighted, T2 = T2-weighted, Gd = T1-weighted with Gd-DTPA.

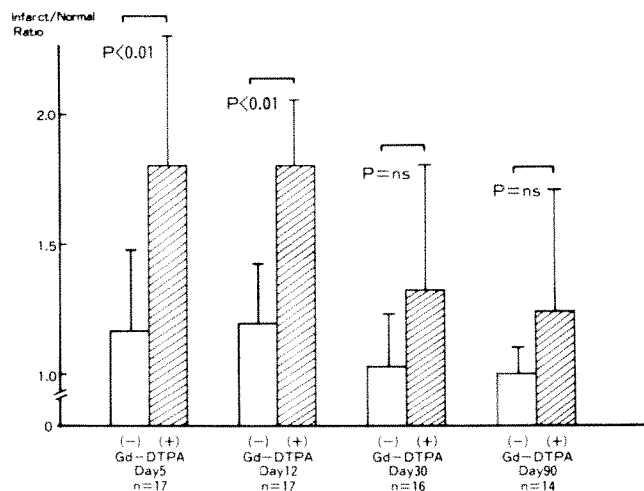


Fig. 7.—Quantitative assessment of area of increased signal intensity in acute myocardial infarction on T1-weighted image by using gated MR imaging from Gd-DTPA. Infarct/normal ratios with (+) and without (-) Gd-DTPA are expressed as mean \pm standard deviation.

the ventricle, as well as artifactual variations of signal intensity in the myocardium due to respiratory or residual cardiac motion [3]. Furthermore, the use of late echo reduces the signal-to-noise ratio, leading to image degradation [6, 7]. These drawbacks, therefore, raise the question of whether gated MR imaging with Gd-DTPA can improve the identification of location and extent of infarct.

Gd-DTPA, which shortens T1 and T2 relaxation times, has been used for the accurate detection of acute myocardial

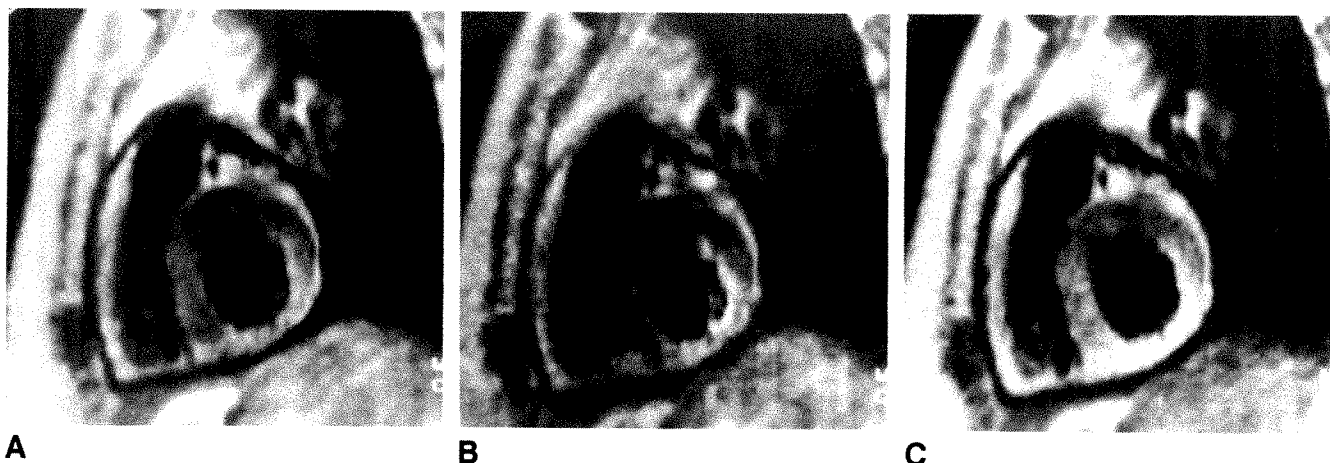


Fig. 8.—MR image shows moderately increased signal intensity at inferoposterior region without Gd-DTPA. Marked contrast enhancement was obtained after Gd-DTPA administration in this region at 12 days from onset of infarction. Pulse sequences were (A) T1, SE 1000/35; (B) T2, SE 1000/70; and (C) T1 with Gd, SE 1000/35.

infarction in dogs [5–7]. In the excised hearts of these animals, the MR contrast was high on the T1-weighted image; the mean T1 values from the infarcted area were significantly shorter than those from the normal area [5, 6]. This contrast enhancement at the infarcted area may be caused by differences in the wash-in and wash-out of Gd-DTPA from the normal myocardium. In acutely damaged myocardium, Gd-DTPA may be delivered to the infarcted area in accordance with the extent of collateral circulation, neovascularization, and cellular damage, all of which cause slow wash-out from the infarct zone [13, 14]. By 10–15 min, however, it has largely washed out of the normal tissue, while it remains in the zone of injury. As MR imaging during the first few minutes is generally impractical, usually it is performed after 10–20 min, when there is more of the agent in the infarcted zone and hence increased signal on T1-weighted images. Contrast enhancement was shown on T1-weighted images after Gd-DTPA administration at 5 and 12 days in 14 (82%) and 16 (94%) of 17 patients, respectively. Of these cases, markedly high signal intensity was shown in eight patients (47%) at 5 days and in nine (53%) at 12 days. Only one patient showed no increase in signal intensity on both studies—a result of a small subendocardial infarction.

Gd-DTPA contrast enhancement was not seen at the chronic stage. Myocardial scar tissue is composed exclusively of connective tissues without viable cells or vessels, hence, influx of the contrast medium does not occur [15, 16]. Persistent high signal intensity at the infarcted area, however, was observed in six patients at 30 days and in three patients at 90 days. The mechanism of persistent high signal intensity in these patients is unknown, because there were no significant differences in serum creatinine phosphokinase level, left ventricular function, and cardiac catheterization data between these patients and those exhibiting no persistent enhancement. The presence or absence of Gd-DTPA contrast enhancement may be caused by differences in the severity and extent of the infarcted area in individual cases. Further stud-

ies, therefore, are needed to evaluate myocardial tissue characterization by using gated MR imaging with Gd-DTPA. As shown in Figure 6, the frequency of high signal intensity at the infarcted area on T2-weighted images without Gd-DTPA was similar to that on T1-weighted images with Gd-DTPA. Although this could be seen as a limitation of gated MR imaging with Gd-DTPA in the detection of infarcted areas, the use of late echo reduces the signal-to-noise ratio, leading to image degradation.

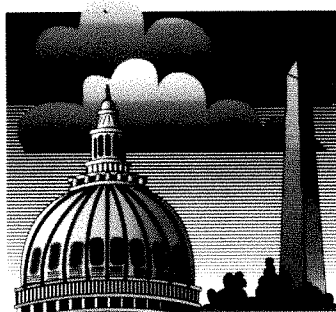
In summary, gated MR imaging with Gd-DTPA could improve identification of recent myocardial infarcts. Uptake of Gd-DTPA in acutely infarcted myocardium may be a positive marker; however, there seems to be no significant enhancement in chronic myocardial infarction.

REFERENCES

1. Wesbey G, Higgins CB, Lanzer P, Botvinick E, Lipton MJ. Imaging and characterization of acute myocardial infarction in vivo by nuclear magnetic resonance. *Circulation* 1984;69:125–130
2. McNamara MT, Higgins CB, Schechtman N, et al. Detection and characterization of acute myocardial infarction in man with the use of gated magnetic resonance. *Circulation* 1985;71:717–724
3. Fisher MR, McNamara MT, Higgins CB. Acute myocardial infarction: MR evaluation in 29 patients. *AJR* 1987;148:247–251
4. Brasch RC, Weinmann HJ, Wesbey GE. Contrast-enhanced MR imaging: animal studies using gadolinium-DTPA complex. *AJR* 1980;142:625–630
5. Wesbey GE, Higgins CB, McNamara T, et al. Effects of gadolinium-DTPA on the magnetic relaxation times of normal and infarcted myocardium. *Radiology* 1984;153:165–169
6. Rehr RB, Peshock RM, Malloy CR et al. Improved in vivo magnetic resonance imaging of acute myocardial infarction after intravenous paramagnetic contrast agent administration. *Am J Cardiol* 1986;57:864–868
7. Nishimura T, Yamada Y, Kozuka T, Nakatani T, Noda H, Tanaka H. Value and limitation of gadolinium-DTPA contrast enhancement in early detection of acute canine myocardial infarction. *Am J Physiol Imag* 1987;2:181–187
8. Nishimura T, Yamada Y, Hayashi M, Kozuka T, Noda H, Tanaka H. Identification of infarct size of acute canine myocardial infarction in dogs by magnetic resonance imaging and gadolinium-DTPA—comparison with indium-111 antimyosin imaging (abstract). *J Nucl Med* 1987;28:590
9. Higgins CB, Herfkens R, Lipton MJ, et al. Nuclear magnetic resonance

imaging of acute myocardial infarction in dogs: alternation in magnetic relaxation times. *Am J Cardiol* **1983**;52:184-192

10. Tscholakoff D, Higgins CB, Sechtem U, Caputo G, Derugin N. Magnetic resonance imaging of reperfused myocardial infarct in dogs. *AJR* **1986**; 146:925-930
11. Pflugfelder PW, Wisenberg G, Prato FS, Turner KL, Carroll E. Serial imaging of canine myocardial infarction by in vivo nuclear magnetic resonance. *J Am Coll Cardiol* **1986**;7:843-849
12. Rokey R, Verani MS, Bolli R, et al. Myocardial infarct size quantification by MR imaging early after coronary occlusion in dogs. *Radiology* **1986**; 158:771-774
13. Tscholakoff D, Higgins CB, Sechtem U, McNamara MT. Occlusive and reperfused myocardial infarcts: effects of Gd-DTPA on ECG-gated MR imaging. *Radiology* **1986**;160:515-519
14. McNamara MT, Tscholakoff D, Revel D, et al. Differentiation of reversible and irreversible myocardial injury by MR imaging with and without gadolinium-DTPA. *Radiology* **1986**;158:765-769
15. Eichstaedt H, Felix R. Use of Gd-DTPA-enhanced magnetic resonance imaging for diagnosis of acute myocardial infarction. In: Runge VM, Clausen C, Felix R, James AE, eds. *Contrast agents in magnetic resonance imaging*. Amsterdam: Excerpta Medica, **1987**:150-154
16. Eichstaedt HW, Felix R, Dougherty FC, et al. Magnetic resonance imaging (MRI) in different stages of myocardial infarction using contrast agent Gadolinium-DTPA. *Clin Cardiol* **1986**;9:527-535



Scientific Program (200 papers)
Instructional Courses (60 hours)

Categorical Course on
Cardiovascular Imaging

The Caldwell Lecture

Award Papers

Scientific Exhibits

Social, Golf, and Tennis Programs

Guest Programs



Come to the
American Roentgen Ray Society

90th

ANNUAL MEETING

Washington, D. C.

Sheraton Washington Hotel

May 13-18, 1990

Cine MR Imaging in Mitral Regurgitation: Comparison with Color Doppler Flow Imaging

Tsunehiko Nishimura¹
 Naoaki Yamada¹
 Akira Itoh²
 Kunio Miyatake²

Cine MR imaging is a new technique that combines short repetition times, limited flip angles, gradient-refocused echoes, and cardiac gating. This procedure was performed in 20 patients in whom mitral regurgitation was shown on left ventriculography, and the results were compared with those of color Doppler flow mapping. In all cases, mitral regurgitation on cine MR imaging was depicted as an area of decreased signal intensity within the left atrium. The extent and severity of the regurgitant jet as seen by the two techniques were classified visually as 4+ (severe), 3+ (moderate), 2+ (mild), and 1+ (minimal). The results of the two methods were the same in 14 (70%) of the 20 patients. In five patients the results differed by one grade and in one patient by two grades. In addition, the maximal intrusion distance and area of the regurgitant jet divided by the area of the left atrium as determined by the two methods were compared. The correlation coefficients between the two methods in regard to the length and area of mitral regurgitation were .74 and .71, respectively.

These data suggest that the accuracy of cine MR imaging in assessing the severity of mitral regurgitation is comparable to that of color Doppler flow imaging.

AJR 153:721-724, October 1989

MR imaging clearly depicts cardiac anatomy in congenital and acquired heart diseases [1-3]. The technique is limited by a long imaging time and low temporal resolution. Recently, cine MR imaging techniques that use a low flip angle and gradient-refocused echoes have been developed [4-7]. They provide a series of images of the heart and great vessels at different phases of the cardiac cycles in which the velocity of flowing blood affects signal intensity. Rapid review of these images, compiled in an endless loop, results in a movie of intracardiac anatomy and flow. Thus, cine MR imaging is useful in evaluating cardiovascular function [6, 7]. A regurgitant jet is identified as a discrete area of low signal intensity extending from the incompetent valve into the respective cardiac chamber [8, 9].

In this study, we compared the extent and severity of mitral regurgitation as determined by cine MR imaging with the results obtained by real-time, two-dimensional color Doppler flow imaging.

Materials and Methods

Cine MR imaging was performed in 34 patients with mitral regurgitation who were hospitalized in the National Cardiovascular Center (Osaka, Japan) between October 1987 and March 1988. Color Doppler flow imaging and left ventriculography were performed within 2 weeks of cine MR imaging in 20 of these patients. There were 12 men and eight women 37-69 years old (mean \pm SD, 54 \pm 12 years). Nine patients had combined valvular heart disease, seven had dilated cardiomyopathy, two had myocardial infarction, and two had hypertensive heart disease. The severity of mitral regurgitation was confirmed by left ventriculography. According to the classification of Sellers et al. [10], seven patients had grade I, six had grade II, three had grade III, and four had grade IV regurgitation.

Received November 14, 1988; accepted after revision April 10, 1989.

¹ Department of Radiology, National Cardiovascular Center, 5-7-1 Fujishirodai, Suita, Osaka, 565 Japan. Address reprint requests to T. Nishimura.

² Department of Cardiology, National Cardiovascular Center, Osaka, 565 Japan.

0351-803X/89/1534-0721

©American Roentgen Ray Society

MR imaging was performed by using a commercially available 1.5-T superconductive magnet (Magnetom H15, Siemens). Images were obtained by means of the FLASH (fast low-angle shot) technique, which uses the low flip angle of 30° and gradient-refocused echoes with an echo time of 16 msec. The repetition time was 30–40 msec. The data acquisition was keyed to the heart rate, with advancement of the phase-encoding gradient with the heartbeat. The acquisition matrix was 128 × 256 interpolated to 256 × 256 for display. The entire heart of each patient was imaged at a 10-mm interval by using one averaging time on the transaxial plane. All images were reconstructed at 21 frames for a cardiac cycle and displayed in a dynamic fashion (Fig. 1). Eleven frames from a 21-image/cardiac cycle sequence at the level of left atrium were assembled into a composite image. Mitral regurgitation on cine MR imaging was defined as an area of decreased signal intensity within the left atrium that originated at the valve plane and coincided with ventricular systole. The total acquisition time was approximately 45 min.

The equipment used included a real-time two-dimensional Doppler flow imaging system (Aloka XA-54 prototype with a 2.5-MHz transducer, Tokyo, Japan) and a commercially available real-time two-dimensional echocardiographic unit (Toshiba SSH-40A, 2.5 MHz transducer, Tokyo, Japan) [11, 12]. The former system allowed visualization of the topography of the intracardiac flow. The flow image was superimposed on the two-dimensional echocardiogram, which was displayed on the same screen. The latter system was used for evaluation of the morphology and dynamic features of the heart. Whether the regurgitant jet was toward the anterior or posterior atrial wall was determined in the long-axis view of the left side of the heart. The total acquisition time was approximately 30 min.

A diagram of the mitral regurgitation as depicted by cine MR imaging and color Doppler flow imaging is shown in Figure 2. The extent and severity of the regurgitant jet were classified on the basis of size as determined by visual inspection. Each technique was scored as 4+ (severe), 3+ (moderate), 2+ (mild), or +1 (minimal). The grading of cine MR imaging and color Doppler flow imaging was done independently by two observers without the knowledge of the other's finding. The maximal intrusion distance of the regurgitant jet signal

from the mitral orifice into the left atrial cavity was used to determine the severity of mitral regurgitation by both techniques. In addition, the maximal area of regurgitant jet divided by the area of the left atrium was also used to determine the severity of mitral regurgitation.

Results

In all cases, mitral regurgitation on cine MR imaging was depicted as an area of decreased signal intensity within the left atrium, and the extent of regurgitant jet was compatible with that seen on color Doppler flow imaging (Figs. 3 and 4).

The severities of mitral regurgitation as determined qualitatively by cine MR imaging and color Doppler flow imaging were compared (Fig. 5). The results of the two methods were the same in 14 patients (70%) and differed by one grade in five and by two grades in one. The results of cine MR and color Doppler flow imaging were correlated with that of left ventriculography.

The maximal intrusion distance and area of the regurgitant jet signal from the mitral orifice into the left atrial cavity were determined by cine MR imaging and color Doppler flow imaging. The interobserver variabilities in cine MR imaging and color Doppler flow imaging were 0.96 and 0.94 in regard to the length and area of mitral regurgitation in 10 selected patients. The correlation coefficient between the length of the mitral jet measured by cine MR imaging and that determined by color Doppler flow imaging was .74 (Fig. 6). The lengths (mean ± SD) of the mitral jet on cine MR imaging in patients with grades I, II, III, and IV regurgitation determined by left ventriculography were 2.3 ± 0.5 cm, 5.0 ± 0.4 cm, 6.1 ± 1.9 cm, and 8.3 ± 1.6 cm, respectively. Those on color Doppler flow imaging were 1.5 ± 0.8 cm, 4.5 ± 1.0 cm, 5.7 ± 0.8 cm, and 8.2 ± 2.2 cm, respectively. In addition, the correlation coefficient between the areas of mitral jet as determined by cine MR imaging and by color Doppler flow imaging was .71

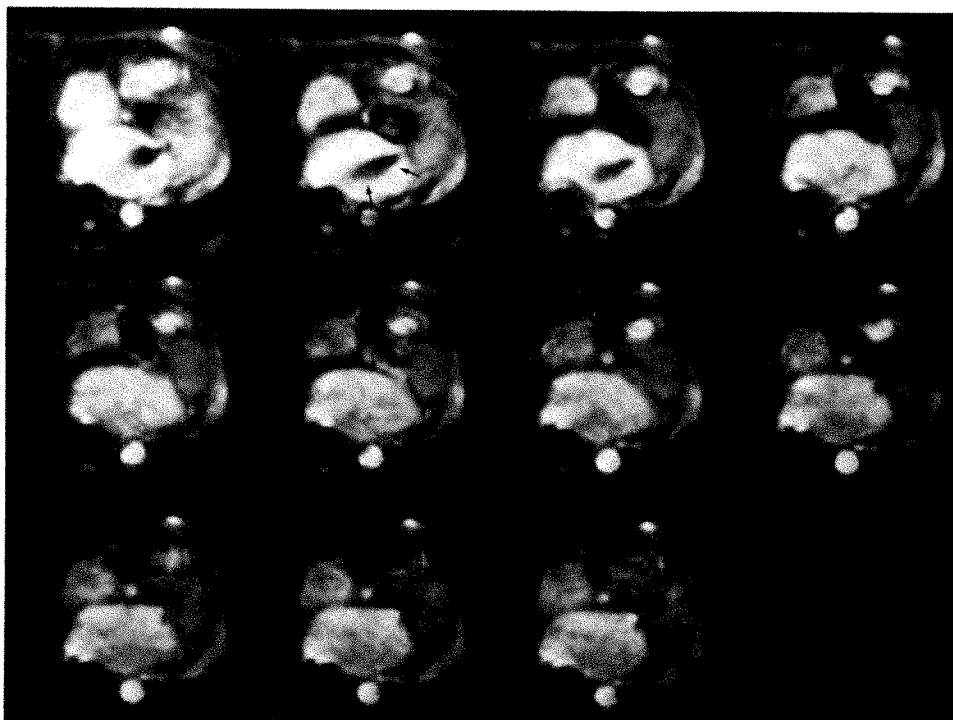


Fig. 1.—Cine MR images of mitral regurgitation at level of left atrium. A composite of 11 frames from 21-image/cardiac cycle sequence is shown. Valvular regurgitation is seen as area of decreased signal intensity within left atrium that appears to originate at valve plane and coincide with ventricular systole (arrows).

(Fig. 7). The areas (mean \pm SD) of mitral jets calculated from cine MR imaging were $8.8 \pm 2.0\%$, $15.9 \pm 6.1\%$, $32.8 \pm 21.9\%$, and $44.2 \pm 5.9\%$ in patients with grades I, II, III, and IV regurgitation as determined by left ventriculography. Those by color Doppler flow mapping were $9.6 \pm 5.2\%$, $19.0 \pm 9.8\%$, $31.6 \pm 8.7\%$, and $39.7 \pm 2.8\%$, respectively.

Discussion

Mitral regurgitation is a common clinical problem in patients with combined valvular disease, ischemic heart disease, and

cardiomyopathy. Left ventriculography has been considered to be the most accurate means for evaluation of mitral regurgitation [10]. This technique, however, requires catheterization and the use of contrast media. Color Doppler flow imaging is now widely used because it is noninvasive and is accurate for the detection of valvular regurgitation [11, 12]. However, this technique is operator dependent and occasionally limited by body habitus. Cine MR imaging has the advantage that the regurgitant jet is visible as a discrete area of low signal intensity and the procedure is not operator dependent [9, 10]. Our studies also show that in all patients the sites and severities of regurgitant jet were similar on cine MR and color Doppler flow imaging. Although our study shows that the low signal intensity caused by the regurgitant jet during systole is specific for mitral regurgitation, normal systolic outflow from the left ventricle into the aorta also tends to have an apparent jet of decreased signal [8]. In addition, flow rates beyond a certain threshold velocity may not be distinguished with cine MR imaging [8].

In our study, the extent and severity of mitral regurgitation determined by cine MR imaging correlated with those measured by color Doppler flow imaging. Therefore, cine MR imaging can be expected to be as accurate as color Doppler flow imaging. Furthermore, cine MR imaging may have potential in the evaluation of the site and severity of mitral regurgitation in any direction, especially in mitral valve prolapse, compared with color Doppler flow imaging. However, the precise anatomic conditions of mitral valve prolapse could not be defined by cine MR imaging, not because of real-time but

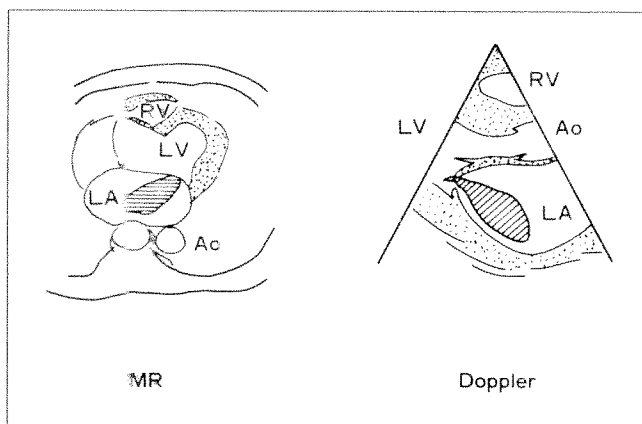


Fig. 2.—Diagram shows mitral regurgitation as detected by cine MR and color Doppler flow imaging. Maximal length and area of regurgitation jet were assessed quantitatively. LV = left ventricle; LA = left atrium; RV = right ventricle; Ao = aorta.

Fig. 3.—48-year-old woman with combined valvular heart disease.

A and B, Cine MR image (A) and Doppler flow image (B) show that mitral regurgitant jet spurts from central area of mitral valve into left atrial cavity (arrows). Both imaging procedures show similar extent and severity of mitral jet, which was confirmed as grade II (I–IV scale) on left ventriculography.

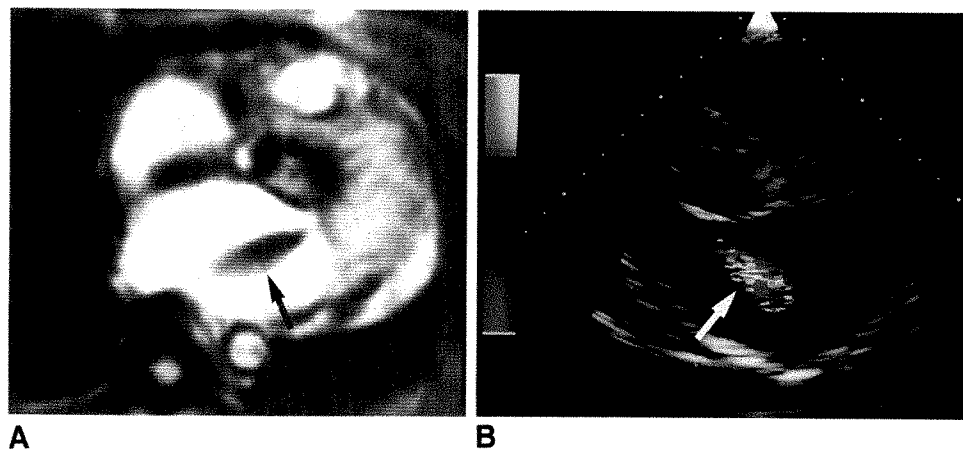
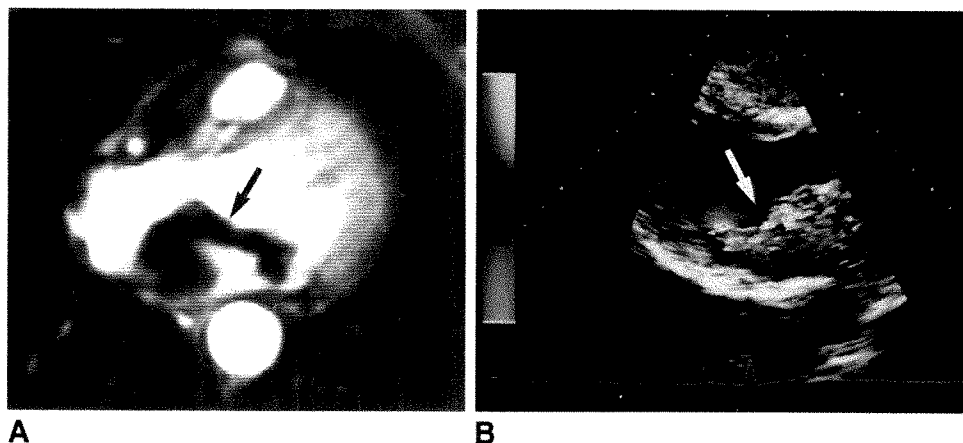


Fig. 4.—57-year-old man with mitral valve prolapse of posteromedial scallops.

A and B, Cine MR image (A) and Doppler flow image (B) show that mitral jet spurts from posteromedial area of valve and toward anterior wall of left atrium (arrows). Extent and severity of mitral jet are similar, which was confirmed as grade IV (I–IV scale) on left ventriculography.



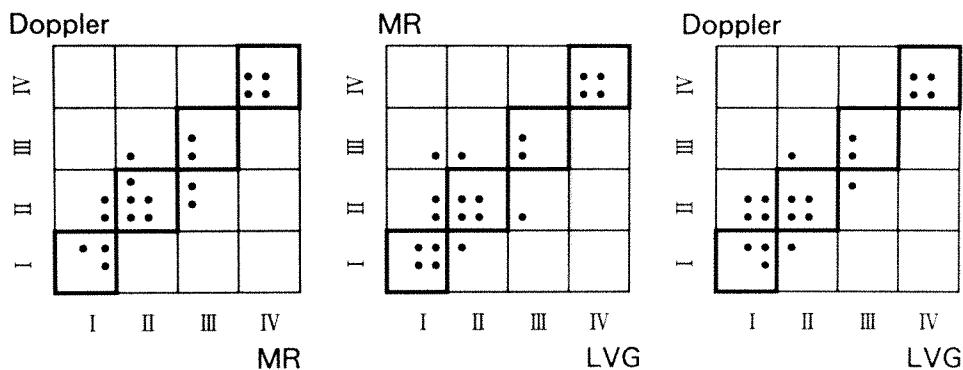


Fig. 5.—Severity of mitral regurgitation determined by cine MR imaging compared with that determined by left ventriculography (LVG) and color Doppler flow imaging. I–IV = degree of mitral regurgitation.

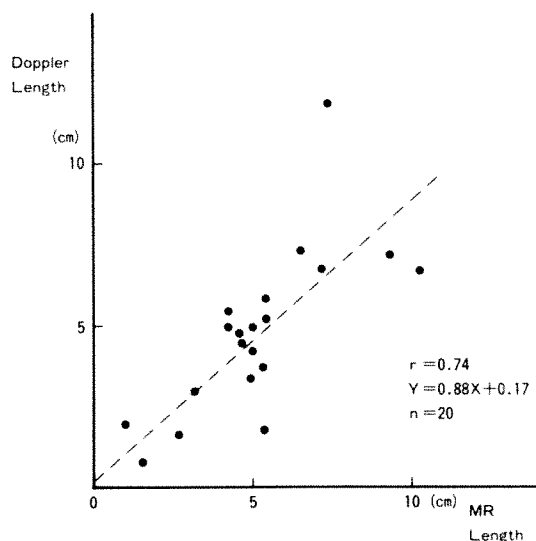


Fig. 6.—Graph shows relationship of maximal length of regurgitant jet as determined by cine MR (x) and color Doppler flow imaging (y). r = correlation coefficient; n = number of cases.

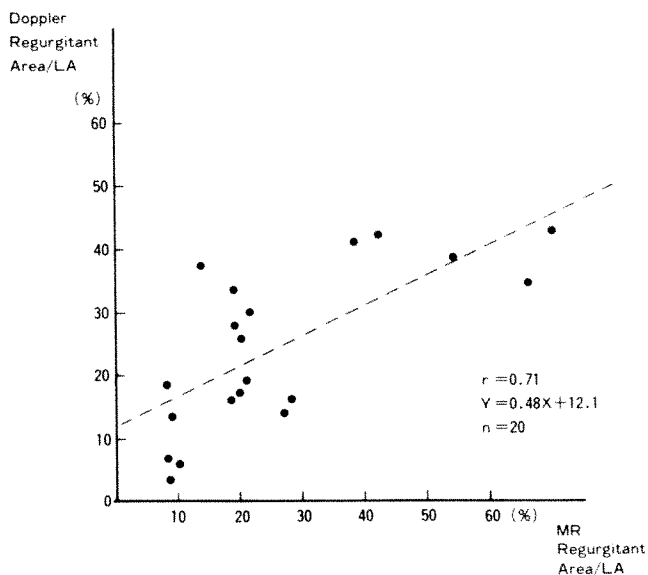


Fig. 7.—Graph shows relationship of maximal area of regurgitant jet as determined by cine MR (x) and color Doppler flow imaging (y). LA = left atrium; r = correlation coefficient; n = number of cases.

because of ECG-gated cardiac imaging. Our cine MR images were obtained in the transaxial plane, whereas color Doppler flow images were obtained in the long-axis plane. The assessment of the integrity and morphology of the valve leaflets is more difficult in transverse section. Although the correlation coefficients of length and area of mitral jet by these two methods were .74 and .71, mitral regurgitation may be assessed more accurately by oblique cine MR imaging [13]. At present, positioning of the patient within the magnet bore is limited, and oblique cine MR imaging is not routinely available with our machine. Oblique cine MR imaging, however, should be investigated further.

In conclusion, cine MR imaging is a promising tool for the noninvasive analysis of mitral regurgitation. The areas of low signal intensity on cine MR imaging were closely correlated with those regions mapped by color Doppler imaging.

REFERENCES

- Herfkens RJ, Higgins CB, Hricak H, et al. Nuclear magnetic resonance imaging of the cardiovascular system: normal and pathologic findings. *Radiology* 1983;147:749–759
- Higgins CB, Byrd BF, McNamara MR, et al. Magnetic resonance imaging of the heart: a review of the experience in 172 subjects. *Radiology* 1985;155:671–679
- Higgins CB. Overview of MR of the heart—1986. *AJR* 1986;146:907–918
- Haase A, Frahm J, Matthaei D, Haenicke W, Merboldt KD. Rapid NMR imaging using low flip-angle pulses. *J Magn Reson* 1986;67:258–266
- Mills TC, Ortendahl DA, Hylton NM, Crooks LE, Carlson JW, Kaufman L. Partial flip angle MR imaging. *Radiology* 1987;162:531–539
- Sechtem U, Pflugfelder PW, White RD, et al. Cine MR imaging: potential for the evaluation of cardiovascular function. *AJR* 1987;148:239–246
- Sechtem U, Pflugfelder PW, Gould RG, Cassidy MM, Higgins CB. Measurement of right and left ventricular volume in healthy individuals with cine MR imaging. *Radiology* 1987;163:697–702
- Schiebler M, Axel L, Reichek N, et al. Correlation of cine MR imaging with two-dimensional pulsed Doppler echocardiography in valvular insufficiency. *J Comput Assist Tomogr* 1987;11:627–632
- Utz JA, Herfkens RJ, Heinsimer JA, Shimakawa A, Glover G, Pelc N. Valvular regurgitation: dynamic MR imaging. *Radiology* 1988;169:91–94
- Sellers RO, Levy MJ, Anplatz K, Lillehei CW. Left retrograde cardioangiography in acquired cardiac disease. *Am J Cardiol* 1964;14:437–447
- Miyatake K, Izumi S, Okamoto M, et al. Semiquantitative grading of severity of mitral regurgitation by real-time two-dimensional Doppler flow imaging technique. *J Am Coll Cardiol* 1986;7:82–88
- Izumi S, Miyatake K, Beppu S, et al. Mechanism of mitral regurgitation in patients with myocardial infarction: a study using real-time two dimensional Doppler flow imaging and echocardiography. *Circulation* 1987;76:777–785
- Askenase A, Chen G, Thompson W, et al. Oblique cine magnetic resonance blood flow imaging to assess changes in wall motion (abstr). *Circulation* 1987;76[suppl IV]:29

Case Report

Diagnosis of a Myocardial Lipoma by Using CT

Dewey J. Conces, Jr.,¹ Vernon A. Vix, and Robert D. Tarver

Cardiac lipomas are rare benign primary tumors of the heart [1]. We describe a case in which the preoperative diagnosis was made by using CT.

Case Report

A 28-year-old man was referred for evaluation of ventricular tachycardia, which had been diagnosed after an episode of syncope. When the patient was 10 years old, he was told he had an enlarged heart, and he underwent a cardiac catheterization at that time, details of which are not available.

Physical examination was normal. A chest radiograph showed an enlarged heart (Fig. 1A). An initial two-dimensional echocardiogram showed normal ventricular size and function. The distal aspect of the ventricular septum had abnormal motion. Cardiac catheterization showed normal right and left ventricular function. The left anterior descending coronary artery was displaced anteriorly by an epicardial mass, which also stretched the septal perforators. A second echocardiogram showed an echogenic mass external to the heart that extended from the anterior intraventricular groove circumferentially to the inferior posterior wall.

To evaluate the mass further, both noncontrast CT and dynamic CT during a 100-ml bolus injection of 61% iopamidol were performed. Scans showed a large, low-density mass located along the left side of the heart, beginning at the anterior intraventricular groove and extending posteriorly to the left atrium. The mass covered the entire anterior wall and most of the lateral wall of the left ventricle. The density of the mass was -107 H. No contrast enhancement of the mass was seen. The left anterior descending coronary artery and smaller branch vessels were displaced away from the ventricular wall by the mass (Figs. 1B and 1C).

At surgery, a large sessile fatty tumor was found arising from the

left ventricle. The mass elevated the coronary arteries from the ventricle. Because the vessels would have had to be sacrificed, the mass could not be resected. A biopsy was performed, and an automatic cardioverter defibrillator was implanted. Histologic examination of the biopsy specimen showed it to be a visceral epicardial lipoma.

Discussion

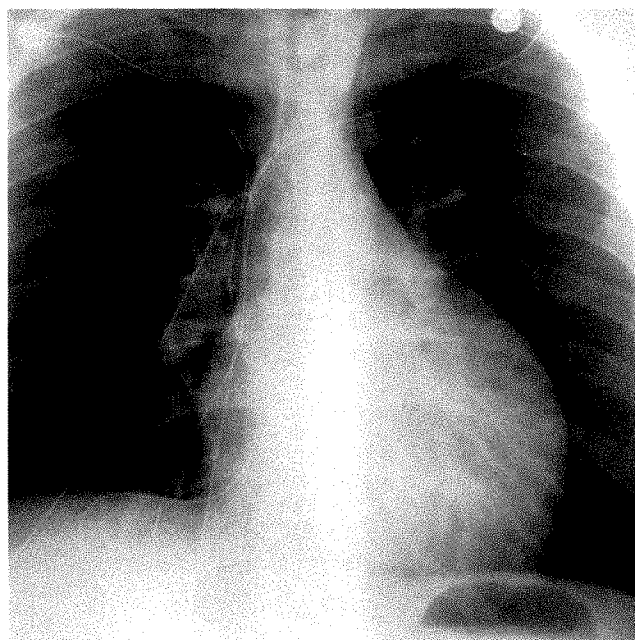
Myocardial lipomas are rare tumors, making up approximately 10% of primary tumors of the heart. They are composed of localized collections of fat surrounded by a capsule. Fifty percent arise subendocardially; the rest are divided between myocardial and epicardial origins. Most patients who have these tumors are asymptomatic. The diagnosis is made at autopsy, or the tumor is detected incidentally on a chest radiograph. The presence and the type of symptoms depends on the size and the location of the tumor [1]. Endocardial lipomas may obstruct the cardiac valves. Large epicardial lipomas may interfere with ventricular function, with resulting dyspnea and fatigue [2-5]. Myocardial lipomas located near the conduction system may produce conduction defects and arrhythmias [6]. In our case, a conduction delay and ventricular arrhythmias were produced either by mass effect or by infiltration of the left ventricular wall by the lipoma.

On chest radiographs, cardiac lipomas typically cause enlargement of the cardiac silhouette and may change the cardiac contour [2-6]. In our case, the cardiac silhouette was enlarged, but nothing suggested the presence of a mass. Echocardiography may show an echogenic mass, as was

Received February 27, 1989; accepted after revision April 14, 1989.

¹ All authors: Department of Radiology, Indiana University School of Medicine, 926 W. Michigan St., Indianapolis, IN 46223. Address reprint requests to D. J. Conces, Jr., Dept. of Radiology, Indiana University Hospital, X-64, 926 W. Michigan St., Indianapolis, IN 46223.

AJR 153:725-726, October 1989 0361-803X/89/1534-0725 © American Roentgen Ray Society



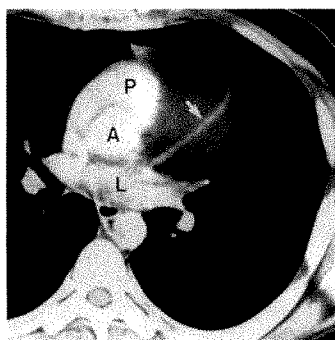
A

Fig. 1.—Myocardial lipoma in a 28-year-old man.
A, Posteroanterior chest radiograph shows an enlarged cardiac silhouette with no suspicion of a cardiac tumor.

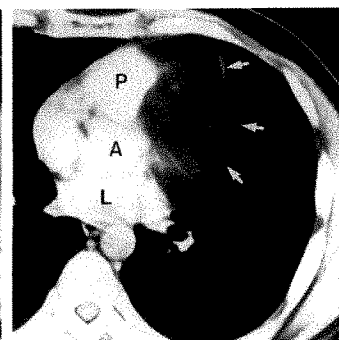
B, CT scan through level of proximal left anterior descending artery shows elevation of artery (arrow) by a large fat-density mass.

C, CT scan at a lower level shows displacement of smaller coronary arteries (arrows) by lipoma.

A = aorta, L = left atrium, P = pulmonary artery/outflow tract.



B



C

seen in our case [5, 6]. It is important to perform coronary arteriography to assess the relationship of the mass to the coronary arteries. This information is needed to determine the feasibility of surgical resection. Moulton et al. [5] reported a case in which the left coronary artery was elevated from the left ventricle. At surgery, the tumor was found to arise from a stalk that displaced the left coronary artery. The tumor was removed except for that part of the stalk that affected the left coronary artery. In our case, coronary arteriography indicated much more extensive involvement, with elevation of the entire left anterior descending artery and stretching of the septal perforators.

CT is ideally suited for use in the diagnosis of myocardial lipomas, especially those arising from the epicardium [6, 7]. The fatty composition of the tumor is readily identified by use of CT. The use of contrast material will increase the density differences between the tumor and the myocardium, cardiac chambers, and coronary arteries. In our case, the size of the tumor could be measured, and its relationship to the ventricular and atrial walls was shown clearly. An important aspect of this case was the clear depiction by CT of the elevation of the coronary arteries away from the ventricular wall by the mass. This extensive elevation of the arteries suggested that it would not be feasible to resect the mass. This was confirmed at surgery; the mass was sessile and covered by the coronary arteries supplying the left ventricle. If the lipoma had arisen from a stalk and not displaced the coronary arteries, its appearance would have been similar to a pericardial lipoma [8]. The absence of coronary artery displacement also would suggest that the lesion might be resectable.

In our case, CT had advantages over echocardiography and arteriography. The tumor was not detected on the initial echocardiogram. The tumor was identified on the second echocardiogram, but coronary artery involvement was not seen. Arteriography showed the mass and its displacement of the coronary arteries, but did not provide information about the nature of the mass. CT, however, clearly depicted the extent of the mass, its fatty composition, and the involvement of the coronary arteries.

MR imaging also may be of use in diagnosing these tumors because of the high signal intensity of fat as compared with myocardium. MR imaging was not done in this case because of the severity of the patient's ventricular arrhythmia.

REFERENCES

- Colucci WS, Braunwald E. Primary tumors of the heart. In: Braunwald E, ed. *Heart disease*. Philadelphia: Saunders, 1984:1457-1469
- Harjola PT, Ala-Kulju K, Ketonen P. Epicardial lipoma. *Scand J Thorac Cardiovasc Surg* 1985;19:181-183
- Maurer ER. Successful removal of tumor of the heart. *J Thorac Surg* 1952;23:479-485
- Shumacker HB, Leshnowar AC. Extracavitary lipoma of the heart. *Ann Thorac Surg* 1974;18:411-414
- Moulton AL, Jaretzki A, Bowman OF, Silverstein EF, Bregman D. Massive lipoma of the heart. *NY State J Med* 1976;76:1820-1825
- Zingas AP, Carrera JD, Murray CA, Kling GA. Lipoma of the myocardium. *J Comput Assist Tomogr* 1983;7:1098-1100
- Williamson BRJ, Sturtevant NV, Black WC, Brenbridge ANAG, Treates CD. Epicardial lipoma: a CT diagnosis. *Comput Radiol* 1985;9:169-171
- Moncada R, Baker M, Salinas M, et al. Diagnostic role of computed tomography in pericardial disease: congenital defects, thickening, neoplasms, and effusions. *Am Heart J* 1982;103:263-282

Chronic Eosinophilic Pneumonia: CT Findings in Six Cases

John R. Mayo¹
Nestor L. Müller¹
Jeremy Road²
John Sisler²
Glen Lillington³

We reviewed the chest radiographs and CT scans in six patients with proved chronic eosinophilic pneumonia. In all patients, the chest radiographs showed patchy air-space consolidation, and in five of six cases, the consolidation was most marked in the middle and upper lung zones. In only one patient was the classic pattern of air-space consolidation that is confined to the outer third of the lungs readily apparent. In three patients, the consolidation appeared to be diffuse, although a slight peripheral predominance was present. In two patients, a peripheral predominance was difficult to appreciate, even in retrospect. The CT scans in all cases showed peripheral air-space consolidation. In addition, mediastinal adenopathy was identified on CT scans in three cases. This has not been described before in association with chronic eosinophilic pneumonia. A follow-up CT scan in one patient showed resolution of the adenopathy and marked improvement in the peripheral air-space disease within 2 weeks.

We conclude that patients with chronic eosinophilic pneumonia show predominantly peripheral air-space consolidation on CT scans, even when this distribution is not readily apparent on the radiograph. CT may be helpful in the diagnosis when the clinical findings are suggestive, but the radiographic pattern is nonspecific.

AJR 153:727-730, October 1989

Chronic eosinophilic pneumonia is an idiopathic condition characterized by chronic infiltration of the lung with eosinophils. It is usually associated with an increased number of eosinophils in the circulating blood. In 50% of cases, the chest radiograph shows nonsegmental air-space consolidation confined to the outer third of the lung, the "photographic negative of pulmonary edema" [1, 2]. This pattern, when associated with blood eosinophilia, is characteristic enough to allow a confident diagnosis. In the remaining cases, the radiographic findings are nonspecific and further investigation is required. This often includes open-lung biopsy.

We report six patients with chronic eosinophilic pneumonia in whom chest radiographs and CT scans were obtained for evaluation of lung infiltrates and assess the potential use of CT in diagnosing this condition.

Subjects and Methods

Six patients with abnormal chest radiographs had chest CT scans made for further evaluation of lung infiltrates. Scans were obtained with either Siemens DR2, GE 8800, or GE 9800 scanners. In two of six patients, IV contrast material was used. Contiguous 8- or 10-mm collimation scans were made through the chest. Mediastinal and lung windows were available at all levels. Additional thin-section collimation scans (1.0 or 1.5 mm) were obtained in two patients at selected levels. All images were obtained within 1 week of diagnosis and before institution of steroid therapy. One patient had a follow-up examination with identical scanning parameters after 2 weeks of therapy.

The patients ranged from 35 to 74 years old (mean, 54 years) and included four men and two women. All complained of a nonspecific prodromal illness consisting of fever, malaise, coughing, or shortness of breath for 2-8 weeks. None of the patients had marked respiratory

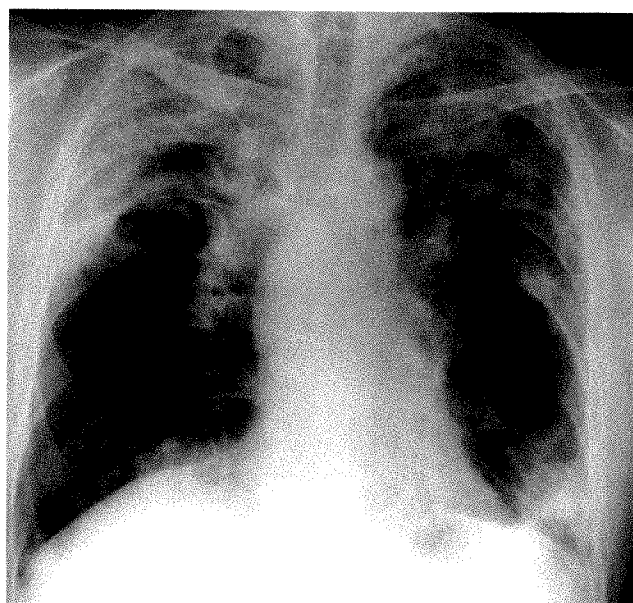
Received April 6, 1989; accepted after revision June 6, 1989.

¹ Department of Radiology, University of British Columbia and Vancouver General Hospital, 855 W. 12th Ave., Vancouver, B.C., Canada V5Z 1M9. Address reprint requests to J. R. Mayo.

² Departments of Radiology and Medicine, University of British Columbia and University Hospital-UBC Site, Vancouver, B.C., Canada V6T 1Y8.

³ Division of Pulmonary-Critical Care Medicine, University of California at Davis, Sacramento, CA 95817.

0361-803X/89/1534-0727
© American Roentgen Ray Society



A

Fig. 1.—A, Chest radiograph shows patchy bilateral air-space consolidation without a definitive peripheral predominance.

B, CT scan at level of right upper lobe bronchus clearly shows peripheral distribution.



B

compromise. A history of asthma for up to 10 years was noted in four cases, with allergic rhinitis in a fifth case. One patient was undergoing treatment with hemodialysis for diabetic chronic renal failure. In none of the patients was any infectious disease identified, and none of the infiltrates had responded to antibiotic therapy. No patient was taking any medication associated with eosinophilic infiltration of the lungs. All had a mild to moderate elevation in WBC count ($9.8\text{--}16.4 \times 10^9/\text{l}$) and mild to severe eosinophilia (6–38%). Laboratory values were obtained within 7 days of diagnosis and before steroid therapy began.

Biopsy was performed in four cases (two open lung, one trans-bronchial, one bronchoscopy with brushings). In two cases, the diagnosis was made on the basis of the clinical findings and the prompt resolution of infiltrates after steroid therapy. Six month follow-up was available in all cases.

Lung infiltrates were classified as peripheral on the chest radiographs and CT scans when the predominant involvement clearly abutted either the lung margins or the major fissures. In only two patients was the peripheral distribution of the infiltrates noticed on the radiograph before the CT scan. The distribution of opacities was classified as upper, mid, or lower lung zones and as predominantly unilateral or bilateral. Mediastinal nodes larger than 1.5 cm were considered enlarged.

Results

The chest radiographs in all patients showed patchy non-segmental areas of consolidation. In five out of six patients, the consolidation was most marked in the mid and upper lung zones, and in one patient it involved mainly the mid and lower lung zones. One case showed a classic peripheral pattern, however the diagnosis of chronic eosinophilic pneumonia was not initially entertained because of concern for an infectious cause. In three cases, patchy air-space consolidation was present with a slight peripheral predominance. In only one of these three patients was the peripheral predominance noticed before the CT scan. However, this was not sufficiently classic to allow a confident plain film diagnosis. Two cases did not show a recognizable peripheral pattern (Fig. 1A). Five radiographs outlined bilateral involvement, and one showed unilateral air-space consolidation. Open-lung biopsy in this case revealed coexistent chronic eosinophilic pneumonia and bronchiolitis obliterans organizing pneumonia.

CT scans unequivocally indicated the peripheral location of infiltrates in all six cases (Figs. 1 and 2). Although all patients



A



B

Fig. 2.—A, CT scan at level of tracheal carina shows bilateral air-space consolidation with a peripheral predominance.

B, High-resolution CT scan at same level better delineates normal from abnormal parenchyma. Two foci of consolidation are subsegmental, and one is 1.5-cm nodular density.

had areas of nonsegmental consolidation, three had additional areas of segmental or subsegmental consolidation and two had nodular areas of consolidation measuring 1–2.5 cm in diameter (Fig. 2). These were better delineated on CT scans than on radiographs. Thin-section scans obtained in two patients showed hazy peripheral densities, which were consistent with peripheral air-space disease (Fig. 2). Although thin-section CT allowed better delineation of normal from abnormal parenchyma it did not provide any additional information. In the patient with additional findings of bronchiolitis obliterans organizing pneumonia, the infiltrates appeared identical but were unilateral in distribution (Fig. 3). Mediastinal adenopathy was seen in three cases. A follow-up scan in one case with identical collimation showed dramatic improvement of the infiltrates and resolution of the mediastinal adenopathy within 2 weeks (Fig. 4).

Discussion

Chronic eosinophilic pneumonia was first described in 1969 [3]. Clinically, the patients present with coughing, weight loss, malaise, or shortness of breath. Life-threatening respiratory compromise may occur [4]. Radiologically, chronic eosinophilic pneumonia is characterized by the presence of homogeneous peripheral air-space consolidation. The pattern remains unchanged for days or weeks unless steroid therapy

is given. Eosinophilic pneumonia is exquisitely sensitive to steroids; lung infiltrates clear within days or weeks of institution of therapy. The combination of blood eosinophilia, peripheral infiltrates on the radiograph, and rapid response to steroid therapy is often sufficiently characteristic to obviate lung biopsy [5, 6].

The diagnosis is sometimes difficult because some patients have minimal blood eosinophilia and the peripheral distribution of infiltrates is not apparent on the plain film. A recent study indicates that the classic radiologic picture is seen in fewer than 50% of cases [1]. The nonperipheral distribution of infiltrates on the chest radiograph could be due to either true variation in the location of the infiltrates or could be a consequence of two-dimensional imaging of a three-dimensional organ. CT scans in our six cases clearly showed that the infiltrates were always peripheral and the failure to perceive this on the radiograph was due to limitations of the technique. The lack of superimposition of shadows on CT scans allows a better assessment of the distribution of infiltrates and determination of their preponderantly peripheral location. The peripheral consolidation on CT scans was illustrated previously in a single case report by Onitsuka et al. [7] and in the textbook by Fraser et al. [8]. The pattern of consolidation on the chest radiograph has been described classically as nonsegmental [8]. However, on CT scans, subsegmental and segmental areas of consolidation were present in three out of six cases and nodular areas of consolidation were present in two cases.

Open-lung biopsy in one patient showed chronic eosinophilic pneumonia in association with bronchiolitis obliterans organizing pneumonia [9]. The CT findings in this case differed only in the unilateral distribution of peripheral infiltrates. However, reports of bronchiolitis obliterans organizing pneumonia have commented on both unilateral and bilateral involvement [10].

The presence of peripheral air-space consolidation can only be considered suggestive of chronic eosinophilic pneumonia in the appropriate clinical setting, in a patient with eosinophilia. The radiologic appearance may be mimicked by a number of other conditions, including bronchiolitis obliterans organizing pneumonia and sarcoidosis [11]. The distribution of infiltrates is identical to that of Loeffler syndrome. In Loeffler syndrome, however, the pulmonary infiltrates are transient and shift in nature over days, whereas chronic eosinophilic pneumonia

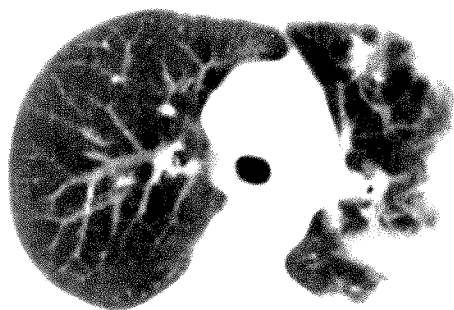


Fig. 3.—CT scan shows unilateral peripheral air-space consolidation. Patient had chronic eosinophilic pneumonia and coexistent bronchiolitis obliterans organizing pneumonia.

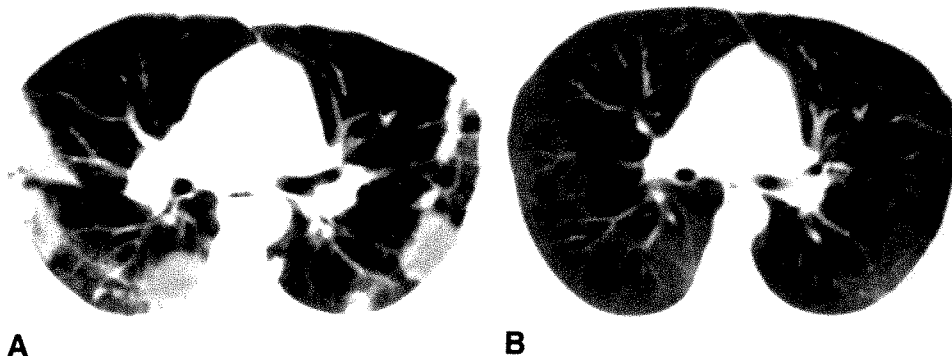


Fig. 4.—A, CT scan at level of bronchus intermedius shows peripheral air-space consolidation.

B, Follow-up CT scan after 2 weeks of steroid therapy shows marked improvement.

has a more protracted course, remaining unchanged over weeks or months. Indeed, in one of our patients the symptoms were of only 2 weeks duration, which would be compatible with Loeffler syndrome. As pointed out by Fraser et al. [8], some overlap occurs between the various eosinophilic lung diseases, and the differential diagnosis of Loeffler syndrome from chronic eosinophilic pneumonia is not critical because both respond readily to corticosteroid therapy.

The high prevalence of patients with atypical radiographic patterns in our series is probably due to patient selection. Patients with blood eosinophilia and air-space consolidation confined to the outer third of the lungs will most likely be diagnosed as having eosinophilic lung disease and treated without any further investigations. These patients are unlikely to undergo CT of the chest.

We conclude that CT is useful in the evaluation of suspected chronic eosinophilic pneumonia when the chest radiograph fails to show clearly the characteristic peripheral air-space consolidation.

ACKNOWLEDGMENT

We thank Pierce Wilcox for assistance in obtaining clinical data.

REFERENCES

1. Jederlinic PJ, Sicilian L, Gaensler EA. Chronic eosinophilic pneumonia: a report of 19 cases and a review of the literature. *Medicine* **1988**;67:154-162
2. Gaensler EA, Carrington CB. Peripheral opacities in chronic eosinophilic pneumonia: the photographic negative of pulmonary edema. *AJR* **1977**;128:1-13
3. Carrington CB, Addington WW, Goff AM, et al. Chronic eosinophilic pneumonia. *N Engl J Med* **1969**;280:787-798
4. Libby DM, Murphy TF, Edwards A, Gray G, King TKC. Chronic eosinophilic pneumonia: an unusual cause of acute respiratory failure. *Am Rev Respir Dis* **1980**;122:497-500
5. Perason DJ, Rosenow EC. Chronic eosinophilic pneumonia (Carrington's). A follow-up study. *Mayo Clin Proc* **1978**;53:73-78
6. Dines DE. Editorial: chronic eosinophilic pneumonia: a roentgenographic diagnosis. *Mayo Clin Proc* **1978**;53:129-130
7. Onitsuka H, Onitsuka S, Yokomizo Y, Matsuura K. Computed tomography of chronic eosinophilic pneumonia. *J Comput Assist Tomogr* **1983**;7:1092-1094
8. Fraser RG, Paré JAP, Paré PD, Fraser RS, Genereux GP, eds. *Diagnosis of diseases of the chest*. Philadelphia: Saunders, **1989**:1290-1298
9. McLoud TC, Epler GR, Colby TV, Gaensler EA, Carrington CB. Bronchiolitis obliterans. *Radiology* **1986**;159:1-8
10. Müller NL, Guerry-Force ML, Staples CA, et al. Differential diagnosis of bronchiolitis obliterans with organizing pneumonia and usual interstitial pneumonia: clinical, functional, and radiologic findings. *Radiology* **1987**;162:151-156
11. Glazer HS, Levitt RG, Shackelford GD. Peripheral pulmonary infiltrates in sarcoidosis. *Chest* **1984**;86:741-744

Gastric Fluid Detected by Sonography in Fasting Patients: Relation to Duodenal Ulcer Disease and Gastric-Outlet Obstruction

Robin H. M. Smithuis^{1,2}
J. Odo Op den Orth¹

We correlated the amount of gastric fluid identified by sonography in 143 fasting patients with the presence of duodenal ulcer disease and gastric-outlet obstruction as seen on barium studies. Unselected consecutive patients who were referred for a barium study of the upper gastrointestinal tract were included in a double-blinded prospective study. Sonograms were obtained in the right lateral decubitus position to allow gastric fluid to accumulate in the antrum, where it was quantified by measuring the maximal cross-sectional area of antral fluid in square centimeters. Sonograms revealed no fluid or a small amount ($<5 \text{ cm}^2$) in 87 (61%) of the patients and a large amount of fluid ($\geq 5 \text{ cm}^2$) in 56 patients (39%). Barium examinations showed a duodenal ulcer in 26 (46%) of the 56 patients with sonographic evidence of a large amount of gastric fluid compared with 10 patients (11%) in the group with little or no fluid on sonography ($p = .001$). Sonographic evidence of a large amount of fluid was found in all five patients who had gastric-outlet obstruction on barium examination ($p = .02$).

The detection of a large amount of fluid in the stomach on sonography appears to be a feature of duodenal ulcer disease and gastric-outlet obstruction.

AJR 153:731-733, October 1989

An excess of gastric fluid in the stomach of fasting patients is suggestive either of gastric hypersecretion, a finding that accompanies duodenal ulcer, or of a gastric-outlet obstruction [1-4]. We used sonography to measure the amount of gastric fluid in a semiquantitative manner to determine if the technique could be used to identify patients with duodenal ulcer or gastric retention. Sonograms were obtained in 143 patients, and the results were correlated with the findings on barium examinations performed on these patients.

Subjects and Methods

One hundred fifty-five consecutive patients who were referred for barium studies of the upper gastrointestinal tract were included in the study. There were 82 men and 73 women, aged 15-86 years (mean age, 53 years). Informed consent was obtained in each case.

After an overnight fast, a sonogram of the abdomen was obtained by a radiologist who had no knowledge of the patient's clinical status. Scans were obtained with a Sonolayer SSA-100A (Toshiba Medical Systems Europe, Delft, the Netherlands) with a 3.5-MHz convex array probe. Patients were examined in the right lateral decubitus position with the head of the table slightly raised. In this position, gastric fluid accumulates in the antrum and gas moves to the fundus (Figs. 1A and 1B).

Adequate sonographic visualization of the antrum was possible in all but five patients. One was morbidly obese, two had large amounts of air in the upper abdomen, and two patients had undergone a partial distal gastrectomy. Seven other patients had to be excluded from the study, because they had been eating or drinking before the examination (chewing gum included, because it stimulates saliva production).

In order to quantify the amount of fluid in the stomach, the maximal cross-sectional area of the antral fluid, assessed in a transverse plane, was measured in square centimeters. The

Received March 13, 1989; accepted after revision May 5, 1989.

¹ Department of Radiology, St. Elisabeth's of Groote Gasthuis, P.O. Box 417, 2000 AK Haarlem, the Netherlands.

² Present address: Department of Radiology, University Hospital Leiden, P.O. Box 9600, 2300 RC Leiden, the Netherlands. Address reprint requests to R. H. M. Smithuis.

0361-803X/89/1534-0731
© American Roentgen Ray Society

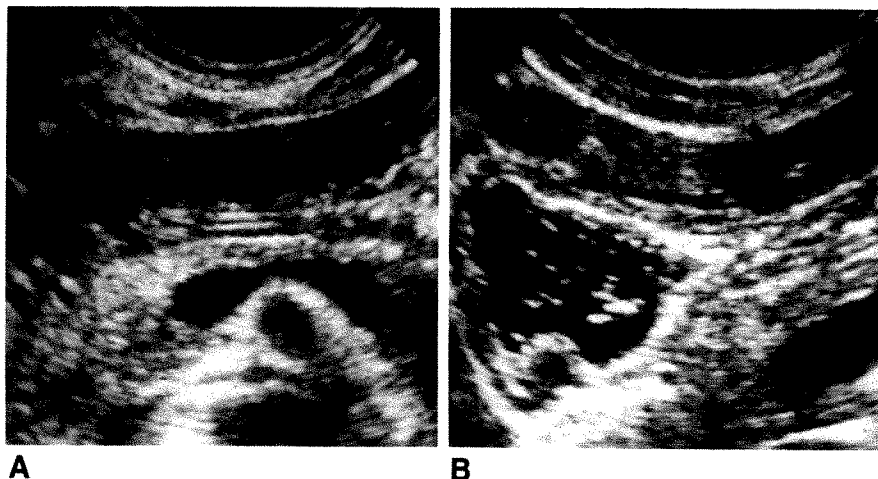


Fig. 1.—Sonograms show gastric fluid in fasting patient.

A, Transverse sonogram of supine patient shows gastric walls in apposition. No fluid can be seen in stomach.

B, Transverse sonogram of same patient in right lateral decubitus position shows fluid in gastric antrum.

measurements were obtained electronically on the sonography unit after tracing around the fluid collection manually with the cursor.

Patients were assigned to one of four categories, depending on the area of antral fluid: 0, <5 , 5–10, and ≥ 10 cm^2 . Patients in the first two categories (<5 cm^2) were regarded as having a small amount of gastric fluid, and patients in the last two categories (≥ 5 cm^2) were regarded as having a large amount of gastric fluid. An antral fluid area of 5 cm^2 was chosen prospectively as a breakpoint, because during the sonographic examination this subjectively seemed to be a breakpoint between small and large collections of gastric fluid. No attempt was made to discover the breakpoint that produced the best statistical results.

A standard biphasic examination of the stomach and duodenum with glucagon was performed within 1 hr by another radiologist, who was unaware of the sonographic findings [5–7].

The results of the two procedures were analyzed. Patients with large amounts of gastric fluid were compared with patients with small amounts for presence of duodenal ulcer and gastric-outlet obstruction. In both cases, the 2×2 tables were analyzed with the chi-square test.

Results

The sonographic examinations in 55 (38%) of the 143 patients showed no detectable fluid in the stomach. Thirty-two patients (22%) had a gastric fluid collection of which the cross-sectional area on the transverse sonogram measured less than 5 cm^2 . In 24 patients (17%), the fluid area measured 5–10 cm^2 , and in 32 patients (22%), it measured more than 10 cm^2 .

The distribution of the duodenal ulcers among the patients with different amounts of fluid in the stomach is shown in Figure 2, in which the patients with gastric-outlet obstruction also are included. The frequency of duodenal ulcer in patients who had large amounts of gastric fluid (antral fluid area ≥ 5 cm^2) differed significantly from the frequency of duodenal ulcer in patients who had small amounts of gastric fluid (antral fluid area <5 cm^2) ($p = .001$).

The biphasic contrast examination detected seven gastric ulcers and four gastric carcinomas (biopsy proved). Most of these patients had no gastric fluid, but in four cases there was a complicating gastric-outlet obstruction. Those four

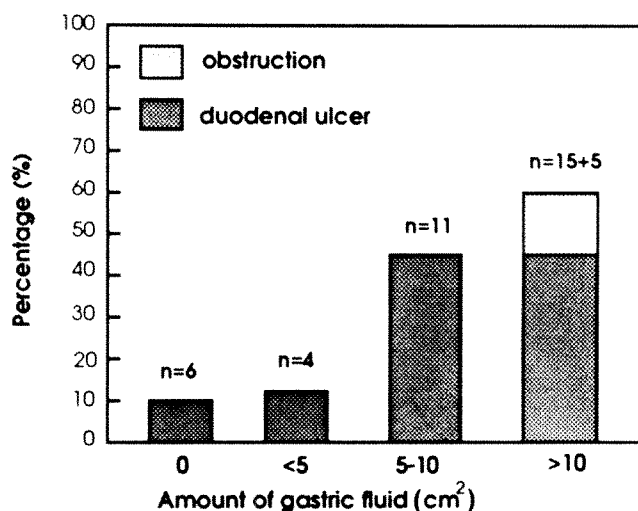


Fig. 2.—Prevalence of duodenal ulcer and gastric outlet obstruction in relation to amount of gastric fluid measured as antral fluid area.

patients all had a large amount of gastric fluid. The obstruction was found to be caused by a pyloric ulcer with stenosis in two cases and by an antral carcinoma with stricture in the other two cases. In the total study group, one other patient had an obstruction. The obstruction was located in the horizontal part of the duodenum and was caused by hematoma formation around an aortic prosthesis. This patient also had a large amount of fluid in the stomach.

In the total study group, 56 patients had a large amount of gastric fluid. Twenty-five (45%) of these patients had neither a duodenal ulcer nor gastric-outlet obstruction. The barium studies in the latter group revealed two gastric ulcers and one gastric ulcer scar.

Discussion

In the fasting patient, the amount of fluid in the stomach depends on gastric secretion, saliva production, pyloric

losses, and duodenogastric reflux [1]. A large amount of fluid usually indicates gastric hypersecretion or gastric-outlet obstruction [2]. In 1932, Henning and Norjsoth [8] reported that the amount of gastric juice aspirated overnight in patients with duodenal ulcer disease was greater than that in normal subjects. Approximately 30–40% of patients with duodenal ulcer disease are true hypersecretors and have acid and volume secretion rates above the upper limits of normal, with the highest output of basal gastric secretion in the morning (5–11 a.m.) [4]. As many patients with a duodenal ulcer have a maximal gastric secretion within the normal range, gastric secretory tests as a single examination are of limited value in the diagnosis of a duodenal ulcer in the individual patient [3]. The purpose of this study was not to investigate whether a duodenal ulcer could be diagnosed by sonography, but to determine if sonography could be used to select patients with a predilection for duodenal ulcer or gastric-outlet obstruction.

The right lateral decubitus position proved to be superior for the detection of gastric fluid. The supine position is not useful, because in this position most of the fluid is in the gastric fundus, where it is often obscured by overlying gas.

To estimate the amount of gastric fluid, we measured the maximal cross-sectional area of the gastric antrum. This method was easy and seemed to be adequate to determine whether a small or a large amount of gastric fluid was present.

The sonographic detection of a large amount of gastric fluid in our patients was associated with a significantly higher prevalence of duodenal ulcer and gastric-outlet obstruction. In the group with the largest amount of gastric fluid (antral fluid area $>10 \text{ cm}^2$), 61% of the patients had either a duodenal ulcer or a gastric-outlet obstruction (Fig. 2).

The practical implications of the results of our study are not unequivocal and cannot simply be translated to other patients. The patients included were referred because their general practitioner or clinician suspected upper gastrointestinal disease, and the high prevalence of duodenal ulcers in

this group of patients has its influence on our results. Thirty-six (25%) of 143 patients in the series had duodenal ulcer shown on the barium studies. This high rate exceeds the number of duodenal ulcers we found recently in another study at our institution, but no extra selection criteria have been used [5]. The results of our study justify undertaking a subsequent study of the correlation between large amounts of fluid and gastric or duodenal disease in a general sonography referral population. The results of that study would indicate what a sonographer should recommend when large amounts of gastric fluid are detected in a patient from an unselected population.

ACKNOWLEDGMENT

The authors thank J. Hermans of the Department of Medical Statistics of the University of Leiden for the statistical analysis.

REFERENCES

1. Hobsley M, Whitfield PF, Faber RG, Parkin JV. Hypersecretion and length of history in duodenal ulceration. *Lancet* 1975;2:101–104
2. Sum DCH, Roth JLA. Tests employed in analysis of the stomach contents and their clinical application. In: Bockus HL, ed. *Gastroenterology*, 3d ed. Philadelphia: Saunders, 1974:419–453
3. Isenberg JL. Gastric secretory testing. In: Sleisenger MH, Fordtran JS, eds. *Gastrointestinal disease*, 2d ed. Philadelphia: Saunders, 1978:714–732
4. Konturek SJ. Gastric secretion: physiological aspects. In: Duthie HL, Wormsley KG, eds. *Scientific basis of gastroenterology*. Edinburgh: Churchill Livingstone, 1979:133–162
5. Dekker W, Op den Orth JO. Biphasic radiologic examination and endoscopy of the upper gastrointestinal tract: a comparative study. *J Clin Gastroenterol* 1988;10:461–465
6. Op den Orth JO, Ploem S. The standard biphasic-contrast gastric series. *Radiology* 1977;122:530–532
7. Op den Orth JO. *The standard biphasic-contrast examination of the stomach and duodenum*. The Hague: Nijhoff, 1979:11–13
8. Henning N, Norjsoth L. Die Magensekretion während des Schlafes. *Dtsch Arch Klin Med* 1932;172:558–563

Videotape Review

RSNA Today, Vol. 3, No. 1. Oak Brook, IL: The Radiological Society of North America, 1989. \$75; by subscription, 4 issues annually at \$225 for RSNA members and \$275 for nonmembers (VHS videotape)

This videotape consists of four segments: a review of interesting technical exhibits at the annual meeting of the Radiological Society of North America (RSNA), a review of award-winning scientific exhibits, a discussion of sonographic aspects of congenital hip dysplasias, and a discussion of Magnevist and its use in MR imaging. In the first part, Joel Gray, chairperson of the committee to evaluate technical exhibits, interviews various vendors in an attempt to highlight specifically those innovations leading to more efficient and less expensive useful new products. Products discussed are a small, self-shielded MR imager that fits into a CT room, a multiformat camera capable of imaging from three different imagers, and a new CT scanner that can fit into 260 sq ft (23.4 m²) and costs no more than a radiographic and fluoroscopic room. Stanley Siegelman then interviews Dr. Gray about questions to ask when purchasing a CT scanner, such as price, dose, speed, cost, size, and installation time. Anthony Proto then reviews the 78 scientific exhibits that received awards at the past RSNA, with a closer look at the four magna-cum-laude winners.

Danielle K. P. Boal then reviews sonography of congenital hip dysplasia. She discusses etiology, pathophysiology, and treatment of this disease along with the advantages (e.g., no radiation, real time) and disadvantages of sonographic examination. Techniques of examination are discussed also, with a helpful real-time demonstration, and Edward Schwentker makes a few comments on the clinical usefulness of sonography.

The last part of the tape is a discussion of Magnevist (gadolinium-DTPA) by Robert Brasch, Gerald Wolf, William Bradley, Jr., and Gordon Sze. The group discusses factors concerning the usefulness of gadolinium, similarities and differences with iodinated contrast material, relaxivity, biodistribution, toxicity, cost, pharmacology, and a postrelease survey on side effects. Indications and contraindications for the use of this drug are discussed also, as are potential areas of usefulness outside the CNS.

The discussion of the technical exhibits is interesting and informative. Of particular note is the fact that equipment is, to some extent, becoming less expensive. Some useful hints are put forth if the viewer happens to be in the market for new equipment. The review of scientific exhibits, although brief, is quite interesting and informative. The part on sonography of the dysplastic hip is well done. The real-time demonstration of the performance of the procedure and the sonographic anatomy is excellent. The discussion on Magnevist is quite interesting and answers many questions about the present uses and potential future uses of gadolinium. In all, the tape is well done, and I recommend it to radiologists, especially those interested in the various fields covered under these topics.

Hano A. Siegel
Mercy Hospital
San Diego, CA 92103

Positive Predictive Value and Posttest Probability of Diagnosis of Colonic Polyp on Single- and Double-Contrast Barium Enema

David J. Ott¹
Eric S. Scharling¹
Yu Men Chen¹
David W. Gelfand¹
Wallace C. Wu²

The positive predictive value for a radiographic diagnosis of colonic polyp, the prevalence of polypoid disease, and posttest probability relative to patient age were studied. The positive predictive value for colonic polyp on single- and double-contrast barium enema was determined for 191 polyps found radiographically in 136 patients who also underwent colonoscopy for confirmation. Of 72 polyps seen in 54 patients on single-contrast examination, 59 were confirmed endoscopically; 110 of 119 polyps seen in 82 patients on double-contrast examination were confirmed similarly, giving positive predictive values of 82% and 92%, respectively. Positive predictive values per patient, disregarding the number of polyps present, were 87% (47/54) and 90% (74/82) for the single- and double-contrast examinations, respectively. False-positive errors were due to stool, air bubbles, haustration, and misinterpretation of an appendiceal stump.

By using specificities derived from our prevalence of polypoid disease and previously reported sensitivities, we drew posttest probability curves showing that predictive values depend both on the chance of disease before the test is done and on the efficacy of the test used.

AJR 153:735-739, October 1989

Although the sensitivity of the barium enema for polypoid disease has been studied extensively, its positive predictive value and posttest probability have received less attention. The positive predictive value and posttest probability for a radiographic diagnosis of colonic polyp are important clinically because they represent the likelihood that a lesion seen by barium enema truly exists. In an earlier study, we determined the positive predictive value of a diagnosis of colonic polyp on the double-contrast barium enema [1]. However, the positive predictive value of the single-contrast barium enema was not investigated, despite the fact that about two thirds of barium enemas done in this country are single-contrast examinations [2]. Therefore, we evaluated the positive predictive values and posttest probabilities for single- and double-contrast barium enemas for the diagnosis of colonic polyps.

Materials and Methods

The radiographic and endoscopic records for a 4-year period were reviewed, and 136 consecutive patients who underwent colonoscopy and had one or more colonic polyps identified by barium enema were studied. All examinations were done at our institution. The single-contrast barium enema was used in 54 patients (28 women; 26 men) with a mean age of 68 years, and double-contrast enema was used in 82 patients (28 women; 54 men) with a mean age of 59 years. Patients were selected for the single-contrast examination on the basis of advanced age, debility, difficulty in retaining a cleansing enema, or a combination of these factors [2].

Colonic preparation for the barium enema was standardized for all patients and included a 24-hr liquid diet, oral hydration, 296 ml magnesium citrate, 59 ml castor oil, and a 2000 ml tap-water enema on the morning of the examination. For the single-contrast barium enema,

Received March 4, 1989; accepted after revision May 30, 1989.

¹Department of Radiology, Bowman Gray School of Medicine, Wake Forest University, Winston-Salem, NC 27103.

²Department of Medicine, Bowman Gray School of Medicine, Wake Forest University, Winston-Salem, NC 27103.

0361-803X/89/534-0735
© American Roentgen Ray Society

a dilute 18% wt/vol barium suspension (Liquid Sol-o-pake, E-Z Em Co., Westbury, NY) was used. Glucagon (0.5 mg IV) was used at the discretion of the examining radiologist. An average of four large and eight small radiographs was obtained, with all accessible areas of the colon compressed on the small films. For the double-contrast enema, a high-density 100% wt/vol barium suspension (Liquid Polibar, E-Z Em Co.) was used, and each patient received 0.5 mg glucagon IV. An average of five large and nine small radiographs was obtained.

Colonoscopy was done with Olympus instruments (Olympus Corp., Lake Success, NY) of various types. After the barium enema, all polyps 5 mm or larger were tabulated. Size determination was based on direct radiographic measurements. The lesions reported radiographically were divided into two size categories: 5–10 mm and larger than 10 mm. Polyps smaller than 5 mm were excluded from the study because we do not routinely report these lesions radiographically, for reasons previously stated [3].

After review of all the barium enema studies and colonoscopic results, the radiographic positive predictive values for individual polyps and patients were calculated. The probable causes for the false-positive errors also were analyzed. Discrepancies between the radiographic and endoscopic findings were resolved by repeated endoscopy, repeated barium enema, or review of the original radiographic study [1, 4]. A radiographic false-positive result was scored retrospectively if the suspected lesion was inconsistent on the available views of the area or if the finding was obviously feces, a diverticulum, an air bubble, or misinterpreted normal anatomy.

At the same time, we reviewed all of our barium enema reports to determine the prevalence of polypoid disease diagnosed on our single- and double-contrast examinations. As most of these patients did not undergo colonoscopy, the initial prevalence figures were refined by determining false-positive and false-negative fractions from our positive predictive values per patient and previously reported sensitivities [5]. By using these various values, we calculated the specificity of our barium enema examinations with the derived formula below [6]:

$$s = \frac{(P)(S)(PPV - 1)}{PPV(1 - P)} + 1$$

where s = specificity, P = prevalence, S = sensitivity, and PPV = positive predictive value. Posttest probability of polypoid disease of the colon when the barium enema yields a positive diagnosis could then be determined by using these sensitivities and specificities [7–10].

Results

For the single-contrast barium enema, 59 of 72 reported lesions were confirmed, giving a positive predictive value of 82%. For 5- to 10-mm polyps, the positive predictive value was 79% (33/42); for polyps greater than 10 mm, it was 87% (26/30). For the double-contrast barium enema, 110 of 119 reported lesions were confirmed, giving a positive predictive value of 92%. For 5- to 10-mm polyps, the positive predictive value was 94% (84/89); for lesions greater than 10 mm it was 87% (26/30). Chi-square analysis showed a statistically significant difference ($p < .05$) in predictive values between the barium enemas for 5- to 10-mm polyps. The positive predictive values per patient, disregarding the number of polyps present, were 87% (47/54) and 90% (74/82) for the single- and double-contrast examinations, respectively ($p > .05$).

False-positive errors were due to air bubbles, stool, diverticula, haustration, and misinterpretation of an appendiceal stump. Of the 13 false-positive errors on the single-contrast examination, six (46%) were due to stool (Fig. 1), five (38%) due to air bubbles (Fig. 2), and two (15%) due to misinterpretation of diverticula and normal anatomy. Of the nine false-positive errors made on the double-contrast examination, six (67%) were due to stool (Fig. 3), two (22%) resulted from confusion of haustral anatomy, and one (11%) was from misinterpretation of an appendiceal stump.

The 22 false-positive errors were distributed widely throughout the colon (Fig. 4). For the single-contrast barium enema, two (15%) errors were made in the cecum and ascending colon; two (15%) in the transverse colon; six (46%) in the descending colon/sigmoid junction; and three (23%) in the rectosigmoid area. Errors due to stool were scattered throughout the colon, whereas those due to air bubbles were mainly in the rectosigmoid and descending colon/sigmoid area. For the double-contrast enema, three (33%) errors were made in the cecum and ascending colon; two (22%) in the transverse colon; one (11%) in the descending colon; and three (33%) in the rectosigmoid area. Errors due to stool were also scattered throughout the colon in the double-contrast studies, whereas those for misinterpretation of haustral anatomy were limited to the sigmoid colon.

The prevalence rates for polypoid disease of the colon in our radiographic population were 8.6% (86/997) and 15.0% (142/947) for the single- and double-contrast barium enema, respectively. By using the patient positive predictive values (87% and 90%) and sensitivities per patient of 93% and 95% for the single- and double-contrast examinations derived from another report [5], we calculated the adjusted prevalence rates to be 8.1% (81/997) and 14.3% (135/947). The specificities calculated from the formula shown earlier are 99% for the single-contrast barium enema and 98% for the double-contrast examination.

Posttest probability of polypoid disease of the colon when the barium enema yields a positive diagnosis is derived from Bayes's theorem and depends on the chance of disease (i.e., pretest probability) before the test is done and on the sensitivity and specificity of the test used [7–10]. By using simple formulas [10] with the sensitivities and specificities derived above, one can show the posttest probability of polypoid disease after a positive radiographic diagnosis to relate graphically to its pretest probability, which depends largely on the age-related prevalence of colonic polyps (Fig. 5). As the prevalence of polypoid disease increases (i.e., as patients age), a correct diagnosis of colonic polyp on barium enema is more likely.

Discussion

In an earlier report on the double-contrast barium enema, we had an 87% positive predictive value for the diagnosis of colonic polyp [1]. In the present study, the positive predictive values for both types of barium enema examination were compared, the causes of error analyzed, and posttest prob-

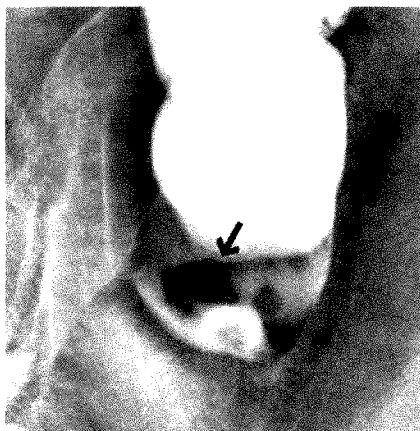
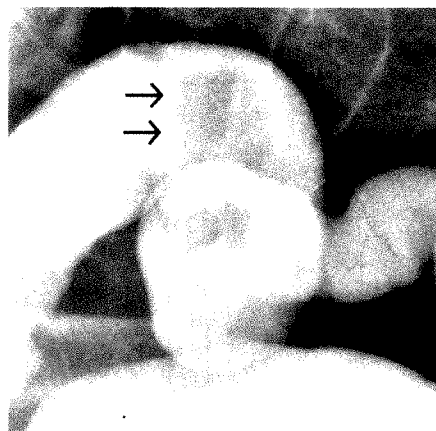
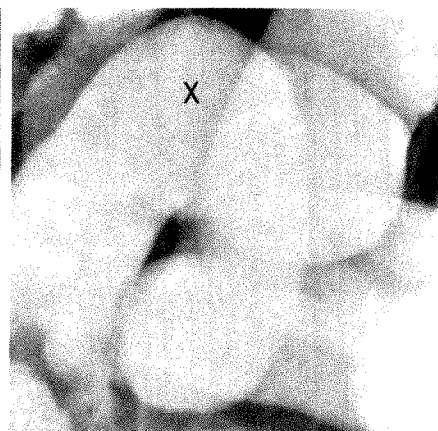


Fig. 1.—Radiograph of sigmoid-descending colon junction after single-contrast barium enema shows a polygonal filling defect (arrow) misinterpreted as a polyp. Two smaller spherical defects laterally are air bubbles.



A



B

Fig. 2.—Radiograph of rectosigmoid region after single-contrast examination with patient in supine left posterior oblique position (A). A large spherical defect (arrows) was identified as a polyp but was not seen in same area (x) on film of prone patient (B).

Fig. 3.—A and B, Radiograph (A) of mid ascending colon after double-contrast enema shows small filling defect (arrow) identified as a polyp. Another view (B) of same area (x) was normal.



A



B

abilities calculated. The positive predictive value for colonic polyps on the single-contrast examination was 82% compared with 92% for the double-contrast barium enema. This difference was significant statistically because of the better predictive value (94% vs 79%) found on the double-contrast examination for 5- to 10-mm polyps. The positive predictive values per patient, however, were not significantly different (87% vs 90%).

Stool was found to be the most common cause of error, accounting for 55% (12/22) of all false-positive diagnoses. Surprisingly, the presence of air bubbles was a cause of five (38%) of the 13 predictive errors made on the single-contrast barium enema, but was not a problem on the double-contrast examination. Indeed, the overall predictive value for the single-contrast study rises to 88% by eliminating errors from air bubbles. Few (23%) of the false-positive errors were due to diverticula or misinterpretation of normal or surgically altered anatomy.

The importance of stool as a cause of false-positive errors must be emphasized. If thorough colonic cleansing is not achieved consistently, the efficacy of any barium enema suffers. The high specificities of our colonic examinations reflect excellent bowel preparation and also our practice of ignoring most filling defects smaller than 5 mm [3]. All patients in this study had an identical colon-cleansing regimen, regardless of the type of barium enema done. In an earlier study to determine the effectiveness of this regimen, a clean colon was found in 97% of 500 patients reviewed [11]. Studies in which the preparation of the colon does not combine various components of this type of regimen effectively will be more prone to radiographic error.

The distribution of false-positive diagnoses was similar for both examinations except that nearly half of the errors made on the single-contrast barium enema occurred in the region of the descending-sigmoid colon. This area was particularly troublesome for misinterpretation of air bubbles as polyps on

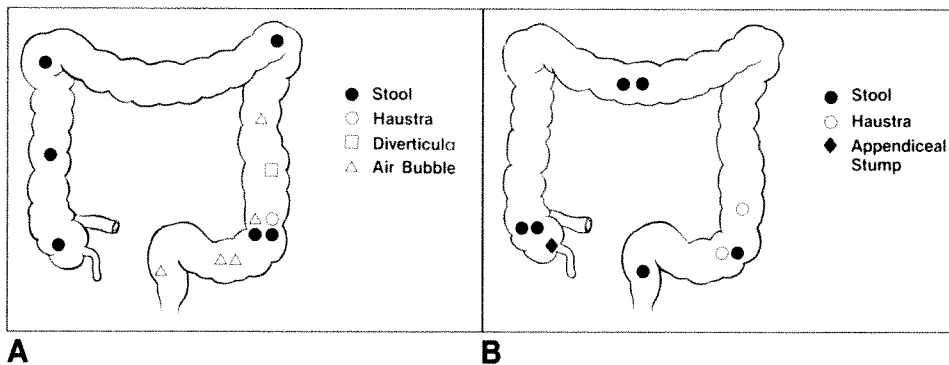


Fig. 4.—A, Distribution of 13 false-positive errors made on single-contrast barium enema.

B, Distribution of nine false-positive errors made on double-contrast barium enema.

the single-contrast examination. With the patient supine, the anteroposterior orientation of the sigmoid-descending colon junction leads to local entrapment of air that may simulate a polyp on the barium-filled colon. Repeated filming with the patient prone or erect usually solves this problem. The sigmoid colon, with its redundancy, also was an important site of radiographic error, as has been well shown [1, 2, 4, 12–14].

Another explanation for the somewhat poorer predictive value of the single-contrast barium enema for smaller colonic polyps may be the age and physical condition of the patients examined. Single-contrast examinations were done on older

and often more debilitated individuals. In an earlier investigation analyzing the sensitivity of the barium enema relative to age of the patient, both examinations showed poorer detection of colonic polyps smaller than 1 cm in patients 70 years old or more [15]. Similarly, in the current investigation, the statistically significant difference in predictive values between the single- and double-contrast barium enemas occurred with the 5- to 10-mm polyps. Excellent bowel preparation and effective positioning and spot-filming with compression are more difficult to accomplish consistently in older patients [2, 11, 15].

The results of this study may be better appreciated by discussing the posttest probability of polypoid disease of the colon when the barium enema yields a positive diagnosis [7–10]. Probability analysis is important because predictive values for colonic polyps are only approximate estimates of the likelihood of disease if the age of the patient and the efficacy of the examinations used are not considered [16]. Posttest probability depends on the chance of disease before the test is done and on the sensitivity and specificity of the test used. The prevalence of polypoid disease of the colon determines its pretest probability and depends primarily on the age of the patient examined. The reported prevalence of colorectal polyps has ranged from 9.5% to 61%, with a mean of 30% [17]. In a composite average of four necropsy reports, the prevalence of colonic adenomas was less than 10% in patients under 40 years old, but gradually increased to 40% by the age of 70 years [18]. In more recent colonoscopic surveys, even higher prevalences were found in the elderly [3].

By using our sensitivities and specificities for single- and double-contrast barium enemas, we found that posttest probability of having polypoid disease after a positive diagnosis varies with the expected age-dependent prevalence of colonic polyps (Fig. 5). The curves show how the chances of having polypoid disease of the colon after a positive barium enema result increases dramatically for prevalence rates above 10%, which occur in patients over 40 years old. For those less than 40 years old, with a low chance of having colonic polyps, the reliability of a positive radiographic diagnosis falls abruptly for both barium enema examinations. For those over 40 years old, a positive diagnosis of colonic polyp is an excellent predictor of the presence of disease. These curves may vary dramatically if different sensitivities and specificities are used [10]. In particular, lower specificities strongly affect the interpretation of a positive test and would shift these curves downward and to the right (Fig. 5).

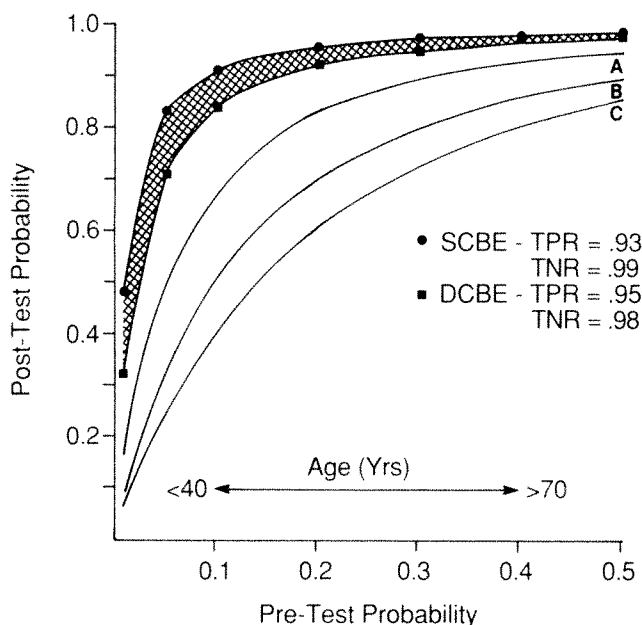


Fig. 5.—Relationship of pretest and posttest probability of a positive diagnosis of polypoid disease of colon determined by using the true-positive rates (TPR) (i.e., sensitivity) and true-negative rates (TNR) (i.e., specificity) shown for single-contrast (SCBE) and double-contrast (DCBE) barium enemas. Pretest probability is expected prevalence of disease before test is done, which mainly depends on age. Patients younger than 40 years old have less than a 10% chance of polypoid disease before test is done, whereas those over 70 years old have a 40% or more prevalence before having barium enema. Two top curves (crosshatched together) were derived from data shown. Curves A, B, and C represent decreasing specificities of .95, .90, and .85, respectively, with sensitivity held constant at .95.

REFERENCES

1. Ott DJ, Ablin DS, Gelfand DW, Meschan I. Predictive value of a diagnosis of colonic polyp on the double-contrast barium enema. *Gastrointest Radiol* 1983;8:75-80
2. Gelfand DW, Chen YM, Ott DJ. Detection of colonic polyps on single-contrast barium enema study: emphasis on the elderly. *Radiology* 1987;164:333-337
3. Ott DJ, Gelfand DW, Wu WC, Munitz HA, Chen YM. How important is radiographic detection of diminutive polyps of the colon? *AJR* 1986;146:875-878
4. Weyman PJ, Koehler RE, Zuckerman GR. Resolution of radiographic-endoscopic discrepancies in colon neoplasms. *J Clin Gastroenterol* 1981;3[suppl 1]:89-93
5. Ott DJ, Scharling ES, Chen YM, Wu WC, Gelfand DW. Barium enema examination: sensitivity in detecting colonic polyps and carcinomas. *South Med J* 1989;82:197-200
6. Phillips WC, Scott JA, Blasczynski G. 1. How sensitive is "sensitivity"; how specific is "specificity"? *AJR* 1983;140:1265-1270
7. Patton DD. Introduction to clinical decision making. *Semin Nucl Med* 1978;8:273-282
8. Black WC, Armstrong P. Communicating the significance of radiologic test results: the likelihood ratio. *AJR* 1986;147:1313-1318
9. Doubilet PM. Statistical techniques for medical decision making: applications to diagnostic radiology. *AJR* 1988;150:745-750
10. Sox HC Jr. Probability theory in the use of diagnostic tests. *Ann Intern Med* 1986;104:60-66
11. Gelfand DW, Chen YM, Ott DJ. Colonic cleansing for radiographic detection of neoplasia: efficacy of the magnesium citrate-castor oil-cleansing enema regimen. *AJR* 1988;151:705-708
12. Ott DJ. Radiographic efficacy. In: Ott DJ, Wu WC, eds. *Polypoid disease of the colon*. Baltimore: Urban & Schwarzenberg, 1986:99-21
13. Ott DJ, Gelfand DW, Ramquist NA. Causes of error in gastrointestinal radiology. II. Barium enema examination. *Gastrointest Radiol* 1980;5:99-105
14. Kelvin FM, Gardiner R, Vas W, Stevenson GW. Colorectal carcinoma missed on double contrast barium enema study: a problem in perception. *AJR* 1981;137:307-313
15. Ott DJ, Chen YM, Gelfand DW, Wu WC, Munitz HA. Single-contrast versus double-contrast barium enema in the detection of colonic polyps. *AJR* 1986;146:993-996
16. Kundel HL. Disease prevalence and radiological decision making. *Invest Radiol* 1982;17:107-109
17. Wu WC. Clinical considerations. In: Ott DJ, Wu WC, eds. *Polypoid disease of the colon*. Baltimore: Urban & Schwarzenberg, 1986:31-42
18. Ott DJ, Gelfand DW. Colorectal tumors: pathology and detection. *AJR* 1978;131:691-695

Book Review

Antibodies in Radiodiagnosis and Therapy. Edited by Michael R. Zalutsky. Boca Raton, FL: CRC Press, 240 pp., 1989. \$124

This book, which has several contributing authors, describes the development of radiolabeled monoclonal antibodies for use in the diagnosis and treatment of cancer. As stated by the editor, the purpose of the book is to provide a basic background on various aspects of this development. The book is divided into 11 chapters. Chapter 1 is an introduction to tumor imaging in nuclear medicine. Chapter 2 gives a review of tumor cell biology, with an extensive list of references. Chapter 3 discusses the methods of production and purification along with some practical considerations of monoclonal antibodies for diagnosis and treatment of tumors.

Radioimmunoscinigraphy is covered in three chapters. Preclinical considerations are discussed in chapter 4. They include the importance of sensitivity and specificity of the monoclonal antibody, cellular location of the antigen, stability of the antigen-antibody complex, and kinetics of the monoclonal antibody-antigen interaction. Clinical evaluations are covered in chapters 8 and 9. Chapter 8 emphasizes regional deliveries of antibodies, such as those via lymphatics, intraperitoneal or intraarterial infusion, and injection into the CSF. Chapter 9 addresses clinical trials of IV administration of the radiolabeled antibody.

Chapter 5 reviews the state-of-the-art in radiohalogenated antibodies and suggests future directions. Chapter 6 discusses the choices

of radionuclides used in labeling, particularly labeling of antibodies with metals by using bifunctional chelates. Physiologic, pharmacologic, and immunologic aspects of antibody targeting are discussed in chapter 7. The last section of this book concentrates on antibody radiotherapy; current status is discussed in chapter 10 and future prospects in chapter 11. Chapter 10 is understandably short, as radiotherapy with antibodies is still in the embryonic stage.

The material presented in the book is thorough and detailed, and it does provide sufficient background on various aspects of the development of labeled monoclonal antibodies. The authors have done a good job in their evaluation of limitations of currently available technologies and approaches, as well as in their suggestions for future research. This book will be a valuable reference for those who are involved in radioimmunoscinigraphy and a worthy addition to nuclear medicine libraries.

Hing-Har Lo
University of Virginia
Charlottesville, VA 22908
Montgomery Radiology Associates, Inc.
Blacksburg, VA 24060

Primary Malignant Tumors in the Small Bowel: A Comparison of the Small-Bowel Enema and Conventional Follow-through Examination

Jeffrey R. Bessette^{1,2}
 Dean D. T. Maglinte³
 Frederick M. Kelvin³
 Stanley M. Chernish⁴

Of 71 patients diagnosed with primary mesenteric malignant tumors in the small bowel over a 21-year period in a community/teaching hospital, 14 underwent small-bowel follow-through, 16 underwent small-bowel enema (enteroclysis), and four patients underwent both studies preoperatively. In a retrospective study, the sensitivity of both the small-bowel enema and the conventional small-bowel follow-through examination were compared on the basis of the original radiologic interpretation. The studies were ordered by clinicians in a clinical setting. Results of the small-bowel follow-through were abnormal in 11 of 18 patients for a sensitivity of 61%, and small-bowel enema showed abnormalities in 19 of 20 patients for a sensitivity of 95% ($p = .0165$). The actual tumor was shown in six (33%) of 18 small-bowel follow-through studies and in 18 (90%) of 20 small-bowel enemas ($p = .0005$). In four patients, normal findings on conventional small-bowel follow-through were followed by abnormal findings on small-bowel enema done for the same reason.

This experience suggests that the small-bowel enema is more sensitive than the conventional follow-through examination for the detection of small-bowel cancers.

AJR 153:741-744, October 1989

The sensitivity of the small-bowel follow-through (SBFT) examination for detecting primary malignant tumors in the small bowel varies widely in the literature. Many studies are limited to a specific tumor type or combine the results of upper gastrointestinal (UGI) and SBFT examinations. Most include direct or indirect evidence of malignancy as criteria for an abnormal finding. SBFT findings have been reported to be abnormal in 53-83% of primary malignant tumors in the small bowel in several series [1-3], and direct evidence of a tumor was present in only 30-44% of cases [3, 4].

The literature includes a few case reports describing the diagnosis of primary malignant tumors in the small bowel by the small-bowel enema (SBE, enteroclysis); however, the sensitivity and the utility of this technique in showing the tumor have not been reported. The SBE has become the standard method of evaluating the small bowel at our institution during the past 12 years, although a modified SBFT is still used in a few cases. We retrospectively analyzed all primary malignant tumors of the small bowel diagnosed at our institution over the past 21 years. The sensitivity of the SBFT and the SBE were analyzed on the basis of both direct evidence (tumor-detection rate) and indirect evidence from the original radiologic interpretation.

Materials and Methods

All the examinations were performed by staff radiologists with various degrees of experience or by residents in various levels of training with staff supervision. The conventional SBFT examination included a series of overhead radiographs made at various intervals until the barium reached the right side of the colon, with spot filming of the terminal ileum.

Received February 3, 1989; accepted after revision May 15, 1989.

¹ Department of Radiology Education, Methodist Hospital of Indiana, Indianapolis, IN 46202.

² Present address: Department of Radiology, University of California, San Diego Medical Center, San Diego, CA 92103.

³ Departments of Radiology, Methodist Hospital of Indiana and Indiana University School of Medicine, Indianapolis, IN 46202. Address reprint requests to D. D. T. Maglinte, Dept. of Radiology, Methodist Hospital of Indiana, 1701 N. Senate Blvd., Indianapolis, IN 46202.

⁴ Department of Medical Research, Methodist Hospital of Indiana, and Dept. of Medicine, Indiana University School of Medicine, Indianapolis, IN 46202.

0361-803X/89/1534-0741
 © American Roentgen Ray Society

Fluoroscopy with manual compression was performed if an abnormality was suspected on the overhead radiographs. Thirteen SBFT examinations (72%) were performed at our institution.

Our method of performing the SBE has been described elsewhere [5]. Briefly, the small bowel is filled with a preselected amount and concentration of barium and methylcellulose infused through a nasoenteric tube with the tip positioned at the junction of the duodenum and jejunum. Single- and double-contrast compression radiographs of all segments of the small bowel are obtained under fluoroscopic control.

Seventy-one patients in whom primary malignant tumor of the small bowel was diagnosed over a 21-year period from 1967 to 1988 were identified through the medical records department. Ileocecal valve tumors and metastatic lesions were excluded. Lymphomas thought to have originated in structures other than the mesentery or small bowel were excluded. Thirty-four (48%) of 71 patients had undergone either an SBFT (14 patients), an SBE (16 patients), or both (four patients) and these 34 form the basis for this study. Patients having undergone only an UGI examination and/or a barium enema were not included.

The patients' charts were reviewed, and the original interpretation of the SBFT or SBE was recorded. All studies were ordered by clinicians in a clinical setting. In patients who underwent both studies, the SBFT preceded the SBE; the clinical indications were similar. Only studies that were considered satisfactory by the original interpreter were used. All SBEs were done after 1976; most SBFTs were done before 1976. History, physical examination, surgical findings, and pathology reports were obtained by reviewing charts. The malignant tumor was confirmed histologically in all cases.

For the tumor-detection rate (direct evidence), results of a study were considered abnormal if a mass was shown and a tumor was suggested on the original report. In some cases, the findings were suggestive of a tumor type; however, because the appearances of different tumor types overlap, a correct histologic diagnosis on the original interpretation was not required for tumor detection. The sensitivity was calculated irrespective of whether or not direct or indirect evidence of the tumor was reported. Indirect evidence included dilated bowel loops, strictures, adhesions, or fistulas. Thus findings from a study were considered abnormal even if the site of the lesion or the lesion itself was not detected (Figs. 1 and 2). Statistical significance was determined with Fisher's exact test for comparing the two techniques.

Results

Findings on SBFT were abnormal in 11 of 18 patients (sensitivity, 61%). A tumor was detected with the SBFT in only six of 18 patients (tumor-detection rate, 33%). Of the five studies with indirectly abnormal results, three were interpreted as showing dilated small-bowel loops, one as Crohn disease, and one as a nonspecific stricture. SBE findings were abnormal in 19 of 20 cases (sensitivity, 95%). A small-bowel tumor was identified on the radiograph after SBE in 18 (90%) of 20 patients. In one SBE with abnormal findings, a narrowed segment was interpreted as an adhesive band, but was found at laparotomy to be an adenocarcinoma (Fig. 2). The one patient with normal SBE results was found to have a 1-cm carcinoid in the midileum (Fig. 3). Two patients with adenocarcinoma, one with carcinoid, and one with lymphoma, had tumors visible on SBE after normal SBFT results. The other three patients with normal SBFT results had malignant

tumors diagnosed at surgery. The sensitivity and tumor-detection rate of the SBE were significantly better than the conventional SBFT ($p = .0165$ and $p = .0005$, respectively).

There were six SBFT and 10 SBE studies performed in patients with adenocarcinoma. The SBFT showed the tumor in two patients; findings were abnormal in two patients and were interpreted as normal in another two. The SBE showed the tumor in nine patients and showed indirect evidence of the tumor in the remaining case. The two patients with normal findings on SBFT were examined subsequently by SBE, at which time the tumor was shown. Of the 14 patients with adenocarcinoma, six had annular strictures, three had polypoid intraluminal masses, and five had ulcerating masses. Pain was a presenting symptom in 12 patients, bleeding in nine, obstruction in eight, and weight loss in nine. All patients had either bleeding or obstructive symptoms, but this combination was present only in three.

Of nine patients with carcinoid tumors, six of the lesions were submucosal and three presented as strictures. The submucosal lesions ranged in size from 1 to 3 cm. The SBE revealed the tumor in five of six patients, and SBE results were reported normal in one. Of the nine carcinoid patients, five had pain, four had bleeding, six had obstructive symptoms, and two had symptoms consistent with the carcinoid syndrome.

Six patients had leiomyosarcoma. SBFT results were abnormal in two patients, normal in one, and the tumor was identified in one. The SBE showed the tumor in two cases. The tumor was necrotic and ulcerated in five patients. Gastrointestinal bleeding was the major symptom in all but one patient. Pain was present in two. None was obstructed.

SBFT results were normal in two patients with lymphoma, two SBFTs showed lymphoma, and two SBEs showed the tumor. Four of the lymphomas were histiocytic and one was Hodgkin type. There were four masses and one annular type of tumor. Two of these patients had bleeding. The patient with the annular lesion had obstructive symptoms.

The SBE studies were all performed after 1976. Ten of the SBFT studies were done before 1976. Of the seven SBFT examinations with normal results, four were done after 1980. The three normal cases before 1980 were not available for review. In retrospect, an intussuscepting carcinoid tumor could be identified in one of the four SBFTs performed after 1980, whereas findings on the other three still were considered normal. Results of one SBE were normal; in retrospect, those results were found to be abnormal (Fig. 3). The retrospective results were not used in determining the sensitivity or the tumor-detection rate.

Discussion

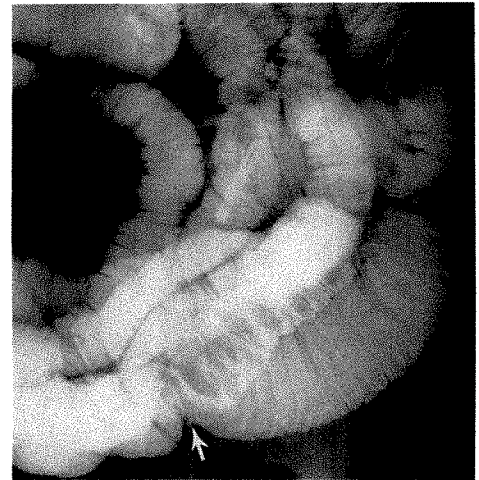
To our knowledge, this is the largest series of primary malignant tumors in the small bowel evaluated with SBE. The SBE in this study was more sensitive than the SBFT both in detecting an abnormality related to the tumor (95% vs 61%) and in depicting the tumor (90% vs 33%). The SBE has a higher sensitivity than does SBFT as reported in the literature.

Fig. 1.—90-min delayed radiograph after small-bowel follow-through examination shows dilated fluid-filled loops of jejunum and ileum. Neither precise point of obstruction nor actual tumor was identified. At surgery, malignant carcinoma was found in distal ileum, causing obstruction.



1

Fig. 2.—Radiograph after small-bowel enema shows partial obstruction caused by what was interpreted as an adhesive band. Patient had circumferential adenocarcinoma of proximal ileum. Both single- and double-contrast phases of study showed difference in caliber of small bowel proximal and distal to narrowing (arrow).

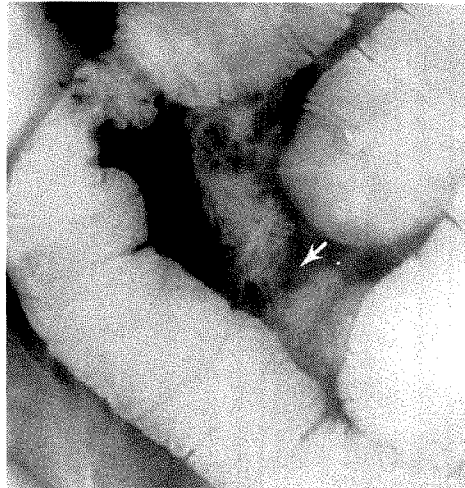


2

Fig. 3.—Small malignant carcinoid missed on small-bowel enema (SBE). Surgery disclosed a bleeding gastric carcinoid, missed by upper gastrointestinal endoscopy done before SBE, and a small ileal carcinoid. This was only false-negative SBE in this series.

A. Oblique radiograph with mild compression during methylcellulose infusion shows small intramural defect (arrow) in distal ileum.

B. Radiograph of supine patient shows persistence of intramural defect (arrow). Defect was noted on several compression radiographs.



A



B

A few small series of patients in whom SBE was used to diagnose small-bowel tumors have been reported. Findings on SBE were abnormal in five (83%) of six patients with malignant tumors in the small bowel [3] and 10 (91%) of 11 patients with lymphoma [6]. Eleven patients with carcinoid and SBE studies were reported, but the sensitivity was not addressed [7]. Ten of the patients in our study who were examined with SBE had adenocarcinomas; 10 (100%) of 10 SBEs had abnormal results and nine (90%) of 10 SBEs detected the tumor. Five (83%) of six carcinoid tumors were detected. In the few cases of leiomyosarcoma and lymphoma, the SBE detected the tumor.

Advantages of the SBE include the ability to test the distensibility of all segments of the small bowel, increased separation of small-bowel loops and a double-contrast see-through effect for evaluating the small-bowel folds, particularly in the pelvis where crowding and overlapping of segments are not infrequent. In obstructed patients, the enteroclysis tube can be used to decompress fluid-distended small-bowel

loops to facilitate the subsequent infusion study [8]. Areas of narrowing or stricture are not easily mistaken for peristalsis or spasm.

The comparison in this series may be considered biased in that a well-performed SBE study was compared with SBFT examinations of variable quality. There is, however, no selection bias on our part in this retrospective analysis because the studies were ordered by clinicians in a clinical setting. They may have been biased in their choice depending on which method they thought would be the most helpful to them. Undoubtedly, the SBE is of prominent interest at our institution. The conventional SBFT exams were performed by staff radiologists and residents with staff supervision before 1976. Four of the examinations with normal results done after 1976 were from smaller community hospitals. These four patients subsequently had abnormal findings on SBE. In retrospect, one SBFT had been misinterpreted. Of those SBFTs available for review, the examinations appear to have been technically adequate (a series of overhead radiographs

with spot films of the terminal ileum and of other segments suspected of being abnormal). Errors on both types of examinations may have been technical, interpretive, or both [9]. Whatever the reason, fewer errors were made with the SBE. More recently, we and others have found that use of a dedicated SBFT (the so-called "fluoroscopic" small-bowel meal) may result in a higher sensitivity of the oral small-bowel examination [10, 11]. Specifically, the performance of thorough compression with fluoroscopy and attention to technical details will improve the SBFT even though limitations of the SBFT related to physiology and anatomy of the gastrointestinal tract are not overcome. None of the SBFT examinations in this analysis were done in this manner. In each case, the original interpretation was used to determine the sensitivity. A retrospective analysis of the films would have been biased because the reviewer was fully aware that a tumor was present.

Few series in the literature have determined the sensitivity of the SBFT in diagnosis of primary mesenteric malignant tumors in the small bowel without including malignant tumors in the duodenum. Reported sensitivities for detecting any abnormality range from 53% to 83% [1-3]. The reported sensitivities for actual detection of tumor are lower, as low as 44% [3]. For specific kinds of tumor, reported sensitivities for indirect evidence of tumor vary with the tumor type; for example, adenocarcinoma 88% [12], carcinoid 40% [13], lymphoma 65% [14], and leiomyosarcoma 29-61% [15-17]. Some authors have reported the sensitivity of a combined UGI-SBFT for adenocarcinoma to be as high as 85-90% [18, 19]; however, these include a large percentage of duodenal lesions that were detected on the UGI study. These reportedly are easier to detect and do exclude other tumor types that have a lower sensitivity. Also, the sensitivity of actual tumor demonstration was not determined in these studies.

In one study, 14 of 29 false-negative results of SBFT examinations were abnormal in retrospect [1]. Most frequently, a narrowing initially was misinterpreted as a peristaltic wave, but overlapping loops, small lesions, and serosal lesions also resulted in false-negatives. Errors in the conventional SBFT have been shown to be primarily due to technical inadequacies (71%) rather than perceptive errors (29%) [9]. The specificities of the SBFT and the SBE were not determined in this study.

On the basis of our experience, we advocate the use of

SBE in patients clinically suspected of having a malignant tumor in the small bowel, particularly when chronic or intermittent abdominal pain with nausea and/or vomiting is present or if there is unexplained gastrointestinal bleeding [20].

REFERENCES

1. Vuori JVA, Vuorio MK. Radiological findings in primary malignant tumors of the small intestine. *Ann Clin Res* 1971;3:16-21
2. Miles RM, Crawford D, Duras S. The small-bowel tumor problem. *Ann Surg* 1979;189:732-740
3. Ekberg O, Ekholm S. Radiography in primary tumors of the small-bowel. *Acta Radiol [Diagn]* (Stockh) 1980;21:79-84
4. Zollinger RM, Sternfeld WC, Schreiber H. Primary neoplasms of the small intestine. *Am J Surg* 1986;151:654-658
5. Maglinte DDT, Herlinger H. Single contrast and biphasic enteroclysis. In: Herlinger H, Maglinte DDT, eds. *Clinical radiology of the small intestine*. Philadelphia: Saunders, 1989:107-118
6. Gourtsoyannis NC, Nolan DJ. Lymphoma of the small intestine: radiological appearances. *Clin Radiol* 1988;39:639-645
7. Jeffrey MA, Barter SJ, Hemingway AP, Nolan DJ. Primary carcinoid tumors of the ileum: the radiological appearances. *Clin Radiol* 1984;35:451-455
8. Maglinte DDT. Small intestinal obstruction: contrast examination. In: Margulis A, Gooding C, eds. *Diagnostic radiology 1988*. San Francisco: Radiology Research and Education Foundation UCSF; 1988:65-76
9. Maglinte DDT, Burney BT, Miller RE. Lesions missed on small-bowel follow-through: analysis and recommendations. *Radiology* 1982;144:727-729
10. Herlinger H, Maglinte DDT. Nonintubation barium methods. In: Herlinger H, Maglinte DDT, eds. *Clinical radiology of the small intestine*. Philadelphia: Saunders, 1989:71-83
11. Maglinte DDT, Lappas JC, Kelvin FM, et al. Small bowel radiography: how, when and why? *Radiology* 1987;163:297-305
12. Williamson RCN, Welch CE, Malt RA. Adenocarcinoma and lymphoma of the small intestine. *Ann Surg* 1983;197:172-178
13. Moertler CG, Saner WG, Dopcherty MB, Baggenstoss AH. Life history of the carcinoid tumor of the small intestine. *Cancer* 1961;14:901
14. Faulkner JW, Dockerty MB. Lymphosarcoma of the small intestine. *Surg Gynecol Obstet* 1952;95:76-84
15. Chiotasso PJP, Fazio VW. Prognostic factors of 28 leiomyosarcomas of the small intestine. *Surg Gynecol Obstet* 1982;155:197-202
16. Skandalakis JE, Gray SW. Smooth muscle tumors of the alimentary tract. In: Arief IM, ed. *Progress in clinical cancer*. New York: Grune and Stratton, 1965:692-708
17. Starr GF, Dockerty MB. Leiomyomas and leiomyosarcomas of the small intestine. *Cancer* 1955;8:101-111
18. Ouriel K, Adams JT. Adenocarcinoma of the small intestine. *Am J Surg* 1984;147:66-71
19. Bruneton JN, Drouillard J, Bourry J, Roux P, Lecomte P. L'adénocarcinome de l'intestin grêle. Etat actuel du diagnostic et du traitement. Etude de 27 cas et revue de la littérature. *J Radiol* 1983;64:117-123
20. Maglinte DDT, Hall R, Miller RE, et al. Detection of surgical lesions of the small-bowel by enteroclysis. *Am J Surg* 1984;147:225-229

Case Report

Typhoid Fever: Diagnosis by Using Sonography

Julien B. C. M. Puylaert,¹ Sjöfn Kristjánsdóttir,² Karen L. Golterman,³ Gerard M. de Jong,³ and Nelly M. Knecht⁴

The diagnosis of typhoid fever is usually obvious, but it can be difficult when the clinical findings are not typical. The disease is curable, but the mortality rate from typhoid fever in the Western world is still about 2%. This is at least partly due to a delay in diagnosis, which occurs either because the disease is initially not considered or because definitive blood cultures require at least 18–36 hr and in 10–30% of patients take over a week to show positive results [1].

Bacterial enteritis caused by other microorganisms, such as *Yersinia enterocolitica* and *Campylobacter jejuni*, appears to have a characteristic sonographic appearance of enlarged mesenteric lymph nodes and mural thickening of the terminal ileum and cecum [2, 3].

We saw three patients with typhoid fever in whom the same sonographic features were found, one of whom is described here.

Case Report

A 12-year-old girl, recently arrived from Pakistan, was admitted to the hospital with high fever, malaise, headache, a dry cough, and abdominal pain. Defecation was normal. The referring physician suspected malaria.

The pulse was 108/min. There was a moderate leukopenia with a marked shift to the left, and the sedimentation rate was 35 mm/hr. Although typhoid fever was considered, a lumbar puncture was done to rule out meningitis. Because of increasing abdominal pain, a

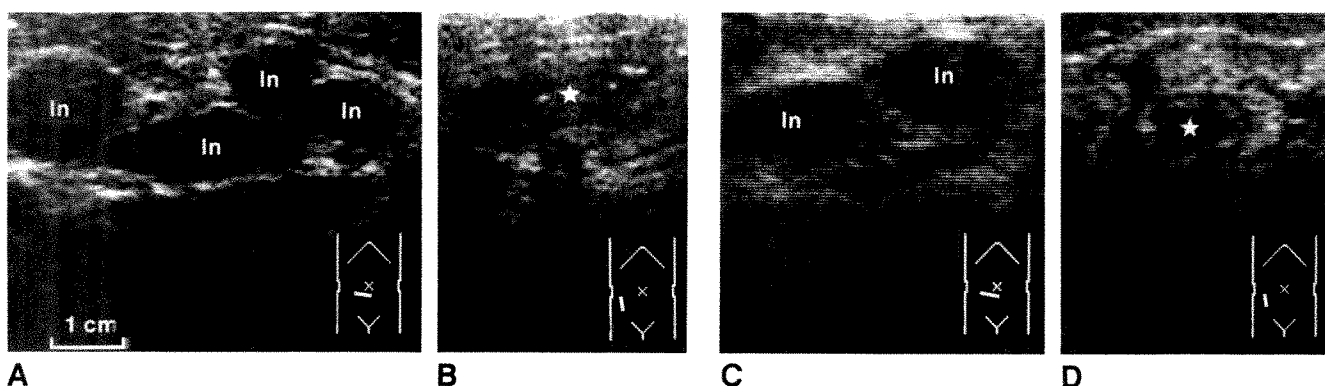


Fig. 1.—A–D, Sonograms show features of bacterial enteritis in two patients with typhoid fever. Enlarged mesenteric lymph nodes (ln) (A, C), in combination with mural thickening of terminal ileum and cecum, give rise to a characteristic axial image of ileocecal valve (star) (B, D).

Received February 1, 1989; accepted after revision March 15, 1989.

¹ Department of Radiology, Westeinde Hospital, Lijnbaan 32, 2512 VA The Hague, the Netherlands. Address reprint requests to J. B. C. M. Puylaert.

² Department of Internal Medicine, Westeinde Hospital, 2512 VA The Hague, the Netherlands.

³ Department of Pediatrics, Westeinde Hospital, 2512 VA The Hague, the Netherlands.

⁴ Department of Bacteriology, Westeinde Hospital, 2512 VA The Hague, the Netherlands.

sonogram was obtained. This showed enlarged mesenteric lymph nodes and mural thickening of the terminal ileum and cecum, compatible with bacterial enteritis (Fig. 1). In addition, enlarged lymph nodes were identified in the porta hepatis and there was moderate splenomegaly. These findings were thought to be consistent with the diagnosis of typhoid fever. The next day, blood cultures were positive for *Salmonella typhi*.

Discussion

We have seen two other patients with typhoid fever in whom identical sonographic features were found in the ileocecal region (Fig. 1). Clinical symptoms in these two patients were not typical of typhoid fever. The sonograms were requested for a suspected amebic abscess in one patient and for unexplained septicemia in the other. Although not specific for any one organism, the sonographic features appear to be specific for bacterial enteritis of the ileocecal region. The differential diagnosis of the sonographic findings includes

Yersinia and *Campylobacter* enteritis, Crohn disease, tuberculous ileitis, and lymphoma. However, the clinical findings of these conditions usually do not mimic those of typhoid fever. Moreover, the sonographic features of Crohn disease are different from those of bacterial enteritis [4], and involvement of the mesenteric lymph nodes in malignant lymphoma is uncommon.

REFERENCES

1. Guerrant RL. Salmonella infections. In: Braunwald E, Isselbacher KJ, Petersdorf RG, Wilson JD, Martin JB, Fauci AS, eds. *Harrison's principles of internal medicine*, 11th ed. New York: McGraw-Hill, 1987:592-596
2. Puylaert JBCM. Mesenteric adenitis and acute terminal ileitis: US evaluation using graded compression. *Radiology* 1986;161:691-695
3. Puylaert JBCM, Lalisang RI, van der Werf SDJ, Doornbos L. *Campylobacter* ileocolitis mimicking acute appendicitis: differentiation with graded-compression US. *Radiology* 1988;166:737-740
4. Puylaert JBCM, Van der Werf SDJ, Ulrich C, Veldhuizen RW. Crohn disease of the ileocecal region: US visualization of the appendix. *Radiology* 1988;166:741-743

Localized Clotted Blood as Evidence of Visceral Trauma on CT: The Sentinel Clot Sign

Dennis Orwig¹
Michael P. Federle^{1,2}

We retrospectively reviewed the CT scans of 116 patients with abdominal trauma who had visceral injuries to determine if identification on CT of focal high-density clotted blood (a "sentinel clot") was an accurate sign of injury to an adjacent organ. The sentinel clot sign was sensitive, present in 101 (84%) of 120 visceral injuries with only three false-positive cases. Whereas CT visualized the visceral injury itself in 86% of cases, the sentinel clot was the only clue as to the source of hemorrhage in 14% of the cases. Splenic and bowel/mesenteric injuries were frequently subtle, and the focal clot helped to focus attention on the traumatic lesion. In 9% of splenic trauma cases and 32% of bowel/mesenteric injuries, the sentinel clot was the only positive finding.

Localized clot is a frequent and accurate sign of injury to an adjacent organ. By facilitating diagnosis of trauma to a specific organ, it may influence the management decision of surgical vs conservative therapy.

AJR 153:747-749, October 1989

CT plays a major role in the evaluation of patients with suspected abdominal trauma. It is accurate in defining visceral injuries and associated hemoperitoneum, but hemoperitoneum frequently is more apparent than the visceral laceration or hematoma itself [1, 2]. Clotted blood has a different CT appearance than lysed blood clot or free-flowing blood because of greater density and hemoglobin content [3-5]. We have reported that perisplenic clot is an important clue in CT diagnosis of splenic injury [6]. Additional experience suggested that localized clotted blood ("sentinel clot") was a consistent and valuable sign in other visceral injuries as well. In order to evaluate the frequency and validity of the sentinel clot sign as an indication of a specific visceral injury, we retrospectively reviewed the medical records of 116 patients with confirmed traumatic abdominal injuries that had been studied by using CT.

Materials and Methods

We retrospectively reviewed the CT log books and surgical registry to find the records of all patients who had CT scans done for blunt abdominal trauma during the period of February 1984 to August 1988. Excluding cases of retroperitoneal injury, incomplete records, or inconclusive proof of diagnosis, we found a total of 130 visceral injuries in 116 patients. CT findings were compared with observations at surgery (114 injuries in 100 patients). In those cases managed nonoperatively (16 injuries in 16 cases), confirmation required unequivocal CT demonstration of a visceral injury; follow-up CT scans frequently provided further confirmatory evidence. If surgery or follow-up did not confirm injury to an additional organ adjacent to the localized clot, the CT scan was considered in error (a false-positive sentinel clot sign).

Hemoperitoneum was identified as free intraperitoneal fluid having an attenuation of greater than 25 H, usually in the range of 35-45 H [1]. Clotted blood was recognized as a heterogeneous focal collection having a mean CT number greater than 60 H when measured by computed region of interest (ROI) cursor readout; if ROI measurements were unavailable, we accepted the presence of a focal heterogeneous collection that was visibly more dense

Received March 27, 1989; accepted after revision: May 30, 1989.

¹ Department of Radiology, University of California, San Francisco, San Francisco General Hospital, San Francisco, CA 94110.

² Present address: Department of Radiology, University of Pittsburgh, One Children's Pl., 3705 Fifth St., Pittsburgh, PA 15213. Address reprint requests to M. P. Federle.

0361-803X/89/1534-0747
© American Roentgen Ray Society

than the other fluid (hemoperitoneum) as evidence of clot. The hyperdense region (sentinel clot) was assigned a relationship to an adjacent solid or hollow viscus as the most likely site of injury and source of hemorrhage.

All scans were obtained on a GE 9800 scanner (General Electric Medical Systems, Milwaukee, WI). All patients received both IV and oral contrast media and were scanned with a 10-mm slice thickness in contiguous slices through the abdomen and at 2-cm intervals through the pelvis.

Results

Of the total 130 visceral injuries in 116 patients, 10 cases had insufficient intraperitoneal blood to evaluate further. Of the remaining 120 injuries, 101 had evidence of a sentinel clot and 19 had generalized hemoperitoneum but no focal clot (Table 1). In 87 (86%) of the 101 cases with sentinel clot, CT also visualized a visceral injury; however, in 14 cases (14%), the sentinel clot was the only clue as to the site of injury. False-positive identification of a sentinel clot was noted in only three cases. In one case, unopacified bowel was falsely interpreted as a clot in the mesentery, whereas in another an extraperitoneal rectus muscle hematoma was misinterpreted as an omental clot. The third case was a predicted splenic injury probably representing misinterpretation because of partial-volume artifact of the enhanced spleen. Distribution of the sites of injury and the relative contribution of the sentinel clot sign are listed in Table 1.

Discussion

Hemoperitoneum is present in nearly all patients with clinically important intraperitoneal injuries and is frequently present in patients with trivial self-limited injuries as well. If a protocol of surgery for all patients having hemoperitoneum, usually determined by diagnostic peritoneal lavage, is used, nontherapeutic laparotomy rates are 10–25% [7, 8]. Minor hepatic and mesenteric injuries are seen most often.

Although peritoneal lavage is a sensitive indicator of intraperitoneal hemorrhage, it fails to detect the source or significance of the bleeding [9]. Nonoperative management of most abdominal visceral injuries is commonly accepted for pediatric patients who are hemodynamically stable. CT has, nevertheless, proved valuable in evaluating the initial injury and the response to therapy [10].

In the adult population, CT has also proved to be extremely accurate in the diagnosis of abdominal visceral trauma [1, 2, 9]. Successful nonoperative management of most patients with hepatic lacerations defined by CT has been demonstrated and is growing in acceptance [11, 12]. Several recent reports have suggested that CT can play an important role in the nonoperative management of adult patients with splenic trauma, based on a scoring system that grades the parenchymal lesion and the extent of hemoperitoneum [13, 14]. CT has also shown promise in distinguishing "surgical" from "nonsurgical" cases of bowel and mesenteric injuries [15, 16]. The potential for CT to demonstrate and quantify hemoperitoneum and to evaluate its source is, therefore, of critical importance.

We found the sentinel clot sign to be a valuable adjunct in CT of abdominal trauma, being both sensitive and specific in identifying the injured organ. Sentinel clot was present in 101 (84%) of 120 visceral injuries, with only three false-positive cases. While CT visualized the parenchymal injury itself in 86% of cases, the sentinel clot sign was the only clue as to the source of hemorrhage in 14% of cases. In many cases, the sentinel clot was much more obvious than the parenchymal injury itself. We propose an analogy to the "fat pad" sign that is so useful in cases of elbow trauma. Just as the positive fat pad sign may be the only abnormality or may draw attention to a subtle underlying fracture, so too can the sentinel clot sign increase the diagnostic accuracy of CT in identifying specific visceral injuries, particularly those of the spleen and bowel/mesentery.

CT has proved accurate in the diagnosis of splenic trauma. Although an accuracy of 95% was reported in an earlier series, the actual splenic laceration or hematoma was visualized in only 71% [6]. The value of noting perisplenic clot, present in 85% of cases, was apparent, and constituted the main or only sign of splenic injury in 11 of 55 cases [6]. Similarly, in the current report, 88% of patients had perisplenic clot, and in six (9%) of 65 total splenic injuries the sentinel clot was the only sign of splenic trauma (Figs. 1 and 2). In such cases, surgical or pathologic findings usually indicated a small peripheral laceration or a central plane of laceration with little parenchymal hematoma.

Intestinal and mesenteric injuries are difficult to diagnose by any means, including imaging, laboratory, physical examination, or peritoneal lavage. Accurate diagnosis with CT has recently been reported [15, 16], but demands excellent scanning technique including the use of oral contrast medium and appropriate CT photography. Although not specifically addressed in the current study, the use of oral contrast medium may allow identification of extravasation (indicating bowel laceration) and may prevent mistaking unopacified bowel loops for hematoma, or vice versa. Despite our caution, two of the three false-positive sentinel clots were in the mesentery or omentum. Because the CT signs of bowel injury may be infrequent (extravasated bowel contrast material or air) or nonspecific (bowel-wall thickening), the sentinel clot sign is particularly valuable. In cases of mesenteric hematoma it is frequently the only sign of injury. In the current series, sentinel clot was the only indication as to the source of hemorrhage in six (32%) of 19 cases of bowel or mesenteric injury. Thus,

TABLE 1: Presence of Sentinel Clot and Site of Injury

Site of Injury	Sentinel Clot Present		Sentinel Clot as:	
	Yes	No	Only Finding	False Positive
Spleen	57	8	6	1
Liver	27	6	0	0
Mesentery/bowel	15	4	6	2
Gallbladder	1	1	1	0
Urinary bladder	1	0	1	0
Total	101	19	14	3

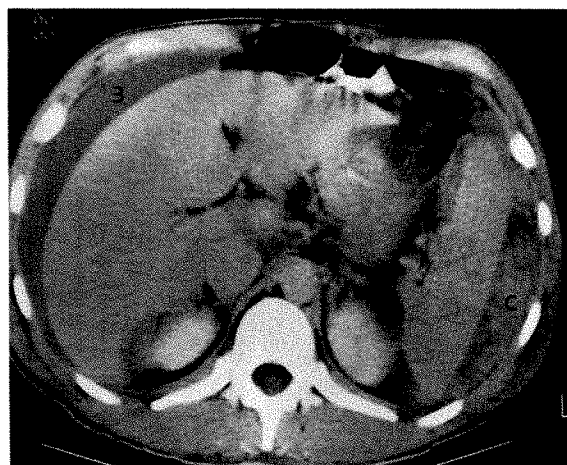


Fig. 1.—Surgically confirmed splenic injury with perisplenic hematomas. CT scan shows hyperdense clot (C) relative to lower density of lysed blood (B) surrounding liver.

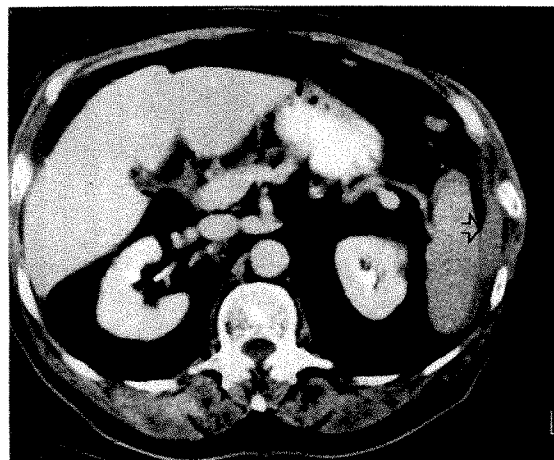


Fig. 2.—Surgically confirmed splenic laceration. CT scan shows focal hyperdense clot (arrow) adjacent to spleen. No parenchymal lesion is evident.

mesenteric hematoma with no other apparent source of hemoperitoneum should suggest an underlying bowel or mesenteric injury (Fig. 3). Close scrutiny of the bowel wall and careful CT techniques are strongly advised.

Hepatic laceration was the second most common injury and was easily diagnosed in most cases. Sentinel clot was a frequent finding (27 [82%] of 33 cases) but in all our cases the hepatic laceration/hematoma was visualized directly. Again, however, the focal clot frequently drew our attention to subtle lesions or lesions that might have been confused with cysts, tumors, or other pathologic entities.

Other injuries were too few to evaluate conclusively. In our few cases of gallbladder or urinary bladder trauma, however, the sentinel clot was present in two of three and was the main or only CT finding in both cases.

We conclude that localized intraabdominal blood clot is an important clue that the bleeding source is an injured adjacent organ, and that this sentinel clot sign is both sensitive and

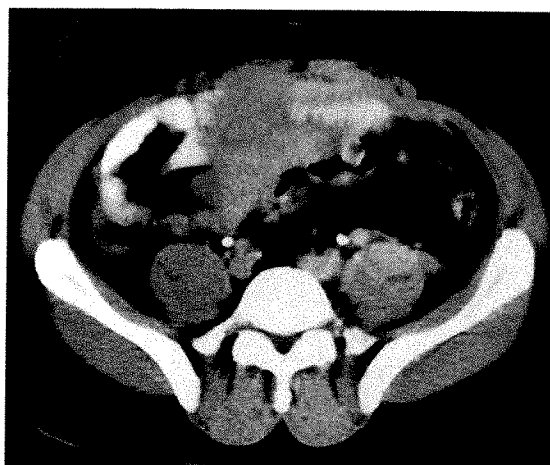


Fig. 3.—Bowel and mesenteric injury. CT scan shows hyperdense mass surrounding ileal loops and extending into mesentery. Bowel-wall thickening and free hemoperitoneum were present on other sections. Surgery confirmed laceration of terminal ileum and a mesenteric hematoma.

specific. Because management of hepatic, splenic, and bowel injuries depends on identification of the source as well as the amount of hemorrhage, CT can have an important influence on management decisions.

REFERENCES

1. Federle MP, Jeffrey RB. Hemoperitoneum studied by computed tomography. *Radiology* 1983;148:187-192
2. Federle MP. CT of upper abdominal trauma. *Semin Roentgenol* 1984;19:269-280
3. Alexander ES, Clark RA. Computed tomography in the diagnosis of abdominal hemorrhage. *JAMA* 1982;248:1104-1107
4. Wolbersson MK, Crepps LF, Sundaram M, et al. Hyperdensity of recent hemorrhage at body computed tomography: incidence and morphologic variation. *Radiology* 1983;149:779-784
5. Swenson SJ, McLeod RA, Stephens DH. CT of extracranial hemorrhage and hematomas. *AJR* 1984;143:907-912
6. Federle MP, Griffiths B, Minagi H, Jeffrey RB Jr. Splenic trauma: evaluation by CT. *Radiology* 1987;162:69-71
7. Thal ER, Shires, GT. Peritoneal lavage in blunt abdominal trauma. *Am J Surg* 1973;125:64-69
8. Root HD, Hauser CW, McKinley CR, et al. Diagnostic peritoneal lavage. *Surgery* 1965;57:633-637
9. Goldstein AS, Sclafani SJA, Kupferstein NH, et al. The diagnostic superiority of computerized tomography. *J Trauma* 1985;25:938-946
10. Kaufman RA, Towbin R, Babcock DS, et al. Upper abdominal trauma in children: Imaging evaluation. *AJR* 1984;142:449-460
11. Meyer AA, Crass PA, Lim R, et al. Selective nonoperative management of blunt liver injury using computed tomography. *Arch Surg* 1985;120:550-554
12. Foley WD, Cates JD, Kellerman GM, et al. Treatment of blunt hepatic injuries: role of CT. *Radiology* 1987;164:635-638
13. Buntain WL, Gould HR, Maull KI. Predictability of splenic salvage by computed tomography. *J Trauma* 1988;28:24-31
14. Rescinti A, Fink MP, Raptopoulos V, Davidoff A, Silva WE. Nonoperative treatment of adult splenic trauma: development of a computed tomographic scoring system that detects appropriate candidates for expectant management. *J Trauma* 1988;28:828-831
15. Donahue JA, Federle MP, Griffiths BG, Trunkay DD. Computed tomography in the diagnosis of blunt intestinal and mesenteric injuries. *J Trauma* 1987;27:11-17
16. Rizzo MJ, Federle MP, Griffiths BG. Computed tomography for bowel and mesenteric injury following blunt abdominal trauma. *Radiology* (in press)

Book Review

Modern Imaging of the Liver. Applications of Computerized Tomography, Ultrasound, Nuclear Medicine, and Magnetic Resonance Imaging. Edited by Michael Andrew Wilson and Francis F. Rucizka, Jr. New York: Dekker, 712 pp., 1989. \$150 (U.S. and Canada); \$180 (all other countries)

The fifth volume in a series of monographs (*Liver: Normal Function and Disease*), this book has been written for "physicians as well as clinical and non-clinical scientists" interested in hepatobiliary diseases. Its main purpose is to "help individuals decide on the relative merits of the various technologies and their potential applications to diseases."

The text is divided into three sections (physical principles, clinical applications, and relative efficacy), each of which is designed to be independent of the others so that chapters in one section "can be read without referring to the others." The first section comprises six chapters, which review the principles and instrumentation of imaging techniques. Topics covered include plain radiography, CT, digital angiography, nuclear scintigraphy, sonography, and MR. This section is meant to be a "general reference source" for imaging techniques, regardless of the anatomic area. The chapters are well written, and the summaries of the principles and instrumentation are useful. Included are several recent developments, such as Doppler sonography and positron emission tomography (PET). However, there is neither a discussion on single-photon emission CT (SPECT) nor a description of contrast agents. Because the chapters are relatively brief, the material presented will be comprehended adequately by only those who are already familiar with the subject matter.

The second section describes the clinical applications of each of the aforementioned imaging tests in examining the liver and biliary tree. Included is a separate chapter on endoscopic retrograde cholangiopancreatography (ERCP). In this section, the chapter on CT of the liver, gallbladder, and bile ducts by Patrick C. Freeny is particularly noteworthy. In general, the image quality is adequate, although a significant proportion of sonograms presented are static images. Because of the small page size, many images are displayed sideways, and often the legends and the images are on different pages. This is inconvenient and it makes image comparison difficult. Missing are

discussions on the role of intraoperative sonography, Doppler sonography, and SPECT.

The final section describes the relative efficacy of each of the imaging techniques in six common clinical conditions (chronic cholecystitis, acute cholecystitis, jaundice, hepatic trauma, liver metastases, and liver abscess). These chapters include useful descriptions on pathophysiology and clinical presentation. However, the material included is not always current. For example, there is only a brief mention of the usefulness of MR imaging for detecting liver metastases. The clinically important issue of differentiating hepatic hemangiomas from metastases is not stressed adequately. Although the need for an "economical diagnosis" was stated as an objective of the text, no explicit discussion is provided on the relative costs of each imaging test.

This text does serve its intended purpose, which is to highlight relative merits of the various imaging tests in diagnosing diseases of the liver and bile ducts (although there is some bias toward nuclear medicine tests). The major limitation of the book is that it has not been edited adequately. Several inconsistent statements in the text result from the book's multiple authorship. For example, the number of cholecystectomies per year in the United States is given as 700,000 in chapter 13 and 500,000 in chapter 14. Similarly, the amount of iodinated contrast medium recommended for evaluating the liver and bile ducts is different in chapters 7 and 15. At least two of the images are displayed incorrectly. The text may be interesting to radiologists, but, given its high cost, it probably will not supplant more comprehensive texts on this topic that already are available.

Sanjay Saini
Massachusetts General Hospital and Harvard Medical School
Boston, MA 02114

Arterial Perfusion Abnormalities of the Liver After Hepatic Arterial Infusion Chemotherapy and Their Correlation with Changes in the Metastases: Evaluation with CT and Angiography

Juergen Roth¹
 Bernd Wallner¹
 Faruk Safi²

We studied the progress of hepatic arterial perfusion abnormalities in 50 patients receiving long-term arterial infusion chemotherapy for palliative treatment of liver metastases from colorectal cancers and correlated the findings with changes in the metastases. Intraarterially and IV enhanced CT scans and digital subtraction angiograms of the liver were made in all patients before chemotherapy and at 3-month intervals during chemotherapy for 1 year. Before the chemotherapy, all patients had normal hepatic arterial perfusion. Arterial perfusion abnormalities were detected in 30 patients (60%) after 6 months of chemotherapy and in 41 patients (82%) after chemotherapy for 1 year. After 6 months of chemotherapy, 36% of the regressive and 39% of the progressive metastases were located in areas with arterial perfusion abnormalities. After 1 year of chemotherapy, 54% of the regressive and 60% of the progressive metastases were situated in portions of the liver with perfusion abnormalities.

Hepatic arterial perfusion abnormalities were found to be progressive during intraarterial infusion chemotherapy. No relationship between arterial perfusion abnormalities and tumor response to chemotherapy could be detected.

AJR 153:751-754, October 1989

Since the introduction of implantable drug infusion pumps, continuous hepatic infusion chemotherapy via the hepatic artery by using 5-fluoro-2-deoxyuridine (FUDR, Roche Laboratories, Nutley, NJ) has gained acceptance for palliative treatment of liver metastases originating from colorectal cancers [1, 2]. However, the procedure is not free of complications. These include liver cell damage, biliary sclerosis, and occlusion of the hepatic artery and its branches [3-6]. Although some of these problems have been described in detail, little is known about hepatic arterial perfusion abnormalities that occur at various times after chemotherapy [7-9].

Therefore, we performed CT and digital subtraction angiography (DSA) on 50 patients who were undergoing continuous intraarterial hepatic infusion of FUDR for treatment of hepatic metastases.

Subjects and Methods

Fifty patients (32 men, 18 women; mean age, 61 years) with histologically proved liver metastases from colorectal cancers were included in the study after informed consent was obtained. The primary tumor had been resected in all patients, and none had clinical or radiologic evidence of extrahepatic metastases. Before the chemotherapy, intraarterial DSA of the celiac mesenteric arteries was performed by using 20 ml of iopamidol given at a rate of 5 ml/sec (Angiotron, Siemens, Erlangen, W. Germany; Solustrast 300, Byk Gulden Konstanz, W. Germany).

A drug-infusion pump was surgically implanted subcutaneously in the anterior abdominal wall (Infusaid, Infusaid Corp., Norwood, MA). When standard arterial anatomy was present, a catheter attached to the pump was inserted surgically into the gastroduodenal artery with the tip of the catheter positioned at the origin of the common hepatic artery. In patients with

Received December 15, 1988; accepted after revision May 17, 1989.

¹ Department of Radiology 1, University Ulm, Steinhövelstrasse 9, 7900 Ulm, W. Germany. Address reprint requests to J. Roth.

² Department of Surgery, University Ulm, Steinhövelstrasse 9, 7900 Ulm, W. Germany.

0361-803X/89/1534-0751
 © American Roentgen Ray Society

two hepatic arteries supplying the liver, catheters were placed in both arteries to allow perfusion of the entire liver. A cholecystectomy also was performed in all patients. After surgery, alternating 2-week continuous infusions of FUDR and heparinized saline (50,000 U/50 ml) were begun. The dosage of FUDR was 0.3 mg/kg/day for 3 months and 0.2 mg/kg/day thereafter.

All patients had complete blood counts, liver chemistry, and carcinoembryonic antigen levels determined at monthly intervals for 1 year. For evaluation of arterial perfusion of the liver, intraarterially enhanced CT scans were made in all patients within 1 week after implantation of the drug-infusion pump and at 3-month intervals thereafter (contiguous 10-mm slices, TCT/GE 8800, Milwaukee, WI). Solustrast 300 was injected via the side port of the drug-infusion pump by using an electrical pump at a constant flow rate of 0.4 ml/sec throughout the examination. Enhancement was assessed visually from the scans. Arterial perfusion of the liver was considered normal when the entire liver parenchyma showed homogeneous enhancement. Perfusion abnormalities or defects were diagnosed when portions of the liver had inhomogeneous enhancement or no enhancement.

Additional enhanced and unenhanced CT studies were performed every 3 months for 1 year. The volume of the metastases on the scans was assessed by delineating the contour of each metastasis with a track-ball device. A change in volume of a metastasis was considered significant when the change amounted to 50% or more of the pretherapeutic volume.

To depict arterial anatomy, flow pattern, and catheter placement, DSA was performed immediately after the intraarterially enhanced CT studies in which contrast material was injected through the side port of the pump (flow rate, 1 ml/sec). Before chemotherapy, intraarterially enhanced CT studies showed homogeneous perfusion of the entire parenchyma of the liver, and DSA revealed normal morphology of the hepatic artery and its branches in all patients.

Four patients died during the study, and the arterial system was explored in detail at autopsy.

Results

Intraarterially enhanced CT scans made after 6 months of infusion chemotherapy showed homogeneous enhancement of the liver in only 20 patients (40%). All of the others had hepatic perfusion abnormalities. In these patients, the regions of the liver showing perfusion abnormalities involved on average 32% of the entire volume of the liver, ranging from 14%

to 48%. Thirty-seven percent of all metastases were located in these areas of the liver.

Hypoperfusion of portions of the liver was found in 24 patients (48%). Hypoperfused areas were located in the right lobe of the liver in 10 patients (20%) and in the left lobe of the liver in seven patients (14%). In seven patients (14%), hypoperfused areas of the liver were seen in both lobes. Complete perfusion defects of areas of the liver were found in six patients (12%). Of these nonperfused areas, three were found in the left and two in the right lobe of the liver. One patient showed perfusion defects in both lobes of the liver (Fig. 1A).

The angiograms made after 6 months of chemotherapy showed similar findings. In patients with homogeneous liver enhancement on CT scans, arteriography showed normal arterial anatomy and perfusion. In patients with inhomogeneous liver enhancement on CT, angiography showed multifocal narrowing of the hepatic arteries. Moreover, in patients with perfusion defects seen on CT scans, peripheral artery occlusions were present, correlating locally to these perfusion defects. In one patient, arteriography showed a significant stenosis of the common hepatic artery close to the tip of the catheter (Fig. 1B).

After 6 months of chemotherapy, the volume of the metastases had decreased in 32 patients (64%) and increased in 11 patients (22%) by more than 50% in comparison with the pretherapeutic volume. In seven patients (14%), no significant changes in tumor burden were found. Thirty-six percent of the regressive and 39% of the progressive metastases were located in hypoperfused areas of the liver. Nine new metastases were found in five of the 11 patients with progressive metastatic disease. Of these nine metastases, two arose in nonperfused areas of the liver. In hypoperfused portions of the liver, two new metastases had emerged. The other five new metastases, however, were located in normally perfused areas of the liver.

Intraarterially enhanced CT scans made after 1 year of chemotherapy showed homogeneous enhancement of the liver in nine patients (18%). None of these patients had hepatic arterial perfusion abnormalities at any time during the follow-up period. Forty-one patients (82%) had arterial perfusion

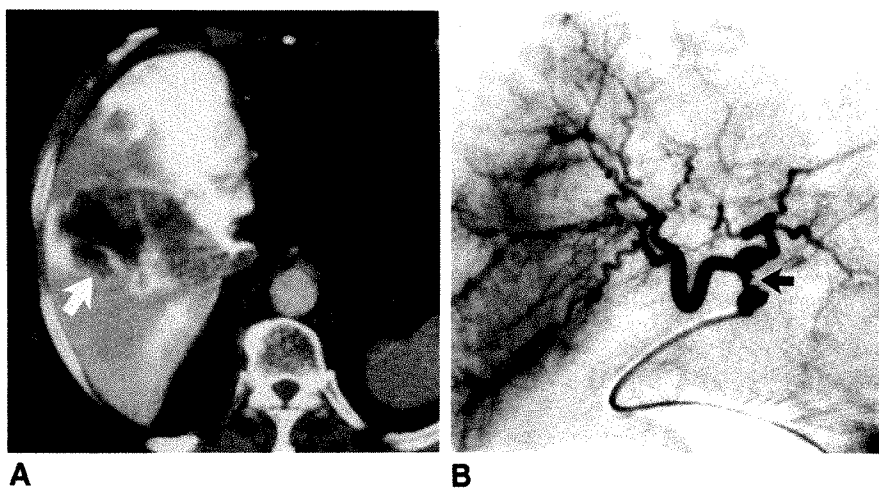


Fig. 1.—A, Intraarterially enhanced CT scan obtained after 6 months of intraarterial infusion chemotherapy. Left lobe of liver has been resected. Arterial perfusion of liver area surrounding large metastases (arrow) is markedly reduced compared with that in anterior portion of liver.

B, Digital subtraction angiogram made at same time as A shows a centrally located stenosis (arrow) and tortuous course of many liver arteries.

abnormalities. In these patients, the average volume of the regions of the liver with perfusion abnormalities amounted to 53% of the total volume of the liver (range, 29–76%). Fifty-five percent of all metastases were situated in these regions of the liver.

Hypoperfused areas of the liver were found in 23 patients (46%). In eight (16%) of these patients, the hypoperfused areas were located in the right lobe and in seven patients (14%) they were in the left lobe of the liver. In eight patients (16%), hypoperfused portions of the liver were found in both lobes. CT showed complete perfusion defects in 18 patients (36%). Perfusion defects were located in the right lobe in four patients (8%), in the left lobe in three (6%), and in both lobes of the liver in four (8%). In seven patients (14%), complete perfusion defects and hypoperfused areas of the liver were found (Fig. 2A).

Comparison of the scans made after 12 months of chemotherapy with those obtained after 6 months of chemotherapy showed different hepatic arterial perfusion patterns in 32 patients (64%). Reperfusion of portions of the liver was found in five patients (10%). Two (4%) of these patients had perfusion defects and three (6%) had hypoperfused areas of the liver on the scans made after 6 months of chemotherapy. Newly developed complete arterial perfusion defects of areas of the liver were found in 11 patients (22%). Five of these perfusion defects were seen in patients with previous homogeneous enhancement. All other new perfusion defects were found in patients with arterial perfusion abnormalities after 6 months of chemotherapy. New arterial hypoperfusions were found in 16 patients (32%). Six (12%) of these patients showed homogeneous enhancement of the liver after 6 months of chemotherapy.

The findings on DSA made after 1 year of chemotherapy were similar to those seen on the CT studies. In all patients with arterial perfusion abnormalities, the described alterations of hepatic arteries such as tortuous courses, stenoses, and occlusions were aggravated in comparison to the 6-month examination. In addition, in seven of the 18 patients with hepatic perfusion defects seen on CT, large liver arteries now were involved and showed stenoses or obliterations. In two

patients with occluded arteries at 6 months, these arteries were recanalized, corresponding to reperfused liver regions seen on CT scans. In four (8%) of the 23 (46%) patients with hypoperfused areas of the liver, arteriography showed a patchy opacification of these areas without sharp delineation of arterial vessels. Neither displacement nor occlusion of the catheter was detected in any patient at any time (Fig. 2B).

After 1 year of chemotherapy, the volume of the metastases had regressed in 19 patients (38%) and had progressed in 26 patients (52%). Regression and progression were defined as changes in volume of metastases of more than 50% when compared to the pretherapeutic volume. In five patients (10%), there was still no significant change in the volume of the metastases. Of the regressive metastases, 47% were located in hypoperfused portions of the liver and 7% were lying in arterially nonperfused areas. Fifty-one percent of the progressive metastases were situated in areas of the liver showing hypoperfusion on CT. Nine percent of the progressive metastases were found in nonperfused regions of the liver. Twenty-one new metastases developed in 17 (34%) of the 26 patients with progressive disease. Of these 17 metastases, seven (41%) were located in hypoperfused areas of the liver. Two (12%) of the 17 newly arisen metastases were found in nonperfused portions of the liver.

Histologic examination of the four livers available from autopsies revealed thrombotic occlusions of hepatic artery branches varying from recent to organized lesions. Sometimes partial recanalization of occluded arteries was detected. Intimal fibrosis of extrahepatic branches of the hepatic artery was a common finding. Cells associated with chronic inflammation were found next to many small arteries, suggesting reactive arteritis.

Discussion

Arterial liver perfusion abnormalities after intraarterial chemotherapy have been examined by Bledin et al. [10], who used ^{99m}Tc -labeled macroaggregated albumin particles. As early as 5 days after chemotherapy was started, irregular perfusion defects of the liver were identified in five of 16 patients [10].

Fig. 2.—A, Intraarterially enhanced CT scan obtained after 1 year of chemotherapy with 5-fluoro-2-deoxyuridine shows extensive arterial hepatic perfusion defects. Metastases located in left lobe of liver are not perfused (arrow).

B, Digital subtraction angiogram made at same time as A shows an occlusion of left hepatic artery (arrow). Peripheral liver regions are deprived of arterial blood flow. Histologic study revealed multiple arterial thrombotic obliterations.



A



B

Little information is known about the pathogenesis of hepatic arterial damage that occurs after intraarterial infusion of FUDR. Arterial injury induced by the catheter would be expected to occur next to the catheter tip. In our series, however, central stenosis of the common hepatic artery close to the tip of the catheter was found in only one patient. All the other arterial stenoses and occlusions observed were located in peripheral liver areas far from the catheter tip.

Distribution of arterial flow depends on the position of the catheter in the hepatic artery. Preferential flow may transport injected substances into a particular region of the organ. Although no changes of catheter position were noted in any patient, this phenomenon may lead to inhomogeneous distribution of the contrast material and of the chemotherapeutic agent.

Arterial thrombosis causing obstruction of arteries may arise from around or within the catheter. Although the system was heparinized and continuously perfused, those thrombi may occur occasionally and cause arterial perfusion abnormalities.

The higher injection rates of the contrast material used for intraarterially enhanced CT scans and for arteriography may result in different arterial perfusion patterns than does the low infusion rate during continuous infusion of the cytotoxic agent. Perfusion abnormalities seen on CT, however, were paralleled by alterations of the hepatic arteries, such as narrowing of the lumen and occlusions, in every patient studied. Thus, distribution of the contrast material may be comparable to that of the chemotherapeutic substance.

As the blood supply of liver metastases is almost exclusively provided by the hepatic artery, metastases act as sumps and may influence the distribution of arterial perfusion. In our series, however, no relationship was found between the occurrence of perfusion abnormalities and the presence of metastases.

Therefore, we hypothesize that the chemotherapeutic agent plays a major role in the development of arterial damage. Toxic arteritis induced by FUDR or its metabolites has been discussed as a possible cause of arterial damage [10]. Furthermore, radiomimetic effects of this antimetabolite of DNA are conceivable, because changes in arteries after exposure to ionizing radiation that are similar to the changes we have seen have been described [11, 12].

The reperfusion of liver regions seen on CT scans after arterial perfusion defects is likely to result from recanalization of previously obliterated arteries. This hypothesis is supported by arteriographic as well as by histologic findings. The recanalization of arteries may be due to reparative processes in the absence of high concentrations of FUDR in occluded vessels.

In patients without recanalization of occluded liver arteries, development of arterial collaterals could account for the observed changing perfusion patterns seen on CT. Existence of intrahepatic collaterals between left and right lobes of the liver has been described by Healey et al. [13]. Moreover, arterial perfusion of liver regions deprived of their original arterial blood supply may be ensured via vasa vasorum or periarterial vessels [14, 15]. Except for the vasa vasorum, these collaterals have been shown by arteriography [16].

Our results remain inconclusive as to whether hepatic arterial perfusion abnormalities have any significant influence on progression or regression of liver metastases. Metastases located in nonperfused liver regions on average did not show an increased tendency to grow when compared to those situated in perfused liver areas. Moreover, metastases did not originate in liver regions deprived of their original arterial blood flow any more frequently than they originated in liver areas without arterial perfusion defects. We suppose that reduction of arterial blood flow can result in ischemic injury of metastases, inhibiting their growth. The reduced arterial nutrition also may be responsible for the low frequency of new metastases emerging in nonperfused liver regions. These results, however, should be viewed as preliminary, because hepatic arterial perfusion can change rapidly during long-term intraarterial infusion chemotherapy and because our observations are based on a relatively short follow-up period in a small number of patients.

REFERENCES

1. Balch CM, Urist MM, Soong SJ, McGregor ML. A prospective trial of continuous FUDR regional chemotherapy for colorectal metastases to the liver using a totally implantable drug infusion pump. *Ann Surg* 1983; 198:567-573
2. Kemeny MM, Goldberg D, Beatty D, et al. Results of a prospective randomized trial of continuous regional chemotherapy and hepatic resection as treatment of hepatic metastases from colorectal primaries. *Cancer* 1986;57:492-498
3. Doria MI, Shepard KV, Levin B, Ridell RH. Liver pathology following hepatic arterial infusion chemotherapy: hepatic toxicity with FUDR. *Cancer* 1986;58:855-861
4. Kemeny N, Daly J, Oderman P, et al. Hepatic artery pump infusion: toxicity and results in patients with metastatic colorectal carcinoma. *J Clin Oncol* 1984;2:595-600
5. Haq M, Valdes LG, Peterson DF, Gourley WK. Fibrosis of extrahepatic biliary system after continuous hepatic artery infusion of floxuridine through an implantable pump. *Cancer* 1986;57:1281-1283
6. Marymont JV, Dakhil SR, Travers H, Housholder DF. Chemical cholecystitis associated with arterial chemotherapy delivered by a permanently implanted pump. *Hum Pathol* 1985;16:986-990
7. Botet JF, Watson RC, Kemeny N, Daly JM, Yeh S. Cholangitis complicating intraarterial chemotherapy in liver metastases. *Radiology* 1985;156:335-337
8. Anderson S, Holley HC, Berland LL, Van Dyke JA, Stanley RJ. Causes of jaundice during hepatic artery infusion chemotherapy. *Radiology* 1986;161:439-442
9. Shea WJ, Demas B, Goldberg HI, Hohn DC, Ferrell LD, Kerlan RK. Sclerosing cholangitis associated with hepatic arterial FUDR chemotherapy: radiographic-histologic correlation. *AJR* 1986;146:717-721
10. Bledin AG, Kim EE, Chuang VP, Wallace S, Haynie TP. Changes of arterial blood flow patterns during infusion chemotherapy as monitored by intra-arterially injected technetium 99m macroaggregated albumin. *Br J Radiol* 1984;57:197-203
11. Berger MR, Henne TH, Aguiar JL, et al. Experiments on the toxicity of locoregional liver chemotherapy with 5-fluoro-2-deoxyuridine and 5-fluorouracil in an animal model. *Recent Results Cancer Res* 1986;100:148-156
12. Danenberg PV, Heidelberger C, Mulkins MA, Peterson AR. The incorporation of 5-fluoro-2-deoxyuridine into DNA of mammalian tumor cells. *Biochem Biophys Commun Res* 1981;102:654-658
13. Healey JE, Schroy PC, Sorensen RJ. The intrahepatic distribution of the hepatic artery in man. *J Int Coll Surg* 1953;20:133-148
14. Mitra SK. The terminal distribution of the hepatic artery with special reference to arterioportal anastomoses. *J Anat* 1966;100:651-663
15. Bookstein J, Boijesen E, Olin T, et al. Angiography after end-to-side portocaval shunt: clinical, laboratory and pharmacoangiographic observations. *Invest Radiol* 1971;6:101-109
16. Charnsangavej C, Chuang VP, Wallace S, Soo CS, Bowers T. Angiographic classification of hepatic arterial collaterals. *Radiology* 1982;144:485-494

MR Angiography and Dynamic Flow Evaluation of the Portal Venous System

Robert R. Edelman¹
 Bin Zhao^{1,2}
 Cheng Liu^{1,2}
 Klaus U. Wentz^{1,3}
 Heinrich P. Mattle⁴
 J. Paul Finn⁴
 Colin McArdle¹

We studied the value of MR angiographic techniques in imaging the portal venous system. Projection angiograms were created by postprocessing a series of two-dimensional, flow-compensated gradient-echo images. Flow velocity was determined by a bolus-tracking method with radiofrequency tagging and multiple data readout periods. Each image was acquired during a breath-hold. MR angiography was applied to six normal subjects and four patients with abnormal hemodynamics in the portal venous system. Flow velocity determined by MR was correlated with the results of duplex sonography. The main portal vein and intrahepatic branches were shown in all cases. Portosystemic collaterals were identified in all patients with portal hypertension. In normal subjects, peak flow velocities (17.9 ± 2.8 cm/sec) on MR correlated well with values determined by duplex sonography (17.5 ± 2.2 cm/sec) ($r = .846$, $p < .04$). Reversed portal blood flow was shown in two patients. One patient with portal vein thrombosis had no evidence of flow by MR angiography.

Our results indicate that MR angiography can provide a three-dimensional display of normal and abnormal vascular anatomy as well as functional information in the portal venous system.

AJR 153:755-760, October 1989

Numerous investigators have used MR to study blood flow [1-4]. Time-of-flight and phase effects can be used to determine the direction and velocity of flow. Recently, methods for obtaining MR angiograms have been described [5-9]. These methods substantially overcome the limitations of two-dimensional tomographic acquisitions by displaying, in a single image, blood vessels within a thick volume, analogous to conventional angiograms. In this article, we describe MR angiography of the portal venous system in normal subjects and in patients with portal hypertension.

Subjects and Methods

Normal Volunteers and Patients

In six healthy male volunteers, portal vein blood-flow velocities were determined by MR angiography and were correlated with the results of duplex sonography. Subjects fasted for at least 4 hr before both studies. The maximum time between completion of MR angiography and duplex sonography measurements did not exceed 30 min.

Four consecutive patients with portal hypertension and abnormal portal venous blood-flow dynamics shown by conventional angiography or duplex sonography were studied. One patient with a history of alcohol abuse had advanced liver cirrhosis. The diagnosis of portal hypertension was based on the finding of abdominal venous collaterals on a sonogram obtained 3 months before admission. A duplex sonogram made at admission suggested portal vein thrombosis, but a second study after the MR examination showed a patent portal vein with reversed flow. The second patient had an enlarged liver, esophageal varices proved by endoscopy, and a patent umbilical vein proved by sonography. In the third patient, the

Received March 31, 1989; accepted after revision May 15, 1989.

¹ Department of Radiology, Beth Israel Hospital, 330 Brookline Ave., Boston, MA 02215. Address reprint requests to R. R. Edelman.

² Shandong Provincial Medical Imaging Research Institute and Dept. of Radiology, Shandong Provincial Hospital, 396 Jing Wu Rd., Jinan, People's Republic of China.

³ Department of Radiology, Klinikum Mannheim, Theodor-Kutzer-Ufer, 6800 Mannheim 1, W. Germany.

⁴ Department of Radiology, New England Deaconess Hospital, 185 Pilgrim Rd., Boston, MA 02215.

0361-803X/89/1534-0755
 © American Roentgen Ray Society

hepatic wedge pressure was elevated. Delayed films after injection of contrast medium into the superior mesenteric artery showed hepatofugal flow in the inferior mesenteric vein and slow hepatopetal flow in the main portal vein. The cause of the portal hypertension in the second and third patients was not known. The fourth patient had a history of alcoholism and showed esophageal varices at endoscopy. Duplex sonography showed thrombosis of the main portal vein, but evaluation for varices was limited by meteorism.

MR Angiography

The MR studies were done with a 1.5-T whole-body imaging system (Siemens, Erlangen, W. Germany). A circularly polarized body coil was used as transmitter and receiver. The peak gradient amplitude of the system was 10 mT/m, and minimum gradient ramp time for this study was 500 μ sec. All studies were done within the guidelines of the institutional review board of the hospital.

Because the portal vein is angled and curved, it is not generally feasible to image its entire length in a single slice. To overcome this problem, a series of overlapping slices was acquired. These images were then postprocessed with a maximum-intensity-projection algorithm [10, 11]. In this technique, the images are viewed by the computer at a user-selected projection angle. The brightest pixel along this angle is placed into the projection image. The process is repeated for 256×128 pixels to produce a spatially resolved projection angiogram. In the MR angiogram, blood vessels appear bright and stationary tissues appear darker.

Breath-hold two-dimensional FLASH (fast low-angle shot) [12] images were acquired at the end of expiration. Images spanning the portal vein were obtained in the axial and coronal planes. In one of the patients, sagittal images also were obtained. First-order (velocity) flow compensation was applied in the frequency-encoding and slice-selection directions [13]. Scan parameters were 30/10/30° (TR/TE/flip angle), with one excitation, 256×256 acquisition matrix, and 6-mm slice thickness. Field-of-view was 42 cm, yielding a pixel dimension of 1.6 mm. Imaging time was 8 sec for each breath-hold acquisition.

Flow Velocity Quantification

This method involved a bolus-tagging phase and a readout phase [14]. In the bolus-tagging phase, a volume of blood was labeled by an RF presaturation pulse. The RF pulse was 2.56 msec in duration

and was computer-optimized to provide a rectangular slice profile [15, 16]. A flip angle of 90° empirically was found to be effective for eliminating signal from flowing blood. The RF pulse was followed by a spoiler gradient (5 mT/m) applied in the slice-selection direction. For evaluation of the main portal vein, the frequency-encoding and phase-encoding gradients were applied simultaneously with the RF pulse. As a result, the presaturation slab (1 cm thick) was oriented at a 45° angle, approximately perpendicular to the main portal vein. The presaturation slab was positioned just distal to the confluence of splenic and superior mesenteric veins.

In the readout phase, the signal was read out four times (generating four images), over an interval of 150 msec, by repeating the FLASH sequence four times. The motion of the tagged bolus was thereby shown at four time points after presaturation. Scanning parameters were 10/20°/1 (TE/flip angle/number of excitations), with a 256×128 acquisition matrix and 6-mm slice thickness. These images were acquired with breath-holding over a 19-sec interval. Neither cardiac nor respiratory gating was used. The excitation flip angle for the FLASH sequence was empirically selected to make the tagged bolus appear dark against a bright background of flowing blood. By changing the orientation and position of the presaturation slab, we could use the same procedure to analyze flow in major portal branches.

In order to overcome potential problems with partial volume averaging, a series of these images was acquired with 1-mm overlap and then was postprocessed as described earlier to produce a projection image spanning the entire thickness of the main portal vein. The projection images then were used for calculation of peak flow velocity.

Calculation of Peak Flow Velocity

In the normal subjects and in one patient, the dynamic bolus-tracking sequence was applied to the portal venous system. For velocity calculations, the MR angiograms were magnified and viewed at narrow windows for the most precise evaluation of the tagged boluses. The distance (D) between the trailing edge of the presaturation slab and the most advanced point in the trailing edge of the tagged bolus was measured for each of the four time points. Peak velocities (V) were calculated by dividing these distances by the time intervals (ΔT) between the center of the presaturation RF pulse and the center of the respective readout periods:

$$V = D/\Delta T \quad (1)$$

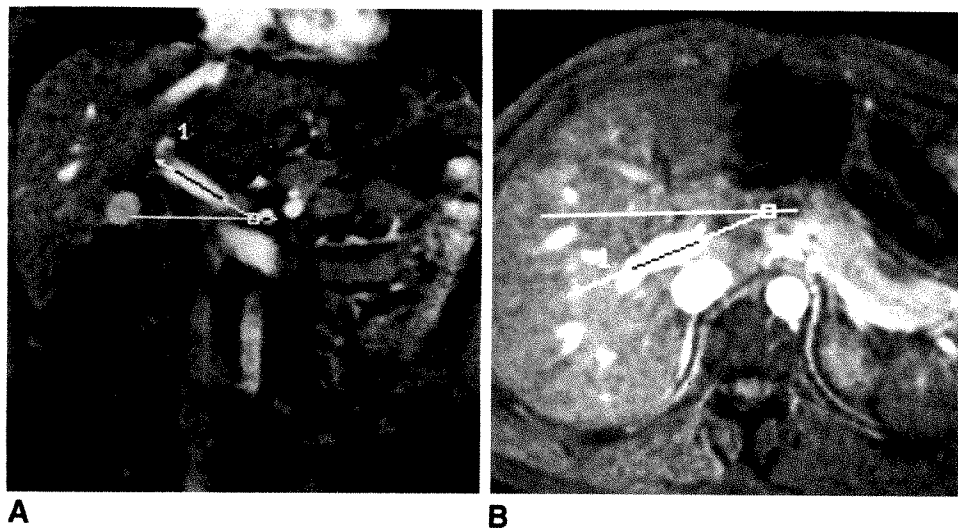


Fig. 1.—A and B, Coronal (A) and axial (B) angiograms created by post-processing a limited series of breath-hold, two-dimensional flow-sensitive images, show determination of angles used for correcting MR flow velocity.

A factor (f) was introduced to correct for the three-dimensional angling of the portal vein with the imaging plane. The angles formed by the portal vein with the coronal (c) and axial (a) planes were measured from the respective projection angiograms (Fig. 1) and the correction factor calculated as:

$$f = \sqrt{(\sin c)^2 + (\cos c / \cos a)^2} \quad (2)$$

The time delays between the presaturation pulse and the different

echos were: $\Delta T_1 = 20.4$, $\Delta T_2 = 58.3$, $\Delta T_3 = 96.3$, $\Delta T_4 = 134.3$ msec. As the distance traveled by the presaturation bolus during ΔT_1 was too short to be determined exactly, this measurement was excluded to avoid errors. The peak velocity of the blood flow in the portal vein was calculated from the average of the velocities corresponding to the other three time intervals.

The sonographic examinations were performed with a computed duplex sonography unit (Acuson-128, Acuson, Mountain View, CA). A phased-array 3.5-MHz sector probe with simultaneous Doppler capacity was used. In all examinations, angle-corrected, time-averaged peak flow velocities were determined. In order to maintain accuracy, the angle between the portal vein and the Doppler beam was kept as acute as possible. In no case was the angle greater than 55° . The main and right portal veins were investigated. All studies were performed without prior knowledge of the results of MR angiography. Mean values were calculated from three measurements in the same subject.

Statistical correlation of MR angiography and duplex sonography results was analyzed by using regression analysis.

Results

The main portal vein and its intrahepatic branches were shown in all six volunteers (Fig. 2). Also the tagged boluses were well delineated, allowing three separate flow-velocity measurements in every case. The mean values and standard deviations, corrected for small samples ($SD_{(n-1)}$), of MR angiography and duplex sonography results are given in Table 1 (next page). Regression analysis showed a high correlation (Fig. 3) between peak velocities obtained by sonography and MR imaging ($r = .846$, $r^2 = .716$). The correlation was significant ($p < .04$) despite the small sample size.

In the first patient, two-dimensional FLASH images and MR angiography showed a patent portal vein, contrary to the original duplex sonography findings. The portal vein had reduced signal intensity, suggesting low flow. MR angiography showed marked dilatation of the left gastric venous plexus,

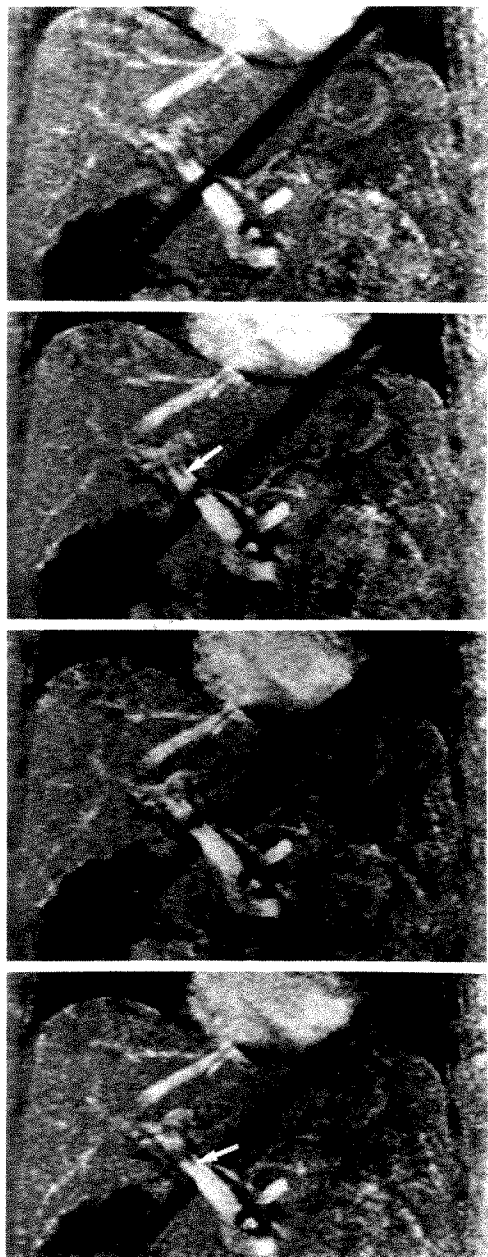


Fig. 2.—Normal subject. MR angiography with dynamic bolus tracking. Presaturation (black stripe) is applied approximately perpendicular to main portal vein and is imaged at four time points (from top to bottom: 20.4, 58.3, 96.3, 134.2 msec). Note hepatopetal motion of tagged bolus within portal vein. Also note dark stripe (arrows). The significance of this is uncertain. However, it may represent phase dispersion due to shear flow at divider separating flow into right and left portal veins.

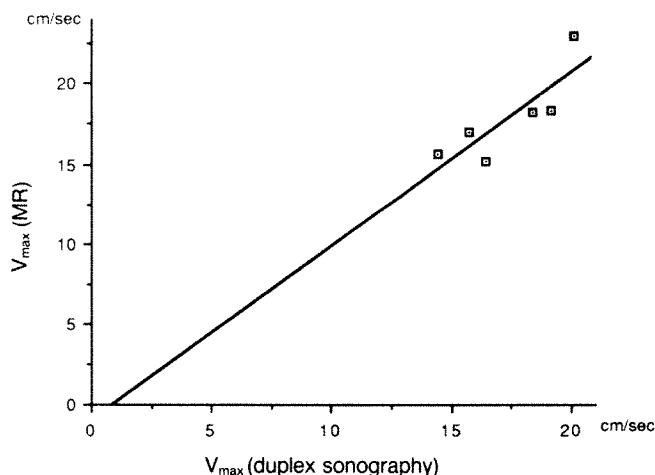


Fig. 3.—Graph showing comparison of peak-velocity measurements assessed by MR bolus tracking vs duplex sonography ($r = .85$, $p < .04$, $y = -0.9075 + 1.0762x$).

TABLE 1: Flow Velocities (V) in the Portal Veins of Six Normal Volunteers

Subject No.	MR Angiography $V_{\max} \pm SD$ (cm/sec)	Duplex Sonography ^a $V_{\max} \pm SD$ (cm/sec)
1	22.9 \pm 1.4	20.2 \pm 2.6
2	18.4 \pm 2.0	19.2 \pm 3.4
3	17.0 \pm 0.4	15.8 \pm 6.4
4	18.2 \pm 1.0	18.5 \pm 4.1
5	15.6 \pm 0.6	14.5 \pm 5.0
6	15.2 \pm 1.1	16.5 \pm 10.2
Mean values	17.9 \pm 2.8	17.5 \pm 2.2

Note.—Correlation coefficient = .846, $r^2 = .716$, $p < .04$.

^a Time-averaged peak velocity.

the superior and inferior mesenteric veins, and the left renal vein, the last findings suggesting splenorenal shunting (Figs. 4A and 4B). MR angiography with dynamic bolus tracking showed reversed flow in the portal vein (Fig. 4C), with a calculated velocity of 6.6 cm/sec. Although duplex sonography showed reversed flow in the portal vein, the examination was technically difficult, and an adequate insonation angle could not be obtained for accurate measurement of velocity.

In the second patient, a patent umbilical vein was shown well in the sagittal MR angiogram, but was not appreciated prospectively in the individual two-dimensional FLASH images (Fig. 5). In the third patient, the anatomy of the portal venous system was shown well. Although dynamic bolus tracking

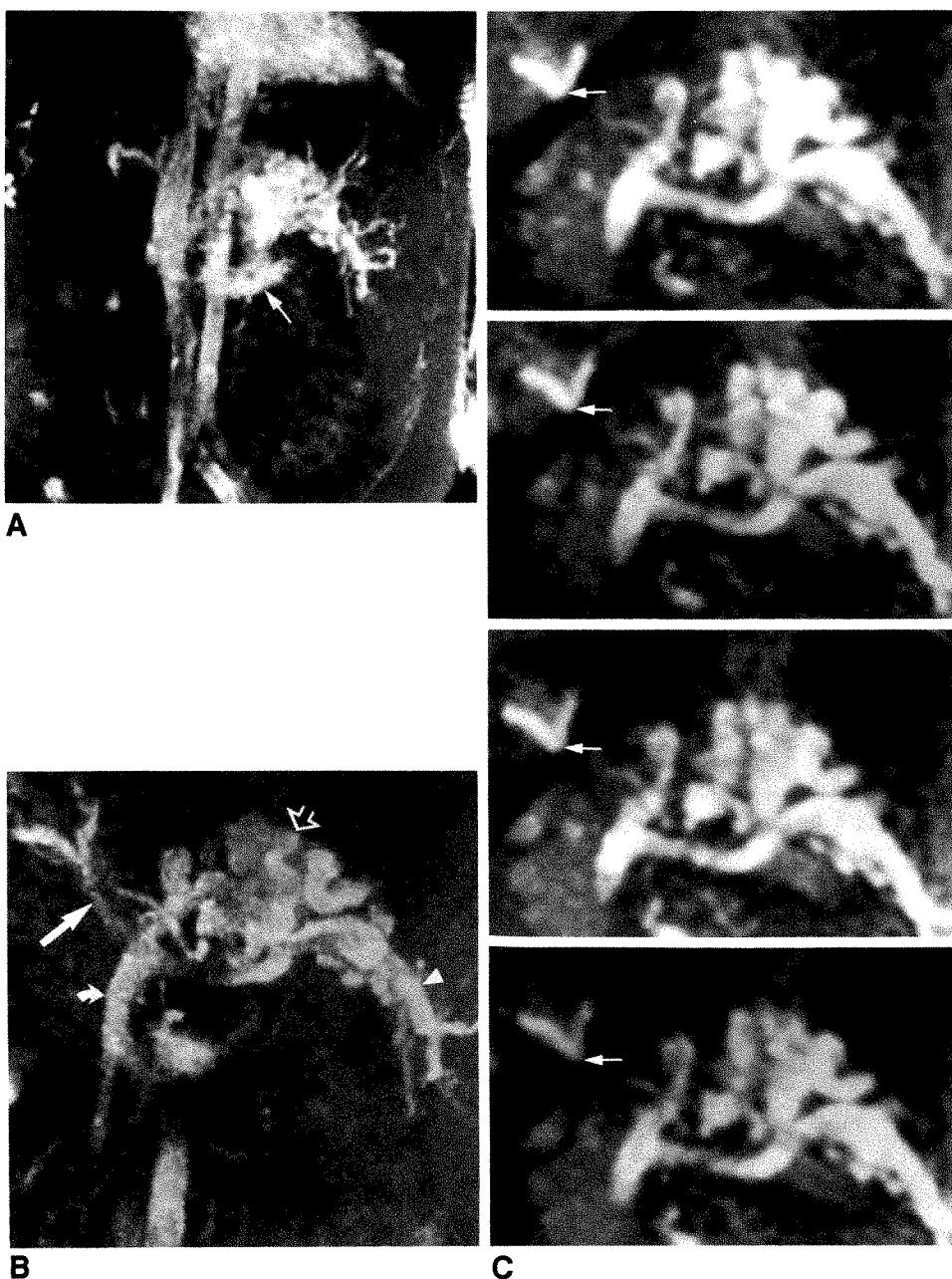


Fig. 4.—Patient with cirrhosis and portal hypertension. Thrombosis of portal vein was suspected on initial duplex sonographic examination.

A, Coronal MR angiogram shows massive collaterals and splenorenal shunting. Note enlarged left renal vein (arrow). Main portal vein is obscured by overlapping aorta and inferior vena cava.

B, MR angiogram created from same acquisition as A. However, slices containing upper abdominal portions of aorta and inferior vena cava were not included among images used for post-processing, thereby eliminating overlap between portal vein and these structures. Angiogram shows a patent portal vein (straight solid arrow) and massive collaterals (open arrow). Note superior mesenteric vein (curved arrow) and splenic vein (arrowhead).

C, Dynamic bolus tracking. Oblique presaturation (black stripe) was positioned just proximal to junction of right and left portal veins. Four time points are shown from top to bottom, as in Fig. 2. Trailing edge of bolus (arrow) is seen to move away from liver, indicating reversed flow.

was not available for this study, the combination of MR angiography with application of presaturation slabs over selected regions was able to show the normal flow direction in the main portal vein and flow reversal in the inferior mesenteric vein. MR angiography of the fourth patient showed extensive esophageal, gastric, and splenic varices. The portal vein was not visualized, consistent with occlusion.

Discussion

MR imaging with conventional spin-echo (SE) pulse sequences has potential for evaluation of abdominal venous abnormalities [17, 18]. The portal venous system is an area of particular clinical interest. However, unlike duplex sonography and conventional angiography, conventional MR imaging methods cannot be used to evaluate the flow dynamics of the portal vein. The clinical application is, for the most part, restricted to showing patency of the portal vein and the presence of portosystemic shunts [19–23].

Currently, duplex sonography represents the best noninvasive technique for assessing portal venous blood flow [24]. However, there are several limitations. The intrahepatic portal venous radicles usually can be identified by duplex sonography, but patient habitus and the presence of ascites and meteorism may prevent adequate visualization of the main portal vein. The accuracy of flow-velocity measurements in the main portal vein may be compromised if the available acoustic window requires imaging at a large angle to the direction of flow. Furthermore, it is difficult to assess flow within the superior and inferior mesenteric veins, and collaterals may not be seen.

The direction of flow also can be determined with conventional or digital angiograms acquired after selective injection of contrast medium into the splenic artery or the mesenteric arteries (indirect portography). This method is currently the

gold standard for evaluation of the portal system. However, it is invasive, and these patients are often at increased risk from coagulopathy, contrast-medium toxicity, and other factors. Moreover, indirect portography can provide portal venous pressures, but generally does not provide a direct measurement of portal flow, which is most likely the more clinically relevant physiologic parameter. The velocity can be determined more accurately by direct portography with transhepatic catheterization [25].

Given these limitations, there is a clinical need for additional noninvasive means for assessing the portal vein. Our results suggest that MR angiography may prove useful in this application. Unlike MR images made by using SE techniques, MR angiography can show patterns of blood flow. Its use for evaluation of the portal venous system is promising because portal flow in most patients is relatively stable, obviating cardiac gating. Also, the velocity of flow is relatively low. This differs from the rapid, turbulent flow in diseased arteries, which causes incoherent phase shifts and nonrecoverable loss of signal. Until recently, respiratory motion precluded the use of MR angiography in the abdomen. However, this problem has been overcome by acquiring a series of breath-hold, flow-sensitive images and postprocessing them to generate a projection angiogram [11].

The flow-velocity quantification method used in this study differs from previously described approaches [14] in the use of postprocessing techniques to create a projection angiogram. As a result, a tagged bolus can be tracked over several centimeters even though the vessel courses through several slices. Moreover, as cardiac gating is not required, flow quantification is achieved rapidly, within a few breath-hold intervals. Instead of using a time-of-flight method to quantify flow, phase-imaging techniques could have been used. However, we found that the dynamic bolus-tracking technique provides a more pleasing visual display of flow patterns. When the angiographic images representing the four time points are played in rapid cine mode, a direct visual representation of portal flow is obtained, similar to a contrast cineangiogram. Another potential use of bolus tracking is to distinguish slow flow from thrombosis (Fig. 4C). This may not always be feasible with standard gradient-echo methods, because slow in-plane flow may fail to produce significant flow-related enhancement.

The breath-hold intervals used in this study for dynamic bolus tracking are probably excessive for some patients, in which case a shorter TR could be used with fewer readout periods after each excitation. The technique also may prove unsatisfactory for flow-velocity quantification in occasional patients with highly pulsatile portal venous blood flow. In these patients, cardiac gating is needed for best results.

In conclusion, our study indicates that MR angiography, enhanced by dynamic bolus-tracking methods, can be used to show portal venous anatomy and flow direction, and to quantify flow velocity in patients with normal and compromised portal venous blood flow. Moreover, varices and splenoportal shunting are readily shown. MR angiography also may prove useful for determining portal, splenic, or mesenteric vein thrombosis and shunt patency.



Fig. 5.—Patient with cirrhosis and portal hypertension. Sagittal MR angiogram shows a patent umbilical vein (solid arrows) originating from left portal vein (open arrow) and extending anteriorly and inferiorly to abdominal wall. Abdominal wall venous collaterals also are shown (curved arrow). Only a small portion of main portal vein, seen end on (arrowhead), was encompassed in images used to create angiogram.

ACKNOWLEDGMENTS

We acknowledge the assistance of Sanjiv Chopra and H. Esterbrook Longmaid in providing patients used in this study, Dennis Atkinson for assistance in pulse-sequence design, and Kathleen Dupuis for performing the patient studies.

REFERENCES

1. Singer JR. NMR diffusion and flow measurements and an introduction to spin-phase graphing. *J Phys [E]* **1978**;11:281-291
2. White EM, Edelman RR, Wedeen VJ, Brady TJ. Intravascular signal in MR imaging: use of phase display for differentiation of blood flow signal from intraluminal disease. *Radiology* **1986**;161:245-249
3. von Schulthess GK, Higgins CB. Blood flow imaging with MR: spin-phase phenomenon. *Radiology* **1985**;157:687-695
4. Axel L. Blood flow effects in magnetic resonance imaging. *AJR* **1984**;143:1157-1166
5. Wedeen VJ, Meuli RA, Edelman RR, et al. Projective imaging of pulsatile flow with magnetic resonance. *Science* **1985**;230:946-948
6. Dumoulin CL, Hart HR. MR angiography. *Radiology* **1986**;161:717-720
7. Laub GA, Kaiser WA. MR angiography with gradient motion rephasing. *J Comput Assist Tomogr* **1988**;12:377-382
8. Dixon WT, Du LN, Faul DD, et al. Projection angiograms of blood labeled by adiabatic fast passage. *Magn Reson Med* **1986**;3:454-462
9. Nishimura DG, Macovski A. MR subtraction angiography. Presented at the fifth annual meeting of the Society of Magnetic Resonance in Medicine, August 19-22, **1986**
10. Lenz GW, Haacke EM, Masaryk TJ, Laub G. In-plane vascular imaging: pulse sequence design and strategy. *Radiology* **1988**;166:875-882
11. Edelman RR, Wentz KU, Mattie H, et al. Projection arteriography and venography: initial clinical results using magnetic resonance. *Radiology* **1989**;172:351-357
12. Frahm J, Haase A, Matthaei D. Rapid NMR imaging of dynamic processes using the FLASH technique. *Magn Reson Med* **1986**;3:321-327
13. Haacke EM, Lenz G. Improving MR image quality in the presence of motion by using rephasing gradients. *AJR* **1987**;148:1251-1258
14. Edelman RR, Mattie H, Kleefield J, Silver MS. Quantification of blood flow with dynamic MR imaging and presaturation bolus tracking. *Radiology* **1989**;171:551-556
15. Edelman RR, Atkinson DJ, Silver MS. FRODO pulses: a new method for elimination of motion, flow and wraparound artifact. *Radiology* **1988**;166:231-236
16. Felmlee JP, Ehman RL. Spatial presaturation: a method for suppressing flow artifacts and improving depiction of vascular anatomy in MRI. *Radiology* **1987**;164:559-564
17. Fisher MR, Wall SD, Hricak H, et al. Hepatic vascular anatomy on MR imaging. *AJR* **1985**;144:739-745
18. Stark DD, Hahn PF, Trey C, et al. MRI of the Budd-Chiari syndrome. *AJR* **1986**;146:1141-1148
19. Cohen JM, Weinreb JC, Redman HC. Pre-operative and postoperative evaluation of the patient with a splenorenal shunt with MRI. *Surgery* **1986**;99:634-636
20. Chezmar JL, Bernadino ME. Mesosplenic shunt for the treatment of Budd-Chiari syndrome: radiologic evaluation in eight patients. *AJR* **1987**;149:707-710
21. Mostbeck GH, Wittich GR, Herold C, et al. Hemodynamic significance of the paraumbilical vein in portal hypertension: assessment with duplex US. *Radiology* **1989**;170:339-342
22. Torres WE, Gaylod GM, Whitemire L, et al. The correlation between MR and angiography in portal hypertension. *AJR* **1987**;148:1109-1112
23. Williams DM, Cho KJ, Aisen AM, Eckhauser FE. Portal hypertension evaluation by MR imaging. *Radiology* **1985**;157:703-706
24. Zoli M, Marchesini G, Cordiani MR, et al. Echo-doppler measurement of splanchnic blood flow in control and cirrhotic subjects. *JCU* **1986**;14:429-435
25. Lunderquist A, Hoevels J, Owman T. Transhepatic portal venography. In: Abrams HL, ed. *Angiography*. 3rd ed. Boston: Little, Brown, **1983**: 1505-1529

Case Report

Idiopathic Cecal Ulcer: CT Findings

Charles S. Marn,¹ Bu-Fan B. Yu,¹ Timothy T. Nostrant,² and James H. Ellis¹

Idiopathic cecal ulcer is an uncommon condition of solitary ulceration in the cecum or ascending colon, first described by Cruveilhier in 1832 [1]. The cause remains unclear. Definitive diagnosis is usually obtained by histologic evaluation of the surgical specimen. Preoperative clinical diagnosis is uncommon, requiring the exclusion of all known causes of cecal or ascending colon ulceration and mass, such as inflammatory bowel disease, neoplasm, appendicitis, tuberculosis, or amebiasis [2–4]. Although difficult to obtain, an accurate preoperative diagnosis would be beneficial in those patients without morbid features such as hemorrhage or perforation, because conservative management is possible [5].

The barium enema findings of this disease often mimic annular carcinoma [6, 7]. To our knowledge the CT findings have not been discussed before. Because CT scans are frequently obtained on patients with either acute or chronic gastrointestinal complaints, we wish to report the CT findings in two surgically proved examples of this disease.

Case Report

A 48-year-old man presented with abdominal cramping, bloody stools, and weight loss of 22 lb. (10 kg). During a similar episode 5 years earlier, barium studies of the colon and small bowel revealed distortion of the ileocecal valve and nodularity and mild narrowing of the terminal ileum. Colonoscopy showed a large ulcer in the ileocecal valve. A presumptive diagnosis of inflammatory bowel disease (probably Crohn disease) was made. Sulfasalazine was given with dramatic

improvement, and the patient was asymptomatic until this recent episode.

The patient was afebrile, with mild tenderness in the right lower quadrant. His hemoglobin was 13.1 g/100 ml, and his white count was 11,100/mm³, with a left shift. Stools were negative for blood, ova, and parasites. A small-bowel follow-through revealed mass effect at the ileocecal valve with a central, irregular barium collection (Fig. 1A). A CT scan showed asymmetric wall thickening throughout the ileocecal region and pericolic stranding (Fig. 1B). Colonoscopy revealed a large cecal wall ulceration with asymmetric distortion of the cecum and ileocecal valve. Results of a biopsy of the ulcer were negative for granulomas or neoplasm.

Because of worsening obstructive symptoms, an ileocecal resection was performed. A 4-cm ileocecal ulcer was evident, with chronic inflammatory changes (Fig. 1C). The diagnosis of idiopathic cecal ulcer was made; the patient remains well after 2 years of follow-up.

Discussion

Idiopathic cecal ulcer is an uncommon condition of unknown cause. It varies markedly in clinical presentation and course. The natural history of the disease is poorly understood because clinical signs, symptoms, and imaging characteristics frequently raise the possibility of cancer or appendicitis, and the correct diagnosis is made only after surgical resection. However, three cases diagnosed without surgery and treated conservatively have been reported recently [5].

The pathogenesis of this disorder has been the subject of considerable discussion and speculation. Although solitary, nonspecific ulcers can occur anywhere in the colon, they are

Received January 13, 1989; accepted after revision March 29, 1989.

¹ Department of Radiology, The University of Michigan Medical Center, University Hospital, 1500 E. Medical Center Dr., Box 0030, Ann Arbor, MI 48109-0030. Address reprint requests to C. S. Marn.

² Department of Gastroenterology, The University of Michigan Medical Center, University Hospital, 1500 E. Medical Center Dr., Box 0030, Ann Arbor, MI 48109-0030.

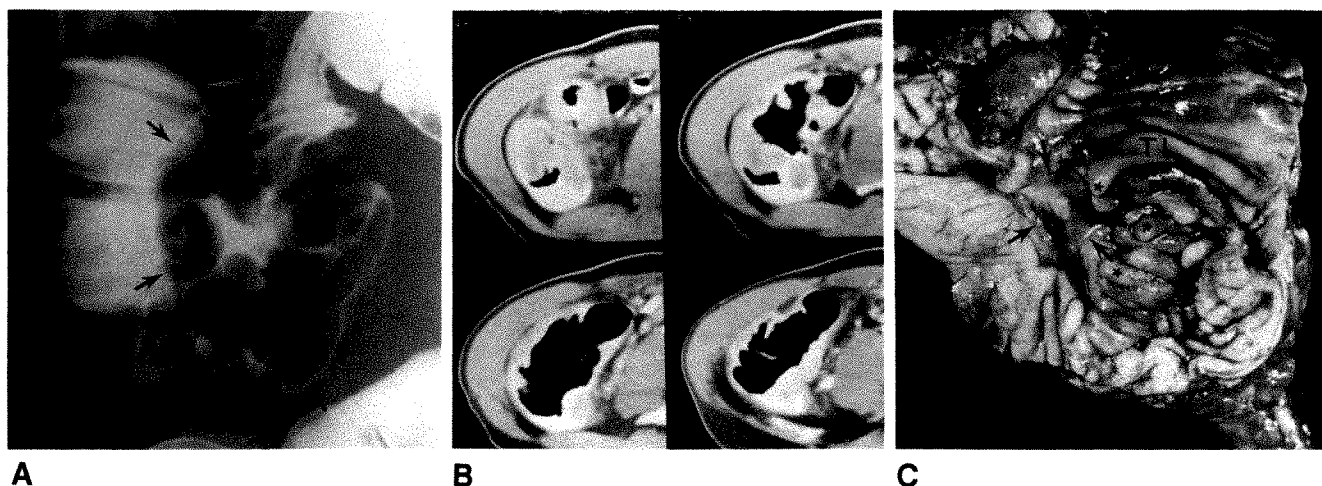


Fig. 1.—Idiopathic cecal ulcer in a 48-year-old man.

A, Small-bowel examination shows a lobular soft-tissue mass centered at ileocecal valve (arrows) with a central irregular barium collection representing ulceration.

B, Four CT images of right lower quadrant show marked lobular soft-tissue thickening of medial portion of cecum. Pericolonic stranding is evident.

C, Surgical specimen is shown with cecum and terminal ileum (TI) opened. An irregular, deep ulcer (arrows) lined with granulation tissue at its base is evident. Inflamed mucosa forms adjacent inflammatory pseudopolyps (asterisks) covering much of ileocecal valve.

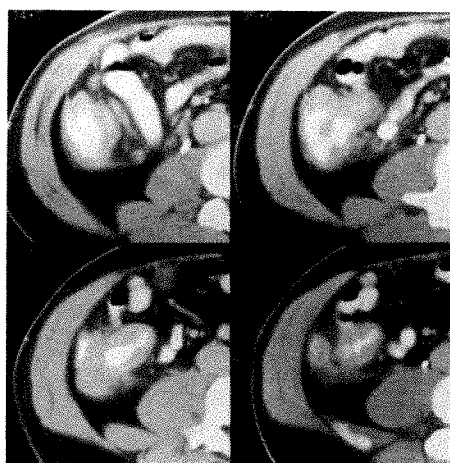


Fig. 2.—Second patient with idiopathic cecal ulcer. Contiguous CT images of cecum and terminal ileum show diffuse homogeneous wall thickening and pericolonic stranding.

most common in the cecum and ascending colon [3, 4]. Hence, colonic irritation by small-bowel contents has been raised as a possible mechanism [2, 4]. Vasculitis or ischemia have been suggested as contributing factors, but this idea has not been confirmed [2]. Drug therapy, including antiinflammatory agents, steroids, or enteric-coated potassium tablets, has been implicated in some cases [2, 4]. As with other gastrointestinal ulcerations, multiple causes are possible.

The radiographic evaluation of idiopathic cecal ulcer by barium studies has been reported [6]. When a barium enema is performed, approximately 75% of cases show some abnormality. However, the ulcer crater itself is infrequently seen.

More commonly, a range of nonspecific features is evident, including segmental narrowing with or without a shelflike defect, spasm and incomplete filling of the involved segment, and mucosal irregularity. Annular lesions have been described, and the incorrect preoperative diagnosis of malignancy is often made. Mesenteric angiography is useful for localizing the site of active bleeding, but this disorder has no specific angiographic features. Intraarterial infusion of vasopressin frequently controls bleeding [7].

The last decade has seen a dramatic increase in the use of CT for bowel-wall abnormalities. The CT findings of inflammatory bowel disease, infection, carcinoma, and lymphoma have been discussed [8]. Our limited experience with CT of idiopathic cecal ulcer shows nonspecific findings. Along with the case presented, we have found one other CT study of this type of lesion from our institution (Fig. 2). This case has somewhat different features, with more diffuse wall thickening of the cecum and involvement of the terminal ileum, whereas the reported case (Fig. 1B) had more mass effect at the ileocecal valve. Bowel-wall thickening with homogeneous attenuation was evident in both patients. In one case, this abnormality was circumferential and involved a significant portion of the terminal ileum. The other case showed asymmetric involvement, with a polypoid mass effect at the ileocecal valve. Both cases showed some degree of stranding in pericolonic fat. None of these findings suggests a specific diagnosis.

Therapy is dictated by both the clinical presentation and the gravity of the major differential diagnostic considerations [2–5]. In the setting of gastrointestinal hemorrhage, perforation, or abscess formation, immediate surgical management is dictated by the seriousness of the patient's acute illness. In more indolent cases, imaging characteristics and endoscopic findings may raise the possibility of malignancy and

provide impetus for surgical exploration. A limited nonsurgical experience with three patients has been reported recently and raises the possibility of nonsurgical management [5]. However, conservative management is based on the presumption that colonoscopic biopsies that reveal only inflammatory cells are indeed representative of the entire mass involving the cecum. These patients obviously require close clinical follow-up, including repeated examinations at times when no symptoms are present.

ACKNOWLEDGMENTS

The authors gratefully acknowledge the assistance of Henry Appleman of the Department of Pathology for review of surgical specimens.

REFERENCES

1. Cruveilhier J. Un beau cas de cicatrisation d'un ulcère de l'intestin gauche datant d'une douzaine d'années. *Bull Soc Anat* **1832**;7:1-2
2. Mark HI, Ballinger WF. Nonspecific ulcer of the colon, report of a case and review of 51 cases from the literature. *Am J Gastroenterol* **1964**;41:266-291
3. Butsch JL, Dockerty MB, McGill DB, Judd ES. "Solitary" nonspecific ulcers of the colon. *Arch Surg* **1969**;98:171-174
4. Ona FV, Allende HD, Vivencio R, Zaky DA, Nadarja N. Diagnosis and management of nonspecific colon cancer. *Arch Surg* **1987**;117:887-894
5. Blundell CR, Earnest DL. Idiopathic cecal ulcer: diagnosis by colonoscopy followed by nonoperative management. *Dig Dis Sci* **1980**;25:494-503
6. Gardiner GA, Bird CR. Nonspecific ulcers of the colon resembling annular carcinoma. *Radiology* **1980**;137:331-334
7. Sutherland D, French RS, Weil R, Najarian JS, Simmons RL. The bleeding cecal ulcer: pathogenesis, angiographic diagnosis, and nonoperative control. *Surgery* **1972**;71:290-294
8. Balthazar EJ. Colon. In: Megibow AJ, Balthazar EJ, eds. *Computed tomography of the gastrointestinal tract*. St. Louis: Mosby, **1986**:274-385

American Roentgen Ray Society Residents' Award Papers, 1990

The ARRS announces competition for the 1990 President's Award and two Executive Council Awards for the best papers concerning the clinical application of the radiologic sciences.

Awards

The winner of the President's Award will receive a certificate and a \$2000 prize. The winners of the two Executive Council Awards will each be given a certificate and a prize of \$1000. The winners will be announced on March 15, 1990. Winning papers will be presented at the ARRS annual meeting at the Sheraton Washington Hotel, Washington, D.C., May 13-18, 1990. Winning papers will be submitted for early publication in the *American Journal of Roentgenology*. All other papers will be returned to the authors.

Regulations

Eligibility is limited to residents or fellows in radiology who have not yet completed 4 years of approved training in a radiologic discipline. A letter from the resident's department chairman attesting to this status must accompany the manuscript. The resident must be the sole or senior author and be responsible for all or most of the project.

Submitted manuscripts must not exceed 5000 words and have no more than 10 illustrations. Four copies of the manuscript and illustrations are required. Submitted manuscripts should not contain previously presented or published material and should not be under consideration for publication elsewhere.

Deadline for submissions is February 16, 1990. Send papers to

B. G. Brogdon, M.D.
Chairman, Committee on Education & Research
American Roentgen Ray Society
Department of Radiology
University of South Alabama Medical Center
2451 Fillingim Street
Mobile, AL 36617

FORTHCOMING ARTICLES

EDWARD B. D. NEUHAUSER MEMORIAL LECTURE

Reflections of men and machines from red goggles and spin wobbles. *Baker DH*

REVIEW ARTICLES

Imaging of the acute abdomen in infants and children. *Franken EA, Kao SC, Smith WL, Sato Y*

Guided percutaneous biopsy of intraabdominal lesions. *Gazelle GS, Haaga JR*

PULMONARY RADIOLOGY

Pulmonary lymphangiomyomatosis: CT findings. *Sherrier RH, Chiles C, Roggli V*

Treatment of loculated pleural effusions with transcatheter intracavitary urokinase. *Moulton JS, Moore PT, Mencini RA*

Pictorial essay. Malignant primary germ cell tumors of the mediastinum: CT features. *Lee KS, Im J, Han CH, Han MC, Kim C, Kim WS*

Case report. Peripheral bronchial involvement in relapsing polychondritis: demonstration by thin-section CT. *Davis SD, Berkmen YM, King T*

BREAST RADIOLOGY

Carcinoma mimicked by the sternal insertion of the pectoralis muscle. *Britton CA, Baratz AB, Harris KM*

Minimal volume excision of nonpalpable mammographic lesions. *Gallagher WJ, Cardenosa G, Rubens JR, McCarthy KA, Kopans DB*

Diagnosis of breast calcifications: comparison of contact, magnified, and television-enhanced images. *Kimme-Smith C, Gold RH, Bassett LW, Gormley L, Morioka C*

GASTROINTESTINAL RADIOLOGY

Contrast-enhanced CT of the liver and spleen: comparison of ionic and nonionic contrast agents. *Nelson RC, Chezmar JL, Peterson JE, Bernardino ME*

The accuracy of sonography in determining the number and size of gallbladder stones before and after lithotripsy. *Mathieson JR, So CB, Malone DE, Becker CD, Burhenne HJ*

Auxiliary partial liver transplantation: imaging evaluation in 10 patients. *Zonderland HM, Lameris JS, Terpstra OT, et al.*

Acute thrombosis of the inferior vena cava and hepatic veins in patients with the Budd-Chiari syndrome: CT demonstration. *Mori H, Maeda H, Fukuda T, et al.*

Sonographically guided paracentesis for palliation of symptomatic malignant ascites. *Ross GJ, Kessler HB, Clair MR, Gatenby RA, Hartz WH, Ross LV*

The lack of sonographic image degradation after barium upper gastrointestinal examination. *Elam EA, Hunter TB, Hunt KR, Fajardo LL, Boren W, Gaines J*

Case report. Microscopic (collagenous) colitis. *Glick SN, Teplitz SK, Amenta PS*

GENITOURINARY RADIOLOGY

The distinction between obstructive and nonobstructive pyelocaliectasis using duplex Doppler sonography. *Platt JF, Rubin JM, Ellis JH*

Technical note. MR imaging of the cervix: off-axis scan to improve visualization of zonal anatomy. *Baumgartner BR, Bernardino ME*

Surgical transposition of the ovaries: imaging findings in 14 patients. *Kier R, Chambers SK*

Case report. Ovarian lipoleiomyoma: a fat-containing mass in the female pelvis. *Dodd GD, Lancaster KT, Moulton JS*

Case report. Fractured penis: sonographic aid to diagnosis. *Forman HP, Rosenberg HK, Snyder HM*

MUSCULOSKELETAL RADIOLOGY

Calcific tendonitis of the long head of the biceps brachii distal to the glenohumeral joint: plain film radiographic findings. *Goldman AB*

Computed arthrotomography of the shoulder: comparison examinations made with internal and external rotation of the humerus. *Pennes DR, Jonsson K, Buckwalter K, Braunstein E, Blasier R, Wojtys E*

Pictorial essay. The radiologic features of eosinophilic granuloma of bone. *David R, Oria RA, Kumar R, et al.*

PEDIATRIC RADIOLOGY

Cranial arteriovenous malformations in neonates: color Doppler imaging with angiographic correlation. *Tessler FN, Dion J, Vinuela F, et al.*

Case report. Hepatic parenchymal and subcapsular gas after hepatic laceration caused by blunt abdominal trauma. *Abramson SJ, Berdon WE, Kaufman RA, Ruzal-Shapiro C*

NEURORADIOLOGY

Frequency and variation of the posterior pituitary bright signal on MR images. *Brooks BS, Gammal TE, Allison JD, Hoffman WH*

MR imaging of the cranial meninges, with emphasis on contrast enhancement and meningeal carcinomatosis. *Sze G, Soletsky S, Bronen R, Krol G*

Topography and identification of the inferior precentral sulcus in MR imaging. *Ebeling U, Steinmetz H, Huang Y, Kahn T*

Acquired spinal subarachnoid cysts: evaluation with MR, CT myelography, and intraoperative sonography. *Sklar E, Quencer RM, Green BA, Montalvo BM, Post MJ*

VASCULAR RADIOLOGY

CT diagnosis of renal artery injury caused by blunt abdominal trauma. *Lupetin AR, Mainwaring BL, Daffner RH*

Takayasu arteritis: angiographic findings and results of angioplasty. *Park JH, Han MC, Kim SH, Oh BH, Park YB, Seo JD*

Case report. Iliac artery endoprosthesis: radiologic and histologic findings after two years. *Rousseau H, Joffe F, Raillat C, Dubouchier C, Glock Y, Escourrou G*

Case report. Percutaneous transhepatic treatment of a large intrahepatic aneurysm. *Rothbarth LJ, Redmond PL, Kump DA*

CONTRAST MATERIAL

Current use of low-osmolality contrast agents: results of a survey. *Bettmann MA, Geller S, McClennan B, Dunnick NR*

COMPUTER PAGE

Automated entry of radiology requisition information with artificial-intelligence techniques. *Kahn CE, Kovatsis PG, Messersmith RN, Lehr JL*

PERSPECTIVES

Restrictive covenants in professional employment contracts. *Roper RR*

New competitive strategies for the practice of radiology in a changing economic environment. *Young SW*

Renal Imaging in Long-term Dialysis Patients: A Comparison of CT and Sonography

Andrew J. Taylor¹
Eric P. Cohen²
Scott J. Erickson¹
David L. Olson¹
W. Dennis Foley¹

Patients undergoing long-term dialysis are subject to cyst formation, hemorrhage, and neoplasia in their native kidneys. Detection of these complications with incremental dynamic CT and detection with sonography were compared prospectively in 41 patients (79 kidneys) who had been undergoing dialysis intermittently for 3 or more years. Acquired cystic kidney disease (five or more cysts per kidney) was identified in 59% of kidneys by use of CT and in 18% by use of sonography. CT showed a complete renal contour definition in all cases, sonography did so in only 57%. Three solid renal tumors (2- to 4-cm diameter) were identified with both techniques with no false-negative evaluations. Four benign hemorrhagic cysts were identified with combined CT (hyperdense mass) and sonography (benign cysts). CT provided the best anatomic image quality and was more accurate for detection of acquired cystic kidney disease. CT and sonography were equivalent for detection of solid tumors.

Our results suggest that dynamic contrast-enhanced CT scanning with the supplemental use of sonography is the best imaging regimen for the evaluation of suspected acquired cystic kidney disease and its potential complications.

AJR 153:765-767, October 1989

Acquired cystic kidney disease refers to the development of cysts in the failing kidney. Although Simon first described the association of cysts with end-stage renal disease in 1847 [1], it was not until 1977 that the concept of acquired cystic kidney disease was formalized by Dunnill et al. [2]. Acquired cystic kidney disease, with its potential complications of hemorrhage and neoplasia, is of growing concern in the expanding population of patients undergoing dialysis. Imaging has become a valuable, although inexact tool for initial evaluation and sequential studies of native kidneys in this population.

Other authors have described the CT and sonographic findings in acquired cystic kidney disease [3-7]. In some cases, the author has attempted to compare the diagnostic accuracies of these two imaging techniques [4, 6, 8]. We report the results of a prospective comparison of CT and sonography, using state-of-the-art equipment and techniques, in patients at risk for acquired cystic kidney disease.

Subjects and Methods

Forty-one patients (20 men, 21 women; age range, 18-75 years) with end-stage renal disease of various causes were included in the study. Forty patients had been treated with maintenance hemodialysis or peritoneal dialysis for 3 years or more; one patient, previously treated with dialysis for more than 3 years, had a functioning renal transplant. These 41 patients had a total of 79 native kidneys. CT and sonography generally were performed on the same day or within 1 week of each other.

CT scans were made with 1-cm sections at 1-cm intervals, both before and after contrast administration. An incremental dynamic scanning technique was used after bolus administration of 100 ml of 60% ionic contrast material. Five-millimeter sections were used at the

Received March 3, 1989; accepted after revision June 6, 1989.

Presented in part at the 21st annual meeting of the American Society of Nephrology, San Antonio, TX, December 1988.

¹ Department of Radiology, Medical College of Wisconsin, Milwaukee, WI 53226. Address reprint requests to A. J. Taylor, Dept. of Radiology, Froedtert Memorial Lutheran Hospital, 9200 W. Wisconsin Ave., Milwaukee, WI 53226.

² Department of Medicine, Medical College of Wisconsin, Milwaukee, WI 53226.

0361-803X/89/1534-0765
© American Roentgen Ray Society

discretion of the radiologist monitoring the examination. In five patients, only unenhanced CT studies were performed. A GE CT 9800 (GE Medical Systems, Milwaukee, WI) was used for 36 examinations and a GE CT 8800 for five examinations. Sonography was performed with a GE R/T 3600 (36 patients) or an Acuson 128 (Mountain View, CA) (five patients) with both 3.5- and 5.0-MHz transducers. Images were acquired in the coronal, sagittal, and axial planes.

Both the CT and sonographic studies were evaluated independently by three radiologists. Identification of patients was removed from all images. Each study was evaluated for presence and degree of acquired cystic kidney disease, definition of renal contour, and presence of a solid renal mass. Renal cystic changes, when present, were graded as follows: grade 0 = no cysts, grade 1 = fewer than five cysts, grade 2 = five to 10 cysts, grade 3 = 11–15 cysts, grade 4 = more than 15 cysts/kidney. This grading scale is modified from that originally proposed by Thomson et al. [9]. Acquired cystic kidney disease was defined as five or more cysts per kidney. Definition of renal contour was characterized as follows: grade 0 = complete renal contour shown, grade 1 = partial loss of renal contour, grade 2 = complete loss of renal contour.

CT scans made before and after contrast administration were compared for anatomic definition and lesion conspicuity.

Results

Identification of Cystic Change

Each technique showed an equal grade of cystic change in 27 (34%) of 79 kidneys. CT showed a higher grade in 52 (66%) of 79 kidneys.

In evaluation for acquired cystic kidney disease, sonography showed only 29% of cases shown by CT. There were no false-positive sonographic diagnoses of acquired cystic kidney disease. The prevalence of acquired cystic kidney disease was 59% as determined by CT, and was 18% as determined by sonography.

Renal Contour Definition

All CT studies were classified as grade 0 (complete renal contour definition). The scores assigned to sonographic examinations were 57% grade 0 (complete renal contour defi-

nition); 32% grade 1 (incomplete renal contour definition); and 11% grade 2 (total loss of renal contour definition).

Detection of Renal Mass Lesions

Evidence of a renal mass lesion was seen with one or both techniques in nine patients. In three patients, solid renal masses that varied in size from 2.0×2.5 cm to 3.0×4.0 cm were shown by both imaging techniques (Fig. 1). All three lesions were later confirmed to be primary malignant tumors by biopsy or nephrectomy. In a fourth patient, two contiguous hyperdense masses, each less than 1 cm in diameter, were seen on precontrast CT scans and had appearances typical for benign renal cysts on sonograms. At subsequent nephrectomy, these lesions were described as retention cysts. In three other patients, small hyperdense masses were shown on precontrast CT scans, whereas sonograms showed typical benign renal cysts. These cases are considered typical hyperdense hemorrhagic renal cysts. In one patient, a 1.5-cm mass was questioned on sonography because of a poorly defined back wall. CT findings were consistent with a simple renal cyst. No cyst puncture or biopsy was performed. In one patient, sonography suggested a solid renal mass, whereas CT findings were consistent with focal hypertrophy in a zone of kidney tissue that enhanced homogeneously after administration of contrast material.

Of 36 patients who had precontrast and postcontrast CT studies, the postcontrast examination was judged superior in 28 (80%).

Discussion

Since the article by Dunnill et al. in 1977 [2], many radiographic imaging surveys for acquired cystic kidney disease and its complications have been reported [3, 4, 6, 7, 10–12]. Various authors have suggested sonography alone [11, 13], sonography and CT [4, 14], or CT alone [7, 10, 12, 15] as the appropriate technique for monitoring patients. Other authors have suggested that either imaging technique is suitable [16]. In this study, state-of-the-art sonographic and CT equip-

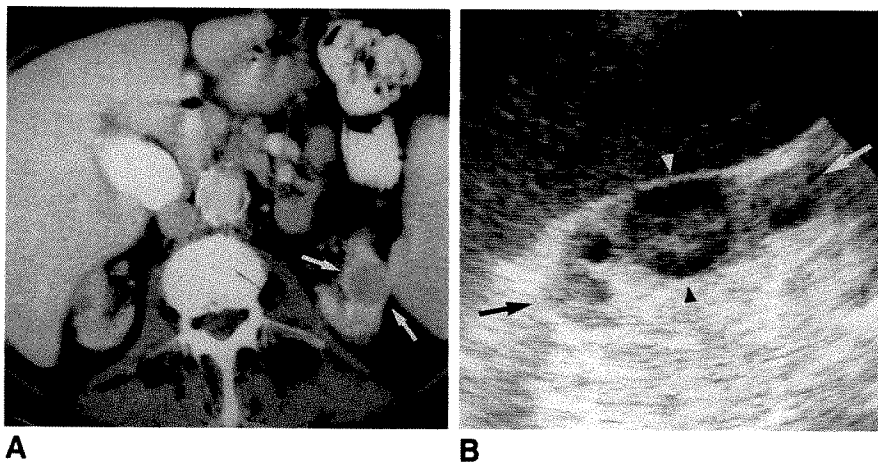


Fig. 1.—Patient with transitional cell carcinoma.

A, CT scan through native kidneys shows solid mass (arrows) in left kidney.

B, Longitudinal sonogram shows mass (arrowheads) in this small, echogenic kidney (arrows). A small cyst is seen just cephalad to mass with a hypoechoic renal pyramid caudally.

ment and technique were used to determine the strengths and weaknesses of each for evaluating patients at risk for acquired cystic kidney disease and its complications.

Contrast-enhanced CT produced the better resolution of renal contour and grading of acquired cystic kidney disease changes in patients with end-stage renal disease. The fibrotic, shrunken kidney seen in patients with end-stage renal disease is difficult to image sonographically. The kidney itself, as well as the fat and bowel that could fill in the renal bed, adds to the difficulty in imaging. These topographic changes do not affect CT imaging.

Contrast-enhanced CT, with a thin-section technique, shows greater resolution than sonography; it can resolve cysts as small as 0.3 cm [6]. Cysts less than 1 cm are difficult to resolve sonographically. The difference in resolution is important, considering that most cysts in acquired cystic kidney disease are 5 mm or less [17]. This difference is reflected in the prevalence of acquired cystic kidney disease shown by CT at 59% compared with a prevalence of only 18% shown by sonography. CT also was able to show a higher grade of cystic change in two thirds of the cases. Although use of CT as the gold standard creates an inherent bias, the differences in these results are substantial.

The definition of cystic change is not only of academic interest. The complications of neoplasia and hemorrhage are associated with acquired cystic kidney disease and, therefore cyst development is an important clinical marker [10, 15, 18].

We believe that IV contrast enhancement is an integral part of the CT scanning technique. Contrast enhancement was judged useful in 80% of the CT examinations in which it was used. The incremental dynamic scanning technique uses contrast material circulating in renal capillaries to provide a tissue "signature." This enhancement helps define small cysts, is useful in defining solid masses, and helps to distinguish focal hypertrophy from solid masses.

Patients with end-stage renal disease with normal cardiovascular function can undergo this bolus-enhanced dynamic scanning technique without risk of fluid overload. In our series, bolus injections of contrast material were given without regard to the subsequent timing of dialysis treatments.

Sonography was clearly inferior to CT for evaluating contour definition and grading acquired cystic kidney disease. However, it is useful for evaluating focal hyperdense masses seen on precontrast CT scans. In our series, four hyperdense masses were characterized as hemorrhagic simple cysts on the basis of sonographic and CT correlation.

Because of the potentially life-threatening complications of hemorrhage or neoplasm in acquired cystic kidney disease, nearly all authors suggest screening patients after 3 years of dialysis. Our data suggest that dynamic contrast-enhanced CT scanning with the supplemental use of sonography is the best imaging regimen. Subsequent progress-imaging studies

done yearly, or possibly every second year, seem appropriate, but long-term studies are needed to show the efficacy of this approach. The symptomatic patient with hematuria, flank pain, abdominal mass on physical examination, or an unexplained drop in hematocrit warrants immediate study.

ACKNOWLEDGMENTS

The authors thank Pam Soberg and Jan Staedler for their help in the preparation of this manuscript.

REFERENCES

1. Simon J. On sub-acute inflammation of the kidney. *Medico-Chirurg Trans Lond* 1847;30:141-164
2. Dunnill MS, Millard PR, Oliver D. Acquired cystic disease of the kidneys: a hazard of long-term intermittent maintenance haemodialysis. *J Clin Pathol* 1977;30:868-877
3. Bommer J, Waldherr R, van Kaick G, Strauss L, Ritz E. Acquired renal cysts in uremic patients—in vivo demonstration by computed tomography. *Clin Nephrol* 1980;14:299-303
4. Narasimhan N, Golper TA, Wolfson M, Rahatzad M, Bennett WM. Clinical characteristics and diagnostic considerations in acquired renal cystic disease. *Kidney Int* 1986;30:748-752
5. Andersen BL, Curry NS, Gobien RP. Sonography of evolving renal cystic transformation associated with hemodialysis. *AJR* 1983;141:1003-1004
6. Levine E, Grantham JJ. The role of computed tomography in the evaluation of adult polycystic kidney disease. *Am J Kidney Dis* 1981;1:99-105
7. Cho C, Friedland GW, Swenson RS. Acquired renal cystic disease and renal neoplasms in hemodialysis patients. *Urol Radiol* 1984;6:153-157
8. Jabour BA, Ralls PW, Tang WW, et al. Acquired cystic disease of the kidneys: computed tomography and ultrasonography appraisal in patients on peritoneal and hemodialysis. *Invest Radiol* 1987;22:728-732
9. Thomson BJ, Jenkins DA, Allan PL, Elton RA, Winney RJ. Acquired cystic disease of the kidney in patients with end-stage chronic renal failure: a study of prevalence and aetiology. *Nephrol Dial Transplant* 1986;1:38-43
10. Ishikawa I, Saito Y, Onouchi Z, et al. Development of acquired cystic disease and adenocarcinoma of the kidney in glomerulonephritic chronic hemodialysis patients. *Clin Nephrol* 1980;14:1-6
11. Minar E, Tscholkoff D, Zazgornik J, Schmidt P, Marosi L, Czemberek H. Acquired cystic disease of the kidneys in chronic hemodialyzed and renal transplant patients. *Eur Urol* 1984;10:245-248
12. Levine E, Grantham JJ, Slusher SL, Greathouse JL, Krohn BP. CT of acquired cystic kidney disease and renal tumors in long-term dialysis patients. *AJR* 1984;142:125-131
13. Weissberg DL, Miller RB. Renal cell carcinoma and acquired cystic disease of the kidneys in a chronically dialyzed patient. *J Ultrasound Med* 1983;2:191-194
14. Kutcher R, Amodio JB, Rosenblatt R. Uremic renal cystic disease: value of sonographic screening. *Radiology* 1983;147:833-835
15. Gehrig JJ Jr, Gottheiner TI, Swenson RS. Acquired cystic disease of the end-stage kidney. *Am J Med* 1985;79:609-620
16. Smith JW, Sallman AL, Williamson MR, Lott CG. Acquired renal cystic disease: two cases of associated adenocarcinoma and a renal ultrasound survey of a peritoneal dialysis population. *Am J Kidney Dis* 1987;10:41-46
17. Hughson MD, Hennigar GR, McManus JF. Atypical cysts, acquired renal cystic disease, and renal cell tumors in end-stage dialysis kidneys. *Lab Invest* 1980;42:475-480
18. Grantham JJ, Levine E. Acquired cystic disease: replacing one kidney disease with another. *Kidney Int* 1985;28:99-105

Imaging Studies for Screening Native Kidneys in Long-term Dialysis Patients

Howard J. Mindell¹

Since the classic paper in 1977 by Dunnill et al. [1], a substantial number of articles have been written concerning the complications of acquired cystic kidney disease and solid neoplasms developing in the native kidneys of patients undergoing long-term hemodialysis or peritoneal dialysis. Patients undergoing renal transplantation also may be so affected, but are far less at risk. From animal experiments and human specimen dissections, consensus has emerged that dialysis fails to clear unknown bioactive substance(s), possibly polyamines [2], which exert renotropic or mitogenic effects on the native kidneys, inducing smooth muscle [3], glomerular, or tubular proliferative processes [4]. Cysts, lined by low cuboidal or columnar epithelium, are thought to develop as fusiform dilatations of the proximal tubules [5]. Solid neoplasms, mostly adenomas, but in some instances carcinomas, may occur also, almost always superimposed on antecedent acquired kidney disease, and arising in some cases from papillary projections off of cyst walls [6].

The risk of these complications is related to the duration of long-term dialysis. Acquired cystic kidney disease has a prevalence of up to 90% of patients after 3 years of long-term dialysis [7]. The solid neoplasms are reported in varying numbers, 7% in the largest available survey [5]. Several reports describe the use of imaging studies in long-term dialysis patients and suggest a variety of management schemes to screen or monitor the status of long-term dialysis patients' native kidneys. Recommendations have included the use of baseline studies right after the start of dialysis [6],

sonography, CT, or both sonography and CT [7]; the use of MR imaging [7] and even prophylactic native-kidney nephrectomy [8] has been considered worth evaluating. The report of Taylor et al. [9] in this issue of *AJR*, however, is only the second blinded prospective study comparing the efficacy of CT and sonography in this setting and is the first to use systematically both sonography and CT in all patients studied. Taylor et al. [9] clearly show CT is better than sonography (59% to 18%) for detecting acquired cystic kidney disease in long-term dialysis patients. Undoubtedly, CT has some margin of superiority over sonography in detecting the small solid renal masses as well, but unfortunately actual data, either from the literature or from this study, are lacking. In the earlier blinded series [7], only one patient had renal cell carcinoma, and the three small renal cell carcinomas in the study of Taylor et al. [9] (7% of 41 patients) were identified by both sonography and CT. Furthermore, Taylor et al. [9] found four hyperdense (CT) masses, shown to be hemorrhagic cysts on sonography, that might have been false-positive for tumor if CT alone had been used. A recent comprehensive blinded study [10], albeit in normal-sized and functioning kidneys, compared sonography, CT, and urography with tomography in detecting small renal masses (<3 cm). CT was used as the gold standard, but sonography showed 82% of lesions 2–3 cm in size, 85% of lesions larger than 3 cm, and was comparable to urography with tomography.

Should routine screening imaging studies be done on long-term dialysis patients? If so, is CT, as suggested by Taylor et

This article is a commentary on the preceding article by Taylor et al.

¹ Department of Radiology, Medical Center Hospital of Vermont, University of Vermont College of Medicine, Burlington, VT 05401. Address reprint requests to H. J. Mindell.

al. [9], the method of choice, with annual examinations in all patients after 3 years of dialysis? To address these questions, one must first consider the medical and socioeconomic milieu of long-term dialysis patients and, second, the clinical significance of either acquired cystic kidney disease or the solid renal masses that might be so detected.

The nearly 100,000 (C. Hill, personal communication) patients in the United States requiring long-term dialysis have a mean age of over 55 years [11] and 5- and 10-year survival rates of 45% and 25%, respectively [12]. The medical complications of long-term dialysis fill an entire page, in small print, in *Harrison's Principles of Internal Medicine* [11]; these patients have an impaired quality of life, with limited mobility, but where medical procedures are commonplace. The actual cost of long-term dialysis is \$26,000 per year (C. Hill, personal communication), and ancillary medical costs may add an additional \$20,000. The long-term dialysis program is funded by Medicare at an annual cost of \$2 billion (C. Hill, personal communication).

As acquired cystic kidney disease occurs in up to 90% of long-term dialysis patients, its presence may be inferred after 3 years of dialysis without any imaging study at all. In any case, acquired cystic kidney disease by itself is of no clinical significance. To be sure, calculi, infection, or hemorrhage may develop in patients with the disease, but the mere diagnosis of acquired cystic kidney disease requires no specific treatment plan—these patients are under close medical supervision, and complications may be dealt with as they arise.

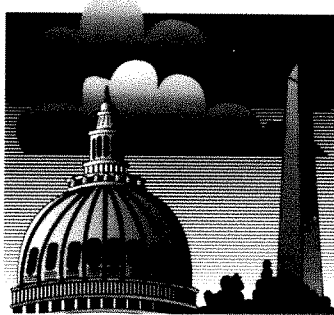
Solid renal masses develop with a prevalence of 7% (43 of 601 patients, multiple series review) [5] in long-term dialysis patients, but most are benign adenomas. The actual incidence of renal cell carcinoma is impossible to determine accurately, given the similar renal tubular histogenesis of adenoma and carcinoma. The natural history of these small tumors is unknown. Ratcliffe et al. [13], for instance, stated that their "malignant potential is uncertain," and Levine et al. [6] observed that the high frequency with which small, single or multiple renal tumors are found at autopsy in long-term dialysis patients "suggests that most remain quiescent." What is known, however, is that only two of 601 patients reported in a review of 14 long-term dialysis series [5] developed metastatic renal cancer, for a prevalence of 0.33%, which is equal to that of the general population. The dilemma posed by these small tumors is best illustrated by the proposal [5] of one group to use a screening CT protocol to find the lesions but then to avoid resection of the tumors, but simply use CT follow-up and intervention only if tumor growth is seen.

Gardner [14] suggested that questions regarding screening native kidneys of long-term dialysis patients cannot be answered until more data are made available by End-Stage Renal Disease Networks and the Health Care Financing Administration. The work by Taylor et al. [9], a carefully designed and executed study, should be given serious attention, but it does not provide the kind of "outcome" data necessary to formulate policy. Annual CT screening of all long-term dialysis patients after 3 years would add \$30 million (60,000 patients at \$500 per CT examination) to the existing Medicare budget,

as well as subjecting a population of fragile patients to the inconvenience of the studies, and the at-least small risk attendant to use of IV contrast medium (CT) in the face of chronic renal failure. Obviously, performing nephrectomies for the solid tumors identified would give incremental additional monetary costs as well as increased morbidity and mortality rates from the surgery. All of this provides no proved or clear improvement in actual outcome for long-term dialysis patients. The work of Taylor et al. [9] certainly shows that when long-term dialysis patients develop signs or symptoms referable to their native kidneys, CT is the imaging method of choice. Sonography is comparable to urography with tomography in normal-sized kidneys for detecting small renal masses [10], 82% as sensitive as CT for masses between 2 and 3 cm in size [10], and equal to CT for the three small carcinomas in the Taylor et al. [9] study. Inexpensive, easily available, with no requirement for IV contrast medium, sonography is most likely the only practical, affordable method to consider for screening 60,000 long-term dialysis patients annually. Even so, "outcome" studies clearly are needed before sonography should be mobilized across the board for this huge population of patients.

REFERENCES

1. Dunnill MS, Millard PR, Oliver D. Acquired cystic disease of the kidneys: a hazard of long-term intermittent maintenance haemodialysis. *J Clin Pathol* 1977;30:868-877
2. Bagdade JD, Subbiah PV, Bartos D, Bartos F, Campbell FA. Polyamines: an unrecognized cardiovascular risk factor in chronic dialysis. *Lancet* 1979;1:412-413
3. McManus JFA, Hughson MD, Fitts CT, Williams AV. Studies on "end stage" kidneys. Nodule formation in intrarenal arteries and arterioles. *Lab Invest* 1977;37:339-349
4. McManus JFA, Hughson MD, Hennigar GR, Fitts CT, Rajagopalan PR, Williams AV. Dialysis enhances renal epithelial proliferations. *Arch Pathol Lab Med* 1980;104:192-195
5. Grantham JJ, Levine E. Acquired cystic disease: replacing one kidney disease with another. *Kidney Int* 1985;28:99-105
6. Levine E, Grantham JJ, Slusher SL, Greathouse JL, Krohn BP. CT of acquired cystic kidney disease and renal tumors in long-term dialysis patients. *AJR* 1984;142:125-131
7. Jabour BA, Ralls PW, Tang WW, et al. Acquired cystic disease of the kidneys. Computed tomography and ultrasonography appraisal in patients on peritoneal and hemodialysis. *Invest Radiol* 1987;22:728-732
8. Kutcher R, Amodio JB, Rosenblatt R. Uremic renal cystic disease: value of sonographic screening. *Radiology* 1983;147:833-835
9. Taylor AJ, Cohen EP, Enckson SJ, Olson DL, Foley WD. Renal imaging in long-term dialysis patients: a comparison of CT and sonography. *AJR* 1989;153:765-767
10. Warshauer DM, McCarthy SM, Street L, et al. Detection of renal masses: sensitivities and specificities of excretory urography/linear tomography, US and CT. *Radiology* 1988;169:363-365
11. Carpenter CB, Lazarus MJ. Dialysis and transplantation in the treatment of renal failure. In: Braunwald E, Isselbacher KJ, Petersdorf RG, Wilson JD, Martin JB, Fauci AS, eds. *Harrison's principles of internal medicine*. New York: McGraw-Hill, 1987:1162-1164
12. Vollmer WM, Wahl PW, Bagg CA. Survival with dialysis and transplantation in patients with end stage renal disease. *N Engl J Med* 1983;308:1553-1558
13. Ratcliffe PJ, Dunnill MS, Oliver DO. Clinical importance of acquired cystic disease of the kidney in patients undergoing dialysis. *Br Med J* 1983;287:1855-1858
14. Gardner KJG. Acquired renal cystic disease and renal adenocarcinoma in patients on long-term hemodialysis (letter). *N Engl J Med* 1984;310:390



Come to the
American Roentgen Ray Society

90th

ANNUAL MEETING

Washington, D. C.

Sheraton Washington Hotel
May 13-18, 1990

Scientific Program (200 papers)

Instructional Courses (60 hours)

Categorical Course on Cardiovascular Imaging

The Caldwell Lecture

Award Papers

Scientific Exhibits

Social, Golf, and Tennis Programs

Guest Programs



In Vivo MR Spectroscopic Imaging of the Adrenal Glands: Distinction Between Adenomas and Carcinomas Larger than 15 mm Based on Lipid Content

Anne Leroy-Willig^{1,2}
 Jacques Bittoun³
 Jean Pierre Luton⁴
 Albert Louvel⁵
 Jean Eric Lefevre³
 André Bonnin⁶
 Jean Claude Roucayrol¹

The usefulness of MR spectroscopic imaging for discriminating between lipid and water was applied to the in vivo differentiation of adrenal adenomas from carcinomas. By using the Dixon sequence in 20 patients, the lipid content of 22 adrenal tumors larger than 15 mm was determined. The mean percentage of lipid in 15 adenomas was 13.4% (standard deviation, 8%), compared with 3.5% lipid (standard deviation, 2%) in seven carcinomas. Only one lesion would have been misclassified on the basis of in vivo measurements of lipid content. After surgery, in vitro MR spectroscopy was used to determine the percentage of lipid in excised samples of nine of the 22 tumors. These in vitro measurements confirmed the in vivo results on lesions larger than 20 mm in diameter. Respiratory artifacts appeared to decrease the accuracy of in vivo measurements in smaller lesions.

In vivo MR spectroscopic imaging of adrenal tumors appears to be useful for differentiating between adrenal carcinomas and adenomas.

AJR 153:771-773, October 1989

In addition to anatomic definition of the adrenal glands [1-3], MR imaging provides some information about the biochemistry of adrenal lesions. However, the signal intensities of different types of lesions overlap on conventional T1- and T2-weighted spin-echo images [4-6], so that a specific diagnosis often is impossible.

We have shown in vitro, by using MR proton spectroscopy, that adrenal cortical lesions (hyperplasia, adenoma, and adrenal carcinoma) differ in their lipid contents [7]. The mean value observed in adenomas and hyperplasias was 17%, whereas it was 1.5% in adrenal carcinomas. The aim of this study is to determine if this distinction can be made with in vivo MR spectroscopic imaging and then to determine if the in vivo estimation of the percentage of lipid in adrenal tumors correlates with the in vitro measurements made on excised samples of the tumors after surgery.

Subjects and Methods

By using a spectroscopic MR imaging sequence in vivo, we measured the lipid content of 22 adrenal lesions with diameters larger than 15 mm in 20 patients (six men, 14 women). Ages of patients ranged from 21 to 69 years (mean, 49 years). There were 15 benign adenomas (seven producing cortisol, three producing aldosterone, five nonfunctioning) and seven adrenal carcinomas (three producing cortisol). The mean diameter of the adenomas was 25 mm. The mean diameter of the carcinomas was 80 mm. The lesions were confirmed pathologically in all cases. In nine patients who underwent surgery after the spectroscopic MR examination (seven with adenomas, two with carcinomas), the in vivo measurements were compared with spectroscopic in vitro measurements on excised samples.

MR examinations were performed at 1.5 T on a GE Signa system at the Centre Inter-Etablissement de Résonance Magnétique (Hopital de Bicêtre, Bicêtre, France). In most cases, a rectangular surface coil (27 × 20 cm) was used. Standard T1-weighted images, 500/20 (TR/TE), and either 1500/30-60 or asymmetric 2000/20-75 images were made in axial and

Received June 6, 1988; accepted after revision May 2, 1989.

¹ Service des Radio-Isotopes, Hopital Cochin, 27 rue du Faubourg Saint-Jacques, 75674 Paris, France.

² Present address: Service Hospitalier Frédéric-Joliot, CEA-DB, Hopital d'Orsay, 91406 Orsay, France. Address reprint requests to A. Leroy-Willig.

³ CIERM, Hopital de Bicêtre, 94270 Kremlin-Bicêtre, France.

⁴ Service d'Endocrinologie, Hopital Cochin, 75674 Paris, France.

⁵ Service d'Anatomie Pathologique, Hopital Cochin, 75674 Paris, France.

⁶ Service de Radiologie A, Hopital Cochin, 75674 Paris, France.

0361-803X/89/1534-0771
 ©American Roentgen Ray Society

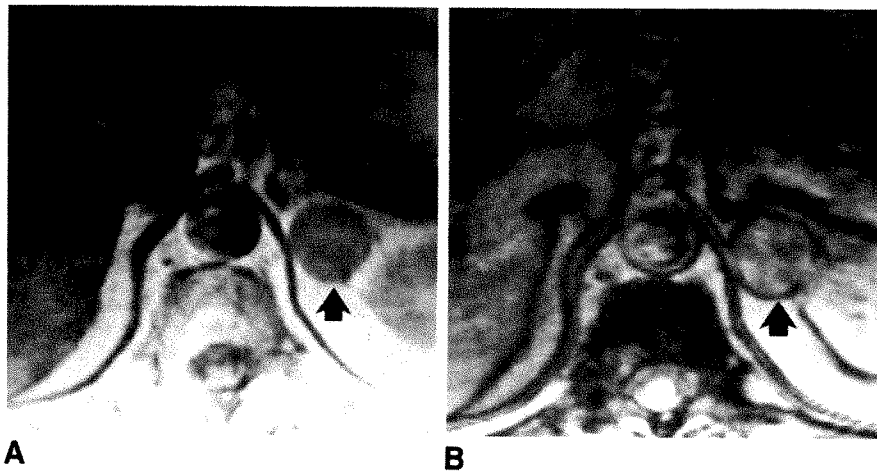


Fig. 1.—A and B, Standard spin-echo (A) and modified Dixon sequence (B) MR images (2000/20) in a patient with a 25-mm-diameter left adrenal adenoma (arrow). Lipid content of tumor measured by using these two images was 14%.

frontal planes. When an adrenal mass larger than 15 mm in diameter was observed, its lipid content was determined by using a spectroscopic imaging sequence. We used a slightly modified version of the sequence published by Dixon [8]. In the original sequence, the 180° refocusing pulse was applied at $(TE - \tau)/2$ instead of $TE/2$. The two abundant chemical species, water and lipid protons, whose resonant frequencies differ by Δf (220 Hz), were refocused in the transverse plane at $TE - \tau$ and then dephased at the acquisition center TE by the angle $\Delta\phi = 2\pi \times \Delta f \times \tau$. This angle was set at a value of 180° by choosing an appropriate value for the time interval τ . In the modified sequence, the refocusing pulse was not shifted; instead, the acquisition and its readout gradient were delayed by the time τ needed to dephase water and lipids after the normal echo time (TE). These two sequences presented only minor differences for T1- and T2-weighting of signals [9].

The values of TR, TE, and the time delay τ were determined from measurements on test media with known amounts of lipids. We used a sequence where TR = 2000 msec, a single echo at TE = 20 msec, and $\tau = 2.5$ msec.

The lipid content of a region of interest (ROI) was measured as follows. A standard spin-echo sequence in which water and lipid magnetizations were added was obtained, giving the mean signal of the ROI, S1. Then the Dixon sequence in which water and lipid magnetizations were opposed was obtained with identical amplification factors (S2 being the mean signal of the same ROI). The ratio $100 \times (S1 - S2)/(2 \times S1)$ gave the lipid percentage of that ROI.

Because we measured the absolute value of magnetization and lost the sign of the difference between water and fat, this ratio was equal to an effective percentage of lipid, G' , when lipids were less abundant than water; it was equal to $100 - G'$ if lipids were more abundant than water. This effective lipid percentage (G') differed from the real lipid content (G) mostly because of the effect of relaxation-time weighting [10]. The systematic error $G' - G$ was calculated to be less than 5% for this data set [9]. Figure 1 shows images obtained with the standard and the Dixon sequences. These two image acquisitions lasted 9 min each. Care was taken to keep the patient motionless during this time. Measurements were made of ROIs of 0.3–1 cm², depending on lesion size. As motion through the selected plane and chemical-shift artifact were two important causes of error, the position of the ROI was critical to the validity of the evaluation of the lipid percentage. The number of measurements done inside a given lesion was related to the size of the lesion. The average of these measurements was taken as representative of the lipid content of the lesion.

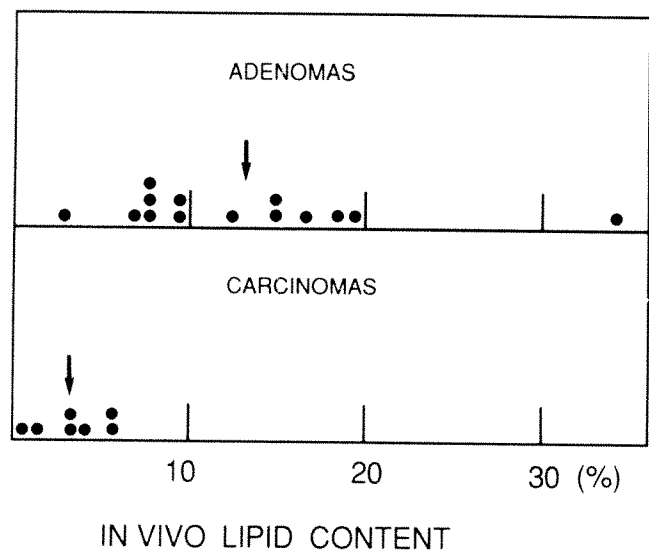


Fig. 2.—In vivo measurement of lipid content of adrenal lesions: histogram of values obtained in 22 lesions, including seven adrenal carcinomas and 15 benign adenomas. Arrows indicate mean values in each class of lesions.

Results

Results of the in vivo measurements for the 22 tumors are plotted in Figure 2. The two populations of tumors are clearly different, as confirmed by the mean values: 13.4% (standard deviation, 8%) for the 15 adenomas and 3.5% (standard deviation, 2%) for the seven carcinomas. This difference is quantified by an unpaired Student's *t* test ($p = .004$).

In vitro and in vivo MR spectroscopic measurements are compared in Figure 3. Discordances are observed in three of the five tumors with diameters less than or equal to 20 mm (plotted as open circles).

Discussion

The results of the in vivo measurements confirmed that the lipid percentage is significantly lower in carcinomas than in

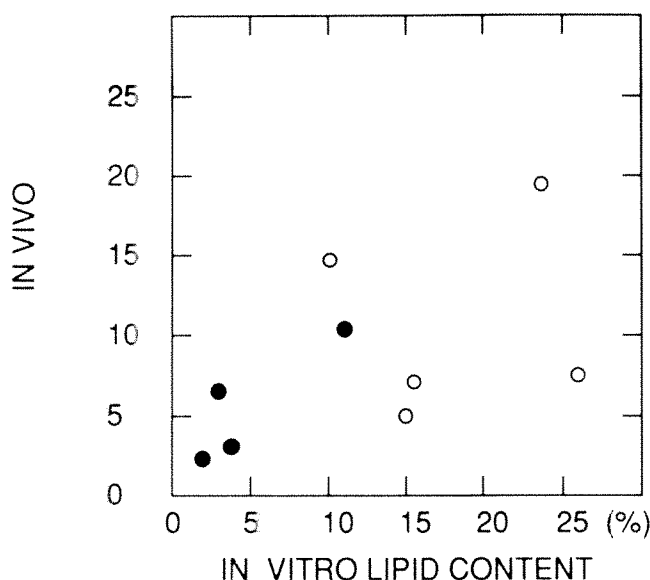


Fig. 3.—In vitro postoperative control of lipid content measured in vivo by MR. Averages of measurements on each lesion by two techniques are compared. (open circles = lesions with diameters less than or equal to 20 mm, solid circles = larger lesions) Correlation between in vivo and in vitro measurements is good for larger lesions and two of smaller lesions in which difference between in vitro and in vivo results is less than 5%. In three small lesions, important deviations are observed between in vivo and in vitro values.

adenomas. Only one adenoma had a lipid content lower than 7%, which overlapped with the carcinomas values. The proportion of incorrectly classified lesions was equal to 4%. In vitro and in vivo measurements correlated well for tumors larger than 20 mm. Discordances for smaller tumors are probably caused by the motion artifact (motion of the lesion during the respiratory cycle) and by the chemical-shift artifact (displacement of water vs fat image). These artifacts are more important at the border of the lesion and thus affect the accuracy for small lesions more. This is clearly shown in Figure 3.

As the number of lesions we could measure in vitro after surgery was low, we compared the in vivo distributions of lipid content of adenomas and carcinomas to the corresponding distributions obtained in vitro in this and earlier studies (Table 1) [7]. An unpaired Student's *t* test showed no significant difference between the mean lipid content in vivo and in vitro of adenomas ($p = .29$) and of carcinomas ($p = .08$).

In clinical practice, it is difficult to identify nonfunctioning adrenal masses. It is commonly accepted [11] that adrenal masses larger than 50 mm are malignant. This size criterion, although effective for our small number of patients with malignant lesions, is not always sufficient. In a series of 35 carcinomas [12], five had a diameter under 25 mm. Although, as stated by Bernardino [13], systematic biopsy is the safest procedure in cancer workup, a less invasive approach may be preferable in other patients with incidentally found adrenal masses.

Several MR methods have been proposed to discriminate nonfunctioning lesions from adrenal metastases on the basis of T2 differences [4], T1 differences [5], or both [6]. These methods currently show overlaps of 21–31% [4] and 31% [5]. We have shown in vitro a nearly complete overlap between T1-weighted images of water in adenomas and carci-

TABLE 1: Mean Lipid Content of Lesions Measured in Vitro and in Vivo

Lesion	In Vitro Lesions		In Vivo Lesions	
	Number	% Lipid	Number	% Lipid
Adrenal carcinoma	9	1.5 ± 2	7	3.5 ± 2
Benign adenoma	15	16.4 ± 7.8	15	13.4 ± 8

Note.—Lipid percentages are mean ± standard deviation.

nomas [7]. The indexes drawn from T1-weighted images, however, are more discriminant probably because of the short T1 of lipid protons contributing to adenoma signals. However, relaxation times are complex parameters, and the presence or absence of lipids in adrenal tissue is conceptually a better index of its benign or malignant characteristics. MR spectroscopic sequences, which alter the contrast between parts of organs where the lipid content is modified by disease, can be used to measure this lipid content. We think that adrenal masses larger than 20 mm can be considered benign if the lipid content measured with this technique is more than 10%. Further studies are needed to improve this technique and to apply it to smaller lesions.

In conclusion, in vivo MR spectroscopic imaging appears to be useful for distinguishing between adrenal carcinomas and adenomas. We now must test its application to the more frequent problem of distinguishing between metastases and incidentally discovered adenomas, because undifferentiated metastatic tissue should contain no lipids.

ACKNOWLEDGMENTS

We thank J. Courtieu (Faculté d'Orsay) for his help with in vitro measurements and P. Jehenson for reviewing the manuscript.

REFERENCES

1. Moon KL, Hricak H, Crooks LE, et al. Nuclear magnetic resonance imaging of the adrenal gland: a preliminary report. *Radiology* 1983;147:155–160
2. Schultz CL, Haaga JR, Fletcher BD, et al. Magnetic resonance imaging of the adrenal glands: a comparison with computed tomography. *AJR* 1984;143:1235–1240
3. Fink LJ, Reinig JW, Dwyer AJ. Magnetic resonance imaging of pheochromocytomas. *J Comput Assist Tomogr* 1985;9:454–458
4. Glazer GM, Woolsey EJ, Borello J, et al. Adrenal tissue characterization using MR imaging. *Radiology* 1986;158:73–79
5. Chezmar JL, Robbins SM, Nelson RC, et al. Adrenal masses: characterization with T1-weighted MR imaging. *Radiology* 1988;166:357–359
6. Reinig JW, Doppman JL, Dwyer AJ, Johnson AR, Knapp RH. Adrenal masses differentiated by MR. *Radiology* 1986;158:81–84
7. Leroy-Willig A, Roucayrol JC, Luton JP, Courtieu J, Louvel A, Niesenbaum N. In vitro adrenal cortex lesions characterization by NMR spectroscopy. *Magn Reson Imaging* 1987;5:339–344
8. Dixon T. Simple proton spectroscopic imaging. *Radiology* 1984;153:189–194
9. Leroy-Willig A, Idy-Peretti I, Laval-Jeantet AM. La quantification des taux de lipides par l'imagerie magnétique en contraste de phase. *J Med Nucl Biophys* 1988;12:49–56
10. Buxton R, Wismer GL, Brady TJ, Rosen BR. Quantitative proton chemical-shift imaging. *Magn Reson Med* 1986;3:881–901
11. Bertagna C, Orth DN. Clinical and laboratory findings and results of therapy in 58 patients with adrenocortical tumors. *Am J Med* 1981;71:855–875
12. Luton JP, Billaud L, Benabed K, et al. Adrénomégalias et autres masses de la loge surrénalienne. *Ann Endocrinol (Paris)* 1988;49:348–352
13. Bernardino M. Management of the asymptomatic patient with a unilateral adrenal mass. *Radiology* 1988;166:121–123

Memorial

Chalmer S. "Bud" Wheeler, 1934–1988



For those who knew and cared for him so much, the life of Bud Wheeler came and went far too quickly. Bud was one of those memorable people whose powerful and flamboyant personality left no room for neutrality. Above all else, he was an individual who gave to others far more than he was ever able to receive for himself.

Bud and his twin sister, Diane, were born in Lexington, KY, in 1934. After moving to Louisville when he was 13 years old, he graduated from Eastern High and the University of Louisville Medical School. Internship was followed by a tour of duty in Vietnam, where he was decorated for heroism and expended considerable effort on behalf of Vietnamese orphans and civilians in his off-duty hours. Bud returned to Louisville for his residency and was an assistant professor at the University of Louisville from 1970 to 1975. He was in private practice at the Jewish Hospital from 1975 until his death.

Bud introduced angiography to Kentucky. Despite his having lost two fingers in a childhood explosion, he was known for his dexterity and phenomenal swiftness in performing his procedures. Many of the angiographers in Kentucky today were trained by him, and he remained the primary source of reference in Louisville for many years.

Bud had wanted to become a physician since childhood. He fulfilled his wish with all the dedication and thoughtfulness that could be hoped for from any person. In addition to his expertise in angiography, he was an out-

standing general radiologist and consultant for any medical problem related to radiology. He also had the well-known capacity to put out a great amount of work.

Bud's most memorable attributes were his dedication and caring for each individual patient. More than any other physician I have known, he was able to create intimate contact that seemed to make the patient feel that the two of them were undergoing the procedure together. Most people do not remember their angiographer 5 years later. His patients frequently did, asking for him again and recounting his kindness.

His favorite pastime was working on his "mini-farm" (as he called it)—a beautiful place in the country where he planted many flowers and fruit trees and kept it like a park. In fact, some balloonists thought it was a park when they landed there once.

A person of legendary generosity, who always put others before himself, Bud was immensely popular with his many, many friends. He is terribly missed. Bud is survived by his sister, Diane.

George F. Drasin
Kansas City, MO 64110

Society of Uroradiology Award Paper

The Pars Infravaginalis Gubernaculi: Importance in the Identification of the Undescended Testis

Arthur T. Rosenfield^{1,2}
Deborah N. Blair^{1,3}
Shirley McCarthy¹
Morton G. Glickman¹
Nancy S. Rosenfield¹
Robert Weiss²

The gubernaculum, a cordlike structure that extends from the testis to the scrotum and guides the testis in its descent, has a bulbous termination, the pars infravaginalis gubernaculi. We reviewed seven surgically proved cases in which the pars infravaginalis gubernaculi was mistaken for an undescended testis on imaging studies. The studies included sonography (five cases), CT (two cases), and MR imaging (two cases). Identification of the mediastinum testis on sonograms or MR images confirms that a structure is testis and not the pars infravaginalis gubernaculi. In two of these patients, testicular venography was used to further identify the undescended testis. In these two patients, the pampiniform plexus, which is used to identify the presence and position of testis, was located adjacent to the pars infravaginalis gubernaculi.

Our experience indicates that the pars infravaginalis gubernaculi can be similar in appearance to the undescended testis on any imaging study. The finding of an apparent cord leading to a testislike structure on caudad sectional imaging does not obviate searching for the testis as far as the renal hila.

AJR 153:775-778, October 1989

Good results have been reported on the use of sonography, CT, and MR imaging for the location of the testes or the demonstration of their absence in patients with undescended testes [1-5]. In the literature, the only false-positive studies for any sectional imaging technique were in two patients in our sonographic series [6]. We describe seven patients in whom the bulbous termination of the gubernaculum testis, the pars infravaginalis gubernaculi (PIG), was mistaken for the testis.

Materials and Methods

From 1976 to 1987 we performed imaging studies in approximately 60 patients for the detection and localization of undescended testes. Seven of these (age range, 4-32 years) had incorrect diagnoses on the basis of sonograms (five patients), CT scans (two patients), and MR images (two patients). Two of the sonographic studies were performed on dedicated high-resolution small-parts equipment at both 10 and 8 MHz (Picker Microview) and three were performed on standard real-time equipment at 7.5 MHz. The CT studies were performed with IV contrast material on a GE 9800 scanner from the bottom of the scrotum to the renal hila, whether or not an apparent testis was identified. MR imaging was performed with a 1.5-T system (GE Signa). Coronal spin-echo (SE), 500/20 (TR/TE), and axial SE 2000/20, 80, 5-mm-thick sections with a 2.5-mm skip, a 128 × 256 matrix and two excitations were acquired through the same anatomic area covered by CT. Testicular venography was performed in two patients using a technique previously described [7]. Histologic sections were obtained from three lesions that proved to be the PIG.

Results

Surgery in all seven cases with false-positive diagnoses of undescended testes on imaging studies disclosed that the structure located at the site of a predicted

Received March 9, 1989; accepted after revision June 12, 1989.

Presented at the annual meeting of the Society of Uroradiology, where it was one of two award-winning papers.

¹ Department of Diagnostic Radiology, Yale University School of Medicine, 333 Cedar St., New Haven, CT 06510. Address reprint requests to A. T. Rosenfield.

² Department of Surgery (Urology), Yale University School of Medicine, New Haven, CT 06510.

³ Present address: Department of Radiology, Alexandria Hospital, 4320 Seminary Rd., Alexandria, VA 22304.

0361-803X/89/1534-0775
© American Roentgen Ray Society

testicle on imaging studies was the PIG. Histologic sections of the PIG from three patients were available for review. In one, the PIG consisted of a gelatinous hyaline material in which the vas deferens originated. In two cases the structure was fibrous. The epididymis was located contiguous to the gubernaculum in one of these three. In the other four cases the PIG was identified at surgery in the region of the apparent testicle but a biopsy was not done.

Sonographically, the PIG was a hypoechoic mass in all five cases, and in each a cordlike structure of similar echogenicity led into it (Figs. 1B and 2). The PIG was less echogenic than the contralateral testis was in each instance. The mediastinum testis, which can be identified in the normally descended and in some undescended testes (Fig. 3), was not seen in any PIG.

The PIG had a CT number similar to that of the undescended testis and the normally descended contralateral testis (Fig. 1A). In one patient with a PIG shown on CT, a more cranial testis was identified on CT as well (Fig. 4).

One of the two MR imaging examinations in this series showed a cordlike gubernaculum with a bulbous termination

in the high scrotum. It was isointense on T1-weighted and hypointense relative to the normal testis on T2-weighted scans. This structure represented the PIG. The testis, which was in the hilum of the pelvic kidney, was not identifiable on MR imaging, even in retrospect. The second MR scan showed a cordlike structure leading to a nubbin of tissue identified in the hemiscrotum on the side of the absent testis. This nubbin was of mixed signal intensity on T2-weighted images (Fig. 5). At surgery, the PIG and epididymis were located together in the scrotum. We assume that the low-signal portion of the nubbin on the T2-weighted images was the PIG and the high-signal area the epididymis.

Testicular venography was performed in two patients. In one who was 6 years old, an apparent testicle was seen in the inguinal region on sonography. The venogram showed a pampiniform plexus on that side, which was in a similar location. At surgery there was no testis. The pampiniform plexus was located adjacent to the PIG. In the second patient two structures were seen on CT, one identified in the external iliac area and the second in the inguinal area (Fig. 4). The testicular venogram localized the pampiniform plexus in the

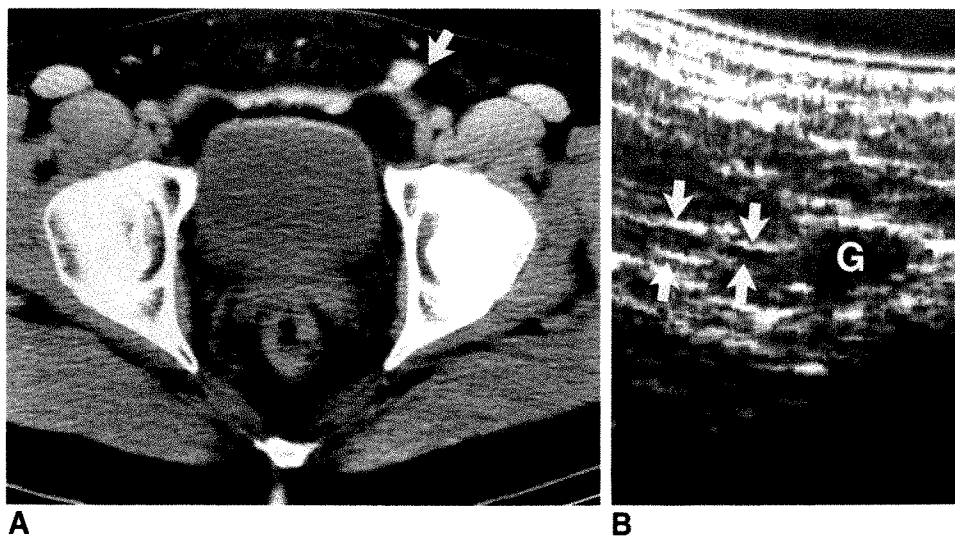


Fig. 1.—Pars infravaginalis gubernaculi mimicking undescended testis in a 16-year-old boy with no palpable testis in left hemiscrotum.

A, CT scan through left inguinal region shows a structure with appearance of atrophic testis (arrow).

B, Sonogram through left inguinal region shows cordlike structure (arrows) leading to bulbous termination (G) in a location similar to that of the structure seen on CT. There are internal echoes within, but it lacks the bright white line representing mediastinum testis seen in most true undescended testes. At surgery, no testis was present in the region, but the pars infravaginalis gubernaculi was.

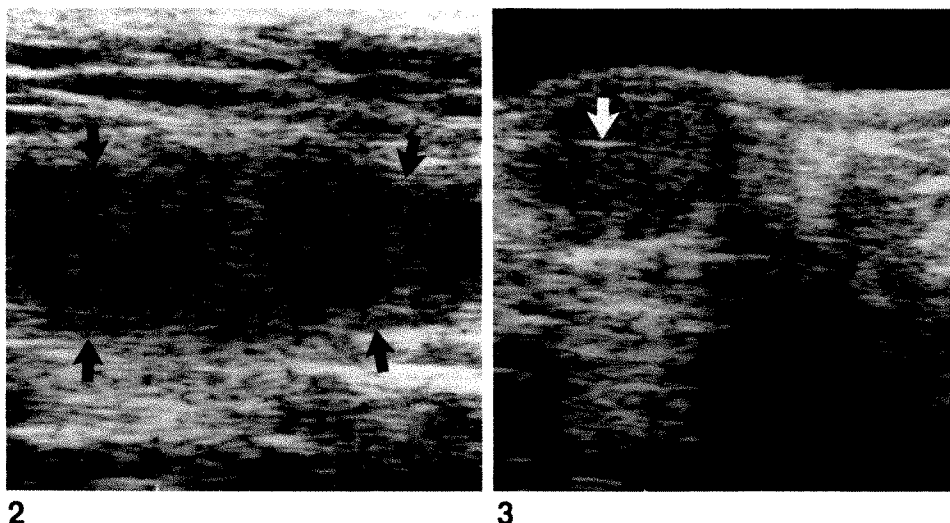


Fig. 2.—Pars infravaginalis gubernaculi mimicking the testis on a longitudinal sonogram in a 6-year-old boy. A left inguinal structure (arrows) is identified that has internal echoes but not a mediastinum testis. This proved at surgery to be the pars infravaginalis gubernaculi. No testis was present on that side.

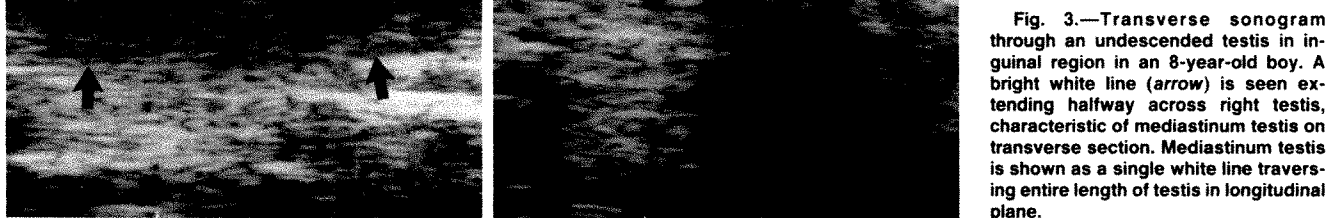


Fig. 3.—Transverse sonogram through an undescended testis in inguinal region in an 8-year-old boy. A bright white line (arrow) is seen extending halfway across right testis, characteristic of mediastinum testis on transverse section. Mediastinum testis is shown as a single white line traversing entire length of testis in longitudinal plane.

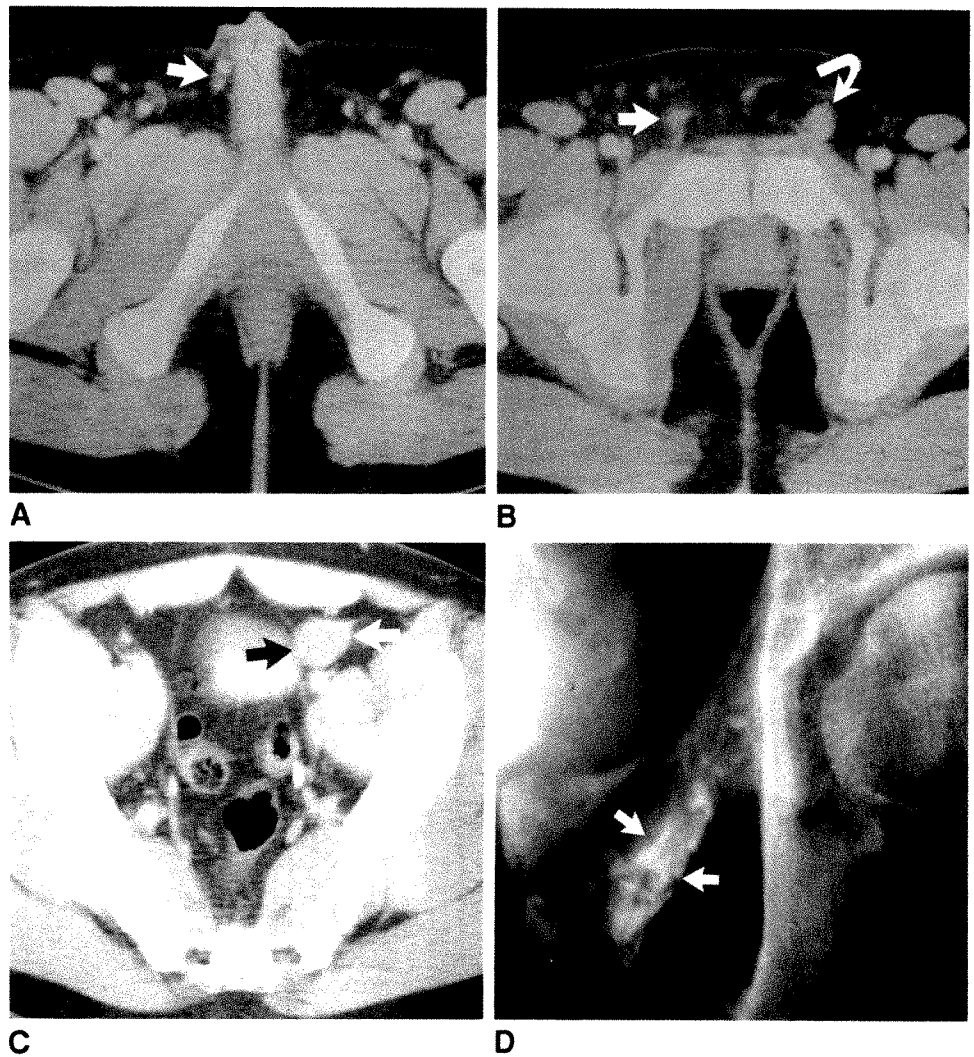
Fig. 4.—Pars infravaginalis gubernaculi and ipsilateral undescended testis in a 29-year-old man with no palpable testis in left hemiscrotum.

A, Axial CT section through inguinal region shows spermatic cord (arrow) that led to a testis on right. No spermatic cord is present on left.

B, More cranial section at level of symphysis pubis shows structure in left inguinal region with appearance of atrophic testis (curved arrow). Note spermatic cord (straight arrow) on right.

C, CT scan at level of external iliac region shows additional structure (arrows) on left that is larger than more caudad structure. Interpretation of CT scan was that more caudad structure was pars infravaginalis gubernaculi and more cranial structure, undescended testis.

D, Testicular venogram shows pampiniform plexus (arrows) to be at level of more caudad inguinal structure. At surgery, pampiniform plexus and pars infravaginalis gubernaculi were found together in inguinal region, whereas testis was in external iliac region.



inguinal area (Fig. 4D). At surgery the testis was in the external iliac area, and the PIG was in the inguinal area along with the pampiniform plexus.

Discussion

The gubernaculum was first described by Hunter [8] as "a substance that runs from the lower end of the testis to the scrotum." In early fetal development, the gubernaculum is soft and jellylike [9]. The distal bulbous segment of the gubernaculum is the pars infravaginalis gubernaculi (PIG). With time the testis moves caudally along the gubernaculum to the scrotum (Fig. 6). When descent is completed, the PIG and the gubernaculum normally atrophy. If the testis fails to descend to the scrotum, the gubernaculum frequently persists as a fibrotic rather than gelatinous remnant. Three pathologic specimens were obtained in our series. In one the PIG was jellylike, and in two it was fibrotic. In all of our examples of the gubernaculum on MR imaging during scanning for undescended testes, the gubernaculum was of low signal intensity on T1- and T2-weighted scans, compatible with fibrosis [5].

Sonography has had some success in the evaluation of the undescended testes [1, 2]. In many undescended testes the mediastinum testis can be identified readily on sonography,

permitting a specific diagnosis (Fig. 3). In others, a discrete mediastinum testis cannot be defined sonographically. The PIG has a sonographic appearance identical to the testis, lacking a discrete mediastinum testis.

CT cannot show the mediastinum testis. Nonetheless, the spermatic cord leading into the testis can be traced. In this series, the CT appearance of the gubernaculum and PIG was indistinguishable from that of the spermatic cord and testis. In the patient in whom the PIG was present distal to a normal testis, CT identified two structures, allowing the correct diagnosis. Therefore, if scanning is started at the scrotum, it is important to continue to the renal hila, because the initial structure identified could be the PIG.

On MR imaging, the testis is typically of low signal on T1- and of high signal on T2-weighted images. Undescended testes that are atrophic may not be of high intensity on T2-weighted scans [4, 5]. In our series, the PIG was of similar intensity as the normal testis on T1-weighted images but was hypointense relative to the normal testis on T2-weighted images. This could not be reliably distinguished from an atrophic ectopic testis. Structures with a long T2 are inconsistent with the PIG but may be lymph nodes instead of undescended testes. The spermatic cord leading to the testis

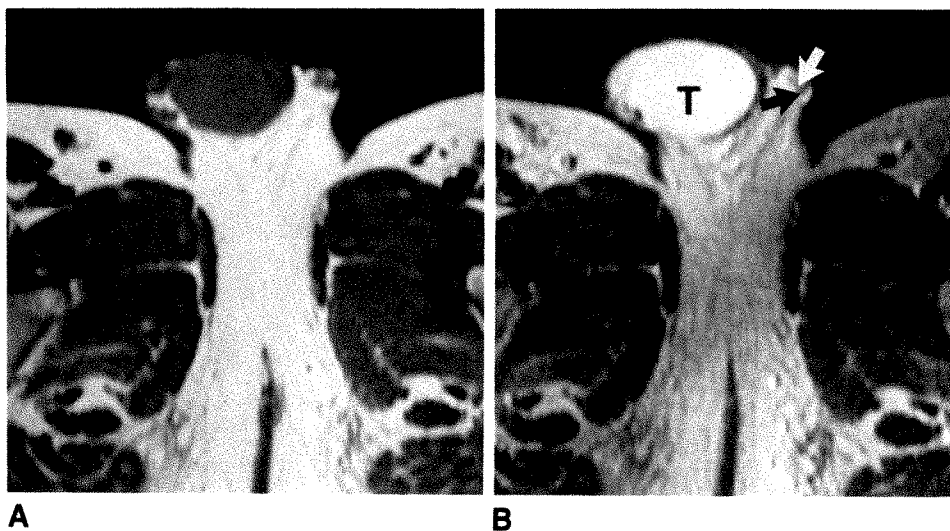


Fig. 5.—Axial MR images of pars infravaginalis gubernaculi show nonpalpable left testis in 5-year-old boy.

A and B, T1-weighted, 500/20 (A), and T2-weighted, 2000/80 (B), scans show pars infravaginalis gubernaculi (black arrow), which is of low signal on both sequences, and centrally located epididymis (white arrow). Note high signal in normal right testis (T) on T2-weighted image.

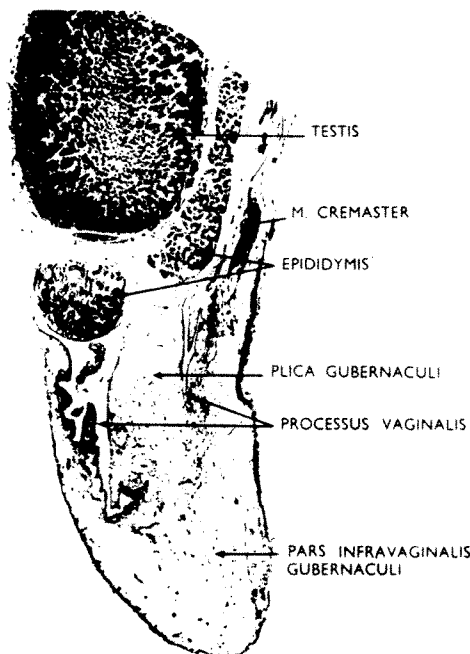


Fig. 6.—Descent of testis on section of testis and gubernaculum in a pig fetus. Note relationship of descended testis to the pars infravaginalis gubernaculi. M. = musculus. (Reprinted with permission from Blackhouse [9].)

and gubernaculum leading to the PIG have identical properties on MR imaging. The mediastinum testis, which sometimes can be seen on MR studies [5], is the only finding that clearly identifies a structure as a testis.

Testicular venography also has pitfalls related to the PIG. This test has been considered definitive if the pampiniform plexus is opacified [7]. It has not received wide acceptance because it is invasive and because failure to opacify the pampiniform plexus is common and nondiagnostic. In one case in this series, the testicular venogram showed the pampiniform plexus in the location of the PIG although the testis was absent. In another patient in whom the testis was proximal to the PIG, the venogram showed the pampiniform plexus at the level of the PIG. Two patients with absent testes but with pampiniform plexus identified on venography have been

reported [10]. In these patients, it is likely that the pampiniform plexus marked the site of a PIG.

The PIG is always located distal to the undescended testis, usually in the scrotum but sometimes craniad to the scrotum. It is in the latter case that the PIG and undescended testis may be confused. Our current approach has been to use MR imaging in children and CT in adults to look for the undescended testis (the techniques provide similar information). If a structure is found that is thought to be the undescended testis, and it is within the range of sonography, sonographic evaluation is performed to look for the mediastinum testis if it has not already been identified on the MR study. Identification of the mediastinum testis is considered absolute evidence that the structure is the undescended testis. If a mediastinum testis is not identified, further studies such as laparoscopy or venography are necessary.

ACKNOWLEDGMENTS

We thank Edmund S. Crelin for advice, Sandra Sudac for the manuscript preparation, and Thomas McCarthy for photography.

REFERENCES

1. Madrazo BL, Klugo R, Parks JA, et al. Ultrasonographic demonstration of the undescended testis. *Radiology* 1979;133:181-183
2. Wolverson MK, Houhuin E, Heiberg E, et al. Comparison of computed tomography with high-resolution real-time ultrasound in the localization of the palpable undescended testis. *Radiology* 1983;146:133-136
3. Lee JK, McClellan BL, Stanley RJ, et al. Utility of computed tomography in the localization of the undescended testis. *J Urol* 1986;135:936-938
4. Fritzsche PJ, Hricak H, Hogan BA, et al. Undescended testis: value of MR imaging. *Radiology* 1987;164:169-173
5. Kier R, McCarthy S, Rosenfield AT, et al. Nonpalpable testes in young boys: evaluation with MR imaging. *Radiology* 1988;169:429-433
6. Weiss R, Carter A, Rosenfield AT. High-resolution real time ultrasonography in the localization of the undescended testis. *J Urol* 1986;135:936-938
7. Glickman MG, Weiss RM, Itzchak Y. Testicular venography for undescended testis. *AJR* 1977;129:67-70
8. Hunter J. Observations on the state of the testis in the fetus, and on the hernia congenita. In: Hunter W. *Medical commentaries part 1*. London: Hamilton, 1762:75-89
9. Blackhouse KM. The gubernaculum testis in utero: testicular descent and maldescent. *Ann R Coll Surg Engl* 1964;35:15-33
10. Greenberg SH, Ring EJ, Pollack HM, et al. The falsely positive gonadal venogram: presence of a pampiniform plexus without a gonad. *J Urol* 1981;125:887-888

Case Report

Benign Prostatic Hypertrophy: Treatment with a Metallic Stent

Lindsay Machan,^{1,2} H. Rolf Jäger,¹ Andreas Adam,¹ Kevin Gill,³ Gordon Williams,³ and David J. Allison¹

We report a patient in whom an expandable metallic stent was inserted under radiologic guidance into the prostatic urethra to treat bladder outflow-tract obstruction due to benign prostatic hypertrophy. To our knowledge, this is the first description of radiologically-guided placement of such a stent.

Case Report

A 74-year-old man presented with a 2-year history of hourly urination during the day, nocturia three times nightly, poor urinary stream with hesitancy and postmicturition dribbling, and a sensation of incomplete emptying of the bladder. He had had two earlier myocardial infarctions and presented with markedly decreased exercise tolerance and borderline congestive heart failure despite medical therapy. In addition to the clinical findings of compensated chronic cardiovascular compromise, he was found to have a moderately enlarged prostate. On transrectal sonography, diffuse parenchymal calcification, but no suspicion of malignancy, was seen. The prostatic volume was 85 ml. A moderate-sized intravesical prostatic protrusion was seen. Bladder outflow-tract obstruction was confirmed by urodynamics, which indicated a peak flow rate of 6 ml/sec (Table 1) and a urethral resistance factor (bladder pressure/peak flow rate²) of 2.8 (normal, ≤ 0.6). Bladder detrusor instability was not seen.

Five months before stent insertion, under fluoroscopic guidance and with mild sedation, the prostatic urethra was dilated with a 25-mm urethroplasty balloon. The patient did not improve symptomatically or by urodynamic assessment. As his cardiac condition was felt to preclude surgery, a long-term indwelling catheter was placed in

the bladder. Three months later the patient suffered another mild myocardial infarction, from which he recovered to his baseline state. He found his urinary catheter to be more distressing than his original symptoms, and was anxious to have a nonoperative procedure to relieve his bladder outflow-tract obstruction. Two weeks before insertion of the stent, the patient developed an asymptomatic urinary tract infection due to *Escherichia coli*. After a 7-day course of ampicillin, the urine became sterile.

After prophylactic ampicillin and sedation with IV diazepam and fentanyl, the urethra was coated with 2% viscous xylocaine, and a retrograde urethrogram was obtained to determine the position of the external sphincter (Fig. 1A). A 12-French steerable catheter (Meditech Inc., Watertown, MA) was passed into the bladder. This was exchanged over a 0.038-in. (0.097 cm) floppy-tipped guidewire for a 16-French Foley catheter with the tip cut away to allow its passage over the guidewire. The Foley balloon was inflated with contrast material and then withdrawn gently against the bladder neck to show the exact position of the bladder outlet. The length of the prostatic urethra was determined to be 2.6 cm by using the bent guidewire technique [1], and a new 0.038-in. (0.097 cm) guidewire was inserted. Over this guidewire, the Foley catheter was exchanged for a 7-French catheter with a preloaded 2-cm-long, 1.4-cm-wide self-expanding stainless steel stent (Medinvent SA, Lausanne, Switzerland). The stent was released by the hydraulically assisted rolling membrane delivery system supplied on the preloaded catheter, positioned so that its superior end was flush with the bladder neck, and the inferior end was immediately above the internal sphincter (Fig. 1B). The delivery catheter was removed over the guidewire, the Foley catheter was reinserted into the bladder, and the balloon was inflated (Fig. 1C). The patient returned the next day for removal of the Foley

Received March 28, 1989; accepted after revision May 30, 1989.

¹ Department of Radiology, Hammersmith Hospital, Du Cane Rd., London, England W12 0HS.

² Present address: Department of Radiology, University of British Columbia Hospital, 2211 Wesbrook Mall, Vancouver, B.C., Canada V6T 2B5. Address reprint requests to L. Machan.

³ Department of Surgery, Hammersmith Hospital, Du Cane Rd., London, England W12 0HS.

AJR 153:779-781, October 1989 0361-803X/89/1534-0779 © American Roentgen Ray Society

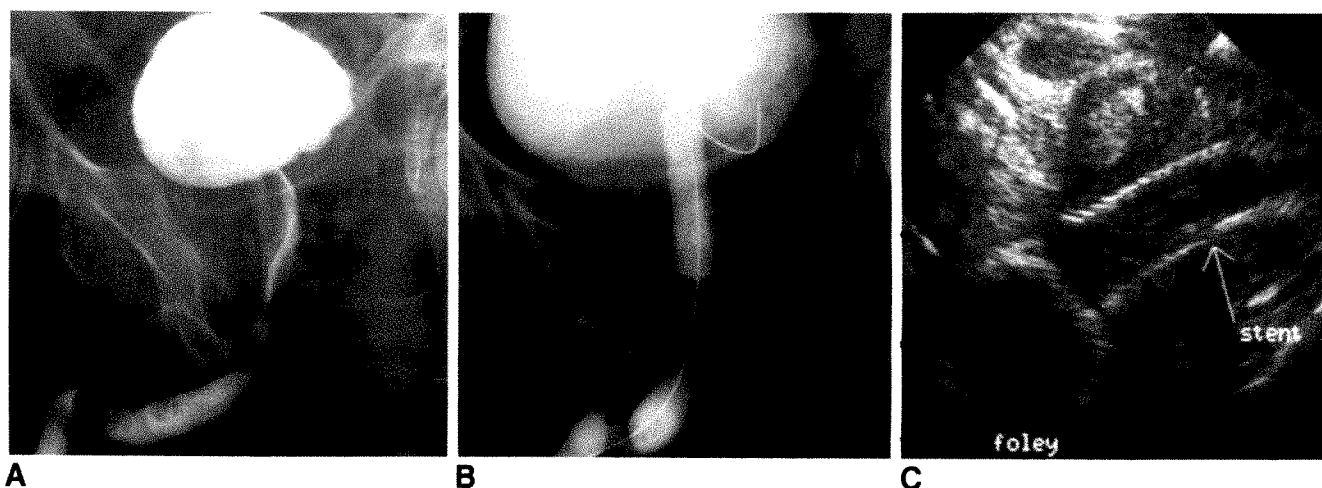


Fig. 1.—A, Retrograde urethrogram before stent insertion to mark position of external sphincter. Residual widening of prostatic urethra from balloon dilatation 5 months earlier is seen.

B, Retrograde urethrogram at end of insertion. Note relationship of each end of stent to internal and external sphincters.

C, Transrectal sonogram, longitudinal projection, after stent insertion. Foley balloon sits on stent, confirming that proximal end is flush with bladder neck.

catheter, and a voiding cystourethrogram was obtained, which showed that the position of the stent was unchanged.

The urine was mildly bloodstained at the time of the procedure, but this cleared by 6 hr later. A mild continuous sensation of urgency persisted for approximately 3 days. Initially, the patient dribbled continuously, but by 48 hr, he had regained continence. At that time, his peak flow rate was 8 ml/sec on a voided volume of only 95 ml. On the second day, the patient developed another asymptomatic urinary tract infection due to *E. coli*, which responded to 2 days of parenteral ampicillin and a further 5 days of oral amoxycillin. Two weeks after implantation, following instructions concerning fluid management and bladder training, the patient was voiding spontaneously at 4-hr intervals. Peak flow rate was 20 ml/sec on a volume of 210 ml, and postvoiding catheter residual urine was 20 ml. Six weeks after insertion, the peak flow rate was 18 ml/sec on a voided volume of 250 ml, and no residual urine was seen by postmicturition sonography.

On follow-up at 3 months, the patient felt much improved from his pretreatment state, voiding every 3 to 4 hr during the day and once at night. He complains of intermittent urgency, which on two occasions has been severe enough to cause urge incontinence, but otherwise he is continent. Peak flow rate is 22 ml/min on a volume of 300 ml, with barely perceptible residual urine seen by sonography. All posttreatment flow rates have shown a nonobstructed pattern. Intermittent bacteruria and occasional pyuria have occurred, but without clinical manifestation, and no further antibacterial treatment has been necessary. The patient is not sexually active, has no spontaneous erections, and was not aware of retrograde ejaculation before or after the stent was inserted.

Discussion

Although most reported uses of expandable stainless steel stents have been in the vascular system [2, 3], they also have been placed in the penile urethra under radiologic [4] and cystoscopic [5] guidance to treat recurrent urethral strictures. In the human penile urethra, the stent becomes covered by urothelium within 4–6 months, effectively becoming incorpo-

TABLE 1: Peak Urine Flow Rates Before and After Treatment

Time	Peak Flow Rate (ml/sec)	Urine Volume (ml)	Bladder Residual (ml)
0	6	—	110
48 hr	8	95	—
2 weeks	20	210	20
6 weeks	18	250	0 ^a
3 months	22	300	Minimal ^a

Note.—Dash (—) = not determined.

^a Seen on postmicturition sonography.

rated into the urethral wall and reducing its potential to act as a nidus for encrustation. No information is available on the long-term effects of stainless steel stents in the bladder outflow tract, nor on the length of time needed for a metallic prosthesis in the prostatic urethra to be covered by urinary epithelium. The device has been placed in the penile urethra of four mongrel dogs [5], and scanning electron microscopy after sacrifice at 2, 4, 6, and 12 months revealed no abnormalities in the deeper tissues of the urethra.

Operative sphincterotomy (incision of the bladder neck) is successful in 78% of patients with bladder outflow-tract obstruction due to benign prostatic hypertrophy [6]. Insertion of a metallic stent mimics this procedure by providing continuous mechanical distention of the internal sphincter. It is important, however, to preserve the external sphincter, which is the most significant factor in maintaining continence, and great care was taken to ensure that the distal end of the stent did not cross over, or even distend, this portion of the urethra by its proximity. Although a device has been designed by the supplier for retrieval of a misplaced stent, it has not been used in vivo. The prosthesis was inserted on the assumption that it probably would not be retrievable. The patient was so distressed by his symptoms that he was willing to accept that

if the external sphincter was interrupted by the stent, he would be left in his original condition, with a permanent indwelling bladder catheter. He was incontinent immediately after the procedure, and his initial voided volumes were low, but this was felt to be a consequence of long-term catheterization. He responded well to bladder retraining. It is of interest that five of eight patients in whom Milroy et al. [5] placed bulbar urethral stents experienced transient postmicturition dribbling immediately after stent insertion.

The development of a urinary tract infection in the presence of a foreign body was of some concern, but it responded immediately to antibiotics. Although intermittent bacteruria has occurred since then, occasionally with pyuria, no treatment is indicated at present. The patient had frequent bacteruria and occasional pyuria when he had a chronic indwelling catheter. He remains afebrile, with no clinical indications of urinary tract infection.

Many designs of metallic stent are currently being manufactured. The device used in this patient is woven from multiple strands of a medical-grade stainless steel alloy. The woven structure allows extreme flexibility, and because it decreases in diameter when it is lengthened, the stent can be stretched and loaded on a delivery catheter significantly smaller than its diameter at full expansion. It is self-expanding, although occasionally the device will not reach its full dimensions without distension by a balloon catheter after it has been discharged.

With our present aging population and the increasing pressure for therapies that lessen the demands on inpatient resources, nonoperative therapy for prostatic disease is an attractive alternative to transurethral resection of the prostate,

particularly in high-risk patients. It was hoped that balloon dilatation of the prostate would fulfill this role, but we have found it to be unsatisfactory in most patients with bladder outflow-tract obstruction due to prostatic disease [7]. Although the long-term efficacy and safety have not been determined, the marked symptomatic and objective improvement in this patient at 3 months has encouraged these authors to feel that the expandable metallic stent warrants further investigation in the treatment of benign prostatic hypertrophy.

REFERENCES

1. Oleaga JA, McLean GK, Freiman DB, Ring EJ. Interventional biliary radiology. In: Ring EJ, McLean GK, eds. *Interventional radiology principles and techniques*. Boston: Little, Brown, 1981:245-378.
2. Sigwart U, Puel J, Mirkovitch B, Joffe F, Kappenberg L. Intravascular stents to prevent occlusion and restenosis after transluminal angioplasty. *N Engl J Med* 1987;316:701-706.
3. Charnsangavej C, Carrasco H, Wallace S, et al. Stenosis of the vena cava: preliminary assessment of treatment with expandable metallic stents. *Radiology* 1986;161:295-298.
4. Sarraon JP, Joffe F, Rousseau H, Puech JL, Wallsten H, El Din A. Early results of a new self-expandable endoluminal prosthesis for the treatment of difficult membranous-bulbar urethral strictures. Presented at the 74th Scientific Assembly, Radiological Society of North America, Chicago, IL, December 1988.
5. Milroy EJG, Cooper JE, Wallsten H, et al. A new treatment for urethral strictures. *Lancet* 1988;226:1424-1425.
6. Nielsen HO. Transurethral prostatotomy vs. transurethral prostatectomy in benign prostatic hypertrophy: a prospective randomized study. *Br J Urol* 1988;61:435-438.
7. Gill KP, Machan LS, Allison DJ, Williams G. Balloon dilatation of the prostate in outflow tract obstruction. Presented at the annual meeting of the American Urological Association, Dallas, TX, May 1989.

Memorial

Fred R. McCrea, 1917–1988



Fred R. McCrea died September 17, 1988, at the age of 70 after an extended illness. He was born in Oil City, PA, on October 28,

1917. He earned his bachelor's and master's degrees from the University of Kentucky and his medical degree from Vanderbilt University. On completion of his internship and residency in radiology at the Indiana University Medical Center, he served as assistant chief of radiology at the Veterans Administration Hospital in Indianapolis.

Dr. McCrea began a private practice in radiology in Terre Haute, IN, in 1952. He served as the director of the department of radiology at the Union Hospital in Terre Haute from 1954 until his retirement in 1981. A capable administrator and radiologist, he guided the department through many renovations, introducing all the new imaging techniques through the years. He was former chief of staff. A diplomate of the American Board of Radiology, he was also a member of the American College of Radiology, the Indiana Roentgen Society, the American Medical Association, and the Indiana State

Medical Association.

His contributions to the community went far beyond radiology. He was a long-standing member of local service organizations and a past-president of the Terre Haute Symphony Orchestra. He was an amputee as the result of an automobile accident that happened when he was a teenager, and he suffered the complications of long-standing diabetes. Consequently, he frequently fulfilled his responsibilities as radiologist, administrator, and teacher while he was in a wheelchair or on crutches. He was an example of courage and determination to all who knew him. He is survived by his wife, Mary, and their children, Patrice, Susan, Michael, and Kevin, as well as his sister, Alice. He is remembered as a kind and fair man who had great compassion for his patients. He will be missed by all who knew him, especially his eldest son.

Michael S. McCrea
South Bend, IN

Technical Note

Biocompatible Copolymer Ureteral Stent: Maintenance of Patency Beyond 6 Months

Marlene E. Rackson,¹ Harold A. Mitty,² Steven V. Lossef,¹ Sol J. Dan,² and John S. Train²

We previously reported our experience [1] with a ureteral stent made of a new biocompatible copolymer, Percuflex (Medi-tech, Watertown, MA). This soft copolymer offers an improved delivery system for ease of antegrade insertion, the largest available inner lumen for a given outside diameter, good tolerance by patients, and thus far more resistance to migration and fracture. In this article, we report our long-term experience in 14 patients whose clinical circumstances resulted in the Percuflex stent not being replaced at the recommended 6-month interval. Thus, we were able to monitor these patients from 1 to 12 months beyond the suggested time for replacement.

Materials and Methods

The design and technique of insertion of the Percuflex stent have been described in detail [1]. The stents are available in 8-French and 10-French diameters. The manufacturer recommends that the stent be replaced every 6 months. However, clinical circumstances or the patients' conditions led to the stents being left in place beyond that time.

Patients were included in this study if their stents had been continuously patent beyond the manufacturer's recommended time for replacement of 6 months. Thus, all patients had patent stents for at least 7 months at the time of elective removal or exchange, death, or the end of the study. Fifty-eight stents were placed in 47 patients between April 1987 and February 1988. Seven patients with one stent each were lost to follow-up. Three stents occluded early (1–5 days), and five stents showed delayed occlusion (within 4 months).

Sixteen stents were electively removed or exchanged between 1 week and 7 months (11 before 6 months, five after 6 months), with only one such case due to stent malfunction. Twenty-one stents were in place when the patient died; five had been in place for longer than 6 months, 16 had not. Sixteen stents in 14 patients were patent for longer than 6 months. These stents were placed because of neoplastic ureteral obstruction in 12 patients; two patients received bilateral stents. Six of the stents were 10-French and eight were 8-French. The remaining two stents were placed for the treatment of nonmalignant strictures: inflammatory stricture due to Crohn disease and ureteroneocystostomy stricture 12 years after cadaveric transplantation. Both of these stents were 10-French.

Stent patency was evaluated with a variety of imaging techniques, including excretory urography, cystography, and sonography. In those patients who died without recent imaging studies, a stent was presumed patent if the cause of death was unrelated to azotemia, sepsis, or clinical signs of stent failure such as decreased urinary output or flank pain.

Results

Follow-up of the patients showed that 16 stents were patent for at least 7 months. Of these, five stents placed for neoplastic obstruction were patent until the patient died (7, 7, 9, 9, and 10 months). Five stents placed for neoplastic obstruction were changed electively (7, 7, 8, 13, and 13 months); these stents were patent at the time of exchange. The stent in a kidney transplantation patient occluded at 18 months. One patient with neoplastic obstruction and bilateral

Received January 17, 1989; accepted after revision April 19, 1989.

¹Department of Radiology, New York Hospital-Cornell University Medical Center, 525 E. 68th St., New York, NY 10021. Address reprint requests to M. E. Rackson.

²Department of Radiology, Mount Sinai School of Medicine of the City University of New York, New York, NY 10029.

AJR 153:783–788, October 1989 0361–803X/89/1534–0783 © American Roentgen Ray Society

stents was lost to follow-up at 11 months. The remaining three stents, which included one stent placed for a nonmalignant stricture, were patent at the end of the study interval (10, 12, and 12 months).

No stent fractured or migrated in this series.

Discussion

Early experience with the somewhat rigid polyethylene and polyurethane stents demonstrated difficulty in transrenal placement, poor tolerance by patients, migration, fracture, and encrustation [2-5]. To avoid such complications, the manufacturer of stents made of biocompatible olefinic copolymer, Percuflex, recommends that the stents be changed every 6 months. In our series, 16 stents remained patent 7 months or longer, with a mean and median of 10 months.

Stents were left in place longer than the manufacturer's recommendation for various reasons, including malignancy with short life expectancy (nine stents), delayed clinical follow-up (five stents), and reluctance on the part of patients with strictures to exchange a functioning stent (two stents). The five patients who died with patent stents were spared the inconvenience and expense of an exchange procedure. The remaining nine patients had the advantage of a longer interval between stent exchanges.

Patency rates did not differ between 8-French and 10-French stents. This implies that the larger diameter stent, which initially requires a larger hole in the renal parenchyma and is mechanically more difficult to insert, does not offer increased protection against encrustation in the long-term setting. Therefore, the 10-French stent might be used for specific indications such as maintaining ureteral diameter after stricture dilatation.

No stent fractured or migrated in this series. Similar results have been noted with C-flex [6], another biocompatible copolymer that is less rigid than polyethylene or polyurethane.

In general, the position of the distal pigtail in the bladder is critical to comfort of the patient when rigid indwelling stents are placed: a stent that is too long may kink or irritate the bladder. The vast majority of stents placed in this series were 22 or 24 cm in length. Inevitably, the distal pigtail came to lie in a variety of locations within the bladder. Nevertheless, no patients complained of discomfort, presumably because of the softer nature of the stent. New copolymer technology has produced materials that are well tolerated by the body.

Some patients are inevitably lost to follow-up, do not return for scheduled cystoscopic procedures, or are too ill for further manipulations. Thus, stents will inevitably be left in place beyond the recommended interval for replacement. It is of interest that the Percuflex stents remained patent and flexible in 14 patients whose clinical circumstances resulted in the same stent remaining in place beyond 6 months. As a routine, one should try to follow the manufacturer's recommendation for the time of stent replacement. However, our experience suggests that Percuflex stents can be left in place beyond this period in appropriate clinical situations.

REFERENCES

1. Mitty HA, Rackson ME, Dan SJ, Train JS. Experience with a new ureteral stent made of a biocompatible copolymer. *Radiology* **1988**;168:557-559
2. Leroy AJ, Williams HJ, Segura JW, Patterson DE, Benson RC. Indwelling ureteral stents: percutaneous management of complications. *Radiology* **1986**;158:219-222
3. Lang EK. Antegrade ureteral stenting for dehiscence, strictures, and fistulae. *AJR* **1984**;143:795-801
4. Abber JC, Kahn RI. Pyelonephritis from severe encrustations on silicone ureteral stents: management. *J Urol* **1983**;130:763-764
5. Pollack HM, Banner MP. Percutaneous nephrostomy and related pyeloureteral manipulative techniques. *Urol Radiol* **1981**;2:147-154
6. Cardella JF, Castañeda-Zuñiga WR, Hunter DW, Hulbert JC, Amplatz K. Urine compatible polymer for long-term ureteral stenting. *Radiology* **1986**;161:313-318

The Enthesopathic Changes of Hypophosphatemic Osteomalacia in Adults: Radiologic Findings

Mark I. Burnstein¹
 Jack P. Lawson²
 Sambasiva R. Kottamasu³
 Burton I. Ellis³
 Joseph Micho⁴

The enthesopathy (bone proliferation at sites of ligament, tendon, joint capsule, and interosseous membrane attachment) that may be present in adults who have long-standing hypophosphatemic osteomalacia, the most common type of osteomalacia, has received little attention in the radiologic literature. These proliferative enthetic changes may be associated with various musculoskeletal symptoms. The spectrum of proliferative enthesopathic changes, involving the axial and appendicular skeleton, is described in six patients 18–63 years old. Proliferative changes at the attachment of the annulus fibrosus were present in six of six patients and ranged in extent from tiny hyperostoses at a few levels to thin marginal symmetric syndesmophytes involving the entire lumbosacral spine and mimicking spondylitis. Thoracic spinal syndesmophytes were present in four patients and cervical hyperostoses of various magnitudes were present in three patients. Changes in the sacroiliac joints were present in four of six patients and varied from mild widening to symmetric intraarticular and anterior paraarticular bony bridging. Proliferative enthesopathy involving the pelvis and proximal femora was present in six of six patients. Appendicular changes included accessory ossicles within the wrist and hands and bony proliferation of the distal radius and metacarpal heads. These were noted in four patients. Ossification of the interosseous membrane of the forearms or the lower extremities was present in six patients and paraarticular bony proliferation about the elbows was noted in four patients.

It is apparent that the severity of the enthesopathy that occurs may vary, and that hypophosphatemic osteomalacia should be recognized as a cause of enthesopathy even if other radiographic findings of osteomalacia may not be present on available radiographs.

AJR 153:785–790, October 1989

Received March 22, 1989; accepted after revision May 18, 1989.

¹ Department of Radiology, University of Wisconsin Hospital and Clinics, 600 Highland Ave., Madison, WI 53792. Present address: Department of Diagnostic Radiology and Medical Imaging, Henry Ford Hospital, 2799 W. Grand Blvd., Detroit, MI 48202. Address reprint request to M. I. Burnstein.

² Department of Radiology, Yale University School of Medicine, 333 Cedar St., New Haven, CT 06510.

³ Department of Diagnostic Radiology and Medical Imaging, Henry Ford Hospital, Detroit, MI 48202.

⁴ Department of Radiology, Indiana University Medical Center, 1001 W. 10th St., Indianapolis, IN 46202.

0361-803X/89/1534-0785
 © American Roentgen Ray Society

The enthesopathy that may be present in adults who have long-standing hypophosphatemic osteomalacia has received little attention in the radiologic literature. These proliferative enthetic changes may result in various musculoskeletal symptoms. The purpose of this article is to illustrate the spectrum of these enthetic changes and to discuss the radiographic differential diagnosis.

Materials and Methods

The radiographs of six adult patients with hypophosphatemic osteomalacia were analyzed retrospectively. Not all of the anatomic areas were radiographed in all patients. Consequently, this report is not meant to be a statistical evaluation of the frequency of changes, but rather a qualitative assessment of the abnormalities that may be encountered in this disorder. Serum levels of calcium, phosphorus, alkaline phosphatase, and creatinine and urine levels of calcium, phosphorus, and creatinine were obtained at a time when the patients were not receiving medication. Clinical and biochemical data are listed in Table 1. Bone biopsies were done after tetracycline (tetracycline hydrochloride capsules, Danbury Pharmacal, Danbury, CT) bone double labeling.

TABLE 1: Clinical and Laboratory Findings in Patients with Hypophosphatemic Osteomalacia

Case No.	Age	Gender	Biochemical Findings (mg/dl) ^a				Family History
			Serum Calcium	Serum Inorganic Phosphate	TmP/GFR		
1	18	M	9.6	2.1	1.6		+
2	22	F	9.3	2.0	1.06		? ^b
3	40	M	9.7	2.0	NA		+
4	36	F	9.3	2.3	NA		+
5	59	F	9.1	1.8	NA		+
6	63	M	9.6	1.4	0.32		? ^b

Note.—All laboratory values were obtained while medical therapy was withheld. TmP = renal tubular maximum reabsorption of phosphate; GFR = glomerular filtration rate; NA = not available.

^a Normal values: serum calcium, 8.5–10.5 mg/dl; serum inorganic phosphate, 2.5–4.5 mg/dl; TmP/GFR = 2.78–4.15 mg/dl.

^b A detailed evaluation of relatives including laboratory values was not possible, so these cases may still represent an X-linked dominant state as opposed to sporadic mutation.

Results

Five of six patients had musculoskeletal symptoms. These symptoms included back rigidity and pain caused by spinal enthesopathy and pain and stiffness of multiple joints, which showed evidence of paraarticular proliferative changes.

Radiologic Findings in the Axial Skeleton

Proliferative changes at the attachment of the annulus fibrosus involving the lumbosacral spine ranged from tiny hyperostoses at several levels to thin marginal symmetric syndesmophytes involving the entire lumbosacral spine (Fig. 1). New bone formation involving the lumbar facets was

identified (Fig. 2). Proliferative marginal changes at the thoracic spine were noted and varied from asymmetric thin hyperostoses at a single level to symmetric marginal syndesmophytes at numerous levels. The changes noted in the cervical spine ranged from nonbridging osteophytosis at two levels to thick flowing hyperostotic changes that were identified anteriorly over contiguous vertebral body levels and occurred in the presence of intact disk spaces (Figs. 3A and 3B). Ossification of interspinous ligaments was shown (Fig. 3C).

The appearance of the sacroiliac joints varied, ranging from symmetrically widened (Fig. 4) or normal to intraarticular ankylosis with ossification of the anterior sacroiliac ligaments (Fig. 5).

The proliferative enthesopathy involving the pelvis and proximal femora consisted of an undulating cortical thickening, which was noted laterally at the supraacetabular margins of the hip joints; "whiskering" along iliac crests and ischia; and bony proliferation at the sites of capsular insertion on the femoral necks (Figs. 4 and 6).

Proliferative changes at the infraglenoid tubercle, at the greater tuberosity of the humeri, along the lateral margin of the scapulae, or at the coracoid attachment of the coracoclavicular ligaments were shown occasionally (Fig. 7).

Radiologic Findings in the Appendicular Skeleton

Accessory ossicles occurring in the hands, wrists, or feet and hooklike projections from the metacarpal heads were identified (Figs. 8 and 9). Radiographic abnormalities in the forearms consisted of cortical thickening at the attachments of the interosseous membrane and proliferative changes about the elbows (Fig. 10). Osseous proliferation involving the lower legs ranged from cortical thickening to pedunculated

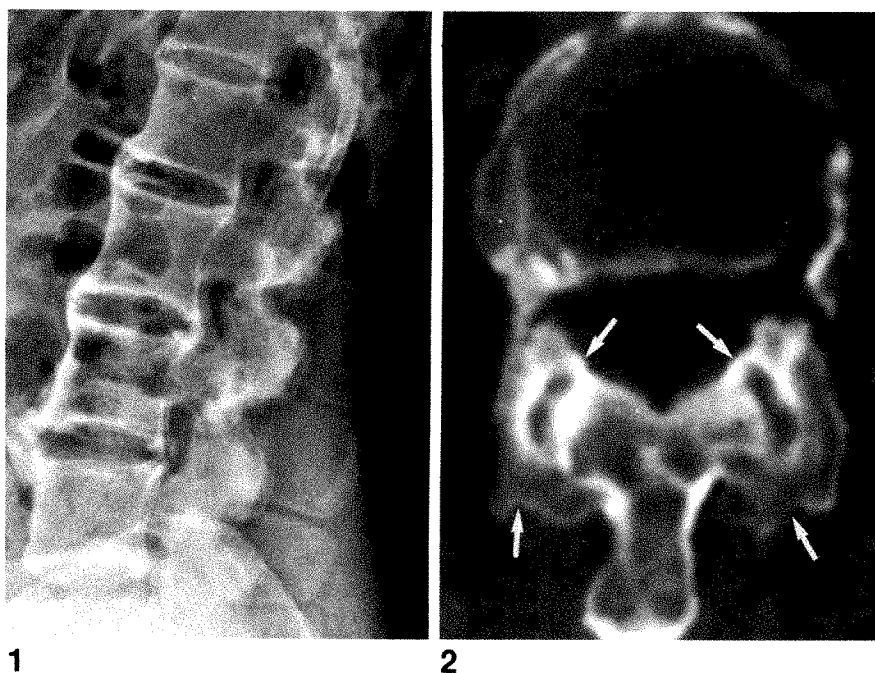


Fig. 1.—Radiograph shows thin marginal syndesmophytes anteriorly and posteriorly from T10 to L3 and larger anterior osteophytes at L3–L4 disk space.

Fig. 2.—Axial CT scan through L1–L2 facet joints shows remodeled facets with paraarticular osseous ankylosis (arrows).

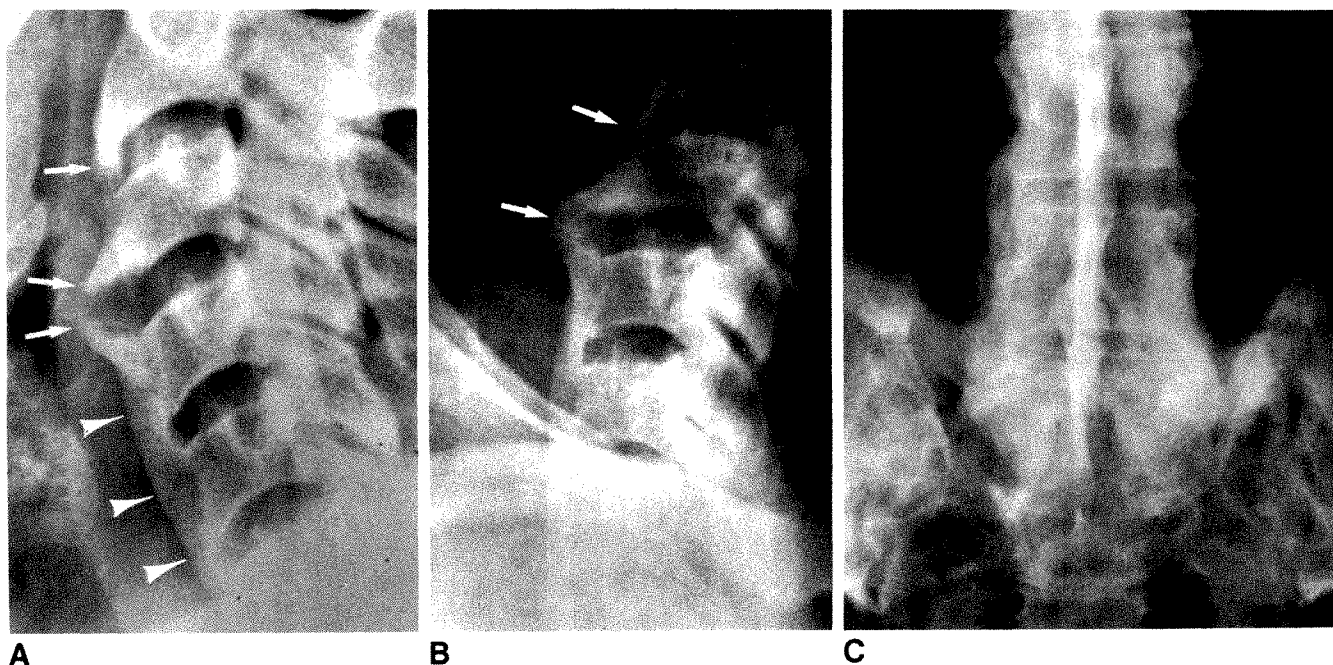


Fig. 3.—Interval bridging of osteophytes.

A, Lateral radiograph of cervical spine shows large, nonbridging anterior osteophytes at C2, C3, and C4 vertebral bodies (arrows) and thick flowing hyperostosis (arrowheads).

B, Radiograph obtained 6 years later shows interval bridging of osteophytes at C2-C3 and C3-C4 levels (arrows).

C, Radiograph shows "dagger sign" of interspinous and supraspinous ligamentous ossification and marginal syndesmophytosis of lumbar spine.

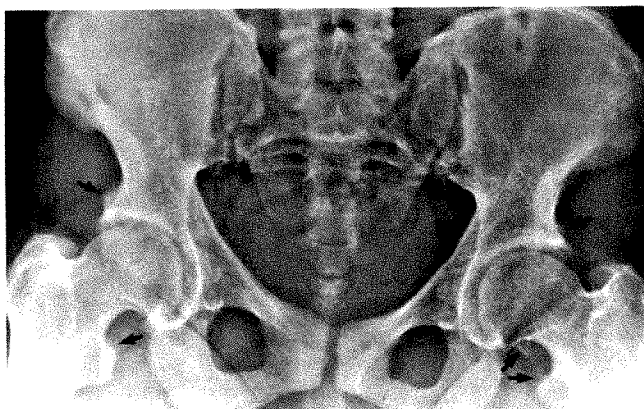


Fig. 4.—Radiograph shows symmetric widening of both fibrous and synovial parts of sacroiliac joints and bony proliferation about hips (arrows).

or sessile projections arising from the attachments of the interosseous membrane and muscular aponeuroses (Fig. 11). Long-bone bowing deformities and/or Looser zones were noted in four patients (Figs. 6 and 11).

Discussion

The most common type of hypophosphatemic osteomalacia is X-linked dominant hypophosphatemia [1]. Rare cases of recessive inheritance and sporadic mutation have also been described [2, 3]. The renal abnormality present in these

patients is a decreased renal tubular transport maximum of phosphate that results in the hypophosphatemia [1]. No other associated renal tubular defects are present, and the glomerular filtration rate is normal. Laboratory values typically seen include normocalcemia, hypophosphatemia, and normal 25-hydroxy-vitamin D₃. It is thought that there may be an inappropriately decreased response of 1,25-vitamin D₃ production to the hypophosphatemic state [1]. Osteomalacia occurs as a result of the mineral imbalance. The severity of clinical and biochemical abnormalities may vary, and a history of growth disturbance or rickets in childhood is common.

In contrast to early-onset hypophosphatemia, patients with adult-onset hypophosphatemia have no history of rickets or childhood growth disturbance, manifest a prominent myopathy, and may have aminoaciduria in addition to a decreased renal tubular transport maximum of phosphate [4, 5].

A radiographic spectrum of calcification of ossification occurring at the attachment of ligaments, tendons, joint capsules, interosseous membranes, and muscular aponeuroses has been described [6, 7]. Despite speculation by many authors, the pathogenesis of the ossific changes remains uncertain [5-10]. It has been shown that these changes are not associated with medical treatment [9, 10]. What remains in doubt is whether the ossifications represent another radiographic manifestation of the genetic disease, as suggested by Polisson et al. [10], or whether the changes are merely a result of the presence of the long-standing mineralization defect. Similar hyperostotic involvement of the spine reported in a patient with long-standing cadmium poisoning and resultant renal tubular disease supports the latter contention [9].

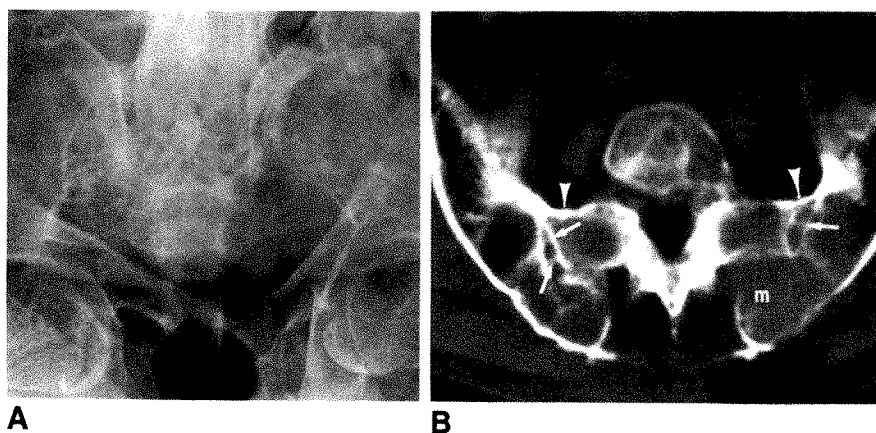


Fig. 5.—Intraarticular and paraarticular sacroiliac joint bone formation.

A, Radiograph shows severe osteopenia and apparent ankylosis of sacroiliac joints.

B, Axial CT scan shows ossification of anterior sacroiliac ligaments (arrowheads) and bone struts crossing within sacroiliac joints (arrows). A metastasis (m) from prostate carcinoma is present.

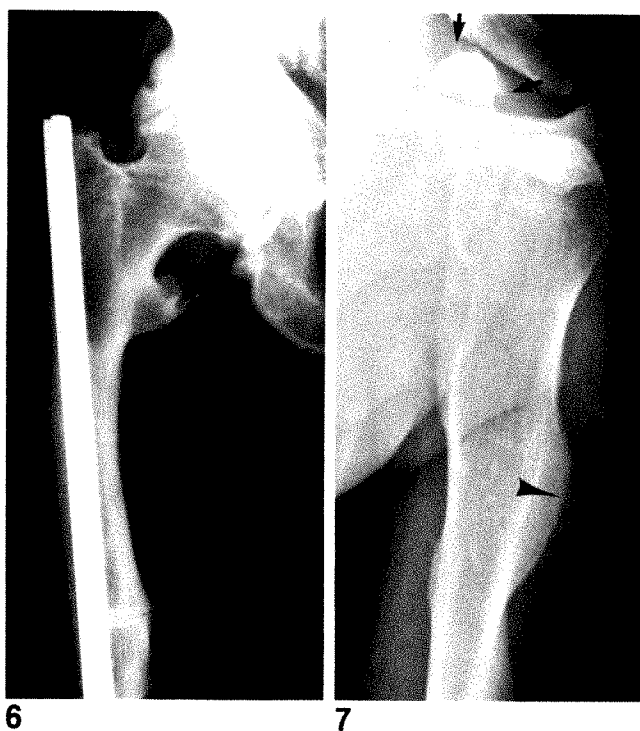


Fig. 6.—Radiograph shows marked bone proliferation involving supra-acetabular cortex and lesser trochanter and Looser zone in mid femur medially.

Fig. 7.—Radiograph shows osseous proliferation at coracoid process (arrows) and marked enlargement of deltoid tuberosity (arrowhead).

Ligamentous calcification has also been described in another long-standing osteomalacic state, hypophosphatasia [11]. In several series of patients with X-linked hypophosphatemia, it has been shown that the prevalence of enthesopathy increases with the age of the patient [10, 12]. The enthesopathy may result in pain or decreased range of motion of the appendicular and axial skeleton [9], and spinal canal encroachment with neurologic symptoms has been reported [13, 14].

With radiologic evidence of Looser zones, bowing, and deformity, there is little to be considered in the differential diagnosis. However, if these features of osteomalacia are not

evident on the available radiographs, the enthesopathic changes shown on the axial or appendicular skeleton may raise the possibility of several disorders.

The radiographic changes that may be identified in the sacroiliac joints may suggest an inflammatory sacroiliitis. Apparent widening of the sacroiliac joints, mimicking an early stage of sacroiliitis, may occur and result from the accumulation of unmineralized osteoid within the subchondral bone [15]. In patients who have been taking phosphate supplements for a long time, hyperparathyroidism and apparent widening of the sacroiliac joint associated with subchondral bone resorption, mediated by elevated parathyroid hormone, may develop. With ossification of the anterior sacroiliac ligaments or true intraarticular bone formation, the radiographic appearance of sacroiliac joint ankylosis may suggest end-stage sacroiliitis [7–9]. The lumbar and thoracic syndesmophytes of hypophosphatemic osteomalacia are marginal and symmetric, which are classically described in ankylosing spondylitis or the spondylitis of inflammatory bowel disease [8], and differ from the paravertebral ossifications associated with spondyloarthropathies of psoriasis, Reiter syndrome, and acne conglobata. Squaring of the vertebral bodies similar to that seen with ankylosing spondylitis may be noted [7–9]. Calcification or ossification of the ligamenta flava and interspinous, supraspinous, anterior, and posterior longitudinal ligaments may occur along with hypertrophy of the facet joints and thickening of the lamina [13, 14].

The radiographic abnormalities described in diffuse idiopathic skeletal hyperostosis have features that are quite similar to those seen in hypophosphatemic osteomalacia. The changes in the appendicular skeleton in patients described by Resnick and Niwayama [16] are essentially the same as those that may occur in hypophosphatemic osteomalacia. The spinal hyperostoses are classically described as thick and flowing and involve at least four contiguous thoracic levels. Similar hyperostotic changes of the cervical vertebral bodies have been described in X-linked hypophosphatemic osteomalacia [9].

Ossification of the posterior longitudinal ligament is another cause of proliferative enthesopathy, which may cause compromise of the spinal canal [17]. This entity has been described most commonly in people of Japanese descent. Ossification of the posterior longitudinal ligament usually involves



Fig. 8.—Radiograph shows multiple intercarpal ossicles and hooklike projections involving metacarpal heads (arrows).



Fig. 9.—Radiograph shows ossicles at several metacarpal phalangeal joints (arrows).

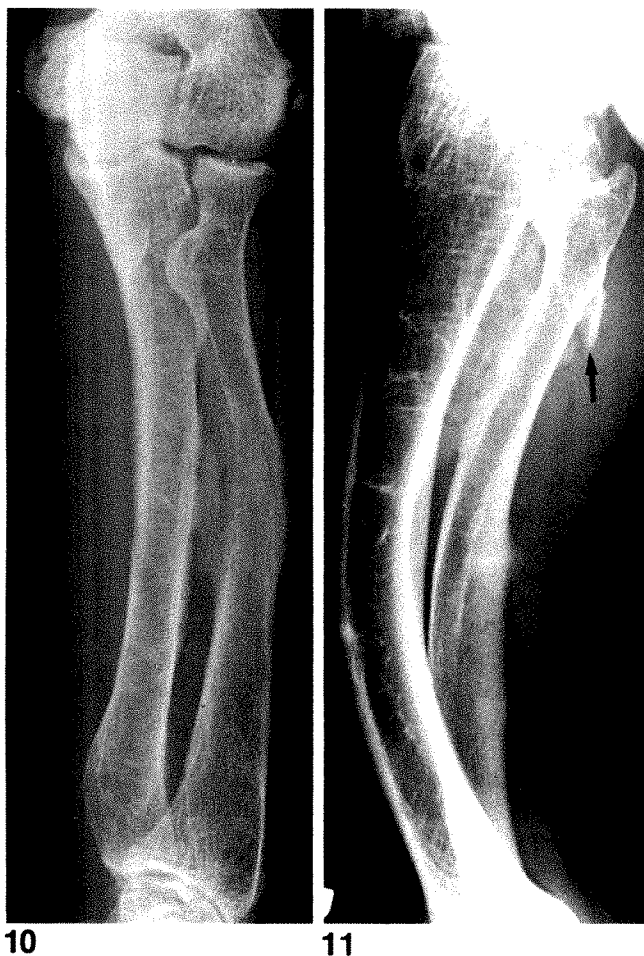


Fig. 10.—Radiograph shows marked cortical thickening at radial attachment of interosseous membrane, prominent radial tuberosity, and proliferative changes at lateral epicondyle with a small accessory ossicle laterally.

Fig. 11.—Radiograph shows marked anterior bowing of tibia and fibula, ossification of proximal part of interosseous membrane, an exostotic projection from proximal fibula (arrow), and healing Looser zones of fibular diaphysis.

the cervical spine with thoracic or lumbar involvement occurring less frequently. Ossification involving the ligaments flava and capsules of the apophyseal joints may occur as seen in hypophosphatemic osteomalacia. Coexistence with diffuse idiopathic skeletal hyperostosis may occur.

The hyperostotic abnormalities of the appendicular skeleton described in idiopathic hypoparathyroidism have many similarities to the proliferative changes seen in hypophosphatemic osteomalacia [18]. Osteosclerosis may be present in both entities. Distinction may be made on the basis of the clinical history and presentation of seizures, cataracts, and skin rash, as well as laboratory values.

Retinoid-induced hyperostosis is a recently recognized cause of enthesopathy [19]. Both axial and appendicular enthesal changes may be present. Radiographically, the spinal syndesmophytes may appear thin initially, yet with continued therapy may progress to changes more characteristic of diffuse idiopathic skeletal hyperostosis.

Finally, fluorosis, which may be associated with osteosclerosis and ligamentous calcification or ossification similar to hypophosphatemic osteomalacia, must be considered in the differential diagnosis [20]. The pathogenesis of fluorosis may relate in part to a mineralization defect with resultant osteomalacia caused by the excess fluoride.

ACKNOWLEDGMENTS

We thank Gloria Storch for secretarial assistance, A. Michael Parfitt for suggestions, and D. S. Burnstein.

REFERENCES

1. Rasmussen H, Anast C. Familial hypophosphatemic rickets and vitamin D dependent rickets. In: Stanbury JB, Wyngarden JB, Fredrickson DS, eds. *The metabolic basis of inherited disease*, 5th ed. New York: McGraw-Hill, 1983:1743-1773
2. Perry W, Samp TCB. Hereditary hypophosphatemic rickets with autosomal recessive inheritance and severe osteosclerosis. *J Bone Joint Surg [Br]* 1978;60—B:430-434
3. Winters RW, McFalls VW, Graham JB. "Sporadic" hypophosphatemia and

- vitamin D-resistant rickets. *Pediatrics* **1960**;25:959-966
4. Dent CE, Stamp TCB. Hypophosphatemic osteomalacia presenting in adults. *Q J Med* **1971**;158:303-329
 5. Parfitt AM. Hypophosphatemic vitamin D refractory rickets and osteomalacia. *Orthop Clin North Am* **1972**;3:653-680
 6. Steinbach HL, Kolb FO, Crane JT. Unusual roentgen manifestations of osteomalacia. *AJR* **1959**;82:875-886
 7. Patton JT. Hip changes in metabolic bone disease. *J R Soc Med* **1966**;59:1231-1236
 8. Patton JT. Skeletal changes in hypophosphatemic osteomalacia. In: Jelliffe AM, Strickland B, eds. *Symposium ossium*. London: Livingstone, **1970**:299-301
 9. Davies M, Stanbury SW. The rheumatic manifestations of metabolic bone disease. *Clin Rheum Dis* **1981**;7:595-645
 10. Polisson RP, Martinez S, Khoury M, et al. Calcification of entheses associated with X-linked hypophosphatemic osteomalacia. *N Engl J Med* **1985**;313:1-6
 11. Bethune JE, Dent CE. Hypophosphatasia in the adult. *Am J Med* **1960**;28:615-622
 12. Hardy DC, Murphy WA, Siegel BA, Reid IR, Whyte MP. X-linked hypophosphatemia in adults: prevalence of skeletal radiographic and scintigraphic features. *Radiology* **1989**;171:403-414
 13. Dugger GS, Vandiver RW. Spinal cord compression caused by vitamin D resistant rickets. *J Neurosurg* **1966**;25:300-303
 14. Adams JE, Davies M. Intra-spinal new bone formation and spinal cord compression in familial hypophosphatemic vitamin D resistant osteomalacia. *Q J Med* **1986**;236:1117-1129
 15. Nagant de Deuxchaisnes C, Krane SM. The treatment of adult phosphate diabetes and Fanconi syndrome with neutral sodium phosphate. *Am J Med* **1967**;43:508-543
 16. Resnick D, Niwayama G. Diffuse idiopathic skeletal hyperostosis (DISH): ankylosing hyperostosis of Forestier and Rotes-Querol. In: Resnick D, Niwayama G, eds. *Diagnosis of bone and joint disorders*, 3rd ed. Philadelphia: Saunders, **1988**:1563-1615
 17. Jones MD, Pais MJ, Omiya B. Bony overgrowths and abnormal calcifications about the spine. *Radiol Clin North Am* **1988**;26:1213-1234
 18. Adams JE, Davies M. Paravertebral and peripheral ligamentous ossification: an unusual association of hypoparathyroidism. *Postgrad Med J* **1977**;53:167-172
 19. Lawson JP, McGuire J. The spectrum of skeletal changes associated with long-term administration of 13-cis-retinoic acid. *Skeletal Radiol* **1987**;16:91-97
 20. Singh A, Dass R, Hayreh SS, Jolly SS. Skeletal changes in endemic fluorosis. *J Bone Joint Surg [Br]* **1962**;44-B:806-815

Radiation-Induced Sarcoma of Bone: CT Findings in 19 Cases

James G. Lorigan¹
Herman I. Libshitz
Martine Peuchot

We reviewed the CT findings in 19 cases of radiation-induced sarcoma of bone. The latent period before development of the sarcoma ranged from 5 to 50 years (mean, 17 years). In all 19 lesions, a soft-tissue extraosseous component was seen on CT, and 18 of them had associated bone destruction. Expansion of the affected bone and tumor-matrix mineralization each were present in 10 patients, but occurred together in only five patients. Periosteal reaction was seen in five patients, one of whom had an associated fracture. Radiation osteitis could not be identified on CT scans in the affected bone of any of the patients when tumor was present, but it was present in contiguous bone in two patients and had been shown 6 years before tumor became apparent in the affected bone in one other patient.

Radiation-induced sarcoma of bone should be considered when bone destruction and an associated soft-tissue mass are shown on CT, or when changes occur in the appearance of previously stable irradiated bone.

AJR 153:791-794, October 1989

Malignant neoplasms are an uncommon, but well-recognized complication of therapeutic irradiation [1]. Radiation-induced sarcomas of bone are estimated to occur in 0.035% of patients treated by irradiation who survive 5 years [2]. The radiographic appearances of these tumors have been well described [3]. However, because CT is now the primary imaging technique in the follow-up evaluation of many cancer patients, it is important that the CT features of radiation-induced sarcoma of bone be recognized. In this report, we describe the CT appearances in 19 patients in whom sarcomas of bone developed after therapeutic irradiation for a variety of nonosseous lesions.

Materials and Methods

The medical records and CT examinations of 19 patients with radiation-induced sarcomas of bone were reviewed. All diagnoses were made after 1980, and all CT scans were obtained with "fast" scanners by using a scan time of 3 sec or less. Seven of these patients, including five with a variety of head and neck tumors, have been included in previous reports [4, 5].

The group was composed of 11 women and eight men; the age range was 16-80 years (mean, 52 years). The average age at irradiation was 35 years (range, 4-67 years). All patients were treated for a nonosseous lesion, and none had had a known abnormality in the affected bone at the time of irradiation. The primary malignancies included breast cancer (five patients), Hodgkin disease (four), ovarian cancer (three), melanoma (one), and prostate cancer (one). The remaining five patients had a variety of head and neck lesions, including cystic hygroma, nasopharyngeal carcinoma, malignant fibrous histiocytoma, and rhabdomyosarcoma. The reason for irradiation of the head and neck in the other patient is unknown.

Treatment of the primary lesion was performed at other institutions in most patients, and details of the radiation therapy were incomplete in nine cases. In the other 10 patients, irradiation was given with cobalt-60; the average dose was 42.8 Gy (4280 rad). Five patients also underwent chemotherapy.

Received March 20, 1989; accepted after revision May 15, 1989.

¹All authors: Department of Diagnostic Radiology, Division of Diagnostic Imaging, University of Texas M. D. Anderson Cancer Center, 1515 Holcombe Blvd., Houston, TX 77030. Address reprint requests to H. I. Libshitz.

0361-803X/89/1534-0791
© American Roentgen Ray Society

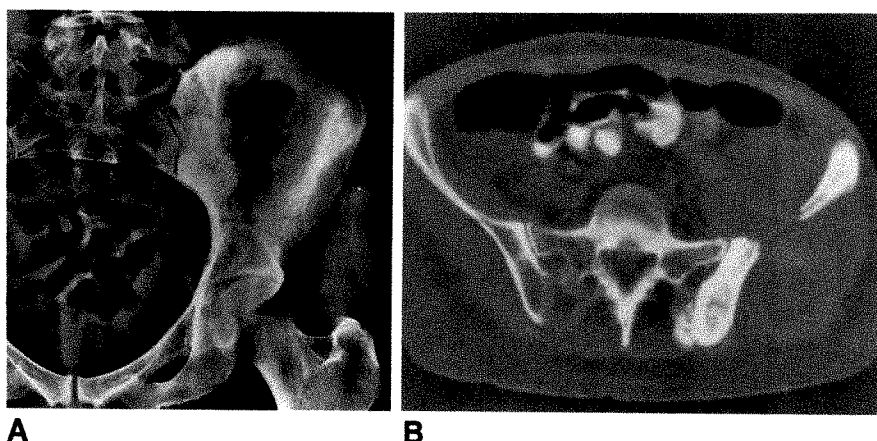


Fig. 1.—Spindle cell sarcoma of ilium in 46-year-old woman 12 years after radiation therapy for ovarian carcinoma.

A, Radiograph of pelvis shows a destructive lesion in left ilium. No soft-tissue mass is seen.

B, CT scan shows bone destruction with a large associated soft-tissue mass in pelvis and buttock, and reactive bone changes in left ilium and periosteal reaction medial to posteromedial aspect of bone.

The diagnosis of radiation-induced sarcoma of bone was made using the criteria originally enumerated by Cahan et al. [6]. These include (1) radiation therapy, (2) development of the neoplasm within the irradiated field, (3) a latent period of some years, and (4) histologic proof of a sarcoma. The average latent period to the development of the sarcoma was 17 years (range, 5–50 years). The radiation-induced malignancies included 14 osteosarcomas, two malignant fibrous histiocytomas, and one case each of chondrosarcoma, malignant chondroblastoma, and spindle cell sarcoma. The tumor occurred in the scapula in six patients, various parts of the maxilla in five, the pelvis in four, the sternum in two patients, and the humerus and clavicle in one patient each.

The CT examinations were evaluated for the presence of soft-tissue mass, destruction and expansion of the affected bone, tumor-matrix mineralization, periosteal reaction, and evidence of radiation osteitis in the affected area.

Results

An extrasosseous soft-tissue mass (19 patients) and bone destruction (18 patients) were the most common features (Figs. 1–5). Bone expansion (Fig. 4) and tumor-matrix mineralization (Figs. 3 and 5) were seen in 10 patients each, but only five patients had evidence of both features. Periosteal reaction was present in five patients (Figs. 1 and 5), one of whom had an associated pathologic fracture of the affected bone (Fig. 4). Associated tumor-matrix mineralization was seen in four of these five patients, and bone expansion was seen in two of them. None of our patients had definite evidence of radiation-induced osteitis in the affected bone on CT examination at the time the tumor was present (Fig. 3). The histology of the underlying neoplasm could not be predicted from the CT appearance (Fig. 3). However, tumor-matrix mineralization was present in each of the four osteosarcomas involving the maxilla but in only four of the other nine osteosarcomas. The other patient with tumor-matrix mineralization had a chondrosarcoma, but we could not distinguish the chondroid matrix of this tumor from the osteoid matrix of the osteosarcomas on CT (Fig. 3).

Discussion

Radiation-induced sarcomas are an infrequent consequence of therapeutic irradiation [1, 2]. Most of the early

cases of radiation-induced sarcoma of bone occurred after irradiation of benign bone lesions, but because this is now rarely done, most of the cases now seen occur after radiation treatment of a soft-tissue neoplasm [2, 3, 5, 7]. The latent period in our patients ranged from 5 to 50 years. This is in keeping with the experience of Huvois et al. [8], who found a latent period ranging from 3.5 to 33 years in 66 patients, and Weatherby et al. [9], who reported a range of 2 years, 9 months to 55 years in 78 patients.

It has been suggested that for radiation to induce malignant change, the injury to individual cells must be sufficient to cause genetic mutation but insufficient to cause cell death [10], a situation that apparently arises at the margins of the radiation field. The anatomic distribution and the preponderance of the bone sarcomas in women in our series reflects the role of therapeutic radiation in the management of breast carcinoma, Hodgkin disease, and gynecologic malignancies.

In 14 (74%) of our patients, the radiation-induced tumor was an osteosarcoma, whereas in the series of Weatherby et al. [9], osteosarcomas (48.7%) and fibrosarcomas (41%) accounted for almost 90% of the tumors. It may be significant that in the series of Weatherby et al., 43 of 78 sarcomas of bone developed at the site of a preexisting bone abnormality. One of the other five neoplasms in our series was a malignant chondroblastoma, a rare tumor that occurs most frequently after curettage or therapeutic irradiation of a benign chondroblastoma [11]. This case is exceptional in that it arose in an area of apparently normal bone, although it may represent malignant transformation of an unrecognized benign chondroblastoma.

The spectrum of conventional radiographic findings in radiation-induced sarcoma of bone are well described [3] and vary from lucent destructive lesions to areas of dense sclerosis or a mixed pattern. Most lesions have an associated soft-tissue mass, although this may not be obvious on conventional radiographs. In Smith's series [3], 19 of 43 patients had radiographic evidence of radiation osteitis involving the affected bone. Five patients in that series had a periosteal reaction, but in three of these, an underlying pathologic fracture was present.

In Smith's series [3], CT was used in 12 patients and was useful for showing the extent of both the bony lesion and the

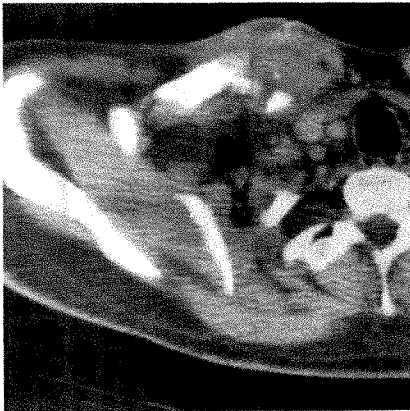
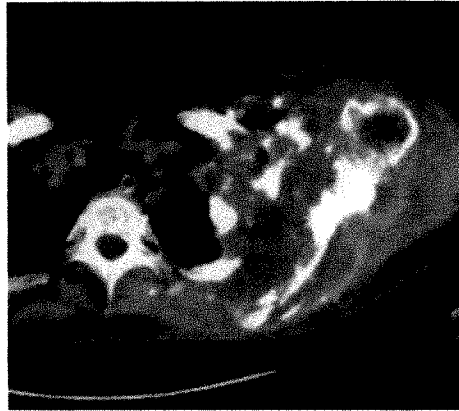


Fig. 2.—Osteosarcoma of right clavicle in 39-year-old man 11 years after radiation therapy for Hodgkin disease. CT scan shows destruction of medial end of right clavicle with an associated soft-tissue mass.



A



B

Fig. 3.—Chondrosarcoma of scapula in 51-year-old woman 24 years after radiation therapy for malignant melanoma.

A, CT scan shows a destructive lesion involving left scapula with an associated soft-tissue mass and tumor-matrix mineralization.

B, CT scan obtained 6 years before **A** shows mottled pattern of radiation osteitis in scapula and no evidence of tumor.

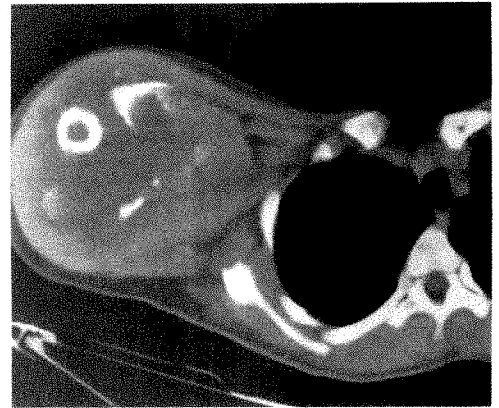
Fig. 4.—Osteosarcoma of proximal right humerus in 16-year-old man 6 years after radiation therapy for Hodgkin disease.

A, Radiograph shows expansile and destructive lesion in proximal humerus with an associated pathologic fracture and periosteal reaction. A large soft-tissue mass is present.

B, CT scan shows large soft-tissue mass in proximal right arm with tumor-matrix mineralization. A bone fragment due to fracture is seen anteriorly.



A

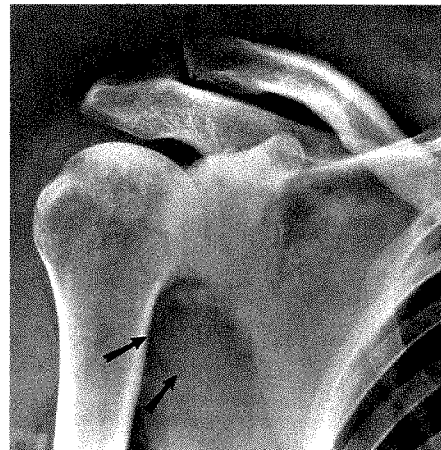


B

Fig. 5.—Osteosarcoma of right scapula in 43-year-old man 13 years after radiation therapy for Hodgkin disease.

A, Radiograph shows tumor-matrix mineralization and suggests presence of a soft-tissue mass (arrows).

B, CT scan shows right scapular lesion, with tumor-matrix mineralization and periosteal reaction and soft-tissue mass.



A



B

soft-tissue mass. Likewise, Sundaresan et al. [7] found that CT was the most useful diagnostic test in radiation-induced sarcomas of the axial skeleton because it frequently showed unsuspected soft-tissue masses.

In our patients, the combination of bone destruction and a soft-tissue mass suggested the correct diagnosis in 18 patients. The remaining patient had a large soft-tissue mass with tumor-matrix mineralization affecting the scapula, without evidence of bone destruction. Bone expansion and tumor-matrix mineralization are good indications of a neoplastic process; they were present, either in combination or singly, in 15 patients. Periosteal reaction was uncommon, and we identified only one associated fracture. Although we could not identify radiation osteitis in tumor-bearing bone on CT, it was seen in a contiguous bone in two of five patients with pelvic tumors. In our experience, however, radiation osteitis is better shown on conventional radiographs than on CT. Likewise, it may be difficult to distinguish true tumor-matrix mineralization from displacement of native bone by expansile bone lesions.

Fractures and subsequent bone resorption are well-recognized complications of radiation injury [12, 13]. These complications can be distinguished from bone destruction due to radiation-induced sarcoma by the absence of a soft-tissue mass [12, 14]; soft-tissue mass was present to some extent in all of our patients. Radiation-induced sarcomas of bone do not differ radiographically from de novo lesions [3, 5]. However, this complication may be suspected when a suspicious bone lesion arises in an area of previous irradiation.

CT is superior to conventional radiography in the evaluation of the intramedullary and soft-tissue extension of osteosarcomas [15, 16]. MR imaging was done in only two of our patients, and we cannot, therefore, adequately assess its role in the evaluation of radiation-induced sarcomas of bone. However, MR may be considered complementary to CT because CT is superior in the evaluation of the bony cortex and new bone formation, whereas MR is superior in the assessment of intramedullary and soft-tissue tumor extension [17].

Radiation-induced sarcoma of bone is a rare occurrence. It should be considered, however, when changes occur in the appearance of previously stable irradiated bone, particularly if an associated soft-tissue mass is present.

ACKNOWLEDGMENT

We thank Debbie Smith for manuscript preparation.

REFERENCES

1. Brady LW. Radiation-induced sarcomas of bone. *Skeletal Radiol* 1979; 4:72-78
2. Tountas AA, Fornasier VL, Harwood AR, Leung PMK. Postirradiation sarcoma of bone: a perspective. *Cancer* 1979;43:182-187
3. Smith J. Radiation-induced sarcoma of bone: clinical and radiographic findings in 43 patients irradiated for soft tissue neoplasms. *Clin Radiol* 1982;33:205-221
4. Souba WW, McKenna RJ Jr, Meis J, Benjamin R, Raymond AK, Mountain CF. Radiation-induced sarcomas of the chest wall. *Cancer* 1986;57: 610-615
5. Lee YY, Van Tassel P, Nauert C, Raymond AK, Edeiken J. Craniofacial osteosarcomas: plain film, CT, and MR findings in 46 cases. *AJR* 1988; 150:1397-1402
6. Cahan WG, Woodard HQ, Higinbotham NL, Stewart FW, Coley BL. Sarcoma arising in irradiated bone: report of eleven cases. *Cancer* 1948;1: 3-29
7. Sundaresan N, Huvos AG, Krol G, Hughes JEO, Cahan WG. Postradiation sarcoma involving the spine. *Neurosurgery* 1986;18:721-724
8. Huvos AG, Woodard HQ, Cahan WG, et al. Postradiation osteogenic sarcoma of bone and soft tissues: a clinicopathologic study of 66 patients. *Cancer* 1985;55:1244-1255
9. Weatherby RP, Dahlin DC, Ivins JC. Postradiation sarcoma of bone: review of 78 Mayo Clinic cases. *Mayo Clin Proc* 1981;56:294-306
10. Cole LJ, Nowell CS. Radiation carcinogenesis: the sequence of events. *Science* 1965;150:1782-1786
11. Bloem JL, Mulder JD. Chondroblastoma: clinical and radiological study of 104 cases. *Skeletal Radiol* 1985;14:1-9
12. Bragg DG, Shidnia H, Chu FCH, Higinbotham NL. The clinical and radiographic aspects of radiation osteitis. *Radiology* 1970;97:103-111
13. Howland WJ, Loeffler RK, Starchman DE, Johnson RG. Postirradiation atrophic changes of bone and related complications. *Radiology* 1975; 117:677-685
14. Skinner WL, Buzdar AU, Libshitz HI. Massive osteolysis of the right clavicle developing after radiation therapy. *JAMA* 1988;260:375-376
15. Lukens JA, McLeod RA, Sim FH. Computed tomographic evaluation of primary osseous malignant neoplasms. *AJR* 1982;139:45-48
16. Rotte KH, Schmidt-Peter P, Kriedemann E. CT evaluation of osseous tumors. *Eur J Radiol* 1986;6:5-8
17. Pettersson H, Gillespy T, Hamlin DJ, et al. Primary musculoskeletal tumors: examination with MR imaging compared with conventional modalities. *Radiology* 1987;164:237-241

Commentary

Optimal Plain Film Imaging of the Shoulder Impingement Syndrome

Ray F. Kilcoyne,¹ Praveen K. Reddy,² Frank Lyons,² and Charles A. Rockwood, Jr.²

The impingement syndrome is a painful condition of the shoulder produced by mechanical pressure on the supraspinatus tendon by the anterior portion of the acromion when the arm is brought into a position of abduction and/or forward flexion [1]. The syndrome can be divided into three stages: (1) edema and hemorrhage into the rotator cuff; (2) fibrosis and tendinitis; and (3) tears of the rotator cuff, biceps tendon rupture, and bony spurs [2].

Early diagnosis and treatment of impingement syndrome may prevent the progression to complete tear of the rotator cuff. Because the impingement is due to an abnormally long anterior portion of the acromion or a spur on this portion, imaging should be directed at visualizing the anterior part of the bone. Radiographic examinations of the shoulder are frequently inadequate when conventional anteroposterior radiographs are used because the anterior part of the acromion is obscured by the body of the acromion. By caudally angling the X-ray beam, the anterior part of the acromion is projected inferiorly to the remainder of the acromion and becomes visible. More sophisticated imaging techniques that can be used to diagnose tears of the rotator cuff are limited in their ability to show the anterior part of the acromion.

Plain Film Diagnosis of Impingement Syndrome

The key to diagnosis of the impingement syndrome is recognition of the acromial abnormality. A congenital deformity with an abnormally long anterior process of the acromion may be present or a spur may develop in this region as a

degenerative process (Fig. 1). Often this part of the acromion is obscured on the conventional anteroposterior radiograph. In a series of patients with the impingement syndrome reported by Hardy et al. [3], 26 (68%) of 38 shoulders showed subacromial bony proliferation on conventional radiographs. Identification of a spur is enhanced by making fluoroscopic

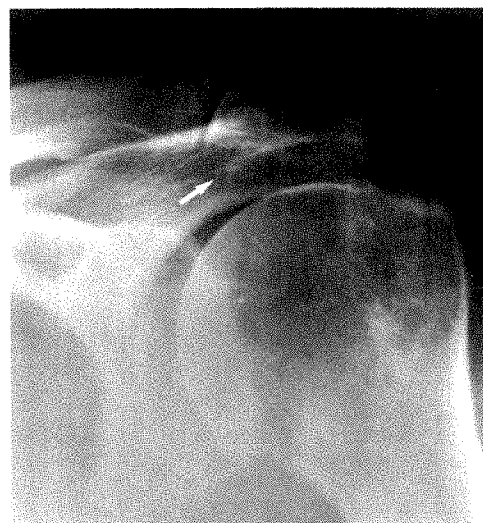


Fig. 1.—Conventional anteroposterior radiograph shows a subacromial spur on anterior-inferior margin of acromion (arrow). Sclerosis of greater tuberosity is thought to be due to cuff degeneration.

Received April 13, 1989; accepted after revision June 5, 1989.

¹ Department of Radiology, University of Texas Health Science Center, San Antonio, TX 78284. Address reprint requests to R. F. Kilcoyne, Radiology Service, VA Medical Center, San Antonio, TX 78284.

² Department of Orthopaedic Surgery, University of Texas Health Science Center, San Antonio, TX 78284.

AJR 153:795-797, October 1989 0361-803X/89/1534-0795 © American Roentgen Ray Society

spot films [4, 5]. When the impingement is long-standing, plain radiographs may show sclerosis or irregularity of the greater tuberosity, acromioclavicular joint abnormalities, and (after rupture of the rotator cuff) superior migration of the humeral head.

To improve early detection of an abnormal acromion, we use an erect anteroposterior projection made at a 30° caudal angle [5, 6]. This view is easy for the technologist to obtain and gives reproducible results (Figs. 2A and 2B). Another alternative is a modified transscapular lateral view at a 5°–10° caudal angle (the supraspinatus outlet view) to show the extent of anterior projection of the acromion [7] (Fig. 2C). This view is more difficult for the technologist to obtain, and

spurs may be more difficult to see because of superimposition of the spine of the scapula or the humeral head (Fig. 3).

Limitation of Other Imaging Procedures in the Diagnosis of Impingement Syndrome

The emphasis in the past has been on diagnosing tears of the rotator cuff, and many methods are available for doing this. We think it is more important to diagnose the impingement syndrome and to treat it before cuff tears develop. Partial as well as complete tears, but not impingement, may be seen by use of sonography [8]. The injection of contrast medium or air into the subacromial bursa allows delineation of the superior surface of the supraspinatus tendon. Subacro-

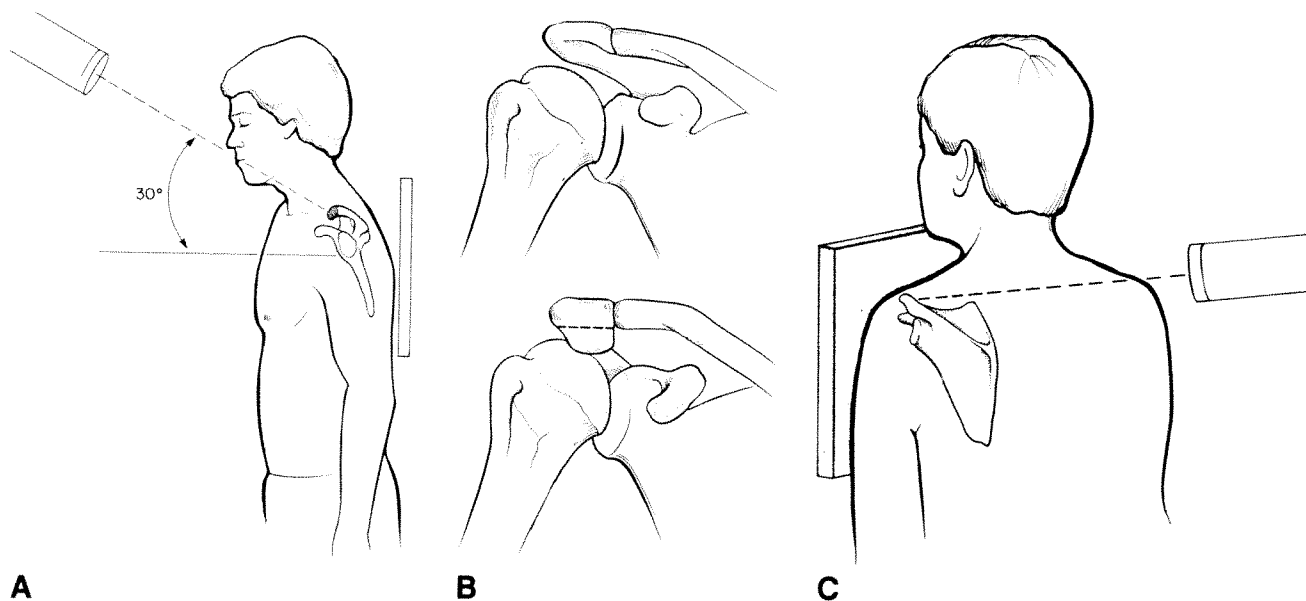


Fig. 2.—A, Diagram shows correct position of patient for 30° caudally angled anteroposterior view to show anterior part of acromion. B, Diagrams show that no abnormality is seen on conventional anteroposterior projection (top), but an abnormally long anterior acromial spur is seen in 30° caudal projection (bottom). Area below dotted line is abnormality. C, Diagram shows correct position of patient for supraspinatus outlet view to show anterior part of acromion in lateral view. Patient is positioned for a transscapular lateral view, and tube is angled 5° caudad.

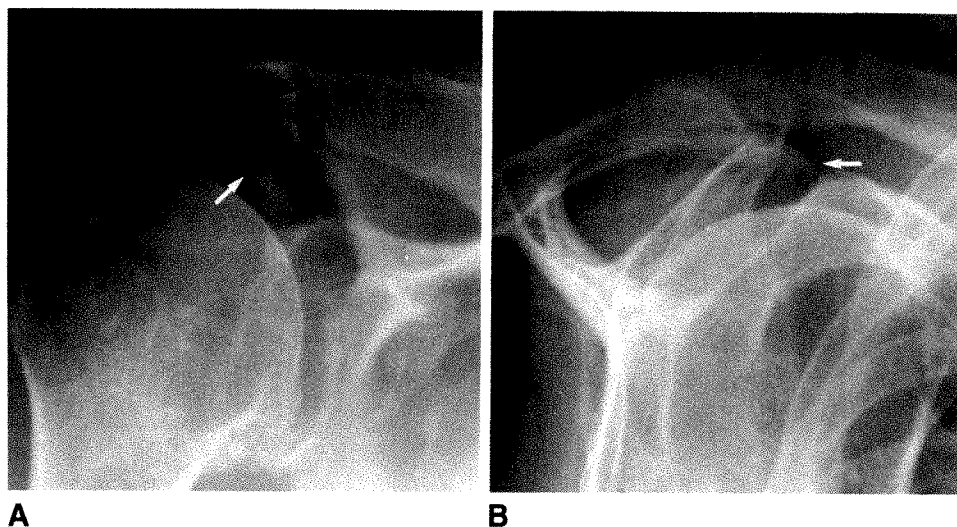


Fig. 3.—A and B, Radiographs show appearance of subacromial spur (arrows) on 30° caudally angled anteroposterior view (A) and on supraspinatus outlet view (B).

Fig. 4.—Shoulder arthrogram shows partial tear (arrow) of rotator cuff. Contrast medium has intravasated into substance of supraspinatus tendon. Subacromial spur is not shown.

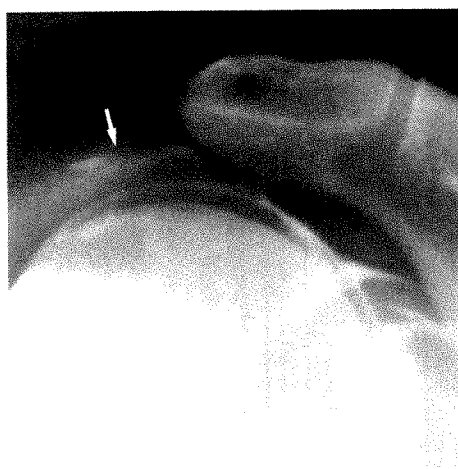


Fig. 5.—T2-weighted MR image (2000/80) shows complete tear (arrows) of rotator cuff. Subacromial spur is not shown.



4

5

mial bursal thickening due to impingement or those incomplete tears that involve the upper surface of the tendon can be diagnosed with this technique. However, in a clinical series of 17 patients undergoing surgery for treatment of impingement, a subacromial bursogram showed abnormalities only in three [9]. Some bursograms have been made with the arm in abduction to show impingement on the bursa by the acromion [5, 9].

Conventional shoulder arthrography is an excellent means of finding complete tears of the rotator cuff. However, impingement cannot be diagnosed and partial tears will not be visible unless they involve the undersurface of the supraspinatus tendon (Fig. 4). Sagittal plane CT arthrography can depict the upper and lower surfaces of the supraspinatus tendon, and impingement on the cuff and partial tears may be seen [10]. The patient's size and inability to assume the necessary position may limit the usefulness of this study.

Recently, authors have described the abnormal tissue characteristics of areas of impingement syndrome or rotator cuff tear by means of MR imaging [11] (Fig. 5). However, it is difficult to distinguish edema from partial or complete tears on the basis of MR images, and the high cost may prohibit use of MR as a screening tool.

Discussion

The presence of a spur or abnormally long anterior process of the acromion may lead to surgical intervention. Beginning with Codman [12] in the 1930s, interest in the surgical treatment of problems involving the rotator cuff has been increasing progressively. Codman thought that tears of the cuff were due to an intrinsic degenerative process. Later authors, including McLaughlin [13] in 1944, have stressed the importance of impingement on the rotator cuff by adjacent structures including an abnormally shaped acromion [14]. Vascular impairment with aging is frequently a contributing factor in degeneration of the cuff [15].

A careful review of patient history and physical examination are key to diagnosis of impingement syndrome. The anteroposterior radiograph at a 30° caudal angle is helpful in confirming the clinical impression and in selecting patients for

surgery. If rest and avoidance of offending maneuvers do not relieve symptoms after 3–5 months, surgery is performed to remove the anterior part of the acromion, the coracoacromial ligament, and/or the subacromial bursa.

In conclusion, in selecting patients for appropriate treatment, the detection of an acromial spur is helpful. Of the available techniques for imaging this spur, the 30° caudally angled anteroposterior radiograph of the shoulder in the erect position is the simplest, cheapest, and most reproducible method. In a busy clinical practice, it offers a distinct advantage over other methods.

REFERENCES

1. Neer CS. Anterior acromioplasty for the chronic impingement syndrome in the shoulder. *J Bone Joint Surg [Am]* 1972;54A:41–50
2. Neer CS. Impingement lesions. *Clin Orthop* 1983;173:70–77
3. Hardy DC, Vogler JB III, White RH. The shoulder impingement syndrome: prevalence of radiographic findings and correlation with response to therapy. *AJR* 1986;147:557–561
4. Newhouse KE, El-Khoury GY, Nepola JV, Montgomery WJ. The shoulder impingement view: a fluoroscopic technique for the detection of subacromial spurs. *AJR* 1988;151:539–541
5. Cone RO III, Resnick D, Danzig L. Shoulder impingement syndrome: radiographic evaluation. *Radiology* 1984;150:29–33
6. Butters KP, Rockwood CA Jr. Office evaluation and management of the shoulder impingement syndrome. *Orthop Clin North Am* 1988;19:755–765
7. Neer CS, Poppen NK. Supraspinatus outlet. *Orthop Trans* 1987;11:234
8. Mack LA, Matsen FA, Kilcoyne RF, Davies PK, Sickler ME. US evaluation of the rotator cuff. *Radiology* 1985;157:205–209
9. Unthoff HK, Hammond DI, Sarkar K, Hooper GJ, Papoff WJ. The role of the coracoacromial ligament in the impingement syndrome. *Int Orthop* 1988;12:97–104
10. Beltran J, Gray LA, Bools JC, Zuelzer W, Weis LD, Unverferth LJ. Rotator cuff lesions of the shoulder: evaluation by direct sagittal CT arthrography. *Radiology* 1986;160:161–165
11. Seeger LL, Gold RH, Bassett LW, Ellman H. Shoulder impingement syndrome: MR findings in 53 shoulders. *AJR* 1988;150:343–347
12. Codman EA. *The shoulder. Rupture of the supraspinatus tendon and other lesions in or about the subacromial bursa*. Brooklyn, NY: G. Miller, 1934:74
13. McLaughlin HL. Lesions of the musculotendinous cuff of the shoulder. I. The exposure and treatment of tears with retraction. *J Bone Joint Surg [Am]* 1944;26A:31–51
14. Morrison DS, Bigliani LU. The clinical significance of variations in acromial morphology. *Orthop Trans* 1987;11:234
15. Rathbun JB, Macnab I. The microvascular pattern of the rotator cuff. *J Bone Joint Surg [Br]* 1970;52B:540–553

John L. Gwinn, 1989 Gold Medalist of The Society for Pediatric Radiology

Fred A. Lee¹



The Society for Pediatric Radiology (SPR) was founded in 1958 by a small group of radiologists with special interest in pediatrics who met to discuss problems and interesting cases around a few viewboxes. It has grown into a 700-member, well-respected organization of a recognized subspecialty of radiology. A major contributor to the rapid, smooth development

of our Society is John L. Gwinn, its second secretary-treasurer, who served in that office for 12 years. His dedication to service and his leadership have been a guiding force for all SPR members.

John was born and raised on a small farm in Gallipolis, OH, and attended Dennison University on a basketball scholarship. He received his M.D. in 1946 from the University of Louisville Medical School under U.S. Navy sponsorship. After a rotating internship at Indianapolis General Hospital, he entered general practice in a small town in southern Indiana. He loves to relate the story of the time he kept a newly delivered, premature baby warm by placing the baby in a shoebox in the oven. From this type of experience came his interest in pediatrics. He began a pediatric residency at the Mayo Clinic, but it was interrupted after 1 year by the outbreak of the Korean War and the Navy's callback to active duty. He served at a Naval hospital in Japan and on ship duty with the Military Sea Transport Service. He was discharged after 2 years. As with many of his involvements, he remained committed to the Navy, serving for 30 years in the Reserve, and retiring with the rank of captain.

After completing his pediatric residency at the Mayo Clinic in 1954, he returned briefly to California to enter the private practice of pediatrics. By this time, however, he had been exposed to the wonders of radiology, and after 1 year he returned to the Midwest for a radiology residency at Indiana with Jack Campbell. Considering John's background in pediatrics, it was only natural that his interest rapidly focused on pediatric radiology.

After radiology training, he accepted a position at the

Childrens Hospital of Los Angeles with Pete Peterson, whose untimely death in 1961 brought John to the post of radiologist-in-chief, a position that he has held with distinction for 28 years. He is professor of both radiology and pediatrics at the University of Southern California Medical School and professor of radiology at the Charles R. Drew Post-Graduate Medical School.

Under his leadership, the Department of Radiology at Childrens Hospital of Los Angeles has grown from a two-man department into a well-respected complete imaging center. John is an excellent teacher, attracting radiology residents for rotation in pediatric radiology in his department from all over Southern California, Nevada, and Arizona. He has written more than 100 papers. He has been bestowed honorary membership in many organizations, in the United States and abroad.

Full-time academicians often are accused of being disinterested or even disdainful of the problems of private practice and medical politics. John has always been farsighted enough to realize that all of medicine must be united to provide the best care to patients. His willingness to participate in local, regional, and national groups has resulted in his election to numerous high offices, including presidency of the Los Angeles Radiological Society, the California Radiological Society, and The Society for Pediatric Radiology. He was founder and first president of the Pacific Coast Pediatric Radiologists' Association. He also has served as vice-president of the American College of Radiology, first vice-president of the American Roentgen Ray Society, and second vice-president of the Radiological Society of North America.

By nature and nurture, John embodies the virtues of Middle America. His sense of commitment extends to his personal life. He met his lovely wife, Patricia, while he was still in medical school, and their 45-year union is blessed with four fine children and two beautiful grandchildren.

John's leadership stems from his talent to see the big picture, and his willingness to quietly discuss problems and make small compromises so as to achieve the larger, long-term goal. The Society for Pediatric Radiology has benefited greatly from his gentle, time-proved guidance and continued wise counsel. It is only fitting that the SPR bestow on John Gwinn its highest honor, the Gold Medal of The Society for Pediatric Radiology, on the eve of his retirement as chairman of his department.

Presented at the annual meeting of The Society for Pediatric Radiology, San Antonio, TX, April 1989.

¹ Department of Radiology, Huntington Memorial Hospital, Pasadena, CA 91105. Address reprint requests to F. A. Lee.

Findings on Chest Radiographs After Prophylactic Pulmonary Surfactant Treatment of Premature Infants

Ewell A. Clarke¹
Robert L. Siegle¹
Alice K. Gong²

Clinical trials are underway that use pulmonary surfactant replacement therapy in an attempt to prevent respiratory distress syndrome (RDS) in premature infants. This study was undertaken to determine the relationship between the clinical course of infants receiving prophylactic "first-breath" endotracheal surfactant and their initial posttreatment radiographs. The study population consisted of 80 premature infants of 24–32 weeks gestational age. All received 3 ml of calf-lung surfactant extract via endotracheal tube at birth. Anteroposterior chest radiographs taken within 1 hr of treatment were reviewed and correlated with gestational age, birth weight, days of endotracheal intubation, mean airway pressure, and days of oxygen requirement greater than 30%. Three distinct patterns of radiographic abnormality were encountered: typical RDS with hypoinflation, diffuse granularity, and air bronchograms (30%); central clearing of RDS (14%); and disproportionate clearing of RDS in the right lung (8%). No significant differences in ventilator requirements or clinical course were seen among these three groups. A fourth group (49%), whose posttreatment radiographs showed no evidence of RDS, required significantly less ventilatory support.

Prophylactic first-breath surfactant treatment of premature infants occasionally results in radiographic patterns that are atypical for RDS. Familiarity with these patterns and their clinical significance will be important if surfactant augmentation becomes prevalent.

AJR 153:799–802, October 1989

The efficacy of exogenous surfactant replacement in the treatment of premature infants with respiratory distress syndrome (RDS) has been shown in several controlled trials [1–6]. Concomitant improvement in the findings on chest radiographs in these infants has been evident [7–9]. If surfactant is approved, it is likely that its use will become commonplace for infants with RDS.

One of the techniques currently under investigation involves endotracheal administration of surfactant to premature infants at the start of respiration in an attempt to prevent RDS from developing. There are indications that this "first breath" method may be the most efficacious [2, 10–12], but it is also technically the most difficult because intubation and surfactant administration must be accomplished in rapid sequence in the delivery room. The purpose of this study was to evaluate the findings on initial posttreatment chest radiographs in these patients and to determine how these findings correlate with the ventilatory requirements and subsequent course.

Subjects and Methods

Eighty premature infants of 24–32 weeks (mean, 29 weeks) gestational age, born at Medical Center Hospital, San Antonio, between April and December 1987 were included in the study. Birth weight ranged from 680 g to 1960 g, with a mean of 1247 g. Infants were not entered in the study if the obstetrical sonogram or maternal menstrual history indicated a gestational age of greater than 32 weeks or if any evidence of dysmorphism was seen.

Received February 27, 1989; accepted after revision: May 23, 1989.

¹ Department of Radiology, The University of Texas Health Science Center at San Antonio, 7703 Floyd Curl Dr., San Antonio, TX 78284. Address reprint requests to E. A. Clarke.

² Department of Pediatrics, The University of Texas Health Science Center at San Antonio, 7703 Floyd Curl Dr., San Antonio, TX 78284.

0361-803X/89/1534-0799
© American Roentgen Ray Society

Prematurity was confirmed with standard parameters for postnatal estimation of gestational age. The protocol was approved by the institutional review board, and informed consent was obtained from the mothers.

The surfactant solution used (Infasurf, Ony Inc., Buffalo, NY) has been characterized in detail [1, 2, 10]. It is prepared by organic solvent extraction from calf lung and contains approximately 98% lipid and 2% protein. A single dose consisted of 90 mg of surfactant in 3 ml of normal saline.

Premature infants were intubated at birth. Surfactant solution (3 ml) was instilled into the trachea of all patients, before the first breath in 69% of cases. This was followed by four deep breaths by hand ventilation. The time from delivery to ventilation was less than 1 min. Further resuscitation measures did not differ from those usually used for premature infants, including placement of an orogastric tube for aspiration of gastric contents. Patients then were taken to the neonatal intensive care unit, where standard protocols for ventilatory assistance and other treatment were followed. Anteroposterior chest radiographs were obtained within 1 hr of surfactant administration and as clinically indicated thereafter.

Radiographs were evaluated simultaneously by two reviewers who did not know the clinical condition of the patient. The patients were then grouped according to the predominant pattern on their initial posttreatment radiograph (Table 1), and the groups were compared retrospectively with the following clinical parameters: gestational age, birth weight, method of delivery, days of intubation, mean airway pressure, and days of oxygen requirement greater than 30%.

Statistical analysis was done by using chi-square tests for incidence data and the unpaired Student's *t* test for continuous variables.

Results

Three distinct patterns of radiographic abnormality were encountered on the initial postsurfactant radiographs. Chest radiographs of 24 patients (30%) showed the bilaterally uniform appearance of RDS with hypoinflation, air bronchograms, and diffuse granularity. A second group of six patients (8%) had chest radiographs showing RDS in the left lung and normal aeration in the right lung (Fig. 1); one of these infants had good aeration of only the right middle and lower lobes (Fig. 2). Chest radiographs of a third group of 11 infants (14%) showed selective central clearing of RDS (Fig. 3). Although

the peripheral density resembled that of pleural effusion, lateral decubitus films and sonograms failed to show pleural fluid in these neonates.

The patterns of asymmetric aeration and central clearing tended to resolve in 1–3 days, after which aeration was uniform, although RDS persisted. These two patterns also were more prevalent early in the study.

A fourth group of 39 patients (49%) had no evidence of RDS on their initial posttreatment chest radiographs. These were either normal or showed an interstitial pattern that cleared rapidly, consistent with retained fetal lung fluid. This group of patients, when compared with the first three groups individually or together, was of significantly greater gestational age and weight, and required significantly less ventilatory support ($p < .05$).

No significant differences in gestational age, weight, and clinical course were found among the groups of infants with RDS, asymmetric aeration, or central clearing.

The results are summarized in Table 1. Some patients breathed before surfactant instillation, and some had surfactant recovered from the stomach, suggesting esophageal instillation. These infants did not display any consistent pattern on chest radiographs and were randomly distributed among the four groups.

Discussion

Surfactant replacement therapy for treatment of RDS in premature infants was first proposed in 1959 by Avery and Mead [13]. Since then, the efficacy of this therapy has been established in numerous controlled, randomized clinical trials that used various surfactant preparations and timing of administration [1–6, 10, 14]. In this series of 80 infants treated with exogenous surfactant at birth, four distinct patterns were noted on posttreatment chest radiographs. Our study attempted to answer questions regarding the clinical significance of these patterns. Efficacy and safety of surfactant treatment were not addressed.

TABLE 1: Characteristics of 80 Surfactant-Treated Infants

	Radiographic Classification			
	Asymmetric Aeration	Central Clearing	Respiratory Distress Syndrome	Normal/Wet Lung
Number of patients ($n = 80$)	6 (8%)	11 (14%)	24 (30%)	39 (49%)
Mean gestation (wk)	28.2	28.3	27.5	30.1 ^a
Mean birth weight (g)	1062	1199	1047	1373 ^a
Range	(780–1680)	(730–1850)	(620–1860)	(780–1960)
Breathing before treatment	3 (50%)	3 (27%)	7 (29%)	12 (31%)
Esophageal instillation	0	0	3 (13%)	2 (5%)
Cesarean delivery	2 (33%)	7 (64%)	9 (38%)	18 (46%)
Mean days $O_2 > 30\%$	21.5	13	21.5	2.6 ^a
Mean days intubated	40	22.5	18.2	2.8 ^a
Mean airway pressure first 24 hr (cm H_2O)	9	5.5	4.5	1.6 ^a

^a Significance $p < .05$ when compared with each of the other three groups and with the other three groups taken together.

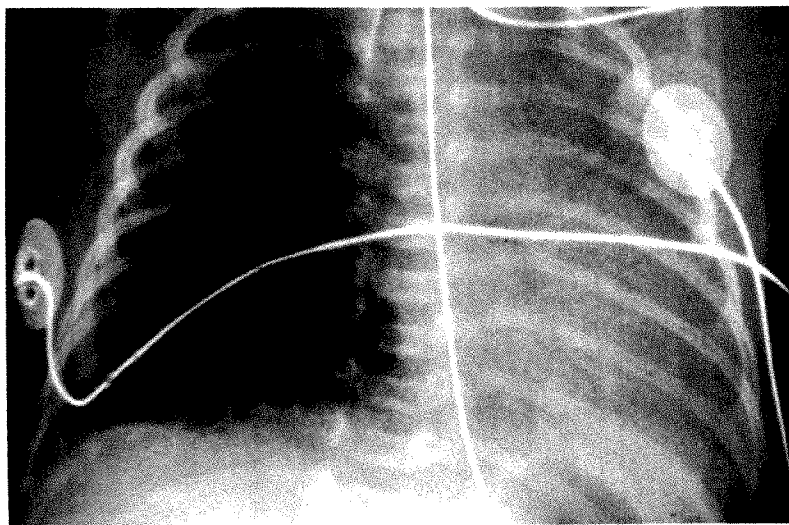


Fig. 1.—Chest radiograph shows selective clearing of respiratory distress syndrome in right lung 6 hr after surfactant administration.

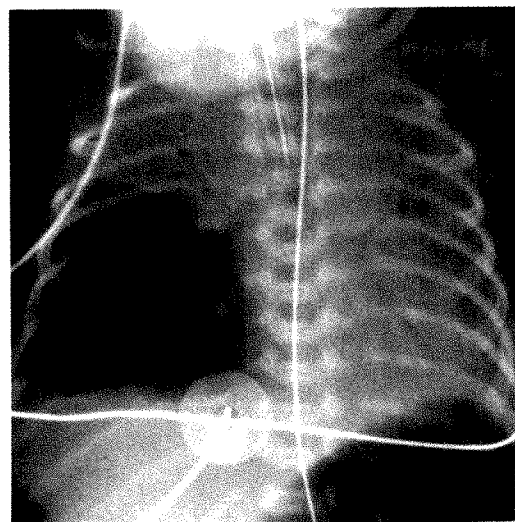
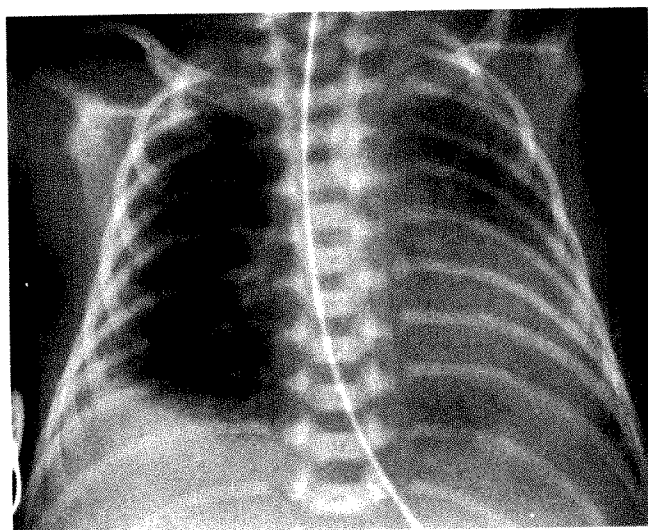
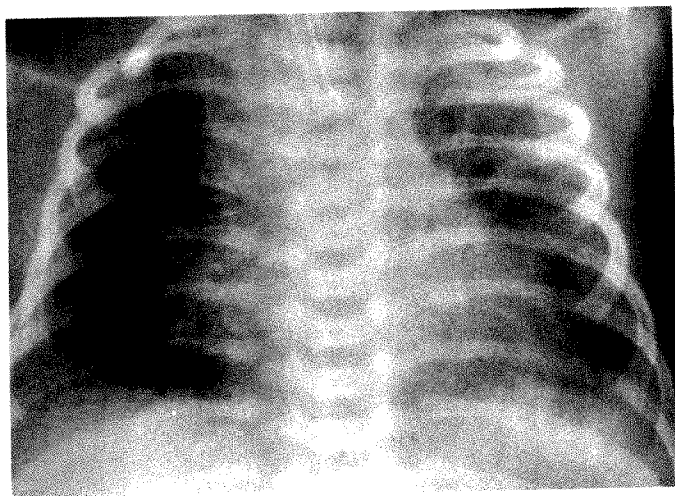


Fig. 2.—Chest radiograph shows selective clearing of severe respiratory distress syndrome in right middle and lower lobes 4 hr after surfactant treatment.

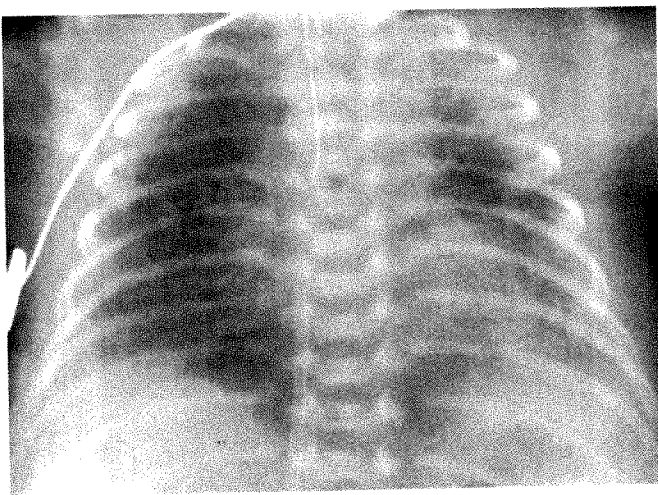
Fig. 3.—A-C, Chest radiographs in three infants show central clearing and residual peripheral atelectasis at 4 hr (A), 5 hr (B), and 8 hr (C) after surfactant administration.



A



B



C

Reports of the radiographic findings after surfactant therapy have focused primarily on differences in the severity of RDS between treated and control groups. However, Edwards et al. [7] noticed asymmetric aeration, greater in the right lung, in three of 18 treated patients. The relevance of this finding to the clinical condition of the patients was not noted, although intubation of the right mainstem bronchus was documented in one case. In our series of 80 treated infants, aeration was better in the right lung in six infants. Because RDS typically affects both lungs equally, right-sided clearing of RDS in these cases suggests that a greater amount of surfactant was delivered to the right lung, possibly because the right mainstem bronchus was intubated. Such a complication is an obvious risk of first-breath administration, because intubation and surfactant instillation must be accomplished in rapid sequence.

The appearance of bilateral, central pulmonary clearing of RDS in 11 patients has not been described before and resembles no other disorder of prematurity. Although we initially thought that the peripheral density might represent pleural effusion, lateral decubitus films and sonograms in six patients showed no fluid. Central clearing probably results from administration of an insufficient amount of surfactant to the airway, or ineffective hand ventilation after surfactant administration, resulting in inadequate distribution of the material to the lung periphery.

Both central clearing and asymmetric aeration were more common early in the study, suggesting that experience is a factor in proper administration of surfactant to the infant. Both patterns improved in 1–3 days to more uniform aeration, although usually with some degree of residual RDS. This correlates with the lack of any significant differences in duration or degree of ventilatory support required by those with asymmetry, central clearing, or typical RDS.

The percentage of patients in our study with no radiographic evidence of RDS after surfactant therapy (49%) is similar to that reported by others [2, 8, 10]. Although some of these infants were quite small and had apnea or other problems necessitating intubation and respirator support, on average these 39 infants were of significantly greater gestational age and birth weight than those with pulmonary disease, and their ventilatory requirements were considerably less (Table 1). Certainly some of these patients would not have developed RDS without surfactant treatment. Results of the controlled trials cited earlier, however, suggest that the absence of significant radiographic abnormality or clinical disease in at least some of these infants is due to the beneficial effects of surfactant therapy. Because treatment occurs before RDS can be diagnosed, all babies receive treatment that only some need. This represents a potential shortcoming of the first-breath method of surfactant delivery.

In summary, first-breath endotracheal instillation of surfactant yielded four distinct patterns on initial posttreatment radiographs. Although most infants showed normal/wet lungs or some degree of RDS, approximately 20% showed asymmetric aeration or central clearing. The last two patterns are felt to be related to technical factors of surfactant delivery; however, the ventilator requirements and clinical course of these infants were not significantly different from those of the infants with RDS. If surfactant augmentation becomes commonplace, familiarity with these patterns and their implications will be important to the radiologist.

REFERENCES

1. Shapiro DL, Notter RH, Morin FC III, et al. Double-blind, randomized trial of a calf lung surfactant extract administered at birth to very premature infants for prevention of respiratory distress syndrome. *Pediatrics* **1985**;76:593–599
2. Enhorning GE, Shennan A, Possmayer F, Dunn M, Chen CP, Milligan J. Prevention of neonatal respiratory distress syndrome by tracheal instillation of surfactant: a randomized clinical trial. *Pediatrics* **1985**;76:145–153
3. Merritt TA, Hallman M, Bloom BT, Berry C. Prophylactic treatment of very premature infants with human surfactant. *N Engl J Med* **1986**;315:785–790
4. Gitlin JD, Soll RF, Parad RB, et al. Randomized controlled trial of exogenous surfactant for the treatment of hyaline membrane disease. *Pediatrics* **1987**;79:31–37
5. Raju TNK, Vidyasagar D, Bhat R, et al. Double-blind controlled trial of single-dose treatment with bovine surfactant in severe hyaline membrane disease. *Lancet* **1987**;1:651–655
6. McCord FB, Curstedt T, Halliday HL, et al. Surfactant treatment and incidence of intraventricular hemorrhage in severe respiratory distress syndrome. *Arch Dis Child* **1988**;63:10–16
7. Edwards DK, Hilton SVW, Merritt TA, Hallman M, Mannino F, Boynton BR. Respiratory distress syndrome treated with human surfactant: radiographic findings. *Radiology* **1985**;157:329–334
8. Wood BP, Sinkin RA, Kendig JW, Notter RH, Shapiro DL. Exogenous lung surfactant: effect on radiographic appearance in premature infants. *Radiology* **1987**;165:11–13
9. Mortenson W, Noack G, Curstedt T, et al. Radiologic observations in severe neonatal respiratory distress syndrome treated with the isolated phospholipid fraction of natural surfactant. *Acta Radiol* **1987**;28:389–394
10. Kwong MS, Egan EA, Notter RH, Shapiro DL. Double-blind clinical trial of calf lung surfactant extract for the prevention of hyaline membrane disease in extremely premature infants. *Pediatrics* **1985**;76:585–592
11. Jobe A, Ikegami M, Jacobs H, et al. Surfactant and pulmonary blood flow distribution following treatment of premature lambs with natural surfactant. *J Clin Invest* **1984**;73:848–856
12. Maeta H, Vidyasagar D, Raju TNK, et al. Early and late surfactant treatments in baboon model of hyaline membrane disease. *Pediatrics* **1988**;81:277–283
13. Avery ME, Mead J. Surface properties in relation to atelectasis and hyaline membrane disease. *Am J Dis Child* **1959**;97:517–523
14. Horbar JD, Soll RF, Sutherland JM, et al. A multicenter randomized, placebo-controlled trial of surfactant therapy for respiratory distress syndrome. *N Engl J Med* **1989**;320:959–965

CT Evaluation of Blunt Abdominal Trauma in Children: Comparison of Ultrafast and Conventional CT

Alan S. Brody¹
F. Glen Seidel²
Jerald P. Kuhn¹

Previous reports describing the use of ultrafast CT have emphasized its value in evaluating the heart, chest, and airway. We describe our experience using this technology on children with blunt abdominal trauma. We retrospectively reviewed 54 consecutive ultrafast CT studies and 30 consecutive conventional dynamic CT studies performed on children after blunt abdominal trauma. Thirty percent of the scans showed abnormalities. CT or pathologic follow-up was available for all abnormal cases. We compared scans made with these two techniques for diagnostic accuracy, amount of visible motion on each slice, and contrast enhancement seen on each study. A protocol of 0.4-sec images and 2 ml/kg IV contrast material administered before scanning was used for the ultrafast CT scans. A standard protocol of 2-sec scanning and 3 ml/kg IV contrast material was used for conventional CT studies. There was no difference in diagnostic accuracy between the two techniques. There was significantly less visible motion ($p < .0001$) and significantly better contrast enhancement ($p < .0001$) seen on the ultrafast CT studies. Two of 54 ultrafast scans had images with sufficient motion to require repeated scanning, compared with 13 of 30 conventional CT studies. In addition, ultrafast scans required less sedation, decreased radiation dose, and improved accessibility of the patient to support personnel.

Ultrafast CT is a valuable technique for abdominal imaging, offering equal diagnostic accuracy with improved image quality and important benefits to the patient.

AJR 153: 803-806, October 1989

The Imatron C-100 ultrafast CT scanner (Imatron, South San Francisco, CA) uses a scanning electron beam instead of an X-ray tube and provides scanning times as much as 40 times shorter than conventional CT scanners [1]. Most reports of this new technique have emphasized its value in the examination of rapidly moving structures that cannot be studied well with other CT scanners [2, 3]. These studies have emphasized the value of 50-msec scanning times, despite lower resolution. However, ultrafast CT can be performed in a high-resolution mode. This mode uses a 512×512 instead of a 256×256 matrix, uses additional collimation, and averages multiple sequential scans at the same level to provide greater photon density. In this manner, the ultrafast CT scanner can perform conventional examinations with resolution comparable to that of conventional scanners [4], but at a rate of 5-20 times faster than conventional scanners.

We have used the Imatron C-100 ultrafast CT scanner for general CT scanning since May 1987. The current study was performed to compare ultrafast CT (UFCT) with conventional dynamic CT (DCT) in the evaluation of acute abdominal trauma in children. CT scanning of the pediatric trauma patient is frequently challenging. There is limited time to prepare the patient, and patients are often uncooperative. Sedation, used extensively in pediatric patients, may be contraindicated. For these reasons, pediatric trauma CT provides an opportunity to evaluate CT scan quality under difficult clinical conditions.

It was our clinical impression that UFCT images were routinely superior to DCT. To assess this impression objectively, we undertook this retrospective review to

Received February 16, 1989; accepted after revision May 22, 1989.

¹ Department of Radiology, Children's Hospital, 219 Bryant St., Buffalo, NY 14222. Address reprint requests to A. S. Brody.

² Department of Radiology, LeBonheur Children's Medical Center, 848 Adams Ave., Memphis, TN 38103.

0361-803X/89/1534-0803
© American Roentgen Ray Society

compare UFCT and DCT, including specific comparison of diagnostic accuracy, visible motion of the patient, and contrast enhancement.

Materials and Methods

All patients included in the study were children in whom CT scans were obtained for the evaluation of acute abdominal trauma. The first 54 examinations performed with the Imatron C-100 (5/22/87 to 1/22/88) and the last 30 studies performed with the Technicare 2020HP (Technicare, Solon, OH) (7/5/86 to 5/19/87) were reviewed. No patients were excluded. The film record of each study was reviewed. While the studies were being done, no changes were made in indications for CT scanning, sedation, or restraint of the patient, and no changes were made in filming practices.

Studies on the ultrafast CT scanner were performed with scanning times of 0.2–0.8 sec/scan with most scans obtained at 0.4 sec. Meglumine contrast material (2 ml/kg 60%) was injected by rapid IV bolus immediately before scanning. Six-millimeter slices at 8-mm intervals were obtained from the bottom of the kidneys to the diaphragm.

Studies on the conventional CT scanner were performed with dynamic 2-sec scans and 3 ml/kg 60% meglumine contrast material. Half the contrast material was administered by rapid bolus immediately before scanning, and the remainder was injected during scanning. Contiguous 1-cm slices were obtained from the bottom of the kidneys to the diaphragm. This standard protocol has been reported [5, 6].

Each study was reviewed by a pediatric radiologist, who made a diagnosis without knowledge of clinical information or follow-up. All images, including repeated slices, were included. This interpretation was then compared with the results of follow-up CT or autopsy.

Contrast enhancement in each study was rated on a three-point scale, identifying the bolus and nonequilibrium phases of contrast enhancement [7]: (1) excellent: good hepatic and aortic contrast on highest slice in the liver, and arteriovenous contrast difference seen on lowest slice in aorta and inferior vena cava; (2) fair: highest or lowest slice (but not both) same as excellent rating; (3) poor: poor

arterial contrast overall. Repeated slices were not included in this analysis.

All slices then were graded for the amount of visible motion. There were 844 images obtained with UFCT and 396 obtained with DCT. A 1-to-4 scale was used: 1 = no motion, all visceral margins were sharply defined; 2 = slight motion with slight blurring of margins, but no loss of diagnostic information; 3 = moderate motion, with interfaces between structures of similar attenuation difficult to determine, causing a loss of subtle diagnostic information; 4 = severe motion, with loss of definition of all structures, causing loss of major diagnostic information. A motion score was determined by adding the above score for each slice in the study and dividing by the number of slices to provide an indicator of average visible motion in each study.

The contrast bolus and motion scores in the two groups were compared by using an unpaired two-tailed t test.

Fifty-four patients were studied with UFCT, 30 boys and 24 girls. Ages ranged from 15 months to 17 years (mean, 9.4 years). Thirty patients were studied with DCT, 21 boys and nine girls. Ages ranged from 4 months to 18 years (mean, 8.1 years). Overall, 25 of 84 cases showed abnormalities. Fifteen (28%) of the 54 UFCT studies showed abnormalities. Eight patients had splenic trauma (Fig. 1A), four had hepatic trauma (Fig. 1B), two had renal trauma (Fig. 1C), and one had abdominal wall trauma. Ten (33%) of the 30 DCT studies showed abnormalities. Four patients had renal trauma (Fig. 2A), three had splenic trauma (Fig. 2B), three had hepatic trauma (Fig. 2C), and one had pancreatic trauma. CT follow-up was available in 24 patients; pathologic follow-up was available in one patient who died.

Results

There was one diagnostic error in the DCT group; a patient whose CT scan was felt to show hepatic trauma (Fig. 3). The patient died from head trauma and had no hepatic abnormality.

The degree of contrast enhancement in UFCT and DCT is compared in Figure 4. Forty-three of 54 UFCT studies had excellent, nine had fair, and two had poor contrast enhancement. Eleven of 30 DCT studies had excellent contrast en-

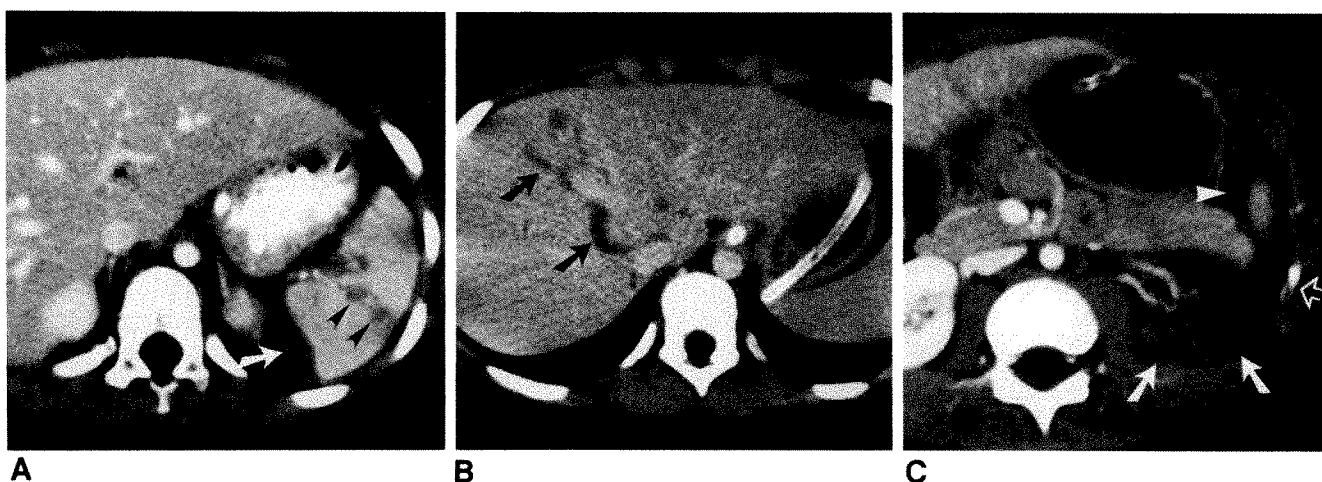


Fig. 1.—Parenchymal trauma shown on ultrafast CT scans. Imatron C-100, 0.4-sec imaging time with 2 ml/kg IV contrast material.
 A, Splenic fracture (arrowheads) with perisplenic hematoma (arrow) sustained by 6-year-old boy in a motor-vehicle accident.
 B, Deep, linear liver laceration (arrows) sustained by 10-year-old girl in a fall.
 C, Partial devascularization of left kidney (arrows) sustained by 8-year-old boy in a motor-vehicle accident. Note lack of enhancement of left kidney with retrograde venous filling compared with normal right kidney. A perisplenic hematoma (arrowhead) and a rib fracture with abdominal wall hematoma (open arrow) also are seen.

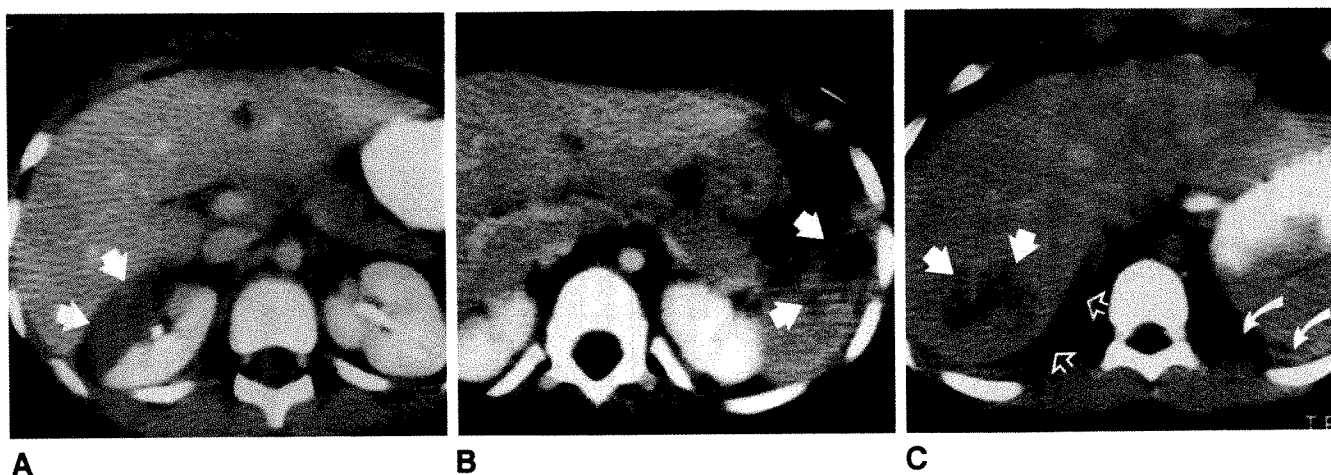


Fig. 2.—Parenchymal trauma shown on conventional CT scans. Technicare 2020HP, 2-sec scanning with 3 ml/kg bolus contrast material. All injuries were sustained in motor-vehicle accidents.

A, Partial devascularization of right kidney in 6-year-old boy. Lateral portion of right kidney does not enhance (arrows).

B, Splenic fracture (arrows) in 3-year-old girl.

C, Stellate laceration of right lobe of liver (straight solid arrows) in 5-year-old girl. Hemoperitoneum (open arrows) and a pulmonary contusion in left lower lobe (curved arrows) also are seen.



Fig. 3.—False-positive conventional CT scan. Low attenuation areas in posterior segment of right lobe (straight arrows) and caudate lobe (curved arrow) of liver were thought to indicate hepatic trauma. Liver was normal at autopsy. Note severe motion artifact and poor contrast enhancement.

hancement. Thirteen studies had fair and six had poor contrast enhancement. Contrast enhancement was significantly better in the UFCT group (unpaired t value = -4.3 , $p < .0001$).

Comparison of the degree of visible motion is shown in Figure 5. Of 844 images obtained with UFCT, 609 showed no motion, 218 slight motion, 15 moderate motion, and two severe motion. Of 54 studies, two included one or more slices with severe motion. Of 396 images obtained with DCT, 53 showed no motion, 255 slight motion, 86 moderate motion, and 32 severe motion. Fourteen of 30 studies included one or more slices with severe motion. Visible motion was significantly less in the UFCT group (unpaired t value = -10.239 , $p < .0001$).

Sedation was used in three patients in the DCT group and in none of the UFCT patients.

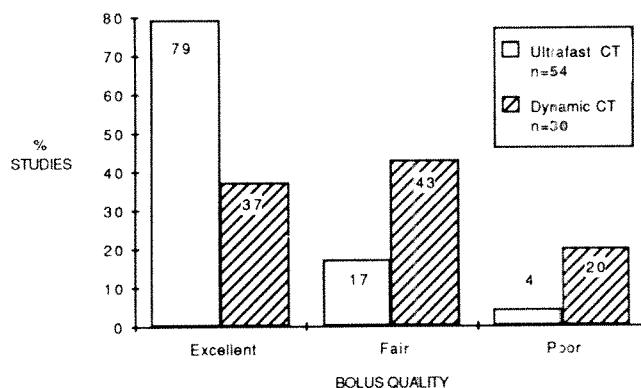


Fig. 4.—Comparison of bolus contrast enhancement in ultrafast and conventional CT. Contrast opacification shown by each study was scored as follows: excellent = good hepatic and aortic contrast on highest slice in liver, and arteriovenous contrast difference seen on lowest slice in aorta and inferior vena cava; fair = highest or lowest section (but not both) same as excellent rating; poor = poor arterial contrast overall. Repeated slices were not included in this analysis.

Discussion

The improved quality of UFCT as compared with DCT is due to shorter scanning time. This reduces movement of the patient, which reduces motion unsharpness and decreases overall examination time, allowing greater contrast enhancement throughout the study. Our findings show that UFCT provides improved image quality.

Because there was only one diagnostic error in the study, we cannot show an increase in diagnostic accuracy. This is not unexpected, because DCT is already a highly accurate means of detecting abdominal injuries [7-9]. However, improvement in image quality with UFCT is still an important advantage. The one diagnostic error occurred in a patient in whom the scans were markedly degraded by motion (Fig. 3).

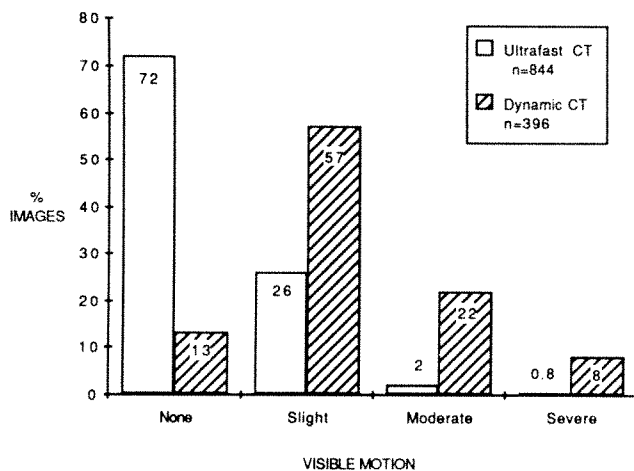


Fig. 5.—Comparison of visible motion of patient in ultrafast and conventional CT. Visible motion on each slice was scored as follows: none = all visceral margins were sharply defined; slight = blurring of margins, but no loss of diagnostic information; moderate = interfaces between structures of similar attenuation difficult to determine, causing a loss of subtle diagnostic information; severe = loss of definition of all structures, causing loss of major diagnostic information.

Repeated scans also were impaired by motion, and there was little contrast enhancement on the repeated images. The study could not be completed satisfactorily because the patient required immediate neurosurgery. Because motion of the patient can be an important factor in showing abdominal trauma, studies involving a large number of patients may well show an improvement in diagnostic accuracy with UFCT.

In addition to improvements in image quality, UFCT has other advantages. The short examination time is valuable when the very ill patient requires a CT scan. The actual scanning time is usually less than 30 sec. Support personnel must leave the patient for only this brief period. Injection of contrast material, scanning, and first and last slice reconstruction can be completed in less than 2 min.

Severe motion, requiring repeated scans, was found in two of 54 UFCT studies and in 13 of 30 DCT studies. If all such slices were repeated, additional imaging would be required in 4% of UFCT studies and in 43% of DCT studies. The need

to repeat slices would increase the time the patient must spend in the radiology department.

Although we were able to use less contrast material for the UFCT studies, a lower dose can be used for DCT examinations. Thus, a lower dose is not an advantage of the UFCT examination. Our study shows that there is less need to sedate patients when UFCT is used than when DCT is used. Image quality was better with UFCT, despite the fact that no sedation was used with UFCT and 10% of the DCT patients were sedated.

The 0.4-sec scan protocol used for the UFCT scans requires a dose of 1.0 rad (0.01 Gy) (32-cm phantom, center dose). This is lower than the 1.3 rad (0.013 Gy) dose measured by the same technique on a GE 9800 CT scanner (General Electric, Milwaukee, WI) with a protocol of 1-cm contiguous slices (R. G. Gould, personal communication). Reported comparisons of different CT scanners also indicate that UFCT uses a smaller X-ray dose than do DCT scanners [4].

REFERENCES

1. Peschmann KR, Napel S, Couch JL, et al. High-speed computed tomography: systems and performance. *Appl Optics* 1985;24:4052-4060
2. Steiner RM, Flicker S, Eldredge WJ, et al. The functional and anatomic evaluation of the cardiovascular system with rapid-acquisition computed tomography (cine CT). *Radiol Clin North Am* 1986;24:503-520
3. Brasch RC, Gould RG, Gooding CA, Ringertz HG, Lipton MJ. Upper airway obstruction in infants and children: evaluation with ultrafast CT. *Radiology* 1987;165:459-466
4. Scanner, computed axial tomography, full body. In: *Diagnostic imaging and radiology. Product comparison system*. Plymouth Meeting, PA: ECRI/McGraw Hill, 1988:13-22
5. Berger PE, Kuhn JP, Brusehaber J. Techniques for computed tomography in infants and children. *Radiol Clin North Am* 1981;19:399-408
6. Kaufman RD, Towbin R, Babcock DS, et al. Upper abdominal trauma in children: imaging evaluation. *AJR* 1984;142:449-460
7. Burgener FA, Hamlin DJ. Contrast enhancement in abdominal CT: bolus vs. infusion. *AJR* 1981;137:351-358
8. Kaufman RA. CT of blunt abdominal trauma in children: a five-year experience. In: Siegel MJ, ed. *Pediatric body CT*. New York: Churchill Livingstone, 1988:313-347
9. Karp MP, Cooney DR, Berger PE, Kuhn JG, Jewett TC Jr. The role of computed tomography in the evaluation of blunt abdominal trauma in children. *J Pediatr Surg* 1981;16:316-323

Reliability of Voiding Cystourethrography to Detect Reflux

Sigrid Jequier¹
Jean-Claude Jequier²

To our knowledge, the reliability of the voiding cystourethrogram for showing vesicoureteral reflux has not been established. Therefore, we evaluated the procedure in 207 children, each of whom underwent voiding cystourethrography with two or more bladder fillings and voidings. The results showed a discrepancy of presence and/or grade of vesicoureteric reflux from one filling to the other in 22 (12%) of 177 patients with two cycles and in six (20%) of 30 patients with three cycles. No changes were observed with cyclic voiding in cases of grade IV reflux (large, tortuous ureters with pelvic dilatation and caliceal clubbing). The grading of reflux was upgraded from 0 to grade I (into ureter only), II (ureter and collecting system), III (distension of pelvis and calices) by a second voiding cycle in only 3% of patients and by a second and third cycle in 4%. Reflux was downgraded by the second or third filling in a similar percentage. Most changes occurred between minor grades of vesicoureteric reflux. With two fillings, the percentage of agreement of the test (including all grades of reflux) for patients with abnormal findings during the first voiding study was 64%; the percentage of agreement for patients with normal results on the first voiding cystourethrogram was 96%.

Voiding cystourethrography is a less reliable test for grading reflux than for documenting the absence of vesicoureteric reflux. Although voiding cystourethrography is a good test to rule out reflux, its diagnostic reliability can be enhanced by a second voiding cycle.

AJR 153:807-810, October 1989

Retrograde voiding cystourethrography (VCUG) with contrast medium came into widespread use around 1958, when fluoroscopes with image intensification and cine recording became generally available [1]. It became the method of choice for detection and grading of vesicoureteric reflux and the standard for comparison with newer methods of assessment of reflux such as isotope VCUG [2, 3] and sonography [4, 5]. Vesicoureteric reflux is an intermittent phenomenon, so differences in presence and degree of reflux on repeated VCUG have been noted [6]. Cyclic voiding has been recommended for improved demonstration of reflux from ureters which insert into the urethra [7]. However, to our knowledge, no study has been done to determine the percentage of agreement between an initial study and subsequent examinations in the diagnosis and grading of reflux.

The purpose of this study was to establish the reliability of VCUG by repeating the VCUG and comparing the results of a consecutive second and/or third cyclic filling and voiding to the first study, with the result of the initial VCUG serving as the standard for the presence and grading of reflux.

Materials and Methods

Between January 1986 and October 30th, 1987, 177 patients had two consecutive bladder fillings and voidings for VCUG, and 30 had three such fillings and voidings. There were 65 boys and 112 girls with two cycles and 17 boys and 13 girls with three cycles. One hundred

Received February 27, 1989; accepted after revision May 25, 1989.

Presented as a scientific exhibit at the meeting of the European Society of Pediatric Radiology in Montreux, Switzerland, April 1988.

¹ Department of Radiology, The Montreal Children's Hospital and McGill University, 2300 Tupper St., Montreal, Quebec H3H 1P3, Canada. Address reprint requests to S. Jequier.

² Institut de Recherche en Santé et Sécurité du Travail du Québec, 505 de Maisonneuve W., Montreal, Quebec H3A 3C2, Canada.

0361-803X/89/134-0807
© American Roentgen Ray Society

sixty-four children were referred because of urinary tract infection, 23 with prenatally or postnatally diagnosed urinary tract malformations (including posterior urethral valves, anal atresia with fistulas into the lower urinary tract, hydronephrosis on prenatal sonograms), 15 with voiding problems (enuresis, dysuria, neurogenic bladder), three with hematuria, and two with familial reflux. All had sonograms made before VCUG.

The age of the patients varied from 4 days to 15 years; the majority (112 patients) were less than 1 year old, 67 were less than 5 years old, and only 18 were school children or adolescents. Most of these 18 patients had voiding problems or came for follow-up of known vesicoureteric reflux and recurrent infections.

In our hospital, children have VCUG done after insertion of a 5- or 8-French infant-feeding tube into the bladder [6]. Renografin 15% warmed to body temperature is instilled by drip infusion. The patient voids around this catheter, which is left in the bladder until the spot films, obtained during fluoroscopy, have been checked. A second study sometimes is done for various medical or technical reasons. No recatheterization is necessary. However, fluoroscopy time is increased usually by 10 sec but sometimes by up to 30 sec. Therefore, repeated VCUG after a normal first study is done only for good clinical or technical reasons. Interpretation of the VCUG usually was done by a radiologist other than the sonographer. Results of the preceding sonography or other examinations, such as previous VCUG or IV pyelography or renal isotope studies, always were available to the radiologist who supervised the VCUG. All images obtained during VCUG and the patients' records were reviewed retrospectively by the authors.

Reasons for the cyclic bladder fillings and voidings with contrast material were intermittent visualization of the distal ureters during a preceding sonographic examination, marked discrepancy in size of the kidneys on sonograms, previously documented reflux and ongoing infections, complex congenital malformations, and occasionally radiographic equipment failure leading to inadequate documentation of reflux that was suspected fluoroscopically. All fluoroscopic examinations were recorded on a closed-circuit videotape. Discrepancy between the initial video image and failed radiographic documentation of a first VCUG and subsequent spot film radiographs on cyclic voiding were considered sufficient evidence of a discrepancy between two consecutive VCUGs.

Vesicoureteric reflux was graded according to the international grading system: grade I = into ureter only, grade II = into ureter and upper collecting system without distension of the renal pelvis, grade III = distension of the renal pelvis and the calices without permanent caliceal clubbing, and grade IV = large, tortuous ureter, pelvic and caliceal dilatation, and caliceal clubbing. (Grade V = all features of grade IV with intrarenal reflux; this did not occur in this group of patients.)

To assess bias in selection of patients, the group of children who underwent cyclic VCUG was compared with a group of 100 consecutive patients who underwent single-filling VCUG. The latter group consisted of 32 boys and 68 girls. Nineteen boys and 53 girls had urinary tract infection (sometimes remote), 19 had voiding problems, four had congenital anomalies, and five had various problems such as hematuria or suspected urethral trauma. In one patient, reflux was seen as an incidental finding during sonographic examination for pyloric stenosis (grade IV reflux was confirmed by VCUG). Twenty-two patients were less than 1 year old, 61 were between 1 and 5 years old, and 17 were between 5 and 15 years old. Only one bladder filling and voiding was done in these patients, because either the first voiding showed significant reflux, the patients were older and therefore less at risk to develop reflux nephropathy, or a preceding sonogram or IV urogram had been normal. All results were reviewed retrospectively by the authors.

Results

In the group of patients who underwent two-filling VCUGs, a discrepancy in the results between two cycles was found in 22 patients and 29 ureters. The second cycle changed the grading from 0 to I in five ureters, from 0 to II in five ureters, from 0 to III in one ureter, from grade I to II in one ureter, from grade I to 0 in nine, from II to 0 in six, from II to I in one, from III to II in another ureter. The results of the initial cycle as compared with the second cycle of all ureters are summarized in Table 1; identical results on both fillings are in boldface type.

Table 2 shows that most differences occurred in minor grades of reflux. No grade IV reflux was missed on either of two voidings. In Table 3, these differences are outlined as positive results, negative results, or difference in results, with the first-filling VCUG as the standard. Differences of results

TABLE 1: Presence and Grading of Vesicoureteric Reflux on Two Consecutive Voiding Cycles

Initial Interpretation	Second Interpretation					Total
	0	I	II	III	IV	
0	292	5	5	1	0	303
I	9	12	1	0	0	22
II	6	1	12	0	0	19
III	0	0	1	7	0	8
IV	0	0	0	0	1	1
Total readings	307	18	19	8	1	353

Note.—Boldface numbers = same grading on both fillings, 0 = no reflux, I = reflux into ureter only, II = reflux into ureter and nondilated pelvis, III = distension of pelvis and calices during reflux, IV = large, tortuous ureter and clubbing of calices. Interpretation = assessment of reflux into a ureter (one patient had a solitary kidney).

TABLE 2: Concordance or Difference in Grading of Vesicoureteric Reflux on Two Consecutive Voiding Cycles

Results of Two Fillings	Grade					Total
	0	I	II	III	IV	
Concordant	292	12	12	7	1	324
Different	11	10	7	1	0	29
Total	303	22	19	8	1	353

Note.—0 = no reflux, I = reflux into ureter only, II = reflux into ureter and nondilated pelvis, III = distension of pelvis and calices during reflux, IV = large, tortuous ureter and clubbing of calices. Total number of interpretations = 353 (one patient had a solitary kidney).

TABLE 3: Positive or Negative Results of the Second Filling Voiding Cystourethrogram Compared with the Initial Study

Initial Interpretation	Second Interpretation		Total
	Positive	Negative	
Positive	32 (agrees)	18 (disagrees)	50
Negative	11 (disagrees)	292 (agrees)	303
Total	43	310	353

Note.—Interpretation = assessment of reflux into a ureter.

of the second and/or third cyclic VCUG are considered false-positive if reflux occurred only on repeated VCUG, the initial one having been normal, and false-negative if initially documented reflux could not be reproduced by repeated VCUG. Concordant-positive reflux was seen and graded the same on each cyclic voiding. Concordant-negative reflux indicated absence of vesicoureteric reflux during all cyclic voidings. This permits calculation of the percentage of agreement for the presence of reflux and also the percentage of agreement for the absence of reflux on cyclic VCUG. In the presence of reflux initially, this percentage is 32 divided by 50, or 64%. In the absence of reflux initially, it is 292 divided by 303, or 96%. The overall percentage of agreement is (32 + 292) divided by 353, or 92%. Because of the unequal number of negative (303) and positive (50) initial cases, the Youden J index was computed [8, 9]. With this better estimate, the overall percentage of agreement drops to 60% from 92%. However, the agreement between initial and second assessment of reflux is fair to good according to the kappa statistics [10], which measure the index of agreement between two assessments and compute the probability of the statistical significance of this index. It equals 67% and, thus, is highly significant ($p < .001$). In other words, the concordance between cyclic voidings outweighs the nonconcordance of the results. The concordance between the first, second, and third assessments of reflux, based on the same calculations done for three cyclic voidings in 30 children (results depicted in Tables 4 and 5), shows an overall percentage of agreement of 91%. In absence of reflux initially, the percentage of agreement is 104/110, or 95%, and in the presence of reflux initially, it is 5/10, or 50%. According to kappa statistics, it equals 47% ($p < .05$).

In the group of 100 children who underwent single-filling VCUG, 77% of the studies were normal, grade I reflux was seen in 1%, grade II in 9%, grade III in 10%, and grade IV in 3%.

Discussion

Most VCUGs in early childhood are obtained in patients with urinary tract infection to detect vesicoureteric reflux. Once the acute infection has resolved and reflux has been

TABLE 5: Concordance or Difference in Grading of Vesicoureteric Reflux on Three Consecutive Voiding Cycles

Results of Three Fillings	Grade				
	0	I	II	III	IV
Concordant	104	1	2	0	2
Different	6	0	4	1	0

Note.—0 = no reflux, I = reflux into ureter only, II = reflux into ureter and nondilated pelvis, III = distension of pelvis and calices during reflux, IV = large, tortuous ureter and clubbing of calices. Interpretation = assessment of reflux into a ureter.

documented, prophylactic treatment will be started to prevent further infections until the reflux has disappeared. In many centers, VCUG is the initial radiographic procedure for investigation of the urinary tract in children with urinary tract infection [11]. Subsequent imaging of the urinary tract by excretory urography or sonography depends on the result of VCUG.

Our study shows that the reliability of showing reflux by VCUG depends on the severity of the reflux. Only grade IV reflux was shown by VCUG with 100% reliability. On the basis of the single case of grade IV reflux in our group of patients, the reliability for detecting this grade of reflux cannot be evaluated statistically. Grade III was modified by a second cyclic voiding in one ureter out of eight (13%), grade II in seven of 19 (37%), and grade I in 10 of 22 (45%). The second voiding upgraded or downgraded the reflux in 12%. The statistical results do not represent the clinical value of the VCUG, which is aimed at detecting, rather than excluding, vesicoureteral reflux. Only initially false-negative results are of clinical importance. If a second voiding showed reflux that was missed during the first one, it was the second one that determined the clinical management of the patient.

In one patient, a second cyclic voiding changed the grading of reflux from 0 to III. The discrepancy of the results between the two cycles could be due to the paraureteric bladder diverticulum next to the refluxing ureter, which filled only during the second cycle. Such diverticula are a known cause for occasionally false-negative VCUGs [12]. As they do not tend to regress with time as does primary reflux and often require surgery, cyclic VCUG was particularly important for this patient.

In one patient in whom three cyclic voidings were done because it was difficult to image the urethra, reflux grade III into a lower moiety of a duplex kidney was seen during the first and last voiding cycle, but not during the second.

By no means do we advocate multiple fillings in all children. Obviously, when grade III or IV reflux is seen on a first-filling VCUG, no cyclic voidings are necessary. This explains the very small number of children in this series of patients with major reflux and multiple-filling VCUG as compared with a much larger number of children with grade III or IV reflux with a single-filling VCUG.

To select patients who might benefit from cyclic voidings, we suggest that in children with urinary tract infection a sonogram be obtained before VCUG. Detection of a marked discrepancy in kidney size and/or intermittent dilatation of the

TABLE 4: Presence and Grading of Vesicoureteric Reflux on Three Consecutive Voiding Cycles

Initial Interpretation	Third Interpretation					Total
	0	I	II	III	IV	
0	104	1	4	1	0	110
I	0	1	0	0	0	1
II	3	1	2	0	0	6
III	1	0	0	0	0	1
IV	0	0	0	0	2	2
Total	108	3	6	1	2	120

Note.—Boldface numbers = same grading on all fillings. 0 = no reflux, I = reflux into ureter only, II = reflux into ureter and nondilated pelvis, III = distension of pelvis and calices during reflux, IV = large, tortuous ureter and clubbing of calices. Interpretation = assessment of reflux into a ureter.

ureters on the sonogram should increase suspicion of the presence of reflux. In these cases, a second filling VCUG should be obtained if the first one is normal, to enhance the diagnostic accuracy of the VCUG. As it is well known that infants and young children are more at risk of developing renal damage with urinary infection than older children, cyclic voiding might benefit patients in the first years of life.

ACKNOWLEDGMENTS

The authors thank L. Moore and M. Quigley for supervising many of the VCUGs and Isabell Webb for efficient secretarial assistance.

REFERENCES

1. Emmett JL, Witten DM. *Clinical urography*. Philadelphia: Saunders, 1972: 70-71
2. Conway JJ, Belmar AB, King LR, et al. Direct and indirect radionuclide cystography. *J Urol* 1975;113:689-693
3. Rizzoni G, Perale R, Bui F, et al. Radionuclide voiding cystography in intrarenal reflux detection. *Ann Radiol (Paris)* 1986;29:415-420
4. Hofmann V, Beyer HJ. Detection of vesicoureteral reflux in infants and children by sonography. *Monatsschr Kinderheilkd* 1985;133:834-839
5. Kessler RM, Altmann DH. Real-time sonographic detection of vesicoureteral reflux in children. *AJR* 1982;138:1033-1036
6. Nogrady MB, Dunbar JS. The technique of roentgen investigation of the urinary tract in infants and children. In: Kaufmann HJ, ed. *Progress in pediatric radiology*, vol. 3. Basel: Karger, 1970:41-42
7. Wyly JB, Lebowitz RL. Refluxing urethral ectopic ureters: recognition by the cyclic voiding cystourethrogram. *AJR* 1984;142:1263-1267
8. Feinstein AR. Clinical biostatistics XXXI. *Clin Pharmacol Ther* 1975; 17:104-116
9. Youden WJ. Index of rating diagnostic tests. *Cancer* 1950;3:33-35
10. Dixon WJ, ed. *BMPD statistical software manual*. Berkeley: University of California Press, 1988:267
11. Blickman JG, Taylor GA, Lebowitz RL. Voiding cystourethrography: the initial radiologic study in children with urinary tract infection. *Radiology* 1985;156:659-662
12. Hernanz-Schulman M, Lebowitz RL. The elusiveness and importance of bladder diverticula in children. *Pediatr Radiol* 1985;15:399-402

Pictorial Essay

Radiographic Evaluation of Velopharyngeal Incompetence in Childhood

Lori L. Barr,¹ C. Keith Hayden, Jr.,¹ Lesley C. Hill,² and Leonard E. Swischuk¹

Velopharyngeal incompetence, inadequate closure of the velopharyngeal portal, includes a spectrum of congenital and acquired abnormalities that usually become apparent with the onset of speech [1]. The opening between the velum or soft palate and the pharynx (velopharyngeal portal) must be closed by coordinated muscular action to permit normal speech and deglutition. Inadequate closure becomes most apparent with the onset of speech. Optimal evaluation of the speech problems is performed when the child is about 5 years old [2].

Technique

A combination of audio-enhanced videofluoroscopy and 105-mm spot films is used; both the radiologist and the speech pathologist are present. This technique has been successful in more than 250 patients with suspected velopharyngeal incompetence at our institution.

Audio-enhanced videofluoroscopy is most important in studying the motion of the velum and the pharyngeal walls during the utterance of certain phrases and connected speech. In both the lateral and frontal projections, patients repeat the phrases, "eat the peach," "pet the pretty puppy," "kick the cat," and "I wear pampers." Hard-copy 105-mm spot films are obtained in the lateral and frontal projections at a frame rate of 2/sec during quiet breathing and prolonged e and s phonation. Subsequent videofluoroscopy and spot filming in the frontal projection (either submentovertex or anteroposterior views) are performed after instillation of 2 ml of barium through the nostrils to coat the nasopharynx.

Physiology

The velum is made up of a number of paired muscles anchored by the pterygoid bones and palatine aponeurosis. In phonation, these muscles lead to combined elevation of the velum, slight anterior displacement of the posterior pharyngeal wall, and inward movement of the lateral pharyngeal walls [2]. During quiet breathing, the velum hangs downward and the pharyngeal walls are relaxed, resulting in the so-called velopharyngeal portal (Figs. 1A and 2A). With phonation, the velum moves upward and posteriorly to assume a right angle configuration and apposes the posterior pharyngeal wall (Figs. 1B and 2B). The posterior pharyngeal wall moves forward, but usually no more than 4 mm. In some cases, a focal elevation of the posterior pharynx develops; this has been termed Passavant's ridge and appears to be a physiologic, accommodative phenomenon to enhance closure of the velopharyngeal portal (Figs. 1C and 2C). On radiographic evaluation, this is identified as a transient bump visualized during phonation but disappearing during rest (Figs. 1C and 2C). Medial movement of the lateral pharyngeal walls at, or just below, the level of the palate is seen on the submentovertex or anteroposterior views (Figs. 3 and 4) [3].

Abnormalities

Congenital abnormalities are responsible most often for velopharyngeal incompetence in children. Most anomalies occur within the spectrum of facial cleft abnormalities, most

Received February 3, 1989; accepted after revision June 5, 1989.

Presented at the annual meeting of the American Roentgen Ray Society, New Orleans, May 1989.

¹ Departments of Radiology and Pediatrics, The University of Texas Medical Branch, Galveston, TX 77550. Address reprint requests to L. L. Barr.

² Department of Speech and Audiology, The University of Texas Medical Branch, Galveston, TX 77550.

of which are apparent at birth. The mildest cleft variant consists of a muscular defect at the midline of the soft palate, or a hypoplastic soft palate, and may go undetected until the onset of speech [1, 2]. These structural abnormalities, consisting primarily of a short, hypoplastic velum and impaired velar and lateral wall motion, are easily identified during radiographic evaluation (Fig. 5) [4].

Hypernasal speech is a common symptom of patients with functional abnormalities resulting in velopharyngeal incompetence. Causes include any condition that leads to dysmotility

or paralysis of the soft palate and pharyngeal muscles, such as cerebral palsy, closed head injury, demyelinating diseases, and muscular dystrophy (Fig. 6).

Children may demonstrate speech deterioration after various surgical procedures such as adenoidectomy. Usually this is caused by a congenitally deep velopharyngeal portal, which is masked by the presence of adenoidal tissue. When the adenoidal bulk is decreased surgically, velopharyngeal incompetence ensues (Fig. 7).

Treatment of velopharyngeal incompetence in children in-

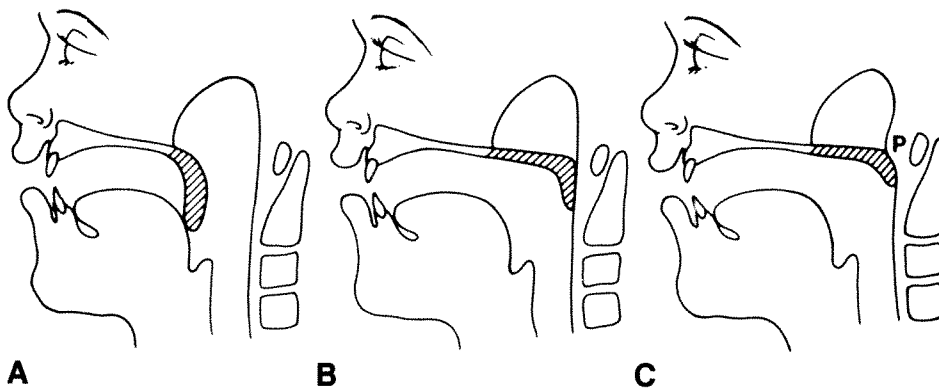


Fig. 1.—Schematic drawings of normal palate, lateral position.

A, During quiet breathing, palate or velum (diagonal hatching) rests on tongue base.

B, With phonation, velum rises and forms a right-angle configuration apposing adenoidal pad.

C, In some patients, an accommodative Passavant ridge (P) arises from posterior pharyngeal wall to meet palate.

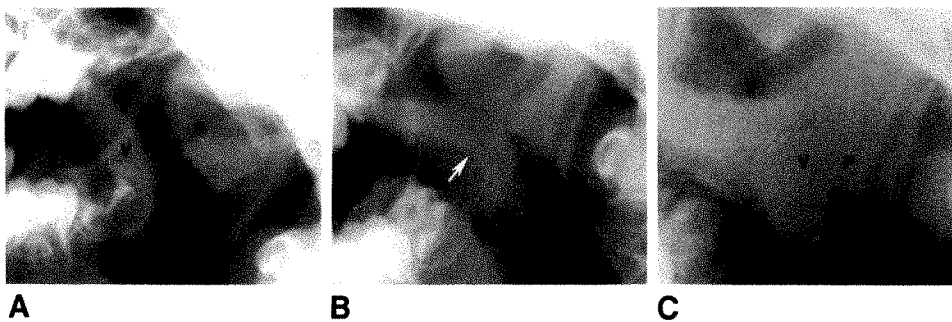


Fig. 2.—Radiographs of normal palate, lateral projection.

A, With quiet breathing, palate or velum (V) rests on tongue base. Adenoidal pad (A) is normal.

B, With phonation, velum rises and forms a right-angle configuration (arrow) as it apposes adenoidal pad.

C, Another patient in whom, with phonation and elevation of velum (V), an accommodative Passavant ridge (P) is seen.

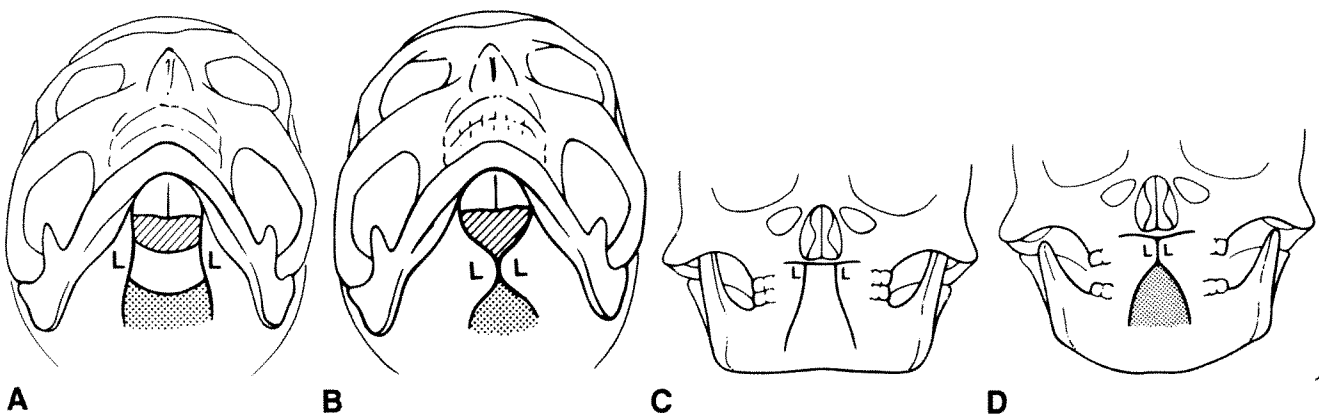


Fig. 3.—Schematic drawings of normal lateral pharyngeal walls, frontal positions.

A, Submentovertex position. With quiet breathing, lateral pharyngeal walls (L) are far apart.

B, Submentovertex position. With phonation, lateral walls approximate at midline and close velopharyngeal portal by meeting velum (diagonal hatching) and posterior pharyngeal wall (stippling).

C, Anteroposterior position. With quiet breathing, lateral pharyngeal walls are far apart.

D, Anteroposterior position. With phonation, walls meet at midline and close velopharyngeal port by meeting posterior pharyngeal wall (stippling).

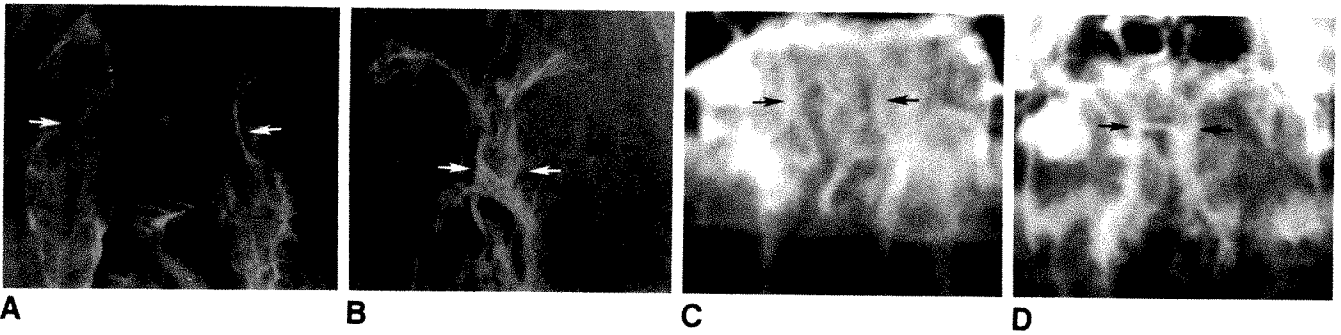


Fig. 4.—Radiographs of normal lateral pharyngeal walls, frontal projections.

A, Submentovertex view. With quiet breathing, lateral pharyngeal walls are far apart (arrows).

B, Submentovertex view. With phonation, walls approximate at midline, markedly narrowing velopharyngeal port (arrows).

C, Anteroposterior view. With quiet breathing, lateral walls are far apart (arrows).

D, Anteroposterior view. With phonation, walls come to midline (arrows).

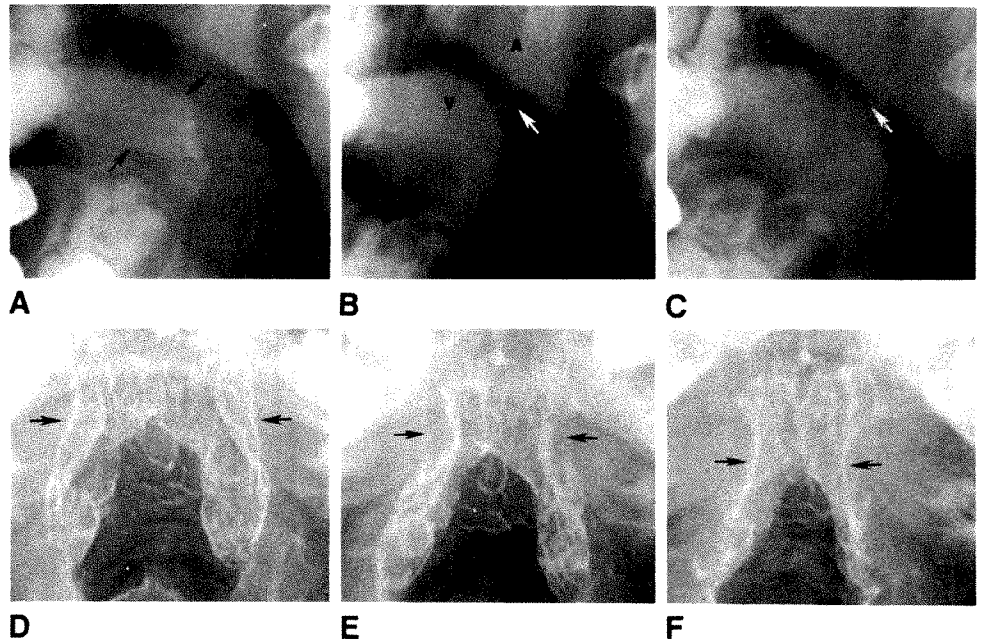


Fig. 5.—Short velum with cleft palate.

A, Lateral view, quiet breathing. Note short, plump velum (arrows).

B, With phonation of letter e, velum (V) rises and forms a reasonable right angle, but fails to meet adenoidal pad (A). An air gap (arrow) persists.

C, With phonation of letter s, the same gap is seen (arrow).

D, Submentovertex view, quiet breathing. Note position of lateral pharyngeal walls (arrows).

E, With phonation of letter e, walls move inward but only slightly (arrows).

F, With phonation of letter s, walls still remain too far apart (arrows). These patients require surgery or a prosthesis.

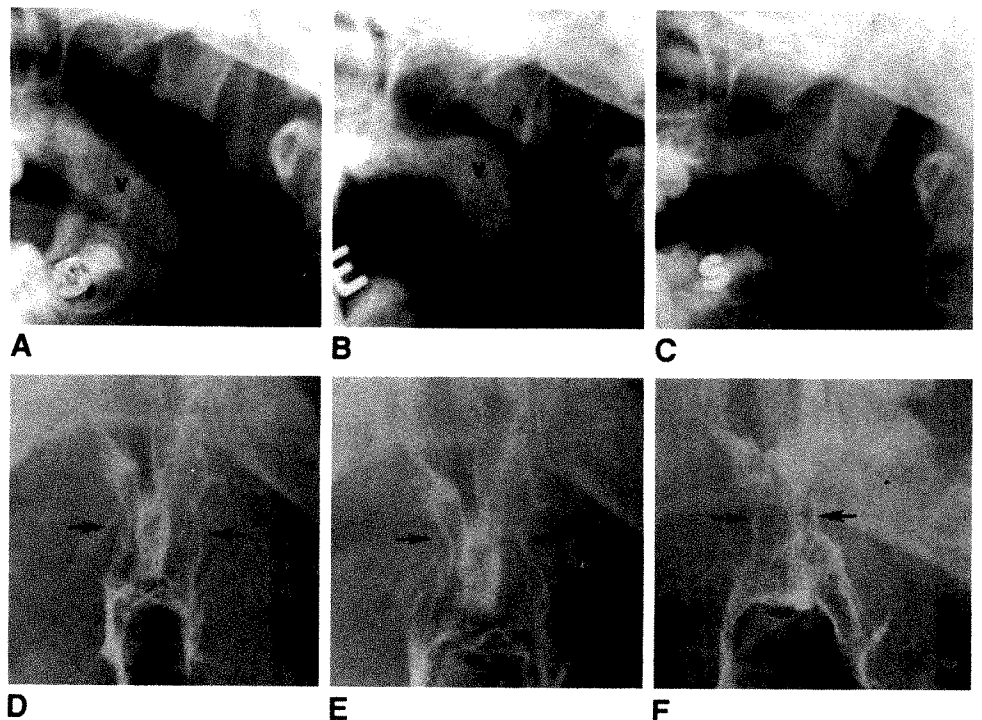


Fig. 6.—Functional abnormality: paralysis of pharynx.

A, Lateral view. Note position of velum (V) on quiet breathing.

B, With phonation of letter e, velum (V) rises, but a small air gap persists between it and adenoids (A).

C, With letter s, air gap is obliterated (arrow).

D, Submentovertex view, quiet breathing. Note normal position of lateral pharyngeal wall (arrows).

E, With phonation of letter e, walls move inwardly (arrows), but not to normal midline position.

F, With letter s, air gap is virtually obliterated (arrows). Treatment in these patients consists of speech therapy and, in some, a prosthesis.

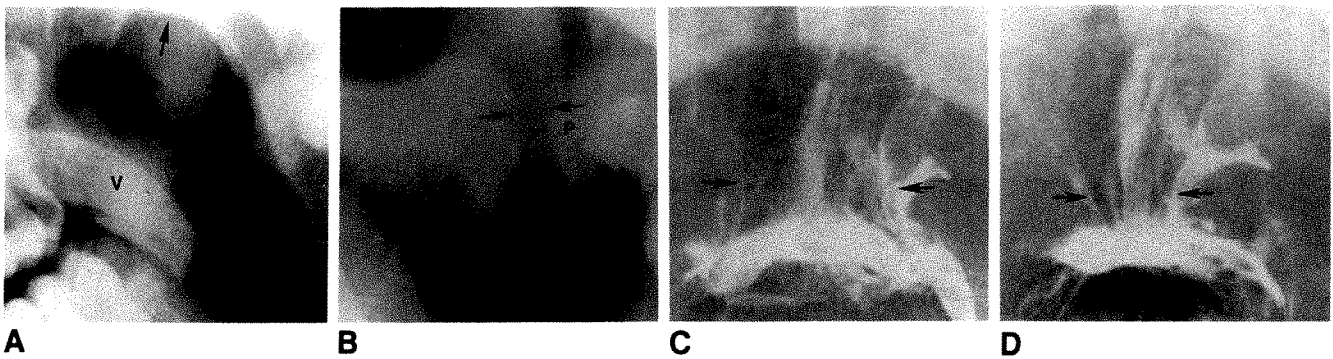


Fig. 7.—Functional abnormality: postadenoidectomy velopharyngeal incompetence.

A, Lateral view, quiet breathing, in postadenoidectomy patient with no adenoidal tissue (arrows). Velum (V) appears normal. Note that posterior pharyngeal wall is flat.

B, With phonation of letter e, velum rises but fails to meet posterior pharyngeal wall; an air gap (arrows) persists. A small bulge in posterior pharyngeal wall represents a small Passavant ridge (P).

C, Submentovertex view. With quiet breathing, lateral walls are far apart (arrows).

D, With phonation of letter e, walls come to midline (arrows). Preferred treatment in these patients is speech therapy.

cludes speech therapy, prosthetic management, and surgical intervention. Speech therapy is the treatment of choice when there is no anatomic cause for velopharyngeal incompetence. A prosthesis is used in cases of paralysis or functionless palate associated with reduced lateral wall mobility. Surgical correction is chosen when the palate is short or cleft and shows decreased motion in the presence of good lateral wall mobility. Optimal function of the modified velopharyngeal portal may not occur for up to 2 years [1].

REFERENCES

1. Cooper H, Harding R, Krogman WM, Mazaheri M, Millard R, eds. *Cleft palate and cleft lip: a team approach to clinical management and rehabilitation of the patient*. Philadelphia: Saunders, 1979
2. McWilliams BJ, Morris H, Shelton R. *Cleft palate speech*. Philadelphia: Decker, 1984
3. O'Hara EA. Roentgen evaluation of patients with cleft palate. *Radiol Clin North Am* 1963;1: 1-11
4. Stringer DA, Witzel MA. Velopharyngeal insufficiency on videofluoroscopy: comparison of projections. *AJR* 1986;146: 15-19

Sonography of Placental Abnormalities and Oligohydramnios in Women with Elevated Alpha-fetoprotein Levels: Comparison with Control Subjects

Richard B. Kelly^{1,2}
David A. Nyberg^{1,3}
Laurence A. Mack¹
Jack Fitzsimmons⁴
Stephanie Uhrich⁴

To evaluate the relationship of placental and amniotic fluid findings to elevated maternal serum alpha-fetoprotein (MS-AFP) levels, we compared sonograms made between 18 and 24 weeks gestational age in 76 women with elevated MS-AFP levels with sonograms of a control group. Patients with fetal malformations, incorrect dates, twins, or lack of follow-up were excluded. Overall, 27 (36%) of 76 patients with elevated MS-AFP levels had placental or amniotic fluid abnormalities compared with only three (3%) of 87 control subjects. Significant differences ($p < .01$) were noted in the frequency of periplacental hemorrhage (9% vs 0%), intraplacental sonolucencies greater than or equal to 1.5 cm in diameter (18% vs 3%) and moderate or severe oligohydramnios (17% vs 0%). More patients with elevated MS-AFP levels had placenta previa (4%) or placental thickness greater than or equal to 3.5 cm (12%) than did those in the control group (1% and 5%, respectively), although these differences did not reach statistical significance. Seven (26%) of the 27 patients had more than one abnormality.

We conclude that placental and/or amniotic fluid abnormalities are frequently shown on sonograms in women who are examined because of elevated MS-AFP levels.

AJR 153:815-819, October 1989

Women with elevated levels of maternal serum alpha-fetoprotein (MS-AFP) commonly undergo prenatal sonography for detection of possible fetal malformations, notably neural tube defects. Other common reasons for elevated MS-AFP levels include incorrect gestational age, multiple gestations, and death of the fetus [1]. However, even when accounting for these conditions, no apparent explanation is found in the vast majority of women with abnormally elevated MS-AFP levels [1].

Recent reports suggest that placental abnormalities [2-6] and oligohydramnios [7-9] may be associated with elevated MS-AFP levels. However, the frequency of such observations is uncertain because of the small number of published series. In order to determine the frequency of placental abnormalities and oligohydramnios in women with an apparently normal fetus and an elevated MS-AFP level, we compared sonographic findings in these patients with findings in a control population.

Materials and Methods

The initial study population consisted of 107 consecutive patients referred for sonographic evaluation during a 3-year period (1985-1987) with the clinical indication of an MS-AFP level greater than or equal to 2.5 multiples of the median level. If necessary, corrections for maternal weight or diabetes were made. All serum samples were obtained between 16 and 20 weeks gestational age. Twenty-two patients were excluded because of fetal anomalies (eight cases), incorrect dates (10 cases), or twins (four cases) that explained the elevated MS-AFP level. Nine other patients were eliminated from the study group because of a lack of follow-up (four cases) or referral to sonography after 24 weeks gestational age (five cases),

Received March 2, 1989; accepted after revision May 23, 1989.

¹ Department of Radiology (SB-C5), University of Washington Hospital, Seattle, WA 98195.

² Present address: Northwest Radiologists, 1800 C St., Ste. F-17, Bellingham, WA 98225-4035.

³ Present address: Swedish Hospital Medical Center, 1229 Madison, Ste. 1150, Seattle, WA 98104-1336. Address reprint requests to D. A. Nyberg.

⁴ Department of Obstetrics and Gynecology, University of Washington Hospital, Seattle, WA 98195.

0361-803X/89/1534-0815
© American Roentgen Ray Society

leaving a total of 76 patients in the study group. All sonograms in these 76 patients were obtained between 18 and 24 weeks gestational age.

The control group consisted of 87 consecutive women who had sonograms made between 18 and 24 weeks gestational age and in whom MS-AFP values were known to be normal. The indications for sonography in these patients included genetic amniocentesis due to advanced maternal age (24 cases), uncertain dates (18 cases), uterine size discordant with dates (14 cases), history of a prior abnormal pregnancy (17 cases), and other routine obstetric indications (14 cases).

Sonograms were obtained with commercially available real-time and static equipment. Each sonogram was reviewed retrospectively and randomly by two experienced sonographers without knowledge of the clinical indication or outcome. When more than one examination was performed, only the first sonogram was evaluated. In each case, the presence of periplacental hemorrhage (retroplacental or subchorionic), placenta previa, intraplacental sonolucencies greater than or equal to 1.5 cm in diameter, and placental thickness greater than or equal to 3.5 cm were noted. A subjective determination of moderate to severe oligohydramnios also was made on the basis of a paucity of amniotic fluid, poor fetal/fluid interfaces, and crowding of fetal parts.

TABLE 1: Comparison of Sonographic Findings in Patients with Elevated Maternal Serum Alpha-fetoprotein (MS-AFP) and Control Subjects

Sonographic Finding	Increased MS-AFP (n = 76)	Control Subjects (n = 87)	p Value ^a
Intraplacental sonolucencies	14 (18%)	3 (3%)	<.01
Periplacental hemorrhage	7 (9%)	0 (0%)	<.01
Oligohydramnios (moderate to severe)	13 (17%)	0 (0%)	<.001
Placenta previa	3 (4%)	1 (1%)	.34
Placental thickness ≥ 3.5 cm	9 (12%)	4 (5%)	.23

^a Fisher two-tailed exact test.

Sonographic findings were then correlated with clinical indications and outcome. The outcome was determined by follow-up sonograms, a review of the medical records, and correspondence with the referring physician.

The statistical significance of sonographic findings was determined with the Fisher two-tailed exact test. Because of the limited size of the study groups, no attempt was made to match abnormal and control populations for maternal factors (i.e., diabetes, hypertension, age, parity, history of tobacco smoking, or previous loss of a pregnancy) that could possibly influence the results.

Results

The results of the study are compiled in Table 1. Intraplacental sonolucencies greater than or equal to 1.5 cm in diameter were noted in 14 women (18%) with elevated MS-AFP levels (Fig. 1) compared with only three women (3%) in the control group ($p < .01$). Seven patients (9%) with an elevated MS-AFP level had evidence of periplacental hemorrhage (Fig. 2), and 13 had evidence of moderate (11 cases) or severe (2 cases) oligohydramnios (Fig. 3). In comparison, none of the control patients had sonographic evidence of periplacental hemorrhage ($p < .01$) or oligohydramnios ($p < .001$).

In all, 27 (36%) of 76 patients with an elevated MS-AFP level had one or more placental abnormalities or oligohydramnios compared with only three (3%) of 87 patients in the control group. Seven (26%) of these 27 patients had more than one abnormality. Four patients had both periplacental hemorrhage and intraplacental sonolucencies, and three patients had periplacental hemorrhage and oligohydramnios.

Placenta previa was identified by sonography in three patients (4%) with elevated MS-AFP levels and in one patient (1%) in the control group. However, when only complete previa at the time of delivery is considered, two patients with

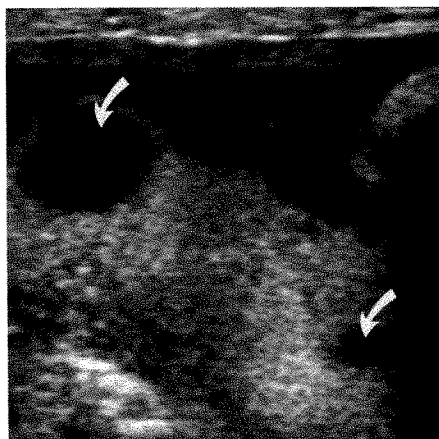
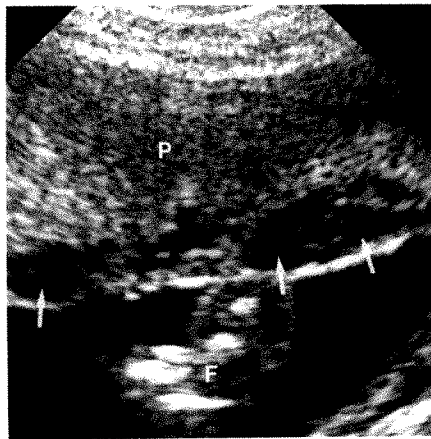
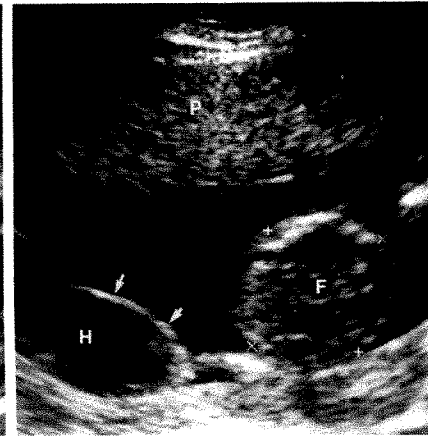


Fig. 1.—Sonogram made at 18 weeks gestational age in a woman with elevated level of maternal serum alpha-fetoprotein shows several intraplacental sonolucencies (arrows). Fetus died at 26 weeks gestation. Placental infarcts were described in pathology report.



A



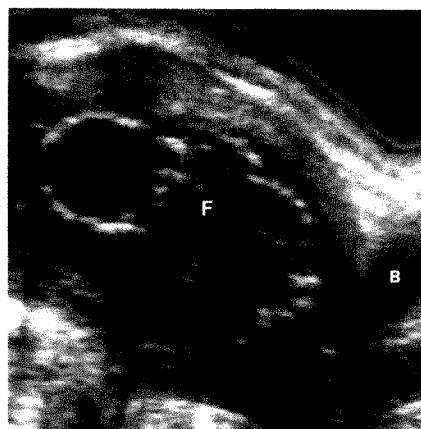
B

Fig. 2.—A, Sonogram made at 18 weeks gestational age shows placental sonolucencies (arrows) beneath chorionic plate in a woman with elevated maternal serum alpha-fetoprotein.

B, Different view of same patient shows a hypoechoic area consistent with hemorrhage (H) beneath chorionic membrane (arrows).

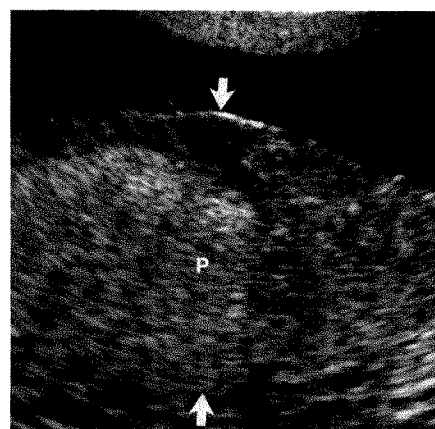
F = fetus, P = placenta.

Fig. 3.—Sonogram made at 17 weeks gestational age shows marked oligohydramnios in a woman with elevated level of maternal serum alpha-fetoprotein. Follow-up sonograms showed no change in these findings, leading to decision to terminate pregnancy at 21 weeks. F = fetus; B = maternal bladder.



3

Fig. 4.—Sonogram made at 19 weeks gestational age in a woman with elevated level of maternal serum alpha-fetoprotein shows marked thickening (arrows) of placenta (P).



4

elevated MS-AFP levels had a previa compared with no control patients ($p = .22$).

An abnormally thickened placenta (≥ 3.5 cm) was found in nine patients (12%) with elevated MS-AFP levels (Fig. 4) compared with four control patients (5%) ($p = .23$).

In patients with elevated MS-AFP levels, clinical outcome included normal delivery in 53 cases (70%), fetal or neonatal death in 11 cases (15%), intrauterine growth retardation in four cases (5%), premature delivery (< 36 weeks gestation) in five cases (7%), and congenital anomalies in three cases (4%). These three anomalies included two cases of cleft lip and palate and one case of amputation of several digits of the hand. No major congenital anomaly such as neural-tube defect or anterior abdominal wall defect was missed by sonography in either the group of patients with elevated MS-AFP levels or the control group.

The clinical outcome of patients with elevated MS-AFP levels was particularly poor in association with oligohydramnios. Of 13 patients with oligohydramnios, the outcome included fetal or neonatal death in seven cases, intrauterine growth retardation in two cases, premature delivery at 25 weeks in one case, and normal term delivery in three cases. Seven patients with oligohydramnios had a history of vaginal bleeding, and two patients had sonographic evidence of periplacental hemorrhage.

Correlation of sonographic findings with pathologic findings was limited because of a lack of adequate examination of the placenta. Also, periplacental and intraplacental hemorrhage often resolve by the time of delivery. We recognize the limitations of pathologic examination, but report that placental blood clots were found at delivery in five cases and placental infarcts were identified in two additional cases. Both patients with placental infarcts had intraplacental sonolucencies. Of the five patients with pathologic evidence of retroplacental clot, sonographic findings suggested periplacental hemorrhage in two cases and marked oligohydramnios in two additional cases. The remaining patient had a normal-appearing placenta at 22 weeks gestational age, but one week later the patient developed acute clinical symptoms consistent with retroplacental abruption. The sonogram at this time showed a markedly thickened and heterogeneous placenta consistent with a retroplacental hemorrhage.

Discussion

Alpha-fetoprotein (AFP) is a fetal-specific protein that is first produced by the yolk sac and later by the fetal gastrointestinal tract and liver [1]. AFP reaches the amniotic fluid by excretion in fetal urine and by diffusion across fetal skin capillaries. In turn, AFP in the amniotic fluid diffuses across placental membranes to reach the maternal circulation. Because of this diffusion gradient, concentrations of AFP in the fetal serum are 100–200 times greater than that found in the amniotic fluid and 100,000 times greater than that found in the maternal serum at 16–20 gestational weeks [1].

Up to 4% of all women with an anatomically normal fetus have elevated levels of MS-AFP [1]. Fetal-maternal hemorrhage has long been suspected as the underlying cause of elevated MS-AFP levels in many of these patients. Because the concentration of AFP in the fetal serum is 100,000 times greater than that in maternal serum at 16–20 weeks gestational age, elevation of the MS-AFP level is a sensitive marker for fetal-maternal hemorrhage [10–12]. Therefore, an elevated MS-AFP level may be a sign of an underlying placental abnormality. Women with elevated MS-AFP levels are known to be at increased risk of placental abruption, intrauterine growth retardation, premature labor, and death of the fetus [1, 3, 7, 13].

As our study shows, placental abnormalities and oligohydramnios are frequently seen in women with elevated MS-AFP levels and an anatomically normal fetus. Intraplacental sonolucencies (Fig. 1) were the most common sonographic abnormal findings in this study. The frequency of intraplacental sonolucencies in women with elevated MS-AFP levels (18%) agrees with the results of Perkes et al. [2], who reported intraplacental sonolucencies in 18.5% of patients with elevated MS-AFP levels and in 2.3% of a control group.

Although intraplacental sonolucencies may represent various pathologic findings, Spirt et al. [14] and others [2, 3, 15–18] have shown that they correlate best with intervillous thrombi. Intervillous thrombi represent intraplacental fetal hemorrhage resulting from rupture of villous capillaries [14, 15]. Devi et al. [18] showed a strong correlation between intervillous thrombi and the presence of fetal RBCs in the maternal circulation. Because intervillous thrombosis repre-

sents a site of fetal-maternal hemorrhage, it also has been associated with Rh sensitization and erythroblastosis in Rh-negative women [15–18]. An association also has been observed between intervillous thrombi and placental abruption, spontaneous abortion, and premature delivery [15–18].

The prevalence and significance of intervillous thrombi appear to vary with gestational age. Javert and Reiss [15] reported pathologic findings of intervillous thrombi in 7.7% of all placentas up to 22 weeks gestation, including 1.2% of placentas from therapeutic abortions and 10.6% from spontaneous abortions. In comparison, these authors found intervillous thrombi in 28.5% of term placentas [15]. Similarly, intraplacental sonolucencies are frequently shown in the third trimester on prenatal sonography, but were observed in only 3% of control subjects before 24 weeks gestation in this study.

As this was a retrospective study, we made no attempt to distinguish intraplacental sonolucencies with blood flow ("maternal lakes") from those without evidence of flow. However, this distinction may be incomplete even when evaluated prospectively because slow flow may be difficult to see on sonography. Also, our own anecdotal experience suggests that maternal lakes seen before 24 gestational weeks also may be associated with elevated MS-AFP levels. We speculate that maternal lakes may form at sites of previous hemorrhage in this situation.

In addition to placental sonolucencies, sonographic evidence of periplacental hemorrhage was associated with elevated MS-AFP levels in the present study (Fig. 2). Seven patients (9%) with elevated MS-AFP levels had evidence of periplacental hemorrhage [19], and all hemorrhages were located near the margin of the placenta or beneath the chorionic membrane (Fig. 2). In comparison, Fleischer et al. [6] reported periplacental hematomas in 16 (64%) of 25 patients with an elevated MS-AFP level and a normal fetus. These authors also reported a high frequency of retroplacental hemorrhage. The reason for these discrepant results is unclear but possibly reflects differences in criteria for selection of patients or in sonographic interpretation. Periplacental hemorrhage apparently leads to an elevated MS-AFP level in a manner similar to that of intraplacental hemorrhage, with transfer of fetal RBCs to the maternal circulation [7, 17, 18]. This notion is supported by an association between circulating fetal RBCs and retroplacental hematomas examined at birth [18].

Thickened placentas (Fig. 4) and placenta previa were observed more often in patients with elevated MS-AFP levels than in the control group in the present study, although these associations did not reach statistical significance. Nevertheless, a thickened placenta or placenta previa in patients with an elevated MS-AFP level may be a helpful ancillary finding in conjunction with other sonographic abnormalities.

The association between midtrimester oligohydramnios and elevated MS-AFP level noted in the present study (Fig. 3) confirms earlier observations [7–9]. In the absence of genitourinary anomalies, the cause of oligohydramnios in these pregnancies is uncertain, but it has been suggested that it reflects an underlying uteroplacental insufficiency [9]. Fetal

hypoxemia may result in shunting of blood away from the fetal kidneys and secondarily in decreased urine production and decreased amniotic fluid volume [9]. The frequent history of vaginal bleeding in association with oligohydramnios and elevated MS-AFP levels also implicates placental dysfunction as a contributing cause.

Regardless of the causes, severe midtrimester oligohydramnios is a predictor of poor fetal outcome due to pulmonary hypoplasia, intrauterine growth retardation, and prematurity [8–10]. In our 13 cases of oligohydramnios and elevated MS-AFP level, seven resulted in fetal or neonatal death, two resulted in intrauterine growth retardation, one resulted in premature delivery at 25 weeks, and only three (23%) resulted in a normal term delivery. A similar outcome has been observed by other authors [8–10]. Richards et al. [9] suggests that the risk of fetal death is increased when severe oligohydramnios persists longer than 2–4 weeks or when there is history of vaginal bleeding or amniotic fluid leakage.

Our findings carry important implications for counseling women found to have an elevated MS-AFP level. Although the protocol for evaluating such patients varies from institution to institution, our approach includes a thorough sonogram to identify possible fetal anomalies before a decision is made to perform amniocentesis. Few anomalies have been missed at our centers, particularly with awareness of characteristic cranial abnormalities that recently have been associated with myelomeningocele [20, 21]. However, amniocentesis is commonly performed to provide additional reassurance that a significant anomaly has not been missed. When placental abnormalities are shown that might explain the elevated MS-AFP level and the fetus appears anatomically normal, many women may decide that the benefits of amniocentesis do not justify its additional risk or expense.

In summary, a significant proportion of women with elevated MS-AFP levels but an anatomically normal fetus have intraplacental sonolucencies, periplacental hemorrhage, and/or oligohydramnios when compared with a control group. Current evidence suggests that these associations reflect fetal-maternal hemorrhage and placental dysfunction. Awareness of these sonographic findings may influence MS-AFP screening protocols.

REFERENCES

1. Main DM, Mennut MT. Neural tube defects: issues in prenatal diagnosis and counseling. *Obstet Gynecol* 1986;67:1–15
2. Perkes EA, Baim RS, Goodman KJ, Macri JN. Second-trimester placental changes associated with elevated maternal serum alpha-fetoprotein. *Am J Obstet Gynecol* 1982;144:935–938
3. Purdie DW, Young JL, Guthrie KA, Piztur CE. Fetal growth achievement and elevated maternal serum alpha-fetoprotein. *Br J Obstet Gynaecol* 1983;90:433–436
4. Salafia CM, Silberman L, Herrera NE, Mahoney MJ. Placental pathology at term associated with elevated midtrimester maternal serum alpha-fetoprotein concentration. *Am J Obstet Gynecol* 1988;158:1064–1066
5. Boyd PA, Keeling JW. Raised maternal serum alpha-fetoprotein in the absence of fetal abnormality—placental findings. A quantitative morphometric study. *Prenat Diagn* 1986;6:369–373
6. Fleischer AC, Kurtz AB, Wapner RJ, et al. Elevated alpha-fetoprotein and a normal fetal sonogram: association with placental abnormalities. *AJR* 1988;150:881–883

7. Hamilton MFR, Abdalla HI, Whitfield CR. Significance of raised maternal serum alpha-fetoprotein in singleton pregnancies with normally formed fetuses. *Obstet Gynecol* 1985;64:465-470
8. Koontz WL, Seeds JH, Adama NJ, Johnson AM, Cefalo RC. Elevated maternal serum alpha-fetoprotein, second-trimester oligohydramnios, and pregnancy outcome. *Obstet Gynecol* 1983;62:301-304
9. Richards DS, Seeds JW, Katz VL, Lingley LH, Albright SG, Cefalo RC. Pregnancy outcome with elevated maternal serum AFP and oligohydramnios: ultrasound evaluation and outcome. *Obstet Gynecol* 1988;72:337-341
10. Lachman E, Hingley SM, Bates G, Ward AM, Stewart CR, Duncan SLB. Detection and measurement of fetomaternal haemorrhage: serum alpha-fetoprotein and the Kleihauer technique. *Br Med J* 1977;1:1377-1379
11. Los FJ, de Wolf BTHM, Huisjes HJ. Raised maternal serum-alpha-fetoprotein levels and spontaneous fetomaternal transfusion. *Lancet* 1979;2:1210-1212
12. Hay DL, Barrie JU, Davison GB, et al. The relation between maternal serum alpha-fetoprotein levels and fetomaternal haemorrhage. *Br J Obstet Gynaecol* 1979;36:516-520
13. Wald NJ, Cuckle H, Stirrat GM, et al. Maternal serum alpha-fetoprotein and low birth weight. *Lancet* 1977;2:268-270
14. Spirt BA, Gordon LP, Kagan EH. Intervillous thrombosis: sonographic and pathologic correlation. *Radiology* 1983;147:197-200
15. Javert CT, Reiss C. The origin and significance of macroscopic coagulation hematomas (red infarcts) of the human placenta. *Surg Gynecol Obstet* 1952;94:257-269
16. Hoogland HJ, de Haan J, Vooys GP. Ultrasonographic diagnosis of intervillous thrombosis related to Rh isoimmunization. *Gynecol Obstet Invest* 1979;10:237-245
17. Wentworth P. A placental lesion to account for foetal haemorrhage into the maternal circulation. *Br J Obstet Gynaecol* 1964;71:379-387
18. Devi B, Jennison RF, Langley FA. Significance of placental pathology in transplacental haemorrhage. *J Clin Pathol* 1968;21:322-331
19. Nyberg DA, Cyr DR, Mack LA, Wilson DA, Shuman WP. Sonographic spectrum of placental abruption. *AJR* 1987;148:161-164
20. Nicolaides KH, Gabbe SG, Campbell S, et al. Ultrasound screening for spina bifida: cranial and cerebellar signs. *Lancet* 1986;1:72-74
21. Nyberg DA, Mack LA, Hirsch J, Mahony BS. Abnormalities of fetal cranial contour in sonographic detection of spina bifida: evaluation of the "lemon" sign. *Radiology* 1988;167:387-392



The Radiology Outreach Foundation (ROF) is a nonprofit corporation whose goal is to help disadvantaged countries improve their health care by providing radiology equipment, books, consultation, education, and training to their practitioners. This assistance is on an application basis that is independent of political, ethnic, or religious orientation of the grantee. It depends on the need of the people and the ability of the ROF to meet that need. The ROF is approved by the U.S. Internal Revenue Service as a tax-exempt organization. It is endorsed by the following radiologic societies: American Association of Women Radiologists, American College of Radiology, American Roentgen Ray Society, Association of University Radiologists, Radiological Society of North America, Society of Chairmen of Academic Radiology Departments, Society for Pediatric Radiology, European Society of Pediatric Radiology.

All donations to the ROF are tax deductible. Persons who would like to contribute financially to the ROF, would be interested in being a visiting professor, would like to send books or journals to any of the institutions supported by the ROF, or would like further information about the ROF should write to Charles A. Gooding, M.D., President, Radiology Outreach Foundation, 3415 Sacramento St., San Francisco, CA 94118 USA.

Book Review

Ultrasound Teaching Cases, vol. 2. By Keith C. Dewbury, David O. Cosgrove, and Hylton B. Meire. New York: Alan R. Liss for Wiley, 193 pp., 1988. \$95.75

A sequel to the first volume of *Ultrasound Teaching Cases*, the current work is intended to complement and expand the type and range of cases. Volume 2 is divided into five sections: liver and biliary system, general abdomen, urinary system, obstetrics and gynecology, and miscellaneous. A total of 232 cases are presented. The format includes a brief clinical history, two to six scans, and a discussion that generally is confined to one-half page of text. Frequently, companion cases are presented in the discussion to illustrate similar or disparate sonographic findings in the same pathologic entity. The entire case presentation is, with few exceptions, confined to two pages.

Although the work covers a broad range of diseases and a spectrum of difficulty, the authors have concentrated on providing information about relatively common entities that has pragmatic clinical value. For example, the section on the liver includes such entities as hepatic metastases, capillary hemangioma, cirrhosis, biliary atresia, liver trauma, liver abscess, and polycystic liver disease. Several cases of hydatid disease of the liver extend the range of entities a bit (at least for the American reader). A similar approach prevails in the remaining sections.

Succinct discussions cover the pertinent sonographic findings, pitfalls, and important clinical considerations. The text is clearly written and reads smoothly and easily throughout. The sonograms

are of first-rate quality, and the pathologic changes are shown clearly in all cases.

Both authors and publisher are to be congratulated on the format, which is kind to the mind and eye; few cases require the turning of a page and the separation of text and illustration. Photographic reproduction is excellent, and each sonogram has an individual homunculus clearly indicating the position of the image. Spacing of images and text is liberal throughout (in fact, even prodigal in some instances); if necessary, the volume could be contracted or cases added. However, neither the size nor the cost of the book is unreasonable. The index provides quite sufficient cross-referencing of pathologic entities.

Volume 2 provides valuable sonographic, clinical, and differential diagnostic information in a highly palatable form for radiologists at all levels of training. Two or three unhurried evenings are easily enough to read the whole book, and its value in a teaching program is unquestionable. The volume already has been circulated to our residents, and the response at all levels of training has been uniformly positive. In short, this is a superb teaching and learning device. I hope that volume 2 is not the last in this series.

Andrew M. Fried
University of Kentucky
Lexington, KY 40536-0084

Intrauterine Shelves in Pregnancy: Sonographic Observations

Douglas L. Brown^{1,2}
 Richard E. Felker¹
 Donald S. Emerson¹

Twenty-five shelves of tissue, all having a free edge within the uterine cavity, were identified by sonography in 24 singleton pregnancies. In no case did the shelf attach to the fetus or restrict fetal motion. The fetus was sonographically normal in 23 pregnancies, and no fetus developed amniotic-band syndrome. One fetus had anencephaly, probably unrelated to amniotic-band syndrome. Although these shelves may be due to synechiae, only eight (32%) of the patients had a history of dilatation and curettage or cesarean delivery, which predispose the patient to formation of synechiae.

This experience suggests that when a shelf of tissue with a free edge is present within the pregnant uterus, there should be no concern for the development of amniotic-band syndrome as long as a complete sonographic survey of the fetus reveals no abnormalities.

AJR 153:821-824, October 1989

Many causes account for membranes or bands within the pregnant uterus. With the exception of the amniotic-band syndrome, and possibly subchorionic hematomas, these structures are usually of little cause for concern. A recent study [1] described the appearance and significance of bands or membranes within the amniotic cavity that were unrelated to the amniotic-band syndrome. In this report, we describe our experience with these bands or shelves and address their significance when the fetus appears normal.

Materials and Methods

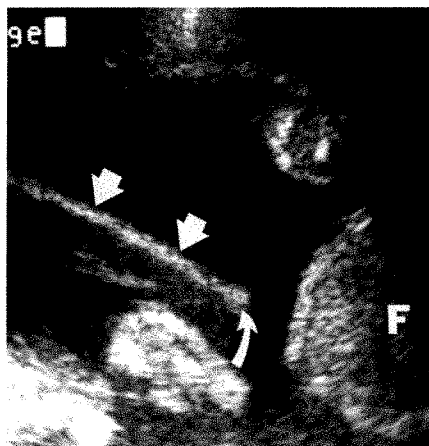
Over a 30-month period, 24 pregnant women who had intrauterine shelves with a free edge (Fig. 1) were seen at our institution. Eight patients were identified by retrospective review of obstetric sonograms obtained over a 1-year period, and 16 more were identified prospectively over the subsequent 18 months. The shelf of tissue had to have a free edge for inclusion in the study. In fact, it was this characteristic that we wanted to stress by use of the name, intrauterine "shelf," although others have referred to these structures as "innocent bands," "intraamniotic bands," or "amniotic sheets." The free edge was sometimes difficult to identify directly, and multiple scanning planes often were attempted before it was shown. The sonograms were obtained on a variety of real-time scanners. Information about previous dilatation and curettage or cesarean delivery for each patient was obtained either by asking the patient or by reviewing the medical chart. In addition to providing a complete survey of the fetus, the sonographic study included evaluation for any attachment of the shelf to the fetus and for the ability of the fetus to move without restriction by the shelf. For each shelf, assessment included its location in the uterus, length, thickness, presence of thickening of the base (that part of the shelf nearest the myometrium) or free edge of the shelf, the presence of placenta on the shelf, and whether the shelf was straight or lax. The length of the shelf is defined as the longest dimension; thickness is the smallest dimension. When follow-up sonograms were obtained, the presence or absence of the shelf was recorded. In all cases, the status of the infant at birth was obtained.

Received February 27, 1989; accepted after revision June 6, 1989.

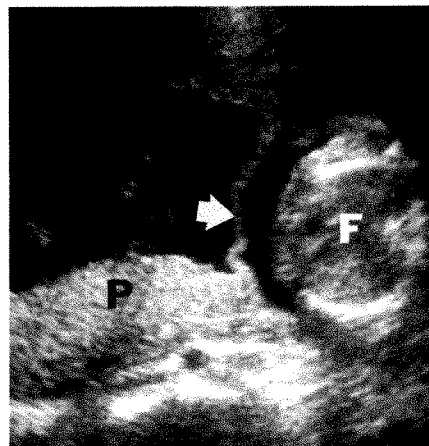
¹ Department of Radiology, University of Tennessee, Memphis, 800 Madison Ave., Memphis, TN 38163. Address reprint requests to R. E. Felker.

² Present address: Department of Radiology, Brigham and Women's Hospital and Harvard Medical School, 75 Francis St., Boston, MA 02115.

0361/803X/89/1534-0821
 © American Roentgen Ray Society



A



B

Fig. 1.—Benign shelf at 24 weeks.

A, Sonogram shows shelf (straight arrows) protruding into uterine cavity. Free edge (curved arrow) is visible. Base of shelf is not seen in this image.

B, Different orientation shows placenta (P) extending up to shelf (arrow). F = fetal body.

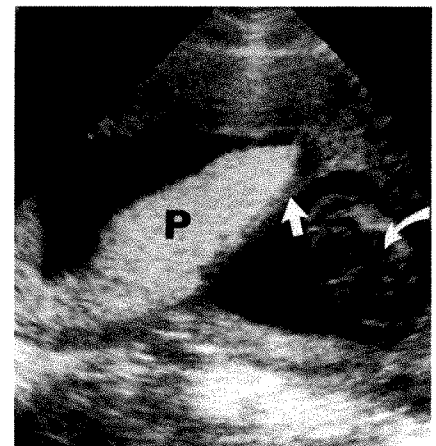


Fig. 2.—Benign shelf at 16 weeks. Sagittal sonogram shows placenta (P) extending well onto shelf (straight arrow) in this patient. This shelf was in lower uterine segment and extended transversely across uterine cavity. This was only case with a fetal anomaly; abnormal cerebral tissue (curved arrow) due to anencephaly is seen.

Results

A total of 25 shelves were identified in 24 women who had singleton pregnancies. One patient had two shelves. Gestational age at which the shelves were first identified ranged from 11 to 35 weeks. Four patients had undergone dilatation and curettage of the uterus, and four had had a cesarean delivery. Five additional patients had had an elective abortion but were uncertain if curettage had been performed.

Evaluation of sonographic characteristics of the shelves revealed that length varied from 1 to 9 cm and thickness ranged from 2 to 8 mm. Thickness often varied in different parts of the shelf; the smallest thickness was recorded. In 16 shelves the base was thickened; thickening of the free edge was observed in one case. Part of the placenta was on the shelf in eight cases. The shelf appeared straight in 22 and lax in three cases. Location of the shelf within the uterus was variable. Twelve shelves were in the lower uterine segment, four were in the body, and nine were in the fundus of the uterus.

The shelf had no connection to the fetus and did not restrict fetal motion in any of the 24 pregnancies. In 23 patients, no abnormality of the fetus was seen sonographically; physical examination of these infants at birth was normal. In one of these 23 cases, one fetal hand remained near the shelf throughout the sonographic examination although no connection to the shelf was identified. The fetus was normal at birth. A fetal anomaly was present in one case; a sonogram performed at 16 weeks revealed anencephaly. No connection of the shelf to the fetus was seen. The placenta extended well onto the shelf (Fig. 2). Pathologic examination of the tissue after subsequent therapeutic abortion did not yield a definitive diagnosis.

Ten patients had a follow-up sonogram. In seven patients, the shelf was no longer present; gestational age at the time

of the negative follow-up study ranged from 19 to 41 weeks. The shelf persisted in three patients on follow-up sonograms at 22, 28, and 38 weeks.

Discussion

Within the pregnant uterus, several types of membranes or bands can be present, including those associated with normal chorioamniotic separation in early pregnancy, subchorionic hematoma, relatively large placental lakes, the separating membrane in a multiple gestation, a septated uterus, and the amniotic-band syndrome [1–3]. Membranes produced by the first three of these causes can be distinguished easily from benign shelves by their delineation of a closed space and their lack of a free or unattached edge. None of our patients had a multiple gestation. In a septated uterus, the septum is usually in the fundus and oriented in a sagittal plane. Although the shelf was in the fundus in nine of our cases, it was not thought to be the septum of a duplicated uterus because the orientation of the shelf was significantly different from the sagittal or near-sagittal orientation expected for such a septum. However, if a benign shelf were located in the fundus and oriented in a sagittal plane, it would probably be difficult to differentiate it sonographically from a septum.

Mahony et al. [4] described seven cases of intrauterine sheets of tissue having a free edge. A similar observation was made by Papp et al. [5] in five cases, although it is unclear whether all their bands had a free edge. Randel et al. [1] recently reported their observations in 17 cases of amniotic sheets that were not associated with amniotic-band syndrome and caused no problem for the fetus. The shelves described in this report probably represent this same type of tissue.

The presence of a band or shelf within the amniotic cavity may raise the possibility of amniotic-band syndrome. This

syndrome is a sporadic abnormality, with the fetus usually having multiple malformations in a nonembryologic distribution [4, 6]. The cause of amniotic-band syndrome is unproved, and whether the bands are the cause or the result of the syndrome is debated [7]. A popular theory is that the malformations are caused by mesodermic bands that develop after rupture of the amnion [8]. Our findings agree with those of earlier studies [1, 4]. The mere presence of shelves within the pregnant uterus does not indicate that the amniotic-band syndrome is present nor that it will subsequently develop. Twenty-four of the 25 shelves in this series were definitely benign. In none of these cases did an initially normal fetus subsequently develop amniotic-band syndrome. Furthermore, we believe that the single shelf in our series that was associated with a fetal anomaly was a benign intrauterine shelf and was not a manifestation of amniotic-band syndrome. The shelf did not connect to the cranial abnormality, the fetal defect itself was an unlikely manifestation of amniotic-band syndrome, and no other abnormalities were seen. Also, one would not expect the placenta, as it did in this case, to extend onto a band that was caused by the amniotic-band syndrome. Moreover, in the unlikely chance that the abnormality was due to the amniotic-band syndrome, the fetal abnormality was obvious on the initial sonogram. As normalcy of the fetus is the prime sonographic consideration, it seems prudent to obtain a follow-up sonogram if a shelf is initially identified in the first trimester, before a complete fetal survey can be obtained. During the time of this study, we saw only three cases of amniotic-band syndrome, diagnosed at 22, 23, and 34 weeks. Although bands are not always visible in amniotic-band syndrome [4], bands were seen in these three cases, with direct attachment of the band to the malformed fetus seen in two of the three cases. The malformations were obvious on the initial sonogram. The bands appeared lax in all three cases.

The cause of these shelves of tissue is unproved. The hypothesis that they are due to intrauterine synechiae [1, 4]

is certainly possible. Synechiae are thought to develop in the uterus after mechanical trauma to the endometrium, primarily during the puerperium or after bacterial infection [9, 10]. That only eight (32%) of our patients gave a definite history of dilatation and curettage or cesarean delivery raises doubt about whether synechiae due to mechanical trauma were the cause in our patients. We did not, however, question the patients regarding past myomectomy or endometritis. Perhaps there is more than one cause for these shelves of tissue. A congenital cause of intrauterine synechiae has been suggested, but never confirmed [10].

In the series of Randel et al. [1], thickening of the base was apparently observed in all cases, and the free edge often appeared bulbous. We observed thickening of the base in 16 cases (64%) and a bulbous appearance to the free edge in only one case (4%). In three cases (with initial sonography at 11, 13, and 15 weeks), the amnion was still separate from the shelf (Fig. 3). This finding, along with the observation of placental tissue on the shelf in eight cases, suggests that the shelf was present before the pregnancy began and therefore was not due to a developmental abnormality of the pregnancy. Comparison with hysterosalpingography would be of interest, but none of our patients had that examination.

Demonstration of normal fetal anatomy is the primary criterion for exclusion of amniotic-band syndrome. Among the sonographic characteristics of shelves, the lack of attachment to the fetus suggests benignity. In our past experience with amniotic-band syndrome, the bands were sometimes lax and undulating and usually very thin; we considered whether these might be discriminating factors in differentiating benign shelves from amniotic-band syndrome. In our three recent cases of amniotic-band syndrome, the bands were all lax and thickness of the bands ranged from 2 to 4 mm. Thus, although the bands in amniotic-band syndrome may more often be lax and on the smaller end of the thickness range, laxity and thickness are probably insufficient for differentiation from intrauterine shelves. In our experience, when bands are seen

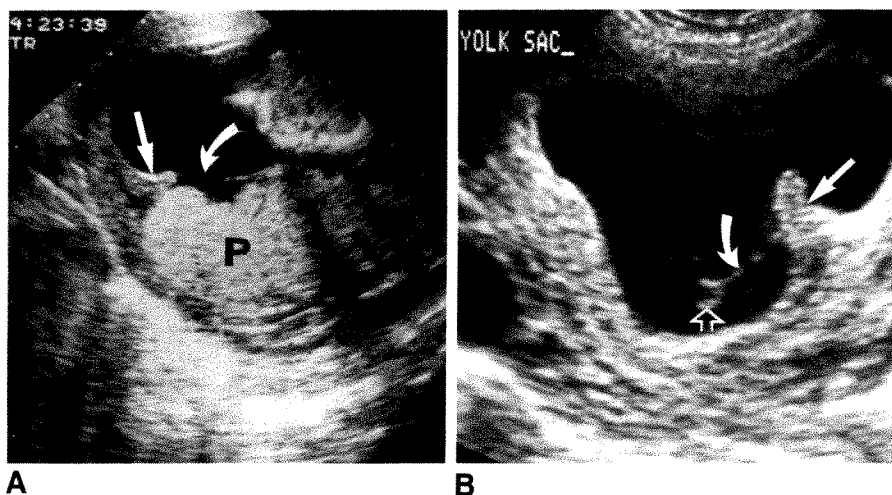


Fig. 3.—Separation of amnion from shelf.

A, Sagittal sonogram of fundus at 15 weeks shows placenta (P) extending to shelf (straight arrow). Amnion (curved arrow) has not yet fused. Maximal length of shelf was 5 cm.

B, Sonogram shows partial separation of amnion (curved arrow) from shelf (straight arrow) in another patient at 11 weeks. Yolk sac (open arrow) also is visible. Maximal length of shelf was 2.5

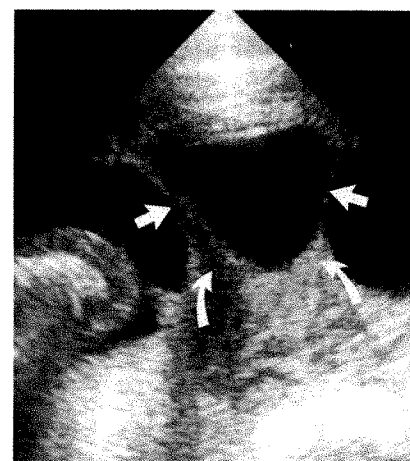


Fig. 4.—Sonogram shows two separate shelves (straight arrows) in body of uterus in this 21-week pregnancy. Note thickening of base (curved arrows) of shelves.

in amniotic-band syndrome, the number of bands is variable, from one to many. In only one of our cases (Fig. 4) was more than one shelf present; multiple benign bands or shelves also were observed by Herbert et al. [3].

In those cases with follow-up sonograms, the shelf often could not be found. As previously speculated, this may be because of rupture or compression of the shelf by the enlarging uterine cavity or fetus [1]. In three cases however, one as late as 38 weeks, the shelf was still present. The force needed to tear adhesions during hysteroscopy seems to be related to the relative amounts of endometrial tissue, fibromuscular tissue, and connective tissue within the synechiae [9]. If these sonographically observed shelves are due to synechiae, perhaps the relative amounts of these tissue components explain why some seem to disappear relatively early and some persist until later in gestation.

In summary, benign shelves of tissue within the pregnant uterus do exist. These shelves have a free edge and do not attach to the fetus. As long as a complete sonographic survey of the fetus can be obtained and reveals no abnormalities, there should be no concern for the subsequent development of amniotic-band syndrome.

REFERENCES

1. Randel SB, Filly RA, Callen PW, Anderson RL, Golbus MS. Amniotic sheets. *Radiology* **1988**;166:633-636
2. Burrows PE, Lyons EA, Phillips HJ, Oates I. Intrauterine membranes: sonographic findings and clinical significance. *J Clin Ultrasound* **1982**; 10:1-8
3. Herbert WNP, Seeds JW, Cefalo RC, Bowes WA. Prenatal detection of intraamniotic bands: implications and management. *Obstet Gynecol* **1985**;65:36S-38S
4. Mahony BS, Filly RA, Callen PW, Golbus MS. The amniotic band syndrome: antenatal sonographic diagnosis and potential pitfalls. *Obstet Gynecol* **1985**;152:63-68
5. Papp Z, Toth Z, Csecsei K, Lindenbaum RH. Are there "innocent" amniotic bands? (letter). *Am J Med Genet* **1986**;24:207-209
6. Romero R, Pilu G, Jeanty P, Ghidini A, Hobbins JC. Prenatal diagnosis of congenital anomalies. Norwalk, CT: Appleton and Lange, **1988**:411-414
7. Lockwood C, Ghidini A, Romero R, Hobbins JC. Amniotic band syndrome: reevaluation of pathogenesis. *Am J Obstet Gynecol* **1989**;160:1030-1033.
8. Torpin R. Fetal malformations caused by amnion rupture during gestation. In: Torpin R, ed. *The human placenta*. Springfield, IL: Charles C Thomas, **1968**:1-76
9. Sugimoto O. *Diagnostic and therapeutic hysteroscopy*. Tokyo: Igaku-Shoin, **1978**:144-158
10. Hunt RB. *Atlas of female infertility surgery*. Chicago: Year Book Medical, **1986**:233-237

Case Report

Sonographic Diagnosis of Omphalocele During 10th Week of Gestation

Douglas L. Brown,^{1,2} Donald S. Emerson,¹ Lee P. Shulman,³ and Sandra A. Carson³

Fetal abdominal wall abnormalities are not usually recognized on sonographic examination until the second or third trimester of pregnancy. With the recent availability of endovaginal transducers, it may be possible to recognize such abnormalities in the first trimester. We report a case of omphalocele diagnosed sonographically during the 10th week of gestation.

Case Report

A 34-year-old, gravida 7, para 1, abortion 5, woman underwent intensive antepartum surveillance because of her history of five spontaneous abortions. She experienced vaginal bleeding 6.5 weeks after her last menstrual period and a sonogram revealed a live intrauterine embryo with a small subchorionic hematoma. Crown-rump length [1] was consistent with age based on last menstrual period.

Weekly sonograms thereafter, all obtained with a 5-MHz endovaginal transducer, showed a decrease in the size of the hematoma. At 10.2 gestational weeks (based on the 6.5-week sonogram) the crown-rump length was 35 mm. During this study, a homogeneous echogenic mass anterior to the fetal abdomen was observed (Fig. 1). Although normally herniated bowel might have accounted for this mass, omphalocele was considered because the circumference of the mass (28 mm) and that of the fetal abdomen (30 mm) were approximately equal. The umbilical cord inserted into the mass. Retrospective review of the previous sonograms obtained at 6, 7.2, 7.3, and 8.8 weeks did not reveal any abnormality.

A sonogram obtained at 14.9 weeks confirmed the diagnosis of omphalocele, with the umbilical cord inserting into the apex of the

mass containing herniated liver and bowel. Amniocentesis was performed at this time and revealed a normal male complement (46, XY) and an amniotic fluid alpha-fetoprotein level within normal limits (2.0 mg%). The patient elected to continue the pregnancy. Sonography at 20 weeks showed no significant change in the omphalocele and no other fetal anomalies.

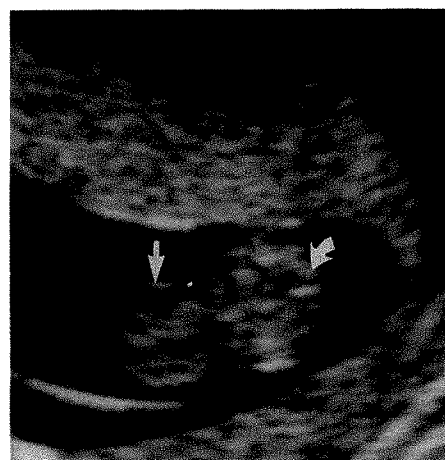


Fig. 1.—Transverse sonogram through fetal abdomen at 10.2 weeks gestational age. Herniated mass of omphalocele (straight arrow) is only slightly smaller than fetal abdomen (curved arrow). Transverse diameters of omphalocele at this level are 8 and 9 mm, and those of abdomen are 9 and 10 mm.

Received February 10, 1989; accepted after revision March 13, 1989.

¹ Department of Radiology, University of Tennessee, Memphis, College of Medicine, 800 Madison Ave., Memphis, TN 38163. Address reprint requests to D. S. Emerson.

² Present address: Department of Radiology, Brigham and Women's Hospital, 75 Francis St., Boston, MA 02115.

³ Department of Obstetrics and Gynecology, University of Tennessee, Memphis, College of Medicine, 800 Madison Ave., Memphis TN 38163.

The patient spontaneously ruptured membranes at 33 weeks gestation. After spontaneous labor, the patient had a vaginal delivery of a 1910-g male with Apgar scores of 4 at 1 min and 9 at 5 min. Examination of the infant revealed a large omphalocele containing bowel, liver, and omentum. In addition, there was postaxial polydactyly of both the right hand and right foot. The extra digits were small and consisted only of soft tissue. No other abnormalities were observed. The first stage of surgical repair was completed 36 hr after birth with no complications.

Discussion

Omphalocele is a surgically correctable malformation that occurs with a frequency of one in 5000 live births [2]. When diagnosed prenatally, it is frequently (73%) associated with other malformations, including cardiovascular, renal, and skeletal anomalies [3]. In addition, over 50% of fetuses with omphalocele have chromosomal abnormalities [3]. The prognosis for isolated omphalocele is excellent; however, cytogenetic or other anatomic abnormalities can worsen fetal outcome [3]. The antenatal detection of omphalocele requires detailed sonographic and cytogenetic evaluation and is necessary for making informed decisions about pregnancy management. First-trimester detection of omphalocele also provides an opportunity to use other diagnostic techniques (e.g., chorionic villus sampling), which could hasten diagnosis of associated abnormalities. However, the ability to detect associated anomalies may be problematic. Specifically, our failure to detect fetal polydactyly, an anomaly not usually associated with omphalocele, illustrates the potential difficulty in detecting certain structural anomalies.

With improving sonographic technology, some anomalies will be recognized during the first trimester. Omphalocele diagnosed as early as 12 weeks of gestation has been reported [2]. The primary problem in diagnosing omphalocele or other abdominal wall defects in the first trimester is not in recognizing the herniated mass, but in distinguishing it from the normal herniation of bowel that occurs during this period. Herniation of the fetal midgut occurs at the beginning of the sixth embryologic week, equivalent to 8 gestational weeks [4]. Classic teaching describes the return of the bowel to the fetal abdomen during the 10th embryologic week (12th ges-

tational week) [4, 5]. Reports differ about when normal bowel herniation is no longer observed sonographically. Cyr et al. [6] believe that reduction of the herniation is complete by 11 gestational weeks. Bowerman et al. [7] observed no herniated midgut after 11.3 gestational weeks. Green and Hobbins [8] report, however, that bowel is still herniated in 20% of fetuses at 12 gestational weeks. The size of the normally herniated bowel has been reported not to exceed 10 mm in one study [6] and 7 mm in greatest diameter in another study [7].

Omphalocele rather than normal bowel herniation into the cord may be suspected when the diameter of the herniation is greater than 7 mm during gestational weeks eight through 12. In our case, the initial suspicion was based on the visual impression that the herniation was too large, because its circumference was approximately equal to that of the abdomen. The presence of liver within the herniated sac, which is sonographically more homogeneous and less echogenic than bowel, provides another clue to the presence of omphalocele [2]. It has been stated that a confident sonographic diagnosis of an anterior abdominal wall defect is possible as early as 12 gestational weeks [7]. However, until more study confirms the gestational age at which physiologic bowel herniation is no longer sonographically identifiable, we believe it is prudent to wait until 14 gestational weeks to confirm the diagnosis [6].

REFERENCES

1. Robinson HP, Fleming JEE. A critical evaluation of sonar "crown-rump length" measurements. *Br J Obstet Gynaecol* 1975;82:702-710
2. Curtis JA, Watson L. Sonographic diagnosis of omphalocele in the first trimester of fetal gestation. *J Ultrasound Med* 1988;7:97-100
3. Gilbert WM, Nicolaides KH. Fetal omphalocele: associated malformations and chromosomal defects. *Obstet Gynecol* 1987;70:633-635
4. Moore KL. *The developing human*, 3rd ed. Philadelphia: Saunders, 1982:239-240
5. Corliss CE. *Patten's human embryology*. New York: McGraw-Hill, 1976: 285-290
6. Cyr DR, Mack LA, Schoenecker SA, et al. Bowel migration in the normal fetus: US detection. *Radiology* 1986;161:119-121
7. Bowerman R, Avila N, Ginsberg H. High resolution sonographic identification of fetal midgut herniation into the umbilical cord: Differentiation from fetal anterior abdominal wall defects. *J Ultrasound Med* 1988;7:Suppl 109
8. Green JJ, Hobbins JC. Abdominal ultrasound examination of the first-trimester fetus. *Am J Obstet Gynecol* 1988;159:165-175

Case Report

Prenatal Sonographic Diagnosis of Harlequin Ichthyosis

Michael Mihalko,¹ Karen K. Lindfors,¹ Arthur W. Grix,² William E. Brant,¹ and John P. McGahan¹

Harlequin ichthyosis is a rare congenital disorder with high perinatal lethality [1]. The skin is thickened and fissured, often dividing into polygonal plaques. It is these plaques, which may resemble the diamond pattern on the costume of the archetypal harlequin (a character in comedy and pantomime with masked face and wooden sword), that are responsible for the name of this disorder. Ectropion (eyelid eversion) and eclabium (eversion of the lips) typically are present. The markedly thickened skin also can produce flexion deformities of the limbs and digital gangrene [2-4]. Most affected neonates die within hours or days after birth. Causes of death include sepsis, mechanical restriction of breathing, and electrolyte imbalance [2]. This abnormality has been diagnosed prenatally by fetoscopy and fetal skin biopsy in two cases with a family history of the disorder [2, 5], but to our knowledge prenatal sonographic diagnosis of harlequin ichthyosis has not been reported. We present such a case and discuss the sonographic findings, with particular reference to differentiation of this anomaly from amniotic bands and sheets.

Case Report

A 35-year-old pregnant woman presented at 28 menstrual weeks in labor after premature rupture of membranes. Sonographic evaluation of the fetus was performed with a 3.5-MHz linear transducer on an Acuson 128 unit (Mountain View, CA). The examination revealed a single fetus in frank breech presentation. The gestational age, based on biparietal diameter, head circumference, abdominal circumference, and femur length, was 28 weeks. The volume of amniotic fluid was normal. A thick discontinuous membrane was floating within

the fluid just anterior to the fetus. The membrane appeared to be fixed to or to arise from the fetal thorax and lower abdominal wall (Fig. 1A). The membrane undulated freely with fetal motion. It did not appear to be continuous with the amnion. The fetal abdominal wall was thickened, but no other evidence of fetal hydrops was seen.

Examination of the fetal face showed bilaterally symmetric cystic masses located anterior to each orbit (Fig. 1B). The fetal scalp was thickened. The fetal limbs were morphologically normal, and their gross movement was unrestricted. The remainder of the survey of fetal anatomy was unremarkable.

Ruptured membranes were confirmed clinically. Findings on amniocentesis were negative for intrauterine infection. Labor could not be controlled, and a cesarean delivery was performed 48 hr after rupture of membranes.

At birth, the infant had characteristics typical of harlequin ichthyosis (Fig. 1C). The skin was thickened and fissured. Ectropion and eclabium were noted. After discussion of the condition and prognosis, the parents elected supportive care only. The infant died 3 hr after birth. Autopsy confirmed the presence of harlequin ichthyosis. No congenital abnormalities of other organ systems were present.

Discussion

Sonographic demonstration of intrauterine membranes implies an established set of diagnostic possibilities. Some, such as amniotic sheets and first trimester chorioamniotic separation, are benign, but others, such as amniotic band syndrome and subchorionic hemorrhage, can be associated with a poor fetal outcome [6-8]. With this case, another possibility is added to the differential diagnosis of intrauterine membranes associated with a poor outcome.

Received March 15, 1989; accepted after revision April 21, 1989.

¹ Department of Radiology, University of California, Davis, Medical Center, Sacramento, CA 95817. Address reprint requests to K. K. Lindfors, [RESEARCH] FOLB II-D.

² Department of Pediatrics, University of California, Davis, Medical Center, Sacramento, CA 95817.

AJR 153:827-828, October 1989 0361-803X/89/1534-0827 © American Roentgen Ray Society

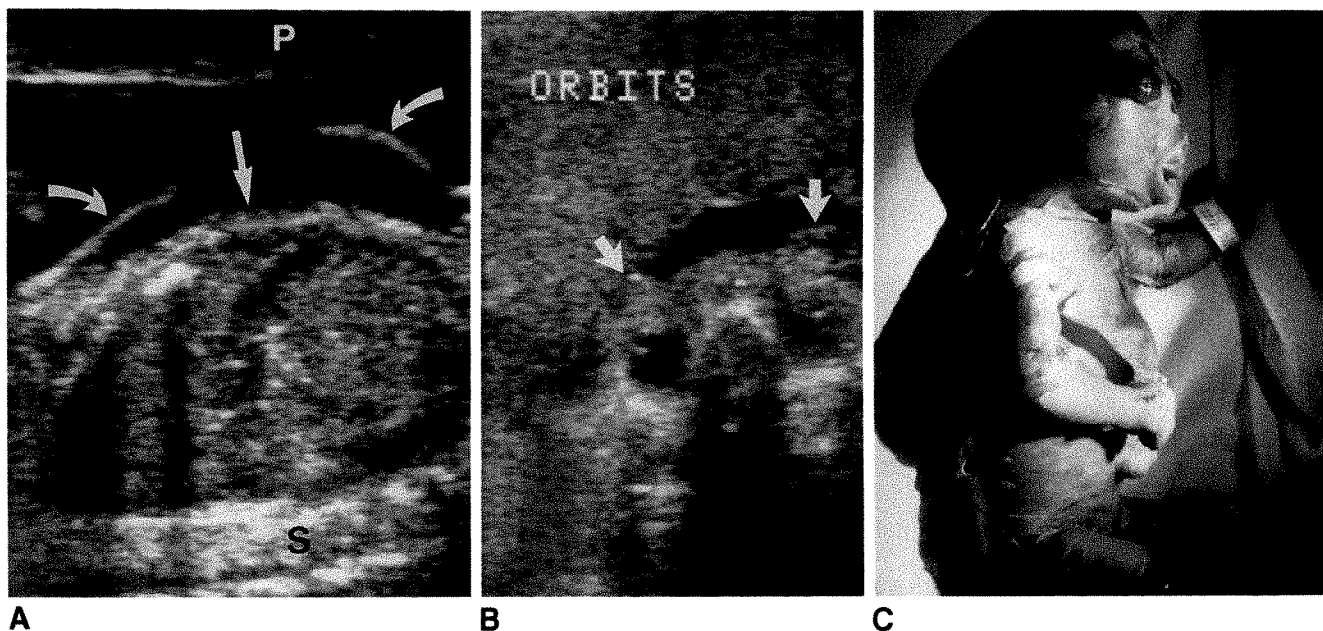


Fig. 1.—Harlequin ichthyosis.
A, Longitudinal sonogram of fetal chest and abdomen with fetal head to left shows thickened abdominal wall (straight arrow) and anterior membrane (curved arrows). P = placenta, S = fetal spine.
B, Semicoronal sonogram through fetal orbits shows hypoechoic mass anterior to each globe (arrows).
C, Autopsy specimen shows ectropion, which produces a mass overlying each orbit. Note also flap of sloughed skin anterior to abdomen.

In this case, the membrane arising from the anterior fetal body was sloughed, abnormally thickened skin. This membrane was distinct from the continuous membrane typical of subchorionic hemorrhage [8]. It also was distinct from an amniotic sheet, which is not fixed to the fetus and has a bulbous free edge [6]. Unlike the amniotic band, we saw no evidence that this membrane arose from a disrupted amnion [7]. However, as with an amniotic band, the membrane in this case was attached to the fetus [7].

In such cases, to avoid confusion with amniotic bands, the sonographer should search for the other anomalies associated with harlequin ichthyosis. These include cystic protuberances over the orbits or absence of normal lips, which indicate ectropion and eclabium, respectively. The abnormally thickened fetal skin, in the absence of hydrops, also should aid in the prenatal diagnosis of harlequin ichthyosis.

This case indicates that prenatal sonography can establish the diagnosis of harlequin ichthyosis in the early third trimester. Survival of neonates with this condition has been reported [1]. However, the intensive treatment appears to necessitate a tertiary level of hospital care with consultants available who are familiar with the condition. It remains to be seen whether the diagnosis can be established sonographically early enough to offer the parents other therapeutic options. Diag-

nosis necessitates genetic counseling, because autosomal recessive transmission has been established [1].

ACKNOWLEDGMENT

Special thanks to Lou McHugh for assistance in manuscript preparation.

REFERENCES

1. Lawlor F. Harlequin baby: inheritance and prognosis. *Br J Dermatol* 1987;117:528
2. Elias S, Mazur M, Sabbagha K, Esterly NB, Simpson JL. Prenatal diagnosis of harlequin ichthyosis. *Clin Genet* 1980;17:275-280
3. Kouskoukis C, Minas A, Tousimis D. Ichthyosis congenital fetalis (harlequin fetus). *Int J Dermatol* 1982;21:347-348
4. Lawlor F, Peiris S. Harlequin fetus successfully treated with etretinate. *Br J Dermatol* 1985;112:585-590
5. Arnold ML, Anton-Lamprecht I. Prenatal diagnosis of epidermal disorders. *Current Probl Dermatol* 1987;16:120-128
6. Randel SB, Filly RA, Callen PW, Anderson RL, Golbus MS. Amniotic sheets. *Radiology* 1988;166:633-636
7. Mahony B, Filly RA, Callen PW, Golbus MS. The amniotic band syndrome: antenatal sonographic diagnosis and potential pitfalls. *Am J Obstet Gynecol* 1985;152:63-68
8. Sauerbei EE, Pham DH. Placental abruption and subchorionic hemorrhage in the first half of pregnancy: US appearance and clinical outcome. *Radiology* 1986;160:109-112

The Cerebellum in Sagittal Plane—Anatomic-MR Correlation:

1. The Vermis

Eric Courchesne¹
 Gary A. Press²
 James Murakami¹
 Dean Berthoty²
 Marjorie Grafe³
 Clayton A. Wiley³
 John R. Hesselink²

Correlation of thin (5-mm) sagittal high-field (1.5-T) MR images of three brain specimens and 11 normal volunteers with microtome sections of the human cerebellar vermis and hemispheres demonstrates that proton-density-weighted (long TR/short TE) and T2-weighted (long TR/long TE) spin-echo pulse sequences provide the greatest contrast between gray and white matter. These images also can display (1) the corpus medullare and primary white-matter branches to the vermician lobules, including the lingula, centralis, culmen, declive, folium, tuber, pyramis, uvula, and nodulus; and (2) several finer secondary branches to individual folia within the lobules. Surface features of the vermis including the deeper fissures (e.g., preculminate, primary, horizontal, and prepymidal) and shallower sulci are best delineated by T1-weighted (short TR/short TE) and T2-weighted images, which provide greatest contrast between CSF and parenchyma. Given that the width of the normal vermis varied from 6 to 12 mm in our volunteers, the acquisition of thin slices (≤ 5 mm) was required to minimize volume averaging of the cerebellar hemispheres with the vermis on a midline sagittal MR section.

Knowledge of the detailed normal anatomy of the cerebellar vermis on sagittal MR images can assist in the identification of various pathologic alterations.

Previous reports provided initial descriptions of normal and pathologic anatomy of the posterior fossa contents at low [1–3], moderate [4, 5], and high [6–9] MR field strengths. Compared with high-resolution CT, MR imaging demonstrates more detailed anatomy of the brainstem, cerebellopontine angles, and internal auditory canals due to its multiplanar imaging capability, absence of beam-hardening artifacts, and greater intrinsic soft-tissue contrast [9].

Although descriptions of the MR appearance of congenital and acquired abnormalities of the cerebellum are included in several reports [2, 4, 10–15], improvements in MR technology including thin (3- to 5-mm) sections, special flow-compensating spin-echo pulse sequences, and cardiac gating now permit display of normal anatomic features of the cerebellum not shown previously. Thus, it seems useful to determine the MR resolution of the cerebellar lobes, lobules, fissures, and related posterior fossa structures by correlating MR with myelin-stained sections of the human cerebellum. Application of these normative data to cerebellar abnormalities, particularly congenital malformations, will be the subject of a separate report.

Materials, Subjects, and Methods

MR studies of three formalin-fixed cadaver brains and 11 normal, healthy adult volunteers, 10 males and one female 13–38 years old (mean age, 24.5 years), were performed in three orthogonal planes by using a 1.5-T superconducting magnet.* All volunteers and specimens were imaged with a standard head coil. In all instances, 5-mm slices with a field of view (FOV) of 12–18 cm and matrix size of 256×256 were acquired using spin-echo sequences. T1-weighted sequences had the parameters, 600/20/4–6 (TR/TE/excitations). All volunteers

This article appears in the July/August 1989 issue of *AJNR* and the October 1989 issue of *AJR*.

Received August 12, 1988; revision requested November 1, 1988; revision received November 25, 1988; accepted December 7, 1988.

This work was supported by National Institute of Neurological Diseases and Stroke grant 5-R01-NS19855 awarded to E. Courchesne.

¹ The Neuropsychology Research Laboratory, Children's Hospital Research Center, San Diego, CA 92123.

² Department of Radiology and Magnetic Resonance Institute, University of California, San Diego, School of Medicine, 225 Dickinson St., San Diego, CA 92103-1990. Address reprint requests to G. A. Press.

³ Department of Pathology, University of California, San Diego, School of Medicine, San Diego, CA 92103-1990.

AJR 153:829–835, October 1989

0361–803X/89/1534–0829

© American Roentgen Ray Society

* General Electric, Milwaukee, WI.

received long TR examinations that were cardiac gated to every other or every third heartbeat. The pulse sequence parameters (2400–3800/20,70/2–4) yielded proton-density- and T2-weighted images, respectively. A presaturation RF pulse for eliminating blood-flow artifacts along the Z axis (flow void=1) was also used. Nongated long TR sequences performed on cadaver brains had the parameters, 1800–3000/20,70/4. Slices obtained in all sequences were separated by a 2.5-mm gap. A 28-sec T1-weighted scout sequence (200/20/1, 24-cm FOV, and 256 × 128 matrix) in the axial and sagittal plane was used to verify precise positioning of the subject or specimen brain prior to performing the protocol sequences.

Before MR, the specimen brains were fixed for 2–4 weeks in 10% neutral-buffered formalin. After MR, the cerebellum and brainstem were separated from the cerebral hemispheres and sectioned in the sagittal plane at a thickness of 5 mm. The tissue blocks were dehydrated in a graded series of alcohols, cleared in xylene, and embedded in paraffin. Sagittal microtome sections of the cerebellum and brainstem were cut at a thickness of 15 μ m by using a Multirange Microtome.[†] Adjacent anatomic sections corresponding closely to the MR sections obtained by our protocol were stained with hematoxylin and eosin and Luxol fast blue–cresyl violet. The normal anatomic features of the cerebellar vermis and hemispheres visualized on MR and on the corresponding anatomic sections were determined by comparison with standard references of neuroanatomy [16, 17], myelin-stained cerebellar sections [18, 19], and cerebellar embryogenesis and development [20–23].

Many systems of nomenclature have been used to describe the normal anatomy of mammalian and human cerebellums [18, 21, 24]. In this report we follow closely the terminologies chosen by Ito [21] and Larsell [24].

Results

Anatomic Features of the Vermis on a Sagittal Microtome Section

The vermis represents the median segment of the cerebellum that is separated from each of the hemispheres by a shallow surface indentation, the paramedian sulcus. On a midline sagittal section (Fig. 1A), the ventral surface of the vermis is separated from the brainstem by three CSF-filled spaces that are oriented vertically [18, 25]. Superiorly, the precentral fissure separates the vermis from the inferior colliculi of the quadrigeminal plate. In the middle, the fourth ventricle separates the vermis from the dorsal surface of the pons and upper medulla. Inferiorly, the vallecule separates the vermis from the inferior medulla. Posteriorly, the cisterna magna separates the vermis from the meninges overlying the inner table of the occipital bone.

Lobar and lobular divisions.—The transverse-oriented primary and posterolateral fissures divide the vermis and cerebellar hemispheres into three major components: the anterior, posterior, and flocculonodular lobes [21] (Table 1). Two important nomenclatures are in common use for the designation of the lobules of the vermis. In one system, the vermis is divided into an anterior lobe containing three lobules (lingula, centralis, and culmen); a posterior lobe with five lobules (declive, folium vermis, tuber vermis, pyramis, and uvula); and

one additional lobule, the nodulus or vermian portion of the flocculonodular lobe [21]. Although these names of the lobules continue to appear in the anatomic literature, another nomenclature widely used in physiologic studies of the cerebellum applies Roman numerals to 10 lobules in the vermis and lateral expansions in the hemispheres [24]. The two nomenclatures are listed in Table 1. In this report the Roman numeral designations are used only when necessary for clarity.

The lobules of the anterior vermis are bounded by the superior medullary velum anteriorly and the primary fissure posteriorly. The precentral fissure separates the lingula and centralis, while the preculminate fissure separates the centralis and culmen (Fig. 1A).

The lobules of the posterior vermis are bounded by the primary fissure (which separates them from the anterior lobe) and the posterolateral fissure (which separates them from the nodulus). Several fissures within the posterior vermis separate its five lobules from one another: the superior posterior fissure separates the declive and folium vermis, the horizontal fissure separates the folium vermis and tuber vermis, the prepyramidal fissure separates the tuber vermis and pyramis, and the secondary fissure separates the pyramis and uvula (Fig. 1A).

The nodulus is a separate lobe of the vermis that contains only one lobule. It represents the vermian portion of the flocculonodular lobe of the cerebellum and is bounded posteriorly by the posterolateral fissure and anteriorly by the vallecule (Fig. 1A).

Sublobular and foliate divisions.—Each lobule of the vermis can be subdivided into one or more sublobules, each containing a variable number of folia. The folium represents the basic structural unit of the cerebellum seen at gross examination and resolved by MR. Each folium is a thin, transverse-oriented fold of cerebellar parenchyma that contains a core of white matter covered by a mantle of gray matter. The unfolded surface of a single folium is a few millimeters wide. The human vermis contains approximately 260 of these structural units [21].

Organization of the white matter.—The white matter of the vermis appears to radiate into the lobules from a central confluence, known as the corpus medullare. The corpus medullare lies posterior to the fourth ventricle (Fig. 1A). Depending on the lobule in which they are located, the white-matter cores of the individual folia of the vermis may represent second-, third-, or even higher-order branches of the white matter emanating from the corpus medullare. To facilitate description, the white-matter tracts that originate from the corpus medullare may be grouped into two major divisions. The anterior division innervates the anterior lobe (lingula, centralis, and culmen) while the posterior division connects with the posterior lobe (declive, folium vermis, tuber vermis, pyramis, and uvula), as well as the nodulus.

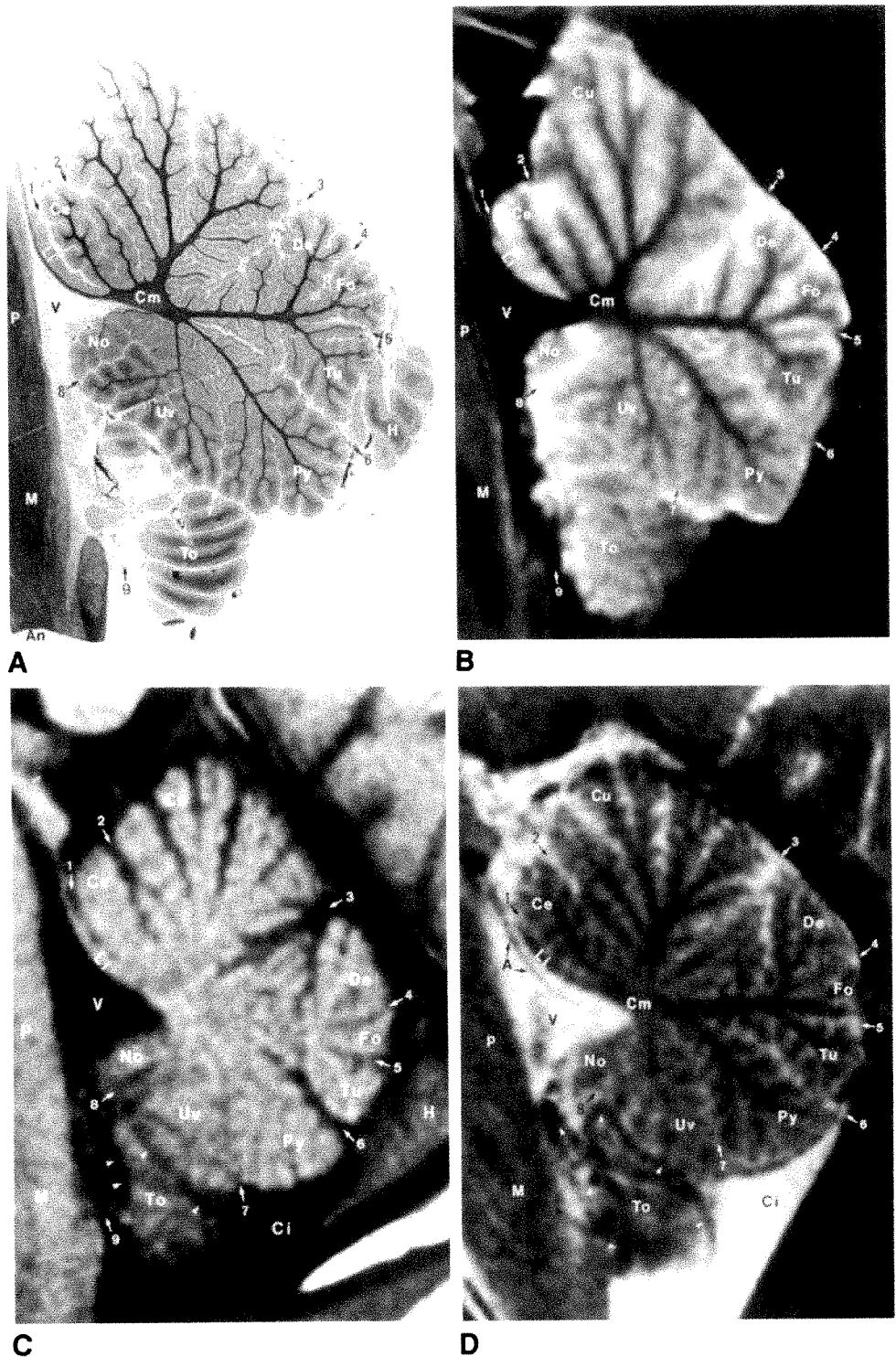
Numerous anatomic variations have been described in the second-, third- and higher-order white-matter branches within the vermis (reviewed in [26]). To avoid confusion, we will emphasize only a description of the branching pattern of the primary white-matter tracts originating from the corpus medullare; this branching pattern was nearly constant in our series of specimen brains and normal volunteers.

[†] LKB, Stockholm, Sweden.

Fig. 1.—Midsagittal sections through cerebellar vermis and brainstem. Sections through vermis must be thin (≤ 5 mm) to minimize volume averaging of adjacent cerebellar hemispheres (H) and tonsils (To).

A and B, Microtome section of specimen brain (Luxol fast blue–cresyl violet myelin stain) (A) and corresponding proton-density-weighted 1.5-T MR image, 3000/20, before sectioning (B). White-matter branching within vermis is seen with remarkable fidelity on MR. Anterior division of white matter of corpus medullare (Cm) innervates lingula (Li), centralis (Ce), and culmen (Cu) of anterior lobe of vermis. Posterior division innervates declive (De), folium vermis (Fo), tuber vermis (Tu), pyramis (Py), and uvula (Uv) of posterior lobe as well as nodule (No) of flocculonodular lobe of cerebellum. Fine secondary and tertiary white-matter branches to some regions (Uv) are shown well. An = anterior aspect of section; P = pons; M = medulla.

C and D, T1-weighted, 600/20 (C), and cardiac-gated T2-weighted 3642/70 (D), images of 38-year-old male volunteer best show surface landmarks of vermis by accentuating signal-intensity difference between cerebellar parenchyma and CSF. Precentral cerebellar (1), preculminate (2), primary (3), superior posterior (4), horizontal (5), prepyramidal (6), secondary (7), and posterolateral (8) fissures around periphery of vermis are readily identified. Valleculla (9) separates vermis from inferior medulla (M), whereas cisterna magna (Ci) separates it from meninges overlying occipital bone. Curvilinear CSF flow artifact (A) may be identified within fourth ventricle (V) anterior to lingula on T2-weighted image. (Absence of curvilinear structure on T1-weighted image confirms its artifactual nature.) T2-weighted image also shows well pattern of white-matter branching within vermis (compare with A and B). Flow void within posterior inferior cerebellar arteries (arrowheads) is seen posterior to medulla in normal volunteer.



1. Anterior division. In the most common arrangement, the lingula is situated along the ventral bank of the precentral fissure and receives a single primary tract from the corpus medullare. This single tract ascends adjacent to the dorsal aspect of the superior medullary velum. Each of our specimen brains (Fig. 1A) and normal volunteers demonstrated this anatomy. Others have reported that the lingula may include

an additional segment between the ventral bank and the lobule centralis, "lingula duplex" [26], receiving an additional primary tract directly from the corpus medullare. This finding was not seen in our series.

The centralis receives one primary tract from the corpus medullare. The culmen also receives a single primary tract from which one or two secondary branches ascend into the

TABLE 1: Components of the Human Cerebellum

Cerebellar Lobe	Vermian Lobule Nomenclature		Hemispheric Lobule Nomenclature	
	Ito [21]	Larsell [24]	Ito [21]	Larsell [24]
Anterior	Lingula	I	—	HI ^a
	Centralis	II, III	Central lobule	III, HIII
	Culmen	IV, V	Quadrangular lobule, anterior portion	HIV, HV
Posterior	Declive	VI	Quadrangular lobule, posterior portion	HVI
	Folium vermis	Superior VIIA	Semilunar lobule, superior portion	HVIIA
	Tuber vermis	Inferior VIIA	Semilunar lobule, inferior portion	HVIIA
		VIIIB	Gracile lobule	HVIIIB
	Pyramis	VIIIA, VIIIB	Biventer	HVIII
	Uvula	IX	Tonsil	HIX
Flocculonodular	Nodulus	X	Flocculus	HX

^a Hemispheric counterpart of vermician lobule I is usually absent in humans [21].

anterior portion of the lobule (lobule IV), and three secondary branches supply the posterior portion of the lobule (lobule V).

2. Posterior division. A single primary tract of the corpus medullare gives rise to several (usually two to four) secondary branches to the declive (lobule VI) and a single secondary branch each to the folium and tuber vermis (combined lobules VIIA and VIIB) (Fig. 1A).

The major white-matter bundle supplying the pyramis may arise either as a primary tract directly from the corpus medullare (Fig. 1A) or as a large secondary branch of the primary tract that innervates also the declive and folium and tuber vermis [26].

Single primary white-matter tracts innervate the uvula and the nodulus along the inferior and antero-inferior surfaces of the vermis. The primary tract to the uvula subsequently splits into two secondary branches, which supply the entire lobule (Fig. 1A).

Overview of MR Imaging of the Vermis

Early in our experience we noted that skull-surface landmarks were unreliable for positioning subjects and anatomic specimens for true sagittal images of the vermis. The small (6- to 12-mm) lateral dimension of the vermis, and its shorter anteroposterior dimension relative to that of the cerebellar hemispheres, can easily result in volume averaging of the hemispheres with the vermis if a tilt of the head remains. We obtained T1-weighted scout images in both the axial and sagittal planes to verify adequate head positioning in all subjects and anatomic specimens. The subsequent acquisition of thin (5-mm) sagittal sections using the protocol sequences provided optimal visualization of the vermis on the midline image.

Spin-echo pulse sequences that maximized the contrast between parenchyma and CSF showed the surface sulci and fissures of the cerebellum to best advantage. T1-weighted images (CSF much lower in signal intensity than parenchyma, Fig. 1C) or T2-weighted images (CSF much higher in signal

intensity than parenchyma, Fig. 1D) were ideal for demonstrating the surface features of the cerebellum in vivo.

Excellent contrast between white and gray matter was obtained with proton-density-weighted (Fig. 1B) and T2-weighted (Fig. 1D) pulse sequences. Such images showed best the deeper anatomy of the vermis including the primary white-matter fiber tracts radiating from the corpus medullare to the individual lobules of the cerebellum. CSF in vivo, or fluid in the subarachnoid space in the postmortem state, was nearly isointense relative to the cortex on proton-density-weighted images, however, thereby obscuring the surface features (sulci and fissures) of the cerebellum.

Superior image quality on the long TR sequence required cardiac gating (every second or every third heartbeat) and a presaturation RF pulse (flow void-1) to further decrease artifacts due to CSF motion in the prepontine cistern and blood flow in the basilar artery and transverse and sigmoid sinuses. Images of eight to 10 5-mm-thick slices could be acquired in a single acquisition (scanning time, 30 or 60 min) using two or four excitations. A 2.5-mm interslice gap was chosen so that the entire cerebellum could be surveyed in the axial or coronal plane, whereas approximately 50% could be examined in the sagittal plane during a single acquisition.

Anatomic Features of the Vermis on Sagittal MR Sections

Surface features.—The cerebellar vermis lies in the midline posterior to the brainstem. The quadrigeminal plate cistern merges inferiorly with the precentral fissure separating the vermis from the midbrain and superior medullary velum (Figs. 1C and 1D). The superior and inferior medullary vela meet at a sharp point called the fastigium to form the roof of the triangular fourth ventricle, which lies between the vermis and the pons. The inferior medullary velum is diaphanous and typically is not resolved on 5-mm-thick images.

Because the great fissures and smaller sulci of the vermis are oriented perpendicular to the midline, sagittal T1-weighted (Fig. 1C) and T2-weighted (Fig. 1D) images display most

accurately the depth of these important surface landmarks. The preculminate, prepymidal, and primary fissures are relatively wide and may be seen easily on MR in normal volunteers. The horizontal and secondary fissures are thinner and more difficult to resolve. Nevertheless, they can be identified confidently in most subjects on T1- and T2-weighted images. The CSF spaces lying between the individual folia of the vermis are shallow and thin. Generally speaking, they can be resolved over the centralis, culmen, declive, folium vermis, tuber vermis, and pyramis, but may be obscured over the lingula, uvula, and nodulus. They are often best seen on T2-weighted images (Fig. 1D).

The cerebellar tonsils have an intimate relationship with the vermis [27]. The tonsils are bilateral, oval-shaped masses of tissue that lie close to the midline. Along their lateral margins they attach to the inferomedial aspects of the cerebellar hemispheres. The other surfaces of each tonsil abut on fissures and cisterns that separate them from the cerebellum, vermis, and brainstem. Several inferior vermicular lobules (nodulus, uvula, and pyramis) are indented to a variable degree by the superior aspects of the tonsils in normal subjects. Moreover, the inferior portions of the tonsils lie within the cisterna magna, and may touch each other in the midline immediately caudal to the vermis. For these reasons, the tonsils can be difficult to distinguish from the nodulus, uvula, and pyramis on midline sagittal images. Helpful clues to identifying a tonsil include its defined ovoid contour, the orientation of its axis parallel to the posterior surface of the medulla, its more sharply convex lower border with greater caudal extent, and the position of the choroid plexus and supratonsillar segment of the posterior inferior cerebellar artery atop the apex of the ovoid [25].

Deep features.—On proton-density-weighted (Fig. 1B) and T2-weighted (Fig. 1D) images, the gray matter overlying the folia of the vermis forms a bright band that is thicker where the surfaces of two lobules are immediately adjacent in the depths of the fissures. The sparse and relatively dark white matter located centrally appears to project radially into the anterior and posterior lobes of the vermis from a small zone just posterior to the fastigium. Sagittal sections through the paramidline hemispheres can be distinguished from those through the vermis due to the greater abundance of white matter, which forms a much larger central body within the hemispheres [27]. Moreover, the gray and white matter of the tonsils, arranged in a regular "hatch-mark" fashion at a 45-90° angle to the posterior surface of the medulla [25], can also be distinguished from the radial arrangement of the vermicular white-matter bundles [27].

Each of the six or seven primary tracts that constitute the anterior and posterior divisions of the vermicular white matter can be distinguished on proton-density-weighted or T2-weighted (Fig. 1D) images *in vivo*. Secondary branches innervating lobules IV and V of the culmen, the declive, and the folium and tuber vermis are also readily detected. In some instances, the tonsils indent the inferior vermis sufficiently to obscure independent visualization of the two secondary white-matter branches within the uvula.

Visualization of the individual white-matter cores distinct

from overlying gray matter of each *folium* of the vermis seems beyond the capability of our *in vivo* MR protocol at present. Nevertheless, proton-density- and T2-weighted images acquired with the specimen brain protocol (four excitations per slice) frequently can resolve many of these most slender white-matter bundles (Fig. 1B).

Discussion

Functional Anatomy and Connections of the Vermis

Somatic motor (midline musculature) and vestibuloocular activities are regulated and coordinated by the vermicular cortex [21, 28]. Cortical (Purkinje) neurons project to the fastigial nuclei, which in turn project to reticular and vestibular neurons of the brainstem. Subsequent ascending pathways controlled by Purkinje cells within the declive, folium, and tuber influence brainstem nuclei governing ocular movements (e.g., oculomotor nucleus); descending (reticulo- and vestibulospinal) pathways controlled by other regions of vermicular cortex reach anterior horn cells of the spinal cord. Cortex of the vermis also influences neural pathways concerned with level of attention [16, 28], sensory function [29], corticostriatal interactions (Ryan LJ, personal communication), autonomic activities [30], motivation [31, 32], memory [33, 34], and behavior [31, 32, 35].

Such functional diversity is reflected in regional specialization of the vermis [28]. For instance, the anterior lobe receives mainly spinal input (from spino- and cuneocerebellar fibers) and relatively little cerebral cortical input. Efferent fibers from the anterior lobe are sent primarily to lower brainstem systems. The posterior lobe receives major input from cerebral cortex (motor, somatosensory, visual, auditory, and association areas), tectum, and hippocampus, but sparse spinal input. Efferents from the posterior lobe connect with the midbrain, thalamus, and hypothalamus, as well as lower brainstem systems [28]. Specialization is epitomized by the declive, folium, and tuber—the auditory and visual areas of the vermis—which are critical for establishing certain types of long-term memory traces [34].

Lesions of the vermis generally result in disorders of eye movements (e.g., horizontal nystagmus), abnormal posture of the head, disturbances of stance and gait, dysmetria, succession deficits, and kinetic tremor [28]. Impairments in memory and consciousness, dysarthria, and past-pointing occur less often [28].

Development Variants

Hypoplasia (undergrowth) and partial or complete agenesis (nongrowth) of the vermis have been reported [36-38]. Although most cases are sporadic, familial agenesis may occur [38]. In all instances of partial agenesis, the anterosuperior portion of the vermis is preserved, presumably because fusion of the vermis proceeds from rostral to caudal during the second month of gestation [27].

The clinical picture of patients with partial or complete agenesis of the vermis is neither uniform nor characteristic

[36]. Although inability to walk, nystagmus, head- and body-turning attacks, and mental retardation are associated frequently with partial vermian agenesis, a minority of patients may be completely asymptomatic [36, 38, 39]. In one sibship, agenesis of the vermis varied from partial to complete; all four patients had mental retardation and developmental delay. Additional abnormalities included hypotonia, episodic hyperpnea, lack of interest in the environment, involuntary facial movements, and abnormal speech and language development [38]. Occasionally, however, psychomotor retardation and neurologic deficits may be absent, even in patients with complete agenesis [36, 38]. Agenesis of the vermis may be accompanied by few or no other CNS abnormalities, or by a spectrum of malformations involving the cerebellar hemispheres and dentate nucleus (e.g., hypoplasia and gray-matter heterotopias) or supratentorial structures (e.g., callosal hypoplasia or agenesis) [36–38]. Symptoms, when present in these patients, may relate to the extravermian locus of abnormality [36, 38].

Hypoplasia of the vermis may be regionally localized (e.g., superoposterior vermis in autism) [40, 41] or diffuse (e.g., Down syndrome) [42]. There are no reports of hypoplasia involving only anterosuperior vermian regions. In all reported cases, vermian hypoplasia is accompanied also by hypoplasia of the cerebellar hemispheres [40, 41, 43, 44].

Atrophic Conditions

After normal development, the vermis may be affected by metabolic or degenerative disorders associated with parenchymal atrophy [45]. In contrast to the developmental anomalies described above, which spare the anterosuperior lobules of the vermis, several common atrophic conditions involve predominantly this portion of vermian cortex. For instance, selective atrophy, most marked in the cortex of the anterior and superior lobules of the vermis and in the paramedian portions of the anterior lobes of the hemispheres, is frequently found in chronic alcoholics [45]. The cortical atrophy is evidenced by wide, deep sulci and thinned folia. Strikingly similar clinical and pathologic findings are demonstrated also in parenchymatous cerebellar atrophy of Holmes, a relatively common degenerative disorder of the cerebellar system [45]. Other degenerative disorders of the cerebellum involve the cerebellar hemispheres to a greater degree than the vermis (e.g., olivopontocerebellar atrophy).

Conclusions

Improvements in MR technology permit the display of many important features of the cerebellar vermis not previously shown. Learning the detailed normal sagittal anatomy of the vermis has helped us to recognize and differentiate the pathologic alterations known to accompany malformations (e.g., hypoplasia and agenesis); genetic (e.g., Down syndrome) and idiopathic (e.g., autism) disorders; metabolic diseases (e.g., alcoholism); and system degenerations (e.g., parenchymatous cerebellar atrophy). Clinical symptomatology may vary depending on the lobules within the vermis that are affected as

well as the time and type of insult. Heretofore, it has not been possible to link with precision active neurologic signs, symptoms, and type of insult to lesion status and extent in vivo. The present MR report opens up this possibility.

REFERENCES

- Han JS, Bonstelle CT, Kaufman B, et al. Magnetic resonance imaging in the evaluation of the brainstem. *Radiology* 1984;150:705–712
- Bradley WG Jr, Waluch V, Yadley RA, Wycoff RR. Comparison of CT and MR in 400 patients with suspected disease of the brain and cervical spinal cord. *Radiology* 1984;152:695–702
- Randell CP, Collins AG, Young IR, et al. Nuclear magnetic resonance imaging of posterior fossa tumors. *AJR* 1983;141:489–496
- Lee BCP, Kneeland JB, Deck MDF, Cahill PT. Posterior fossa lesions: magnetic resonance imaging. *Radiology* 1984;153:137–143
- New PFJ, Bachow TB, Wismar GL, Rosen BR, Brady TJ. MR imaging of the acoustic nerves and small acoustic neuromas at 0.6 T: prospective study. *AJNR* 1985;6:165–170
- Daniels DL, Millen SJ, Meyer GA, et al. MR detection of tumor in the internal auditory canal. *AJNR* 1987;8:249–252
- Gentry LR, Jacoby CG, Turski PA, et al. Cerebellopontine angle-petromastoid mass lesions: comparative study of diagnosis with MR imaging and CT. *Radiology* 1987;162:513–520
- Enzmann DR, O'Donohue J. Optimizing MR imaging for detecting small tumors in the cerebellopontine angle and internal auditory canal. *AJNR* 1987;8:99–106
- Press GA, Hesselink JR. MR imaging of cerebellopontine angle and internal auditory canal lesions at 1.5 T. *AJNR* 1988;9:241–251
- Spinos E, Laster DW, Moody MD, Ball MR, Witcofski RL, Kelly DL Jr. MR evaluation of Chiari I malformations at 0.15 T. *AJNR* 1985;6:203–208
- Lee BCP, Deck MDF, Kneeland JB, Cahill PT. MR imaging of the cranio-cervical junction. *AJNR* 1985;6:209–213
- Barkovich AJ, Wippold FJ, Sherman JL, Citrin CM. Significance of cerebellar tonsillar position on MR. *AJNR* 1986;7:795–799
- Wolpert SM, Anderson M, Scott RM, Kwan ESK, Runge VM. Chiari II malformation: MR imaging evaluation. *AJNR* 1987;8:783–792
- Naidich TP, Zimmerman RA. Common congenital malformations of the brain. In: Brant-Zawadzki M, Norman D, eds. *Magnetic resonance imaging of the central nervous system*. New York: Raven, 1987:131–150
- van der Knaap MS, Valk J. Classification of congenital abnormalities of the CNS. *AJNR* 1988;9:315–326
- Nieuwenhuys R, Voogd J, Huijzen C. *The human central nervous system: a synopsis and atlas*, 2nd ed. New York: Springer-Verlag, 1981
- Carpenter MB. *Human neuroanatomy*, 7th ed. Baltimore: Williams & Wilkins, 1976
- Angvine JB Jr, Mancall EL, Yakovlev PI. *The human cerebellum. An atlas of gross topography in serial sections*. Boston: Little, Brown, 1961
- DeArmond SJ, Fusco MM, Dewey MM. *Structure of the human brain: a photographic atlas*. New York: Oxford University, 1976
- Fox CA, Snider RS, eds. *The cerebellum*. Amsterdam: Elsevier, 1967
- Ito M. *The cerebellum and neural control*. New York: Raven, 1984
- Lemire RJ, Loeser JD, Leech RW, Alvord EC Jr. *Normal and abnormal development of the human nervous system*. Hagerstown, MD: Harper & Row, 1975
- Larsell O. The development of the cerebellum in man in relation to its comparative anatomy. *J Comp Neurol* 1947;87:85–129
- Larsell O. The cerebellum. A review and interpretation. *Arch Neurol Psychiatry* 1937;38:580–607
- Yousefzadeh DK, Naidich TP. US anatomy of the posterior fossa in children: correlation with brain sections. *Radiology* 1985;156:353–361
- Larsell O, Jansen J. *The comparative anatomy and histology of the cerebellum*, vol. 3. *The human cerebellum, cerebellar connections and cerebellar cortex*. Minneapolis: University of Minnesota, 1972
- Press GA, Murakami J, Courchesne E, et al. The cerebellum in sagittal plane—atomic-MR correlation: 2. The cerebellar hemispheres. *AJNR* 1989;10:667–676
- Gilman S, Bloedel J, Lechtenberg R. *Disorders of the cerebellum*. Philadelphia: Davis, 1981

29. Crispino L, Bullock TH. Cerebellum mediates modality-specific modulation of sensory responses of midbrain and forebrain in rat. *Proc. Natl. Acad. Sci USA* **1984**;81:2917-2920
30. Haines DE, Dietrichs E. On the organization of interconnections between the cerebellum and hypothalamus. In: King JS, ed. *New concepts in cerebellar neurobiology*, vol. 12. New York: Liss, **1987**:113-149
31. Supple WF, Leaton AN, Fanselow MS. Effects of cerebellar vermal lesions on species-specific fear responses, neophobia, and taste-aversion learning in rats. *Physiol Behav* **1987**;39:579-586
32. Ball G, Micco DJ Jr, Berntson G. Cerebellar stimulation in the rat: complex stimulation-bound oral behaviors and self-stimulation. *Physiol Behav* **1974**;13:123-127
33. Newman PP, Reza H. Functional relationships between the hippocampus and the cerebellum: an electrophysiological study of the cat. *J. Physiol (Lond)* **1979**;287:405-426
34. Leaton RN, Supple WF. Cerebellar vermis: essential for long-term habituation of the acoustic startle response. *Science* **1986**;232:513-515
35. Reis DJ, Doba N, Nathan MA. Predatory attack, grooming, and consummatory behaviors evoked by electrical stimulation of cat cerebellar nuclei. *Science* **1973**;182:845-847
36. Macchi G, Bentivoglio M. Agenesis or hypoplasia of cerebellar structures. In: Vinken PJ, Bruyn GW, eds. *Congenital malformations of the brain and skull*. Amsterdam: North-Holland, **1977**:367-393
37. Mercuri S, Curatolo P, Giuffrè R, DiLorenzo N. Agenesis of the vermis cerebelli and malformations of the posterior fossa in childhood and adolescence. *Neurochirurgia (Stuttg)* **1979**;22:180-188
38. Joubert M, Eisenring JJ, Robb JP, Andermann F. Familial agenesis of the cerebellar vermis. *Neurology* **1969**;19:813-825
39. DeMorsier G, Laville F. Etudes sur les dysraphies cranio-encéphaliques. VIII. Dysraphies du diencephale de la loge hypophysaire, du telencephale inferieur et du cervelet. *Acta Neurol Belg* **1962**;23:443-453
40. Courchesne E, Hesselink JR, Jernigan TL, Yeung-Courchesne R. Abnormal neuroanatomy in a nonretarded person with autism: unusual findings with magnetic resonance imaging. *Arch Neurol* **1987**;44:335-341
41. Courchesne E, Yeung-Courchesne R, Press GA, Hesselink JR, Jernigan TL. Hypoplasia of cerebellar vermal lobules VI and VII in infantile autism. *N Engl J Med* **1988**;318:1349-1354
42. Benda CE. *Down's syndrome. Mongolism and its management*. New York: Grune & Stratton, **1969**:134-166
43. Jervis GA. Early familial cerebellar degeneration (report of three cases in one family). *J Nerv Ment Dis* **1950**;111:398-407
44. Sarnet HB, Alcalá H. Human cerebellar hypoplasia. *Arch Neurol* **1980**;37:300-305
45. Adams JH, Corsellis JAN, Duchon LW, eds. *Greenfield's neuropathology*, 4th ed. New York: Wiley, **1985**

Book Review

Craniospinal Magnetic Resonance Imaging. By Stephen J. Pomeranz. Philadelphia: Saunders, 677 pp., 1989. \$125

Advances in MR imaging technology and knowledge are occurring at an astonishingly rapid rate. Currently, 85–90% of MR studies are of the brain and spine. Thus, there is a need for a concise and comprehensive introductory text covering the broad and complex topic of MR imaging of the craniospinal axis.

The stated objective of *Craniospinal Magnetic Resonance Imaging* is to provide a clinical reference for those engaged in MR imaging. This book attempts to present the most current data on this imaging technique and to integrate the various concepts of MR imaging so that clinicians of every level of sophistication in the field, from medical students to experienced neuroradiologists, can understand its applications in the diagnosis of lesions of the brain and spine. Allowing for the fact that current developments in MR far exceed the most timely publication, the authors have, to a great degree, succeeded in their objective. *Craniospinal Magnetic Resonance Imaging* is a well-written, comprehensive introduction to this complicated subject.

This book has 20 contributors and 22 chapters and spans 677 pages, yet it is not bulky. The first four chapters cover MR physics, flow effects, and fast-scan imaging and give an introduction to craniospinal MR. This last chapter provides an understanding of the operator-dependent variables that determine image contrast and quality as they relate to daily clinical implementation of MR imaging.

One chapter focuses on MR anatomy of the head and spine. Succeeding chapters are devoted to the different disease processes, both congenital and acquired, that affect the brain and spine in adults and in children. The final three chapters cover MR of the orbit, nasopharynx, and temporomandibular joint. The book has two appendixes at the end. Appendix 1 is a summary of examination preferences (CT, MR) for evaluation of the cranium, spine, ears, nose, and throat. Recommended protocols for MR examination in different areas and for different clinical problems in the craniospinal axis, orbit, and temporomandibular joints are summarized in appendix 2.

Each chapter is extensively illustrated, and effective use is made

of tables. The text is well organized and concise but readable. The material, with a few exceptions, is current. Although the book has 20 different contributors, it is written in a manner that flows from one subject to another. Each chapter is supported by an abundant, but not exhaustive, reference list.

The chapters discussing MR physics and related topics and the chapter on MR imaging of hemorrhage explain some of the more difficult concepts of MR. Because of its contrast properties, MR has unusual pitfalls not typical of other imaging techniques. These may be due to canting or tilting of the head or to MR artifacts. An excellent chapter highlights this important topic.

However, the book has a number of important deficiencies. Overcrowding and excessive labeling are detractors in the chapter on MR anatomy of the head and spine, although the anatomic sections are displayed with reasonable clarity. The discussion and illustration of MR contrast agents, specifically gadolinium, is limited.

Although most of the illustrations are of a reasonable quality and standard, perhaps the most glaring shortcoming of this book is the poor quality of some of the images, which are significantly inferior to those that can be produced in routine daily practice. Furthermore, some of the images are not much larger than a postage stamp, and these miniature illustrations detract from the overall quality of the book.

In spite of the deficiencies, *Craniospinal Magnetic Resonance Imaging* is a worthwhile purchase for those involved in the interpretation of neurologic MR images. It fills the void between the more detailed, bulkier texts and the smaller, less comprehensive primers in the field. This text should be a welcome addition to the library of everyone involved in the neurosciences.

Solomon Batnitzky
University of Kansas Medical Center
Kansas City, KS 66103

The Cerebellum in Sagittal Plane—Anatomic-MR Correlation:

2. The Cerebellar Hemispheres

Gary A. Press¹
 James Murakami²
 Eric Courchesne²
 Dean P. Berthoty¹
 Marjorie Grafe³
 Clayton A. Wiley³
 John R. Hesselink¹

Thin (5-mm) sagittal high-field (1.5-T) MR images of the cerebellar hemispheres display (1) the superior, middle, and inferior cerebellar peduncles; (2) the primary white-matter branches to the hemispheric lobules including the central, anterior, and posterior quadrangular, superior and inferior semilunar, gracile, biventer, tonsil, and flocculus; and (3) several finer secondary white-matter branches to individual folia within the lobules. Surface features of the hemispheres including the deeper fissures (e.g., horizontal, posterolateral, inferior posterior, and inferior anterior) and shallower sulci are best delineated on T1-weighted (short TR/short TE) and T2-weighted (long TR/long TE) sequences, which provide greatest contrast between CSF and parenchyma. Correlation of MR studies of three brain specimens and 11 normal volunteers with microtome sections of the anatomic specimens provides criteria for identifying confidently these structures on routine clinical MR.

MR should be useful in identifying, localizing, and quantifying cerebellar disease in patients with clinical deficits.

The major anatomic structures of the cerebellar vermis are described in a companion article [1]. This communication discusses the topographic relationships of the cerebellar hemispheres as seen in the sagittal plane and correlates microtome sections with MR images.

Materials, Subjects, and Methods

The preparation of the anatomic specimens, MR equipment, specimen and normal volunteer scanning protocols, methods of identifying specific anatomic structures, and system of anatomic nomenclature are described in our companion article [1]. The pulse sequences illustrated in this article comprise proton-density-weighted images, 3000/20/4 (TR/TE/excitations); T1-weighted images, 600/20/4; and cardiac-gated T2-weighted images, 3642/70/2.

Results

Gross Anatomic Features of the Cerebellar Hemispheres

Lobar and lobular divisions.—The cerebellar hemispheres are two large, lateral masses separated from the midline vermis by paired shallow surface indentations, the paramedian sulci [2]. The tentorium cerebelli, a transverse fold of the dura mater, stretches horizontally over the superior aspect of the hemispheres separating them from the overlying occipital lobes of the cerebrum. The posterior, inferior, and lateral surfaces of the hemispheres lie adjacent to the meninges overlying the occipital bone. The precentral fissure separates the anterior paramedian aspect of each hemisphere from the posterior aspect of the pons and junction of the pons and midbrain [1]. Further laterally, the cerebellopontine angle cistern separates the anterior surface of each cerebellar hemisphere from the dorsal aspect of the petrous ridge [2].

This article appears in the July/August 1989 issue of *AJNR* and the October 1989 issue of *AJR*.

Received August 12, 1988; revision requested November 1, 1988; revision received November 25, 1988; accepted December 7, 1988.

This work was supported by National Institute of Neurological Diseases and Stroke grant 5-RO1-NS19855 awarded to E. Courchesne.

¹ Department of Radiology and Magnetic Resonance Institute, University of California, San Diego, School of Medicine, 225 Dickinson St., San Diego, CA 92103-1990. Address reprint requests to G. A. Press.

² The Neuropsychology Research Laboratory, Children's Hospital Research Center, San Diego, CA 92123.

³ Department of Pathology, University of California, San Diego, School of Medicine, San Diego, CA 92103-1990.

AJR 153:837-846, October 1989
 0361-803X/89/1534-0837
 © American Roentgen Ray Society

Key to Abbreviations Used in Figures

An	anterior aspect of section
Ant Lobe	anterior lobe of hemisphere
ao	atlantooccipital joint
Bi	biventer
Ce	centralis
cl	clivus
Cm	corpus medullare
CP	collicular plate
cpa	cerebellopontine angle cistern
Cu	culmen
D	dentate nucleus
De	declive
F	flocculus
FF	floor of fourth ventricle
fm	foramen magnum
Fo	folium vermis
Gr	gracile lobule
hpr	hemisphere primordium
iac	internal auditory canal
IC	inferior colliculus
icp	inferior cerebellar peduncle
jv	jugular vein
Li	lingula
M	medulla
mcp	middle cerebellar peduncle
No	nodulus
P	pons
pb	petrous bone
PF	pontine flexure
pr	cerebellar primordium
pt	primary white-matter tract
Py	pyramis
Qu P	quadrangular lobule, posterior portion
Rh	rhombic lip
Ro	roof of fourth ventricle
sc	semicircular canal
Se I	semilunar lobule, inferior portion
Se S	semilunar lobule, superior portion
tmj	temporomandibular joint
To	tonsil
Uv	uvula
Tu	tuber vermis
vpr	vermis primordium
1	precentral fissure
2	preculminate fissure
3	primary fissure
4	superior posterior fissure
5	horizontal fissure
6	prepyramidal fissure (vermis only)
6'	inferior posterior fissure (hemisphere only)
6''	inferior anterior fissure (hemisphere only)
7	secondary fissure
8	posterolateral fissure

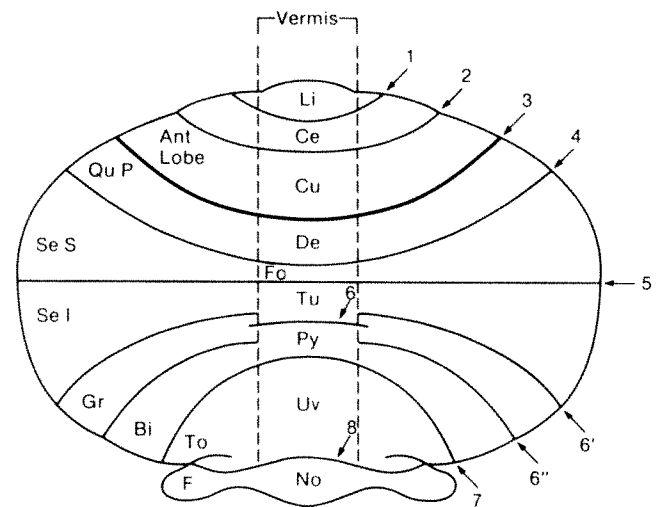


Fig. 1.—Diagram of lobar and lobular structures of cerebellum. This modification of a standard anatomic diagram of the human cerebellum [3] permits rapid identification of the locus of any given term used here and in our companion report [1]. Abbreviations used to designate the anterior lobe of the hemisphere as a whole, and each of the individual lobules of the posterior lobe of the hemisphere and flocculus, are positioned on the left side of the diagram. Arranged on the right side of the diagram are the numerals used to designate the major fissures subdividing the cerebellum. Confined by the central pair of broken lines are abbreviations used to designate the lobules of the vermis. The **bold line** of the primary fissure (3) represents the boundary between the anterior and posterior lobes of the cerebellum. See key for abbreviations.

The deep primary and posterolateral fissures extend outward from the vermis into the cerebellar hemispheres dividing them also into three portions: the anterior and posterior lobes and the hemispheric component of the flocculonodular lobe, the flocculus (HX) (Fig. 1) [1, 3]. Additional, shallower fissures subdivide the anterior and posterior lobes of the hemispheres into a series of lobules (HII–HIX). No hemispheric counterpart of vermicular lobule I exists in humans [3, 4].

The lobules of the anterior lobe of the hemisphere (HII–HV) are bounded by the precentral cerebellar fissure and cerebellopontine angle cistern anteriorly and the primary fissure posteriorly (Fig. 1). The preculminate fissure separates the central lobule (HII and HIII) from the anterior quadrangular lobule (HIV and HV) [3, 4].

The lobules (HVI–HIX) of the posterior lobe of the cerebellum are bounded by the primary fissure (which separates them from the anterior lobe) and the posterolateral fissure (which separates them from the flocculus). Three additional fissures within the vermis extend also into the hemispheres to separate several of the five lobules of the posterior lobe of the hemisphere from one another: the superior posterior fissure separates the posterior quadrangular lobule (HVI) from the superior semilunar lobule (HVIIA), the horizontal fissure separates the superior semilunar lobule from its inferior component (also HVIIA), and the secondary fissure separates the biventer (HVIII) and tonsil (HIX). Two remaining fissures are present within the hemispheres only and subdivide the remainder of the lobules of the posterior lobe: the inferior posterior fissure separates the inferior semilunar lobule and

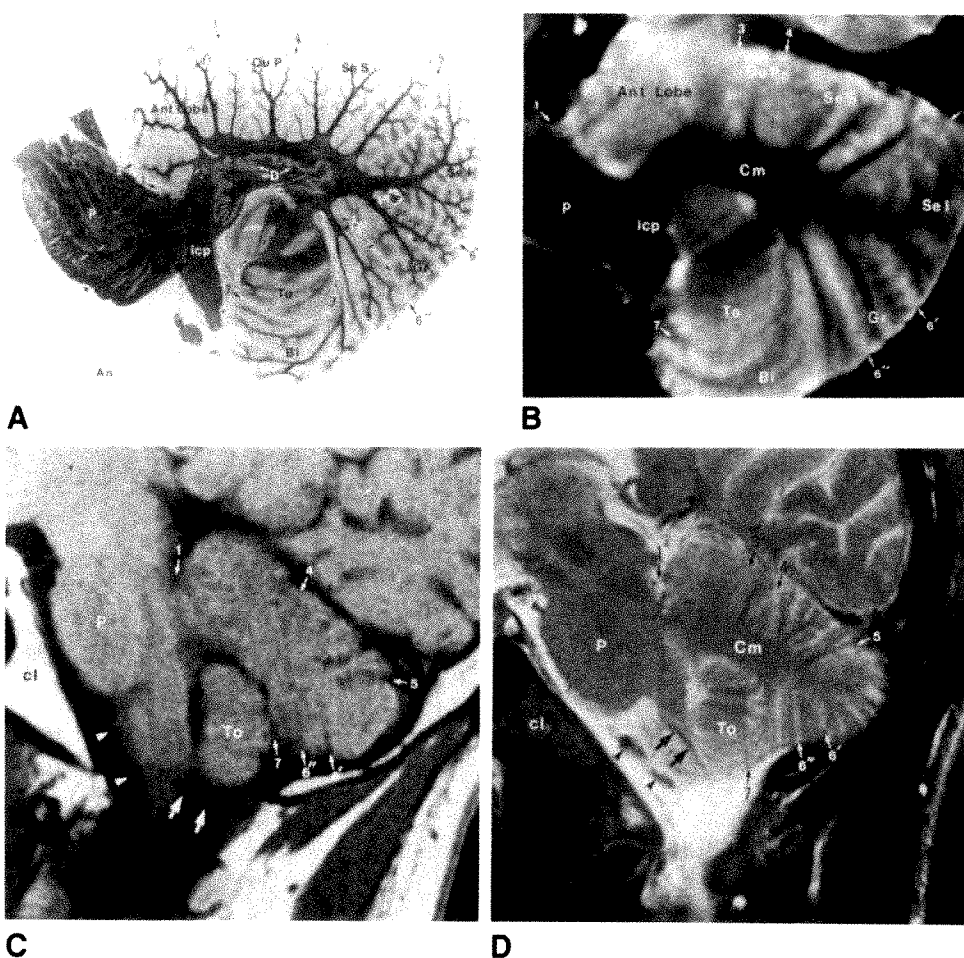
Fig. 2.—Plane 1, through the brain-stem and anterior and posterior lobes of the cerebellum. See key for abbreviations.

A, Sagittal microtome section of specimen brain. (Luxol fast blue-cresyl violet myelin stain)

B, Corresponding sagittal proton-density-weighted image (3000/20/4) of same specimen brain before sectioning.

C and D, Sagittal T1-weighted, 600/20/4 (C), and cardiac-gated T2-weighted, 3642/70/2 (D), images of 38-year-old male volunteer.

Pons and cerebellar hemisphere are continuous. Corpus medullare and superior and inferior cerebellar peduncles arch over tonsil. Primary white-matter tracts innervating posterior quadrangular, semilunar, and gracile lobules and posterior portion of the biventer are well delineated on proton-density-weighted image of anatomic specimen and T2-weighted image of volunteer. Note hatchmarklike arrangement of gray and white matter within tonsil (A, B, and D). Several primary white-matter tracts to anterior lobe of hemisphere are obscured due to volume averaging on B and D. For the same reason, characteristic undulating contour of dentate nucleus is identifiable only on thin (15- μ m) anatomic image (A). Gray and white matter have similar signal intensity on T1-weighted image; however, margins of hemisphere and fissures are well defined on this image. Extra-parenchymal landmarks in this plane include a paramidline section through the clivus, intraarachnoid course of vertebral artery (arrowheads), and lateral medullary segment of posterior inferior cerebellar artery (arrows).



gracile lobule (HVIIIB) and the inferior anterior fissure separates the gracile lobule and biventer (Fig. 1) [3, 4].

The flocculus is a separate lobe of the cerebellar hemisphere and contains only one lobule (HX). It represents the hemispheric component of the flocculonodular lobe of the cerebellum and is bounded posteriorly by the posterolateral fissure and anteriorly by the cerebellopontine angle cistern [3, 4].

Two prominent fissures that do *not* form a boundary between hemispheric lobules are mentioned here to avoid confusion when viewing the anatomic and MR sections: (1) the intrabiventral fissure divides the biventer into anterior and posterior portions and (2) the intracural sulcus 1 divides the superior semilunar lobule (HVIIA) into anterior and posterior portions [5].

Sublobular and folial divisions.—Each lobule of the cerebellar hemispheres contains from one to three sublobules; each of these contains many folia. As is the case with the vermis of the cerebellum, the folium represents the minimum unit of structure of the cerebellar hemispheres [1, 4]. Each cerebellar hemisphere in humans contains 330 folia [4]. A more detailed description of the sublobular divisions of the hemispheres can be found in other sources [4, 5].

Organization of the white matter.—The white matter of each cerebellar hemisphere radiates proximally into the brain-stem and distally into the lobules of the hemisphere from a central confluence known as the corpus medullare. This central body of white matter extends posterolateral to the fourth ventricle on each side and is much larger within the hemispheres than within the vermis [1, 3].

Three major white-matter bundles emanate from the anterior aspect of each corpus medullare to connect the cerebellar hemispheres with the three segments of the brainstem [3]. Axons of the superior cerebellar peduncles slope gently upward adjacent to the superolateral aspect of the fourth ventricle to decussate within the midbrain just beneath the red nuclei. Fibers of the middle cerebellar peduncles project anteromedially as they exit the cerebellum to decussate in the tegmentum of the pons. Fibers of the inferior cerebellar peduncles turn sharply inferiorly just medial to the middle cerebellar peduncles to enter the posterolateral aspect of the low pons and medulla (Figs. 2A and 3A).

Smaller bands of white matter radiate from the corpus medullare to the hemispheric lobules. Thin (15- μ m) paramedian sagittal microtome sections reveal that three primary tracts enter the anterior lobe (HII–HV) (Figs. 2A, 3A, and 4A).

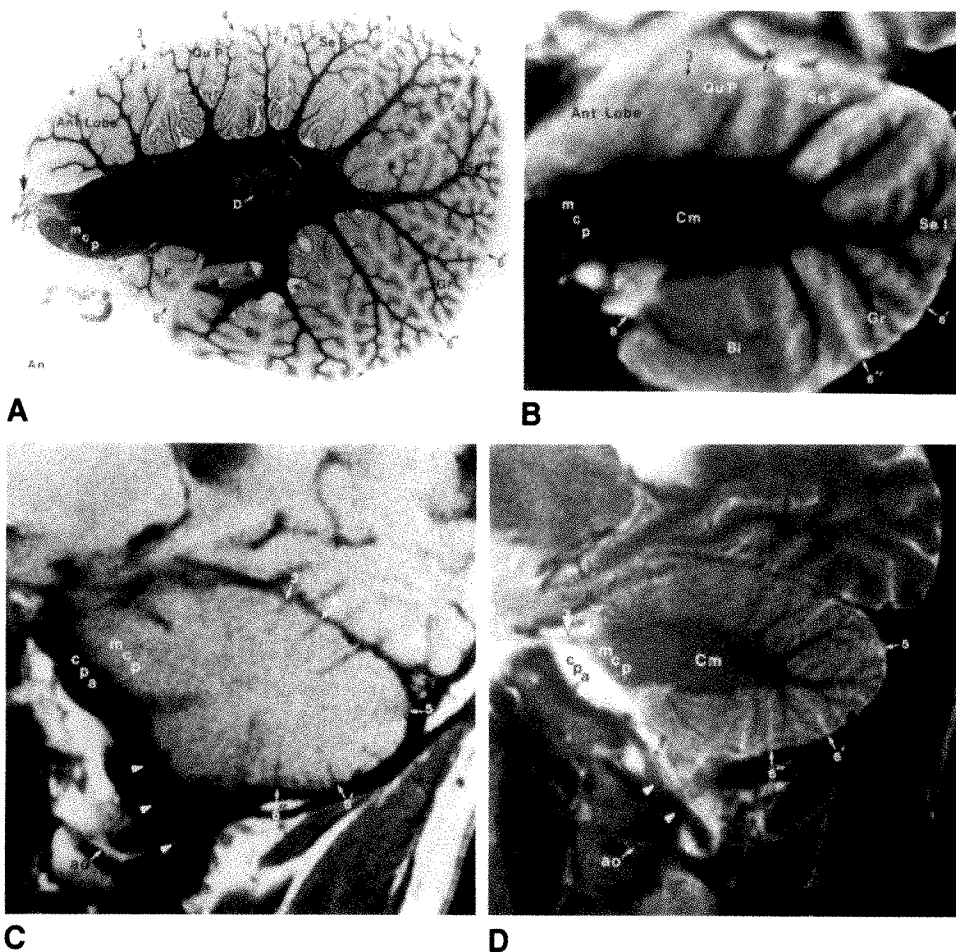


Fig. 3.—Plane 2, through anterior and posterior lobes of cerebellum, middle cerebellar peduncle, and trigeminal root and/or flocculus. See key for abbreviations.

A, Sagittal microtome section of specimen brain. (Luxol fast blue-cresyl violet myelin stain)

B, Corresponding sagittal proton-density-weighted image (3000/20) of same specimen brain before sectioning.

C and D, Sagittal T1-weighted, 600/20 (C), and cardiac-gated T2-weighted, 3642/70 (D), images of 38-year-old male volunteer.

In plane 2, lateral to brainstem and tonsil, corpus medullare becomes oval in shape. Middle cerebellar peduncle extends from corpus medullare to anterior aspect of hemisphere. Biventer alone is sectioned at anteroinferior aspect of hemisphere (compare with Figs. 1A and 1B). Anterior lobe of hemisphere is smaller than in plane 1. Flocculus may appear as a small, globular lobule at anteroinferior aspect of corpus medullare (A and B). Posterolateral aspect of dentate nucleus appears as a complete ring within corpus medullare and is best seen on anatomic image (A). Within superior aspect of cerebellopontine angle cistern is trigeminal nerve root (arrows, A and D), which courses over petrous bone to end in Meckel cave (D). Extraparenchymal landmarks identified *in vivo* include atlantooccipital joint and vertebral artery (arrowheads) passing over posterior arch of C1 to enter cranial cavity.

whereas six or seven primary tracts enter lobules HVI–HVIII of the posterior lobe (Fig. 3A). Both the tonsil (lobule HIX of the posterior lobe) and the flocculus (HX) receive a single primary tract from the corpus medullare (Figs. 2A and 3A) [3].

Anatomic Features of the Cerebellar Hemispheres on Sagittal Microtome and MR Sections

Inspection of the cerebellar hemispheres revealed that sagittal sections would display its lobules and white-matter tracts in discontinuous segments. There are three reasons for this:

1. The complex organization of the cerebellum as a whole. The greater portion of the cerebellum is a composite of multiple transverse lobules, each of which is crescent-shaped with a wedgelike cross section that widens toward the periphery (Fig. 1). The cerebellar parenchyma may be thought of as a stack of such crescents, with the spaces between them analogous to the various fissures. At the center of the stack of crescents lies the fourth ventricle and cerebellar vermis forming its roof. Posterolateral to the fourth ventricle on each side are the paired corpora medullare, which send white-matter tracts into each of the hemispheric lobules.

2. The varying radii of curvature of the different lobules. The anterior lobules (e.g., HII and HIII), having a smaller radius of curvature than the posterior lobules, would be seen on the

most medial sagittal sections only (Figs. 2A, 3A, and 4A), whereas the larger posterior lobules (e.g., HVIIA and HVIIIB) would be present on all sagittal sections (Figs. 2A, 3A, 4A, 5A, 6A, and 7A).

3. Unlike the stacked crescent-shaped lobules, the flocculus and tonsil are significantly smaller, ovoid lobules that protrude from the anterior and inferomedial surfaces of the hemispheres, respectively, and would be seen on a limited number (one or two) of sagittal images (Figs. 3A and 4A) only.

Analysis of the anatomic relationships of the cerebellar hemisphere in six sagittal sections revealed sequential and reproducible changes in the contours and relationships of the individual lobules, corpus medullare and smaller white-matter branches, brainstem, adjacent cisterns, and cerebellar fissures. The individual components of the hemispheres could be identified confidently and consistently on sagittal MR sections by using the intrinsic configurations and signal intensities of these structures and by using secondary clues from the positions and configurations of the surrounding noncerebellar structures.

Several observations can be made if the sagittal anatomic or MR sections are considered in sequence from the paramedian plane (plane 1) toward the lateral plane (plane 6).

Surface features:

1. The shape of the normal hemisphere in plane 1 (Fig. 2) is similar to an isosceles triangle with rounded corners. The

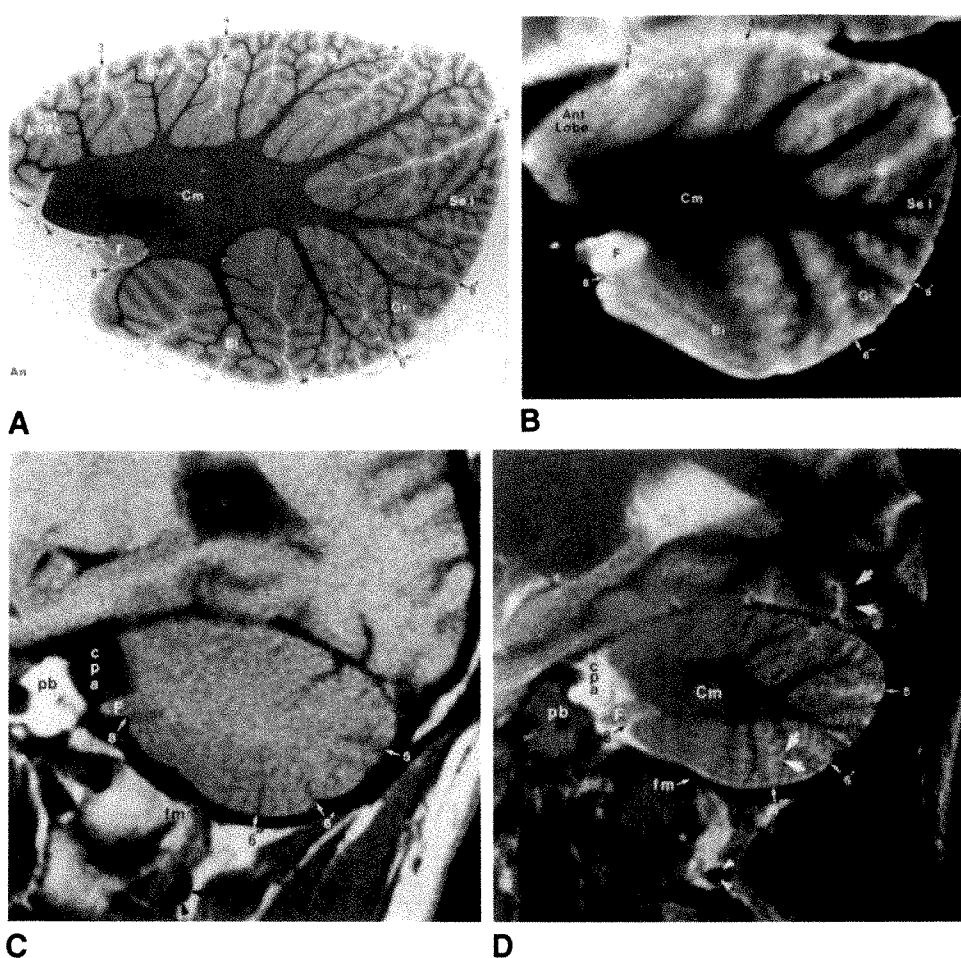
Fig. 4.—Plane 3, through anterior and posterior lobes of hemisphere (lateral to middle cerebellar peduncle), and through flocculus (hemispheric portion of flocculonodular lobe). See key for abbreviations.

A, Sagittal microtome section of specimen brain (Luxol fast blue-cresyl violet myelin stain)

B, Corresponding sagittal proton-density-weighted image (3000/20) of same specimen brain before sectioning.

C and D, Sagittal T1-weighted, 600/20 (C) and cardiac-gated T2-weighted, 3642/70 (D), image of 38-year-old male volunteer.

This is the final section to include a portion of the anterior lobe of the hemisphere. Dentate nucleus is not present in A. Flocculus protrudes tongue-like into inferior aspect of cerebellopontine angle cistern (C and D). Three-layered cortex of cerebellum is thinner than six-layered cortex of inferior occipital lobe (arrows, D). Extraparenchymal landmarks identified in this plane in vivo include apex of petrous bone anterior to porus acusticus, lateral edge of foramen magnum, and vertebral artery (arrowheads).



side of the triangle adjacent to the brainstem (anterior leg) is formed by the upper margin of lobules HII and HIII superiorly, the anterior aspect of the cerebellar peduncles in the middle, and the anterior aspect of the cerebellar tonsil (HIX) inferiorly. The superior aspect of lobules HIV–HVIIA forms the superior leg of the triangle. The inferior leg is formed by the inferior aspect of lobules HVIIA–HIX.

In plane 2 (Fig. 3), the anteroposterior diameter of the cerebellar hemisphere exceeds the superoinferior diameter, and the hemisphere acquires an oval shape. The shape of the hemisphere becomes more rounded in planes 4–6 (Figs. 5–7) due to the progressive shortening of its anteroposterior diameter exceeding the shortening of its superoinferior diameter.

2. Because the inferior aspect of the tonsil may lie slightly closer to the midline than its superior aspect does, a variable portion of the adjacent biventer often appears as an arch beneath the tonsil in plane 1 (Fig. 2).

3. The cerebellopontine angle cistern is most prominent in planes 2 and 3. Traversing the superior aspect of the cistern is the trigeminal nerve root proceeding from its origin in the lateral tegmentum of the pons/middle peduncle junction region to Meckel cave (Figs. 3A and 3D). The flocculus extends into the inferior aspect of the cerebellopontine angle cistern; it appears as a tubular or globular, <1-cm mass protruding from the anterior aspect of the hemisphere at the lower margin

of the corpus medullare (Figs. 3A, 3B, and 4). The flocculus and cisternal segment of the trigeminal nerve are seen only in planes 2 or 3 or both.

4. The lower midbrain, pons, and corpus medullare are continuous in plane 1, joined by fibers of the cerebellar peduncles (Fig. 2). Depending on the precise plane of section and the size of the various structures in each patient, different portions of the peduncles will be included in this immediately paramedian section. Fibers proceeding anterosuperiorly from the cerebellum to the midbrain and pons within a thin (<1-cm transverse diameter) white-matter band are part of the superior peduncle. Fibers within a larger bundle proceeding antero-inferiorly toward the pons and medulla represent portions of the middle and inferior peduncles. This region is variable in appearance. No midbrain, lower brainstem, or tonsillar tissue is present on the more lateral sections.

Deep features:

1. Frequently, the white matter of the corpus medullare and cerebellar peduncles is seen as an arch over the top of the ovoid contour of the tonsil (HIX) in plane 1 (Fig. 2). The shape of the corpus medullare is distinctly different in planes 2 and 3 (Figs. 3 and 4), becoming a biconvex low-signal region within the center of the hemisphere. The fibers of the middle cerebellar peduncle are sectioned obliquely and form the anterior margin of the central white-matter mass in plane 2 (Fig. 3). In plane 4, the appearance of the corpus medullare

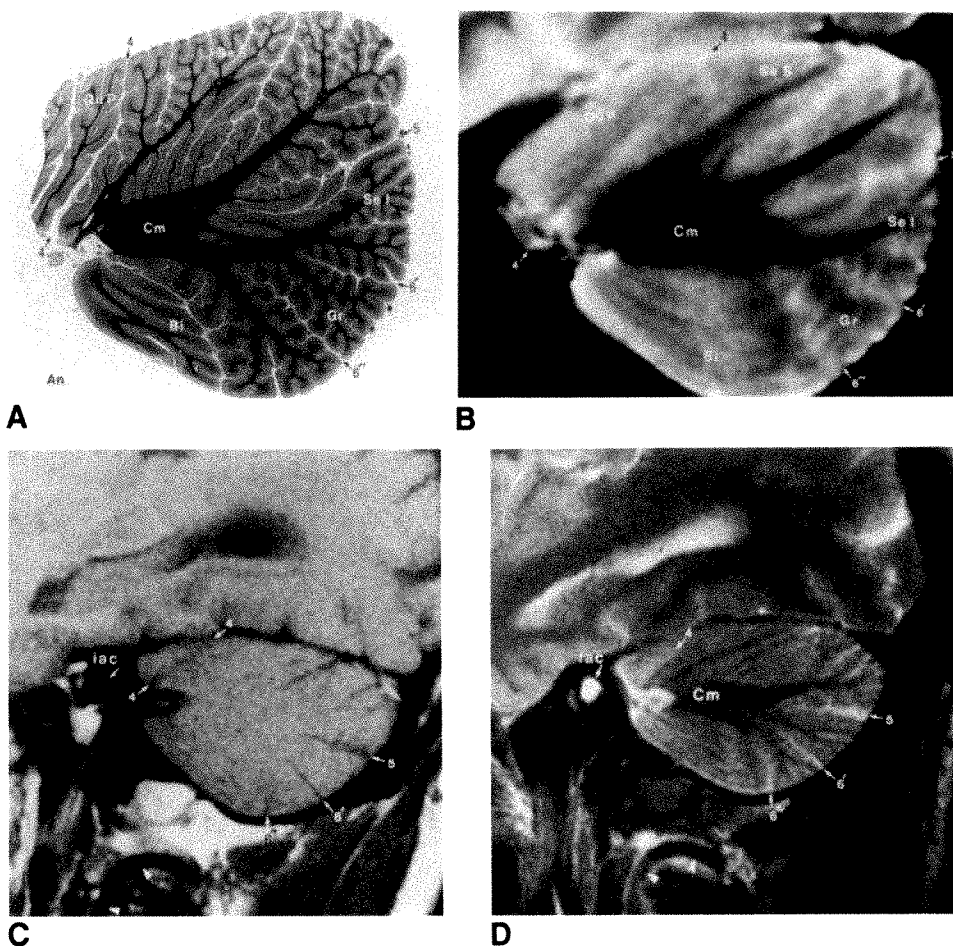


Fig. 5.—Plane 4, through posterior lobe of hemisphere and corpus medullare. See key for abbreviations.

A, Sagittal microtome section of specimen brain. (Luxol fast blue-cresyl violet myelin stain)

B, Corresponding sagittal proton-density-weighted image (3000/20) of same specimen brain before sectioning.

C and D, Sagittal T1-weighted, 600/20 (C), and cardiac-gated T2-weighted, 3642/70 (D), images of 38-year-old male volunteer.

Lateral to anterior lobe of hemisphere, corpus medullare becomes smaller, with linear upper and lower margins. Profile of hemisphere as a whole is more rounded. Flocculus is no longer present. Extraparenchymal landmarks identified in this plane in vivo include cranial nerves VII and VIII within internal auditory canal and vertebral artery (arrowheads) coursing posteromedially from transverse foramen to posterior arch of atlas.

changes again, becoming much smaller with linear upper and lower margins from which primary branches radiate into the superior and inferior semilunar lobules (Fig. 5). Planes 5 and 6 (Figs. 6 and 7) (beyond the lateral aspect of the corpus medullare) section obliquely along primary tracts of white matter within the superior and inferior semilunar lobules. Situated above and below the horizontal fissure, these primary tracts appear as diverging hypointense bundles surrounded by mantles of gray matter having higher signal intensity.

2. The gray-/white-matter distinction within lobules HII–HV of the anterior lobe and HVI and HVIII of the posterior lobe as well as the primary and superior posterior fissures may be obscured on sagittal MR images (Figs. 2B, 2D, 3B, and 3D) in comparison with gross and microtome sections (Figs. 2A and 3A). The reasons for this are (1) the relatively small radius of curvature of these structures, which causes them to be sectioned most obliquely on sagittal images; combined with (2) volume averaging inherent in obtaining 5-mm-thick MR sections. Thinner (15- μ m) microtome sections minimize these difficulties and depict the smallest anatomic details.

3. Situated within the corpus medullare posterolateral to the fourth ventricle are the paired deep nuclear structures of the cerebellum. From medial to lateral they are the fastigial, globose, emboliform, and dentate nuclei. In 5-mm-thick sag-

ittal MR images the deep nuclei of the cerebellum may be difficult to resolve due to their small size (fastigial, globose, and emboliform), serpentine configuration (dentate), and low signal intensity due to iron deposition (dentate); nevertheless, thinner anatomic sections display the dentate nuclei well. Each dentate nucleus has a characteristic undulating margin and a convex upward contour in paramidline plane 1 (Fig. 2A); the nucleus becomes a complete oval in plane 2 (Fig. 3A). The dentate is no longer present on sagittal sections lateral to plane 2 (Figs. 4A, 5A, 6A, and 7A).

4. Unique to the cerebellum is a relatively thin (0.7-mm) three-layered cortex consisting of a deep cellular (granular) layer containing closely packed granule cells; a middle monolayer (Purkinje) layer containing Purkinje cells; and a superficial (molecular) layer containing mainly a feltwork of nerve fibers, dendrites, and glial processes [6, 7]. In contrast, the large majority of the cerebral cortex comprises thicker (1.45–4.5 mm) iso- (or neo-) cortex that contains six layers [7]. This histologic difference is detected on anatomic and MR sagittal sections as a thinner cortical mantle overlying the cerebellar vermis and hemispheres when compared with that overlying the adjacent gyri of the occipital lobes (Fig. 4D).

Imaging landmarks on sagittal MR.—Nonparenchymal landmarks consistently identified in each of the six imaging planes in our volunteers included (1) plane 1 (Figs. 2C and 2D):

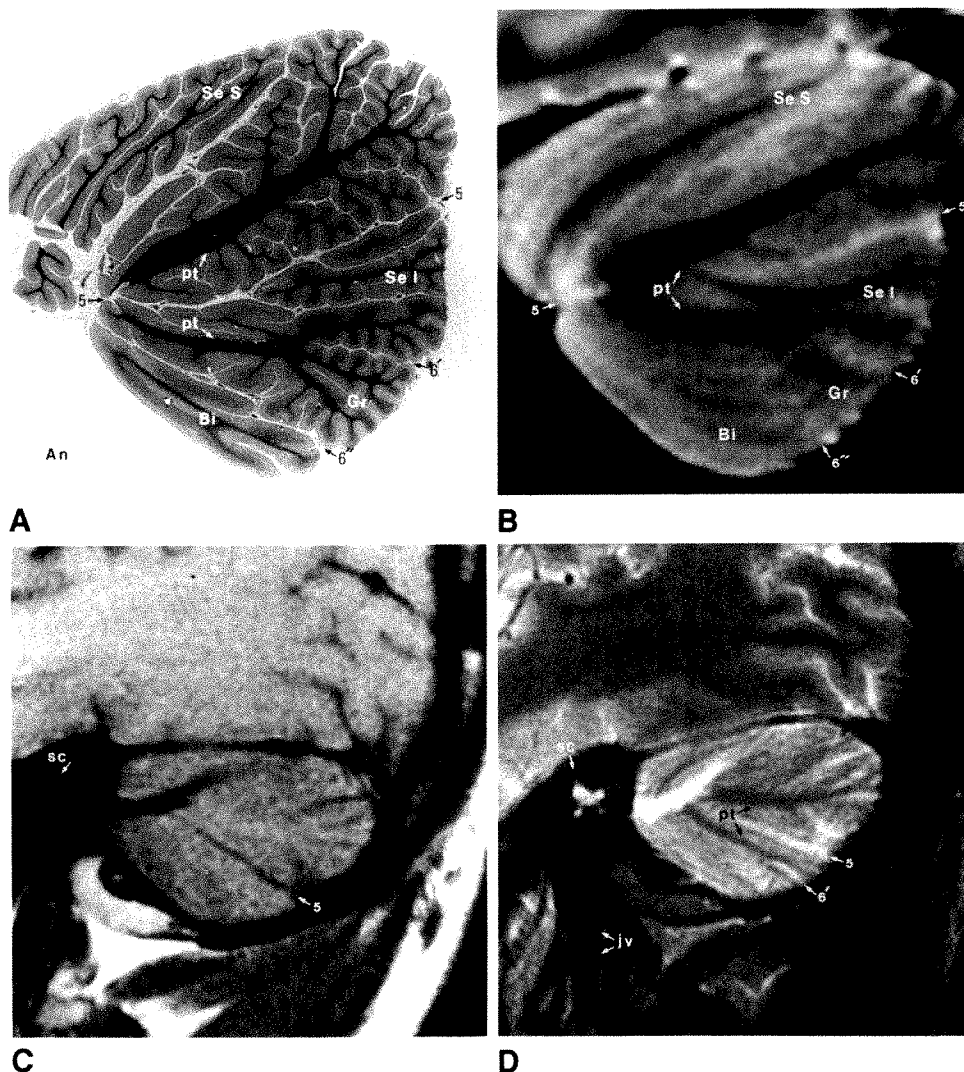
Fig. 6.—Plane 5, through posterior lobe of hemisphere lateral to corpus medullare. See key for abbreviations.

A, Sagittal microtome section of specimen brain. (Luxol fast blue–cresyl violet myelin stain)

B, Corresponding sagittal proton-density-weighted image (3000/20) of same specimen brain before sectioning.

C and D, Sagittal T1-weighted, 600/20 (C), and cardiac-gated T2-weighted, 3642/70 (D), images of 38-year-old male volunteer.

Primary white-matter tracts innervating superior and inferior portions of semilunar lobule diverge posteriorly. This is the final section to include a portion of the biventer and gracile lobules. Extraparenchymal landmarks identified in this plane include semicircular canals and vestibule within petrous bone and internal jugular vein.



paramedian section through clivus, intraarachnoid course of the vertebral artery, and lateral medullary segment of the posterior inferior cerebellar artery; (2) plane 2 (Figs. 3C and 3D): atlantooccipital joint and vertebral artery coursing over the posterior arch of C1; (3) plane 3 (Figs. 4C and 4D): petrous apex medial to porus acusticus and lateral edge of foramen magnum; (4) plane 4 (Figs. 5C and 5D): seventh and eighth cranial nerves within CSF-filled internal auditory canal and vertebral artery coursing superiorly and posteriorly through the transverse foramen of the atlas to reach the sulcus arteriosus on the superior surface of the posterior arch of C1; (5) plane 5 (Figs. 6C and 6D): semicircular canals and vestibule and internal jugular vein; and (6) plane 6 (Figs. 7C and 7D): temporomandibular joint. The vertical portion of the sigmoid sinus appears on the sagittal section just lateral to the cerebellar hemisphere.

Discussion

Development of the Cerebellum

A brief review of key stages in the development of the cerebellum will contribute greatly to understanding its adult

appearance on sagittal MR. Neuroblasts, which form the cerebellum, derive ultimately from symmetric "alar plates" on both sides of the rhombencephalon beneath the roof of the fourth ventricle, sites of intense neuroblastic activity [6, 8]. At the beginning of the second month of life, the proliferating neuroblasts form paired rhombic lips (cerebellar rudiments) that thicken, project further into the fourth ventricle, and extend progressively toward the midline (Figs. 8A and 8B). At the end of the second month of gestation, the rhombic lips of the two sides fuse in the midline beginning rostrally, and the anterior lobe of the vermis is thereby formed before the posterior lobe. During the third month, the cerebellum acquires additional cells at such a rate that it begins to bulge extraventricularly (Figs. 8C and 8D). The middle regions of the vermis and hemispheres proliferate more extensively than the rostral or caudal extremes, and the simple linear structure of the developing cerebellum becomes mushroom-shaped [6, 8].

The growth of the cerebellum posterior to the roof of the fourth ventricle creates the posterolateral fissure early in the third month [6, 8]. All of the remaining horizontally oriented fissures, which divide the cerebellar vermis and hemispheres

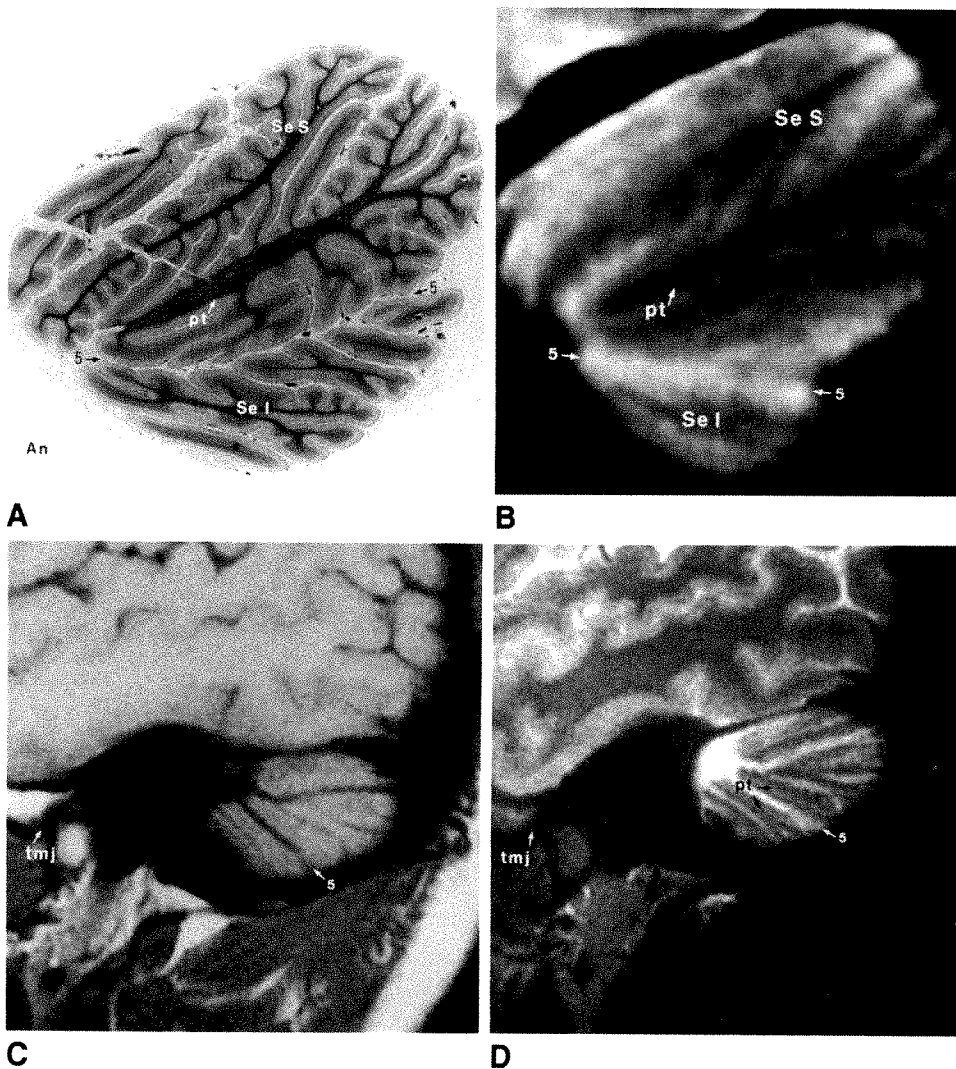


Fig. 7.—Plane 6, through superior and inferior portions of semilunar lobule. See key for abbreviations.

A, Sagittal microtome section of specimen brain. (Luxol fast blue-cresyl violet myelin stain)

B, Corresponding sagittal proton-density-weighted image (3000/20) of same specimen brain before sectioning.

C and D, Sagittal T1-weighted, 600/20 (C), and cardiac-gated T2-weighted, 3642/70 (D), images of 38-year-old male volunteer.

Horizontal fissure divides completely the remainder of the hemisphere into upper and lower portions containing lateral-most aspects of superior and inferior semilunar lobules, respectively. Temporomandibular joint is extraparenchymal landmark consistently identified in this plane in vivo.

into transverse lobules, are visible by the end of the fourth month (Figs. 8E and 8F). Eventually, continued hemispheric growth outstrips growth of the vermis, creating the sagittally directed paravermian sulci between the hemispheres and the vermis (Fig. 8F). Moreover, to accommodate the expansion of lobules HVIIA and HVIIIB, a shift in the hemispheric lobules occurs—the biventral lobules (HVIII), tonsils (HIX), and flocculi (HX) are pushed anteriorly, inferiorly, and medially from their initially lateral position, attaining their final position along the anteroinferior aspect of the hemispheres (Figs. 8E–8G). This shifting process, together with growth of the tonsils themselves, results in a sagittally directed furrow between them and the vermis [6–8].

Functional Anatomy and Connections of the Cerebellar Hemispheres

A major responsibility of the cerebellum is the coordination of motor responses. Through its synergistic action, reflex and voluntary motor acts become coordinated and effective [7].

In broad general terms, distinct clinical abnormalities can be referred to two major sagittal zones of function (midline and lateral) within the cerebellum that correspond closely to its anatomic organization. These zones have distinct (but overlapping) functions [10]. The midline zone, containing the vermis and fastigial nuclei, is related mainly to activities of the midline musculature of the body [10]. The functional anatomy, connections, and disorders of the midline zone are described more fully in our companion article [1].

The lateral (hemispheric) zone of the cerebellum consists of the hemisphere and the dentate, globose, and emboliform nuclei of each side. The cerebellar hemispheres are phylogenetically younger than the midline structures, and are concerned with movements of the proximal and distal extremities. Neurons of the lateral hemispheric cortex (including the most lateral region of the anterior lobe and the lateral portions of the superior and inferior semilunar lobules, HVIIA) project to the dentate nuclei, which then project to the ventrolateral thalamic nucleus [10]. Nerve fibers from this portion of the thalamus ascend to the precentral gyrus and influence finely coordinated movements of the distal extremities. Cortical

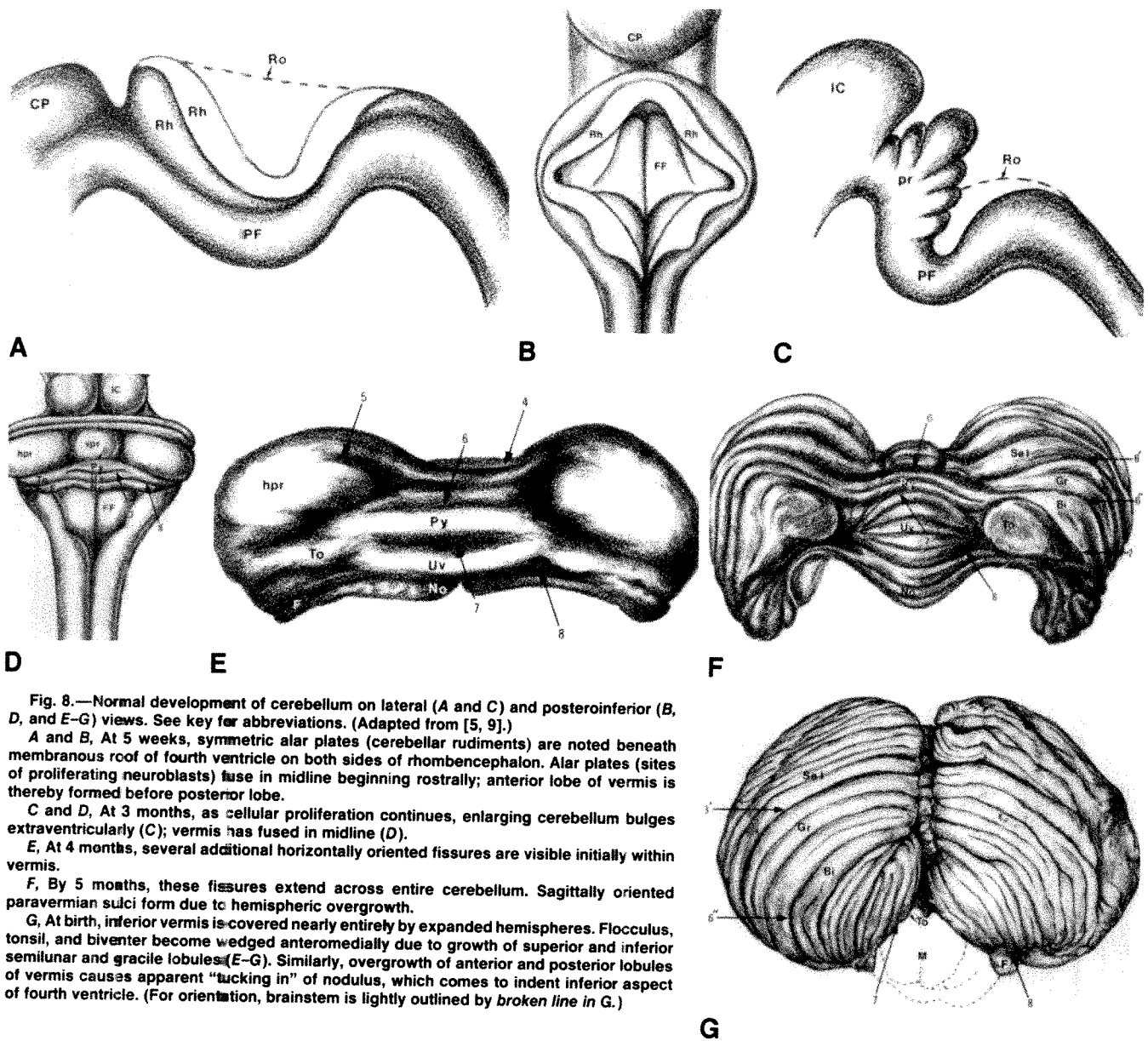


Fig. 8.—Normal development of cerebellum on lateral (A and C) and posteroinferior (B, D, and E-G) views. See key for abbreviations. (Adapted from [5, 9].)

A and B, At 5 weeks, symmetric alar plates (cerebellar rudiments) are noted beneath membranous roof of fourth ventricle on both sides of rhombencephalon. Alar plates (sites of proliferating neuroblasts) fuse in midline beginning rostrally; anterior lobe of vermis is thereby formed before posterior lobe.

C and D, At 3 months, as cellular proliferation continues, enlarging cerebellum bulges extraventricularly (C); vermis has fused in midline (D).

E, At 4 months, several additional horizontally oriented fissures are visible initially within vermis.

F, By 5 months, these fissures extend across entire cerebellum. Sagittally oriented paravermian sulci form due to hemispheric overgrowth.

G, At birth, inferior vermis is covered nearly entirely by expanded hemispheres. Flocculus, tonsil, and biventer become wedged anteromedially due to growth of superior and inferior semilunar and gracile lobules (E-G). Similarly, overgrowth of anterior and posterior lobules of vermis causes apparent "tucking in" of nodulus, which comes to indent inferior aspect of fourth ventricle. (For orientation, brainstem is lightly outlined by broken line in G.)

neurons of the medial portions of the cerebellar hemispheres project to the globose and emboliform nuclei. These nuclei project subsequently to the red nucleus and ventrolateral thalamic nucleus. The rubrospinal tract (originating from cells of the red nucleus) synapses with both medial and lateral groups of anterior horn cells of the spinal cord, thereby influencing the activity of proximal and distal limb musculature, respectively. This pathway is involved in several motor functions including phasic limb movements, maintained positions of an extremity, stance, gait, and posture [10].

Motor signs accompanying lesions involving mainly the cerebellar hemispheres include ipsilateral static and kinetic tremors of the extremities, dysmetria, dysdiadochokinesia (abnormal rapid alternating movements), excessive rebound, impaired check reflex, decomposition of movements, past-pointing, and hypotonia [10].

Clinical and basic research indicates that the cerebellum (particularly the posterior lobe of the hemispheres and vermis) regulates, integrates, and coordinates a wide variety of additional, nonmotor concerns including level of consciousness, learning, memory, and motivated behavior. For example, early investigators recognized that cerebellar damage occurring in adulthood may be associated with lethargy and coma [10] or psychosis [10, 11]. Others observed that retarded intellectual functioning is typically associated with developmental disorders of the cerebellum ranging from hypoplasia [12-14] to near total agenesis [15, 16]. In many such instances, lesions found in the CNS outside the cerebellum were insufficient to explain the severity of the mental retardation [12]. More recently, in a test of word meaning and association, the cerebellum was one of three sites of significant neural activity defined by positron emission tomography (Petersen SE, Fox

PT, Posner MI, Mintun MA, Raichle ME, personal communication). In addition, the posterior lobe of the cerebellum has been shown to be an "obligatory part" of the discrete adaptive response circuit for associative learning; the cerebellum may be the locus of the memory trace for learned responses of this kind [17, 18].

Such clinical data and experimental observations require a reassessment of the role of the cerebellum in normal CNS functioning. Indeed, one investigator has proposed that the role of the cerebellum may extend far beyond regulation of simple motor activities to encompass global coordination of many additional types of behavior for the purpose of optimizing information acquisition (sensory reception) during active exploration of the environment (Bower J, personal communication). MR will likely facilitate defining the bounds of the "expanding" role of the cerebellum by providing improved in vivo identification, localization, and quantification of cerebellar disease in patients whose clinical deficits can be thoroughly tested [19].

REFERENCES

1. Courchesne E, Press GA, Murakami J, et al. The cerebellum in sagittal plane—atomic-MR correlation: 1. The vermis *AJNR* **1989**;10:659-665
2. Carpenter MB. *Human neuroanatomy*, 7th ed. Baltimore: Williams & Wilkins, **1976**
3. Angevine JB Jr, Mancall EL, Yakovlev PI. *The human cerebellum: an atlas of gross topography in serial sections*. Boston: Little, Brown, **1961**
4. Ito M. *The cerebellum and neural control*. New York: Raven, **1984**
5. Larsell O, Jansen J. *The comparative anatomy and histology of the cerebellum*, vol. 3. *The human cerebellum, cerebellar connections and cerebellar cortex*. Minneapolis: University of Minnesota, **1972**
6. Lemire RJ, Loeser JD, Leech RW, Alvord EC Jr. *Normal and abnormal development of the human nervous system*. Hagerstown, MD: Harper & Row, **1975**
7. Crosby EC, Humphrey T, Lauer EW. *Correlative anatomy of the nervous system*. New York: Macmillan, **1962**
8. Larsell O. The development of the cerebellum in man in relation to its comparative anatomy. *J Comp Neurol* **1947**;87:85-129
9. Pansky B. *Review of medical embryology*. New York: Macmillan, **1982**
10. Gilman S, Bloedel J, Lechtenberg R. *Disorders of the cerebellum*. Philadelphia: Davis, **1981**
11. Keddie KMG. Hereditary ataxia, presumed to be of the Menzel type, complicated by paranoid psychosis in a mother and two sons. *J Neurol Neurosurg Psychiatry* **1969**;32:82-87
12. Jervis GA. Early familial cerebellar degeneration (report of three cases in one family). *J Nerv Ment Dis* **1950**;111:398-407
13. Joubert M, Eisenring JJ, Robb JP, Andermann F. Familial agenesis of the cerebellar vermis. *Neurology* **1969**;19:813-825
14. Sarnet HB, Alcalá H. Human cerebellar hypoplasia. *Arch Neurol* **1980**;37:300-305
15. Rubinstein HS, Freeman W. Cerebellar agenesis. *J Nerv Ment Dis* **1943**;92:489-502
16. Mercuri S, Curatolo P, Giuffrè R, DiLorenzo N. Agenesis of the vermis cerebelli and malformations of the posterior fossa in childhood and adolescence. *Neurochirurgia (Stuttg)* **1979**;22:180-188
17. McCormick DA, Thompson RF. Cerebellum: essential involvement in the classically conditioned eyelid response. *Science* **1984**;223:296-299
18. Thompson RF. Neuronal substrates of simple associative learning: classical conditioning. *Trends Neurosci* **1983**;6:270-275
19. Press GA, Courchesne E, Yeung-Courchesne R, Hesselink JR. Cerebellar hypoplasia and autism (letter). *N Engl J Med* **1988**;319:1154

MR Imaging of Muscles of Mastication

Kurt P. Schellhas¹

High-field MR imaging was used to study structural and physiologic alterations involving the muscles of mastication in 46 patients. Muscular abnormalities were often detected incidentally in conjunction with lesions of the CNS, cranial nerves, facial bones, and/or temporomandibular joint (TMJ). Specific pathologic alterations observed included anomalies of musculoskeletal development, muscle hypertrophy, atrophy (disuse and denervation), inflammatory disorders, injuries (including contusions, tears, and muscle rupture), posttraumatic musculoskeletal deformities, and reflex sympathetic dystrophy. Atrophy, fatty replacement, fibrosis, and contracture of selected muscles of mastication may accompany internal derangement of the TMJ in the absence of traumatic deformity.

We conclude that MR is a highly accurate imaging method for detecting masticatory muscle disease. Nontraumatic anatomic and physiologic abnormalities of the muscles of mastication are uncommon disorders. Demonstrable muscle alterations frequently accompany fracture dislocations of the mandibular condyle neck and related facial bones onto which masticatory muscles attach.

Imaging of the trigeminal nerve and TMJ has been revolutionized by thin-section CT and MR [1-15]. The normal and abnormal muscles of mastication and cranio-mandibular apparatus may be routinely studied with head- and surface-coil MR imaging techniques. We investigated the MR characteristics of various structural and physiologic alterations within the muscles of mastication by using high-field MR imaging.

Materials and Methods

We selected for retrospective study 46 patients (14-69 years old) in whom abnormalities of the muscles of mastication were demonstrated with high-field MR imaging. Cases of radiologically demonstrable muscle abnormalities were selected from over 2600 surface-coil studies of the temporomandibular joint (TMJ) (over 1500 patients) and 1400 MR studies of the brain, head, salivary glands, and facial region (over 2800 total patients) obtained at an outpatient imaging center during a 28-month period. All cases in the study were either formally interpreted or reviewed by a single investigator. At least 100 patients had both surface-coil MR studies of the TMJ and head-coil studies of the brain, masticatory muscles, and face. In many cases, masticatory muscle abnormalities were observed incidentally during evaluation of the brain, head, and neck; however, muscle disease was prospectively considered in all patients, especially those with a history of mandible-facial trauma and those having surface-coil TMJ imaging [8, 10-12].

Indications for brain-head imaging studies (performed with the head coil) where muscle lesions were found incidentally were diverse and included headache; facial pain; otalgia; decreased hearing; cranial nerve deficits; recent head and/or facial injury; suspicion of demyelinating disease; and question of CNS, skull base, temporal bone, salivary gland, or paranasal sinus neoplasia and/or inflammatory disease.

Indications for TMJ surface-coil studies included headache; TMJ and/or ipsilateral facial pain; otalgia; decreased hearing; TMJ clicking; crepitus and/or locking; asymmetric jaw movement during either speech or mastication; recent TMJ and/or mandibular injury; facial

This article appears in the July/August 1989 issue of *AJNR* and the October 1989 issue of *AJR*.

Received September 7, 1988; revision requested November 1, 1988; revision received December 5, 1988; accepted December 6, 1988.

Presented in part at the annual meeting of the Society for Magnetic Resonance Imaging, Boston, March 1988.

Presented at the annual meeting of the American Society of Neuroradiology, Chicago, May 1988.

¹ Center for Diagnostic Imaging, 5775 Wayzata Blvd., Suite 190, St. Louis Park, MN 55416. Address reprint requests to K. P. Schellhas.

AJR 153:847-855, October 1989

0361-803X/89/1534-0847

© American Roentgen Ray Society

asymmetry, where muscle pathology was a major consideration; and recent change in skeletal occlusion within 12 months of imaging. Most patients who underwent MR study of the TMJ had been screened with submentovertex and anteroposterior, jaw-protruded radiographs and tightly collimated closed- and open-mouth lateral TMJ tomograms to assess osseous structures.

Three normal volunteers (22–38 years old) underwent both head and TMJ MR studies for the purpose of providing normal muscle images (Figs. 1 and 2). In addition, a normal 61-year-old woman had surface-coil TMJ imaging to assess muscle size and morphology (Fig. 3). The masticatory muscles were carefully studied in normal volunteers and compared with cases of suspected abnormality. Side-to-side symmetry in muscle size, length, and intrinsic signal characteristics was assessed in each patient. Care was taken to clearly identify each muscle within each patient and compare cases of suspected abnormality with relatively age-matched (± 5 years) normal individuals when normal controls were available.

All studies were performed with a 1.5-T superconducting G.E. magnet. Each head study was performed with a commercially available head coil and tailored toward the specific anatomy and complaints in question. A typical study of the brain, trigeminal ganglia, and masticator muscles included a sagittal, 5-mm-thick MR image, 500–600/20/1, 2 (TR range/TE/excitations) with a 256×128 matrix and a 24-cm field of view (FOV), followed by multiecho axial (2000–3200/30, 80–100/1, 2) and coronal (600–900/20/1) or multiecho (2400–2800/30, 800–100/1, 2) 3–5-mm-thick images with 1–2.5-mm interspaces, respectively, between images.

Surface-coil studies of the TMJ were performed with either a single, commercially available 8.9-cm round, receive-only surface coil or a dual 8.9-cm round, bilateral, receive-only surface-coil apparatus, with coupled coils designed to prevent radiofrequency feedback. A typical screening TMJ study employed a preliminary axial, 300–600/20/1, sequence with three to eight 5-mm-thick images obtained for mandibular condyle localization and morphology, followed by seven to nine nonorthogonal, 3-mm-thick images (500–2500/20–25, 80–100/1, 2) with a 1-mm interspace, 256×192 – 256 matrix, and 12–13-cm FOV through the full width of each condyle, scanning perpendicular

to the long condylar axis. Short GRASS (gradient-recalled acquisition in the steady state) scans were routinely performed with the mouth closed, partially open, and fully open after closed-mouth multiecho long TR/short and long TE pulse sequences. Further details of surface-coil single- and dual-coil TMJ studies have been previously described [8, 11–15].

Results

Eight patients exhibited anomalous craniomandibular development such as acquired, nontraumatic facial asymmetry with either enlarged (hypertrophic) (Figs. 4 and 5) or small (hypoplastic-atrophic) (Fig. 6) muscles of mastication either unilaterally or bilaterally (Table 1). We observed either old or recent traumatic injuries affecting the muscles of mastication in 18 patients; these injuries included muscle laceration, contusion, rupture, alteration in length, fibrosis, and focal tears (Figs. 7–9). Two patients exhibited findings compatible with reflex sympathetic dystrophy (RSD) involving the entire unilateral masticatory musculature in conjunction with a history of previous trauma, including skull fracture requiring craniotomy (Fig. 10) and fracture dislocation of the mandibular condyle neck (Fig. 11). Five patients with diffuse masticatory muscle atrophy had an underlying systemic illness such as myasthenia gravis (Fig. 12), polymyositis, progressive systemic sclerosis, or rheumatoid arthritis (Fig. 13). Three patients had unilateral muscle atrophy associated with mass lesions arising either within or adjacent to and externally compressing the ipsilateral trigeminal ganglion (Fig. 14). Nine patients exhibited such findings as muscle hypoplasia, atrophy, and/or fatty replacement of the superior belly of the lateral pterygoid muscle (SBLP) in conjunction with internal derangements of the TMJ (Figs. 15–19). One patient with a 3-month history of severe TMJ pain and a documented (with

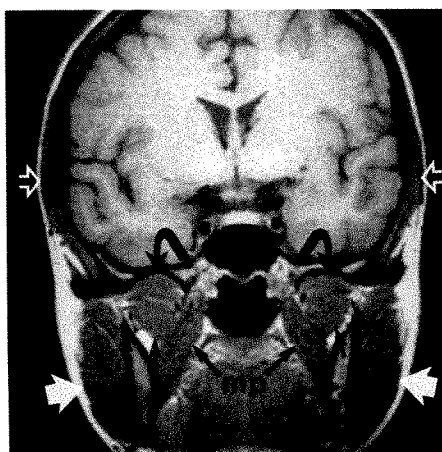


Fig. 1.—Normal muscles of mastication in 32-year-old female volunteer with medium build. Closed-mouth coronal 3-mm-thick MR image, 800/20, with head coil shows normal temporalis (open arrows), masseters (solid white arrows), and medial pterygoids (mp), representing the muscles of jaw closure. Superior (curved arrows) and inferior (small black arrows) bellies of lateral pterygoids function in mouth opening.

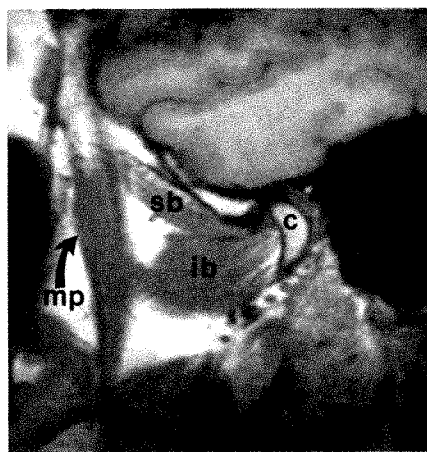


Fig. 2.—Normal pterygoid muscles and TMJ in 37-year-old male volunteer with average build. Sagittal, 3-mm-thick MR image, 500/20, with surface coil (with mouth closed in centric occlusion) reveals normal superior (sb) and inferior (ib) bellies of lateral pterygoids. mp = medial pterygoid, c = mandibular condyle.

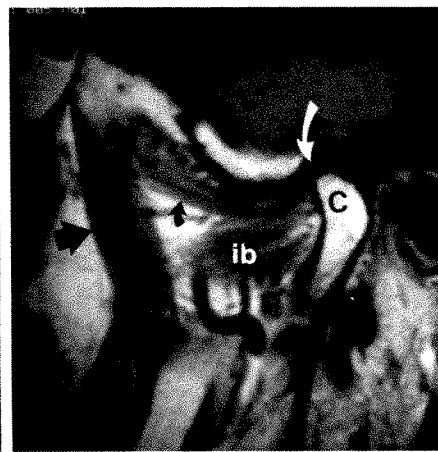


Fig. 3.—Normal pterygoids and TMJ in 61-year-old female volunteer with average build. Sagittal MR image, 600/20, with mouth closed, shows normal medial (large black arrow) pterygoid. Superior (curved black arrow) and inferior (ib) bellies of lateral pterygoids control TMJ meniscus (curved white arrow) and mandibular condyle (c), respectively.

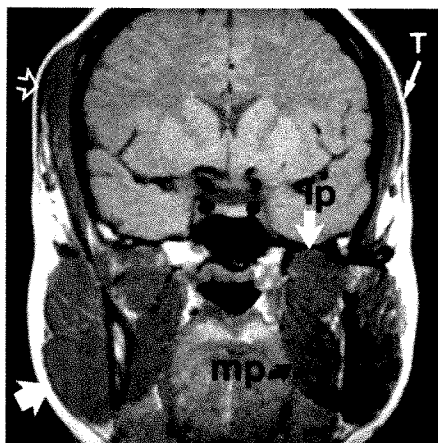
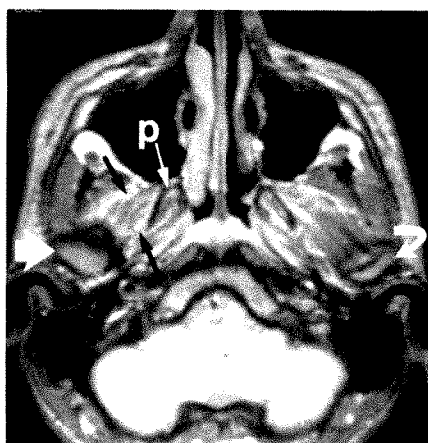
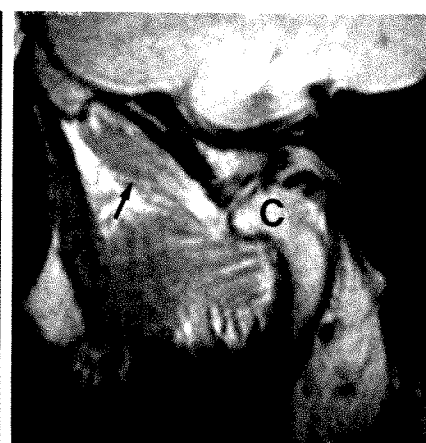


Fig. 4.—Hypertrophic muscles of mastication in 24-year-old woman with right-sided temporal headaches, tender temporalis muscles, and long history of nocturnal bruxism. Coronal, 3-mm-thick MR image, 800/20, reveals asymmetric hypertrophy between left- and right-sided temporalis (T), masseter (M), lateral (Ip), and medial pterygoid (mp) muscles. Note massively hypertrophic right temporalis (open arrow) and masseter (solid arrow) compared with moderately hypertrophic left side (compare with Fig. 1).



A

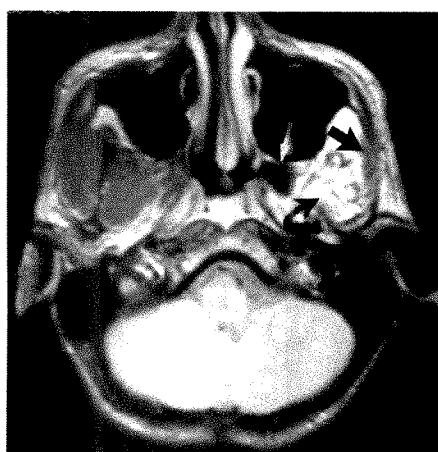


B

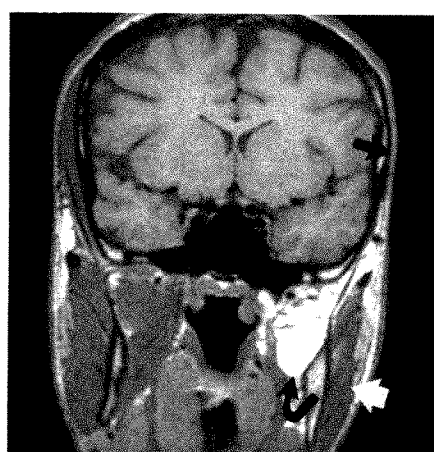
Fig. 5.—Asymmetric lateral pterygoid muscle length resulting from developmentally hypertrophic mandibular condyle in 32-year-old man with long history of right-sided headache, facial pain, and TMJ dysfunction.

A, Axial MR image, 2000/30, shows enlarged right condyle (large white arrow) with shortened superior belly of right lateral pterygoid muscle (black arrows). Curved arrow = normal left condyle, p = normal right pterygoid plate.

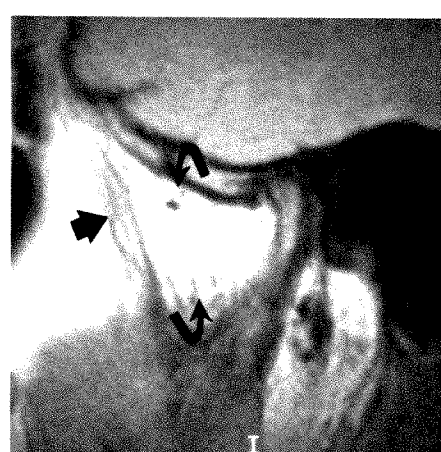
B, Closed-mouth sagittal TMJ MR image, 600/20, shows enlarged and deformed condyle (C) with shortened superior belly of right lateral pterygoid (arrow).



A



B



C

Fig. 6.—Severe developmental masticatory muscle atrophy and contracture in 17-year-old boy with asymmetric jaw motion and severely restricted left condylar motion resulting from childhood facial injury. Coronoid process (not shown) is severely hypoplastic.

A, Axial, 5-mm-thick MR image, 2400/30, shows fatty replacement of pterygoids (curved arrow) and atrophy of masseter (straight black arrow). Note asymmetrically enlarged and aerated left pterygoid plate (white arrow).

B, Coronal, 3-mm-thick MR image, 800/20, shows complete fatty replacement and fibrosis of temporalis (straight black arrow) and pterygoids (curved arrow). Left masseter (white arrow) is atrophic but less involved than temporalis and pterygoids. Right-sided muscles slightly hypertrophic (compare with Figs. 1 and 4).

C, Closed-mouth sagittal TMJ MR image, 700/20, with surface coil reveals severe atrophy and fatty replacement of medial (straight arrow) and lateral (curved arrows) pterygoids.

MR imaging) inflammatory TMJ arthropathy exhibited ipsilateral atrophy of the entire masticatory musculature, suggesting pain-induced RSD. Fascial-space fluid was observed above and surrounding the SBLP in association with inflammatory TMJ arthropathy and large upper-joint-compartment effusions (Fig. 20) [15].

Discussion

The major muscles of mastication receive motor innervation from the mandibular division (V-3) of the trigeminal nerve. The larger jaw-closure muscles include the medial pterygoid, temporalis, and masseter. Muscles of jaw opening include the

superior and inferior belly of the lateral pterygoid, innervated by V-3, and the platysma and anterior belly of the digastric, both of which receive motor supply from the 7th cranial nerve. Normal and hypertrophic masticatory muscles are usually well visualized with both head- and surface-coil MR studies, appearing mildly hypointense and of uniform intrinsic signal intensity with either T1-weighted or long TR/short TE images (Figs. 1-4, 19) [2, 7, 8, 11]. Tendons are well delineated by their very low intrinsic signal, which contrasts sharply with adjacent muscle and fat. Side-to-side symmetry of muscle size, morphology, and intrinsic signal characteristics within

each individual is most important, since marked variation between patients is the rule. Variations between individuals relate to a broad range of factors, including skeletal size (genetic and/or growth related), age, masticatory habits, and general health (Figs. 1-6, 12, 13). Factors that might influence masticatory muscle appearance should be sought in patients exhibiting muscle abnormalities on MR studies.

Normal and abnormal masticatory muscles may be studied with sequential MR images during various stages of the masticatory cycle with either T1-weighted or GRASS fast scans to simulate dynamic muscle function (Fig. 9) [8, 9, 11, 12]. Anomalous musculoskeletal development, such as either facial or mandibular hemihypertrophy/hemiatrophy may result in demonstrable asymmetry in masticatory muscle size and length (Figs. 5 and 6). Alterations of muscle length and/or mass may result in a decreased force (amplitude) and length (distance) of contraction, which might secondarily affect mastication and/or phonation by causing asymmetric jaw motion and function. Internal derangements of the TMJ may cause similar clinical afflictions by interfering with normal joint and masticatory muscle function.

Atrophic muscles on occasion exhibit increased signal on short and long TR/short TE images due to dystrophic changes and/or fatty replacement (Figs. 6, 8, 10-15). Familial masticatory muscle hypertrophy has been described [16, 17]. Mandibular coronoid process hypertrophy is known to result in chronic restriction of TMJ mobility, in many instances leading to atrophy and contracture of the muscles of jaw closure due to decreased range of motion and the lack of periodic muscle stretching [18].

Atrophy, fatty replacement, and fibrosis of the muscles of mastication occur with either disuse or denervation. Disuse atrophy is frequently observed after immobilization, in debili-

TABLE 1: Diagnoses Associated with MR Alterations in the Muscles of Mastication ($n = 46$, ages = 14-69 years)

Diagnosis	Number of Patients
Anomalous development	8
Trauma	
Old	10
Recent	8
Posttraumatic reflex sympathetic dystrophy	2
Systemic illness	
Myasthenia gravis	1
Polymyositis	1
Progressive systemic sclerosis	1
Rheumatoid arthritis	2
Mass lesion affecting trigeminal ganglion	3
Internal derangement of TMJ (no associated fracture of traumatic deformity)	9
Reflex sympathetic dystrophy accompanying inflammatory TMJ arthropathy	1
Total	46



Fig. 7.—Lateral pterygoid muscle shortening 3 weeks after fracture dislocation of mandibular condyle (C) in 14-year-old boy. Closed-mouth sagittal TMJ MR images, 2200/25 (top) and 2200/80 (bottom), reveal shortening of superior belly of right lateral pterygoid (curved arrows). TMJ meniscus (large white arrows) remains normally positioned relative to condyle, separating upper- and lower-joint-compartment fluid collections (small arrows).



Fig. 8.—Severe muscle atrophy and contracture resulting from old, healed bilateral condylar neck fracture dislocations in 44-year-old man with only 4 mm of vertical mouth opening.

A, Axial, 5-mm-thick, adjacent MR images, 500/20, obtained with dual TMJ surface-coil apparatus, show displaced condyles (C) with large calluses (open arrows) originating from healed condylar neck fractures. Medial pterygoids (curved black arrows) and masseters (solid black arrows) are severely atrophic.

B, Closed-mouth, sagittal, 3-mm-thick, surface-coil MR image, 2200/25, of left TMJ reveals atrophic medial pterygoid (curved arrow) with severe fibrosis of superior belly of right lateral pterygoid (straight arrow). (Compare with lower image in A.) TMJ meniscus (M) is normally positioned relative to deformed mandibular condyle (C).



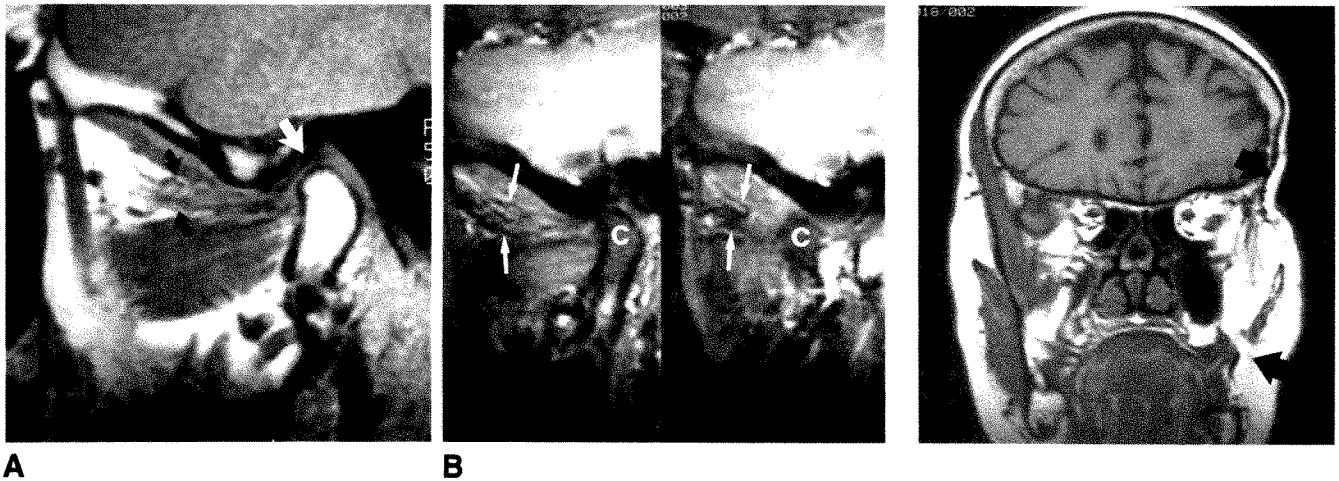


Fig. 9.—Partial muscle tear in 56-year-old woman who experienced severe TMJ and facial pain after posterior molar extractions performed under general anesthesia.

A, Sagittal closed-mouth MR image, 600/20, shows partial tear and retraction of inferior fibers (curved black arrows) of superior belly of right lateral pterygoid (compare with Figs. 2, 3, and 5). TMJ meniscus (white arrow) is normal in position and morphology.

B, Closed- (left) and open-mouth (right) sagittal GRASS images show nonfunction of torn muscle fibers (arrows) during mouth opening. C = mandibular condyle.

Fig. 10.—Severe muscle atrophy suggesting posttraumatic reflex sympathetic dystrophy in 65-year-old woman with severe left-sided headache, facial pain, and restricted jaw motion 20 years after left-sided skull fracture and craniotomy. Coronal, 3-mm-thick MR image shows complete fatty replacement of masticatory muscles (arrows). Opposite side is normal for age.

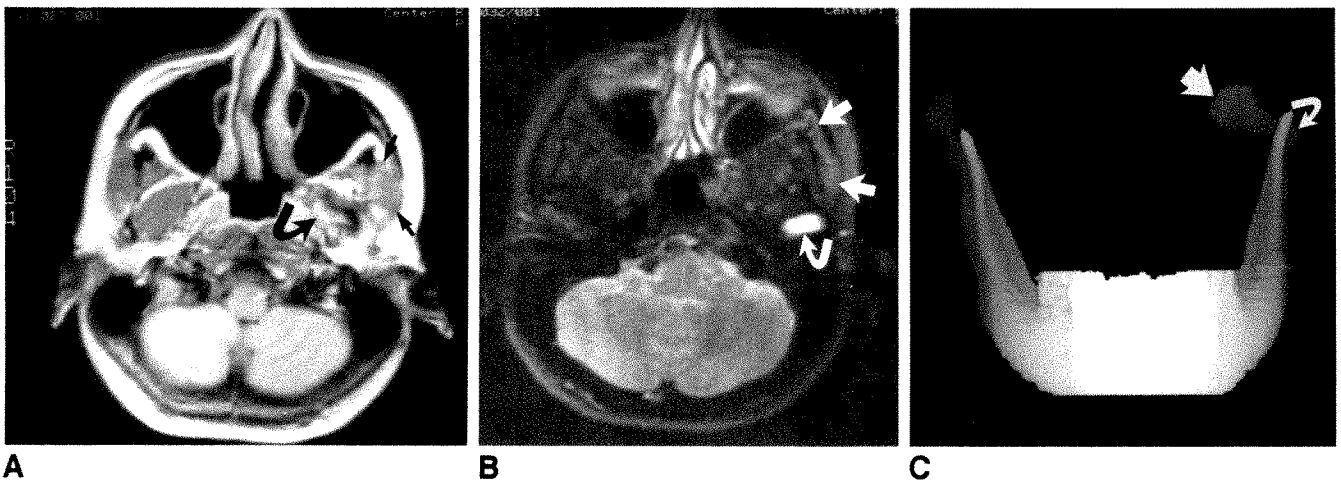


Fig. 11.—Posttraumatic reflex sympathetic dystrophy 3 months after fracture dislocation of mandibular condyle in 46-year-old woman with severe, constant left-sided facial pain, unilateral muscle wasting, and complete loss of mouth-opening ability.

A, Axial, 5-mm-thick MR image, 2000/20, shows dislocated condyle (curved arrow) with normal intrinsic marrow signal. Masseter (straight arrows) exhibits higher signal than opposite side. (Reprinted with permission from [10].)

B, Axial MR image, 2000/80, above that in A, reveals signal-intense fluid (curved arrow) within empty glenoid fossa and slightly increased signal within clinically atrophic and tender left masseter (straight arrows).

C, Frontal view of three-dimensional CT scan of disarticulated mandible shows displaced condyle (straight arrow) and callus (curved arrow) at site of healed condylar neck fracture. Severe pain, muscle wasting, and avascular necrosis of left mandibular condyle was noted 18 months after MR imaging. Patient has refused follow-up MR study because of claustrophobia. Avascular necrosis was diagnosed with radiography and tomography.

tating diseases, and with advanced age [19]. Muscle fibrosis and contracture may follow prolonged immobilization and disuse. Denervation atrophy may occur with either structural lesions (masses) affecting the brain, trigeminal ganglion (Fig. 14) and/or peripheral trigeminal nerve branches, in generalized inflammatory diseases (Fig. 13), and in cases of biochemical denervation, such as myasthenia gravis (Fig. 12) [1, 20]. Simultaneous fatty replacement and muscle edema may be

observed with multiecho, long TR/short and long TE images during the active phase of muscle resorption following denervation (Fig. 14).

Traumatic injuries to the brain, face, mandible, and TMJ may all affect either the trigeminal neuraxis or the muscles of mastication [8, 10, 14, 15]. Muscle tears, alterations in muscle length, contusions, and tendon ruptures are all demonstrable posttraumatic sequelae. The radiologic diagnosis of both

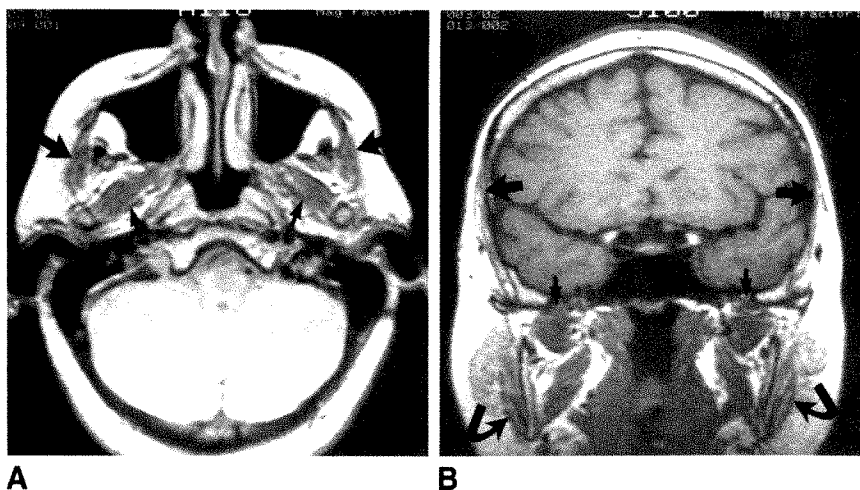


Fig. 12.—A and B, Muscle atrophy caused by myasthenia gravis in 49-year-old woman with masticatory muscle weakness and wasting scanned for suspected brainstem disease. Axial (A), 2000/20, and coronal (B), 800/20, MR images reveal severe atrophy affecting the temporalis (*large straight arrows*) and masseters (*curved arrows*). Lateral pterygoids (*small arrows*) are moderately atrophic. Myasthenia gravis was diagnosed after muscle atrophy was noted and brainstem disease ruled out.

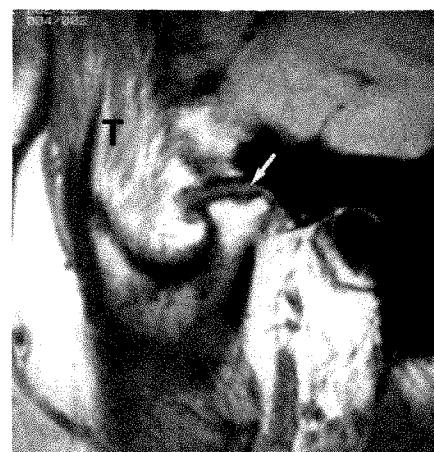


Fig. 13.—Temporalis atrophy and fatty replacement associated with long-standing rheumatoid arthritis and painful, degenerated TMJ. Sagittal, closed-mouth MR image, 600/20, reveals increased fat within temporalis (T) muscle. Note absence of meniscus from fluid-filled joint compartment (*arrow*) and flattening of mandibular condyle. Meniscus (not seen) was dislocated anteromedially on more medial images.

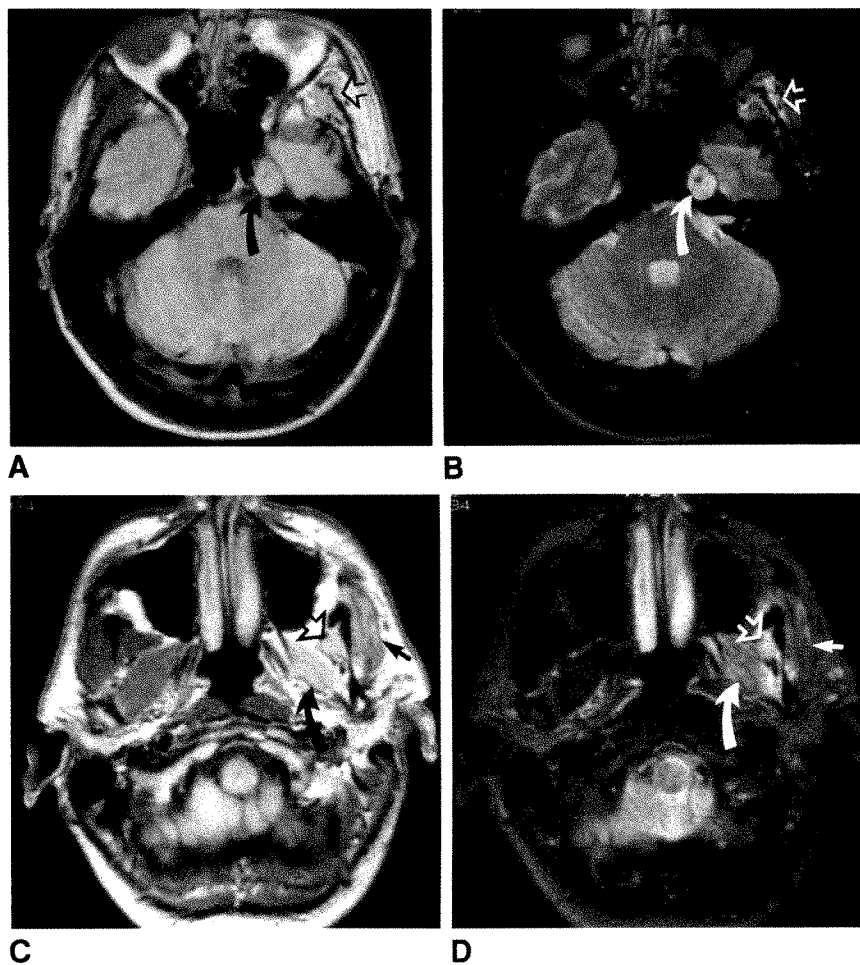


Fig. 14.—Subacute denervation atrophy caused by surgically confirmed schwannoma of the trigeminal ganglion in 31-year-old man with progressive, unilateral jaw weakness and externally visible muscle wasting of 3–5 months duration.

A and B, Axial MR images, 2000/20 (A) and 2000/80 (B), reveal mass (*curved arrows*) within Meckel's cave. Muscle atrophy and increased signal (*open arrows*) are thought to reflect fatty replacement and cellular–extracellular inflammation and edema.

C and D, Masseter (*small straight arrows*), temporalis (*open arrows*), and lateral pterygoid (*curved arrows*) exhibit fatty replacement and increased fluid caused by proximal denervation.

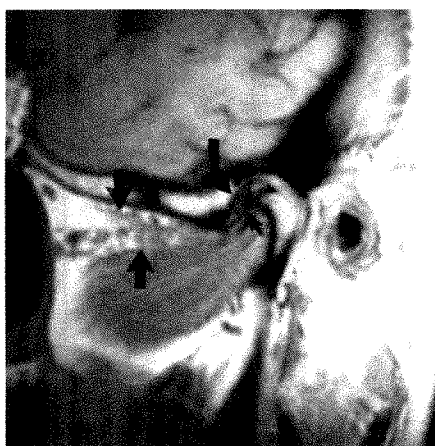


Fig. 15.—Atrophy and fatty replacement of superior belly of right lateral pterygoid in 24-year-old man with chronic TMJ pain and dysfunction. Superior belly of right lateral pterygoid (*large straight arrows*) is atrophic. TMJ meniscus (*small straight arrow*) is anteriorly displaced. Glenoid fossa articular surface (*curved arrow*) is nearly vertical. Mechanical joint symptoms and pain resolved completely after meniscectomy.



A



B

Fig. 16.—A and B, Developmental muscular hypoplasia versus acquired atrophy and fibrosis of superior belly of right lateral pterygoid associated with unusually deep glenoid fossa configuration in 24-year-old woman with TMJ clicking, facial pain, and episodic joint locking. Closed- (A) and open-mouth (B) sagittal TMJ MR images, 600/20, reveal a deep glenoid fossa and steep articular eminence (*straight arrows*). Superior belly of right lateral pterygoid (*curved arrows*) is small and either severely underdeveloped or atrophic.

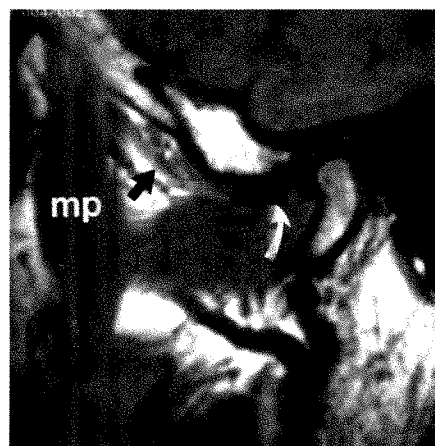


Fig. 17.—Atrophy, fibrosis, and contracture of superior belly of right lateral pterygoid associated with chronic displacement of TMJ meniscus. Sagittal, closed-mouth TMJ MR image, 600/20, reveals atrophy and fibrosis of superior belly of right lateral pterygoid (*straight arrow*) with anterior displacement, thickening, and deformity of TMJ meniscus (*curved arrow*). Adjacent medial pterygoid (mp) muscle is normal.



Fig. 18.—Atrophy, fibrosis, and contracture of superior belly of right lateral pterygoid (*straight arrow*) after 4 years of TMJ therapy with progressive, anterior-repositioning intraoral splints in 39-year-old woman with long history of TMJ pain and worsening malocclusion during treatment. No pretreatment imaging. Sagittal, closed-mouth MR image, 600/20, without splint shows widened space (*curved arrow*) behind condyle (C). Note normal meniscus and anterior position of condyle due to iatrogenic occlusal changes (compare with Figs. 2, 3, and 17).

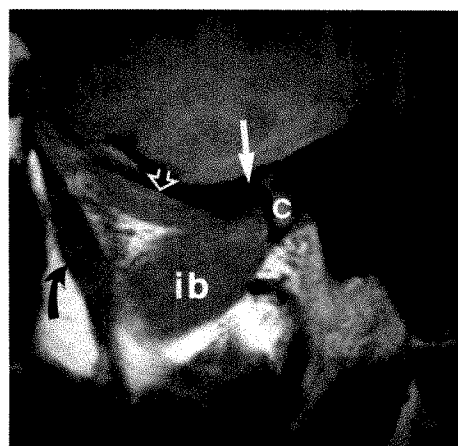


Fig. 19.—Normal pterygoid muscles with anterior displacement of TMJ meniscus. Closed-mouth sagittal MR image through medial pole of mandibular condyle (c) reveals anteromedial displacement of meniscus (*white arrow*) with normal pterygoid muscles. Open arrow = superior belly of right lateral pterygoid, ib = normal inferior belly of lateral pterygoid, curved arrow = normal medial pterygoid.

acute and chronic traumatic muscle alterations is important, since changes in muscle function often occur after muscle tear, shortening, and/or rupture (Figs. 7–9). Muscle injuries and alterations in muscle length that result from fracture dislocations of the mandible may result in significant disability (Figs. 8–11). Localized edema and fascial-space inflammation

may accompany contusions, direct muscle injuries, and TMJ inflammation (Fig. 20). We have observed muscle tears after pharyngeal surgery and posterior dental extractions due to overdistraction and/or excessive lateral mobilization of the jaw under general anesthesia (Fig. 9). RSD of the masticator muscles is a poorly understood posttraumatic sequela of

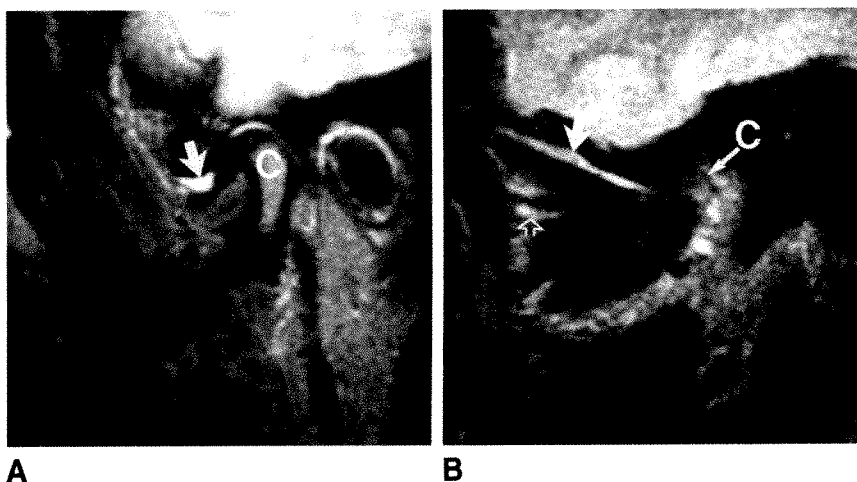


Fig. 20.—Fascial-space edema caused by non-infectious, inflammatory TMJ arthropathy in adult woman with recent onset of facial/TMJ pain, otalgia, and ipsilateral open bite. Closed-mouth, adjacent, sagittal MR images, 2500/100, through center of condyle (A) and medial pole of condyle (B). A, Large, signal-intense, upper-compartment effusion (arrow) is present. C = mandibular condyle. B, Fluid is seen above (solid arrow) and below (open arrow) superior belly of right lateral pterygoid. C = medial pole of condyle.

craniomandibular injury that results in pain, muscle wasting, skeletal demineralization, and disability as it does in the appendicular skeleton (Figs. 10 and 11) [21–24].

It is theorized that RSD results from excessive sympathetic stimulation and/or parasympathetic nonfunction causing vasoconstriction and ischemia in the affected anatomic region, leading to pain and dystrophic changes such as muscle atrophy and skeletal demineralization. RSD often follows either peripheral nerve or nerve plexus injury in the extremities, where it is observed by neurologists, orthopedists, and rehabilitation specialists. The exact frequency of RSD is not known.

Anomalous development, atrophy, fibrosis, and muscle contracture are all observed in conjunction with internal derangements of the TMJ (Figs. 15–18) [4–8, 11, 18, 25]. Hypoplasia versus acquired atrophy of the SBLP muscle is a commonly observed but poorly understood finding associated with unusually deep glenoid fossa configurations, with or without accompanying internal derangement and/or displacement of the TMJ meniscus (Figs. 15 and 16). Atrophy, fibrosis, and contracture of the SBLP are found in selected cases of meniscus derangement and anterior displacement, although this finding is not constant and merits further investigation (Figs. 17–19) [7, 8, 11, 25]. We have noted SBLP fibrosis and contracture associated with the prolonged use of anterior-repositioning intraoral splints used for treatment of TMJ afflictions (Fig. 18). Fascial-space edema surrounding the pterygoid musculature is observed with inflammatory TMJ arthropathy, as intraarticular fluid from the superior joint compartment drains anteromedially toward the pterygopalatine fossa, within and around distended lymphatics, above and between the lateral pterygoids (Fig. 20). This drainage pathway for upper-joint-compartment fluid (or contrast material) has been observed commonly during two-compartment TMJ arthrography with inadvertent rupture of the superior compartment capsule [11]. Atrophy, contracture, and disability of masticatory muscles may occur as sequelae of chronic TMJ and/or facial pain, without history of trauma, suggesting the existence of pain-induced reflex sympathetic dystrophy [22, 24].

In conclusion, structural and physiologic lesions involving the muscles of mastication may be observed with MR imaging

in association with a variety of head and neck disorders. Masticatory muscle abnormalities are most often observed with trauma and less often with anomalous development and internal derangements of the TMJ. The recognition of muscle alterations may lead to a correct diagnosis and improved understanding of the clinical symptomatology and disease pathophysiology under investigation.

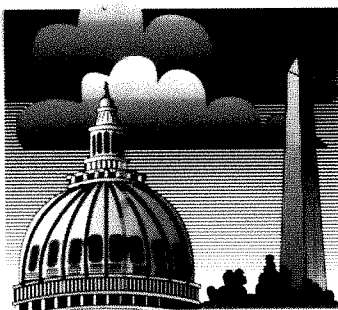
ACKNOWLEDGMENTS

Thanks to Mark R. Omlie, C. Randall Nelms, Elizabeth A. Reid, James C. Block, Robert J. Keck, John J. Norton, and Eric L. Schiffman for individual case contributions. Special thanks to Clyde H. Wilkes for over half of the 46 cases in the series and to Mark A. Piper for his consultation. The contributions of Kenneth B. Heithoff, Hollis M. Fritts, Becky Borgerson, and the technical staff at the Center for Diagnostic Imaging are sincerely appreciated.

REFERENCES

- Harnsberger HR, Dillon WP. Major motor atrophic patterns in the face and neck: CT evaluation. *Radiology* 1985;155:665–670
- Daniels DL, Pech P, Pojunas KW, Kilgore DP, Williams AL, Haughton VM. Trigeminal nerve: anatomic correlation with MR imaging. *Radiology* 1986;159:577–583
- Seltzer SE, Wang AM. Modern imaging of the masseter muscle: normal anatomy and pathosis on CT and MRI. *Oral Surg Oral Med Oral Pathol* 1987;63:622–629
- Harms SE, Wilk RM, Wolford LM, et al. The temporomandibular joint: magnetic resonance imaging using surface coils. *Radiology* 1985;157:133–136
- Katzberg RW, Bessette RW, Tallents RH, et al. Normal and abnormal temporomandibular joint: MR imaging with surface coil. *Radiology* 1986;158:183–189
- Schellhas KP, Wilkes CH, Heithoff KB, Omlie MR, Block JC. Temporomandibular joint: diagnosis of internal derangements using magnetic resonance imaging. *Minn Med* 1986;69:516–519
- Harms SE, Wilk RM. Magnetic resonance imaging of the temporomandibular joint. *RadioGraphics* 1987;7:521–542
- Schellhas KP, Wilkes CH, Fritts HM, Omlie MR, Heithoff KB, Jahn JA. Temporomandibular joint: MR imaging of internal derangements and post-operative changes. *AJNR* 1987;8:1093–1101, *AJR* 1988;150:381–389
- Burnett KR, Davis CL, Read J. Dynamic display of the temporomandibular joint meniscus using “fast scan” MR imaging. *AJR* 1987;149:959–962
- Schellhas KP, El Deeb M, Wilkes CH, et al. Three dimensional computed tomography in maxillofacial surgical planning. *Arch Otolaryngol Head Neck Surg* 1988;114:438–442
- Schellhas KP, Wilkes CH, Omlie MR, et al. The diagnosis of temporomandibular joint disease: two-compartment arthrography and MR. *AJNR*

- 1988;9:579-588, *AJR* 1988;151:341-350
12. Schellhas KP, Fritts HM, Heithoff KB, Jahn JA, Wilkes CH, Omlie MR. Temporomandibular joint: MR fast scanning. *J Craniomand Pract* 1988; 6:209-216
 13. Schellhas KP, El Deeb M, Wilkes CH, et al. Permanent proplast temporomandibular joint implants: MR imaging of destructive complications. *AJR* 1988;151:731-735
 14. Schellhas KP, Wilkes CH, Fritts HM, Lagrotteria LB, Omlie MR. MR of osteochondritis dissecans and avascular necrosis of the mandibular condyle. *AJNR* 1989;10:3-12, *AJR* 1989;152:551-560
 15. Schellhas KP, Wilkes CH. Temporomandibular joint inflammation: comparison of MR fast scanning with T1- and T2-weighted imaging techniques. *AJNR* 1989;10:589-594, *AJR* 1989;153:(in press)
 16. Gorlin RJ, Pindborg JJ, Cohen MM. *Syndromes of the head and neck*, 2nd ed. New York: McGraw-Hill, 1976:341-343
 17. Martinelli P, Fabbri R, Gabellini AS, Mazzini G, Rasi F. Familial hypertrophy of masticatory muscles. *J Neurol* 1987;164:811-816
 18. Isberg A, Isacson G, Noh K-S. Mandibular coronoid process locking: a prospective study of frequency and association with internal derangement of the temporomandibular joint. *Oral Surg Oral Med Oral Pathol* 1987; 63:275-279
 19. Ramon Y, Samra H, Oberman M. Mandibular condylosis and apertognathia as presenting symptoms in progressive systemic sclerosis (scleroderma). Pattern of mandibular bony lesions and atrophy of masticatory muscles in PSS, presumably caused by affected muscular arteries. *Oral Surg Oral Med Oral Pathol* 1987;63:269-274
 20. Rigamonti D, Spetzler RF, Shetter A, Drayer BP. Magnetic resonance imaging and trigeminal schwannoma. *Surg Neurol* 1987;28:67-70
 21. Markoff M, Farole A. Reflex sympathetic dystrophy syndrome. Case report with a review of the literature. *Oral Surg Oral Med Oral Pathol* 1986;61: 23-28
 22. Jaeger B, Singer E, Kroening R. Reflex sympathetic dystrophy of the face. Report of two cases and a review of the literature. *Arch Neurol* 1986; 43:693-695
 23. Schwartzman RJ, McLellan TL. Reflex sympathetic dystrophy: a review. *Arch Neurol* 1987;44:555-561
 24. Talacko AA, Reade PC. Hemifacial atrophy and temporomandibular pain-dysfunction syndrome. *Int J Oral Maxillofac Surg* 1988;17:224-226
 25. Wilkes CH. Internal derangement of the temporomandibular joint: pathologic variations. *Arch Otolaryngol Head Neck Surg* 1989;115:469-477



Scientific Program (200 papers)

Instructional Courses (60 hours)

Categorical Course on
Cardiovascular Imaging

The Caldwell Lecture

Award Papers

Scientific Exhibits

Social, Golf, and Tennis Programs

Guest Programs



Come to the
American Roentgen Ray Society

90th

ANNUAL MEETING

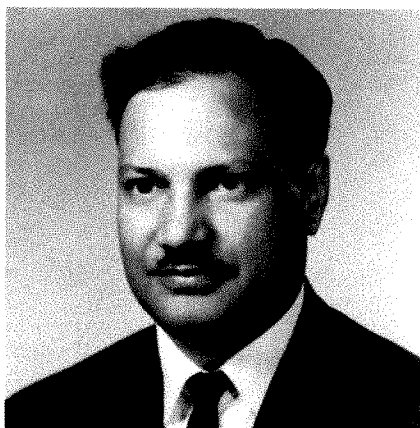
Washington, D. C.

Sheraton Washington Hotel

May 13-18, 1990

Memorial

Satya Pal Aggarwal, 1925–1989



Dr. Satya Pal Aggarwal died in Delhi on January 19, 1989, after a 13-month heroic struggle against cancer. During his illness, he never lost hope, and he fought courageously and with remarkable patience.

After graduation from Glancy Medical College, Amritsar, he followed in the footsteps of his illustrious father, Diwan Chand Aggarwal, who, even in his own lifetime, was a legend in radiology. After the partition of the country, the Aggarwals moved from Lahore in West Pakistan to Delhi, and young Satya

Pal and his father soon established one of the most modern and well-equipped radiology clinics at Delhi. During this time, Satya Pal went to Vienna to work with the famous radiologist, Professor Zsvonsky, and obtained his postgraduate qualification. His tireless efforts ultimately created the largest and most modern radiology and imaging clinic in India, the Dr. Diwan Chand Aggarwal X-Ray Clinic at Delhi. Despite the large number of patients and the high costs of sophisticated machinery, Satya Pal Aggarwal ensured that the clinic would provide every diagnostic procedure to patients at an affordable cost. He was an ardent follower of Bhagvad Gita and lived the life of a "Karma Yogi."

Dr. Aggarwal served the Indian Radiological & Imaging Association (IRIA) in various capacities: first as secretary and then twice as president of the Delhi Branch of IRIA. Later, he was the general secretary of IRIA for several years and then was elected president. He was also deeply involved with the Indian Medical Association. He was the architect of its new wing, the Indian Academy of Medical Specialties, and was its general secretary. He was an astute organizer and had successfully organized several national conferences at Delhi with distinction.

In 1977, he was nominated as a director of the Hindustan Photo Films Mfg. Co. Ltd., a Government of India Undertaking, and

served this organization fruitfully with his vast knowledge of all spheres of radiology: academics, organization, and equipment.

He distinguished himself in the academic field, too, and was always ahead of his colleagues in the teaching institutions. In recognition, he was elected unopposed for the coveted "Sir Jagadish Chandra Bose Memorial Oration" for his outstanding contribution to radiology and imaging.

He was deeply involved with patient care and was dedicated to his patients. He had endeared himself to them so much that they approached him like a friend and went home with a smile on their lips.

Dr. Satya Pal Aggarwal was a simple man at heart. His deep insight into human nature stood him in good stead in making friends all over the world. He was soft-spoken, kind-hearted, and selfless. His sincerity won him many admirers. He was never in the habit of mincing words and spoke his mind clearly about the affairs of the IRIA, but his words never hurt anyone. With his death, we have lost a towering personality—a man with pioneering zeal, endless energy, and unaffected warmth of heart. He leaves behind his devoted wife, Raj, four brothers and four sisters, and countless friends and admirers.

S. K. Dhawan
New Delhi-110001, India

MR Imaging of Neurocysticercosis

George P. Teitelbaum^{1,2}
 Ronald J. Otto^{1,3}
 Mimi Lin⁴
 Alyssa T. Watanabe⁵
 Margaret A. Stull²
 Herbert J. Manz⁶
 William G. Bradley, Jr.¹

This article appears in the July/August 1989 issue of *AJNR* and the October 1989 issue of *AJR*.

Received April 6, 1988; revision requested June 16, 1988; revision received January 5, 1989; accepted January 5, 1989.

Presented at the annual meeting of the American Society of Neuroradiology, New York City, May 1987.

¹ Huntington Medical Research Institutes, 10 Pico St., Pasadena, CA 91105. Address reprint requests to W. G. Bradley, Jr.

² Department of Radiology, Georgetown University Hospital, 3800 Reservoir Rd., N.W., Washington, DC 20007.

³ Riverside Radiology Medical Group, 6941 Brockton Ave., Riverside, CA 92506.

⁴ Department of Radiology, Kaiser-Permanente Medical Center, Sunset Blvd., Los Angeles, CA 90039.

⁵ Department of Radiology, University of California, Los Angeles, School of Medicine, Los Angeles, CA 90024.

⁶ Department of Pathology, Georgetown University Hospital, Washington, DC 20007.

AJNR 153:857-866, October 1989

0361-803X/89/1534-0857

© American Roentgen Ray Society

Twenty-six patients with neurocysticercosis were studied with MR imaging to correlate their clinical presentation with the location and appearance of their neurocysticercosis lesions. Intraventricular cysts were present in 14 patients (54%), parenchymal cysts were present in 18 (69%), and intraventricular together with parenchymal cysts were present in six (23%). Intraventricular cysts were detected by mass effect, ventricular obstruction, detection of a cyst rim, and/or CSF flow void adjacent to the cyst. The intensity of most intraventricular and parenchymal cysts presumed to be viable was similar to that of CSF on both T1- and T2-weighted sequences. Cysts presumed to be degenerated had increased signal intensity on T1-weighted images, probably resulting from increased protein content. Pericystic high signal intensity surrounding lesions of various ages was seen on both proton-density- and T2-weighted images and represents gliosis, edema, and inflammation. Patients with parenchymal cysts had symptoms of seizures, while those with intraventricular cysts generally had symptoms related to obstructive hydrocephalus. Aqueductal stenosis, seen in 10 patients (38%), was possibly due to ependymal inflammation or adhesions caused by prior ventricular infection by neurocysticercosis. One patient with the racemose form of neurocysticercosis demonstrated abundant cyst wall proliferation resulting in obstructive hydrocephalus. In six patients scanned 1-6 months after oral praziquantel therapy, there was no change in the MR appearance of intraventricular cysts, while some parenchymal cysts showed evidence of degeneration.

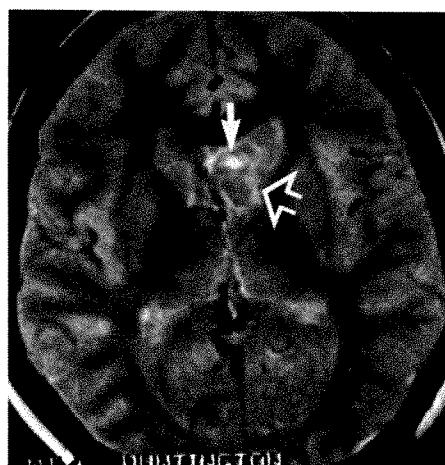
We found MR to be useful in detecting the cysts of neurocysticercosis and the accompanying signs of cyst degeneration and pericystic inflammation. MR was inferior to CT in the detection of parenchymal calcifications.

Neurocysticercosis is an infection of the CNS by the larval stage of the pork tapeworm *Taenia solium*. The disease is prevalent in developing nations, particularly in regions of poor sanitation and hygiene. It is the most common cause of seizures in young adults in endemic areas [1]. With immigration of individuals from endemic areas, cysticercosis is becoming increasingly prevalent in the United States [1].

The diagnosis of neurocysticercosis often depends on a combination of clinical symptoms, CSF analysis, and radiologic findings [2]. CSF antibody or antigen titers are useful, but the findings can be nonspecific [2-4]. Radiologic findings are the most sensitive [2]. CT is beneficial in identifying parenchymal calcifications associated with neurocysticercosis; however, intraventricular cysts often are difficult to identify with CT owing to the similarity of densities between cyst fluid and CSF. MR imaging, with its multiplanar imaging capabilities, excellent depiction of tissue contrast, and sensitivity to flow effects, is a powerful technique for the evaluation of neurocysticercosis, particularly in the presence of intraventricular cysts. The present study analyzes the location and MR appearance of neurocysticercosis lesions in 26 patients and correlates these findings with clinical presentation.

TABLE 1: Summary of Findings in Patients with Neurocysticercosis

Variable	Type of Cyst			Total
	Parenchymal	Intraventricular	Mixed Parenchymal/ Intraventricular	
Cyst characteristics				
Total no.	12	9	26	47
Locations of intraventricular				
Third ventricle	–	3	3	6
Fourth ventricle	–	2	2	4
Lateral ventricle	–	3	1	4
Subarachnoid cistern	–	1	4	5
MR intensities				
Isointense relative to CSF	2	7	14/10 ^a	33
Hyperintense relative to CSF	10	2	2/0 ^a	14
Patient characteristics				
Total no.	12	8	6	26
Presenting symptoms				
Seizures	10	0	3	13
Nausea/vomiting and/or headache	2	8	3	13
Patients with aqueductal stenosis	1	6	3	10
Means of diagnosis				
CSF analysis	8	6	4	18
Surgery	4	2	2	8

^a Parenchymal/intraventricular.

1



2

Fig. 1.—Axial MR image (SE 2000/60) through lateral ventricles. Cysticercosis cyst in anterior horn of left lateral ventricle displays rim of hyperintensity (open arrow) caused by ependymal inflammation. Scolex (solid arrow) is well defined as focus of hyperintensity within cyst.

Fig. 2.—Axial section (SE 2000/60) through level of third ventricle. A 1-cm cyst within third ventricle (arrow) displays prominent hyperintensity suggestive of cyst degeneration. Scolex cannot be identified.

Materials and Methods

Between May 1983 and July 1988, 26 patients, 18 males and eight females 7–69 years old, with a diagnosis of neurocysticercosis underwent cranial MR imaging. The clinical records of these patients were reviewed retrospectively to determine the presenting symptoms; that is, seizures vs signs of hydrocephalus (e.g., headache, ataxia, and nausea and vomiting). Diagnoses of neurocysticercosis were corroborated by findings at surgery and/or CSF analysis. All MR studies were performed on a 0.35-T,* 0.5-T† or 1.5-T‡ superconducting MR unit. All patients were initially scanned in the axial plane with dual-echo spin-echo (SE) technique, 2000–3000/30–100/2–4 (TR range/TE range/excitations). Sagittal and coronal SE images (1000/30–80/

2) were obtained in most cases to further characterize lesions observed during the initial axial sequences. Slice thicknesses of either 5 or 10 mm were used. The matrix size was either 128 × 256 or 256 × 256. Each MR study was evaluated for the site(s), number, and signal pattern of intracranial cysts. Cysts within the subarachnoid cisterns were included within the intraventricular group. The cyst rim was assessed for thickness, the presence and extent of pericystic high signal intensity, and alterations in ependymal signal intensity.

The ventricular system was evaluated for evidence of obstruction manifested by general ventricular dilatation (out of proportion with sulcal enlargement), third ventricular enlargement, temporal horn enlargement, and periventricular high signal (on T2-weighted images) suggestive of transependymal CSF flow. Aqueductal stenosis, as evidenced by a diminutive area of aqueductal low signal, was evaluated on both sagittal and axial MR images.

MR results were correlated with brain CT scans and pathologic findings when available. Correlation was made between the clinical presentation of the patients and the MR pattern of neurocysticercosis.

* Diasonics, Milpitas, CA.

† Siemens, Erlangen, W. Germany.

‡ General Electric, Milwaukee, WI.

Six patients received oral praziquantel therapy at a dosage of 60 mg/kg/day for up to 2 weeks and underwent a repeat MR examination 6 weeks to 6 months after the completion of therapy. MR examinations were evaluated for changes in the number and appearance of cysts.

Results

The MR findings of the 26 patients are summarized in Table 1.

Intraventricular Cysts

Fourteen (54%) of the 26 patients in our series had intraventricular cysts. In eight (31%) of the 26 patients, intraventricular cysts were present without parenchymal cysts. In each of these eight (and in a total of 11 of the 14 patients with intraventricular cysts), there was a clinical history of nausea and vomiting or headaches or both. The symptoms were believed to be related to elevated intracranial pressure caused by the cysts. Eight patients required the placement of a ventriculoperitoneal shunt for varying degrees of hydrocephalus. Two patients each had cysts in the fourth, third, and lateral ventricles, while one patient had a cyst in both the third and lateral ventricles. The intraventricular cysts were typically 1–2 cm in diameter. Eleven (79%) of the 14 patients had evidence of a pericystic ependymal inflammatory reaction,

as manifested by a hyperintense rim best seen on T2-weighted images (Fig. 1). The cysts generally had a signal intensity similar to that of CSF on T2-weighted images. Mass effect, visualization of the cyst rim, and CSF flow void adjacent to these cysts aided in their identification. Two of the intraventricular cysts had fluid that on T2-weighted images was hyperintense relative to CSF (Fig. 2).

Six (23%) of the 26 patients had both intraventricular and parenchymal cysts. Three of these six patients presented with nausea, vomiting, and headaches. Four of these six patients had multiple parenchymal cysts; one patient had a total of five. One patient had an unusually large fourth ventricular cyst and three identifiable parenchymal cysts (Fig. 3). Although three of the six patients presented with seizures, cyst degeneration was thought to be present in only two of the three. Prominent pericystic ependymal reaction was seen in two of the three seizure patients.

Parenchymal Cysts

Eighteen (69%) of 26 patients presented with parenchymal cysts that involved the gray/white-matter junction in all but one case. Twelve (46%) of the 26 patients had MR evidence of parenchymal cysts only. Ten patients (83%) in this subgroup of 12 patients had a history of recent seizures. All of these 10 patients had MR findings of pericystic high signal intensity suggesting gliosis and/or edema (Fig. 4). In one

Fig. 3.—Sagittal sections (SE 1000/40) in patient with large fourth ventricular cyst.

A, Scolex (straight solid arrow) is well demonstrated. Dilated cerebral aqueduct, with central flow void (curved arrow), probably is due to to-and-fro CSF flow caused by obstructive effects of subjacent fourth ventricular cyst (open arrow).

B, Section 5.5 mm lateral to A shows superiorly located 1-cm parenchymal cyst with central scolex (arrow). Signal intensity of cyst fluid is similar to that of CSF on this sagittal image. No pericystic edema is present, suggesting cyst viability.

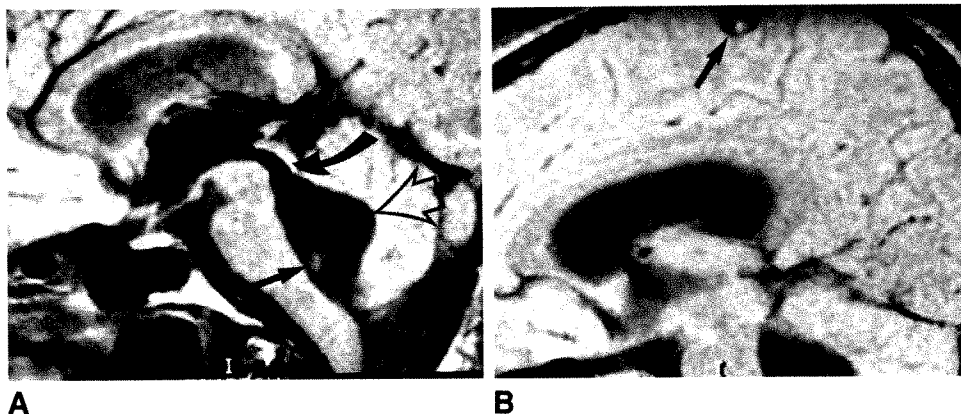
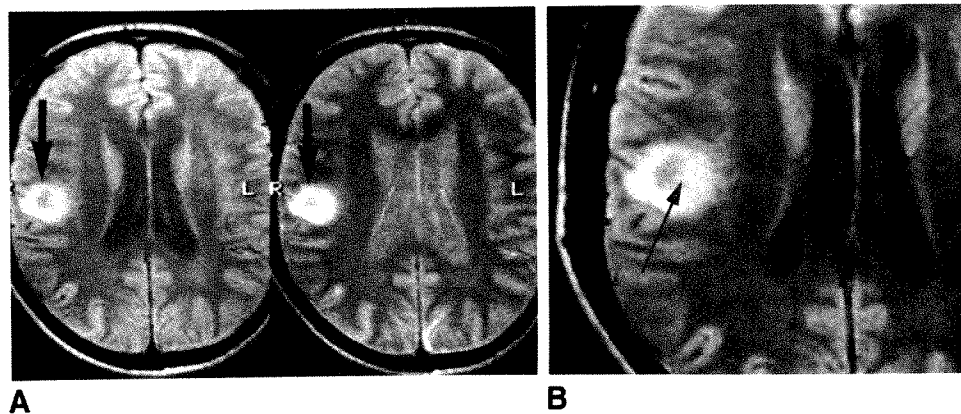


Fig. 4.—Patient with recent onset of seizures.

A and B, Axial MR images, SE 2000/30 (left) and SE 2000/60 (right), show right parietal cystic lesion with pericystic rim of hyperintensity (arrows) suggestive of inflammatory reaction with gliosis and/or edema. Cyst fluid is isointense relative to CSF.

B, Magnified view of first-echo image. What appears to be scolex can be faintly visualized along medial cystic wall (arrow).



case, the extensive pericystic inflammatory reaction simulated a glioma (Fig. 5). Pathologic examination of the surgical specimen from this lesion and another cyst with extensive pericystic high-signal change revealed surrounding gliosis (Fig. 6). One (8%) of these 12 patients with parenchymal cysts presented with only headaches, and another (8%) had unrelated clinical findings in which the neurocysticercosis cyst was found incidentally. One patient in this group who presented with headaches and ataxia was found to have an unusually large 4-cm cyst in the cerebellum that was surgically resected (Fig. 6). Typically, the cysts in these 12 patients were 1–2 cm in diameter. A central or eccentric high-signal focus, suggestive of a scolex, could be identified in only six cysts. Pathologic correlation was available in two patients with this appearance.

In both cases, a scolex was identified (Fig. 7). In one of these cases, the organism appeared viable. However, there was a significant amount of pericystic high signal indicating an inflammatory reaction (Fig. 7).

Aqueductal Stenosis

In 10 (38%) of 26 patients (nine of 14 patients with intraventricular cysts and one of 12 patients with parenchymal cysts only) cerebral aqueductal stenosis was identified that was best appreciated on sagittal images (Fig. 8) as an absence of the normal aqueductal CSF flow void on midline slices. This finding may be associated with ependymal inflammation (granular ependymitis with subependymal gliosis) or

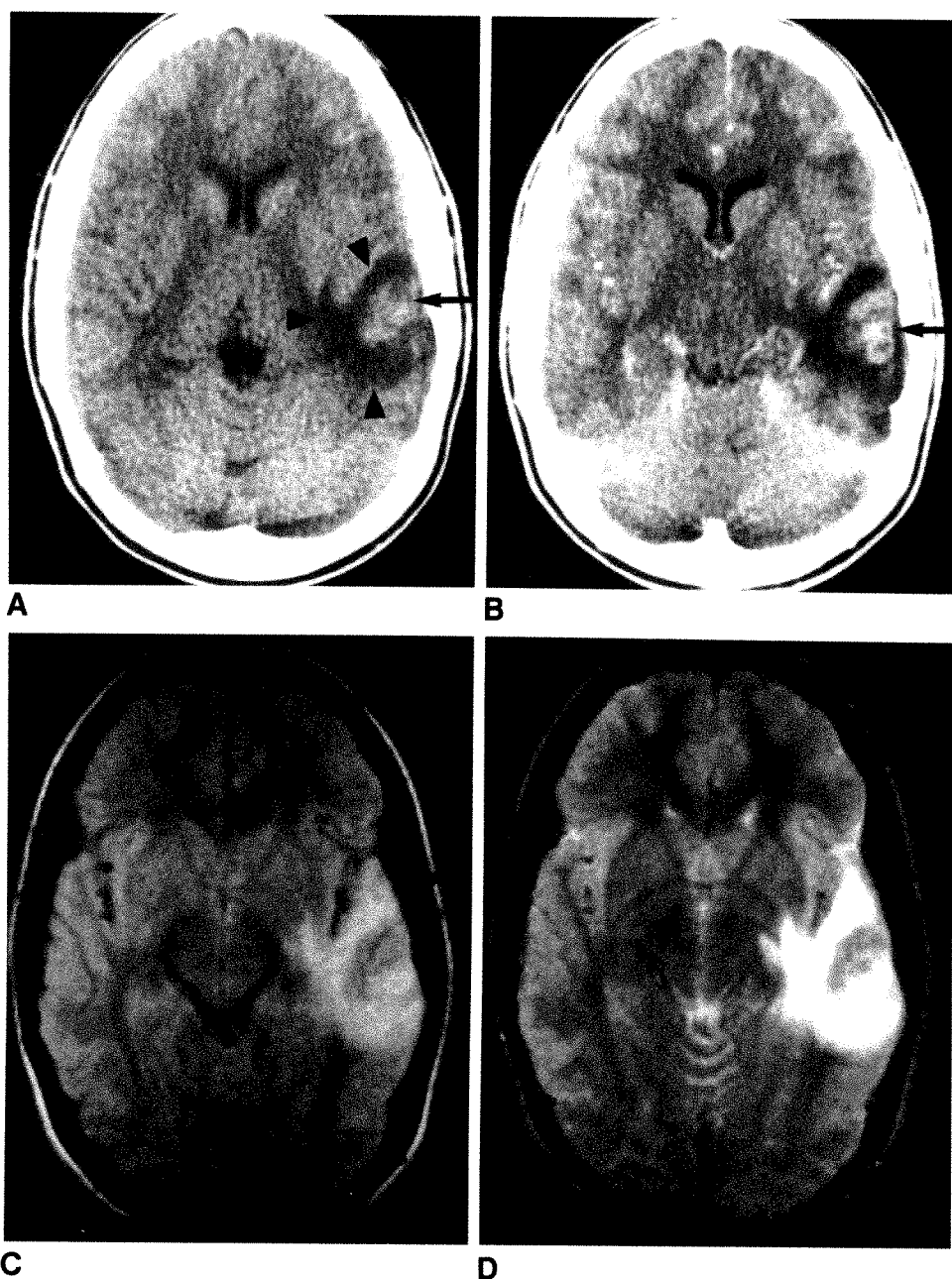


Fig. 5.—CT and MR findings in patient with seizures.

A, Nonenhanced brain CT scan shows left posterior temporal mass (arrow) with surrounding area of low attenuation (arrowheads) consistent with parenchymal edema.

B, Contrast-enhanced CT scan shows enhancement within mass (arrow).

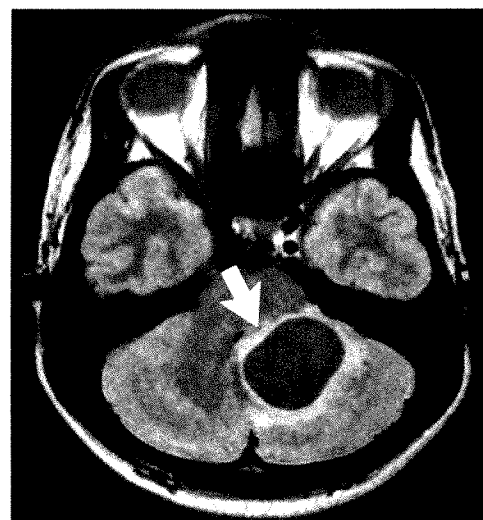
C, First-echo image of axial MR brain study (SE 2450/30) shows large area of increased signal intensity surrounding this same lesion representing edema.

D, Edematous changes appear more intense on second-echo image (SE 2450/100). Preoperative diagnosis was glioma. However, at surgery, a degenerated cysticercosis cyst was found with extensive edema and gliosis surrounding the lesion.

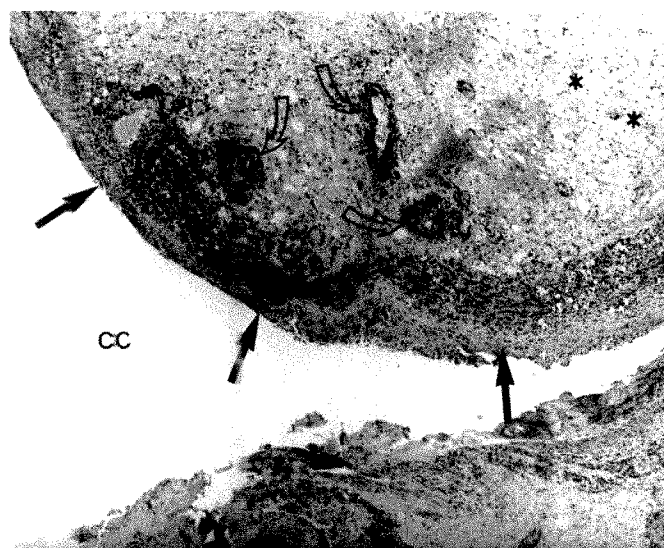
Fig. 6.—A, Axial section (SE 2000/40) shows atypically large 4-cm cerebellar parenchymal cyst. Note pericystic rim of hyperintensity (arrow), indicating inflammatory reaction. Cyst was removed at surgery.

B, Histopathologic specimen from excised tissue shows cyst cavity (CC), host-derived cyst wall and adjacent inflammation (solid arrows), perivascular inflammation (open arrows), as well as inflammatory reaction with gliosis and edema in surrounding cerebellar tissue (asterisks). (H and E, $\times 68$)

C, Nonviable larva found in same surgical specimen. Note poorly defined internal chitinous wall within parasite (solid arrows). Also seen are adjacent inflammatory infiltrate (open arrows) and cerebellar gliosis and edema (asterisks). (H and E, $\times 134$)



A



B



C

adhesions due to prior ventricular infestation. Seven of the 10 aqueductal stenosis patients were judged to have some degree of hydrocephalus.

One of these 10 patients presented with abundant cyst wall proliferation within the quadrigeminal plate cistern, associated with the racemose form of neurocysticercosis, which resulted in obstructive hydrocephalus and required shunting. The proliferative changes in the cyst wall were well demonstrated on both T2-weighted axial and coronal images (Fig. 9). The cyst fluid intensity was similar to that of CSF on both T1- and T2-weighted images. This patient also had a history of presumed bacterial meningitis that was unresponsive to therapy.

CT Correlation

CT brain scans were obtained (at comparable times) in 10 (38%) of the 26 patients. Seven (70%) of the 10 CT examinations demonstrated parenchymal calcifications (Fig. 10A). MR was less sensitive than CT in demonstrating the size and

number of calcifications. In only three (43%) of these seven MR studies was there evidence of calcifications (small signal-void areas) (Fig. 10B). In seven (70%) of 10, CT demonstrated ventriculomegaly consistent with hydrocephalus; however, CT could not define the cause of hydrocephalus. MR was able to identify the cause of hydrocephalus in six of these seven patients (usually an intraventricular cyst) (Fig. 11). MR was more sensitive than CT in showing the extent of pericystic gliotic/edematous changes (Fig. 7).

Changes After Praziquantel Therapy

Among the seven parenchymal cysts in six patients, there was evidence of degeneration, manifested by increased signal on T1-weighted images, in only three cysts (in two patients) after praziquantel therapy (Fig. 12). One of the seven parenchymal cysts regressed and was no longer visible after therapy. All six patients had intraventricular cysts also. In one of these patients, an intraventricular cyst was removed sur-

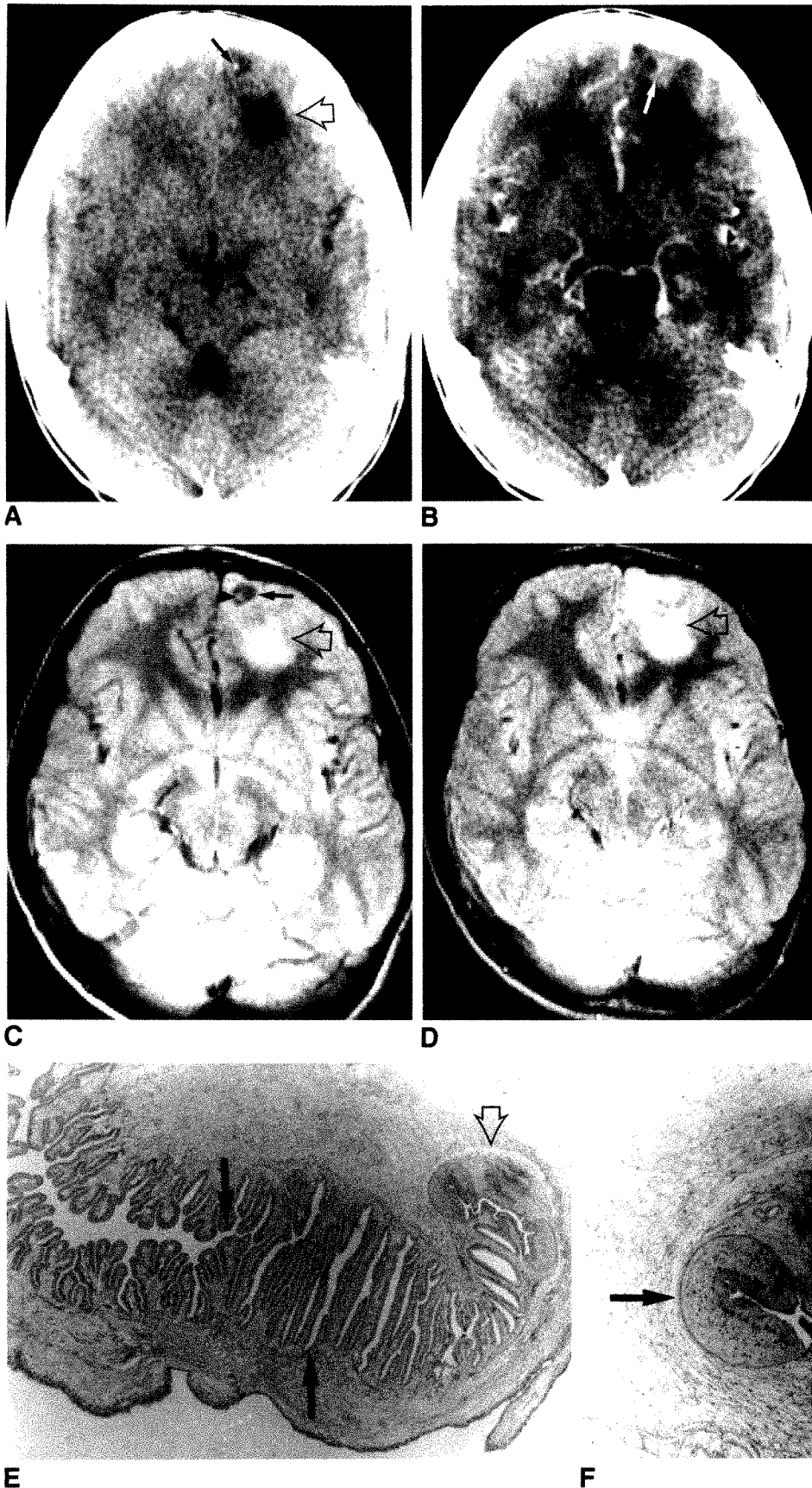


Fig. 7.—A, Nonenhanced axial CT image shows left frontal cysticercosis lesion in patient with seizures. Central calcification (solid arrow) is present within cyst, and there is a small adjacent area of decreased attenuation consistent with parenchymal edema (open arrow).

B, After administration of IV contrast material, CT shows only small region of pericystic enhancement (arrow).

C and D, Proton-density-weighted, SE 2500/30 (C), and T2-weighted, SE 2500/80 (D), axial MR images show left frontal pericystic inflammatory reaction—high-signal-intensity area (open arrows)—with better definition than on CT. These changes were more pronounced on second-echo image (D). Cyst, with fluid isointense relative to CSF (solid arrow), and central scolex (arrowhead) are better seen on first-echo image (C). Calcification was not visible on MR images. Lesion was surgically removed.

E, Histopathologic specimen from excised tissue shows invaginated scolex with well-defined, highly convoluted, and internalized cell membrane (chitinous wall) (solid arrows). This extends to muscular suckers at right of photograph (open arrow). (H and E, $\times 180$)

F, Magnified view of E depicts three muscular suckers (arrows). (H and E, $\times 500$)

gically. No signal or morphologic changes were noted in intraventricular cysts after praziquantel therapy.

Discussion

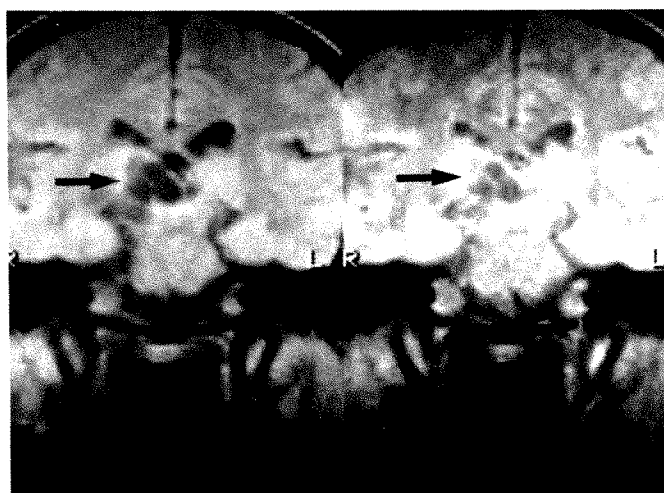
When the embryonated ova of *T. solium* are ingested, usually as a result of fecal contamination of food or water or autoinfection in tapeworm carriers, gastric acid releases the hexacanth larvae from their encasement, thus creating the



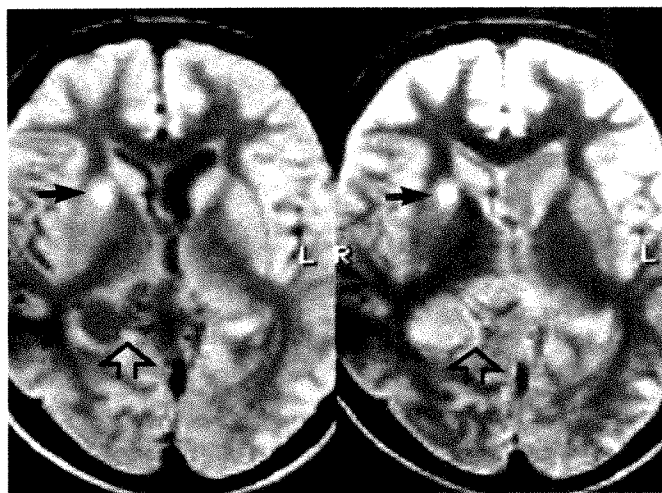
Fig. 8.—Midline sagittal 5-mm section (SE 1000/40) shows cerebral aqueduct stenosis (arrow) in patient with intraventricular infestation. (Aqueductal narrowing was identified in nine of 14 patients with intraventricular cysts and may be related to ependymal inflammatory reaction or adhesions from previous infestation.)

intermediate host state. Once the hexacanth larvae penetrate the intestinal mucosa, they are transported via the lymphatics or venules to the systemic circulation. The blood-borne organisms have a predilection for localization in skin and muscle, where they are asymptomatic, and in the CNS (particularly the cerebral gray matter, periventricular tissues, and leptomeninges), where they may present with a variety of clinical manifestations. The hexacanth larval cells proliferate, eventually producing cysts, typically 1–2 cm in diameter. A small invagination develops along one margin of the cyst and proliferates and differentiates to become the scolex. Cyst fluid is usually clear. Cloudiness of the cyst fluid usually indicates death of the parasite. With death of the parasite, there is resultant cyst degeneration and a striking host inflammatory cell and gliotic reaction. It is probable that during the life span of the cysticercus, there is active suppression of host defenses by factors secreted by the parasite; as the organism loses viability, host immune and inflammatory responses are brought into play, thereby accounting for the marked brain edema about degenerating cysticerci [5].

The diagnosis of neurocysticercosis is confirmed by clinical history, serology and CSF analysis, CT and MR findings, and occasionally, surgical findings. A history of travel to or immigration from an endemic area assists in making the diagnosis. Serology and CSF analysis can be helpful in the case of intraventricular infestation [3, 4, 6]. The CT identification of multiple focal brain parenchymal calcifications [7] and the demonstration of the actual cyst (and the scolex within it) with CT and/or MR [2] are particularly valuable in arriving at a diagnosis. However, in some cases (Fig. 5), the CT and MR findings may still be inconclusive, necessitating surgical resection and histopathologic diagnosis. CT and MR can also



A



B

Fig. 9.—A and B, Coronal, SE 1000/28 (left) and SE 1000/56 (right) (A), and axial, SE 2000/28 (left) and SE 2000/56 (right) (B), sections in patient with racemose form of cysticercosis. Multiple cysts are present in ambient cistern on coronal images (A, arrows). Cysts were observed extending from quadrigeminal plate cistern into right retropulvinar cistern (open arrows) on axial images (B). Axial images also demonstrated an additional hyperintense lesion within right globus pallidus (solid arrows). On both echoes, during coronal and axial imaging, cysts remained isointense relative to CSF and produced little evidence of ependymal reaction. Racemose form of neurocysticercosis is believed to be a proliferative reaction of cyst in which no scolex is formed, but cyst infiltrates subarachnoid spaces irregularly and conforms to their peculiar configurations in various locations. The patient received a ventriculoperitoneal shunt to relieve obstructive hydrocephalus.

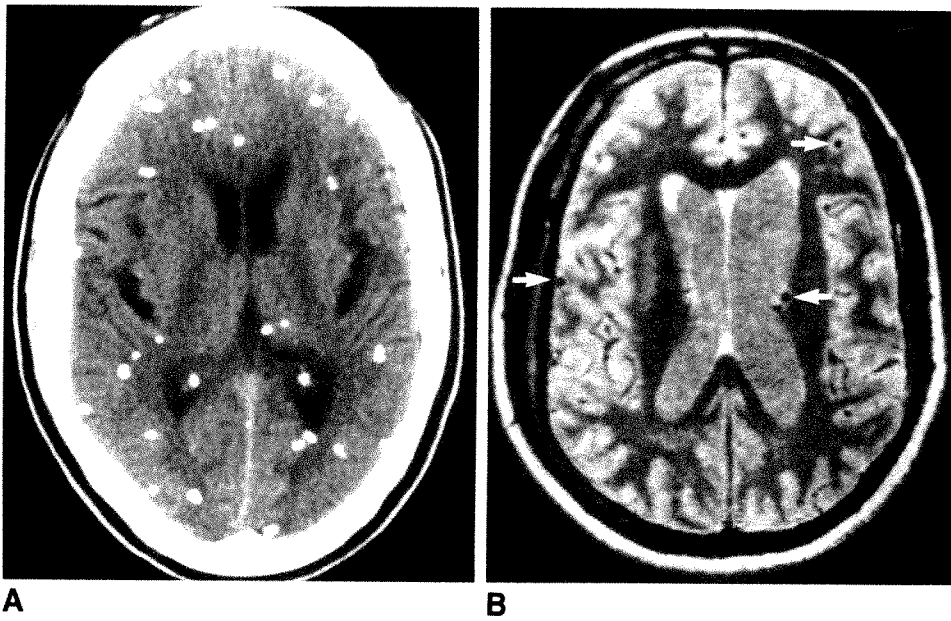


Fig. 10.—A, Nonenhanced brain CT scan reveals numerous small parenchymal calcifications caused by old cysticercosis lesions.

B, Axial MR brain scan (SE 2000/60) displays calcific foci as small signal-void zones (arrows). Parenchymal calcifications of neurocysticercosis are better detected with CT than with SE MR imaging.

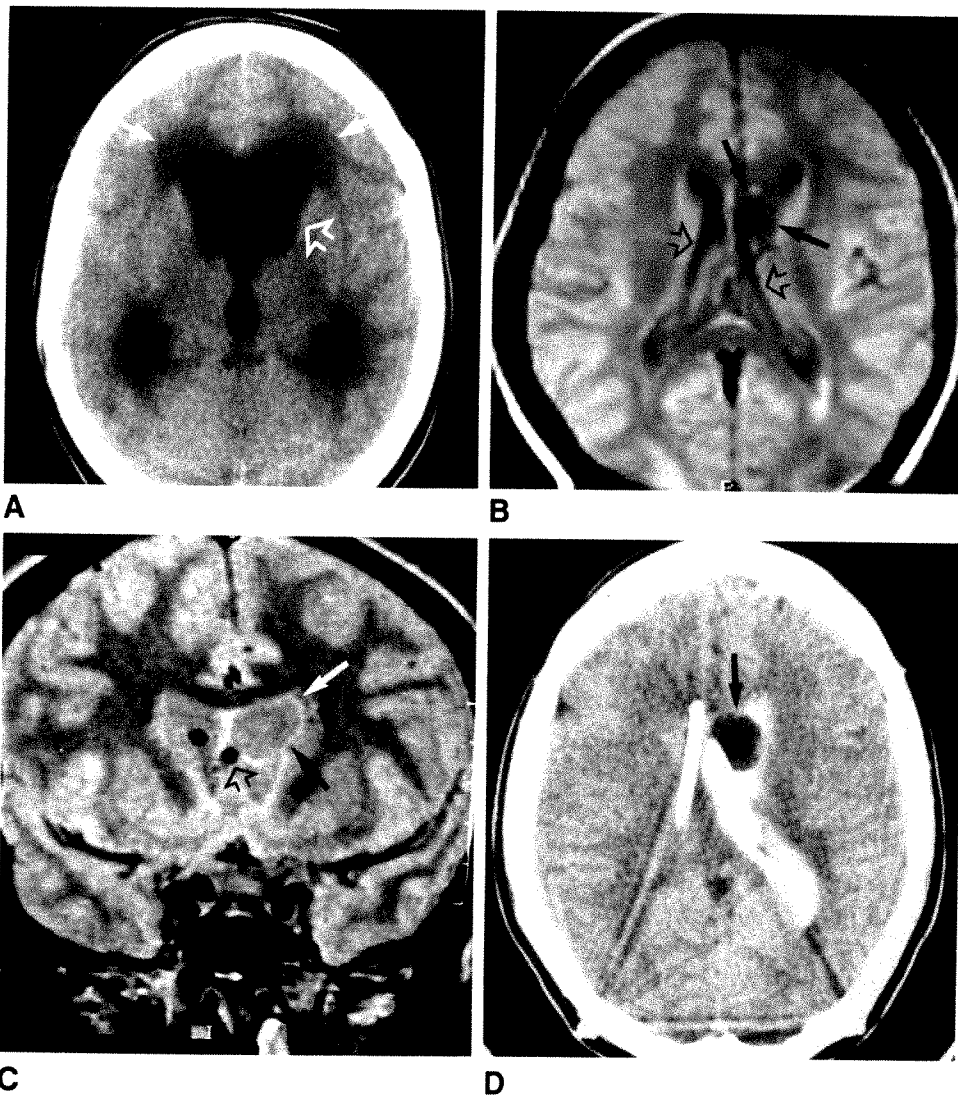


Fig. 11.—A, Nonenhanced brain CT scan shows third and lateral ventricular dilation as well as periventricular low attenuation (solid arrows) consistent with hydrocephalus with transependymal CSF flow. Frontal horn dilation is slightly more prominent on left side (open arrow).

B, Axial first-echo MR brain scan (SE 2000/30) after placement of bilateral ventriculoperitoneal shunt tubes (open arrows). There is left frontal horn intraventricular cysticercosis cyst (solid arrows) with well-defined cyst rim. Ventriculoperitoneal shunt tubes display low signal intensity (open arrows).

C, Coronal MR scan (SE 3000/40) further defines left frontal horn cyst (solid arrows), which displaces left shunt tube medially and inferiorly (open arrow).

D, Contrast ventriculography performed during follow-up brain CT scan confirms presence of cyst (arrow).

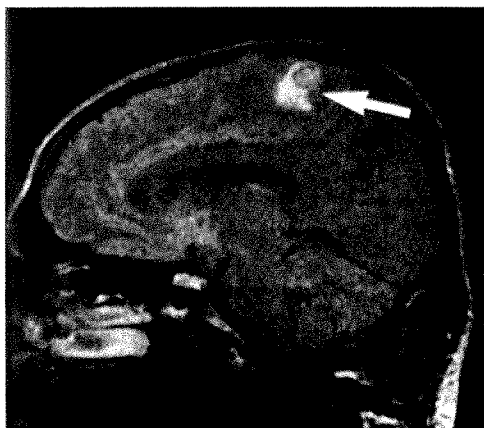


Fig. 12.—Sagittal section (SE 1000/80) of patient in Fig. 3 after surgical resection of fourth ventricular cyst and subsequent oral praziquantel therapy. There is now evidence of pericystic edema, consistent with adjacent inflammatory reaction, surrounding superiorly located parenchymal cyst (arrow).

be of assistance in the follow-up evaluation of patients. Intraventricular cysts were encountered in 14 (54%) of the 26 patients. The cyst fluid was generally isointense relative to CSF; however, in two cases, slightly increased cyst fluid intensity (relative to CSF) was present, which may have been related to cyst degeneration or lack of flow effects within the cyst fluid or both. Mass effect, a cyst rim, adjacent CSF flow void, and ventricular outflow obstruction were all beneficial in confirming the presence of intraventricular cysts. Eleven (79%) of the 14 patients with intraventricular cysts showed evidence of pericystic edema. This finding may be a sign of initial cyst degeneration or may be the result of cystic attachment to the ependyma, eliciting a granulomatous response [8]. Nine (90%) of the 10 patients with aqueductal stenosis had intraventricular cysts. The aqueductal stenosis may have been the result of prior intraventricular cyst degeneration resulting in ependymal scarring and adhesions [9]. The direct sagittal imaging capabilities of MR were vital in diagnosing aqueductal stenosis. Eleven patients (79%) with intraventricular cysts had symptoms of frequent headaches, nausea, and vomiting, which may have been related to increased intracranial pressure. Intraventricular cysts may remain clinically silent until they degenerate, inciting an ependymal reaction, or until they cause obstructive hydrocephalus [9–12].

One patient (Fig. 9) presented with the racemose form of neurocysticercosis. Racemose cysts usually lack a scolex and are typically found in the cisterns around the rostral brainstem or the sylvian fissure [1]. They may produce obstructive hydrocephalus [1]. The degenerating cyst may incite an excessive leptomeningeal fibroblastic and inflammatory reaction, causing extensive cyst wall proliferation. In our patient, the proliferative changes in the cyst wall were well demonstrated by MR. The patient also had a history of meningitis. The racemose form of neurocysticercosis is known to be associated with chronic meningitis [9].

Parenchymal cysts were present in 18 (69%) of the 26 patients and were noted to involve the gray/white-matter

junction almost invariably. No cases of meningeal neurocysticercosis were encountered in our series. Typically, the parenchymal cysts that were considered viable were isointense relative to CSF on T1- and T2-weighted images. It is known that with cyst degeneration, cyst fluid becomes more proteinaceous and gelatinous [9]. This was manifested on MR images as increased signal intensity of the cyst fluid on T1- and proton-density-weighted sequences, probably due to T1-shortening effects of increased protein solutes and surface-layer effects of water molecules interacting with macromolecules within the cyst fluid [13].

Viable parenchymal larvae survive for approximately 5 years and then die for unknown reasons [14]. Upon the death of the parasites, a more pronounced host immune response is initiated with inflammation and edema. This inflammatory reaction often causes seizures [5, 9]. Correlation with pathologic specimens in two patients with marked pericystic inflammatory reaction (evidenced by increased signal intensity) demonstrated gliosis and edema (Figs. 5 and 6). Secondary astrocytic gliosis of variable intensity has been described as the most common pathologic change in the parenchyma immediately surrounding the cyst [9]. Because marked pericystic high signal was seen in one patient with a histopathologically demonstrated cysticercus (Fig. 7), the presence of pericystic hyperintensity may not always be a reliable indicator of the stage of cyst degeneration. Most of the parenchymal cysts encountered were 1–2 cm in diameter. However, one patient was found to have a cerebellar cyst 4 cm in diameter with a rim of pericystic edema (Fig. 6).

Although the advantages of MR in neurocysticercosis were obvious—that is, better tissue characterization, multiplanar imaging capabilities, etc.—SE MR imaging was insensitive to parenchymal calcifications that were well demonstrated on CT (Fig. 10) [7]. Gradient-echo MR imaging may display greater sensitivity to the presence of parenchymal calcifications. However, when compared with CT, MR better demonstrated the extent of pericystic inflammation (Fig. 7).

Praziquantel is a heterocyclic pyrazinoisoquinoline oral anthelmintic agent that is most effective against the *Schistosoma* species [15]. In some cases, it has been shown to be effective in the treatment of cysticercosis and typically is administered with a total daily oral dosage of 60 mg/kg for 4 days to 2 weeks [16–18]. Praziquantel acts by increasing the permeability of the organism's cell membranes to calcium ions, causing massive muscle contraction and paralysis followed by disintegration. Dexamethasone is often given in combination with praziquantel to reduce the inflammatory reaction (with accompanying edema) arising from larval degeneration, which can itself result in additional clinical symptoms, such as seizures or elevated intracranial pressure [12, 16].

One difficulty with praziquantel therapy is that patients with neurocysticercosis, especially those with parenchymal cysts, often do not present until cyst degeneration has already begun. The viable larvae tend not to cause appreciable symptoms, thus making evaluation of drug effectiveness difficult [9].

In the present series of six patients who received praziquantel therapy, two of the patients with parenchymal cysts demonstrated either a reduced number of detectable cysts or

evidence of the development of pericystic edema and cyst degeneration on follow-up MR studies (Fig. 12). None of the intraventricular cysts showed appreciable changes on repeat MR examinations performed 6 weeks to 6 months after a full course of therapy. These preliminary findings suggest that the CSF concentration of praziquantel may not have been sufficiently high to effect the destruction of viable larvae, and that a longer period of treatment may be required for the eradication of intraventricular cysts.

We conclude that MR is useful in evaluating neurocysticercosis, especially in the case of intraventricular cysts, not only because of MR's ability to actually detect cysts, but also because of its ability to detect signs of cyst degeneration and pericystic inflammation. Cerebral aqueductal stenosis due to periaqueductal ependymal inflammation was well demonstrated with MR. However, MR was insensitive to parenchymal calcifications that are typically seen well with CT. In our series of neurocysticercosis patients, treatment with praziquantel did not appear to appreciably affect intraventricular cysts.

ACKNOWLEDGMENTS

We thank K. E. Kortman, B. D. Klein, and E. Helmer for assisting in the collection of clinical material for this article and Edith E. Scott for manuscript preparation.

REFERENCES

- McCormick GF, Zee CS, Heiden J. Cysticercosis cerebri: review of 127 cases. *Arch Neurol* 1982;39:534-539
- Suss RA, Maravilla KR, Thompson J. MR imaging of intracranial cysticercosis: comparison with CT and anatomopathologic features. *AJNR* 1986;7:235-242
- Rydzewski AK, Chrisholm ES, Kagan IG. Comparison of serologic tests for human cysticercosis by indirect hemagglutination, indirect immunofluorescent antibody, and agar gel precipitin test. *J Parasitol* 1975;61:154-155
- Miller B, Goldberg MA, Heiner D, Myers A, Goldberg A. A new immunological test for CNS cysticercosis. *Neurology* 1984;34:695-697
- Rickard MD, Williams JF. Hydatidosis/cysticercosis: immune mechanisms and immunization against infection. *Adv Parasitol* 1982;21:229-296
- Flisser A, Larralde C. Cysticercosis. In: Walls KW, Schantz PM, eds. *Immunodiagnosis of parasitic diseases*, vol. 1. *Helminthic disease*. New York: Academic Press, 1986:109-161
- Bentson JR, Wilson GH, Helmer E, Winter J. Computed tomography in intracranial cysticercosis. *J Comput Assist Tomogr* 1977;1:464-471
- Scaravilli F. Parasitic and fungal infections of the nervous system. In: Adams JH, Corsellis JA, Duchon LW, eds. *Greenfield's neuropathology*, 4th ed. New York: Wiley, 1984:315-317
- Escobar A. The pathology of neurocysticercosis. In: Palacios E, Rodriguez-Carbajal J, Taveras JM, eds. *Cysticercosis of the central nervous system*. Springfield, IL: Thomas, 1983:27-54
- Marquez-Monter H. Cysticercosis. In: Marcial-Rojas, ed. *Pathology of protozoal and helminthic diseases with clinical correlation*. Baltimore: Williams & Wilkins, 1971:592-617
- Shanley JD, Jordan MC. Clinical aspects of CNS cysticercosis. *Arch Intern Med* 1980;140:1309-1313
- Apuzzo MLJ, Dopkin WR, Zee C-S, Chan JC, Giannotta SL, Weiss MH. Surgical considerations in treatment of intraventricular cysticercosis. An analysis of 45 cases. *J Neurosurg* 1984;60:400-407
- Fullerton GD. Physiologic basis of magnetic relaxation. In: Stark DD, Bradley WG Jr, eds. *Magnetic resonance imaging*. St. Louis: Mosby, 1988:36-55
- Handler LC, Mervis B. Cerebral cysticercosis with reference to the natural history of parenchymal lesions. *AJNR* 1983;4:709-712
- Praziquantel—a new antiparasitic drug. *Med Lett Drugs Ther* 1982;24:108-109
- Spina-Franca A, Nobrega JPS, Livramento JA, Machado LR. Administration of praziquantel in neurocysticercosis. *Trop Med Parasitol* 1982;33:1-4
- Sotelo J, Escobedo F, Rodriguez-Carbajal J, Torres B, Rubio-Donnadieu F. Therapy of parenchymal brain cysticercosis with praziquantel. *N Engl J Med* 1984;310:1001-1007
- deGhetaldi LD, Norman RM, Douville AW. Cerebral cysticercosis treated biphasically with dexamethasone and praziquantel. *Ann Intern Med* 1983;99:179-181

CT of Nasopharyngeal Carcinoma: Significance of Widening of the Preoccipital Soft Tissue on Axial Scans

John Hoe¹

Axial CT scans of 60 patients with biopsy-proved nasopharyngeal carcinoma were reviewed with particular reference to sites of origin and routes of spread of disease. In all patients there was involvement of the pharyngeal space with blunting of the fossa of Rosenmuller and usually associated thickening of the adjacent levator veli palatini muscle. Tumor infiltration through the pharyngobasilar fascia manifested by obliteration or displacement of the parapharyngeal fat space was seen in 65% of the patients. T-staging by CT showed T1 (28%), T2 (20%), T3 (5%), and T4 (47%) involvement. In three patients there was bilateral symmetric blunting of the fossa of Rosenmuller with no evidence of tumor infiltration into the parapharyngeal space. The scans were initially interpreted as normal except for widening of the preoccipital soft-tissue area in the midline of more than 1.5 cm and up to 2.0 cm in the anteroposterior plane. Biopsy of the postnasal space was positive for tumor in these patients. With symmetric, early stage nasopharyngeal carcinoma, a confident radiologic diagnosis on CT can be difficult. If there is asymmetry of pharyngeal mucosal space or evidence of deep infiltration this should not be a problem.

Although lymphoid adenoid tissue can sometimes result in widening of the preoccipital area, it is proposed that widening of this area of greater than 1.5 cm is an additional CT sign of nasopharyngeal carcinoma not previously emphasized. It is the result of early submucosal infiltration of the disease, and a patient with clinically suspected nasopharyngeal carcinoma should have aggressive deep biopsies of the fossa of Rosenmuller.

CT has been the most reliable and well-established imaging technique for staging and assessing the extent of nasopharyngeal carcinoma (NPC) [1-3], although MR imaging is now replacing CT as the examination of choice in the nasopharynx. NPC has a tendency for submucosal spread, and diagnosis of the disease is usually not difficult on CT scans. The typical finding is asymmetry of the fossa of Rosenmuller manifested as blunting or obliteration, often with associated thickening of the deglutitional muscle layer caused by tumor infiltration [4] (Fig. 1). As NPC characteristically results in deep infiltration, there is often obliteration or displacement of the parapharyngeal space (Fig. 2).

Materials and Methods

Axial CT scans of 68 patients with clinically suspected NPC were reviewed. All scans were obtained to aid in the diagnosis and to assess extent of disease infiltration. In 18 patients, scans were acquired to reassess recurrence of disease after radiotherapy. All patients underwent postnasal space biopsy of the fossa of Rosenmuller to confirm the presence of disease. In 60 patients disease was proved histologically. These patients consisted of 40 males and 20 females, 11 to 76 years old (mean, 48 years).

All scans were performed on a Picker 1200SX scanner. Contiguous axial scans, 5-mm thick, were obtained parallel to the hard palate, from a level of about 2 cm below the hard palate and extending cranially to the base of the skull up to the inferior orbital margin. Only contrast-enhanced scans were obtained, immediately after a bolus IV injection of contrast medium (50 ml Urografin 76).^{*} Owing to demands on scanner time, scans were not routinely

This article appears in the July/August 1989 issue of *AJNR* and the October 1989 issue of *AJR*.

Received July 19, 1988; revision requested September 9, 1988; revision received November 25, 1988; accepted December 7, 1988.

¹ Department of Diagnostic Radiology, National University Hospital, 5 Lower Kent Ridge Rd., Singapore 0511. Address reprint requests to J. Hoe.

AJR 153:867-872, October 1989
0361-803X/89/1534-0867

© American Roentgen Ray Society

^{*}Schering AG, West Germany.



Fig. 1.—Example of early nasopharyngeal carcinoma. There is blunting of left fossa of Rosenmuller and enlargement of levator palatini muscle. Although there is asymmetry of superficial mucosal contours of nasopharynx, the changes can be quite subtle.

Fig. 2.—Tumor has spread through pharyngobasilar fascia to involve parapharyngeal fat space. Note that normal fat density of this space is partly obliterated and that there is obvious asymmetry of the fossa of Rosenmuller.

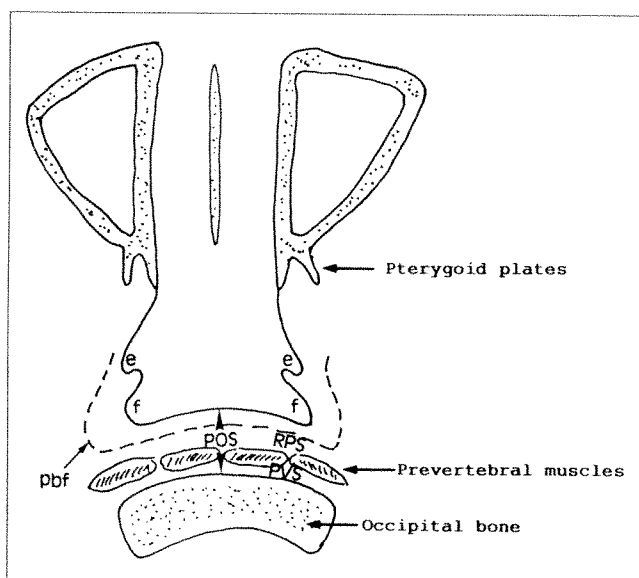


Fig. 3.—Diagram showing preoccipital soft tissue in midline at mid-nasopharyngeal level. (e = eustachian orifice, f = fossa of Rosenmuller, pbf = pharyngobasilar fascia, RPS = retropharyngeal space, PVS = prevertebral space, POS = preoccipital space.)

extended down the neck, and coronal scans were obtained only when the findings on the axial scans were subtle.

Axial CT scans of the 60 patients with NPC were reviewed with particular reference to the site of origin and regions of spread of tumor. In three patients, there was bilateral, fairly symmetric blunting of the fossa of Rosenmuller with no evidence of tumor infiltration into the parapharyngeal space. There was initial difficulty in diagnosing confidently the axial scans as abnormal. An associated widening of the preoccipital soft tissue in the midline at the mid-nasopharyngeal level of more than 1.5 cm on axial scans was found in these patients (Fig. 3). Although physiologic maneuvers and coronal scanning may help in differentiating normal from abnormal superficial mucosal masses of the nasopharynx, it appears that this widening of the preoccipital soft tissue is a useful additional sign to aid in the CT diagnosis of early NPC, which has not been emphasized previously.

Results

In assessing the spread of tumor, infiltration was evaluated in terms of involvement of spaces of the nasopharynx, which are spaces compartmentalized by the deep cervical fascia. In all 60 patients there was involvement of the pharyngeal mucosal space with blunting of the fossa of Rosenmuller. Bilateral blunting of the fossa was seen in six patients.

Once the disease has invaded the pharyngobasilar fascia there is involvement of the parapharyngeal space. This was seen in 65% of patients in whom there was obliteration of the normal fat density of the space or lateral displacement. Beyond this area direct spread of NPC can be anteriorly to the masticator space, laterally to the parotid and carotid spaces, posteriorly to the retropharyngeal and prevertebral spaces, or superiorly to the skull base.

Superior intracranial extension was the most common region of spread of disease and was seen in 48% of patients. Opacification of the sphenoid sinus, infiltration of the cavernous sinus, and bony destruction of the base were common findings in most patients (Fig. 4). The most common areas of bony destruction were the base of the sphenoid bone and the clivus, the foramen lacerum, with the adjacent middle cranial fossa, and the foramen jugulare. Posterior spread of NPC to the retropharyngeal space was the next most common site and seen in 40% of patients. More posterior spread to the prevertebral spaces was seen in 15%, while spread to the masticator space, parotid space, and inferior spread of disease deep to the tonsillar pillars was less common.

In three patients, bilateral, fairly symmetric blunting of the fossa of Rosenmuller was seen with no definite evidence of a soft-tissue density tumor mass either laterally or in the midline anterior to the prevertebral muscles. There was no evidence of tumor infiltration into the parapharyngeal spaces, which appeared to be preserved (Fig. 5). There was initial difficulty in diagnosing confidently the axial scans as abnormal, although in one patient there was suspicion of an en-

Fig. 4.—A and B, On axial scan (A) there is opacification of the sphenoid sinus. Destruction of sphenoid sinus floor by direct infiltration of tumor is confirmed on coronal scan (arrow in B).

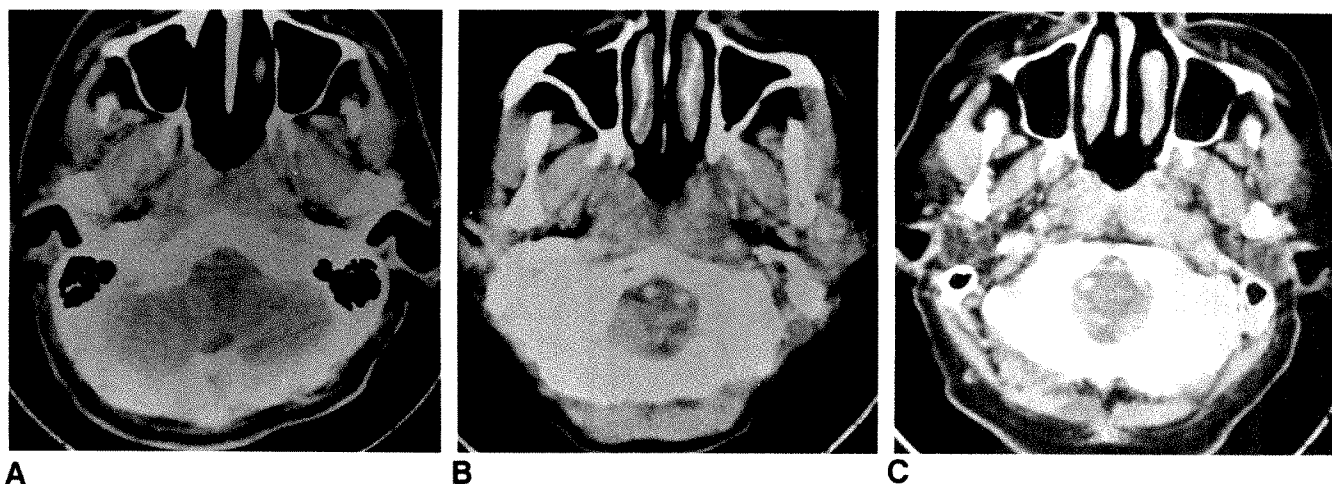
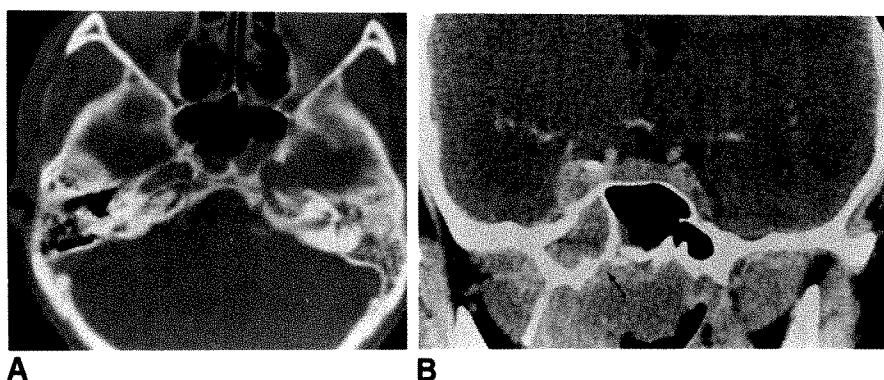


Fig. 5.—A–C, In the three cases shown, all biopsy-proved nasopharyngeal carcinoma, there is bilateral blunting of the fossa of Rosenmüller and no obvious asymmetry of mucosal airway contour. The preoccipital space is widened. In C, on the left side, there is a soft-tissue density lateral to the prevertebral muscles near the carotid artery. It could represent a metastatic retropharyngeal lymph node.

larged retropharyngeal lymph node (Fig. 5C). The preoccipital soft-tissue width (POS) was reviewed in all patients. This was defined as the maximum anteroposterior width of the soft-tissue density in the midline, at the mid-nasopharyngeal level, with the anterior border being the mucosal surface of the pharyngeal mucosal space and the posterior border being the occipital bone (Fig. 3).

An associated widening of the preoccipital soft tissue of more than 1.5 cm on the axial scans was found in these three patients, the POS measuring 1.5 cm, 2.0 cm, and 1.8 cm, respectively. Postnasal space biopsy was positive for NPC in these three patients who had positive biopsies bilaterally. Abnormality of the mucosa of the postnasal space bilaterally in these patients was also visualized by the surgeon at the time of biopsy. When the POS was measured in the other 57 patients, the average width was 1.47 cm (range, 0.4–3.0 cm). Note that this widening of the POS could not be identified on the lateral scout views.

Of the 68 patients reviewed in this study, two were biopsy-negative for NPC, although their scans showed apparent blunting of the fossa bilaterally with no widening of the POS (Fig. 6).

T-staging of the disease by CT was also recorded. Criteria used for T-staging NPC were as specified by the American Joint Committee for Cancer (AJCC) and also after Ho's classification [5, 6] (Table 1). The results of T-staging by CT are as shown in Table 2.

Table 3 lists the compartments and spaces of the nasopharynx. The medial compartment of the nasopharynx contains the pharyngeal mucosal space. For involvement of this space, asymmetry of the fossa of Rosenmüller was looked for, especially with associated enlargement of the levator veli palatini muscle.

The lateral compartment of the nasopharynx contains the parapharyngeal space, the masticator space, and the parotid and carotid spaces. The masticator space is situated anteriorly and contains the infratemporal fossa in its cephalic aspect. It is bounded medially and laterally by the superficial layer of deep cervical fascia and contains the muscles of mastication and body of the mandible [7]. The parotid space is posterolateral to the parapharyngeal space and contains the parotid gland. The carotid space is retrostyloid and formed by the carotid sheath; it contains the internal carotid artery and jugular vein and lymph nodes of the deep cervical chain.

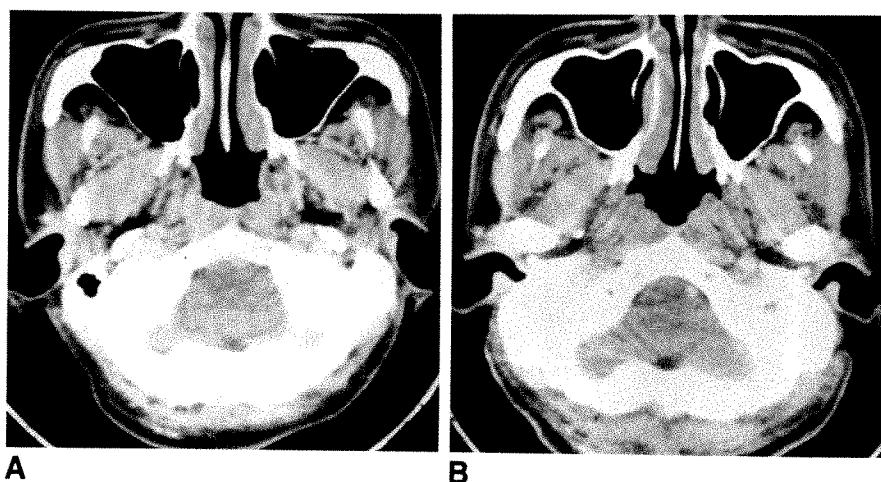


Fig. 6.—A and B, In these two cases there is bilateral blunting of the fossa of Rosenmuller. The preoccipital space is less than 1 cm. Biopsies of the postnasal space were negative for tumor.

TABLE 1: T-Staging of Nasopharyngeal Carcinoma

American Joint Committee Classification		Ho's Classification	
T1	Tumor confined to one site within nasopharynx	T1	Tumor confined to nasopharynx
T2	Tumor involving two sites within nasopharynx	T2	Tumor extends to nasal fossa, oropharynx or adjacent muscles, or nerves below base of skull
T3	Tumor extension beyond nasopharynx to neighboring soft tissues (oropharynx, nasal cavity)	T3a	Bone involvement below base of skull (floor of sphenoid sinus is included in this category)
		T3b	Involvement of base of skull
		T3c	Involvement of cranial nerves
		T3d	Involvement of orbits, laryngopharynx, or infratemporal fossa
T4	Osseous (skull base) or cranial nerve involvement		

The posterior compartment of the nasopharynx contains the retropharyngeal space and prevertebral space. The retropharyngeal space is the most anterior of the fascia-enclosed spaces of the posterior compartment and is formed anteriorly by the buccopharyngeal fascia and posteriorly by the prevertebral fascia. Posterior spread of disease to this space was identified by the presence of a soft-tissue density tumor mass in the midline and anterior to the prevertebral muscles. More posterior spread to the prevertebral space was identified by presence of tumor in the prevertebral muscles and in the midline.

Discussion

NPC has its highest incidence (20 to 30 per 100,000 per year in males) in the southern provinces of China and in emigrant Chinese populations in Southeast Asia, Hong Kong,

TABLE 2: Results of T-Staging by CT

American Joint Committee Classification			Ho's Classification		
	No. of Patients	%		No. of Patients	%
T1	17	28	T1	14	23
T2	12	20	T2	15	25
T3	3	5	T3a	5	8
T4	28	47	T3b	25	42
			T3c	—	—
Total	60	100	T3d	1	2
			Total	60	100

TABLE 3: CT Findings of Nasopharyngeal Carcinoma Infiltration

		No. of Patients	%
A.	Involvement of pharyngeal mucosal space	60	100
	• Blunting of fossa of Rosenmuller	60	
	• Thickening of levator veli palatini	55	
B.	Involvement of parapharyngeal space	39	65
	• Parapharyngeal space obliterated	33	
	• Parapharyngeal space displaced	7	
	Involvement of masticator space	9	15
	• Infiltration of infratemporal fossa	7	
	• Infiltration of pterygopalatine fossa	1	
	• Destruction of pterygoid plates	7	
	Involvement of parotid space	1	2
	Involvement of carotid space	14	23
	• Styloid process displaced	5	
C.	Involvement of retropharyngeal space	24	40
	Involvement of prevertebral space	9	15
D.	Evidence of superior intracranial spread	29	48
	• Involvement of cavernous sinus, parasellar area	14	
	• Destruction of base of skull	20	
E.	Evidence of inferior spread	6	10
	• Disease deep to tonsillar pillars	3	
F.	Anterior spread to nasal cavity (beyond posterior choanal orifice)	1	2

and elsewhere. In Singapore, with its predominantly Chinese population, this neoplasm is commonly encountered [8].

CT is well established as the most reliable method of staging and assessing the extent of NPC, since CT allows more precise staging than is possible clinically [1]. It cannot only demonstrate tumor, which may be entirely submucosal in location, but also allows assessment of areas not easily assessable clinically, such as the parapharyngeal and retropharyngeal areas [9].

The findings on CT of NPC have been previously described [1, 4, 10], but these findings do not appear to be well documented in many large series of patients. The CT appearances of the 60 patients with NPC reviewed here confirmed most of the previous findings.

NPC arises most often posterosuperiorly in the postnasal space in the region of the fossa of Rosenmuller. NPC may be entirely submucosal in-site and in its early stages when it has not infiltrated through the pharyngobasilar fascia. The earliest sign on CT is usually asymmetry of the fossa of Rosenmuller with blunting of the fossa. In the patients reviewed here this finding was present in all patients, confirming that NPC originates in this region of the pharyngeal mucosal space.

NPC has a tendency for deep infiltration, and this can occur by direct extension of disease through the tough pharyngobasilar fascia or by tumor extending through the sinus of Morgagni, a gap in the superior margin of the pharyngobasilar fascia. The eustachian tube passes through this defect. Once through this fascia with tumor in the parapharyngeal space, disease spread can occur anteriorly, laterally, or superiorly. Superior intracranial spread of disease to the skull base and middle cranial fossa, which was the most common site of deep infiltration seen in this series of patients, can occur by direct extension through the skull base. Perivascular or perineural spread through the foramen lacerum and foramen ovale into the cavernous sinus area is, however, more commonly seen. Recently, MR has allowed inference of specific routes through which NPC extends from the nasopharynx to the middle cranial fossa [11]. It was suggested that extension of disease to the middle cranial fossa occurred most commonly along the eustachian tube, following it to the foramen lacerum and ovale and then into the cavernous sinus. Less commonly, tumor may extend into the middle cranial fossa via the pterygoid canal or sphenopalatine foramen. With CT it is not possible to ascertain whether tumor is infiltrating along the eustachian tube through the sinus of Morgagni or directly through the pharyngobasilar fascia. Among the patients reviewed here, in whom there was evidence of cavernous sinus and middle cranial fossa disease, associated infiltration of the pterygoid plates and pterygopalatine fossa was an uncommon finding, and disease spread to the cavernous sinus was seen most commonly after there was involvement of the foramen lacerum and foramen ovale.

Intracranial extension of NPC is best identified by the presence of infiltration of the cavernous sinus and destruction of the bony skull base. Opacification of the sphenoid sinus or the presence of a fluid level is common and can occur from concomitant inflammatory sinusitis or from decreased mucus drainage from an obstructed nasopharyngeal airway, but early

direct superior extension of tumor should be looked for. Coronal scans are mandatory and can usually document bony destruction of the sphenoid sinus, which can indicate the need for a change of T-staging of the disease [6].

Direct anterolateral spread of tumor to the masticator space was present in 15% of the patients. The nasopharyngeal component of masticator space contains the infratemporal fossa and the pterygoid plates and pterygopalatine fossa. Infiltration of the latter has been shown to be one of the routes by which NPC high in the nasopharynx can infiltrate into the middle cranial fossa through the sphenopalatine fossa [11]. Direct lateral extension of disease to the parotid space from the parapharyngeal space is a rare finding in NPC and was seen in only one of the patients in this series.

Direct invasion of NPC into the retropharyngeal space is identified by the presence of a mass anterior to the prevertebral muscles. As the medial retropharyngeal nodes are medial to the carotid sheath, it was often difficult to distinguish lymph node involvement here from direct extension of tumor. The tissue planes of the retropharyngeal space are not normally as distinct as the others so that its involvement may be manifested only by asymmetric thickening of the posterior wall of the nasopharynx. Direct tumor invasion into the carotid space formed by the carotid sheath was also often difficult to distinguish from enlargement of the deep cervical nodes. Displacement of the styloid process posterolaterally may indicate direct extension of tumor from the nasopharynx, since enlarged nodes alone tend to displace the styloid process anterolaterally [7]. MR is superior to CT in the detection of carotid sheath adenopathy [12]. Adenopathy has homogeneous low signal intensity on T1-weighted images and can have a high signal intensity on T2-weighted images if necrosis is present.

T-staging of NPC by CT is widely recognized as being superior to clinical evaluation [3]. CT has been shown to upstage 55% of clinical T2 NPC lesions and 36% of clinical T3 lesions [9]. Tumor, node, metastasis (TNM) staging of NPC can be by several methods: the International Union Against Cancer (UICC) Classification system, the American Joint Committee for Cancer (AJCC) system, and Ho's classification, although the T-staging of the UICC and AJCC is now the same [5]. In the Far East, where the bulk of the disease experience lies, Ho's classification tends to be more popular. This may be because it subclassifies the tumors with bone destruction according to the site of involvement and hence influences the size of the radiation portal used for treatment [3]. Currently, there is no international agreement of the best staging system, and to allow comparison of treatment experience between different centers it has been recommended that each patient have simultaneous recording of the AJCC and Ho's staging systems [13].

As already described, the earliest sign on CT of NPC is asymmetry of the fossa of Rosenmuller with blunting of the fossa. However, the fossa of Rosenmuller is of variable size, and asymmetry of the fossa can occur normally. Hypertrophied and normal lymphoid tissue is not uncommonly seen in the nasopharynx and can fill the fossa, resulting in blunting of the fossa. If there is doubt as to whether the asymmetric

blunting of the fossa is benign or pathologic, certain additional features may help in the differentiation. Physiologic measures, such as opening the mouth widely, can be used to distend the airways, as there is often variation in the distension of the fossa from side to side in NPC [14]. IV contrast medium may also be used to help distinguish adenoid tissue from tumor tissue, as with adenoid tissue the capillary bed adjacent to the pharyngobasilar fascia may enhance after contrast in a gull-wing type pattern [15]. It has also been stated that the mass effect of the adenoids should always be limited to the mucosa and submucosa and that if the deep planes are intact, then the process is most likely a benign one and limited to the mucosa [15]. As NPC has a tendency for deep infiltration, one should look for associated submucosal tumor infiltration of the adjacent deglutitional muscle, usually identified as thickening or enlargement of the levator veli palatini muscle, as well as for involvement of the parapharyngeal fat space [10]. If there is still doubt then coronal scans should be obtained.

However, the diagnosis of NPC by axial CT can be difficult if there is early disease that is limited to the submucosal area with bilateral blunting or obliteration of the fossa and no evidence of associated deep infiltration into the parapharyngeal space. In the three patients described, the only apparent other abnormality was the widened preoccipital soft-tissue width. The soft-tissue thickness of this area has been previously measured on axial scans, with the mean thickness at a scanning angle of 0° to Reid's baseline, being 6 mm in normal patients and up to 12 mm, with scan angulation of 25° [16]. Scans angled 20° or more off Reid's baseline do not apparently cause significant thickening of the soft-tissue space [14]. Our scans were done parallel to the hard palate, which is approximately 10° off Reid's baseline. The importance and significance of a widened POS width has not been emphasized in most previous reports of the CT appearances of NPC, most likely because there is usually evidence of deep infiltration of disease [2, 4, 10].

On axial CT scans of the nasopharynx, the various components and spaces of this POS area are often difficult to differentiate because there is no reliable fat plane in this region. Even with high-resolution scans, the prevertebral muscles are often the only structures that can be reliably identified, and even then these muscles may not always be easily seen. The increase in POS width in the three patients described is most likely due to the presence of tumor in the pharyngeal mucosal space, which originated in one fossa and extended submucosally across the midline to the contralateral fossa without having yet infiltrated through the pharyngobasilar fascia. The disease spread in these patients would appear to be atypical, since the normal vector of spread of disease originating from the pharyngeal mucosal space is from medial to lateral with a tendency to displace the parapharyngeal space and styloid process posterolaterally [7].

In addition, the CT density of adenoidal tissue is similar to muscle, making it difficult to differentiate from surrounding superficial nasopharyngeal musculature. On T2-weighted axial MR scans, adenoidal tissue has high signal intensity and can be clearly separated and identified by a sharp interface with the prevertebral muscles. The difficulty with CT in differentiating tumor infiltration from the prevertebral muscles can be resolved with MR imaging. MR provides improved contrast between muscles and tumor tissue. In general, where MR is available it has replaced CT as the examination of choice in the nasopharynx.

ACKNOWLEDGMENT

The author thanks Claire Lim for secretarial assistance.

REFERENCES

1. Mancuso AA, Hanafee WN. *Computed tomography and MRI of the head and neck*, 2nd ed. Baltimore: Williams & Wilkins, 1985:428-444
2. Smoker WRK, Gentry LR. Computed tomography of the nasopharynx and related spaces. *Semin Ultrasound CT MR* 1986;7:107-130
3. Yamashita S, Kondo M, Hashimoto S. Conversion of T-stages of nasopharyngeal carcinoma by computed tomography. *Int J Radiat Oncol Biol Phys* 1985;11:1017-1021
4. Silver AJ, Sane P, Hilel SK. CT of the nasopharyngeal region. *Radiol Clin North Am* 1984;22:161-176
5. American Joint Committee on Cancer. In: Beahrs OH, Myers MH, eds. *Manual for staging of cancer*, 3rd ed. Philadelphia: Lippincott, 1988
6. Ho HC. Nasopharynx. In: Halnan KE, ed. *Treatment of cancer*. London: Chapman & Hall, 1982:249-267
7. Harnsberger HR. CT and MRI of masses of the deep face. *Curr Probl Diagn Radiol* 1987;16(3):141-173
8. Shanmugaratnam K. Nasopharynx. In: Schottenfeld D, Fraumeni JF, eds. *Cancer epidemiology and prevention*. Philadelphia: Saunders, 1982: 536-553
9. Yu ZH, Xu GZ, Hwang YR, et al. Value of computed tomography in staging the primary lesion of nasopharyngeal carcinoma: an analysis of 54 patients with special reference to the parapharyngeal space. *Int J Radiat Oncol Biol Phys* 1985;11:2143-2147
10. Silver AJ, Mawad ME, Hilel SK, et al. Computed tomography of the nasopharynx and related spaces. II. Pathology. *Radiology* 1983;147: 733-738
11. Teresi LM, Lufkin RB, Vinuela F, et al. MR imaging of the nasopharynx and floor of the middle cranial fossa. Part II. Malignant tumors. *Radiology* 1987;164:817-821
12. Dillon WP, Mills CM, Kjos B, et al. Magnetic resonance imaging of the nasopharynx. *Radiology* 1984;152:731-738
13. Pagano JS, Shanmugaratnam K. Recommendation for future international studies. In: Prasad U, Ablashi DV, Levine PH, et al. eds. *Nasopharyngeal carcinoma: current concepts*. Kuala Lumpur: Univ. Malaya Press, 1983: 455-458
14. Mancuso AA, Bohman LG, Hanafee WN, et al. Computed tomography of the nasopharynx: normal and variants of normal radiology. *Radiology* 1980;137:113-121
15. Mancuso AA, Som PM. The upper aerodigestive tract (nasopharynx, oropharynx and floor of the mouth). In: Bergeron RT, Osborn AG, Som PM, eds. *Head and neck imaging, excluding the brain*. St Louis: Mosby, 1984:374-401
16. Nicholson RL, Kreel L. CT anatomy of the nasopharynx, nasal cavity, paranasal sinuses and intratemporal fossa. *J Comput Tomogr* 1979;3: 13-23

MR Signal Intensity of Parathyroid Adenomas: Correlation with Histopathology

Wolfgang Auffermann¹
Margot Guis²
Nuno J. Tavares¹
Orlo H. Clark³
Charles B. Higgins¹

Recent experience has shown that parathyroid adenomas vary in their MR signal intensity, which raises the question of whether the signal intensity is related to different histologic characteristics. In order to address this question, 10 patients who had MR imaging studies (four at 0.35 T, six at 1.5 T) showing large- to medium-sized parathyroid adenomas and who subsequently underwent surgery with histologic proof of the lesion were evaluated. The MR appearance was compared with histologic characteristics. The adenomas were classified into three groups according to the MR appearance: group I, low signal intensity on short TR/TE images, high signal intensity on long TR/TE images ($n = 5$); group II, low signal intensity on short and long TR/TE images ($n = 3$); group III, high signal intensity on short and long TR/TE images ($n = 2$). Histologic analysis revealed that the major features of each group were different. High cellularity without degeneration or fibrosis was observed for all five adenomas from group I. In group II, all three adenomas showed cellular degenerative changes, old hemorrhage with hemosiderin-loaded macrophages, and/or fibrosis. In group III, both adenomas showed evidence of acute hemorrhage without significant degenerative or fibrotic changes.

These data suggest that the signal intensity of parathyroid adenomas on T1- and T2-weighted images corresponds at least in part to differences in histologic composition.

AJR 153:873-876, October 1989

MR imaging has been shown to be effective in demonstrating abnormal parathyroid glands [1-12]. According to these reports, the characteristic MR appearance of most parathyroid adenomas is low to medium signal intensity on short TR/TE images and high signal intensity on long TR/TE images. However, it has been noted that this typical MR intensity pattern is not observed in all cases [12]. About 30% of parathyroid adenomas have either high intensity on short TR/TE images or low to medium intensity on long TR/TE images [12].

MR intensity patterns of parathyroid adenomas have not been correlated with histologic features. Thus, the histologic substrate for the differences in MR appearance is not known. The aim of this study was to determine whether certain MR intensity patterns correspond to specific histologic features.

Subjects and Methods

Patients

Seventy patients with hyperparathyroidism were studied with MR imaging (38 at 0.35 T and 32 at 1.5 T) between 1984 and 1988. Sixty-two of these patients had surgically verified parathyroid adenomas or parathyroid hyperplasia. Ten patients who had histologically proved parathyroid adenomas and had undergone MR imaging before surgery were selected for study. All 10 had MR images that unequivocally showed one of three imaging patterns on T1- and T2-weighted images and showed adenomas that completely filled the section thickness. The three patterns were low to medium intensity on short TR/TE images and high intensity on long TR/TE images (group I); low to medium intensity on both short and long

Received January 6, 1989; accepted after revision April 14, 1989.

W. Auffermann also is associated with the Department of Radiology, University of Münster (West Germany) and is supported by Grant #Au-70/2-2 from Deutsche Forschungsgemeinschaft, Bonn (West Germany). N. J. Tavares is supported by Grant #Proc. 3.3/P. 517 from the Luso-American Development Foundation, Lisbon (Portugal).

¹Department of Radiology (C-309), School of Medicine, University of California, San Francisco, San Francisco, CA 94143-0628. Address reprint requests to C. B. Higgins.

²Department of Pathology, School of Medicine, University of California, San Francisco, San Francisco, CA 94143-0628.

³Department of Surgery, School of Medicine, University of California, San Francisco, San Francisco, CA 94143-0628.

0361-803X/89/1534-0873

© American Roentgen Ray Society

TR/TE images (group II); and high intensity on both short and long TR/TE images (group III).

The study comprised four men and six women ranging from 38 to 88 years old (mean, 60 years). The time interval between the MR imaging and parathyroidectomy was 1 day to 5 weeks (mean, 12 days). Four patients were studied in an 0.35-T and six patients in a 1.5-T cryogenic MR unit.

MR Imaging Technique (0.35 T)

Multislice images were obtained with repetition times (TR) from 0.5 to 2.0 sec and echo times (TE) of 30 msec (first echo) and 60 msec (second echo). Two sets of multislice transverse images were obtained: a single-echo TR 0.5-sec sequence and a dual-echo TR 2.0-sec sequence. Standard slice thickness (z-axis) was 5–10 mm with approximately a 1-mm gap between slices. The standard resolution mode was used, which has a 256×256 image matrix and produces an in-plane spatial resolution of 1.7 mm. The number of excitations per line was two for TR 2.0-sec sequences and four for TR 0.5-sec sequences. An elliptical RF coil with a y-axis of 30 cm and an x-axis of 58 cm was used for the 0.35-T unit. Images were considered T1 weighted with a TR of 0.5 sec and TE of 30 msec. Images were considered T2 weighted with a TR of 2.0 sec and TE of 60 msec.

MR Imaging Technique (1.5 T)

Multislice images were obtained with TR ranging from 0.6 to 2.5 sec and TE of 20–30 msec (first echo) and 60–80 msec (second echo). Two sets of transverse images were obtained: a single echo, TR 0.6- to 0.7-sec sequence and a dual-echo, TR 2.0- to 2.5-sec sequence. Standard slice thickness (z-axis) was 5 mm, with a 1-mm gap between slices. The standard resolution mode was used, which has a 256×128 image matrix, producing an in-plane spatial resolution of 0.95 mm in a 16-cm field of view. The number of excitations per line was two for both TR 2.0-sec and TR 0.5-sec sequences. A collar-shaped RF coil (11.5×16 cm) was used for neck imaging, and a circular body coil was used for chest imaging. T1-weighted images were obtained with a TR of 0.6 sec and a TE of 20–30 msec. Images

were considered T2-weighted with a TR of 2.0–2.5 sec and a TE of 60–80 msec. The upper mediastinum was imaged from the base of the heart to the thoracic inlet with an elliptical RF body coil and ECG-gated acquisitions.

Image Analysis

Signal intensities of parathyroid tissue were defined qualitatively as *high* if greater than or equal to the intensity of fat, *medium* if greater than the intensity of muscle but less than that of fat, and *low* if less than the intensity of muscle. According to their MR appearance, the adenomas were classified into three groups: I = low intensity on short TR/TE images, high intensity on long TR/TE images ($n = 5$); II = low intensity on short and long TR/TE images ($n = 3$); III = high intensity on short and long TR/TE images ($n = 2$).

Pathologic Evaluation

After formalin fixation and paraffin embedding, one to four hematoxylin-eosin-stained slides of each parathyroid adenoma were examined. The pathologist did not know the MR findings. The material was evaluated for the following characteristics: primary and secondary architectural pattern (trabecular, endocrine, diffuse), primary and secondary cell type (oncocyctic, chief, clear cell), presence of a rim sign, sclerosis, fatty infiltration, sinusoids or cystic changes, vascularity, nuclear and cytoplasmic atypias, mitotic activity, cell degeneration, fibrosis, and hemorrhage. The semiquantitative grading system for histologic features was 0 = not present (or normal); + = minimal frequency of abnormalities; ++ = mild frequency; +++ = moderate frequency; ++++ = marked frequency.

Results

The three groups showed no apparent histologic difference in vascularity, fatty infiltration, presence of the rim sign, architectural pattern, or main cell type. Only a single case showed very rare mitoses. The results of histopathologic evaluation are given for each patient in Table 1.

TABLE 1: Correlation of MR Imaging with Histopathology in 10 Patients with Hyperfunctioning Parathyroid Tissue

Case No.	Hemorrhage		Degeneration	Fibrosis	Sinusoids	Pleomorphism
	Acute	Chronic				
Group I (L/H)						
1	0	0	0	0	0	0
2	0	0	0	0	0	0
3	0	0	0	0	0	0
4	0	0	0	0	dil, F	++
5	0	0	0	0	0	++, F
Group II (L/L)						
6	0	+	++++	++	0	0
7	0	0	++	0	0	++++
8	0	+++	+	+++	dil, F	+++
Group III (H/H)						
9	++	0	0	+	dil	++
10	+	0	0	0	dil	++

Note.—L/H = low intensity on short TR/TE images and high intensity on long TR/TE MR images; L/L = low intensity on short and long TR/TE MR images; H/H = high intensity on short and long TR/TE MR images. Symbols are given as amount of the specimen involved. 0 = normal; + = minimal; ++ = mild; +++ = moderate; ++++ = marked; dil = dilated; F = focal.

The adenomas in group I (low to medium intensity on short TR/TE images and high intensity on long TR/TE images, Fig. 1) had high cellularity without remarkable degenerative changes. They were without necrosis, marked cytologic atypia, cystic or degenerative changes, or inflammation.

Group II (low to medium intensity on short and long TR/TE images, Fig. 2) showed atypical or degenerative changes in all three cases, including extensive cellular degeneration with hemosiderin, macrophages, and surrounding fibrosis (case 6); marked nuclear and/or cytoplasmic pleomorphism with diffuse individual cell degeneration (cases 7 and 8); and dense central fibrosis with abundant hemosiderin, suggesting old hemorrhage or necrosis (case 3).

Group III (high intensity on short and long TR/TE images, Fig. 3) showed extensive acute hemorrhage and minimal fibrosis with cystic changes and mild atypia (case 9) or dilated sinusoids and focal acute hemorrhage (case 10).

Discussion

This study describes the various patterns of intensity of abnormal parathyroid glands in relation to the TR and TE of spin-echo images and the relationship of this diversity to differences in histologic features of abnormal parathyroid glands. The most frequent pattern in the literature [1, 3, 6, 7, 10, 12] is low to medium intensity on short TR/TE images

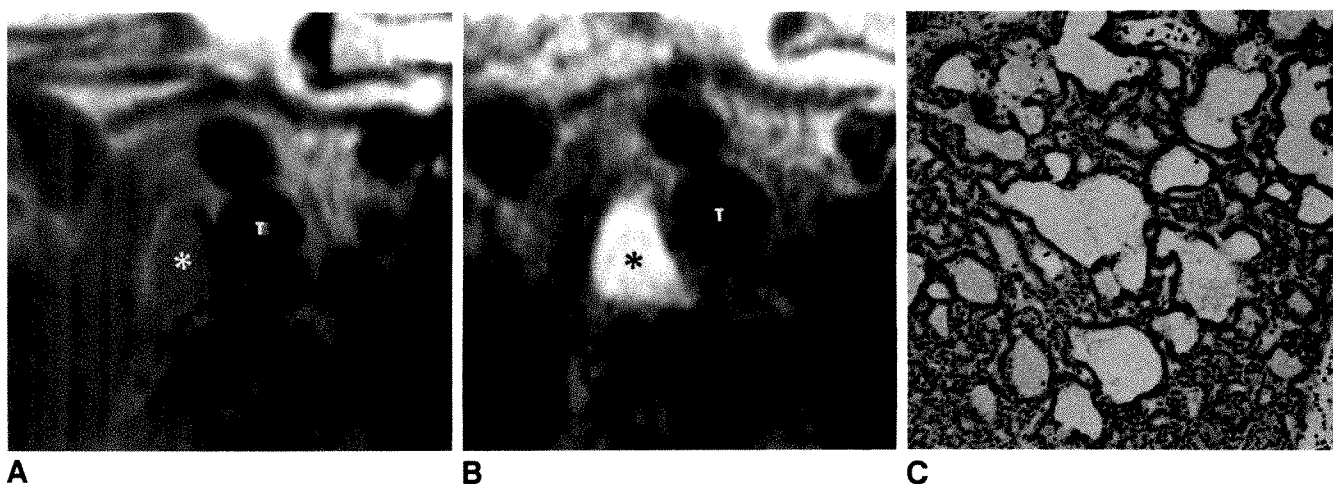


Fig. 1.—A and B, MR images obtained at 1.5 T show a surgically proved parathyroid adenoma (asterisks) 1.5 × 2 cm. Parathyroid adenoma is of low intensity on short TR/TE image, SE 700/20 (A), and of high intensity on long TR/TE image, SE 2000/70 (B). It is representative of group I. T = trachea. C, Photomicrograph of histologic specimen shows a highly cellular parathyroid adenoma (H and E, ×100).

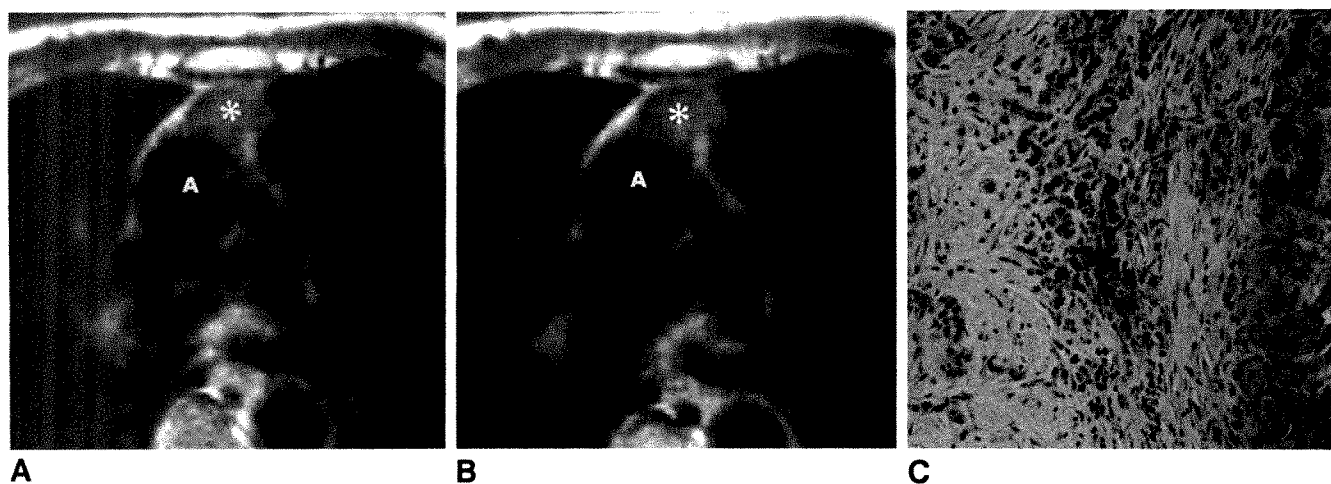


Fig. 2.—A and B, MR images obtained at 1.5 T show a surgically proved parathyroid adenoma (asterisks) 1 × 1 cm. Parathyroid adenoma is located in anterior mediastinum and shows low intensity on both short TR/TE image, SE 500/30 (A), and long TR/TE image, SE 2000/60 (B). It is representative of group II. A = aorta. C, Photomicrograph of histologic specimen shows extensive fibrosis, old hemorrhage with hemosiderin-loaded macrophages and cellular degeneration (H and E, ×100).

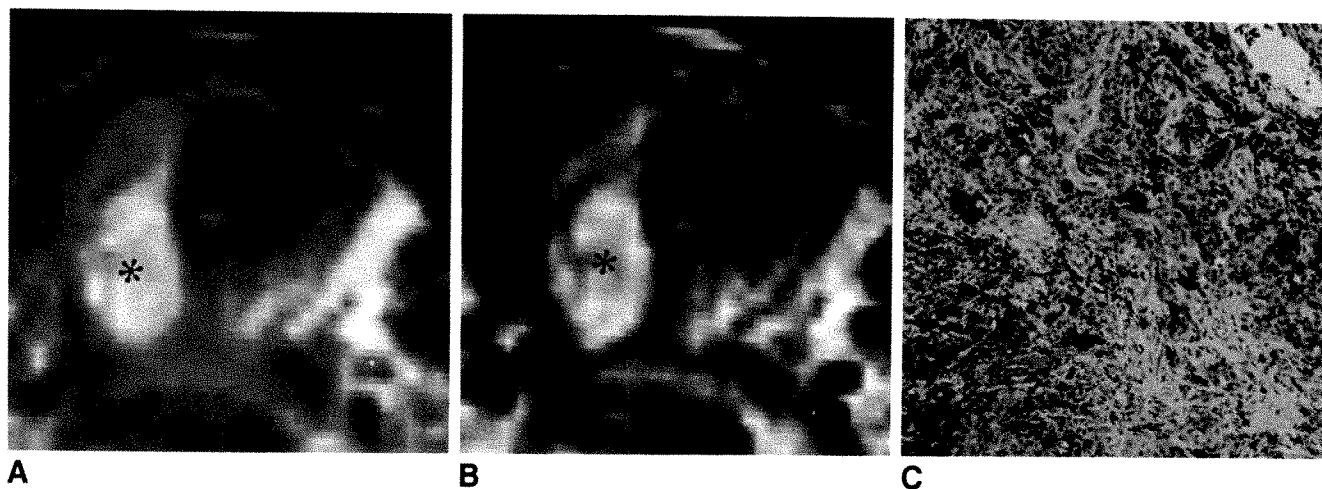


Fig. 3.—A and B, MR images obtained at 0.35 T show a surgically proved parathyroid adenoma (asterisks) 2×1.5 cm. Adenoma shows high intensity on both short TR/TE image, SE gated, TE = 30 msec (A), and long TR/TE image, SE 2000/60 (B). It is representative of group III. C, Photomicrograph of histologic specimen shows extensive fresh hemorrhage without fibrosis or cellular degeneration (H and E, $\times 100$).

and high intensity on long TR/TE images. The number of patients in the current study does not reflect the frequencies of the three patterns in our study population because patients with each of the patterns were specifically selected for inclusion in the current study. Other factors that also can influence signal intensity of adenomas at different field strengths and using different parameters may have been precluded by the selection criteria in the current study and the fact that only histologic features of the abnormal glands were studied.

The most frequent pattern (i.e., low intensity on short TR/TE images and high intensity on long TR/TE images) was characterized histologically by parathyroid adenomas of high cellularity that lacked degenerative or hemorrhagic changes. A less frequent MR pattern (i.e., no signal enhancement with longer TR/TE) was associated with degenerative and/or fibrotic changes in the gland. Cellular degeneration with replacement of normal parenchymal tissue by fibrosis has been known to cause low signal intensity on short and long TR/TE images in various organs of the neck, chest, abdomen, and pelvis [13–15]. The present study suggests that cellular degeneration, including fibrosis of parathyroid adenomas, follows a similar MR intensity pattern.

High intensity on T1- and T2-weighted images reflects short T1 and long T2 relaxation times. This pattern might be caused by highly proteinaceous fluid, subacute hematoma, fat, or paramagnetic material within the gland. In parathyroid adenomas, this pattern seems to be associated with subacute hemorrhage.

In conclusion, the appearance of abnormal parathyroid glands on spin-echo MR images is variable. The intensity pattern on T1- and T2-weighted images seems to be associated with differences in tissue composition. However, these observations do not indicate tissue specificity of MR based on cell type or cell atypia. The number of cases examined is small, and further experience is necessary to support these initial observations.

REFERENCES

1. Stark DD, Moss AA, Gamsu G, Clark OH, Gooding GAW, Webb WR. Magnetic resonance imaging of the neck. II. Pathologic findings. *Radiology* 1984;150:455–461
2. Kier R, Herfkens RJ, Blinder RA, et al. MRI with surface coils for parathyroid tumors: preliminary investigation. *AJR* 1986;147:497–500
3. Hemmingsson A, Ericsson A, Ljunghall S, et al. Technical aspects of magnetic resonance imaging in parathyroid gland lesions. *Acta Radiol [Diagn]* (Stockh) 1986;27:595–597
4. Vogl T, Hefele B, Hahn D, Nieden Z, Muhlig HP. Results of a comparative study of MR, CT and sonography of patients with primary hyperparathyroidism. *ROFO* 1986;145:167–172
5. Wang C, Gaz RD, Moncure AC. Mediastinal parathyroid exploration: a clinical and pathologic study of 47 cases. *World J Surg* 1986;10:687–695
6. Kneeland JB, Krubsack AJ, Lawson TL, et al. Enlarged parathyroid glands: high-resolution local coil MR imaging. *Radiology* 1987;162:143–146
7. Peck WW, Higgins CB, Fisher MR, Ling M, Okerlund MD, Clark OH. Hyperparathyroidism: comparison of MR imaging with radionuclide scanning. *Radiology* 1987;163:415–420
8. Levin KE, Gooding GA, Okerlund M, et al. Localizing studies in patients with persistent or recurrent hyperparathyroidism. *Surgery* 1987;102:917–925
9. Miller DL, Doppman JL, Shawker TH, et al. Localization of parathyroid adenomas in patients who have undergone surgery. Part 1. Noninvasive imaging methods. *Radiology* 1987;162:133–137
10. Spritzer CE, Gefter WB, Hamilton R, Greenberg BM, Axel L, Kressel HY. Abnormal parathyroid glands: high-resolution MR imaging. *Radiology* 1987;162:487–491
11. Hamilton R, Greenberg BM, Gefter W, Kressel H, Spritzer C. Successful localization of parathyroid adenomas by magnetic resonance imaging. *Am J Surg* 1988;155:370–373
12. Auffermann W, Clark OH, Gooding GAW, et al. Diagnosis of recurrent hyperparathyroidism: comparison of magnetic resonance with other imaging modalities. *AJR* 1988;150:1027–1033
13. Auffermann W, Clark OH, Thurnher S, Galante M, Higgins CB. Recurrent thyroid carcinoma: characteristics on MR images. *Radiology* 1988;168:753–757
14. Schmidt HC, Tscholakoff D, Hricak H, Higgins CB. MR image contrast and relaxation times of solid tumors in the chest, abdomen and pelvis. *J Comput Assist Tomogr* 1985;9:738–748
15. Ebner F, Kressel HY, Mintz MC, et al. Tumor recurrence versus fibrosis in the female pelvis: differentiation with MR imaging at 1.5 T. *Radiology* 1988;166:333–340

Cost-effective Development of a Computer-Assisted Instruction System

Robert B. McGhee, Jr.,¹ William F. Bennett,¹ Christopher S. Morris,¹ and Larry S. Witanowski²

Computer-assisted instruction (CAI) is becoming an important and practical method for radiologic education. The importance of radiologic knowledge for medical students continues to grow, but many academic radiologists find it difficult to devote large amounts of time to teaching [1]. CAI systems can provide interactive instruction for medical students, residents, and others, augmenting other learning methods such as reading and lectures [2]. Until recently, development of such systems required considerable expertise in programming and a large financial investment to produce images of reasonable quality. The rapid improvements in graphics capabilities as well as other aspects of personal computers have now made possible the intradepartmental production of high-quality, low-cost CAI systems. We have developed such a system for use by medical students, residents, and practicing radiologists.

System

Our system is based on the Commodore-Amiga personal computer (Commodore-Amiga, Inc., West Chester, PA), an inexpensive microcomputer with high-quality graphics. Individual floppy disk-based tutorials are produced by using a commercially available digitizer and various software packages. This tutorial system is presently designed for use only on the Commodore Amiga. The cost of the computer system, including two floppy disk drives, one megabyte of memory,

and color monitor, is less than \$1300. The total cost of hardware and software for the actual production of tutorials is less than \$1000.

Images are digitized by using a standard black-and-white video camera (Fig. 1). With the same camera, color images (as might be used for correlative gross pathology) can be produced by using a color filter wheel supplied with the digitizer. Original radiographs, 35-mm slides, or prints can be used as source material. These images are then saved on floppy disks, combined with text, and incorporated into a question-and-answer format (Fig. 2). The question screen is constructed with Deluxe Paint III (Electronic Arts, San Mateo, CA), a commercially available "paint program" that enables the user to manipulate graphics and add text. The answers for the answer screen are entered by using WordPerfect (WordPerfect Corp., Orem, UT), commercially available word-processing software. The Director (Right Answers, Torrance, CA), a high-level authoring language, was used to create the interactive environment. This software package is an easy-to-use programming language designed for producing interactive graphics-oriented programs. Our program was written by two radiologists (R. McGhee and W. Bennett) with no professional programming experience.

Each tutorial, which is contained on two floppy disks, consists of 15–20 interactive questions on a particular subject and takes from 1 to 2 hr for the student to complete. A combination of visual and textual information is provided, with appropriate explanations for both correct and incorrect re-

Received April 20, 1989; accepted after revision June 7, 1989.

This work was supported by grants from Commodore-Amiga, Inc. and the Eastman Kodak Co.

¹ Department of Radiology, S-209 Rhodes Hall, Ohio State University Hospitals, 410 W. 10th Ave., Columbus, OH 43210.

² Department of Radiology, State University of New York Health Science Center at Syracuse, 750 E. Adams St., Syracuse, NY 13210.

sponses. All images and questions are accessible from any point within the tutorial. Color is incorporated into all screens to add visual appeal. Our system has become a part of the core curriculum for medical students on the radiology rotation at Ohio State University. These tutorials are intended as a learning resource, rather than a testing tool, and test scores are not recorded. The system is also used by radiology residents, nonradiology residents, radiologic technologists, and practicing radiologists. Because the tutorials are on floppy disks, reproduction and distribution to interested parties is easy.

Discussion

Interactive CAI provides a unique self-paced learning environment that complements the traditional approaches of lec-

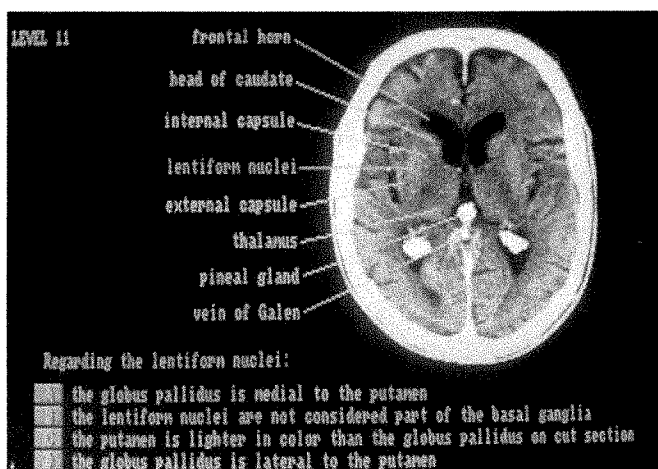
tures and printed media. Many studies have suggested that CAI-based learning is at least as effective as traditional methods [3]. In addition, the amount of time required to learn a given amount of material appears to be less with CAI methods. Lectures are often interactive but require the physical presence and time of the teacher-expert. Books and journals generally are not interactive in nature, although they certainly are an essential tool in radiologic education. In a questionnaire completed by medical students using our CAI system, most indicated they liked using the system because it is interactive and because it offers an enjoyable change of pace from reading books or reviewing teaching files. Most felt CAI in general is a welcome addition to, but not a replacement for, other methods of learning radiology.

There are many potential applications for CAI within radiology. Education of medical students and residents is an obvious application. Instruction for radiologic technologists or other hospital personnel such as nurses is another possibility. Patients undergoing an imaging procedure would most likely find an interactive explanation of the procedure interesting and helpful. Finally, practicing radiologists might find CAI-based learning, if incorporated into the continuing medical education system, to be an attractive option.

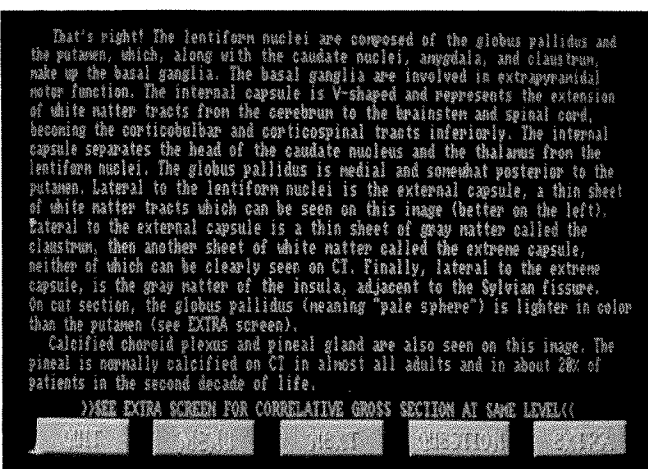
Various approaches in the development of CAI systems for radiologic education are possible, each with its own advantages and drawbacks. A floppy disk-based system such as ours is quite inexpensive, both for the production and the use of CAI material. For the student, no equipment besides the computer system is needed. This makes it possible to use CAI materials at home for those who own the appropriate computer system. Because the teaching material is produced in small, separate modules, new tutorials can be added easily and used as soon as they are completed. With this approach, a library of tutorials on floppy disks can be developed, providing a logical and inexpensive system for distribution of specific tutorials to interested parties. Radiographic images, dia-



Fig. 1.—Images are digitized by using a black-and-white video camera connected to computer via digitizer (arrow). Filter wheel for reproduction of color images is in front of camera lens.



A



B

Fig. 2.—Sample question.

A, Question screen has one or more radiographic images with multiple-choice question. Correct answer to this question is "A."

B, Correct answer ("A") has been chosen and detailed information is now given. If the wrong answer is chosen, a brief explanation is given and user is encouraged to choose another answer. Additional screens are available for correlative images or other pertinent material.

grams, and text can be combined easily on individual screens. A disadvantage of this approach is the limited number of images (approximately 30–80) that can be included in each tutorial. Another drawback is the poor reproduction of plain films, limiting applications primarily to MR imaging, CT, sonography, and nuclear medicine education.

Another approach that has been used in the development of a CAI system is the use of a videodisk player in conjunction with a microcomputer. Advantages of such a system include storage of thousands of images on a single videodisk, faster access to images, and better reproduction of plain films. The large image capacity of videodisks and rapid access makes feasible the production of moving images, an advantage in some areas such as echocardiography. One disadvantage to videodisk-based CAI systems is that they are considerably more expensive, both for the developer and for the user. In addition to the computer and videodisk player, a second monitor may be necessary. The videodisk itself can be produced in-house by using more expensive systems. Less expensive systems usually require material to be sent out for the production of the videodisk, making addition of new material or corrections much more difficult.

The choice of a CAI system depends on the needs and resources available to the user. A large teaching institution may find the image storage capacity and other aspects of a videodisk-based system desirable, whereas a smaller institu-

tion or an individual may feel an inexpensive but flexible floppy disk-based system is more suitable. A videodisk would be more appropriate for the production of a comprehensive textbooklike teaching environment, whereas a floppy disk system would work better in the development of a subscription-based periodical CAI system for continuing medical education. As microcomputer technology progresses and as other high-capacity storage formats, such as compact disk read-only memory (CD-ROM), become more widely available, the number of options will grow and they will most likely become more affordable.

In summary, interactive CAI is a useful adjunct to other learning methods, with many present and potential applications. The capabilities of microcomputers and related electronic devices have progressed, and the costs of such systems have decreased, to the point that development or use of CAI systems in radiologic education is possible for nearly all who are interested.

REFERENCES

1. Squire LF. On teaching radiology to medical students: challenges for the nineties. *AJR* 1989;152:457–461
2. Jacoby CG, Smith WL, Albanese MA. An evaluation of computer-assisted instruction in radiology. *AJR* 1984;143:675–677
3. Kulik CC, Kulik JA, Shwalb BJ. The effectiveness of computer-based adult education: a meta-analysis. *J Educ Comp Res* 1986;2:235–252

Book Review

Alimentary Tract Radiology, 4th ed., vols. 1 and 2. Edited by Alexander R. Margulis and H. Joachim Burhenne. St. Louis: Mosby, 2147 pp., 1989. \$299

The origin of this respected text had an unexpected beginning. When Alexander Margulis was at Washington University in St. Louis, he was dissuaded from book authorship by his chief. Dr. Hugh Wilson said that time was better spent with original research. C. V. Mosby was disappointed. When Dr. Margulis was appointed department chairman at UCSF, it was possible to reconsider.

Joachim Burhenne, then director of radiology at Childrens Hospital and Adult Medical Center of San Francisco, an acknowledged expert on radiology of the postoperative stomach, wanted to write a monograph on that subject. After talking it over, he and Dr. Margulis decided to take on the whole gastrointestinal tract.

Pediatric radiology and neuroradiology already had achieved subspecialty status with the texts of Caffey and Pancoast-Pendergrass-Chamberlain. Gastrointestinal radiology was just part of the "general" workload. The young professors, in a desire to both inform and dignify this area, took on the task of creating a multiauthor text in the field of alimentary tract radiology.

The initial edition was published in 1967 and received critical acclaim. It made instant subspecialists out of the contributors, who were honored by Dr. Burhenne's idea of having each author's name on the cover. The publication of the first edition created an increase in intellectual interest in gastrointestinal radiology. In retrospect, the first edition suffered considerably from a lack of editorial discipline, but this was understandable as the youngish editors were faced with senior contributors with delicate egos.

Each subsequent edition has been an improvement. The editors are now the seniors, and they exercise rigid control over the content. What is surprising is that these two strong personalities have been able to avoid professoricide. Their product continually improves while their own personal careers have ascended to high levels. They swear to a totally noncombative relationship. Certainly this must be equal to or better than any conventional marriage based on love, honor, and fidelity.

Your reviewer was fortunate to be on sabbatical leave and thus was able to read the entire text rather than just skim through it as is ordinarily necessary with a textbook of this size. It was fun and educational.

The new edition has 111 names on the cover!

The organization of this edition is similar to the past. There is an introductory section of history, equipment, contrast media, pharmacology, and basic examination methods. Some of this material, such as that on radiographic-fluoroscopic equipment by Capp and Ovitt, is not readily available from other sources.

You will immediately understand that dogmatism is avoided when reading back-to-back chapters by Laufer on the double-contrast examination and Gelfand on the fluoroscopically controlled single-contrast examination. Both are powerful contributions.

Anatomy, physiology, and embryology are in Part II, and the color sectional anatomic illustrations along with their imaging counterparts are outstanding. As might be expected, this comes from the New York Hospital-Cornell Medical Center group.

In Part III, Mindelzun and McCort borrow generously from their excellent monograph and present the value of the plain film in evaluating the acute abdomen. Federle adds a chapter on abdominal trauma taken from his extensive experience at San Francisco General Hospital. The value and importance of CT are nicely documented.

Then it is on to the tubular gut from lips to anus. Each section starts with a review of pathology followed by the radiologic information and concluded with an overview. It is almost 700 pages of pure gold. The chapter by Wylie J. Dodds incorporates his investigative findings into a brilliant report on what our strengths and limitations are in imaging the esophagus. If you didn't like what you read from Gelfand and Laufer you have Burhenne and Facche to tell you how to study the stomach and duodenum. They are not bashful in explaining their methods. Peptic disease by Kressel and Levine and gastric neoplasia by Shirakabe and Maruyama provide excellent updates of these important conditions. For pure aesthetics, the chapter on the duodenum by J. Odo Op den Orth wins the barium prize. If we could achieve his level of imaging quality on all our examinations, fiberoptics would be used almost exclusively for telecommunications. R. F. Thoeni presents a balanced view of the options for small-bowel examination. The chapters on the pathophysiology of the small bowel are concise and well illustrated. The section on the colon presents the Thoeni-Margulis approach to the colon, which is similar to the philosophy of Laufer. A short chapter on defecography is an introduction to this examination that so many of us seem to be avoiding. This filming of what is considered a private, unaesthetic event will probably never prove popular, but clearly the problems cannot be ignored.

What criticisms are there of volume 1? The chapter on pharmacology seems unfocused. This would be better written by a knowledgeable radiologist. I was disappointed by some of the pathology chapters until I came to Tailbot. He has done an excellent job of both simplifying and illustrating. Discussion of diversion colitis and intramural edema-hemorrhage in the small bowel was not found in the text.

Volume 2 takes you away from barium and into the liver, pancreas, spleen, and retroperitoneum, with concluding chapters related to pediatric radiology, interventional radiology, and miscellaneous topics. Because of the recent advances in these areas, more new information appears in volume 2.

The pancreas section is sensational. Freeny and Rohrmann take the nonneoplastic diseases, present a broad view of all the imaging techniques available, and do not spare clinical advice. Stephens does the same in the chapter on the neoplastic diseases. It is concise but complete.

The authors on the liver, gallbladder, and biliary tract are covered by a paraphrase from the movie *Casablanca*, "round up the usual experts." All of the methods of imaging are covered. Since there are so many, some duplication occurs. The only area that might need augmentation is CT of the liver. It was not given full coverage.

With his usual finesse, Singleton spilled a little barium into this volume in a chapter on the gastrointestinal tract in kids. The chapter by Rosenberg and Goldberg on pediatric sonography was an even greater delight. It gives one a new feeling about the power of sonography when used in the infant and child. Their illustrations are outstanding.

Keller, Rösch, and Freeny contribute the chapters on angiography, and these take the prize for aesthetically pleasing illustrations in volume 2. Although the authors acknowledge that the use of angiography is diminishing, the value and the standards of performance of these methods are clearly presented. The spleen may be viewed as

somewhat of a boring organ, but the contributions on the spleen are important and well done. There is great emphasis on proper diagnosis so that the spleen, once considered a throwaway organ, remains in situ and functioning.

Meyers, Ajzen, Allen, Cooperberg, Demas, Hricak, and Castellino invaded the retroperitoneum but attempted to avoid the genitourinary tract. Although the avoidance was not complete, the important imaging contributions in this area are explained and illustrated.

While interventional radiology is the least stable of any field of alimentary tract radiology, the current state of the art is covered for now. Don't rely on this information in 1990.

Criticism of volume 2 is limited to a desire for better integration. There is liver served at almost every course of the meal and that does dull the appetite.

It is impossible to cover every aspect and author of this 2000+ page treatise, but the global assessment is that this is an unusually effective multiauthored text. Many of the authors have written the best monograph in their area, so it is like an anthology of the best short stories of 1988. Don't look for *Alimentary Tract Radiology* to be on the *New York Times* best-seller list, but be a reader if you want the best current information in this field.

John R. Amberg
University of California, San Diego, Medical Center
San Diego, CA 92103



AMERICAN JOURNAL OF ROENTGENOLOGY

MELVIN M. FIGLEY FELLOWSHIP IN RADIOLOGY JOURNALISM

The American Roentgen Ray Society announces a one-month fellowship in radiology journalism in the La Jolla editorial office of the AJR. Board-certified radiologists with special academic promise are invited to apply.

PURPOSE

The purpose of the fellowship is (1) to stimulate bright young radiologists to continue with an academic career, to accelerate their progress, and to stimulate their interest in good radiology journalism, and (2) to improve the quality of radiology journals by teaching the fundamentals of medical journalism to academicians, training manuscript reviewers and future editors, and providing core teachers of medical journalism in radiology departments around the country.

CURRICULUM

The fellow will be taught the fundamentals of medical writing, manuscript preparation, peer review, manuscript editing, the ethics of scientific journalism, and journal publication and printing in personal tutorials given by the AJR editors and editorial staff through hands-on experience in the editorial office. He or she will visit Williams & Wilkins in Baltimore to observe the publication and printing process.

STIPEND

The successful candidate will be awarded \$10,000, which includes the cost of travel to La Jolla and Baltimore, living expenses for the month, and an honorarium.

APPLICATIONS

Candidates should apply in writing to Robert N. Berk, M.D., Editor-in-Chief, AJR Editorial Office, 2223 Avenida de la Playa, Suite 200, La Jolla, CA 92037. The letter must include a curriculum vitae and a description of the candidate's goals during the fellowship. Letters of recommendation from his or her department chairman and one other senior person are required. Deadline for receipt of applications is Nov. 1, 1989. The successful candidate will be notified Dec. 1, 1989, and may choose one of the following months for the fellowship training: Jan., Feb., March, April 1990.

Letters

Error in Meeting News Report

The *AJR* report [1] of the proceedings of the recent annual meeting of the Society of Cardiovascular and Interventional Radiology is a valiant attempt to bridge the gap between the ponderous but accurate peer-reviewed scientific journals and the fast but distorted journalism of unscientific newspapers and "throw-away" magazines. This report carries the imprimatur of a highly regarded scientific journal, the *AJR*, and will be indexed and may be cited in future publications. The Journal thus has a major responsibility to ensure the accuracy of the contents. Errors may be very damaging.

In the section on vena caval filters, the presentation of Ernest J. Ferris is misquoted. The lower inferior vena cava is not "studied easily by sonography," nor is the newer bird's nest filter "easier to remove." The terms "effective" and "safe" normally are not applied to investigational devices. The Simon Nitinol filter (without quotes or parentheses) currently is undergoing clinical trial. It has not been submitted to the U. S. Food and Drug Administration yet and thus could not have been "precluded approval" [2]. Its clinical complication rate is comparable with that of other filters, particularly as they previously could not be followed with MR imaging. A significant omission, since other introducers are cited, is that it passes through a slim 7-French introducer. The Greenfield titanium filter is stated by Dr. Cho to have shown "a success rate of 100% in 47 patients." If so, the filter recall noted in the final sentence seems a disturbing non sequitur.

I hope that future attempts at reporting meeting news will be better. An obvious suggestion would be to send galleys of each section to the speaker being quoted, for editing and approval. The speaker need be given only a few days to respond. Furthermore, the entire report should receive the overall professional review and approval of the chair of the meeting's program committee. Finally, the report should not be anonymous. The author should be recognized and should take appropriate responsibility for his or her work. Regrettably, these minimal requirements have not been met in this initial venture.

Morris Simon
Beth Israel Hospital
Harvard Medical School
Boston, MA 02215

REFERENCES

1. Meeting news. Society of Cardiovascular & Interventional Radiology: 14th annual meeting, March 1989. *AJR* 1989;152:1147-1151
2. Simon M, Athanosoulis CA, Kim D, et al. Simon nitinol inferior vena cava filter: initial clinical experience. Work in progress. *Radiology* 1989;172:99-103

Reply

The meeting news article [1] in the June issue of the *AJR*, about the March meeting of the Society of Cardiovascular and Interventional Radiology, was the first in a new series of papers summarizing important national meetings. The purpose of the series is to provide Journal readers with the latest information promptly and in an interesting fashion. Because of the nature and intent of these articles, they are not subject to the peer review required of other papers.

From the outset, we recognized that there is a risk of publishing erroneous information in such articles. Real possibilities exist that we can fail to report accurately what was said at the meeting or that the authors of the papers can present erroneous information.

As the first article was being published, we already had decided that the papers must be reviewed for accuracy of content by more than just the Journal editors. As many persons as possible will be included, despite the time constraints we have imposed. At the very least, galleys will be sent to the meeting directors and the members of the Journal's publication committee. When the number of persons involved allows it, galleys will be sent to all those who presented papers. Also, after the first article, we decided not to publish the reports anonymously. The author of the summary article will be noted in print even if he or she is an employee of the Journal.

If we continue to receive letters like the one from Dr. Simon as future meeting news articles appear in the Journal, or if readers find the reports of little interest and value, the series will not be continued. We encourage readers to let us know what they think about the series.

Robert N. Berk
Editor-in-Chief

REFERENCE

1. Meeting news. Society of Cardiovascular & Interventional Radiology: 14th annual meeting, March 1989. *AJR* 1989;152:1147-1151

Partial Flip-Angle Spin-Echo Imaging: Clinical Applications

One of the major problems in MR imaging is the time required for acquisitions. This limits the number of patients that can be imaged each day and may result in motion artifacts in critically ill patients. Use of fast imaging techniques with partial flip-angle refocused echoes has resolved this problem somewhat by providing rapid T2-weighted sequences [1-3]. However, these sequences have some limitations: (1) The contrast obtained is T2*-weighted rather than T2-weighted. This difference is more than academic, as the T2-weighted

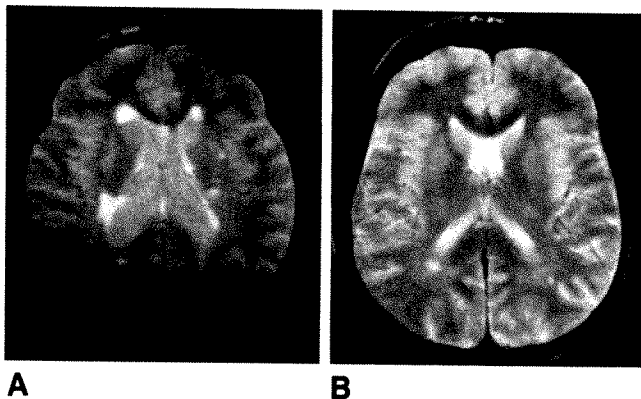


Fig. 1.—A and B, Comparison of two 1500/100 spin-echo MR images with flip angles of 90° (A) and 65° (B) at about same brain level in two patients with multiple sclerosis. B has more T2-weighted contrast than A.

images seem to show parenchymal abnormalities in the brain better than T2*-weighted gradient-echo images. (2) The number of slices per acquisition time is limited. (3) There is no evolution from spin-density to T2-weighted contrast as seen with the use of several echoes in long TR spin-echo (SE) sequences, which are particularly useful in brain examinations.

To reduce the overall acquisition time per patient, we applied partial flip angles to SE sequences on a 0.5-T magnet. We compared these sequences with long TR acquisitions and concluded that the sequences gave comparable information without degradation in image quality. The late echo of such sequences provides the same level of intensity in the CSF and the same contrast with gray and white matter as those seen with 2000/120 SE sequences.

These sequences are performed with a paired number of echoes (needed because of the nutation angles) by using RF refocusing pulses. With a 65° flip angle (approximately near the Ernst angle for most tissues), proton-density and T2-weighted contrasts are obtained with a TR of 1500 msec and TEs of 50 and 100 msec, respectively. This sequence allows 11 slices per acquisition; the time required is less than 13 min with two averages and a 256 × 256 acquisition matrix (Fig. 1).

The same contrasts can be obtained with a flip angle of 35°, a TR of 1100 msec, and TEs of 40 and 80 msec without important loss in the signal-to-noise ratio. The same number of slices is available, and this acquisition takes less than 9.3 min.

In patients who cannot stay in the magnet long, we also use an SE sequence with a partial flip angle of 30°, a TR of 600 msec, TEs of 35 and 70 msec, and two averages, but the signal-to-noise ratio is weaker, and only seven slices per unit time are obtained. Despite these pitfalls, this sequence is performed to give information on signal abnormalities rather than on anatomic detail and is achieved in 5.3 min with a 256 × 256 acquisition matrix.

During the past 6 months, about 500 patients have been examined by using these sequences. The savings in time has been approximately 8% compared with the long TR, spin-echo sequences usually performed.

J. P. Laissy
Hôpital Charles Nicolle
76031 Rouen Cedex, France
P. Hugonet
IRM Paris Nord
95200 Sarcelles, France

REFERENCES

1. Buxton RB, Edelman RR, Rosen BR, Wisner GL, Grady TJ. Contrast in rapid MR imaging: T1 and T2 weighted imaging. *J Comput Assist Tomogr*

1987;11:7-16

2. Mills TC, Ortendahl DA, Hylton NM, Crooks LE, Carlson JW, Kaufman L. Partial flip angle MR imaging. *Radiology* 1987;162:531-539
3. Winkler ML, Ortendahl DA, Mills TC, et al. Characteristics of partial flip angle and gradient reversal MR imaging. *Radiology* 1988;166:17-26

Focal Nodular Hyperplasia of the Liver: Features on Gd-DTPA-Enhanced MR

A 33-year-old woman had severe dysmenorrhea and abdominal pain in the right lower quadrant. Physical examination revealed a mobile palpable mass in the right upper quadrant. At laparoscopy, in addition to a myoma of the uterus and a benign cyst of the right ovary, a pedunculated tumor attached to the liver was found. Sonography showed a well-defined, subcapsular, hypoechoic, solid mass 6 cm in diameter attached to the liver. CT showed a well-defined, homogeneous, hypodense, solid, pedunculated tumor of the liver. Ateriography and scintigraphy showed typical findings of focal nodular hyperplasia. On T1-weighted MR images, the tumor was hypointense compared with normal liver parenchyma (lesion:liver ratio, 0.8), and the signal intensity of the center was low (Fig. 1). On T2-weighted images, the tumor was isointense compared with normal liver parenchyma (lesion:liver ratio, 1.0-1.1), and the signal intensity of the center was high. Delineation of the tumor from normal liver paren-

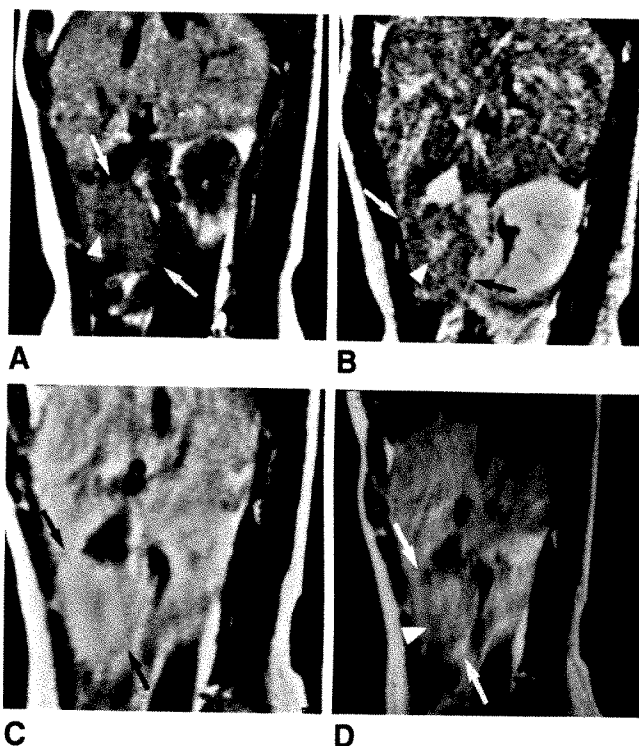


Fig. 1.—Focal nodular hyperplasia of liver.

A and B, Unenhanced sagittal MR images show pedunculated tumor (arrows) attached caudally and ventrally to right lobe of liver is hypointense compared with normal liver parenchyma on T1-weighted image, SE 20/300 (A), and isointense on T2-weighted image, SE 100/2000 (B). Signal intensity of centrally located scar (arrowheads) is low on T1-weighted image and high on T2-weighted image.

C and D, MR images obtained immediately (C) and 6 min (D) after IV bolus infusion of Gd-DTPA show enhancement of tumor (arrows), which has high signal intensity. Image obtained at 6 min also shows nodular lobules of high signal intensity separated by septa of low signal intensity (arrowhead), consistent with pathologic appearance of focal nodular hyperplasia.

chyma was difficult. T1-weighted images obtained after an IV bolus infusion of Gd-DTPA (0.1 mmol/kg) showed a vascular tumor. The tumor was hyperintense (lesion:liver ratio, 1.2) immediately after the infusion of Gd-DTPA because of the high vascularity of the lesion. Six minutes after the infusion, radiating septa were seen as structures with low signal intensity that separated the nodular lobules of high signal intensity within the tumor. The contrast-enhanced MR findings were consistent with the diagnosis of focal nodular hyperplasia. The patient was treated surgically, and pathologic examination of the tumor confirmed the diagnosis.

To our knowledge, only two MR studies [1, 2] of patients with focal nodular hyperplasia have been reported, and neither study included contrast enhancement. As reported, focal nodular hyperplasia can be visualized on unenhanced MR imaging as a homogeneous isointense lesion on all pulse sequences, a hypointense lesion on T1-weighted sequences, or a homogeneous hyperintense lesion on T2-weighted sequences. The typical central stellate scar is seen as a dark region on T1-weighted images and as a bright region on T2-weighted images. This may be due to the presence of bile ducts and slowly flowing blood within the scar [1]. In our case, the central scar and septa were depicted on MR only. The superior soft-tissue contrast of Gd-DTPA-enhanced MR enabled visualization of the lobules of normal liver tissue, which were separated from one another by the fibrous septa. This was consistent with the typical pathologic findings [3]. The lobules are hyperplastic nodules of normal liver tissue. The fibrous trabecular strands occupy the center and extend to the periphery to form a stellate structure with compartments of various sizes and shapes [3]. Microscopically, focal nodular hyperplasia is composed of areas of normal-appearing liver cells that are subdivided into pseudolobules by the fibrous strands, which may coalesce at the center. The proliferative mass may have a centric or eccentric arrangement. The pattern seen on contrast-enhanced MR may provide an important diagnostic clue for this disorder and may help in differentiating it from other focal hepatic tumors.

Richenel T. O. Tjon A. Tham
Herma C. Holscher
Theo H. M. Falke
Jan-Willem Arndt
Cornelis B. H. W. Lamers
University Medical Centre Leiden
2333 AA Leiden, the Netherlands

REFERENCES

- Butch FJ, Stark DD, Malt RA. MR imaging of hepatic focal nodular hyperplasia. *J Comput Assist Tomogr* 1986;10:874-877
- Mattison GR, Glazer GM, Quint LE, Francis IR, Bree RL, Ensminger WD. MR imaging of hepatic focal nodular hyperplasia: characterization and distinction from primary malignant hepatic tumors. *AJR* 1987;148:711-715
- Edmondson MA, Craig JR. Neoplasms of the liver. In: Schiff L, Schiff ER, eds. *Diseases of the liver*. Philadelphia: Lippincott, 1987:1109-1158

Focal Nodular Hyperplasia of the Liver on Delayed Enhanced CT

Recent reports [1, 2] have described the value of delayed contrast-enhanced CT of the liver for the detection of hepatic lesions. With this technique, focal hepatic lesions appear as low-attenuation defects within the surrounding liver. We describe a case of hepatic focal nodular hyperplasia in which the lesion had higher attenuation than surrounding liver on delayed contrast-enhanced scans, a finding that may be specific for this disease.

A 36-year-old woman noted a palpable abdominal mass in the right upper quadrant with no associated symptoms. Findings on liver sonography were normal. Examination of a needle-biopsy specimen of the mass showed focal nodular hyperplasia. CT was performed 8

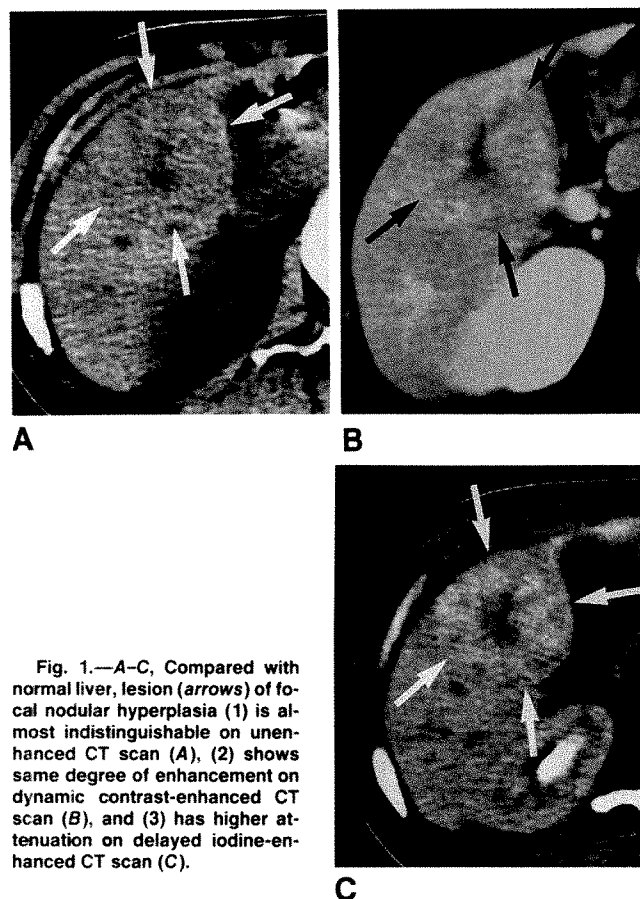


Fig. 1.—A-C, Compared with normal liver, lesion (arrows) of focal nodular hyperplasia (1) is almost indistinguishable on unenhanced CT scan (A), (2) shows same degree of enhancement on dynamic contrast-enhanced CT scan (B), and (3) has higher attenuation on delayed iodine-enhanced CT scan (C).

days later to assess the extent of the lesion. Although a central focal scar was seen on both unenhanced and dynamic enhanced (150 ml Renografin 60% [methylglucamine diatrizoate] at 2 ml/sec) CT scans (Fig. 1), the extent of the lesion was seen best as a high-attenuation area on scans made 4 hr later. Whereas normal liver attenuation increased from 67 H on unenhanced CT to 88 H on delayed enhanced CT, attenuation of the lesion increased from 67 to 96 H.

Most lesions of focal nodular hyperplasia are hypodense to surrounding liver on unenhanced CT, becoming isodense or transiently hyperdense after infusion of IV contrast material, depending on the rate of infusion. A central scar may be a relatively specific CT feature, but it was noted in only two (14%) of 23 cases in a recent series [3]. To date, focal lesions in the liver on delayed enhanced scans uniformly have been described as having lower attenuation than normal liver [1, 2]. Because normal hepatocytes secrete 1% to 2% of the injected iodine load into the biliary system, on delayed scans most hepatic lesions will be hypodense compared with surrounding parenchyma [1]. However, the presence of functioning hepatocytes within lesions of focal nodular hyperplasia may be an exception to this pattern. Hyperfunctioning hepatocytes may be present in cases such as this one, with hypersecretion of iodine leading to a hyperdense lesion on delayed contrast-enhanced scans. The same process would account for the focally increased uptake of the radionuclide seen within lesions of focal nodular hyperplasia on biliary scintigraphy [4]. We conclude that focal nodular hyperplasia, unlike other focal hepatic lesions, may be hyperdense to normal liver parenchyma on delayed contrast-enhanced CT.

Ruben Kier
Arthur T. Rosenfield
Yale New Haven Hospital
New Haven, CT 06504

REFERENCES

1. Bernardino ME, Erwin BC, Steinberg HV, Baumgartner BR, Torres WE, Gedgudas-McClees RK. CT scanning: increased confidence and improved detection of hepatic metastases. *Radiology* 1986;159:71-74
2. Miller DL, Simmons JT, Chang R, et al. Hepatic metastasis detection: comparison of three CT contrast enhancement methods. *Radiology* 1987;165:785-790
3. Welch TJ, Sheedy PF II, Johnson CM, et al. Focal nodular hyperplasia and hepatic adenoma: comparison of angiography, CT, US, and scintigraphy. *Radiology* 1985;156:593-595
4. Tanasescu D, Brachman M, Rigby J, et al. Scintigraphic triad in focal nodular hyperplasia. *Am J Gastroenterol* 1984;79:61-64

Direct Sagittal CT of the Foot

Most commonly, CT scans of the foot are acquired in axial or, less frequently, coronal projections [1]. As noted by Solomon et al. [2], "It is not always possible with conventional radiographic techniques to show foot pathology to the best advantage." Because CT can show cortical detail best when the plane of the CT section is at right angles to the cortex in question, in some situations reformations in the two other anatomic planes may be necessary to solve difficult imaging problems. Compared with direct scanning in the desired plane, reformation has several disadvantages: Spatial resolution is decreased, patients absorb higher doses of radiation, and a longer examination time often is required because of the large number of thin sections needed to study the region of interest. Reformation also requires

increased technician and computer time, resulting in additional expense. Because of these limitations, we devised a method to obtain direct sagittal CT of the foot.

Figure 1 shows how patients are positioned for direct sagittal CT of the foot. A firm, wedge-shaped cushion 4 ft. (1.2 m) long and approximately 18 in. (45.7 cm) high at the apex is placed on the CT table. Relative to the foot to be scanned, the patient is placed in the contralateral decubitus position with the long axis of that foot parallel to the scanning beam. Care is taken to support the extended torso comfortably. A box or block taped or clamped to the CT table keeps the foot in position and prevents external rotation. The foot is taped along its dorsum to prevent dorsiflexion and motion during scanning. If necessary, the angle of the gantry can be adjusted to facilitate precise sagittal sectioning. Anatomic localization with a topogram and appropriate section thickness and technique can be used then.

Recently [3], we saw a 33-year-old woman in whom severe disabling pain developed approximately 1 month after a total implant arthroplasty of the first right metatarsophalangeal joint. CT was planned to evaluate sesamoid entrapment into the prosthesis, but a sagittal plane was desired for optimal detail. The patient was positioned as shown in Figure 1, and three sets of sagittal sections through the first metatarsophalangeal joint were performed with the patient's great toe in the flexed, extended, and neutral positions (Fig. 2).

F. A. Mann

L. A. Gilula

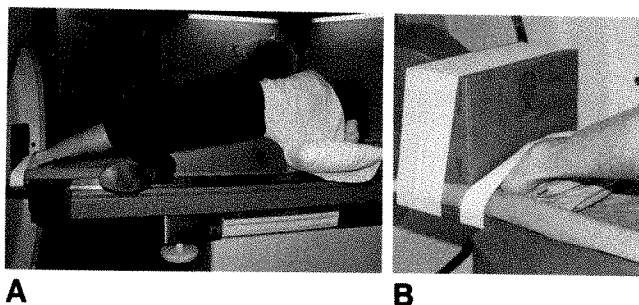
Mallinckrodt Institute of Radiology
St. Louis, MO 63110

Fig. 1.—A and B, Positioning of patient for direct sagittal CT of foot.

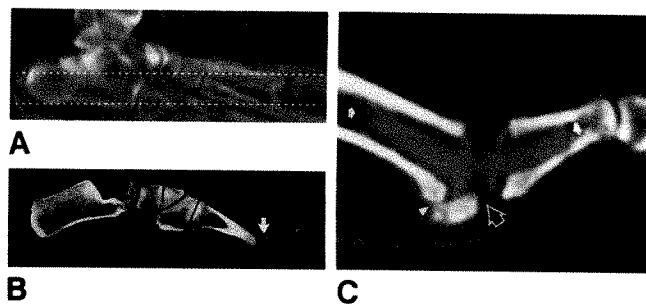


Fig. 2.—Sagittal CT scans of metatarsophalangeal (MTP) joint silastic implant in great toe.

A, Scanogram shows area (between dashed lines) in which sections were obtained.

B, Direct sagittal section of entire foot clearly shows anatomy through medial side of foot and part of MTP joint prosthesis (arrow).

C, Scan of great toe in dorsiflexion shows MTP joint prosthesis (between closed arrows). Tibial sesamoid is drawn into prosthesis (open arrow), and bone-bone (without space for sesamoid cartilage) articulation is present between sesamoid and residual first metatarsal cortex (arrowhead).

REFERENCES

1. Smith RW, Staple TW. Computerized tomography scanning technique for the hindfoot. *Clin Orthop* 1983;177:34-38
2. Solomon MA, Gilula LA, Oloff LM, Oloff J. CT scanning of the foot and ankle. 2. Clinical applications and review of the literature. *AJR* 1986;146:1204-1214
3. Hamilton SA, Boberg J, Gilula LA. The Lawrence design first metatarsophalangeal prosthesis: a complication. *J Am Podiatr Med Assoc* (in press)

The Lateral Ankle Index

It is always exciting for an emergency department radiologist to read about a new soft-tissue sign that may aid in the diagnosis of fractures. The lateral ankle index (LAI) reported by Finck and Jones [1] appeared to be just such a sign, totally new and not too complex to be practical. (The index is derived by dividing the sagittal length of the distal tibial articulating surface by the distance from the anterior tibial articulating surface to the anterior border of the pre-Achilles fat as shown on the lateral radiograph.)

I immediately pulled out my teaching envelope of radiographs of ankle injuries to test the sign. Each of the first three fractures of the fibula had an index of 0.66 or 0.67, right at the borderline of one standard deviation from the fracture mean and the same from the "no fracture" mean. If two standard deviations are used, these results are even more inconclusive. I then looked at the radiographs of two severe fractures of the fibula. The LAIs were 0.60 and 0.62, clearly indexes indicating "no fracture."

These observations may help to better define the usefulness of the LAI for further testing. A sign in which the value in a person without trauma is in the same range as the value in a person with a fracture is clearly not a sign for discovering fractures. Rather, if no obvious (severe) fracture is present and the LAI is below the fracture range, indicating extensive soft-tissue swelling, then a diagnosis of "no fracture" can be made.

It is hoped that the index will be valid for excluding fractures of the distal fibula. Only time will determine if enough energy can be transmitted to both the bone and the soft tissue to cause both a subtle fracture and a lot of soft-tissue swelling.

A final point to remember: The LAI will not exclude fractures of the mid or proximal fibula, which may occur with ankle-twisting injuries.

Stanley P. Bohrer

Bowman Gray School of Medicine
Winston-Salem, NC 27103

REFERENCE

1. Finck S, Jones MD. The lateral ankle index: its usefulness in detecting lateral malleolar fractures. *AJR* 1989;152:895

Reply

We thank Dr. Bohrer for his letter about our recent article [1]. He cites examples of five patients with fibular fractures who have lateral ankle indexes (LAI) ranging from 0.60 to 0.67. In our experience, these values are low for patients with isolated lateral adduction fractures of the ankle who had radiographs taken promptly after their injury. The LAI may be less accurate in patients who have multiple or severe ankle fractures or in patients who did not have radiographs taken shortly after their injury. The LAI is most accurate when used to confirm the presence or absence of a subtle lateral malleolar fracture.

Saul Finck

Malcolm D. Jones

University of California, Irvine, Medical Center
Orange, CA 92668

REFERENCE

1. Finck S, Jones MD. The lateral ankle index: its usefulness in detecting lateral malleolar fractures. *AJR* 1989;152:895

Spinal Cord Compression by Unusual Epidural Air Accumulation After Continuous Epidural Analgesia

Continuous epidural analgesia, a palliative method for relief of acute sciatic pain, causes surprisingly few neurologic complications [1]. Lumbar root compression usually is attributed to hematoma or formation of an abscess, but signs and symptoms due to injection of air have been reported only recently [2].

A 40-year-old woman was admitted 10 days after the appearance of disabling radiating pains in her right leg. She had had similar sciatic pains 5 years earlier. On admission, she had marked motor weakness and sensory loss in her right leg. An epidural catheter was installed at the level of L3-L4, and 40 mg of methylprednisolone acetate and 4 ml of 0.5% bupivacain hydrochloride were administered. The pain in her right leg was relieved after 15 min., and the same amount of bupivacain was injected every 4 hr. The next day, the epidural catheter became occluded and was replaced. Myelography showed extradural compression of the thecal sac at the level of L5-S1 on the right side. CT with metrizamide confirmed the level of the herniated disk, and a few air bubbles were seen in the epidural space and between the paraspinal muscles of the lumbar region. Despite the relief achieved by the use of continuous epidural analgesia, the patient began to complain of increasing motor weakness and numbness in her left leg. Reocclusion of the epidural catheter occurred 2 days later, and the catheter was replaced again. Headaches, increasing

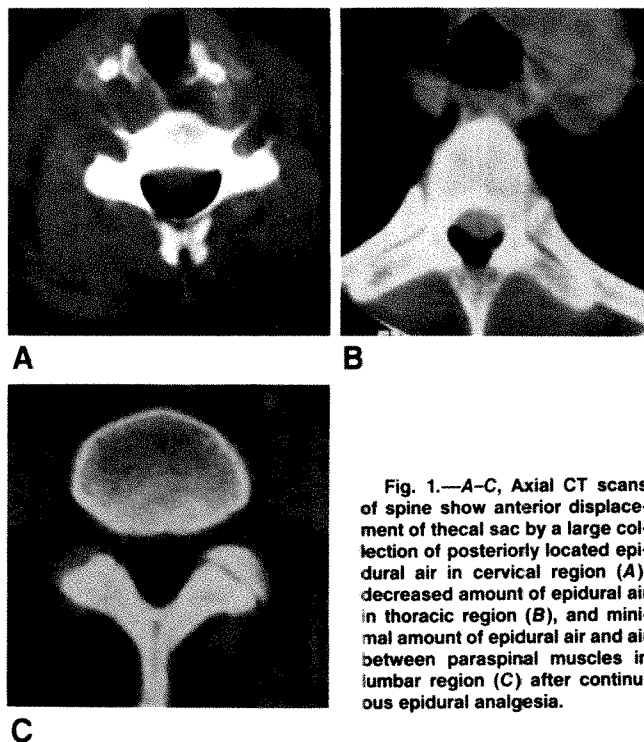


Fig. 1.—A–C, Axial CT scans of spine show anterior displacement of thecal sac by a large collection of posteriorly located epidural air in cervical region (A), decreased amount of epidural air in thoracic region (B), and minimal amount of epidural air and air between paraspinal muscles in lumbar region (C) after continuous epidural analgesia.

motor weakness, and hyposensitivity in the upper extremities appeared a few hours later. Removal of the epidural catheter led to slow relief of her headaches. CT scan of the cervical spine showed a fairly large amount of posteriorly located epidural air displacing the thecal sac anteriorly in the cervical and thoracic spine (Fig. 1) and, to a lesser amount, in the lumbar area. After the catheter was removed, the neurologic signs and symptoms disappeared gradually, first in the upper extremities and later in the left leg. CT of the spine performed at this time showed a decreased amount of epidural air. A week later, the patient had right discectomy at the L5-S1 level.

Many of the complications of epidural analgesia are related to technique, as correct insertion of the epidural catheter can be verified only by the ensuing neural blockade [3]. Subcutaneous emphysema is a known, but rare, complication [4]. Presumably, the repeated replacement of the catheter in our case, requiring testing by injection of air, led to the epidural collection of air along the spine. The virtual absence of anterior epidural space in the spinal canal limited the accumulation of air to the posterior epidural space. The CT evidence of anterior displacement of the thecal sac by the large epidural collection of air supported the clinical manifestations of spinal cord compression, which vary with the severity of the pressure and the rapidity of its induction [1]. These neurologic sequelae are reversible after removal of the epidural catheter.

M. Hirsch

Y. Katz

A. Sasson

Soroka Medical Center
Ben-Gurion University of the Negev
Beer-Sheva 84101, Israel

REFERENCES

1. Usubiaga JE. Neurological complications following epidural anesthesia. *Int Anesthesiol Clin* 1975;13:1-153

2. Kennedy TM, Ullman DA, Harte FA, Saberski LR, Greenhouse BB. Lumbar root compression secondary to epidural air. *Anesth Analg* 1988; 1184-1186
3. Koch J, Nielsen JU. Rare misplacements of epidural catheters. *Anesthesiology* 1986;65:556-557
4. Prober A, Tverskoy M. Soft-tissue emphysema associated with epidural anesthesia. *AJR* 1987;149:859

Gd-DTPA-Enhanced MR Detection of Diffuse Leptomeningeal Metastases

A 3-year-old girl had a 1-month history of lethargy and vomiting. The results of a physical examination and routine blood tests were normal. Cranial CT with and without contrast enhancement showed hydrocephalus without evidence of an obstructing lesion. After placement of a ventriculoperitoneal shunt, the patient improved dramatically.

Two months later, the patient returned because of recurrent vomiting. Contrast-enhanced CT showed normal ventricles, multiple areas of low attenuation within both cerebral hemispheres and the cerebellum, and abnormal enhancement of the basal cisterns. Cranial MR imaging showed multiple, well-circumscribed areas of decreased signal on T1 sequences and of increased signal on T2 sequences. The largest lesion was in the right temporal lobe (Fig. 1). After IV administration of Gd-DTPA (0.1 mmol/kg), marked diffuse enhancement of the basilar cisterns, sylvian and interhemispheric fissures, and cortical sulci occurred. MR examination of the spinal areas showed an enhancing intradural lesion at the T9 level.

Laboratory evaluation of CSF showed increased protein, slight leukocytosis, and cytologic evidence of dysplastic cells. All microbiologic cultures were negative. Biopsy of the lesion in the right temporal lobe was performed, and histopathologic examination of the specimen showed a primitive neuroectodermal tumor.

Leptomeningeal metastases occur with a number of intra- and extracranial neoplasms. These include leukemia, lymphoma, and extracranial solid tumors. Primitive neuroectodermal or embryonal tumors are undifferentiated, highly malignant, primary CNS neoplasms that occur in young patients. Medulloblastoma, cerebral neuroblastoma, pineal parenchymal tumors (pineoblastoma and pineocytoma), ependymoblastoma, and retinoblastoma are some of the neoplasms included in the classification of primitive neuroectodermal tumors [1]. These tumors, as well as ependymomas, have a propensity to seed through the CSF.

Leptomeningeal metastases may be diffuse or may produce focal deposits. Clinically, this produces neurologic symptoms and signs at several levels of the CNS. Analysis of CSF is useful in confirming the diagnosis and may show increased protein, leukocytosis, and abnormal cytologic findings.

The findings on contrast-enhanced CT can be abnormal in approximately 35% of patients with known leptomeningeal metastatic disease [2]. CT findings include enhancement of the basal cisterns, sulci, and tentorium. Ependymal-subependymal enhancement occurs with ventricular involvement, and communicating hydrocephalus may be present.

MR imaging without contrast enhancement is less sensitive than contrast-enhanced CT in detection of leptomeningeal metastases [3]. Abnormal findings on nonenhanced MR include hydrocephalus, focal cisternal masses, and possible signal changes in the CSF of the basal cisterns. As both iodinated contrast media and Gd-DTPA are postulated to produce enhancement in areas of breakdown of the blood-brain barrier, it might be expected that administration of contrast material would result in cisternal and sulcal enhancement on

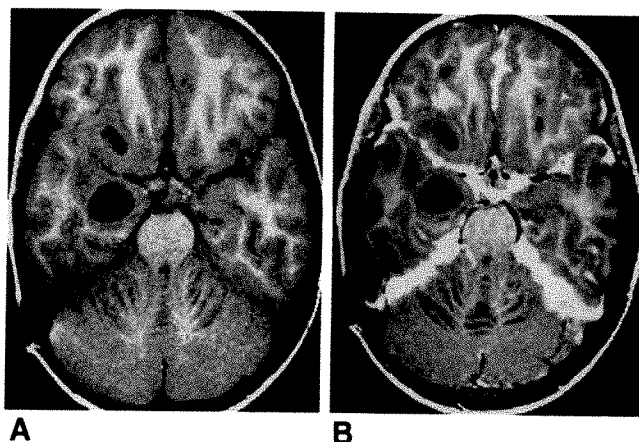


Fig. 1.—Diffuse leptomeningeal metastases in a 3-year-old girl with primitive neuroectodermal tumor.

A and B, Axial MR images, 650/25, obtained before (A) and after (B) administration of Gd-DTPA show multiple low-signal parenchymal lesions (A) and diffuse enhancement of cisterns and tentorium (B).

MR, as in our case. Meningitis also may produce hydrocephalus and leptomeningeal and subependymal enhancement, similar to the findings in metastatic disease [4].

Our case shows that, as with CT, Gd-DTPA MR enhancement is needed to detect leptomeningeal metastasis not evident on standard images. Consequently, Gd-DTPA-enhanced MR imaging should be mandatory in patients who have neoplasms known to metastasize commonly to the leptomeninges, such as primitive neuroectodermal tumors, or who have hydrocephalus of unknown cause.

Peter A. Cooley
David J. Czarnecki
St. Luke's Medical Center
Milwaukee, WI 53215
John R. Sty
Children's Hospital of Wisconsin
Milwaukee, WI 53226

REFERENCES

1. Okazaki H, Scheithauer BW. *Atlas of neuropathology*. New York: Gower Medical, 1988
2. Lee Y, Glass JP, Geoffroy A, Wallace S. Cranial computed tomographic abnormalities in leptomeningeal metastasis. *AJNR* 1984;5:559-563
3. Davis PC, Friedman NC, Fry SM, Malko JA, Hoffmann JC, Braum IF. Leptomeningeal metastasis: MR imaging. *Radiology* 1987;163:449-454
4. Mathews VP, Kuharik MA, Edwards MK, D'Amour PG, Azzarelli B, Dreesen RG. Gd-DTPA-enhanced MR imaging of experimental bacterial meningitis: evaluation and comparison with CT. *AJR* 1989;152:131-136, *AJNR* 1988;9:1045-1050

Normal Location of Conus Medullaris in Childhood

The study by Wilson and Prince [1] on the normal level of the conus medullaris in childhood had flawed methodology. The retrospective analysis was circular, and the sample was biased. The authors state, "The study group consisted of 184 children ranging in age from newborn to 20 years who had a normal conus level as reported by the radiologist of record." The objective of the article, however, was to determine what a normal conus level is. It does not make sense to assume certain criteria for normality in selecting the sample group and then study that same sample to determine the

criteria for normality. In addition, the study was to "determine the location of the conus medullaris in normal children," but the subjects chosen were not normal. The sample included, among others, patients with low back pain or back injury, possible infection or tumor of the spine or cord, poor bowel and/or bladder control, scoliosis, abnormal muscle tone or gait, and spina bifida. A study of this nature should not include patients with spinal orthopedic or neurologic dysfunction. Children imaged for unrelated conditions that incidentally revealed the location of the conus would have been more appropriate. Although the objective of the article is worthwhile, less potentially biased data need to be analyzed.

Dvorah Balsam
Mark Lodespoto
Nassau County Medical Center
East Meadow, NY 11554

REFERENCE

1. Wilson DA, Prince JR. MR imaging determination of the location of the normal conus medullaris throughout childhood. *AJR* 1989;152:1029-1032, *AJNR* 1989;10:259-262

Reply

We appreciate the interest that Drs. Balsam and Lodespoto have shown in our research. We also are fully aware of the bias inherent in any retrospective study. Our analysis was not, however, circular. For our group of "normal" infants and children, we chose 85 subjects who were referred for MR scans because of back pain, back injury, leukemia, possible spinal tumor or inflammation, or abdominal tumor (mostly Wilms tumors and liver tumors). All of these studies were interpreted as normal by the radiologist of record in so far as involvement of the spine was concerned. In other words, there was no gross evidence of infection, tumor, or significant trauma involving the spine or cord that might alter the level of the conus medullaris. There was

also no evidence in this group for spinal dysraphism, dysplastic conus, thickened filum terminale, or adherence of the cord to the thecal sac. Only those subjects with back pain might be considered to have a slightly increased prevalence of tethered cord.

The second group of subjects was studied because of possible symptoms of tethered cord, and indeed this diagnosis was made and surgically confirmed in 40 children during the course of our study. After eliminating the subjects who had proved tethered cord, we were left with a group of 99 subjects. We used rigorous statistical analysis to evaluate the findings in this group and determined that the location of the conus did not differ significantly from that in the "normal" subjects in the first group. Only then did we combine the groups for further analysis. We suppose it is possible that one or more patients with a morphologically normal cord, conus medullaris, and filum terminale could have had a tethered cord. The probability of this occurring must be quite small, but if it did occur, the statistical effect of such an error on our results and conclusions would be miniscule. In a 1-year follow-up of our entire "normal" group (combined groups 1 and 2), the diagnosis of a tethered cord has not been made subsequently in any of the subjects. We concluded the following: (1) The conus medullaris does not ascend throughout childhood but reaches the adult level sometime during the first few months of life. (2) A conus medullaris at or above L2-L3 is normal at any age. (3) The conus occasionally can occur at L3 in a normal child or adult. We remain confident in the accuracy of our results.

A prospective study is clearly the next step in confirming our findings. There are, however, difficulties inherent in obtaining adequate numbers of healthy children whose parents will permit MR with the requisite risk of sedation. This type of study also would be expensive, costing approximately \$80,000 at our institution for the same number of subjects.

Don A. Wilson
John R. Prince
Magnetic Resonance Center
Oklahoma Medical Center
Oklahoma City, OK 73126

Letters are published at the discretion of the Editor and are subject to editing.

Letters to the Editor must not be more than two *double-spaced*, typewritten pages. One or two figures may be included. Abbreviations should not be used. See Author Guidelines, page A5.

Material being submitted or published elsewhere should not be duplicated in letters, and authors of letters must disclose financial associations or other possible conflicts of interest.

Letters concerning a paper published in the *AJR* will be sent to the authors of the paper for a reply to be published in the same issue. Opinions expressed in the Letters to the Editor do not necessarily reflect the opinions of the Editor.

Review of Current Literature

Initials and addresses of corresponding authors are provided in parentheses for each article so that the reader can obtain reprints directly. Abstracts are printed verbatim from each journal.

The New England Journal of Medicine

A controlled trial of dexamethasone in preterm infants at high risk for bronchopulmonary dysplasia. Cummings JJ, D'Eugenio DB, Gross SJ (JJC, Children's Hospital of Buffalo, 219 Bryant St., Buffalo, NY 14222). *N Engl J Med* 320(23):1505-1510, June 1989

We evaluated the use of dexamethasone in preterm infants to decrease morbidity associated with bronchopulmonary dysplasia in a randomized, double-blind, placebo-controlled trial. Thirty-six preterm infants (birth weight, ≤ 1250 g and gestational age, ≤ 30 weeks) who were dependent on oxygen and mechanical ventilation at two weeks of age received a 42-day course of dexamethasone ($n = 13$), an 18-day course of dexamethasone ($n = 12$), or saline placebo ($n = 11$). The starting dose of dexamethasone was 0.5 mg per kilogram of body weight per day, and it was progressively lowered during the period of administration.

Infants in the 42-day dexamethasone group, but not those in the 18-day group, were weaned from mechanical ventilation significantly faster than control infants (medians 29, 73, and 84 days, respectively; $P < 0.05$), and from supplemental oxygen (medians 65, 190, and 136 days, respectively; $P < 0.05$). No clinical complications of steroid administration were noted. Follow-up of all 23 survivors at 6 and 15 months of age showed good outcome (normal neurologic examinations and Bayley Developmental Indexes ≥ 84) in 7 of the 9 infants in the 42-day dexamethasone group, but in only 2 of the 9 infants in the 18-day dexamethasone group and 2 of the 5 in the placebo group ($P < 0.05$).

We conclude that dexamethasone therapy for 42 days improves pulmonary and neurodevelopmental outcome in very-low-birth-weight infants at high risk for bronchopulmonary dysplasia.

A randomized, controlled trial of very early prophylactic ligation of the ductus arteriosus in babies who weighed 1000 g or less at birth. Cassady G, Crouse DT, Kirklin JW, et al. (GC, Children's Hospital of San Francisco, 3850 California St., San Francisco, CA 94118). *N Engl J Med* 320(23):1511-1516, June 1989

We speculated that prophylactic ligation of the ductus arteriosus would reduce mortality and morbidity in very-low-birth-weight infants. To test this hypothesis, we randomly assigned 84 babies who weighed 1000 g or less at birth and required supplemental oxygen either to receive standard treatment ($n = 44$) or to undergo prophylactic surgical ligation of the ductus arteriosus on the day of birth ($n = 40$). The ductus was ligated in babies in the control group only if

the shunt was hemodynamically important. All the babies were followed for one year.

The incidence of necrotizing enterocolitis was reduced in the group that underwent prophylactic ligation (3 of 40 [8 percent]) as compared with the control group (13 of 44 [30 percent]; $P = 0.002$). The frequency of death, bronchopulmonary dysplasia, retinopathy of prematurity, and intraventricular hemorrhage was similar in both groups. Because early enteral feeding may have increased the incidence of necrotizing enterocolitis, we analyzed separately the babies who were fed early. Among the infants who were fed within 14 days of birth, those who underwent prophylactic ligation had a lower incidence of necrotizing enterocolitis (1 of 11 [9 percent]) than those who did not (13 of 24 [54 percent]; $P = 0.001$). Within the control group, the infants who were fed within 14 days of birth and whose ductus was ligated for medical reasons within 5 days of birth had a lower incidence of necrotizing enterocolitis (2 of 10 [20 percent]) than those whose ductus was ligated later or not at all (11 of 14 [79 percent]; $P = 0.004$).

We conclude that early surgical closure of the ductus arteriosus reduces the risk of necrotizing enterocolitis in infants of very low birth weight who require supplemental oxygen.

Cancer

Relationship between carotenoids and cancer: the multiple risk factor intervention trial (MRFIT) study. Connett JE, Kuller LH, Kjelsberg MO, et al. (JEC, Coordinating Centers for Biometric Research, Ste. 508, 2829 University Ave., S. E., Minneapolis, MN 55414). *Cancer* 64:126-134, 1989

We evaluated the baseline serum levels of beta carotene, total carotenoids, vitamin A and E, and retinol-binding protein among 156 initially healthy men who participated in the Multiple Risk Factor Intervention Trial (MRFIT) and who subsequently died of cancer and 311 controls individually matched for age, smoking status, randomization group, date of randomization, and clinical center. Both total carotenoids and beta carotene levels were lower in the 66 lung cancer cases than in their matched controls. For all cancer deaths combined, there were no significant differences in total carotenoids or beta carotene between cases and controls. The relationship between lower serum carotenoid levels and lung cancer persisted after adjusting for the number of cigarettes, alcohol intake, serum thiocyanate levels, and cholesterol levels in the blood. Serum levels of retinol, alpha tocopherol, and retinol-binding protein were not related to any cancer site. The results of this study provide further evidence for a possible protective effect of beta carotene against lung cancer among cigarette smokers.

Reprinted by permission from the American Cancer Society.

Relationship between cirrhosis, liver cancer, and hepatic metastases: an autopsy study. Melato M, Laurino L, Mucli E, Valente M, Okuda K (MM, Istituto di Anatomia Patologica, University of Trieste, Ospedale Maggiore, I 34100 Trieste, Italy). *Cancer* 64:455-459, 1989

Consecutive autopsies (5241) performed in the Trieste area and consecutive autopsies (6511) performed in the Tokyo-Chiba area were analyzed to study the frequency of liver metastases in cirrhotics. The Italian material included 500 cases and the Japanese material included 529 cases of liver cirrhosis. Both of these groups were matched for sex and age with a control group. The results were similar in both areas and confirmed the widely held but disputed opinion that metastases in cirrhotic liver are rare. These results seem to be clinically important since they agree with the fact that most neoplasms in cirrhotic liver are primary. From a biologic and epidemiologic point of view, these results call for reconsideration of the complex relationship existing between cancer and liver cirrhosis, in relation to major causative factors such as alcohol and hepatitis B virus (HBV) infection.

Reprinted by permission from the American Cancer Society.

Chest

Roentgenographic evidence for predominant left-sided location of unilateral pleural plaques. Withers BF, Ducatman AM, Yang WN (AMD, Environmental Medical Service, MIT, 18 Vassar St., Cambridge, MA 02139). *Chest* 95:1262-1264, 1989

The roentgenographic prevalence and anatomic distribution of pleural plaques were studied in the US Navy Asbestos Medical Surveillance Program population (105,064 individuals as of July 17, 1985). "Definite" or "probable" pleural plaques were noted in 4.4 percent of films. These were unilateral in 19.3 percent of roentgenograms with "definite" pleural plaque and 33.9 percent of films with "probable" pleural plaque. Unilateral findings were more often left-sided than right-sided; a ratio of 287:82 in the "definite" group and 625:287 in the "probable" group. Left-sided predominance of unilateral plaque is a consistent and unexplained epidemiologic finding that may provide clues to pleural pathogenesis following asbestos exposure.

Gastroenterology

Enteroclysis in the evaluation of suspected small intestinal bleeding. Rex DK, Lappas JC, Maglinte DDT, Malczewski MC, Kopecky KA, Cockerill EM (DKR, Dept. of Medicine, Division of Gastroenterology, Indiana University School of Medicine, Indianapolis, IN). *Gastroenterology* 97:58-60, 1989

One hundred twenty-five consecutive enteroclysis studies performed for the indication of gastrointestinal bleeding were reviewed. The overall yield of positive studies was low (10%) but important lesions were found. Patients with unequivocally normal evaluations of the upper gastrointestinal tract and colon had the highest yield of positive enteroclysis studies (20%). Neither the specific type of bleeding, the presence or absence of abdominal symptoms or physical examination findings, nor the results of laboratory tests were associated with a positive or negative enteroclysis study.

Reprinted with permission by the American Gastroenterological Association.

Digestive Diseases and Sciences

Detection of biliary origin of acute pancreatitis: comparison of laboratory tests, ultrasound, computed tomography, and ERCP. Schölmerich J, Gross V, Johannesson T, et al. (JS, Medizinische Universitätsklinik, Hugstetter Str. 55, D-7800 Freiburg, West Germany). *Dig Dis Sci* 34(6):830-833, June 1989

Fifty consecutive patients with acute pancreatitis were assessed with respect to a biliary origin of the disease. Endoscopic retrograde cholangiopancreatography, surgery, and autopsy were used to define biliary pancreatitis. Ultrasound, computed tomography, and several laboratory tests (SGOT, SGPT, alkaline phosphatase, and bilirubin) were analyzed for their ability to detect a biliary origin of the disease. Ultrasound and computed tomography could not reliably make the diagnosis in the 10 patients found to have biliary disease. Receiver-operator-characteristic curves revealed that none of the laboratory tests assessed had sufficient sensitivity and specificity to determine the diagnosis, although all tests showed higher mean values in biliary pancreatitis. SGPT gave the best discrimination (positive predictive value 53%, negative predictive value 94%, cut off 40 units/liter). Therefore, initial ERCP is suggested for a reliable diagnosis of biliary origin of acute pancreatitis.

Clinicopathological features and natural history of gastric hamartomatous polyps. Iishi H, Tatsuta M, Okuda S (HI, Dept. of Gastrointestinal Oncology, The Center for Adult Diseases, 3-3, Nakamichi 1-chome, Higashinari-ku, Osaka 537, Japan). *Dig Dis Sci* 34(6):890-894, June 1989

The clinicopathological features, chromoendoscopic findings, and natural history of hamartomatous polyps of the stomach were compared with those of gastric hyperplastic polyps. Hamartomatous polyps were found significantly more frequently in adult females than adult males, and all were located in the gastric body or the fundus. In general, the number of polyps per patient was less in older patients. Histologically, all these polyps were formed of cystically dilated oxyntic glands and irregularly deformed oxyntic glands. Chromoendoscopic examinations using Congo red showed that the polyps were associated with extensive acid-secreting areas, were all located in acid-secreting areas, and had an acid-secreting function. Colonoscopy and/or radiologic examinations showed that one or a few polyps were frequently also present in the colons of these patients, but none of the families of the patients had a history of gastrointestinal polypoid. One to 11 years after the initial endoscopy, in seven (50.0%) of 14 patients with hamartomatous polyps followed up, the number of polyps decreased significantly.

Detection of esophageal motor disorders by radionuclide transit studies: a reappraisal. Holloway RH, Lange RC, Plankey MW, McCallum RW (RWM, Division of Gastroenterology, University of Virginia School of Medicine, Box 145, Charlottesville, VA 22908). *Dig Dis Sci* 34(6):905-912, June 1989

Radionuclide measurement of esophageal transit has been proposed as a screening test for esophageal motor dysfunction. In this study we evaluated the radionuclide esophageal transit test in 49 consecutive patients undergoing esophageal manometry for esophageal motor disorders. Esophageal transit was assessed using a 10-ml water bolus labeled with 250 μ Ci technetium-99m sulfur colloid. In preliminary studies in 14 healthy controls, mean transit time was 9.6 ± 2.1 (SD) sec. Prolonged transit (>15 sec) was observed in two of 28 swallow sequences in the control subjects. Transit times were prolonged in all patients with achalasia or diffuse esophageal spasm, and in five of seven patients with nonspecific abnormalities of peristaltic progression. The test was abnormal in only three of seven patients with high-amplitude peristalsis (nutcracker esophagus) and in none of three patients with hypertensive lower esophageal sphincter. Additionally, prolonged transit was seen in two of 18 patients with normal manometry. We conclude that the radionuclide transit test using a liquid bolus successfully identifies motor disorders characterized by defective peristaltic progression but not disorders in which peristalsis is intact. A major limiting factor appears to be the small number of swallow sequences tested. The test may not, therefore, be accurate enough to consider adopting as a sensitive and noninvasive screening test in the evaluation of patients with suspected esophageal motor disorders.

The Journal of Bone and Joint Surgery

Evaluation of magnetic resonance imaging in the diagnosis of osteonecrosis of the femoral head: accuracy compared with radiographs, core biopsy, and intraosseous pressure measurements. Robinson HJ Jr, Hartleben PD, Lund G, Schreiman J (HJR, Mayo Memorial Bldg., 420 Delaware St. S. E., Minneapolis, MN 55455). *J Bone Joint Surg [Am]* 71-A(5):650-663, June 1989

The accuracy of magnetic resonance imaging in the detection of osteonecrosis of the femoral head was compared with that of other diagnostic methods in current use: plain radiography, bone-marrow pressure determinations, intramedullary venography, and histological examination of core-biopsy bone specimens. In the first phase of the study, forty-eight patients (ninety-six hips) who were at high risk for avascular necrosis were studied. Abnormal patterns on magnetic resonance imaging, consistent with those seen in necrosis, were found in all hips that were suspected of having Ficat Stage-2 or 3 changes on the basis of radiographic evidence of the disease. Abnormal patterns on magnetic resonance imaging that were characteristic of avascular necrosis were also observed in 17 per cent of the hips that were suspected of having Ficat Stage-0 changes and in 64 per cent of those that showed Stage-1 changes, all with no radiographic changes.

In the second phase of the study, twenty-three of the ninety-six hips that were suspected of having early-stage necrosis of the femoral head but showed slight or no radiographic changes were studied by repeat radiographs, Ficat functional evaluations of bone, core biopsies of the femoral head, and magnetic resonance imaging. Of the twenty-three hips, eighteen (78 per cent) had positive changes on magnetic resonance imaging; nineteen (83 per cent) had positive histological evidence of necrosis; and fourteen (61 per cent) had positive findings by bone-marrow pressure studies and intramedullary venography. Although false-negative and false-positive results were observed with magnetic resonance imaging, the over-all results of this study suggest that magnetic resonance imaging may be useful for the early diagnosis of avascular necrosis.

Clinical Orthopaedics and Related Research

Benign metastasizing giant-cell tumor of bone: report of three cases and review of the literature. Maloney WJ, Vaughan LM, Jones HH, Ross J, Nagel DA (WJM, 300 Pasteur Dr., Division of Orthopaedic Surgery, R171, Stanford, CA 94305-5326). *Clin Orthop* 243:208-215, June 1989

Three cases of benign giant-cell tumor (GCT) of bone with pulmonary metastasis are reported. In addition, 28 cases from the literature are reviewed. The patients were followed for a mean of 7.8 years (range from two to 29 years). The interval to metastasis ranged from zero to ten years with a mean of 3.2 years. Metastasis was not related to the number of previous operations. The local recurrence rate in the tumors that metastasized was 63%, suggesting that GCTs that metastasize may be an aggressive form of the tumor. The overall mortality rate was 16%. Persistent pulmonary disease does not carry a poor prognosis; surgical resection of accessible pulmonary nodules is recommended to provide histologic confirmation of the diagnosis, and prevent future complications secondary to local growth of the implants, as well as provide a potential cure. Chemotherapy has not improved survival and is associated with significant morbidity and is thus not recommended. Adjuvant radiation is recommended only for control of surgically unresectable lesions because of its potential association with sarcomatous degeneration in GCT.

The Journal of Urology

Selective use of excretory urography in women with acute pyelonephritis. Sandberg T, Stokland E, Brolin I, Lidin-Janson G, Eden

CS (TS, Dept. of Infectious Diseases, Ostra Hospital, S-416 85 Göteborg, Sweden). *J. Urol* 141:1290-1294, June 1989

The outcome of excretory urography was analyzed in 103 non-pregnant women followed prospectively after community acquired acute pyelonephritis. Radiological abnormality was found in 40 per cent of the patients (17 per cent had major abnormalities, including renal scarring, calculi and obstruction). All 5 women with surgically correctable lesions had rapid bacteriological relapse or recurrent acute pyelonephritis.

Neither a history of urinary tract infection, the acute inflammatory response nor infection due to *Escherichia coli* with or without adhesions specific for Gal α 1 \rightarrow 4Gal β -containing receptors was efficient in predicting major radiographic lesions or the outcome of treatment. Bacteremia was detected in 27 per cent of the patients but in the absence of obstruction. These results suggest that excretory urography is dispensable in most women with acute pyelonephritis, and that those needing such investigation may be identified by failure to respond to antibiotic treatment or by the recurrence pattern.

The Journal of Pediatrics

High-output cardiac failure in fetuses with large sacrococcygeal teratoma: diagnosis by echocardiography and Doppler ultrasound. Schmidt KG, Silverman NH, Harrison MR, Callen PW (NHS, University of California, San Francisco, Rm. M342 A, Box 0214, San Francisco, CA 94143). *J Pediatr* 114:1023-1028, June 1989

With two-dimensional echocardiography and Doppler ultrasound, we demonstrated high-output cardiac failure in three fetuses with large sacrococcygeal teratomas. All fetuses had normal cardiac structure, dilated ventricles maintaining a normal fractional shortening index, a dilated inferior vena cava reflecting the increased venous return from the lower body, pericardial and pleural effusions as a manifestation of fetal hydrops, and a markedly thickened placenta. When fetal hydrops was present, the combined ventricular output was very high (mean 1280 ml/min/kg; normal 553 ± 153 (SD)). Descending aortic flow was also sharply increased (mean 930 ml/min/kg; normal 184 ± 20), as was placental flow (mean 480 ml/min/kg, normal 110 ± 26). High-velocity arterial flow signals were also found within the tumor. In one fetus studied serially, placental thickness and tumor diameter increased rapidly; placental flow as a percentage of descending aortic flow decreased, indicating a further increase of flow to the tumor. These abnormal hemodynamic changes were reversed after the fetus's teratoma was surgically removed. We conclude that the sacrococcygeal teratoma acts as a large arterio-venous fistula, which causes high-output cardiac failure. Surgical removal of the teratoma in a pre-viable fetus with such hemodynamic findings may prove to be the most effective treatment.

Journal of Thoracic Imaging

The Fleischner Lecture: computed tomography of diffuse pulmonary disease. Genereux GP (E. N. C. Milne, M.D., Professor of Radiological Sciences and Medicine, University of California, Irvine Medical Center, 101 City Dr., Orange, CA 92668-3297). *J Thorac Imaging* 4(3):50-87, 1989

The current level of computed tomography (CT) scanner resolution is such that CT is possibly the best radiographic procedure available for viewing gross pulmonary anatomy and pathology. CT densitometry, in contrast, is of limited value in assessing diffuse lung disease because of partial volume errors created by the wide range of intrathoracic tissue densities. Anteroposterior density gradients and total mean lung density can be used advantageously in a select group of patients with suspected high-density disease.

The morphologic patterns of diffuse high-density lung disease as viewed on conventional roentgenograms correlate closely with those depicted on CT images.

Density measurements in normal and abnormal patients suggest that the medulla of the lung may be a reservoir zone that accommodates increased blood flow via distention and recruitment of vessels under appropriate conditions.

Pulmonary diseases that cause oligemia can be identified and distinguished by their combined CT densitometric and morphologic characteristics. Combined high- and low-density disease may need total integration of plain radiographs, isotopic scans, and CT scans for proper interpretation.

Pediatric Radiology

The natural history of reflux into the lower pole of duplicated collecting systems: a controlled study. Ben-Ami T, Gayer G, Hertz M, Lotan D, Boichis H (TB-A, Dept. of Diagnostic Imaging, The Chaim Sheba Medical Center, Tel Hashomer, Israel). *Pediatr Radiol* 19:308-310, 1989

Thirty two children with reflux into the lower pole of duplicated collecting systems, followed non-operatively for one to five years, were compared to a carefully selected control group of similar children who had reflux into a single collecting system. There were no significant differences between the two groups, either in the outcome of reflux or in the incidence of new renal scars. We conclude that reflux into the lower pole of a duplex kidney does not in itself constitute an indication for early surgical treatment.

Mastoid abnormalities in Down syndrome. Glass RBJ, Yousefzadeh DK, Roizen NJ (RBJG, Dept. of Radiology, Loyola University Medical Center, Maywood, IL). *Pediatr Radiol* 19:311-312, 1989

Hearing loss and otitis media are commonly associated with Down syndrome. Hypoplasia of the mastoids is seen in many affected children and sclerosis of mastoid bones is not uncommon in Down syndrome. Awareness and early recognition of mastoid abnormality may lead to appropriate and timely therapy, thereby preserving the child's hearing or compensating for hearing loss; factors which are important for learning and maximum development.

Journal of Ultrasound in Medicine

Sonography of the distal cystic duct. Parulekar SG (SGP, Mount Sinai Medical Center, Dept. of Radiology, Division of Ultrasound, 1 Mount Sinai Dr., Cleveland, OH 44106). *J Ultrasound Med* 8:367-373, July 1989

This prospective study of 139 patients was performed for evaluation of the normal and abnormal distal cystic duct and cystic duct remnant after cholecystectomy. The normal distal cystic duct could be demonstrated in 51% of the patients with normal common bile duct and normal gallbladder. The average diameter of the normal distal cystic duct was 1.8 mm. In 95% of the patients, the distal cystic duct was located posterior to the common bile duct and, in 5% of the patients, anterior to the common duct. Echoes produced by cystic duct insertion into the common bile duct occasionally can be mistaken for stones in the common bile duct. These echoes, however, are not associated with acoustic shadowing. Sludge and stones could be demonstrated in the distal cystic duct as well as in the cystic duct remnant after cholecystectomy.

Reprinted with permission by the American Institute of Ultrasound in Medicine.

Journal of Computer Assisted Tomography

Gadolinium-DOTA enhanced MR imaging of intracranial lesions. Parizel PM, Degryse HR, Gheuens J, et al. (PMP, Dept. of Radiology,

Universitair Ziekenhuis Antwerpen, University of Antwerp, Wilrijkstraat 10, B-2520 Edegem, Belgium). *J Comput Assist Tomogr* 13(3):378-385, May/June 1989

Gadolinium 1,4,7,10-tetraazacyclododecane-N,N',N'',N'''-tetraacetic acid (Gd-DOTA) is the first of a new class of macrocyclic paramagnetic magnetic resonance (MR) contrast agents (gadolinium cryptelates) to be used in clinical practice. Gadolinium-DOTA possesses relaxation properties similar to those of gadolinium diethylene triamine pentaacetic acid (Gd-DTPA). We report our initial clinical experience in 38 patients with intracranial lesions studied with MR before and after injection of Gd-DOTA. Diseases included primary and metastatic brain tumor, cerebral infarct, vascular malformation, meningioma, hemangiopericytoma, schwannoma, and pituitary macroadenoma. Gadolinium-DOTA was administered intravenously in a dosage of 0.1 mmol/kg body weight. All studies were performed on a superconductive 0.5 T system. As compared to noncontrast T1- and T2-weighted images (WI), Gd-DOTA enhanced T1 W1 were useful in defining the anatomy of malignant intraaxial tumors (high-grade glioma, metastasis) and in tumor versus edema differentiation. Low-grade gliomas did not enhance; in these cases the precontrast T2-weighted sequence was found to be more informative. In post-operative patients, Gd-DOTA allowed us to demonstrate residual tumor or tumor recurrence. Extraaxial tumors (meningioma, hemangiopericytoma, neuroma) enhanced markedly, presumably reflecting tumor vascularity. In our experience, the use of Gd-DOTA improves the anatomic definition of cerebral lesions and in some cases increases both MR sensitivity and specificity. We found Gd-DOTA to be a well tolerated and effective paramagnetic contrast agent. Gadolinium-DOTA can be considered as an alternative water-soluble MR contrast agent to Gd-DTPA.

Computed tomography in pulmonary sarcoidosis. Lynch DA, Webb WR, Gamsu G, Stulberg M, Golden J (DAL, Dept. of Radiology, University of California at San Francisco, San Francisco, CA 94143-0628). *J Comput Assist Tomogr* 13(3):405-410, May/June 1989

We studied the high resolution CT (HRCT) scans of 15 patients with biopsy-proven sarcoidosis and correlated the findings with pulmonary function tests (12 patients), ⁶⁷Ga scans (10 patients), bronchoalveolar lavage (five patients), recent transbronchial biopsy (six patients), and recent open lung biopsy (three patients). The HRCT features included small nodules, thickened interlobular septa, patchy focal increase in lung density, honeycombing, and central conglomeration of vessels and bronchi. Active alveolitis was present by gallium scanning criteria in 5 of 10 cases. By bronchoalveolar lavage criteria, activity was present in three of five cases. Patchy increase in density may correlate with active alveolitis as seen on ⁶⁷Ga scanning. High resolution CT was better than chest X-radiography for demonstration of patchy increase in density and for distinguishing nodules from septal thickening. Both nodules and patchy density were partly reversible following therapy. Nodular densities seen on CT correlated with the presence of granulomata on histology. Resting pulmonary function tests correlated poorly with presence and extent of lung disease on HRCT. The presence on HRCT of focal fine nodules, patchy focal increase in lung density, and central crowding of bronchi and vessels should suggest the diagnosis of sarcoidosis. In some patients, HRCT can identify unsuspected parenchymal lung disease and document the reversible components of sarcoid lung disease.

Computed tomography of inflation-fixed lungs: the beaded septum sign of pulmonary metastases. Ren H, Hruban RH, Kuhlman JE, et al. (D. M. Hutchins, Dept. of Pathology, Johns Hopkins Hospital, Baltimore, MD 21205). *J Comput Assist Tomogr* 13(3):411-416, May/June 1989

Radiographic identification of pulmonary metastases has proved to be a challenging problem. We applied high resolution CT (HRCT) to 180 postmortem lung specimens prepared by a method that allows for direct one-to-one pathologic-radiologic correlation. Of the 180

lungs, 32 had pulmonary metastases. The location, number, size, and interstitial changes were evaluated in 32 cases with pulmonary metastases. The pulmonary metastases were peripheral lesions in 94% of these 32 patients, and multiple tumors were found in 91% of these cases. The metastases were <1 cm in diameter in 78%. Twenty-two of the 32 cases (69%) had obvious interstitial changes. In 19 of these 22 cases the interstitial change was characterized by the appearance of a "beaded septum" on HRCT. This beaded septal change corresponded directly to tumor growth in pulmonary capillaries and lymphatics and the septal interstitium. This sign was not noted in any of the specimens with pulmonary edema or fibrosis or in normal lungs. We believe that detection of the beaded septum sign on HRCT is highly suggestive of pulmonary metastases.

Magnetic Resonance Imaging

Magnetic resonance imaging of malignant fibrous histiocytoma.

Mahajan H, Kim EE, Wallace S, Abello R, Benjamin R, Evans HL (EEK, Division of Diagnostic Imaging, Box 057, The University of Texas M. D. Anderson Cancer Center, 1515 Holcombe Blvd., Houston, TX 77030). *Magn Reson Imaging* 7:283-288, 1989

The magnetic resonance imaging (MRI) changes in 39 patients with malignant fibrous histiocytoma (MFH) were reviewed retrospectively. Twenty-one sarcomas were in the lower extremity, five each in the upper extremity and trunk, two each in the neck and heart, and one each in the maxillary sinus, sella turcica, tongue, and spermatic cord.

The examinations were performed with spin-echo sequences on a 1.5 Tesla Signa Scanner (GE, Milwaukee WI). Twenty-two tumors

exhibited intermediate signal intensity on T_1 -weighted images and 23 were of high signal intensity on T_2 -weighted images. There was no significant difference in signal intensity of 12 preoperative and 13 recurrent neoplasms. Twelve of 13 patients were correctly diagnosed as having postoperative changes.

The MR sensitivity and specificity for detecting a neoplasm were 96% and 83% respectively, but the signal changes were nonspecific for MFH. When compared to CT in 14 patients, MR better defined the extent of the MFH, its relationship to surrounding tissues and vessels, and best differentiated residual or recurrent disease from postoperative changes when examined at least 3 months after surgery.

Biological effects of weak electromagnetic fields from 0 Hz to 200 MHz: a survey of the literature with special emphasis on possible magnetic resonance effects. Beers GJ, (GJB, Dept. of Radiology, Boston University Medical Center, 88 E. Newton St., Boston, MA 02118). *Magn Reson Imaging* 7:309-331, 1989

The literature on biological effects of weak electromagnetic fields of a frequency of 200 MHz or less is surveyed. The topic has been extraordinarily controversial, in part because of disputed assertions about a role for electromagnetic fields in carcinogenesis or production of abnormalities in growth and development. There is fairly widespread acceptance of certain beneficial effects, particularly the stimulation of healing. An increasing number of reports point to interactions between static magnetic fields and time-varying fields in the production of some effects. Safety implications are noted along with the hypothetical possibility of production of experimental artifacts by electromagnetic fields in MRS research.

News

Society for Medical Decision Making Annual Meeting

The 11th annual meeting of the Society for Medical Decision Making will be Oct. 15-18 at the Radisson University Hotel, Minneapolis, MN. The program will include a symposium, Medical Decision Making and Public Policy; presentations of seven categories of current scientific work; poster sessions; and discussions for special interest groups. One-day courses in medical decision making will be held Oct. 15, including Practical Applications of Medical Decision Making, Advanced Decision Psychology, Confidence Profiles, and Influence Diagrams. Information: John C. Tomeny, Administrative Director, Society for Medical Decision Making, P. O. Box 447, West Lebanon, NH 03784; (603) 298-9929.

Principles and Practice of MRI

The Johns Hopkins Medical Institutions are sponsoring Principles and Practice of MRI, Nov. 10-12, at the Sheraton Inner Harbor Hotel, Baltimore, MD. Program directors: Elias A. Zerhouni, R. Nick Bryan, and Clare M. C. Tempany. Category 1 credit: 20.5 hr. Fee: physicians, \$395; persons in training, \$200. Information: Office of Continuing Education, The Johns Hopkins Medical Institutions, Turner Bldg., 720 Rutland Ave., Baltimore, MD 21205-2195; (301) 955-2959.

Diagnostic Radiology and Nuclear Medicine

The Dept. of Radiology, Bowman Gray School of Medicine, Wake Forest University, will hold its 9th Annual Winter Continuing Education Meeting, Jan. 27-Feb. 3, 1990, at the Frenchman's Reef Beach Resort, St. Thomas, U. S. Virgin Islands. The course will provide the practicing radiologist a survey of contemporary topics pertaining to key subspecialties and techniques. A special feature will be a seminar on financial planning. Category 1 credit: 17 hr. Fee: \$500. Information: Pat Rice, Dept. of Radiology, Bowman Gray School of Medicine, 300 S. Hawthorne Rd., Winston-Salem, NC 27103; (919) 748-2470.

Intermountain Imaging Conference

The Medical College of Wisconsin will hold its 11th annual Intermountain Imaging Conference, Feb. 10-17, 1990, in Steamboat Springs, CO. This 6-day program will discuss the application of digital imaging to clinical programs. Morning lectures and afternoon seminars will explore the use of computer-based imaging systems in problem solving and their relationship to other conventional diagnostic techniques. A series of focused seminars will cover Doppler vascular imaging, neurologic imaging, and imaging in obstetrics and gynecology. Category 1 credit: 33 hr. Fee: \$475. Information: Thomas L.

Lawson, M.D., 6420 N. Lake Dr., Milwaukee, WI 53217; (414) 257-6024 or 257-7201.

Interventional Radiology 1990: Vascular and Biliary Updates

The Dept. of Radiology, University of Utah, School of Medicine, is sponsoring Interventional Radiology 1990: Vascular and Biliary Updates, Feb. 11-16, 1990, at Snowbird, UT. Course director: Franklin J. Miller. Category 1 credit: 22 hr. Fee: practicing physicians, \$395; residents and fellows, \$150. Information: Judy Gallegos, CME Coordinator, Dept. of Radiology, University of Utah, School of Medicine, 1A71 Medical Center, Salt Lake City, UT 84132; (801) 581-8699.

Imaging the Central Nervous System (Including the Spine)

The Medical College of Wisconsin and Continuing Medical Education, Inc., will present Imaging the Central Nervous System (Including the Spine), Feb. 18-23, 1990, at the Westin La Paloma Resort, Tucson, AZ. The course is designed for radiologists and others who are interested in MR and state-of-the-art conventional imaging. Topics will include applications of MR, CT, sonography, myelography, and angiography. Anatomic-radiologic correlations will be featured. Program chairmen: Victor Haughton, Thomas Naidich, Robert Quencer, and Joachim Seeger. Category 1 credit: 25 hr. Fee: through Dec. 31, 1989; \$425; after Dec. 31, \$475. Information: Continuing Medical Education, Inc., 11011 W. North Ave., Milwaukee, WI 53226; (414) 771-9520.

The American Board of Radiology Examinations

Written examinations for the American Board of Radiology (ABR) are scheduled for Oct. 12-13, 1989, and Sept. 27-28, 1990. Oral examinations will be held at the Executive West Hotel in Louisville, KY, June 4-8, 1990. The ABR will accept applications for admission to the examinations after July 1, but not later than Sept. 30, in the year preceding the year in which the examination is to be taken. For application forms and further information: Office of the Secretary, The American Board of Radiology, 300 Park, Ste. 440, Birmingham, MI 48009.

Wanted: Radiologists to Teach in India in December

Radiologists are needed to teach mammography in India for the month of December 1989. All expenses will be paid. Information: Lillian Stern, M.D., Dept. of Diagnostic Medical Imaging, Methodist Hospital, 2301 S. Broad St., Philadelphia, PA 19148; (215) 952-9151.

Meeting and Course Review

For the reader's convenience, a summary of upcoming meetings and courses is provided. Detailed listings are given in the *AJR* issue given in parentheses.

Basic and Advanced Training in MRI, times arranged, Baltimore (Dec 1988)

Visiting Fellowships in Radiology at MGH, times arranged, Boston (April)

Biliary Lithotripsy Visiting Fellowships, times arranged, Philadelphia (April)

Visiting Fellowship in Interventional Radiology, times arranged, Baltimore (Sept)

Visiting Fellowships in UCSF, times arranged, San Francisco (Sept)

Preceptorships in Transrectal Ultrasound of the Prostate, Ann Arbor, MI (Sept)

Radiology on Ischia, Sept. 23–Oct. 1, Lacco Ameno, Island of Ischia, Bay of Naples, Italy (May)

Registry Preparation Courses for Sonographers: Physics, Sept. 29–Oct. 1, Los Angeles; Oct. 6–8, Chicago; **Doppler Physics**, Oct. 2, Los Angeles (May)

Tutorial Course in Ireland, Oct. 1–5, Adare, Ireland (Sept)

MR Course in Riyadh, Saudi Arabia, Oct. 2–5, Riyadh, Saudi Arabia (June)

Current Trends in Diagnostic Radiology, Oct. 2–5, Boston (June)

Update in Pediatric Imaging, Oct. 2–5, Laguna Niguel, CA (June)

Clinical Magnetic Resonance Imaging, Oct. 2–6, San Francisco (Sept)

MRI: Clinical State of the Art, Oct. 4–7, New York (Sept)

Seminar in Diagnostic Ultrasound, Oct. 5–7, Ann Arbor, MI (May)

Biomedical Image Processing with Microcomputers, Oct. 5–7, St. Louis (Aug)

Breast Imaging: Problems and Solutions, Oct. 6, Boston (June)

Pediatric Neuroradiology Seminar, Oct. 7, San Francisco (Sept)

Practical Radiology, Oct. 9–12, Charlottesville, VA (May)

Introduction to Comparative Imaging for Urologic Lithotripsy, Oct. 12, Denver (Aug)

Color Doppler 1990, Oct. 12–14, Beverly Hills, CA (Sept)

Practical Magnetic Resonance Imaging 1989, Oct. 12–15, Las Vegas, NV (April)

Renal and Biliary Lithotripsy, Oct. 12–15, Denver (Aug)

The Lungs and Heart: Imaging Answers to Clinical Problems, Oct. 14–29, Bangkok, Chiangmai, and Phuket, Thailand; Hong Kong; and Taipei, Taiwan (July)

Organ Imaging Review 1989, Oct. 15–20, Toronto, Ontario (Aug)

Clinical MR Imaging Course, Oct. 16–18, New Haven, CT (Sept)

Chest Disease, Oct. 16–19, Boston (July)

World Congress for Bronchology, Oct. 18–20, Tokyo, and Oct. 21–22, Kyoto, Japan (Nov 1988)

Farwest Image Perception Conference, Oct. 19–20, Tucson, AZ (June)

Neonatal Neurosonography, Oct. 19–20, Philadelphia (Sept)

CT and MR of the Brain, Head, Neck, and Spine, Oct. 19–20, Chicago (Sept)

Royal Australasian College of Radiologists Annual Meeting, Oct. 19–23, Melbourne, Australia (March)

MRI Review '89, Oct. 20–22, Toronto, Ontario (Aug)

Automated Percutaneous Discectomy Workshops, Oct. 21–22, 1989, and April 7–8, 1990, Washington, DC; Nov. 18–19, 1989, Nashville, TN; Dec. 9–10, 1989, Jan. 13–14 and Feb. 17–18, 1990, San Francisco (Sept)

Mammography for the General Radiologist, Oct. 23–26, Boston (March)

Visiting Fellowship in Mammography, Oct. 23–27, Los Angeles (March)

Practicums in MR Imaging: Basic Practicum, Oct. 23–27, Baltimore (March)

Magnetic Resonance Imaging and CT Update, Oct. 23–27, Boston (July)

Advanced Neuroradiology Seminar, Oct. 26–28, Orlando, FL (June)

Advanced Imaging of the Musculoskeletal System, Oct. 28–29, Coronado (San Diego), CA (June)

San Diego Postgraduate Course, Oct. 30–Nov. 3, Coronado (San Diego) (July)

Obstetrics and Gynecology, Oct. 30–Nov. 3 and Dec. 4–8, Philadelphia (Sept)

International Seminar of Medical Imaging, Oct. 30–Nov. 5, Shatin, Hong Kong, the New Territories (May)

Interventional Radiology, Nov. 3–5, Coronado (San Diego) (July)

New Orleans Fall Radiology Conference, Nov. 6–8, New Orleans (Sept)

Diagnostic Radiology Seminar in Hawaii, Nov. 6–10, Maui, HI (Sept)

Magnetic Resonance Imaging: Techniques and Imaging Methodology, Nov. 6–10, Philadelphia (Sept)

Color Doppler Ultrasound, Nov. 13, Philadelphia (Sept)

Abdominal Ultrasound, Nov. 13–16, Philadelphia (Sept)

3-D Imaging in Medicine, Nov. 16–19, San Diego (Aug)

Prostate Ultrasound, Nov. 17, Philadelphia (Sept)

Advances in Chest, Interventional, and Ultrasound, Nov. 25–Dec. 10, South America (Caracas, Isla Margarita, Manaus, Recife, Rio de Janeiro, Buenos Aires, and Bariloche) (March)

Advanced Seminars in Diagnostic Imaging, Dec. 8–10, Laguna Niguel, CA (July)

CT and MRI—Head to Toe, Dec. 11–16, New York (Sept)

MR Imaging Seminar, Dec. 14–16, New York (Sept)

Genitourinary Radiology, Dec. 15–17, Scottsdale, AZ (Aug)

Thoracic Imaging '90, Jan. 7–11, 1990, Naples, FL (Sept)

Society of Gastrointestinal Radiologists Annual Meeting and Postgraduate Course, Jan. 14–19, 1990, Hawaii (Sept)

Diagnostic Radiology Seminar in Ixtapa, Mexico, Jan. 22–26, 1990, Ixtapa, Mexico (Sept)

Midwinter Radiological Conference, Jan. 26–28, 1990, Los Angeles (Sept)

Coronary Atherosclerosis: New Diagnostic and Therapeutic Approaches, Jan. 28–Feb. 1, 1990, Orlando, FL (Sept)

Mid-Pacific Radiological Conference, Jan. 30–Feb. 3, 1990, Maui, HI (Sept)

XV Interamerican Congress of Radiology, Feb. 11–16, 1990, Caracas, Venezuela (Aug)

International Conference on Gallstones and Their Management, Feb. 25–28, 1990, Jerusalem, Israel (May)

Interventional Radiology in Cardiovascular Pathology, Feb. 28–March 2, 1990, Toulouse, France (Aug)

Congress of the European Federation of Societies for Ultrasound in Medicine and Biology, May 6–11, 1990, Jerusalem, Israel (May)

AJR carries announcements of courses, symposia, and meetings of interest to its readers if received a minimum of 5 months before the event. There is no charge; receipt of items by the *AJR* Editorial Office is not acknowledged. Submit items for publication typed double-spaced. Provide title, date, location, brief description, sponsor, course directors, fees, category I credit, and address and telephone number for additional information. Faculty from the host institution will not be listed. Guest faculty names will appear **only** if initials are provided. Mail news items to *AJR* Editorial Office, 2223 Avenida de la Playa, Suite 200, La Jolla, CA 92037-3218.

Books Received

Receipt of books is acknowledged as a courtesy to the sender. Books considered of sufficient interest are reviewed as space permits. If the book has been reviewed in the *AJR*, the date of its review is given in parentheses.

Imaging in Clinical Practice. By Alan G. Chalmers, James H. McKillop, and Philip J. A. Robinson. Dobbs Ferry, NY: Sheridan House, 340 pp., 1988. \$35, softcover (7/89)

Practical Ultrasound. Edited by R. A. Lerski. Washington, DC: IRL Press, 255 pp., 1988. \$50, softcover; \$76, hardcover (7/89)

Cerebral Vascular Disease in Children and Adolescents. Edited by Michael S. B. Edwards and Harold J. Hoffman. (Part of the series Current Neurosurgical Practice. Series editor: Charles B. Wilson.) Baltimore: Williams & Wilkins, 480 pp., 1989. \$99.50 (7/89)

Interventional Radiology in Bone and Joint. Edited by Michel Bard and Jean-Denis Laredo. New York: Springer-Verlag, 273 pp., 1988. \$179.50 (7/89)

MRI Physics for Physicians. By Alfred L. Horowitz. New York: Springer-Verlag, 113 pp., 1989. \$19.50 (7/89)

Computed Tomography of the Lung. An Approach Based on Signs. By S. Galluzzi, C. Ruffalo, and L. Forzini. Padua: Piccin, 186 pp., 1988. (7/89)

The Radiologic Clinics of North America. Radiology of the Pancreas. Guest Editor: Patrick C. Freeny. Philadelphia: Saunders, January 1989; 27(1):1-193. \$25; by subscription, 6 issues annually for \$93 (7/89)

The Use of Gd-DTPA in the Central Nervous System. By Murray Solomon. (Videotape 2 of Murray Solomon's Magnetic Resonance Video Review.) Burlingame, CA: Murray Solomon's MRVR, (415) 692-8230, 1989. Single tape, \$125; series of 6 tapes, \$495 (7/89)

Basic Physics for Medical Imaging. By Edwin G. A. Aird. Stoneham, MA: Butterworths, 262 pp., 1988. \$49.95 (7/89)

Radiologic Oncology of the Abdomen and Pelvis. An Atlas and Text. Edited by Ali Shirkhoda. Chicago: Year book Medical, 1374 pp., 1988. \$195 (7/89)

Basic Physics for Medical Imaging. By Edwin G. A. Aird. Oxford, United Kingdom: Heinemann, 262 pp., 1988. £17.50, softcover (8/89)

Imaging of the Newborn, Infant, and Young Child. 3rd ed. By Leonard E. Swischuk. Baltimore: Williams & Wilkins, 1053 pp., 1989. \$136.95 (8/89)

Computed Body Tomography. With MRI Correlation, 2nd ed. Edited by Joseph K. T. Lee, Stuart S. Sagel, and Robert J. Stanley. New York: Raven, 1184 pp., 1989. \$140 (8/89)

Endoscopic Ultrasonography in Gastroenterology. Edited by Kei-ichi Kawai. New York: Igaku-Shoin, 161 pp., 1988. \$65 (8/89)

Radiology of the Esophagus. By Marc S. Levine. Philadelphia: Saunders, 373 pp., 1989. \$95 (8/89)

Renal Cystic Disease. By David S. Hartman. (Fascicle 1 of AFIP Atlas of Radiologic-Pathologic Correlations. Series editor: Alan J. Davidson.) Philadelphia: Saunders, 160 pp., 1989. \$50 (8/89)

Biliary Lithotripsy. Edited by Joseph T. Ferrucci, Michael Delius, and H. Joachim Burhenne. Chicago: Year Book Medical, 309 pp., 1989. \$85 (8/89)

Enhanced Magnetic Resonance Imaging. Edited by Val M. Runge. St. Louis: Mosby, 356 pp., 1989. \$69 (8/89)

Key Anatomy for Radiology. By Simon Westacott and John R. W. Hall. Oxford, United Kingdom: Heinemann, 227 pp., 1988. £17.50 (8/89)

Correlative Imaging. Nuclear Medicine, Magnetic Resonance, Computed Tomography, Ultrasound. By Martin P. Sandler, James A. Patton, Max I. Shaff, Thomas A. Powers, and C. Leon Partain. Baltimore: Williams & Wilkins, 660 pp., 1989. \$110 (8/89)

Atlas of Film-Screen Mammography. By Ellen Shaw de Paredes. Baltimore: Urban & Schwarzenberg, 364 pp., 1989. \$108 (8/89)

Quantitative Methods in Bone Densitometry. By Alan L. Huddleston. Boston: Kluwer, 217 pp., 1988. \$90 (8/89)

Appropriate Diagnostic Technology in the Management of Cardiovascular Diseases. Report of WHO Expert Committee (Technical Report Series, No. 772). Geneva: World Health Organization, 41 pp., 1988. \$4.80 (8/89)

Radiology of the Esophagus. By Dieter N. Hüpscher. New York: Thieme, 121 pp., 1988. \$65 (8/89)

Computed Tomography of the Abdomen in Adults. 85 Radiological Exercises for Students and Practitioners. By A. Wackenheim and A. Badoz. (Translated by Marie-Therese Wackenheim.) New York: Springer-Verlag, 159 pp., 1988. \$19.50 (9/89)

Magnetic Resonance Imaging. 2nd ed.; vol. 1, Clinical Principles. By C. Leon Partain, Ronald R. Price, James A. Patton, Madan V. Kulkarni, and A. Everette James, Jr. Philadelphia: Saunders, 967 pp., 1988. \$400/2-vol. set (9/89)

Endovaginal Ultrasound. By Steven R. Goldstein. New York: Alan R. Liss, 175 pp., 1988. \$55 (9/89)

Diagnostic Imaging of the Acute Abdomen. A Clinico-Radiologic Approach. By Dieter Beyer and Ulrich Mödder. (Translated by Terry C. Telger.) New York: Springer-Verlag, 445 pp., 1988. \$130 (9/89)

Atlas of Duplex Scanning. Carotid Arteries. By John J. Cranley, William S. Karkow, and E. Douglas Baldrige, Jr. Philadelphia: Saunders, 352 pp., 1989. \$125 (9/89)

Digital Subtraction Imaging in Infants and Children. Edited by Eric N. Faerber. Mount Kisco, NY: Futura, 193 pp., 1989. \$42 (9/89)

Applied Pathology for Radiographers. By Paul F. Laudicina. Philadelphia: Saunders, 326 pp., 1989. \$32.95 (9/89)

General Thoracic Surgery. 3rd ed. Edited by Thomas W. Shields. Philadelphia: Lea & Febiger, 1251 pp., 1989. \$150 (9/89)

Catalog of Prenatally Diagnosed Conditions. By David D. Weaver. Baltimore: The Johns Hopkins University Press, 251 pp., 1989. \$45

Measurements of Radon and Radon Daughters in Air. (NCRP Report No. 97.) Bethesda, MD: National Council on Radiation Protection and Measurements, 174 pp., 1988. \$15

The Radiologic Clinics of North America. Hyperthermia. Guest Editor: Richard A. Steeves. Philadelphia: Saunders, May 1989; 27(3):401-630. \$25; by subscription, 6 issues annually for \$93

Blood Flow in the Brain. Edited by W. J. Angerson, C. D. Sheldon, J. C. Barbenel, A. C. Fisher, and J. D. S. Gaylor. New York: Oxford University Press, 138 pp., 1989. \$49.95

Blood Flow in Artificial Organs and Cardiovascular Prostheses. Edited by J. C. Barbenel, A. C. Fisher, J. D. S. Gaylor, W. J. Angerson, and C. D. Sheldon. New York: Oxford University Press, 266 pp., 1989. \$75

A Primer on Theory and Operation of Linear Accelerators in Radiation Therapy. By C. J. Karzmark and Robert J. Morton. Madison, WI: Medical Physics Publishing, 44 pp., 1989. \$12

Principles of Microsurgery for Lumbar Disc Disease. By John A. McCulloch. New York: Raven, 317 pp., 1989. \$98

American Roentgen Ray Society 90th Annual Meeting May 13-18, 1990, Washington, DC Sheraton Washington Hotel

Registration and Hotel Reservations

Forms for advance registration and hotel reservations will be in the February and March 1990 issues of the *AJR*.

Scientific Program

Abstracts of papers to be considered for the program must be submitted by December 1, 1989. Forms on which to submit abstracts are in this issue of the *AJR*. The ARRS Program Committee will select papers and notify authors in early January. The *AJR* has first rights to all papers accepted for presentation at the ARRS meeting. Send abstract, application, and four copies of the abstract to

M. Paul Capp, M.D.
c/o Paul R. Fullagar
American Roentgen Ray Society
1891 Preston White Dr.
Reston, VA 22091

Refresher Course Program

A summary of the refresher courses will appear in the *AJR* in February along with advance registration forms. Early registration is an advantage in assuring preferred courses in this popular program. Dr. J. T. Ferrucci, Jr., is program director.

Scientific Exhibits

Proposals for scientific exhibits must reach the Chairman of Exhibits by December 1, 1989. Forms, which may be photocopied, are in this issue of the *AJR*. Send completed form to

John E. Madewell, M.D.
The Pennsylvania State University
The Milton S. Hershey Medical Center
P.O. Box 850
Hershey, PA 17033
Telephone (717) 531-8044

Caldwell Lecture

Sandra Day O'Connor, U.S. Supreme Court Justice, will be giving the Caldwell Lecture. The title of her lecture and the date and time will be announced in a future issue of the *AJR*.

Local Program

A program of sightseeing, shopping, and entertainment will be developed by the Local Arrangements Chairman, Dr. Abner M. Landry, Jr. Information and advance registration forms will be in the February issue of the *AJR*.

Residents' Award Papers

The society offers several cash awards for the best scientific papers prepared by residents in radiology. The President's Award has a \$2000 prize. There are two Executive Council awards of \$1000 each. All are presented at the annual meeting. Papers should be submitted by February 16, 1990, for consideration in this competition. Send entries to

B. G. Brogdon, M.D.
Dept. of Radiology
University of South Alabama Medical Center
2451 Fillingim Street
Mobile, AL 36617

Deadlines

Abstracts of papers: December 1, 1989
Scientific exhibit proposals: December 1, 1989
Residents' Award papers: February 16, 1990

Call for Papers

American Roentgen Ray Society 1990 Annual Meeting: May 13-18, 1990, Washington, DC

ADDRESS OF PRESENTING AUTHOR

Department _____

Institution _____

Street _____

City, State _____

Zip _____

Phone: _____

Type title, authors, and abstract in the space provided below. (Instructions are on reverse side of this page. Abstract should not exceed 300 words.)

Select one category: _____Angio/Interventional _____Breast _____Chest _____CT _____Gastrointestinal Tract _____Genitourinary Tract _____MR
_____Neuroradiology _____Skeletal _____Sonography

Projection Requirements: _____35 mm, single or double (circle one) _____16 mm silent film _____1/2" VHS _____3/4"

Has this been presented elsewhere? _____yes _____no. If yes, please describe on reverse side of this page.

Instructions for Scientific Abstracts

1. Type the information single-spaced within the lines. Underline the name of the presenting author. Append as a last line of the abstract any research grant support, if applicable (e.g., Supported by USPHS Grant HE-80144). If the abstract is accepted, it will not be proofread; it will appear exactly as typed. Use the following format:

MR IMAGING OF THE SPINE AND NECK
F. S. Lau, M.D., A. N. Kirk, M.D., and R. A. Beck, Ph.D.
University of California, Bakersfield, Bakersfield, CA 92338
2. Abstracts should include four paragraphs devoted sequentially to the following topics: (1) object or purpose of the study, (2) materials, methods, and procedures, (3) results, (4) significance of the results and conclusions. The text should not exceed 300 words. Specific data are essential. The abstract should be a succinct summary of work done rather than a promissory note.
3. The Program Committee will grade each abstract and determine acceptance. Further information will be forwarded to those whose abstracts are accepted for presentation.

Deadline for submission of abstract is December 1, 1989. Mail abstract and two copies to

M. Paul Capp, M.D.
c/o Paul R. Fullagar
American Roentgen Ray Society
1891 Preston White Dr.
Reston, VA 22091

Call for Scientific Exhibits

**American Roentgen Ray Society
1990 Annual Meeting:
May 13-18, 1990, Washington, DC**

FOR COMMITTEE USE ONLY

Date Received _____ Application No. _____

Subject _____ Score _____

Rejected _____ Accepted _____

Assigned _____ Space No. _____

Principal Exhibitor's Mailing Address

Name _____ Institution _____

Department _____ Street Address _____ City _____

State _____ Zip Code _____ Telephone: office () home ()

Names of Exhibitors (List principal exhibitor first and telephone number of each person.)

Last	First	Middle	Telephone	Degree (one only)	Member ARRS?
------	-------	--------	-----------	----------------------	--------------

_____	_____	_____	_____	_____	_____
_____	_____	_____	_____	_____	_____
_____	_____	_____	_____	_____	_____
_____	_____	_____	_____	_____	_____
_____	_____	_____	_____	_____	_____

Title of Exhibit _____

Type abstract single-spaced in the space provided below. (See instructions on the reverse side of this page.)

Instructions for Abstract

The abstract should be a brief paragraph that states the purpose, principal information, and conclusions of the exhibit. Promissory statements are not acceptable. Type single-spaced in the space provided on the reverse side. Brevity is desirable but not at the expense of specific information. **The abstract will appear in the program book as submitted.** Please use typewriter and complete the application form on both sides. List space requirements.

What Sort of Exhibit Is Proposed? (Check one and fill in all appropriate blanks.)

_____ **Free-standing.** This is a self-contained display created in total by the exhibitor. It may be a fold-open unit, a unit shipped in cases and assembled on site, or a tabletop unit. Linear feet required _____.

_____ **Poster Board (backboard panels).** Backboard panels are 4×6 or 4×8 ft. (1.2×1.8 or 1.2×2.5 m). Number of panels required _____ 4×6 or _____ 4×8 . If two panels are needed, there will be a $\frac{1}{4}$ -in. frame separating the panels, thus requiring a separation in the presentation.

_____ **Viewbox.** Mounted materials (radiographs and other transparencies) for display on the society's illuminators. Each illuminator is 39.5×59.5 in. (100×151 cm). Number of illuminators required _____. Slides should not be glass mounted.

_____ **Audiovisual.**

Please Indicate Most Appropriate Category.

Diagnostic Radiology

_____ Bone _____ Cardiovascular System _____ Chest _____ Pediatric Radiology _____ Gastrointestinal Tract
_____ Genitourinary Tract _____ Neuroradiology _____ Mammography

Other

_____ Medical Physics _____ Nuclear Medicine _____ Radiation Oncology _____ Radiobiology _____ Sonography

Has the exhibit been shown in whole or in part at any previous meeting? _____ (Previous display does not preclude acceptance.)

If so, where? _____ When? _____

Nature of meeting or name of society _____

Signature of Principal Exhibitor _____

Exhibitors will receive instructions for exhibit preparation.

Applications must be received no later than December 1, 1989. Mail original and five copies to

John E. Madewell, M.D.
The Pennsylvania State University
The Milton S. Hershey Medical Center
P. O. Box 850
Hershey, PA 17033

Telephone: (717) 531-8044

American Roentgen Ray Society

Officers, Committees, and Membership Information

Officers

President: Ronald G. Evens
President-elect: M. Paul Capp
1st Vice-president: John A. Kirkpatrick, Jr.
2nd Vice-president: A. Everette James, Jr.
Secretary: Glen W. Hartman
Treasurer: Beverly P. Wood

Executive Council: R. J. Alfidi, R. N. Berk, B. G. Brogdon, M. P. Capp, W. J. Casarella, R. G. Evens, J. T. Ferrucci, Jr., R. A. Gagliardi, G. W. Hartman, J. A. Kirkpatrick, Jr., A. Landry, Jr., G. R. Leopold, J. E. Madewell, A. A. Moss, L. F. Rogers, J. H. Thrall, K. H. Vydareny, B. P. Wood, A. K. Poznanski, chairman

Committees

Editorial Policy: R. N. Berk, S. V. Hilton, C. A. Rohrman, Jr., S. S. Sagel, R. J. Stanley, J. M. Taveras, N. O. Whitley, W. J. Casarella, chairman

Education and Research: C. B. Higgins, B. J. Hillman, R. A. McLeod, W. M. Thompson, B. G. Brogdon, chairman

Finance and Budget: R. J. Alfidi, R. C. Gedgaudas-McClees, G. R. Leopold, J. R. Thornbury, J. Thrall, chairman

Nominating: R. A. Gagliardi, N. O. Whitley, R. J. Alfidi, chairman

Publications: C. A. Rohrman, Jr., S. S. Sagel, R. J. Stanley, N. O. Whitley, W. J. Casarella, chairman

Membership: R. J. Alfidi, A. A. Moss, K. H. Vydareny, G. R. Leopold, chairman

Representatives to Other Organizations

American Board of Radiology: J. A. Kirkpatrick, Jr., E. C. Klatte, L. F. Rogers

American College of Radiology: R. A. Gagliardi, G. A. Kling, J. E. Madewell, L. F. Rogers

American Medical Association House of Delegates: S. F. Ochsner, K. L. Krabbenhoft, alternate

American National Standards Institute: M. Haskin

National Council on Radiation Protection and Measurements: H. L. Friedell, E. L. Saenger

Meeting Arrangements

Annual Meetings: May 13-18, 1990, Sheraton Washington Washington, DC; May 5-10, 1991, Sheraton Boston, Boston

Annual Meeting Committee: H. C. Carlson, J. K. Crowe, G. P. Janetos, R. R. Lukin, A. Landry, Jr., chairman

Instruction Courses: R. J. Stanley, associate chairman, J. T. Ferrucci, Jr., chairman

Scientific Program: R. J. Alfidi, E. Buonocore, D. O. Davis, K. B. Hunter, T. C. McCloud, W. A. Murphy, Jr., A. E. Robinson, L. B. Talner, J. H. Thrall, M. P. Capp, chairman

Scientific Exhibits: R. J. Churchill, A. A. Moss, R. G. Ramsey, J. E. Madewell, chairman

ARRS Membership

An application form is printed in this issue of the Journal. For consideration at the 1990 ARRS meeting, send completed forms before February 1, 1990, to American Roentgen Ray Society, 1891 Preston White Dr., Reston, VA 22091. Active members are graduates of an approved medical or osteopathic school or hold an advanced degree in an allied science. They must practice radiology or work in an associated science in the United States or Canada and be certified by the American Board of Radiology, American Osteopathic Board of Radiology, or Royal College of Physicians of Canada or otherwise adequately document training and credentials. Corresponding members are foreign radiologists or scientists who are active in radiology or an allied science. Members-in-training are residents or fellows in radiology or postgraduate students in an allied science. Additional application forms can be obtained from the ARRS offices in Reston, VA.

Business Office

Paul Fullagar, Executive Director, American Roentgen Ray Society, 1891 Preston White Dr., Reston, VA 22091; (703) 648-8900

Information and Application for Membership in the American Roentgen Ray Society

General Information

The American Roentgen Ray Society, founded in 1900, has been a forum for progress in radiology since shortly after the discovery of x-rays. From its beginning and continuing to today, the ARRS has been guided by dedication to the goal of the advancement of medicine through the science of radiology and its allied sciences.

The goal of the ARRS is maintained through an annual scientific and educational meeting, and through publication of the *American Journal of Roentgenology*.

The annual meeting consists of instructional courses, scientific sessions, a symposium, scientific exhibits, and commercial exhibits. A special categorical course is also offered. Category I CME credits are available on an hour-for-hour basis.

The monthly *American Journal of Roentgenology* is a highly respected peer review journal with a worldwide subscription base. For over 75 years the *AJR* has been accepted as one of the best specialty journals available in the world, and this reputation grows each month.

A recently developed quarterly ARRS newsletter keeps members informed of events and general Society news.

Application Instructions

Candidates for Active Membership

1. An Active member must be a graduate of an approved medical school or hold an advanced degree in one of the physical, chemical or biological sciences and be certified by the American Board of Radiology, the American Osteopathic Board of Radiology, the Royal College of Physicians of Canada, or document training and credentials that are adequate to qualify for membership. Active members shall actively practice radiology or one of its branches in the United States or Canada. Such members are eligible to participate in all activities of the Society, including membership on committees, and have full voting privileges.
2. Application must be on an official form, signed by the applicant and at least two members of the American Roentgen Ray Society, active or emeritus, in good standing, who endorse the applicant.
3. Application fee is \$50 (payable when billed for dues).
4. Annual dues are \$125, payable on January 1 of each year following the initial year. First year dues will be invoiced following candidate election at the annual meeting. Of this amount, \$50 is for a 1-year subscription to the *American Journal of Roentgenology*, beginning with the July issue following election to membership.
5. Application must be received by February 1 for action during the current year's meeting.

Candidates for In-Training Membership

1. In-training members must be serving in a radiology residency program approved by the Radiology Residency Review Committee, the American Osteopathic Board of Radiology, or the Royal College of Physicians of Canada, or in an approved post-residency fellowship, or be a postgraduate student in an allied science. Training status must be verified by the program director. In-training members have special consideration in fees and subscription rates to the Society journal. Such members cannot hold Society offices or vote.
2. Application must be on an official form and signed by the applicant and by the applicant's training or residency program director.
3. In-training status is limited to a maximum of five years starting with the entrance date into the radiology residency. In the last year, each in-training member will receive an application for active membership from the Society. Those who do not apply for transfer to active membership shall be dropped from membership at the end of the fifth year, but can later apply as a new member through the process outlined for active status.
4. There is no application fee. Annual dues are \$25. Membership includes a subscription to the *American Journal of Roentgenology* and admission to the annual meeting without payment of the registration fee.
5. Membership applications will be acted on when received.

Corresponding Membership

A corresponding member must meet the qualifications of active membership, but reside and practice in a foreign country. Corresponding members shall pay dues and fees, but shall not have the privileges of voting nor of holding elective office.

All Applicants

1. Do not remit application fee or dues until requested.
2. Send completed forms to: American Roentgen Ray Society
1891 Preston White Drive
Reston, Virginia 22091

For ARRS
Office Use

Date Rec'd _____

I.D.# _____

AMERICAN ROENTGEN RAY SOCIETY APPLICATION FOR MEMBERSHIP

Date: _____

Category of Membership: ☐ Active
(Check One) ☐ Corresponding
☐ In-Training

Name (Please Print) _____ Degree(s) _____
First Initial Last

Mailing Address _____ Date of Birth _____
Street/Box

City/State/Country _____ Zip Code _____ Telephone () _____

A. Education: (List name of institution, years attended, and degree and type received.)

Undergraduate: _____

Graduate (Medical School, Graduate School, etc.):

Postgraduate [Internship, Residency, Fellowship, etc.):

B. Licensure:

Licensed to practice _____ in _____ since _____
(Type) (State, Province, etc.)

C. Appointments/Memberships: (In-Training applicants: skip to Section F on reverse.)

Present Appointments: Academic _____

Hospitals _____

Memberships in Scientific Societies: _____

Offices or Committee Assignments: _____

Government Service (Military or Civilian) _____ (Position) _____ (Years)

D. Credentials:

I hereby certify that I was issued a certificate of qualification in _____
(Specialty)

in _____ by the _____
(Year) (Name of Qualifying Board)

Other Credentials: _____

Signature: _____

E. References:

We, active or emeritus members in good standing of the American Roentgen Ray Society, and acquainted with the applicant, do recommend him/her for membership in the Society. (Two references are required.)

Name (Please Print) 1. _____ 2. _____

Address _____

Signatures: _____

F. IN-TRAINING APPLICANTS MUST COMPLETE THIS SECTION**Credentials:**

I certify that I am serving as a Resident/Fellow in _____
(Specialty)

at _____ Date program began (begins): _____;
(Name of Institution)

date program to end: _____. I understand that in-training membership is limited to a maximum of 5 years.

Applicant Signature: _____

Verification: (Program Director or Department Chairman *only*)

I certify that the applicant is in training at the institution named and qualifies for enrollment as a member-in-training of the American Roentgen Ray Society.

Name (Please Print) _____

Address: _____

Signature _____

Send completed form to: **American Roentgen Ray Society**
1891 Preston White Drive
Washington, D.C. 20037

Classified Advertisements

Positions Available

PACIFIC NORTHWEST—Extraordinary opportunity for BC diagnostic radiologist interested in joining private, office-based practice in Seattle suburb. Expertise and interest in CT and ultrasound required. Address inquiries, including CV to Harold Shulman, M.D., Talbot Rd. Radiology, 4300 Talbot Rd. S., Renton, WA 98055; (206) 228-6000. 10a.

OPPORTUNITY FOR YOUNG, WELL-TRAINED, AGGRESSIVE RADIOLOGIST to join 5-person group in a small, midwestern city near St. Louis. Excellent equipment including mobile MRI. Competitive salary leading to early partnership. Reply to Box U40, AJR (see address this section). 10xap

ANDREWS, LYNCH & FIELD, RADIOLOGISTS, P.A., a 15-radiologist group based in Bangor, ME, is currently working with 2 hospitals in coastal "Downeast" Maine to recruit radiologists. The hospitals, located in Calais and Machias, are 90 mi. from Bangor in areas noted for outdoor recreation, natural beauty, and a slower pace of life. Each hospital has R/F, ultrasound, and new dedicated mammography units and will begin to receive mobile CT and nuclear medicine services in the near future. Wide flexibility exists in practice arrangements to meet the needs of the radiologists, and the goal of the hospitals to secure stable, long-term radiologist support. If you would like to learn more about these opportunities, contact Peter Holman, Administrator, Andrews, Lynch & Field, Radiologists, P.A., 276 State St., Bangor, ME 04401; (207) 945-6877. 10ap

STAFF RADIOLOGIST—The Colmery-O'Neil VA Medical Center, Topeka, KS, is recruiting for a board-certified radiologist to work with 2 staff radiologists in a modern diagnostic imaging dept. Activities include routine radiography, fluoroscopy, limited angiography, CT, ultrasound, percutaneous biopsy, and PTC. This 609-bed medical center is affiliated with the Oral Roberts School of Medicine which provides physicians with teaching opportunities. An excellent school system, several universities within a 60-mi. radius, and a wide variety of cultural and recreational programs are available. Federal benefit package includes liberal holiday and leave programs, malpractice insurance coverage, and tax-deferred retirement options. Please send inquiries to Harold M. Voth, M.D., Chief of Staff (11), VA Medical Center, 2200 Gage Blvd., Topeka, KS 66622. EOE. 10a

BODY IMAGER—We are seeking a board-certified radiologist with postgraduate training and experience in body imaging, CT, ultrasound, MRI, and interventional radiology. Experience in mammography is desirable. This 550-bed hospital is in an attractive suburban setting 25 mi. from New York City with university-affiliated residency. Negotiable terms leading to full partnership. Please send CV to P. E. Moriarty, M.D., 151 Summit Ave., Summit, NJ 07901. 10-12ap

FULL- AND PART-TIME DIAGNOSTIC RADIOLOGIST positions available immediately at the VA Medical Center, Allen Park, MI. All modalities except MR available. Dept. is actively affiliated with the Wayne State University College of Medicine's radiology residency rotation program. Flexible schedules available for part-time radiologists. Must be board-certified/eligible with licensure in any state. Salary \$80,000-\$90,000 for full-time, depending on qualifications. Liberal vacation time (30 days/yr), sick leave (13 days/yr) and medical education leave. Contact L. Jean Bronn, M.D., Chief, Diagnostic Radiology Service, VA Medical Center, Southfield & Outer Dr. Allen Park, MI 48101; (313) 562-6000, ext. 3256. Equal opportunity employer. 10a

DIAGNOSTIC RADIOLOGIST—BC radiologist interested in group practice in central Maine. Candidates must have strong diagnostic skills in R/F, CT, ultrasound, and mammography. The 52-bed hospital is located in a beautiful rural community 35 mi. from Bangor. Radiologist will be supported by 15-member, Bangor-based group. Partnership is offered after completion of 3 yr employment. Liberal vacation and CME leave, and outstanding fringe benefits are included. Contact Peter Holman, Administrator, Andrews, Lynch & Field, Radiologists, P.A., 276 State St., Bangor, ME 04401; (207) 945-6877. 10ap

THE ABDOMINAL SECTION OF EMORY UNIVERSITY, DEPT. OF RADIOLOGY, is seeking an abdominal radiologist. The position is an exciting opportunity for an individual with teaching, clinical, and/or research interest. The individual will have access to state-of-the-art equipment in fluoroscopy, ultrasound, CT, and MRI. Interested candidates should contact Michael E. Bernardino, M.D., Professor of Radiology, Director, Abdominal Division and Magnetic Resonance Imaging, Dept. of Radiology, Emory University Hospital, 1364 Clifton Rd., N.E., Atlanta, GA 30322. Emory University is an equal opportunity/affirmative action employer. 10-12a

FACULTY NEURORADIOLOGIST, THOMAS JEFFERSON UNIVERSITY HOSPITAL—The Dept. of Radiology at Thomas Jefferson University Hospital and Jefferson Medical College, Philadelphia, will have a new faculty neuroradiology position available July 1, 1990. This is due to rapid growth in our neuro/ENT division and the opening of 3 additional MRI units by that date. Jefferson has very large and active neurology, neurosurgery, and ENT clinical services, as well as strong commitments to research and teaching. Our Neurosciences Imaging Center includes angio, myelography, CT, and MRI units together in a discrete area of the dept. The current neuro/ENT division includes 5 full-time faculty and 4 fellows. Candidates can be either at the junior or senior level; rank and compensation will be determined by previous experience. Excellent salary and benefits are provided. Contact David C. Levin, M.D., Chairman, Dept. of Radiology, Thomas Jefferson University Hospital, Philadelphia, PA 19107. Jefferson is an equal opportunity/affirmative action employer. 10xa

DIAGNOSTIC RADIOLOGISTS—Roswell Park Memorial Institute (RPMI) is seeking board-certified radiologists with special interest in gastrointestinal imaging, including barium radiography, CT, and ultrasound. At this renowned comprehensive cancer center, currently entering a period of renewed growth, opportunity for research and academic activity is outstanding. A faculty appointment at the School of Medicine and Biomedical Sciences, SUNY at Buffalo, depends on professional qualifications. CV should be submitted to Andrew A. Gage, M.D., Roswell Park Memorial Institute, Elm and Carlton Sts., Buffalo, NY 14263. RPMI is an affirmative action/equal opportunity employer. 10a

DIAGNOSTIC RADIOLOGISTS—Roswell Park Memorial Institute (RPMI) is seeking board-certified radiologists with special interest in CT/MRI. At this renowned comprehensive cancer center, currently entering a period of renewed growth, opportunity for research and academic activity is outstanding. A faculty appointment at the School of Medicine and Biomedical Sciences, SUNY at Buffalo, depends on professional qualifications. CV should be submitted to Andrew A. Gage, M.D., Roswell Park Memorial Institute, Elm and Carlton Sts., Buffalo, NY 14263. RPMI is an affirmative action/equal opportunity employer. 10a

THE DEPT. OF RADIOLOGY AT TRIPLER ARMY MEDICAL CENTER, HONOLULU, HI, is recruiting academically oriented radiologists for several divisions of the dept.: ultrasound, CT and/or MRI, interventional radiology, chest radiology, neuroradiology, and general diagnostic radiology. Our dept. offers a fully accredited residency program with 16 residents and 16 attending full-time staff. Numerous consultants from across the country lecture on a continuing and regular basis. The hospital is a modern, tertiary-care center servicing Hawaii and the entire Pacific basin. A strong residency program, a diverse and interesting patient population, excellent equipment, and a tropical lifestyle are positive aspects of the practice. Academic credentials and/or experience are necessary. Recently graduated fellows are encouraged to apply. Board certification is mandatory. Candidates should be particularly interested in patient care, teaching, and research. Salary and benefits are competitive and generous. Tripler is an EO/EEOE employer. Please contact Dr. Mark F. Hansen, Col. MC, Chief, Dept. of Radiology, TAMC, HI 96859-5000; (808) 433-6393. 10a

RADIOLOGISTS—New York City combined private radiology practice and fee-for-service hospital practice has an immediate opening for 2 BC/BE radiologists with experience in CT, ultrasound, and interventional radiology. In addition, MRI and mammography experience is preferred. This well-established practice has 3 private offices on the upper east side of Manhattan as well as operations in 3 hospitals in Manhattan. Other studies performed in the practice are diagnostic radiology, nuclear imaging, and vascular duplex imaging. The practice continues to expand in all imaging modalities with its recent opening of a second state-of-the-art MRI unit. Excellent benefit package includes health, life, disability, and malpractice insurance, profit-sharing plan, continuing medical education, and a travel and entertainment account for professional use. Send CV to Box U48, AJR (see address this section). 10ap

IMMEDIATE OPENING FOR BC/BE RADIOLOGIST to join 6 radiologists in practice at 300-bed, teaching hospital in greater Boston area. Should have some interest in special procedures and interventional procedures. Salary negotiable, leading to partnership. Send CV to Herbert D. Weintraub, M.D., Framingham Union Hospital, 115 Lincoln St., Framingham, MA 01701; (508) 626-3525. 10-1ap

BELOIT, WI—Three board-certified radiologists seek a fourth for a dynamic diagnostic and interventional practice in a community hospital, multi-specialty clinic, and private office. All imaging modalities are represented. The hospital is affiliated with the University of Wisconsin. Beloit is on the Illinois-Wisconsin state line not far from Madison, Milwaukee, and Chicago. Write or call Thomas J. Lisk, M.D., Beloit Radiology, Ltd., 1969 W. Hart Rd., Beloit, WI 53511; (608) 364-5266 or (815) 623-6010. An excellent opportunity. 10-1ap

KENNER ARMY COMMUNITY HOSPITAL, a 120-bed facility, is seeking a second full-time, board-certified/eligible radiologist trained in ultrasound, mammography, CT, and general radiology. The dept. consists of 5 examination rooms, 10 technicians, support staff, and modern equipment. Located on Fort Lee in Petersburg, VA, the hospital is situated 25 mi south of Richmond and within 3 hr of historic Williamsburg, Washington, DC, and Virginia Beach. Paid vacation; salary negotiable. Submit inquiries to Lt. Col. Gayle Humm, Deputy Commander for Clinical Services, Kenner Army Community Hospital, Fort Lee, VA 23801; (804) 734-5058. Fort Lee is an equal opportunity employer. 10a

DIAGNOSTIC RADIOLOGIST—Eight board-certified radiologists in expanding, hospital-based, private practice seek BC/BE general radiologist to associate. Competence in all modalities expected, with need for interventional and/or MRI training emphasized. Opportunity in midwestern city of 72,000 people offers generous compensation/vacation. Full partnership after 2 yr. Reply to Box U44, *AJR* (see address this section). 10-1a

THE SECTION OF URORADIOLOGY, DEPT. OF RADIOLOGY, HOSPITAL OF THE UNIVERSITY OF PENNSYLVANIA, is seeking a third, full-time staff urologist to join its faculty in Aug. or Sept. 1990. Although experience in diagnostic and interventional urology is preferable, consideration will be given to less experienced radiologists anxious for a career in academic urology. For further information, contact Howard M. Pollack, M.D., Section of Uroradiology, Dept. of Radiology, Hospital of the University of Pennsylvania, 3400 Spruce St., Philadelphia, PA 19104; (215) 662-3278. 10a

DIAGNOSTIC RADIOLOGY, PLYMOUTH, MA—Successful group of 4 radiologists in seacoast community 40 mi. south of Boston seeks compatible fifth diagnostic radiologist for July 1990. Busy practice at hospital and offices includes all modalities. We seek an excellent general radiologist with expertise in MRI/neuro. At least 6 mo full-time MRI experience is necessary. Excellent benefits and vacation leading to full partnership. Please send letter of inquiry with CV to D. Dougherty, M.D., or R. Goldberg, M.D., 139 Sandwich St., Plymouth, MA 02360. 10-12ap

DIAGNOSTIC RADIOLOGIST—Immediate opening for a board-certified/eligible general diagnostic radiologist at the VA Medical Center, Atlanta, GA. Must be proficient in body CT, ultrasound, and related interventional procedures. We offer a full range of federal employee benefits. Qualified applicants will receive a clinical faculty appointment at the Emory University Medical School. For further information, call Jeanie McCleary at (404) 728-7637 or write VA Medical Center, 1670 Clairmont Rd., Atlanta (Decatur), GA 30033. EOE. 10-11a

THE RADIOLOGY DEPT., University of Massachusetts Medical Center, is seeking a full-time radiologist with interest in trauma, emergency room, and musculoskeletal radiology. The Medical Center is a 370-bed university hospital and medical school located in Worcester, MA, approximately 40 mi. west of Boston. The dept. consists of 19 clinical staff, 12 residents, and 3 fellows and does approximately 120,000 exams/yr. The dept. is well-equipped with 2 fourth-generation CT scanners, two 1.5-T GE MR scanners, and a 2.0-T small-bore unit for animal research. The hospital is a major trauma center and is serviced by 2 Life Flight helicopters. The candidate must be board-eligible/certified and have a clinical background in skeletal radiology. Please send CV/requests to Dr. Edward H. Smith, Chair, Dept. of Radiology, University of Massachusetts Medical Center, 55 Lake Ave. N., Worcester, MA 01655. The University of Massachusetts Medical Center is an equal opportunity employer. 10a

PACIFIC NORTHWEST—Ten-member, hospital-based group seeks 2 radiologists (a fellowship-trained chest radiologist and a general radiologist with optional fellowship training) for a modern, 625-bed, tertiary-care medical center and on-campus office practice in Spokane, WA, a progressive community with outstanding recreational opportunities. Forward inquiry or CV to Hal Holte, M.D., Dept. of Radiology, Sacred Heart Medical Center, W. 101 - 8th, Spokane, WA 99204; (509) 455-3352 or 455-3330. 10xap

DIRECTOR, DIAGNOSTIC RADIOLOGY—Roswell Park Memorial Institute (RPMI) is seeking a board-certified radiologist to serve as director of the Dept. of Diagnostic Radiology. Substantial academic credentials and an interest in research are highly desired. At this renowned comprehensive cancer center, currently entering a period of renewed growth, opportunity for research and academic activity is outstanding. A faculty appointment at the School of Medicine and Biomedical Sciences, SUNY at Buffalo, is associated with the appointment. CV should be submitted to Andrew A. Gage, M.D., Roswell Park Memorial Institute, Elm and Carlton Sts., Buffalo, NY 14263. RPMI is an affirmative action/equal opportunity employer. 10a

NEW ORLEANS RADIOLOGY GROUP seeks board-certified radiologist interested in part-time position. No angiography is required. Long-term commitment is desired. Responsibilities include general radiography, mammography, CT, and ultrasound. Ideal practice situation for a semi-retired radiologist. Send CV to Harold R. Neitzschman, M.D., 440 General Meyer Ave., Ste. 211, New Orleans, LA 70131. 10-12ap

ISRAEL, DIAGNOSTIC RADIOLOGY. Opportunities for 3-4 week or longer working vacations in a number of Israeli medical centers, on a volunteer basis. Positions varied, arrangements flexible. For information contact: Jonathan H. Fish, M.D., 1844 San Miguel Dr., #302, Walnut Creek, CA 94596; (415) 947-0560. 8-10ap

DIAGNOSTIC RADIOLOGIST, ABDOMINAL IMAGING—The University of Missouri-Columbia Hospital and Clinics is seeking a radiologist with expertise in abdominal imaging (GI, CT, ultrasound, and MRI). Board certification required. Fellowship desirable. Tenured and nontenured tracks available at assistant and associate professor levels. Address inquiries to Robert J. Churchill, M.D., Dept. of Radiology, University of Missouri-Columbia Hospital and Clinics, One Hospital Dr., Columbia, MO 65212. An equal opportunity/affirmative action employer. 9-12a

NEURORADIOLOGIST—The University of Missouri-Columbia Hospital and Clinics is seeking a second neuroradiologist. Board certification required. Junior or senior member of ASNR. Tenured and nontenured tracks available at assistant and associate professor levels. Address inquiries to Robert J. Churchill, M.D., Dept. of Radiology, University of Missouri-Columbia Hospital and Clinics, One Hospital Dr., Columbia, MO 65212. An equal opportunity/affirmative action employer. 9-12a

NEURORADIOLOGIST—A position is available in the Dept. of Radiology, at the University of Rochester Medical Center, Strong Memorial Hospital, a 750-bed tertiary-care facility. An appointment as assistant professor or higher is available at a level appropriate to experience. A fellowship is required. Research and teaching opportunities are available in a strong academic dept. with state-of-the-art radiologic equipment. Send CV to Daniel K. Kido, M.D., Diagnostic Radiology, Box 648, University of Rochester Medical Center, Rochester, NY 14642. EO/AA/M-F employer. 9-11a

VASCULAR RADIOLOGIST—Board-certified vascular radiologist to join dept. in a university-affiliated hospital in western Pennsylvania. Applicant should have fellowship training or past residency experience in vascular and interventional procedures. The radiologists are organized as a professional corporation offering excellent salary and fringe benefits. Send inquiries and CV to Radiologist-in-Chief, Montefiore Hospital, 3459 Fifth Ave., Pittsburgh, PA 15213. 9-12ap

PEDIATRIC RADIOLOGIST—The University of Rochester Medical Center, Strong Memorial Hospital, a 750-bed tertiary-care facility has an opening within the Pediatric Section of the Dept. of Radiology. State-of-the-art equipment, a high volume of neonatal and oncology work, research, and teaching opportunities are available in a strong academic dept. Faculty rank depends on qualifications. Send CV to Robert E. O'Mara, M.D., Chairman, Dept. of Radiology, Box 648, University of Rochester Medical Center, Rochester, NY 14642. EO/AA/M-F employer. 9-11a

DIAGNOSTIC RADIOLOGIST WITH SPECIAL INTEREST IN ANGIOGRAPHY AND INTERVENTIONAL RADIOLOGY—The Dept. of Radiology at The University of Texas Medical School at Houston has an immediate opening for an experienced interventionist/angiographer with strong interest in patient care and teaching. Research interest and experience are important, but not essential. While the principal responsibilities will be in intervention/angiography, there will be an opportunity to be involved in other clinical areas of the candidate's interest. The position will include teaching at the medical student and resident levels. Candidate must be a diplomate of the American Board of Radiology and have completed at least a 1-yr interventional/angiography fellowship, have a Texas state medical license, and have had at least 1 yr post-fellowship experience. Candidates with the qualifications for a senior assistant professor or associate professor appointment are preferred. Academic rank and salary will be commensurate with qualifications. Please submit CV, along with the names and addresses of 3 references to John H. Harris, Jr., M.D., Dept. of Radiology, The University of Texas Medical School of Houston, 6431 Fannin St., Ste. 2.132, Houston, TX 77030. The University of Texas Health Science Center at Houston is an equal opportunity employer. Women and minorities are encouraged to apply. 9-12a

TWO DIAGNOSTIC RADIOLOGISTS—Four-person, private practice group seeks 2 BC/BE radiologists with expertise in CT, angio/interventional, ultrasound, and mammography. MRI/neuro/trauma experience helpful. Practice includes 225-bed private hospital plus 2 smaller hospitals. University affiliation, some teaching. Duluth is a pleasant northern community which combines proximity to outdoor recreation with the advantages of a small urban center. Competitive salary/fringe leading to early partnership. Send CV or call F. Ekberg, M.D., 915 E. 1st St., Duluth, MN 55805; (218) 726-5222. 9-11ap

SOUTH FLORIDA, IMMEDIATE OPENING—Rapidly expanding, 10-person group with 3 hospitals, MRI center, and imaging office desires an additional well-trained radiologist. Interventional radiology fellowship and/or equivalent interventional experience a must. This is a highly desirable private practice with partnership potential. Please send CV to Lee M. Katims, M.D., Dept. of Radiology, 21644 State Rd. 7, Boca Raton, FL 33428. 9-11ap

DIAGNOSTIC RADIOLOGIST—Immediate opening for a board-certified radiologist to join young, dynamic, 4-person group in the Miami area. All modalities including special procedures, CT, nuclear medicine, and MRI. Community hospital-based practice with adjacent outpatient facility. Competitive salary and benefits with partnership opportunity. Location convenient to Florida Keys, with easy access to downtown, cultural, and recreational facilities. Please contact Roberto J. Calderon, M.D.P.A., 730 N.W. 107 Ave., Ste. 108, Miami, FL 33172. 9-11ap

INTERVENTIONAL RADIOLOGIST—A tenure-track position at the rank of assistant professor to professor is available in the Dept. of Radiology at the University of Virginia Health Sciences Center. Salary and academic rank commensurate with experience and qualifications. Minimum requirements include M.D. with board certification in radiology and competence in angiography, interventional radiology, and special procedures. Starting date is negotiable. Please provide CV and names and addresses of 3 references. Contact Charles J. Tegtmeier, M.D., Professor and Director, Division of Angiography, Interventional Radiology and Special Procedures, Box 170, University of Virginia Health Sciences Center, Charlottesville, VA 22908; (804) 924-9401. Equal opportunity/affirmative action employer. 9-11a

POSITION AVAILABLE—Two diagnostic radiologists seek a BE/BC radiologist to join them in a growing practice in northeast Michigan. Our 176-bed, regional referral hospital serves an area population of 80,000-100,000. All diagnostic modalities with the exception of MRI are represented. Equipment includes Acuson ultrasound, Siemens Somatom CT, and dedicated Phillips mammography. Our location on Lake Huron offers immediate access to sailing, fishing, scuba diving, etc. Excellent hunting, snowmobiling, and cross-country skiing are favorite fall and winter activities. This is an outstanding opportunity for someone seeking a small town atmosphere, a dynamic radiology practice with early partnership in a beautiful outdoor area. Please respond to Box T5, AJR (see address this section). 9-11a

DIAGNOSTIC RADIOLOGIST—State-of-the-art practice includes ultrasound, nuclear medicine, digital subtraction angiography, CT, and MRI. Excellent practice. Excellent financial package. Send CV to Robert L. Dever, M.D., 1416 Big Bend Rd., Poplar Bluff, MO 63901; (314) 785-0125. 9-12ap

CHIEF, BREAST IMAGING CENTER—The Dept. of Diagnostic Radiology at William Beaumont Hospital is seeking a radiologist with mammography experience to head its modern breast imaging center which includes breast ultrasound. There will be some rotation in general radiology. Beaumont Medical Center is a 940-bed, modern, tertiary-care teaching hospital in southeastern Michigan with residency and fellowship in most subspecialties including radiology. Excellent remuneration and fringe benefits. For further information, write to Jalil Farah, M.D., Chairman, Diagnostic Radiology, William Beaumont Hospital, 3601 W. 13 Mile Rd., Royal Oak, MI 48072; (313) 551-6064. 9-11a

ASSISTANT PROFESSOR OF NEURORADIOLOGY—The University of Texas Medical School at Houston has an opening for a neuroradiologist who will perform clinical neuroradiology. Candidate will participate in resident and medical student teaching and will have the opportunity to do basic or clinical research. Candidates must have completed an approved residency in diagnostic radiology and must have successfully completed 2 yr of a neuroradiology fellowship. Candidates must be board-certified by the American Board of Radiology or equivalent and must have a Texas medical license. Applicants should send a CV, along with the names and addresses of 3 references, to John H. Harris, Jr., M.D., D.Sc., Professor and Chairman, Dept. of Radiology, The University of Texas Medical School at Houston, 6431 Fannin St., Ste. 2.132, Houston, TX 77030. The University of Texas Health Science Center at Houston is an equal opportunity employer. Women and minority candidates are encouraged to apply. 9-12a

ULTRASONOLOGIST—Board-certified radiologist with fellowship training in ultrasound to join dept. in a university-affiliated hospital in western Pennsylvania. Position immediately available. The radiologists are organized as a professional corporation offering excellent salary and fringe benefits. Send inquiries and CV to Radiologist-in-Chief, Montefiore Hospital, 3459 Fifth Ave., Pittsburgh, PA 15213. 9-12ap

IMMEDIATE OPENING, DIAGNOSTIC RADIOLOGIST—Large, private practice, 3 hospitals, northeast Philadelphia suburbs and Trenton, NJ, between Philadelphia and Princeton. Two positions to start preferably Dec. 1989 or later. Practice requires all areas of diagnostic radiology; expertise in angio-interventional, MRI, or cross-sectional imaging desired. Fellowship or practice experience preferred. Send letter and CV to S. Meshkov, M.D., 838 W. State St., Trenton, NJ 08618. 9-11ap

APPROVED "B" READER to interpret chest x-rays on- or off-site in central New Jersey. Contact Joel Namm, M.D., 838 W. State St., Trenton, NJ 08618. 9-11ap

IMMEDIATE OPENING IN PHILADELPHIA, PA—Excellent opportunity for diagnostic radiologist to join newly formed private group in 260-bed, south Philadelphia hospital. Prefer starting date Dec. 1989; would consider later. Expertise in angio-interventional or cross-sectional imaging desired. Practice requires all areas of diagnostic radiology. Fellowship or practice experience preferred. Send letter and CV to Box T7, AJR (see address this section). 9-11ap

RADIOLOGIST, IMMEDIATE OPENING—New York City imaging center seeks board-certified radiologist, specialty MRI, with experience in CT. General Electric equipment. Replies to Box T9, AJR (see address this section). 9-11ap

MAINE—General radiologist to join busy practice affiliated with modern, 92-bed, acute-care hospital. Diagnostic modalities include ultrasound, mammography, angiography, nuclear medicine, and mobile CT. Beautiful 4-season recreation area close to skiing, hunting, and fishing. Excellent school system. Competitive first yr salary with partnership available by the second yr. For further information, send CV to New England Health Search, 63 Forest Ave., Orono, ME 04473; (207) 866-5680 or (207) 866-5658. 8-11ap

VASCULAR/INTERVENTIONAL RADIOLOGIST—The Dept. of Radiology of Emory University Hospital, Atlanta, GA, has a faculty position available for a board-certified vascular/interventional radiologist with fellowship training. Academic rank depends on qualifications and experience. A strong interest in care of patients, teaching, and research is required. Submit application and CV to Stephen L. Kaufman, M.D., Director of Vascular and Interventional Radiology, Emory University Hospital, 1364 Clifton Rd., N.E., Atlanta, GA 30322. Emory University is an equal opportunity/affirmative action employer. 8-10a

EUGENE, OR—BC/BE, general, and axial imaging radiologist. Group of 9 radiologists in Pacific Northwest seeking a new associate for a growing radiology practice. All imaging modalities represented are state-of-the-art. Practice is in a 400-bed hospital with an excellent referring staff. A very democratic, fair radiology group and a great environment to raise a family make this opening especially desirable. Two yr to full partnership. Prepartnership compensation negotiable, commensurate with experience. Prefer fellowship experience in MRI, CT, or ultrasound with Doppler. Please send CV to L. Paul Wilson, M.D., 667 E. 12th Ave., Ste. 110, Eugene, OR 97401. 8-10ap

DIAGNOSTIC RADIOLOGIST, GEORGIA—Group of 5 board-certified radiologists affiliated with 300-bed, acute-care hospital in Savannah, GA, seeks BC/BE associate. Excellent facilities include CT, nuclear medicine with SPECT, general and vascular ultrasonography, mammography, neuro/angio/interventional, and MRI. Practice includes new private office, liberal benefits, and early partnership. Demographics include an expanding economy in an attractive community with outstanding recreational resources. Please include CV with letter of inquiry to Thomas Philbrick, M.D., Savannah Radiologists, P. O. Box 14444, Savannah, GA 31499. 9-11ap

THE DEPT. OF RADIOLOGY, VIRGINIA COMMONWEALTH UNIVERSITY/MEDICAL COLLEGE OF VIRGINIA, Richmond, VA, seeks faculty for positions in diagnostic radiology: chest, GI, mammography, CT/ultrasound/MRI, neuroradiology, pediatrics, ER, angio/interventional, and general radiology. Our 1058-bed facility (205 for pediatric patients) is a Level 1 trauma center. ABR certification of eligibility required. Academic rank and salary commensurate with experience. Submit CV to A. V. Proto, M.D., Diagnostic Radiology, Medical College of Virginia, MCV Box 47, Richmond, VA 23298-0047. VCU/MCV is an equal opportunity/affirmative action employer. Women and minorities are encouraged to apply. 9-12a

DIAGNOSTIC RADIOLOGIST, NORTHEASTERN PENNSYLVANIA—Opportunity available for board-certified/eligible general radiologist with experience in MRI, ultrasound, CT scanning, nuclear medicine, and mammography in a 130-bed, community hospital located in the pleasant Pocono Mountain Resort region of northeast Pennsylvania. Competitive salary and early partnership. The area offers outstanding recreational opportunities and is within a reasonable distance of New York and Philadelphia. Contact Fred C. Van Natta, M.D., Dept. of Radiology, Wayne County Memorial Hospital, Honesdale, PA 18431. 9-10a

THE OREGON HEALTH SCIENCES UNIVERSITY, Dept. of Radiology, Portland, OR, invites applications for faculty positions in MRI, neuroradiology, general radiology, skeletal radiology, vascular and interventional radiology, GU radiology, pediatric radiology, computed body tomography, and ultrasound. A second Ph.D. NMR scientist also is being sought. The Oregon Health Sciences University is an affirmative action, equal opportunity employer. Send CV to Richard W. Katzberg, M.D., Chairman of Diagnostic Radiology, L340, The Oregon Health Sciences University, 3181 S.W. Sam Jackson Park Rd., Portland, OR 97201-3098. 5-4ap

NEW HAMPSHIRE—Excellent opportunity for young, BC/BE, general radiologist with MRI experience to join well-established, busy, small group. Live and work in beautiful Connecticut Valley Region close to lakes and skiing. Competitive compensation package leading to partnership. Please send CV to New England Health Search, 63 Forest Ave., Orono, ME 04473; (207) 866-5680 or (207) 866-5685. 8-10ap

RADIOLOGIST—Expanding radiology practice has an opening for a radiologist with fellowship or postgraduate experience in interventional radiology. Exceptional general radiology talents also needed. Special competency in nuclear medicine and MRI a plus, but not mandatory. Practice is located in Albuquerque, NM and consists of 13 physicians serving 3 major hospital facilities and a separate MRI center. Climate and living conditions are outstanding. Qualified applicants may send CV and references to Radiology Associates of Albuquerque, P.A., 4001 Indian School Rd., N.E., Ste. 300, Albuquerque, NM 87110, Attn: J. R. Ellison, Business Manager. 8-10ap

INTERVENTIONAL/DIAGNOSTIC RADIOLOGIST—Immediate opening for a board-certified diagnostic radiologist in Providence, RI. Well-established private practice of 5 radiologists encompassing a tertiary-care hospital and 1 private office. Interventional fellowship, interest in general diagnostic radiology, and teaching skills required. Address CV and inquiries to Allan M. Deutsch, M.D., Director, Dept. of Radiology, Miriam Hospital, 164 Summit Ave., Providence, RI 02906; (401) 274-3700, ext. 4408. 8-10ap

ULTRASOUND STAFF RADIOLOGIST, THOMAS JEFFERSON UNIVERSITY HOSPITAL—The Dept. of Radiology at Thomas Jefferson University Hospital in Philadelphia has an immediate faculty opening in its Division of Diagnostic Ultrasound. This is an exciting opportunity for a person with combined clinical, research, and teaching interests. Our ultrasound division is 1 of the largest and best-equipped in the world, with responsibility for the full range of ultrasound exams, including obstetrical, vascular, endorectal and endovaginal, interventional, Doppler, operative, and gallstone and kidney stone lithotripsy. Excellent salary and benefits are provided. Interested applicants should contact Barry Goldberg, M.D., Director of Diagnostic Ultrasound, or David Levin, M.D., Chairman, Dept. of Radiology, Thomas Jefferson University Hospital, Philadelphia, PA 19107. Thomas Jefferson University is an equal opportunity/affirmative action employer. 8-1ap

ALEXANDRIA, VA GROUP seeks BC associate for hospital/office practice. Candidate should have expertise in all areas of noninterventional radiology including nuclear medicine and MR. Present 8-person group staffs 400-bed hospital, MR center, and active offices. Submit CV to William V. Hindle, M.D., Chairman, Dept. of Radiology, Alexandria Hospital, 4320 Seminary Rd., Alexandria, VA 22304. 8-10ap

DIAGNOSTIC RADIOLOGIST—Two positions: 1 full-time leading to early partnership; 1 full-time salary for 1 yr. We are a private practice group of 7 full- and 2 part-time board-certified radiologists, all with prior fellowship and/or faculty status, practicing general radiology with specialty interests accommodating all diagnostic and interventional modalities, including MRI. Our 350-bed hospital is a primary teaching affiliate of University of Massachusetts Medical School with year-round medical students and house staff in several dept. The Berkshire Mountains are a desirable summer, winter, and fall foliage resort community, less than 3 hr drive to all major northeastern cities. Quality of our practice, hospital, affiliated office, and style of life are superior. Please respond with CV to Stuart Masters, M.D., Chairman, Dept. of Radiology, Berkshire Medical Center, 725 North St., Pittsfield, MA 01201. 8-11ap

DIAGNOSTIC RADIOLOGIST sought to join a fee-for-service group practice in a 458-bed Bronx hospital. Board certification with expertise in ultrasound, MRI, CT, special procedures, and general diagnostic radiology preferred. Send CV to St. Barnabas Radiological Associates, P. O. Box 4332, Great Neck, NY 11027, or call M. Gade, M.D.; (212) 960-6171. 8-1ap

SAN FRANCISCO BAY AREA, DIAGNOSTIC RADIOLOGY—Full-time position available as of July 1989 for BC/BE radiologist to join established group based in growing SF Bay area communities. Competence in all modalities including MRI and angiography required; fellowship training desirable. Contact J. Fish, M.D., c/o Walnut Creek Radiology, 1844 San Miguel Dr., #302, Walnut Creek, CA 94596; (415) 947-0560. 10-12xa

ON JULY 1, 1990 THE FACULTY OF THE UNIVERSITY OF TEXAS MEDICAL SCHOOL AT HOUSTON will assume clinical practice, teaching, and research at the Lyndon Baines Johnson (LBJ) General Hospital, newly constructed by the Harris County Hospital District, in Houston, TX. LBJ General will be a principal medical student teaching affiliation of the UTMSH, is certified for 307 beds, and is projected to perform approximately 130,000 imaging procedures the first yr. The Dept. of Radiology at LBJ is fully-equipped with new state-of-the-art GE equipment, including a 9800 Quick CT scanner with 3-D software and an LU angiographic unit, comparable routine, R and F, ultrasound, and nuclear equipment. Full-time UTMSH faculty positions exist for 5 associate professors and 10 assistant professors with clinical, teaching, and research interests in all aspects of diagnostic imaging. Compensation, based upon the most recent AAMC survey, will be commensurate with training and experience. Candidates must be diplomates of the American Board of Radiology or its equivalent, and must have a Texas medical license. Applicants are requested to send their CV to John H. Harris, Jr., M.D., D. Sc., Professor and John S. Dunn, M.D., Chairman, Dept. of Radiology, the University of Texas Medical School at Houston, 6431 Fannin, Ste. 2.132, Houston, TX 77030. The University of Texas Health Science Center at Houston is an equal opportunity employer. Women and minorities are encouraged to apply. 8-11a

RADIOLOGIST—The Elko Regional Medical Center seeks a BC/BE general diagnostic radiologist to work at the medical center as well as the local community hospital. CT, mammography ultrasound, nuclear medicine, and some interventional training or experience required. Guaranteed salary for 6 mo leading to full partnership. Excellent benefits package including malpractice insurance. Elko is a thriving community surrounded by mountains and wilderness areas. Recreation yr round. Please send CV to Cherie Atwood, Administrator, Elko Regional Medical Center, 762 14th St., Elko, NV 89801; (702) 738-3111. 10-12ap

TWO RADIOLOGISTS, BC/BE to join 2 others in N.E. Florida location of St. Augustine. Two hospitals, imaging center, and mobile MRI. Excellent salary in lovely beach community. Send CV to Dr. Lewis or Dr. Mendenhall, St. Augustine General Hospital, U.S. 1 South, Box 2208, St. Augustine, FL 32085; (904) 824-8431. 7-10ap

TEXAS, DIAGNOSTIC RADIOLOGIST—Three board-certified radiologists seek compatible associate for growing group practice in attractive N.E. Texas community. Excellent health resources. Modalities include MRI and angiography. Comfortable call arrangement; good salary and benefits. Early partnership. Area has strong, diversified economy, excellent schools, and many social and recreational opportunities. Enjoy great location, weather, and people. Extraordinary opportunity! Please send CV in confidence, or call Vicki Truitt, Physician Resource Network, P. O. Box 37102, Fort Worth, TX 76117; (817) 595-1128. 7-10ap

RADIOLOGIST—Board-certified/eligible radiologist wanted to join 3 board-certified radiologists in busy, university-affiliated, community hospital near Boston. Area offers many educational and recreational opportunities. We seek a general radiologist with demonstrated ability in mammography, angio/interventional, ultrasound, and CT. MR experience a plus. Liberal benefits, vacation, and educational leave. Competitive salary leading to full partnership in professional corporation. Address inquiries to Steven Sitzman, M.D., The Malden Hospital, One Hospital Rd., Malden, MA 02148; (617) 322-7560, ext. 5164. 7-10ap

DIAGNOSTIC RADIOLOGIST—Radiologists seek board-certified radiologist with experience in CT, nuclear medicine, general radiology, and ultrasound including Doppler, for a hospital-based, private practice in 225-bed general hospital in Forest Hills, NY. MRI pending. Immediate opening leading to partnership. Contact M. Tartell, M.D.; (718) 544-5858. 9-10ap

NEURORADIOLOGIST—The University of Texas Health Science Center at San Antonio is seeking a qualified academic neuroradiologist to fill an immediate opening. Send cover letter and CV to John R. Jenkins, M.D., Director of Neuroradiology, University of Texas Health Science Center, 7703 Floyd Curl Dr., San Antonio, TX 78284-7800. 6-11ap

BREAST IMAGING RADIOLOGIST, THOMAS JEFFERSON UNIVERSITY HOSPITAL—The Dept. of Radiology at Thomas Jefferson University Hospital in Philadelphia has an immediate opening in a faculty position with emphasis on mammography and breast ultrasound. Some work in the general diagnostic division also is included. Jefferson has a large new Breast Imaging Center currently averaging about 85 studies/day, as well as active research and teaching programs. Excellent salary and benefits are offered. Contact either Stephen A. Feig, M.D., Director of Breast Imaging, or David C. Levin, M.D., Professor and Chairman, Dept. of Radiology, Thomas Jefferson University Hospital, Philadelphia, PA 19107. Thomas Jefferson University is an equal opportunity/affirmative action employer. 6-11ap

PEDIATRIC RADIOLOGIST—Vacancies are available in various parts of the Pediatric Radiology Dept. at The Hospital for Sick Children, Toronto. The hospital is a 560-bed, tertiary-care, pediatric center situated in downtown Toronto and affiliated with the University of Toronto. 100,000 exams are performed each yr, and the staff includes 17 full-time pediatric radiologists and 7 fellows. Positions are available in general pediatric radiology areas as well as in more specialized areas such as neuroradiology. The dept. is equipped with state-of-the-art equipment. Applicants must have pediatric radiology experience, including 1- and preferably 2-yr fellowship, and staff radiologists with greater experience are certainly most welcome. For further information, please contact A. Daneman, M.D., Radiologist-in-Chief, Dept. of Radiology, The Hospital for Sick Children, 555 University Ave., Toronto, Ontario, M5G 1X8, Canada; (416) 598-6026. 9-12a

ATLANTA, GA—One radiology position. The Southeast Permanente Medical Group, Inc., Georgia Region, is seeking an additional radiologist for a growing radiology dept. serving several medical centers throughout the Atlanta area. Interested and qualified candidates must be board-certified in radiology with expertise in general radiology to include CT, ultrasound, and mammography. Address inquiries and CVs to Alex Daley, M.D., Chief of Radiology, c/o The Southeast Permanente Medical Group, Inc., 3355 Lenox Rd., Ste. 1000, Atlanta, GA 30326; (404) 233-0555, ext. 192. 5-10ap

DIAGNOSTIC RADIOLOGIST—Combined hospital/office position available at a large, tertiary-care hospital in Phoenix, AZ. The radiology group seeks a new associate who is board-certified, and preferably has had an imaging fellowship and/or academic experience. Competitive salary and benefits leading to partnership offered. Please call Theodore Ditchek, M.D., or Aubrey Palestrant, M.D.; (602) 239-4601 or write c/o Dept. of Radiology, Good Samaritan Regional Medical Center, 1111 E. McDowell Rd., Phoenix, AZ 85006. 8-12ap

POSITION OPEN IMMEDIATELY—Forty-physician multispecialty clinic, serving central and western Kansas, is seeking a board-eligible/certified radiologist. Excellent facilities include diagnostic radiology, CT, diagnostic ultrasound, nuclear medicine, and mobile MR services. An excellent opportunity in a dynamic practice setting. Please send CV to Administrator, Hutchinson Clinic, 2101 N. Waldron, Hutchinson, KS 67502; (316) 663-6121. 6-12ap

Positions Desired

SEEKING FELLOWSHIP in angiography and interventional radiology. 43-yr-old, university-trained diagnostic radiologist with 10-yr experience in angiography and interventional procedures. Please respond to Box U42, AJR (see address this section). 10-11bp

BC RADIOLOGIST, UNIVERSITY-TRAINED IN MRI—Experienced diagnostic radiologist (all modalities) with administrative and organizational experience, and 1 yr university training in MRI, is interested in a private/academic practice with primary MRI/CT responsibility in a quality medical community. Prefer Southern California but will consider all opportunities. Reply to Box U46, AJR (see address this section). 10bp

Fellowships and Residencies

FELLOWSHIP IN ULTRASOUND AND BODY CT/MRI—July 1, 1991 to June 30, 1992, at the New York Hospital/Cornell Medical Center. Dept. provides state-of-the-art equipment, including Acuson ultrasound, GE 9800 CT, and GE Signa 1.5-T MR. Wide variety of ultrasound exams include abdominal, OB-GYN, color Doppler, small parts, neonatal head, transvaginal, and transrectal. Applicants should be ABR eligible or certified. Send CV to Elias Kazam, M.D., Dept. of Radiology, The New York Hospital/Cornell Medical Center, 525 E. 68th St., New York, NY 10021. 10-12cp

NEURORADIOLOGY FELLOWSHIP, THOMAS JEFFERSON UNIVERSITY HOSPITAL—An unexpected opening for a neuroradiology fellow is available in the Dept. of Radiology at Thomas Jefferson University Hospital, beginning July 1990. The Division of Neuroradiology has close clinical and research relationships with Jefferson's very active neurology, neurosurgery, orthopedic surgery, and otolaryngology depts. Complete training in ENT radiology is part of this program. Five full-time faculty members currently staff this division. Clinical facilities include 2 dedicated CT scanners, a myelography room, a biplane angiography room with DSA, and a GE 1.5-T MRI unit. Two more MRI units will be operational by the summer of 1990. Contact Carlos Gonzalez, M.D., Director of Neuroradiology, 1009 Main Bldg., Thomas Jefferson University Hospital, Philadelphia, PA 19107; (215) 928-5447. Jefferson is an affirmative action/equal opportunity employer. 10xc

MRI FELLOWSHIP AT THOMAS JEFFERSON UNIVERSITY HOSPITAL—A new MRI fellowship position has been created in the Dept. of Radiology of Thomas Jefferson University Hospital, Philadelphia. This 1-yr position encompasses a full range of clinical and research activities. The MRI division includes 6 staff physicians, 2 MRI physicists, and 3 Signa systems (1.5 T). The position is available as of Jan. 1990, but applications will also be taken for the academic year beginning July 1990. Send inquiries to Matthew Rifkin, M.D., Dept. of Radiology, Thomas Jefferson University Hospital, Philadelphia, PA 19107. Jefferson is an equal opportunity/affirmative action employer. 9-6c

FELLOWSHIP IN MUSCULOSKELETAL RADIOLOGY—The Emory University, School of Medicine, Dept. of Radiology, offers a 1-yr fellowship in musculoskeletal radiology starting July 1, 1990. Clinical activities include MRI, CT, needle biopsies, arthrography, and QCT. The musculoskeletal section is staffed by 3 full-time radiologists. Experience includes a wide range of musculoskeletal disease and trauma through a 600-bed university hospital, a 1000-bed county hospital, a 160-bed pediatric hospital, and 2 outpatient clinics. Candidates should be eligible for Georgia medical licensure. Contact Terry M. Hudson, M.D., Dept. of Radiology, Emory University School of Medicine, Atlanta, GA 30322; (404) 248-4354. Emory University is an equal opportunity/affirmative action employer. 10-12c

UNIVERSITY OF MASSACHUSETTS MEDICAL CENTER, Dept. of Radiology, has an opening for a 1-yr vascular/interventional radiology fellowship beginning July 1, 1990. The Medical Center is a major trauma center with approximately 360 beds. It is located 40 mi. west of Boston, in central Massachusetts. The clinical service is very active. An average of 650 vascular/interventional procedures are performed during an academic yr. Facilities include 2 dedicated vascular/interventional radiology suites with Siemens and Toshiba equipment. Both conventional and digital subtraction imaging capabilities are present. The staff consists of 2 fellowship-trained, cardiovascular/interventional radiologists. Numerous radiological, clinical, and basic science conferences are scheduled on a daily basis, and there is ample time during the course of the yr to attend many of these presentations. A 1-mo rotation on ultrasound and/or body CT is also available. The fellowship position carries the title of instructor of radiology. For further information, contact David A. Phillips, M.D., Associate Professor, Director Vascular and Interventional Radiology, UMMC, 55 Lake Ave. N., Worcester, MA 01655; (508) 856-5740. An equal opportunity employer. 10c

FELLOWSHIPS IN NEURORADIOLOGY—The Dept. of Radiology at The University of Texas Medical School at Houston has openings for 1- and 2-yr fellowships to begin in July 1990 and July 1991 in neuroradiology. Under faculty supervision, candidates will be responsible for neuroradiologic exams and procedures (i.e., angiograms, myelograms, CT and MR imaging, and *in vivo* spectroscopy). The candidate will participate in teaching at the medical student and resident levels and will conduct basic or clinical research. Candidate must be a graduate of an approved U.S. medical school or its equivalent, must have completed an approved residency in diagnostic radiology, must be a diplomate of the American Board of Radiology, and must have a Texas medical license. Please submit CV, along with the names and addresses of 3 references to John H. Harris, Jr., M.D., Dept. of Radiology, The University of Texas Medical School at Houston, 6431 Fannin, Ste. 2.132, Houston, TX 77030. The University of Texas Health Science Center at Houston is an equal opportunity employer. Women and minorities are encouraged to apply. 9-12c

CARDIOVASCULAR AND INTERVENTIONAL RADIOLOGY—Two-yr fellowship starting July 1, 1990. Peripheral and coronary angiography, cardiac catheterization, digital vascular imaging, all types of interventional procedures, noninvasive vascular techniques, and cardiovascular MRI. Research time available for participation in original or ongoing clinical and/or laboratory projects. Contact Donald P. Harrington, M.D., Dept. of Radiology, Harvard Medical School, Brigham and Women's Hospital, 75 Francis St., Boston, MA 02115. 9-10c

RADIOLOGY RESIDENCY IN SAN FRANCISCO BAY AREA—Unexpected, immediate opening available at 2nd, 3rd, or 4th yr level. Please send CV to Edward A. Lebowitz, M.D., Dept. of Diagnostic Radiology, Santa Clara Valley Medical Center, 751 S. Bascom Ave., San Jose, CA 95128; (408) 299-6370. 9-10cp

FELLOWSHIPS AT THOMAS JEFFERSON UNIVERSITY HOSPITAL—The Dept. of Radiology at Thomas Jefferson University Hospital in Philadelphia offers 6 different fellowship programs each yr: ultrasound/CT/MRI - contact Barry Goldberg, M.D.; cardiovascular/interventional - contact Geoffrey Gardiner, Jr., M.D.; neuroradiology/ENT - contact Carlos Gonzalez, M.D.; chest/breast imaging - contact Robert Steiner, M.D. or Stephen Feig, M.D.; MRI - contact Matthew Rifkin, M.D.; and musculoskeletal (including MRI) - contact David Karasick, M.D. We have a large and well-equipped dept. performing 180,000 exams/yr. Our ultrasound division occupies a spacious new facility and provides training in all phases of ultrasound, including obstetrical, vascular, lithotripsy, and endoluminal. The dept. has 3 modern CT scanners and operates 3 GE 1.5-T MRI units also. The interventional radiology division recently has opened an entirely new angio suite housing state-of-the-art Philips units with DSA. This division performs the full range of both vascular and nonvascular interventional procedures. The neuroradiology division is housed in a neurosciences imaging center containing all imaging modalities in a single comprehensive facility. A large new breast imaging center now operates 5 mammography units and performs breast ultrasound studies also. All program directors listed above can be contacted at the Dept. of Radiology, Thomas Jefferson University Hospital, Philadelphia, PA 19107. Jefferson is an equal opportunity/affirmative action employer. 9xc

FELLOWSHIP IN ULTRASOUND/CT/ANGIO-INTERVENTIONAL—Available July 1, 1990. A 1-yr fellowship program is available at the Lehigh Valley Hospital Center in Allentown, PA, a 492-bed, acute-care facility with Level I Trauma Center designation. The fellowship program offers training in CT (head and body), ultrasound, angiography (neuro and visceral), and interventional radiography. MRI experience also is available. For further information, contact Robert Kricun, M.D., Dept. of Radiology, Lehigh Valley Hospital Center, P. O. Box 689, Allentown, PA 18105. 10cp.

FELLOWSHIPS IN ABDOMINAL IMAGING—The Dept. of Radiology at The University of Texas Medical School at Houston has openings for 2 fellowships to begin in July 1991 in abdominal imaging. Under faculty direction and supervision, candidates will further their training in the specialty of abdominal imaging including CT, ultrasound, and MRI through 4-mo rotations in each service. Candidates will participate in teaching in each section at the medical student and resident levels, will have the opportunity to conduct basic or clinical research, and will be expected to prepare and submit at least 1 scientific article to an appropriate refereed journal. Candidate must be a graduate of an approved U.S. medical school or its equivalent, must have completed an approved residency in diagnostic radiology, must be a diplomate of the American Board of Radiology, and must have a Texas medical license. Please submit CV, along with the names and addresses of 3 references to John H. Harris, Jr., M.D., Dept. of Radiology, The University of Texas Medical School at Houston, 6431 Fannin, Ste. 2.132, Houston, TX 77030. The University of Texas Health Science Center at Houston is an equal opportunity employer. Women and minorities are encouraged to apply. 9-12c

FELLOWSHIP POSITIONS—Applications are invited now for July 1991. Positions are available in neuroradiology, vascular/interventional radiology, and body imaging (CT/ultrasound/MRI). For information, contact James R. Schmidgall, M.D. or Richard W. Katzberg, M.D., Chairman, Dept. of Radiology, L-340, Oregon Health Sciences University, 3181 S. W. Sam Jackson Park Rd., Portland, OR 97201. 7-6c

Other

EIGHTH WINTER CONGRESS: DAVOS, SWITZERLAND—March 10-17, 1990. Category I accreditation; international faculty. MRI, CT, ultrasound, and interventional. For information, contact Medical Seminars, 9800 D Topanga Canyon Blvd., Ste. 232, Chatsworth, CA 91311; (818) 700-9821. 10-2e

AJR Classified Advertisements Information

Box Responses and Address for Ad Placement

Write Box _____, AJR, 2223 Avenida de la Playa, Suite 200, La Jolla, CA 92037-3218; (619) 459-2229; FAX: (619) 459-8814.

How to Place an Ad

AJR accepts classified advertising for Positions Available, Positions Desired, Fellowships and Residencies, and Tutorials/Courses. Ads are accepted by mail or FAX.

Rates: \$6.00/line with a \$30 minimum charge. Box service is \$10 additional for each month the ad appears. There are discounts for multiple insertions: 10% for 2-3 insertions; 20% for 4 or more. To estimate lines, count all words and divide by 7.

Billing: Ads *must* be prepaid, or advertisers will be billed after the ad appears *providing* a purchase order number is submitted with the advertising copy. Terms are net 30 days.

Deadlines: 6 weeks prior to issue date. For specific deadlines, telephone the AJR editorial office.

Estimating Ad Charges

Line charge: divide total words by 7 and multiply by \$6.00	\$ _____
Multiple insertions? If so, multiply by number	× _____
Subtotal	\$ _____
Discount applies to two or more insertions. Subtract 10% if ad appears 2-3 months, 20% if 4 months or more	- _____
Subtotal	\$ _____
Box response requested? If so, multiply number of months by \$10.00	+ _____
Approximate advertising charge	\$ _____

SIEMENS

RSNA
1915•1989

75
years

Advancing
Patient Care
through Science
and Education



Beyond Imaging

Beyond each imaging modality and support service we offer there is a commitment to be in touch with the state of your art...and with you, the professionals who practice it.

Once a year the RSNA gives us that opportunity.

A time for professional enrichment. The exchange of ideas. A welcome chance to learn more about your requirements for tomorrow. And the opportunity to show you the technological advancements and services we have today.

Computed tomography • PACS • Lithotripsy • Linear accelerators • Magnetic resonance • Therapy planning • Mobile image intensifier • Diagnostic ultrasound • X-ray mammography • R/F systems • Data management • Education programs • Digital imaging • Therapy simulator • Uro-radiology • Mobile MR • Nuclear medicine • Site planning • Service plans • Mobile CT • Cardiovascular imaging • Financial services • Mobile X-ray • Preventive maintenance • Special procedures • Health physics • Diagnostic imaging centers • In-service education • Positron emission tomography • Bone mineral densitometry

1989 ARRS AWARD PAPERS

- 687 President's award. The validity and utility of sonography in the diagnosis of appendicitis in the community setting. Larson JM, Peirce JC, Ellinger DM, et al.
- 693 Executive council award. Exercise-enhanced MR imaging of variations in forearm muscle anatomy and use: importance in MR spectroscopy. Fleckenstein JL, Bertocci LA, Nunnally RL, Parkey RW, Peshock RM

PROGRESS IN RADIOLOGY

- 699 High-resolution carotid sonography: past, present, and future. O'Leary DH, Polak JF
- 705 Sonography of the male genital tract. Benson CB, Doubilet PM, Richie JP

CARDIOPULMONARY RADIOLOGY

- 715 Serial assessment of myocardial infarction by using gated MR imaging and Gd-DTPA. Nishimura T, Kobayashi H, Ohara Y, et al.
- 721 Cine MR imaging in mitral regurgitation: comparison with color Doppler flow imaging. Nishimura T, Yamada N, Itoh A, Miyatake K
- 725 Case report. Diagnosis of a myocardial lipoma by using CT. Conces DJ Jr, Vix VA, Tarver RD
- 727 Chronic eosinophilic pneumonia: CT findings in six cases. Mayo JR, Müller NL, Road J, Sisler J, Lillington G

GASTROINTESTINAL RADIOLOGY

- 731 Gastric fluid detected by sonography in fasting patients: relation to duodenal ulcer disease and gastric-outlet obstruction. Smithuis RHM, Op den Orth JO
- 735 Positive predictive value and posttest probability of diagnosis of colonic polyp on single- and double-contrast barium enema. Ott DJ, Scharling ES, Chen YM, Gelfand DW, Wu WC
- 741 Primary malignant tumors in the small bowel: a comparison of the small-bowel enema and conventional follow-through examination. Bessette JR, Maglinte DDT, Kelvin FM, Chernish SM
- 745 Case report. Typhoid fever: diagnosis by using sonography. Puylaert JBCM, Kristjānsdóttir S, Golterman KL, de Jong GM, Knecht NM
- 747 Localized clotted blood as evidence of visceral trauma on CT: the sentinel clot sign. Orwig D, Federle MP
- 751 Arterial perfusion abnormalities of the liver after hepatic arterial infusion chemotherapy and their correlation with changes in the metastases: evaluation with CT and angiography. Roth J, Wallner B, Safi F
- 755 MR angiography and dynamic flow evaluation of the portal venous system. Edelman RR, Zhao B, Liu C, et al.
- 761 Case report. Idiopathic cecal ulcer: CT findings. Marn CS, Yu B-FB, Nostrant TT, Ellis JH

GENITOURINARY RADIOLOGY

- 765 Renal imaging in long-term dialysis patients: a comparison of CT and sonography. Taylor AJ, Cohen EP, Erickson SJ, Olson DL, Foley WD
- 768 Commentary. Imaging studies for screening native kidneys in long-term dialysis patients. Mindell HJ
- 771 In vivo MR spectroscopic imaging of the adrenal glands: distinction between adenomas and carcinomas larger than 15 mm based on lipid content. Leroy-Willig A, Bittoun J, Lutton JP, et al.
- 775 The pars infravaginalis gubernaculi: importance in the identification of the undescended testis. Rosenfield AT, Blair DN, McCarthy S, Glickman MG, Rosenfield NS, Weiss R
- 779 Case report. Benign prostatic hypertrophy: treatment with a metallic stent. Machan L, Jäger HR, Adam A, Gill K, Williams G, Allison DJ
- 783 Technical note. Biocompatible copolymer ureteral stent: maintenance of patency beyond 6 months. Rackson ME, Mitty HA, Lossef SV, Dan SJ, Train JS

MUSCULOSKELETAL RADIOLOGY

- 785 The enthesopathic changes of hypophosphatemic osteomalacia in adults: radiologic findings. Burnstein MI, Lawson JP, Kottamasu SR, Ellis BI, Micho J

- 791 Radiation-induced sarcoma of bone: CT findings in 19 cases. Lorigan JG, Libshitz HI, Peuchot M
- 795 Commentary. Optimal plain film imaging of the shoulder impingement syndrome. Kilcoyne RF, Reddy PK, Lyons F, Rockwood CA Jr

PEDIATRIC RADIOLOGY

- 798 John L. Gwinn, 1989 gold medalist of The Society for Pediatric Radiology. Lee FA
- 799 Findings on chest radiographs after prophylactic pulmonary surfactant treatment of premature infants. Clarke EA, Siegle RL, Gong AK
- 803 CT evaluation of blunt abdominal trauma in children: comparison of ultrafast and conventional CT. Brody AS, Seidel FG, Kuhn JP
- 807 Reliability of voiding cystourethrography to detect reflux. Jequier S, Jequier J-C
- 811 Pictorial essay. Radiographic evaluation of velopharyngeal incompetence in childhood. Barr LL, Hayden CK Jr, Hill LC, Swischuk LE

FETAL AND OBSTETRIC RADIOLOGY

- 815 Sonography of placental abnormalities and oligohydramnios in women with elevated alpha-fetoprotein levels: comparison with control subjects. Kelly RB, Nyberg DA, Mack LA, Fitzsimmons J, Uhrich S
- 821 Intrauterine shelves in pregnancy: sonographic observations. Brown DL, Felker RE, Emerson DS
- 825 Case report. Sonographic diagnosis of omphalocele during 10th week of gestation. Brown DL, Emerson DS, Shulman LP, Carson SA
- 827 Case report. Prenatal sonographic diagnosis of harlequin ichthyosis. Mihalko M, Lindfors KK, Grix AW, Brant WE, McGahan JP

NEURORADIOLOGY

- 829 The cerebellum in sagittal plane—anatomic-MR correlation. 1. The vermis. Courchesne E, Press GA, Murakami J, et al.
- 837 The cerebellum in sagittal plane—anatomic-MR correlation. 2. The cerebellar hemispheres. Press GA, Murakami J, Courchesne E, et al.
- 847 MR imaging of muscles of mastication. Schellhas KP
- 857 MR imaging of neurocysticercosis. Teitelbaum GP, Otto RJ, Lin M, et al.
- 867 CT of nasopharyngeal carcinoma: significance of widening of the preoccipital soft tissue on axial scans. Hoe J
- 873 MR signal intensity of parathyroid adenomas: correlation with histopathology. Auffermann W, Guis M, Tavares NJ, Clark OH, Higgins CB

COMPUTER PAGE

- 877 Cost-effective development of a computer-assisted instruction system. McGhee RB, Bennett WF, Morris CS, Witanowski LS

OTHER CONTENT

- Book and videotape reviews 714, 734, 740, 750, 820, 836, 880
- 763 ARRS 1990 resident award papers information
- 764 Forthcoming articles
- 774 Memorial, Chalmer S. "Bud" Wheeler
- 782 Memorial, Fred R. McCrear
- 856 Memorial, Satya Pal Aggarwal
- 883 Letters
- 890 Review of current literature
- 895 News
- 897 Books received
- 898 ARRS 1990 meeting announcement, calls for papers and exhibits
- 903 American Roentgen Ray Society information
- 904 ARRS application for membership
- 907 Classified advertisements
- A3 Guidelines for authors
- A8 AJR business and subscriber information